DISSERTATION

FORMATION OF THE HURRICANE EYE

Submitted by

Jonathan L. Vigh

Department of Atmospheric Science

In partial fulfillment of the requirements

For the Degree of Doctor of Philosophy

Colorado State University

Fort Collins, Colorado

Spring 2010

COLORADO STATE UNIVERSITY

January 29, 2010

WE HEREBY RECOMMEND THAT THE DISSERTATION PREPARED UNDER OUR SUPERVISION BY JONATHAN L. VIGH ENTITLED FORMATION OF THE HURRICANE EYE BE ACCEPTED AS FULFILLING IN PART REQUIREMENTS FOR THE DEGREE OF DOCTOR OF PHILOSOPHY.

Committee on Graduate Work

William R. Cotton

Takamitsu Ito

Mark DeMaria

David Krueger

Advisor: Wayne H. Schubert

Department Head: Richard H. Johnson

ABSTRACT OF DISSERTATION

FORMATION OF THE HURRICANE EYE

This dissertation consists of three distinct studies which investigate aspects of eye formation. The first study reviews eye phenomenon in a variety of vortices ranging from simple vortices to the menagerie of geophysical vortices, emphasizing similarities and differences to the eyes formed in hurricanes. The hurricane eye is found to be a paradoxical structure imposed by conservation of angular momentum and the boundaries of the vortex. A comprehensive definition for hurricane eye formation is proposed and various eye formation mechanisms are summarized.

The next study presents a simple theoretical argument to isolate the conditions under which a tropical cyclone can rapidly develop a warm-core thermal structure and subsequently approach a steady state. The theoretical argument is based on the balanced vortex model and, in particular, on the associated transverse circulation equation and the geopotential tendency equation. The transverse circulation and the temperature tendency in a tropical vortex depend not only on the diabatic forcing, but also on the spatial distributions of the static stability, the baroclinity, and the inertial stability. The vortex response to diabatic heating depends critically on whether the heating occurs in the low inertial stability region outside the radius of maximum wind or in the high inertial stability region inside the radius of maximum wind. This result suggests that rapid intensification is favored for storms which have at least some of the eyewall convection inside the radius of maximum wind. The development of an eye partially removes diabatic heating from the high inertial stability region of the storm center, yet rapid intensification may continue if the eyewall heating continues to become more efficient. As the warm core matures and static stability increases over the inner core, conditions there become less favorable for deep upright convection and the storm tends to approach a steady state.

The final study characterizes the kinematic and thermodynamic changes that occur before, during, and after the initial eye formations of a broad set of Atlantic tropical cyclones. To obtain the requisite structure and intensity parameters, a new data set has been synthesized from the Vortex Data Messages

transmitted by routine aircraft reconnaissance from 1989-2008. Intensity ranges are determined for the times when the eye/eyewall structure first appears in aircraft radar and infrared satellite imagery. The mean intensity at which an eye is first observed in both aircraft or satellite imagery is found to be 58 kt, somewhat lower than reported in previous studies. Changes about the time of eye formation are examined for intensity, the radius of maximum winds, the minimum Rossby radius of deformation, eye temperature and dew point temperature depression. Storms are found to intensify most rapidly near the time of eye formation, especially when a persistent eye is observed in infrared satellite imagery. Many storms which are forming eyes are found to undergo a substantial and rapid contraction in the radius of maximum winds during the 24-h period before the eye is observed; once the eye is present, this contraction slows or ceases. Strong warming at lower levels (850 or 700 hPa) of the eye is not observed to correlate well with the time in which the eye is first observed. Finally, observations suggest that the dynamical heating efficiency of the resulting eyewall increases even as the physical scale of the efficient heating region decreases. This allows the storm to continue intensifying even though the total inner core diabatic heating may decrease. The answer to why some storms fail to form eyes may shed light on whether eye formation is a stochastic process involving constructive and destructive mesoscale interactions – or whether it is a manifold attractor of the system sometimes stymied by an unfavorable environment.

Jonathan L. Vigh
Department of Atmospheric Science
Colorado State University
Fort Collins, Colorado 80523-1371
Spring 2010

ACKNOWLEDGEMENTS

I thank all of the teachers and mentors who have opened the world of knowledge to me over the years. In particular, I owe a debt of gratitude to my advisor Wayne Schubert. His infectious love for atmospheric dynamics combined with an unparalleled willingness to repeatedly explain complex dynamical phenomenon and discuss all manner of other topics have made it an absolute pleasure to work for him. His unflappable dedication, continual curiosity, and extraordinary patience are inspirational and worthy of emulation. He has not only been a great research advisor to me, but also a close mentor and friend. I count myself very blessed to have had the opportunity to work with him.

I also thank the members of my committee members for their patience, guidance, and helpful suggestions. These persons include Mark DeMaria (who has also been a good mentor), William Cotton, Takamitsu Ito, David Krueger, and Michael Montgomery (former committee member).

The other members of the Schubert Research Group, past and present, have also contributed substantially to my understanding of hurricanes and tropical meteorology. These include Christopher Rozoff, Kate Musgrave, Levi Silvers, Brian McNoldy, Eric Hendricks, Paul Ciesielski, Matthew Masarik, Kevin Mallen, Alex Gonzalez, Gabriel Williams, Gabriela Mora, James Kossin, Ricardo Prieto, and Jack Dostalek. I appreciate the many insightful discussions I have had with them over the years. Their humor has helped make the journey more enjoyable. Rick Taft and Gail Cordova have provided amazing computer and administrative support which has also been greatly appreciated.

Several other people have provided helpful guidance, suggestions, and ideas which helped shape this work over the years. These include John Knaff, Greg Holland, Margie Kieper, Christopher Landsea, Frank Marks, Jr., Hugh Willoughby, Raymond Zehr, Jim Kossin, Joanne Simpson, and Naomi Surgi.

Since each major chapter has been written so as to be published as a stand-alone paper, the following acknowledgments are listed by chapter.

For chapter 2, we thank John Knaff, Mark DeMaria, Greg Holland, William Gray, Christopher Rozoff, William Cotton, David Krueger, Takamitsu Ito, Michael Montgomery, Frank Marks, Jr., Hugh Willoughby, Brian McNoldy, Kate Musgrave, and Levi Silvers for their advice and helpful comments.

For chapter 3, we thank Christopher Rozoff, Timothy Dunkerton, Mary Haley, Paul Ciesielski, Mark DeMaria, Levi Silvers, Eric Hendricks, Kevin Mallen, Brian McNoldy, Kate Musgrave, Rick Taft, Ed Zipser, and an anonymous reviewer for their advice and helpful comments.

For chapter 4, we owe an enormous debt to the brave flight crews of the 53rd Weather Reconnaissance Squadron and NOAA's Aircraft Operation Center who put themselves at risk each and every time they go out to collect these vital data. Without their dedication and diligence, this study would not have been possible. We also thank the following people for their assistance in obtaining the comprehensive VDM archive used in this study: Steve Feuer, Barry Damiano, John Pavone, Chris Sisko, Christopher Juckins, Mark Zimmer, Christopher Landsea, and Neal Dorst. Our many questions about the VDM contents, format, history, and usage have been graciously answered by the previous people, and also by Eric Blake, Jonathan Talbot, Jack Parrish, and Nicholas Carrasco. Mary Haley and David Brown provided very helpful advice on some of the programming aspects of this project. The first author would also like to thank Christopher Landsea for his encouragement to undertake this project in the first place — never underestimate the power of a timely word of encouragement.

For chapter 5 and chapter 6, we thank Raymond Zehr for his role in developing the CIRA GOES IR satellite archive. We also appreciate the efforts of the fine folk (including Jeff Hawkins, Tommy Lee, and many others) at the Naval Research Lab–Monterey who have worked diligently to create innovative visualizations of microwave imagery and make this available for download on the NRL Tropical Cyclone web page portal. We are grateful to Mark DeMaria, Takamitsu Ito, William Cotton, and David Krueger for their helpful comments and suggestions on the manuscript. Chris Fogarty provided helpful feedback on the structure and intensity plots. Mary Haley, Dennis Shea, and David Brown provided helpful debugging support on some issues with the programming language used to process the data and create plots.

Finally, I thank my family, friends, and church for their love, encouragement, and support through this long journey.

This research was supported by NASA/TCSP Grant NNG06GA54G and NSF Grants ATM-0332197 and ATM-0837932. The revisions of this dissertation were completed with the support of a Postdoctoral Fellowship of the Advanced Study Program at the National Center for Atmospheric Research. The National Center for Atmospheric Research is operated by the University Corporation for Atmospheric Research under sponsorship of the National Science Foundation and other agencies. Opinions, findings, conclusions, or recommendations expressed in this publication do not necessarily reflect the views of any of UCAR's sponsors.

DEDICATION

Soli Deo gloria!

CONTENTS

FIGURES

TABLES

Chapter 1

INTRODUCTION

> "The scope and detail of the conflicts is likely to astonish the meteorologist working on high-latitude problems, accustomed as he is to a large measure of agreement on the fundamental descriptions of temperate and high-latitude weather. In the tropics there is not even agreement on the common forms of tropical clouds or on the meteorological conditions accompanying precipitation. It has become the custom to generalize in haste and to reject inconvenient observations at leisure. Large areas of the tropical atmosphere have not been explored by observation and even the better-known areas have not yet yielded statistics of sufficient scope or reliability to justify the tropical parts of the "models" which are incorporated into the textbook descriptions of the general circulation of the atmosphere. In synoptic meteorology, conditions are little better than in climatology. The role of water substance in the genesis of tropical depressions is a matter of dispute, the existence or nonexistence of fronts the subject of irreconcilable speculations. A dynamical meteorology of the tropics can hardly be said to exist." — from the article "Tropical Meteorology" by C. E. Palmer, published in the Compendium of Meteorology (American Meteorological Society, 1951).

1.1 Opening remarks and motivation

The massive disruption and havoc wreaked by the hyperactive 2004 and 2005 Atlantic hurricane seasons graphically and painfully illustrated that even advanced technological societies can be extremely vulnerable to tropical cyclones. While the past several decades have witnessed steady – no, even remarkable – improvements in track forecasts (McAdie and Lawrence, 2000), progress in predicting storm intensity and structure have lagged significantly (Avila, 1998). Predictions of secondary storm effects such as storm surge and rainfall depend to a large degree on accurate foreknowledge of a storm's intensity and structure. Eye formation strongly impacts both intensity and structure, so an increased understanding of eye formation should have positive implications for intensity and structure prediction. Indeed, the eye and eyewall act as the "Rosetta stone" of hurricane dynamics — when this structure is present in a storm, the movement and transformation of the ocean's thermal energy into atmospheric latent, sensible, and

kinetic energy are greatly enhanced and the storm can reach a very high intensity. When this structure is lacking or disrupted, the storm often (but not always) falters and weakens.

The empirical Dvorak technique of intensity estimation (Dvorak, 1975, 1984) has been widely and successfully applied in basins around the world. The underpinning assumption of the standard visible technique and the later Enhanced InfraRed (EIR) technique is that the present intensity of a system is related to its convective organization and vigor. Similar objective methods, such as the Objective Dvorak Technique (ODT, Velden et al., 1998) are also based on this assumption, relating intensity to the structural 'scene' (e.g., curved banding, central dense overcast, embedded eye, eye, etc.). When an eye is present, the ODT technique relates overall storm intensity to the coldness and symmetry of the convective ring surrounding the eye and the eye temperature (a colder, more symmetric ring surrounding a warmer eye yields a higher intensity estimate). Such objective measures are proxies for (1) the height to which the convection reaches (as inferred from cloud top temperatures), (2) the definition of the eye degree of symmetry, and (3) the strength of the associated eye subsidence (inferred the warmness of the eye temperature). Yet the physical processes that cause such a strong relationship are not well understood (Elsberry et al., 1992). This dissertation seeks to shed light on this enigma by expanding the observational knowledge base upon which better intensity estimation and prediction techniques may eventually be built.

1.2 Scope and introduction of research questions

This dissertation details a comprehensive investigation into *some* aspects of the formation and subsequent development of the hurricane eye. The starting point for this investigation is taken to be a tropical cyclone that has undergone the genesis process. Tropical cyclogenesis seems to involve a finite amplitude threshold – once the storm has intensified beyond this threshold,[1] intensification can continue as long as the environment remains favorable or the storm reaches its maximum potential intensity. The stopping point for this study is taken to be the time when a storm reaches its maximum intensity. At this point, the storm has either matured into a steady state with a well-developed eye/eyewall structure, or

[1] Operationally, tropical cyclogenesis is defined in the best track as the first point at which a system satisfies the criteria for a tropical cyclone: a closed surface wind circulation and sustained deep convection. Genesis often occurs when maximum sustained surface winds reach $25-30$ kt.

alternatively, it has for some reason failed to form an eye and begun the decay process. This research seeks to explain the structural and dynamical changes that occur during this time period which may last anywhere from a day in the most extreme of rapid intensification cases, to over a week in slowly developing systems.

To further limit the scope of this study, two main research foci are chosen. The first involves a theoretical investigation into the conditions for the development of the warm core in a barotropic vortex. The second involves a broad observational study of the inner core structural and thermodynamic characteristics of storms forming eyes. There are, of course, many other potentially fruitful avenues of research on this topic, chief of which would involve process modeling studies to examine in detail the several eye formation mechanisms which have been put forward by past researchers. This dissertation limits its attention of these proposed mechanisms to a literature review and to the extent that observational data support the proposed processes. Much of the focus will be placed on seeing what observations can tell us about the structure and intensity changes that occur during eye formation.

Complete research requires the exploration of the widest possible range of avenues of inquiry, knowing full well that some avenues may prove unproductive. While no research can ever truly be complete, practical thoroughness is a worthy aim. *Good* research tries to fully explore the productive ones while wasting as little time as possible in unproductive directions. With this awareness, a broad battery of research questions were formulated at the outset of this work, with modifications as the research progressed. In the interest of focus, the original list of 75 questions has been pared down to a smaller subset of main questions this dissertation attempts to address. For the interested (and tireless) reader, the full list of questions and some answers can be found in appendix A.

- **Questions of definition:** What is the most useful way to define the eye from a dynamical perspective? From an observational perspective? At what point can the eye be said to have formed?
- **Questions about eye formation processes:** What are the salient mechanisms and dynamics that drive a single-cell vortex structure to a two-cell vortex structure? What role does central subsidence play in eye formation? What forces the subsidence? How important is it that convective heating occur inside the inertially stable core of the storm? Are there multiple dynamical pathways to eye formation, or do all intensification routes lead to one common eye formation pathway, perhaps dictated purely by geometry and friction? Putting it another way: Is eye formation essentially a stochastic process or a manifold attractor of the system? Does the eye play a passive or an active role in intensifying the storm?

- **Observational questions:** At what intensities do these various stages of eye formation occur at? Do observations show the existence of a general intensity threshold for eye formation? What is the least intense tropical cyclone to sport a bona fide eye? What is the most intense storm to not possess a clearly defined eye? What are the size characteristics of the initial eye at the time it is first detected? What can observations tell us about the development of the warm core and thermodynamic structure across the eye/eyewall interface? How does the radius of maximum winds change before and after eye formation? Does it always contract as the storm intensifies? Does a dynamical length scale such as the minimum Rossby length have utility?

- **Questions related to the interaction of the storm and its environment:** Why do some storms rapidly intensify as they form eyes, yet others do not? Is it merely that some storms exist in favorable environments while others do not? What is the effect of land on eye formation? Can a storm form a "true" eye over land if it didn't previously have one?

1.3 Outline of dissertation

This dissertation's three main parts (a review, a theoretical study, and an observational study) are comprised of five major chapters, each of which has been written in a style amenable for publication as a stand-alone journal article. The author has attempted to meld these separate works into a cohesive whole without much if any duplication. Each chapter is self-contained, with its own introduction and summary or conclusions, and can therefore be read as a separate entity. An overview of the remaining chapters is now given along with the current publication status of the respective journal articles that will be derived from this dissertation.

The first main part of this dissertation, chapter 2, explores the intersection of the cross section of inquiries listed above and the broad body of literature on tropical cyclones and dynamics. This chapter reviews the extant theories on eye formation and supplies a new, cohesive definition for eye formation. Early historical ideas on eye formation are traced through to the era of modern observations. Competing dynamical theories on the causes of the central subsidence are examined and reconciled. Results from numerical modeling and laboratory studies are surveyed, and several possible eye formation mechanisms are explored in detail. Following further work, this chapter will be submitted for publication as a review article in the *Quarterly Journal of the Royal Meteorological Society* as Vigh et al. (2010d).

In the second main portion of this dissertation, chapter 3, we supply a theoretical argument developed from the balanced vortex model to understand how a barotropic storm can rapidly develop a warm core structure and approach a steady state. This chapter provides further illumination on the well-known

idea that heating must occur within the region of high inertial stability in order to efficiently intensify the storm. We accomplish this by calculating the vertical motion response to heating in a simplified vortex which allows the inertial stability to vary in the radial direction. In this chapter, we will also explore the paradoxical influence of eye formation in both stabilizing the inner core, yet contributing to rapid intensification in some situations. This chapter is essentially a reproduction of a paper that has already been published in the *Journal of Atmospheric Science* as Vigh and Schubert (2009).

The third and final part of this dissertation consists of three chapters which explore observations of eye formation. Chapters 4 through 6 are meant to comprise a three-part observational paper which examines the initial eye formations of a broad set of Atlantic tropical cyclones to characterize the kinematic and thermodynamic changes that occur before, during, and after eye formation. To obtain the requisite structure and intensity parameters, a new data set has been synthesized from the Vortex Data Messages (VDM) transmitted by routine aircraft reconnaissance from 1989-2008. The first part of this 3-part paper series, chapter 4, documents the VDM and other data sets used throughout the study, and sets forth the observational philosophy and background. This chapter will be submitted for publication to *Monthly Weather Review* as Vigh et al. (2010a).

The second part of this 3-part paper series, chapter 5, determines the intensity thresholds at which the eye/eyewall structure is first observed in aircraft radar, microwave satellite imagery, and infrared satellite imagery. These time points are then used to determine a characteristic timescale for the eye formation process. The trend in intensity is quantified. Environmental conditions are examined near the time of eye formation for storms which successfully formed eyes and went on to rapidly intensify, and those which failed to form eyes and subsequently weakened. A goal is to determine if eye formation is essentially a stochastic process involving constructive and destructive mesoscale interactions – or whether it is a manifold attractor of the dynamical system sometimes stymied by an unfavorable environment. This chapter will be submitted for publication in *Monthly Weather Review* as Vigh et al. (2010b).

The third part of this 3-part paper series, chapter 6, examines the structural and thermodynamical changes which occur during and after eye formation. Trends are computed for the radius of maximum winds, eye temperature and dew point depression, and the minimum Rossby radius of deformation. This chapter will be submitted for publication to *Monthly Weather Review* as Vigh et al. (2010c).

Chapter 7 highlights the main results of this work and provides some unifying discussion and concluding remarks.

The Vortex Data Message data set has proven to be a veritable gold mine for a more general exploration of the inner core structure of tropical cyclones. Because these data have not been previously available to the broader research community, extensive summary tables have been prepared to document various aspects of hurricane structure and intensity. These appear as three separate appendices. Appendix B provides supplementary tables which have been referred to in the main text. Appendix D contains additional tables not specifically referred to by the main text which may be of general interest or utility to the broader research community. Appendix C contains the seedlings for a future paper[2] which will conduct a systematic observational study of warm rings, eye moats, and hub clouds.

In order to visualize and quality-control the VDM data, the author has also created a suite of specialized figures that illustrate temporal changes in intensity and structure over the storm's lifetime. These plots have been created for all 180 storms that were reconnoitered by aircraft in the Atlantic basin from 1989 to 2008. Since some of these figures (especially for the more notable storms) may be of interest to the broader research community, they are included in appendix E.

[2] After considerable work beyond this dissertation additional flight level data, the author plans to submit this material for publication to *Quarterly Journal of the Royal Meteorological Society* as Vigh and Schubert (2010).

Chapter 2

A REVIEW OF EYE FORMATION IN TROPICAL CYCLONES

> It is a well-known fact in meteorology that in the centre of the most violent hurricanes there is an area of very light winds, or absolute calm. Over this area the torrential rain of the hurricane ceases, and the clouds frequently break away, showing blue sky, with the sun, or the moon and stars. On account of its peculiar clearness this spot has received the name, "eye of the storm." — Sidney Ballou (1892)

2.1 Introduction

A plethora of genesis mechanisms result in tropical cyclone formation. Gray (1998b) purports that *hundreds* of tropical cyclogenesis theories have been put forward. Some genesis mechanisms or influences include low level wind surges (Gray, 1993), barotropic breakdowns of the Intertropical Convergence Zone (Ferreira and Schubert, 1997), Madden-Julian Oscillation twins (Ferreira et al., 1996), upscale vorticity and energy cascade from the diabatic merger of "vortical hot towers" (Hendricks et al., 2004; Hendricks and Montgomery, 2006), eddy fluxes of angular momentum and heat from environmental asymmetries (Pfeffer and Challa, 1992), development via convectively-forced Vortex Rossby Waves (Montgomery and Kallenbach, 1997; Montgomery and Enagonio, 1998), or a combined interaction between several large scale influences (e.g. Briegel and Frank, 1997).

Yet, all storms which subsequently intensify into mature tropical cyclones eventually sport the characteristic hurricane 'eye': a central region characterized by relatively calm winds, diminished precipitation, and subsiding air. Indeed, viewed from space, the eye is one of the most distinctive features of the mature hurricane, appearing as a broad cloud-free funnel whose lower portions contain clouds more often than not, sometimes whipped into fantastic patterns by mesovortices. Figure 2.1 shows such a scene, captured by a U-2 flyover of Supertyphoon Ida. The edges of the funnel often slope outward

with height, and are defined by a towering, swirling wall of clouds of generally rising air. At the top of the storm, most of the air turns outward, flowing away from the center in a thick cirrus canopy sometimes punctuated by vigorous updrafts from beneath, but some of this exhaust air turns inward over the eye and sinks. Figure 2.2 shows the extremely tight eye funnel shape exhibited by Hurricane Wilma (2005), as viewed from space. The success of the Dvorak technique (Dvorak, 1975, 1984) in estimating tropical cyclone intensity from satellite imagery points to the fact that storm structure and intensity are inextricably linked.

Tropical cyclones which form eyes are often observed to rapidly intensify with a concomitant increase in structural organization. During eye formation, convection begins to concentrate into an annular ring at some preferred radial distance from the storm center while a region of subsiding air develops over the center. Latent heat released by eyewall convection and adiabatic warming due to central subsidence both contribute to the storm's warm core structure, causing surface pressure falls near the center. Outside the core, surface pressure gradients increase as a result, strengthening the low level radial inflow, leading to increased convergence of moisture and angular momentum, invigorated convection, and an overall intensification of the storm. The dynamical and kinematic response of the vortex to warming of its central column engenders even stronger subsidence and increased eyewall latent heat release: a synergistic positive feedback process. Thus, the importance of the eye/eyewall structure in maintaining and intensifying the storm to a mature state is readily seen. This explains why the eye feature is common to all intense convective cyclones – without an eye and eyewall, these systems would not be able to reach such a high intensity.[1]

While the intensification role of the eye/eyewall structure is well appreciated in the literature,

[1] As an aside, we must accede to the fact that some oceanic non-tropical weather systems have been observed to attain central low pressure deficits that are almost comparable to those of the most intense tropical cyclones. To give a couple examples, the North Atlantic cyclone of December 1986 reached at least 916 hPa (Burt, 1987) while the North Atlantic cyclone of January 1993 deepened to between 912 and 915 hPa (Burt, 1993). These minimum central pressures, if observed in a hurricane, would indicate a storm of Category 5 intensity on the Saffir-Simpson Hurricane Scale (SSHS, Simpson, 1974). Of course, these systems are not tropical cyclones — they are extratropical cyclones, and their pressure gradients are not as large as those found in a tropical cyclone [although geostrophic winds well in excess of 100 kt were computed in the 1993 storm (Burt, 1993)]. Furthermore, while some extratropical cyclones do exhibit an *eye-like* feature, examination of the satellite imagery for the January 1993 storm (presented in Fig. 3 of McCallum and Granhame 1993) does not show a marked eye feature during its most intense period (there is however a pronounced notch and what could be considered a partial eye in the cloud field). It is not the purpose of this review to examine the dynamics of non-tropical systems, but the extremely low pressures achieved by these systems are no doubt due to extreme latent heat release in a zone of intense baroclinity. While an eye may not be present, subsident warming still likely played a role in helping the storm to achieve these record low intensities.

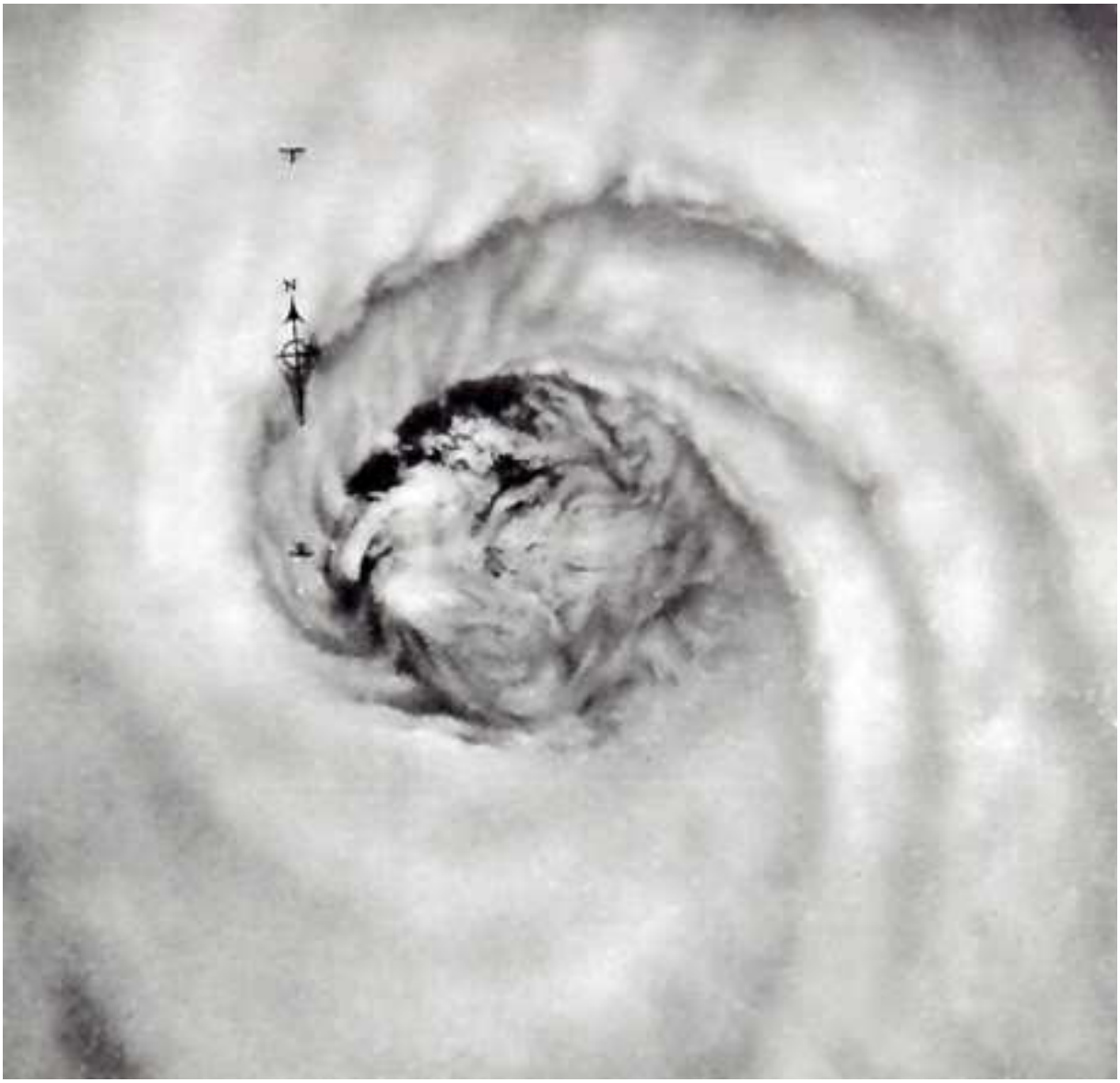

Figure 2.1: A high altitude aerial photograph of Supertyphoon Ida taken from a U-2 spy plane on 25 September 1958 (c.f. Fletcher et al. 1961). Photo courtesy of Frank Marks (NOAA/AOML/HRD). [Photo has been digitally enhanced to remove dust specks.]

relatively few studies have examined the fundamental causes of the transition from a single-cell vortex – in which the secondary radial circulation extends inward to the central axis – to a two-cell vortex, in which the eyewall separates the outer radial circulation from an inner radial circulation of the opposite sense. Several studies have sought the dynamical causes of the central subsidence, which are indeed a natural and key piece of the eye formation puzzle. Yet, because such subsidence is also a forced response to intensification of the vortex, it may be counterproductive to label it as a causative factor

Figure 2.2: The tight eye funnel of Hurricane Wilma. Photo taken from the International Space Station at 8:22 AM CDT, 19 October 2005. Wilma was near peak intensity at this time, with a minimum sea level pressure of 882 hPa and maximum sustained surface winds of 160 kt. [NASA Photo ISS012-E-5241].

in isolation. Likewise, it would be naive to try to explain eye formation by appealing to any of the reinforcing structural characteristics and intensification dynamics of the mature eye (Anthes, 1982). A complete understanding of eye formation must delineate cause from effect, which may be a difficult task given the coupled nature of intensity and structure. While this review will unfortunately not provide a complete understanding of this topic, we will attempt to shed further light on the subject. The next subsection puts this review into context by relating the current work to previous reviews and setting forth new questions to be answered.

2.1.1 Scope of this review

At the outset, we restrict this review to the formation of the *primary* (first) eyewall that forms in a hurricane. The phenomenon of secondary eyewall formation, in which a concentric convective band and associated secondary wind maximum form into a new eyewall at a larger radius than the original eyewall,

has been the subject of much observation interest and study over the years (Willoughby et al., 1982; Black and Willoughby, 1992; Kossin et al., 2000; Nong and Emanuel, 2003; Kuo et al., 2004; Terwey and Montgomery, 2008; Rozoff et al., 2008; Kossin and Sitkowski, 2009). The secondary eyewall often contracts, choking off the inner eyewall and eventually replacing it, often causing significant changes to the intensity and size of the inner core of the storm. Up until recently, numerical modelers had great difficulty simulating the details of concentric eyewall formation. Primary eye formation has perhaps received less attention because it has been easy to simulate a storm which forms an eye.

Although a comprehensive review of primary eye formation has not yet been undertaken until now, several good reviews of tropical cyclone structure and intensity have already been accomplished and touch on the problem of eye formation. Anthes (1982) was probably the first to review the eye formation problem (see his chapter 3) and provides a good summary of the state of the knowledge of eye subsidence ideas at the time as well as the role of the boundary layer in eye formation. Willoughby (1995) provides a detailed review of the dynamics of tropical cyclone structure change and reviews his substantial contribution on the role of contracting convective rings. Along this vein, he postulates that eye formation may occur as the primary band wraps around the storm. Wang and Wu (2004) provides an updated review on structure and intensity change, but does not consider the eye formation problem explicitly. In 2005, a short exchange of notes in the nontechnical journal *Weather* examined the question of 'Why must hurricanes have eyes?' (Pearce, 2005; Smith, 2005), but like many problems in hurricane dynamics, it did not seem that the authors of those notes agreed.

Much energy has already been expended in determining the causes of the central eye subsidence, but an updated summary of the current state of knowledge is in order. Some questions still remain as to the degrees of contribution from these various subsidence mechanisms and whether the air in the eye is actively cycling through the storm, or whether it has remained relatively undisturbed since the eye formed. Willoughby (1995) broached a related question — Does the eye play an active or passive role in intensifying the storm? Several convincing arguments have been put forward, but there is still some disagreement here as well. We will try to sort this out as we go along. Several eye formation mechanisms have been proposed. We will attempt to categorize these arguments and comment on the validity with respect to what is known from observations.

Certain aspects relating to the eye formation problem are reviewed in other chapters of this dissertation. To avoid duplication, they will not be repeated here. Please note the following links to these mini-reviews:

- Balanced vortex theory and the role of the secondary circulation are briefly reviewed in chapter 3.1.
- A review of observations concerning the location of diabatic heating relative to the radius of maximum wind in observed storms can be found in chapter 3.7.1.
- The maturation of the warm core as the storm approaches a steady state is discussed in chapter 3.7.3.
- The effects of eye formation and contraction are considered in chapter 3.7.2.
- The issue of whether an eye is necessary to reach a high intensity is reviewed in chapter 4.1.
- Historical practices for determining when an eye is present by aircraft, radar, or satellite imagery are covered in chapter 4.2.
- The relation between eye formation and tropical cyclogenesis will be touched on in chapter 6.

2.1.2 Purpose and outline

While few studies have examined the causative factors behind eye formation directly, much work has been done on related aspects and it seems that many of the pieces of the puzzle have already been put forward. The purpose of this chapter[2] is to review previous work on eye formation and evaluate the various proposed mechanisms and ideas with a hope of synthesizing a more complete view on the subject. Since a comprehensive definition for the eye/eyewall structure does not yet exist, a second goal is to put forward a definition that will be useful from the observational, dynamical, and operational forecasting perspectives.

This review is structured as follows. The next section provides background to the problem of tropical cyclone eye formation by surveying vortex eye phenomena in simple vortices, other geophysical vortices, and laboratory analogs and numerical simulations. The remainder of the chapter will focus solely on eye phenomena in tropical cyclones. Section 2.3 traces the development of observational

[2] This chapter will be submitted for publication to *Quarterly Journal of the Royal Meteorological Society* as Vigh et al. (2010d).

knowledge on the nature of tropical cyclone structure down to the modern era. In section 2.4, we use these observational insights to construct a new, comprehensive definition for determining what constitutes an eye. Section 2.5 examines possible symmetric mechanisms for eye formation, with a focus on the various causes of the central subsidence in the eye. The role of boundary layer forcing in initiating the eyewall will also be considered. Section 2.6 will review the various asymmetric eye formation mechanisms that have been proposed in the literature, some of which may provide a 'shortcut' route to eye formation. Section 2.7 concludes with a discussion of what has been learned and surveys the next challenges.

2.2 Overview of vortex eye phenomena

In this section, we describe the fundamental essence of an eye and then describe the eyes that form in a variety of vortices ranging from some simple vortices and more complex geophysical vortices. Afterward, we undertake a non exhaustive review of the literature involving theoretical, laboratory, and modeling studies which examine the question of what controls the transition between one- and two-cell vortices. Our goal here is to find what (if any) relevance the eye formations in these geophysical and laboratory vortices have to the eyes formed in tropical cyclones.

2.2.1 What is an eye?

Before discussing the essence of what constitutes an eye, it helps first to review a few basics of vortex dynamics. The flow in a vortex can be described as a force balance between an inward-directed pressure gradient force (owing to the central pressure deficit of the vortex) and an outward-directed centrifugal force.[3] There may be other forces involved, but these are the two basic ones. When the PGF and centrifugal forces are equal, the vortex is said to be in *cyclostrophic balance*. If the Coriolis force is also included in the force balance, the vortex is said to be in *gradient balance*. The balanced swirling (tangential) flow is referred to as the cyclostrophic and gradient winds, respectively.

It was perhaps Leonardo Da Vinci who first realized that all vortices contained a vortex within the

[3] Is it proper to call this force 'centrifugal' or 'centripetal'? The answer depends on the reference frame chosen. In an inertial frame, the constant directional acceleration required by rotational motion necessitates a radially-inward directed force to keep the parcel from flying off on a tangent. But when viewed in a non inertial frame moving with the rotating fluid parcel, the apparent force is outward.

vortex, i.e., an inner region of the vortex with properties that differed from those of the outer vortex. In the outer vortex, the swirling flow v increases *inward* with radius r up to a maximum value known as the *radius of maximum winds* (r_{max}). In contrast, the inner vortex features tangential flow which increases *outward* with radius. If v increases linearly with r, the inner vortex is said to be in *solid body rotation*. Thus, r_{max} separates the two vortex regions and arises as a consequence of the conservation of angular momentum, M, where $M = rv$.

The necessity of the existence of r_{max} can be understood by considering what happens if a fluid parcel in the outer vortex moves inward towards the vortex axis. If the fluid's initial velocity is v_0 at radius r_0, its angular momentum will be $M_0 = r_0 v_0$. In the absence of other forces, its angular momentum M_1 at a new radius r_1 will be the same as M_0, so $r_0 v_0 = r_1 v_1$, so $v_1 = \frac{r_0 v_0}{r_1}$. Thus, the parcel's v increases proportionally to the inverse of r. Thus, a parcel in the outer vortex cannot reach the vortex center because that would require an infinite velocity. So as a result of the conservation of angular momentum, the inner vortex is 'protected' from the outer vortex in that fluid parcels cannot cross r_{max} (although r_{max} could move inward).

Should this protected region be considered an eye? Please consider the vortex shown in Fig. 2.3. A passing aircraft generated a wingtip vortex which was made visible by a mixing cloud that formed from the water vapor emitted by a nearby industrial source. The cloud matter wraps throughout the outer vortex, but does not penetrate to the protected inner vortex. For now, we will reserve judgment on whether this is a bona fide eye, but this example clearly illustrates that eye-like behavior is by no means limited to hurricanes. To some extent, all vortices have this general feature which arises purely due to the conservation of angular momentum.

2.2.2 Simple vortices

The simplest possible vortex is a symmetric 2-dimensional (2-D) vortex, such as a vortex tube generated by speed shear in a unidirectional flow. The wingtip vortex just cited is essentially a 2-D vortex apart from the draft of the passing plane. Yet, there is something unsatisfactory about designating the clear, protected regions of these vortices an 'eye'. The reason will become apparent as we consider slightly more complicated 3-dimensional (3-D) vortices which allow variations along the radial axis of

Figure 2.3: The ‘eye’ of a wing tip vortex generated by a passing Boeing 747 aircraft at Kai Tak Airport, Honk Kong. An additional image in the sequence can be found at: `http://www.sydneyparagliding.com/articles.htm#Wing_tip_Vortices`.

the vortex.

Tea cup vortex

Anyone who has vigorously stirred a cup of tea has observed the central lowering of the fluid surface due to the centrifugal force imparted by the high tangential velocity of the fluid. In response to the stirring, the pressure in the center of the vortex lowers (as manifested by the lowering of the free surface) so that the inward-directed pressure gradient force (PGF) comes into balance with the outward-directed centrifugal force. The tea cup vortex is actually not so simple, as it has an Ekman boundary layer due to friction with the lower surface. This produces a secondary circulation which spins down the vortex and is responsible for collecting the tea leaves at the bottom center of the cup Greenspan and Howard (1963).

Spin table vortex

An even simpler 'centrifugal' vortex is one in which the fluid is spun up slowly on a rotating turntable. Due to friction with the vortex boundaries, a slight secondary circulation will occur during the spin-up process, but once equilibrium is reached, $\frac{V}{r} = \omega$ everywhere so that the fluid is in solid body rotation. Once this occurs, the vortex will be unaffected by friction because the lower and side boundaries are also in solid body rotation. At this point, the centrifugal and pressure gradient forces will exactly balance, so that the slope of the free surface is defined by a parabola whose curvature depends solely on ω. If the fluid is rotating rapidly enough, the free surface will drop all the way down to the lower boundary in the center of the vortex — in effect, forming an 'eye'.[4] The essential difference between the protected region of a 2-D vortex and the situation in these 3-D vortices is that *the spin up of a 3-D vortex requires a vertical rearrangement of mass in order to drive the vortex back towards force balance*. If taken far enough, this vertical rearrangement process will result is the formation of an eye.

With this concept in mind, we may now distinguish between *eye formation* and *eye maintenance*. Specifically, in the spin-table vortex the maintenance of cyclostrophic balance requires that the fluid rise near the outer boundary and sink near the center for any incremental increase in vortex intensity.

[4] If one were so inclined, he or she could call this a *centrifugal eye*.

However, once the vortex reaches solid body rotation, no further vertical motion is required, yet the result of this mass adjustment (e.g., the eye structure) is still apparent. Thus, the formation of an eye and the processes which maintain an eye can be separated Malkus (1958a). Thus, we reserve the term ‘eye’ to refer only to those vortices which have undergone a dichotomy of vertical motion in the vortex core (sinking motion in the eye and rising motion outside of it) in order to come into balance as they spun up. A two-cell vortex then is considered to have an eye; a one-cell vortex does not. The fact that a 3-D vortex may transition back and forth between these two circulatory regimes is what makes eye formation an interesting problem.

Bathtub Vortex

The addition of a mass sink complicates the picture. As anyone who has taken a bath or washed dishes in a sink well knows, when fluid is evacuated from the bottom of the vortex, the associated vortex stretching tends to spin up the fluid near the radial axis until a narrow, columnar ‘eye’ forms. This eye can be considered to have formed when the free surface extends down to the sink hole. If the fluid possess a small tangential rotation at the time the mass sink is introduced, the ‘eye’ remains on a small scale with a steep funnel slope near the top. The fluid in the outer regions will only spin up slowly. On the other hand, if the fluid already has a large tangential rotation when the sink is introduced, the eye formed will be larger and its influence on the vortex will be greater. The slope of the funnel will not be as great and extend out to greater radius. The analogies to tropical cyclone eye behavior will be explored later when we discuss the theory of Kuo (1959). We also note that whirlpools such as the Norwegian ‘maelstrom’ is a variations on the ‘bathtub vortex.’

2.2.3 Geophysical vortices

Besides occurring in tropical cyclones, eyes or “eye-like” phenomena have been noted across a broad spectrum of geophysical vortices:

- topographically-generated mesoscale cyclones,
- dust devils,
- tornadoes,

- waterspouts,
- supercell thunderstorms,
- convective mesolows,
- polar lows,
- extratropical cyclones,
- and hybrid cyclones.

Some examples of the eye phenomena found in these cyclone types are now surveyed, with a brief comparison on how the eye in each vortex type is similar or dissimilar to tropical cyclones. While the essential vortex dynamics are largely the same irrespective of media, significant differences arise related to the driving force of the vortices and how the boundaries are expressed to the vortex.

Topographically-generated mesoscale cyclones

This first cyclone type includes mesoscale lows that are formed in the lee of topographical barriers such as the the Denver Cyclone and the island of Hawai'i. Szoke (1991) examines a case of the Denver Cyclone from 4 October 1988 in which a clear area formed in the stratocumulus cloud field. This feature coincided with the center of the vortex circulation and surface observations showed a distinct wind shift as the feature passed. Various modeling work on the Denver Cyclone (see references in Szoke 1991) suggest that the mesoscale vortex may indeed be weakly warm core with central subsidence. Modeling studies suggest that the thermal stratification of the upstream atmosphere may play a crucial role in controlling the vortex dynamics, and that friction has little effect. In comparison to tropical cyclones, this is a weak, shallow cyclone with little to no internal sources of energy (the vorticity is generated by flow past a barrier). Evidently, the low intensity of the vortex does not preclude the clear area from forming, as seen in Fig. 5b of Szoke (1991), reproduced here as Fig. 2.4. While convection later fired around the periphery, it did not seem to be important to its formation. Overall, this example is a rather marginal case and does not look very much like the eye of a tropical cyclone; certainly, there is nothing like an eyewall present. Thus, this type probably has little relevance to the problem of tropical cyclone eye formation and likely falls under the category of "eye-like feature" rather than a "true eye". It can

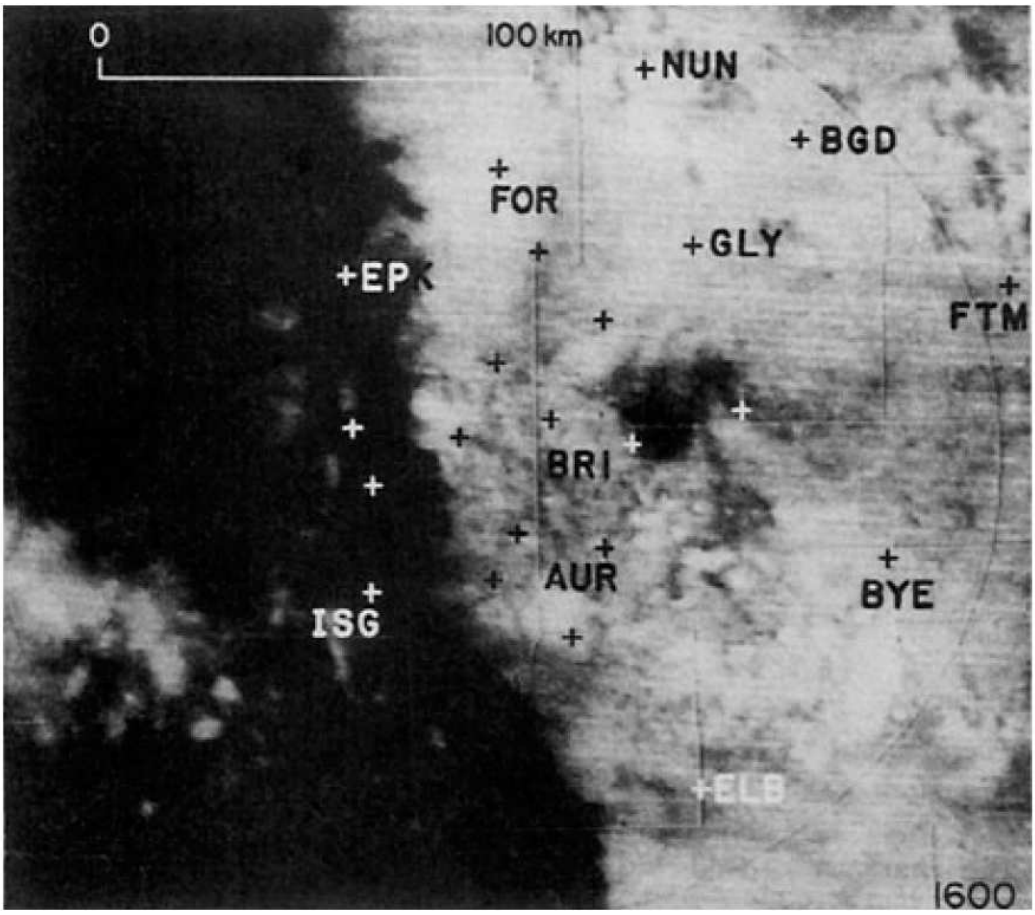

Figure 2.4: Visible satellite photo of the 'eye' feature in the Denver Cyclone at 1600 UTC on 4 October 1988. This image has been reproduced from Fig. 5b of Szoke (1991).

sometimes be difficult to distinguish between the two, even in tropical cyclones. Later in this review, we will propose a thorough definition to help.

Dust devils

Although they have a much larger aspect ratio than tropical cyclones (so that the vortex height is much greater than its length, $H << L$), dust devils are similar to tropical cyclones in that they are both driven by surface fluxes and convective updrafts. Of course there is no latent heating in a dust devil — the vortex derives its energy by releasing buoyant energy supplied from the super-adiabatic near-surface air that has been heated by solar insolation. Using an instrumented mobile tower, Sinclair (1973) made direct measurements of dust devils and found maximum temperature variations of 4 to 8 °C within the lower (at a height of 7 ft) portion of the dust devil. Temperature anomalies rapidly declined to values

about half the lower values by a height of 31 ft as cooler environmental air was mixed in from outside the vortex core. Pressure deficits ranged from 2.5 to 4.5 hPa (one dust devil had a deficit of 7.0 hPa). Vertical wind velocities in the updraft often approach $10\,\mathrm{m\,s^{-1}}$. Tangential wind velocities tend to be the same order of magnitude, perhaps approaching 20 to $25\,\mathrm{m\,s^{-1}}$ in some strong dust devils.

Dust-free eye columns are sometimes observed in dust devils due both to the centrifugal force on the dust particles, and to the spiraling current of air that descends from above. Because the air in the surrounding toroidal updraft is superadiabatic, the descending current (which is merely dry adiabatic) ends up slightly cooler (by 0.5 to 1.0 °C) than the surrounding rising air, but is still warmer than the environment so dust devils are still warm core vortices (Sinclair, 1973). Like tropical cyclones, the surface friction plays a vital role in promoting radial inflow and hence, convergence of the thermally energetic air that feeds the vortex. Due to the decay with height of the strong radial inflow, the vortex column slopes outward with height. Doppler-radar observations give insights into the structures of both one- and two-cell vortices. The one-cell dust devils resemble a relatively narrow, Rankine combined vortex while the two-cell vortices have a broad, calm eye which on occasion displays Rossby-like wave motion and multiple vortex structure (Bluestein et al., 2004; Bluestein, 2005). Fig. 2.5 shows the reflectivity eye observed in a dust devil. The broad eye had a diameter of 80 m.

Waterspouts

Nontornadic waterspouts have much in common with dust devils in their basic vortex structure, although their energy sources differ. A waterspout often forms as the updraft associated with a cumulus cloud draws in air from near the surface. The mass sink from above (the updraft into the cumulus cloud base) spins up local vorticity, and increases the sensible and latent heat fluxes from the ocean. These fluxes are important in intensifying the updraft as they enhance the buoyancy. Increasing wind speeds increases the fluxes even more, so in this way, waterspouts are similar to tropical cyclones. Since waterspouts occur in moist environments, condensation occurs in their funnel releasing latent heat, although on a much different scale than in a tropical cyclone.

Leverson et al. (1977) used instrumented aircraft to penetrate waterspouts off of the Lower Florida Keys and found that the waterspout funnel structure did indeed have a slight warm core that was sur-

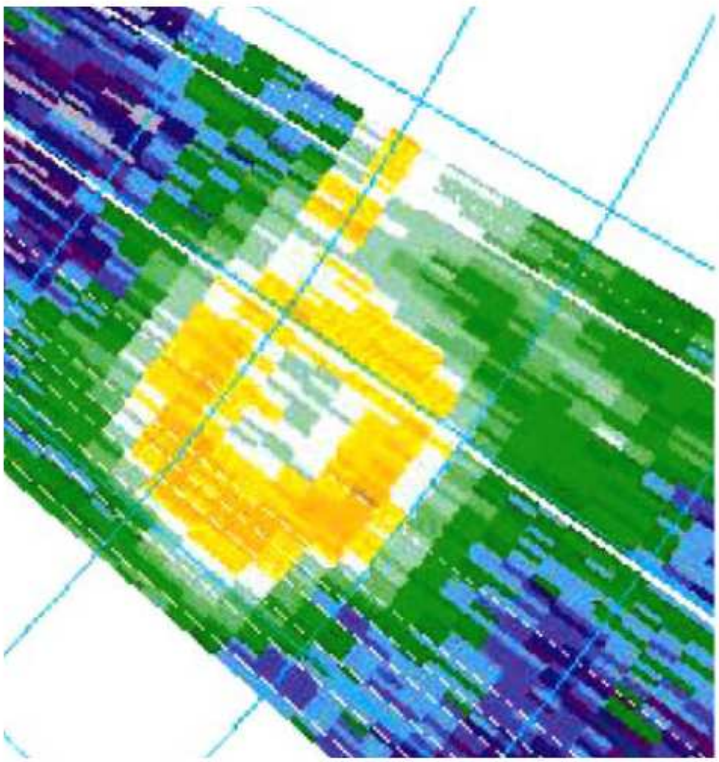

Figure 2.5: The reflectivity eye of a broad, two-cell dust devil. TX.The dust devil were observed by Doppler radar near Tell, TX on 25 May 1999. This image has been reproduced from Fig. 19 of Bluestein (2005).

rounded by strong updrafts of 5 to $10\,\mathrm{m\,s^{-1}}$ that were 0.2 to 2.5 °C warmer than the surrounding environment. Tangential velocities ranged from 5 to $28\,\mathrm{m\,s^{-1}}$ and the maximum central pressure deficits of up to 8.5 hPa were observed. Both the tangential winds and horizontal pressure gradients were stronger than observed in dust devils. The core downdraft is usually weak, but a more intense rain-cooled downdraft is often found outside the waterspout funnel. Velocities in this outer downdraft may approach $3.5\,\mathrm{m\,s^{-1}}$.

Tornadoes

Tornadoes can generally be split into two categories:[5] supercell and non-supercell tornadoes (sometimes called landspouts). As the name suggests, landspouts have some commonalities with waterspouts in that they form by concentrating ambient vorticity in association with the updrafts and downdrafts from a local cloud feature or gust front. Often, but not always, the parent feature is an ancillary feature to a larger thunderstorm complex. In contrast, a supercell tornado has a much stronger connection to its rapidly rotating mesoscale cyclone parent storm. Much of a supercell tornado's energy and vorticity is derived from the parent storm, and like hurricanes, theories have been put forward to find the "thermodynamic speed limit" that a tornado can achieve and the factors that influence this (Fiedler and Rotunno, 1986). Latent heat release often occurs in at least part of the tornado's funnel, and this may play some roles in the thermodynamics and energetics of the vortex.

Unlike waterspouts or dust devils, surface *fluxes* of sensible and latent heat have little if any impact on tornadoes, but surface friction on the other hand, is very important in modifying the lower tornado vortex structure. A wide range of shapes, scales, and behaviors has been observed, ranging from narrow, sinuous columnar vortices just tens of meters across, to broad, turbulent multivortex tornadoes spanning several kilometers. Often the same tornado will undergo drastic changes during its lifetime. This has elicited much study by researchers. Various studies have reported that the nondimensional swirl parameter controls the structure of dust devil- and tornado-like laboratory vortices (Davies-Jones, 1973; Church et al., 1979; Walko, 1988). Friction with the surface plays a vital role in depleting the angular momentum in the boundary layer, and this seems to have important implications for the vortex intensity near the surface Lewellen et al. (2000). Hydraulic jumps or collapse processes brought on by the temporary cutoff of inflowing air (Lewellen and Lewellen, 2007) can cause violent intensification in the so-called "corner" region where the near-surface inflowing air turns upward. For brief periods, the wind speeds in this region may be ten times those of the core vortex, drastically exceeding any tornado 'speed limit'.

[5] Agee and Jones (2009) have recently proposed a tri-fold tornado taxonomy based on genesis mechanism. Their scheme includes 15 tornado subtypes and includes several types of tornadoes that are generated within the hurricane eyewall, outer bands, or mini-supercells.

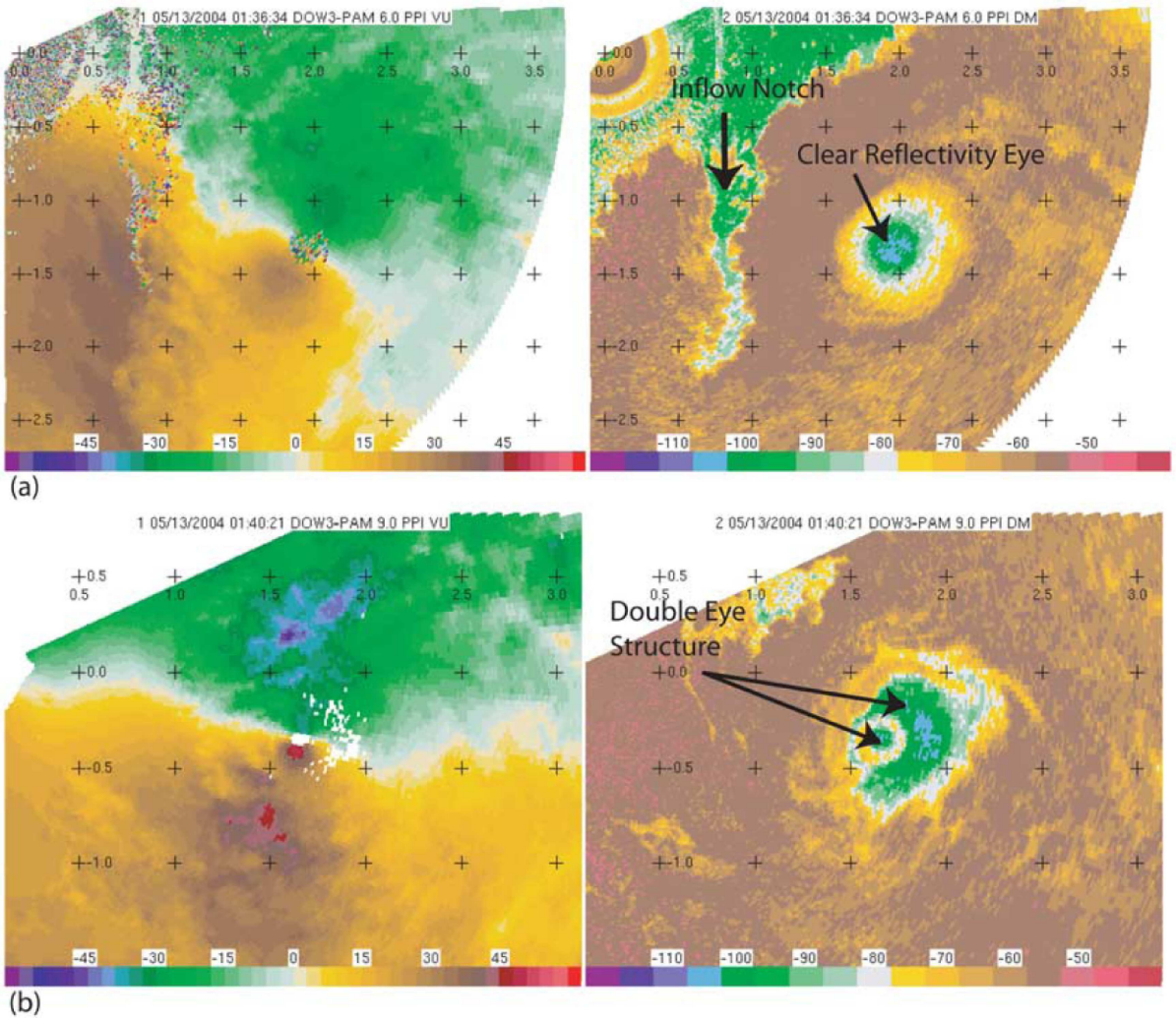

Figure 2.6: Harper, KS tornado, 12 May 2004. Left panel shows Doppler velocity, while right panel shows the radar reflectivity. In panel a), a clear hole can be seen in the reflectivity field, and the maxima couplet in the velocity field are located near the reflectivity gradient on the inner edge of high reflectivity. In panel b), the tornado exhibits a double eye structure. Reproduced from Fig. 1 of Kosiba et al. (2008).

Tornadoes exhibit morphologies similar to hurricanes, with spiral bands and eyes (Bluestein, 2005). The 'eyewalls' of tornadoes often exhibit smaller-scale waves or vortices on their inner edge. An example of the clear reflectivity eye of a tornado is reproduced in Fig. 2.6.

Supercell thunderstorms

Supercell thunderstorms themselves may take on the appearance of an eye, although it is unclear whether this really should be considered an eye. In one example, a tornado-producing supercell over Duplin County, NC, was seen to take on the appearance of a hurricane, complete with eye and spiral

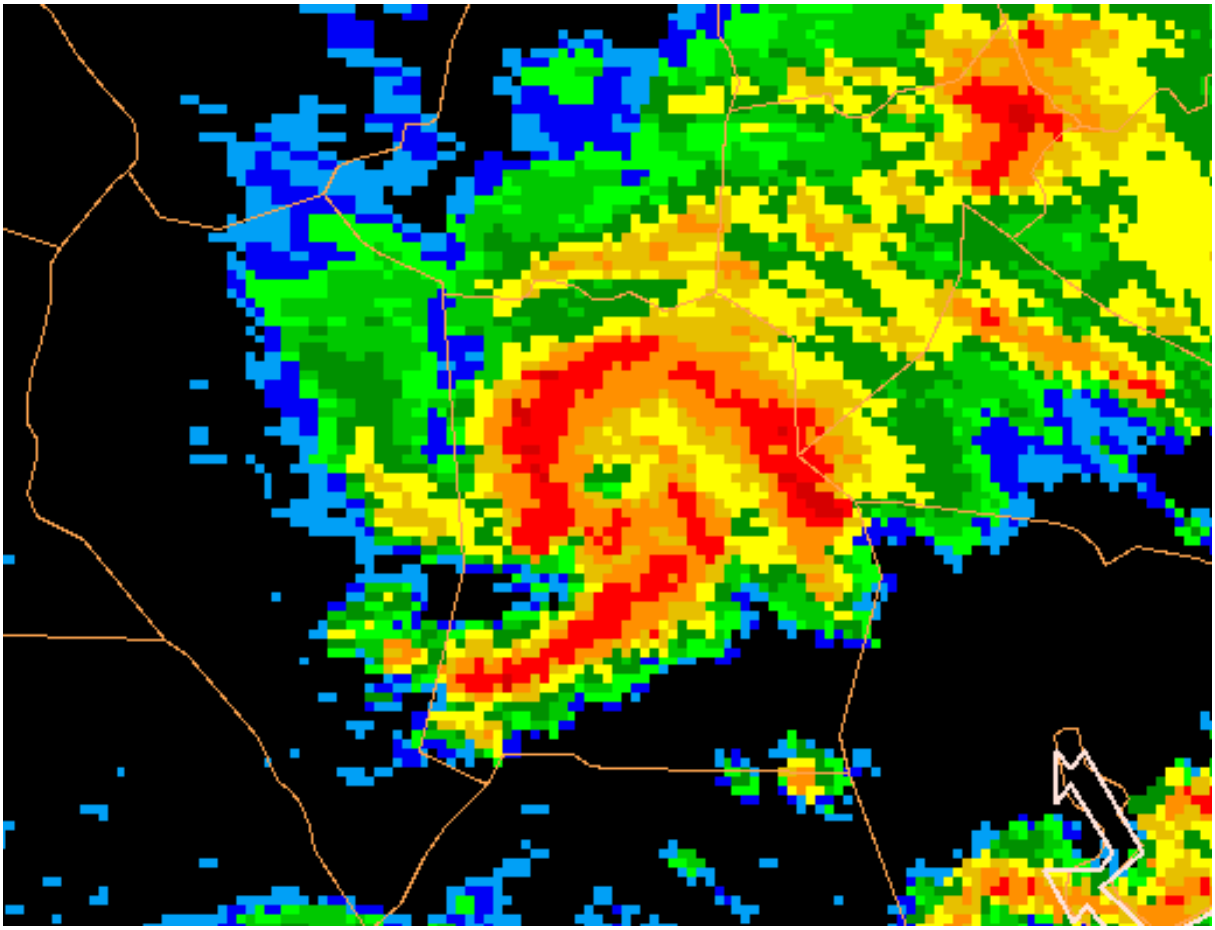

Figure 2.7: Base reflectivity from the Wilmington, NC radar of a hurricane-shaped, tornado-producing supercell thunderstorm complex over Duplin County, NC at 0139 UTC on 16 Apr 1999. This image has been downloaded from an online writeup by David Roth, available online at: `http://www.hpc.ncep.noaa.gov/research/roth/landcane.html`.

convective bands. This is shown in Fig. 2.7. Animation of the radar composite imagery showed that the eye-like structure was fleeting and didn't persist as the storm rapidly evolved. Supercells often exhibit a bounded weak echo region (BWER) created when the intense updraft core lofts all precipitation-sized particles up and out of the BWER region. It would be erroneous to mistake this radar feature for the clearing of an eye, as the dynamics are very different. Nevertheless, on at least one occasion, the central vortex associated with a tornado appeared to extend all the way to the top of the supercell. Thus, it may be possible for supercells to have an eye.

Convective mesolows

A more interesting and hurricane-like eye/eyewall structure can develop on rare occasions from within a long-lived Mesoscale Convective System (MCS). The eye and eyewall develop from a mesolow and can persist for more than several hours. The scale of this feature is comparable to that in a hurricane, except that these developments have occurred over land. A recent instance (8 May 2009) was modeled in real-time by one member of a real-time Advanced Research Weather and Research Forecasting (WRF-ARW) ensemble that was being run for a convective field experiment. Diagnosis of that simulation revealed a significant warm core aloft (M. Weissman, personal communication). The actual system was associated with very strong winds and a large swath of wind damage. Fig. 2.8 shows another example, a 'landcane' which developed over several days from an MCS that originated in Iowa. Another example might be the strong eye/eyewall feature that developed in association with the remnants of Tropical Storm Erin (2008) over Oklahoma.[6] These systems need more study, but their mere existence suggests that it may be possible for an inland convective system to form a hurricane-like eye/eyewall structure. If this is the case, this has implications for the relevant and salient dynamics of hurricane eye formation. The strong surface fluxes and lower friction provided by an ocean surface may not be a *necessary* component of eye formation.

Polar lows, extratropical cyclones, and hybrid cyclones

Concerning the last three cyclone types (polar lows, extratropical cyclones, and hybrids), it is evident that some cyclones cannot be grouped into neat categories. Rather, there exists a continuum of cyclones ranging from fully extratropical to fully tropical and some cyclones which have characteristics of both. Cyclones in this continuum derive their energy from a variety of sources, ranging from storms which largely feed off energy obtained from strong baroclinic zones, to cyclones which derive the bulk of their energy through surface fluxes from the ocean. In most or all of these cyclones, the energy is mediated and expressed to the atmosphere through the release of latent heat via moist convection.

[6] Although this might be considered a redevelopment from a system which had tropical origins, Erin did not have a well-defined eye before landfall. The eyewall was associated with wind gusts to near 40 m s^{-1} and tropical-storm like rainfall tallies of 25 cm.

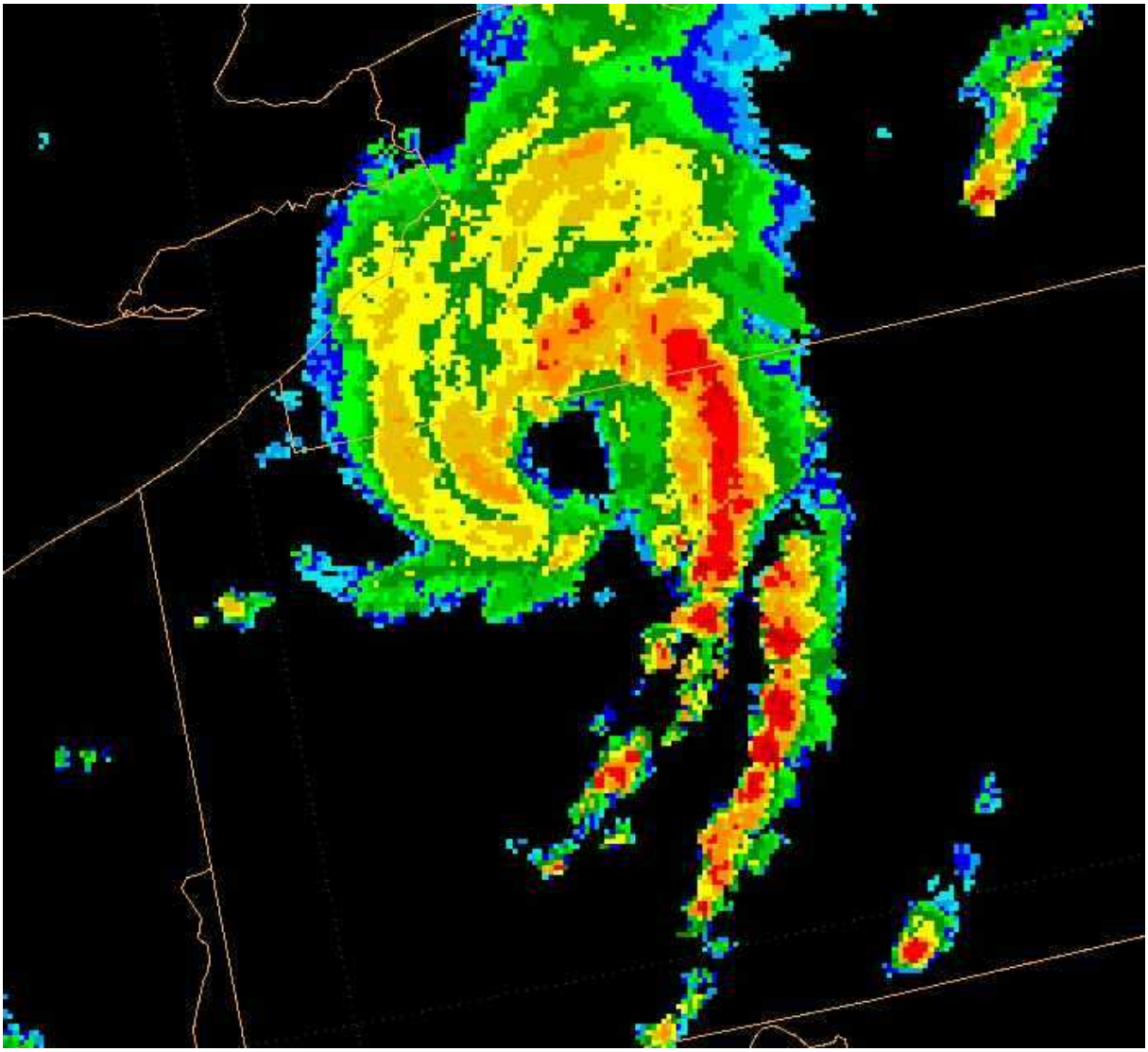

Figure 2.8: A radar composite of the “landcane” mesoscale convective system which occurred over the upper Ohio Valley at 2036 UTC on 21 Jul 2003. This image has been downloaded from an online writeup by David Roth, available online at: `http://www.hpc.ncep.noaa.gov/research/roth/landcane.html`.

Vortices having much in common with tropical cyclones — including eye features, upper level outflow, and spiral bands — have been noted over the Mediterranean (Reale and Atlas, 2001; Emanuel, 2005) and even Lake Huron (Miner et al., 2000; Sousounis et al., 2001). Fig. 2.9 reproduces a satellite photograph of the hybrid system which formed over Lake Huron from a cutoff upper low in a region of weak baroclinity in September 1996. The storm was fed by large (over $600\,\mathrm{W\,m^2}$) surface fluxes of sensible and latent heat from the aggregated Great Lakes (Sousounis et al., 2001).

Out of all the geophysical vortices considered so far, polar lows are probably the closest to their

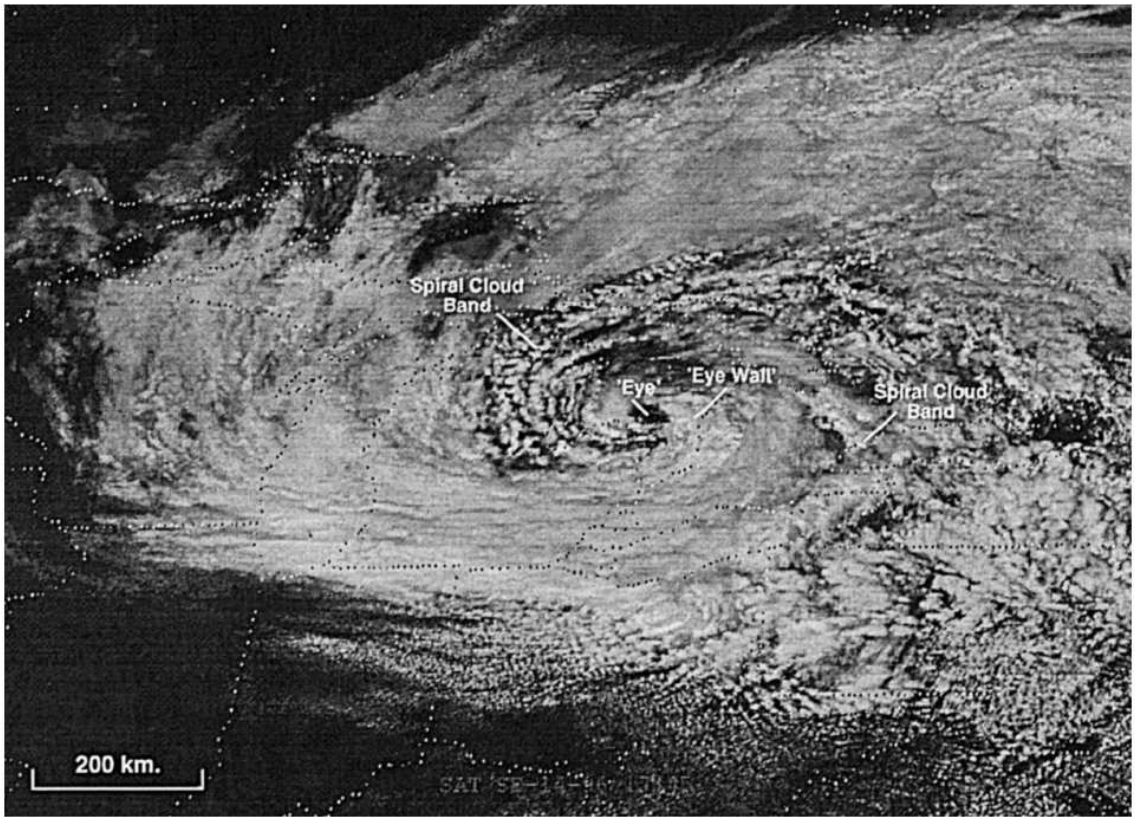

Figure 2.9: A satellite photograph of “Hurricane Huron” near the time of peak surface intensity at 1745 UTC on 14 Sep 1996. This image has been adapted from Fig. 1 of Miner et al. (2000).

tropical cousins. Emanuel (1989) goes so far to say that *some* polar lows are actually Arctic hurricanes. Yet even amongst polar lows, there is a continuum — many polar lows do not have much in common with tropical cyclones and most do not sport eyes. According to Yarnal and Henderson (1989), there are two main polar low types: a *comma cloud* type which feeds from moist baroclinity, and a *spiraliform* type which grows from Conditional Instability of the Second Kind (CISK). It is the spiraliform type that are most similar to tropical hurricanes and which sometimes sport bona fide eyes. An example of a spiraliform polar low with a clear eye is reproduced in Fig. 2.10.

Gray (1998a) studied the eyes formed in numerically-simulated hurricanes and polar lows. She found eye size to be relatively insensitive to initial relative and planetary vorticity for rapidly rotating eyes. This was not true of eye simulations in polar lows, which tended to produce weakly-rotating eyes. Polar low eye size was found to be related to the rate of subsidence in the core, with increased subsidence

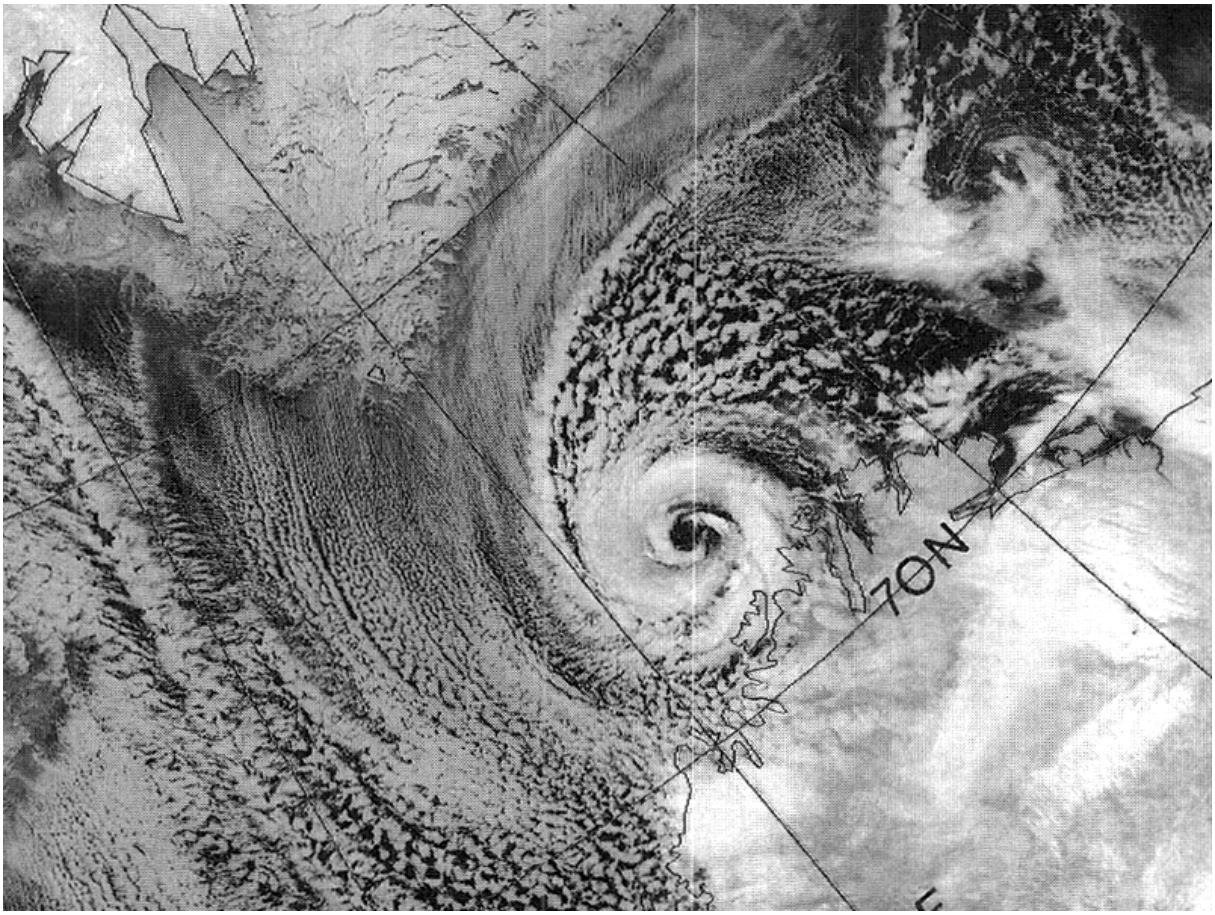

Figure 2.10: A NOAA-9 satellite image of the Bear Island polar low on 0831 UTC 27 February 1987. This image has been adapted from Fig. 3 of Nordeng and Rasmussen (1992). Photograph courtesy of Department of Electrical Engineering and Electronics, University of Dundee.

producing larger eyes.

Can an extratropical cyclone form a 'true eye'? These systems are by nature cold-core cyclones throughout the lower and middle troposphere, but the tropopause often dips down so that a stratospheric warm core sits above the cold core. This warm anomaly has some dynamical analogy to the eye in a hurricane. In a hurricane, the thermally indirect circulation driven by eyewall diabatic heating serves to strengthen the storm by causing further warming in the region that is already warm. In contrast, the thermally direct circulation in the lower portions of an extratropical storm act against storm intensification by warming the cold core (Palmén, 1948). Yet occasionally, strong extratropical cyclones appear to form eyes. Fig. 2.11 shows the apparent 'eye' of the Blizzard of 2006 as it passed offshore the Delmarva Peninsula. On the morning of 12 February, the storm appeared to have a clear, circular eye embedded

within what seems to be a rather symmetric central dense overcast. However, upon closer inspection of the 'shadows' cast by the 'eyewall', one can show herself that the implied sun angle is incorrect (contrast this with actual shadows cast by a higher cloud band to the southeast of the storm). A higher resolution time series of images (not shown) reveal that this 'eye' was actually an uneven erosion in a low-lying stratocumulus deck. This case illustrates that an 'eye-like feature' is not always indicative of 'eye-like dynamics'. Similar 'eyes' have been noted in other extratropical cyclones such as the President's Day Snowstorm of 18-19 February 1979 (not shown, see Fig. 16 of Bosart 1981) and the "QE II" storm of 10-11 September 1978 (Gyakum, 1983). In the President's Day Snowstorm, the eye feature appeared in a shallow cloud deck while the overall storm took on a distinct comma shape. Extratropical cyclones are normally quite asymmetric with the storm circulation dominated by warm and cold moist conveyor belt circulations — these structures are hardly conducive to eye formation. However, it is possible for storm of extratropical origin to form a 'true' eye if deep convection near the center becomes organized into an eyewall by the strong circulation, similar to many of the eye formations observed in subtropical storms. An example is shown in Fig. 2.12. Another mode of eye formation can occur once the storm has completely occluded and undergone a tropical transition. The genesis of the Unnamed Hurricane in the "Perfect Storm" (which had itself absorbed Hurricane Grace previously) of October 1991 is a good example, as a true tropical cyclone formed in the center of the larger, decaying extratropical cyclone. The system later went on to form an eye (not shown, see `http://www.ncdc.noaa.gov/oa/satellite/satelliteseye/hurricanes/unnamed91/unnamed91.html`). Thus, in most cases in which an eye appears to form in an extratropical cyclone, one can surmise that it is either a false eye — or that the storm has become dominated by surface fluxes and taken on at least some hybrid characteristics.

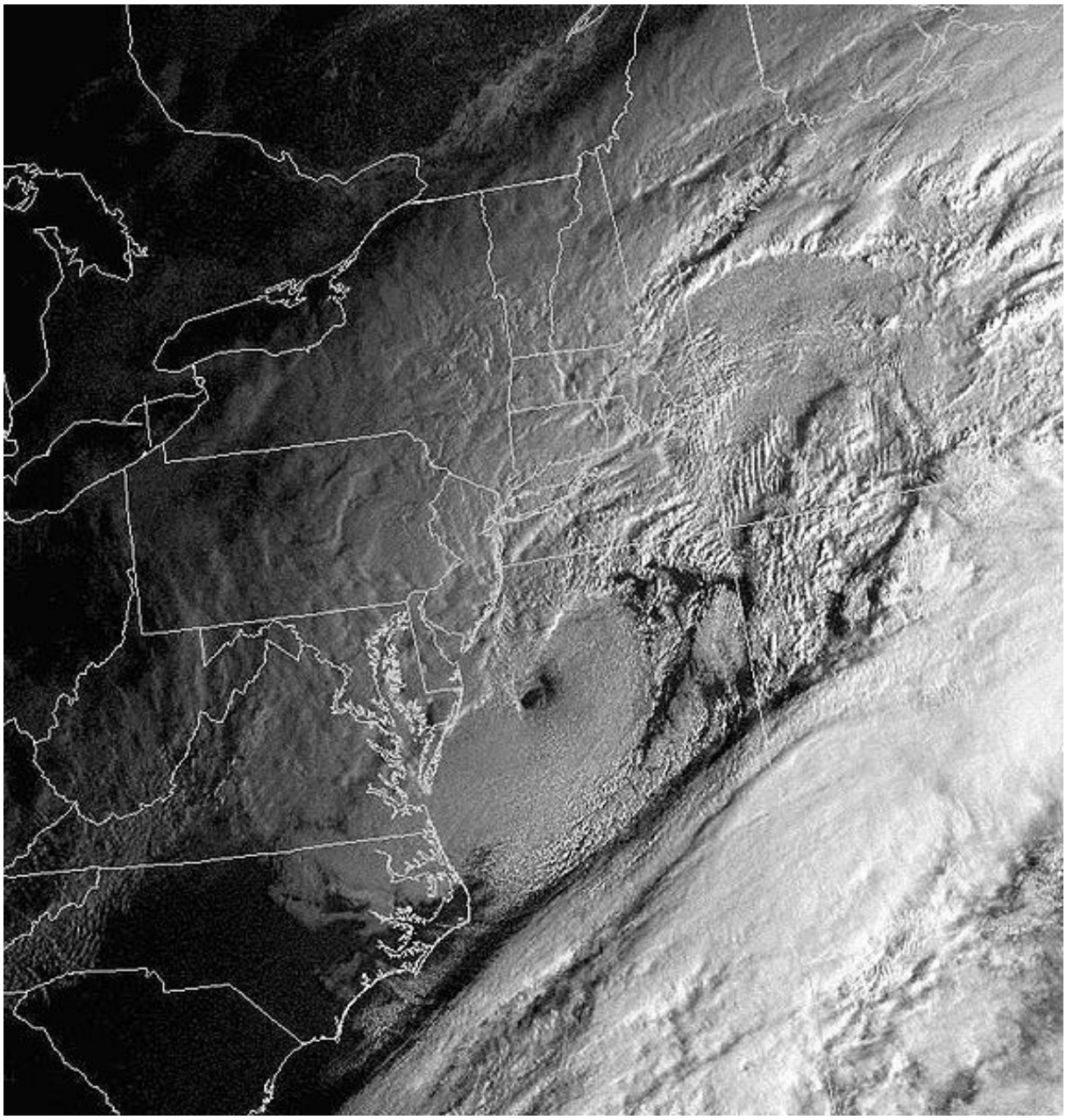

Figure 2.11: NOAA GOES satellite image of the “eye” of the Blizzard of 2006, as seen on 1245 UTC on 12 Feb 2006. Photo credit: NASA GSFC.

2.3 Observations of tropical cyclone structure and eye phenomena

2.3.1 Discovery of the warm core

Before the age of aircraft and radiosonde observations, the thermal structure of the tropical cyclone was somewhat of a mystery. Early observers noted little variation of surface temperature during the

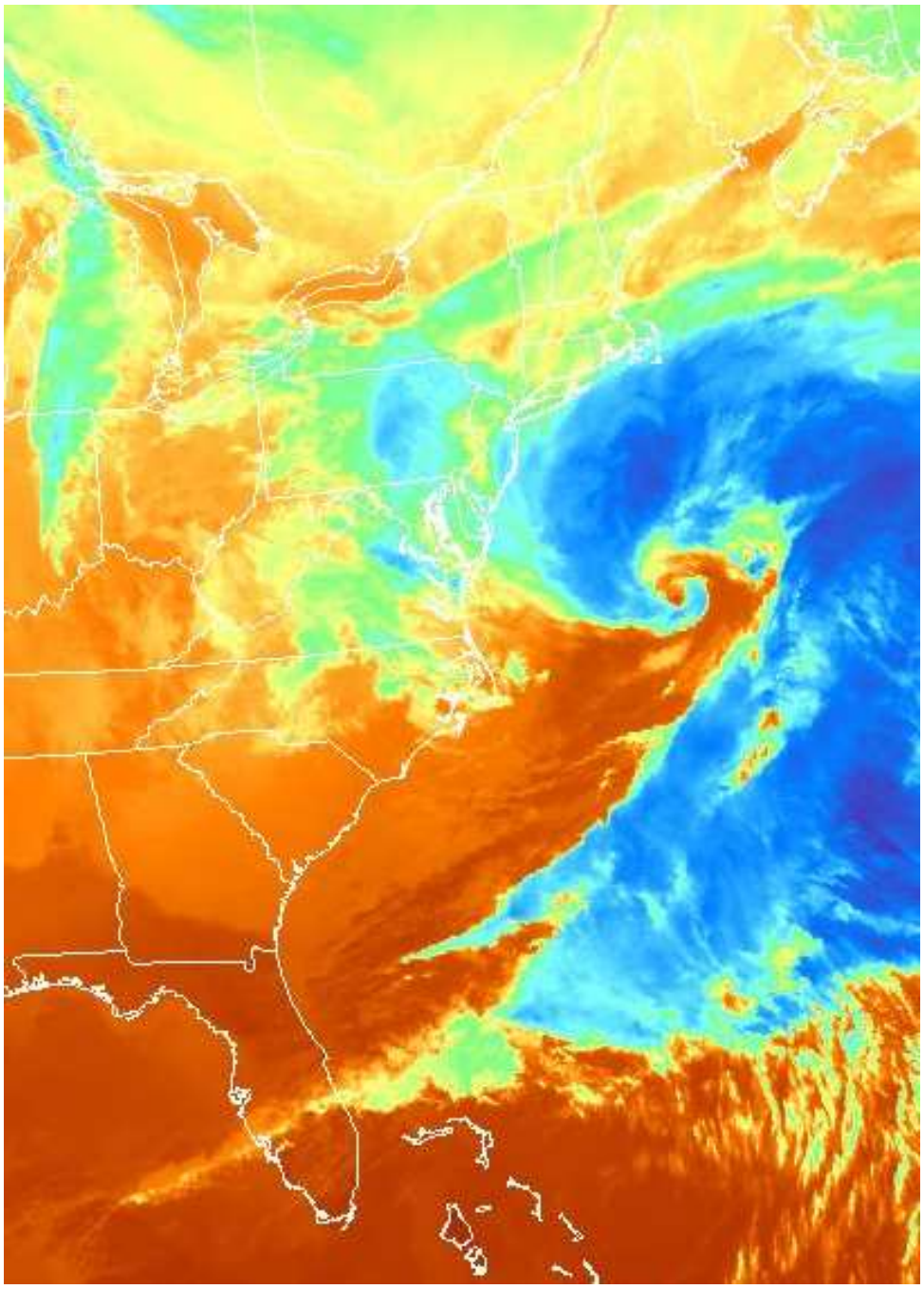

Figure 2.12: GOES IR satellite image of the forming eye of an extratropical cyclone at 1545 UTC on 22 January 2010. Downloaded from `http://www.rap.ucar.edu/weather/satellite/g12.2010022.1545_US_ir.jpg`.

passages of tropical cyclones over the southeast United States (Cline, 1926) and the Philippines (Deppermann, 1937a), yet there had been isolated reports of relatively warmer or even "scorching" air in the eyes of some storms. One well-documented example occurred during the 20 October 1882 passage of a

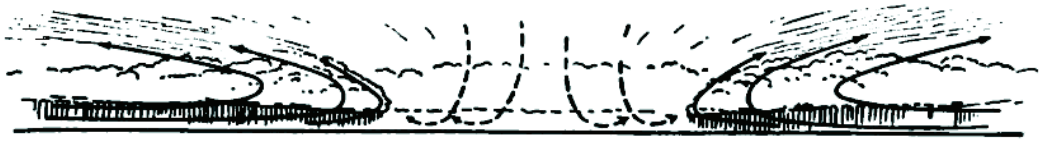

Figure 2.13: Late 19th century schematic of the radial structure of a hurricane's inner core, showing radial inflow at low levels, ascent in a sloping, convectional eyewall, and outflow aloft. Slowly subsiding currents and clearing are displayed in the eye. Reproduced from Fig. 60 of (Davis, 1899, p. 204)

typhoon eye over Manila. As the city entered the calm of the eye around noon, the sky cleared considerably but for a thin cloud veil, and the surface temperature suddenly rose from 25 °C (77 °F) to 31.5 °C (88.7 °F). The relative humidity dropped from near saturation to 49% (or 43% depending on account), which was considerably drier than what would be expected if the surface air had simply warmed sensibly. Afterwards the temperature and relative humidity returned to their previous values (Algué, 1904, p. 57). While some questioned the validity of this measurement (e.g. Deppermann, 1937b), it seems that this singular report of warm, dry air in the eye tipped off meteorologists to the likelihood that the warm core was an integral feature of mature tropical cyclones.[7] Controversies ensued as to whether the core sometimes contained descending air currents in addition to the widely regarded predominance of ascending motions (e.g., Davis, 1899, pp. 202-208). As Davis's schematic hurricane cross section shows (his Fig. 60, reproduced here as Fig 2.13), the gross structure of the hurricane had been surmised by the close of the 19th century.

In the 1930s, workers fleshed out some dynamical aspects of the warm core. Haurwitz (1935) assembled the afore-mentioned puzzle pieces and used the hydrostatic equation to convincingly demonstrate that the mature tropical cyclone must indeed contain a deep warm core structure that extends to great height.[8] Using some simple assumptions and a time trace of surface observations, he ascertained the outward-sloping funnel-shape of the eye/eyewall interface, reproduced here in Fig. 2.14. Durst and Sutcliffe (1938) added to this view by analyzing the equations of motion applied to a symmetric vortex.

[7] Even later, some researchers have cast doubt on whether the warm air ever properly reaches the surface. Dunn (1951) discusses that observer's reports of "oppressive", "sultry", and "suffocating" air is apparently a psychological effect caused by the rapid transition from high winds and torrential rains to the relative calm and high humidity of the eye. He attributes the few cases of noticeable temperature rise to insolation or the foehn effect.

[8] Previously, the height of the hurricane circulation had been a question of intense debate.

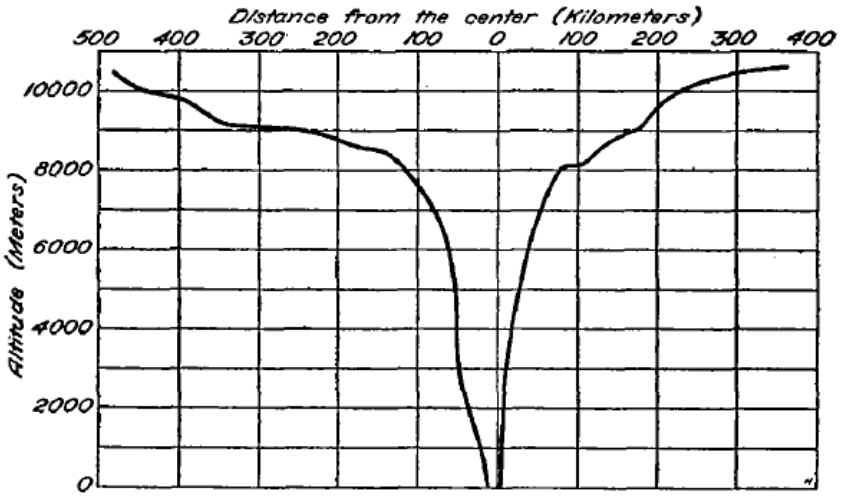

Figure 2.14: Shape of the funnel of the Manila cyclone, computed from surface observations as it passed over a station during 19-20 October 1882. Reproduced from Fig. 2 of Haurwitz (1935).

They suggested that the eviction of air from the center is accomplished by an upper warm-core anticyclone whose excess pressure is maintained through subsidence warming via the "vertical term." Palmén (1948) expanded on this understanding, establishing that the high temperatures in the eye results from the tendency of the vortex to establish thermal wind balance, a combined hydrostatic and geostrophic-cyclostrophic balance.

2.3.2 Modern observations of the eye and warm core structure

The advent of routine radiosonde observations, radar, and aircraft reconnaissance established the ubiquitous nature of the tropical cyclone warm core. Schacht (1946) computed a mean hurricane sounding from radiosonde ascents in Caribbean hurricanes during 1941–1944, confirming that the storm's low pressure anomaly and winds decrease with height. The radial pressure gradient reverses sign at about 10 km, with anomalously high pressures over the storm center and outflow in the 10-14 km layer.

Compelling observational proof for the existence of the warm core and the necessity of dry adiabatic subsidence came when the first radiosonde ascent was made in the eye of a hurricane near Tampa (19 October 1944). Temperatures above 600 hPa were by far the warmest on record for that area and, it seemed, were produced "by prolonged descent of originally high-tropospheric air" (Riehl, 1948). Jordan (1952) used dropsonde data from reconnaissance aircraft to show that the eye subsidence does not usually extend all the way to the surface; below a temperature inversion, the eye is often cloud-filled and comprised of air with properties similar to air in the eyewall. Observations of warm, dry air reaching the surface are exceedingly rare, but this can happen if the inversion crashes all the way to the surface. Jordan (1961) discusses an over-ocean sounding in Typhoon Ida (1958) which had a surface temperature of 92 °F and a relative humidity of 50%. A later study by Jordan and Jordan (1954) composited over 300 radiosonde observations in hurricanes and showed that the anomalous eye warmth only becomes appreciable above 700 hPa. They also found that the upper portion of the warm core may extend laterally for hundreds of kilometers regardless of the size of the inner core of rain and high winds. From aircraft observations taken in extremely intense Supertyphoon Marge (1951), Simpson (1952) found that significant temperature gradients were confined primarily near the eye/eyewall interface at lower levels, but spread outward into the eyewall region at higher levels. A remarkable horizontal temperature gradient of about 18 °C was measured over just 60 mi at 17, 000 ft, showing that the warm core may be enclosed by a very strong baroclinic zone. By using radar observations of the height of bright band echoes in Hurricane Edna (1954), Kessler (1958) assumed a given lapse rate and also found that the strongest temperature gradients were concentrated near the eye of Hurricane Edna (1954). That the pronounced warm core structure occurs within the space bounded by the radius of maximum winds is a key observational result.

Subsequent studies uncovered more details about the warm core's structure, magnitude, and relation to storm intensity and intensification rate. Palmén (1956) discussed how the hydrostatic effect of latent heating of the entire column up to 150 hPa is only sufficient to drop the surface pressure by about 15 hPa. Therefore, the formation of the eye is critical in allowing the storm to reach such great intensity. LaSeur and Hawkins (1963) constructed a cross section of the warm core of Hurricane Cleo (1958) which revealed that the warmest temperatures are not always found in the center of the eye, but sometimes occur near the eyewall, forming a warm ring structure (the dynamical reasons for this are

treated by Schubert et al. 2007 and in chapter 3). Cleo's maximum temperature anomaly of $+11$ K was found above 250 hPa. In contrast, the tight warm core of intense Hurricane Inez (1966) displayed a double maximum in height, with temperature anomalies of $+9$ K centered at 650 hPa and 300 hPa on one day, and $+11$ and $+16$ K on another day (see Fig. 6 and 14 of Hawkins and Imbembo 1976; their Fig. 14 is reproduced in chapter 6 as Fig. 6.8). Recent NASA/CAMEX field campaigns mapped the three-dimensional warm cores of a sheared storm (Erin, 2001) and a storm with strong "hot towers" embedded in the eyewall (Bonnie, 2001). An unprecedented battery of data was gathered from the low-level P-3's, the DC-8, and the high altitude ER-2 aircraft with its unique EDOP radar system. These data show that the warm core may be asymmetric and tilted due to vertical shear, and that some convective bursts may produce episodic eye warnings via a mesoscale descending current of several meters per second (Heymsfield et al., 2001; Halverson et al., 2006). This last fact has possible implications for eye formation and and will be discussed later.

Of particular interest for the eye formation problem is the question of whether the warm core builds upward or downwards. Yanai (1961) examined radiosondes from Kwajalein Island Typhoon Doris. He thought that the warm core built downwards, and that rapid development of the storm did not being until this upper warm core had formed. This may be true of developing storms in general, however, the warming observed by Yanai may be different from the more concentrated warming that occurs during eye formation. It is generally thought that active convection deepens the vortex, causing it to build upward as convective fluxes transport angular momentum upwards in the storm. If so, then it would seem natural for the subsidence to also build upwards with the convection. There are not many observations of the vertical progression of warm core development because high level sorties through the hurricane are not normally undertaken. Some good data on the upper levels of hurricanes was taken during the 1950s however, when Air Force bombers were used for some missions. Alaka and Rubsam (1965) studied multilevel aircraft data from Hurricane Ella and did observe a case in which the warm core built upwards.

2.3.3 Investigations of the eyewall

One of the first aircraft eye penetrations and the advent of radar challenged early ideas on the nature of the eyewall. On 14 September 1944, Colonel Floyd B. Wood and his crew of two flew into the eye of a 940 hPa hurricane off of Cape Henry, Virginia (Wood, 1945). They encountered a strong, steady downward current as they flew through the stratiform rain region at 3000 ft. As they approached the eyewall, the rain grew heavier, the sky dimmer, and the air was very turbulent. They were quite surprised when their plane began rising at 2000 ft per minute, reaching 5000 ft by the time they broke into the eye. In the eye, the sky brightened and there was almost no rain. Wexler (1945) prepared a cross section schematic showing the general storm structure as far as they could tell. This is reproduced here as Fig. 2.15 and shows descending motion at low levels through the rain area, with just a narrow 'throat' of strong updrafts feeding the immense hurricane cloud system. The observations of this flight surprised early researchers since it had been previously thought that the hurricane contained general ascending motion everywhere except the area of descent in the eye. Also that month, the first known picture of a hurricane eye was photographed on the radar scope at the U. S. Naval Air Station in Lakehurst, New Jersey Maynard (1946). That and subsequent photographs of Pacific typhoons later that year confirmed the eye as a dark area 'surrounded by curved bands of echoes with featured edges and trailing wisps.' In some of the photographs presented in Maynard's paper, the eyewall is seen as thicker with stronger echoes and sometimes separated from the curved bands. Thus, the eyewall was found to be a distinct and unique feature different from the typical curved bands. Deppermann (1946) conducted a simple geometrical and kinematic analysis to estimate the speed of upward motion in the eyewall and came up with a figure of $5\,\mathrm{m\,s^{-1}}$. He went on to make an argument about how wide the updraft should be and how this should narrow for a more peaked wind profile.

By the early 1950s, much information was being gathered in the eye of the storm, but not many observations were being taken in the surrounding eyewall due to the turbulence and strong gradients — the rapid change of values made it difficult for observers to record. The introduction of automatic recording equipment lead to detailed profiles of wind and temperature, leading to the aforementioned result that the eyewall was a region of intense baroclinity, with a sharp temperature rise as the eye was approached.

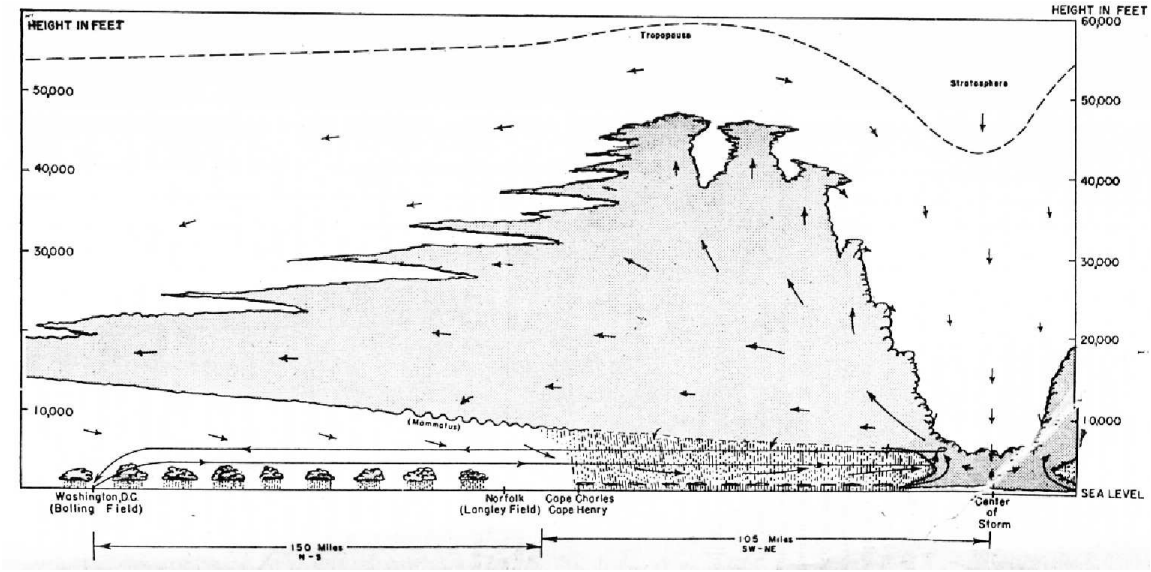

Figure 2.15: Schematic of showing the narrow 'throat' of the eyewall updraft that fed the immense convective cloud of the storm. Reproduced from Fig. 4 of Wexler (1945).

The composite study of Shea and Gray (1973); Gray and Shea (1973) found the warmest temperature occurred well inside $r_{\max}$, and that the largest temperature gradients occurred at $r_{\max}$ where the gradient averaged $1.5\,^{\circ}\mathrm{C}(5\,\mathrm{n\,mi})^{-1}$). Their schematic, shown here as Fig. 2.16, displays these findings. In their study, they found that $r_{\max}$ occurred within the cloud area, normally $5-6\,\mathrm{n\,mi}$ outside of the inner eyewall edge. This displacement from the inner eye edge tended to narrow for more intense storms (see Fig. 18 of Shea and Gray 1973). Their cross section of kinematically computed vertical motion relative to $r_{\max}$(not shown, see Fig. 5 of Gray and Shea 1973) showed that the eye/eyewall boundary was demarcated by a strong reversal in vertical motion, with the strongest upward motion occurring near $r_{\max}$ in the eyewall, and the strongest downward motion located just inside the inner edge of the eye. Thus, the eye/eyewall boundary is found to be a semi-vertical surface of zero divergence (cf. their Fig. 4).

Shea and Gray found little slope in $r_{\max}$, contending that appreciable slope of the eyewall tended to occur mainly in weaker storms. They surmised that stronger eyewall convection transported horizontal momentum to upper levels, resulting in a more vertical eyewall. This was in contrast to theoretical arguments for a large eyewall slope by Palmén (1956). The near-vertical eyewall idea was challenged by a later observational study involving multiple aircraft flights various levels of intense storms. Jorgensen (1984a,b) showed convincingly that even in intense storms, the eyewall convection sloped outward with

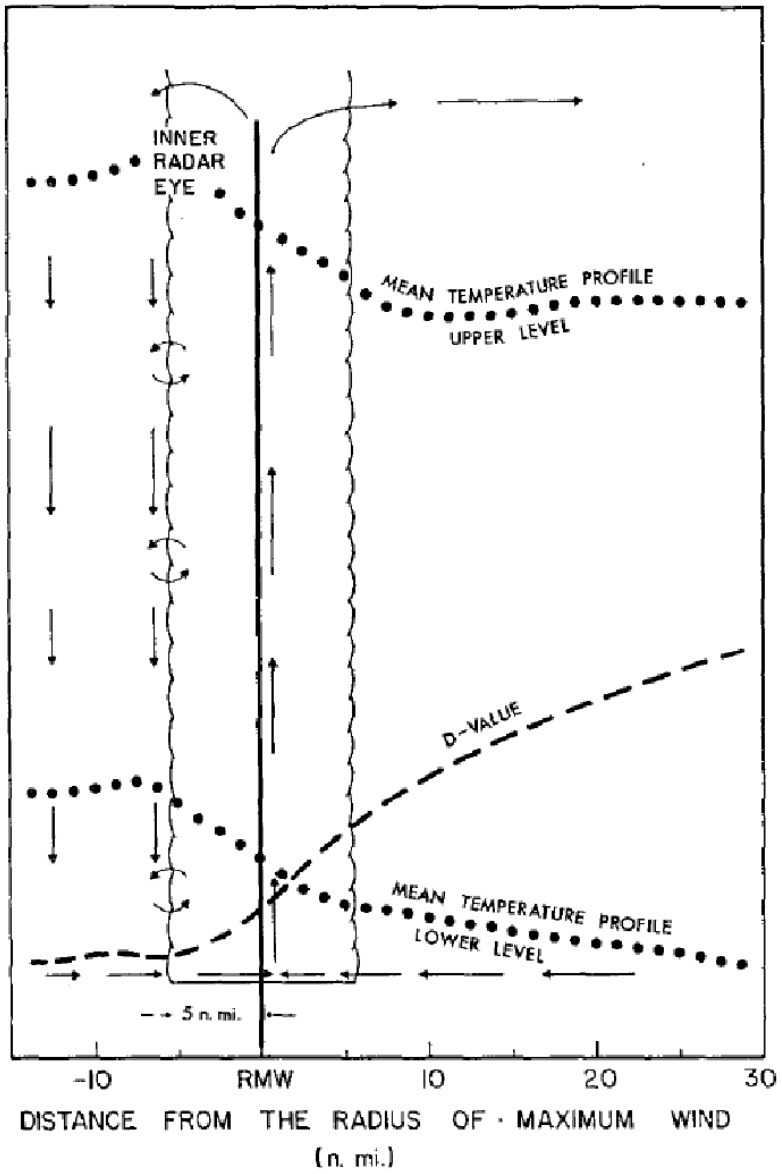

Figure 2.16: The schematic portrayal of the variations across the eyewall for the D-value, the mean temperature profile at upper and lower levels, and the radial and vertical motion. Reproduced from Fig. 19 of Shea and Gray (1973).

height (with slopes ranging from 27° to 45°), implying a sloping updraft. The steepness of the slope was apparently related to the eye diameter and storm strength, with steeper slopes occurring in stronger storms that have smaller eyes. His study confirmed Shea and Gray's findings that the strongest wind tended to occur within $r_{\max}$, finding typical values of $1-6$ km. His schematic of eyewall structure is reproduced as Fig. 2.17, and shows a sloping eyewall updraft inward from $r_{\max}$, with the heaviest precipitation located just outside of $r_{\max}$. Interestingly, he found strong outflow from the eye into the eyewall at lower

levels. The implications of this last finding will be discussed shortly in relation to the hypothesis that eye formation involves a centrifuging of air by the eyewall. Most recently, Stern and Nolan (2009) find that eyewall slope does increase with radius, confirming the outward flaring funnel shape first surmised observationally by Haurwitz (1935). They also confirm that $r_{\max}$ closely approximate a constant angular momentum surface, but find little relationship between eye slope and the intensity of the storm. Instead, they find that the slope of $r_{\max}$ is a function of the size of the storm, with larger storms displaying a larger slope.

Finally, Willoughby (1990b) conducted an important study on eyewall dynamics in which further examined the contracting ring of convection discussed in Shapiro and Willoughby (1982). Using many radial profiles of tangential wind, he showed observationally that convective rings are a frequent mode of tropical cyclones and are associated with strong intensification of the system as the strongest height falls just inside the radius of maximum winds.

Now that the basic structure of the eye and eyewall structure have been reviewed, in the next section we offer a definition for determining the moment when an eye forms in a tropical cyclone.

2.4 Definition of tropical cyclone eye formation

Forecasters are sometimes unsure whether an eye has developed in a tropical storm. Their operational storm discussions sometimes refer to the presence of an "eye-like feature." The initial stages of eye development can be rather marginal and ephemeral, and a forming eye may not immediately satisfy all the criteria one might expect of a "true" eye. It seems that a clear and straightforward definition for the hurricane eye does not yet exist, at least in the literature on tropical cyclones. Historically, the eye has been defined according to its properties — the region of light or calm winds found in the center of a tropical cyclone. As an example, the *Glossary of Meteorology* gives the following definition for the *eye*:

> In meteorology, usually the eye of the storm (hurricane, typhoon), that is, the roughly circular area of comparatively light winds found at the center of a severe tropical cyclone and surrounded by the eyewall. The winds increase gradually outward from the center but can remain very light up to the inner edge of the eyewall. No rain occurs and in intense tropical cyclones the eye is clear with blue sky overhead. Most, but not all, tropical cyclones with maximum winds in excess of $40\,\mathrm{m\,s^{-1}}$(78 kt) have eyes visible on satellite imagery. Eye diameters vary from 10 to more than 100 km.

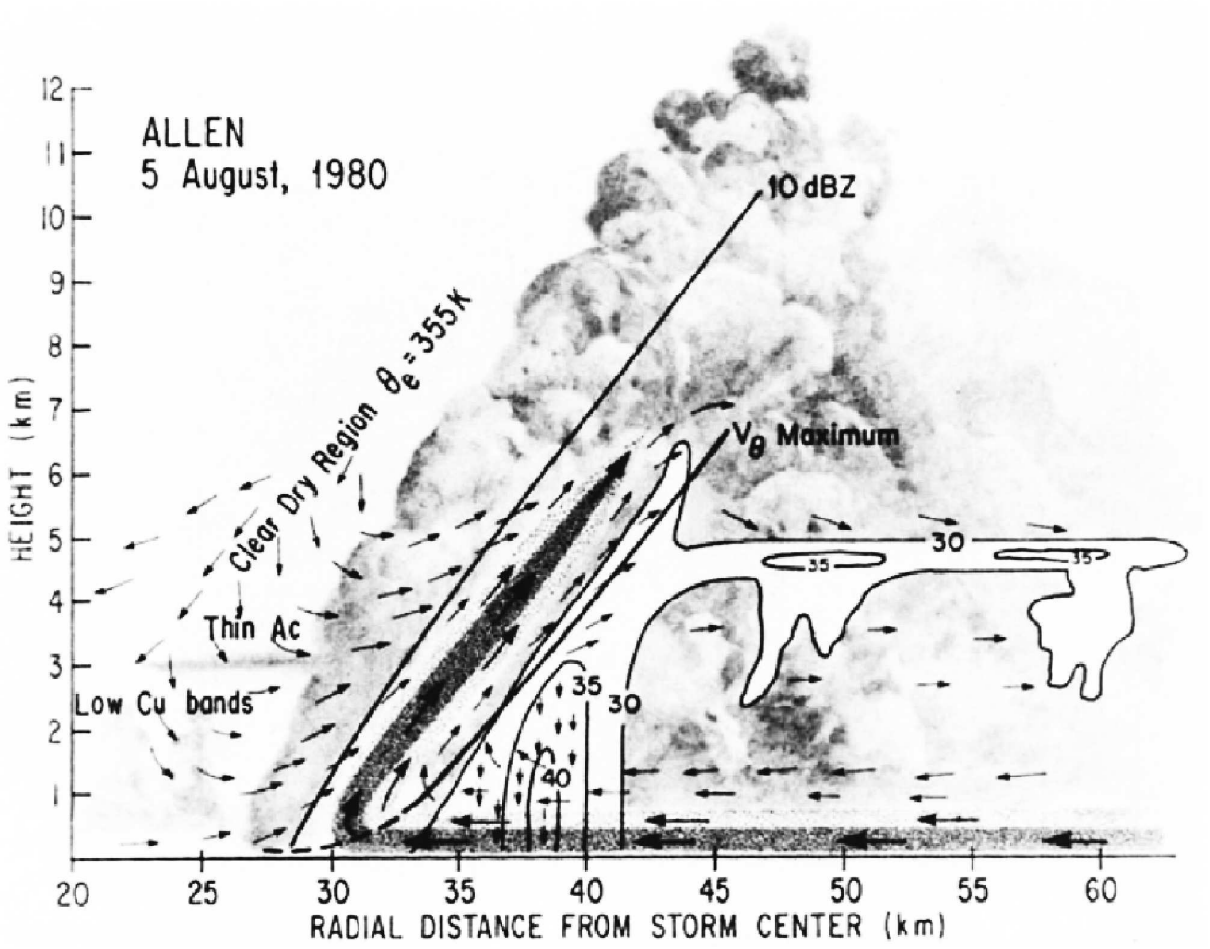

Figure 2.17: Schematic of Hurricane Allen's eyewall structure. Reproduced from Fig. 19 of Jorgensen (1984b).

The *eyewall* is defined as:

> A ring of cumulonimbus that encircles the eye of a tropical cyclone. In radar depictions, the clouds must occupy at least 180° of arc to be called an eyewall.

The observational criteria used to determine the presence of an eye are reviewed in chapter 4, but basically require that a continuous eyewall be visible on aircraft radar, subtending at least half of the eye. The ill-defined use of the term eyewall in the literature has been noted recently by Stern and Nolan (2009). Thus, both of these definitions are still lacking as several questions illustrate. What determines the eye/eyewall boundary? How well defined and complete must the eyewall be to consider it to contain an eye? Does the eyewall convection have to attain a certain height? Is the vertical structure of the warm core a necessary requisite? If the near-calm of the surface winds is important to the definition,

where does the eye begin for storms in which the center is near solid body rotation? Should an eye be considered such if the winds are are far less than hurricane force?

Our review of tropical cyclone structure in the previous section suggests many possible ways to define the eye/eyewall boundary:

- the region of near calm at the surface
- the cloud field (or inner boundary of precipitation)
- the horizontal gradient of temperature
- the horizontal gradient of humidity (relative or specific)
- the radius of maximum winds
- the horizontal gradient of inertial stability
- the horizontal gradient of vertical motion

The region of near calm can be discounted, as quite high winds can sometimes occur near the eyewall edge. Using the boundary of clouds at the eyewall is helpful when the provisional eye region is clear, but many hurricane eyes are cloud filled, especially below the inversion that typically resides at a height of about 1.5 km. The horizontal gradient of temperature typically becomes pronounced for intense storms, but storms just forming an eye may not possess such a strong gradient if the eye warm core is not yet strong. The gradient in humidity suffers from the same troubles as the cloud field and temperature gradient criteria — these require that the subsidence warming already be quite strong and might miss weak eyes. The radius of maximum winds, as was previously shown to be a consequence of angular momentum conservation, is ubiquitous to all vortices, and is typically found several kilometers into the precipitating eyewall in the hurricane, thus is not very helpful here. The horizontal gradient of inertial stability may be useful, as the high inertial stability of the cyclone core acts as a 'wall' to inflowing air. Finally, the horizontal gradient of vertical motion seems promising, as many of the other criteria above arise from the subsidence, at least eventually. Actually, Walko (1988)'s study on tornadoes has already defined the eye as "an inner cell separated by a streamsurface from the outer meridional circulation of the storm, and is heated by subsidence at its center." In his paper, he specifically discusses the warm eyes formed in hurricanes in reference to this definition, so we take this as the most straightforward definition for a tropical cyclone eye yet.

The idea that the eye and eyewall have some dynamical significance in allowing the storm to intensify has so far been implicit in our discussion on definitions, but is not brought forth as we consider whether the surrounding eyewall must be vertically deep. The National Hurricane Center (NHC) normally requires that the eyewall convection have a brightness temperature colder than $-50\,^{\circ}\mathrm{C}$ (J. Franklin, personal communication 2008). Tropical cyclones which have been strongly sheared may sometimes still have a central clear spot and even a residual warm core aloft, but without an eyewall, their potential for future intensification is quite dubious. Such systems are often observed in the Eastern Pacific basin. It is difficult to make a case that such a system should be considered to have an eye. Including a vertical depth requirement may be warranted. If the NHC criterion is used, then the eyewall convection must extend through a good portion of the troposphere. A more dynamically relevant criterion could involve the use of the Rossby penetration depth, but for now, we just require that the eyewall cloud extend through a substantial portion of the troposphere (perhaps more than half).

Ambiguity arises also at the lower eye region, as that is normally filled with moist, cloudy air beneath a temperature inversion. Air may or may not be crossing into this lower eye region from beneath the eyewall. Due to the friction with the surface, an Ekman-type boundary circulation may actually promote a gentle updraft up to the height of the inversion. Should this lower region be considered part of the eye? As a matter of practicality and to be compatible with historical usage, we will consider this to be part of the eye. Then it should be referred to as the 'lower eye'.

Combining Walko's definition with the previous observational definition and adding a few criteria from common sense considerations, we arrive at the following definition for tropical cyclone eye formation. The eye is said to have formed in a tropical cyclone when:

- the candidate eye contains the primary wind center of the vortex and the area of lowest pressure,
- the eye region is generally delimited by a streamsurface that separates it from the outer meridional circulation; this surface is typically manifested by a sharp radial discontinuity of vertical motion so that the eye is filled with subsidence extending through most of the mid to upper troposphere,
- the eye region is at least 50% surrounded by an annular cloudy, precipitating eyewall region which fills a substantial portion of the troposphere, and
- the eyewall region contains the ascending branch of the secondary circulation, a peak in tangential wind (e.g., $r_{\max}$), and *often* features decreasing temperature with radius.

No definition is perfect, so we offer the following caveats. The use of a streamsurface can be confounded by several effects. First of all, both upward and downward motion may occur in the eye from transient wave-like motions (Yamasaki, 1983; Willoughby, 2009). Mixing episodes associated with eyewall mesovortices may also distort the vertical motion field locally.

This definition does *not* require the eye to be precipitation-free. After a secondary eyewall formation has taken place, a hub cloud or relict eye (the remnants of the former eye) may remain for some time within the larger secondary eyewall. This definition does not preclude disturbance by eyewall mesovortices or a requirement for symmetry (elliptical eyes are often observed). The 50% completeness of the eyewall is retained however — the dynamical signficance of this is that whatever the mechanism for forcing the eye subsidence, it must depend in some way on the presence of an eyewall. Sheared storms often display a strong wavenumber-1 asymmetry in the eyewall convection, so that an open eyewall is present. From a dynamical perspective, having at least half of an eyewall appears to be sufficient to generate most or all of the properties of an eye. This definition does not require the eye to form over water, allowing for the possibility the eye could form over land. Finally, no persistence or "self-reinforcing" criteria are included, allowing for the possibility that this structure may appear and then dissipate after a short while. The eye/eyewall structure seems to normally be reinforcing, but we allow for the possibility that it could be disrupted by other factors, such as vertical shear.

Thus, the moment of eye formation occurs from a *dynamical* standpoint when the subsidence fills the eye region and the eyewall has become sufficiently well defined to be recognized as such. From a *practical* standpoint, the observational requirement for a precipitating eyewall cloud to subtend at least $180°$[9] appears to be sufficient to reliably indicate the presence of an eye, so long as there is some evidence of accompanying subsidence in the eye region. Cloud clearing associated with a transition to general subsidence in the eye region is normally a sure giveaway that an eye has formed — this is the point in which an eye is considered to have definitely formed from an operational perspective.

Now that a comprehensive definition for the eye has been developed, the next sections of this chapter will survey the mechanisms and causes of eye formation that have been proposed. We start by considering mechanisms which do not involve azimuthal variations.

---

[9] The historical observational definition for an eye will be discussed in much more depth in chapter 4.

2.5 Symmetric mechanisms of eye formation

As previously mentioned, it is important to distinguish between the processes of eye formation and the processes of eye maintenance. Once an eyewall has formed, it is relatively straightforward to understand why there is subsidence in the eye. It is also important to realize that eye formation is a process, not necessarily an "event". Yet some eyes seem to form very rapidly and theoretical work by Carrier (1971) suggests that the *e*-folding time for eye formation itself can occur on a much shorter time scale of as little as 20 min. Certainly, satellite observations have shown that the cloud clearing of the eye can occur in short order, although it is less likely that the eyewall develops that quickly.

2.5.1 Forced subsidence theories

Nevertheless, we will follow the progression of ideas about the eye subsidence as they developed in the literature. The causes of forced axial subsidence falls mainly into two categories:[10] dynamically-forced or convectively-forced.

Dynamically-forced subsidence: the centrifugal hypothesis

Many have mistakenly attributed the centrifuging hypothesis to Malkus (1958a) and Kuo (1959), calling this the Malkus-Kuo hypothesis. This is actually incorrect. It turns out that the basic idea of centrifuging was around long before (e.g., Byers, 1944; Sawyer, 1947; Syōno, 1951). Perhaps the earliest (and most lucid) description is offered by Ballou (1892):

> "What then is the cause of the clearness of the eye? The following is proposed as a rational hypothesis, which appears to be borne out by the facts.
>
> The wind of the cyclone is prevented from reaching the centre by two causes. First, as the wind velocity increases, the deflective force of the earth's rotation increases, until around the centre the hurricane winds blow in a circle. Secondly, the air is carried upward and outward by the convectional circulation before reaching the centre.
>
> Thus we have a revolving circumference of violent winds, with a calm in the centre. But the winds by their friction must tend to drag the calm air adjacent to them into the cyclonic whirl. Possibly, also, there is a tendency of the circumference of winds to expand by centrifugal force. In either case, there would be a deficiency of air at the outer edge of the calm, which would have to be supplied by a gradual settling of air

[10] Although a third possibility will be discussed later.

over the whole area. Such a settling would be sufficient to dissolve the cloud stratum and to show blue sky."

Thus, the idea that the eye air mixes with high angular momentum eyewall air and causes it to be centrifuged out of the eye at low levels was not original to Malkus or Kuo, although they certainly elaborated and expanded on this idea. This argument explains the presence of the eye subsidence as required to maintain mass balance. Malkus (1958a) proposed that eye air began its descent at high levels, where the angular momentum was weak, but acquired angular momentum as it descends in the eye, arriving to the 800 to 900 hPa level with supergradient wind speeds and a peak descent rate of 10 to 15 $\mathrm{cm\,s^{-1}}$. Owing to the the excessive centrifugal and Coriolis accelerations, this air would then flow outward into the eyewall. She suggested that the resulting strong divergence in the lowest kilometer of the eye was responsible for the large and remarkable calm often observed at the surface. She constructed a detailed thermodynamic and angular momentum budget for a hypothetical storm which assumed various rates of mixing between the eye and eyewall as the eye air descended. Applying the model to some real storm examples gave reasonable values, but the questions of how much entrainment occurs and how much water substance is introduced into the eye air (thereby having a substantial cooling effect) are important 'tunable' parameters of the model. The requirement of a vertical eyewall is another limitation which she noted. It should be pointed out that she recognized this hypothesis was not necessarily a means of forming the eye, but rather applied to the maintenance.

Kuo (1959) elaborated further on Malkus's idea by considering integral constraints on the energy and angular momentum of the inflowing air, essentially defining a Bernoulli equation[11] along a streamline of the inflowing air. Considering that the total (internal, potential, and kinetic) energy of inflowing air is limited, yet that the conservation of absolute angular momentum requires the tangential velocity (and thus the kinetic energy) to continually increase as air approaches the center, he showed that there exists a limiting radius beyond which the converging current cannot pass. This air is then forced upward. Kuo used this theory to make calculations of eye radius with and without surface friction and came up

[11] The classical Bernoulli theorem states that intersections of surfaces of potential temperature and constant Bernoulli function yield streamlines of the flow. Schär (1993) has given a generalization to Bernoulli's Theorem in recent years, finding that "in the presence of frictional and diabatic effects, these intersections yield the flux lines along which potential vorticity is transported."

with reasonable eye sizes. The effect of surface friction is to deplete the angular momentum of the inflowing air, allowing further radial penetration and hence, smaller eyes. As a side note, Carrier et al. (1971) also constructs a model of the mature hurricane which considers the role of the frictionally-driven recirculation of the eye in maintaining the intense storm.

In retrospect, it is perhaps unfortunate that some (e.g., Anthes, 1982) have grouped Kuo and Malkus together. While Kuo does remark on the centrifugal idea and actually attributes the idea to earlier papers such as Byers (1944) and Syōno (1951), the main contribution of his paper is the fundamental explanation for the reason for the existence of the eye in the first place, harking back to our discussion of Da Vinci's observations of all vortices. Kuo's combination of energy and angular momentum conservation certainly gets at the root of the problem of why there is a limiting radius. Kuo's theory is quite appealing from a parcel perspective as well. The idea resurfaced recently in the modeling study of (Zhang et al., 2005) who successfully modeled the record 370 km diameter secondary eyewall of Typhoon Winnie (1997). Somewhat reminiscent of Kuo's (1959) theory, they suggest eye size is constrained by the distribution of environmental angular momentum and the maximum kinetic energy that is achieved by the inflowing air. Basically, if the absolute angular momentum of the source air is greater, the eye will form at larger radius, so larger wind circulations *favor* a larger radius of maximum winds (and hence, a larger eye), but do not uniquely determine eye size. They point to the importance of kinetic energy production, frictional loss of angular momentum of inflow, and other factors such as static stability and vertical mixing of momentum. Oddly however, Zhang et al. (2005) seemed to be unaware of Kuo's work as they did not cite his paper.

Emanuel (1997) contributed further to idea that turbulent momentum diffusion acts to mechanically spin up the eye to solid body rotation, playing an indirect role in intensifying the tropical cyclone. According to his MPI theory (Emanuel, 1986, 1988, 1991, 1995, 1997; Bister and Emanuel, 1998), the ultimate intensity of the storm depends solely on the thermodynamic imbalance between the ocean surface and the radiative sink to space. He concludes that the mechanical spin up of the eye helps to intensify the storm more rapidly than it would have otherwise, but the final intensity does not depend on this effect. Eye formation then is viewed as a frontogenetic collapse, causing the eyewall to appear as an atmospheric front in θ_e. He views the eye then, as a merely passive response to the intensification of the

storm driven solely by the dynamics in the eyewall and outer region.

Convectively-forced subsidence

Although not applied to hurricanes at first, Eliassen's 1952 balanced vortex theory proved foundational for understanding how sources of heat and momentum drive the vortex via a secondary circulation.[12] Willoughby (1979b) and Shapiro and Willoughby (1982) performed a scaling analysis of Eliassen's balanced vortex model to show that secondary circulation leads to a slow evolution of the axisymmetric vortex. They posit that "subsidence in the eye is forced by radial gradients of convective heating"; specifically, this is the latent heat released by convective rings. In weak systems (tangential winds of less than $35\,\mathrm{m\,s^{-1}}$, the restraining influences of structure and boundaries lengthen vortex evolution time scales, but for higher wind speeds, these influences diminish in importance resulting in faster evolution. For maximum winds speeds greater than $35\,\mathrm{m\,s^{-1}}$, they report "recirculation of air within the vortex core tends to form an eye." This theory also offers a nice dynamical description of convective ring contraction, explaining a portion of the concentric eye phenomenon. (Schubert and Hack, 1982) also used the balanced vortex model and found that the efficiency of a storm's response is greatly increased as the Rossby radius of deformation decreases in the core and becomes similar in scale to the core of heating. To be effective in causing the central subsidence, the heating should occur within the radius of maximum winds. Using aircraft data in several storms, Willoughby (1990b) provided an expanded view of contracting convective rings and showed how their contraction relates to the profile of the wind tendency due to the convective heating that occurs inside the radius of maximum wind.

An alternative view on eye subsidence

Smith (1980) proposed a subsidence mechanism somewhat different from both the dynamically- or convectively-forced theories. He suggested that central subsidence "is driven by an imbalance between vertical gradient of perturbation pressure, the buoyancy force and the vertical stress." The downward axial pressure gradient force almost exactly opposes the vortex-scale upward buoyancy force of the warm eye air, so that the rate of subsidence is just what is required to warm the air to maintain its buoyancy

[12] For more on the role of eyewall heating in developing the warm core, see chapter 3.

close to hydrostatic balance with the perturbation pressure gradient associated with the vortex. This perturbation pressure gradient arises mainly due to the vertical decay of tangential winds with height and/or the radial spread of these winds. In other words, this force (which balances buoyancy) is just what is required to maintain local thermal wind balance with the eyewall at each level. Any buoyancy sink, such as radiative cooling or surface friction would then require subsidence to maintain the buoyancy of the warm core at the value that the vortex intensity requires. Smith points out that his idea refers to a *local* balance, while Shapiro and Willoughby's convectively-forced hypothesis is based on a *global* balance (thermal wind balance) in an slowly evolving system. Smith's theory allows for supergradient winds near r_{max}, but does not require suction of the eye air to be *caused* by the turbulent mixing of angular momentum or the vertical transport of angular momentum by the convection. In some senses, his theory is complimentary to both the dynamically-forced and convectively-forced theories.

Which theory is correct and how does this relate to eye formation?

Some have questioned the importance of the centrifugal effect or even whether it occurs at all. If air was being centrifuged out of the eye, it should be evident by supergradient winds near the intersection of the lower eyewall and the lower eye. Whether supergradient winds actually exist became a contentious issue in the literature. Shea and Gray's composite study of flight level winds (Shea and Gray, 1973; Gray and Shea, 1973) showed supergradient winds, so they cited this as evidence in support of the centrifugal hypothesis. They postulated that eye formation is dependent on supergradient winds and offered as evidence the fact that most eyewalls form at radii of $20-35$ n mi, which coincides with the radial region where supergradient winds are possible. Willoughby (1990a) pointed out that the compositing method used by Shea and Gray, in which the radial profiles of tangential winds were positioned relative to the radius of maximum winds rather than absolute radius, will tend to artificially cause supergradient winds in the composite. Gray (1991) replied with a battery of evidence from individual storms that an important imbalance does exist at the eyewall base near r_{max}. Previous work (Gray, 1967) had also found that the observed temperature gradients were substantially larger than required by the vertical shear of the tangential wind, suggesting a significant imbalance in the thermal wind, especially for intensifying cyclones. He attributed this imbalance in part to the upward transport of angular momentum by the

convective mass flux in the eyewall.

Recent observational work has verified that substantial supergradient flows do indeed exist in tropical cyclones (Kepert, 2006). Essentially, the supergradient flow is associated with an overshoot at the top of the frictional boundary layer where the air turns upward into the eyewall; a similar effect has long been noted in tornadoes. The radial inflow is maintained against the outward gradient imbalance by vertical diffusion, vertical advection, and horizontal advection Kepert (2001); Kepert and Wang (2001). Observations of eyewalls certainly do support the idea of a frontogenetic collapse (Emanuel, 1997), so turbulent momentum diffusion does seem to be an important effect. Meanwhile, it is difficult to assail the idea of convective heating forcing eye subsidence. So what is to prevent all of these theories from being correct? And if they are, what proportion of the eye subsidence is contributed by each effect?

The answer to the above questions depends in part to the issue of how rapidly the air actually recycles through the eye. The dynamically-forced theories would seem to require a steady recycling of air through the eye, and this is what was envisioned by Malkus (1958a). In particular, the movement of the eye seemed to require substantial recycling according to early understandings, but Willoughby and Chelmow (1982) showed that the eye air could move kinematically with the storm, so rapid storm motion did not seem to be a great impediment by requiring extraordinary recycling. But Willoughby (1998) brought out a conflicting view, maintaining that the air within the eye experiences the bulk of its subsidence as the eye forms and then is essentially undisturbed, acting as a 'containment vessel'. This was motivated in part by some chemical tracer studies (e.g., Newell et al., 1996) which seemed to suggest that the upper eye air had been in place and essentially undisturbed for many days. Willoughby proposed that mixing at the eyewall interface prevented a complete frontogenetic collapse from occurring. A recent modeling Cram et al. (2007) examined whether the eye should be viewed as such; Lagrangian parcel trajectories showed that significant mass recycling does actually occur in the mid and upper levels of the eye, and of course, that shear ventilated the eye.

A numerical modeling study of Hurricane Andrew Zhang et al. (2000, 2002) has possibly reconciled the three theories we have been discussing. This study analyzes the vertical momentum budget of absolute angular momentum and inverts the three-dimensional perturbation pressures to obtain the buoyancy- and dynamically induced perturbation pressure gradient forces (PGF). They find that the ver-

tical acceleration in the eyewall depends on a balance between the perturbation PGF, buoyancy, and water loading and most notably, so that the upward motion in the eyewall is mostly forced by this perturbation PGF. In the eye, the perturbation PGF is partitioned into a buoyant PGF (which largely opposes the buoyancy of the warm eye air) and a dynamically-driven PGF analogous to the centrifugal effect of a spinning column of water in a tank. The dynamically-driven PGF points downward in the eye, and thus is largely responsible for the downward motion there. They find that buoyancy perturbation pressure due to the warming by moist-adiabatic ascent in the eyewall is responsible for 70% of the total pressure deficit in their simulation (55 hPa out of the 80 hPa). The dynamically-driven perturbation pressure is reponsible for the other 30% (25 hPa) of the pressure deficit. If this is correct, an immediate conclusion we could draw would be that the centrifugal effect is important in intense hurricanes, and may be responsible for helping an intense hurricane reach Category 4 or 5 intensity, but the convectively-driven subsidence accounts for most of the eye warming. Another of their conclusions is that the negative vertical shear in the eyewall is caused by the subsidence warming, not the other way around (so Smith (1980) had it backwards). But most importantly, they find that it is the radial shear of the tangential winds (actually, the radial gradient of V^2 weighted by radius) that increases and induces a deep layer of downward dynamically-forced PGF. Thus, eye formation could occur simply as the wind profile becomes more peaked during intensification; as this occured, the induced subsidence would overwhelm the ascent in the nascent eye and clear it of clouds. The role of inertial stability in confining the vortex response to heating has been cited by many authors (Shapiro and Willoughby, 1982; Schubert and Hack, 1982; Jorgensen, 1984b; van Delden, 1989; Schubert et al., 2007; Vigh and Schubert, 2009).

2.5.2 Two-layer models

Two-fluid models can be useful heuristic tools to explore eye formation, but such models are simplistic because the real tropical atmosphere is continuously stratified. Furthermore, the eye is stably stratified, but the eyewall tends to be close to moist neutrality. But such models may provide a glimpse of the relevant physics of the problem, so they are mentioned briefly for completeness. Pearce (1998) presents a two-layer theory and then extends it to a compressible fluid in Pearce (2004). Gravity waves, vortex tilting, and production of azimuthal vorticity have been cited by some as important factors for eye

formation (see Pearce, 2005), but the interpretation of these are still under debate (see Smith, 2005).

2.5.3 Eye formation due to boundary layer effects

While the dynamics associated with convective heating and the perturbation pressure field may be key in forcing central eye subsidence, the tendency for convection to organize into an annulus could still be adequately explained through other means. The frictional boundary layer beneath the storm may provide such a preferential ring of upward mass forcing. Eliassen (1971) examined the boundary layer of a circular vortex and found that the distribution of upward motion obtained depends critically on the boundary condition – a turbulent Ekman layer (appropriate to real vortices) produces a maximum of upward motion out at some radial distance from the center. In contrast, laminar Ekman layers provide a more or less radially-constant upward mass flux near the vortex center. This work was expanded by Eliassen and Lystad (1977), who computed spindown rates in relation to the Rossby number and the drag coefficient. The spindown rate is important to a hurricane (and the question of eye formation), because any intensification mechanisms must overcome the spindown tendency of the boundary layer.

Eliassen (1959) viewed the low level frictional convergence from the boundary layer as in competition with the subsidence forced by the convective heating of the eyewall and proposed that an eye may form when the subsidence overwhelms the upward boundary layer forcing near the center. Wirth and Dunkerton (2006, 2009) have recently explored this using a simple analytic model that includes the boundary layer Ekman forcing and convective heating (included as a radiative-like relaxation towards a thermal equilibrium). They found that the transition to an eye occurred suddenly and depended on the ratio of the surface friction and the relaxation rate. Their means of parameterizing the convective heating seems a bit dubious, but their results show that the formation of an eye (or a similar process) can be a rather simple dynamical process that is related to the diabatic heating of the vortex and the boundary layer forcing.

Closely related to the boundary layer theory, it is possible that the sea state itself may exert an important influence on eye formation. The intensity threshold at which an eye forms (surface winds of approximately 30 to 40 $\mathrm{m\,s^{-1}}$, Andreas 2004) is also the threshold at which sea spray becomes significant. These wind speeds may also decrease the aerodynamic drag coefficient (C_d) of the surface layer as

the short waves (which cause the greatest drag) are damped (Moon et al., 2004). Gedzelman et al. (2003) examined stable isotope ratios of water and found that the a large amount (modeling results suggested about 50%) of the eyewall water content was actually from sea spray. Significant amounts of sea spray change air-sea interface from a well-defined interface into an emulsion (Emanuel, 2003), also modifying the transfer coefficients for drag and heat. Additionally, the growing wave field in an intensifying storm may exert an important asymmetric forcing during eye formation.

2.5.4 Eye formation as a frontogenetic collapse

As already mentioned, Emanuel (1997) proposes that eye formation occurs as a frontogenetic collapse, but the idea may have been around, at least in part much earlier. Sawyer (1947) had studied hurricanes and was aware of the centrifugal hypothesis, and had also published some theoretical works on frontogenesis (Sawyer, 1952, 1956), but it is unclear whether he made the connection that the developing eyewall of a hurricane is a form of frontogenesis. Eliassen (1959) did make the connection however, as was previously noted. Frisius (2006) has modeled eyewall formation as a frontogenetic collapse, and did not find that momentum diffusion accelerated the development, as Emanuel (1997) had reported.

2.6 Asymmetric mechanisms of eye formation

While the symmetric mechanisms of eye formation are interesting and the imposition of eye subsidence is certainly important to the problem, it seems that the storms are hardly axisymmetric when they form eyes, as they often contain a strong primary band or spiral banding. The impact of asymmetric heating has been studied generally (Möller and Shapiro, 2005; Nolan et al., 2007; Raymond and Sessions, 2007; Yang et al., 2007; Shin and Smith, 2008; Peng et al., 2008; Van Sang et al., 2008), but we will focus here on aspects of the storm's convective morphology that tend to produce an eyewall or in some way contribute to the development of the warm core. These have been explored in somewhat less quantitative detail in the literature, since asymmetric theories can be considerably more complex than symmetric theories. Nevertheless, some of these seem promising and will be briefly reviewed now.

2.6.1 Encircling rainband hypothesis

As a starting point, consider the "encircling rainband theory" put forth by Willoughby (1979a, 1990a, 1988, 1995). Like their parent hurricanes, spiral rainbands also exhibit an in-up-and-out radial circulation, with upward motion in the vicinity of the rainband, and subsiding motion in the near-environment. Due to the curved geometry of spiral bands, the general idea is that since subsidence is favored and concentrated on the inside of the band, a spiral band encircling the center of a developing system will favor central subsidence. Conversely, if an outer band encircles an already formed eye, the effect may be to force subsidence over that eye, weakening it (Samsury and Zipser, 1995). This conceptual picture may be valid, but currently there is little quantitative or observational evidence to support this hypothesis.

2.6.2 Eye formation via the primary band

A somewhat related idea involves the primary band, which is often observed in moderate strength tropical storms before they form eyes. Indeed, the appearance of curved banding is used in the Dvorak method Dvorak (1984) as an indication of a trend towards increasing organization. Willoughby (1988) points out that the orientation of a primary band may be a type of bow shock caused by the storm's movement through its environment (Sherman, 1956), but vertical shear may be another influence in determining its location (J. Knaff, personal communication 2009). Willoughby et al. (1984b) suggested that a tropical cyclone has two dynamical regimes with respect to rainbands: (1) a high Rossby number (Ro), low Richardson number (Ri) regime found in the inner core, and (2) an outer regime of low Ro and high Ri. In the inner core, the local Rossby radius of deformation is of the same magnitude as the distance to the center so that convection can intensify the symmetric vortex efficiently and accelerations are dominated by relative rotation (rather than the Coriolis force). In the outer regime, heating was less efficient and the accelerations due to rotation and Coriolis were comparable. In between the two regimes, a collection of spiral banding occurred, which they termed the 'stationary band complex.' (SBC) As a weak storm strengthens and the first regime develops, this principle band sometimes formed into a convective ring.

Mathur (1997) modeled the development of an eyewall-like structure from a primary band, finding that an outer arcing band at large radius dies out, and a new band forms at smaller radius. Intense heating rates, strong vertical motion, and areas of upper divergence formed in association with this inner band, apparently as slantwise convection started up. The anvil-like outflow caused the storm's cloud field to take the appearance of a comma shape about the time the eyewall was established. His simulation did not simulate subsidence over the center however; it was concentrated on the outside of the band. According to Dvorak (1984), a comma cloud appearance is an important clue that the storm is continuing to develop.

Kieper (2008) has also linked a primary band morphology with the development of a low level convective ring in her study of 37 GHz microwave imagery. She finds that a thin connecting band often develops between the primary band and the nascent eyewall.

2.6.3 Inertially-confined subsidence by hot towers or induced through vortex stretching of mesocyclones

Other convective asymmetries may also help or inhibit eye formation. Simpson et al. (1998) report that hot towers were present in the nascent eyewall structures of some developing storms and that these features contributed substantially to the development of the warm core. Simpson et al. (1997) and Reasor et al. (2005) advance the view that the latter stages of tropical cyclone formation are a stochastic process, whereby interacting mesoscale circulations interact to build up the vortex-scale circulation. Relating this view to the present problem, eye formation may likewise be thought of as a stochastic process, depending sensitively on the evolution and ecology of the convective morphology.

One open question is whether local mesoscale subsidence can be enhanced by high inertial stability associated with sub-vortex scale features. Intense convective bursts often occur during the genesis and tropical storm stage of a cyclone, and have been implicated in intensification (Steranka et al., 1986; Zehr, 1992). Marks, F. D., Jr. and Houze, Robert A., Jr. (1984) observed a mesocyclone in the developing eyewall of Hurricane Debby and noted that occasionally the aircraft seemed to find secondary centers, perhaps associated with prototypical warm cores. Stossmeister and Barnes (1992) observed an even more illuminating case in which an MCS complex was associated with dry, subsident warming and formed a secondary circulation center, reminiscent of a midlatitude heat burst or the wake low that forms

from the downdraft beneath an anvil.

Several observational studies further developed the idea that local subsidence could be enhanced by convective features. Stewart and Lyons (1996) used ground-based NEXRAD Doppler radar to observe Tropical Storm Ed (1993) in the Western North Pacific. An embedded mesovortex circulation was observed to contribute to the eye formation of Ed. The authors formulate a "shortcut" theory of rapid eye formation, whereby a locally enhanced convective burst (or hot tower) very near the wind center stretches the wind circulation, increasing the vorticity. This feature induces supergradient winds which then force subsidence over the storm center, rapidly clearing an eye. The unbalanced flow within the radius of maximum winds turns divergent and leads to the formation of a low level convergence zone, triggering the development of the convective eyewall.

Heymsfield et al. (2001) have investigated a similar mechanism in much more detail from a very well-observed case study of Hurricane Bonnie (1998). In this case, a series of strong convective bursts formed and advected around the circulation center. Fig. 2.19 displays this sequence from IR satellite imagery. At times, these convective bursts were associated with strong mesoscale descent on the order of several meters per second, contributing to the warming in the nascent eye. Based on their observations, they construct a conceptual model in which the hot towers detrain a downdraft over the core, leading to warming of several Kelvins and contributing to the eventual eye formation. A schematic of this is shown in Fig. 2.19.

We end this section by noting that another possible mode of rapid eye formation may occur when a strong convective cell moves very close to the cyclone center so that its circulation rapidly intensifies due to the very efficient heating, and thus grows to dominates the overall storm circulation. A footnote in Jorgensen (1984b) discusses an interesting case which occurred in Hurricane Gladys (1975), relayed to him by Peter Black. A single convective cell dominated the wind field such that an "eye" of just a few hundred meters diameter was observed by the low-level aircraft. The modeling study of Nolan (2007) noted a similar sequence of events in several runs. In each case, a strong convective feature with a large updraft moved very near to the vortex center and 'captured' it. Very rapid intensification of the wind field ensued, so that in a couple hours, the storm was well on the way to becoming a hurricane. In at least one simulation, an eye formed directly from this central convective cell.

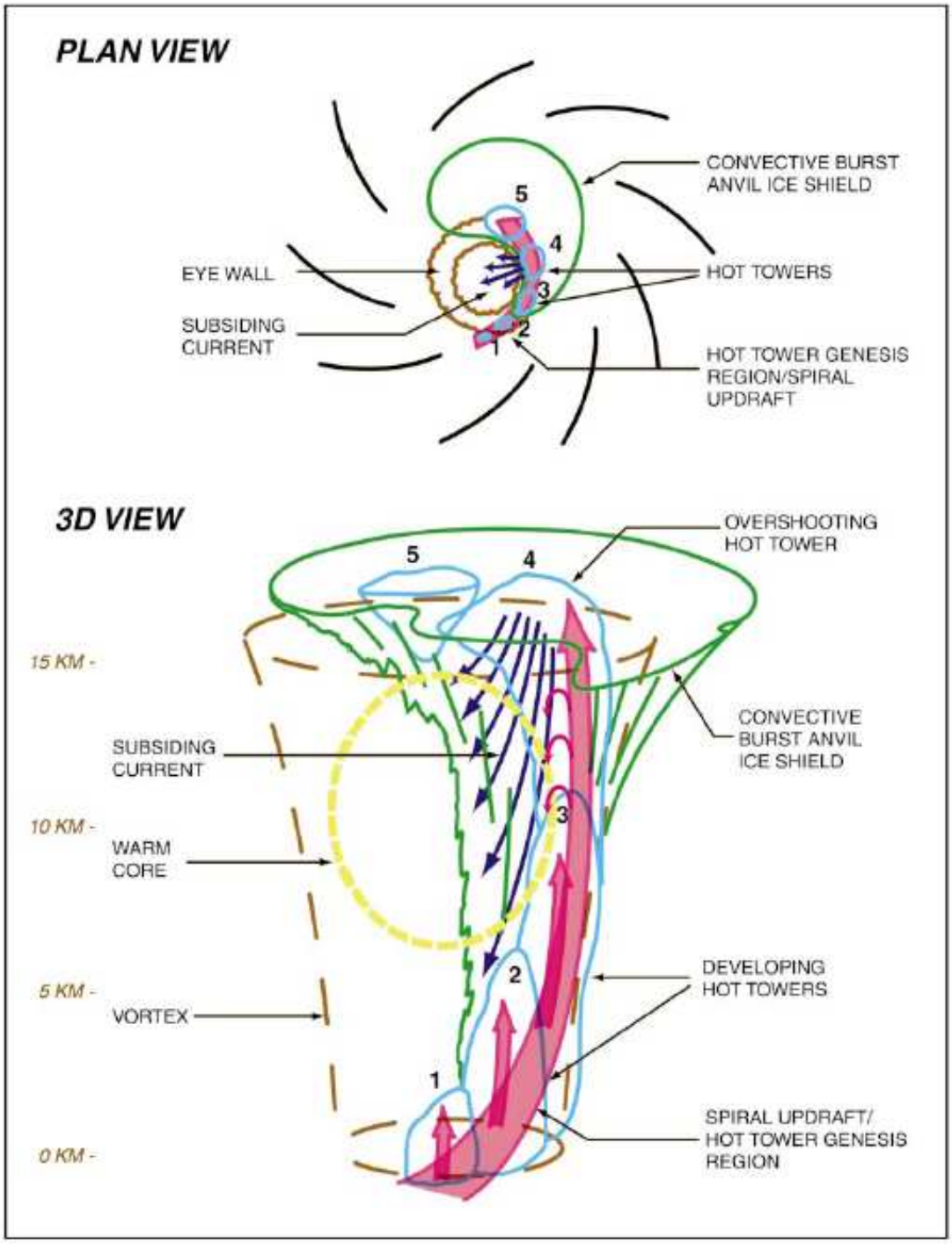

Figure 2.18: A schematic showing the situation in Hurricane Bonnie (1998). Reproduced from Heymsfield et al. (2001).

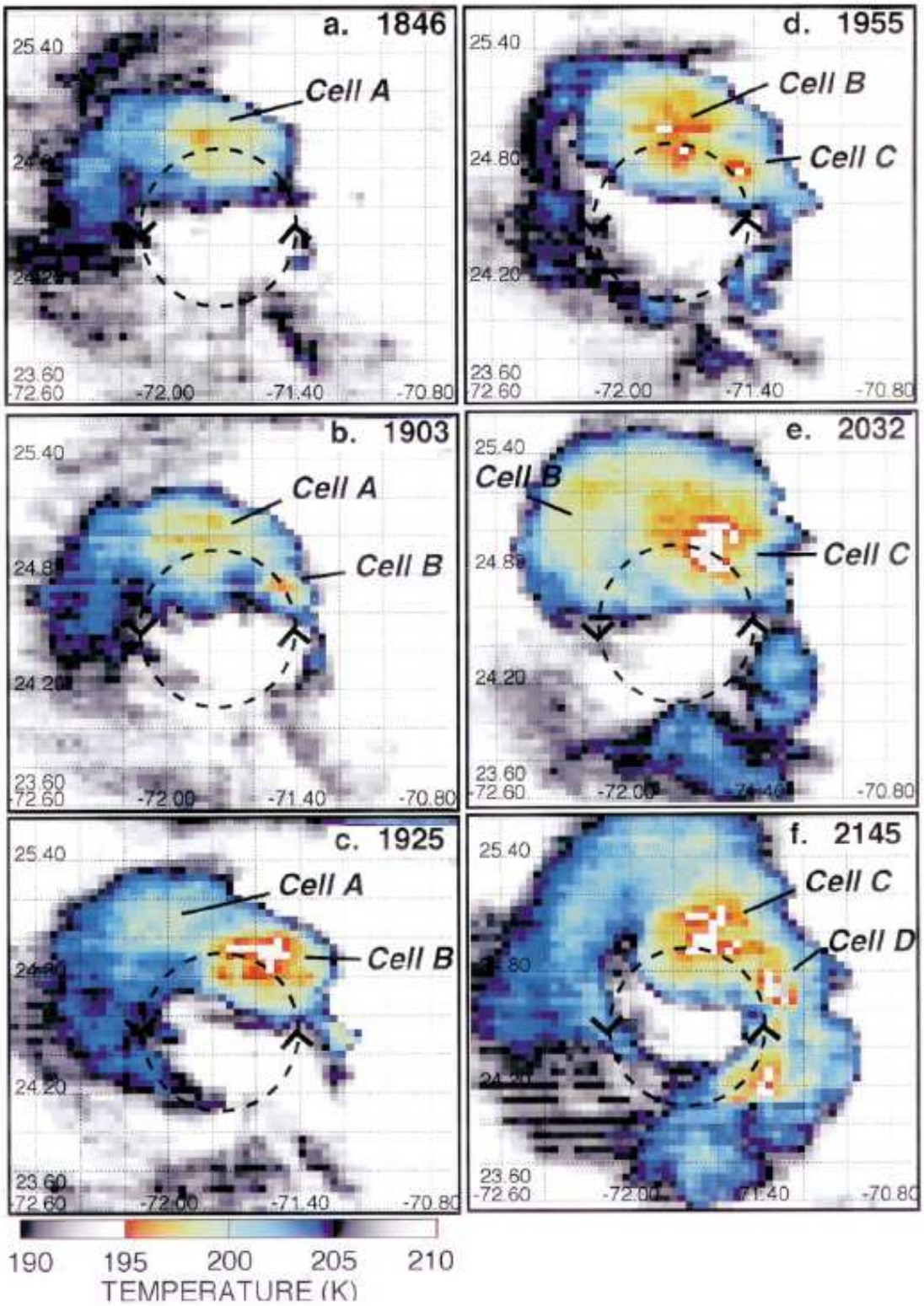

Figure 2.19: A sequence of IR images from Hurricane Bonnie on 23 August 1998. Reproduced from Heymsfield et al. (2001).

2.6.4 Other proposed mechanisms

To round out our review, we consider a few of the other proposed mechanisms for eye formation that are either likely not a factor, or have been viewed as somewhat eccentric and of unknown utility. Abdullah (1954) attempted to explain eye formation as a series of hydraulic jump waves which retarded the flow in the inner cyclone. While novel, this likely has little bearing on the problem. Dickerson (2006) has an even more novel, but physically plausible explanation for the development of central subsidence in a tropical cyclone: a downward magnetohydrodynamical (MHD) force caused by the rotation of an electrically-charged cloud field (the eyewall). MHD effects certainly are important in electrically-charged flows such as in the solar atmosphere, but in hurricanes the magnitude of such effects may be so small as to be insignificant. It seems however that the development of strong charge separation presupposes an eyewall structure, so if magnetohydrodynamic effects actually are important, they probably have less bearing on the problem of initial eye formation and more bearing on the subsequent eye development and maintenance processes. In an apparently independent study, Patton et al. (2008) recently proposed that this effect could serve as mechanism for tornadogenesis.

Finally, it has been suggested that since the eye acts as a barrier to potential vorticity (PV) mixing, perhaps the development of such a boundary could be relevant to the problem of eye formation. Vortices involve the dynamical processes of advective transport and mixing. The polar stratospheric vortex is observed to form an ozone “hole” during polar night because of a transport barrier at the vortex edge. This barrier prevents mixing across the vortex boundary, isolating the low ozone air inside from higher ozone air outside the vortex. Mizuta and Yoden (2001) examine such transport barriers for an idealized stratospheric polar vortex, finding that one type of transport barrier is related to steep gradients of potential vorticity. As previously discussed, the rapidly rotating eye of a hurricane may likewise act as a containment vessel (Willoughby, 1998; Cram et al., 2007). Thus, it may be possible to interpret eye formation as the manifestation of a physical barrier to mixing at the eyewall edge. Several recent papers (Shuckburgh and Haynes, 2003; Nakamura, 2004) give some methods which may be helpful for diagnosing such transport and mixing processes.

2.7 Concluding Remarks

We started this review by highlighting the understanding of how conservation of angular momentum leads to a protected region within the radius of maximum winds of all vortices. We then developed the fundamental concept that eye phenomena involve a vertical rearrangement of mass in the cyclone core of 3-D vortices as they are spun up. This rearrangement is required in order to drive the vortex back towards a combined vertical and horizontal force balance. The eyes formed in a variety of geophysical vortices were reviewed, and it was found that many similarities existed between the eyes formed in dust devils, waterspouts, tornadoes, mesolows, and polar lows and hybrids. In all cases, the details of the eyes produced depended on the nature of the boundaries of the vortex. For most vortices, the lower boundary is very important, as surface friction depletes angular momentum and causes supergradient winds to develop near the radius where the winds turn upward into the eyewall. In the larger scale vortices (extratropical cyclones, polar lows, and especially hurricanes), the upper boundary (the tropopause) becomes important in modifying the vortex upper structure and causing a substantial warm core to develop. The upper and lower boundaries will be felt more strongly as the local Rossby penetration depth increases in the vortex core.

Observations of tropical cyclone structure have been reviewed with respect to the development of the warm core and the structure of the eyewall. From these insights, a comprehensive definition for determining the moment of eye formation has been proposed. Next symmetric mechanisms for eye formation were considered, with a careful review of the causes of central subsidence which include dynamically-forced subsidence (the centrifugal hypothesis), convectively-forced driven subsidence, and forcing due to a perturbation PGF. Recent modeling work has at least partially reconciled these competing viewpoints and in some sense, it seems that many of these views are actually related to each other. It has been difficult to recognize this due to the differing frameworks each view is built on. Nonetheless, the moist-adiabatic warming in the eyewall seems to be the main cause of the eye subsidence, providing 70% of the central pressure deficit (and probably a greater proportion in weaker storms). In very strong storms, the centrifugal effect may provide 30% of the central pressure deficit. It seems that the actual subsidence is expressed in the eye as a result of the intensifying vortex circulation through the local

perturbation PGF. The boundary layer forcing may play a role in setting the preferred radius of updraft forcing. Asymmetric mechanisms for eye formation were also examined. It seems that these may provide a shortcut to eye formation by providing a reduced Rossby radius of deformation and inertially-confined subsidence which may jumpstart warm core development.

The influence of the radial shear of the tangential wind profile has been highlighted by various authors. This was found to be crucial in driving the perturbation PGF that causes subsidence in the eye. This complements the ideas on how the reduced Rossby deformation length (which is also synonymous with high inertial stability) focuses the vortex response to heating. A further investigation on this aspect will be considered in the next chapter. The literature is mostly lacking though, in how the Rossby penetration depth may control how the vortex feels the upper and lower boundaries. This may be just as important for the issue of eye formation.

2.7.1 Remaining questions

There are many remaining questions which are left for future investigations. The first is whether there is actually a trigger for eye formation. If so, what is the trigger? The role of humidity in the core is also another intriguing aspect, as the storm does not typically undergo genesis until the inner core has become saturated (Nolan, 2007). The genesis process seems to be dominated by convective adjustment to the stratiform heating of the central rain area, so what preconditions a tropical cyclone vortex to undergo frontogenetic collapse? What is the role of the distribution of hydrometeors? What causes the eyewall to slope, and how does this influence the storm's intensification? Nong and Emanuel (2003) have proposed that such rings are an attractor to the system for *secondary* eye formation, such that a wind maximum grows into an eyewall through the wind induced surface heat exchange mechanism (WISHE). It is left as an open question whether the convective ring (e.g., Willoughby, 1990b) is an attractor to the system for primary eye formation.

Chapter 3

RAPID DEVELOPMENT OF THE TROPICAL CYCLONE WARM CORE

"The hurricane eye is a spectacular and never-to-be-forgotten phenomenon. It is a clear, often wholly cloud-free, spot of quiet 10–30 miles across; an oasis of calm surrounded by a circular wall of towering thunderheads and raging squalls. Surface winds within it are light and variable." — Joanne Malkus (1958)

The contents of this chapter have been published as:

Vigh, J. L. and W. H. Schubert, 2009: Rapid development of the tropical cyclone warm core. *J. Atmos. Sci.*, **66**, 3335–3350, doi:10.1175/2009JAS3092.1.

3.1 Introduction

One of the goals of the National Aeronautics and Space Administration's Tropical Cloud Systems and Processes (NASA/TCSP) research program is to understand the conditions under which a tropical cyclone can rapidly intensify, i.e., rapidly decrease its central surface pressure and rapidly increase its azimuthal wind and inner core temperature. Understanding changes in the wind and thermal structure of a tropical cyclone is not a straightforward matter. As can be seen from (3.2) and (3.5), for an inviscid axisymmetric vortex the azimuthal wind tendency depends on the radial and vertical advection of angular momentum, while the temperature tendency depends on the diabatic heating, in addition to the radial and vertical advection terms. If the vortex is balanced in the sense that it is continuously evolving from one gradient-balanced state to another, then the transverse circulation is determined by the solution of a second order partial differential equation in the (r, z)-plane. According to this "transverse circulation equation," first derived by Eliassen (1951) and given below in (3.11), the streamfunction for the radial and vertical motion is determined by the radial derivative of the diabatic heating and the three variable coefficients A, B, and C, which are the static stability (3.8), the baroclinity (3.9), and the inertial stability

(3.10). Although solutions of (3.11) generally yield radial and vertical velocities that are much weaker than the azimuthal velocity, the radial and vertical directions are the directions of large gradients, so the relatively weak transverse circulation is crucial for vortex evolution (Ooyama, 1969; Willoughby, 1979b). If vortex evolution is the main focus of understanding, it may be preferable to consider solutions of the geopotential tendency equation, which can be derived by similar means and is given below in (3.21). Note that the geopotential tendency equation is also a second order partial differential equation with the same three variable coefficients A, B, and C.

In his classic 1951 paper Eliassen presented the principal part of the Green's function solutions of the constant coefficient version of the transverse circulation equation for the case in which $\partial Q/\partial r$ is localized and for the case in which Q itself is localized in the (r, z)-plane. These Green's function solutions clearly illustrate how the strength and shape of the transverse circulation depend on the coefficients A, B, and C. However, for applications to tropical cyclones, there are several disadvantages to Eliassen's approach: (i) The effects of top and bottom boundary conditions and the circular geometry are not included; (ii) The important spatial variability of the inertial stability coefficient C is not included; and (iii) The diabatic heating is localized in z, whereas in tropical cyclones it is rather smoothly distributed over the whole troposphere (for examples of satellite-observed vertical profiles of diabatic heating see Fig. 6 of Rodgers et al. 1998 and Fig. 9 of Rodgers et al. 2000). In the present chapter, we remove these limitations through a somewhat different analysis of the balanced vortex model.

We consider an idealized vortex structure and an idealized vertical structure of Q that allows the transverse circulation equation and the geopotential tendency equation to be solved by separation of variables. This leads to the radial structure equations (3.24) and (3.25). Then, considering the diabatic heating as localized in r, we find the Green's functions for these ordinary differential equations, taking into account the circular geometry and the far-field boundary conditions. This simple theoretical argument isolates the conditions under which a warm-core thermal structure can rapidly develop in a tropical cyclone and thereby elaborates on the vortex heating efficiency ideas discussed in Shapiro and Willoughby (1982), Schubert and Hack (1982), Hack and Schubert (1986), and Nolan et al. (2007). The unique aspect of the present approach is its emphasis on the geopotential tendency equation as the most direct route towards understanding the rapid development of the warm core.

The chapter is organized in the following way. In section 3.2 the balanced vortex model and the associated transverse circulation equation and geopotential tendency equation are presented, followed by a discussion of how the right hand side of the geopotential tendency equation can be written in a compact and physically interpretable form via introduction of potential vorticity concepts, and by a discussion of the separation of variables to reduce the partial differential equations into ordinary differential equations for the radial structure. Section 3.3 discusses the general solution of the radial structure problem in terms of Green's functions. The actual Green's functions are derived for a resting atmosphere in section 3.4 and for a Rankine-like vortex in section 3.5. The results of calculations from these solutions are shown in section 3.6 to illustrate how the temperature tendency depends on the eyewall geometry and the radial distribution of inertial stability. In section 3.7 we discuss observations of the radial distribution of heating and inertial stability in real storms; the implications of the impact of subsequent structure change on intensification rate are also considered. Some concluding remarks are presented in section 3.8.

3.2 Tropical cyclone theory

3.2.1 Balanced vortex model

We consider inviscid, axisymmetric, quasi-static, gradient-balanced motions of a stratified, compressible atmosphere on an f-plane. As the vertical coordinate we use $z = H \ln(p_0/p)$, where $H = RT_0/g$ is the constant scale height, and where p_0 and T_0 are constant reference values of pressure and temperature. We choose $p_0 = 100\,\mathrm{kPa}$ and $T_0 = 300\,\mathrm{K}$, the latter of which yields $H \approx 8.79\,\mathrm{km}$. The governing equations for the balanced vortex model are

$$\left(f + \frac{v}{r}\right) v = \frac{\partial \phi}{\partial r}, \tag{3.1}$$

$$\frac{\partial v}{\partial t} + u\left(f + \frac{\partial (rv)}{r\partial r}\right) + w\frac{\partial v}{\partial z} = 0, \tag{3.2}$$

$$\frac{\partial \phi}{\partial z} = \frac{g}{T_0} T, \tag{3.3}$$

$$\frac{\partial (ru)}{r\partial r} + \frac{\partial (\rho w)}{\rho \partial z} = 0, \tag{3.4}$$

$$\frac{\partial T}{\partial t} + u\frac{\partial T}{\partial r} + w\left(\frac{\partial T}{\partial z} + \frac{RT}{c_p H}\right) = \frac{Q}{c_p}, \tag{3.5}$$

where u and v are the radial and azimuthal components of velocity, w is the "log-pressure vertical velocity", ϕ is the geopotential, f is the constant Coriolis parameter, c_p is the specific heat at constant pressure, $\rho(z) = \rho_0 e^{-z/H}$ is the pseudodensity, $\rho_0 = p_0/(RT_0) \approx 1.16$ kg m^{-3} is the constant reference density, and Q is the diabatic heating.

3.2.2 *Transverse circulation equation*

Multiplying the thermodynamic equation by g/T_0 and the tangential wind equation by $f + (2v/r)$, and then making use of the gradient and hydrostatic relations, we obtain

$$\frac{\partial \phi_t}{\partial z} + A\rho w - B\rho u = \frac{g}{c_p T_0} Q, \tag{3.6}$$

$$\frac{\partial \phi_t}{\partial r} - B\rho w + C\rho u = 0, \tag{3.7}$$

where $\phi_t = \partial\phi/\partial t$ denotes the geopotential tendency, and where the static stability A, the baroclinity B, and the inertial stability C are defined by

$$\rho A = \frac{g}{T_0}\left(\frac{\partial T}{\partial z} + \frac{RT}{c_p H}\right), \tag{3.8}$$

$$\rho B = -\frac{g}{T_0}\frac{\partial T}{\partial r} = -\left(f + \frac{2v}{r}\right)\frac{\partial v}{\partial z}, \tag{3.9}$$

$$\rho C = \left(f + \frac{2v}{r}\right)\left(f + \frac{\partial (rv)}{r\partial r}\right). \tag{3.10}$$

One way of proceeding from (3.6) and (3.7) is to eliminate ϕ_t to obtain an equation for the transverse circulation. This equation takes the form

$$\frac{\partial}{\partial r}\left(A\frac{\partial(r\psi)}{r\partial r} + B\frac{\partial \psi}{\partial z}\right) + \frac{\partial}{\partial z}\left(B\frac{\partial(r\psi)}{r\partial r} + C\frac{\partial \psi}{\partial z}\right) = \frac{g}{c_p T_0}\frac{\partial Q}{\partial r}, \tag{3.11}$$

where we have used the mass conservation principle (3.4) to express the transverse circulation in terms of ψ via the relations

$$\rho r u = -\frac{\partial(r\psi)}{\partial z} \qquad \text{and} \qquad \rho r w = \frac{\partial(r\psi)}{\partial r}. \tag{3.12}$$

Here we consider only vortices with $AC - B^2 > 0$ everywhere, which ensures that (3.11) is an elliptic equation. For boundary conditions on (3.11), we require that $\psi = 0$ at $z = 0$, at $z = z_T$, and at $r = 0$, and that $r\psi \to 0$ as $r \to \infty$.

3.2.3 *Geopotential tendency equation*

Another way of proceeding from (3.6) and (3.7) is to eliminate u and w to obtain an equation for ϕ_t. Thus, eliminating w between (3.6) and (3.7), we obtain

$$A\frac{\partial \phi_t}{\partial r} + B\frac{\partial \phi_t}{\partial z} + (AC - B^2)\rho u = \frac{g}{c_p T_0} BQ. \tag{3.13}$$

Similarly, eliminating u between (3.6) and (3.7), we obtain

$$B\frac{\partial \phi_t}{\partial r} + C\frac{\partial \phi_t}{\partial z} + (AC - B^2)\rho w = \frac{g}{c_p T_0} CQ. \tag{3.14}$$

Through the use of the mass continuity equation (3.4) we can now eliminate u and w between (3.13) and (3.14) to obtain

$$\frac{\partial}{r\partial r}\left(r\frac{A}{D}\frac{\partial \phi_t}{\partial r} + r\frac{B}{D}\frac{\partial \phi_t}{\partial z}\right) + \frac{\partial}{\partial z}\left(\frac{B}{D}\frac{\partial \phi_t}{\partial r} + \frac{C}{D}\frac{\partial \phi_t}{\partial z}\right) = \frac{g}{c_p T_0}\left[\frac{\partial}{r\partial r}\left(r\frac{B}{D}Q\right) + \frac{\partial}{\partial z}\left(\frac{C}{D}Q\right)\right], \tag{3.15}$$

where $D = AC - B^2$. Equation (3.15) is a second order partial differential equation for ϕ_t, and the boundary conditions imposed on it should be consistent, via (3.6) and (3.7), with the boundary conditions for (3.11). Here we simply require that $\partial\phi_t/\partial r$ vanish at $r = 0$, that $\partial\phi_t/\partial z$ vanish at the bottom and top isobaric surfaces $z = 0$, $z = z_T$, and that $r\phi_t \to 0$ as $r \to \infty$.

We shall refer to the right hand side of (3.15) as the "tropical cyclogenesis function," since it gives the interior forcing function associated with nonzero ϕ_t. Because of the rather complicated mathematical form given in the right hand side of (3.15), physical interpretation is difficult. However, using potential vorticity concepts, the tropical cyclogenesis function can be transformed into a simpler form that allows straightforward physical interpretation. To accomplish this transformation we first note that the potential vorticity equation, derived from (3.1)–(3.5), is

$$\frac{DP}{Dt} = \frac{1}{\rho}\frac{\partial(m,\dot{\theta})}{r\partial(r,z)} = \frac{1}{\rho}\frac{\partial(m,\theta)}{r\partial(r,z)}\frac{\partial(m,\dot{\theta})}{\partial(m,\theta)} = P\left(\frac{\partial\dot{\theta}}{\partial\theta}\right)_m, \tag{3.16}$$

where

$$P = \frac{1}{\rho}\frac{\partial(m,\theta)}{r\partial(r,z)} = \frac{1}{\rho}\left[-\frac{\partial v}{\partial z}\frac{\partial\theta}{\partial r} + \left(f + \frac{\partial(rv)}{r\partial r}\right)\frac{\partial\theta}{\partial z}\right] \tag{3.17}$$

is the potential vorticity, $m = rv + \frac{1}{2}fr^2$ is the absolute angular momentum per unit mass, $\theta = T(p_0/p)^\kappa$ is the potential temperature, $D/Dt = (\partial/\partial t) + u(\partial/\partial r) + w(\partial/\partial z)$ is the material derivative,

$(\partial/\partial\theta)_m$ is the partial derivative with respect to θ along the absolute angular momentum surface, and $\dot{\theta} = Q/\Pi$, with $\Pi = c_p(p/p_0)^\kappa$ denoting the Exner function. Using (3.17) and (3.8)–(3.10) we can easily show that

$$D = AC - B^2 = \frac{g\Pi}{c_p T_0 \rho}\left(f + \frac{2v}{r}\right)P, \tag{3.18}$$

so that (3.11) and (3.15) are elliptic if $[f + (2v/r)]P > 0$. Using (3.18) we can also easily show that

$$\frac{g}{c_p T_0} r \frac{B}{D} Q = -\frac{\partial m}{\partial z}\frac{\dot{\theta}}{P} \quad \text{and} \quad \frac{g}{c_p T_0}\frac{C}{D} Q = \frac{\partial m}{r\partial r}\frac{\dot{\theta}}{P}. \tag{3.19}$$

These last two relations allow us to write

$$\begin{aligned}\frac{g}{c_p T_0}\left[\frac{\partial}{r\partial r}\left(r\frac{B}{D}Q\right) + \frac{\partial}{\partial z}\left(\frac{C}{D}Q\right)\right] &= -\frac{\partial v}{\partial z}\frac{\partial(\dot{\theta}/P)}{\partial r} + \left(f + \frac{\partial(rv)}{r\partial r}\right)\frac{\partial(\dot{\theta}/P)}{\partial z} = (\boldsymbol{\zeta}\cdot\nabla)(\dot{\theta}/P) \\ &= \frac{\partial(m,\dot{\theta}/P)}{r\partial(r,z)} = \frac{\partial(m,\theta)}{r\partial(r,z)}\frac{\partial(m,\dot{\theta}/P)}{\partial(m,\theta)} = \rho P\left(\frac{\partial(\dot{\theta}/P)}{\partial\theta}\right)_m,\end{aligned} \tag{3.20}$$

where $\boldsymbol{\zeta}$ is the projection of the vorticity vector onto the (r,z)-plane. This allows (3.15) to be rewritten as

$$\frac{\partial}{r\partial r}\left(r\frac{A}{D}\frac{\partial\phi_t}{\partial r} + r\frac{B}{D}\frac{\partial\phi_t}{\partial z}\right) + \frac{\partial}{\partial z}\left(\frac{B}{D}\frac{\partial\phi_t}{\partial r} + \frac{C}{D}\frac{\partial\phi_t}{\partial z}\right) = \rho P\left(\frac{\partial(\dot{\theta}/P)}{\partial\theta}\right)_m. \tag{3.21}$$

The right hand side of (3.21) is the compact form of the cyclogenesis function, which can now be interpreted as being proportional to the product of potential vorticity with the θ-derivative of $\dot{\theta}/P$ along an absolute angular momentum surface. If the cyclogenesis function vanishes everywhere, we conclude from (3.21), with the aid of the boundary conditions discussed above, that $\phi_t = 0$ everywhere and the storm is in a steady state. Hausman et al. (2006) have used an axisymmetric, nonhydrostatic, full-physics model to demonstrate how a tropical cyclone approaches a steady state in which the P and $\dot{\theta}$ fields become locked together in a thin leaning tower on the inner edge of the eyewall cloud.

It should be noted that, for the balanced vortex model, only one second order elliptic partial differential equation need be solved (see Haynes and Shepherd 1989 and Wirth and Dunkerton 2006 for illustrations of this point). Depending on the particular formulation, that elliptic equation could be the transverse circulation equation (3.11) or the geopotential tendency equation (3.21). Since our particular interest here is in the rapid development of a warm core, we find it convenient to focus much of our attention on the geopotential tendency equation.

3.2.4 *Idealized vortex and the separation of variables*

For real hurricanes the coefficients A, B, and C can have complicated spatial distributions (e.g., Fig. 6 of Holland and Merrill 1984 illustrates the radial and vertical variations of inertial stability and static stability computed from their composite tropical cyclone), which would preclude analytical solution of (3.11) and (3.21). To obtain analytical solutions we shall consider an idealized vortex that leads to a drastic simplification of the coefficients A and B, but retains the crucial radial dependence of the inertial stability C. Thus, we consider a barotropic vortex ($B = 0$) with a static stability given by $\rho A = N^2$, where the square of the Brunt-Väisälä frequency, N^2, is a constant. The inertial stability (3.10) can then be written in the form $\rho C = \hat{f}^2$, where $\hat{f}(r) = [f + (2v/r)][f + \partial(rv)/r\partial r]^{1/2}$ is the "effective Coriolis parameter". Under the above assumptions, (3.11) reduces to

$$N^2 \frac{\partial}{\partial r}\left(\frac{\partial(r\psi)}{r\partial r}\right) + \hat{f}^2 \rho \frac{\partial}{\partial z}\left(\frac{1}{\rho}\frac{\partial \psi}{\partial z}\right) = \frac{g\rho}{c_p T_0}\frac{\partial Q}{\partial r}, \tag{3.22}$$

and (3.21) reduces to

$$N^2 \frac{\partial}{r\partial r}\left(\frac{r}{\hat{f}^2}\frac{\partial \phi_t}{\partial r}\right) + \frac{\partial}{\rho \partial z}\left(\rho \frac{\partial \phi_t}{\partial z}\right) = \frac{g}{c_p T_0}\frac{\partial(\rho Q)}{\rho \partial z}. \tag{3.23}$$

We now assume that the diabatic heating and the streamfunction have the separable forms $e^{-z/H} Q(r,z) = \hat{Q}(r)\mathcal{Z}(z)$ and $\psi(r,z) = \hat{\psi}(r)\mathcal{Z}(z)$, where $\mathcal{Z}(z) = e^{-z/2H}\sin(\pi z/z_T)$. Since $e^{-z/H}(e^{z/H}\mathcal{Z}')' = -(\pi/z_T)^2 + (2H)^{-2}\mathcal{Z}$, where the prime denotes a derivative with respect to z, the partial differential equation (3.22) reduces to the ordinary differential equation

$$r^2\frac{d^2\hat{\psi}}{dr^2} + r\frac{d\hat{\psi}}{dr} - \left(\mu^2 r^2 + 1\right)\hat{\psi} = \frac{g\rho_0 r^2}{c_p T_0 N^2}\frac{d\hat{Q}}{dr}, \tag{3.24}$$

with $\mu^2(r) = [\hat{f}^2(r)/N^2][(\pi/z_T)^2 + (2H)^{-2}]$ denoting the inverse Rossby length squared. The corresponding separable forms for the temperature and geopotential tendencies are $T_t(r,z) = \hat{T}_t(r)e^{z/H}\mathcal{Z}(z)$ and $\phi_t(r,z) = (z_T/\pi)\hat{\phi}_t(r)e^{z/H}\mathcal{Z}'(z)$. Because of hydrostatic balance, the radial structure functions $\hat{T}_t(r)$ and $\hat{\phi}_t(r)$ are related by $(g/T_0)\hat{T}_t(r) = -(z_T/\pi)[(\pi/z_T)^2 + (2H)^{-2}]\hat{\phi}_t(r)$. Using these results, it immediately follows that the partial differential equation (3.23) reduces to the ordinary differential equation

$$\hat{T}_t - \frac{d}{rdr}\left(\frac{r}{\mu^2}\frac{d\hat{T}_t}{dr}\right) = \frac{\hat{Q}}{c_p}. \tag{3.25}$$

Note that, although it has a certain resemblance to the thermodynamic equation, (3.25) follows directly from (3.21), which has been obtained through a combination of all the original equations (3.1)–(3.5).

The remainder of this chapter deals with the physical insights revealed by analytical solutions of (3.24) and (3.25). As is easily shown by integration of (3.25) and use of the boundary conditions, these solutions have the integral property

$$\int_0^\infty \hat{T}_t \, r \, dr = \int_0^\infty \frac{\hat{Q}}{c_p} \, r \, dr, \tag{3.26}$$

so the integrated local temperature change is equal to the integrated diabatic heating. However, the crucial question for hurricane intensification is whether the local temperature change occurs primarily in the region of diabatic heating or is spread over a much larger region. This question can be answered by examining the solutions of (3.25), which show the following general properties. If the diabatic heating $\hat{Q}/c_p$ is localized to a region of large Rossby length (i.e., a region where μ^{-2} is large), then $d^2\hat{T}_t/dr^2$ tends to be small, so that $\hat{T}_t$ tends to be spread over a large area but with values much smaller than the peak value of $\hat{Q}/c_p$. In contrast, if the diabatic heating occurs in a region of small Rossby length (i.e., a region where μ^{-2} is small), then $d^2\hat{T}_t/dr^2$ tends to be larger, so that $\hat{T}_t$ tends to be confined to a smaller area, with values more comparable to the peak value of $\hat{Q}/c_p$. The former case tends to occur when a vortex is weak, i.e., when the effective Coriolis parameter $\hat{f}(r)$ is small and the Rossby length $\mu^{-1}(r)$ is large. However, as the vortex becomes stronger, $\hat{f}(r)$ becomes larger and $\mu^{-1}(r)$ becomes smaller, so that the diabatic heating results in a tendency $\hat{T}_t(r)$ that is more localized to the region where $\hat{Q}(r)$ is confined. This process can result in the rapid development of a tropical cyclone warm core. In the following sections we attempt to provide a more quantitative understanding of these simple qualitative arguments.

3.3 General solution in terms of the Green's function

The solution of (3.25) can be written in the form

$$\hat{T}_t(r) = \int_0^\infty G(r, r') \frac{\hat{Q}(r')}{c_p} r' \, dr', \tag{3.27}$$

where the Green's function $G(r, r')$ satisfies the differential equation

$$G(r, r') - \frac{d}{r dr}\left(\frac{r}{\mu^2}\frac{dG(r, r')}{dr}\right) = \frac{\delta(r - r')}{r'}, \tag{3.28}$$

with $\delta(r - r')$ denoting the Dirac delta function localized at radius r'. The validity of (3.27) and (3.28) can easily be confirmed by substituting (3.27) into (3.25) and noting that $\int_0^\infty \hat{Q}(r')\,\delta(r-r')\,dr' = \hat{Q}(r)$. The Green's function $G(r, r')$ gives the radial distribution of the temperature tendency when the diabatic heating is confined to a very narrow region at radius r'. It satisfies the boundary conditions

$$\frac{dG(r,r')}{dr} = 0 \text{ at } r = 0, \quad rG(r,r') \to 0 \text{ as } r \to \infty, \tag{3.29}$$

and the jump conditions

$$\left[G(r,r')\right]_{r=r'-}^{r=r'+} = 0 \quad \text{and} \quad \left[\frac{r}{\mu^2}\frac{dG(r,r')}{dr}\right]_{r=r'-}^{r=r'+} = -1, \tag{3.30}$$

the latter of which is derived by integrating (3.28) across a narrow interval centered at radius r'.

The solution of (3.24) could be obtained in an analogous way. However, it is simpler to determine $G_\psi(r, r')$, the Green's function for ψ, directly from $G(r, r')$, the Green's function for the temperature tendency. This can be accomplished by noting that the thermodynamic equation (3.6), with the assumptions given in section 3.2, leads to

$$\frac{d[rG_\psi(r,r')]}{rdr} = -\frac{g\rho_0}{T_0 N^2}G(r,r') \qquad \text{for} \quad r \neq r'. \tag{3.31}$$

Thus, once we have determined $G(r, r')$, we can obtain $G_\psi(r, r')$ by integration of (3.31).

The differential equation (3.28) for the Green's function $G(r, r')$ can be solved analytically only if $\mu(r)$ takes some simple form. Here we present two simple cases. In the first case (section 3.4) the atmosphere is assumed to be at rest, so that μ is a constant. In the second case (section 3.5) we consider a Rankine-like vortex, so that μ is piecewise constant, with a large value of μ in the vortex core and a small value of μ in the far-field.

3.4 Green's functions for a resting atmosphere

We first consider the case where $v = 0$, so that $\hat{f}(r) = f$ and $\mu(r)$ takes on the constant value μ_f. Then, (3.28) reduces to the order zero modified Bessel equation (Abramowitz and Stegun, 2006, Chapter 9) when $r \neq r'$. The general solution of the problem is constructed from a combination of the order zero modified Bessel functions $I_0(\mu_f r)$ and $K_0(\mu_f r)$. Because of the boundary conditions (3.29), only the $I_0(\mu_f r)$ solution is valid for $r < r'$ and only the $K_0(\mu_f r)$ solution is valid for $r > r'$.

Matching these solutions across $r = r'$ involves the jump conditions (3.30), which can be enforced with the aid of the derivative relations $dI_0(x)/dx = I_1(x)$ and $dK_0(x)/dx = -K_1(x)$, and the Wronskian $I_0(x)K_1(x) + K_0(x)I_1(x) = 1/x$. The final result is

$$G(r, r') = \mu_f^2 \begin{cases} K_0(\mu_f r')I_0(\mu_f r) & \text{if } 0 \le r \le r' \\ I_0(\mu_f r')K_0(\mu_f r) & \text{if } r' \le r < \infty. \end{cases} \tag{3.32}$$

Integrating (3.31), using (3.32) and the derivative relations $d[rI_1(\mu r)]/rdr = \mu I_0(\mu r)$ and $d[rK_1(\mu r)]/rdr = -\mu K_0(\mu r)$, we obtain

$$G_\psi(r, r') = \frac{g\rho_0\mu_f}{T_0 N^2} \begin{cases} -K_0(\mu_f r')I_1(\mu_f r) & \text{if } 0 \le r < r' \\ I_0(\mu_f r')K_1(\mu_f r) & \text{if } r' < r < \infty. \end{cases} \tag{3.33}$$

To compute the actual temperature tendency associated with the Green's function (3.32), we return to (3.27) with the condition $\hat{Q}(r') = 0$ for $r' \neq r_h$. Then (3.27) becomes

$$\hat{T}_t(r) = G(r, r_h) \int_{r_h-}^{r_h+} \frac{\hat{Q}(r')}{c_p} r'\, dr'. \tag{3.34}$$

Note that, according to (3.34), the spatial distribution of $\hat{T}_t(r)$ is given by $G(r, r_h)$ and the magnitude by $\int_{r_h-}^{r_h+} [\hat{Q}(r')/c_p] r'\, dr'$, which is somewhat arbitrary. We have chosen this normalization factor to be

$$\int_{r_h-}^{r_h+} \frac{\hat{Q}(r')}{c_p}\, r'\, dr' = \left(26 \text{ K h}^{-1}\right)(25 \text{ km})(10 \text{ km}) \equiv S, \tag{3.35}$$

which is the same normalization used by Schubert et al. (2007) in their study of the distribution of subsidence in the hurricane eye. With this normalization, the $\psi(r, z)$ and $T_t(r, z)$ fields can be written as

$$\psi(r, z) = SG_\psi(r, r_h)e^{-z/(2H)} \sin\left(\frac{\pi z}{z_T}\right), \tag{3.36}$$

$$T_t(r, z) = SG(r, r_h)e^{z/(2H)} \sin\left(\frac{\pi z}{z_T}\right). \tag{3.37}$$

Figure 3.1 shows contours of $r\psi$ and T_t in the (r, z)-plane for this resting atmosphere case. These plots have been constructed from (3.36) and (3.37) using the Green's function formulas (3.32) and (3.33). Note that $r\psi$ is negative for $r < 25$ km and is positive for $r > 25$ km, which means that the transverse mass flux is counterclockwise for $r < 25$ km and clockwise for $r > 25$ km. The discontinuity of $r\psi$ at

$r = 25\,\text{km}$ means that infinite upward vertical velocity occurs there. However, the vertical mass flux is finite since

$$\rho \int_{r_h-}^{r_h+} w(r,z)\, r\, dr = r_h\, [\psi(r_h+,z) - \psi(r_h-,z)] = \frac{g\rho_0 S}{T_0 N^2} e^{-z/(2H)} \sin\left(\frac{\pi z}{z_T}\right), \tag{3.38}$$

which follows from (3.33), (3.36), and the Wronskian. The minimum value of $r\psi$, which occurs just inside $r = 25\,\text{km}$, is given in the sixth column of the first row in Table 3.1, while the maximum value of $r\psi$, which occurs just outside $r = 25\,\text{km}$, is given in the seventh column. Thus, at the level of maximum vertical mass fluxes, the downward mass flux inside $r = 25\,\text{km}$ is $0.5339 \times 10^6\,\text{kg s}^{-1}$, while the downward mass flux outside $r = 25\,\text{km}$ is $448.38 \times 10^6\,\text{kg s}^{-1}$. Defining $\eta = (r\psi)_{\max}/[(r\psi)_{\max} - (r\psi)_{\min}]$ as the fraction of the upward mass flux that is compensated by far-field subsidence, we see (eighth column of Table 3.1) that approximately 99.88% of the upward mass flux is compensated by downward mass flux outside $r = 25\,\text{km}$ and only 0.12% is compensated by downward mass flux inside $r = 25\,\text{km}$. As can be seen in the right panel of Fig. 3.1, there is very little variation of the temperature tendency on a fixed isobaric surface. In other words, the Dirac delta function in the diabatic heating leads to a transverse circulation that raises the temperature on a given isobaric surface nearly uniformly over a large area. The production of very weak horizontal temperature gradients and corresponding weak vertical shears of the azimuthal wind is consistent with the well-known result that diabatic heating on a horizontal scale smaller than the Rossby length is a very inefficient way to produce rotational flow (e.g., Schubert et al., 1980; Gill, 1982; Shapiro and Willoughby, 1982; Schubert and Hack, 1982).

Although the assumption of a resting atmosphere is too restrictive for our present goals, the idealized Green's functions (3.32) and (3.33) provide useful comparisons for the more general results of section 3.5.

3.5 Green's functions for a nonresting atmosphere

3.5.1 A Rankine-like vortex

To treat radial variations of $\mu(r)$ in a simple manner, we consider the specific barotropic vortex in which the square of the absolute angular momentum is given by $m^2(r) = [rv(r) + \frac{1}{2} f r^2]^2 = \frac{1}{4} f_c^2 r^4$ for $0 \le r \le r_c$ and by $m^2(r) = m^2(r_c) + \frac{1}{4} f^2 (r^4 - r_c^4)$ for $r_c \le r < \infty$, where r_c and f_c are specified

Table 3.1: Parameters for the resting case (first row) and the Rankine-like vortex cases (remaining rows): radius of the vortex core, r_c; maximum azimuthal wind, $v(r_c)$; dimensionless effective Coriolis parameter in the vortex core, f_c/f; and Rossby length in the vortex core, μ_c^{-1}. The last four columns show the minimum value of $r\psi$ (which occurs just inside $r = r_h$), the maximum value of $r\psi$ (just outside $r = r_h$), the fraction (η) of the downward mass flux that occurs in the region $r > r_h$, and the maximum value of T_t.

Case	r_c (km)	$v(r_c)$ ($\mathrm{m\,s^{-1}}$)	f_c/f	μ_c^{-1} (km)	$(r\psi)_{\min}$ ($\times 10^6\,\mathrm{kg\,s^{-1}}$)	$(r\psi)_{\max}$ ($\times 10^6\,\mathrm{kg\,s^{-1}}$)	η (%)	$(T_t)_{\max}$ ($\mathrm{K\,h^{-1}}$)
R0	-	0	1.0	1000.0	−0.5339	448.38	99.88	0.0411946
A10	20	10	21.0	47.6	−0.5266	448.39	99.88	0.0411952
A20	20	20	41.0	24.4	−0.5081	448.41	99.89	0.0411969
A30	20	30	61.0	16.4	−0.4830	448.44	99.89	0.0411992
A40	20	40	81.0	12.3	−0.4557	448.46	99.90	0.0412018
B10	30	10	14.3	69.8	−5.5922	443.31	98.75	0.43832
B20	30	20	27.7	36.1	−18.099	430.75	95.97	1.47819
B30	30	30	41.0	24.4	−35.154	413.61	92.17	3.05366
B40	30	40	54.3	18.4	−53.852	394.81	88.00	5.04679

constants giving the radius and strength of the vortex core. It can easily be shown that

$$\hat{f}(r) = \left(\frac{\partial m^2}{r^3 \partial r}\right)^{1/2} = \left\{\left(f + \frac{2v}{r}\right)\left(f + \frac{\partial (rv)}{r\partial r}\right)\right\}^{\frac{1}{2}} = \begin{cases} f_c, & \text{if } 0 \le r < r_c \text{ (vortex core)}, \\ f, & \text{if } r_c < r < \infty \text{ (far-field)}, \end{cases} \tag{3.39}$$

so that f_c can be interpreted as a specified constant giving the effective Coriolis parameter in the vortex core. Because of (3.39), the inverse Rossby length $\mu(r)$ also has the piecewise constant form

$$\mu(r) = \begin{cases} \mu_c & \text{if } 0 \le r < r_c \text{ (vortex core)}, \\ \mu_f & \text{if } r_c < r < \infty \text{ (far-field)}, \end{cases} \tag{3.40}$$

where the constants μ_c and μ_f are defined in terms of the constants f_c and f via $\mu_c = (f_c/N)[(\pi/z_T)^2 + (2H)^{-2}]^{1/2}$ and $\mu_f = (f/N)[(\pi/z_T)^2 + (2H)^{-2}]^{1/2}$. Plots of $v(r)$, computed using the parameters listed in the second (sixth) through the fifth (ninth) rows of Table 3.1, are shown in the left column of Fig. 3.2 (Fig. 3.3). In constructing Table 3.1 and Figs. 3.2 and 3.3, we have used $f = 5 \times 10^{-5}\,\mathrm{s^{-1}}$ and $\mu_f^{-1} = 1000\,\mathrm{km}$. Note that the $v(r)$ profiles are Rankine-like, and that the strength of the tangential winds range from tropical depression, through tropical storm, to Category 1 on the Saffir-Simpson scale. The Rossby length in the vortex core, given by μ_c^{-1} and listed in the fifth column of Table 3.1, is less than 20 km for the stronger vortices.

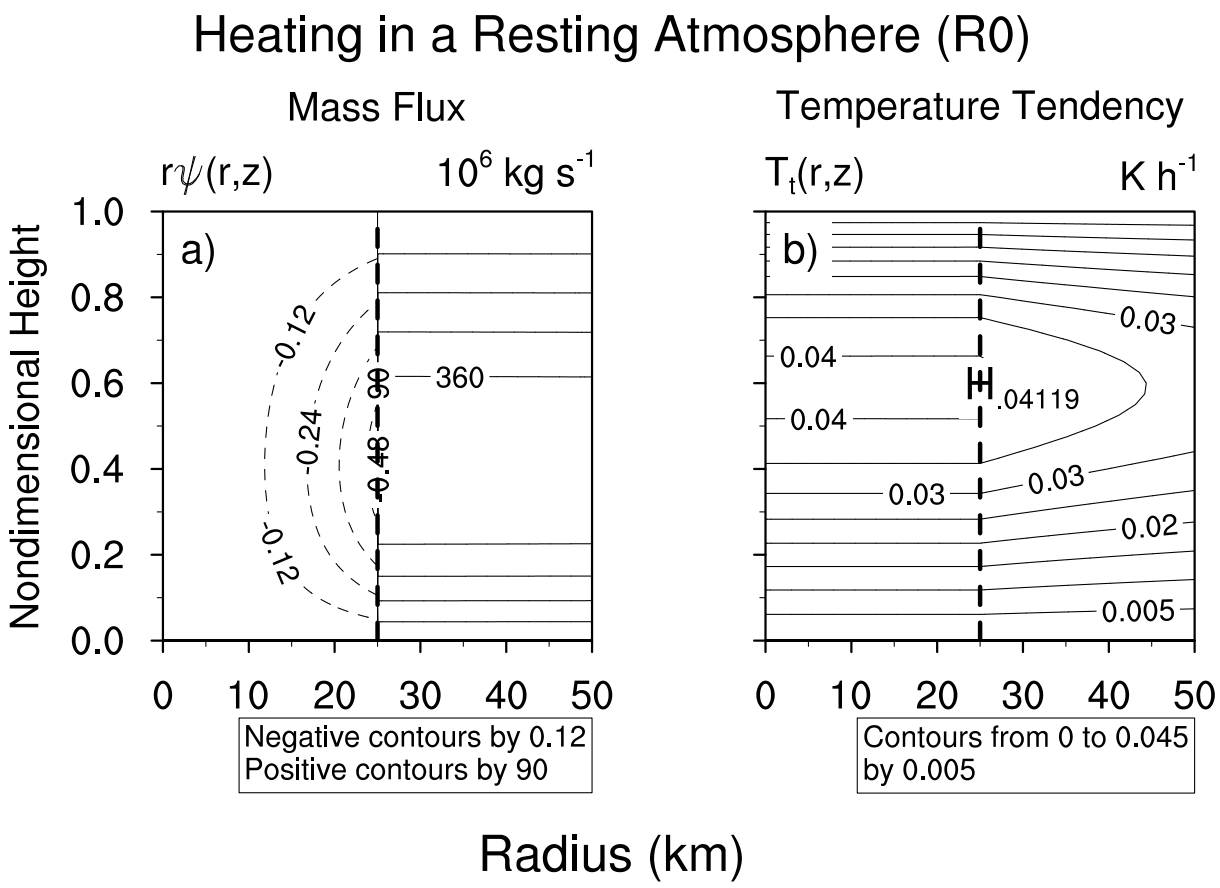

Figure 3.1: Isolines of $r\psi$ and temperature tendency T_t in the (r, z)-plane for the resting atmosphere case. The radial axis is labeled in km and the vertical axis in the dimensionless vertical coordinate z/z_T. The radius of diabatic heating is $r_h = 25$ km (as indicated by the vertical dashed line).

3.5.2 Diabatic heating outside the vortex core ($r_c < r_h$)

To solve the Green's function problem (3.28)–(3.30) for this Rankine-like vortex, we first consider the case $r_c < r_h$. Then, (3.28) reduces to

$$\begin{aligned} &\frac{d}{rdr}\left(r\frac{dG(r,r_h)}{dr}\right) - \mu_c^2 G(r,r_h) = 0 \quad \text{if} \quad 0 \le r < r_c, \\ &\frac{d}{rdr}\left(r\frac{dG(r,r_h)}{dr}\right) - \mu_f^2 G(r,r_h) = 0 \quad \text{if} \quad r_c < r < \infty \quad \text{but} \quad r \neq r_h. \end{aligned} \tag{3.41}$$

Now, in addition to the boundary conditions (3.29) and the jump conditions (3.30), we require

$$[G(r,r_h)]_{r=r_c-}^{r=r_c+} = 0 \quad \text{and} \quad \left[\frac{r}{\mu^2}\frac{dG(r,r_h)}{dr}\right]_{r=r_c-}^{r=r_c+} = 0, \tag{3.42}$$

the latter of which is derived by integrating (3.28) across a narrow interval centered at $r = r_c$. The solution of (3.41) consists of linear combinations of the zeroth-order modified Bessel functions $I_0(\mu_c r)$

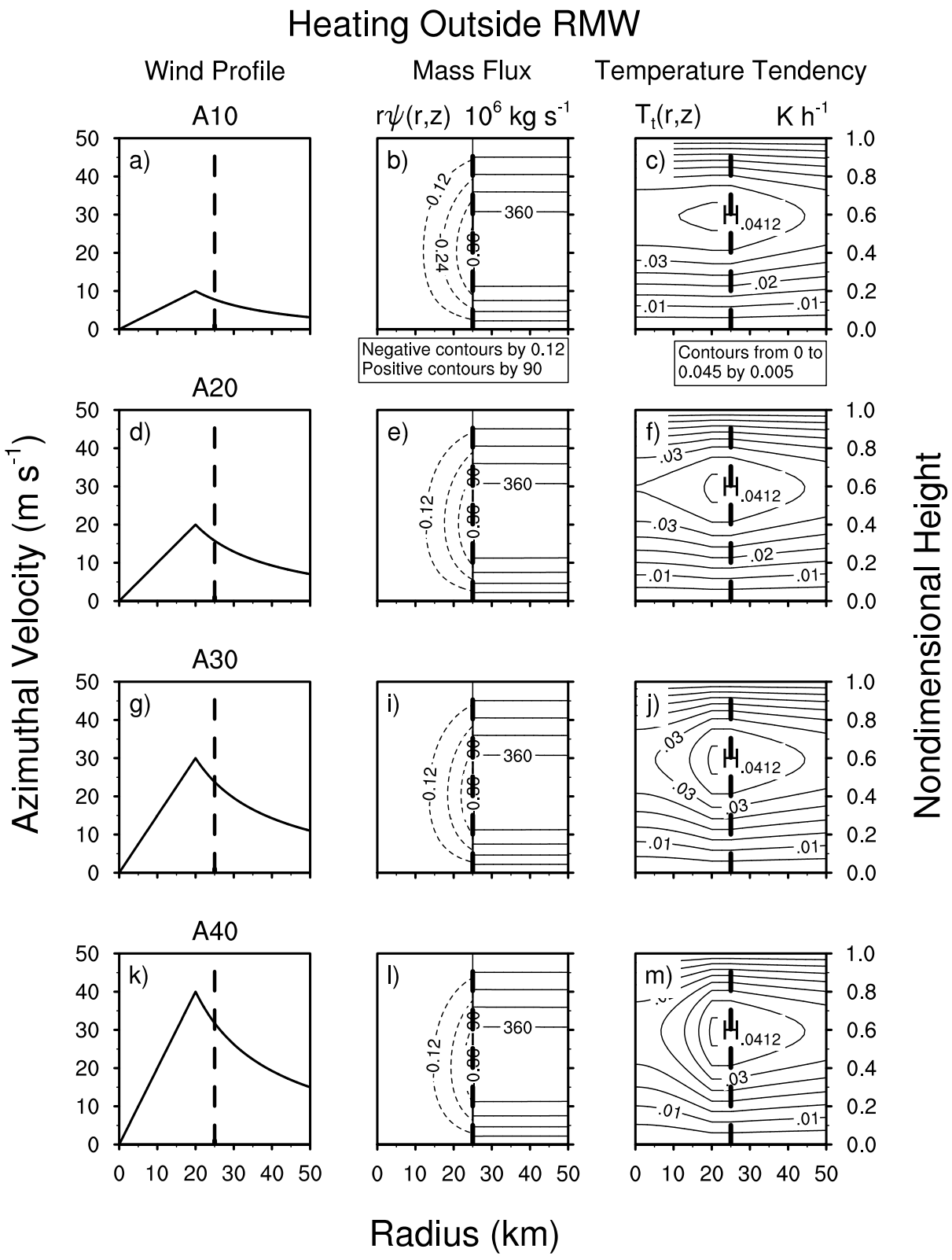

Figure 3.2: Isolines of $r\psi(r,z)$ and temperature tendency $T_t(r,z)$ for the four Rankine-like vortices shown in the left column. The radius of maximum wind is $r_c = 20$ km and the radius of diabatic heating is $r_h = 25$ km (as indicated by the vertical dashed line).

and $K_0(\mu_c r)$ in the region $0 \le r < r_c$, and linear combinations of $I_0(\mu_f r)$ and $K_0(\mu_f r)$ in the region $r_c < r < \infty$. Because our boundary condition requires that $dG(r, r_h)/dr = 0$ at $r = 0$, we can discard the $K_0(\mu_c r)$ solution in the inner region. Similarly, because $rG(r, r_h) \to 0$ as $r \to \infty$, we can discard the $I_0(\mu_f r)$ solution in the outer region. The solution of (3.41) can then be written as

$$G(r, r_h) = \mu_f^2 \begin{cases} F_1(r_c, r_h) K_0(\mu_f r_h) I_0(\mu_c r) & 0 \le r \le r_c \\ F_1(r, r_h) K_0(\mu_f r_h) I_0(\mu_c r_c) + \gamma_1 F_1(r_c, r) I_0(\mu_f r_h) K_0(\mu_f r_h) & r_c \le r \le r_h \\ \gamma_1 F_1(r_c, r_h) I_0(\mu_f r_h) K_0(\mu_f r) & r_h \le r < \infty, \end{cases} \tag{3.43}$$

where

$$F_1(x, y) = \frac{I_0(\mu_f x) K_0(\mu_f y) - K_0(\mu_f x) I_0(\mu_f y)}{I_0(\mu_c r_c) K_0(\mu_f r_h) - \gamma_1 K_0(\mu_f r_c) I_0(\mu_f r_h)} \tag{3.44}$$

and

$$\begin{aligned} \gamma_1 = {} & \mu_f r_c \left[I_0(\mu_c r_c) K_1(\mu_f r_c) + \frac{\mu_f}{\mu_c} I_1(\mu_c r_c) K_0(\mu_f r_c) \right] \\ & + \mu_f r_c \left[I_0(\mu_c r_c) I_1(\mu_f r_c) - \frac{\mu_f}{\mu_c} I_1(\mu_c r_c) I_0(\mu_f r_c) \right] \frac{K_0(\mu_f r_h)}{I_0(\mu_f r_h)}. \end{aligned} \tag{3.45}$$

Since $F_1(r_c, r_c) = 0$ and $F_1(r_h, r_h) = 0$, (3.43) guarantees that $G(r, r_h)$ is continuous at $r = r_c$ and $r = r_h$, so that the first entry in (3.30) and the first entry in (3.42) are both satisfied. The jump condition on the derivative at $r = r_h$ (i.e., the second entry in (3.30)) and the jump condition on the derivative at $r = r_c$ (i.e., the second entry in (3.42)) can be confirmed by using the Bessel function derivative relations and the Wronskian. The Green's function for ψ can be obtained by integrating (3.31), using (3.43) for $G(r, r_h)$. The result is

$$G_\psi(r, r_h) = \frac{g\rho_0 \mu_f}{T_0 N^2} \begin{cases} -\dfrac{\mu_f}{\mu_c} F_1(r_c, r_h) K_0(\mu_f r_h) I_1(\mu_c r) & 0 \le r \le r_c \\ -K_0(\mu_f r_h) \left[I_0(\mu_c r_c) \hat{F}_1(r_h, r) - \gamma_1 I_0(\mu_f r_h) \hat{F}_1(r_c, r) \right] & r_c \le r < r_h \\ \gamma_1 F_1(r_c, r_h) I_0(\mu_f r_h) K_1(\mu_f r) & r_h < r < \infty, \end{cases} \tag{3.46}$$

where

$$\hat{F}_1(x, y) = \frac{K_0(\mu_f x) I_1(\mu_f y) + I_0(\mu_f x) K_1(\mu_f y)}{I_0(\mu_c r_c) K_0(\mu_f r_h) - \gamma_1 K_0(\mu_f r_c) I_0(\mu_f r_h)}. \tag{3.47}$$

To summarize for the case $r_c < r_h$, after specifying μ_c, μ_f, r_c, and r_h, we can compute γ_1 from (3.45), and then $G(r, r_h)$ from (3.43) and $G_\psi(r, r_h)$ from (3.46). Note that, when $\mu_c = \mu_f$, (3.45) reduces to $\gamma_1 = 1$, the first two lines of (3.43) become identical, the first two lines of (3.46) become identical, and (3.43) reduces to (3.32) while (3.46) reduces to (3.33).

3.5.3 Diabatic heating within the vortex core ($r_h < r_c$)

Now consider the case $r_h < r_c$. The Green's function for the temperature tendency is

$$G(r, r_h) = \mu_c^2 \begin{cases} \gamma_2 F_2(r_h, r_c) K_0(\mu_c r_h) I_0(\mu_c r) & 0 \le r \le r_h \\ \gamma_2 F_2(r, r_c) K_0(\mu_c r_h) I_0(\mu_c r_h) + F_2(r_h, r) I_0(\mu_c r_h) K_0(\mu_f r_c) & r_h \le r \le r_c \\ F_2(r_h, r_c) I_0(\mu_c r_h) K_0(\mu_f r) & r_c \le r < \infty, \end{cases} \tag{3.48}$$

where

$$F_2(x, y) = \frac{I_0(\mu_c x) K_0(\mu_c y) - K_0(\mu_c x) I_0(\mu_c y)}{I_0(\mu_c r_h) K_0(\mu_f r_c) - \gamma_2 K_0(\mu_c r_h) I_0(\mu_c r_c)} \tag{3.49}$$

and

$$\begin{aligned} \gamma_2 = {} & \mu_c r_c \left[K_0(\mu_f r_c) I_1(\mu_c r_c) + \frac{\mu_c}{\mu_f} I_0(\mu_c r_c) K_1(\mu_f r_c) \right] \\ & + \mu_c r_c \left[K_0(\mu_f r_c) K_1(\mu_c r_c) - \frac{\mu_c}{\mu_f} K_0(\mu_c r_c) K_1(\mu_f r_c) \right] \frac{I_0(\mu_c r_h)}{K_0(\mu_c r_h)}. \end{aligned} \tag{3.50}$$

Note that the continuity of $G(r, r_h)$ at $r = r_h$ and $r = r_c$ follows directly from $F_2(r_h, r_h) = 0$ and $F_2(r_c, r_c) = 0$. The Green's function for ψ is

$$G_\psi(r, r_h) = \frac{g\rho_0\mu_c}{T_0 N^2} \begin{cases} -\gamma_2 F_2(r_h, r_c) K_0(\mu_c r_h) I_1(\mu_c r) & 0 \le r < r_h \\ I_0(\mu_c r_h) \left[-\gamma_2 K_0(\mu_c r_h) \hat{F}_2(r_c, r) + K_0(\mu_f r_c) \hat{F}_2(r_h, r) \right] & r_h < r \le r_c \\ \dfrac{\mu_c}{\mu_f} F_2(r_h, r_c) I_0(\mu_c r_h) K_1(\mu_f r) & r_c \le r < \infty, \end{cases} \tag{3.51}$$

where

$$\hat{F}_2(x, y) = \frac{K_0(\mu_c x) I_1(\mu_c y) + I_0(\mu_c x) K_1(\mu_c y)}{I_0(\mu_c r_h) K_0(\mu_f r_c) - \gamma_2 K_0(\mu_c r_h) I_0(\mu_c r_c)}. \tag{3.52}$$

When $\mu_c = \mu_f$, (3.50) reduces to $\gamma_2 = 1$, the last two lines of (3.48) become identical, the last two lines of (3.51) become identical, and (3.48) reduces to (3.32) while (3.51) reduces to (3.33).

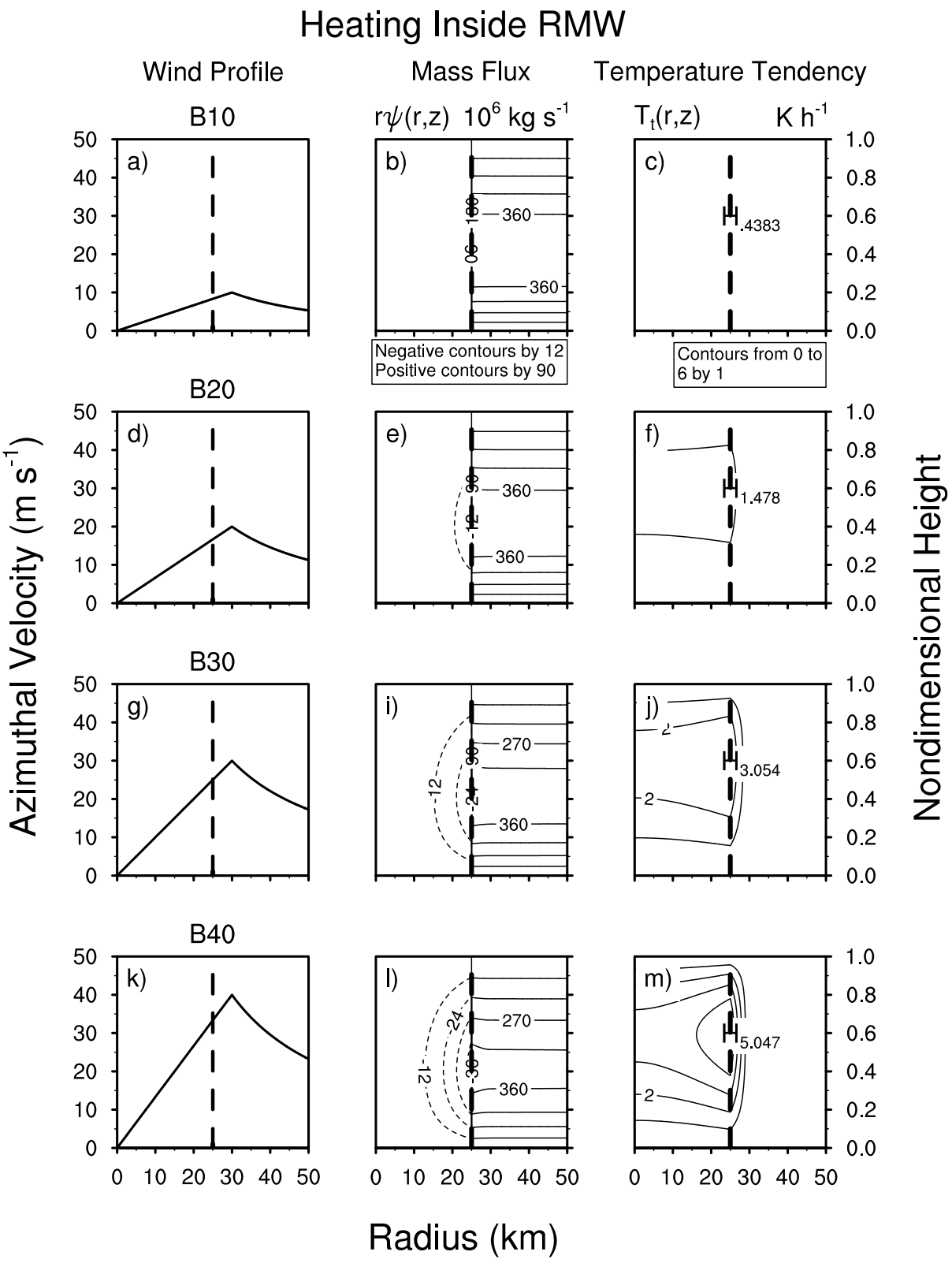

Figure 3.3: Same as Fig. 3.2 except $r_c = 30$ km, so that the diabatic heating occurs inside the radius of maximum wind. Note the change in isoline intervals from those used in Fig. 3.2.

3.6 Conditions for rapid development of a warm core

3.6.1 Inner core response to heating

Plots of mass stream function $r\psi(r,z)$ and temperature tendency $T_t(r,z)$ can now be constructed from (3.36) and (3.37) using either (3.43) and (3.46) for $r_c < r_h$ or (3.48) and (3.51) for $r_h < r_c$. It can be shown that the $r\psi(r,z)$ field constructed in this way also satisfies the mass flux normalization relation (3.38).

We first consider the case $r_c = 20\,\text{km}$ and $r_h = 25\,\text{km}$, which is typical of cases in which the diabatic heating lies outside the radius of maximum wind. In the second and third columns of Fig. 3.2 we show isolines of $r\psi(r,z)$ and $T_t(r,z)$ for the four vortices displayed in the left column. These vortices all have a maximum wind at $r_c = 20\,\text{km}$, but with $v(r_c) = 10, 20, 30,$ and $40\,\text{m s}^{-1}$. The corresponding values of f_c/f and μ_c^{-1} are given in the fourth and fifth columns of Table 3.1, along the rows labeled A10, A20, A30, and A40. The most obvious feature of Fig. 3.2 is the similarity of the four $r\psi(r,z)$ fields and the four $T_t(r,z)$ fields, and the fact that they differ little from the resting case shown in Fig. 3.1. For example, the peak value of $T_t(r,z)$ is $0.041195\,\text{K h}^{-1}$ for Case A10 and $0.041202\,\text{K h}^{-1}$ for Case A40. Since the vortex core is more inertially stable in Case A40, the compensating subsidence does not extend as far inward, which means the subsidence is not as large at $r = 0$ and thus T_t is not as large at $r = 0$. This explains why the temperature tendency in Fig. 3.2m is somewhat more localized than the temperature tendency in Fig. 3.2c. This "warm-ring effect" has been observed in real storms, e.g. Hurricane Isabel (2003; see Fig. 10 of Schubert et al. 2007). However, the main conclusion to be drawn from Fig. 3.2 is that diabatic heating in the low inertial stability region outside the radius of maximum wind produces a temperature tendency that is nearly uniform horizontally and similar to that found for a resting atmosphere. In other words, diabatic heating outside the radius of maximum wind is very inefficient at producing rotational flow, no matter how small the Rossby length inside the radius of maximum wind.

Now consider the case $r_h = 25\,\text{km}$ and $r_c = 30\,\text{km}$, which is typical of cases in which the diabatic heating lies inside the radius of maximum wind. In the second and third columns of Fig. 3.3 we show isolines of $r\psi(r,z)$ and $T_t(r,z)$ for the four vortices displayed in the left column. These vortices all have

a maximum wind at $r_c = 30\,\text{km}$, but with $v(r_c) = 10, 20, 30,$ and $40\,\text{m s}^{-1}$. The corresponding values of f_c/f and μ_c^{-1} are given in the fourth and fifth columns of Table 3.1, along the rows labeled B10, B20, B30, and B40. The most obvious features of Fig. 3.3 are the much larger and more localized values of $T_t(r,z)$ near $r = 25\,\text{km}$. The values are approximately ten ($0.4383\,\text{K h}^{-1}$ for Case B10) to one hundred ($5.047\,\text{K h}^{-1}$ for Case B40) times the values in Fig. 3.2. *Thus, when diabatic heating occurs within the high inertial stability region that lies inside the radius of maximum wind, there is enhanced subsidence inside the radius of heating*[1] *and a tendency to rapidly form a warm core.*

It should be noted that while all results shown here represent the heating as a Dirac delta function, these results could be extended for a more general distribution of heating of finite width. Because of the linearity of the geopotential tendency equation and the transverse circulation equation, we can construct solutions for general diabatic heating fields by superposition of the Green's functions $G(r,r')$ and $G_\psi(r,r')$ for different values of r'. This allows us to argue as follows. Suppose that the diabatic heating field consists of an annular ring of finite width, and that the radius of maximum wind occurs somewhere between the inner and outer edges of this ring. In this case, the portion of the diabatic heating that occurs inside the radius of maximum wind contributes much more efficiently to warm core formation and vortex intensification than the portion of the diabatic heating that occurs outside the radius of maximum wind. A consequence is that the inward or outward movement of the radius of maximum wind relative to the annular ring of convection can have a large effect on the vortex intensification rate.

3.6.2 Outer core response to heating

Further physical insight may be gained by noting a subtle difference between Figs. 3.1, 3.2, 3.3. Isolines of $r\psi(r,z)$ for the B40 vortex in Fig. 3.3l possess a discernible slope between r_h and r_c, whereas they do not in Fig. 3.1 and Fig. 3.2l. This slope indicates significant subsidence (and therefore adiabatic warming) occurs locally outside of the diabatic forcing region where the inertial stability remains high. As a word of caution, it should be recognized that our idealized vortex has a very large change of inertial stability at the radius of maximum winds and thereby accentuates the difference between the efficiency of diabatic heating just inside and just outside this radius. In real hurricanes the variation of inertial stability

[1] See the values of η listed in Table 3.1. Smaller η values indicate that more of the mass flux recirculates into the eye.

with radius (Mallen et al., 2005; Holland and Merrill, 1984) is somewhat smoother, so there is a more gradual change from the inefficient response to diabatic heating outside the radius of maximum wind to the efficient response inside this radius. In Holland and Merrill's composite tropical cyclone, inertial stability peaks at approximately $1000 f^2$ at $r \approx 30$ km, decreases rapidly to $100 f^2$ at $r \approx 80$ km, and then drops off more gradually to $10 f^2$ at $r \approx 200$ km. The corresponding Rossby length at $r \approx 200$ km is approximately 300 km, or one third that of the far-field value (1000 km), so the heating there will still be considerably more efficient than in the far-field. Thus, heating in this transition region can still spin up the local tangential wind and radially constrain the circulation response — despite the fact that the heating is occurring outside of the radius of maximum wind. This causes strong subsidence warming and increased static stability outside of the inner core which will tend to inhibit convection. According to the authors, this effect likely explains the relatively clear doughnut-shaped region sometimes observed surrounding intense storms following a period of rapid intensification.[2] Annular hurricanes have been noted to lack significant outer rainbands (Knaff et al., 2003) and may also possess a vortex "skirt" outside of the radius of maximum winds. Our simple analytic results suggest that the enhanced outer subsidence associated with such a "vortex skirt" may be implicated in suppressing these outer rainbands. This effect has also been suggested by a recent full-physics modeling study by Wang (2008).

3.6.3 Far-field response to heating

In passing, we note that the outer core ($r \approx 50$ km) temperature tendencies are qualitatively similar between all three figures,[3] but the far-field tendencies (e.g., $r \sim 500$ km, not shown) of Fig. 3.3 are slightly less than the tendencies in Figs. 3.1 and 3.2. This difference is easily explained by recalling from (3.26) that the integrated local temperature tendency must be equal to the integrated diabatic heating. So in Fig. 3.3, the large temperature tendencies of the small inner core region are exactly compensated for by the slightly reduced tendencies (compared to Fig. 3.1 and Fig. 3.2) over the expansive far-field region.

[2] For an example, see the remarkable clear "moat" that surrounded Hurricane Allen (1980) shown in Fig. 1e of Jorgensen (1984a).

[3] This difference is not very apparent from the figures because the isoline levels have been changed in Fig. 3.3 in order to highlight the enhanced inner core tendency response.

3.7 Comparison to observed storms and further discussion

In light of these results, we would be remiss if we did not inquire as to the radial distributions of diabatic heating and inertial stability in real storms. In particular, does the location of the radius of maximum wind relative to the heating really play a prominent role in controlling intensification rates in observed storms? Seeking to answer this question, we turn our attention to observational studies which have shed some light on this issue.

3.7.1 Location of diabatic heating relative to the radius of maximum wind in observed storms

Shea and Gray (1973) conducted a landmark study in which they examined 533 radial flight legs from Atlantic hurricanes over a 13-year period. They characterized the radius of maximum wind as the boundary between two dynamically-disparate regions of the storm. Outside the radius of maximum winds, convergence and high winds dominate, while high winds, high vorticity, and subsidence are found inside the radius of maximum winds. At low levels, air flowing in towards the radius of maximum wind meets air flowing outwards from the eye, forcing a strong updraft at or near the radius of maximum wind. Thus, in the overwhelming majority of cases, the radius of maximum wind occurs *within* the eyewall cloud.[4] In fact, on average, the radius of maximum wind was located 8–10 km outward from the inner edge of the eyewall (as observed by aircraft radar). Jorgensen (1984a) made additional observations of mature hurricanes which possessed contracting eyewalls; his results show that the maximum convective scale updrafts (which correspond to the maximum diabatic heating) are typically located between 1 and 6 km inward from the radius of maximum wind. These observations indicate that significant diabatic heating normally occurs within the high inertial stability region of most storms. Thus, the typical tropical cyclone structure clearly supports intensification, but the more interesting question still remains: what controls how rapidly a storm will intensify?

It is not a trivial matter to resolve the radial distribution of diabatic heating in a tropical cyclone.

[4] In a small number of cases, the radius of maximum wind was found *inside* the eye. This suggests that diabatic heating associated with the eyewall updraft may occur entirely outside of the high inertial stability region. Our Fig. 3.2 suggests that any such distribution of heating will be very inefficient at intensifying the storm.

Several past studies have used satellite-based passive microwave radiometer data or aircraft to examine the relationship between inner core diabatic heating and intensity change. Some general findings of those studies are summarized here. (i) As a storm develops and intensifies from a disturbance to the hurricane stage, inner core diabatic heating tends to increase and concentrate towards the center (Adler and Rodgers, 1977; Lonfat et al., 2004). (ii) Episodes of enhanced heating seem to precede periods of intensification, with perhaps a lag of a day or two (Rodgers and Adler, 1981; Steranka et al., 1986; Rao and MacArthur, 1994). (iii) The storm tends to become more responsive to increases in inner core diabatic heating as the intensity increases (Rodgers et al., 1998); hurricanes may need less of an increase in heating to intensify as compared with tropical storms (Rodgers et al., 1994). (iv) In the mature stage however, Marks (1985) observed no relationship between Hurricane Allen's (1980) intensity changes and inner core diabatic heating over a 5 d period. Increases in latent heat seemed to be related to areal increases in rainfall caused by rainband activity or the presence of multiple eyewalls.

Most of the above studies share several common weaknesses. First of all, it is difficult to separate the intensification response due to increased inner core diabatic heating from the general tendency of the diabatic heating to concentrate near the center as the storm intensifies. Additionally, the early satellite-based estimates of diabatic heating could not adequately resolve the radial distribution of diabatic heating. Finally, these studies did not include any information on the distribution of heating relative to the radius of maximum winds.

One study has overcome some of these limitations. Corbosiero et al. (2005, see their Fig. 6) have performed a detailed investigation of Hurricane Elena (1985) data during a 28 h period when it was well observed by both ground-based radar and aircraft. These data show that, during Elena's period of most rapid intensification, the radius of maximum wind contracted to approximately 30 km and the inner edge of the eyewall convection remained at approximately 20 km, while there appeared to be periods of intense convection in the region between 20 and 30 km. According to the analysis presented here, the portion of the diabatic heating that occurred between 20 and 30 km was most responsible for the intensification of Elena. Because this is just one case, and the intensification rate appears to be constant during this period (as indicated from the best track, which only gives intensity values every 6 h), it is difficult to tell whether the concentration of diabatic heating within the radius of maximum winds actually affected

Elena's intensification rate.

Returning to the study of Shea and Gray, their Fig. 18 plots the difference between the radius of maximum wind and the inner eye radius as a function of intensity. This distance measures how far within the cloud area the radius of maximum wind resides, and can be thought of as a crude proxy for the amount of efficient diabatic heating. According to the figure, storms near minimal hurricane intensity exhibit a wide variation in this quantity (with the radius of maximum wind sometimes occurring near the inner cloud edge, but in other cases lying more than 40 km outward from the inner cloud edge). Their figure bolsters the view that the proportion of diabatic heating located within the radius of maximum winds decreases as a storm intensifies. But clearly, an observational challenge remains to continue to document, for a broad set of storms with widely-varying intensification rates, the relation between the radius of maximum wind and the inner edge of eyewall convection.

3.7.2 Effects of eye formation and contraction

Because the formation of an eye[5] must necessarily remove some of the diabatic heating from the high inertial stability region of a storm, Schubert and Hack (1982) viewed eye formation as a stabilizing factor which prevents run-away intensification. On the other hand, observations suggest that storms often intensify most rapidly during or immediately following the formation of an eye (Mundell, 1990). The argument for eye formation as a stabilizer to storm intensification can be summarized thusly. Convective heating in the consolidating eyewall forces central axial subsidence, increasing static stability in the nascent eye. At the same time, the increased inertial stability associated with the intensifying swirling flow of the developing eyewall acts as a barrier to moist air flowing towards the center. With the moisture-rich low level source air becoming "locked-out" from the center, and any remaining convection "locked-down" by the increasing static stability, diabatic heating is removed from the high inertial stability region and an eye appears. All things being equal, this change in the radial distribution of heating should decrease a storm's overall heating efficiency, thereby retarding the intensification rate.

However, all other things are clearly not equal when an intensifying storm forms an eye. While it is

[5] The dynamical mechanisms responsible for eye formation are not discussed here, but most surely involve the remarkable property for the boundary layer Ekman pumping to maximize at a finite radius rather than at $r = 0$ (see Eliassen and Lystad 1977).

true that the development of an eye must necessarily remove diabatic heating from the center, significant heating still occurs between the inner edge of the eyewall and the radius of maximum winds. During intensification both the radius of maximum winds and the inner edge of diabatic heating tend to move inward in accordance with the convective ring hypothesis discussed by Willoughby et al. (1982, 1984a) and Willoughby (1990b). While the area of efficient heating may shrink in physical space, when viewed in potential radius coordinates, the "dynamic size" of the heated area may actually increase if the angular momentum surfaces move inward faster than the edge of the convective heating (Schubert and Hack, 1983). Since the reduction in the radius of maximum wind and the increase in tangential winds both act to dramatically shrink the local Rossby length in the eyewall, *the intensification rate of a storm increases as its spatial scale shrinks and its intensity increases.* This has been shown recently by Pendergrass and Willoughby (2009), who used a more general framework to solve the Sawyer−Eliassen equation for a piecewise-continuous balanced mean vortex which includes a realistic vertical shear. Their realistic vortex case (their Fig. 9a) shows that the tangential wind tendency experiences a rapid increase as the maximum wind crosses the 30–35 $\mathrm{m\,s^{-1}}$ threshold. As Shapiro and Willoughby (1982) note, this is the threshold at which a tropical cyclone tends to form an eye.

In addition to the effects of spatial scale and intensity, the eyewall heating rate likely increases as the eyewall organization improves. Thus, the storm concentrates its diabatic heating in the area where the inertial stability is most rapidly increasing. As a result, continued increases in the efficiency of the eyewall heating can offset the losses in efficiency which result from removal of diabatic heating from the eye. Neglecting other factors, it seems likely that the net effect of eye formation is to increase the storm's intensification rate.

3.7.3 Maturation of the warm core and approach to a steady state

As the storm continues to intensify and warm air overspreads the inner core, several factors begin to act against further intensification. First of all, rising air parcels require increasing amounts of energy to overcome the warmer temperatures aloft; this tends to hinder deep upright convection (Ooyama, 1969). Secondly, the increased static stability imposes an additional source of resistance to the secondary circulation. This tends to reduce the convergence of moisture and angular momentum into the inner core.

Both of these factors decrease the inner core heating, countering the increased efficiency gains which occur due to eye contraction. Eventually, the maturation of the warm core should cause the storm to approach a steady state. These negative influences may be minimized if the storm is able to concentrate the warming as high as possible, and as close to the center as possible (Mundell, 1990). The details of the vertical distribution of the warm core response depend on the influence of baroclinity, an effect which is not included in our mathematical framework, but which is likely very important (van Delden 1989 suggests that baroclinity enhances deepening rates when the maximum winds speed exceeds $30\,\mathrm{m\,s^{-1}}$). Eventually, the region of efficient heating in the eyewall collapses to a small finite area through which only a certain amount of mass flux can occur to drive diabatic heating. These ideas suggest that the ultimate intensity achieved by the storm may depend in part on the vertical and spatial distribution of the warm core and on the amount of diabatic heating which remains in the efficient region of the eyewall. This "dynamical limit" view of intensification is surely not the whole picture, but may offer further avenues of investigation by models of intermediate complexity.

3.7.4 Analogy to stratospheric sudden warming

Dr. T. Dunkerton (personal communication, 2009) has pointed out the existence of a useful analogy between the hurricane problem considered here and the stratospheric sudden warming problem considered by Matsuno and Nakamura (1979) and Dunkerton (1989). In the idealized hurricane problem the secondary circulation is driven by a "vertical delta surface" of diabatic heating, while in the idealized stratospheric sudden warming problem, the Lagrangian mean circulation is driven by an Eliassen-Palm flux convergence that is singular at a given height, i.e., by a "horizontal delta surface" that provides a "zonal force" which drives a transformed Eulerian mean circulation. An important difference between the two problems is that quasi-geostrophic theory is a useful dynamical framework for studying stratospheric sudden warming, but the gradient balanced vortex model is necessary for the highly curved, large Rossby number flows in hurricanes.

3.8 Concluding remarks

It has been known for several decades that one of the necessary conditions for hurricane development is that diabatic heating occur in the region of high inertial stability. Compared to past studies, the present study is unique in that it has analytically solved for the temperature tendency associated with a vertical delta surface of diabatic heating in a vortex with a simple radial dependence of inertial stability. The solutions emphasize the fact that diabatic heating in the low inertial stability region outside the radius of maximum wind is inefficient at generating a warm core, no matter how large the current storm intensity. In contrast, diabatic heating in the high inertial stability region inside the radius of maximum wind is efficient at generating a localized temperature tendency, and this efficiency increases dramatically with storm intensity. In other words, the present results emphasize that the vortex intensification rate depends *critically* on how much of the heating is occurring inside the radius of maximum wind. However, when a tropical cyclone reaches a minimum surface pressure of approximately 985 hPa and a maximum tangential wind of approximately $35\,\mathrm{m\,s^{-1}}$, an eye forms, and diabatic heating becomes at least partially locked out of the high inertial stability region. Thus, it can be argued that storms which continue rapid intensification after eye formation are those in which at least some of the diabatic heating persists in the high inertial stability region inside the radius of maximum wind. Our results suggest that the shrinking effect on the local Rossby length, due to the decreasing spatial scale and increasing tangential winds, compensates for the loss of efficiency due to eye formation.

In closing it is interesting to note that we have derived the Green's functions for the transverse circulation equation (3.11) and the geopotential tendency equation (3.21) in the special case of a resting atmosphere and the special case of a height-independent Rankine-like vortex. In these special cases the differential operators in (3.11) and (3.21) simplify considerably. Obviously, it would be useful to obtain the corresponding Green's functions for a general baroclinic vortex. Such baroclinic Green's functions would aid in understanding the role of eyewall slope and in understanding how a steady state is approached as the ratio of $\dot{\theta}$ to P becomes constant along each absolute angular momentum surface. One approach to this more difficult baroclinic problem is to transform (3.11) and (3.21) from (r, z)-coordinates to either (R, z)-coordinates (where $\frac{1}{2} f R^2 = m$) or (r, θ)-coordinates. In both cases, the

operators on the left hand sides of (3.11) and (3.21) are considerably simplified, so that simple analytical solutions can be found.

Chapter 4

OBSERVATIONS OF HURRICANE EYE FORMATION. PART I: BACKGROUND AND DATA

> "Thus the 'point of no return' in hurricane formation is probably the appearance of the eye. Prior to that the warmest temperatures have their upper limit set by that of the undilute rain-band, and the lowest pressure (governing the inflow and wind development) is prescribed by that limit. Winds thus cannot reach speeds greater than about 45 mph. Once eye descent enhances the low central pressure beyond this point, velocities may wind up to hurricane fury in a few hours; the lid is off, so to speak, and indeed we wonder what sets the upper boundary to the intensification. The closed low central-vortex now dominates and takes over from the former easterly wave circulation; the storm acquires a girl's name; becomes the subject of radio broadcasts and intensive aircraft reconnaissance, and continues her baleful and much-publicized way: All this is apparently conditional on her ability to develop an eye!" — Joanne Malkus (1958)

4.1 Introduction

The formation of an eye has long been viewed as the hallmark of a storm that has reached hurricane intensity.[1] Long before the era of modern observations, sailors and coastal residents associated the eerie, central calm of the eye with the most ferocious of hurricanes. Ships unlucky enough to experience the eye firsthand, but fortunate enough to survive the encounter, have reported oppressive but calm air (or nearly so), little if any precipitation, breaks in the low clouds with blue skies or stars overhead, chaotic seas tumbling in every direction, and exhausted birds and butterflies. These clues led early researchers to surmise that the eye region must contain descending air (Ballou, 1892). As knowledge of the machinations of hurricanes increased, various workers pointed out that the hydrostatic pressure drop caused by the temperature rise from the latent heat of condensation is insufficient to support the

[1] In this dissertation, the term *hurricane* is used generically to reference any tropical cyclone whose maximum surface winds exceed $32\,\mathrm{m\,s^{-1}}$ (64 kt), while the term *storm* is used to reference a tropical cyclone of any intensity.

surface pressure drop found in a hurricane (Palmén, 1956) — the development of an extreme low pressure deficit requires adiabatic warming by forced subsidence in the eye (Anthes, 1982). High above the center, this 'warm core' of air results in higher pressures than in the storm's surroundings at a given height; this pressure excess pushes the storm's convective exhaust outward at upper levels, away from the center. Without such outflow, the low-level inflow would 'fill up' the storm center (Malkus, 1958b). So structurally, the formation of an eye paves the way for intensification and further organization of the storm. Observationally, the appearance and definition of an eye figure prominently in the very successful Dvorak technique for estimating a tropical cyclone's intensity using satellite imagery — the eye often develops when the storm nears hurricane strength (Dvorak, 1984). These concepts and observations lend support to the idea that hurricane structure and intensity are inextricably linked.

In addition to the observation that storms readily form eyes as they near hurricane intensity, several researchers have associated the formation of an eye with a period of rapid intensification. Malkus (1958b) brought forward the idea that a storm's intensity is limited to moderate tropical storm strength *until* the storm forms an eye. Once this structure is achieved however, the upper limit of intensity is set much higher by some other factor — she suggested that the formation of an eye may represent a 'point of no return' with regard to a storm's development and intensification. In his detailed study of Typhoon Doris (1958), Yanai (1961) expanded on this view by noting that the pressure did not drop rapidly until *after* the warm core had become established; i.e., the storm rapidly intensified once the eye had formed. Mundell (1990, p. 26, 31) studied 119 rapidly intensifying typhoons in the western North Pacific from 1956–1987 and found that most (87.4%) of these rapid intensifiers commenced their rapid rate of intensity change when the central pressure was in the range of 987 to 962 mb. Using the Atkinson-Holliday pressure-wind relationship (Atkinson and Holliday, 1977), this range of central pressures is equivalent to maximum sustained surface winds of 26 to 41 $\mathrm{m\,s^{-1}}$ (50 to 80 kt). Mundell states that "this range of initial intensities is significant because it closely approximates the point at which a tropical cyclone develops a central eye which is apparent on radar and satellite imagery (Weatherford and Gray, 1988b)."

Willoughby (1990b)'s study of convective rings offers further observational support to the idea that eye formation is associated with intensification. Expanding on the ideas discussed in Shapiro and Willoughby (1982), he used radial profiles of tangential wind and heights that convective rings are a

frequent mode of tropical cyclones and are often associated with strong intensification. The strongest height falls tend to occur just inside the radius of maximum winds, the region of high inertial stability.

Yet, the presence of an eye is not a guarantee that the storm will achieve a high intensity. Malkus (1958b) points out that many storms repeatedly attempt to form eyes, but do not succeed. When discussing the abortive or marginal eyes formed in Tropical Storm Alma and Hurricane Becky during the 1970 Atlantic hurricane season, (Robert) Simpson and Pelissier (1971) wrote that it is a fact, "well-known to the forecasters, that a radar eye is not a sufficient condition for the existence of a hurricane." They observed that it is not uncommon for one or more spiral bands to temporarily wrap themselves into an apparent eye that fails to persist. Much later, Joanne Simpson and coauthors advanced the view that mesoscale interactions leading up to eye formation are essentially stochastic in nature, with some interactions having a constructive effect, while others tend to disrupt the eye formation process (Simpson et al., 1997, 1998).

Putting the results of these previous studies together, some questions naturally arise. First of all, we might expect that adverse environmental conditions (e.g., vertical wind shear and proximity to land) play a key role in disrupting eye formation in some storms. If we can set these obvious factors aside, are there other environmental or internal structural differences between the storms which easily form eyes and those which do not? Secondly, what is the relationship between intensification and eye formation? Does the formation of the eye (and warm core) really precede significant intensification? Or is it a natural response to intensification? What structural and thermodynamic changes does a storm undergo during the eye formation process? Are there any commonalities amongst the cases which continue to rapidly intensify to major hurricanes (category 3 and above on the Saffir-Simpson Hurricane Wind Scale)?

This chapter[2] frames the challenge of observing eye formation and develops a strategy to do so from 20 y of aircraft reconnaissance data. The remainder of this chapter is organized as follows. Section 4.2 discusses the merits of a reconnaissance-based approach and lays out the conditions under which an eye is reported during surveillance missions. Section 4.3 documents the various data sets used in this study with particular focus on how the reconnaissance data has been transformed into a usable data set. Section 4.4 provides an overview of various intensity and structure parameters for the period of aircraft

[2] This chapter will be submitted for publication to *Monthly Weather Review* as Vigh et al. (2010a).

observations for all of the storms which were reconnoitered from 1989 – 2008. Section 4.5 offers some concluding remarks.

4.2 Observational background

4.2.1 Challenges

One of the longstanding challenges of studying hurricane eye formation is that most storms form an eye while well out at sea. The occasional ship, buoy, or island can provide surface data from which one may ascertain the storm's intensity or pressure deficit, but these data do not possess the spatial resolution necessary to characterize even the surface wind field, let alone the kinematic and thermal structure of the higher regions of the storm.[3] Time composites of radiosonde data (e.g., Jordan and Jordan, 1954) can reveal the upper regions of the storm, but these observations are generally too sparse over the oceans to study the inner core. Geostationary earth-orbiting (GOES) satellites provide frequent and detailed top-down views of the storm cloud structure, but the initial and intermediate stages of eye formation are very often obscured from satellite view by a central dense overcast which often precedes the appearance of an eye in satellite imagery (Dvorak, 1984; Zehr, 1992; Steranka et al., 1986). The advent of space-based radar and passive microwave radiometers remove this impediment by revealing the distribution of warm rain and ice particles in the storm. From imagery constructed from multiple channels, one can infer rainbands and the presence of an eyewall (if it exists) beneath the upper cloud shield. Because there are now many satellites with microwave radiometers, such a view of the storm's convective morphology is available every few hours (the time between overpasses typically ranges between 1 and 7 hrs). Despite these advancements, the intensity of storms which are observed only by satellites can be quite uncertain.

On the other hand, aircraft, with their on-board radar, *in situ* observations at flight level, and dropsondes, provide a much more definite characterization of both a storm's intensity and structure. Over the years, coordinated aircraft research missions have done much to advance the understanding of hurricane dynamics and energetics, but many of these campaigns have focused on intense storms which already possessed well-defined eyes (e.g. Hawkins and Rubsam, 1968; Hawkins and Imbembo,

[3] Although with some proper assumptions, one can deduce much about the upper thermal structure just from surface observations; see Haurwitz (1935).

1976; Jorgensen, 1984a,b). Only a handful of storms have been studied *in situ* during the period after genesis but before they formed an eye. This list includes Daisy in 1958 (Malkus et al., 1961; Riehl and Malkus, 1958), Isabel in 1985 (Stossmeister and Barnes, 1992), Irma in 1987 (Ryan et al., 1992), and Oliver in 1993 (Simpson et al., 1997, 1998). And of these, not all were well-observed during the actual period of eye formation. In addition to the dearth of good cases, the logistics of aircraft (e.g. crew rest requirements, limited fuel capacity, and the small number of aircraft) generally prohibit continuous research missions longer than thirteen hours (including ferry times to and from the storm, Henderson 1978). Yet the period of interest for eye formation may be closer to 12 to 24 h in duration,[4] so more frequent observations are needed.

4.2.2 Reconnaissance aircraft observations

The extensive aircraft reconnaissance over the last twenty years offers a veritable goldmine of data for studying storm structure and intensity. Whenever a storm threatens land in the Atlantic, Eastern Pacific, and Central Pacific basins, the United States Air Force Reserve's (AFRES) 53rd Weather Reconnaissance Squadron Hurricane Hunters[5] flies sorties primarily to determine the storm's location and intensity. The civilian National Oceanic and Atmospheric Administration Aircraft Operations Center (NOAA-AOC) planes are often tasked for dedicated reconnaissance missions as well. Due to the preponderance of Caribbean islands, the nearly land-locked Gulf of Mexico, and the vulnerable U. S. East Coast, storms in the Atlantic basin are normally reconnoitered every 6 to 12 h once they move west of 55° or 60°W. Before an impending U. S. landfall, storms may be monitored even more frequently. A typical reconnaissance mission flies an α-shaped pattern and penetrates the vortex center 4 times. The resulting meteorological data gathered during each "vortex fix" is transmitted in a Vortex Data Message (VDM). These messages provide a detailed but basic summary of the storm's gross kinematic and thermodynamic parameters every hour or two during the period the plane is in the storm (the contents of the VDMs will

[4] Theoretical work by Carrier (1971) suggests that the *e*-folding time for eye formation itself may occur on a much shorter time scale, possibly as little as 20 min. There are many instances of storms clearing out eyes (as observed in satellite imagery) in just a couple hours.

[5] Previously, reconnaissance was also conducted by the 54th, 55th, and 815th Weather Reconnaissance Squadrons (Henderson, 1978).

be described in further detail in section 4.3.5).

The instrumentation and data-gathering procedures of reconnaissance aircraft have undergone substantial improvements in recent years. During the 1970s and 80s, the determination of aircraft flight level winds relied on Doppler radar estimates of the plane's ground speed (see Henderson, 1978). During high wind conditions, these measurements were inherently uncertain due to the movement of the sea surface (Sheets, 1990). Much of the sensors had to be eye-balled by the flight meteorologist and converted to meteorological values using a hand calculator. The resulting data messages were transmitted by high frequency radio (personal communication, J. Talbot). By 1991, the onboard instrumentation and recording system of all AFRES WC-130Hs had been upgraded to the Improved Reconnaissance Weather System (IRWS, Gray et al., 1991). That system's superior inertial navigation system allowed flight level wind speed to be measured more accurately since the ground speed was known to greater certainty. The IRWS data system automated some of the data-gathering tasks and displayed the meteorological values onscreen. Data messages were prepared on a PC workstation and transmitted via a satellite communications link. Starting in 2001 the AFRES fleet was upgraded[6] to WC-130J aircraft with an even more advanced computerized data collection system which augments the Inertial Navigation System (INS) with Global Positioning Satellites (GPS). The new system includes angle of attack and side slip in its wind calculation so that flight level wind speeds are even more accurate, especially in light winds (personal communication, J. Talbot 2009). Much of the data gathering and data message generation tasks are now automated with the flight meteorologist providing quality control. The NOAA WP-3D research aircraft have undergone similar instrumentation improvements over the years (Jorgensen, 1984a; Griffin et al., 1992). Until recently, the surface wind speed on both the AFRES and NOAA planes was estimated visually by the sea state, but in 2005, the WP-3D planes were outfitted with an operational version of the Stepped Frequency Microwave Radiometer (SFMR, Uhlhorn et al., 2007); in 2008, SFMR sensors were installed on the entire AFRES fleet of new C-130J aircraft (Rappaport et al., 2009). These sensors allow for a much more accurate measurement of surface wind speed, allowing for more precise determination of the radius of maximum winds at the surface. As a result of these improvements (and

[6] The entire AFRES fleet had been upgraded to the new WC-130J aircraft by the start of the 2005 season (personal communication, J. Talbot 2009).

others not mentioned here), the last twenty years of Atlantic reconnaissance data are more accurate than were available to previous studies which used reconnaissance data from earlier eras. Previous landmark studies have examined general relationships of storm structure and intensity (e.g., Shea and Gray, 1973; Gray and Shea, 1973), while others have looked specifically at outer core strength and its relation to eye size (Weatherford and Gray, 1988a,b) and the associated climatology and statistical properties of these size parameters (Kimball and Mulekar, 2004). Yet others have focused on rapid intensification in considerable detail (e.g., Mundell, 1990; Fitzpatrick, 1996), but no study has yet explicitly examined the question of intensity and structure changes during eye formation. Thus, this study fills a unique void.

4.2.3 Definition for the aircraft eye

The keystone of this study is the use of reconnaissance aircraft to establish whether an eye was present or not for all time periods. This aircraft-only approach is important because reconnaissance aircraft have used a consistent and reliable method for determining eye presence over the entire 20-y period (1989-2008) studied in the current chapter and chapters 5 and 6. *An eye is only reported if a circular, precipitating, inner-cloud feature is observed to subtend at least half of the candidate eye region* (Weatherford and Gray, 1988b) on the aircraft's forward-pointing 3-cm (X-band) weather avoidance radar. If the eyewall feature completely encircles the eye region, a *closed eye* is reported. If the eyewall subtends at least 180° of the eye with no breaks, an *open eye* is reported. If the eyewall feature does not encircle at least half the central region, no eye is reported, but the flight meteorologist[7] may put a mention of *partial eyewall* in the remarks. As also described by Weatherford and Gray (1988b), to be considered an eyewall, the circular convective feature must also be distinct from the adjacent spiraling bands. If the convection is not separate from these bands, the descriptor *spiral banding* (or simply *banding*) is often given.

All of the AFRES C-130J and NOAA WP-3D aircraft have similar nose radars with comparable operating characteristics.[8] On this radar, the second reflectivity threshold level (31 dBz, yellow) is

[7] On the AFRES aircraft, the flight meteorologist duties are conducted by the Aerial Reconnaissance Weather Officer.

[8] The nose radar is subject to attenuation and cannot see behind the aircraft. Thus, the radar interpreter must keep in mind that attenuation may cause a symmetric eyewall feature to appear asymmetric before passing through to the eye. The NOAA WP-3Ds have a lower fuselage radar (and a tail radar) which gives better coverage, since it has a 360° view about the plane.

normally used to identify eyewall structure because reflectivity returns at the lower threshold (21 dBz) may sometimes occur from precipitation aloft or cloud features not part of the eyewall (personal communication 2009, J. Parish). Though this method of determining an eye is still subjective and relies on the judgment of the onboard flight meteorologist, it is more consistent than any other method available which possesses the frequency and reliability of aircraft reconnaissance observations. Apart from incremental improvements in radar technology (e.g., the C-130J aircraft now have a digital Doppler nose radar which is enhanced in many ways over the old system on the C-130H aircraft, personal communication, J. Talbot 2009), this general methodology of determining eye presence has not changed substantially since the 1950s.

4.2.4 Comparison between the aircraft eye and the microwave eye

Apart from limited horizontal resolution and the intermittency issues, space-based passive microwave radiometers are ideal for discerning the eyewall structure beneath the storm's cirrus canopy because small ice crystals are not strong emitters or scatterers at typical microwave frequencies (Glass and Felde, 1989). The 85-GHz channel is sensitive to scattering by *precipitation-sized* ice particles and is thus ideal for observing deep convection in the upper regions of the storm, including the eyewall and convectively-deep rainbands. The lower levels of a storm are dominated by rain precipitation, liquid cloud water, and water vapor. Since the 85-GHz channel saturates for liquid water paths greater than about 0.3 mm (Weng and Grody, 1994), it is not as useful for seeing structure at lower altitudes. On the other hand, the 37-GHz channel has enhanced sensitivity for liquid water paths in the range of 0 to 0.5 mm. Comparisons of 37-GHz brightness temperatures with rain rates derived from WSR-57 radars over the Gulf of Mexico show that the microwave brightness temperatures explain a large percentage of the variance of rain rates (Spencer et al., 1983; Spencer, 1986). Thus, the 37-GHz channel is particularly effective at resolving the low-level ring of thick clouds and rain which corresponds to the lower eyewall structure (Lee et al., 2002).

Once inside the eye, it can more easily verify whether the eyewall is symmetric and encircles at least half the eye. Thus, the WP-3Ds may have a somewhat better ability to detect an eye (personal communication, J. Parrish 2009).

Kieper (2008) examined the utility of 37-GHz microwave imagery for predicting rapid intensification (RI). In her study of 82 North Atlantic tropical cyclones from 2003-2007, 34 of these storms displayed the low level convective ring pattern at least once in their lifetime. These statistics include 7 cases of rings appearing more than once in a storm's lifetime, but exclude 7 cases which hit land within 24 h of displaying the ring pattern. Of the resulting 34 cases, 23 storms experienced rapid intensification[9] . The appearance of the ring pattern reliably indicated the beginning of all RI periods for these 23 storms. The other 11 storms which displayed the ring pattern did not undergo RI, however, often due to negative environmental factors. By requiring that the storm's intensity be at or above a minimum intensity threshold of 45 kt and that environmental conditions be conducive to intensification [by using the Statistical Hurricane Intensity Prediction Scheme (SHIPS) Rapid Intensification Index], a simple forecast RI scheme was developed which had a rate of success (95%), a low false alarm rate (5%), and a good probability of detection (83%).

Edson and Ventham (2008) have also examined the microwave imagery for clues to RI. They found that the formation of a convective ring around the wind center was a prerequisite to intensification. Like Kieper (2008), this ring did not have to be comprised of deep convection, as it was normally seen in 37-GHz imagery before showing up as a deeper convective ring in the 85-GHz imagery. They called it a "pre-eyewall" and noted that it seemed to be a key feature for storms commencing RI at an early stage (lower intensity). They also noted that a 'convective burst' within the ring signaled the start of RI in all of their cases (and was best seen in the 85-GHz imagery). When available, QuikSCAT surface wind observations often showed strong low level convergence into the inner convective ring.

4.3 Data sources and processing

This study uses several existing data sets, including the Best Track and Extended Best Track data sets, the SHIPS developmental data set, and also develops a new data set of storm structure parameters based on the VDMs. Additional information on the timing of eye formation is obtained through a subjective analysis of the infrared and microwave channels of satellite imagery. This section describes the characteristics of these data sets, how the eye is defined for the satellite imagery, and the processing

[9] Rapid intensification was defined as a 30 kt increase in the best track maximum winds over a 24 h period.

methods that will be used to obtain the results presented in chapters 5 and 6.

4.3.1 Best Track (BT) data set

The National Hurricane Center (NHC) maintains a data set of storm positions, wind speeds, and pressures for Atlantic tropical cyclones since 1851 (and for Eastern Pacific tropical cyclones since 1949). This storm information is synthesized from a post-season analysis of all available observational data[10] subject to the then-current observational practices and standards. The resulting "best tracks" contain the smoothed storm positions (latitude and longitude), storm intensities (estimated 1-minute maximum sustained surface wind speeds, in knots), and the minimum central pressure (hPa) of the storm for every 6 h (at 00, 06, 12, and 18 UTC) during its lifetime. Smoothing is necessary to remove small-scale fluctuations of the storm center which are unrepresentative of the path of the larger-scale circulation (Jarvinen et al., 1984). As observing technologies have advanced and more platforms have become available, the quality of the best tracks has generally improved over the years (for an extensive history of the best track data set, see McAdie et al. 2009). Over the years, changes in operational practice and knowledge of storm structure (e.g., improved understanding of reducing flight level winds to the surface as documented by Franklin et al., 2003) have also led to epochal variations in the quality of the best track storm positions and (especially) intensities.

The original best track data set (HURDAT) consists of one file containing just the positions, intensities, pressures, and storm type (e.g., tropical storm, hurricane, non-tropical, etc.) for each storm, as well as some very brief summary information on landfalls (Jarvinen et al., 1984). More recently, the Automated Tropical Cyclone Forecasting (ATCF) System has been implemented and used by various tropical prediction centers including the Joint Typhoon Warning Center and NHC (Miller et al., 1990; Sampson and Schrader, 2000). The ATCF file format for storing best tracks[11] is capable of also storing

[10] From McAdie et al. (2009), these data include surface observations from ocean buoys, land stations, and ships; upper air measurements from radiosondes; aircraft reconnaissance; coastal radars; and space-based polar-orbiting and geostationary satellite measurements of the cloud field in the visible and infrared channels, the distribution of hydrometeors as seen by the active radar on the Tropical Rainfall Measuring Mission satellite (TRMM, Kummerow et al. 1998) and passive microwave sensors, thermal profiles from the Advanced Microwave Sounder Unit (AMSU, Kidder et al. 2000), and the surface wind field from spaced-based scatterometers such as QuikSCAT.

[11] The ATCF best track files are called the "b-decks", while the files containing the operational model guidance are called the "a-decks". The combined abr-deck format is described at:

Table 4.1: A summary of Best Track parameters used in this study. The first column gives the symbolic notation used in this and the following chapters, the second column gives the parameter description, and the third column gives the native units of the data set.

Best Track Parameters		
Parameter	Description	Units
BT LAT	Latitude of Best Track storm center	degrees North positive
BT LON	Longitude of Best Track storm center	degrees West positive
BT $p_{\min}$	Best Track minimum sea level pressure	mb
BT $v_{\max}$	Best Track 1-min maximum sustained surface wind speed	kt
BT $r_{\max}$	Best Track radius of maximum winds at the surface	n mi

size parameters which specify the storm's wind profile, such as the radius of maximum winds, the radius of the last closed isobar, the pressure of the last closed isobar, and the radii of 34, 50, and 64 kt winds in each quadrant of the storm. Some other important information is also stored, including the storm type, the level of development (tropical, extratropical, subtropical, wave, disturbance, etc.), and the radii of various wave height thresholds in each quadrant of the storm. Table 4.1 summarizes the BT parameters used in this study.

This study uses NHC's archive best tracks[12] to establish the storm's position, maximum sustained wind speed, minimum sea level pressure, and radius of maximum wind. It is important to keep in mind that these BT data are best estimates which are inherently smoothed in time. Throughout chapters 5 and 6, trends in BT quantities will be compared with trends computed from the directly-observed VDM quantities.

4.3.2 Extended Best Track (EBT) data set

NHC's archive best tracks (b-decks) do not include the additional size parameters prior to 2001, so the Extended Best Track (EBT) data set[13] is used to supplement the BT radius of maximum wind values back to 1989. The base data of the EBT data set are obtained from the best track and operational

`http://www.nrlmry.navy.mil/atcf_web/docs/database/new/abrdeck.html`.

[12] The NHC archive best tracks are available for download at:
`ftp://ftp.tpc.ncep.noaa.gov/atcf/archive/`.

[13] The Extended Best Track data set and accompanying documentation may be downloaded at: `http://rammb.cira.colostate.edu/research/tropical_cyclones/tc_extended_best_track_dataset/`. This data set was prepared by M. DeMaria with partial support from the Risk Prediction Initiative.

advisories containing wind radii information from the databases maintained in the Automated Tropical Cyclone Forecast (Sampson and Schrader, 2000) databases at the National Hurricane Center and the Joint Typhoon Warning Center (Demuth et al., 2006). The EBT parameters not contained in the BT data set have come from operational data sources including ship and buoy observations, aircraft observations (when available), satellite-derived measures, and operational analyses. As such, the EBT is a composite data set derived from sources of varying quality, so the extra EBT parameters have *not* necessarily benefited from any post-season analysis (Demuth et al., 2006). Some of the radius of maximum wind values are simply the values chosen by the duty forecaster for the purpose of initializing the bogus cyclone in the operational numerical models [14] Thus, these values do not always reflect fidelity to the forecaster's best estimate of the actual radius of maximum wind in the storm. It should be noted that the EBT data set does contain an estimate of eye diameter, and could therefore have been used to determine eye presence as was done in the detailed climatological study of storms size in Kimball and Mulekar (2004). These values are not only given during periods when the storm was observed by aircraft, but also during periods when the storm was only observed by satellite. However, since the aircraft estimates normally supersede the satellite estimates, the definitions for an eye and its diameter are not consistent in the EBT data set.[15]

4.3.3 Statistical Hurricane Intensity Prediction Scheme (SHIPS) Developmental data set

A secondary goal of this study is to determine whether hostile environmental conditions can be implicated in cases in which an eye forms but fails to persist. Since the statistical-dynamical SHIPS forecast aid incorporates a wide array of environmental, satellite, and model-based parameters to make skillful predictions of tropical cyclone intensity (DeMaria and Kaplan, 1994, 1999; DeMaria et al., 2005), the developmental data set on which its predictor relationships are developed provides a convenient way for studies such as the present one to access information about the changing environmental conditions for

[14] These r_{max} values are actually stored in the a-decks. In the vast majority of cases, these values have simply been copied over to the b-decks by the ATCF system (personal communication, B. Sampson 2010).

[15] Indeed, the desire for a consistent and stable definition for when an eye was present is a primary motivator behind the aircraft-only approach of the current study.

Table 4.2: Summary of a subset of the SHIPS environmental parameters.

SHIPS Environmental Parameters		
Parameter	Description	Units
VMPI	Maximum Potential Intensity from Bister and Emanuel (1998)	kt
RSST	Reynolds SST	°C
E000	1000 mb θ_E (200-800 km average)	Kelvins
D200	200 mb divergence (0-1000 km average)	10^{-7} s^{-1}
T200	200 mb temperature	°C
SHDC	850-200 mb shear magnitude with vortex removed (0-500 km average)	kt
VVAV	Average (0 − 15 km vertical velocity of a parcel lifted from the surface accounting for entrainment, ice phase, and condensate weight	m s^{-1}

past storms. This data set[16] covers all NHC-designated tropical cyclones (1982-2008) which reached at least tropical storm intensity in the Atlantic and Eastern Pacific basins. Unnamed Atlantic depressions are also included back to 1989. For the period 1982-2000, the predictors are derived from NCEP Reanalysis fields.[17] From 2001 onward, the predictors are obtained from the operational analyses and forecasts of the real-time runs of the Global Forecast System (GFS) model. Approximately 50 predictors are available from 0 out to 120 h at 6-h intervals relative to the time and date of each particular case.

This study only uses a small subset of these predictors to ascertain the favorableness of the storm environment at $t = 0$ h (the analysis time of the operational model; no model forecasts are used here). The most important environmental parameters are vertical wind shear and some gross measure of convective instability. There are several options for computing the convective instability from these SHIPS quantities. One option is to estimate the instability by proxy from the environmental values of SST, the 200 mb temperature, and the low level θ_E. Alternatively, a parcel-based calculation can be undertaken to compute the convective instability. A third option is to use the Maximum Potential Intensity (MPI) calculation of Emanuel (1988). Table 4.2 summarizes the SHIPS parameters used in this study.

[16] The SHIPS developmental data set and additional documentation may be downloaded at: `http://rammb.cira.colostate.edu/research/tropical_cyclones/ships/`.

[17] It should be noted that the relative humidity predictors from the NCAR reanalysis (1982-2000) are biased low by perhaps 10% (personal communication, M. DeMaria, 2009).

4.3.4 Cooperative Institute for Research in the Atmosphere (CIRA) GOES IR satellite archive

The CIRA GOES IR archive includes Atlantic tropical cyclones from 1995 to the present and consists of brightness temperatures from the IR channel 4 (10.3 μm) in a window centered on the moving storm center. To provide a comprehensive cloud-top view of the storm during eye formation, 60,574 images were generated from the brightness temperature data. The IR cloud fields of these images have been subjectively analyzed to obtain the date/time and coldest brightness temperature anywhere in the scene for the following stages of development of the IR eye:

(1) *IR1: First open warm spot:* This stage is reported when a warm spot is first observed in the cold cloud shield – or a clear area was first noted near the storm center with surrounding convection. In either case, colder clouds or deep convection must surround the warm spot at least two thirds of the way around. Not infrequently, the IR satellite image of a storm may display a cold central cloud cover with a few warm pixels. In some cases (especially in the case of strong vertical wind shear), these are warm overshoots and are not believed to be dynamically significant to the process of eye formation. As such, these instances have not been classified as warm spots in this analysis. If, on the other hand, the warm spot is near the center and persisted for several images, then it usually has been classified here. The classification of this first stage is rather liberal, so as to pick up on the first clues of a possible developing eye. Thus, many of the IR1 classifications may be false alarms.

(2) *IR2: First closed warm spot:* This stage is reported when the warm spot was first completely surrounded by colder cloud tops. In the instance when a storm develops an embedded eye, the time of this stage sometimes coincides with the time of the first open warm spot. In some cases when the storm was developing an obvious embedded eye, the eye structure is quite obvious but the brightness temperatures thresholds of the first eye (IR3) stage are not satisfied. In these instances, the IR2 stage provides the first sign that an eye is developing. The analysis of this stage is less liberal than the IR1 stage.

(3) *IR3: First eye:* This stage is reported when a closed warm spot first exceeds $-50\,^{\circ}$C or is at least

15 °C warmer than the surrounding convection. At this stage, many (but perhaps not all) casual observers would agree that an eye has developed.

(4) *IR4: First persistent eye:* This stage starts at the beginning time point of an eye which persists for at least 6 h using the same criterion as the *first eye* stage. Once an eye persists, there is usually no doubt that an eye has formed amongst reasonable observers. Thus, this stage provides a definite confirmation that the storm has formed an eye. Because it is not known in advance how long the eye will last, this stage cannot be verified until the appropriate time interval has completed. In some cases in this analysis, the eye became ill-defined and may have not met the precise definition of an eye for an image or two. As long as the eye generally persisted and was still definite by the end of the 6 h period, this classification stage stood.

(5) *IR5: First strong eye:* This stage is reported when the warmest brightness temperature in the eye exceeds $-30\,^{\circ}$C *and* the eye is at least three quarters surrounded by a ring of convection with brightness temperatures colder than $-70\,^{\circ}$C. In general, the eye should be fairly symmetric. In some pinhole eye cases (e.g., Hurricane Opal in 1995), the storm was never classified with a strong eye because a pixel warmer than $-30\,^{\circ}$C could not be seen. In these cases, the satellite resolution and especially, zenith angle, could affect whether a strong eye classification is made.

In addition to the times and coldest brightness temperatures recorded for the above stages, a description of the storm is made at the time in which the aircraft eye was first reported, and the coldest brightness temperature in the scene is recorded. Finally, a general description of the storm morphology is made up until the time of definite eye development.

4.3.5 Vortex Data Message (VDM) data set

The VDMs contain a wealth of information about the storm's intensity and structure; these data form the backbone of this study. Each VDM contains data associated with a single vortex fix made by the aircraft. Once the fix center location has been determined, a VDM is transmitted back to the Chief, Aerial Reconnaissance Coordination, All Hurricanes (CARCAH) at NHC in near real-time, providing the operational forecasters with rapidly updated information on the storm. A detailed guide to decoding

the VDMs is available in Table 5-2 of the National Hurricane Operations Plan (2009, available online at: `http://www.ofcm.gov/nhop/09/nhop09.htm`), but for the convenience of the reader an example VDM from Hurricane Rita (2005) is given in Fig. 4.1 and decoded here (decoded values are indicated in parentheses). As a side note, this VDM was taken when Rita was near peak intensity. This VDM indicates that the maximum flight level temperature at 700 mb in Rita's eye was 31 °C at the time. The dew point at that location was −3 °C, resulting in a dew point depression of 34 °C. To the authors' knowledge, this is the highest eye temperature, the lowest dew point temperature, and the greatest dew point depression ever measured in a tropical cyclone at the 700 mb flight level.

VDM format

The first line of the VDM gives information about the mission including the message code (URNT12 indicates this is a VDM for a storm in the Atlantic basin), the supervising office (KNHC), and the day of the month and time that the message was transmitted (0739 UTC on the 22nd day). The next line indicates that this is a full VDM.[18] The main section of the VDM contains regular items preceded by letters from the phonetic alphabet.[19] Item ALPHA gives the day of the month (22) and the time (07:14:30 UTC) that the vortex center was fixed. Item BRAVO gives the latitude and longitude of this fixed storm center (hereafter, the term *fix center* references the location of the storm center as determined by the aircraft at the vortex fix time). The minimum height (2208 m) at a standard atmospheric surface (in this case, the 700 mb pressure surface) is given in item CHARLIE. The flight level variables reported in the remainder of the VDM are generally taken from this standard surface. Items DELTA and ECHO give the estimated maximum surface wind speed observed[20] on the inbound leg (not available in this case) and bearing and distance from the center to the location of the maximum surface wind speed, respectively. Item FOXTROT gives the direction (228°) and magnitude (148 kt) of the maximum flight level wind speed observed on the inbound leg. If a higher surface or flight level wind speed is subsequently

[18] Abbreviated VDMs are occasionally transmitted with some lines left out.

[19] Before modern satellite communications became available, VDMs were relayed by voice via shortwave radio, so unambiguous vocal identifiers were used.

[20] Before 2005, nearly all of the surface wind speed measurements were visual estimates based on the sea state. Starting in 2005, the SFMR was used to obtain these values from the NOAA WP-3Ds, and in 2008, operational SFMRs were installed on all of the AFRES C-130J aircraft.

```
URNT12 KNHC 220739
VORTEX DATA MESSAGE
A. 22/07:14:30Z
B. 24 deg 48 min N
  087 deg 46 min W
C. 700 mb 2208 m
D. NA  kt
E. NA  deg     nm
F. 225 deg 148 kt
G. 134 deg 013 nm
H.         899 mb
I.   9 C/ 3047 m
J.  31 C/ 3043 m
K.  -3 C/ NA
L. CLOSED WALL
M. C16
N. 12345/ 7
O. 0.02 / 1  nm
P. AF307 1618A RITA         OB 11
MAX FL WIND 165 KT NE QUAD 05:34:00 Z
STADIUM EFFECT VERY VISIBLE IN MOONLIGHT
FREQUENT LIGHTNING WITHIN EYEWALL
```

Figure 4.1: An example VDM from Hurricane Rita for the vortex fix taken at 0714 UTC on 22 September 2005. See text for further explanation of the VDM contents.

observed on the outbound leg, a corrected VDM is sent with the updated values noted in the remarks section. Item GOLF gives the bearing (134°) and range (14 n mi) from the fix center to the location of the maximum flight level wind.

Item HOTEL gives the minimum sea level pressure (899 mb) observed during the vortex fix. This value is either computed from a dropsonde (which may not fall in the exact center of the eye), or extrapolated from flight level. Item INDIA gives the representative maximum flight level temperature (9 °C) and the pressure altitude (3047 m) immediately *outside* of the eyewall or maximum wind band. Item JULIET gives the maximum flight level temperature (31 °C) and pressure altitude (3043 m) observed *inside* the eye and within 5 n mi of the fix center. If a higher maximum temperature is observed more than 5 n mi from the fix center, a supplementary maximum temperature reading is given in the remarks section.[21] Item KILO gives the dew point temperature at the location of the maximum flight level tem-

[21] A supplementary maximum temperature report provides a strong indication that the storm may have a *warm ring* structure, rather than a more simple warm core structure. Appendix C provides more information about how warm rings are defined and

perature (−3 °C) and the SST (not available in this case) observed by a downward-pointing radiometric thermometer.

Item LIMA describes the character of the eyewall. If the radar eyewall feature completely surrounds the eye, 'CLOSED WALL' or simply 'CLOSED' is given. If the eyewall feature surrounds at least 50% of the eye, but less than 100%, 'OPEN' is given and the direction of the break(s) will be indicated. If eyewall coverage is less than 50%, 'NA' is given to indicate Not Available and a mention of a partial eyewall or hub cloud may be given in the remarks section. Other characterizations may be given such as 'RAGGED' or 'POORLY DEFINED'. Item MIKE gives the eyewall diameter (16 n mi) and whether the eye was circular 'C', elliptical 'E', or concentric 'CO'. If the eye is elliptical, both the major and minor diameters are given as well as the orientation of the major axis. Likewise, if concentric eyewalls are observed, diameters for both the inner eyewall and outer eyewall are given. Item NOEL indicates the methods which were used to fix the center; these include penetration '1', radar-indicated banding or curvature consistent with fix center '2', wind '3', pressure '4', and temperature '5'. The fix level is also given (700 mb in this case) and whether the surface center and flight level center are the same. Item OSCAR gives the navigational accuracy (0.02 n mi) and meteorological accuracy (1 n mi) of the center fix.

Item PAPA gives remarks that enhance or supplement the regular data items of the VDM. Five types of remarks are mandatory and must always be given if conditions warrant. The first required remark is the mission identifier, which includes the agency and aircraft number (AF307, an AFRES plane in this case), the mission and storm system indicator (the 16th sequential mission into storm number 18 in the Atlantic basin), the designated storm name or mission type (RITA), and the observation number for the current mission. The second required remark is the maximum flight level wind speed (165 kt) observed during the latest pass through any part of the storm, along with the time (05:34:00 UTC) and quadrant (northeast) of that observation. The third required remark is the maximum flight level wind just obtained on the outbound leg (if higher than the maximum from the inbound leg). The fourth required remark is the method of deriving the minimum sea level pressure (if extrapolated). The fifth required remark is the bearing and range of the surface center and/or the maximum flight level temperature if either of these are

---

includes a table of observed warm ring cases.

not within 5 n mi of the flight level center. In addition to these required remarks, the flight meteorologist may also provide optional remarks describing any other aspects of the storm which are unusual or which he/she thinks may be of use to the forecasters. These may include additional descriptors of the appearance of the eye, the presence of lightning, hail, or turbulence, and the presence of a secondary wind maximum in either the surface or flight level winds.

Processing of VDMs into a usable data set

The creation of a usable data set from the raw VDMs was an involved and time-intensive process. In total, 183 variables are derived from the contents of the VDMs, including all of the data from the regular sections, all of the data from the required remarks, and many of the more important free-form optional remarks. Since this data set has substantial applicability beyond this study, this subsection provides an overview of the procedures which have been used to automatically read and process the VDMs. Nevertheless, because a complete documentation of the code is beyond the scope of this dissertation (the code set itself comprises more than 30,000 lines which is roughly equivalent to 400 pages of text), the author recommends the code itself as the most complete source of documentation for the particulars on how the parameters from the VDMs are translated into the variables of this data set. For this purpose, the code has been modularized and documented internally.

Before data processing could be accomplished, it was first necessary to collect the VDMs from various sources. These sources include the 'old' and 'new' archives of reconnaissance data located on NHC's ftp and http servers[22] , an alternate archive maintained at Florida State University, and several archives maintained by Mark Zimmer and Steve Feuer. For several years of the study period, some VDMs from the pre-tropical storm stage may be missing. It also appears that a number of VDMs from NOAA research missions may be missing.[23] Once a common archive had been created of all available VDMs, the VDMs were organized into separate files by storm.[24] Many VDMs had to be "cleaned"

[22] NHC's old recon archive can be accessed at: `ftp://ftp.nhc.noaa.gov/pub/products/nhc/recon/`; the new archive can be accessed at: `http://www.nhc.noaa.gov/archive/recon/`.

[23] The missing NOAA VDMs may exist in hard copy form at AOC but they were not available at the time of this study (personal communication, B. Damiano 2008).

[24] These storm-organized VDMs have been made available to the research community at:

(by script) to remove non-printable characters. In total, the collected VDMs comprise approximately 133,000 lines.

To accomplish the task of reading, processing, and combining the resulting VDM contents into a usable data set, a program was written in NCAR Command Language (NCL[25]). Building an automated and robust code to accurately read the VDMs proved difficult and time-consuming for several reasons: VDM formats have undergone several changes over the years, the VDMs contain many irregularities and human-coding errors, and a great deal of string parsing is necessary to extract the desired data from both the regular sections and the free-form remarks. An alternative approach would have been to manually code the VDMs into a data set. This approach may actually have taken less time since it does not require teaching a computer how to interpret the intricacies and idiosyncrasies of the VDM format. Indeed, one previous study did use the manual approach. In his climatology of eye characteristics, Piech (2007) examined the aircraft reconnaissance data for 1989-2005 and chose to manually compile a VDM data set. Perhaps due to the tedious nature of this task, he only examined a subset of the VDM parameters (items DELTA, ECHO, FOXTROT, GOLF, and OSCAR are missing, as are the remarks). Most notably, his data set does not include the flight level wind data, which are essential to this study. His study also excluded VDMs for storms with an intensity less than 45 kt. Since this study focuses on the eye formation period which begins at or just below this intensity threshold, it was necessary to compile a completely new VDM data set. Thus, an automated strategy was undertaken to read and process the VDMs. This approach has several advantages, including consistency in translating VDMs for the entire data set – if a translation error is discovered, or one would like to include additional parameters, the entire data set can be regenerated relatively painlessly. Another advantage of an automated code is that this opens the door to predictive applications which can use these data in real-time. Finally, a code approach will allow the data set to be extended in future years with minimal additional effort. Thus, a robust code has been written to automatically read and process the VDMs.

Once the VDMs were collected, the processing from raw data to finished results are accomplished in four stages: (1) each VDM is translated; (2) all of the translated VDMs for a particular storm undergo

---

`http://euler.atmos.colostate.edu/~vigh/hurricanes/vdm/`.

[25] NCL is a free data processing and visualization language available for download at: `http://www.ncl.ucar.edu/`.

some initial processing, are combined with other storm data, and written out to a network Common Data Form (netCDF[26]) file; (3) all of the individual storm files are aggregated into one combined structure and intensity data set; and finally (4) additional post-processing and analysis steps are undertaken to arrive at the finished results, tables, and figures used in this study.

In the translation stage of processing (stage 1), each individual VDM is read and parsed to extract 183 VDM variables. Twenty of these variables are simply a copy of the raw data lines from the VDM. This information is included in the finished data set so that any future user can go back and check whether a particular VDM parameter has been read and translated correctly. Several more of the VDM variables are strings which have been parsed and expanded from individual data lines which contain multiple data items. The purpose for retaining these variables is again mainly for checking and debugging. Once the regular VDM data lines have been dissected into the expected data 'fields', these are parsed and read into the appropriate variables. Some basic checks are done at this stage (for instance, to ensure that expected units are present and that numerical items are in fact numerical). Many abbreviations have been used in the VDMs, some of which are mis-abbreviated or nonstandard. An 'abbreviation map' was created to expand all abbreviations into standard word sequences that the code keys off of. Because there were many non-standard spelling errors or human-coding errors (such as using the number '0' and the letter 'O' interchangeably), some additional logic was necessary to accomplish the full translation, or in some cases, offending VDM errors had to be corrected by hand. Several 'shorthand codes' in the VDMs (such as flight levels and fix methods) have been translated to more user-friendly variables. Finally, it should be noted that the VDMs use a combination of nautical units (knots, nautical miles, millibars) and SI units. To allow for more effective quality control of these data, all of the translated VDM variables of this data set retain the original units of the raw VDMs. The original units of the VDMs will be used throughout the current chapter and chapters 5 and 6. Note that $1\,\mathrm{kt} = 0.51444\,\mathrm{m\,s^{-1}}$, $1\,\mathrm{n\,mi} = 1.852\,\mathrm{km}$, $1\,\mathrm{mb} = 1\,\mathrm{hPa}$, and $^\circ\mathrm{C} = \mathrm{Kelvins} - 273.15$.

In the next processing stage (stage 2), the 183 VDM variables are read for all the vortex fixes for a given storm. Additionally, 14 BT variables are read from the NHC b-deck file for that storm and checked

[26] netCDF is a set of software libraries and machine-independent data formats that support the creation, access, and sharing of array-oriented scientific data. These libraries are freely available for download at: `http://www.unidata.ucar.edu/software/netcdf/`.

against the equivalent values from the EBT data set; if the BT and EBT values differ, the EBT value has been used.[27] Likewise, when the BT radius of maximum wind value is missing, the EBT value is used. The 57 SHIPS environmental and dynamical variables (at $t = 0$ h) for the storm are also read. The non-VDM data (BT, EBT, and SHIPS variables) are snapped onto a common time dimension which corresponds to the BT time points for that storm (normally these are every 6-h for the duration of the storm, however off-synoptic time points may be included at the times when a storm makes landfall). The VDM data, on the other hand, exist on an irregular time dimension determined by the fix times of the VDMs. Once the VDMs have been read into memory, several additional steps are necessary to sort and merge the VDMs. First of all, some VDMs do not contain the storm name, the storm identification string, or any other obvious way of associating a VDM with a particular storm.[28] Additionally, none of the VDMs contain complete date information: the month is missing, and many VDMs also do not contain the year. A combination of time and space matching has been used to ensure that a particular VDM corresponds to the known best track of a given storm. Once the complete date, time, storm, and storm number are known, a unique identifier is assigned to each VDM message. Using these identifiers, the messages are sorted chronologically by fix time. Any VDM of a given fix time which was subsequently corrected by another VDM of the same fix time is superseded by the values from the corrected VDM.

Special effort has been made to extract all of the available maximum wind speed information from each VDM. Up to four maximum flight level wind speeds may be reported in each VDM. These include the inbound maximum flight level speed reported in item GOLF, the maximum flight level wind speed reported in the remarks, the outbound maximum flight level wind speed reported in the remarks, and the secondary maximum flight level wind speed reported in the remarks. Most of the non-wind VDM variables do not have a date/time associated with them, so these other variables are assumed to

[27] The EBT values were preferred because some of the b-deck files do not contain all of the size parameters. In actuality, the b-deck files should serve as the 'final' authoritative best track. Apart from missing data values, very few differences were found between the two data sets. When values did differ, most instances were minor differences that resulted because the version of the EBT data set used here includes the provisional best tracks for 2008, whereas the b-decks from that year contain the finalized best tracks. Only two differences were found for the parameter of $r_{\max}$, and these were both in Eastern Pacific storms.

[28] The storm name is always included in the VDM once a storm has reached tropical storm intensity, but depression-stage or 'INVEST' (investigations of suspect areas) VDMs are troublesome in this regard. In NHC's old VDM archive, the individual file names of the individual VDM messages provided the necessary association to match VDMs to the correct storms. In NHC's new VDM archive however, VDMs have not grouped by storm. Starting in 2007, the storm identification string is explicitly included in the VDM message, so VDMs from the depression stage onward are always associated with that storm. VDMs from the invest stage may still be missing.

be valid at the time the center fix was taken. In contrast, the maximum wind speed information usually *does* have a separate observation time. Not infrequently, one of the maximum flight level wind speeds given in the remarks section (which is supposed to be from the latest pass) is actually several hours old, but may be the highest wind speed value. If one were to simply choose the highest wind speed, more recent wind information would sometimes be replaced (and therefore lost) by old wind information which was already included in the data set at a previous fix time. To prevent this from occurring, the date/time of every maximum wind report was determined (if possible) and the values were compared. The "combined" maximum wind speed value was stored at its indicated time (which does not necessarily correspond to the fix time). The individual maximum wind speed values are also retained so that no information is excluded. A similar method was used to arrive at a combined maximum surface wind speed.

The final part of stage two involves the calculation of derived quantities from VDM and BT data. These derived variables include the Coriolis parameter for the storm location, the minimum Rossby radius of deformation (calculated from the maximum wind speed and the associated radius of this maximum wind) at the surface and at flight level, the associated dynamical eye size, and the difference between the radius of maximum winds and the eye radius. All of the VDM, BT, EBT, and SHIPS variables (276 variables in total) for a particular storm are written out to an individual netCDF file. Table 4.3 provides a summary of many of the VDM parameters and the notation that will be used through the remainder of this chapter.

The aggregation stage (stage 3) involves reading in the 276 variables for all of the fixes and BT points of each storm and storing these in two-dimensional arrays (dimensioned by storm and either the number of fixes or BT time points). The combined arrays are then written out to one large netCDF data file approximately 469 MB in size (or 205 MB for just the Atlantic). The combined intensity and structure data set contains approximately 413,000 valid, nonmissing data values.

The post-processing and analysis stage (stage 4) accomplishes a variety of 'lower level' tasks before the final results are obtained. First of all, minimum and/or maximum values are determined and stored for the lifetime of the storm for a variety of flight level variables including the maximum wind

Table 4.3: A summary of some of the VDM-derived parameters commonly used in this study. The first column gives the symbolic notation which will be used in the remainder of this dissertation, the second column gives the parameter description, the third column gives the corresponding section that this variable comes from, and the last column gives the native units of the data set. The shorthand notation 'FL' indicates that the observation pertains to flight level.

VDM-derived Parameters			
Parameter	Description	VDM section	Units
FL SAS	Standard atmospheric surface of flight level for current fix	CHARLIE	mb or ft
FL $H_{\min}$	Minimum height of the flight level SAS observed inside the center	CHARLIE	m
surface $v_{\max,\text{in}}$	Maximum surface wind speed observed during the inbound leg of current fix	DELTA	kt
surface $r_{\max}$	Radius of maximum surface winds (range of surface $v_{\max,\text{in}}$ from center fix coordinates)	ECHO	n mi
surface $v_{\max,\text{out}}$	Maximum surface wind speed observed during the outbound leg of current fix	remarks	kt
surface $v_{\max}$	Combined maximum surface wind speed (may be a wind speed from a recent previous fix)	DELTA or remarks	kt
FL $v_{\max,\text{in}}$	Maximum flight level wind speed observed during the inbound leg of current fix	FOXTROT	kt
FL $r_{\max}$	Radius of maximum flight level winds (range of flight level $v_{\max,\text{in}}$ from center fix coordinates)	GOLF	n mi
FL $v_{\max,\text{out}}$	Maximum flight level wind speed from outbound leg of current fix	remarks	kt
FL $v_{\max}$	Combined maximum flight level wind speed (may be a wind speed from a recent previous fix)	FOXTROT or remarks	kt
VDM $p_{\min}$	Minimum sea level pressure (obtained by extrapolation or dropsonde)	HOTEL	mb
T_{out}	Maximum flight level temperature observed just outside the eyewall or maximum wind band	INDIA	°C
T_{eye}	Maximum flight level temperature observed within 5 n mi of center fix coordinates	JULIET	°C
T_{sup}	Supplementary maximum flight level temperature observed more than 5 n mi from center fix coordinates	remarks	°C
$T_{\text{d,eye}}$	Dew point temperature observed at same location as T_{eye}	KILO	°C
d_{eye}	Diameter of primary eye	MIKE	n mi
$T_{\text{DEP,eye}}$	Dew point depression in the eye at location and flight level of T_{eye}	calculated	°C
$\Delta T_{\text{eyewall}}$	Temperature difference between eye and outside eyewall ($T_{\text{eye}} - T_{\text{out}}$)	calculated	°C
FL $\lambda_{\text{R,min}}$	Minimum Rossby length computed from flight level $v_{\max,\text{in}}$ and flight level $r_{\max}$	calculated	n mi
Ξ	Dynamical eye size calculated from d_{eye} and flight level $\lambda_{\text{R,min}}$	calculated	dimensionless

speed, the radius of maximum wind, the primary eye diameter,[29] the calculated minimum Rossby radius, the calculated dynamical eye size, the dew point depression in the eye, and the horizontal temperature difference across the eyewall (defined as the difference between the maximum flight level temperature in the eye and the flight level temperature just outside the eyewall). The BT maximum surface wind speed and BT minimum sea level pressure are also stored. These data will be summarized later in section 4.4.

Next, the presence of an eye is determined for each fix time following the principles outlined

[29] Note that in the case of elliptical eyes, the major and minor eye diameters have been averaged together to obtain one diameter value. This average primary diameter is used in the tabulation of the maximum and minimum statistics, the calculation of the minimum Rossby radius of deformation, and the determination of the presence of an eye.

in section 4.2.3. For this study, an *aircraft eye* is considered to be observed if either of the following conditions are met:

- The eyewall completeness descriptor contains either ‘open’ or ’closed’.
- The aircraft reports an eye diameter descriptor (item MIKE) *and* the eyewall completeness descriptor (item LIMA) contains one of the following: ‘poor’, ‘weak’, or ‘ragged’.[30]

Since it is unclear how to interpret the eyewall definition descriptors ‘poor’, ‘weak’, and ‘ragged’ without additional information, this study assumes that cases correspond to valid ’open’ eyes *if* the eye was defined well enough to also report an eye diameter.

Reconnaissance missions are conducted at several different flight levels (e.g., 1500 ft, 925 mb, 850 mb, 700 mb, and a handful at 500 mb) with 850 mb being the most common flight level flown near the time of eye formation. In order to remove differences due merely to the data being on different levels, some adjustments are made to the wind speed and temperature data. This allows statistics and trends to be computed consistently, irregardless of flight level. First of all, the flight level wind speeds are reduced to surface equivalent wind speeds following Franklin et al. (2003). The following reduction factors were used for each flight level: 0.90 for 700 mb, 0.80 for 850 mb, and 0.75 for 925 mb and 1500 ft. These flight-level-to-surface adjustments allow the intensity of the storm to be directly compared to the best track intensity estimate.

It is important to note that flight level winds in this study have *not* been adjusted to a frame of reference centered on the moving storm. Due to trochoidal motions and other short-period fluctuations, such an adjustment would require a careful analysis of the motion of the storm’s flight level center, not just the motion vector calculated from the smoothed best track. Since our study’s focus is on the computation of trends, and we do not *a priori* expect a change in storm motion during the time of eye formation, the intensity trends calculated from these data should not be strongly affected by not taking storm motion into account. Storms typically move between 5 and 15 kt while forming eyes. Drastic changes in storm speed are often associated with a significant change in the storm environment, and

[30] Note that the occasional descriptors ‘broken’, ‘breaks’, and ‘semi-circle’ have already been mapped to the ‘open’ descriptor in this data set.

Table 4.4: The mean inner core thermal characteristics of all storms in the VDM data set.

Mean thermal characteristics of VDM data set				
Flight Level	# of fixes	Mean T_{eye}	Mean $T_{d,eye}$	Mean T_{out}
1500 ft	1198	24.5	22.7	23.3
925 mb	48	22.8	20.6	21.1
850 mb	1482	20.8	17.0	17.5
700 mb	2097	16.6	10.9	10.8
500 mb	7	9.3	8.3	7.2

would likely be accompanied by significant vertical wind shear. A storm is not likely for form an eye during significant storm accelerations.

The flight level temperature data are adjusted for some portions of this study. Rather than reducing the temperature values to the surface, which would be suspect due to the changing thermal stratification below the eye inversion, all flight level temperatures are adjusted to an equivalent temperature at the 700 mb. This adjustment is accomplished by determining the mean flight level temperature *inside the eye* for all study data at each flight level. The adjustment factor for a given flight level is calculated as the difference between the mean eye temperature at that level, and the mean eye temperature at 700 mb. That adjustment factor is then added to all the temperature values at that flight level. The adjustment factors used are given in Table 4.4. In most cases, 850 mb temperatures are being adjusted up to 700 mb.

4.4 VDM data by storm

From 1989-2008, a total of 4924 unique VDMs were available from 205 tropical cyclones in the Atlantic, Eastern Pacific, and Central Pacific basins. Table 4.5 provides a summary of all storms in the VDM data set (1989-2008) which underwent aircraft reconnaissance for at least two center fixes. In the table, the storm identification (STORMID) is used to uniquely identify storms. STORMID consists of an 8-character sequence which uniquely identifies a storm based on the basin in which it formed ('AL' for Atlantic, 'EP' for Northeast Pacific, 'CP' for Central Pacific), the final designated two-digit storm number it was assigned by the warning agency, and the 4-digit year in which the storm formed.

Table 4.5: Summary of all storms in the VDM data set (1989-2005) for which there are at least two vortex fixes. The BT values are summarized for the entire storm lifetime. All remaining VDM quantities are summarized only for the periods when the storm was under aircraft surveillance, so higher maxima and lower minima may have occurred during periods with no reconnaissance.The columns of this table are as follows: (1) designated storm name; (2) storm identification ('STORMID', see text); (3) number of aircraft fixes; (4) lowest BT minimum sea level pressure ($p_{\min}$, mb); (5) highest aircraft-observed flight level temperature measured within 5 n mi of the storm center fix (T_{eye}, °C; note that this maximum value is only computed from observations at the 700 mb) flight level; (6) lowest aircraft-observed dew point temperature ($T_{\text{d,eye}}$, °C; note that this minimum value is only computed from observations at the 700 mb flight level; also note that $T_{\text{d,eye}}$is measured at the location of T_{eye}); (7) highest aircraft-observed dew point depression measured at any flight level ($T_{\text{d,eye}}$, °C); (8) highest aircraft-observed horizontal temperature difference across the eyewall at any flight level, defined as $\Delta T_{\text{eyewall}}$, where $T_{\text{out}}$is the representative flight level temperature just outside the eyewall (°C); (9) highest BT maximum sustained surface wind speed ('VMAX BT', kt); (10) highest aircraft-observed maximum flight level wind speed ('VMAX FL', kt); (11) smallest flight level minimum Rossby length ($\lambda_{\text{R,min}}$, n mi); (12 and 13) smallest and largest radii of maximum wind as determined from location of the maximum inbound flight level wind speed ('FL RMW', n mi); (14) most complete eyewall stage; (15 and 16) smallest and largest primary eye diameters (n mi); and (17 and 18) smallest and largest dynamical eye sizes. Summary statistics follow beneath the main table.

				Max FL	Min FL	Max	Max	**Maximum**		Min	**FL**		Most	**Primary eye**		**Dynamical**	
		# of	BT	700 mb	700 mb	$T_{\text{eye}}-$	$T_{\text{eye}}-$	**wind speed**		FL	**RMW**		complete	**diameter**		**eye size**	
Name	STORMID	fixes	$p_{\min}$	T_{eye}	$T_{\text{d,eye}}$	$T_{\text{d,eye}}$	T_{out}	BT	FL	$\lambda_{\text{R,min}}$	Min	Max	eyewall	Min	Max	Min	Max
			mb	°C	°C	°C	°C	kt	kt	n mi	n mi	n mi	stage	n mi	n mi		
1	2	3	4	5	6	7	8	9	10	11	12	13	14	15	16	17	18
BARRY	AL031989	2	1005			2	1	45	48	21.6	10	15					
CHANTAL	AL041989	14	984			5	3	70	82	30.0	12	50	closed	5	25	0.1	0.4
DEAN	AL051989	18	968	18	7	10	7	90	84	14.3	10	90	closed	15	25	0.2	1.3
GABRIELLE	AL101989	29	937	19	10	7	7	125	139	15.8	20	95	closed	15	50	0.4	1.9
HUGO	AL111989	44	918	24	3	19	13	140	162	2.4	5	60	closed	6	40	0.2	4.3
IRIS	AL121989	12	1001			5	3	60	72	14.7	10	75	open	18	18	0.6	1.1
JERRY	AL141989	22	983			6	9	75	73	15.3	6	85	open	10	10	0.2	0.6
KAREN	AL151989	25	1000			6	5	50	65	18.3	8	78	open	10	10	0.4	0.5
ARTHUR	AL021990	12	995			18	9	60	87	7.7	6	70	open	9	9	0.8	0.8
BERTHA	AL031990	24	973	15	6	9	5	70	88	61.9	22	133	closed	21	50	0.4	0.4
DIANA	AL051990	13	980	15	7	8	7	85	111	10.9	13	83	open	28	30		
GUSTAV	AL081990	14	956	22	1	21	12	105	107	13.1	12	71	closed	23	40	0.2	1.5
KLAUS	AL131990	38	985			9	7	70	72	10.9	8	115	open	5	25	0.1	0.4
LILI	AL141990	12	987			5	3	65	76	45.7	10	70	open	25	25	0.5	0.5
MARCO	AL151990	16	989			5	3	55	62	19.6	5	28					
NANA	AL161990	24	989	14	2	15	7	75	89	3.4	2	40	closed	8	28	0.1	0.9
AKA	CP011990	2				1	1	55	39	36.5	26	83					
MARIE	EP161990	24	944			7	6	120	76	27.2	18	113					
BOB	AL031991	43	950	18	10	8	10	100	119	4.8	2	70	closed	9	22	0.1	1.9
CLAUDETTE	AL061991	18	946	19	11	8	9	115	115	5.7	5	39	closed	6	22	0.2	1.6
GRACE	AL111991	16				3	3	85	71	34.8	15	63	closed	25	35	0.3	0.7

continued on next page

Table 4.5: *continued*

Name	STORMID	# of fixes	BT p_{min} mb	Max FL 700 mb T_{eye} °C	Min FL 700 mb $T_{d,eye}$ °C	Max $T_{eye}-T_{d,eye}$ °C	Max $T_{eye}-T_{out}$ °C	**Maximum wind speed** BT kt	FL kt	Min FL $\lambda_{R,min}$ n mi	**FL RMW** Min n mi	Max n mi	Most complete eyewall stage	**Primary eye diameter** Min n mi	Max n mi	**Dynamical eye size** Min	Max
ANDREW	AL041992	64	922	22	3	19	12	150	170	3.5	2	89	closed	6	30	0.3	2.7
DANIELLE	AL071992	23	1001			14	5	55	77	32.7	7	100	open	10	15	0.1	0.2
EARL	AL091992	36	990			5	4	55	65	54.7	20	107	closed	10	10	0.1	0.2
ARLENE	AL021993	14	1000			3	2	35	42	60.6	21	115					
BRET	AL031993	11	1002			2	3	50	58	5.1	6	70					
CINDY	AL041993	10	1007			5	3	40	51	11.2	5	89					
EMILY	AL051993	59	960	15	4	10	8	100	132	11.2	5	87	closed	2	45	0.0	2.4
FLOYD	AL071993	5	966			5	3	70	58	29.7	9	138					
GERT	AL081993	15	970	18	8	10	9	85	101	28.3	29	90	closed	4	40	0.1	1.0
KEONI	CP011993	14		18	6	12	8	115	118	4.3	6	46	closed	10	30	0.4	5.0
FERNANDA	EP071993	16	934	16	10	6	6	125	94	27.8	24	101	closed	28	50	0.8	1.5
ALBERTO	AL011994	23	993			5	5	55	67	21.6	11	101	closed	12	25	0.1	0.9
BERYL	AL031994	9	1000			1	2	50	61	87.4	20	77					
CHRIS	AL041994	14	979	13	3	10	3	70	61	24.2	8	73					
FIVE	AL051994	13				4	2	30	44	11.1	4	75	open	40	40	0.5	0.5
DEBBY	AL061994	5	1006			4	4	60	66	26.8	15	42					
FLORENCE	AL111994	2	972	11	5	6	4	95	72	44.2	21	29	closed	30	30	0.5	0.6
GORDON	AL121994	50	980	15	5	9	9	75	96	2.9	2	105					
DANIEL	EP041994	8	993			5	4	55	49	13.0	5	53	open	30	30	1.0	2.1
EMILIA	EP051994	33	926	19	3	16	11	135	151	2.4	6	34	closed	10	45	0.4	5.8
GILMA	EP071994	21	920	22	7	14	12	140	113	3.8	6	49	closed	16	30	0.5	4.3
JOHN	EP101994	26	929	21	8	13	11	150	157	4.2	6	27	closed	15	35	1.6	4.2
KRISTY	EP131994	6	992	17	8	9	6	90	55	14.9	6	57					
ALLISON	AL011995	25	982	16	7	11	7	65	74	3.2	2	98					
BARRY	AL021995	4	989			2	2	60	79	28.3	11	41	open	35	35	0.6	0.9
CHANTAL	AL031995	40	991			12	8	60	67	8.5	3	105	closed	8	20	0.0	0.1
DEAN	AL041995	17	999			5	3	40	55	44.0	16	120					
ERIN	AL051995	44	974	14	6	12	8	80	92	13.6	6	102	closed	20	40	0.3	1.6
SIX	AL061995	6				3	1	30	38	22.1	7	60					
FELIX	AL071995	70	929	19	11	8	6	120	140	5.3	6	117	closed	10	70	0.1	3.1
GABRIELLE	AL081995	11	990			4	3	60	73	15.6	3	105					
IRIS	AL101995	49	957	21	7	14	11	95	94	3.7	3	106	closed	15	35	0.4	1.2
JERRY	AL111995	9	1002			2	7	35	45	87.2	15	88					
LUIS	AL131995	47	935	21	10	10	10	120	146	11.1	14	80	closed	20	58	0.4	3.1
MARILYN	AL151995	56	950	24	4	18	12	100	123	6.1	6	81	closed	10	40	0.1	3.3

continued on next page

Table 4.5: *continued*

Name	STORMID	# of fixes	BT p_{min} mb	Max FL 700 mb T_{eye} °C	Min FL 700 mb $T_{d,eye}$ °C	Max $T_{eye}-T_{d,eye}$ °C	Max $T_{eye}-T_{out}$ °C	**Maximum wind speed** BT kt	FL kt	Min FL $\lambda_{R,min}$ n mi	**FL RMW** Min n mi	Max n mi	Most complete eyewall stage	**Primary eye diameter** Min n mi	Max n mi	**Dynamical eye size** Min	Max
OPAL	AL171995	38	919	26	11	14	14	130	152	5.8	4	94	closed	5	30	0.1	1.6
ROXANNE	AL191995	72	958	20	7	11	10	100	111	9.1	4	108	closed	7	40	0.1	2.8
SEBASTIEN	AL201995	10	1001			6	3	55	50	6.5	3	97					
ARTHUR	AL011996	12	992			4	2	45	45	97.3	27	73					
BERTHA	AL021996	58	960	19	6	13	11	100	122	13.8	8	104	closed	12	35	0.1	1.7
CESAR	AL031996	15	990			5	4	70	74	19.9	24	88	closed	15	15	0.2	0.2
DOLLY	AL041996	18	989			5	5	70	78	14.0	8	92	closed	10	25	0.1	0.4
EDOUARD	AL051996	67	933	22	7	14	10	125	140	7.3	7	101	closed	10	60	0.1	2.8
FRAN	AL061996	71	946	18	8	12	8	105	114	10.8	7	86	closed	18	45	0.1	1.7
HORTENSE	AL081996	17	935	14	7	7	6	120	89	16.0	8	82	closed	6	18		
JOSEPHINE	AL101996	24	970			5	7	60	74	29.3	14	94	open	20	25	0.1	0.8
KYLE	AL111996	2	1001			2	1	45	49	15.4	8	14					
LILI	AL121996	35	960	18	9	8	9	100	112	6.4	3	77	closed	5	40	0.2	1.3
MARCO	AL131996	41	983	15	5	22	11	65	71	2.0	2	106	open	5	5	0.8	0.8
ANA	AL021997	4	1000			2	3	40	54	93.2	31	77					
BILL	AL031997	3	987			2	2	65	47	34.2	8	32					
CLAUDETTE	AL041997	8	1003			3	2	40	50	30.1	6	56	open	30	30	0.9	0.9
DANNY	AL051997	43	984			5	5	70	82	4.4	2	56	closed	6	20	0.2	1.4
ERIKA	AL071997	33	946	19	6	14	9	110	111	14.9	13	98	closed	10	55	0.1	1.8
LINDA	EP141997	4	902	15	14	1	4	160	84	36.7	25	43	closed	6	18	0.1	0.3
ALEX	AL011998	4	1002			2	0	45	43	130.4	35	66					
BONNIE	AL021998	75	954	21	9	8	8	100	116	6.2	4	102	closed	10	50	0.1	1.7
CHARLEY	AL031998	7	1001			3	1	60	71	29.0	7	93					
DANIELLE	AL041998	43	960	17	8	9	7	90	97	9.0	6	89	closed	8	20	0.1	1.6
EARL	AL051998	23	964	16	5	28	5	85	104	34.4	8	94					
FRANCES	AL061998	14	990			4	5	55	59	68.1	23	130					
GEORGES	AL071998	79	937	24	6	17	15	135	146	5.6	5	105	closed	12	65	0.2	5.0
HERMINE	AL081998	24	999			4	3	40	56	8.8	2	86					
MITCH	AL131998	48	905	22	5	17	12	155	168	2.9	6	94	closed	8	35	0.9	5.5
LESTER	EP141998	7	965	19	7	12	10	100	93	7.2	9	23	closed	15	20	0.9	2.4
MADELINE	EP151998	4	979	16	9	7	7	75	76	12.2	10	48	closed	10	15	0.7	1.1
ARLENE	AL011999	8	1006			1	2	50	55	114.8	45	107					
BRET	AL031999	42	944	20	9	10	9	125	134	5.1	2	102	closed	7	20	0.2	2.3
DENNIS	AL051999	84	962	20	3	14	12	90	110	23.3	10	111	closed	20	45	0.1	1.3
EMILY	AL061999	14	1004			4	3	45	55	3.7	2	45					

continued on next page

Table 4.5: *continued*

Name	STORMID	# of fixes	BT p_{min} mb	Max FL 700 mb T_{eye} °C	Min FL 700 mb $T_{d,eye}$ °C	Max $T_{eye}-T_{d,eye}$ °C	Max $T_{eye}-T_{out}$ °C	**Maximum wind speed** BT kt	FL kt	Min FL $\lambda_{R,min}$ n mi	**FL RMW** Min n mi	Max n mi	Most complete eyewall stage	**Primary eye diameter** Min n mi	Max n mi	**Dynamical eye size** Min	Max
FLOYD	AL081999	69	921	26	4	22	15	135	149	10.4	12	107	closed	17	50	0.4	2.6
GERT	AL091999	13	930	17	12	4	6	130	127	14.6	18	94	closed	18	35	0.2	2.1
HARVEY	AL101999	15	995			8	4	50	58	16.2	1	61					
ELEVEN	AL111999	12				3	3	30	44	27.4	11	176					
IRENE	AL131999	44	960			14	7	95	93	11.8	5	110	closed	3	20	0.0	0.4
JOSE	AL141999	31	979	23	6	13	14	85	99	10.5	7	106	closed	20	40	1.0	3.1
KATRINA	AL151999	5	999			11	3	35	43	25.0	16	52					
LENNY	AL161999	44	933	25	5	18	14	135	145	4.5	6	96	closed	15	55	0.8	6.1
DORA	EP071999	18	943	18	5	13	10	120	114	6.2	6	38	closed	18	30	0.5	2.9
EUGENE	EP081999	14	964	17	5	12	8	95	68	23.0	23	58	closed	18	40	0.3	1.0
FOUR	AL042000	6				2	2	30	47	19.7	6	33					
BERYL	AL052000	9	1007			4	4	45	55	38.1	20	89					
CHRIS	AL062000	3	1008			2	0	35	23	58.6	19	110					
DEBBY	AL072000	26	993	16	5	11	9	75	88	13.1	4	123	closed	15	25	0.4	1.4
FLORENCE	AL102000	22	985			9	6	70	79	32.3	12	119	open	3	25	0.1	0.1
GORDON	AL112000	29	981	19	2	16	13	70	89	3.9	3	75	closed	30	30	0.2	0.7
HELENE	AL122000	15	986			9	7	60	67	36.3	10	58					
JOYCE	AL142000	3	975			2	0	80	40	48.4	16	58					
KEITH	AL152000	34	941	25	2	23	16	120	133	4.2	4	87	closed	15	40	0.2	4.4
LESLIE	AL162000	11	973			7	6	60	52	53.7	9	124					
MICHAEL	AL172000	6	965			8	6	85	89	21.4	10	50	open	20	40	0.7	1.7
SUBTROP	AL192000	4	978			4	3	55	60	63.8	20	72					
DANIEL	EP062000	20	954	14	6	10	7	110	86	19.3	12	108	closed	15	30	0.6	1.0
ROSA	EP192000	2	993			4	3	55	46	27.9	15	15	closed	20	20	0.7	0.7
ALLISON	AL012001	3	1000			2	1	50	55	47.0	13	55					
BARRY	AL032001	30	990	18	6	12	7	60	66	13.2	6	105					
CHANTAL	AL042001	29	997			9	4	60	82	10.8	3	110					
DEAN	AL052001	2	994			1	1	60	65	11.3	4	36					
ERIN	AL062001	21	968	18	4	14	11	105	118	13.6	4	77	closed	28	50	0.8	2.0
GABRIELLE	AL082001	20	975	19	9	9	8	70	85	22.5	5	113					
HUMBERTO	AL102001	8	970	21	0	21	13	90	86	24.3	11	37	closed	20	40	0.6	1.5
IRIS	AL112001	30	948	18	7	9	8	125	134	0.8	1	53	closed	3	20	0.2	5.5
JERRY	AL122001	3	1004			5	2	45	56	22.2	22	70					
MICHELLE	AL152001	39	934	23	2	14	9	120	135	5.3	7	93	closed	9	50	0.6	3.0
JULIETTE	EP112001	6	923	19	12	7	6	125	131	3.0	3	9	closed	7	15	1.3	3.3

continued on next page

Table 4.5: *continued*

Name	STORMID	# of fixes	BT p_{min} mb	Max FL 700 mb T_{eye} °C	Min FL 700 mb $T_{d,eye}$ °C	Max $T_{eye}-T_{d,eye}$ °C	Max $T_{eye}-T_{out}$ °C	**Maximum wind speed** BT kt	FL kt	Min FL $\lambda_{R,min}$ n mi	**FL RMW** Min n mi	Max n mi	Most complete eyewall stage	**Primary eye diameter** Min n mi	Max n mi	**Dynamical eye size** Min	Max
BERTHA	AL022002	3	1008			2	2	35	47	64.0	13	34					
CRISTOBAL	AL032002	8	999			4	1	45	59	27.8	6	96					
EDOUARD	AL052002	23	1002			10	8	55	57	8.8	2	79					
GUSTAV	AL082002	22	960			5	4	85	91	17.0	5	112	open	18	35	0.2	0.6
HANNA	AL092002	26	1001			7	8	50	59	21.1	5	108					
ISIDORE	AL102002	73	934	23	9	13	11	110	122	5.0	5	158	closed	8	22	0.6	2.8
KYLE	AL122002	12	980			3	2	75	52	13.8	3	144					
LILI	AL132002	67	940	26	6	20	13	125	141	4.8	2	94	closed	8	25	0.3	2.5
KENNA	EP142002	4	913	19	6	13	11	145	146	2.1	4	30	closed	10	20	0.9	4.3
BILL	AL032003	8	997			2	5	50	66	33.7	10	94					
CLAUDETTE	AL042003	57	982	16	6	10	11	75	85	3.2	3	119	closed	9	40	0.3	2.6
SEVEN	AL072003	2	1016			3	1	30	24	77.7	14	45					
ERIKA	AL082003	16	988	16	8	8	7	65	67	5.3	1	101	closed	12	20	0.1	0.5
FABIAN	AL102003	30	939	22	10	12	11	125	140	7.3	8	35	closed	20	40	0.4	3.1
GRACE	AL112003	5	1007			8	2	35	40	46.9	7	136					
HENRI	AL122003	27	997			7	4	50	46	19.5	4	120	open	22	22		
ISABEL	AL132003	35	915	21	12	8	11	145	158	11.2	15	73	closed	20	60	0.3	2.7
LARRY	AL172003	23	993			7	6	55	66	11.2	6	92					
MINDY	AL182003	10	1002			8	4	40	54	8.0	3	93					
ODETTE	AL202003	10	993	14	8	6	9	55	60	12.6	2	49					
JIMENA	EP102003	12	970	19	4	15	9	90	71	21.1	6	57	open	18	20	0.5	0.5
OLAF	EP152003	2	987			7	6	65	64	14.4	12	57	closed	25	30		
ALEX	AL012004	25	957	19	8	11	9	105	105	20.6	10	118	closed	10	60	0.3	1.2
BONNIE	AL022004	29	1001	13	6	10	7	55	72	6.7	3	91	closed	8	20	0.2	0.8
CHARLEY	AL032004	39	947	20	6	13	11	125	148	0.8	1	84	closed	5	40	0.3	5.5
FRANCES	AL062004	73	937	24	5	17	14	125	138	6.4	8	97	closed	12	60	0.2	3.3
GASTON	AL072004	4	986			1	3	65	60	22.3	10	27	closed	35	42	0.8	0.9
IVAN	AL092004	107	910	24	7	12	13	145	161	2.3	4	44	closed	6	60	0.4	4.4
JEANNE	AL112004	58	951	18	5	7	7	105	113	11.3	7	103	closed	10	60	0.3	2.1
MATTHEW	AL142004	10	997			5	4	40	50	11.8	2	75					
ESTELLE	EP072004	2	989			4	3	60	35	118.8	64	93					
ARLENE	AL012005	21	990			9	4	60	75	43.1	21	121	poor				
CINDY	AL032005	8	992			11	5	65	66	29.6	11	55					
DENNIS	AL042005	53	930	21	8	11	12	130	150	3.8	4	97	closed	8	30	0.0	2.7
EMILY	AL052005	68	929	23	4	19	16	140	153	2.9	4	99	closed	8	60	0.4	4.2

continued on next page

Table 4.5: *continued*

Name	STORMID	# of fixes	BT $p_{\min}$ mb	Max FL 700 mb T_{eye} °C	Min FL 700 mb $T_{\text{d,eye}}$ °C	Max $T_{\text{eye}}-T_{\text{d,eye}}$ °C	Max $T_{\text{eye}}-T_{\text{out}}$ °C	**Maximum wind speed** BT kt	FL kt	Min FL $\lambda_{\text{R,min}}$ n mi	**FL RMW** Min n mi	Max n mi	Most complete eyewall stage	**Primary eye diameter** Min n mi	Max n mi	**Dynamical eye size** Min	Max
FRANKLIN	AL062005	19	997			11	8	60	62	19.2	6	81	open	10	15	0.2	0.6
IRENE	AL092005	23	970			7	8	90	88	26.1	10	69	closed	8	80	0.1	0.9
KATRINA	AL122005	56	902	29	6	23	16	150	166	8.3	7	58	closed	6	50	0.2	2.1
NATE	AL152005	2	979	14	8	6	7	80	85	35.8	18	27	open	34	35	0.6	0.9
OPHELIA	AL162005	96	976	16	6	13	10	75	84	22.3	10	134	closed	10	90	0.1	1.0
PHILIPPE	AL172005	4	985	16	7	9	9	70	83	6.2	6	9	closed	16	20	1.6	2.4
RITA	AL182005	71	897	31	−3	34	22	155	165	4.9	7	92	closed	14	50	0.4	3.8
STAN	AL202005	12	977	18	7	9	9	70	69	5.4	2	111	open	16	16	2.0	2.0
TAMMY	AL222005	4	1001			1	3	45	53	190.0	75	143					
WILMA	AL252005	56	882	24	8	14	14	160	168	1.1	2	97	closed	2	75	0.1	4.1
BETA	AL272005	4	962	15	10	5	5	100	67	5.7	6	15	closed	10	15	1.1	1.6
GAMMA	AL282005	6	1002			2	6	45	49	16.1	8	77					
ADRIAN	EP012005	2	983			11	11	70	83	4.1	6	8	open	20	25	3.6	4.5
ALBERTO	AL012006	19	969	13	7	6	7	60	74	37.3	21	120					
BERYL	AL032006	19	1000			5	6	50	67	61.3	23	71	open	35	35	0.3	0.3
CHRIS	AL042006	32	1001			13	12	55	67	7.8	5	110					
ERNESTO	AL062006	55	985	14	3	16	8	65	78	6.6	3	99	open	6	25	0.2	0.5
FLORENCE	AL072006	13	963	17	7	10	9	80	96	44.7	27	73	closed	25	45	0.4	0.4
HELENE	AL092006	7	955	19	13	6	4	105	111	16.2	12	30	open	40	50	1.8	2.3
JOHN	EP112006	7	948	20	7	13	11	115	107	4.0	5	12	closed	10	15	1.0	2.8
LANE	EP132006	4	952	20	11	6	13	110	110	5.8	6	24	closed	8	9	0.2	1.3
PAUL	EP172006	4	970	18	7	11	6	90	88	7.6	9	27					
ANDREA	AL012007	2	998			6	1	65	39	212.8	71	78					
BARRY	AL022007	2	990			4	3	50	54	17.4	8	10					
DEAN	AL042007	47	907	23	9	12	12	150	165	2.9	5	86	closed	11	25	0.4	4.8
ERIN	AL052007	4	995			10	13	50	43	16.4	3	75					
FELIX	AL062007	23	930	26	4	22	17	150	162	1.7	3	52	closed	8	30	0.3	4.3
GABRIELLE	AL072007	13	1004			11	9	50	66	40.7	17	74					
INGRID	AL082007	2	1002				4	40	40	55.3	30	55	poor				
HUMBERTO	AL092007	4	985			27	10	80	79	7.9	4	10	closed	6	17	0.3	2.0
KAREN	AL122007	5	988	16	8	8	6	65	68	44.2	29	96	poor				
NOEL	AL162007	21	965	15	7	10	7	75	90	34.1	22	155	poor				
BERTHA	AL022008	8	952	13	5	8	5	110	99	45.3	34	78	closed	50	55	0.6	1.1
CRISTOBAL	AL032008	13	998			6	3	55	54	140.6	33	82					
DOLLY	AL042008	33	963	18	5	9	10	85	92	14.3	9	105	closed	11	25	0.2	1.0

continued on next page

Table 4.5: *continued*

Name	STORMID	# of fixes	BT $p_{\min}$ mb	Max FL 700 mb T_{eye} °C	Min FL 700 mb $T_{\text{d,eye}}$ °C	Max $T_{\text{eye}}-T_{\text{d,eye}}$ °C	Max $T_{\text{eye}}-T_{\text{out}}$ °C	**Maximum wind speed** BT kt	FL kt	Min FL $\lambda_{\text{R,min}}$ n mi	**FL RMW** Min n mi	Max n mi	Most complete eyewall stage	**Primary eye diameter** Min n mi	Max n mi	**Dynamical eye size** Min	Max
EDOUARD	AL052008	16	996			5	7	55	68	39.7	11	100					
FAY	AL062008	43	986	9	9	6	7	60	63	23.0	11	95	closed	8	50	0.2	0.8
GUSTAV	AL072008	56	941	23	5	16	12	130	143	8.4	6	93	closed	6	32	0.0	2.5
HANNA	AL082008	39	977			17	7	75	90	24.7	9	109					
IKE	AL092008	70	935	22	5	12	9	125	129	7.4	4	99	closed	4	60	0.0	2.6
KYLE	AL112008	14	984	19	4	12	6	75	82	32.7	12	90					
OMAR	AL152008	19	958	21	5	12	13	115	132	4.1	3	69	closed	10	32	0.8	2.7
SIXTEEN	AL162008	2	1004			2	2	25	34	8.3	3	105					
PALOMA	AL172008	27	944	23	5	24	16	125	142	5.8	8	77	closed	16	30	0.2	3.7
N		205	199	107	107	204	205	205	205	205	205	205		127	127	123	123
minimum		2		9	−3	1	0	25	23	0.8	1	8		2	5	0.0	0.1
maximum		107	1016	31	14	34	22	160	170	212.8	75	176		50	90	3.6	6.1
average		24.0	966.5	19.0	6.5	9.2	7.0	81.4	86.9	24.01	10.7	79.7		14.2	34.4	0.43	2.02
std. dev.		21.5	74.5	3.9	2.8	5.8	4.1	33.9	35.9	29.58	10.6	32.6		9.0	16.1	0.47	1.47

4.5 Concluding remarks

This chapter has laid the groundwork for the first extensive study of tropical cyclone eye formation using aircraft reconnaissance data. It has also presented an extensive summary of various aircraft-observed structure and thermodynamic parameters for the 205 storms which occurred in the Atlantic, Eastern Pacific, and Central Pacific basins from 1989–2008. The consistent aircraft-based method of determining when an eye is present proves key to the results which are presented in chapters 5 and 6. Chapter 5 explores the intensity characteristics near the time of eye formation, including the range of intensities at which an eye has been observed to form and the intensification trends that occur before, during, and after eye formation. Chapter 6 looks at the characteristics and changes of other structural and dynamic quantities during and after eye formation.

In the present study, it was earlier mentioned that two recent studies Kieper (2008) and Edson˙Ventham2008˙preprint had associated the appearance of a 'low level convective ring' with subsequent rapid intensification of tropical cyclones. This fact deserves more detailed consideration. Of particular interest is the timing between the appearance of an eye in microwave imagery and the first report of an eye by reconnaissance aircraft. Both platforms are essentially observing the same ring pattern, which is the storm's forming eyewall around a central area of reduced precipitation. Microwave observations suggest that the eyewall structure develops upward in time, as seen by the progression of the ring pattern first in the 37-GHz and then later in the 85-GHz imagery. At the same time, from the lower 37-GHz brightness temperatures in the center, one can infer that total column water vapor is already depressed in the center of the ring. Apparently, drying by central subsidence 'hollows' out the forming eye region even while the eyewall is still shallow. It seems plausible that the eye subsidence builds upwards over time in association with the vertically-deepening eyewall. Eventually, this subsidence reaches the top of the storm, clears out the cirrus shield, and reveals the formed eye in IR imagery. From an operational perspective, this latter milestone (a cleared eye in satellite imagery) has traditionally been the point when the storm was considered to have developed an eye. Aircraft eyes and microwave eyes have often been referred to in operational discussions as 'eye-like' features (personal communications, M. Kieper and J. Franklin 2010). According to the definition for eye formation proposed in chapter 2, and in light

of the operational definition discussed in the current chapter, both the aircraft eye and the microwave eye should certainly should be considered a bona fide eye. Since several past studies (Karyampudi et al., 1999; Hawkins et al., 2001) have noted that the eye often appears first in the microwave imagery and later in the visible and IR imagery, early recognition of microwave eyes as actual eyes could provide forecasters with a substantial early notice that strong intensification could be underway. Future work is planned to better establish the timing of this sequence of events using a combination of microwave, IR, and aircraft data. A goal will be to establish a timescale for eye formation and identify morphological precursors to both eye formation and rapid intensification.

In closing, we would like to point out other possible uses of the VDM data set that was developed in this chapter. Besides eye formation, these data can also be used to study other structural phenomenon in tropical cyclones, such as eyewall replacement cycles. A future paper will delve into the somewhat rare occurrence for the storm to take on a *warm ring* structure, as opposed to the more typical *warm core* structure. In that study, the VDM data will serve as a road map to a more detailed investigation with research-grade flight level data.

Finally, real-time VDM data may be eventually be used to enhance predictions of intensity, and to also predict structure and size changes. These prediction aids could be developed using statistical-dynamical methods (e.g., a 'SHIPS'-type model for structure change) or perhaps through simplified dynamical models of reduced complexity. Recently, Kossin and Sitkowski (2009) developed an empirical method to predict secondary eyewall formation using environmental and satellite parameters. They noted that their prediction method could be refined using the high temporal frequency aircraft reconnaissance observations, but did not attempt to do so because these were not available in a convenient form. The development of the VDM data set in the current chapter has now filled this gap. The inclusion of routine reconnaissance data in the future, such as recently added High Density Observations (HDOBS), should allow for even more structure data to be utilized in future research endeavors.

Chapter 5

OBSERVATIONS OF HURRICANE EYE FORMATION. PART II: INTENSITY RANGES AND CHANGES

> "[Those] who have an excessive faith in their theories or in their ideas are not only poorly disposed to make discoveries, but they also make very poor observations." — Claude Bernard (1813–1878).

5.1 Introduction

From 1989-2008, reconnaissance aircraft made a total of at least 4924 vortex fixes in 205 tropical cyclones in the Atlantic, Eastern Pacific, and Central Pacific basins. Since storms in the Eastern and Central Pacific basins do not often threaten land, they are not normally reconnoitered frequently enough to be of use for this study. Thus, the remainder of this study focuses on the 4662 unique Vortex Data Messages (VDMs) taken from the 180 tropical cyclones which occurred in the Atlantic basin during this period.

Chapter 4 gave the observational basis for using aircraft reconnaissance data to study eye formation and documented the data sources used herein. In the current chapter[1] we aim to quantify the intensity thresholds at the various stages of eye development for a broad set of Atlantic hurricanes. Another goal is to compute the intensification rates which occur before and after the time when the eye is first observed by reconnaissance aircraft and in infrared satellite imagery. This chapter is organized as follows. Section 5.2 explains how the eye formation cases have been selected and the method of calculating intensity trends. Section 5.3 provides a brief climatology of the selected eye formation cases. The intensity thresholds at which eyes have formed are tabulated in section 5.4, while section 5.5 calculates

[1] This chapter will be submitted for publication to *Monthly Weather Review* as Vigh et al. (2010b).

the intensification rates before, during, and after the time of eye formation. The role of environmental influences on eye formation is examined in section 5.6. Section 5.7 discusses the implications of these results, and section 5.8 gives some concluding remarks.

5.2 Methods

5.2.1 Case selection

The primary focus of this study are the intensity statistics and trends associated with the 72-h period before and following the first aircraft reconnaissance report of the eye in each storm's lifetime. We purposely neglect the issue of subsequent eye reformations so as to make our results applicable to the forecasting perspective of developing storms which have not yet formed eyes. In order to make the selection of cases as objective as possible, valid cases must satisfy the following dual criteria: (1) at least one aircraft fix must be taken prior to the first aircraft report of an eye, and (2) the time interval between the prior fix and the prospective eye formation fix can not be more 12 h. The first criterion ensures that an eye was not already present before aircraft observations commenced, while the second criterion excludes cases in which the eye may have actually formed a considerable length of time before the fix in which it was first recorded. Since this chapter seeks to calculate trends about the specific point in time when the eye is first reported, this guideline is a compromise between including as many cases as possible, but not allowing too much uncertainty as to when the eye actually formed.

To further stratify this study, eye formation cases are objectively classified[2] according to the duration and persistence of the initial eye (or subsequently reformed eyes) during the 72-h period following the first eye report by aircraft. For this study, an eye formation event is considered to be successful if the eye persists for $\geq$ 24 h; otherwise, it is considered to be a failure. These case categories are described as follows (the number of cases that fall in each category are indicated in parentheses):

(1) **No attempt (73)**: an eye was never reported in the storm during the period of aircraft observation (although it is possible that an eye formed at some other time).

(2) **Insufficient Data (37)**: the storm possessed an aircraft-observed eye for at least part of its

[2] While these criteria were made as objective as possible, two of the storms which were objectively classified as valid cases were deemed to lack sufficient aircraft data for the classification to be considered reliable. These storms (Gaston 2004 and Beta 2005) were moved to the "insufficient data" category.

lifetime, but either the initial eye formed before the period of aircraft observations began, it formed after observations ceased, or aircraft fixes were too infrequent to determine the time of formation to within 12 h.

(3) **Complete failure (17)**: the initial eye was reported for less than 24 h and then dissipated without further formation attempts.

(4) **Intermittent failure (24)**: an eye formed, dissipated, and subsequently reformed (possibly multiple times) without any of these eyes persisting longer than 24 h.

(5) **Delayed success (12)**: an eye formed and then dissipated, or was intermittent for a time, but eventually an eye formed and persisted for at least 24 h.

(6) **Complete success (17)**: an eye formed and persisted for at least 24 h without interruption.

5.2.2 Data masking

There are many possible reasons why a storm may fail at forming an eye, but two chief causes are landfall and high vertical wind shear. In order to remove the effect of periods when storms were influenced by land or experiencing high vertical wind shear, data masks have been constructed and applied so that the various intensity and structure data are set to "missing" so as to not influence the trend statistics presented later in this chapter. To determine the time periods when a storm was over land, the best track positions have been interpolated to 1-h intervals during the storm's lifetime. Then the distance to nearest land point is calculated from a coastline data set which includes major islands and continents. If the distance was negative, then the storm was over land and the land mask is set accordingly. A vertical wind shear mask has likewise been constructed from the SHIPS 'SHDC' environmental parameter so that data points can be excluded from the time periods when the storm was in a hostile vertical wind shear environment. Except where explicitly mentioned, the statistics of this chapter will be computed using the full unmasked intensity data.

5.2.3 Calculation of intensity trends

Due to the difficulty of computing trends from the noisy aircraft data, many past studies have used the best track intensity for trend analysis. The best track intensity estimates are comprised not just of aircraft data, but of all available intensity information. A human analyst integrates all of these data into a cohesive picture to construct a reasonable trace of storm intensity and track. Due to the standard 6-h time

interval used in the best track, and the subjective process of incorporating various data, the best track intensity inherently smooths the intensity signal. Rapid fluctuations on timescales shorter than 6 to 12 h are not preserved. This study computes intensity trends from both the best track intensity and from the reconnaissance aircraft data.

Several aspects of the reconnaissance aircraft data require careful attention in order to compute intensity trends. First of all, the aircraft fixes are taken at highly irregular intervals. While the plane is in the storm, fixes are typically taken every couple hours, but once the plane leaves, it may be 6 or 12 h, or sometimes even a day or more, before the next reconnaissance sortie. Apart from the irregular time sampling, another sampling issue also makes it difficult to construct a representative record of storm intensity from aircraft-measured maximum flight level wind speeds. Past researchers have noted that the reported maximum flight level wind speeds oscillate from fix to fix (e.g., Dvorak, 1984). This often occurs when a storm possesses a distinct wavenumber-1 asymmetry with intense convection and high winds on one side of the eyewall, and weaker convection and lighter winds on the other side. As the plane samples the storm at various azimuths in the usual α-shaped flight pattern, it often samples the strong and weak sides of the eyewall on alternating fixes.

To compute robust intensity trends, it is desirable to somehow smooth these rapid short-term fluctuations (which sometimes exceed 20 or even 40 kt), but still preserve the overall character of intensity change. A simple centered or weighted average is not useful here, because we do not wish to include information from the lower values – these values are not representative of the maximum storm intensity. What is needed, rather, is for some automated method to accomplish what a child could do — to connect the dots in an intelligent fashion so as to pick out the changes in the upper bound of storm intensity, while ignoring the noise of the lower points. To accomplish this, a filtering algorithm has been designed to eliminate all relatively low values while leaving only the points which essentially contribute to the upper bound of storm intensity.

The algorithm works by constructing sloping lines from the current point (c) to all remaining points (j) in the forward time direction (where $j = c + 1$ to N and N is the total number of fixes for a

storm). The formula for slope is the usual one:

$$\text{slope} = \frac{V_j - V_c}{t_j - t_c} = \frac{\Delta V}{\Delta t} \tag{5.1}$$

where V is the maximum flight level wind speed observed during each fix and t is the time of each fix. The basic idea is adjust the actual slopes in some fashion so as to assign a higher weighting to points which could contribute to the upper bound, while assigning lower weightings to points which do not contribute to this upper bound. The point which has the highest adjusted slope is then chosen as the 'survivor' out of the remaining points. Once the survivor has been identified, all points between the current point and the survivor point are eliminated (set to 'missing'). Then the algorithm steps forward, skipping past the just-eliminated points to the just-identified-survivor point. This becomes the new current point and the process repeats, a new survivor is identified, and so on. In this manner, all points which do not contribute to the upper bound are eliminated.

The formula for slope adjustment is as follows:

$$\text{slope}_{\text{adj}} = \begin{cases} \text{slope} \times \frac{6\,\text{h}}{\Delta t} - \frac{\Delta t}{9\,\text{h}\,\text{s}\,\text{m}^{-1}} & \text{if} \quad \text{slope} \ \geq 0 \\ \text{slope} - \frac{\Delta t}{9\,\text{h}\,\text{s}\,\text{m}^{-1}} & \text{if} \quad \text{slope} \ < 0 \end{cases} \tag{5.2}$$

This adjustment has a component which applies in all cases (whether the actual slope is positive or negative), and another component which only applies to points with positive slopes (i.e., to future points that have a greater intensity than the current point). The common adjustment component subtracts a linear factor from the slopes of all points. This factor is proportional to the time difference Δt between the current point and the jth point. The constant of proportionality of this subtractive factor is set equal to $\left[\,\text{m}\ (9\,\text{h}\,\text{s})^{-1}\right]$ so that the adjusted slope decreases by unity for every 9 h that the jth point is ahead in time from the current point.

For positive slopes, an additional adjustment is made: the actual slope is boosted or flattened *before* subtracting the aforementioned factor. If the jth point is 6 h or less from the current point, the slope is boosted. The degree of the slope increase depends on how close the point is (e.g., a point three hours ahead will have its sloped boosted by a factor of 2 while a point just one hour ahead will have its slope boosted by a factor of 6). When the jth point is more than 6 h from the current point, the slope is instead decreased. Points more than a day or two into the future have their slopes strongly

flattened towards zero. Once the slope has been boosted or flattened, the previously described adjustment component is subtracted. At the first and last points, the algorithm cannot be applied because there is not enough information. Instead, a simple check is done. If the slope from the first point to the next point exceeds $+6.67\,\mathrm{kt\,h^{-1}}$, the first point is eliminated. Likewise, if the slope from the next to last point to the last point is less than $-8.33\,\mathrm{kt\,h^{-1}}$, the last point is eliminated. This prevents spurious trends from arising due to unrepresentative end points.

This algorithm has the nice property that each point will normally be retained as long as the intensity of the storm is continually increasing. Thus, the resulting upper bound is capable of representing the parabolic upward curves that may occur as the intensification rate accelerates. When the intensity decreases however, the algorithm gives some additional weight to distant points which have a positive slope. This prevents sudden downward spikes to nearby low wind speed points which may not be representative of the upper bound. Because of the potential for long-period data gaps, the flattening of slopes toward zero for distant points, in conjunction with the subtraction of a factor proportional to Δt, ensures that the algorithm will not completely ignore intermediate points which are strongly suggestive of a decreasing intensity trend. This is because the subtractive component drags down the slopes of distant points more than nearby points, making it unlikely that the algorithm will 'jump' to a far point which would have otherwise had a positive slope. Without this subtraction, the algorithm would still ignore a nearby point that had a negative slope. The subtractive and boosting factors have been tuned to provide a reasonable balance between screening out the noise of low points, but still capturing significant downtrends in a timely and reasonable fashion. The resulting upper bound often corresponds well with the best track intensity curve, but is also able to capture the more rapid changes that occur when the intensity is in an uptrend. Since a storm is generally intensifying when the eye is forming, the upper bound produced by this algorithm should work well for calculating trend statistics.

Trend statistics for the intensity and structure parameters are calculated using the following observational baseline times:[3]

- **First aircraft eye (A):** the time of the VDM fix for which reconnaissance aircraft first reports any radar eye (open or closed).

[3] The full criteria for obtaining these baseline times are explained in chapter 4.

- **First open aircraft eye (A1):** the time of the fix for which reconnaissance aircraft first reports an open radar eye.
- **First closed aircraft eye (A2):** the time of the fix for which reconnaissance aircraft first reports a closed radar eye.
- **First open warm spot (IR1):** the time of the GOES IR satellite image when an open warm spot first appears near the storm center.
- **First closed warm spot (IR2):** the time of the GOES IR satellite image when a closed warm spot first appears near the storm center.
- **First eye (IR3):** the time of the GOES IR satellite image when an eye is first observed. To be considered a bona fide eye, the warmest eye brightness temperature ($T_{\mathrm{b,IR}}$) exceed $-50\,^{\circ}\mathrm{C}$ or be at least $15\,^{\circ}\mathrm{C}$ warmer than a nearby cold cloud top in the eyewall. Also, the ring of convection must be at least somewhat colder than the eye temperature all the way around.
- **First persistent eye (IR4):** the beginning point of the time period when the storm first maintains an eye (according to the criterion of IR3) for at least 6 h.
- **First strong eye (IR5):** the time when the warmest eye $T_{\mathrm{b,IR}}$ exceeds $-30\,^{\circ}\mathrm{C}$ and is surrounded by cold cloud tops colder than $-70\,^{\circ}\mathrm{C}$ for at least three out of four quadrants.

To compute the actual intensity trend from aircraft data, the upper bound maximum flight level wind speeds are linearly interpolated to a time grid which stretches from 72 h before the baseline time to 72 h after the baseline time in 6-h increments. The intensity trend for a given time is calculated by subtracting the interpolated intensity from that of the previous 6-h period. The best track intensity trends are calculated in a similar fashion.

5.3 Climatology of Atlantic hurricane eye formations

5.3.1 Frequency

Out of the 310 Atlantic tropical cyclones (including all named systems, tropical depressions, and designated subtropical depressions and storms) which occurred from 1989 to 2008, 180 had sufficient data to be included in the VDM data set. The CIRA IR satellite imagery archive covers a shorter period from 1995 to 2008, during which 204 storms occurred. Only 193 of these storms had usable satellite data however, because significant gaps in imagery occurred during key periods of some early storms. Table 5.1 shows the number of storms for various stages of eye development, as well as the associated frequencies of occurrence for each stage. All frequencies are computed by dividing the number of storms in each observing class by the total number of storms with valid observations for that particular observing

platform (i.e., 180 for aircraft and 193 for IR satellite imagery). Since this table seeks to estimate the true frequency of eye formations in the full population of Atlantic tropical cyclones, all aircraft data are included whether or not the storm was regarded as being under aircraft observation at the time of eye formation (so the insufficient data cases are included in this table).

An aircraft eye (A, open or closed)[4] was reported in 107 (59.4%) of these systems. This number should not be taken as an estimate of the true frequency of whether a storm will form an eye during its lifetime, however, since these statistics only apply to the storms which were sampled by aircraft. Storms may form eyes before or in between periods of reconnaissance and subsequently lose their eye before an aircraft is able to observe it; or the storm may form an eye as it recurves out to sea (after reconnaissance has ended because the storm is no longer a threat to land). Because of these factors, this number represents a lower bound on the true frequency of eye formation for Atlantic tropical cyclones.

The IR satellite imagery covers the entire basin and does not suffer from the data gap issues of aircraft, so the frequency of eye observations from this platform are more applicable to the broad population of Atlantic storms. An IR satellite eye (IR3) was observed in 118 (61.1%) of the systems which had usable IR imagery. Meanwhile, 82 (42.5%) of IR-observed systems developed a persistent eye (IR4) at some point in their lifetimes.

During the study period, 126 storms observed by both aircraft and IR satellite imagery. Of these, an aircraft eye was reported for 73 (57.9%) storms, while an IR3 eye was reported for 86 (66.7%) storms. An eye was observed by both aircraft and IR satellite imagery in 69 storms (54.8%).

5.3.2 Spatial distribution

Fig. 5.1 presents the spatial distribution of eye formations stratified by the case types described in section 5.2.1. Note that this climatology excludes cases in which the storm did not attempt to form an eye (73 storms) and cases for which there were insufficient aircraft data to determine the time of eye formation (37 storms). This leaves 70 storms out of the 180 aircraft-observed storms that were available. Each panel displays the best tracks which correspond to storms from one the four remaining case types: “complete failure”, “intermittent failure”, “delayed success”, and “complete success”. The

[4] The conditions under which an aircraft eye is reported are given in chapter 4.

Table 5.1: Frequency of various observations of eye formation for Atlantic tropical cyclones for various observing platforms. First group: aircraft-observed storms displaying banding. Middle group: aircraft-observed storms for which an eye was reported. Last group: various stages of eye development obtained from subjective classification of IR satellite images.

Frequency of Eye Formation

Code	Observational baseline	# of storms	
	Aircraft observations of banding		
B1	Banding without subsequent eye	16	8.9%
B2	Banding and subsequent eye	62	34.4%
B	Any banding (B1 ∪ B2)	78	43.3%
	Aircraft observations of eyes		
A1	Poorly-defined aircraft eye	3	1.6%
A2	Open aircraft eye	104	57.7%
A3	Closed aircraft eye	84	46.7%
A	Any aircraft eye (A1 ∪ A2 ∪ A3)	107	59.4%
	IR satellite observations of eyes		
IR1	Open warm spot	176	91.2%
IR2	Closed warm spot	147	81.7%
IR3	Eye	118	61.1%
IR4	Persistent eye	82	42.5%
IR5	Strong eye	41	21.2%

line segments of each track are colored to indicate portions of the track before and after the period of aircraft reconnaissance (black), data gaps of 18-h or greater within the reconnaissance period (white), periods when the storm was regularly reconnoitered but an eye was not reported (gray), periods of active reconnaissance when an open eye was reported (blue), and likewise, periods when aircraft reported a closed eye (red). Specific fixes when aircraft reported banding (but not eye) or poorly defined eyes are indicated by orange and green dots, respectively. Additionally, polymarkers indicate the locations when a storm first attained to the following stages in IR satellite imagery: open warm spot (IR1, hollow circle), closed warm spot (IR2, hollow square), first eye (IR3, filled square), first persistent eye (IR4, filled circle), and the first strong eye (IR5, filled star).

The first panel (Fig. 5.1a) shows the tracks of the 17 complete failure cases. These storms formed an eye which then dissipated in short order with no attempt at reformation. One cluster of irregular-looking tracks have their origins off the U. S. East Coast. These are suggestive of storms of subtropical origin, which tend to develop early and/or late season. These storms often have a well-defined surface circulation, but struggle to close off enough deep convection to be considered an eyewall. Several other

of these complete failure cases formed eyes but then their development was arrested when they made landfall on the Gulf Coast.

The second panel (Fig. 5.1b) displays the 24 intermittent failure cases in which a storm made several attempts to form an eye, but could not get an eye to persist for more than 24 h over the following 3-d period. Four of these cases formed eyes and were likely developing but then hit the Gulf Coast. Another subset of storms formed short-lived eyes near the Leeward Islands. The Tropical Tropospheric Upper Trough (TUTT) has a mean summer position in this area, so it is likely that the eye formations of these storms were disrupted by adverse vertical wind shear.

In the third panel (Fig. 5.1c), the 12 delayed success cases are shown. In these cases, a storm forms an eye which then dissipates after only a few hours, but within the next couple days an eye reforms and persists for at least 24 h. The broad sweeping tracks of these storms suggest a favorable upper level environment (an absence of shearing troughs or cold lows) and/or a mid-tropospheric steering ridge to the north which provides a consistent storm environment. It seems that even when environmental conditions are generally favorable, some storms may make several attempts at eye formation before succeeding. The final panel (Fig. 5.1d) shows the 17 complete success cases, in which a storm forms an eye on its first attempt and that eye persists for at least 24 h. Again, out in the Atlantic there are many straight-running or broadly-curving tracks suggestive of favorable environments. However, a significant cluster of storms originate in the western Caribbean and have odd or atypical recurving tracks. These tracks are from late season storms (e.g., Mitch 1998, Michelle 2001, and Paloma 2008) that rapidly developed and then recurved into the westerlies. Interestingly, in both this panel and in the third panel, there is a distinct absence of subtropical-looking tracks. During the subjective analysis of the IR satellite image archive, it was noted that many subtropical systems did in fact successfully form eyes in the Eastern Atlantic, but these storms do not appear in the present climatology because they were not reconnoitered.

It should be noted that land does not always prevent eye formation. On rare occasions, the increased surface friction over land may actually aid eye formation. Fig. 5.1b shows the track of Fay (2008) which hit southwest Florida just after forming an open aircraft eye. While over the south Florida mainland[5] a very distinct satellite eye appeared and persisted until after the storm moved back over wa-

[5] Granted, much of the 'land' in South Florida is rather marginal — consisting of the Everglades and Lake Okeechobee.

ter. Several other systems also seem to have formed their first IR3 eye while over land (see filled squares over the Yucatan Peninsula, Nicaragua, and the Mississippi River Delta).

5.3.3 Temporal distribution

We now turn our attention to the distribution of eye developments in time. In order to compare the eye formations of each storm to all the others, it is necessary to choose a common reference time point. Taking this point to be the time when each storm first reaches tropical storm intensity (the point when best track wind speeds first exceed 34 kt), we have subtracted these reference time from the baseline times observed for the various stages of eye development. The resulting timeline shows the relative timings of the various eye development stage for each storm in days since the storm reached tropical storm strength. These timelines have been grouped by case type and are shown in Fig. 5.2.

Examining the complete failure cases first, we immediately notice that many of these storms were only observed by aircraft for a few days and all of their eye formations were brief (which must be the case, by the definition of this case category). While many of these storms did form an IR3 eye (IR imagery are only from 1995 onward), none of them formed a persistent eye (IR4). While this case category does not include reformation cases, the scattered presence of banding (orange dots) indicates that some storms were trying to form (or attempting to maintain) an eye for an extended time period.

The storms of the intermittent failure cases generally lasted longer than the complete failure storms. Some of these cases did eventually form eyes which lasted longer than our 24 h criterion, albeit outside of the 3-d time window allowed from the first attempt. For most of these cases, aircraft initially reported an open eye; this suggests that the eye definition was somewhat marginal. Even though these cases were considered failures, a persistent eye (IR4) appeared in 3 of the 24 storms during the 3-d time window. Taken together, these timelines are suggestive of slowly developing systems which had difficulty forming an eye. Some eventually succeed, including Ophelia, which took nearly 8 days from the first hint of an eye (IR1) to a persistent eye (IR4). Notably, a strong eye was seen in just one storm in this group, so very few of these systems went on to become intense hurricanes.

The delayed success cases were longer lived, became more intense (nearly all eventually displayed a strong eye, IR5), and in some cases, showed signs of eye development a day or two before aircraft

observations began. This latter situation can occur if a storm in the east Atlantic has started to form an eye, but then takes a few days to come into aircraft range. Nevertheless, all of these storms had their eye developments interrupted by some factor. It appears that once the inhibiting factor was removed, the storms developed consistently and in some cases rapidly, seemingly no worse for the wear. Interestingly, some of these storms took longer to form eyes after reaching tropical storm intensity (even 3 or 4 days in some cases). This also bolsters the view that the environment or some other factor was not initially favorable for development.

In contrast to the delayed success cases, the complete success cases often formed eyes within a day of attaining tropical storm strength. In many of these cases, the first reported aircraft eye was closed. Not only did these storms form eyes quickly, but their eyes also tended to have better definition when they appeared. Some of these storms rapidly intensified, progressing all the way to a strong eye (IR5) within a day of first forming an eye. All of this evidence suggests that these storms developed in a very favorable environment. Another interesting aspect of the complete success cases is that quite a few storms displayed open or closed warm spots (IR1 and IR2) and even actual eyes (IR3) before reaching tropical storm intensity. These early formers may represent a special class of eye formation distinct from normal development. Perhaps the best example of an early former is Erin (2001), which formed an IR3 eye in the far east Atlantic just as it was designated as a tropical depression. A distinct warm spot surrounded by a ring of curved deep convection appeared and persisted for several hours before being obscured by deep convection. Erin still displayed some signs of eye structure for several more hours but then came under hostile vertical wind shear. Almost a week later, a persistent (IR4) eye formed and the storm continued developing into an intense storm.

5.4 Intensity thresholds for eye formation

Perhaps the most basic questions this study can address are: "At what intensity does the eye tend to form?" and "What are the ranges of intensities at which storms have formed eyes?" To find quantitative answers to these questions, each storm's best track maximum sustained surface wind speed (BT v_{max}) and maximum flight level wind speed (FL v_{max}) values are interpolated to the baseline times described

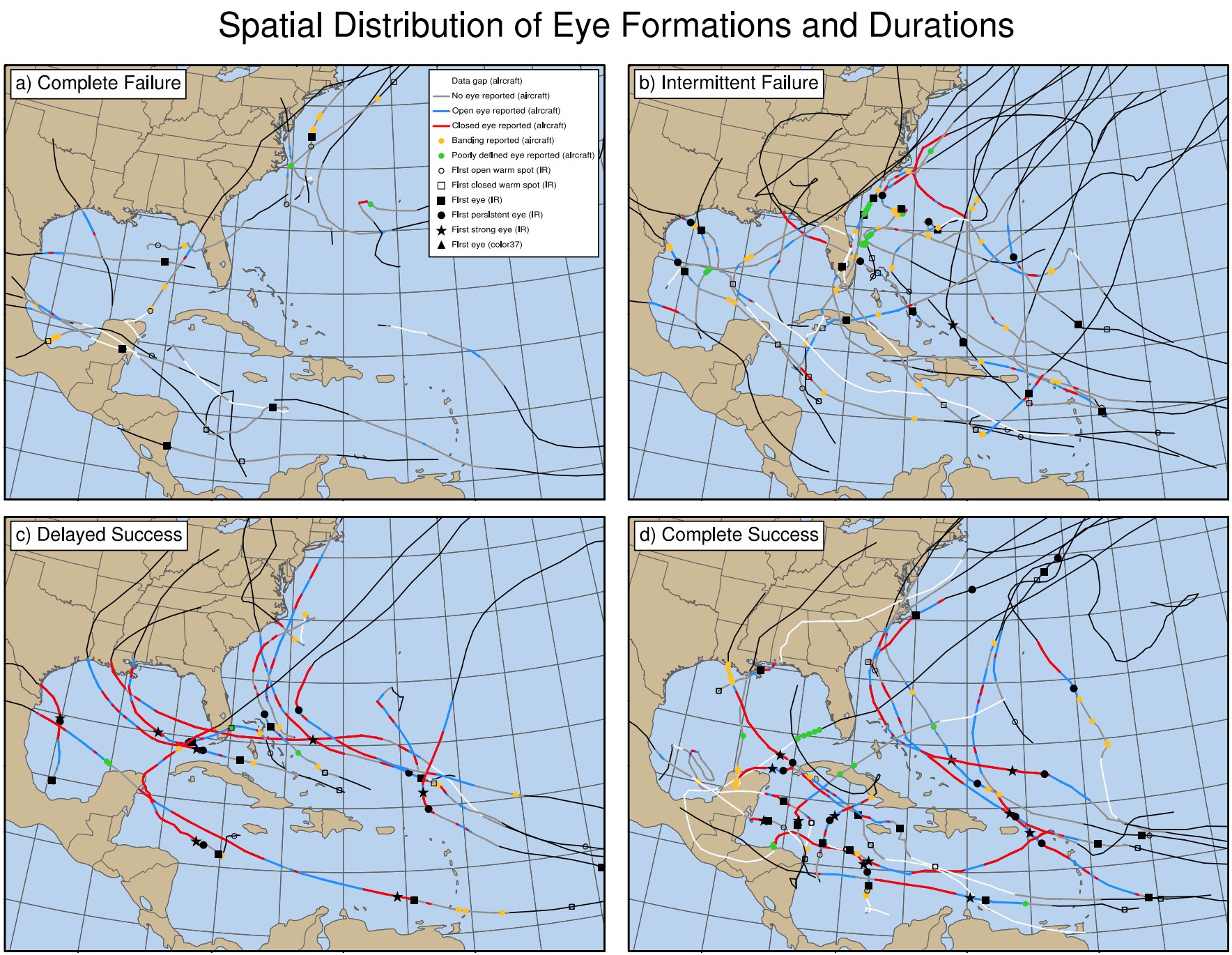

Figure 5.1: Spatial distribution of all Atlantic storms which formed eyes during the period of aircraft reconnaissance. See text for full description.

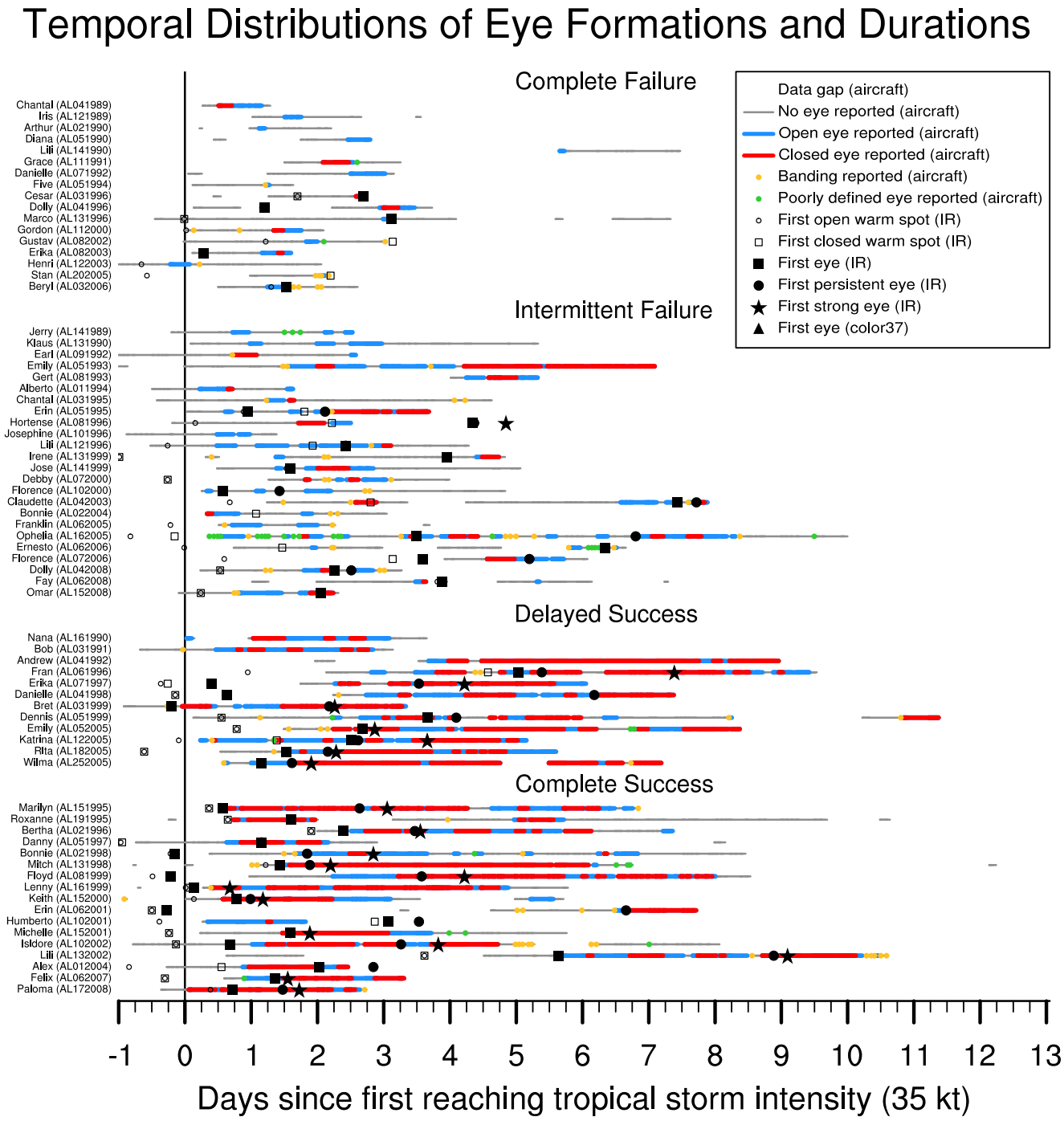

Figure 5.2: Temporal distribution of all Atlantic storms which formed eyes during the period of aircraft reconnaissance. See text for full description.

in section 5.2.3 (e.g., first aircraft eye, first IR satellite eye, etc.).[6] A statistical summary of the resulting distributions of intensity at each baseline is presented in Table 5.2. The first part of the table displays the summary statistics for the interpolated BT v_{max} values, while the second part of the table displays statistics computed from the interpolated upper bound of the FL v_{max} values which were first reduced to surface equivalent wind speeds (hereafter, these reduced aircraft wind speeds are denoted by 'rFL v_{max}').[7] No insufficient data cases are included in the statistics presented in this section. For the second part of the table, the upper bound rFL v_{max} are used, but only when the baseline time falls in between aircraft fixes no more than 12 h between the baseline time and each of the fix times. This criterion cuts the sample sizes significantly, but helps ensure that the interpolated values are representative of the storm intensity at that point in time. Box-and-whisker plots are provided in Figs. 5.3 (for BT v_{max}) and 5.4 (for rFL v_{max}) to visually illustrate the characteristics of the intensity ranges obtained for each baseline.

5.4.1 Intensity distributions obtained from BT v_{max}

Looking first at the sample mean ($\bar{y}$) intensity statistics obtained from BT v_{max}, we immediately note that intensity increases consistently as storms progress from the observational baselines associated with less defined organization [such as open warm spots (IR1, 38 kt), closed warm spots (IR2, 45 kt, and the first aircraft observation of banding (B, 50 kt)], to baselines associated with more defined eye structure: the open aircraft eye (A1, 56 kt), the first satellite eye (IR3, 58 kt, the first closed aircraft eye (A2, 68 kt), the first persistent satellite eye (IR4, 77 kt), and finally, the first strong satellite eye (IR5, 101 kt). This progression broadly supports the view that storm intensity increases concomitantly with increasing structural organization. The median M is a more robust measure of the distribution center than the sample mean; in this case, the medians of the distributions at each baseline track the means quite closely. These statistics clearly show that many of the storms which form eyes begin doing so at an intensity substantially less than the hurricane threshold. Although the first persistent satellite eye is not noted until higher intensities, it is interesting to note that the first signs of the satellite eye appear at an

[6] A full table of all of the observational baseline times determined in this study is given in Table B.1 of Appendix B.

[7] The individual interpolated intensity values for every baseline and each storm that, on which the summary statistics Table 5.2 is based, are available as Table B.2 and Table B.3 in Appendix B.

average intensity that is near that at which the aircraft eye is first observed.

Turning our attention to measures of the broadness of the distribution of intensities at each baseline, we see a general broadening of the intensity distributions with increased structural organization. This can seen by the increase in sample standard deviations in Table 5.2 and the increase in interquartile ranges shown by the the widening of the boxes in Figs. 5.3 and 5.4. Notable exceptions to this trend are the broader distributions associated with the closed aircraft eye (A2) and the first satellite (IR3) eye. The broadness of A2 is probably due to fact that the first eye report *may* occur as a closed eye at lower intensity, but if the storm instead forms an open eye first, it will normally develop a closed eye at some later time if the intensity continues to increase. This has the effect of broadening the A2 distribution. IR3 does not suffer from this dual-classification issue, so the broadness of this distribution could suggest that the subjective classifications of the first satellite eye are less reliable (more uncertain) than those for the persistent eye (IR4) and strong eye (IR5) baselines. Given the high potential for false IR3 identifications, this is entirely possible.

5.4.2 Comparison to intensity distributions obtained from rFL v_{max}

Now we compare the statistics obtained from the BT $v_{\max}$ to those gathered from the rFL $v_{\max}$ in the second part of Table 5.2. For the sample mean obtained from the upper bound rFL $v_{\max}$, we see that the first open aircraft eye occurs at 54 kt, the first closed aircraft eye at 63 kt, while the first satellite eye forms at 64 kt and the first persistent eye forms at 82 kt. Curiously, for the aircraft baselines (B, A, A1, and A2) the mean intensities based on the aircraft winds are about 4 to 5 kt *lower* than those obtained from the BT $v_{\max}$. For the satellite baselines (IR1 through IR5) however, the aircraft-based mean intensities are 5 to 6 kt *higher* (an exception being at IR5 where the aircraft-based $\bar{y}$ is somewhat lower than the BT-based $\bar{y}$[8]). Comparing the medians reveals a similar story, with slightly larger differences. What could cause this strange discrepancy? Several factors are likely involved, but let us first note the differences in sample sizes. Because the aircraft observational baselines require the presence of an aircraft, the distributions obtained for them from the BT $v_{\max}$ and rFL $v_{\max}$ are more directly comparable. The

[8] The sample sizes of IR5 are small enough for both the BT $v_{\max}$ and rFL $v_{\max}$ that the discrepancy may simply be due to sampling errors.

previously-mentioned representativeness criterion reduces the number of points in the latter distribution somewhat, but these two distributions are substantially similar. Assuming for a moment that they are exactly the same, we would then be forced to assume that any discrepancies here arise from one or a combination of the following factors: (1) errors in the method of calculating an upper bound and interpolating this to specific time points, (2) errors in the reduction of flight level winds to surface equivalent wind speeds, or (3) systematic biases in the best track intensity estimates caused either by early timing errors (on an upsloping intensity trend) or an overall high bias at these intensities.

Now we examine the differences between the distributions for the satellite-based observational baselines (IR1 through IR5). For this group, the mean intensities based on the rFL v_{max} are *higher* than the mean intensities obtained from the BT v_{max}. Note that there is a large difference in sample sizes: the BT v_{max} distributions contain substantially more data points than the rFL v_{max} distributions for the IR1 (173 vs. 33) through IR4 (80 vs. 36) baselines. Thus, it is easier to argue that discrepancies are due to underlying differences in the two populations that are being sampled. The much larger sample size of the BT-based distributions are due to the preponderance of frequent satellite observations across the entire basin, whereas aircraft normally only sample storms that reach the western half of the basin. When aircraft reconnaissance observations are available, the "ground truth" of aircraft carry a large weight in the BT intensity estimates. When aircraft observations are unavailable, the intensity estimate must be made from limited surface observations (ocean buoys, island stations, and the occasional ship of opportunity) and a plethora of satellite observations. Satellite-based intensity estimates may be obtained from the visible and enhanced IR Dvorak technique, estimates of the upper warm core anomaly derived from thermal wind calculations based on AMSU temperature retrievals, and estimates of the surface wind speed obtained from passive and active scatterometry. Some of these satellite intensity measures have only become available in the last decade. Undoubtedly, the Dvorak intensity estimates carry a large weight in the best track when aircraft observations were unavailable. It is no accident then that the first persistent eye occurs at 77 kt in the BT distribution of Table 5.2 — it occurs right at the intensity the Dvorak method says it should. The objective Dvorak T-number of 4.5 corresponds to 77 kt and is the intensity assigned by the technique when a storm first displays the eye scene.[9] Because storms

[9] The Dvorak technique assigns an objective T-number of T4 to storms when they display a banding eye pattern. The T4

Table 5.2: Statistical summary of intensity ranges obtained from interpolating BT $v_{\max}$ and the upper bound of rFL $v_{\max}$ to the various observational baseline times (see text). Statistical measures included are the sample size (N), sample mean ($\bar{y}$), sample standard deviation s, the sample minimum (min), the lower quartile (Q_1, the median (M), the upper quartile (Q_3), and the sample maximum (max). The aircraft baseline stages are as follows: first aircraft eye (open or closed, 'A'), first open aircraft eye ('A1'), first closed aircraft eye ('A2'). Note that aircraft baseline stages are only reported for valid cases ('insufficient data' cases have been excluded). The baseline stages obtained subjectively from IR satellite imagery are as follows: first open warm spot ('IR1'), first closed warm spot ('IR2'), first eye ('IR3'), first persistent eye ('IR4'), first strong eye ('IR5'). For the second portion of this table, the interpolation is done from the upper bound of the reduced FL $v_{\max}$ values. To see the individual interpolated intensity values at the observational baseline times for each storm (on which the current table is based), see Table B.2 and Table B.3 in Appendix B.

Intensity Ranges for Eye Formation

	B	A	A1	A2	IR1	IR2	IR3	IR4	IR5
				Interpolated from BT $v_{\max}$					
N	23	70	48	52	173	143	114	80	40
$\bar{y}$	50.2	58.1	56.4	67.6	37.8	44.7	58.1	77.1	101.1
s	12.4	11.9	11.5	16.7	11.3	14.7	16.7	14.4	14.7
min	29	29	29	38	19	19	23	44	67
Q_1	39	50	49	58	29	31	47	66	93
M	50.0	58.0	55.5	66.0	34.0	44.0	59.0	77.0	98.0
Q_3	59	66	63	79	44	56	69	88	109
max	80	88	88	112	77	81	99	114	141
				Interpolated from FL $v_{\max}$					
N	21	57	38	45	33	34	38	36	24
$\bar{y}$	44.8	53.9	53.6	62.6	42.6	50.1	63.6	82.3	98.3
s	11.1	12.3	12.0	17.8	12.3	13.3	15.6	15.5	16.8
min	26	26	26	32	25	30	33	52	59
Q_1	38	44	44	48	33	39	53	66	85
M	44.3	51.9	51.5	59.6	41.3	47.4	61.6	83.8	98.6
Q_3	49	62	62	72	47	60	69	93	108
max	67	78	74	110	83	82	101	116	128

generally intensify as they travel westward, one may be tempted to try to explain the higher aircraft-based intensities as a result of stronger storms, or alternatively, that storms further east tend to be weaker. But if our subjective satellite classifications truly reflect storm structure, and if certain storm structures and appearances generally occur at the same intensities, this should not be the cause of this discrepancy. Further analysis is needed to resolve this conundrum.

designation corresponds to an intensity of 65 kt. Because the objective T-number includes several adjustments based on other factors, it is possible for a storm to be assigned a T3.5 when it displays a banded eye. The T3.5 designation corresponds to an intensity of 55 kt).

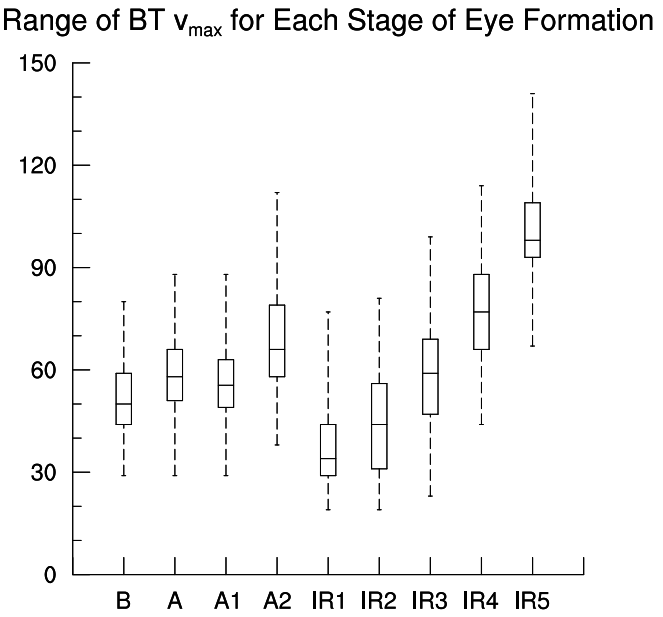

Figure 5.3: Box-and-whisker plot showing the intensity range characteristics obtained from BT $v_{\max}$ interpolated to the various observational baseline stages of eye formation. The center line of each box gives the median value, while the upper and lower box edges correspond to the upper and lower hinges of the distribution (hinges are nearly the same as the quartiles of the distribution. The endpoints of the whiskers correspond to the extreme values of the distribution.

5.4.3 Explanation of the structure and intensity plots

A special type of plot is presented to visualize the key data values contained in the VDMs. These 'structure and intensity' plots will be presented throughout the remainder of this dissertation so a detailed description is now provided. Fig. 5.5 presents the structure and intensity plot for Hurricane Wilma (2005) as an example for the following discussion. This plot displays selected aircraft-based intensity, structure, and thermodynamic parameters for all the fixes taken in a particular storm during its lifetime. This allows for the voluminous aircraft data to be visually synthesized and is also quite useful for quality-control purposes. The plot consists of five panels, each of which is placed on a common time grid. Vertical lines and background shading run through each of the panels to indicate key structural developments such as any instance of banding (black) or poorly-defined eyes (green), the first report of an open aircraft eye (dark blue), and the first report of a closed aircraft eye (red). For the periods when an open aircraft eye is observed, the area in between fixes is shaded in light gray.[10] Similarly, time periods in which the

[10] If an open eye was observed for just one fix, the shading only extends for one hour afterward. Otherwise, shading extends between consecutive fixes in which an open aircraft eye was reported. If more than 18 h elapsed between consecutive fixes

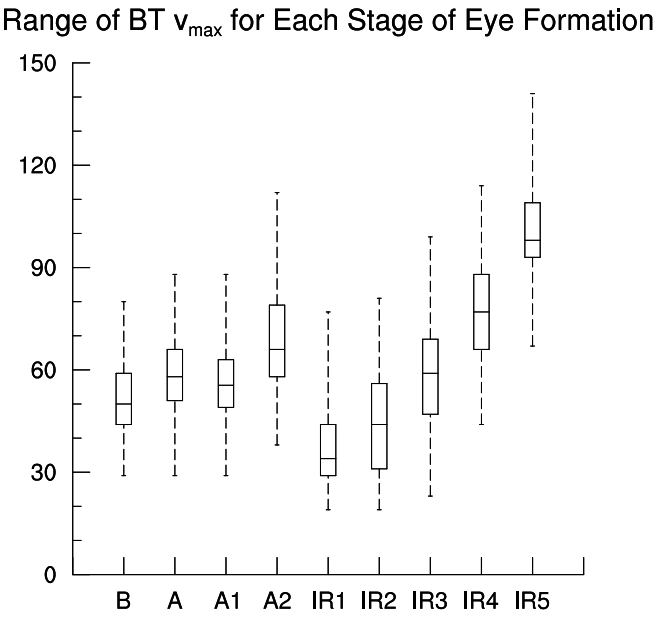

Figure 5.4: As in Fig.5.3, except that the intensity ranges are obtained by interpolating the reduced FL v_{max} winds to the observational baseline times.

storm possessed a closed aircraft eye are indicated with light blue shading. Pink shading highlights the time period just before the aircraft eye appeared (from the last observation without an eye to the first observation with an eye). This represents the timing uncertainty associated with the identification of the first aircraft eye. This vertical coherence between panel plots allows the various parameters to be compared with each of the other parameters in relation to the key structure changes (e.g., eye formation). Tick marks on the inside top edge of each panel indicate the fix times that these data correspond to. These various shading and tick mark conventions allow the reader to evaluate the impact of gaps in aircraft data on interpretations made from these data.

where aircraft reported an eye, the shading ends one after the fix at the beginning of the time gap.

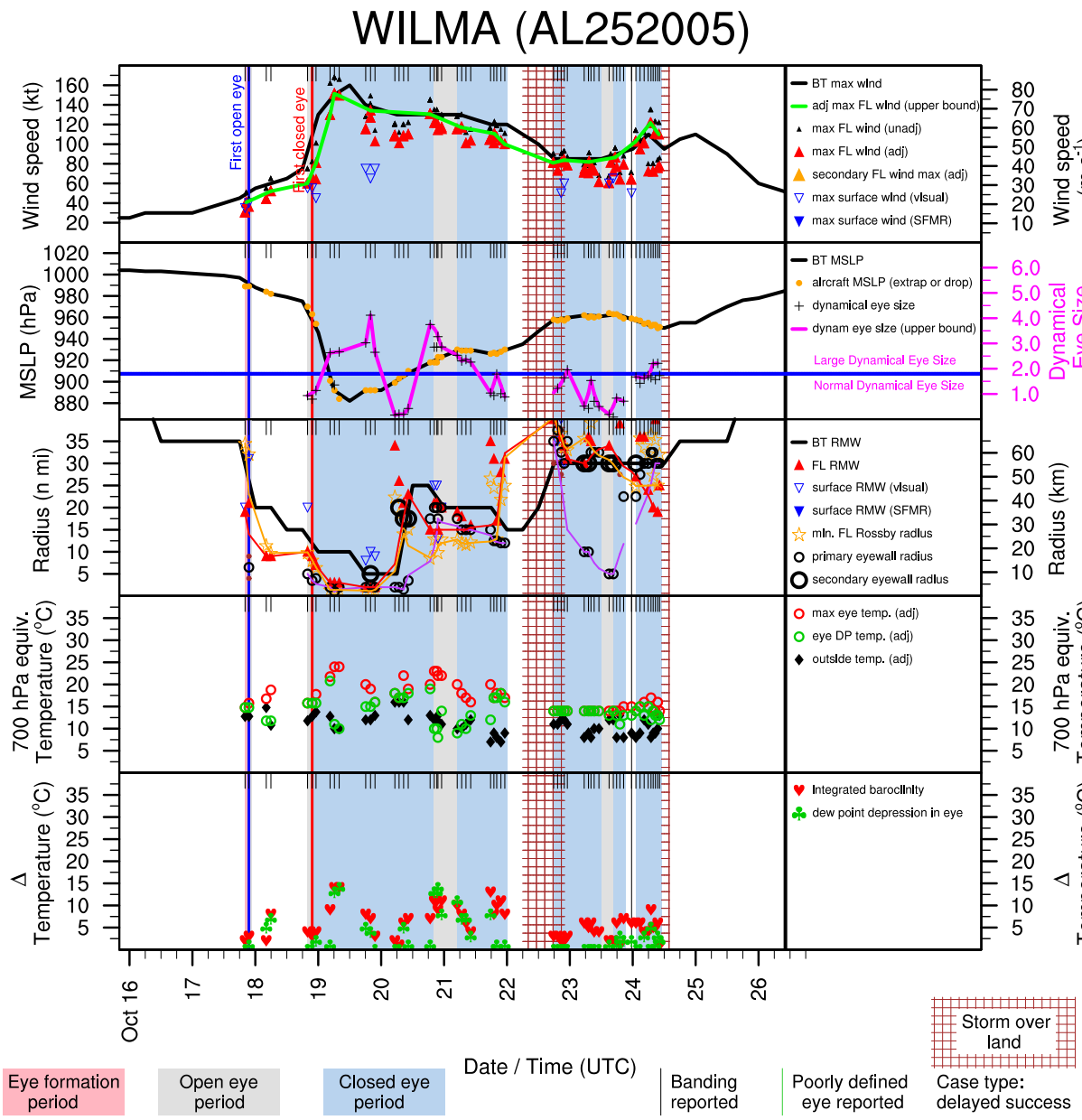

Figure 5.5: Structure and intensity parameters for Hurricane Wilma (2005).

Intensity parameters are presented in the first ('intensity') panel of the structure and intensity plot. The raw (unadjusted) FL v_{max} values are indicated by small black up-pointing triangles, while the rFL v_{max} values are indicated by larger red down-pointing triangles. When a secondary wind maximum occurs, the surface-equivalent secondary v_{max} are indicated by large orange down-pointing triangles. The visually-estimated surface wind estimates are indicated by hollow blue down-pointing triangles, while the SFMR-based surface wind estimates are shown by filled blue down-pointing triangles. The filtered upper bound of rFL v_{max} is shown by a solid green line. For comparison, the BT v_{max} is shown by a black line.[11]

The second ('pressure') panel displays pressure data and the dynamical eye size. Aircraft-derived pressure measurements are indicated by orange dots. For comparison, the BT p_{min} is shown by a black line. When an eye is present, this panel uses plus symbols to show the dynamical eye size for each fix.[12] Because these data can be quite noisy, an upper bound has been constructed using the same filtering algorithm used for the upper bound of FL v_{max} (except the adjustment weights have been tuned differently).

The middle ('structure') panel displays the storm's structural parameters including the radius of maximum wind r_{max}, the eye radius r_{eye}, and minimum Rossby length $\lambda_{R,min}$. A similar convention to the intensity panel has been used in this panel: the FL r_{max} are shown by red down-pointing triangles, the r_{max} of the visually-estimated surface wind are shown by hollow blue down-pointing triangles, and the r_{max} of the SFMR surface wind by filled blue down-pointing triangles. The minimum $\lambda_{R,min}$ computed from the FL wind parameters is indicated by hollow orange stars. The primary eye radius is shown by small thick open circles. When a concentric eye is present, the radius of the outer (secondary) eye is shown by a larger thick open circle, while the radius of the inner (primary, or sometimes relict) eye is shown by the normal small thick open circle. When an elliptical eye is present, the average radius is shown using the normal small thick open circle, but small brown dots are also placed to indicate the major and minor diameters. For comparison with the aircraft data, the BT r_{max} is shown by a black line.

[11] In most cases, the upper bound rFL v_{max} and BT v_{max} correspond track fairly closely, which gives confidence that our method for computing the upper bound rFL v_{max} is robust, despite occasional data gaps.

[12] As a reminder, dynamical eye size is computed by dividing the eye radius by $\lambda_{R,min}$.

Lower bounds have been computed and are displayed using thin solid lines for the FL r_{max} (red), the r_{eye} (purple), and the $\lambda_{R,min}$ (orange).

The fourth ('temperature') panel shows thermodynamic parameters related to the warmness and dryness of the eye. All temperatures have been adjusted to 700 hPa-equivalent values using the method described in chapter 4.3.5. The maximum 700 hPa-equivalent FL temperature reported within 5 n mi of the center (normally inside the eye when an eye is present) is $T_{eye}$and is indicated by red thick open circles. The FL dew point temperature $T_{d,eye}$ is reported for the same location as T_{eye} and is indicated by green thick open circles. The FL temperature representative of the region just outside of the eyewall $T_{out}$is indicated by filled black diamonds.

The last ('temperature difference') panel displays the computed dew point temperature depression ($T_{DEP,eye}$, green cloverleaves) and the horizontal temperature difference across the eyewall ($\Delta T_{eyewall}$, red hearts). High dew point temperature depressions are an excellent indicator of dry adiabatic subsidence warming associated with a strong eye. Large horizontal temperature differences across the eyewall also indicate the presence of a strong warm core and imply the presence of high inertial stability (the subject of chapter 3). The large baroclinity across the eyewall likely plays a very significant dynamical role in controlling the storm's intensification response to convective latent heating.

When the structure and intensity plots of specific storms are referred to within the dissertation text, the plot will appear within the next few pages. As a service to the broader research community, structure and intensity plots for *all* of the 205 storms in the VDM data set (1989-2008) have been included in Appendix E.

5.4.4 Lower intensity bound for eye formation

Now we investigate the lower extrema of the eye formation intensity distributions. From Table 5.2, the lowest interpolated BT v_{max} at the first report of an open (closed) aircraft eye was 29 kt (38 kt). If the rFL v_{max} are used instead, an open (closed) aircraft eye was observed at the extreme low value of 26 kt (32 kt). For the IR3 baseline, the lowest BT v_{max} (rFL v_{max}) intensity was 23 kt (32 kt). Due to the subjective nature of the IR satellite imagery classifications, the IR4 baseline provides a more definitive signal that the storm has formed an eye — the corresponding BT v_{max} (rFL v_{max}) of the least intense

storm to form a persistent eye was 44 kt (52 kt). The minimum BT v_{max} (rFL v_{max}) at which a storm formed a strong eye (IR5) was 67 kt (59 kt). These intensities seem remarkably low, so Table 5.3 (first part) has been prepared to summarize the storms which formed aircraft (A) eyes while at exceptionally low intensity. Besides the interpolated BT and rFL v_{max} at the time the aircraft eye was first reported, this table also provides the maximum intensity reached during each storm's lifetime and some other structural (e.g., r_{max}) and thermodynamic information (such as the maximum observed dew point depression, $T_{DEP,eye}$) that may be useful in evaluating whether the reported aircraft eye was a 'true' eye. The four least intense storms of this table are analyzed next in greater detail.

The least intense system to form an aircraft-reported eye was not even a tropical storm, but rather a tropical depression — TD5 in 1994. At the time the eye was reported, the depression had an interpolated BT v_{max} (rFL v_{max}) of 29 kt (26 kt). Fig. 5.6 shows the structure and intensity plot for TD5. Aircraft reported an eye at just one fix (1835 UTC on 30 Aug). At this time 35 kt FL v_{max} was observed (equivalent to 26 kt at the surface), the p_{min} was 1007 hPa, and surface winds were visually estimated at 35 kt. On the day before the eye formed, FL v_{max} winds were as high as 44 kt (33 kt surface equivalent). One might question whether the aircraft misidentified the eye structure in this case. This is possible, but the report of banding about 90 min before the first eye was reported is another indication that the eye was forming. Pressures were slowly falling and NHC's preliminary storm report noted that the system seemed to have some development potential. The eye did not persist however, and the storm hit land the next day without appreciable intensification.

The second least intense storm to form an eye was Tropical Storm Nana (1990), with an interpolated BT v_{max} of 36 kt (there were not enough aircraft observations to obtain an interpolated rFL v_{max}). Fig. 5.7 shows the structure and intensity plot for Nana. Aircraft first reported an eye in the 2027 UTC fix on 16 October. At the time, p_{min} was 1005 hPa, FL v_{max} was 48 kt, and the visual surface wind was estimated at 50 kt. These values suggest that Nana may have been a bit stronger than the interpolated BT v_{max} computed here: it is possible that Nana did not really form an eye at exceptionally low intensity.

Tropical Storm Henri (2003) was the third least intense storm to form an eye, with a BT v_{max} (rFL v_{max}) of 27 kt. Fig. 5.8 shows the structure and intensity plot for Henri. The eye was first reported in the 0742 UTC fix on 5 Sep with a FL v_{max} of just 31 kt. The highest FL v_{max} reported by aircraft at any

Table 5.3: Ten least intense storms to form an aircraft-observed eye; ten most intense storms to not form an aircraft-observed eye. Storms have been ranked by their interpolated BT v_{max} at the time of eye formation (first part) or their lifetime maximum BT v_{max} (second part). Columns 6 through 13 summarize maximum or minimum values for the entire storm lifetime (or for the entire period of aircraft observations. Columns are as follows: number of aircraft fixes (third column); BT v_{max} interpolated to time of first aircraft eye report (kt, fourth column); reduced FL v_{max} interpolated to time of first aircraft eye report (kt, fifth column); highest BT v_{max} (kt, sixth column); highest observed maximum flight level wind speed reduced to surface equivalent ("rFL", kt, seventh column) and unadjusted ("FL", kt, eighth column); smallest observed radius of maximum winds ("r_{max}", ninth column); smallest observed minimum Rossby length (n mi, tenth column); lowest BT minimum sea level pressure (p_{min}, hPa, eleventh column); largest flight level dew point temperature depression, $T_{DEP,eye}$, measured within 5 n mi of the storm center (°C, twelfth column); best stage of completeness of the formed aircraft eyewall (last column).

			Interpolated Intensity		**Maximum wind speed**							
Storm	Year	# of fixes	BT kt	rFL kt	BT kt	rFL kt	FL kt	Min r_{max} n mi	Min Rossby length n mi	Min BT p_{min} hPa	Max $T_{DEP,eye}$ °C	Eyewall Completeness?
Least Intense Storms to Form an Aircraft-Observed Eye												
FIVE	1994	13	29	26	30	33	44	4	11.1	1005	4	open
NANA	1990	24	36		75	71	89	2	3.4	989	15	closed
HENRI	2003	27	36		50	37	46	4	19.5	997	7	open
BRET	1999	42	38	32	125	121	134	2	5.1	944	10	closed
ALBERTO	1994	23	39	35	55	50	67	11	21.6	993	5	closed
KATRINA	2005	56	40	35	150	149	166	7	8.3	902	23	closed
BONNIE	2004	29	43	40	55	58	72	3	6.7	1001	10	closed
ANDREW	1992	64	44	58	150	153	170	2	3.5	922	19	closed
LILI	2002	67	44	40	125	127	141	2	4.8	940	20	closed
CHANTAL	1995	40	45	38	60	51	67	3	8.5	991	12	closed
Most Intense Storms to Not Form an Aircraft-Observed Eye												
EARL	1998	23			85	83	104	8	34.4	964	28	
KYLE	2008	14			75	74	82	12	32.7	984	12	
NOEL	2007	21			75	81	90	22	34.1	965	10	poor
GORDON	1994	50			75	86	96	2	2.9	980	9	(banding)
ANDREA	2007	2			65	29	39	71	212.8	998	6	
ALLISON	1995	25			65	67	74	2	3.2	982	11	
ALBERTO	2006	19			60	56	74	21	37.3	969	6	
BARRY	2001	30			60	59	66	6	13.2	990	12	(banding)
GABRIELLE	1995	11			60	55	73	3	15.6	990	4	(banding)
EDOUARD	2008	16			55	54	68	11	39.7	996	5	(banding)

time before eye formation was just 38 kt (or a surface equivalent 30 kt). At the time the eye appeared, the aircraft-measured p_{min} was 1000 hPa. After the initial eye report, the intensity increased and the r_{max} continued to contract for about 6 h with one report of banding, but no eye was reported again.

The fourth least intense storm to form an eye was Tropical Storm Bret in 1999, with an interpolated BT v_{max} of 42 kt (32 kt). A structure and intensity plot for Bret is shown in Fig. 5.9. A definite aircraft eye was first noted at the 2320 UTC fix on 19 Aug, with FL v_{max} of 35 kt (28 kt surface equivalent) and

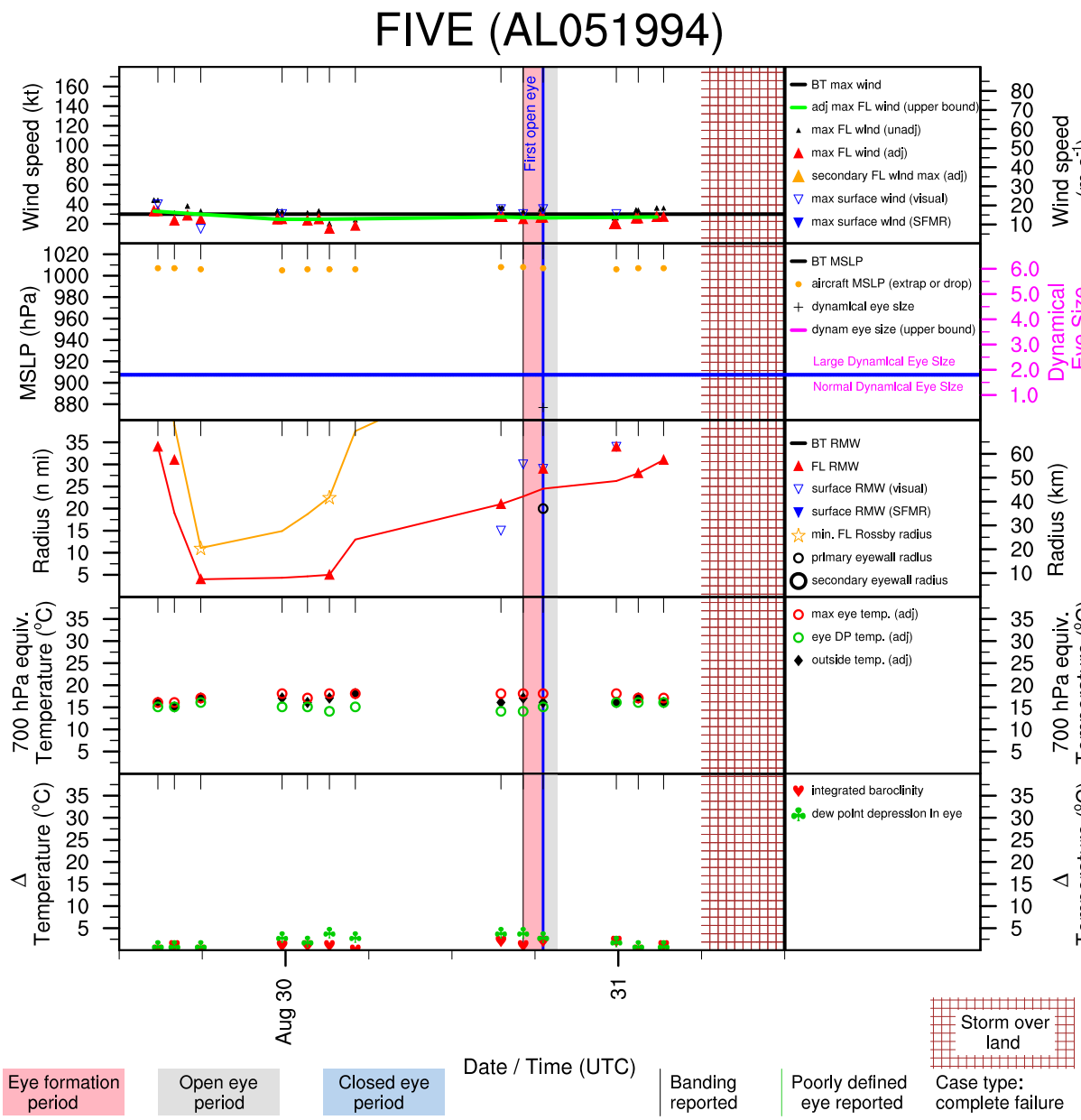

Figure 5.6: Structure and intensity parameters for Tropical Depression Five (1994) which was the least intense storm in the VDM data set for which an aircraft reported an eye. See 5.4.3 for a detailed description of the VDM parameters displayed in this plot.

a $p_{\min}$ of 1000 hPa. The $r_{\max}$ reached a very small value of 2 n mi at the time the eye appeared. Twelve hours previously, aircraft had noted banding. Nine hours before the eye was reported, FL $v_{\max}$ winds reached 45 kt (36 kt surface equivalent) and $p_{\min}$ was measured at 1008 hPa. The surface wind had been visually estimated at 35 kt at various times before the eye formed.

Synthesizing the above results, the lowest intensity bound for eye formation (based on the aircraft-

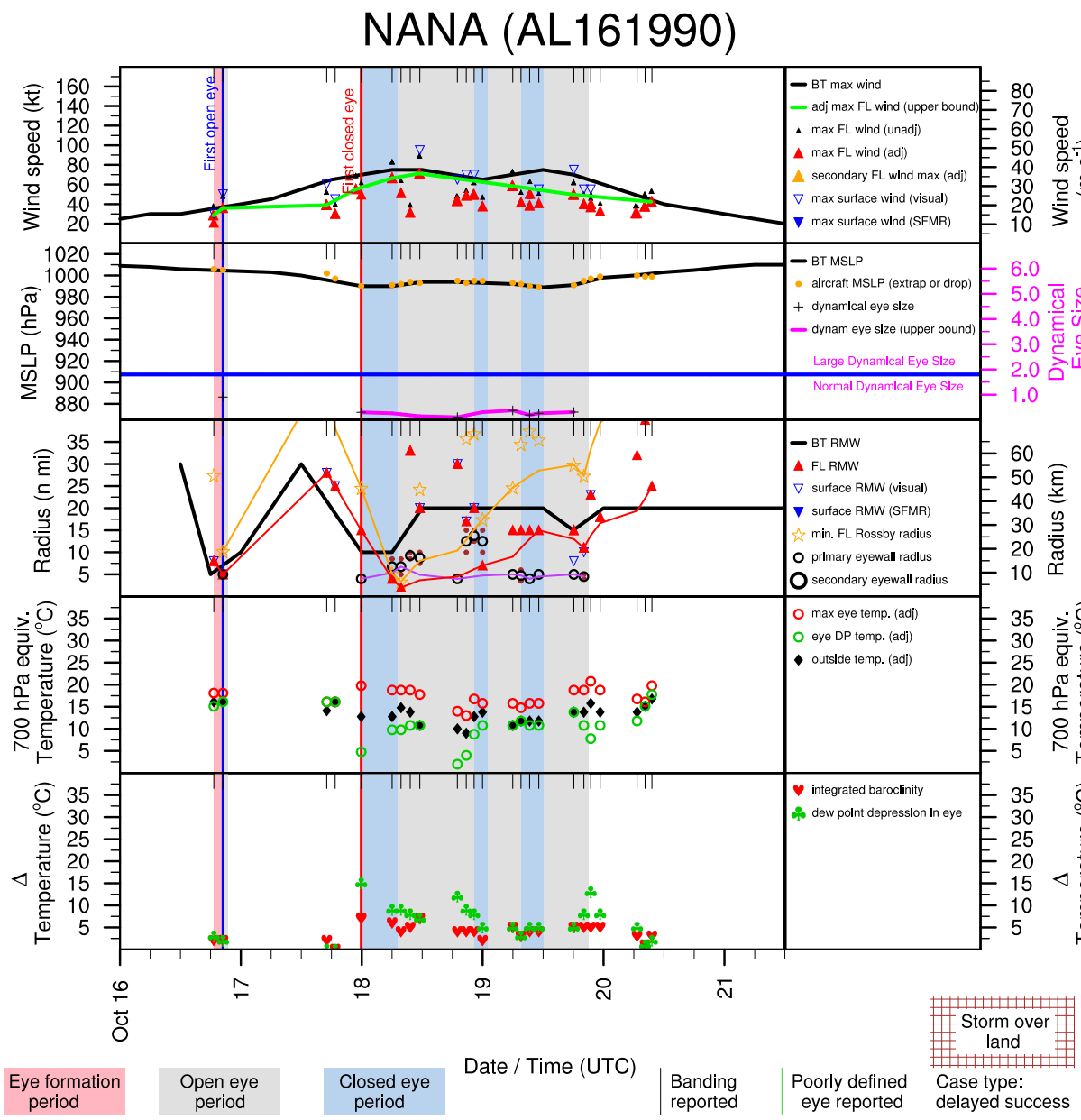

Figure 5.7: Structure and intensity parameters for Hurricane Nana (1990).

reported eye) corresponds to minimal tropical storm intensity with maximum sustained surface winds of 35 kt. For all of these early eye formers, FL v_{max} attained 38 to 45 kt either before or at the time the eye was reported. The highest pressures observed in these early eye-forming storms ranged from 1007 to 1000 hPa. Five of these storms failed to develop much further, one became a moderate hurricane, and the other four became major hurricanes. All of these storms achieved quite small r_{max} and minimum $\lambda_{R,min}$ at some point during their lifetimes. Also, all of the storms except Henri and Alberto attained a

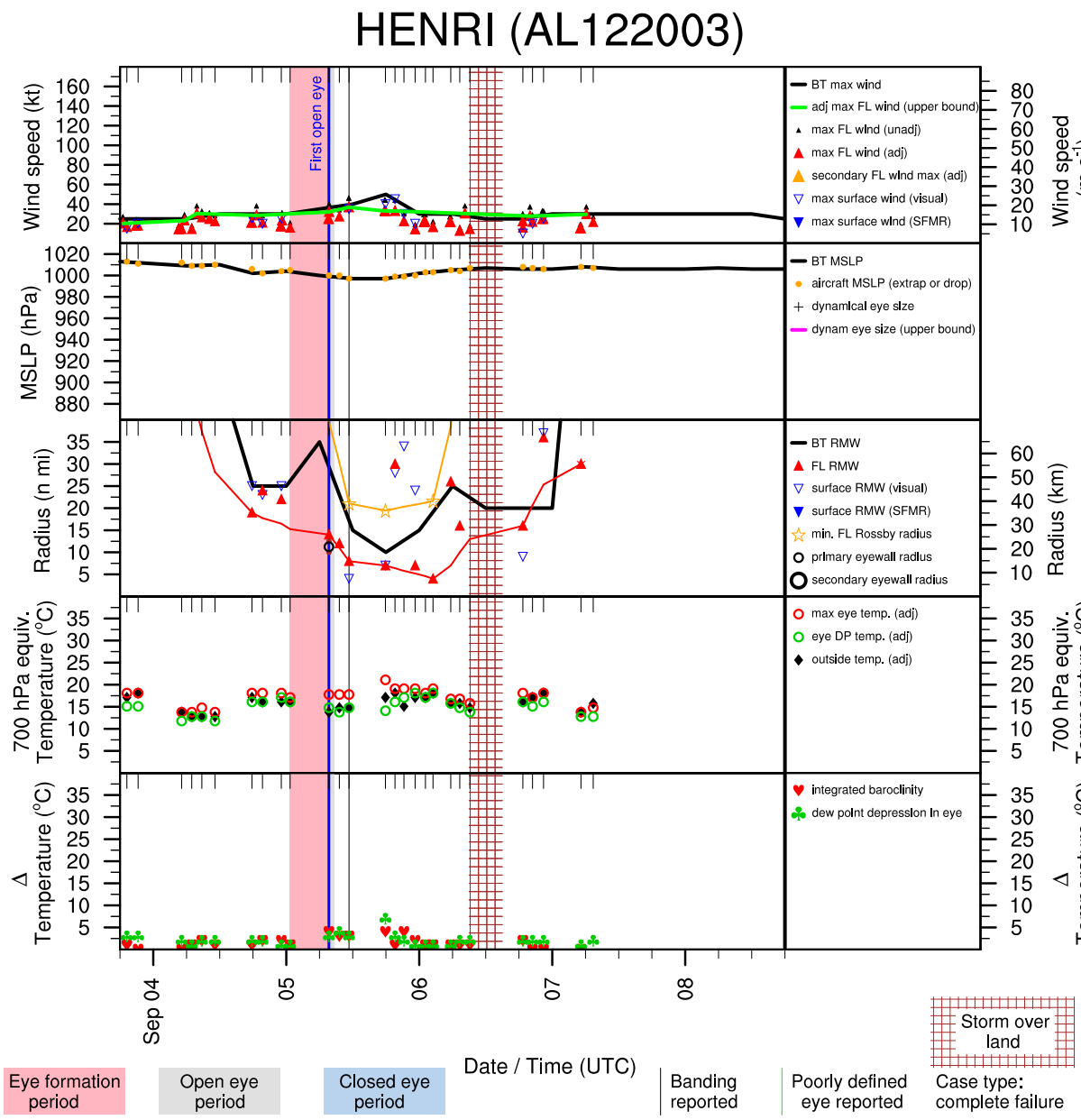

Figure 5.8: Structure and intensity parameters for Tropical Storm Henri (2003).

$T_{\mathrm{DEP,eye}}$ of at least 10 °C, which is indicative of the substantial central drying normally associated with a developed eye.

5.4.5 *Upper intensity bound for eye formation*

What is the most intense storm to not possess a clearly defined eye? This subsection examines storms which did not form an eye even at exceptionally high intensity. Starting first with the maximum

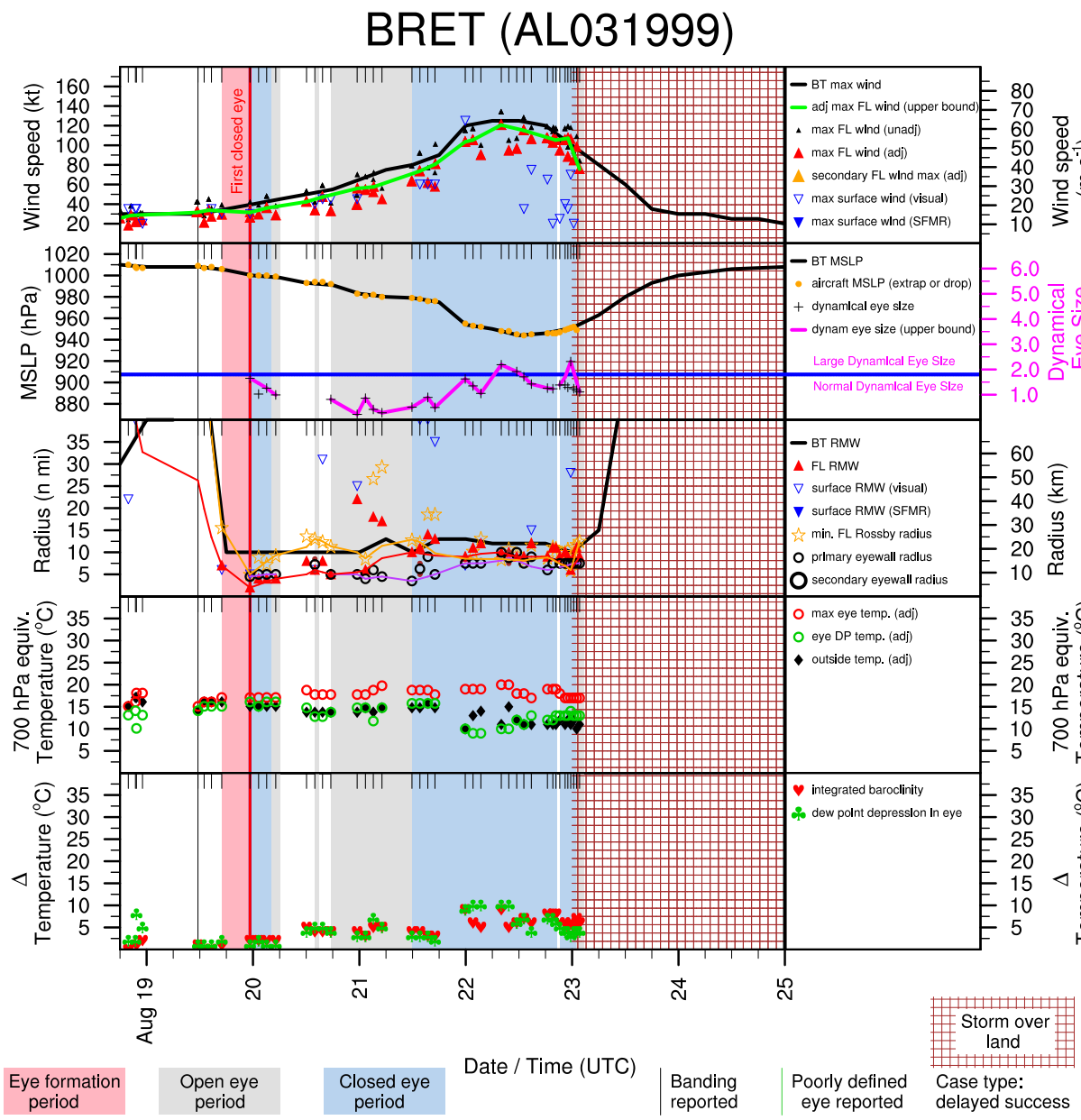

Figure 5.9: Structure and intensity parameters for Hurricane Bret (1999).

interpolated intensities given in Table 5.2, the highest interpolated BT $v_{\max}$ (rFL $v_{\max}$) at the first report of an open aircraft eye was 88 kt (74 kt). The maximum BT $v_{\max}$ (rFL $v_{\max}$) intensity for the first report of a closed eye was 112 kt (110 kt). A word of caution is warranted though. These maximum values cannot properly be used to estimate the upper intensity bound for eye formation because these intensity values were interpolated from the time the aircraft eye was first *reported*. Because a time lag of up to 12 h has been allowed between fixes for determining the first eye report (so as to include as many cases as

possible), it is possible and even probable that a few storms formed their eyes quite some time *before* the aircraft reported them. When storms were intensifying throughout this period, the intensity interpolated from the aircraft eye baseline time must then be an *overestimate* of the upper bound for eye formation.[13]

A safer approach is to examine the maximum lifetime intensities achieved by all storms which did not form an eye. The second part of Table 5.3 provides such a list, ranked by the maximum observed BT v_{max}. Storms have been excluded from this table if they were not adequately observed by aircraft (to reasonably ensure that an eye did not form during a data gap) or if the storm developed an IR3 eye in satellite imagery. Three case studies are now given to evaluate these 'eye-less hurricanes'.

Hurricane Earl (1998) was the most intense storm (in the VDM data set) to never form an aircraft-observed eye during its lifetime. On 2 September, the storm attained a maximum BT v_{max} of 85 kt while FL v_{max} reached 104 kt. Fig. 5.10 displays the evolution of Earl's structure and intensity. Earl developed in the Gulf of Mexico, reaching tropical storm strength at 1800 UTC on 31 August. The storm intensified to 50 kt on 1 September while encountering westerly vertical wind shear. By 1400 UTC, IR satellite images show that the storm had developed vigorous deep convection near the center while displaying a few hints of banding and rotation (banding and rotation of the cold cloud features sometimes indicate that eye formation may be occurring). At this time, aircraft reported FL v_{max} of 54 kt at a r_{max} of 93 n mi. The central p_{min} was 1000 hPa. Extremely dry dew points (less than 0 °C) were reported at this time, but it is likely that the dew point sensor was malfunctioning for this specific flight as neither satellite imagery nor the other dew point measurements from other aircraft missions indicate exceptionally dry air during this time. During the afternoon, the deep convection developed into a strong Central Dense Overcast (CDO) pattern. A closed warm spot appeared at 1945 UTC, but this did not appear to migrate with the low level center which was moving northeastward at the time – instead the warm spot moved off to the southwest across a band of deep convection that was becoming quasilinear at the time. It is possible that this warm spot was either a warm overshoot or a 'wake depression' in the cloud field caused by the interaction of the deep convection with the westerly shear.

[13] This time delay factor could also apply to the lower bound estimates for eye formation reported in the previous subsection, and indeed must be considered for all of the statistics reported for the aircraft baseline times in Table 5.2. It is less likely to be a factor in the determination of the lower bound intensity, however, because many of the early eye-forming storms were intensifying only slowly or hardly at all when they first formed their eyes.

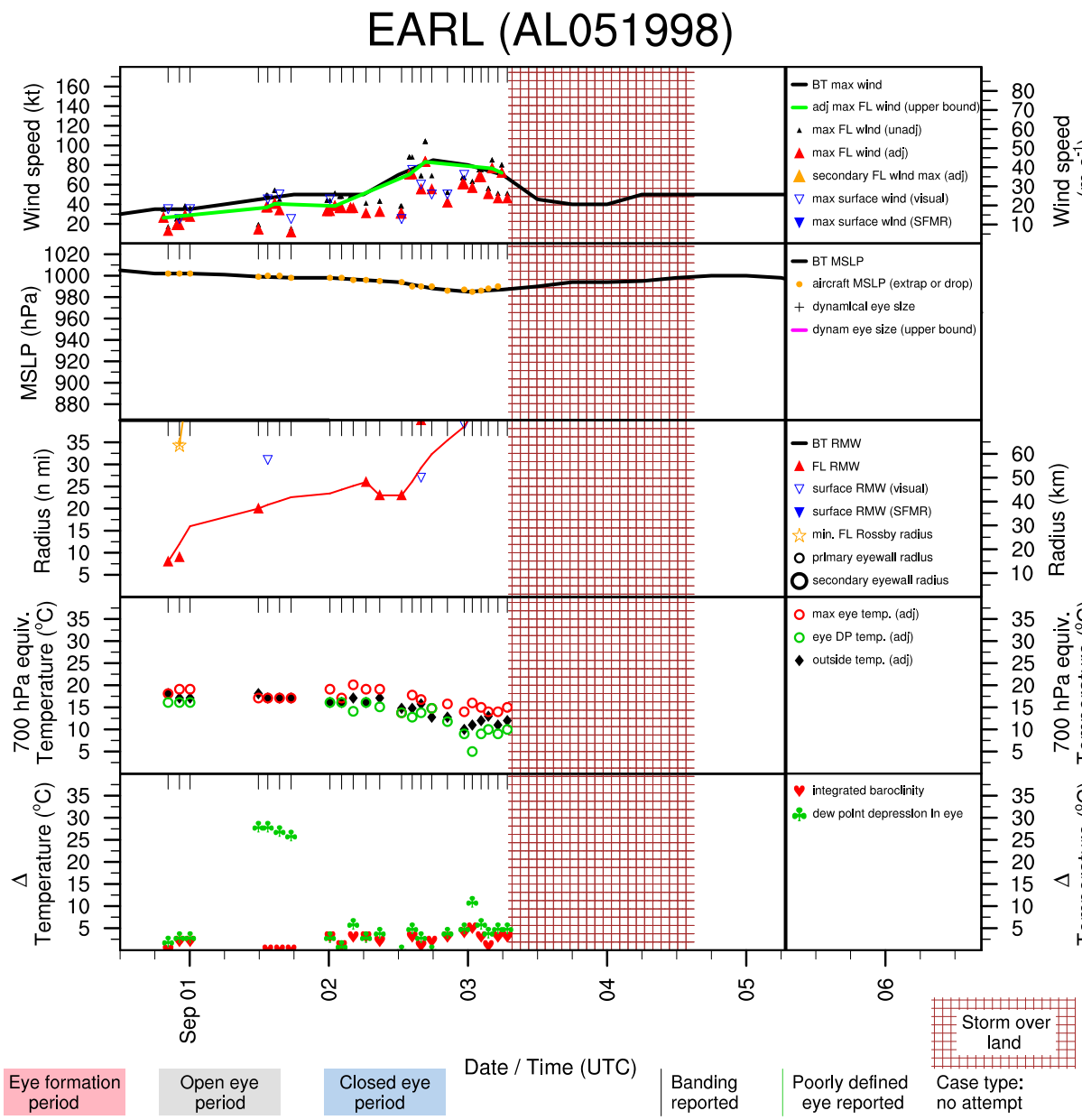

Figure 5.10: Structure and intensity parameters for Hurricane Earl (1998).

A new CDO developed over the storm center at 0045 UTC on 2 September. Overnight, the storm rapidly intensified from a BT $v_{\max}$ of 50 kt at 0600 UTC to 85 kt by 1800 UTC. Just before this rapid intensification another closed warm spot appeared at 0345 UTC, but shortly afterward the convection again took on a linear appearance and shifted to the east side of the storm. At the 0625 UTC fix, the VDM remarks section describe the system as having a poorly-defined pressure wind field with an erratic center position. Flight level winds were only 41 kt but the central pressure had decreased to 996 hPa and

r_{max} had contracted to 26 n mi. At the 0847 UTC fix aircraft reported multiple vortices near the center. At the 1233 UTC fix the system center was still described as poorly defined and maximum flight level winds were just 38 kt at a r_{max} of 23 n mi. The 1423 UTC fix showed a dramatic change, with FL v_{max} of 88 kt at a r_{max} of 93 n mi to the southeast of the center. Surface winds were estimated visually at 75 kt in this general vicinity. The central pressure had dropped to 990 hPa. Peak flight level winds of 104 kt (83 kt surface equivalent) were observed at the 850 hPa flight level at 1638 UTC in the east quadrant of the storm. At 1715 UTC IR satellite images showed a distinct curl developing simultaneously at both the lower and upper levels as the storm attempted to wrap convection around the center towards the north and west. The center of the upper curl was displaced from the lower curl by nearly a degree. This trend did not persist and deep convection waned shortly thereafter. By 2028 UTC aircraft data showed that p_{min} had decreased to 985 hPa, but was now located 22 n mi south-southwest of the center. A supplementary maximum FL temperature of 21 °C was also reported at this location; this was 4 °C warmer than the maximum FL temperature reported near the center. From this point on, Earl showed signs of becoming extratropical as strong vertical wind shear continued to push most of the deep convection to the east of the storm. Earl made landfall by about 0000 UTC on 3 September. After crossing the southeastern U. S. the storm moved back over the Atlantic and strengthened into a deep (964 hPa) extratropical storm near Newfoundland.

To summarize this case, eye-less Earl reached a quite high BT v_{max} of 85 kt and a respectable p_{min} of 985 hPa, but never formed an aircraft-reported or an obvious eye in satellite imagery. The r_{max} experienced a big jump as the storm intensity rapidly increased. At one point, the storm tried to form an eye, but strong westerly vertical wind shear seemed to disrupt or mask this process and the storm began the transition to an extratropical system. During the time when it might have formed on 2 September, Earl was well-observed by aircraft with no data gaps exceeding 4 h. Thus, this storm establishes a lower estimate for the true upper bound of intensity for an eye-less hurricane.

The 2008 Atlantic season featured another eye-less hurricane. Kyle formed near the Dominican Republic on 25 September. A structure and intensity plot for Kyle is given in Fig. 5.11. Later that day, deep convection consolidated into a CDO and the storm displayed some signs of banding in IR satellite imagery. A col-type warm spot also appeared. The storm reached a BT v_{max} of 45 kt and a p_{min} of

998 hPa by 0000 UTC on the 26th. Kyle's intensity gradually increased over the next few days, but the storm was repeatedly disrupted by strong vertical wind shear. The low level center was nearly exposed on the 26th, but strong deep convection was maintained just to the east. On the 27th, deep convection became more circular and had the appearance of "rolling over" the north side of the storm. Thereafter, the convection became more centrally-located, so the storm displayed a CDO pattern. A strong burst of convection with $T_{b,IR}$ colder than $-80\,^{\circ}$C occurred right at the center around 1700 UTC. At 1841 UTC, aircraft reported 850 hPa winds of 78 kt at a r_{max} of 39 n mi northeast of the center. The central pressure was 995 hPa and SFMR-observed surface winds were measured at 74 kt 55 n mi from the center. The surface center and maximum FL temperature were both displaced from the flight center. After this time, strong upper level winds impacted the storm from the southwest, but the storm attempted to roll the deep convection over the top of the storm again on 28 Sep. At 1117 UTC the final aircraft fix in Kyle reported FL v_{max} of 82 kt at 700 hPa (74 kt surface equivalent) at a r_{max} of 65 n mi. SFMR-measured surface winds were 77 kt and the p_{min} was 991 hPa. The BT v_{max} peaked at 75 kt at this time. Shortly thereafter the storm began extratropical transition.

Noel (2007) is an example of a hurricane which almost developed an eye (actually, a 'poorly defined' eye was reported at one fix) and appeared to have lots of opportunities to form an eye, but never did. Fig. 5.12 provides an overview of Noel's intensity and structure history. Noel developed late in the season (24 October) near the U. S. Virgin Islands, then dipped southwestward into the Caribbean and was sheared by strong upper level westerly winds for a couple days. It reached tropical storm intensity on the 28th as it developed a very large and strong CDO pattern as it turned north towards the Dominican Republic. The storm displayed some precursors to eye formation including signs of banding and rotation of the cold cloud features. The CDO also appeared to "roll over" and Noel's BT reached v_{max} 50 kt before making island-fall. Vertical wind shear increased about this time and the storm was disrupted for a couple days. On the 31st, deep convection intensified and became more involved with the low level center. At 2309 UTC, aircraft reported a poorly-defined eye (but no eye diameter), a p_{min} of 996 hPa and a FL v_{max} of 42 kt with a 39 n mi r_{max}. By 0215 UTC on 2 November, a large CDO developed and displayed several small cold rings with $T_{b,IR}$ approaching $-90\,^{\circ}$C. The first cold ring (with a minor warm spot) appeared at 0215 UTC and only lasted for only about 45 min. An aircraft fix at 0346 UTC showed

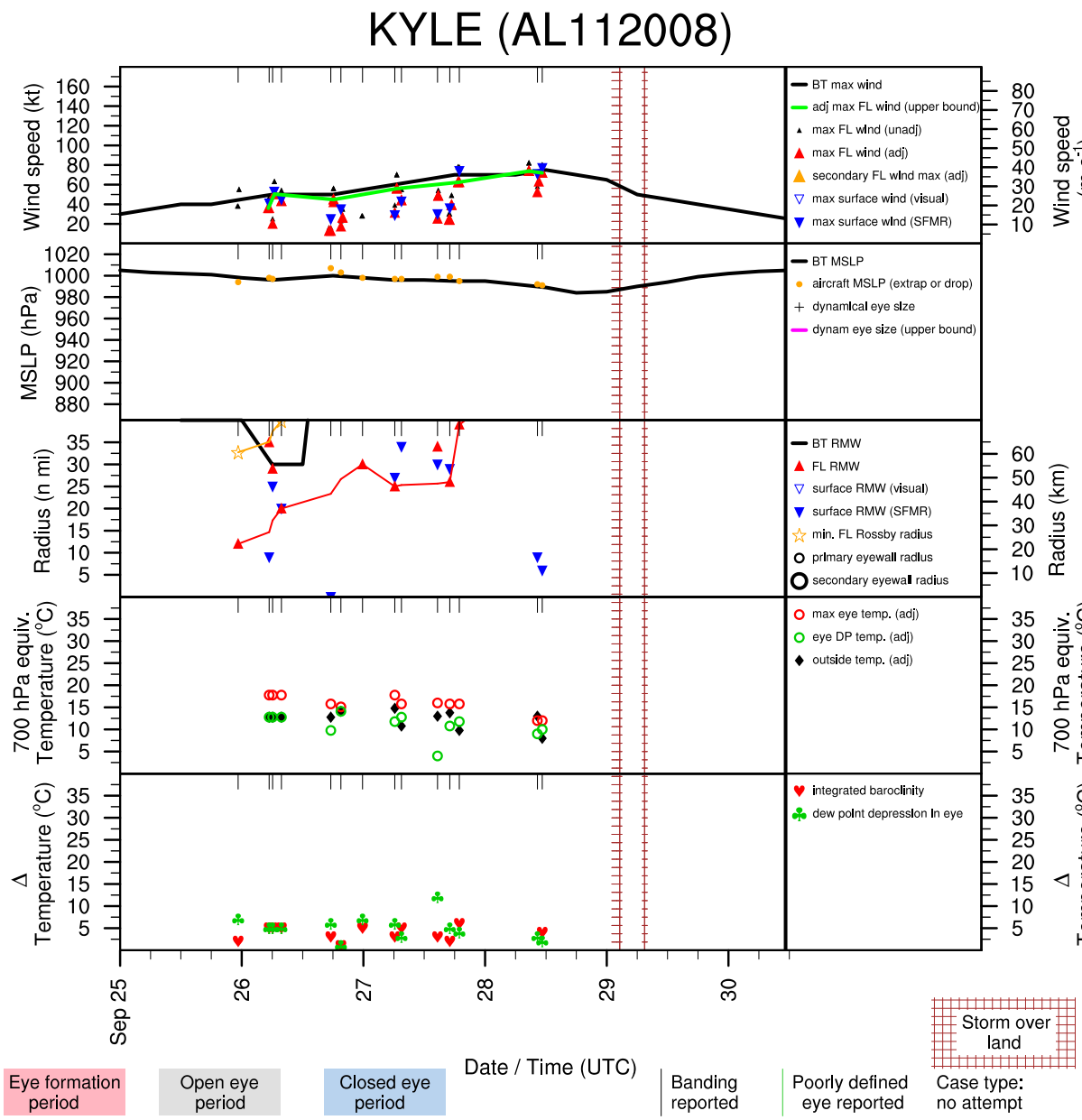

Figure 5.11: Structure and intensity parameters for Hurricane Kyle (2008).

that $p_{\min}$ had dropped to 994 hPa. A FL $v_{\max}$ of 54 kt was measured at 0433 UTC.

The second cold ring appeared to develop from a single convective tower which penetrated the CDO at about 0632 UTC. This quickly expanded into a cold ring with a warm spot by 0715 UTC. The ring pattern appeared to move eastward while the general storm circulation was presumed to be traveling northward at the time. By 0735 UTC, the local cloud shield began to warm and the ring pattern was no longer evident. An hour later, aircraft reported $p_{\min}$ of 993 hPa with just 41 kt winds to the northeast of

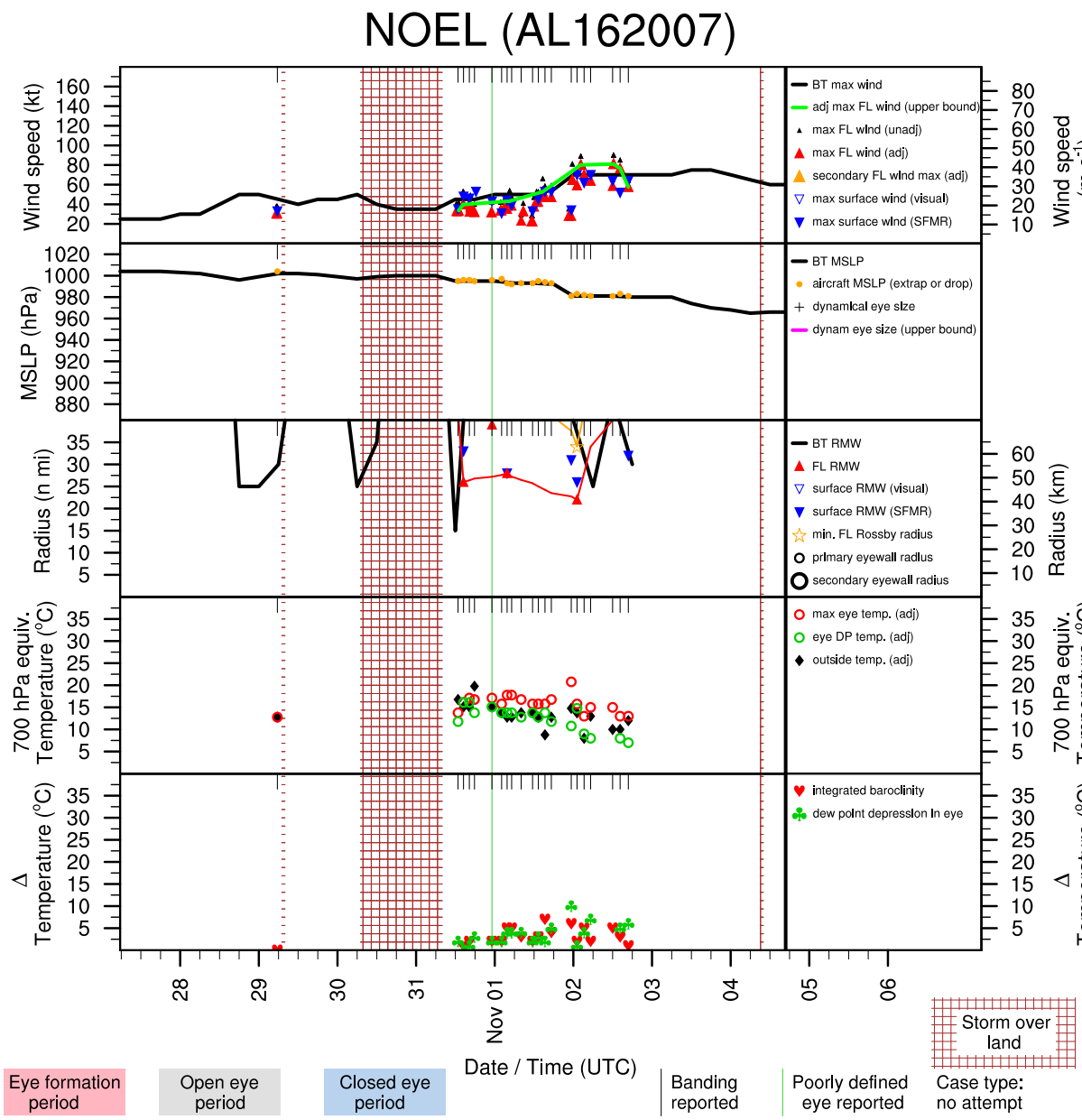

Figure 5.12: Structure and intensity parameters for Hurricane Noel (2007).

the center. $r_{\max}$ had jumped to 107 n mi in the previous fix, but was now 57 n mi. Shortly thereafter, deep convection developed closer to the center and consolidated into a new CDO as the storm traversed the Bahamas. FL $v_{\max}$ increased to 66 kt at 1439 UTC fix but pressure held relatively steady at 994 hPa. This CDO grew in size and the inner cold cloud features displayed signs of banding and rotation. By 2322 UTC, the $p_{\min}$ had dramatically deepened to 981 hPa. Shortly thereafter, an 81 kt FL $v_{\max}$ was reported. Early on the 2nd, the CDO "rolled over" — a development pattern which has often been observed prior

to eye formation. Near this time, aircraft reported 89 kt flight level winds (80 kt surface equivalent) and an unremarkable 4 °C dew point temperature depression at flight level (700 hPa. The pressure had not deepened further however. Shortly afterward, the cloud shield warmed, the CDO dissipated, and the center became largely free of deep convection as the storm moved rapidly to the north. This storm illustrates why the CDO pattern in the Dvorak pattern is called the "pattern of last resort". Because the CDO often obscures the low level cloud features, the center is hard to locate and it can be very difficult, if not impossible, to distinguish an eye from the occasional warm spots (or even cold rings) that may develop in the cloud shield. In this case, it appears that these dramatic cold rings were *not* associated with eye development in Noel. When the CDO displayed more classical signs of a developing eye, none appeared and the storm weakened. With a BT $v_{\max}$ of 70 kt during this time period, Noel is yet another example of an eye-less hurricane.

Rounding out the rest of the storms in the second part of Table 5.3, Hurricane Gordon (1994) was relatively well-observed (although no satellite imagery is available) and came close to forming an eye after a rapid increase in intensity. Banding was observed and a FL $v_{\max}$ wind reached 96 kt. Hurricane Andrea (2007) began as a subtropical development and had difficulty gathering enough convection about its center to be considered an eyewall. Several other storms reported banding which indicates that they may have been close to forming an eye.

To summarize, the upper bound of intensity for a storm to not achieve an eye appears to be at least $80-85$ kt, with a corresponding lower bound for $p_{\min}$ of about 980 hPa. From our few brief case studies, it seems that storms that fail to form an eye are often being disrupted by vertical wind shear,[14] the influence of land (e.g., Noel 2007), or possibly due to disruptive deep convection (e.g., Noel 2007) or the presence of multiple low level centers (e.g., Earl 1998). Some of these eyeless hurricanes went on to become powerful extratropical storms later in their lifetime.

[14] Using satellite imagery alone, it is often difficult to tell whether a storm is really being disrupted by shear or whether cloud debris advecting into the eye region are merely obscuring the eye. Of course, if sufficient cloud debris enter the eye region, evaporational cooling can substantially weaken the warm core and also act to weaken the storm. Once the low level center becomes exposed however, this issue becomes clear.

5.5 Intensification rates before, during, and after eye formation

This section examines the trend in intensity during the eye formation process. We will seek to answer the following questions: "What is the relationship between intensification and eye formation? Does the formation of the eye (and warm core) really precede significant intensification? Which eye formation baselines are associated most strongly with intensification?"

5.5.1 Intensity curves for aircraft-based eye formation baselines

Fig. 5.13 shows storm intensity interpolated to a 6-day time window centered on various observational baseline times for eye formation. This particular figure shows both the BT (blue) and rFL (red) v_{max} interpolated for the four aircraft baselines: first banding (B), first eye (open or closed, A), first open eye (A1), and first closed eye (A2). The individual storm intensities are displayed by thin solid lines (light blue for BT v_{max} and light pink for rFL v_{max}). This 'spaghetti plot' allows the reader to assess changes in the intensity distribution over time. The mean intensities for the B baseline (Fig. 5.13a) show that storms generally intensify steadily but slowly up until about 12 h before the first report of banding, with a relatively quick pickup in intensity up until the time in which banding is actually observed. Then the intensification rate slows and eventually levels off. Over the 6 d time window, the average intensity rises from about 27 kt at the beginning (72 h before B) to 77 kt by the end of the period. Examining the individual storm intensity curves, a significant bifurcation is seen at the time of B. A small subset of storms rapidly intensify to high intensity while many others intensify more slowly. After a day or two, some of these moderate intensifiers keep intensifying steadily while others begin to decrease in intensity. A small subset of storms which display B at quite low intensities ($v_{max} < 35$ kt exhibit little or no intensification afterward. This bifurcation behavior illustrates the general behavior of the distribution of storm intensities as storms either succeed in forming eyes and continuing to intensify, or fail to form an eye.

Fig. 5.13a shows the intensity curves for the A baseline (first aircraft eye, open or closed). The reader may notice that many of the individual curves look similar to those for B. This, is of course, because they are the same curves (from the same general set of storms) — but shifted left or right in the plot depending on the difference in timing between when the B and A baselines were observed for

each storm. This baseline has a larger number of cases near the edges of the time window, so the mean intensity curve should be more reliable. Overall it is quite similar to that of B, except it is smoother.[15] The reader should keep in mind that the A baseline includes both cases in which the initial eye was open, and cases in which it was closed. To better resolve the intensity trend information, the lower panels display the intensity curves for open and closed eyes separately. By comparing the two panels, it can be seen that the A2 storms are intensifying more rapidly at the baseline time. Furthermore, three days after the baseline is reached, the storms that initially formed closed eye had an average intensity between 5 and 14 kt stronger (using the BT and rFL curves, respectively). An interesting divergence occurs between the BT and rFL v_{max} mean curves in all four panels. In general, BT v_{max} is 2 to 4 kt greater than rFL v_{max} up until a day or so after the baseline time. After this point, the rFL tends to be a few knots greater than BT v_{max}, except in the A2 case where it is more than 10 kt greater. These differences might be due to our method of reducing the flight level winds to surface equivalents (the 'real' reduction factors may change as a storm reaches hurricane intensity) — or they could be due to systematic biases in the BT winds.

To better understand the impact of the failure or success of eye formation on storm intensification, we now present interpolated intensity curves composited for all the storms for each of the four eye formation case types. The resulting panel plot is shown in Fig. 5.14 for the A baseline. Splitting the 70 valid cases into 4 categories results in fewer storms for each composite, but the intensity 'signals' obtained are significantly stronger. The complete failure composite intensity displays a very clear pattern of strengthening in the 24-h period leading up until A, then peaking followed by weakening. The intensity over the 6 d period rises from 30 kt to a peak of 56 to 60 kt about 6 to 12 h after the time the first eye is reported, then decreases to just 35 kt 3 d after A. The individual curves display some variations on this theme, but no storm ended the period above 55 kt. The number of cases after this baseline decreases as storms either hit land or ceased to be designated as tropical storms.

The intermittent failure cases (Fig. 5.14b) display a similar intensity evolution up until the baseline, but rather than decreasing, the intensity remains rather flat with a slow downward drift. The peak intensity occurs about 24 h after A and the mean storm intensity ends the period at 55 kt. One storm keeps

[15] The limited number of rFL v_{max} curves 72 h after the B baseline means that the mean intensity there may be less reliable and more subject to noise. Thus, the B storms may not necessarily exhibit higher intensities than the A storms — this could be a statistical artifact.

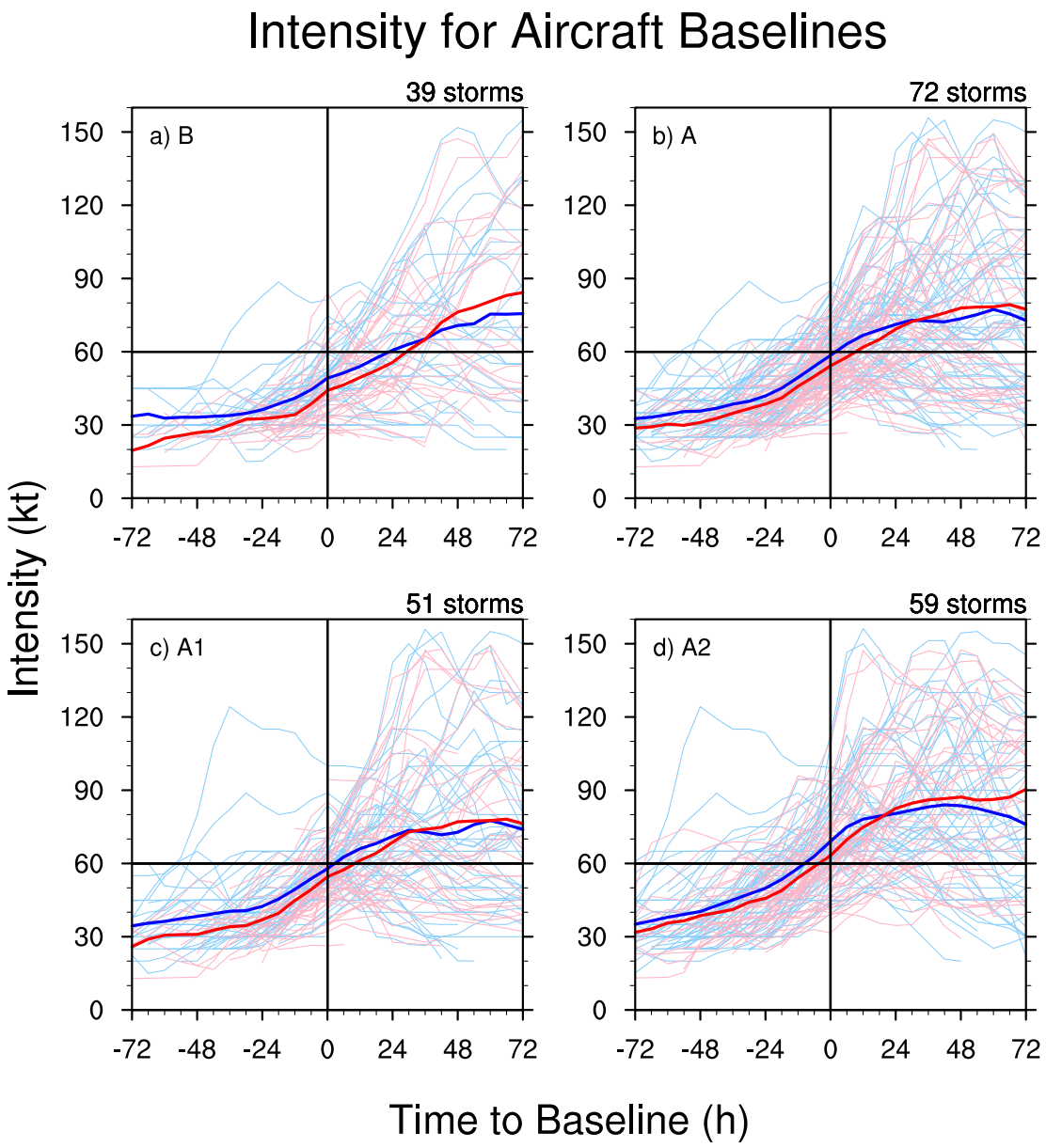

Figure 5.13: BT v_{max} and rFL v_{max} interpolated to various times before and after the following aircraft-based eye formation baselines: first report of banding (B), first report of any eye (open or closed, A), first report of an open eye (A1), and first report of a closed aircraft eye (A2). Each panel shows all of the individual intensities of storms for that particular baseline for both the BT v_{max} (thin light blue lines) and the rFL v_{max} (thin light pink lines). The mean intensities computed from the individual storms are also shown for both the BT v_{max}(thick blue line) and the rFL v_{max}(thick red line). Data from periods when a storm was over land are not included for the BT v_{max}. For the reader's convenience, a vertical reference line has been added at zero on the time coordinate to indicate the time when aircraft first reported an eye. Similarly, a horizontal baseline has been added at $v_{max} = 60$ kt. Results are paneled for the following case types: a) complete failure, b) intermittent failure, c) delayed success, d) complete success.

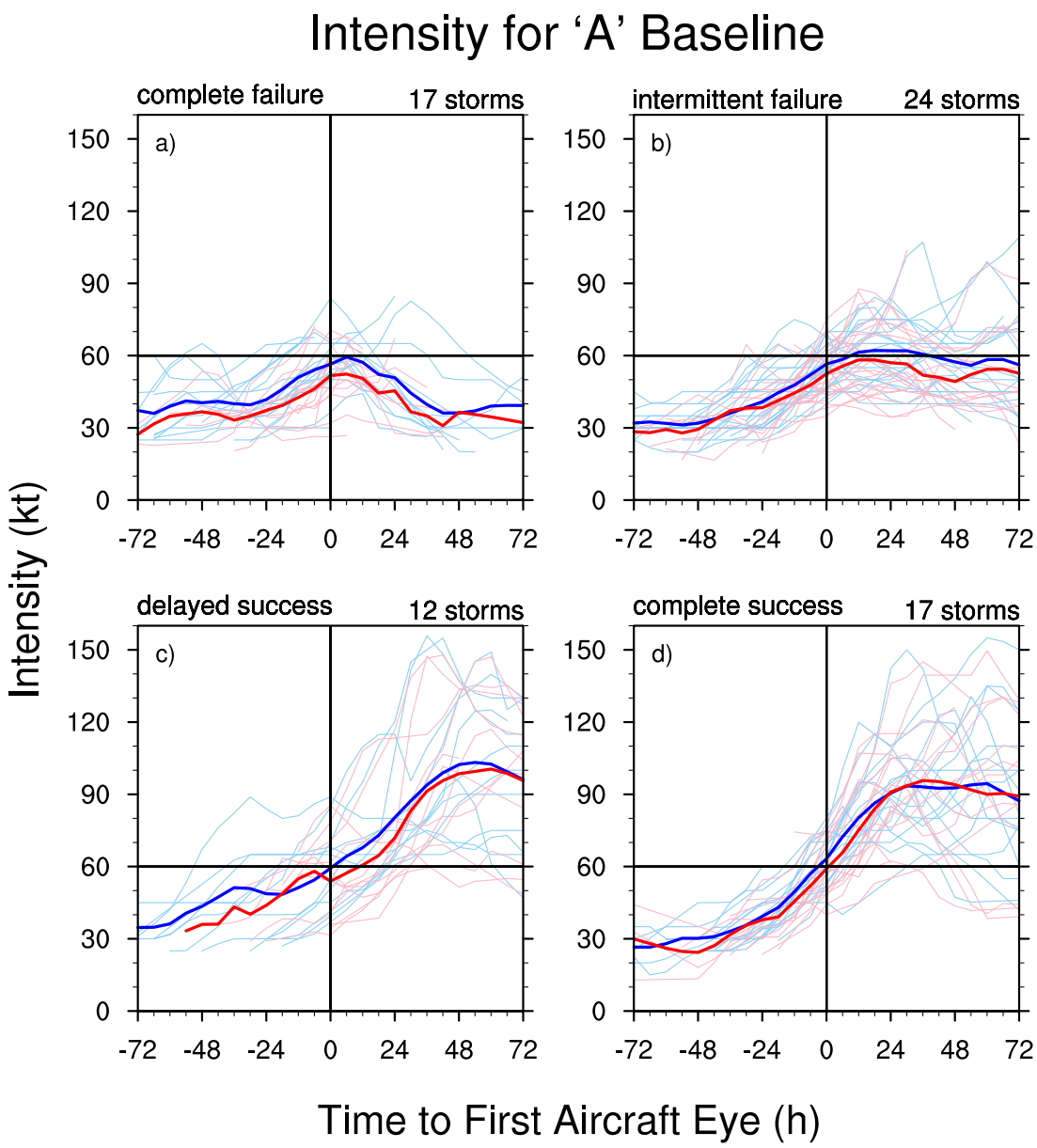

Figure 5.14: BT v_{max} and rFL v_{max} interpolated to various times before and after the first report of an open or closed aircraft eye (A). Each panel shows the individual intensity curves of storms in the designated eye formation case type and the mean composite intensity of those cases. Line colors and thicknesses are as in Fig. 5.13. Data from periods when a storm was over land are not included for the BT v_{max}. Results are paneled for the following case types: a) complete failure, b) intermittent failure, c) delayed success, d) complete success.

intensifying rapidly at the end of the period - this storm likely formed an eye successfully after the 3 d time window from the first attempt. The mean intensity curve is skewed upwards by these intensifying late eye-formers, but the majority of storms end the period at lower intensities than the mean.

The delayed success cases (Fig. 5.14c) comprise just 12 storms and are therefore more susceptible

to statistical noise. Nevertheless, these cases display intensification both before and after forming the eye (although the rates are quite uneven). Some storms intensify and then level off or decrease before the baseline, while others are flat for part of the period. A small number of storms intensify rapidly straight through A. This case type also includes a substantial subset of storms which reach A at relatively low intensities of 30 to 45 kt, but then rapidly intensify from 12 to 36 h after A. These "early eye-formers" seem to have a very significant and strong intensification signal. The composite mean rFL $v_{\max}$ experiences the strongest rate of increase between 18 and 36 h after A. During this period, it rises from 65 kt to 95 kt, an intensification rate of about $40\,\mathrm{kt\,d^{-1}}$. The composite intensity is influenced in part by the extreme intensification of Hurricane Wilma (2005). A structure and intensity plot for Wilma has been given in Fig. 5.5 and shows that the storm began intensifying very rapidly starting about 24 h after the aircraft eye was first reported. The mean intensity of the delayed success storms peaks at about 105 K around 48 h after A and then decreases thereafter.

The complete success storms (Fig. 5.14d) show the most consistent intensity trend with rapid intensification from 18 h before A until 18 h afterward. Unlike the varied and halting intensifications of the delayed success cases, nearly all of the complete success storms intensify gradually starting 48 h before A. The intensification rate picks up significantly about 16 h before A and continues at a blistering pace. Peak intensity is reached in a fairly wide time window from 12 to 60 h after A. The composite intensity peaks at 95 kt by about 36 h after A and then slowly decreases to 90 kt by the end of the period. Comparing these complete success storms to the delayed success cases, a greater proportion of the complete success storms have decreasing intensities by the end of the period. The maximum intensity is also about 10 kt lower.

Putting all this together, the storms which fail to form an eye experience intensification up until (or just after) the formation attempt, then have flat or decreasing intensities. Storms which successfully form an eye tend to experience strong intensification once a persistent eye has formed[16] and reach a higher overall intensity. Storms which form eyes successfully and maintain them intensify the most rapidly for the longest time, but peak earlier and reach a lower intensity than storms which experienced a delay

[16] This is built into the definition of our case types and explains why the delayed success cases experience their peak intensification rate a day or so after reaching A

in their formation process. Finally, we note that eye failures tend to occur at lower intensities than the successful eye formations. As previously noted, this may be entirely due to the fact that the storms are being sampled only every few hours and the successful storms may simply be intensifying more rapidly — or this may be a legitimate and important result which deserves further scrutiny.

5.5.2 Intensity curves for satellite-based eye formation baselines

The use of aircraft-based eye formation baselines reduces the number of available cases since a storm has to be under active aircraft reconnaissance to be included in the 70 valid eye formation cases. We can eliminate this impediment by examining the intensity trends interpolated to a time window centered on the satellite-based eye formation baselines. Fig. 5.15 plots the intensity traces for all the storms and the resulting mean composite intensity curves for the IR2, IR3, IR4, and IR5 baselines. The number of cases for IR2 is about double that for A, while the number of IR3 cases is more than 60% greater. These greater number of cases should yield very reliable composite means.

Before going into the actual results of this plot, let us first turn our attention back to the curious discrepancy between rFL $v_{\max}$ and BT $v_{\max}$ that was noted previously. While the number of individual rFL curves must be less than the number of BT curves (since many of these additional cases were not observed by aircraft), in all four panels, the two composite intensity curves track quite closely up until 24 to 72 h after the baseline time. After this time however, the differences are considerable for all four IR baselines. In IR3, rFL $v_{\max}$ is more than 10 kt greater than BT $v_{\max}$. Since this baseline has 117 storms, this is unlikely to be merely a statistical artifact. What could be causing this? The astute reader may now realize that the discrepancy is most prominent *after* storms have reached their peak intensity. It seems likely that the higher rFL winds manifest the very strong circulation that occurs in the middle levels of the storm even as the lower level winds have begun to spin down. Storms often seem to intensify from the bottom upward as momentum is carried aloft by deep convection. It seems that they also weaken from the bottom up as well.[17] Because our method of reducing the flight level winds to surface equivalents does *not* take the storm life cycle into account, this effect may solve our conundrum. Following this

[17] When a storm begins decaying, friction spins down the boundary layer winds faster than at midlevels. Since the convection tends to be weaker at this stage, the lower angular momentum near the surface is not communicated to the midlevels right away.

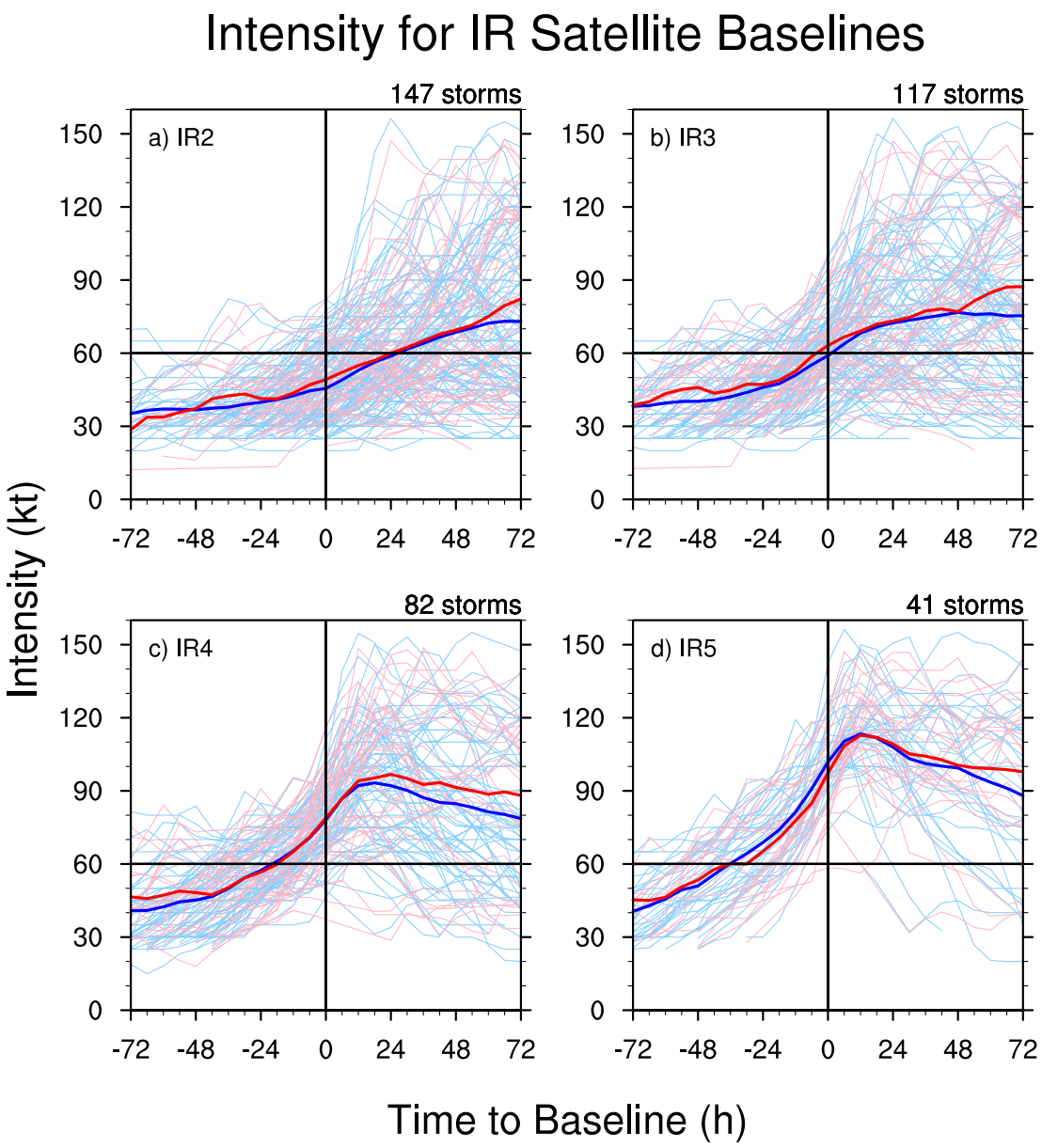

Figure 5.15: As in Fig. 5.13, but for the IR satellite baselines: IR2, IR3, IR4, and IR5.

reasoning, one might expect that rFL v_{max} should be below BT v_{max} before this time period, and it is, but not by very much. This is likely due to the fact that aircraft usually fly developing storms at lower flight levels (925 hPa and 850 hPa) when the storm is still weak. Once the storm has reached hurricane intensity, the flights usually occur at the 700 hPa level. So this proposed *reduction factor* effect is likely a real, physical effect and only becomes apparent in these plots after the storms reach peak intensity.

Looking now at the individual panels of Fig. 5.15, we first note that the intensity distributions are

considerably greater than for the aircraft baselines. This suggests that the the IR satellite-based baselines contain less 'information' (or more uncertainty). The very wide range of intensities at the end of the 6-day time window imply that intensity for these baselines is not nearly as constrained. The tightly clustered intensity curves based on the IR5 baseline are an exception to this general guideline, however. This suggests that storms displaying a strong eye tend to follow a well-defined intensity evolution. Comparing the IR2 and IR3 composite curves, little difference can be seen overall, except that the mean intensity curve for IR3 is about 5 to 10 kt higher and exhibits a bit more intensification from 24 h before the baseline until 12 h afterward. The IR4 composite curve displays a much more robust intensification trend, going from about 55 kt at 36 h before the IR4 baseline, to more than 90 kt by 12 h after IR4. The composite curve then abruptly levels off, reaching a peak of about 95 kt at 24 h and then decaying thereafter. Unlike the IR3 curves, nearly all storms that reached the IR4 baseline reach a peak intensity of at least 60 kt. Many intensify very rapidly to peaks of 100 to 150 kt about 18 h after IR4. The IR5 curves are similar with respect to the timing of peak intensity and the gradual decay afterward, but the IR5 curves exhibit even more rapid intensification starting around 60 h before the baseline time. The peak intensity occurs just a bit sooner than IR4 — about 6 h after the IR5 baseline. This makes sense, as storms which exhibit strong eyes have already been intensifying for longer and reach a higher intensity than when they exhibit the persistent eye. The mean intensity reached by these IR5 storms is an incredible 110 kt.

Synthesizing these results for the IR baselines, we note that storms displaying *any* of these tend to continue to develop, on average. The greater uncertainty inherent in the IR2 and IR3 classifications likely results in some false positives in eye detection. This can be seen by the great number of non-intensifying curves at the later time periods. The appearance of a persistent eye, on the other hand, is a very definite guidepost in the storm's development and portends strong intensification in many cases. Since our IR4 classification requires that the eye persist for 6 h (and the IR4 baseline is taken at the beginning of this period), the utility of a persistent eye is somewhat diminished by this delay. This is because most storms reach their intensity peaks just 12 h after the IR4 baseline is verified (18 h from when the eye first is persistent). The IR4 baseline may be most useful as an indication that the storm is currently in its most rapid intensification phase. The IR5 baseline on the other hand tends to occur at about the time the intensification is beginning to slow — these results suggest that the appearance of a strong eye indicates

that the storm will reach peak intensity in 6 to 12 h.

To compare the aircraft and IR satellite baselines to each other, the mean intensity curves for all baselines (B, A, A1, A2, IR1, IR2, IR3, IR4, IR5) are displayed together on Fig. 5.16 for all available cases for both the BT v_{max} (upper panel) and the rFL v_{max} (lower panel). The corresponding intensification rates, computed by subtracting the current intensity from the intensity 6 h previous, are shown in Fig. 5.16. In general, the baselines which correspond to a lower level of storm development (B, IR1, and IR2) show flat to low intensification rates up until the baseline time, then modest rates of up to 4 kt in a 6-h period after that time.[18] These baselines are the first indications of possible eye development and structural organization, so it is significant that intensification rates trend upward near the baseline time (sometimes intensification begins up to a day before the baseline). The intensity curves of the IR1 baseline seems to possess the weakest signal. The IR1 baseline likely contains just a small amount of information about storm development and is probably not very useful. The A1 intensity curve corresponds closely with the A baseline (Fig. 5.16) and follows trends as discussed previously. The A2 and IR3 composite intensities coincide at the beginning, middle, and end of the period, but the A2 storms display a stronger intensification signal from the baseline time until about 48 h later.

Looking at the quantitative intensification rates more closely (Fig. 5.16), we see that the intensification rates for all the baselines resemble a cosine curve with the peak rate near the baseline time (a phase of zero in the cosine curve). The reason for this is due to in part due to statistics. Storms which hit a given baseline tend to be developing and intensifying. Once the baseline has been achieved, the storms become part of the data sample for that baseline, but after this baseline all sorts of (bad) things can happen to the storm — it may hit land (and thus be masked out), it may encounter a hostile environment (strong vertical wind shear, dry air, or low SSTs), or it may simply weaken. At the time the storm achieves the given baseline, it is mostly likely to be intensifying. Further away from the baseline time, it is less likely that intensification is occurring. Therefore it is no surprise that nearly all the baselines exhibit a peak intensification rate near or on the actual baseline — selection bias causes it to be so. This

[18] From here on, we will give intensification rates with units of knots change per 6-h period [$\mathrm{kt\,(6\,h)^{-1}}$]. The main reason for using a 6-h period is that the most rapid intensifications do not normally last a full 24-h period. Intensification rates are not usually constant over a 24-h period anyway. Since warning advisories are issued every 6 h, this period is a natural one to use for expressing intensification rate.

effect is not entirely overwhelming, however. The peak intensification rate of IR1 occurs almost a day after the baseline, for instance. The intensification rates for all baselines drop by 3 d after the baseline however. In general, this is because most storms only last between 4 and 10 days, so the longer one looks out, the more likely he or she will be seeing the decay stage of the storm. The lower baselines (B, IR1, A1) decay more slowly because these include a much larger sample of storms that may or may not have intensified much previously. The IR4 and IR5 baselines display the strongest and most rapid drops in intensity — the storms which reach these baselines have a high intensity to decay from. There is a suggestion of a 'bounce' in the IR5 intensification rate curve however. If reliable, this indicates that once a storm has rapidly intensified, it tends to decay a bit, but then reaches a steady state (on average). The conventional wisdom is that storms often rapidly intensify until either an eyewall replacement halts intensification, or a horizontal vorticity mixing event occurs pushing the storm into Kossin and Eastin 'regime 2' (2001. The peak intensification rates calculated here (using the smoother BT $v_{\max}$) are $3\,\mathrm{kt}\,(6\,\mathrm{h})^{-1}$ for IR1, $4\,\mathrm{kt}\,(6\,\mathrm{h})^{-1}$ for B and A1, $5\,\mathrm{kt}\,(6\,\mathrm{h})^{-1}$ for IR3, $6\,\mathrm{kt}\,(6\,\mathrm{h})^{-1}$ for A2, almost $9\,\mathrm{kt}\,(6\,\mathrm{h})^{-1}$ for IR4, and more than $12\,\mathrm{kt}\,(6\,\mathrm{h})^{-1}$ for IR5.

5.6 Environmental role during eye formation

Since it is observed that all storms will form an eye eventually if they get strong enough (e.g., an intensity exceeding 90 kt), it is interesting to question the fundamental nature of eye formation. Is eye formation a manifold attractor of the dynamical system or is a stochastic process whose success or failure is dependent on random interactions between the convection? The role of environmental influences during eye formation may offer a partial answer to this question. If the eye/eyewall structure is an attractor of the system, then the reasons for failure should be external to the system.

As a preliminary test of this idea, the environmental vertical wind shear has been subjected to a stratification analysis about the time of eye formation in the same manner as intensity. The SHDC parameter is used from the SHIPS development data set. This variable measures the vertical shear between 850 and 200 hPa and is calculated from global model analyses for an annulus about the storm. The result is shown in Fig. 5.18. The composite mean shear is fairly low in the days leading up to eye formation, with most individual storms experiencing less than 20 kt of shear before they form eyes. The actual shear

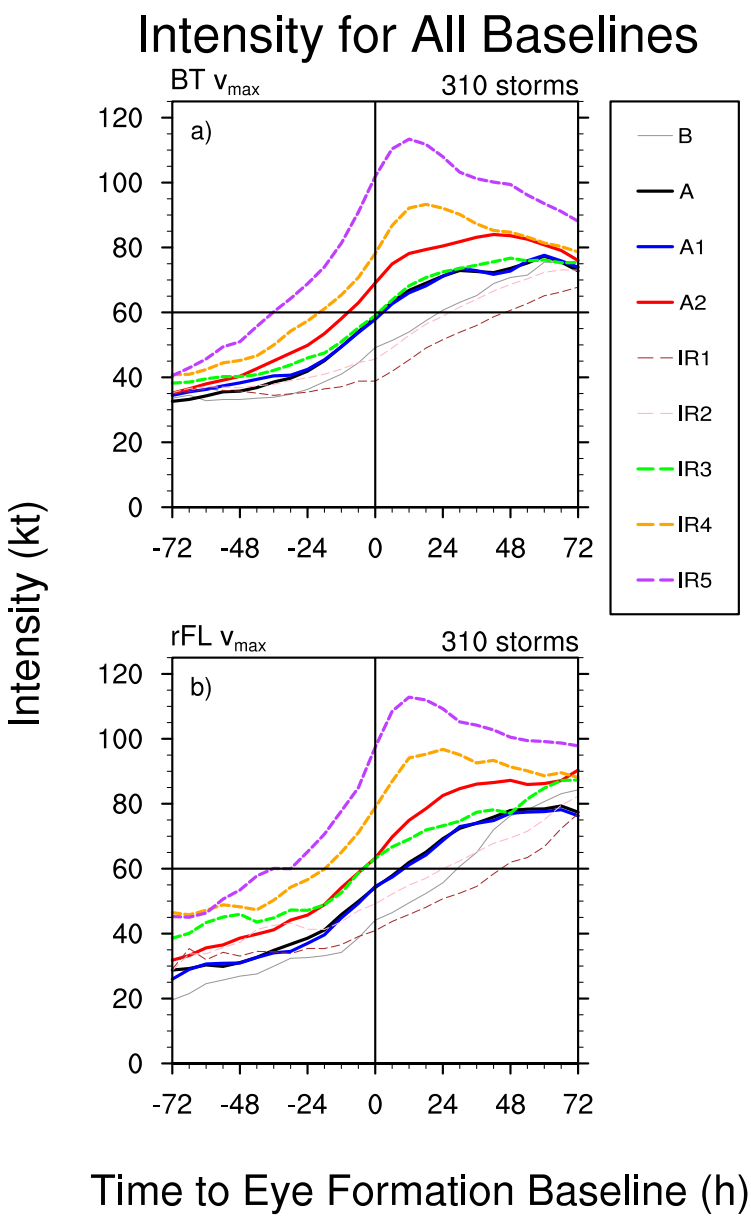

Figure 5.16: Composite mean intensity curves for each of the aircraft and IR satellite baselines (B, A, A1, A2, IR1, IR2, IR3, IR4, and IR5) for BT v_{max} (upper panel) and rFL v_{max} (lower panel).

value is quite low for all of the formation case types at the time of eye formation, ranging from 15 kt for the complete failure and intermittent failure cases, to 11 to 12 kt for the delayed success and complete success cases. The shear was less than 25 kt at the time of eye formation for nearly all the storms in this data set. After the initial formation attempt, the shear increases rapidly to greater than 20 kt in a number of the complete failure cases. For the cases which succeed, the shear stays low, allowing continued development. An initial conclusion is that the high environmental vertical shear has a strong disruptive

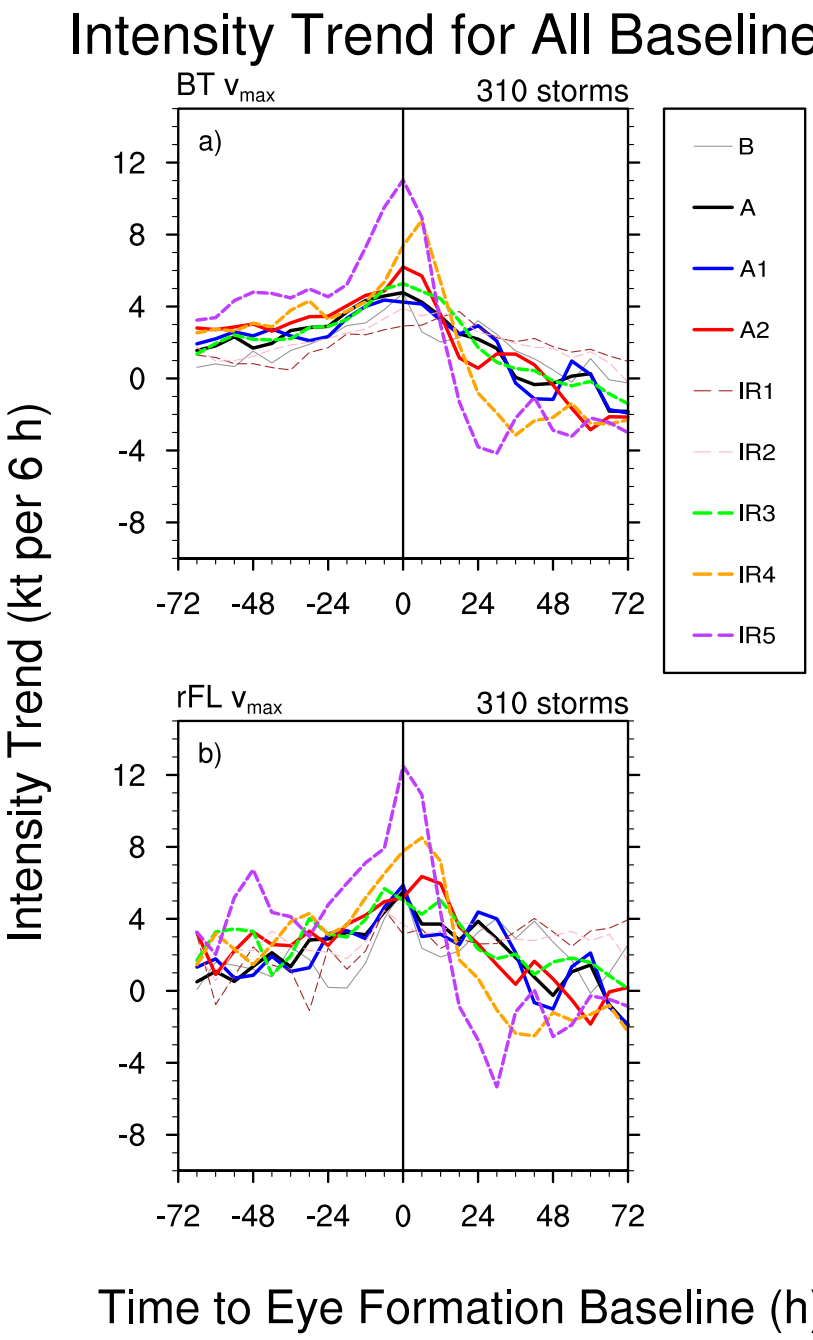

Figure 5.17: As in Fig. 5.16, but for composite mean *intensification rates*.

influence on eye formation. The influence of other environmental factors and an answer to our overall question requires further analysis.

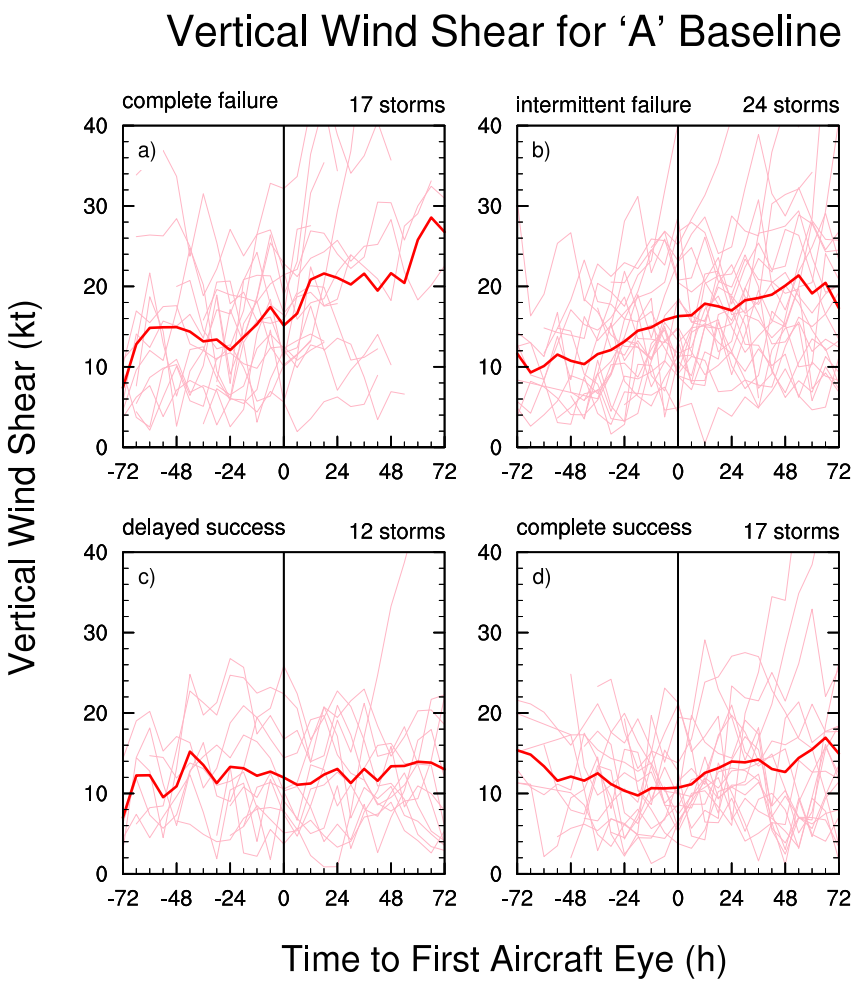

Figure 5.18: Vertical wind shear (SHDC) for the ‘A’ baseline, stratified by eye formation case type. The composite mean of the respective cases is indicated by the thick, solid line.

5.7 Discussion

As discussed in chapter 4.1, the idea that storm intensity is limited until it has formed an eye held currency with early pioneers in the field such as Malkus (1958b) and Yanai (1961). Subsequent observational work by Mundell (1990) showed that Pacific typhoons generally begin their rapid intensification period in the range of intensities and pressures at which the eye generally forms. The most common intensity at which rapid intensification commenced was 67 kt; approximately two-thirds of the storms which underwent rapid intensification began their RI episode at intensities ranging from 55 kt to 78 kt. With the development of a warm core and the concentration of diabatic heating into an eyewall, it is easy to see how this could be a positive for storm intensification. Yet, some researchers, namely Schubert and

Hack (1982), suggested that the formation of an eye should stabilize a storm to run-away intensification. Their argument was based on the idea that the development of an eye must necessarily remove diabatic heating from the high inertial stability region of the inner core, thereby preventing the overall storm efficiency from becoming singular. In chapter 3, an attempt was made at reconciling these competing ideas by postulating that the eyewall heating may still boost storm efficiency (making it dynamically-large with respect to the area of heating) even as the physical scale and the overall amount of heating may shrink as the eye contracts. This idea has some support from the numerical results of Pendergrass and Willoughby (2009).

The present study has shown that storms are intensifying slowly before the B, IR1, and IR2 baselines. Intensification accelerates for a storm which reaches the eye formation baselines corresponding to greater eye definition and structural organization, so that a storm on average is intensifying most rapidly *during* eye formation. The intensification rate slows down once the eye has matured and becomes visible in satellite imagery. Some storms however keep on intensifying rapidly for another 36 h. So it seems that the start of the eye formation process is a response to the gradual intensification of the storm. If the eye formation is successful, storm intensity responds strongly. Peak intensity represents the end of the eye formation process.

5.7.1 Comparison with previous work on the intensity threshold for eye formation and subsequent intensification rates

Now we compare our results for the intensity threshold for eye formation to those from cited in previous studies. While there are some references to the eye forming at relatively low intensities (e.g., about 45 kt in Malkus 1958b), an oft-cited value is the 'myth' (perpetuated by Shapiro and Willoughby 1982) that storms tend to form eyes when the pressure reaches 985 hPa and $35\,\mathrm{m\,s^{-1}}$ (68 kt). This is actually not so misleading, however, if this value refers to the maximum wind speeds anywhere in the vortex, rather than the surface value. Regardless, the present work clearly shows that the eye begins forming at a significantly lower intensity.

Figure 5.19 shows the Dvorak model of tropical cyclone development, where various stages of structural organization and the corresponding intensity indicated by a model 'T-number'. Comparing our

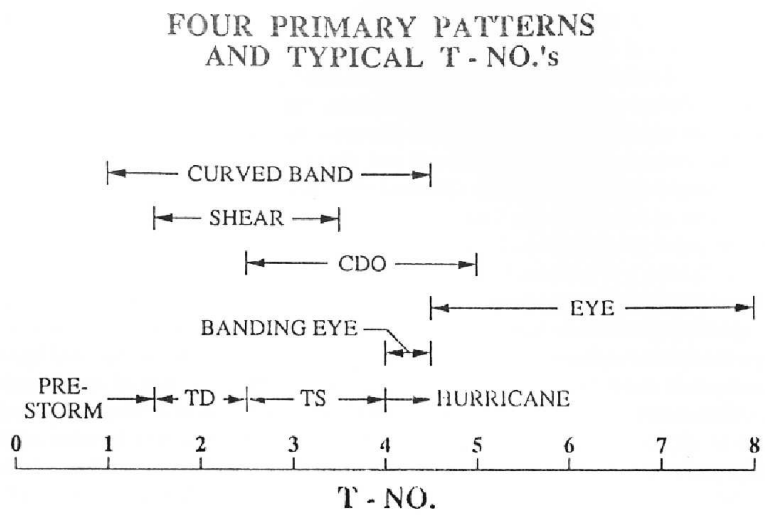

Figure 5.19: The Dvorak model of tropical cyclone development, showing intensity at each stage of storm development. A typical progression is one T-number per day. Reproduced from Karyampudi et al. (1999).

results to the Dvorak method (Dvorak, 1984), our intensity threshold for eye formation is lower than the Dvorak model. In that model, a banded eye scene can appear at a Dvorak T number of 4.0 65 kt, but the eye scene (an obvious cleared eye) is typically evident at T4.5 (77 kt). This latter value corresponds precisely to the intensity we observe for the persistent eye baseline (IR4): BT $v_{\max}$ of 77 kt (the rFL $v_{\max}$ is a bit higher, at 82 kt). The lowest intensity Dvorak allows for a poorly defined ragged eye is T3 (45 kt). Thus, the lowest possible eye designation allowed by Dvorak is still higher than the lowest intensity we found of an eye forming near tropical storm intensity (35 kt). It is possible that at least part of this discrepancy is due to changing understanding of the reduction factors for obtaining a surface wind estimate from flight level winds. If so, this suggests that the Dvorak method could be recalibrated. Looking at the upper bound for eye formation, the Dvorak technique allows for a storm to be as strong as 102 kt without an IR eye (personal communication, R. Zehr 2009).

While this study has not examined rapid intensification explicitly, our results are consistent with what have been found by some previous workers. Specifically, Mundell (1990) asserted (p. 31, 34) that "Rapid intensification commences once a central eye develops." Weatherford and Gray (1988b) found that rapid deepeners formed eye at a higher intensity than normal (985 hPa compared with the normal value of 981 hPa). According to Mundell, the "prediction of a rapid intensification event should only be

made after development to at least 26 m/s (50 kt or until an eye is apparent on satellite or radar." A recent rapid intensification (RI) forecast scheme (Kieper, 2008) requires that a storm achieve an intensity of at least 45 kt before RI can be predicted.

5.8 Summary and conclusions

This study has examined the eye formations for a broad set of Atlantic tropical cyclones that occurred from 1989 to 2008. Out of the 180 tropical cyclones, 70 were reconnoitered during the time when the initial eye formed. Using a novel method to determine the upper bound curve of the flight level maximum wind speeds obtained from VDMs, a surface equivalent intensity time series was obtained for each storm and interpolated to a 6-day window centered on the time when the aircraft or satellite first reported an eye.

Here is a summary of some of the major findings and conclusions of this chapter:

(1) **Banding found to be a precursor to eye formation**: Banding was often noted by aircraft before an aircraft eye appeared and was observed in 43% of all storms. Of the storms which displayed banding, 79% went on to form an aircraft eye. Clearly, banding is a strong precursor to eye formation, but since it is only reported some of the time, its usefulness to a forecaster may be somewhat limited.

(2) **Eyes are more frequently seen in satellites than by aircraft**: 59% of reconnoittorred storms reported an aircraft eye. Closed aircraft eyes (A2, 47%) were less commonly observed than open aircraft eyes (A1, 58%), as expected. 61% of all storms reported an eye in IR satellite imagery (IR3), but only 43% developed an IR eye which lasted longer than 6 h, and just 21% displayed a strong eye (IR5). Out of the storms which were well observed by both aircraft and satellite, eyes were more frequently observed by satellite (IR3, 67%) than by aircraft (A, 58%). This result was unexpected since it has been generally thought that the convective ring of the developing eyewall should be apparent before the eye is observed by satellite. It is unclear whether this statistic is simply due to the less frequent observations of aircraft, or whether perhaps the indications of a forming eye are more apparent than previously thought.

(3) **Storms which form aircraft eyes tend do so quickly after reaching tropical storm threshold**: The temporal distribution of the observed eye formation baselines shows that most of the storms which form eyes (whether successful or not), tend to do so with 24 h of reaching tropical storm strength (35 kt). This is somewhat quicker than the Dvorak model and seems to suggest that there is about a 1 d window during which a storm which has recently undergone genesis can quickly form an eye. If the environmental conditions are not favorable so that the initial attempt fails, the storm may take days and days to form an eye. But the failure of the initial eye is not necessarily detrimental — a sizable subset of storms form an eye which does not persist, but upon reforming an eye within a day or so, continue on a rapid development. This suggests that environmental conditions may play a key role in the success or failure of the eye. If adverse conditions improve, the storm development can be rapid.

(4) **Many storms which form an eye begin doing so at intensities substantially lower than hurricane intensity**: Eye formation often occurs at a significantly lower intensity threshold than some of the mythological values that appear in the literature. For our 70-storm sample, both the 'A' eye and the IR3 eye appear at a mean BT intensity of 58 kt. This is considerably below some values which have been reported, such as the oft-cited 68 kt from Shapiro and Willoughby (1982) or the 65 to 77 kt given by the Dvorak model (Dvorak, 1984).

(5) **An increasing intensity trend is seen with improving structural organization**: Storms intensify as they progress from the baselines associated with less structural organization [such as open warm spots (IR1, 38 kt), closed warm spots (IR2, 45 kt, and the first aircraft observation of banding (B, 50 kt)], to baselines associated with more defined eye structure: the open aircraft eye (A1, 56 kt), the first satellite eye (IR3, 58 kt, the first closed aircraft eye (A2, 68 kt), the first persistent satellite eye (IR4, 77 kt), and finally, the first strong satellite eye (IR5, 101 kt).

(6) **The lower bound intensity for eye formation is near minimal tropical storm strength**: The least intense tropical cyclones to sport a bona fide eye was TD5 (1994) and Henri (2003), both of which were close to minimal tropical storm strength with maximum sustained surface wind speeds of 30 to 35 kt.

(7) **The upper bound intensity for eye formation is at least 80 to 85 kt**: The most intense tropical cyclone in the data set to not form an eye was Hurricane Earl (1998), which was being disrupted by high shear and about to undergo extratropical transition. Storms which do not form eyes at high intensity often display some of the commonly-observed precursors to eye formation, such as a distinct 'curl' of a deep convective 'blob' as it rotates and rolls over the north side of the center. Some storms will even display cold rings in the IR imagery, but it seems that these are local mesoscale features associated with the deep convection that do not persist or have a strong dynamical influence on the resulting storm evolution.

(8) **Storms which form eyes successfully and maintain them intensify the most rapidly *once a persistent eye has formed***: These successful cases intensify the longest and reach the highest overall intensity. An interesting subset of success cases experience very rapid intensifications. These are storms in which an eye forms, but then is stymied until a persistent eye can form later (usually about a day or so). Many of these rapid intensifiers seem to be late season tropical cyclones in the Caribbean which were held back by unfavorable environmental conditions. Once the conditions improved, development and intensification occurred rapidly.

(9) **Vertical wind shear is highly disruptive to eye formation**: Preliminary analysis suggests that eyes generally do not form if the vertical wind shear is above 25 kt. Most eyes form when the vertical shear is between 10 and 20 kt. This results suggests that environmental influences to play an important role, so the possibility that eye formation is a dynamical attractor of the system is not precluded, although more analysis is needed.

One of the key results of this study is that it confirms with observations the long-suspected idea that the formation of an eye is often associated with rapid intensification of the storm. The quantification of intensification rates associated for each of the eye development pathways (both satellite-based and aircraft-based) should be helpful for forecasters faced with the exceedingly challenging problem of real-time intensity prediction. Much more work is needed to quantify the timescales for eye formation and

rapid intensification episodes and to categorize the various eye development pathways using the convective morphology as seen in radar, satellite, and microwave imagery. Such results may offer the chance to refine the Dvorak model of tropical cyclone development and provide better intensity forecasts when aircraft data are unavailable.

Many more insights to the problem of eye formation may be gained by looking beyond just intensity or the environment. The next chapter will examine the kinematic and thermodynamic changes that occur in the inner core of the storm during eye formation.

Chapter 6

OBSERVATIONS OF HURRICANE EYE FORMATION: PART III: DYNAMIC AND THERMODYNAMIC CHANGES

> "I often say that when you can measure what you are speaking about, and express it in numbers, you know something about it; but when you cannot measure it, when you cannot express it in numbers, your knowledge is of a meagre and unsatisfactory kind."
> — Lord Kelvin (William Thomson, 1st Baron, 1824-1907).

6.1 Introduction

D. Nolan's idealized modeling study (Nolan, 2007) revealed several structural precursors to tropical cyclogenesis — the point in time when a mesoscale convective disturbance transitions into a self-sustaining tropical cyclone with the potential to intensify into a hurricane. His cloud-resolving simulations showed that the pre-storm disturbance undergoes an incubation period of 36 to 72 h or more, during which time scattered deep convective elements moisten the central column until it nears saturation through great depth (12 km or more). As this moistening occurs, there is little change in pressure or intensity of the simulated system, but the updrafts become more persistent and a mid-level vortex forms (if one did not already exist) and increases in depth. At the time of genesis, a small scale vortex forms very near to the surface within the broader mid-level vortex. This smaller vortex seems to form in association with a strong and persistent updraft that moves near to the center of the overall vortex. As such an arrangement is highly efficient at converting latent heat into kinetic energy, this smaller vortex rapidly intensifies in just a couple hours to become the core of the incipient tropical cyclone. In at least one of his simulations, an eye formed directly from this small scale vortex. This sequence of events was robust across a variety of initial vortices, so Nolan suggests that the moistening of the inner core may indeed be a trigger for the genesis of the tropical cyclone. The rapid contraction of the radius of maximum winds

(r_{max}) seems to provide an early signal that the storm has finished the genesis stage and has commenced the intensification phase. It is at this point that a storm is ready to start developing an eye.

The appearance of a small scale intense surface-based vortex is difficult to observe given the small scale nature of the updraft core (just 10 to 20 km across) and the very short time frame involved (1 to 2 h). When a disturbance is nearing tropical storm strength, reconnaissance aircraft typically fly low-level investigation missions ('invests') to see if a defined low level circulation has formed, as this is believed to be crucial for a developing storm. While it is generally known that r_{max} decreases as a tropical storm strengthens toward hurricane strength, the relation between r_{max} and eye formation has not been carefully examined through observations. Similarly, the development of the warm core is known to coincide with eye development, yet how rapidly does the warm core develop and at which levels? Does the warm core build upward as the eyewall develops, or does it build downwards from above? When does the peak warming of the eye column occur?

This chapter[1] computes trends for various structural and thermodynamical parameters obtained from VDMs before, during, and after the eye formation period for a broad set of Atlantic storms. The following flight level parameters are investigated: radius of maximum wind, minimum Rossby radius, central eye temperature, dew point temperature depression in the eye, horizontal temperature difference between the eye and the region outside the eyewall, and subsequent changes in size of the newly formed eye. The goal of this chapter is to quantitatively trace the structural and thermodynamic changes that occur during the eye formation process in the hopes of identifying structural precursors to eye formation. We would like to determine whether observations support Nolan's proposed sequence of events and whether there are other modes of eye formation. The theoretical argument of chapter 3 suggested that inertial stability plays a crucial role in facilitating the development of the warm core. In this chapter, we will examine whether *in situ* observations support this conjecture.

[1] This chapter will be submitted for publication to *Monthly Weather Review* as Vigh et al. (2010c).

6.2 Structural trends during eye formation

6.2.1 Radius of maximum wind

It is generally known that the radius of maximum wind (r_{max}) contracts as a young tropical storm intensifies, but is there a clear relationship between r_{max} contraction and eye formation? Once an eye has formed, does r_{max} stop shrinking? The flight level r_{max} is given in the VDM as the range (from the fix center) of the maximum flight level wind speed reported during the inbound leg of the fix. These r_{max} data are then interpolated to a time window centered on the various eye formation baselines described in chapter 5. The individual storm r_{max} traces and composite mean r_{max} are computed for both the BT and FL values and are shown for the aircraft baselines (B, A, A1, and A2) in Fig. 6.1.

Before attempting to interpret the physical meaning of the data presented in this figure, some discussion is in order on the considerable discrepancy between the BT and FL r_{max} values. For all panels of Fig. 6.1, and throughout the entire 6-day window, FL r_{max} is significantly less than BT r_{max}. The difference is greatest from 72 to 36 h before eye formation, during which time BT r_{max} exceeds FL r_{max} by approximately 15 to 20 n mi. In relative terms, the BT r_{max} values are approximately 30 to 90% greater than the FL r_{max} values. In the 24 h leading up to eye formation, the absolute difference narrows somewhat, but the relative differences are still as great since both the BT and FL r_{max} have contracted. 36 h after the eye formation baseline has been observed, the difference narrows to as little as 5 n mi. What could cause such a large discrepency?

Several factors may be responsible. First we consider the characteristics of the BT r_{max} data. These values are supposed to reference the radius of the maximum *surface* wind speed. Barring a highly sloped eyewall, a strongly tilted vortex, or a very incoherent vortex, it might be expected that the surface r_{max} should occur in the same general radial vicinity as the FL r_{max} for typical reconnaissance flight levels (925 hPa, 850 hPa, and 700 hPa). Given the propensity for the storm's angular momentum surfaces to slope *outwards* with height (Jorgensen, 1984a,b), one should expect the FL r_{max} to actually be somewhat *greater* than the surface r_{max}, not smaller. Indeed, a study which compared flight level and SFMR-measured surface winds found that on average, the surface radius of maximum winds was 0.875 the radius of the maximum flight level wind (Powell et al., 2009). Thus a normal outward slope

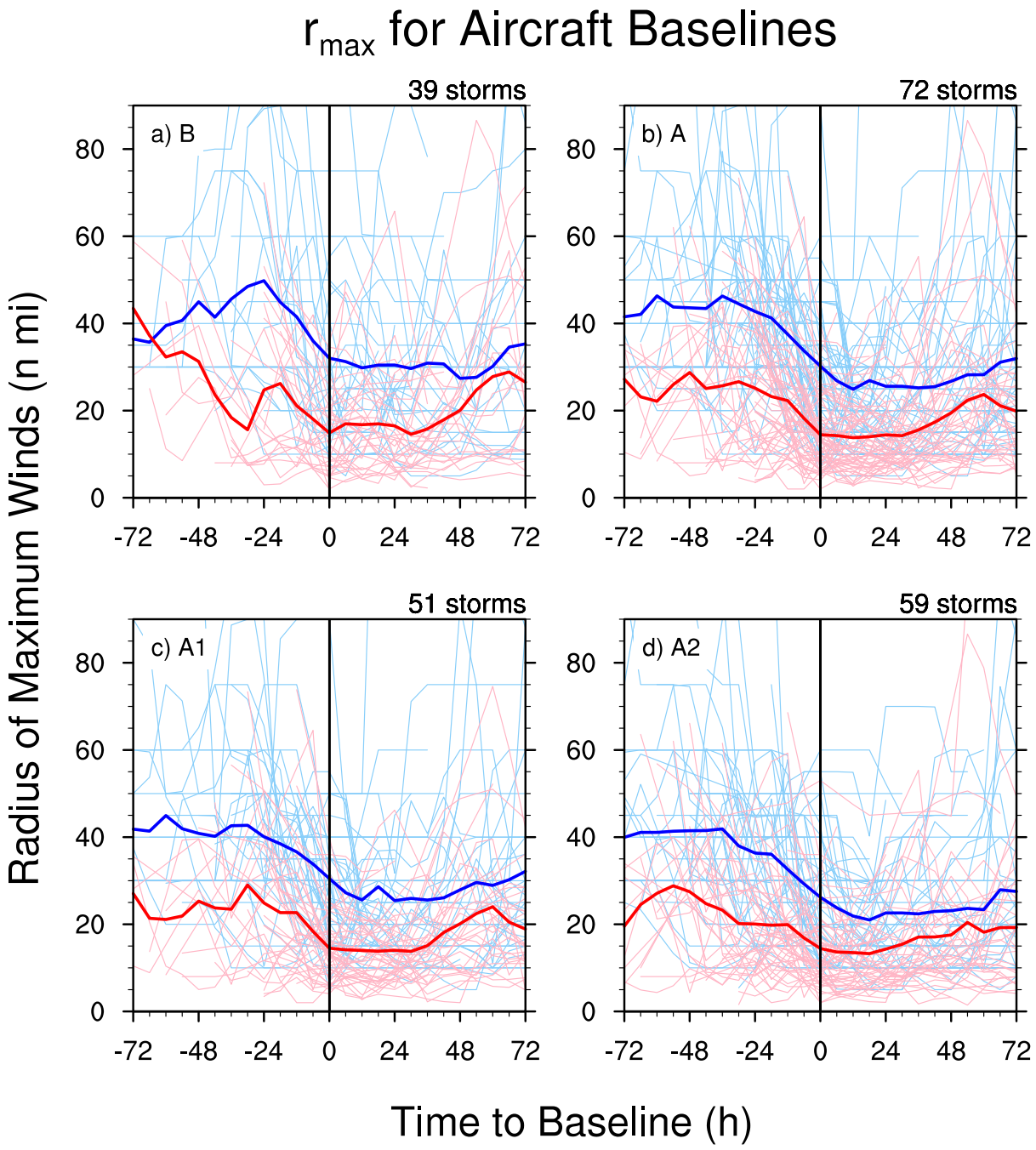

Figure 6.1: BT and FL radii of maximum wind (r_{max}) for aircraft baselines (B, A, A1, A2) for a 6-day window centered on the respective baseline. Thick lines indicate the composite mean r_{max} of the BT (blue) and FL (red) winds. Thin lines indicate the individual storm r_{max}traces for the BT winds (light blue) and FL winds (pink).

of r_{max} surfaces with height cannot help to resolve this discrepancy — if anything, the real difference between the surface r_{max} and flight level r_{max} could be even larger than indicated here.

Chapter 4 has discussed some of the vagaries of the best track r_{max} data, in particular, how these

values are sometimes chosen by the operational forecaster for the sole purpose of initializing the operational forecast models. Thus, at least for some cases, these values do not represent a 'best track' estimate of *observed* radius of maximum wind information. To obtain a better read on how often this may have occurred, a quick visual inspection was conducted for the 180 structure and intensity plots of storms with at least some aircraft data during the study period. These plots are provided in Appendix E. This comparison reveals that occasionally the BT $r_{\max}$ estimates remained constant throughout large portions of a storm's lifetime. This suggests that sometimes forecasters were not using *any* of the available data to estimate BT $r_{\max}$. Notable examples include Bob (1991), Andrew (1992), Chantal (1995), Luis (1995), Marilyn (1995), Hermine (1998), and Lili (1996). In many other cases however, the BT $r_{\max}$ curve follows the FL $r_{\max}$ curve to at least some degree, so it is quite evident that in these cases, forecasters did base their $r_{\max}$ estimates on observed data. Some examples where the BT $r_{\max}$ seems to be well correlated with the FL $r_{\max}$ data include: Emily (1993), Lenny (1995), Mitch (1998), Bret (1999), Iris (2001), Isidore (2002), Isabel (2003), Ivan (2004), and Wilma (2005). Generally, the quality of BT $r_{\max}$ estimates seems to be higher in the second half of the study period than in the first half. Quality seems to be higher for stronger systems, perhaps especially if a field campaign was in progress. On the other hand, quality seems to be lower for weak systems. In addition, many systems without aircraft data (not included in Appendix E) display much less variation in BT $r_{\max}$ over their lifetime. Clearly, the BT $r_{\max}$ data set is subject to large variations in quality and reliability.

Yet, the varied quality of the BT $r_{\max}$ data does not explain why it would have a high bias relative to observations. Considering that the primary purpose of choosing these values was to initialize the numerical models, we speculate that the limited resolution of the operational models may have played a role. Since these models have not been able to resolve scales smaller than 20 to 40 n mi for most of the 20-y period of our study,[2] , operational forecasters may have shied away from giving extremely low values of $r_{\max}$, as they knew that the model would not be able to initialize a storm with such a small inner core. Thus, it is easy to comprehend why a high bias in $r_{\max}$ could occur for this reason alone. Even

[2] It is important to remember that due to aliasing and other effects, the minimum horizontal grid spacing in a model is not equivalent to the minimum resolvable scale of that model. Generally, the smallest resolvable scale is considered to be 4 times the minimum grid increment. In 1995, the GFDL hurricane model became operational with an inner nest mesh size of 1/6○, or an effective resolution of about 40 n mi. In 2005, a third mesh was added with a mesh size of 1/12○, or an effective resolution of 20 n mi (Bender et al., 2007).

for the cases in which the forecasters appeared to follow the data, they often followed more of the upper bound of r_{max} than some weighted average. As the storm strengthens and achieves an eye, however, the forecaster's operational estimates of r_{max} values probably decreased since forecasters understand and anticipate a contracting r_{max} as the storm intensifies. The appearance of a definite eye undoubtedly also helps to constrain the forecaster's r_{max} estimates to lower values since remote sensing views provide forecasters with more concrete cues as to the size of the inner core of the storm. This may explain why the discrepancy between BT r_{max} and FL r_{max} narrows somewhat after the eye has formed.

In compiling the FL r_{max} data from the VDMs, we must note that the *lower bound* of FL r_{max} has been used, rather than some sort of azimuthal averaging over time. This should naturally lead to smaller r_{max} values than would be obtained if some sort of azimuthal averaging had been done in a moving time window.[3] . This factor may therefore be partly responsible for the high bias of BT r_{max}. However it is doubtful that this is responsible for all of the difference. In summary, it is difficult to escape the conclusion that the observed BT r_{max} have a large high bias when compared with the FL r_{max}.

Given the deficiencies of the BT r_{max}, we may wonder if the FL r_{max} are more representative of the storm's maximum wind radius. Certainly, they do represent the observed r_{max} at the given flight level and this is probably close to the true surface r_{max}. The mean composites in Fig. 6.1 still deserve some caution, however. The reason is due to the small number of storms that contribute to the composite in the early periods before eye formation. Looking at the 'A' baseline in panel b, we see that the time period from 72 to 48 h before eye formation has few individual storm traces. The composite curve is noisy and trendless during this period. Starting around 24 h before eye formation, however, many more individual traces can be seen and the composite curve decreases from 25 n mi to about 16 n mi at the time the first aircraft eye is observed. Looking at the individual storm traces, we see that many of the individual FL curves (pink thin lines) dive steeply from r_{max} values of 50 to 70 n mi down to 10 to 20 n mi by the time the eye is observed. In a few storms, r_{max} begins contracting sharply 48 h before eye formation, but in the vast majority of storms here, the contraction starts 24 h before eye formation.

Given that chapter 5 showed that the storm begins a steady and increasing rate of intensification at

[3] Because of the issue of data gaps, such an approach was viewed to be problematic, and for this study, the lower bound of r_{max} was viewed to be the most important from a dynamical perspective, since this represents some measure of the maximum inward penetration of inflowing air parcels.

about this time, the conjecture of Nolan (2007) appears to be well supported by these data. His idealized study initialized a mid-level vortex with an r_{max} of 100 km (about 55 n mi). The smaller scale vortex had an r_{max} on the order of 20 km (10 n mi). Many of the individual storms in the VDM data set attain an r_{max} of less than 10 n mi by the time the eye has formed. For what its worth, the BT r_{max} show a similar evolution, just biased to higher radii. Yet, not all of the storms forming eyes follow this pathway. Many of the storms observed 48 h before eye formation already have relatively small FL r_{max} values of less than 25 n mi. It seems that these may represent a different mode or class of eye-forming systems — storms that already have a r_{max} on relatively smaller scales.

About 12 and 24 h after the eye has formed, r_{max} reaches its smallest radius of between 5 and 15 n mi when the eye is first observed. By 36 h after 'A', the composite mean FL r_{max} increases somewhat. This increase is caused in part by a few storms which have rapidly increasing r_{max} after eye formation — these skew the composite mean upwards. For the majority of storms though, r_{max} remains small or increases modestly. Storms undergoing extratropical transition often display a marked and rapid increase in r_{max}, which probably explains the rapidly rising curves in this figure. Storms which decay while remaining tropical may tend to 'relax' to a larger r_{max}, but the maximum winds do not grow appreciably outward.

Next we examine the behavior of observed r_{max} for the IR satellite-based eye formation baselines. Fig. 6.2 shows the evolution of r_{max} for the IR2, IR3, IR4, and IR5 baselines. The general pattern is largely the same as for the aircraft baselines. Again, BT r_{max} are higher and do not decrease as rapidly as FL r_{max}. There is considerably more scatter in the BT r_{max} values, especially for the IR2 and IR3 baselines. This is probably because these baselines are more prone to 'false positives' in identifying the time of eye formation. The cluster of rapidly decreasing r_{max} is less apparent in these figures, with many storms having already undergone the rapid decrease before the IR eye formation baselines. The mean composite FL r_{max} is 16 n mi at the time the first IR eye appears (IR3), and 12 n mi when the first strong eye (IR5) is noted. In the absence of aircraft data, these mean values may be helpful to operational forecasters if no other r_{max} information is available.

To analyze the behavior of r_{max} for the various degrees of eye formation success, the data are

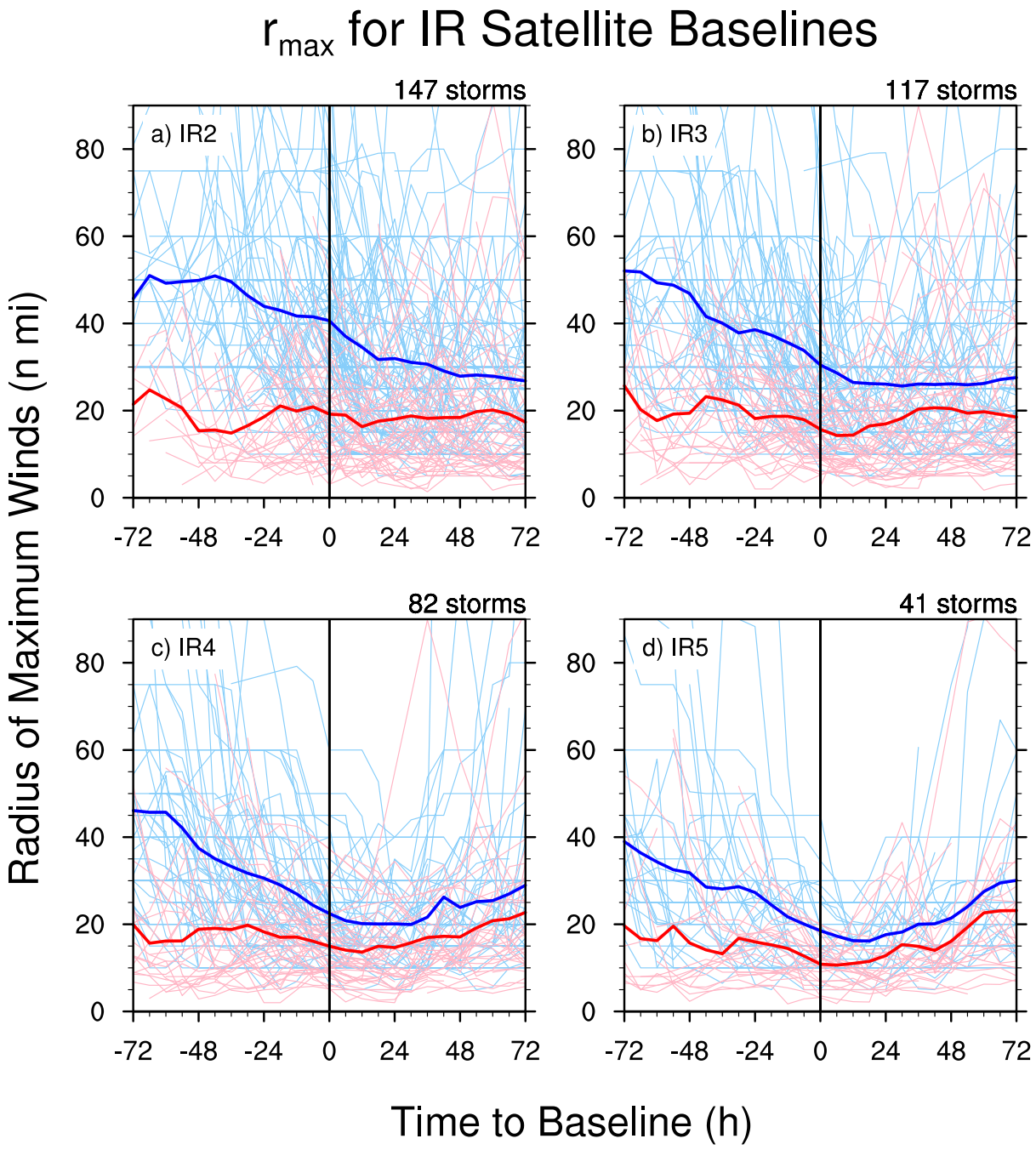

Figure 6.2: BT and FL r_{max} for IR satellite baselines (IR2, IR3, IR4, and IR5). Plotting conventions are the same as in Fig. 6.1.

now stratified for the aircraft eye baseline 'A' by the four eye formation case types:[4] complete failure, intermittent failure, delayed success, and complete success. The result is shown in Fig. 6.3. Ignoring the composite mean when there are insufficient data, we see that the for the complete failure cases, r_{max} un-

[4] The definitions for the case types were set forth in chapter 5.

dergoes a sharp decrease in the 24 h before eye formation. During this period the FL r_{max} composite mean contracts from over 30 n mi to 17 n mi. The eye forms just a few hours after this low r_{max} threshold is reached. All of the individual storm r_{max} are less than 30 n mi by the time the aircraft eye is first observed. Within 24 h after eye formation, nearly all the individual r_{max} values increase and the composite mean also increases. The intermittent failure cases show a similar pattern, but with an even more pronounced 'U'-shaped pattern: after 'A', FL r_{max} holds steady for 18 h and then begins a steady increase. For the delayed success cases, the composite mean r_{max} contracts all the way to 12 n mi at the time of eye formation and then holds steady through 36 h. The complete success cases show a steady drop until eye formation and then a continued slowly decreasing r_{max} through 30 h. Very few of the individual storm r_{max} curves increase substantially in the 72 h after eye formation.

Summarizing these results, r_{max} undergoes a consistent decrease starting 24 h to 30 h before the aircraft eye is observed. Minimum values of r_{max} occur about the time that the first eye is reported, with values ranging from 12 to 17 n mi. Gray and Shea (1973) put forward the idea that supergradient winds are important to eye formation. In keeping with this idea, they observed that eye formation is typically restricted to radii $< 20 - 35$ n mi where supergradient winds are possible. The findings of the present study — both the sharp decrease in r_{max} before eye formation and the fact that nearly all eyes formed when $r_{max} < 40$ n mi — offer support for this idea.

If the eye fails to persist, r_{max} tends to relax back to larger sizes. If the eye formation succeeds, r_{max} remains steady at small radius or decreases even further for some time before increasing. This late increase in r_{max} could be caused by the eyewall replacement phenomenon as an outer wind maxima becomes dominant. The greatest contraction in r_{max} occurs in the day or so before eye formation. During the subsequent intensification, r_{max} does not contract much more than the r_{max} achieved at the time the eye forms. This result seems to support Kuo (1959), who posits that there is a limiting radius for inflowing air that is imposed by the conservation of angular momentum. As the relative angular momentum increases for an inflowing parcel, the kinetic energy required eventually exceeds the energy available for transformation in the parcel. Once the maximum velocity is attained, the air parcel turns upward, forming an eyewall. The above results showing that the contraction of r_{max} ceases or slows at the time eye formation is in keeping with this general idea. A more quantitative analysis would be needed to verify

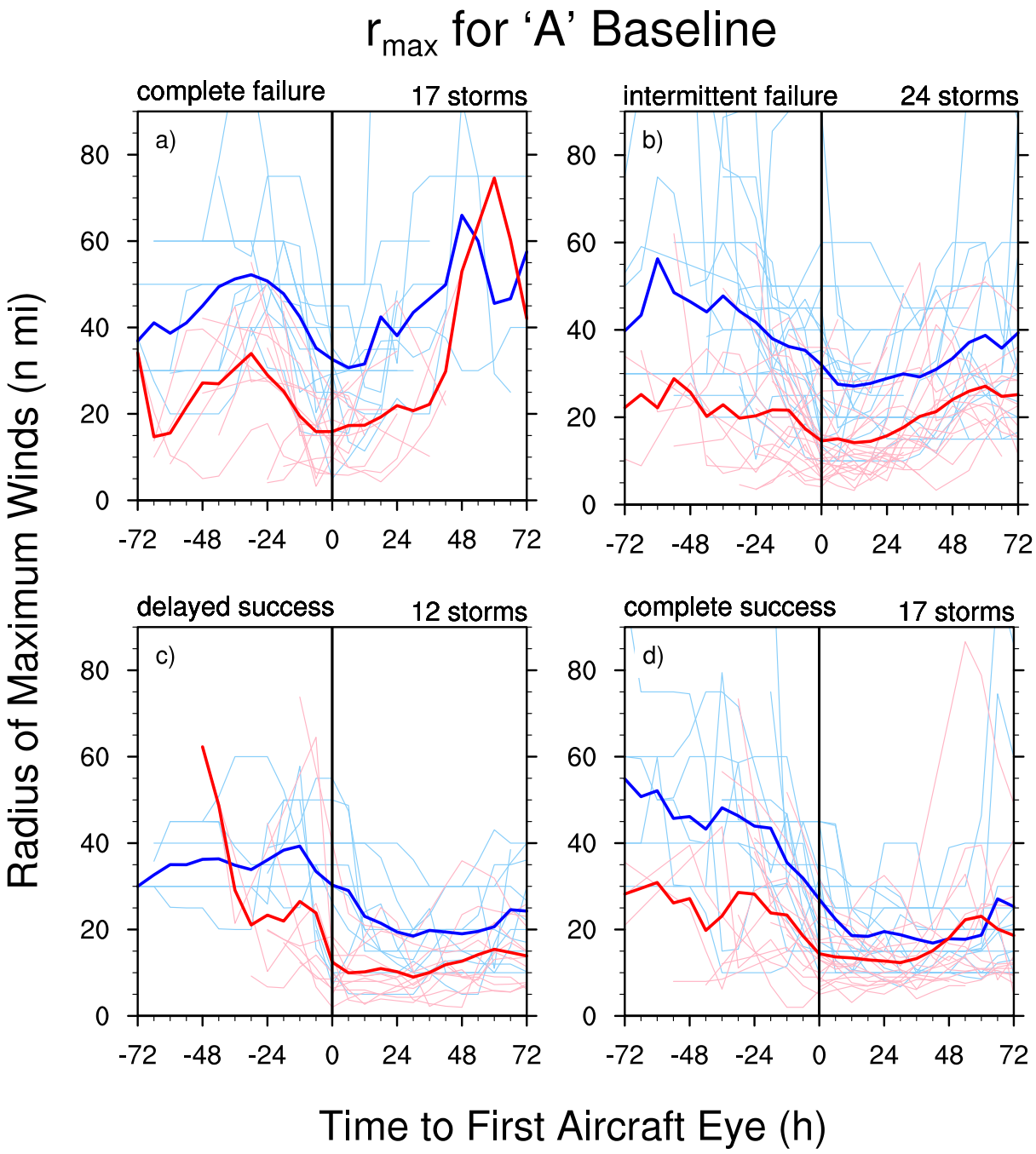

Figure 6.3: BT and FL r_{max} stratified by eye formation case type for the 'A' baseline: a) complete failure, b) intermittent failure, c) delayed success, d) complete success. The individual storm $r_{max}$are shown by thin lines for the BT (light blue) and FL (pink) values, while the composite mean is shown by thick lines for BT (blue) and FL (red).

Kuo's theory.

6.2.2 *Minimum Rossby length*

To compare the evolution of $r_{\max}$ about the time of eye formation, it is helpful to have a dynamical length scale to use as a reference for comparison. The Rossby length (λ_R) is the appropriate dynamical length scale to use, as this indicates how far away the surrounding atmosphere adjusts to a forcing such as latent heating. Chapter 3 made substantial use of Rossby length ideas, except that inverse Rossby length, μ, was used instead of λ_R. To remind the reader, the basic idea is this: when the Rossby length is much larger than the scale of the heating (L_h) so that $\lambda_R >> L_h$, much of the latent heating is dissipated to the far-field via inertia-gravity waves so that very little energy remains to spin up the rotational flow in the final adjusted state. When $\lambda_R \sim L_h$ however, a substantial portion of the latent heating is retained within the confines of the storm and is manifested as a local warming. The resulting hydrostatic pressure drop spins up the tangential winds and so the storm is said to be 'efficient' at converting heat energy to kinetic energy. In the tropics (with latitude of ~ 20 deg), the background λ_R is O(500 n mi), but the core of active heating in a developing tropical storm is O(100 n mi). Out of all the storms in this study, the one with the largest $\lambda_{\text{R,min}}$ during its lifetime (a tropical storm with small $v_{\max}$ and large $r_{\max}$) was still just 239 n mi. Thus, even the weakest tropical storms still have $\lambda_{\text{R,min}}$ which are considerably smaller than the background value in the tropics.

Using the VDM data, $\lambda_{\text{R,min}}$ is computed from the maximum inbound FL wind speed and the $r_{\max}$ associated with that specific wind speed report. This provides the smallest Rossby length observed in the storm and an estimate for how well-confined the response to heating will be within the core of the storm. Plots of the individual and composite mean $\lambda_{\text{R,min}}$ are shown for the aircraft baselines in Fig. 6.4. At first glance, this plot looks remarkably similar to the $r_{\max}$ curves shown in Fig. 6.1. It should since a reduction in $r_{\max}$ also reduces $\lambda_{\text{R,min}}$. Increasing $v_{\max}$ also decreases $\lambda_{\text{R,min}}$. Because storms are usually intensifying when they form eyes, $\lambda_{\text{R,min}}$ drops a little quicker than $r_{\max}$. Whereas the $r_{\max}$ values decrease to about 15 n mi by the time the aircraft eye was first reported, here $\lambda_{\text{R,min}}$ decreases to about 26 n mi by the 'A' baseline. For many of the individual storms however, $\lambda_{\text{R,min}}$ decreases to below 15 n mi. As a result, the warming response due to latent heating will be confined to the roughly the same scale as the nascent eyewall. A few eyes do form at higher $\lambda_{\text{R,min}}$ (30 to 45 n mi) however,

so there does *not* seem to be an absolute value of $\lambda_{R,min}$ that triggers eye formation. After the eye has formed, the composite mean $\lambda_{R,min}$ ceases contraction within a few hours. But this average masks what is happening with the individual storms. Storms which continue intensifying continue to contract their $\lambda_{R,min}$ due to the effect of increasing v_{max} in the $\lambda_{R,min}$ calculation. By the time a strong eye is observed, the composite mean $\lambda_{R,min}$ reaches a very small radius of 10 n mi (not shown). For many individual storms however, $\lambda_{R,min}$ undergoes a sharp increase after eye formation. These are weakening storms with slowly expanding r_{max} and decreasing wind speeds. This combination rapidly expands $\lambda_{R,min}$ and makes the storm much less efficient.

In Fig. 6.5, $\lambda_{R,min}$ are stratified by eye formation case type. Many of the complete failure cases do in fact achieve small $\lambda_{R,min}$, but the composite mean is skewed upwards because some eye-formations occur at considerably higher $\lambda_{R,min}$ (off the scale of the figure). In the complete failure cases, $\lambda_{R,min}$ decreases before the eye formation attempt and then rapidly increases afterward in all cases. The composite mean $\lambda_{R,min}$ bottoms out at about 34 n mi at the time of the eye is reported. The intermittent failure cases display a similar pattern, except the composite mean $\lambda_{R,min}$ reaches 28 n mi by the time of eye formation and then remains steady or even decreases for about 18 h afterward. Apparently, the storm may make several attempts at forming an eye while $\lambda_{R,min}$ remains low. The delayed success cases display a more marked decrease in the 24 h before eye formation, reaching 20 n mi by the time the eye is first reported. $\lambda_{R,min}$ continues decreasing for another 24 to 30 h afterward. The composite mean $\lambda_{R,min}$ undergoes the sharpest pre-formation decrease for the complete success cases. After eye formation, some of the storms maintain very low $\lambda_{R,min}$, while others begin rising by 36 to 48 h (note that this rise occurs later than the delayed success cases). This last point is in keeping with the result (chapter 5) that the complete success storms tend to peak earlier than the delayed success storms.

6.3 Thermodynamic trends during eye formation

The minimum Rossby length also serves as a proxy for the inertial stability in the storm. When $\lambda_{R,min}$ is low, the corresponding inertial stability is high and the vortex resists radial motions more strongly. The theoretical argument of chapter 3 proposed that the warm core will develop rapidly when a substantial portion of the latent heating occurs within the region of high inertial stability in the core of

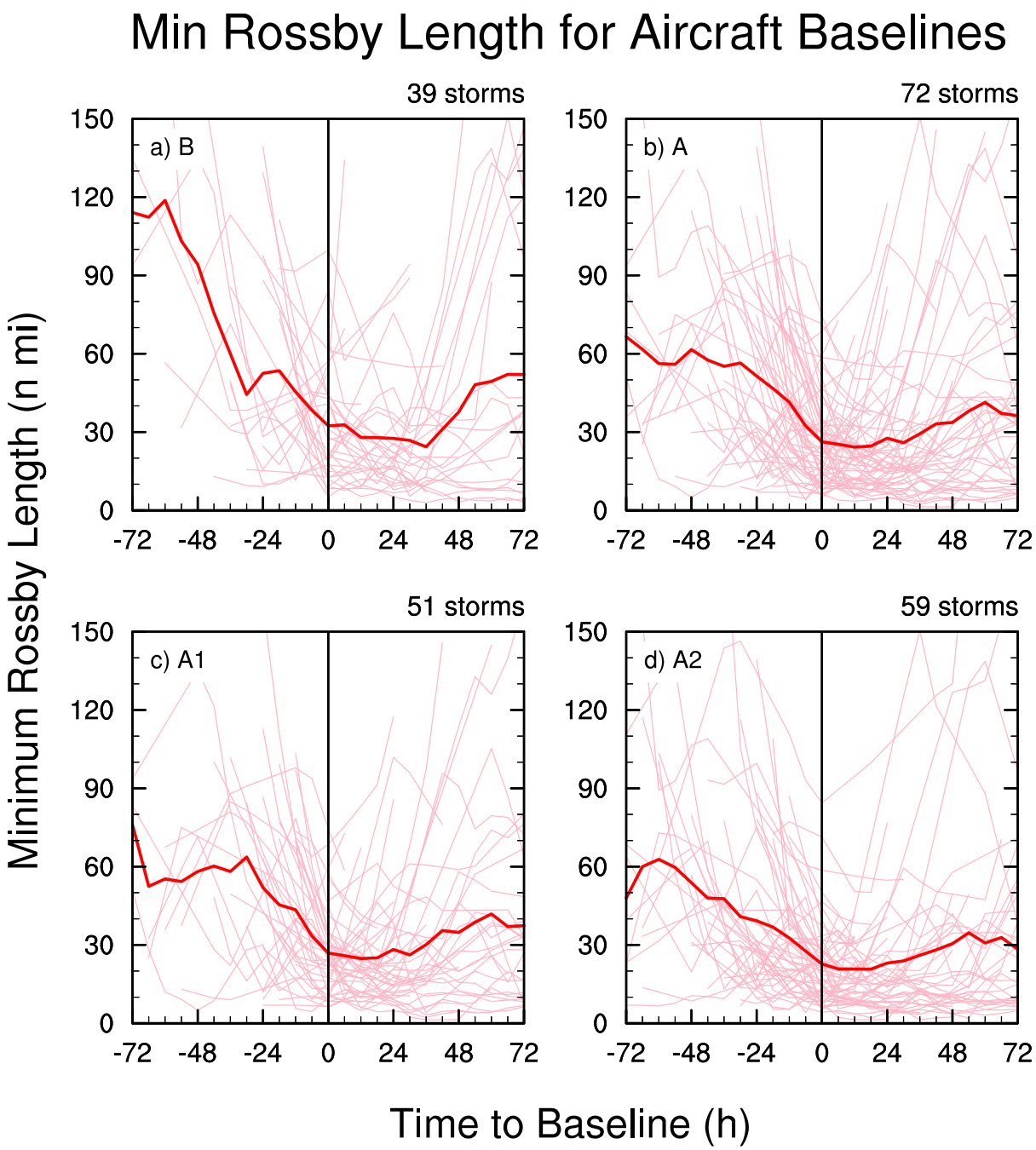

Figure 6.4: FL minimum Rossby length ($\lambda_{R,min}$) for aircraft baselines (B, A, A1, A2) for a 6-day window centered on the respective baseline. The composite mean $\lambda_{R,min}$is indicated by the thick red line, while the individual storm $\lambda_{R,min}$ values are shown using thin pink lines.

the cyclone. For the idealized barotropic vortices considered in that chapter, the region of high inertial stability resides within the radius of maximum winds. In real storms however, the transition from low inertial stability to high inertial stability is not always sudden, but may occur over a distance of tens of

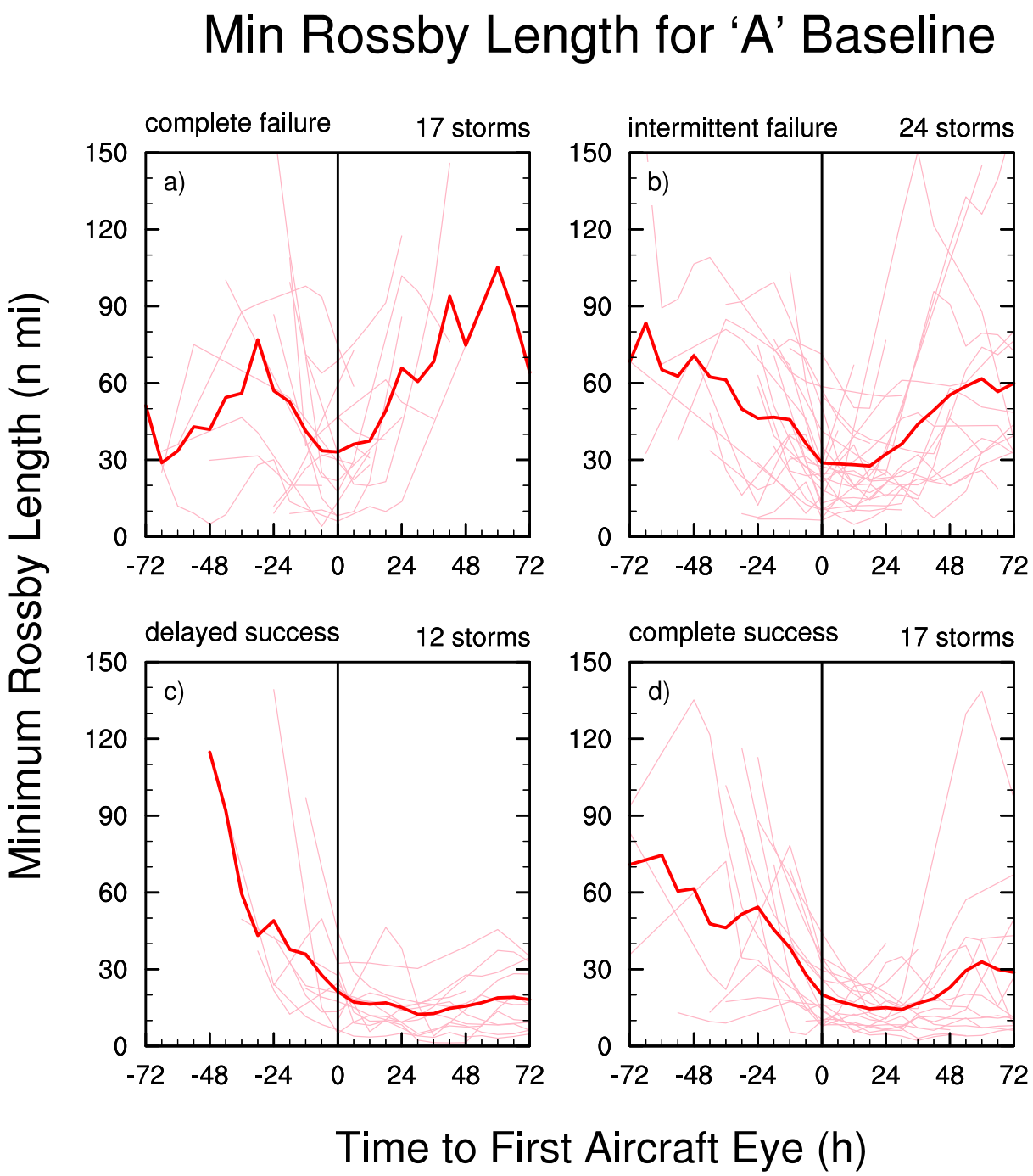

Figure 6.5: FL $\lambda_{R,min}$ stratified by eye formation case type for the 'A' baseline: a) complete failure, b) intermittent failure, c) delayed success, d) complete success. The individual storm FL $\lambda_{R,min}$ are shown by thin pink lines and the composite mean is shown by thick red lines.

kilometers.[5] In this section, we examine the development of the warm core as indicated by increasing

[5] Fig. 6 of (Holland and Merrill, 1984) shows the vertical and radial distribution of inertial stability computed from a composite of observed storms. Instead of increasing suddenly, as in the idealized vortices considered in chapter 4, inertial stability may ramp up over several tens of kilometers.

temperature and lowering dew point temperature in the eye, and by an increasing temperature difference across the eyewall.

6.3.1 Central eye temperature

The maximum flight level temperatures observed within 5 n mi of the VDM fix center are taken at various flight levels during the life of each storm, so these values have been converted to 700 hPa equivalent temperatures using the method described in chapter 4.3.5. The T_{eye} values have been interpolated to the window about the time of eye formation and are shown for the various aircraft baselines in Fig. 6.6. Unexpectedly, the composite mean temperature is fairly steady both before and after the time of eye formation, with just a slight increase from about 16 °C before the time of eye formation, to 17 °C at the time of eye formation. Afterward, the mean temperature increases slightly more to about 17.5 °C, but begins declining about 36 h after 'A'. The reason for the muted changes in temperature will be discussed further, but first we must allow for the possibility that our adjustment of the flight level temperatures to a 700 hPa-equivalent temperature may be faulty. To arrive at the adjusted temperature, we have simply computed an adjustment factor by subtracting the mean maximum FL temperature for the 700 hPa level for all storms from the mean FL maximum temperature at the level the adjustment is being made from. This assumes a constant thermal stratification for all storms and through all stages of a storm's lifetime, including periods in which the storm was strengthening as well as weakening. If the adjustment factor used here is too large, the warming associated with eye formation may be masked when the plane begins flying the storm at the higher flight levels. These uncertainties aside, we will now interpret the results.

The individual storm T_{eye} display a wide range of behaviors. In general, the variance of eye temperature increases after the baseline eye formation time in each panel. In many of the storms, the eye temperature does rise sharply after eye formation to reach the warmest temperature at any point in the storm's life, but then T_{eye} falls nearly as rapidly. This spike and decline takes place over an 18 to 36 h period. The rapid declines in T_{eye} after the storm reaches its 'warm core peak' help explain why the composite mean temperature does not increase appreciably after eye formation. This behavior is consistent with the finding of Jordan (1961), whose dropsonde study in Western Pacific typhoons found that temperature and moisture conditions in the eye below 700 hPa undergo rather large changes at the

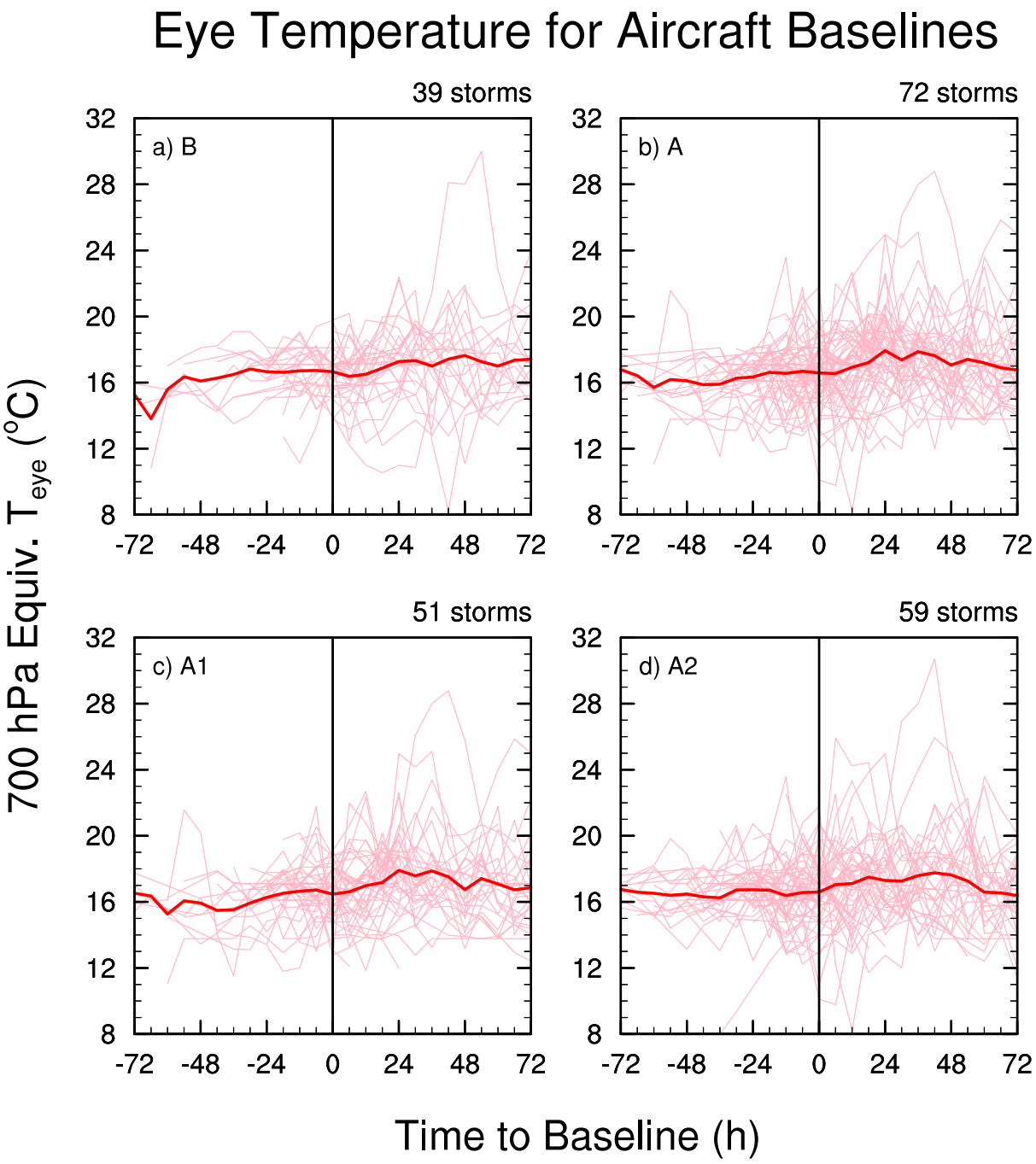

Figure 6.6: 700 hPa-equivalent maximum eye temperature (T_{eye}) observed within 5 n mi of the fix center for aircraft baselines (B, A, A1, A2) for a 6-day window centered on the respective baseline. The composite mean T_{eye} is indicated by the thick red line, while the individual storm T_{eye} values are shown using thin pink lines.

time of lowest pressure (maximum intensity). Before peak intensity, the eye is abnormally warm and dry, as the pressure is falling rapidly. After peak intensity, dropsondes showed the eye to be moist. This effect was studied further by Kossin and Eastin (2001). Their observational study examined radial

profiles of temperature and tangential wind and showed that the eye is warm and dry during a storm's initial intensification (their 'regime I'). During this time, the tangential wind profile is often U-shaped. At some point, the horizontal shear across the eyewall becomes so great that a horizontal mixing event occurs, so that the storm exchanges eye air and eyewall air. This results in an eye that is close to solid body rotation (a more V-shaped profile in tangential wind) and considerably cooler and moister than before (their 'regime II'). The shift from regime I to regime II often coincides with the peak intensity of the storm, so that the mixing event acts as a brake on intensification. Some details of the mixing process have been examined recently by (Rozoff et al., 2009).

A few storms display temperature spikes of 4 to 5 °C *before* eye formation. This has possible relevance to one proposed mechanism for eye formation. In Hurricane Bonnie (1998), Heymsfield et al. (2001) observed several mesoscale descending currents with strong adiabatic warming. These currents developed in association with some vigorous hot towers in the nascent eyewall. They postulated that the enhanced wind velocities about these convective elements shortened the local Rossby length, thereby concentrating the subsidence within the core of the storm. It is possible that these pre-formation temperature spikes may occur in conjunction with this mechanism, but a more detailed analysis would be needed to either confirm or reject this hypothesis.

A more substantial eye warming is observed for some of the infrared satellite baselines. Fig. 6.7 shows the individual and composite mean T_{eye} curves for the IR2, IR3, IR4, and IR5 baselines. The IR2 baseline shows very little change, with just a slight hint at warming 48 h after the first closed IR warm spot has been observed. The T_{eye} curves for the IR3 baseline are also nearly trendless, but several storms display large spikes after the first satellite eye has been observed. The warming is even more pronounced during the 24 h after the first persistent eye appears (IR4), but the appearance of a strong eye holds the strongest association with eye warming. Beginning about 6 h before IR5, the composite mean T_{eye} rises from about 16 °C to nearly 19 °C about 12 to 18 h after the baseline. In chapter 5 we saw that this period also corresponded to the time when the storm was intensifying most rapidly.

The individual storm T_{eye} curves show a general rise at and after IR5, but only a handful of storms feature 700 hPa temperatures of > 25 °C. Clearly, a storm can become fairly intense (> 105 kt) and display a strong eye without displaying a remarkable eye warming. Since the warming at upper levels

accounts for most of the pressure drop, and therefore deepening of the storm, strong warming at the lower and middle levels of the storm is not absolutely required to reach an intense stage. Yet some storms do experience strong warming in their lower eye. Inez (1966), comes to mind as an example. That storm was well-observed by multiple aircraft at several different levels as discussed in Hawkins and Imbembo (1976). In their Fig. 14, reproduced here as Fig. 6.8, a double warm anomaly can be seen. The greatest warm anomaly of 16 °C was found in the upper eye near 200 hPa. A substantial warm anomaly also exists in the middle eye near the 600 hPa-level. Several early pioneers (Ballou, 1892; Malkus, 1958a; Kuo, 1959) suggested that the momentum diffusion across the eye/eyewall interface would act to centrifuge air out of the eye, thereby forcing subsidence in the eye. Later workers showed that at least a portion of the eye warming could be accounted for by other means, namely as a response to the forcing of latent heating in a ring (Willoughby, 1990b) or as a consequence of maintaining thermal wind balance in a baroclinic vortex (Smith, 1980). Thus, the idea of a centrifugal 'pump' had seemed to lose traction in the past few decades. But is it possible that this 'momentum diffusion pump' actually does operate in some of the strongest storms? Perhaps this can account for the instances of very strong warming at 700 hPa such as has been observed the eyes of storms like Inez, Hurricane Rita (2005), Supertyphoon Ida (1958), and many others.

6.3.2 Central eye dew point temperature and dew point temperature depression

The dew point temperature taken at the location of the maximum flight level temperature within 5 n mi of the eye provides another view of the warm adiabatic descent associated with the subsidence in the eye. The dew point temperatures have been adjusted to 700 hPa-equivalent values using the same adjustment factors that were used for the FL temperatures. Although this adjustment may be somewhat crude, the results are shown interpolated to the eye formation period in Fig. 6.9. This figure shows that the dew point temperature slowly declines from near 15 °C three days before the first aircraft eye, to about 13.5 °C at the time 'A' is observed, to 12 °C about 24 h later. In individual storms, the decline in $T_{d,eye}$ tends to be quite significant (with many storms getting down to 7 °C) and takes place over about a day. But the timing of the drying episodes in individual storms is not very coherent with regard to eye formation. It appears that substantial $T_{d,eye}$ declines can occur anywhere from 12 h before eye formation

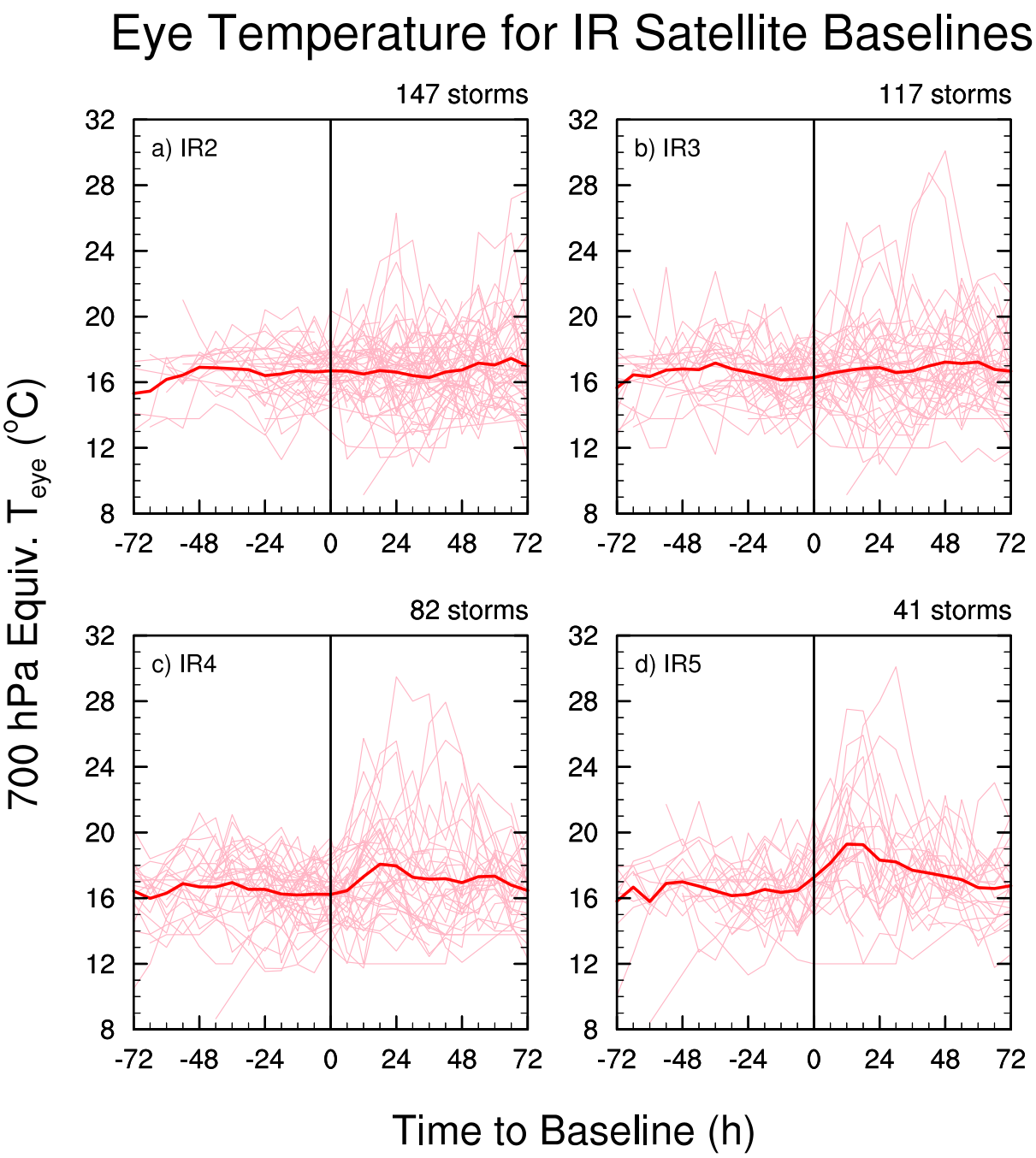

Figure 6.7: T_{eye} for the IR satellite baselines. Plotting conventions are the same as in Fig. 6.6.

to 72 h afterward. The fact that the center of some storms is drying before the eye is observed suggests that in some cases, significant central subsidence can precede eye formation. This suggests that central subsidence may not necessarily be just a simple response to the convective heating of an eyewall (e.g., Shapiro and Willoughby 1982).

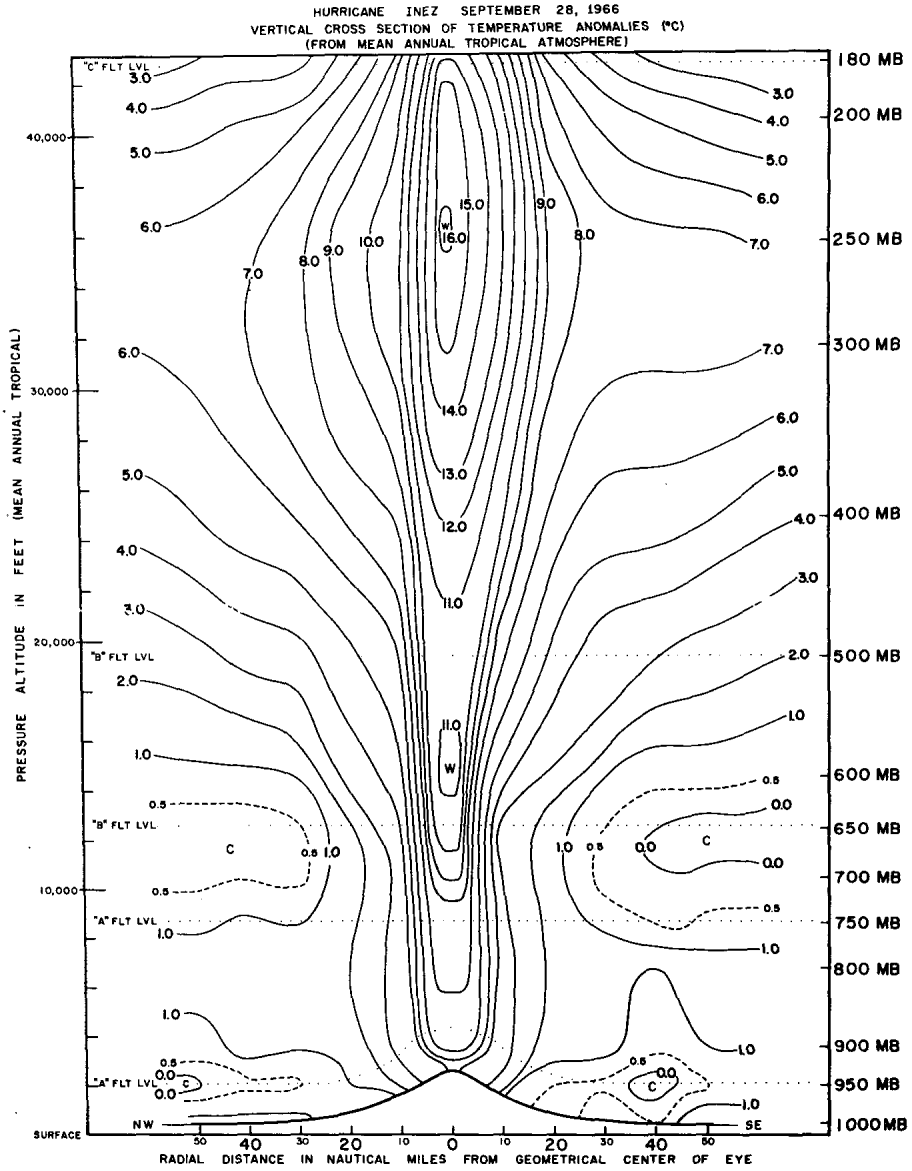

Figure 6.8: Temperature anomalies in Hurricane Inez on 28 September 1966. Note that temperatures were near normal outside the eye around 550 hPa, but warmer elsewhere. The eye displays a double maxima of warmness, with the main warm anomaly centered near the 250 hPa level, and another warm anomaly centered near 600 hPa. Reproduced from Fig. 14 of Hawkins and Imbembo (1976).

The dew point depression $T_{\mathrm{DEP,eye}}$ does not suffer from our rather temperature dubious adjustments. Given that the core is near saturation through a great depth near the time of genesis (so that $T_{\mathrm{DEP,eye}}$ should be near zero), the development of large $T_{\mathrm{DEP,eye}}$ offers perhaps the clearest view of the subsident warming associated with eye formation and subsequent deepening of the storm. A plot of $T_{\mathrm{DEP,eye}}$ for the four aircraft baselines is shown in Fig. 6.10. For the 'A' baseline, $T_{\mathrm{DEP,eye}}$ rises from 2 °C

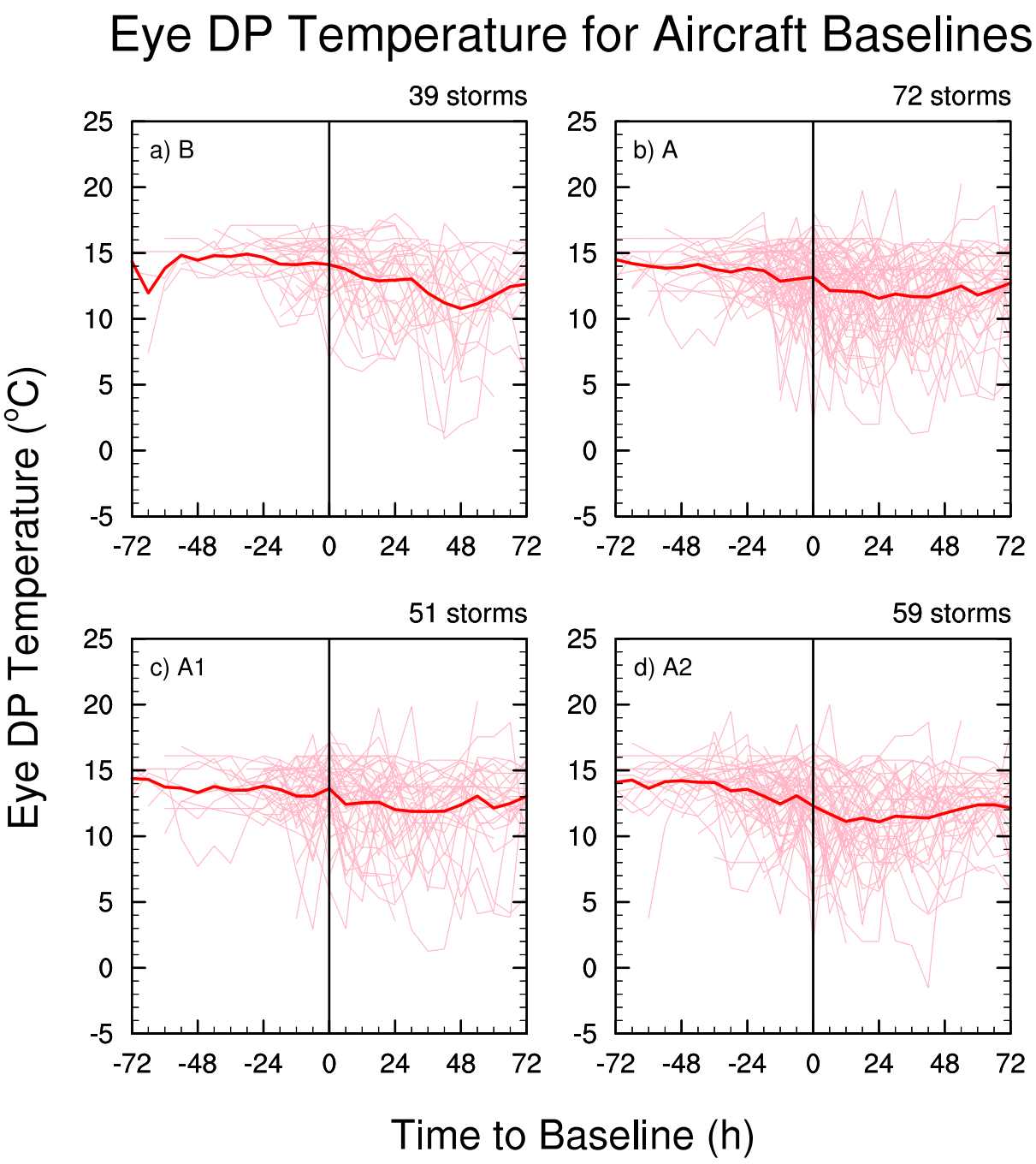

Figure 6.9: As in Fig. 6.6, but for 700 hPa-equivalent maximum eye dew point temperature $T_{d,eye}$ observed at the location of T_{eye}.

three days before eye formation, to 3.5 °C at A, to 6.5 °C 24 h after 'A'. Like the plot of T_{eye} given earlier in Fig. 6.6, a pattern of spikes are seen in the individual storm traces; the interpretation is the same. It appears that while extraordinary dew point temperature depressions of greater than 20 °C do occur in a few storms, these are by no means necessary to obtain an intense storm.

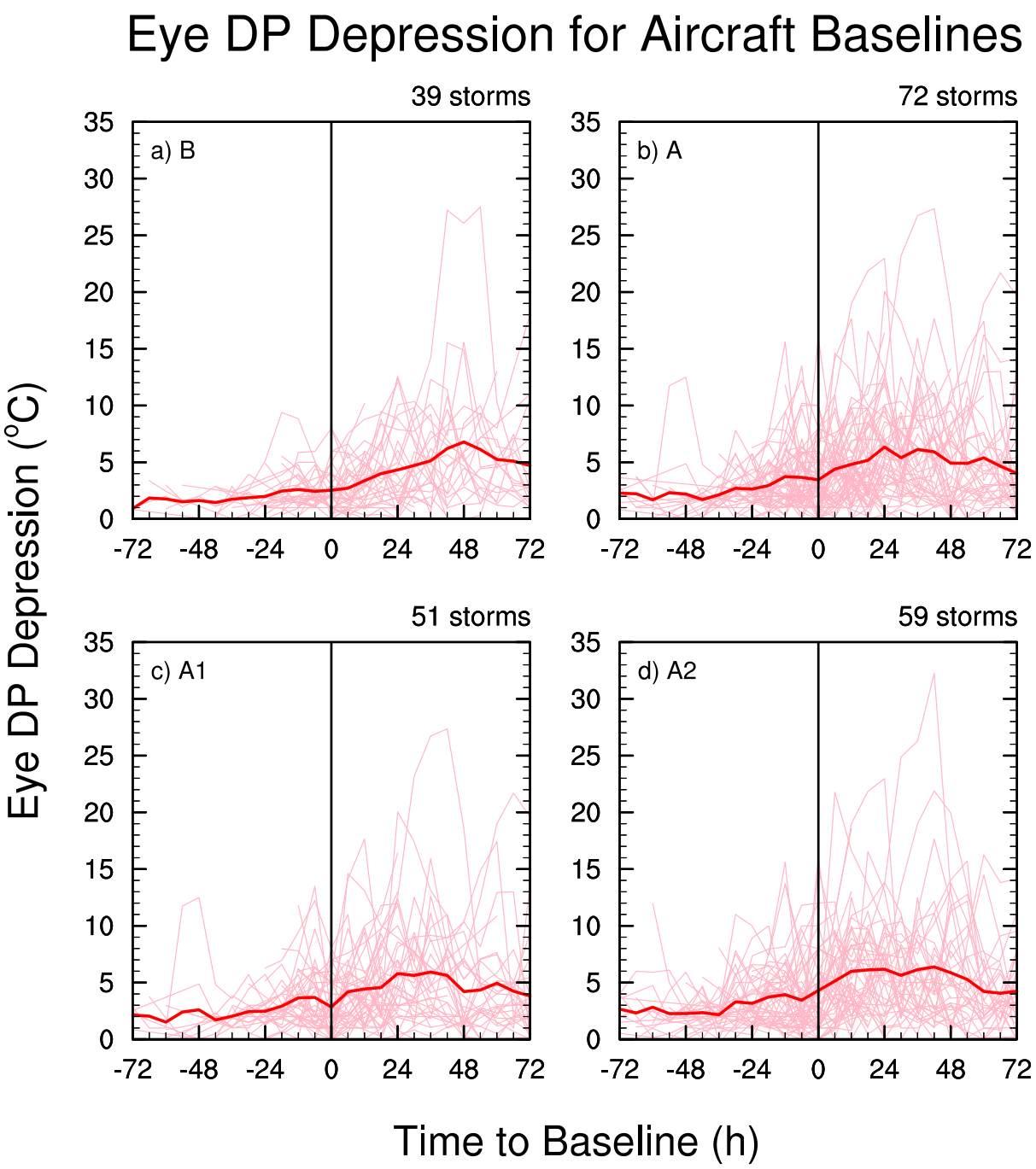

Figure 6.10: Maximum eye dew point temperature depression ($T_{\mathrm{DEP,eye}}$) for aircraft baselines. Plotting conventions are the same as in Fig. 6.6.

Table 6.1 shows all the cases in which $T_{\mathrm{DEP,eye}}$ exceeded 20 °C along with some other thermodynamic and kinematic information from the same time. First note two storms (Rita 2005; Katrina 2005) are responsible for 14 out of these 25 high $T_{\mathrm{DEP,eye}}$ cases! Clearly, extraordinary $T_{\mathrm{DEP,eye}}$ do not occur in all very intense tropical cyclones and some extremely intense storms (e.g., Wilma 2005, with a $p_{\mathrm{min}}$of

882 hPa is not in this table). Looking at the $p_{\min}$ column though, it seems that with the exception of a couple storms (Humberto 2001 and Gustav 1990), storms with high $T_{\mathrm{DEP,eye}}$ are normally very intense. Also take note that all of these cases were taken at the 700 hPa flight level. Even though strong subsidence warming can extend below the 850 hPa level (and even reach the surface in very rare instances), it seems that the largest dew point depressions will always be found at higher of the two routinely available flight levels (e.g, 700 hPa). While a pure subsiding current would become warmer and even dryer the lower it went, the moister lower levels observed in hurricanes may be due in part to effect of boundary layer dynamics (Kepert, 2001; Kepert and Wang, 2001; Kepert, 2006). According to that body of work, inflowing air near the top of the boundary layer becomes supergradient and 'overshoots' into the eye. This would tend to moisten the eye at those levels. Finally, notice that none of these extreme $T_{\mathrm{DEP,eye}}$ cases have small eyewalls. All of the eye diameters for these cases are between 15 and 28 n mi. This could be described as within the 'normal' range. Storms with very small eyes are conspicuously absent from this list. Since such small-eye storms can still be very intense, there must be some aspect(s) of eye structure, size, or shape that prevent those storms from achieving large $T_{\mathrm{DEP,eye}}$. Assuming that the eyewall mixing arguments of (Malkus, 1958a) are valid (in that work, moisture and angular momentum budgets were constructed using hypothetical soundings of eye, eyewall, and environmental). If the eyewall were nearly vertical and of a small radius, then the volume of descending air would be more easily moistened by mixing with the eyewall and the evaporation of hydrometeors falling in from above. If the eye on the other hand is of moderate size with a highly sloped eyewall, it will be more difficult for hydrometeors to fall in from above and there will be a larger volume of subsidence so that the effect of eyewall mixing will not be as much, at least near the center of the eye. Thus, it would seem that extremely large $T_{\mathrm{DEP,eye}}$ may be found with fairly large eyes with highly sloping eyewalls. Hurricanes Rita and Katrina certainly fit this description at these times. Interestingly, no storms with eyes larger than 28 n mi had an extremely large $T_{\mathrm{DEP,eye}}$. This may be because $\lambda_{\mathrm{R,min}}$ is quite low ($\sim$ 5 n mi) for intense storms. As the eye diameter becomes appreciably larger than this, the eye becomes 'dynamically large' and the strongest subsidence will tend to concentrate near the outer rim of the eye (Schubert et al., 2007). Since this is also where eyewall mixing would tend to moisten the eye air, it seems that eye diameters above 30 n mi preclude extreme $T_{\mathrm{DEP,eye}}$.

Table 6.1: All cases in the VDM data set for which the flight level central dew point depression ($T_{DEP,eye}$) exceeded 20 °C. The storm name, basin (AL = Atlantic, EP = Eastern Pacific), and date and time (UTC) of fix are given in the first, second, and third columns, respectively. The fourth column gives the flight level of the aircraft fix. The minimum sea level pressure ("MSLP", hPa) measured during the fix is given fifth column. The maximum flight level temperatures reported just outside the eyewall ("Outside") and within 5 n mi of the center ("Eye") are given in the sixth and seventh columns, respectively. The corresponding dew point temperature at the location of maximum flight level temperature in the eye is given in the eighth column.The flight level dew point temperature depression, $T - T_d$, at the location of maximum flight temperature (°C, measured within 5 n mi of the storm center) is given in the ninth column. The flight level baroclinity (°C, tenth column). The diameter of the primary eye and the radius of maximum wind ("RMW", given by the radius of the maximum inbound flight level wind speed reported for the fix), are given in the eleventh and twelfth columns, respectively. The thirteenth column gives the maximum inbound flight level wind speed ("VMAX"), while the fourteenth column lists the minimum Rossby length. The dynamical eye size is given in the final column.

Storm	Basin	Fix date / time UTC	Fix flight level	MSLP hPa	Outside T °C	Eye T °C	Eye T_d °C	T - T_d °C	Baro-clinity °C	Eye diameter n mi	RMW n mi	VMAX kt	Min Rossby length n mi	Dynamical eye size
RITA	AL	22 Sep 2005 / 07:14	700 mb	899	9	31	−3	34	22	16	13	148	5.2	1.5
RITA	AL	21 Sep 2005 / 21:16	700 mb	904	9	30	−1	31	21	20	9	145	3.6	2.8
RITA	AL	21 Sep 2005 / 23:13	700 mb	899	8	28	1	27	20	20	11	142	4.5	2.2
RITA	AL	21 Sep 2005 / 23:09	700 mb	899	8	28	1	27	20	20	11	142	4.5	2.2
RITA	AL	22 Sep 2005 / 05:38	700 mb	898	9	28	3	25	19	16	12	165	4.3	1.9
RITA	AL	21 Sep 2005 / 19:36	700 mb	914	8	27	2	25	19	20	16	161	5.7	1.7
PALOMA	AL	08 Nov 2008 / 21:23	700 mb	961	10	26	2	24	16	18	10	102	4.8	
RITA	AL	21 Sep 2005 / 17:53	700 mb	920	9	26	3	23	17	20	7	153	2.7	3.8
KATRINA	AL	28 Aug 2005 / 17:55	700 mb	902	14	29	6	23	15	25	22	160	8.5	1.5
KEITH	AL	01 Oct 2000 / 18:16	700 mb	950	11	25	2	23	14	20	8	103	3.4	3.0
FELIX	AL	02 Sep 2007 / 23:07	700 mb	936	25	26	4	22	1	15	12	152	2.6	2.9
RITA	AL	22 Sep 2005 / 11:10	700 mb	907	11	27	5	22	16	18	9	133	4.0	
KATRINA	AL	28 Aug 2005 / 20:38	700 mb	903	16	28	6	22	12	28	14	130	6.8	2.1
FLOYD	AL	13 Sep 1999 / 11:21	700 mb	921	11	26	4	22	15	20	19	142	7.6	1.3
RITA	AL	22 Sep 2005 / 09:12	700 mb	902	14	29	8	21	15	18	10	134	4.4	2.0
HUMBERTO	AL	24 Sep 2001 / 07:43	700 mb	989	8	21	0	21	13	25	20	66	23.1	
KEITH	AL	01 Oct 2000 / 07:34	700 mb	942	9	23	2	21	14	15	12	114	4.6	1.6
GUSTAV	AL	29 Aug 1990 / 05:10	700 mb	984	12	22	1	21	10		40	78	26.8	
KATRINA	AL	28 Aug 2005 / 15:00	700 mb	907	11	27	7	20	16	22	18	154	7.2	1.5
KATRINA	AL	28 Aug 2005 / 14:17	700 mb	907	12	26	6	20	14	22	14	140	6.1	1.8
KATRINA	AL	28 Aug 2005 / 12:57	700 mb	908	10	26	6	20	16	22	18	145	7.6	1.5
LILI	AL	02 Oct 2002 / 23:24	700 mb	940	14	26	6	20	12	9	7	89	4.9	0.9
FLOYD	AL	13 Sep 1999 / 17:35	700 mb	926	13	25	5	20	12	25	12	111	6.2	2.0

6.3.3 Horizontal temperature difference across the eyewall

Another measure of the warm core strength can be obtained by measuring the temperature change across the eyewall at flight level. This horizontal temperature difference is obtained by subtracting the representative temperature of the region just outside the eyewall from the maximum temperature reported from within 5 n mi of the center: $\Delta T_{\text{eyewall}} = T_{\text{eye}} - T_{\text{out}}$. While this measure is immune from the vagaries of our temperature adjustment scheme, changes in flight levels during the reconnaissance period may still introduce difficulties in interpretation. This is because the lower flight levels may pass through the cooler, moist portion of the eye beneath the inversion which typically resides between 850 and 700 hPa. This would cause the aircraft-reported warm anomaly values to be quite low. In the strongest storms, the eye inversion may reach all the way down to the surface in the eye[6] . Fig. 6.11 shows the interpolated temperature differences for the aircraft baselines. The curves for the 'A' baseline show that the FL warm anomaly begins rising about 36 h before 'A'. Starting from 1 °C, the composite mean warm anomaly increases to about 3 °C by 'A' and reaches 5 °C about 36 h after 'A'. Most of the individual storm curves range from −1 °C (i.e., "cool core") before 'A' to 5 to 6 °C by 'A'. Between 12 and 48 h after 'A', many storms achieve a warm anomaly of at least 6 °C while a few exceed 12 °C. In a large number of storms, the $\Delta T_{\text{eyewall}}$ is still small at the time of eye formation. Unlike $T_{\text{DEP,eye}}$, $\Delta T_{\text{eyewall}}$ does not decrease much after the peak warm core strength is reached. If T_{eye} does in fact decline, then the small change in $\Delta T_{\text{eyewall}}$ must be due to a decrease in T_{out}. In our adjustment scheme, however, T_{out} was adjusted in the same manner as T_{eye}. Whether T_{out} actually decreases is a matter left for further analysis.

Fig. 6.12 stratifies $\Delta T_{\text{eyewall}}$ by eye formation case type. A slight increase is seen for the intermittent failure cases. For the delayed success cases, the composite mean $\Delta T_{\text{eyewall}}$ increases steadily both before and after the aircraft eye is observed. In contrast, the complete success cases show a distinct uptrend which begins exactly at the time of eye formation.

---

[6] A remarkable example of the eye inversion reaching the surface is discussed in chapter 2.3.2

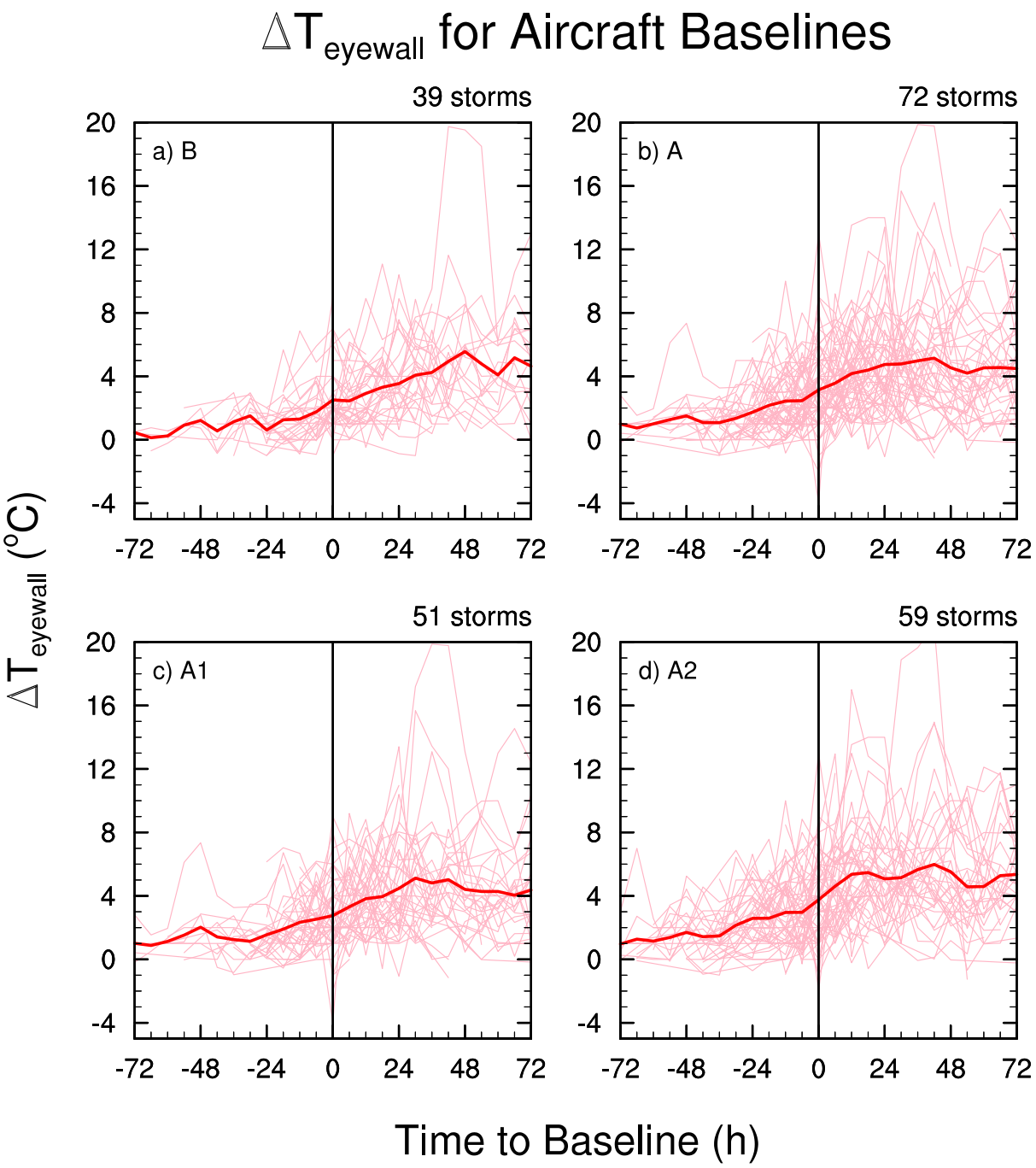

Figure 6.11: Horizontal temperature difference across the eyewall ($\Delta T_{\text{eyewall}}$) for aircraft baselines. Plotting conventions are the same as in Fig. 6.6.

Fig. 6.13 shows a similar plot for the IR satellite baselines. The mean composite $\Delta T_{\text{eyewall}}$ for IR2 shows a slow but steady increase reaching 5 °C by the end of the 6 d period. The mean composite curve for the IR4 baselines shows a similar steady increase in the warm anomaly (except it starts from a higher

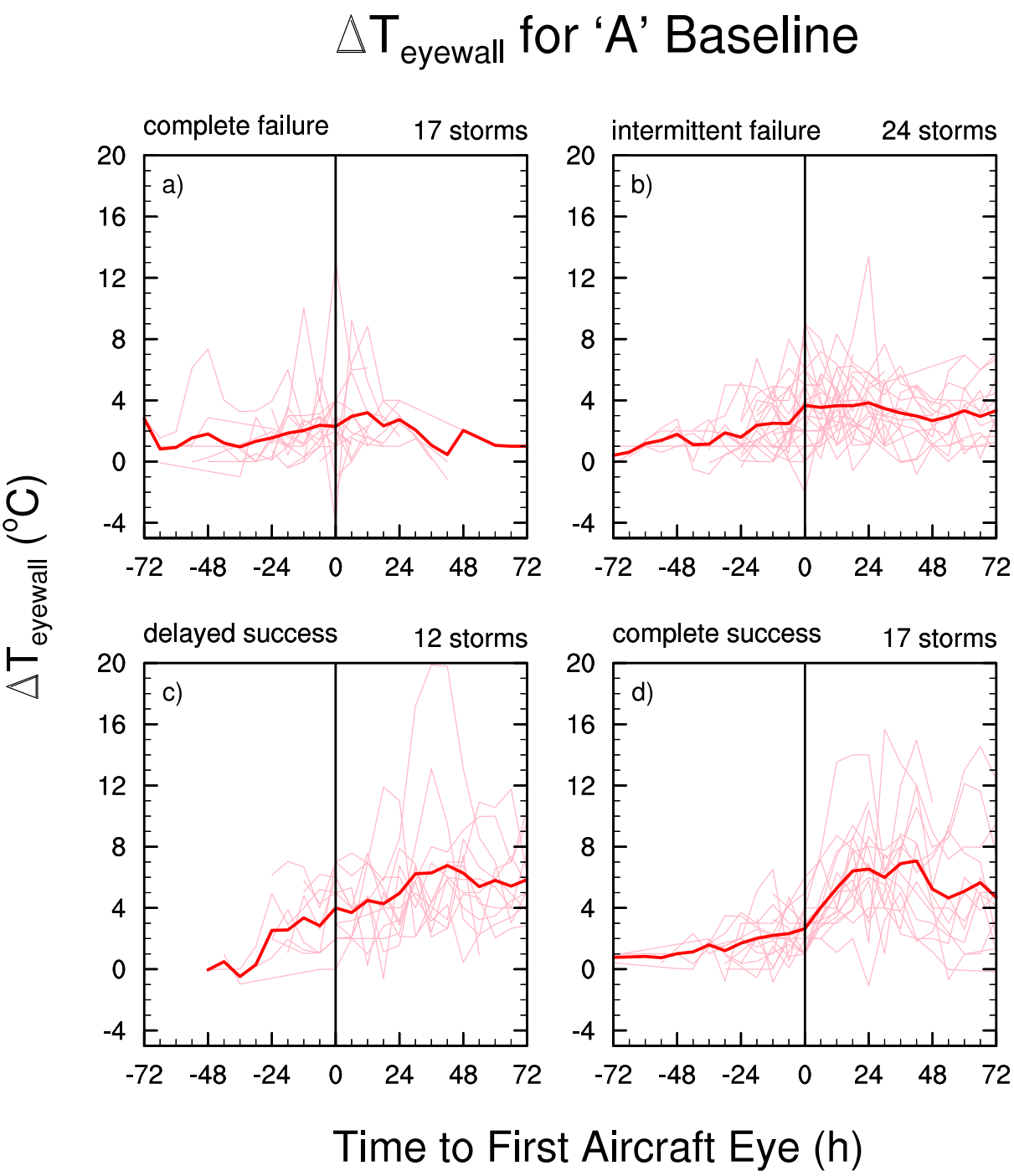

Figure 6.12: $\Delta T_{\text{eyewall}}$ for the 'A' baseline, stratified by eye formation case type.

level of 3 °C 72 h before the baseline). $\Delta T_{\text{eyewall}}$ rises a couple more degrees until about 18 h, when a decline starts. The IR5 composite mean starts rising appreciably 12 h before the baseline, from 4.5 °C to 8 °C about 12 h after the baseline. Oddly, at least one storm had a warm core anomaly of 3 °C at the time

the strong eye was reported. It is unclear whether this is simply because the FL in that particular case was at a level below the inversion of the eye or whether that particular storm just had a weak warm core in the mid levels. Finally, we note from this figure and our previous analysis of intensity (see Fig. 5.15) that the peak warm anomaly seems to coincide with peak intensity, in line with Kossin and Eastin (2001).

6.4 Subsequent eye size changes and the role of eyewall heating efficiency

This section examines the physical eye size changes of the newly formed eyes and changes in eyewall heating efficiency that occur as the physical scale of the system shrinks in size.

6.4.1 Physical scale of newly formed eyes

Eye size is determined by the flight crews by measuring the distance from the eye center to the inner edge of the eyewall convection as seen on radar. Fig. 6.14 shows eye radius r_{eye} interpolated to the 6-day time window centered on the aircraft baselines. At the time the aircraft eye is first observed, the composite mean r_{eye} is 9 n mi. The mean r_{eye} holds steady, with just a slight increase to 10 n mi over the next 3 d, but the individual storm r_{eye} show a wide range of variations. Dramatic jumps upward are very likely due to eyewall replacement cycles, during which an outer secondary eye forms and replaces the inner eyewall. The outer eyewall often contracts and sometimes the cycle repeats several times on a time scale ranging from 6 h to up to 3 d. The eyes of other storms continue contracting as the storm intensifies. These competing factors result in a basically trendless mean composite r_{eye}.

6.4.2 Physical scale of the efficient heating region

While both r_{eye} and r_{max} normally contract as a storm intensifies, it is generally believed that r_{max} contracts more than r_{eye}, so that the dynamically-efficient region of heating (which resides between the edge of the eye and the radius of maximum winds) reduces in physical scale. A plot of $r_{\text{max}} - r_{\text{eye}}$ is shown in Fig. 6.15. Varied behavior is shown for the various eye formation case types, but the impor-

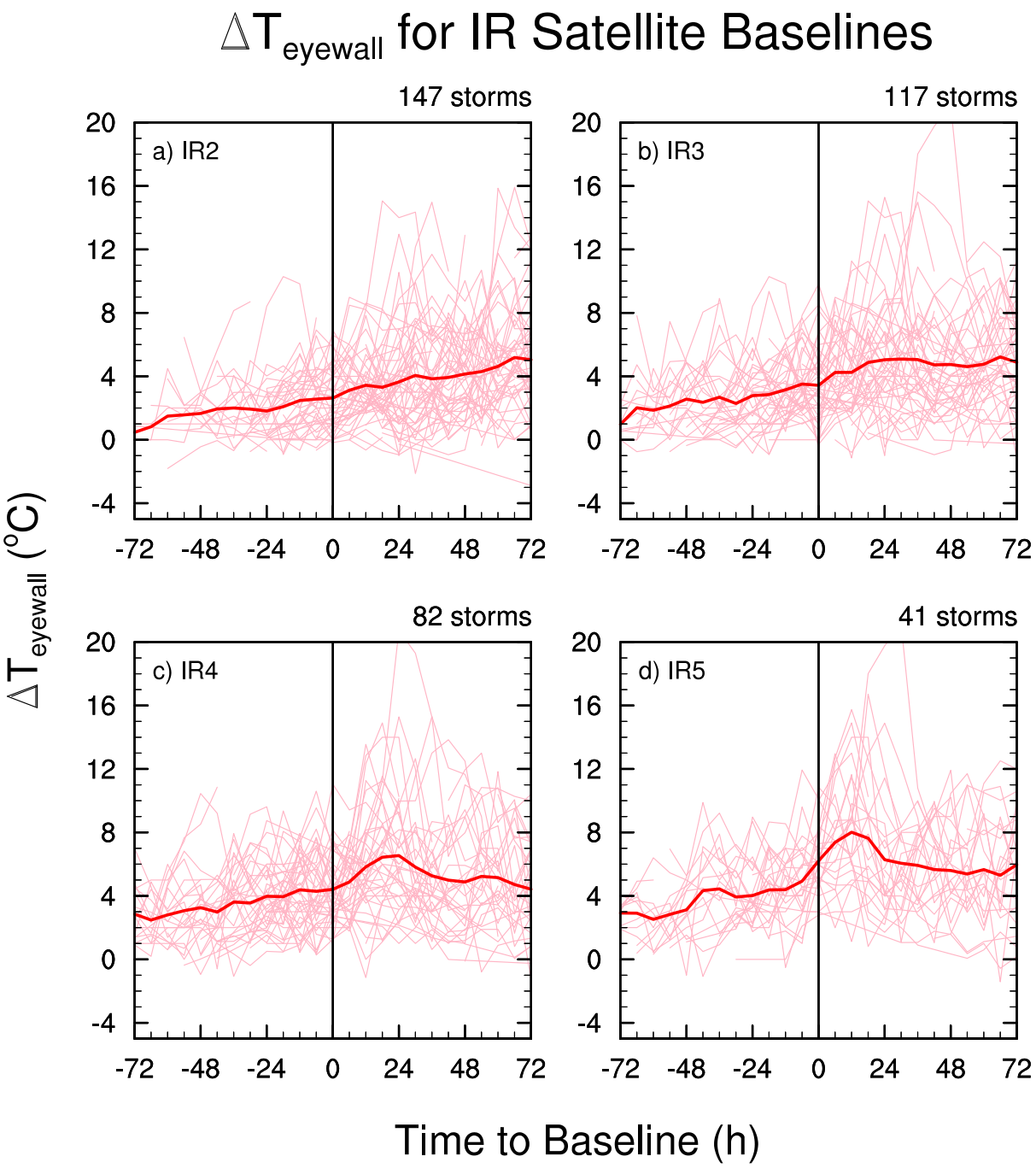

Figure 6.13: Horizontal temperature difference across the eyewall ($\Delta T_{\text{eyewall}}$) for IR satellite baselines. Plotting conventions are the same as in Fig. 6.13.

tant thing to notice is that the area of dynamically-efficient heating ranges from a few nautical miles, to 10 n mi for a good number of the storms, with an average of about 5 n mi. During the 24 to 36 h that the storm is intensifying, the dynamically-efficient region reduces down to 1 to 3 n mi. This corrobo-

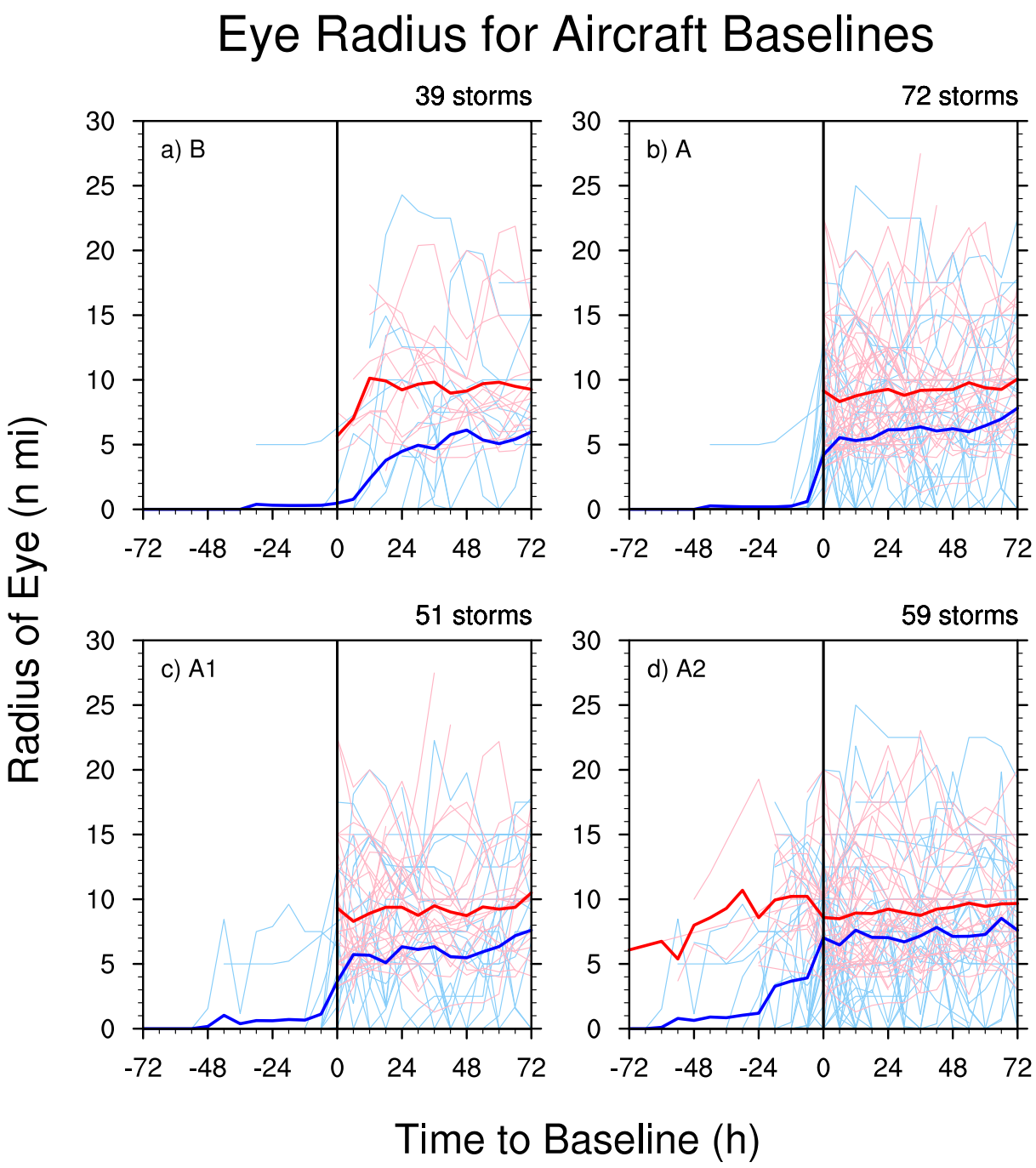

Figure 6.14: Radius of the formed eye (r_{eye}) for aircraft baselines. Plotting conventions are the same as in Fig. 6.1.

rates Shea and Gray (1973) who found that this distance decreased with increasing intensity (see their Fig. 18). After peak intensity is reached, this region expands. Obviously, the storm is not intensifying during this expansion, so other dynamics besides the efficient heating hypothesis of Schubert and

Hack (1982) are involved. Interestingly, this $r_{\max} - r_{\text{eye}}$ is negative for some storms at various times. This means that $r_{\max} < r_{\text{eye}}$ and there should therefore be *no* efficient eyewall heating in the azimuthal mean (though it is possible that there could be some azimuths where the heating is efficient). It seems unclear how this situation can arise, and some have suggested it is physically impossible (or at least unreasonable) Kimball and Mulekar (2004).

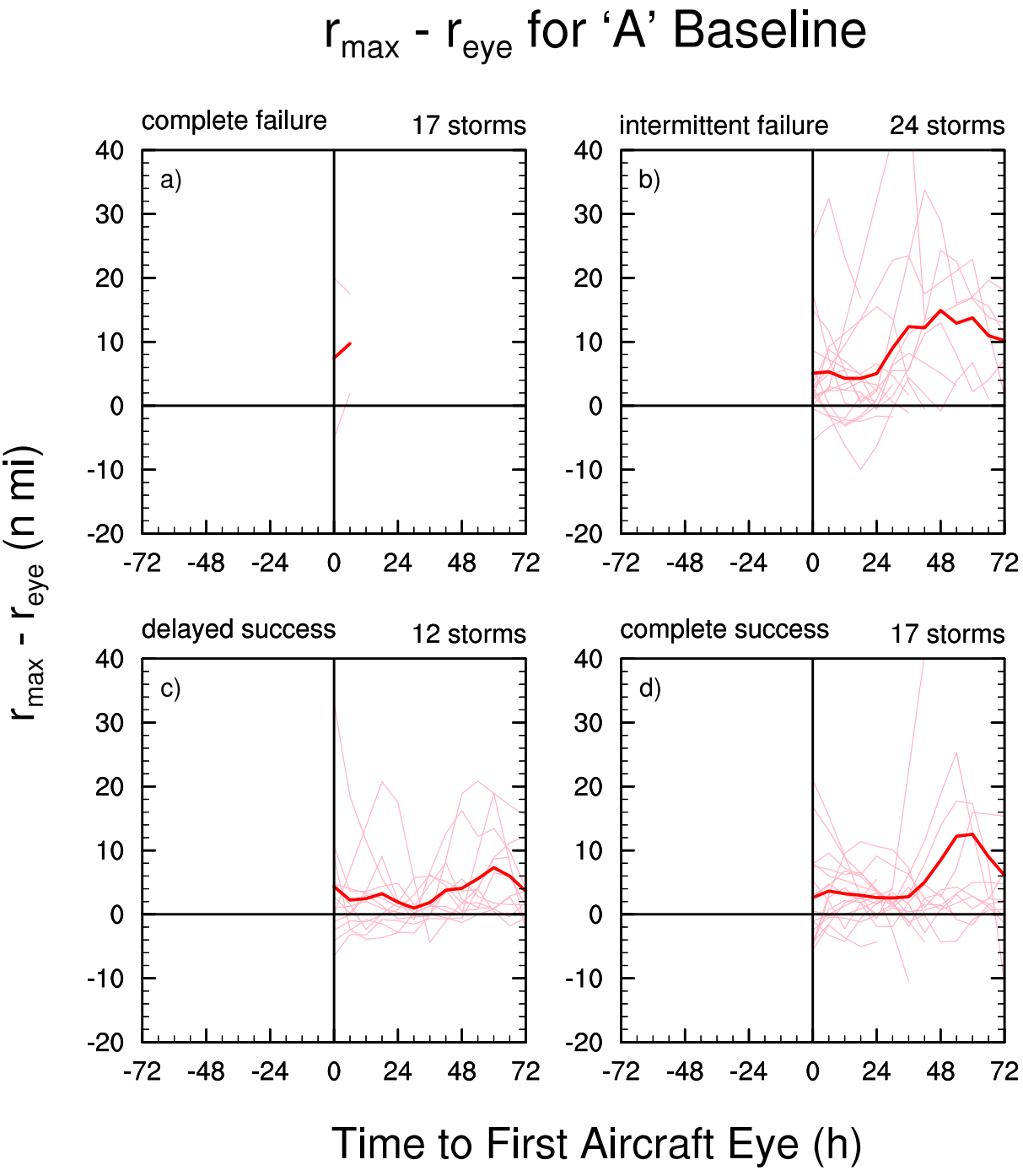

Figure 6.15: The physical scale of efficient heating ($r_{max} - r_{eye}$) for aircraft baselines, stratified by eye formation case type.

6.4.3 Dynamic scale of the heating region

Schubert and Hack (1982) suggested that the formation of an eyewall should eventually stabilize the vortex to rapid intensification as heating becomes 'locked out' of the high inertial stability region in the core. Observations however show that many storms continue intensifying rapidly after eye formation, which seems at odds with their theoretical argument. A possible solution has been discussed by some, in which the 'dynamical size' of the efficient heating region of the eyewall increases, even as the physical scale contracts (Fritsch, 1975; van Delden, 1989; Pendergrass and Willoughby, 2009). This of course occurs because $\lambda_{R,min}$ contracts even faster than the physical area of efficient heating decreases. Chapter 3 explains how a storm might continue rapidly intensifying due to the increase in dynamic efficiency of the heating region, even as the physical scale and total diabatic heating of this region decreases.

Fig. 6.16 shows the quantity $r_{max}/\lambda_{R,min}$, which we take as the nondimensional *dynamic vortex scale*, a measure of the size of the core of high inertial stability divided by the characteristic length scale over which the influence of heating will spread to the surrounding atmosphere. A wide variety of behaviors is displayed for storms which fail at their eye formations, but the dynamic vortex scale stays mostly below 0.6. In contrast, the delayed success cases show a rising trend, but then a setback right before the time of eye formation, with a subsequent recovery to higher values a couple days later. The complete success cases show a steady rise from 24 h before the time of eye formation, to 24 h afterward. This supports the idea (elucidated in chapter 3) that the increasing efficiency of the eyewall heating more than counteracts the decreasing physical scale of the efficient heating, allowing the storm to keep intensifying rapidly even while diabatic heating is 'locked out' of the core.

6.5 Summary and conclusions

This chapter opened by considering the proposed sequence of Nolan (2007) which proposes that genesis proceeds when the inner core of a tropical cyclone saturates. In his simulations, a small scale

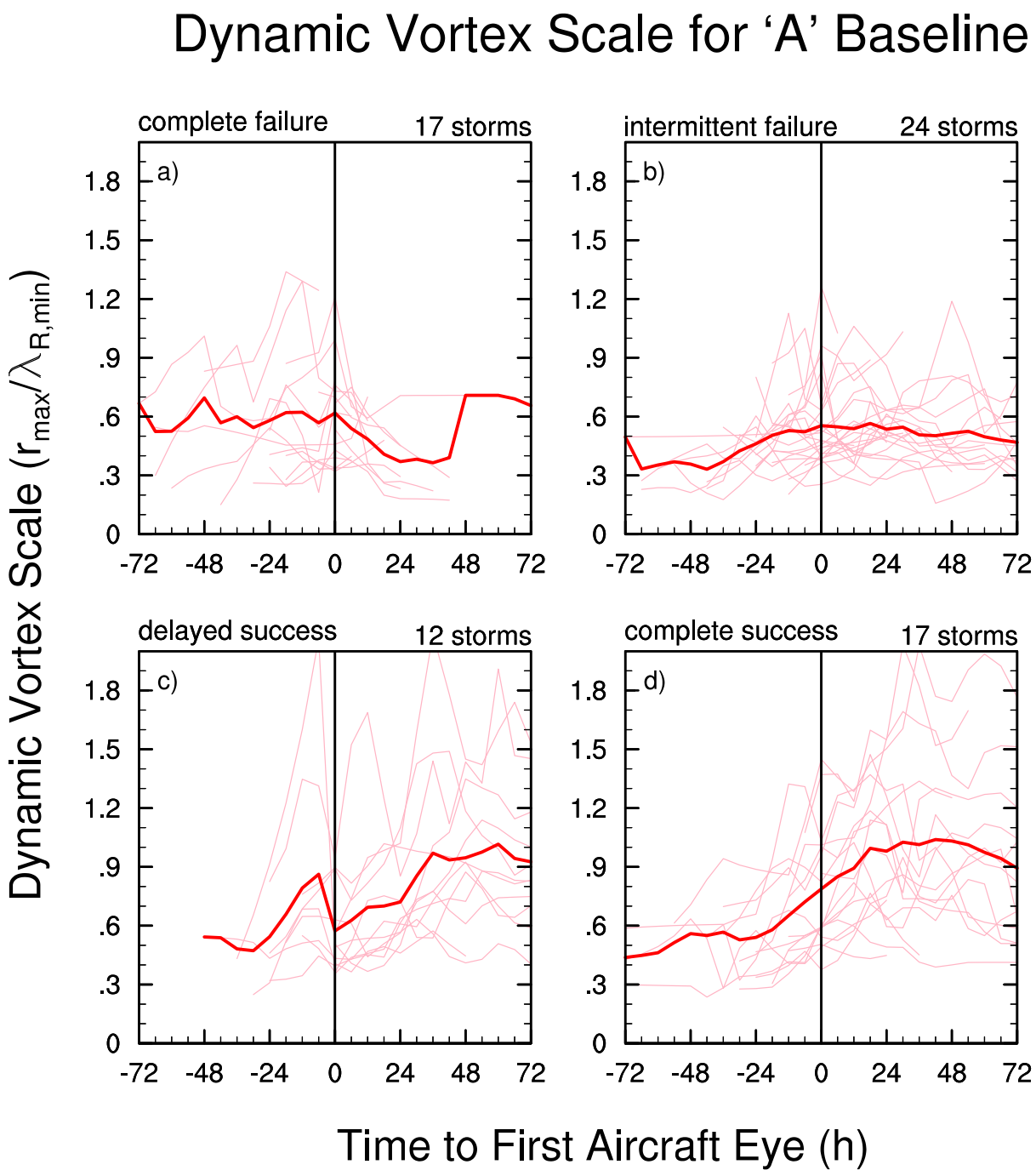

Figure 6.16: Dynamic vortex scale (r_{max}/r_{eye}) for aircraft baselines, stratified by eye formation case type.

vortex forms near the surface within the broad mid-level vortex. This occurs when a strong updraft element ‘captures’ the storm center and quickly intensifies to dominate the subsequent vortex evolution. To be fair, Nolan’s study does not even speak to the question of eye formation, but storms following that

sequence of events are certainly brought into a state in which eye formation would seem likely. Nolan's hypothesis has been tested by considering a battery of various structural and thermodynamic parameters from the eye formations of a broad subset of Atlantic tropical cyclones. Perhaps slightly more than half of these eye-forming storms do in fact undergo a substantial and rapid decrease in r_{max} during the 24 h before the aircraft eye is observed. Thus, we can say that the evidence broadly supports Nolan's proposed sequence of events for *some* of the cases. The fact that other storms already possess a small r_{max} well before their eye formations suggests however, that there are other pathways to eye formation.

Some other major conclusions of this chapter include the following:

(1) **BT r_{max} is found to have an erroneous and substantial high bias**: The r_{max} values contained in the best track 'bdecks' and the extended best track data set are not actually 'best tracked' radius values — that is, they have not undergone the scrutiny and vetting that the intensity values undergo in the post season. Rather, the BT r_{max} values are simply what was given by the operational forecaster, who is tasked with choosing a value of the storm's radius of maximum winds to initialize the numerical models with. Since those best of those models has had a relatively low resolution of 40 n mi until recently, it seems likely that this may be why forecasters were reluctant to assign smaller values of r_{max} to a given storm. If the FL r_{max} values are taken as "truth" and no tilt of the vortex is assumed, the BT r_{max} values are biased high by 30 to 90%.

(2) **About half of the storms studied undergo a substantial and rapid contraction in FL r_{max} starting during the 24-h period before the eye forms**: In these eye-forming systems, FL r_{max} contracts from 40 n mi or greater to between 5 and 20 n mi by the time an aircraft eye is observed. The mean r_{max} at that time is 15 n mi.

(3) **Minimum FL r_{max} is reached at or soon after the eye forms, supporting Kuo's idea of a limiting radius**: Storms which continue to rapidly intensify may contract slowly for some time after eye formation, but in many storms r_{max} is steady after eye formation until peak intensity is reached. r_{max} experiences a substantial expansion in storms in which the eye formation failed.

(4) **There is no absolute value of $\lambda_{R,min}$ that triggers eye formation, but many storms undergo a sharp contraction in $\lambda_{R,min}$ in the 24 h before the eye forms**: The average $\lambda_{R,min}$ at the time of eye formation is just 26 n mi, but a few storms form eyes at considerably higher values (30 to 45 n mi). $\lambda_{R,min}$ continues to contract for storms that continue intensifying after forming eyes, but increases rapidly for storms in which eye formation fails. Storms that form a strong (IR5) eye $\lambda_{R,min}$ averages 10 n mi.

(5) **Many storms undergo a 'spike' in the 700 hPa-equivalent FL eye temperature which lasts between 18 and 36 h, but this period of strong eye warming is not well correlated with the time at which the *aircraft* eye is observed**: A few storms have strong central warming *before* eye formation, while others experience it considerably later. Because of the varied times in relation to eye formation, the overall composite mean T_{eye} shows little change. The appearance of these spikes supports the findings of Jordan (1961); Kossin and Eastin (2001) and the idea that a storm's peak intensity is caused by a regime change in eye structure.

(6) **The appearance of a persistent (IR4) or strong (IR5) satellite eye *does* have a strong correlation to the timing of the peak eye column warming**: T_{eye} rises an average of 2 to 4 °C for these baselines, but individual storms show much greater increases of 8 to 14 °C. The strongest warming of T_{eye} begin right at the time an IR5 eye is observed. These storms experience their peak eye temperatures between 12 and 36 h afterward. *Thus, the eye clearing and well-defined cold ring of eyewall cloud top temperature associated with the strong eye 'scene' is strongly associated with warming in the lower eye.*

(7) **A handful of storms exhibit substantial $T_{\text{DEP,eye}}$ of greater than 8 °C before forming an eye, suggesting that the subsidence may not necessarily just be a simple response to the establishment of an eyewall**: In some cases, signs of central subsidence precede the actual eye formation by 12 to 24 h. Most storms experience their greatest $T_{\text{DEP,eye}}$ between 1 and 2 d after forming an eye.

(8) **The largest $T_{\text{DEP,eye}}$ are always found at the 700 hPa level in storms with moderate-sized eyes**: This suggests that below this level, mixing with inflowing eyewall air or modification through contact with the ocean air moistens the air — or perhaps that total subsidence is just not as strong at this lower level due to air leaving the eye below 700 hPa. Such eyewall mixing undoubtedly occurs, so storms with smaller eyes (and therefore smaller eye volumes) are more strongly affected (and moistened). Storms with very large eyes also do not reach large $T_{\text{DEP,eye}}$ values because the subsidence tends to be confined near the eyewall boundary by the low value of $\lambda_{\text{R,min}}$.

(9) **While extraordinary dew point depressions of greater than 20 °C are in some storms, by no means is this a requirement for a storm to reach a high intensity — many storms reach high intensity without such signals of subsidence**. It appears that only *some* storms experience strong warming in their lower eye regions, and that this is by no means required to have an intense storm. The greatest hydrostatic impact of warming occurs when the warming is at high levels, so of course all storms which reach high intensity possess a significant warm core aloft. But for whatever reason, strong warming is not always observed lower down. A possible cause is that the proposed 'momentum diffusion pump' (basically, the centrifugal effect) may only become substantial for the more intense storms. If so, then the mixing event which finally spins up the eye to solid body rotation would 'break' this pump, resulting in the peak of maximum intensity and subsequent weakening. Elements of this idea are discussed in more detail by Kossin and Eastin (2001) and Rozoff et al. (2009).

(10) **The temperature difference across the eyewall undergoes a strong increase on average only for the storms which are completely successful in their eye formations, supporting to some degree the idea that eye formation involves a frontogenetic collapse (Emanuel, 1997).** However, the strongest average $\Delta T_{\text{eyewall}}$ increases occur later when the persistent (IR4) and strong (IR5) eyes are observed. Thus, as just noted above, it seems that the 'momentum diffusion pump' becomes most relevant for the latter stages of eye formation. In this view then, the so-called 'centrifugal effect' is the strongest mainly after the eye has already formed and contributes to storm intensification up until peak intensity. More analysis is needed however to verify or disprove this idea.

(11) **Observations of the storms which experienced complete success in their eye formations support the idea that the dynamic efficiency of the eyewall heating increases even as the physical scale of the efficient heating region shrinks**: This effect is important in allowing a storm to continue intensifying, even as the diabatic heating becomes 'locked out' of the high

inertial stability of the core. Efficiency gains in the eyewall appear to more than counteract the reduction in total diabatic heating that occurs as the eyewall contracts.

There are several questions that this chapter was not able to answer due to the nature of the observational data used. One of these questions is whether the warm core of the eye builds upwards with the eyewall, downwards, or whether the eye column warms simultaneously (following Willoughby 1998). Another aspect not considered by this chapter is the role of potential vorticity (PV) dynamics in the developing eyewall. Again, the basic parameters from the Vortex Data Messages do not lend themselves to calculation of the three-dimensional PV field. The ideas of inertial stability are closely related to PV however, and this chapter has shown these inertial stability ideas have been shown to be useful by verifying several conjectures from the literature. Finally, this chapter did not even touch on the issue of the slope of the eyewall. To get better answers to our questions, observations of the radial profiles of tangential wind and temperature are needed. The Hurricane Research Division (HRD) flight level data sets contain a wealth of data, although there are still very few research flights made in storms near the time of eye formation. Future work will seek out some eye formation cases to study in more detail using full *in situ* data from the flight level data sets.

Finally, the high bias discovered in the BT r_{max} data point to the substantial need for better inner core size data. A 'better best track' of reliable r_{max} data would have great utility for many applications including wind risk engineering, past and real-time catastrophe modeling, storm surge modeling, and the validation and diagnosis of numerical weather prediction models.

Chapter 7

CONCLUSIONS

"Science is not a democracy.
The majority is often wrong..."
- Dr. Joanne Simpson - First Woman PhD in Meteorology

7.1 Introduction

This dissertation has examined the problem of hurricane eye formation by conducting three distinct studies over five chapters, each of which stands alone as a separate work with its own summary and conclusions sections. The goal of this chapter is not to reiterate the detailed summaries that have already been given in those chapters, but rather to highlight the main new results and to offer some unifying conclusions on the work as a whole. The reader is invited to refer to chapter 2.7 to review the general conclusions of the extensive review of vortex eye literature. The conclusions of the theoretical study can be found in chapter 3.8. Detailed summaries of the conclusions of the observational components of this study are given in chapter 5.8 (intensity changes) and chapter 6.5 (structure changes).

This chapter is organized as follows. The next section highlights the most important results of this work. The relation between primary eye formation and secondary eyewall formation is discussed in section 7.3. Future observational, theoretical, and modeling work are discussed in section 7.4, and some concluding remarks and a dedication are given in section 7.5.

7.2 Highlights

This work began with an comprehensive review of eye phenomenon in vortices ranging from simple vortices (e.g., a tea cup vortex) to complex hurricane-like geophysical vortices (e.g., dust devils and

polar lows). From these examples, the following fundamental understanding of eye formation was developed: *subsidence is required in 3-D vortices because the spin up of such a vortex requires a vertical rearrangement of mass in order to drive the vortex back towards force balance*. If taken far enough, this vertical rearrangement process will result is the formation of an eye. With this insight in hand, a comprehensive new definition for eye formation was put forward which melds the historic observational definition[1] with the dynamical understanding that the eye region is generally delimited by a streamsurface that separates its inner meridional circulation from that of the outer meridional circulation. This surface is typically manifested by a sharp radial discontinuity of vertical motion so that the eye is filled with subsidence extending through most of the mid to upper troposphere. With this understanding, 'aircraft eyes' and 'microwave eyes' do in fact satisfy the requisites of actual eyes (or nearly so). Thus, forecasters should not wait until an eye has appeared in satellite imagery to key off of the potential for increased intensification and further structural organization.

In the theoretical portion of this work, the role of diabatic heating in intensifying the storm was investigated in the framework of Eliassen's classic balanced vortex model. While previous approaches involved solutions of the transverse circulation equation, this approach is unique in that it analytically solves for the temperature tendency directly (via the geopotential tendency equation) associated with a vertical delta surface of diabatic heating in a vortex with a simple radial dependence of inertial stability. Calculations were made for some simple vortex wind profiles that had diabatic heating located within and without the region of high inertial stability. Our results showed that diabatic heating in the low inertial stability region outside the radius of maximum wind is inefficient at generating a warm core, no matter how large the current storm intensity. In contrast, diabatic heating in the high inertial stability region inside the radius of maximum wind is efficient at generating a localized temperature tendency, and this efficiency increases dramatically with storm intensity. These results emphasized that the vortex intensification rate depends *critically* on how much of the heating is occurring inside the radius of maximum wind. The formation of an eye tends to partially lock diabatic heating out of the highly efficient heating region of high inertial stability, leading to a striking paradox: Why do many storms intensify

[1] Historically, the eye region has been identified on aircraft radar when the candidate eye region is at least 50% surrounded by an annular cloudy, precipitating eyewall region which fills a substantial portion of the troposphere.

most rapidly during or after eye formation when the area of efficient heating is decreasing? We argue that the shrinking effect on the local Rossby length (due to the decreasing spatial scale and increasing tangential winds) more than compensates for the loss of efficiency due to eye formation and that this allows a hurricane to continue intensifying rapidly even after forming an eye.

The observational portion of this work characterized the kinematic and thermodynamic changes that occur before, during, and after the initial eye formations of a broad set of Atlantic tropical cyclones. An extensive new data set of inner core structure and intensity parameters was synthesized from the little-used Vortex Data Messages routinely transmitted from reconnaissance aircraft from 1989-2008. The first major finding was that storms form their first eyes (as observed by aircraft or IR satellite imagery) over a wide range of intensities ranging from a lower bound intensity of 30 to 35 kt to an upper bound of 80 to 85 kt. The mean intensity at which an eye is first reported was found to be 58 kt, which is considerably lower than what has been reported in some previous studies such as the oft-cited 68 kt from Shapiro and Willoughby (1982) or the 65 to 77 kt given by the Dvorak model (Dvorak, 1984). Clearly, the organization of an eyewall often begins *well below* hurricane intensity and has largely completed by the storm reaches the hurricane threshold. An increasing intensity trend is seen with improving structural organization, and banding was found to be a precursor to eye formation. Perhaps the most important result of this study, however, is that it observationally confirms the long-suspected idea that storms are intensifying most rapidly during and after eye formation. Storms which continue developing displayed even higher intensification rates at the eye development baselines associated with improved eye presentation. The best signal of imminent or currently occurring rapid intensification was found to occur when a *persistent*[2] eye is observed on satellite imagery. When the *strong*[3] eye signature appears, the most rapid intensification phase is often nearing its end.

Vertical wind shear was found to be highly disruptive to eye formation, but most storms form eyes in environments in which the vertical wind shear is between 10 and 20 kt. The temporal distribution

[2] A persistent eye is noted at the beginning of time period when a storm first maintains an eye for at least 6-h period according to the following criterion: the warmest eye brightness temperature must exceed −50 °C or be at least 15 °C warmer than a nearby cold cloud top in the eyewall and the ring of convection must be at least somewhat colder than the eye temperature all the way around.

[3] A strong eye was defined to have an IR brightness temperature in the eye of greater than −30 °C surrounded (in at least three out of four quadrants) by a cold cloud band of brightness temperatures colder than −70 °C.

of observed eye formation shows that most storms that form eyes tend to do so within 24 h of reaching tropical storm strength. From this we conclude that there is a fairly narrow time window of opportunity in which storms which have undergone genesis may quickly develop an eye. If eye formation fails, much more time may be required for a storm to reach a state of high organization and intensity. Yet, the failure of the initial eye may not necessarily be detrimental as a sizable number of storms reform an eye within a day or so of the initial failure and go on to rapidly intensify. This suggests that environmental conditions often play a key role in the success or failure of an eye.

Regarding the structural changes that occur during eye formation, many eye-forming storms experienced a substantial and rapid contraction in the radius of maximum winds during the 24-h period before the eye was observed. Once the eye appeared, the contraction of radius of maximum winds slowed or halted. The fact that the minimum radius of maximum winds is reached at or soon after the eye forms offers strong support to Kuo's idea that eye formation results from the existence of a limiting radius for inflowing air parcels. Looking at thermodynamic changes, strong warming at lower levels (850 or 700 hPa) of the eye is not observed to correlate well with the time in which the eye is first observed. Some warming episodes were observed *before* eye formation, suggesting that in some cases, subsidence can precede the appearance of an eye. This suggests that subsidence may not always be merely a response to the presence of an eyewall — it may directly contribute to the formation of the eye. Strong warming at lower levels lasts for a period of between 18 and 36 h and seems to more strongly associated with storm's intensification rate rather than the appearance of the eye itself. This supports the findings of previous studies and also the idea that a storm's peak intensity is caused by a regime change in eye structure. Finally, observations confirm the idea that the dynamical heating efficiency of the resulting eyewall increases even as the physical scale of the efficient heating region decreases. As argued previously from theoretical considerations, this allows the storm to continue intensifying even though the total inner core diabatic heating is decreasing.

7.3 Relation to the problem of secondary eyewall formation

This work has focused exclusively on the problem of primary eye formation, but it is natural to ask how this relates to the problem of secondary eyewall formation. Intense tropical cyclones are often

observed to undergo eyewall replacement cycles, during which an outer convective ring and associated tangential wind maximum forms and undergoes contraction. As the new, outer eyewall contracts, its convection imposes a new meridional circulation cell which opposes that of the primary eyewall's outer cell. This tends to cut off moist inflow and forces subsidence over the inner eye. Over time, the subsident warming and reduced inflow inhibit the convection of the inner eyewall and eventually kills it, leaving a relict circulation within the larger new primary eye. This cycle has been well-documented by following the temporal evolution of radial profiles of tangential wind obtained from aircraft (Willoughby et al., 1982; Black and Willoughby, 1992) and recently examined in a analytic framework similar to that used in chapter 3, but in a vortex with five regions (Rozoff et al., 2008). Although the relevant dynamics of ring contraction are well understood (Shapiro and Willoughby, 1982), the mechanism by which convective rings form is not, although Willoughby (1990b) suggests that the convective ring structure may be a normal mode, or attractor, of the system. Follow up work by Nong and Emanuel (2003) suggests that convective rings undergo amplification through a Wind-Induced Surface Heat Exchange (WISHE) mechanism if the lower atmosphere is moist enough. Due to cool downdrafts and thermal stability in the outer regions of storms, their modeling results suggest that large scale external forcings are necessary to initiate convective rings. Eddy angular momentum fluxes caused by interactions between the storm and the environment (e.g. an upper trough) could provide such a forcing (Molinari and Vollaro, 1990; Molinari et al., 1995), yet concentric eyewall phenomena are commonly observed in storms that are highly axisymmetric. This fact suggests that internal dynamics play a critical role (Rozoff et al., 2009). Rapid filamentation zones (Rozoff et al., 2006) and the role played by a vortex Rossby wave stagnation radius (Montgomery and Kallenbach, 1997) appeal to the internal dynamics view, since both apply to strongly-rotating vortices. In contrast, primary eye formation occurs in a weak-to-moderate rotation regime. Secondary eyewall formations have long been a difficult problem to model, but successful simulations have recently been conducted (Terwey and Montgomery, 2008). While the dynamics that organize convection into an eyewall may be somewhat different for inner and outer eyewalls, both primary and secondary eyewalls may share similarities with respect to the air-sea exchange regime under the nascent eyewall, where winds range from 20 to 40 $\mathrm{m\,s^{-1}}$. Further work is needed on many aspects of this problem.

7.4 Future work

All human endeavors must eventually come to a stopping point. Many fruitful avenues have been left unexplored in this dissertation. Other avenues were followed a ways before circumstances forced a detour. This section focuses on the main unresolved issue of the problem and how to proceed with new analyses, new observations, and theoretical and modeling studies.

7.4.1 Unresolved issues

The first major unresolved issue involves the actual causes of the central subsidence. Chapter 2 reviewed several somewhat competing theories, such as the global balance theories, the local force balance ideas, and mechanically-forced or turbulent diffusion of momentum ideas. In some sense, these theories are not necessarily in competition, but could rather be complimentary as there could undoubtedly be several contributive factors to subsidence. More careful study is needed to determine whether these theories are actually describing some of the same effects, but in such different dynamical frameworks that they seem completely different due to a type of 'balance degeneracy.'

Another unresolved problem involves the self-organization of convection into an eyewall and whether a transition from upright-dominated convection to slantwise convection is important in this process. Before the eye appears, satellite imagery often shows one or more 'blobs' of convection rotating around the nascent eyewall with strongly spreading anvils. While some shortcut mechanisms have been proposed based on inertial confinement of subsidence by a locally enhanced Rossby radius of deformation, the role of slantwise motions is unclear. There is no doubt however that the mature hurricane eyewall can involve such motions, and that before the appearance of an eyewall, convective motions are more vertical. The development of the warm core probably is key to this process, but the details are quite unclear.

Other unresolved issues include the role of the frictional boundary layer and air-sea interaction. The next paragraphs offer some potential steps that could be taken to make further progress on these unresolved issues.

7.4.2 Further observational work

Many aspects of this dissertation have highlighted the critical role of the radial increase in tangential wind shear as a parcel approaches the center. To better understand this effect, high resolution radial profiles of the tangential wind are needed for cases of storms strengthening from a minimal tropical storm through minimal hurricane intensity. A dearth of such data currently exists because many research missions to date have focused on storms that were already intense. Also, due to the passing of Ed Rahn, the Willoughby-Rahn data set has not been updated for storms after 2001, so many of the fantastic data that were gathered during the hyperactive 2004 and 2005 Atlantic hurricane seasons have been largely inaccessible to researchers. To this end, the author is working to process the varied HRD flight level data formats into a common format where data are transformed into a coordinate system relative to the moving storm center. In the Willoughby-Rahn data set, the radial legs were parsed 'by hand' — by visually examining each radial leg and picking off the starting and ending times to subset the data by — this is a tedious and time consuming process. The author has developed a novel algorithm to parse the radial legs automatically by objective criterion. The end goal of initial efforts is to produce an extended flight level data set which includes all the storms from 1977 down to the present, in one common and standardized netCDF file format. Once these data are in hand, the next step forward is to examine the role of the radial gradient in tangential wind (or, similarly, the absolute angular momentum gradient) in forcing the axial subsidence of the hurricane vortex. Related questions are how rapidly the warm core develops and whether a frontogenetic collapse actually occurs during eyewall formation. Radial profiles of moist entropy should be helpful for the latter, while quantitative measures of temperature tendency data should help with the former.

As the VDM data set was developed, it was recognized that this data set provided a unique opportunity to explore the phenomenon of 'warm ring' structures in hurricanes. Such structures are predicted theoretically when a storm's dynamical eye size becomes large (Schubert et al., 2007). Some observational evidence exists, but a detailed study has not yet been done. The VDM data set is ideal for examining where in a storm's life cycle warm rings occur, and what the relation is to intensity and structure change. Because this did not quite fit with the focus of the current work, this work not included

(apart from Appendix C. Future efforts will use the VDM data set to mine the HRD extended flight level data set for more detailed cases for further examination.

The role of convective morphology is another unresolved issue of hurricane eye formation. As discussed in chapter 4, the space-based microwave imagery contain a wealth of information, and in some cases give early clues as to the existence of an eye. The next step forward is to obtain the baseline times for eye formation from the 85 GHz and 37 GHz color composite imagery and incorporate these as extension of the current study (chapters 4 through 6). Due to the vertical differences in attenuation and sensing capabilities of the 85 GHz and 37 GHz channels,[4] , these data should also be very helpful in determining whether the eyewall structure and associated subsidence form at low levels (the 'low level convective ring') and builds upwards, develop downwards, or develop simultaneously throughout the eye column. These data will also be quite helpful in understanding the characteristic timescales for eye development and how these relate to the subsequent intensification path taken by the storm.

Finally, more detailed observations are needed of the boundary layer, particularly in the overshoot region where the winds become supergradient and turn upwards into the eyewall (personal communication, F. Marks Jr. 2010). It is very difficult to gather data in this region due to the severe and dangerous conditions that exist, but perhaps a combination of Doppler radar, unmanned aerial vehicles, and dropsondes can be used to investigate this interesting region which could be key to the eye formation problem.

7.4.3 Suggested steps towards a theoretical approach

Various theories (such as MPI) have examined the hurricane problem from a thermodynamics viewpoint, but a comprehensive analytic theory for the structure changes involved in eye formation does not yet exist, apart from some two-layer models and some of the boundary layer ideas and frontogenetic collapse ideas reviewed in chapter 2. Of course, to develop such a theory could be very challenging, if it is even possible, but this is a worthy goal. In the meantime, there are other avenues which may offer quicker results.

A very recent observational study Stern and Nolan (2009) has shed more light on the issue of

[4] The 85 GHz imagery is better able to sense the ice scattering by deep cold convective structure of the storm, while the 37 GHz imagery is good for examining the low level structure of moisture and hydrometeors.

eyewall slope, finding that at least one long-held myth (that eye slope is related to a storm's intensity) is not supported by the observations. They did find that eye slope was a function of storm size however, and that the radially-outward slope of the funnel was also a function of radius. We wonder, however, whether the slope is actually more of a function of the *age* of the storm and the cumulative influence of warm core development, rather than the intensity or size. Storms typically grow in size after maturing. After the small-eye stage, very intense storms often develop larger eyes and develop a more shallow eyewall slope. Eyewall width also changes as the amount of mass flow in the storm's secondary circulation changes. Annular hurricanes represent an extreme state in which the eyewall becomes a very thick annulus with a very shallow slope Wang (2008).

Another related problem is to better understand the influence of baroclinity and eyewall slope on the storm's evolution. The transformation of an idealized baroclinic vortex into potential radius coordinates should allow analytic solutions of the vortex response to a delta-surface of heating. Then the results of chapter 3 could be extended to a baroclinic vortex which includes the important radial variation in inertial stability as well as baroclinity. The mathematical solution would be directly analogous to the methods used in chapter 3. For comparison, numerical solutions could be computed using multigrid methods for an idealized vortex with spatially-varying coefficients for the static stability, the baroclinity, and the inertial stability. If realized, this work will be published as Schubert et al. (2010).

7.4.4 Suggested steps towards a modeling approach

Modern weather prediction and simulation models such as the Advanced Hurricane Weather Research and Forecasting (AHW-WRF[5]) model offer a comprehensive numerical platform on which to test the various eye formation theories. In the first step, a sensitivity study should be conducted to understand how the propensity of the modeled storm to form an eye is affected by variations of environmental parameters such as the mean thermodynamic profile, vertical wind shear, SST, and the Coriolis parameter. It would be particularly interesting to find whether eye formation helps a storm resist vertical wind shear. Next, a variety of process modeling experiments should be executed to examine some of the

[5] The ARW-WRF model features a dynamical core with an Eulerian mass solver and fully nonhydrostatic, compressible dynamics. For a description of the ARW and its numerics, see Klemp et al., 2000; Wicker and Skamarock, 2002; and Skamarock et al., 2005).

eye formation mechanisms that have been proposed. An experiment should test the boundary layer ideas of Eliassen (1959) by diagnosing the storm's convective response to parameterized or actual boundary forcing. Another experiment should measure the response of a storm to varying convective morphologies associated with eye formation. These morphologies include the primary band pathway, the pathway proposed by Nolan (2007) involving the formation of a central small scale vortex, and the morphology in which one or more large convective elements (hot towers?) rotate in the nascent eyewall, eventually forming a closed eyewall. Another modeling experiment should examine the impact of asymmetric wave drag and the role of sea spray. Finally, the eye formations in real storms (such as Hurricane Rita 2005, which was well observed by radar) should be diagnosed.

Simulations should be analyzed using a variety of methods. The evolution of the momentum, θ_E, and potential vorticity (PV) fields should be examined, but attention should also be focused on diagnosing the strength of the induced axial subsidence so as to determine the contributive mechanisms following the methods similar to Zhang et al. (2000). Of particular interest is whether the centrifugal mechanism is actually important for the dynamics of intense storms. Extremely high resolution simulations conducted by G. Bryan have shown that the diffusion mixing length parameter has a large control on the intensity of the storm. This may be directly related to the 'momentum diffusion pump' mechanism. Another very useful analysis might involve the computation of absolute angular momentum, thermodynamic energy, moisture, kinetic energy, and PV of the eye and eyewall air following Lagrangian parcel trajectories following Cram et al. (2007). To obtain trajectories with the highest possible accuracy and fidelity, the trajectory calculations should be computed on-line if possible.

7.5 Closing remarks

The author suspects that a dynamical systems viewpoint of eye formation should be advanced. In this view, eye formation process is viewed as an manifold attractor of the system, not merely a stochastic interaction of convective elements which are constructive or destructive. Eye formation then is an *end result of the genesis process*, with most if not all failed eye formations due to the disruptive role of the environment rather than the inner core disruptions. Of course, the competing and cooperative interaction of the smaller scale convective elements, the larger vortex, and the environment are by no means a solved

problem, and the author earnestly recognizes that his view could be in error.

The tropical cyclone genesis problem offers analogies which may be helpful here. Many have attempted to explain the cyclogenesis problem as an upscale cascade of energy and vorticity from vortical hot towers. Through merger processes, and cooperative interaction with the parent vortex, it has been proposed that these build up the parent vortex until genesis is achieved (Hendricks et al., 2004; Hendricks and Montgomery, 2006; Montgomery et al., 2006). While this is a very useful view, and no doubt captures important aspects of the underlying vortex dynamics, the current author tends to agree with Nolan (2007) that genesis involves a large scale adjustment of the vortex to the mean heating through a gradual evolution which includes the smaller scale convective elements, but is perhaps not so dependent on the details. The idea that saturation and cooling of the vortex core is a necessary prerequisite to genesis was proposed by Emanuel and Bister (1997). In that view, the cooling and saturation of the core is vital in maintaining thermal wind balance as the mid-level vortex strengthens and serves to destabilize the vortex to deep moist convection. Vortical hot towers may indeed play a role as the inner core spins up, and the capture of the center by a hot tower may indeed be a valid pathway to eye formation. The establishment of slantwise convection may be another pathway. The hot-tower induced warm core boost mechanisms of (Stewart and Lyons, 1996; Simpson et al., 1997, 1998; Heymsfield et al., 2001) likely offer shortcuts to eye formation. While many pathways to eye formation may exist, given favorable conditions, the author suspects that the end result is always the same: the storm intensifies into an intense vortex with an annular tower of PV and a spectacular, well-defined eye.

7.5.1 Dedication

As mentioned in the acknowledgments, science is a collaborative endeavor involving the combined thought and efforts of many, many people. This work is no different, and I again thank all who have contributed ideas and suggestions along the way. To paraphrase Isaac Newton, if I have seen further than anyone before, it is because I have stood on the shoulders of giants. The author is acutely aware of the many defects in this work and takes full responsibility for any errors of omission or commission. To the extent that this dissertation contains anything good, the author dedicates it to the benefit of mankind and to the glory of God.

This dissertation concludes with possibly the earliest known reference to the eye of a storm, found in Job 38:1-11, reproduced here in a standard standard translation and a modern paraphrase:[6]

From the New King James Version:

1 Then the LORD answered Job out of the whirlwind, and said:

2 Who is this who darkens counsel
By words without knowledge?

3 Now prepare yourself like a man;
I will question you, and you shall answer Me.

4 Where were you when I laid the foundations of the earth?
Tell Me, if you have understanding.

5 Who determined its measurements?
Surely you know!
Or who stretched the line upon it?

6 To what were its foundations fastened?
Or who laid its cornerstone,

7 When the morning stars sang together,
And all the sons of God shouted for joy?

8 Or who shut in the sea with doors,
When it burst forth and issued from the womb;

9 When I made the clouds its garment,
And thick darkness its swaddling band;

10 When I fixed My limit for it,
And set bars and doors;

11 When I said,
This far you may come, but no farther,
And here your proud waves must stop!

And from *The Message*:

And now, finally, God answered Job from the eye of a violent storm. He said:

”Why do you confuse the issue?
Why do you talk without knowing what you’re talking about?
Pull yourself together, Job!
Up on your feet! Stand tall!
I have some questions for you,
and I want some straight answers.
Where were you when I created the earth?

[6] The book of Job may have been written by Moses around 1500 B. C., but Job himself may have lived as early as 2200 B. C.

Tell me, since you know so much!
Who decided on its size? Certainly you'll know that!
Who came up with the blueprints and measurements?
How was its foundation poured,
and who set the cornerstone,
While the morning stars sang in chorus
and all the angels shouted praise?
And who took charge of the ocean
when it gushed forth like a baby from the womb?
That was me! I wrapped it in soft clouds,
and tucked it in safely at night.
Then I made a playpen for it,
a strong playpen so it couldn't run loose,
And said, 'Stay here, this is your place.
Your wild tantrums are confined to this place.'

BIBLIOGRAPHY

Abdullah, A. J., 1954: A proposed mechanism for the development of the eye of a hurricane. *J. Meteor.*, **11**, 189–195.

Abramowitz, M. and I. A. Stegun, 2006: *Handbook of Mathematical Functions*. Dover Publications, 1046 pp.

Adler, R. F. and E. B. Rodgers, 1977: Satellite-observed latent heat release in a tropical cyclone. *Mon. Wea. Rev.*, **105**, 956–963.

Agee, E. and E. Jones, 2009: Proposed conceptual taxonomy for proper identification and classification of tornado events. *Wea. Forecasting*, **24**, 609–617.

Alaka, M. A. and D. T. Rubsam, 1965: Evolution of the kinematic and thermal fields during the development of hurricane Ella (1962). *Mon. Wea. Rev.*, **93**, 673–686.

Algué, J., 1904: The cyclones of the Far East, 2nd (revised) ed. Bureau of Printing, Manila, 283 pp.

Andreas, E. L., 2004: Spray stress revisited. *J. Phys. Oceanogr.*, **34**, 1429–1440.

Anthes, R. A., 1982: *Tropical Cyclones: Their Evolution, Structure, and Effects*. No. 41 in Meteor. Monogr., Amer. Meteor. Soc., 208 pp.

Atkinson, G. D. and C. R. Holliday, 1977: Tropical cyclone minimum sea level pressure/maximum sustained wind relationship for the Western North Pacific. *Mon. Wea. Rev.*, **105**, 421–427.

Avila, L. A., 1998: Forecasting tropical cyclone intensity changes: An operational challenge. Preprints, *Symp. on Tropical Cyclone Intensity Change*, Phoenix, AZ, Amer. Meteor. Soc., 1–3.

Ballou, S. M., 1892: The eye of the storm. *American Meteorological Journal*, **9 (2)**, 67–84, 121–127.

Bender, M. A., I. Ginis, R. Tuleya, B. Thomas, and T. Marchok, 2007: The operational GFDL coupled hurricane-ocean prediction system and a summary of its performance. *Mon. Wea. Rev.*, **135**, 3965–3989.

Bister, M. and K. A. Emanuel, 1998: Dissipative heating and hurricane intensity. *Meteorol. Atmos. Phys.*, **65**, 233–240.

Black, M. L. and H. E. Willoughby, 1992: The concentric eyewall cycle of Hurricane Gilbert. *Mon. Wea. Rev.*, **120**, 947–957.

Bluestein, H. B., 2005: A review of ground-based, mobile, W-band Doppler-radar observations of tornadoes and dust devils. *Dynam. Atmos. Oceans*, **40**, 163–188.

Bluestein, H. B., C. C. Weiss, and A. L. Pazmany, 2004: Doppler radar observations of dust devils in Texas. *Mon. Wea. Rev.*, **132**, 209–224.

Bosart, L. F., 1981: The President's snowstorm of 18–19 February 1979: A subsynoptic-scale event. *Mon. Wea. Rev.*, **109**, 1542–1566.

Briegel, L. M. and W. M. Frank, 1997: Large-scale influences on tropical cyclogenesis in the Western North Pacific. *Mon. Wea. Rev.*, **125**, 1397–1413.

Bryan, G. H. and R. Rotunno, 2009: The influence of near-surface, high-entropy air in hurricane eyes on maximum hurricane intensity. *J. Atmos. Sci.*, **66**, 148–158.

Burt, S., 1987: A new North Atlantic low pressure record. *Weather*, **42**, 53–56.

Burt, S., 1993: Another new North Atlantic low pressure record. *Weather*, **48**, 98–103.

Byers, H. R., 1944: *General Meteorology*. McGraw-Hill, New York, 645 pp.

Carrier, G. F., 1971: The intensification of hurricanes. *J. Fluid Mech.*, **49**, 145–158.

Carrier, G. F., A. L. Hammond, and O. D. George, 1971: A model of the mature hurricane. *J. Fluid Mech.*, **47**, 145–170.

Church, C. R., J. T. Snow, G. L. Baker, and E. M. Agee, 1979: Characteristics of tornado-like vortices as a function of swirl ratio: A laboratory investigation. *J. Atmos. Sci.*, **36**, 1755–1776.

Cline, I. M., 1926: *Tropical Cyclones*. MacMillan, 301 pp.

Corbosiero, K. L., J. Molinari, and M. L. Black, 2005: The structure and evolution of Hurricane Elena (1985). Part I: Symmetric intensification. *Mon. Wea. Rev.*, **133**, 2905–2921.

Cram, T. A., J. Persing, M. T. Montgomery, and S. A. Braun, 2007: A Lagrangian trajectory view on transport and mixing processes between the eye, eyewall, and environment using a high-resolution simulation of hurricane Bonnie (1998). *J. Atmos. Sci.*, 1835–1856.

Davies-Jones, R. P., 1973: The dependence of core radius on swirl ratio in a tornado simulator. *J. Atmos. Sci.*, **30**, 1427–1430.

Davis, W. M., 1899: *Elementary Meteorology*. Ginn & Company, 395 pp.

DeMaria, M. and J. Kaplan, 1994: A statistical hurricane intensity prediction scheme SHIPS for the Atlantic basin. *Wea. Forecasting*, **9**, 209–220.

DeMaria, M. and J. Kaplan, 1999: An updated statistical hurricane intensity prediction scheme (SHIPS) for the Atlantic and eastern North Pacific basins. *Wea. Forecasting*, **14**, 326–337.

DeMaria, M., M. Mainelli, L. K. Shay, J. A. Knaff, and J. Kaplan, 2005: Further improvements to the statistical hurricane intensity prediction scheme (SHIPS). *Wea. Forecasting*, **20**, 531–543.

Demuth, J. L., M. DeMaria, and J. A. Knaff, 2006: Improvement of Advanced Microwave Sounding Unit tropical cyclone intensity and size estimation algorithms. *J. Appl. Meteor. Climatol.*, **45**, 1573–1581.

Deppermann, C. E., 1937a: Are there warm sectors in Philippine typhoons? Tech. rep., Bureau of Printing, Manila, 20 pp.

Deppermann, C. E., 1937b: Temperature conditions in the eyes of some typhoons. Tech. rep., Bureau of Printing, Manila, 19 pp.

Deppermann, C. E., 1946: Is there a ring of violent upward convection in hurricanes and typhoons? *Bull. Amer. Meteor. Soc.*, **27**, 6–8.

Dickerson, R. A., 2006: Phemonenological analysis of forces in hurricane dynamics. Preprints, *27th Conf. on Hurricanes and Tropical Meteorology*, Monterey, CA, Amer. Meteor. Soc., Paper 3B.2, [Available online at `http://ams.confex.com/ams/pdfpapers/107571.pdf`].

Dunkerton, T. J., 1989: Body force circulations in a compressible atmosphere: Key concepts. *Pure Appl. Geophys.*, **130**, 243–262.

Dunn, G. E., 1951: Tropical cyclones. *Compendium of Meteorology*, Amer. Meteor. Soc., 887–900.

Durst, C. S. and R. C. Sutcliffe, 1938: The importance of vertical motion in the development of tropical revolving storms. *Quart. J. Roy. Meteor. Soc.*, **64**, 75–84.

Dvorak, V. F., 1975: Tropical cyclone intensity analysis and forecasting from satellite imagery. *Mon. Wea. Rev.*, **103**, 420–430.

Dvorak, V. F., 1984: Tropical cyclone intensity analysis using satellite data. NOAA Tech. Rep. NESDIS 11, 47 pp., Washington, D. C.

Edson, R. T. and J. D. Ventham, 2008: Signs of rapid intensification as depicted in the microwave imagery. *Extended Abstract, 28th Conf. on Hurricanes and Tropical Meteorology*, Orlando, FL, Amer. Meteor. Soc., Paper 15A.2, [Available online at `http://ams.confex.com/ams/pdfpapers/137258.pdf`].

Eliassen, A., 1951: Slow thermally or frictionally controlled meridional circulations in a circular vortex. *Astrophys. Norv.*, **5**, 19–60.

Eliassen, A., 1959: On the formation of fronts in the atmosphere. *The Atmosphere and the Sea in Motion: Scientific Contributions to the Rossby Memorial Volume*, B. Bolin, Ed., Rockefeller Institute Press, New York, 277–287.

Eliassen, A., 1971: On the Ekman layer in a circular vortex. *J. Meteor. Soc. Japan*, **49**, 784–788.

Eliassen, A. and M. Lystad, 1977: The Ekman layer of a circular vortex. A numerical and theoretical study. *Geophys. Norv.*, **31**, 1–16.

Elsberry, R. L., G. J. Holland, H. Gerrish, M. DeMaria, C. P. Guard, and K. Emanuel, 1992: Is there any hope for tropical cyclone intensity prediction? – a panel discussion. *Bull. Amer. Meteor. Soc.*, **73**, 264–275.

Emanuel, K., 1986: An air-sea interaction theory for tropical cyclones. Part I: Steady-state maintenance. *J. Atmos. Sci.*, **43**, 585–604.

Emanuel, K., 1988: The maximum intensity of hurricanes. *J. Atmos. Sci.*, **45**, 1143–1155.

Emanuel, K., 1989: Polar lows as Arctic hurricanes. *Tellus*, **41A**, 1–17.

Emanuel, K., 1991: The theory of hurricanes. *J. Atmos. Sci.*, **23**, 179–196.

Emanuel, K., 1995: Sensitivity of tropical cyclones to surface exchange coefficients and a revised steady-state model incorporating eye dynamics. *J. Atmos. Sci.*, **52**, 3969–3976.

Emanuel, K., 1997: Some aspects of hurricane inner-core dynamics and energetics. *J. Atmos. Sci.*, **54**, 1014–1026.

Emanuel, K., 2003: A similarity hypothesis for air-sea exchange at extreme winds speeds. *J. Atmos. Sci.*, **60**, 1420–1428.

Emanuel, K., 2005: Genesis and maintenance of "Mediterranean hurricanes". *Adv. Geosci.*, **2**, 217–220.

Emanuel, K. and M. Bister, 1997: Reply. *J. Atmos. Sci.*, **54**, 2778–2779.

Ferreira, R. N. and W. H. Schubert, 1997: Barotropic aspects of ITCZ breakdown. *J. Atmos. Sci.*, **54**, 261–285.

Ferreira, R. N., W. H. Schubert, and J. J. Hack, 1996: Dynamical aspects of twin tropical cyclones associated with the Madden-Julian Oscillation. *J. Atmos. Sci.*, **53**, 929–945.

Fiedler, B. H. and R. Rotunno, 1986: A theory for the maximum windspeeds in tornado-like vortices. *J. Atmos. Sci.*, **43**, 2328–2340.

Fitzpatrick, P. J., 1996: Understanding and forecasting tropical cylone intensity change. Dept. of Atmos. Sci. Paper No. 598, Colorado State University, 346 pp. [Available from Dept. of Atmospheric Science, Colorado State University, Fort Collins, 80523.].

Fletcher, R. D., J. R. Smith, and R. C. Bundgaard, 1961: Superior photographic reconnaissance of tropical cyclones. *Weatherwise*, **14**, 102–109.

Franklin, J. L., M. L. Black, and K. Valde, 2003: GPS dropwindsone wind profiles in hurricanes and their operational implications. *Wea. Forecasting*, **18**, 32–44.

Frisius, T., 2006: Surface-flux-induced tropical cyclogensis within an axisymmetric atmospheric balanced model. *Quart. J. Roy. Meteor. Soc.*, **132**, 2603–2623, doi:10.1256/qj.06.03.

Fritsch, J. M., 1975: Cumulus dynamics: Local compensating subsidence and its implementation for cumulus parameterization. *PAGEOPH*, **113**, 851–867.

Gedzelman, S., et al., 2003: Probing hurricanes with stable isotopes of rain and water vapor. *Mon. Wea. Rev.*, **131**, 1112–1127.

Gill, A. E., 1982: *Atmosphere-Ocean Dynamics*, International Geophysics Series, Vol. 30. Academic Press, 662 pp.

Glass, M. and G. Felde, 1989: Structure of tropical cyclones and surrounding regions as determined by OLS and SSM/I imagery analysis. Preprints, *4th Conf. on Satellite Meteorology and Oceanography*, Amer. Meteor. Soc., San Diego, CA.

Gray, S. L., 1998a: Analysis of the eyes formed in simulated tropical cyclones and polar lows. *Quart. J. Roy. Meteor. Soc.*, **124**, 2357–2375.

Gray, W. M., 1967: The mutual variation of wind, shear, and baroclinicity in the cumulus convective atmosphere of the hurricane. *Mon. Wea. Rev.*, **95**, 55–73.

Gray, W. M., 1991: Comments on "gradient balance in tropical cyclones". *J. Atmos. Sci.*, **48**, 1201–1208.

Gray, W. M., 1993: Tropical cyclone formation and intensity change. *ICSU/WMO International Symp. on Tropical Cyclone Disasters*, J. Lighthill, Z. Zhemin, G. Holland, and K. Emanuel, Eds., Peking University Press, Beijing, 116–135.

Gray, W. M., 1998b: The formation of tropical cyclones. *Meteorol. Atmos. Phys.*, **67**, 37–69.

Gray, W. M., C. Neumann, and T. L. Tsui, 1991: Assessment of the role of aircraft reconnaissance on tropical cyclone analysis and forecasting. *Bull. Amer. Meteor. Soc.*, **72**, 1867–1883.

Gray, W. M. and D. J. Shea, 1973: The hurricane's inner core region. II. Thermal stability and dynamic constraints. *J. Atmos. Sci.*, **30**, 1565–1576.

Greenspan, H. P. and L. Howard, 1963: On a time-dependent motion of a rotating fluid. *J. Fluid Mech.*, **17**, 385–404.

Griffin, J. S., R. W. Burpee, Marks, F. D., Jr., and J. L. Franklin, 1992: Real-time airborne analysis of aircraft data supporting operational hurricane forecasting. *Wea. Forecasting*, 480–490.

Gyakum, J. R., 1983: On the evolution of the EQ II storm. I: Synoptic aspects. *Mon. Wea. Rev.*, **111**, 1137–1155.

Hack, J. J. and W. H. Schubert, 1986: Nonlinear response of atmospheric vorticies to heating by organized cumulus convection. *J. Atmos. Sci.*, **43**, 1559–1573.

Halverson, J. B., J. Simpson, G. Heymsfield, H. Pierce, T. Hock, and L. Ritchie, 2006: Warm core structure of Hurricane Erin diagnosed from high alitude dropsondes during CAMEX-4. *J. Atmos. Sci.*, **63**, 309–324.

Haurwitz, B., 1935: The height of tropical cyclones and of the "eye" of the storm. *Mon. Wea. Rev.*, **63**, 45–49.

Hausman, S. A., K. V. Ooyama, and W. H. Schubert, 2006: Potential vorticity structure of simulated hurricanes. *J. Atmos. Sci.*, **63**, 87–108.

Hawkins, H. F. and S. M. Imbembo, 1976: The structure of a small, intense hurricane–Inez 1966. *Mon. Wea. Rev.*, **104**, 418–442.

Hawkins, H. F. and D. T. Rubsam, 1968: Hurricane Hilda, 1964. II Structure and budgets of the hurricane on October 1, 1964. *Mon. Wea. Rev.*, **96**, 617–636.

Hawkins, J. D., T. F. Lee, J. Turk, C. Sampson, J. Kent, and K. Richardson, 2001: Real-time internet distribution of satellite products for tropical cyclone reconnaissance. *Bull. Amer. Meteor. Soc.*, **82**, 567–578.

Haynes, P. H. and T. G. Shepherd, 1989: The importance of surface pressure changes in the response of the atmosphere to zonally-symmetric thermal and mechanical forcing. *Quart. J. Roy. Meteor. Soc.*, **115**, 1181–1208.

Henderson, R. S., 1978: USAF aerial weather reconnaissance using the Lockheed WC-130 aircraft. *Bull. Amer. Meteor. Soc.*, **59**, 1136–1143.

Hendricks, E. A. and M. T. Montgomery, 2006: Rapid scan views of convectively generated mesovortices in sheared tropical cyclone Gustav (2002). *Wea. Forecasting*, **21**, 1041–1050.

Hendricks, E. A., M. T. Montgomery, and C. A. Davis, 2004: The role of "vortical" hot towers in the formation of tropical cyclone Diana (1984). *J. Atmos. Sci.*, **61**, 1209–1232.

Heymsfield, G. M., J. B. Halverson, J. Simpson, L. Tian, and T. P. Bui, 2001: ER-2 Doppler radar investigations of the eyewall of Hurricane Bonnie during the Convection and Moisture Experiment-3. *J. Appl. Meteor.*, **40**, 1310–1330.

Holland, G. J. and R. T. Merrill, 1984: On the dynamics of tropical cyclone structural changes. *Quart. J. Roy. Meteor. Soc.*, **110**, 723–745.

Jarvinen, B. R., C. J. Neumann, and M. A. S. Davis, 1984: A tropical cyclone data tape for the North Atlantic basin, 1886-1983: Contents, limitations, and uses. NOAA Tech. Memo. NWS/NHC 22, 21 pp. [Available from NOAA/NWS/NHC, Miami, FL 33165.].

Jordan, C. L., 1952: On the low-level structure of the typhoon eye. *J. Meteor.*, **9**, 285–290.

Jordan, C. L., 1961: Marked changes in the characteristics of the eye of intense typhoons between the deepening and filling stages. *Mon. Wea. Rev.*, **18**, 779–789.

Jordan, C. L. and E. S. Jordan, 1954: On the mean thermal structure of tropical cyclones. *J. Meteor.*, **11**, 440–448.

Jorgensen, D. P., 1984a: Mesoscale and convective-scale characteristics of mature hurricanes. Part I: General observations by research aircraft. *J. Atmos. Sci.*, **41**, 1268–1285.

Jorgensen, D. P., 1984b: Mesoscale and convective-scale characteristics of mature hurricanes. Part II: Inner core structure of Hurricane Allen (1980). *J. Atmos. Sci.*, **41**, 1287–1311.

Karyampudi, V. M., J. D. Hawkins, E. B. Rodgers, R. M. Zehr, C. S. Velden, J. Simpson, and S. Huntrakul, 1999: Tropical cyclone structure and intensity change. *Estimating the Amount of Rainfall Associated with Tropical Cyclones Using Satellite Techniques*, WMO Tech. Doc. No. 975, Report No. TCP-42, 11–92, [Available from Secretariat of the World Meteorological Organization, Publications Sales Unit, Case Postale 2300, CH-1211 Geneva 2, Switzerland].

Kepert, J., 2001: The dynamics of boundary layer jets within the tropical cyclone core. Part I: Linear theory. *J. Atmos. Sci.*, **58**, 2469–2484.

Kepert, J. and Y. Wang, 2001: The dynamics of boundary layer jets within the tropical cyclone core. Part II: Nonlinear enhancement. *J. Atmos. Sci.*, **58**, 2485–2501.

Kepert, J. D., 2006: Observed boundary layer wind structure and balance in the hurricane core. Part II: Hurricane Mitch. *J. Atmos. Sci.*, **63**, 2194–2211.

Kessler, III, Edwin, 1958: Eye region of hurricane Edna, 1954. *J. Meteor.*, **15**, 264–270.

Kidder, S. Q., M. D. Goldberg, R. M. Zehr, M. DeMaria, J. F. W. Purdom, C. S. Velden, N. C. Grody, and S. J. Kusselson, 2000: Satellite analysis of tropical cyclones using the Advanced Microwave Sounding Unit (AMSU). *Bull. Amer. Meteor. Soc.*, **81**, 1241–1259.

Kieper, M. E., 2008: A technique for anticipating initial rapid increases in intensity in tropical cyclones using 37 GHz microwave imagery. *Extended Abstract, 28th Conf. on Hurricanes and Tropical Meteorology*, Orlando, FL, Amer. Meteor. Soc., P2B.15, [Available online at `http://ams.confex.com/ams/pdfpapers/140605.pdf`].

Kimball, S. K. and M. S. Mulekar, 2004: A 15-year climatology of North Atlantic tropical cyclones. Part I: Size parameters. *J. Climate*, **17**, 3555–3575.

Klemp, J. B., W. C. Skamarock, and J. Dudhia, 2000: Conservative split-explicit time integration methods for the compressible nonhydrostatic equations, [Available online at `http://box.mmm.ucar.edu/people/skamarock/wrf_equations_eulerian.pdf`].

Knaff, J. A., J. P. Kossin, and M. DeMaria, 2003: Annular hurricanes. *Wea. Forecasting*, **18**, 204–223.

Kosiba, K. A., R. J. Trapp, and J. Wurman, 2008: An analysis of the axisymmetric three-dimensional low level wind field in a tornado using mobile radar observations. *Geophys. Res. Lett.*, **35**, L05805, doi:10.1029/2007GL031851.

Kossin, J. P. and M. D. Eastin, 2001: Two distinct regimes in the kinematic and thermodynamic structure of the hurricane eye and eyewall. *J. Atmos. Sci.*, **58**, 1079–1090.

Kossin, J. P., W. H. Schubert, and M. T. Montgomery, 2000: Unstable interactions between a hurricane's primary eyewall and a secondary ring of enhanced vorticity. *J. Atmos. Sci.*, **57**, 3893–3917.

Kossin, J. P. and M. Sitkowski, 2009: An objective model for identifying secondary eyewall formation in hurricanes. *Mon. Wea. Rev.*, **137**, doi:10.1175/2008MWR2701.1.

Kummerow, C., W. Barnes, T. Kozu, J. Shiue, and J. Simpson, 1998: The Tropical Rainfall Measuring Mission (TRMM) sensor package. *J. Atmos. Ocean. Technol.*, **15**, 809–817.

Kuo, H. C., L.-Y. Lin, C.-P. Chang, and R. T. Williams, 2004: The formation of concentric vorticity structures in typhoons. *J. Atmos. Sci.*, **61**, 2722–2734.

Kuo, H. L., 1959: Dynamics of convective vortices and eye formation. *The Atmosphere and the Sea in Motion: Scientific Contributions to the Rossby Memorial Volume*, B. Bolin, Ed., Rockefeller Institute Press, New York, 413–424.

LaSeur, N. E. and H. F. Hawkins, 1963: An analysis of hurricane Cleo (1958) based on data from research reconnaissance aircraft. *Mon. Wea. Rev.*, **91**, 694–709.

Lee, T. F., F. J. Turk, J. Hawkins, and K. Richardson, 2002: Interpretation of TRMM TMI images of tropical cyclones. *Earth Interactions*, **6**, 1–17.

Leverson, V. H., P. C. Sinclair, and J. H. Golden, 1977: Waterspout wind, temperature and pressure structure deduced from aircraft measurments. *Mon. Wea. Rev.*, **105**, 725–733.

Lewellen, D. C. and W. S. Lewellen, 2007: Near-surface vortex intensification through corner flow collapse. *J. Atmos. Sci.*, **64**, 2195–2209.

Lewellen, D. C., W. S. Lewellen, and J. Xia, 2000: The influence of a local swirl ratio on tornado intensification near the surface. *J. Atmos. Sci.*, **57**, 527–544.

Lonfat, M., Marks Jr., F. D., and S. S. Chen, 2004: Precipitation distribution in tropical cyclones using the Tropical Rainfall Measuring Mission TRMM microwave imager: A global perspective. *Mon. Wea. Rev.*, **132**, 1645–1660.

Malkus, J. S., 1958a: On the structure and maintenance of the mature hurricane eye. *J. Meteor.*, **15**, 337–349.

Malkus, J. S., 1958b: Tropical weather disturbances — why so few become hurricanes. *Weather*, **13**, 75–89.

Malkus, J. S., C. Ronne, and M. Chaffee, 1961: Cloud patterns in hurricane Daisy, 1958. *Tellus*, **13**, 9–30.

Mallen, K. J., M. T. Montgomery, and B. Wang, 2005: Reexamining the near-core radial structure of the tropical cyclone primary circulation: Implications for vortex resiliency. *J. Atmos. Sci.*, **62**, 408–425.

Marks, F. D., Jr., 1985: Evolution of the structure of precipitation in Hurricane Allen. *Mon. Wea. Rev.*, **113**, 909–930.

Marks, F. D., Jr. and Houze, Robert A., Jr., 1984: Airborne Doppler radar observations in hurricane Debby. *Bull. Amer. Meteor. Soc.*, **65**, 569–582.

Mathur, M. B., 1997: Development of an eye-wall like structure in a tropical cyclone model simulation. *Dynam. Atmos. Oceans*, **27**, 527–547.

Matsuno, T. and K. Nakamura, 1979: The Eulerian- and Lagrangian-mean meridional circulations in the stratosphere at the time of a sudden warming. *J. Atmos. Sci.*, **36**, 640–654.

Maynard, R. H., 1946: Radar and weather. *J. Meteor.*, **2**, 214–226.

McAdie, C. J., C. W. Landsea, C. J. Neumann, J. E. David, E. S. Blake, and G. R. Hammer, 2009: Tropical cyclones of the North Atlantic, 1851–2006 (6th ed.). Historical Climatology Series 6-2. [Available from the National Climatic Data Center, 151 Patton Avenue, Room 120, Asheville, NC 28801-5001. Also available online at: `http://www.nhc.noaa.gov/abouttrackbooks.shtml`].

McAdie, C. J. and M. B. Lawrence, 2000: Improvements in tropical cyclone track forecasting in the Atlantic basin, 1970-98. *Bull. Amer. Meteor. Soc.*, **81**, 989–997.

McCallum, E. and N. S. Granhame, 1993: The Braer storm – 10 january 1993. *Weather*, **48**, 103–107.

Miller, R. J., A. J. Scrader, C. R. Sampson, and T. L. Tsui, 1990: The automated tropical cyclone forecast system (atcf). *Wea. Forecasting*, **5**, 653–660.

Miner, T., P. J. Sousounis, J. Wallman, and G. Mann, 2000: Hurricane Huron. *Bull. Amer. Meteor. Soc.*, **81**, 223–236.

Mizuta, R. and S. Yoden, 2001: Chaotic mixing and transport barriers in an idealized stratospheric polar vortex. *J. Atmos. Sci.*, **58**, 2616–2629.

Molinari, J., S. Skubis, and D. Vollaro, 1995: External influences on hurricane intensity. Part III: Potential vorticity structure. *J. Atmos. Sci.*, **52**, 3593–3606.

Molinari, J. and D. Vollaro, 1990: External influences on hurricane intensity. Part II: Vertical structure and response fo the hurricane vortex. *J. Atmos. Sci.*, **47**, 1902–1918.

Möller, J. D. and L. J. Shapiro, 2005: Influences of asymmetric heating on hurricane evolution in the MM5. *J. Atmos. Sci.*, **62**, 3974–3992.

Montgomery, M. T. and J. Enagonio, 1998: Tropical cyclogensis via convectively forced vortex Rossby waves in a three-dimensional quasigeostrophic model. *J. Atmos. Sci.*, **55**, 3176–3207.

Montgomery, M. T. and R. J. Kallenbach, 1997: A theory for vortex Rossby waves and its application to spiral bands and intensity changes in hurricanes. *Quart. J. Roy. Meteor. Soc.*, **123**, 435–465.

Montgomery, M. T., M. E. Nicholls, T. A. Cram, and A. B. Saunders, 2006: A vortical hot tower route to tropical cyclogenesis. *J. Atmos. Sci.*, 355–386.

Moon, I.-J., I. Ginis, and T. Hara, 2004: Effect of surface waves on air-sea momentum exchange. Part II: Behavior of drag coefficient under tropical cyclones. *J. Atmos. Sci.*, **61**, 2334–2348.

Mundell, D. B., 1990: Prediction of tropical cyclone rapid intensification. M.S. thesis, Dept. of Atmospheric Science, Colorado State University, 186 pp., Fort Collins, Colorado, 80523.

Nakamura, N., 2004: Quantifying asymmetric wave breaking and two-way transport. *J. Atmos. Sci.*, **61**, 2735–2748.

Newell, R. E., et al., 1996: Atmospheric sampling of Supertyphoon Mireille with NASA DC-8 aircraft on September 27, 1991, during PEM-West A. *J. Geophys. Res.*, **101 (D1)**, 1853–1871.

Nolan, D. S., 2007: What is the trigger for tropical cyclogensis? *Aust. Meteorol. Mag.*, **56**, 241–266.

Nolan, D. S., Y. Moon, and D. P. Stern, 2007: Tropical cyclone intensification from asymmetric convection: Energetics and efficiency. *J. Atmos. Sci.*, **64**, 3377–3405, doi:10.1175/JAS3988.1.

Nong, S. and K. Emanuel, 2003: A numerical study of the genesis of concentric eyewalls in hurricanes. *Quart. J. Roy. Meteor. Soc.*, **129**, 3323–3338.

Nordeng, T. E. and E. A. Rasmussen, 1992: A most beautiful polar low. a case study of a polar low development in the Bear Island region. *Tellus*, **44A**, 81–99.

Ooyama, K., 1969: Numerical simulation of the life cycle of tropical cyclones. *J. Atmos. Sci.*, **26**, 3–40.

Palmén, E., 1948: On the formation and structure of tropical hurricanes. *Geophysica*, **3**, 26–38.

Palmén, E., 1956: Formation and development of tropical cyclones. *Paper No. 13, Tropical Cyclone Symposium*, Brisbane, 19.

Patton, F. S., G. D. Bothun, and S. L. Sessions, 2008: An electric force facilitator in descending vortex tornadogenesis. *J. Geophys. Res.*, **113**, D07106, doi:10.1029/2007JD009027.

Pearce, R. P., 1998: A study of hurricane dynamics using a two-fluid axisymmetric model. *Meteorol. Atmos. Phys.*, **67**, 71–81.

Pearce, R. P., 2004: An axisymmetric model of a mature tropical cyclone incoporating azimuthal vorticity. *Quart. J. Roy. Meteor. Soc.*, **130**, 259–293.

Pearce, R. P., 2005: Why must hurricanes have eyes? *Weather*, **60**, 19–24.

Pendergrass, A. G. and H. E. Willoughby, 2009: Diabatically induced secondary flows in tropical cyclones. Part I: Quasi-steady forcing. *Mon. Wea. Rev.*, **137**, 805–821, doi:10.1175/2008MWR2657.1.

Peng, J., M. S. Peng, and T. Li, 2008: Dependence of vortex asymmetrization on the characterization of the asymmetry. *Quart. J. Roy. Meteor. Soc.*, **134**, 1253–1268, doi:10.1002/qj.281.

Persing, J. and M. T. Montgomery, 2003: Hurricane superintensity. *J. Atmos. Sci.*, **60**, 2349–2371.

Pfeffer, R. L. and M. Challa, 1992: The role of environmental asymmetries in Atlantic hurricane formation. *J. Atmos. Sci.*, **49**, 1051–1059.

Piech, D. J., 2007: Atlantic reconnaissance vortex messsage climatology and composities and their use in characterizing eyewall cycles. M.S. thesis, Dept. of Meteorology, Florida State University, 123 pp., Tallahassee, Florida, 32306.

Powell, M. D., E. W. Uhlhorn, and J. D. Kepert, 2009: Estimating maximum surface winds from hurricane reconnaissance measurements. *Wea. Forecasting*, **24**, 868–883.

Rao, G. V. and P. D. MacArthur, 1994: The SSM/I estimated rainfall amounts of tropical cyclones and their potential in predicting the cyclone intensity changes. *Mon. Wea. Rev.*, **122**, 1568–1574.

Rappaport, E. N., et al., 2009: Advances and challenges at the National Hurricane Center. *Wea. Forecasting*, **24**, 395–419.

Raymond, D. J. and S. L. Sessions, 2007: Evolution of convection during tropical cyclogenesis. *Geophys. Res. Lett.*, **34**, L06811, doi:10.1029/GL028607.

Reale, O. and R. Atlas, 2001: Tropical cyclone-like vortices in the extratropics: Observational evidence and synoptic analysis. *Wea. Forecasting*, **16**, 7–34.

Reasor, P. D., M. T. Montgomery, and L. F. Bosart, 2005: Mesoscale observations of the genesis of hurricane Dolly (1996). *J. Atmos. Sci.*, **62**, 3151–3171.

Riehl, H., 1948: A radiosonde observation in the eye of a hurricane. *Quart. J. Roy. Meteor. Soc.*, **74**, 194–196.

Riehl, H. and J. Malkus, 1958: Some aspects of hurricane Daisy, 1958. *Tellus*, **13**, 181–213.

Rodgers, E., W. Olson, J. Halverson, J. Simpson, and H. Pierce, 2000: Environmental forcing of Supertyphoon Paka's (1997) latent heat structure. *J. Appl. Meteor.*, **39**, 1983–2006.

Rodgers, E. B. and R. F. Adler, 1981: Tropical cyclone rainfall characteristics as determined from a satellite passive microwave radiometer. *Mon. Wea. Rev.*, **109**, 506–521.

Rodgers, E. B., S. Chang, and H. F. Pierce, 1994: A satellite observational and numerical study of precipitation characteristics in Western North Atlantic tropical cyclones. *J. Appl. Meteor.*, **33**, 129–139.

Rodgers, E. B., W. S. Olson, V. M. Karyampudi, and H. F. Pierce, 1998: Satellite-derived latent heating distribution and environmental influences in Hurricane Opal (1995). *Mon. Wea. Rev.*, **126**, 1229–1247.

Rozoff, C. M., J. P. Kossin, W. H. Schubert, and P. J. Mulero, 2009: Internal control of hurricane intensity variability: The dual nature of potential vorticity mixing. *J. Atmos. Sci.*, **66**, 133–147, doi:10.1175/2008JAS2717.1.

Rozoff, C. M., W. H. Schubert, and J. P. Kossin, 2008: Some dynamical aspects of tropical cyclone concentric eyewalls. *Quart. J. Roy. Meteor. Soc.*, **134**, 583–593, doi:10.1002/qj.237.

Rozoff, C. M., W. H. Schubert, B. D. McNoldy, and J. P. Kossin, 2006: Rapid filamentation zones in intense tropical cyclones. *J. Atmos. Sci.*, **63**, 325–340.

Ryan, B. F., G. M. Barnes, and E. J. Zipser, 1992: A wide rainband in a developing tropical cyclone. *Mon. Wea. Rev.*, **120**, 431–447.

Sampson, C. R. and A. J. Schrader, 2000: The automated tropical cyclone forecasting system (version 3.2). *Bull. Amer. Meteor. Soc.*, **81**, 1231–1240.

Samsury, C. E. and E. J. Zipser, 1995: Secondary wind maxima in hurricanes: Airflow and relationship to rainbands. *Mon. Wea. Rev.*, **123**, 3502–3517.

Sawyer, J. S., 1947: Notes on the theory of tropical cyclones. *Quart. J. Roy. Meteor. Soc.*, **73**, 101–126.

Sawyer, J. S., 1952: Dynamical aspects of some simple frontal models. *Quart. J. Roy. Meteor. Soc.*, **78**, 170–178.

Sawyer, J. S., 1956: The vertical circulation at meteorological fronts and its relation to frontogenesis. *Proc. Roy. Soc. A.*, **234**, 346–362.

Schacht, E. J., 1946: A mean hurricane sounding for the Caribbean area. *Bull. Amer. Meteor. Soc.*, **27**, 324–327.

Schär, C., 1993: A generalization of Bernoulli's Theorem. *J. Atmos. Sci.*, **50**, 1437–1443.

Schubert, W. H. and J. J. Hack, 1982: Inertial stability and tropical cyclone development. *J. Atmos. Sci.*, **39**, 1687–1697.

Schubert, W. H. and J. J. Hack, 1983: Transformed Eliassen balanced vortex model. *J. Atmos. Sci.*, **40**, 1571–1583.

Schubert, W. H., J. J. Hack, P. L. Silva Dias, and S. R. Fulton, 1980: Geostrophic adjustment in an axisymmetric vortex. *J. Atmos. Sci.*, **37**, 1464–1484.

Schubert, W. H., C. M. Rozoff, J. L. Vigh, B. D. McNoldy, and J. P. Kossin, 2007: On the distribution of subsidence in the hurricane eye. *Quart. J. Roy. Meteor. Soc.*, **133**, 595–605, doi:10.1002/qj.49.

Schubert, W. H., J. L. Vigh, C. M. Rozoff, and P. E. Ciesielski, 2010: A numerical and theoretical investigation of the relation between hurricane eye slope, intensity, and intensification rate. *Dynam. Atmos. Oceans, in preparation.*

Shapiro, L. J. and H. E. Willoughby, 1982: The response of balanced hurricanes to local sources of heat and momentum. *J. Atmos. Sci.*, **39**, 378–394.

Shea, D. J. and W. M. Gray, 1973: The hurricane's inner core region. I. Symmetric and asymmetric structure. *J. Atmos. Sci.*, **30**, 1544–1564.

Sheets, R. C., 1990: The National Hurricane Center – past, present, and future. *Wea. Forecasting*, **5**, 185–232.

Sherman, L., 1956: On the wind asymmetry of hurricanes. *J. Meteor.*, 500–503.

Shin, S. and R. K. Smith, 2008: Tropical cyclone intensification and predictability in a minimal three-dimensional model. *Quart. J. Roy. Meteor. Soc.*, **134**, 1661–1671, doi:10.1002/qj.327.

Shuckburgh, E. and P. Haynes, 2003: Diagnosing transport and mixing using a tracer-based coordinate system. *Phys. Fluids*, **15**, 3342–3357.

Simpson, J., J. B. Halverson, B. S. Ferrier, W. A. Petersen, R. H. Simpson, R. Blakeslee, and S. L. Durden, 1998: On the role of "hot towers" in tropical cyclone formation. *Meteorol. Atmos. Phys.*, **67**, 15–35.

Simpson, J., E. Ritchie, G. J. Holland, J. Halverson, and S. Stewart, 1997: Mesoscale interactions in tropical cyclone genesis. *Mon. Wea. Rev.*, **125**, 2643–2661.

Simpson, R. H., 1952: Exploring eye of Typhoon "Marge," 1951. *Bull. Amer. Meteor. Soc.*, **33**, 286–298.

Simpson, R. H., 1974: The hurricane disaster-potential scale. *Weatherwise*, **27**, 169, 186.

Simpson, R. H. and J. M. Pelissier, 1971: Atlantic hurricane season of 1970. *Mon. Wea. Rev.*, **99**, 269–277.

Sinclair, P. C., 1973: The lower structure of dust devils. *J. Atmos. Sci.*, **30**, 1599–1619.

Skamarock, W. C., J. B. Klemp, J. Dudhia, D. O. Gall, D. M. Barker, W. Wang, and J. G. Powers, 2005: A description of the Advanced Research WRF Version 2. NCAR Tech. Note NCAR/TN-468+STR, 20 pp., Boulder, CO. [Available online at `http://www.mmm.ucar.edu/wrf/users/docs/arw_v2.pdf`].

Smith, R. K., 1980: Tropical cyclone eye dynamics. *J. Atmos. Sci.*, **37**, 1227–1232.

Smith, R. K., 2005: "Why must hurricanes have eyes" – revisited. *Weather*, **60**, 326–328.

Sousounis, P. J., J. Wallman, G. Mann, and T. Miner, 2001: "hurricane Huron": An example of an extreme lake-aggregate effect in Autumn. *Mon. Wea. Rev.*, **129**, 401–419.

Spencer, R. W., 1986: A satellite passive 37-GHz scattering-based method for measuring oceanic rain rates. *J. Climate Appl. Meteor.*, **25**, 754–766.

Spencer, R. W., B. B. Hinton, and W. S. Olson, 1983: Nimbus-7 37 GHz radiances correlated with radar rain rates over the Gulf of Mexico. *J. Climate Appl. Meteor.*, **22**, 2095–2099.

Steranka, J., E. B. Rodgers, and R. C. Gentry, 1986: The relationship between satellite measured convective bursts and tropical cyclone intensification. *Mon. Wea. Rev.*, **114**, 1539–1546.

Stern, D. P. and D. S. Nolan, 2009: Reexamining the vertical structure of tangential winds in tropical cyclones: Observations and theory. *J. Atmos. Sci.*, **137**, 3579–3600, doi:10.1175/2009JAS2916.1.

Stewart, S. R. and S. W. Lyons, 1996: A WSR-88D radar view of Tropical Cyclone Ed. *Wea. Forecasting*, **11**, 115–135.

Stossmeister, G. J. and G. M. Barnes, 1992: The development of a second circulation center within Tropical Storm Isabel (1985). *Mon. Wea. Rev.*, **120**, 685–697.

Sy ̄ono, S., 1951: On the structure of atmospheric vortices. *J. Meteor.*, **8**, 103–110.

Szoke, E. J., 1991: Eye of the Denver cyclone. *Mon. Wea. Rev.*, **119**, 1283–1292.

Terwey, W. D. and M. T. Montgomery, 2008: Secondary eyewall formation in two idealized, full-physics modeled hurricanes. *J. Geophys. Res.*, **113**, D12112, doi:10.1029/2007JD008897.

Uhlhorn, E. W., P. G. Black, J. L. Franklin, M. Goodberlet, J. Carswell, and A. S. Goldstein, 2007: Hurricane surface wind measurements from an operational stepped frequency microwave radiometer. *Mon. Wea. Rev.*, **135**, 3070–3085.

van Delden, A., 1989: On the deepening and filling of balanced cyclones by diabatic heating. *Meteorol. Atmos. Phys.*, **41**, 127–145.

Van Sang, N., R. K. Smith, and M. T. Montgomery, 2008: Tropical-cyclone intensification and predictability in three dimensions. *Quart. J. Roy. Meteor. Soc.*, **134**, 563–582, doi:10.1002/qj.235.

Velden, C. S., T. L. Olander, and R. M. Zehr, 1998: Development of an objective scheme to estimate tropical cyclone intensity from digital geostationary satellite infrared imagery. *Wea. Forecasting*, **13**, 172–186.

Vigh, J. L., J. A. Knaff, and W. H. Schubert, 2010a: Observations of hurricane eye formation. Part I: Background and data. *Mon. Wea. Rev.*, *in preparation*.

Vigh, J. L., J. A. Knaff, and W. H. Schubert, 2010b: Observations of hurricane eye formation. Part II: Intensity ranges and changes. *Mon. Wea. Rev.*, *in preparation*.

Vigh, J. L., J. A. Knaff, and W. H. Schubert, 2010c: Observations of hurricane eye formation: Part III: Dynamic and thermodynamic structure. *Mon. Wea. Rev.*, *in preparation*.

Vigh, J. L. and W. H. Schubert, 2009: Rapid development of the tropical cyclone warm core. *J. Atmos. Sci.*, **66**, 3335–3350, doi:10.1175/2009JAS3092.1.

Vigh, J. L. and W. H. Schubert, 2010: Observations of warm rings, eye moats, and hub clouds. *Mon. Wea. Rev., in preparation*.

Vigh, J. L., W. H. Schubert, and G. Holland, 2010d: A review of eye formation in tropical cyclones. *Quart. J. Roy. Meteor. Soc., in preparation*.

Walko, R. L., 1988: Plausibility of substantial dry adiabatic subsidence in a tornado core. *J. Atmos. Sci.*, **45**, 2251–2267.

Wang, Y., 2008: Structure and formation of an annular hurricane simulated in a fully compressible, nonhydrostatic model—TCM4. *J. Atmos. Sci.*, **65**, 1505–1527, doi:10.1175/2007JAS2528.1.

Wang, Y. and C.-C. Wu, 2004: Current understanding of tropical cyclone structure and intensity changes – a review. *Meteorol. Atmos. Phys.*, **87**, 257–278.

Weatherford, C. L. and W. M. Gray, 1988a: Typhoon structure as revealed by aircraft reconnaissance. Part I: Data analysis and climatology. *Mon. Wea. Rev.*, **116**, 1032–1043.

Weatherford, C. L. and W. M. Gray, 1988b: Typhoon structure as revealed by aircraft reconnaissance. Part II: Structural variability. *Mon. Wea. Rev.*, **116**, 1044–1056.

Weng, F. and N. C. Grody, 1994: Retrieval of cloud liquid water using the Special Sensor Microwave Imager (SSM/I). *J. Geophys. Res.*, **99 (D12)**, 25,535–25,551.

Wexler, H., 1945: The structure of the September, 1944, hurricane when off Cape Henry, Virginia. *Bull. Amer. Meteor. Soc.*, **26**, 156–159.

Wicker, L. J. and W. C. Skamarock, 2002: Time-splitting methods for elastic models using forward time schemes. *Mon. Wea. Rev.*, **130**, 2088–2097.

Willoughby, H. E., 1979a: Excitation of spiral bands in hurricanes by interaction between the symmetric mean vortex and a shearing environmental steering current. *J. Atmos. Sci.*, **36**, 1226–1235.

Willoughby, H. E., 1979b: Forced secondary circulations in hurricanes. *J. Geophys. Res.*, **84**, 3173–3183.

Willoughby, H. E., 1988: The dynamics of the tropical cyclone core. *Aust. Meteorol. Mag.*, **36**, 183–191.

Willoughby, H. E., 1990a: Gradient balance in tropical cyclones. *J. Atmos. Sci.*, **47**, 265–274.

Willoughby, H. E., 1990b: Temporal changes of the primary circulation in tropical cyclones. *J. Atmos. Sci.*, **47**, 242–264.

Willoughby, H. E., 1995: Mature structure and evolution. *Global Perspectives on Tropical Cyclones*, WMO Tech. Doc. No. 693, Report No. TCP-38, 21–62, [Available from Secretariat of the World Meteorological Organization, Publications Sales Unit, Case Postale 2300, CH-1211 Geneva 2, Switzerland. Also available online at `http://www.bom.gov.au/bmrc/pubs/tcguide/globa_guide_intro.htm`].

Willoughby, H. E., 1998: Tropical cyclone eye thermodynamics. *Mon. Wea. Rev.*, **126**, 3053–3067.

Willoughby, H. E., 2009: Diabatically-induced secondary flows in tropical cyclones. Part II: Periodic forcing. *Mon. Wea. Rev.*, **137**, 822–835, doi:10.1175/2008MWR2658.1.

Willoughby, H. E. and M. B. Chelmow, 1982: Objective determination of hurricane tracks from aircraft observations. *Mon. Wea. Rev.*, **110**, 1298–1305.

Willoughby, H. E., J. A. Clos, and M. G. Shoreibah, 1982: Concentric eye walls, secondary wind maxima, and the evolution of the hurricane vortex. *J. Atmos. Sci.*, **39**, 395–411.

Willoughby, H. E., H.-L. Jin, S. J. Lord, and J. M. Piotrowicz, 1984a: Hurricane structure and evolution as simulated by an axisymmetric, nonhydrostatic numerical model. *J. Atmos. Sci.*, **41**, 1169–1186.

Willoughby, H. E., Marks, F. D., Jr., and R. J. Feinberg, 1984b: Stationary and moving convective bands in hurricanes. *J. Atmos. Sci.*, **41**, 3189–3211.

Wirth, V. and T. J. Dunkerton, 2006: A unified perspective on the dynamics of axisymmetric hurricanes and monsoons. *J. Atmos. Sci.*, **63**, 2529–2547.

Wirth, V. and T. J. Dunkerton, 2009: The dynamics of eye formation and maintenance in axisymmetric diabatic vortices. *J. Atmos. Sci.*, **66**, 3601–3620.

Wood, F. B., 1945: Flight into the September, 1944, hurricane off Cape Henry, Virginia. *Bull. Amer. Meteor. Soc.*, **26**, 153–156.

Yamasaki, M., 1983: A further study of the tropical cyclone without parameterizing the effects of cumulus convection. *Pap. Meteorol. Geophys.*, **34**, 221–260.

Yanai, M., 1961: A detailed analysis of typhoon formation. *J. Meteor. Soc. Japan*, **39**, 187–214.

Yang, B., Y. Wang, and B. Wang, 2007: The effect of internally generated inner-core asymmetries on tropical cyclone potential intensity. *J. Atmos. Sci.*, **64**, 1165–1188, doi:10.1175/JAS3971.1.

Yarnal, B. and K. G. Henderson, 1989: A climatology of polar low cyclogenetic regions over the North Pacific Ocean. *J. Climate*, **2**, 1476–1491.

Zehr, R. M., 1992: Tropical cyclogenesis in the western North Pacific. NOAA Tech. Rep. NESDIS 61, 181 pp., Washington, D. C.

Zhang, D.-L., Y. Liu, and M. K. Yau, 2000: A multiscale numerical study of Hurricane Andrew (1992). Part III: Dynamically induced vertical motion. *Mon. Wea. Rev.*, **128**, 3772–3788.

Zhang, D.-L., Y. Liu, and M. K. Yau, 2002: On the formation of the hurricane eye. *Selected Papers of the Fourth Conference on East Asia and Western Pacific Meteorology and Climate, Vol. 1 of World Scientific Series on Meteorology of East Asia*, C.-P. Chang, G. Wu, B. Jou, and C.-Y. Lam, Eds., World Scientific Publishing Company, Hangzhou, China, 219–227.

Zhang, Q.-H., S.-J. Chen, Y.-H. Kuo, K.-H. Lau, and R. A. Anthes, 2005: Numerical study of a typhoon with a large eye: Model simulation and verification. *Mon. Wea. Rev.*, **133**, 725–742.

Appendix A

ADDITIONAL QUESTIONS

The following list provides the broad cross section of the potential avenues of inquiry that were formulated at the outset and during this research effort. Although not all questions fit neatly into categories, they have been grouped into the following clusters: questions of definition and description, interrogations of eye formation mechanisms and processes, questions pertaining to what can be shown through observations, inquiries about the dynamics of internal processes, the control they exert on various aspects of storm structure, and questions related to the interaction of the storm and its environment. Questions may overlap somewhat in scope.

A.1 Research questions

- **Questions of definition and description (D)**

  D1 What is the most useful way to define the eye?

  D2 At what point can the eye be said to have formed?

  D3 Are there different types or general classes of eyes?

- **Questions about eye formation mechanisms and processes (F)**

  F1 What are the salient mechanisms and dynamics that drive a single-cell vortex structure to a two-cell vortex structure?

  F2 What role does central subsidence play in eye formation? What forces the subsidence? Does the subsidence build upwards or downwards — or does it appear all at once throughout the eye column? Does the subsidence follow as a result of eye formation? Or does it actually trigger eye formation?

  F3 The distribution and concentration of convection must obviously play an important role in eye formation, but what role? How important is it that convective heating occur inside the inertially stable core of the storm?

  F4 What processes lead to the geometrical arrangement of convective elements into rings, spiral bands, or clusters? Why do some bands or rings become true eyewalls while others do not?

F5 It is also believed that friction plays a critical role in eye formation. What is that role? As the storm intensifies, are feedbacks between the sea state and the resulting frictional drag exerted on the atmosphere important for eye formation? What are the microphysical effects of increasing sea spray on the storm's cloud and precipitation microphysics?

F6 Is eye formation a bifurcation phenomenon, with multiple states of equilibria? If so, what mechanisms are responsible for pushing a storm back and forth between equilibria states? Can a phase space diagram be constructed for eye formation? What are the relevant parameters of this phase space?

F7 Are there multiple dynamical pathways to eye formation, or do all intensification routes lead to one common eye formation pathway, perhaps dictated purely by geometry and friction? Putting it another way: Is eye formation essentially a stochastic process or a manifold attractor of the system?

F8 If there are multiple modes of eye formation, which one is optimal for the greatest intensification rate? How much of the storm's actual realized maximum intensity depends on the storm's initial structure and the route it took to get there?

F9 What role do asymmetries play in eye formation? As the storm strengthens, when do asymmetric mixing processes become important?

F10 On a related note, do inertia-gravity waves play a role during eye formation? Vortex Rossby Waves?

F11 Is eye and eyewall buoyancy necessary for eye formation?

F12 Does the eye play a passive or an active role in intensifying the storm?

F13 What role does intensification play during eye formation? Is eye formation an instability process triggered at an intensity threshold? If so, what is the nature of the trigger?

- **Observational questions (O)**

O1 Viewing eye formation as a process rather than an event, what are the common stages a storm passes through as it forms an eye? Can these be routinely and reliably observed?

O2 At what intensities do these various stages of eye formation occur at? Do observations show the existence of a general intensity threshold for eye formation?

O3 What is the least intense tropical cyclone to sport a bona fide eye? What is the most intense storm to not possess a clearly defined eye?

O4 What are the size characteristics of the initial eye at the time it is first detected? When it reaches a mature state?

O5 Likewise, what can observations tell us about the development of the warm core and thermodynamic structure across the eye/eyewall interface?

O6 After forming an eye, how does the radius of maximum winds change in relation to eye size as the storm intensifies? Does it always contract as the storm intensifies?

O7 What are the common convective morphologies displayed in satellite and radar imagery as eyes develop? Can we identify any precursors to rapid development and intensification?

O8: How does the wind profile change during eye formation? Can quantitative measurements of inertial stability be obtained?

- **Questions related to internal control and dynamics of structure change (S)**

S1 What observable internal and external factors control the size of the initial eye?

S2 What is the utility of a dynamical length scale such as the minimum Rossby length? Are there other length or depth scales which may be useful?

S3 What are the relationships between overall storm size and initial eye size? Eye size and intensification rate? Eye size and a storm's ultimate realized intensity?

S4 How much of a constraint does the storm's initial structure place on its *final* mature structure?

S5 What determines the eye shape and eyewall slope in real storms? How is eye shape and slope affected by intensity or rate of intensification? Movement? Shear?

S6 How does the slope of the eyewall affect storm intensity and structure? Does the baroclinity in the eyewall ultimately control how intense a storm can get? What brings the eye to a mature state?

S7 Are there commonalities in the developing eyes of storms which subsequently undergo rapid intensification in the hurricane stage?

- **Questions related to the interaction of the storm and its environment (E)**

E1 Why do some storms rapidly intensify as they form eyes, yet others do not? Is it merely that some storms exist in favorable environments while others do not?

E2 Which environmental factors are favorable for eye formation? Which ones are disruptive? Are these the same factors that are generally positive and negative for storm intensification?

E3 Does the value of angular momentum at the inflow source radius constrain the size of the eye that is formed? What other environmental factors affect eye size?

E4 What is the effect of land on eye formation? Is it always detrimental? Can a storm form a "true" eye over land if it didn't previously have one?

A.2 Some answers

Returning full circle, the questions put forward are now revisited to see what progress has been made in light of this work. Only selected questions are answered in light of what has been found, while other questions are left for future work.

- **Questions which have been answered to some degree:**

D1 *What is the most useful way to define the eye?* A comprehensive new definition for the hurricane eye has been put forth in chapter 2.4. The fundamental property that makes an eye an eye is the existence of a second inner meridional circulation cell that resides radially inside the outer in-up-out secondary circulation. Many or all of the general properties of the hurricane eye (such as the warm core, the clear skies, the near calm of the center, etc.) follow directly from this definition.

D2 *At what point can the eye be said to have formed?* The eye is considered to form once a two-cell flow regime has been established throughout most of the depth of the troposphere in the vortex center, so that the eye region contains subsidence and is more than halfway surrounded by an eyewall.

D3 *Are there different types or general classes of eyes?* Yes, eye/eyewall structure can be grouped into classes by: (1) whether the eye is rapidly rotating or weakly rotating, as seen by the shape of the wind profile (U-shaped vs. V-shaped), (2) by whether eyewalls are sloped or erect, (3) by whether the eyewall is symmetric (circular) or asymmetric (e.g., elliptical or ragged), or (4) by the radial and vertical structure of the warm core and cloud field (e.g., warm ring vs. warm core or warm cylinder, cloud-filled vs. clear).

F1 *What are the salient mechanisms and dynamics that drive a single-cell vortex structure to a two-cell vortex structure?* Eye formation has been found to be a fundamental property of three-dimensional vortices which involves a rearrangement of mass to maintain the force balance of the vortex. Various ideas exist as to the why this regime change occurs. For laboratory vortices, the swirl ratio is found to be important, although this is less well defined for hurricanes. Various symmetric and asymmetric processes have been put forward to explain how subsidence can be forced in the hurricane vortex. But the fundamental answer is that the eye formation occurs as a consequence of the need to conserve angular momentum for inflowing air parcels (in the absence of other effects). Diabatic heating, the shape of the vortex wind profile, and the nature of the upper and lower boundaries all add complications to the pristine picture of a simple limiting radius in which air must turn upwards upon reaching.

F2 *What role does central subsidence play in eye formation? What forces the subsidence? Does the subsidence follow as a result of eye formation? Or does it actually trigger eye formation?* The causes of the subsidence have been discussed in chapter 2.5.1 and fall into two basic categories: subsidence forced by the diabatic heating of the eyewall, and subsidence forced dynamically by the vortex. The historic 'centrifuging' hypothesis, in which air is centrifuged into the eyewall at lower levels, or the somewhat complimentary 'momentum diffusion pump', are variations of dynamical forcing idea, but questions still remain as to how important these are. Some theoretical work Smith (1980) and modeling work Zhang et al. (2000) has partially reconciled the differing viewpoints on the causes of the subsidence by describing the subsidence as being forced by a local perturbation pressure gradient force such as is required to maintain thermal wind balance in the cyclone at the given level. This idea is analogous a rotating cylinder of water which experiences changes in the free surface height to bring the fluid into hydrostatic and centrifugal balance. A common feature in the various frameworks put forward for hurricane eye subsidence involves the radial gradient of the tangential wind and the convective heating profile. One modeling study found that convectively-forced subsidence (due to moist adiabatic ascent in the eyewall) was responsible for roughly 70% of the central pressure deficit, with the dynamical forcing responsible for the remaining 30%. The observational results of this study were inconclusive in whether the subsidence triggers eye formation, or merely follows as a consequence of the establishment of an eyewall. The idea of eyewall formation as a frontogenetic collapse shows that these two ideas need not be in competition. Please see the future work section for more.

F3 *The distribution and concentration of convection must obviously play an important role in eye formation, but what role? How important is it that convective heating occur inside the inertially stable core of the storm?* Chapter 3 reiterated the historical view that it is very important for heating to occur within the high inertial stability of the core. The formation of an eye was previously viewed to stabilize the vortex, but observations show that many storms still intensify rapidly after forming eyes. This paradox is resolved by considering that the rapidly decreasing Rossby length in the eyewall of a developing hurricane increases the eyewall heating efficiency, even as the physical scale of the efficient heating

region shrinks. Observational evidence supporting this conclusion were shown in chapter 6.4.

F5 *It is also believed that friction plays a critical role in eye formation. What is that role?* The role of friction is to deplete absolute angular momentum as air flows towards the vortex center at low levels. The decreased angular momentum allows the air to penetrate further inward than it would have otherwise. Strong inflow near the top of the boundary layer can cause the air to 'overshoot' and become supergradient. While it is now clear that a supergradient jet does exist in many hurricanes, the exact influence on the storm circulation is still a matter of debate. The view of Eliassen (1971); Eliassen and Lystad (1977) in which the boundary layer forces energetically-rich air upwards at a preferred radius may indeed play a key role.

F9 *What role do asymmetries play in eye formation? As the storm strengthens, when do asymmetric mixing processes become important?* The symmetric eye formation mechanisms seem plausible and capable of forming an eye. The asymmetric mechanisms may act as shortcuts, allowing the eye to form more quickly than it would have otherwise. Initial subjective analysis of a variety of eye formation morphologies in the IR satellite imagery suggests that asymmetries are nearly ubiquitous and thus surely play a role. Mixing processes may delay eyewall formation or development if the frontogenetic collapse is prevented from occurring.

F11 *Is eye and eyewall buoyancy necessary for eye formation?* Hurricanes are convectively-driven vortices, but some researchers have shown and others have shown that the eyewall region is often moist neutral. The analysis of Zhang et al. (2000) suggests that the perturbation PGF forces air upward in the outer eyewall in addition to causing the central subsidence. Thus, convective instability may not be required. The current author speculates that an important aspect of eye formation may be the establishment of slantwise convection.

F12 *Does the eye play a passive or an active role in intensifying the storm?* The eye and eyewall should be thought of as a single structure. The low pressures in the eye are a hydrostatic result of the intense warming anomaly aloft, and various work has shown this to be mainly a consequence of the dynamics and structure of the tangential wind profile and heating. Arguments involving an active role for the eye via surface fluxes and mixing due to the 'superintensity' hypothesis Persing and Montgomery (2003) have been strongly questioned Bryan and Rotunno (2009).

F13 *What role does intensification play during eye formation? Is eye formation an instability process triggered at an intensity threshold? If so, what is the nature of the trigger?* There seems to be no single intensity, $r_{\max}$, or $\lambda_{\mathrm{R,min}}$trigger that causes eye formation. It is unclear that eyewall formation is an instability process. If the frontogenetic view is true, then the formation of an eyewall could be viewed in some ways as an instability. However, the development of an eyewall *might* be more properly thought of as a transition from buoyant convection to slantwise convection. If so, eye formation is not so much an instability as a somewhat gradual transition facilitated by the peakedness of the tangential wind profile and the properties of the inflowing air.

O2 *At what intensities do these various stages of eye formation occur at? Do observations show the existence of a general intensity threshold for eye formation?* The Dvorak method of intensity estimation has associated various stages of development with various intensities. This work has determined the various statistics for various eye formation baselines (e.g., aircraft banding, open and closed eyes, the first satellite eye, first persistent eye, and the first strong eye). If the intensity thresholds are robust (since some differences were found

between the best track $v_{max}$and the reduced flight level v_{max}), the results of this work suggest that some minor refinements may be in order for the Dvorak model (see chapter 5.7. The first aircraft eye was generally found to occur between 50 and 60 kt. All observed eyes formed when the storm intensity was in the range of about 30 kt to 85 kt.

O3 *What is the least intense tropical cyclone to sport a bona fide eye? What is the most intense storm to not possess a clearly defined eye?* Chapter 5 answered this question in depth. The least intense tropical cyclones to sport a bona fide eye was TD5 and Henri (2003), both of which were close to minimal tropical storm strength with maximum sustained surface wind speeds of 30 to 35 kt. The most intensity tropical cyclone in the data set to not form an eye was Hurricane Earl (1998), which was being disrupted by high shear and about to undergo extratropical transition.

O4 *What are the size characteristics of the initial eye at the time it is first detected?* Most eyes form with an initial radius of between 5 and 15 n mi, with a mean radius of 9 n mi. The eye radius tends to stay fairly constant up through peak intensity.

O5 *Likewise, what can observations tell us about the development of the warm core and thermodynamic structure across the eye/eyewall interface?* The lower warming tends to occur in an 18- to 36-h period 'spike' which coincides with the most rapid intensification of the storm. Some storms exhibit signatures of subsidence even *before* eye formation, but most of the time, the peak warming occur about a day or so after forming an eye.

O6 *After forming an eye, how does the radius of maximum winds change in relation to eye size as the storm intensifies? Does it always contract as the storm intensifies?* In many storms, r_{max}undergoes a strong and market decrease in the day before eye formation. Upon forming an eye, the contraction in r_{max}often ceases or slows. This supports the idea that the eye does represent a limiting radius to the storm. If the storm intensifies, the difference between $r_{max}$and r_{eye}tends to decrease to about 1 to 5 n mi.

S2 *What is the utility of a dynamical length scale such as the minimum Rossby length? Are there other length or depth scales which may be useful?* As discussed in chapter 3, the role of the minimum Rossby length (and the related concept of inertial stability) have been shown to be crucial in confining the vortex warming response to localized diabatic heating. Chapter 6 has provided observational confirmation of this result. But other related scales, such as the Rossby penetration depth scale may be just as useful and essential. The penetration depth scale controls how a vortex 'feels' the influence of the lower and upper boundaries. As the depth scale increases, the vortex will be more strongly confined by the lower boundary, resulting in an additional restraint on the freedom of the mass flow in the secondary circulation.

E1 *Why do some storms rapidly intensify as they form eyes, yet others do not? Is it merely that some storms exist in favorable environments while others do not?* This work has shown that vertical shear has a highly disruptive impact on the outcome of eye formation. Storms which failed to form eyes were found to have experienced increasingly high vertical wind shear starting around the time of the initial attempt.

E3 *Does the value of angular momentum distribution at the inflow source radius constrain the size of the eye that is formed? What other environmental factors affect eye size?* The limiting radius idea of Kuo appears to be very valid, so the angular momentum of the source air should play a crucial role in setting the eye radius. The environment of a hurricane is never completely symmetric however (due to the variations in Coriolis force), so the idea of a hurricane 'swirl ratio' is ill defined.

E4 *What is the effect of land on eye formation? Is it always detrimental? Can a storm form a "true" eye over land if it didn't previously have one?* The increased surface friction due to

landfall has a profound effect on eye formation, namely by causing the eye to contract or even disappear. Storms that move back over water experience reduced surface friction and often reform eyes much larger than before they made landfall. There are a few instances of eyes forming over land in tropical storms (e.g., Fay 2008), tropical storm remnants (e.g., Erin 2007), or convective mesolows associated with MCSs.

Appendix B

SUPPLEMENTARY TABLES

This appendix provides supplementary tables which have been referenced by the main text of this dissertation. Most importantly, this appendix contains the observational baseline times for the various stages of eye formation. Since some of these baseline times have been obtained from a time-consuming subjective classification of tens of thousands of satellite images, these data are vital for anyone attempting to reproduce the results presented in this dissertation. While the author doubts anyone will actually go to the trouble to attempt to reproduce these results (since that would be very time consuming), reproducibility is an important aspect of the scientific endeavor. Other tables in this appendix present extended tables which form the basis for shorter summary tables presented in the main text.

Table B.1: Dates and times for various observational baseline stages of eye formation. The aircraft baseline stages are as follows: first aircraft eye (open or closed, 'A'), first open aircraft eye ('A1'), first closed aircraft eye ('A2'). Note that aircraft baseline stages are only reported for valid cases ('insufficient data' cases have been excluded). The baseline stages obtained subjectively from IR satellite imagery are as follows: first open warm spot ('IR1'), first closed warm spot ('IR2'), first eye ('IR3'), first persistent eye ('IR4'), first strong eye ('IR5'). See chapter 4 for a description of these observational baselines.

Storm	Year	B	A	A1	A2	IR1	IR2	IR3	IR4	IR5
ONE	1989									
ALLISON	1989									
BARRY	1989									
CHANTAL	1989		23:00 07/31		23:00 07/31					
DEAN	1989									
SIX	1989									
ERIN	1989									
FELIX	1989									
NINE	1989									
GABRIELLE	1989									
HUGO	1989									
IRIS	1989		14:12 09/19	14:12 09/19						
THIRTEEN	1989									
JERRY	1989		23:12 10/13	23:12 10/13						
KAREN	1989									
ONE	1990									
ARTHUR	1990		17:00 07/25	17:00 07/25						
BERTHA	1990				18:03 07/30					
CESAR	1990									
DIANA	1990		17:19 08/07	17:19 08/07						
EDOUARD	1990									
FRAN	1990									
GUSTAV	1990									
HORTENSE	1990									
ISIDORE	1990									
ELEVEN	1990									
JOSEPHINE	1990									
KLAUS	1990		21:38 10/04							
LILI	1990		23:29 10/11	23:29 10/11						
MARCO	1990	11:09 10/11								
NANA	1990		20:27 10/16	20:27 10/16	23:54 10/17					
ANA	1991									
TWO	1991									

continued on next page

Table B.1: *continued*

Storm	Year	B	A	A1	A2	IR1	IR2	IR3	IR4	IR5
BOB	1991	17:16 08/16	11:42 08/17	11:42 08/17	14:26 08/17					
FOUR	1991									
FIVE	1991									
CLAUDETTE	1991									
DANNY	1991									
ERIKA	1991									
FABIAN	1991									
TEN	1991									
GRACE	1991		12:11 10/28		12:11 10/28					
UNNAMED	1991									
SUBTROP	1992									
ONE	1992									
TWO	1992									
ANDREW	1992		06:13 08/21	06:13 08/21	13:12 08/21					
BONNIE	1992									
CHARLEY	1992									
DANIELLE	1992		11:33 09/25	11:33 09/25						
SEVEN	1992									
EARL	1992	05:11 09/30	13:59 09/30		13:59 09/30					
FRANCES	1992									
ONE	1993									
ARLENE	1993									
BRET	1993									
CINDY	1993									
EMILY	1993	23:32 08/26	11:53 08/27	11:53 08/27	13:41 08/27					
DENNIS	1993									
FLOYD	1993									
GERT	1993		00:20 09/20	00:20 09/20	04:01 09/20					
HARVEY	1993									
TEN	1993									
ALBERTO	1994		11:47 07/02	11:47 07/02	17:15 07/02					
TWO	1994									
BERYL	1994									
CHRIS	1994									
FIVE	1994	17:08 08/30	18:35 08/30	18:35 08/30						
DEBBY	1994									
ERNESTO	1994									

continued on next page

Table B.1: *continued*

Storm	Year	B	A	A1	A2	IR1	IR2	IR3	IR4	IR5
EIGHT	1994									
NINE	1994									
TEN	1994									
FLORENCE	1994									
GORDON	1994	23:56 11/17								
ALLISON	1995									
BARRY	1995	20:43 07/07								
CHANTAL	1995	05:30 07/15	11:52 07/15	11:52 07/15	15:35 07/15					
DEAN	1995									
ERIN	1995		15:46 07/31	15:46 07/31	16:10 08/02	21:15 07/31	19:15 08/01	22:45 07/31	02:45 08/02	
SIX	1995									
FELIX	1995					11:45 08/09	12:15 08/09	21:45 08/09	22:15 08/11	22:45 08/11
GABRIELLE	1995	11:13 08/10								
HUMBERTO	1995					09:00 08/23	09:00 08/23	06:00 08/24		
IRIS	1995					04:50 08/29	07:15 08/30	07:15 08/30	16:15 08/31	
JERRY	1995	16:34 08/23				23:45 08/22	23:45 08/22	23:45 08/22		
KAREN	1995									
LUIS	1995									
FOURTEEN	1995									
MARILYN	1995		18:01 09/13		18:01 09/13	08:45 09/13	08:45 09/13	13:45 09/13	15:15 09/15	01:15 09/16
NOEL	1995									
OPAL	1995					15:15 10/01	16:15 10/01	00:15 10/04	00:15 10/04	
PABLO	1995									
ROXANNE	1995	19:24 10/09	19:24 10/09		19:24 10/09	15:31 10/09	15:31 10/09	14:31 10/10	14:31 10/10	
SEBASTIEN	1995									
TANYA	1995									
ARTHUR	1996					12:45 06/20				
BERTHA	1996		02:54 07/08	02:54 07/08	07:00 07/08	09:45 07/07	09:45 07/07	21:15 07/07	23:15 07/08	01:15 07/09
CESAR	1996		02:56 07/28		02:56 07/28	04:45 07/27	04:45 07/27	04:45 07/28		
DOLLY	1996		17:51 08/22	17:51 08/22	23:16 08/22	22:45 08/20	22:45 08/20	22:45 08/20	22:45 08/20	
EDOUARD	1996					20:45 08/23	20:45 08/23	07:45 08/24	07:45 08/24	18:45 08/24
FRAN	1996		09:14 08/30	09:14 08/30	08:59 08/31	10:45 08/28	01:45 09/01	12:45 09/01	21:15 09/01	21:15 09/03
GUSTAV	1996					23:15 08/28	19:45 08/31			
HORTENSE	1996		08:29 09/09		08:29 09/09	09:45 09/07	11:15 09/09	14:15 09/11	14:45 09/11	02:15 09/12
ISIDORE	1996					15:15 09/25	15:45 09/25	06:45 09/26	10:45 09/27	19:15 09/27
JOSEPHINE	1996		11:35 10/07	11:35 10/07						
KYLE	1996									

continued on next page

Table B.1: *continued*

Storm	Year	B	A	A1	A2	IR1	IR2	IR3	IR4	IR5
LILI	1996		23:25 10/16	23:25 10/16	08:39 10/19	23:45 10/15	04:15 10/18	16:15 10/18	16:15 10/18	
MARCO	1996		07:27 11/22	07:27 11/22		05:45 11/19	05:45 11/19	08:45 11/22		
SUBTROP	1997									
ANA	1997					09:45 07/01	13:45 07/03	13:45 07/03		
BILL	1997					15:15 07/11	04:45 07/12	15:45 07/12		
CLAUDETTE	1997					14:15 07/14	09:45 07/16			
DANNY	1997		05:07 07/18	05:07 07/18	12:27 07/18	12:45 07/16	13:15 07/16	15:45 07/18	15:45 07/18	
FIVE	1997									
ERIKA	1997		02:01 09/06	02:01 09/06	03:53 09/06	09:15 09/03	11:45 09/03	03:45 09/04	06:45 09/07	23:15 09/07
FABIAN	1997					07:15 10/08	08:15 10/08			
GRACE	1997					20:45 10/16				
ALEX	1998					12:00 07/27	12:00 07/27	12:00 07/27		
BONNIE	1998	23:51 08/21	05:35 08/22	05:35 08/22	01:24 08/23	06:46 08/20	08:15 08/20	08:15 08/20	08:15 08/22	08:15 08/23
CHARLEY	1998					09:15 08/21	09:45 08/21	10:45 08/21		
DANIELLE	1998	01:41 08/27	13:19 08/27	13:19 08/27	01:26 08/28	14:30 08/24	14:30 08/24	09:15 08/25	22:15 08/30	
EARL	1998					19:45 09/01	19:45 09/01	19:45 09/01		
FRANCES	1998					09:45 09/09	09:15 09/11			
GEORGES	1998					02:15 09/17	05:00 09/17	15:45 09/17	01:15 09/18	18:46 09/19
HERMINE	1998	18:27 09/17								
IVAN	1998					07:45 09/21	13:45 09/23	13:45 09/23	13:45 09/23	
JEANNE	1998					01:00 09/22	04:30 09/23	04:30 09/23		
KARL	1998					00:15 09/24	00:15 09/24	08:15 09/24	19:15 09/26	
LISA	1998					01:15 10/06	01:15 10/06			
MITCH	1998	20:10 10/23	07:53 10/24	07:53 10/24	17:38 10/24	23:15 10/23	04:15 10/24	04:15 10/24	15:15 10/24	22:45 10/24
NICOLE	1998					05:00 11/24	16:30 11/24	16:30 11/24	17:45 10/30	
ARLENE	1999					00:15 06/13				
TWO	1999									
BRET	1999	23:20 08/19	23:20 08/19		23:20 08/19	13:15 08/19	13:15 08/19	13:15 08/19	22:15 08/21	00:15 08/22
CINDY	1999					07:15 08/25	18:45 08/25	18:45 08/25	16:45 08/27	07:15 08/28
DENNIS	1999	15:14 08/25	20:19 08/26		13:43 08/27	01:15 08/25	01:15 08/25	03:45 08/28	14:15 08/28	
EMILY	1999	04:10 08/26				18:15 09/07	00:15 09/08	01:15 09/08	20:15 09/11	11:15 09/12
SEVEN	1999									
FLOYD	1999		18:17 09/10	18:17 09/10	17:41 09/11	18:15 09/07	00:45 09/08	00:45 09/08	19:45 09/11	11:15 09/12
GERT	1999					08:00 09/12	00:15 09/13	00:15 09/13	13:15 09/13	23:45 09/14
HARVEY	1999					20:15 09/20	20:15 09/20			
ELEVEN	1999	20:15 10/05								
TWELVE	1999									

continued on next page

Table B.1: *continued*

Storm	Year	B	A	A1	A2	IR1	IR2	IR3	IR4	IR5
IRENE	1999	21:36 10/13	22:10 10/14	22:10 10/14	01:08 10/18	12:15 10/12	12:15 10/12	10:45 10/17		
JOSE	1999		17:04 10/19	17:04 10/19	11:39 10/20	18:46 10/19	20:15 10/19	20:15 10/19		
KATRINA	1999					04:15 10/29				
LENNY	1999	21:24 11/14	06:00 11/15		06:00 11/15	12:15 11/14	13:15 11/14	15:15 11/14		04:15 11/15
ONE	2000									
TWO	2000									
ALBERTO	2000					16:00 08/04	16:00 08/04	17:00 08/04	11:15 08/06	00:45 08/12
FOUR	2000	20:22 08/09								
BERYL	2000					18:15 08/14				
CHRIS	2000									
DEBBY	2000		03:05 08/22		03:05 08/22	23:45 08/19	23:45 08/19			
ERNESTO	2000									
NINE	2000									
FLORENCE	2000		21:35 09/11	21:35 09/11		01:45 09/12	01:45 09/12	01:45 09/12	22:15 09/12	
GORDON	2000	03:11 09/16	11:38 09/17		11:38 09/17	00:26 09/16				
HELENE	2000					23:45 09/20	23:45 09/20	00:45 09/21		
ISAAC	2000					01:15 09/23	00:45 09/23	14:15 09/23	14:15 09/23	22:15 09/23
JOYCE	2000					02:30 09/26	02:30 09/26	19:45 09/26		
KEITH	2000		18:08 09/30		18:08 09/30	21:15 09/29	12:45 09/30	12:45 09/30	17:45 09/30	22:15 09/30
LESLIE	2000					07:45 10/05				
MICHAEL	2000					16:45 10/16	01:15 10/17	01:15 10/17	06:45 10/17	
NADINE	2000					00:45 10/20				
SUBTROP	2000									
ALLISON	2001					12:45 06/05				
TWO	2001									
BARRY	2001	11:54 08/05				17:15 08/02	04:15 08/05			
CHANTAL	2001					09:15 08/16	01:45 08/19	09:45 08/19		
DEAN	2001					22:15 08/23	22:15 08/23	14:45 08/27		
ERIN	2001	06:20 09/07	19:30 09/08	19:30 09/08	06:10 09/09	18:01 09/01	18:01 09/01	23:30 09/01	21:45 09/08	
FELIX	2001					11:45 09/10	02:15 09/11	11:45 09/12	06:45 09/13	
GABRIELLE	2001					07:15 09/12	10:15 09/12	16:15 09/18		
NINE	2001									
HUMBERTO	2001		06:48 09/23	06:48 09/23	19:14 09/23	02:45 09/22	08:45 09/25	13:45 09/25	00:45 09/26	
IRIS	2001				20:45 10/06	12:15 10/04	20:45 10/05	20:45 10/05	06:45 10/08	20:45 10/08
JERRY	2001					03:15 10/07	03:15 10/07			
KAREN	2001					00:15 10/12	00:15 10/12	00:15 10/12	07:15 10/13	
LORENZO	2001					05:45 10/31				

continued on next page

Table B.1: *continued*

Storm	Year	B	A	A1	A2	IR1	IR2	IR3	IR4	IR5
MICHELLE	2001		18:11 11/02		18:11 11/02	18:15 10/31	18:15 10/31	14:15 11/02	14:15 11/02	21:15 11/02
NOEL	2001					05:15 11/04	17:15 11/04			
OLGA	2001					22:45 11/23	01:15 11/24	13:15 11/24	17:15 11/26	
ARTHUR	2002					22:15 07/14	02:15 07/15			
BERTHA	2002									
CRISTOBAL	2002					22:45 08/05	22:45 08/05			
DOLLY	2002					15:15 08/30	15:15 08/30			
EDOUARD	2002	13:53 09/03								
FAY	2002					18:15 09/05	18:15 09/05			
SEVEN	2002									
GUSTAV	2002		14:49 09/10	14:49 09/10		23:15 09/09	21:15 09/11			
HANNA	2002	04:41 09/13								
ISIDORE	2002	08:03 09/19	08:03 09/19	08:03 09/19	17:54 09/19	02:45 09/18	02:45 09/18	22:15 09/18	12:15 09/21	01:45 09/22
JOSEPHINE	2002									
KYLE	2002					06:45 09/24	17:45 09/24	17:45 09/24	03:15 09/26	
LILI	2002		23:56 09/28		03:38 09/29	14:45 09/26	14:45 09/26	15:15 09/28	21:15 10/01	02:15 10/02
FOURTEEN	2002									
ANA	2003					07:45 04/19				
TWO	2003									
BILL	2003					04:15 06/30	02:45 07/01			
CLAUDETTE	2003	05:36 07/09	12:01 07/10		12:01 07/10	10:15 07/08	13:15 07/10	04:15 07/15	11:15 07/15	
DANNY	2003					03:15 04/17	17:45 04/18	17:45 04/18	21:15 07/18	
SIX	2003									
SEVEN	2003									
ERIKA	2003		02:20 08/16	02:20 08/16	05:22 08/16	00:45 08/15	00:45 08/15	00:45 08/15		
NINE	2003					03:45 08/22				
FABIAN	2003					03:45 08/28	03:45 08/28	02:15 08/30	16:15 08/30	01:15 08/31
GRACE	2003					18:45 08/30				
HENRI	2003		07:42 09/05	07:42 09/05		14:15 09/04				
ISABEL	2003					03:15 09/06	03:15 09/06	17:15 09/07	17:15 09/07	02:45 09/08
FOURTEEN	2003									
JUAN	2003					11:15 09/26	13:15 09/26	13:15 09/26	17:15 09/26	
KATE	2003					12:15 09/26	21:15 09/26	08:15 10/01	08:15 10/01	
LARRY	2003					19:15 10/04				
MINDY	2003									
NICHOLAS	2003					03:45 10/14	03:45 10/14	17:15 10/15		
ODETTE	2003					12:45 12/06				

continued on next page

Table B.1: *continued*

Storm	Year	B	A	A1	A2	IR1	IR2	IR3	IR4	IR5
PETER	2003					09:15 12/09	14:45 12/09	14:45 12/09		
ALEX	2004		17:04 08/02	17:04 08/02	00:18 08/03	21:45 07/31	07:15 08/02	18:45 08/03	14:15 08/04	
BONNIE	2004		21:54 08/09		21:54 08/09	16:15 08/03	13:45 08/10			
CHARLEY	2004				14:13 08/11	12:45 08/09	06:45 08/12	16:45 08/12	22:15 08/12	14:45 08/13
DANIELLE	2004					09:00 08/15	09:00 08/15	09:00 08/15	17:15 08/15	
EARL	2004					21:45 08/14				
FRANCES	2004					01:15 08/25	06:15 08/26	03:45 08/27	08:15 08/27	09:45 08/28
GASTON	2004		20:51 08/28	20:51 08/28	22:28 08/28	17:15 08/27	22:45 08/28	22:45 08/28		
HERMINE	2004					22:45 08/29	22:45 08/29			
IVAN	2004					03:45 09/03	19:45 09/03	06:45 09/05	06:45 09/05	21:45 09/05
TEN	2004									
JEANNE	2004					22:45 09/13	23:45 09/15	23:45 09/15	23:45 09/15	10:45 09/16
KARL	2004					16:00 09/16	16:00 09/16	16:00 09/16	06:45 09/18	11:45 09/19
LISA	2004					18:00 09/19	18:00 09/19	07:30 09/20	08:45 10/01	
MATTHEW	2004					21:15 10/09				
NICOLE	2004									
OTTO	2004					03:15 11/30	03:15 11/30	03:15 11/30		
ARLENE	2005					20:45 06/09	08:45 06/10	18:15 06/11		
BRET	2005					01:15 06/29				
CINDY	2005					09:45 07/04	09:45 07/04	23:15 07/05		
DENNIS	2005				09:39 07/07	12:15 07/05	14:45 07/05	14:45 07/05	18:45 07/07	11:45 07/08
EMILY	2005	13:35 07/13	11:49 07/14		11:49 07/14	18:45 07/12	18:45 07/12	16:15 07/14	16:15 07/14	20:45 07/14
FRANKLIN	2005	14:20 07/22	01:48 07/23	01:48 07/23		18:45 07/21				
GERT	2005					19:15 07/24				
HARVEY	2005					00:45 08/04	02:45 08/05	03:45 08/05		
IRENE	2005					10:45 08/11	17:45 08/14	17:15 08/14	12:45 08/16	
TEN	2005									
JOSE	2005									
KATRINA	2005		19:49 08/24	19:49 08/24	23:05 08/24	09:45 08/24	21:15 08/25	00:15 08/27	02:45 08/27	03:45 08/28
LEE	2005					06:15 08/29	23:15 08/30	23:15 08/30		
MARIA	2005					08:45 09/02	16:15 09/02	21:45 09/03	07:15 09/05	
NATE	2005					23:45 09/05	02:45 09/07	16:15 09/07	16:15 09/07	
OPHELIA	2005		01:45 09/08	01:45 09/08	02:24 09/09	10:15 09/06	02:15 09/07	17:45 09/10	01:15 09/14	
PHILIPPE	2005					12:15 09/17				
RITA	2005	02:13 09/20	12:03 09/20	12:03 09/20	13:30 09/20	03:15 09/18	03:15 09/18	06:45 09/20	21:45 09/20	00:45 09/21
NINETEEN	2005									
STAN	2005	05:19 10/04	08:48 10/04	08:48 10/04		16:15 10/01	10:45 10/04			

continued on next page

Table B.1: *continued*

Storm	Year	B	A	A1	A2	IR1	IR2	IR3	IR4	IR5
UNNAMED	2005									
TAMMY	2005					09:45 10/05	18:45 10/05			
TWENTY-TWO	2005									
VINCE	2005					19:30 10/08	04:30 10/09	10:45 10/09	10:45 10/09	
WILMA	2005		21:32 10/17	21:32 10/17	21:42 10/18	05:15 10/16	09:45 10/18	09:45 10/18	20:45 10/18	03:45 10/19
ALPHA	2005					12:15 10/22	01:15 10/24			
BETA	2005		20:20 10/28	20:20 10/28	20:01 10/29	03:15 10/27	10:45 10/27	15:45 10/29	00:45 10/30	
GAMMA	2005					07:45 11/14	07:45 11/14			
DELTA	2005					00:45 11/23	18:45 11/23	18:45 11/23		
EPSILON	2005					17:15 11/29	19:15 11/29	13:15 11/30	11:45 12/02	
ZETA	2005					16:45 12/30	04:45 01/01	05:15 01/04		
ALBERTO	2006					10:15 06/06	10:15 06/06			
NONAME	2006									
BERYL	2006		05:36 07/20	05:36 07/20		01:15 07/20	06:45 07/20	06:45 07/20		
CHRIS	2006	00:09 08/02				07:45 08/02				
DEBBY	2006					22:00 08/21	22:00 08/21	08:45 08/23		
ERNESTO	2006		11:30 08/27	11:30 08/27		11:45 08/25	23:15 08/26	20:15 08/31		
FLORENCE	2006		05:24 09/10		05:24 09/10	20:15 09/05	09:15 09/08	20:15 09/08	10:45 09/10	
GORDON	2006					02:45 09/11	21:15 09/11	22:15 09/12	12:15 09/13	
HELENE	2006					17:45 09/12	17:45 09/12	03:45 09/17	03:45 09/17	
ISAAC	2006					02:45 09/27	09:15 09/30	09:15 09/30	19:15 09/30	
ANDREA	2007					12:15 05/09				
BARRY	2007									
CHANTAL	2007					10:45 07/31	10:45 07/31			
DEAN	2007					00:15 08/15	06:15 08/16	08:45 08/16	20:15 08/17	23:15 08/17
ERIN	2007					13:32 08/15				
FELIX	2007		22:41 09/01	22:41 09/01	17:24 09/02	16:45 08/31	16:45 08/31	08:45 09/02	08:45 09/02	13:15 09/02
GABRIELLE	2007	11:07 09/09								
INGRID	2007					20:45 09/12				
HUMBERTO	2007					10:45 09/12	14:30 09/12	11:02 09/13		
TEN	2007									
JERRY	2007					15:15 09/24				
KAREN	2007					01:15 09/25	05:00 09/25	14:45 09/26		
LORENZO	2007					18:15 09/25	18:15 09/25			
MELISSA	2007					10:15 09/28	08:45 10/01			
FIFTEEN	2007									
NOEL	2007					02:15 10/28	10:45 10/28			

continued on next page

Table B.1: *continued*

Storm	Year	B	A	A1	A2	IR1	IR2	IR3	IR4	IR5
OLGA	2007									
ARTHUR	2008					09:15 05/31	09:15 05/31			
BERTHA	2008					18:45 07/03	23:15 07/06	05:45 07/07	05:45 07/07	
CRISTOBAL	2008					14:02 07/22				
DOLLY	2008	17:11 07/21	11:29 07/22		17:06 07/22	00:45 07/21	00:45 07/21	18:15 07/22	00:15 07/23	
EDOUARD	2008	20:44 08/04				18:15 08/04				
FAY	2008		06:54 08/19	06:54 08/19		13:25 08/19	15:15 08/19	15:15 08/19	15:15 08/19	
GUSTAV	2008					13:15 08/25	23:15 08/25	01:15 08/26	06:55 08/30	08:02 08/30
HANNA	2008	19:16 09/01					02:25 09/02	03:15 09/02		
IKE	2008			18:56 09/05	06:55 09/06	19:45 09/01	14:15 09/03	14:15 09/03	20:45 09/03	00:15 09/04
JOSEPHINE	2008					12:15 09/02	12:15 09/02	15:15 09/02		
KYLE	2008					11:32 09/25				
LAURA	2008					12:45 09/29	11:45 09/30			
MARCO	2008									
NANA	2008									
OMAR	2008	19:06 10/14	19:53 10/14	19:53 10/14	23:17 10/15	05:45 10/14	05:45 10/14	01:15 10/16	01:15 10/16	
SIXTEEN	2008									
PALOMA	2008		17:07 11/06		17:07 11/06	15:15 11/06	23:15 11/06	23:15 11/06	17:25 11/07	23:25 11/07

Table B.2: The best track intensity interpolated to the various observational baseline times (as in Table B.1; see chapter 4 and chapter 5 for a full description).

Storm	Year	Case Type	# of fixes	B	A	A1	A2	IR1	IR2	IR3	IR4	IR5
ONE	1989	no aircraft data										
ALLISON	1989	no aircraft data										
BARRY	1989	no attempt	2									
CHANTAL	1989	complete failure	14		63		63					
DEAN	1989	insufficient data	18									
SIX	1989	no aircraft data										
ERIN	1989	no aircraft data										
FELIX	1989	no aircraft data										
NINE	1989	no aircraft data										
GABRIELLE	1989	insufficient data	29									
HUGO	1989	insufficient data	44									
IRIS	1989	complete failure	12		60	60						
THIRTEEN	1989	no aircraft data										
JERRY	1989	intermittent failure	22		53	53						
KAREN	1989	insufficient data	25									
ONE	1990	no aircraft data										
ARTHUR	1990	complete failure	12		58	58						
BERTHA	1990	insufficient data	24									
CESAR	1990	no aircraft data										
DIANA	1990	complete failure	13		83	83						
EDOUARD	1990	no aircraft data										
FRAN	1990	no aircraft data										
GUSTAV	1990	insufficient data	14									
HORTENSE	1990	no aircraft data										
ISIDORE	1990	no aircraft data										
ELEVEN	1990	no aircraft data										
JOSEPHINE	1990	no aircraft data										
KLAUS	1990	intermittent failure	38		54							
LILI	1990	complete failure	12		64	64						
MARCO	1990	no attempt	16									
NANA	1990	delayed success	24		36	36	69					
ANA	1991	no aircraft data										
TWO	1991	no aircraft data										
BOB	1991	delayed success	43	33	54	54	58					
FOUR	1991	no aircraft data										

continued on next page

Table B.2: *continued*

Storm	Year	Case Type	# of fixes	B	A	A1	A2	IR1	IR2	IR3	IR4	IR5
FIVE	1991	no aircraft data										
CLAUDETTE	1991	insufficient data	18									
DANNY	1991	no aircraft data										
ERIKA	1991	no aircraft data										
FABIAN	1991	no aircraft data										
TEN	1991	no aircraft data										
GRACE	1991	complete failure	16		64		64					
UNNAMED	1991	no aircraft data										
SUBTROP	1992	no aircraft data										
ONE	1992	no aircraft data										
TWO	1992	no aircraft data										
ANDREW	1992	delayed success	64		44	44	50					
BONNIE	1992	no aircraft data										
CHARLEY	1992	no aircraft data										
DANIELLE	1992	complete failure	23		53	53						
SEVEN	1992	no aircraft data										
EARL	1992	intermittent failure	36	39	46		46					
FRANCES	1992	no aircraft data										
ONE	1993	no aircraft data										
ARLENE	1993	no attempt	14									
BRET	1993	no attempt	11									
CINDY	1993	no attempt	10									
EMILY	1993	intermittent failure	59	60	59	59	61					
DENNIS	1993	no aircraft data										
FLOYD	1993	no attempt	5									
GERT	1993	intermittent failure	15		54	54	61					
HARVEY	1993	no aircraft data										
TEN	1993	no aircraft data										
ALBERTO	1994	intermittent failure	23		39	39	44					
TWO	1994	no aircraft data										
BERYL	1994	no attempt	9									
CHRIS	1994	no attempt	14									
FIVE	1994	complete failure	13	29	29	29						
DEBBY	1994	no attempt	5									
ERNESTO	1994	no aircraft data										
EIGHT	1994	no aircraft data										

continued on next page

Table B.2: *continued*

Storm	Year	Case Type	# of fixes	B	A	A1	A2	IR1	IR2	IR3	IR4	IR5
NINE	1994	no aircraft data										
TEN	1994	no aircraft data										
FLORENCE	1994	insufficient data	2									
GORDON	1994	no attempt	50									
ALLISON	1995	no attempt	25									
BARRY	1995	insufficient data	4									
CHANTAL	1995	intermittent failure	40	44	45	45	44					
DEAN	1995	no attempt	17									
ERIN	1995	intermittent failure	44		57	57	56	64	74	67	74	
SIX	1995	no attempt	6									
FELIX	1995	insufficient data	70					44	44	47	96	97
GABRIELLE	1995	no attempt	11									
HUMBERTO	1995	no aircraft data						67	67	85		
IRIS	1995	insufficient data	49					77	70	70	81	
JERRY	1995	no attempt	9					23	23	23		
KAREN	1995	no aircraft data										
LUIS	1995	insufficient data	47									
FOURTEEN	1995	no aircraft data										
MARILYN	1995	complete success	56		59		59	49	49	55	82	90
NOEL	1995	no aircraft data										
OPAL	1995	insufficient data	38					47	48	99	99	
PABLO	1995	no aircraft data										
ROXANNE	1995	complete success	72	52	52		52	47	47	85	85	
SEBASTIEN	1995	no attempt	10									
TANYA	1995	no aircraft data										
ARTHUR	1996	no attempt	12					29				
BERTHA	1996	complete success	58		74	74	73	57	57	72	79	83
CESAR	1996	complete failure	15		69		69	57	57	69		
DOLLY	1996	complete failure	18		49	49	54	44	44	44	44	
EDOUARD	1996	insufficient data	67					67	67	79	79	102
FRAN	1996	delayed success	71		64	64	62	53	64	70	74	89
GUSTAV	1996	no aircraft data						39	34			
HORTENSE	1996	intermittent failure	17		69		69	38	69	91	91	101
ISIDORE	1996	no aircraft data						47	47	69	88	95
JOSEPHINE	1996	intermittent failure	24		58	58						
KYLE	1996	no attempt	2									

continued on next page

Table B.2: *continued*

Storm	Year	Case Type	# of fixes	B	A	A1	A2	IR1	IR2	IR3	IR4	IR5
LILI	1996	intermittent failure	35		53	53	94	29	73	80	80	
MARCO	1996	complete failure	41		55	55		34	34	56		
SUBTROP	1997	no aircraft data										
ANA	1997	no attempt	4					38	32	32		
BILL	1997	no attempt	3					42	57	64		
CLAUDETTE	1997	insufficient data	8					40	34			
DANNY	1997	complete success	43		63	63	69	24	25	69	69	
FIVE	1997	no aircraft data										
ERIKA	1997	delayed success	33		66	66	67	29	29	46	74	94
FABIAN	1997	no aircraft data						34	34			
GRACE	1997	no aircraft data						34				
ALEX	1998	no attempt	4					25	25	25		
BONNIE	1998	complete success	75	64	69	69	91	30	31	31	71	96
CHARLEY	1998	no attempt	7					27	27	28		
DANIELLE	1998	delayed success	43	80	88	88	79	31	31	57	67	
EARL	1998	no attempt	23					49	49	49		
FRANCES	1998	no attempt	14					29	41			
GEORGES	1998	insufficient data	79					46	48	60	71	125
HERMINE	1998	no attempt	24									
IVAN	1998	no aircraft data						34	56	56	56	
JEANNE	1998	no aircraft data						40	73	73		
KARL	1998	no aircraft data						34	34	36	81	
LISA	1998	no aircraft data						40	40			
MITCH	1998	complete success	48	50	67	67	88	54	62	62	82	97
NICOLE	1998	no aircraft data						34	56	56		
ARLENE	1999	no attempt	8					49				
TWO	1999	no aircraft data										
BRET	1999	delayed success	42	38	38		38	30	30	30	111	120
CINDY	1999	no aircraft data						54	60	60	89	116
DENNIS	1999	delayed success	84	49	67		64	39	39	72	86	
EMILY	1999	no attempt	14									
SEVEN	1999	no aircraft data										
FLOYD	1999	complete success	69		69	69	90	24	30	30	87	102
GERT	1999	insufficient data	13					31	54	54	65	98
HARVEY	1999	no attempt	15					49	49			
ELEVEN	1999	no attempt	12									

continued on next page

Table B.2: *continued*

Storm	Year	Case Type	# of fixes	B	A	A1	A2	IR1	IR2	IR3	IR4	IR5
TWELVE	1999	no aircraft data										
IRENE	1999	intermittent failure	44	51	59	59	81	19	19	64		
JOSE	1999	intermittent failure	31		63	63	84	64	66	66		
KATRINA	1999	no attempt	5					29				
LENNY	1999	complete success	44	62	75		75	40	42	47		73
ONE	2000	no aircraft data										
TWO	2000	no aircraft data										
ALBERTO	2000	no aircraft data						37	37	38	69	90
FOUR	2000	no attempt	6									
BERYL	2000	no attempt	9					44				
CHRIS	2000	no attempt	3									
DEBBY	2000	intermittent failure	26		67		67	29	29			
ERNESTO	2000	no aircraft data										
NINE	2000	no aircraft data										
FLORENCE	2000	intermittent failure	22		64	64		63	63	63	64	
GORDON	2000	complete failure	29	44	65		65	40				
HELENE	2000	no attempt	15					24	24	25		
ISAAC	2000	no aircraft data						50	49	74	74	98
JOYCE	2000	no attempt	3					34	34	42		
KEITH	2000	complete success	34		75		75	42	65	65	73	91
LESLIE	2000	no attempt	11					31				
MICHAEL	2000	insufficient data	6					34	36	36	45	
NADINE	2000	no aircraft data						29				
SUBTROP	2000	no attempt	4									
ALLISON	2001	no attempt	3					41				
TWO	2001	no aircraft data										
BARRY	2001	no attempt	30					42	38			
CHANTAL	2001	no attempt	29					29	55	59		
DEAN	2001	no attempt	2					24	24	56		
ERIN	2001	complete success	21	29	63	63	89	29	29	29	68	
FELIX	2001	no aircraft data						29	29	53	75	
GABRIELLE	2001	no attempt	20					24	24	58		
NINE	2001	no aircraft data										
HUMBERTO	2001	complete success	8		55	55	80	26	64	64	65	
IRIS	2001	insufficient data	30					24	46	46	93	119
JERRY	2001	no attempt	3					37	37			

continued on next page

Table B.2: *continued*

Storm	Year	Case Type	# of fixes	B	A	A1	A2	IR1	IR2	IR3	IR4	IR5
KAREN	2001	no aircraft data						59	59	59	59	
LORENZO	2001	no aircraft data						34				
MICHELLE	2001	complete success	39		79		79	29	29	73	73	84
NOEL	2001	no aircraft data						44	48			
OLGA	2001	no aircraft data						45	49	49	64	
ARTHUR	2002	no aircraft data						29	31			
BERTHA	2002	no attempt	3									
CRISTOBAL	2002	no attempt	8					29	29			
DOLLY	2002	no aircraft data						49	49			
EDOUARD	2002	no attempt	23									
FAY	2002	no aircraft data						29	29			
SEVEN	2002	no aircraft data										
GUSTAV	2002	complete failure	22		51	51		44	81			
HANNA	2002	no attempt	26									
ISIDORE	2002	complete success	73	52	52	52	64	32	32	48	99	109
JOSEPHINE	2002	no aircraft data										
KYLE	2002	no attempt	12					45	54	54	66	
LILI	2002	complete success	67		44		41	29	29	44	89	93
FOURTEEN	2002	no aircraft data										
ANA	2003	no aircraft data						34				
TWO	2003	no aircraft data										
BILL	2003	no attempt	8					44	37			
CLAUDETTE	2003	intermittent failure	57	59	69		69	39	66	63	73	
DANNY	2003	no aircraft data									64	
SIX	2003	no aircraft data										
SEVEN	2003	no attempt	2									
ERIKA	2003	complete failure	16		56	56	58	40	40	40		
NINE	2003	no aircraft data						29				
FABIAN	2003	insufficient data	30					29	29	66	94	109
GRACE	2003	no attempt	5					34				
HENRI	2003	complete failure	27		36	36		29				
ISABEL	2003	insufficient data	35					31	31	69	69	86
FOURTEEN	2003	no aircraft data										
JUAN	2003	no aircraft data						63	65	65	69	
KATE	2003	no aircraft data						29	29	51	51	
LARRY	2003	no attempt	23					49				

continued on next page

Table B.2: *continued*

Storm	Year	Case Type	# of fixes	B	A	A1	A2	IR1	IR2	IR3	IR4	IR5
MINDY	2003	no attempt	10									
NICHOLAS	2003	no aircraft data						29	29	44		
ODETTE	2003	no attempt	10					54				
PETER	2003	no aircraft data						45	54	54		
ALEX	2004	complete success	25		49	49	60	24	41	84	88	
BONNIE	2004	intermittent failure	29		43		43	24	48			
CHARLEY	2004	insufficient data	39					29	75	87	89	108
DANIELLE	2004	no aircraft data						77	77	77	84	
EARL	2004	no aircraft data						34				
FRANCES	2004	insufficient data	73					25	45	72	79	102
GASTON	2004	insufficient data	4					24	53	53		
HERMINE	2004	no aircraft data						39	39			
IVAN	2004	insufficient data	107					32	44	66	66	112
TEN	2004	no aircraft data										
JEANNE	2004	insufficient data	58					24	59	59	59	67
KARL	2004	no aircraft data						33	33	33	85	104
LISA	2004	no aircraft data						30	30	32	56	
MATTHEW	2004	no attempt	10					39				
NICOLE	2004	no aircraft data										
OTTO	2004	no aircraft data						44	44	44		
ARLENE	2005	no attempt	21					36	46	48		
BRET	2005	no aircraft data						34				
CINDY	2005	no attempt	8					26	26	63		
DENNIS	2005	insufficient data	53					34	36	36	102	128
EMILY	2005	delayed success	68	50	84		84	44	44	94	94	104
FRANKLIN	2005	intermittent failure	19	44	46	46		31				
GERT	2005	no aircraft data						35				
HARVEY	2005	no aircraft data						49	54	54		
IRENE	2005	insufficient data	23					43	59	58	85	
TEN	2005	no aircraft data										
JOSE	2005	no aircraft data										
KATRINA	2005	delayed success	56		40	40	44	32	64	89	91	115
LEE	2005	no aircraft data						24	24	24		
MARIA	2005	no aircraft data						32	38	57	80	
NATE	2005	insufficient data	2					34	56	67	67	
OPHELIA	2005	intermittent failure	96		45	45	61	24	31	69	65	

continued on next page

Table B.2: *continued*

Storm	Year	Case Type	# of fixes	B	A	A1	A2	IR1	IR2	IR3	IR4	IR5
PHILIPPE	2005	insufficient data	4					29				
RITA	2005	delayed success	71	59	69	69	73	24	24	60	90	96
NINETEEN	2005	no aircraft data										
STAN	2005	complete failure	12	63	66	66		28	68			
UNNAMED	2005	no aircraft data										
TAMMY	2005	no attempt	4					38	44			
TWENTY-TWO	2005	no aircraft data										
VINCE	2005	no aircraft data						44	48	53	53	
WILMA	2005	delayed success	56		50	50	108	29	62	62	99	141
ALPHA	2005	no aircraft data						29	29			
BETA	2005	insufficient data	4					31	42	74	90	
GAMMA	2005	no attempt	6					29	29			
DELTA	2005	no aircraft data						44	49	49		
EPSILON	2005	no aircraft data						44	44	53	59	
ZETA	2005	no aircraft data						44	49	49		
ALBERTO	2006	no attempt	19									
NONAME	2006	no aircraft data										
BERYL	2006	complete failure	19		49	49		49	49	49		
CHRIS	2006	no attempt	32					54				
DEBBY	2006	no aircraft data						30	30	41		
ERNESTO	2006	intermittent failure	55		55	55		34	54	59		
FLORENCE	2006	intermittent failure	13		69		69	40	39	46	73	
GORDON	2006	no aircraft data						29	45	62	79	
HELENE	2006	insufficient data	7					29	29	72	72	
ISAAC	2006	no aircraft data									70	
ANDREA	2007	no attempt	2					44				
BARRY	2007	no attempt	2									
CHANTAL	2007	no aircraft data						42	42			
DEAN	2007	insufficient data	47					49	70	73	114	122
ERIN	2007	no attempt	4					30				
FELIX	2007	complete success	23		63	63	112	28	28	87	87	94
GABRIELLE	2007	no attempt	13									
INGRID	2007	no attempt	2					29				
HUMBERTO	2007	insufficient data	4					32	38	66		
TEN	2007	no aircraft data										
JERRY	2007	no aircraft data						32				

continued on next page

Table B.2: *continued*

Storm	Year	Case Type	# of fixes	B	A	A1	A2	IR1	IR2	IR3	IR4	IR5
KAREN	2007	no attempt	5					30	34	64		
LORENZO	2007	no aircraft data						24	24			
MELISSA	2007	no aircraft data						28	24			
FIFTEEN	2007	no aircraft data										
NOEL	2007	no attempt	21					29	37			
OLGA	2007	no aircraft data										
ARTHUR	2008	no aircraft data						38	38			
BERTHA	2008	insufficient data	8					35	53	64	64	
CRISTOBAL	2008	no attempt	13					52				
DOLLY	2008	intermittent failure	33	44	53		59	44	44	59	64	
EDOUARD	2008	no attempt	16					40				
FAY	2008	intermittent failure	43		54	54		56	57	57	57	
GUSTAV	2008	insufficient data	56					37	58	62	88	93
HANNA	2008	no attempt	39						70	69		
IKE	2008	insufficient data	70					44	65	65	88	105
JOSEPHINE	2008	no aircraft data						34	34	40		
KYLE	2008	no attempt	14					38				
LAURA	2008	no aircraft data						49	49			
MARCO	2008	no aircraft data										
NANA	2008	no aircraft data										
OMAR	2008	intermittent failure	19	60	61	61	92	39	39	98	98	
SIXTEEN	2008	no attempt	2									
PALOMA	2008	complete success	27		51		51	47	62	62	79	97
Summary statistics for all valid eye formation case types												
N			180	23	70	48	52	173	143	114	80	40
mean			25.9	50.2	58.1	56.4	67.6	37.8	44.7	58.1	77.1	101.1
std. dev.			22.1	12.4	11.9	11.5	16.7	11.3	14.7	16.7	14.4	14.7
minimum			2	29	29	29	38	19	19	23	44	67
lower quartile			9	39	50	49	58	29	31	47	66	93
median			19.0	50.0	58.0	55.5	66.0	34.0	44.0	59.0	77.0	98.0
upper quartile			39	59	66	63	79	44	56	69	88	109
maximum			107	80	88	88	112	77	81	99	114	141

continued on next page

Table B.2: *continued*

Storm	Year	Case Type	# of fixes	B	A	A1	A2	IR1	IR2	IR3	IR4	IR5
Summary statistics for only 'Complete Failure' cases												
N			17	3	17	13	6	9	7	5	1	0
mean			18.5		57.1	54.5	62.2	40.6	53.3	51.6		
std. dev.			7.9		12.5	13.4	5.3	9.4	16.6	11.4		
minimum			12	29	29	29	54	28	34	40	44	−999
lower quartile			12		49	49	54	29	34	40		
median			16.0		58.0	55.0	63.5	40.0	49.0	49.0		
upper quartile			19		64	58	64	44	57	49		
maximum			41	63	83	83	69	57	81	69	44	−999
Summary statistics for only 'Intermittent Failure' cases												
N			24	8	24	16	17	16	15	13	10	1
mean			35.0	50.1	55.6	54.1	64.7	39.8	51.4	67.8	73.9	
std. dev.			18.5	8.5	8.7	7.1	16.1	14.8	17.4	14.2	12.8	
minimum			13	39	39	39	43	19	19	46	57	101
lower quartile			22	44	46	46	46	29	31	59	64	
median			32.0	47.5	54.5	54.5	61.0	38.5	54.0	64.0	73.0	
upper quartile			43	59	61	59	69	44	66	67	74	
maximum			96	60	69	64	94	64	74	98	98	101
Summary statistics for only 'Delayed Success' cases												
N			12	6	12	9	12	9	9	9	9	7
mean			54.6	51.5	58.3	56.8	66.3	34.6	43.0	64.4	87.3	108.4
std. dev.			17.9	16.7	17.5	16.6	18.9	9.1	16.3	19.9	13.8	18.2
minimum			24	33	36	36	38	24	24	30	67	89
lower quartile			42	33	40	40	50	29	29	46	74	89
median			56.0	49.5	59.0	54.0	65.5	31.0	39.0	62.0	90.0	104.0
upper quartile			68	50	67	64	73	32	44	70	91	115
maximum			84	80	88	88	108	53	64	94	111	141
Summary statistics for only 'Complete Success' cases												
N			17	6	17	10	17	17	17	17	16	12
mean			46.0	51.5	62.3	62.4	73.4	35.9	42.5	59.2	79.8	92.4
std. dev.			21.0	12.5	10.5	8.1	17.9	11.2	14.7	18.8	9.3	9.4
minimum			8	29	44	49	41	24	25	29	65	73

continued on next page

Table B.2: *continued*

Storm	Year	Case Type	# of fixes	B	A	A1	A2	IR1	IR2	IR3	IR4	IR5
lower quartile			25	29	52	52	59	26	29	44	71	84
median			44.0	52.0	63.0	63.0	75.0	30.0	41.0	62.0	80.5	93.5
upper quartile			58	52	69	67	80	42	49	69	87	97
maximum			75	64	79	74	112	57	65	87	99	109

Table B.3: As in Table B.2, but for the rFL intensity.

Storm	Year	Case Type	# of fixes	B	A	A1	A2	IR1	IR2	IR3	IR4	IR5
ONE	1989	no aircraft data										
ALLISON	1989	no aircraft data										
BARRY	1989	no attempt	2									
CHANTAL	1989	complete failure	14		48		48					
DEAN	1989	insufficient data	18									
SIX	1989	no aircraft data										
ERIN	1989	no aircraft data										
FELIX	1989	no aircraft data										
NINE	1989	no aircraft data										
GABRIELLE	1989	insufficient data	29									
HUGO	1989	insufficient data	44									
IRIS	1989	complete failure	12		71	71						
THIRTEEN	1989	no aircraft data										
JERRY	1989	intermittent failure	22									
KAREN	1989	insufficient data	25									
ONE	1990	no aircraft data										
ARTHUR	1990	complete failure	12		65	65						
BERTHA	1990	insufficient data	24									
CESAR	1990	no aircraft data										
DIANA	1990	complete failure	13									
EDOUARD	1990	no aircraft data										
FRAN	1990	no aircraft data										
GUSTAV	1990	insufficient data	14									
HORTENSE	1990	no aircraft data										
ISIDORE	1990	no aircraft data										
ELEVEN	1990	no aircraft data										
JOSEPHINE	1990	no aircraft data										
KLAUS	1990	intermittent failure	38									
LILI	1990	complete failure	12		59	59						
MARCO	1990	no attempt	16									
NANA	1990	delayed success	24				57					
ANA	1991	no aircraft data										
TWO	1991	no aircraft data										
BOB	1991	delayed success	43	38	40	40	46					
FOUR	1991	no aircraft data										
FIVE	1991	no aircraft data										

continued on next page

Table B.3: *continued*

Storm	Year	Case Type	# of fixes	B	A	A1	A2	IR1	IR2	IR3	IR4	IR5
CLAUDETTE	1991	insufficient data	18									
DANNY	1991	no aircraft data										
ERIKA	1991	no aircraft data										
FABIAN	1991	no aircraft data										
TEN	1991	no aircraft data										
GRACE	1991	complete failure	16		46		46					
UNNAMED	1991	no aircraft data										
SUBTROP	1992	no aircraft data										
ONE	1992	no aircraft data										
TWO	1992	no aircraft data										
ANDREW	1992	delayed success	64		58	58						
BONNIE	1992	no aircraft data										
CHARLEY	1992	no aircraft data										
DANIELLE	1992	complete failure	23		43	43						
SEVEN	1992	no aircraft data										
EARL	1992	intermittent failure	36	40	41		41					
FRANCES	1992	no aircraft data										
ONE	1993	no aircraft data										
ARLENE	1993	no attempt	14									
BRET	1993	no attempt	11									
CINDY	1993	no attempt	10									
EMILY	1993	intermittent failure	59									
DENNIS	1993	no aircraft data										
FLOYD	1993	no attempt	5									
GERT	1993	intermittent failure	15		59	59	65					
HARVEY	1993	no aircraft data										
TEN	1993	no aircraft data										
ALBERTO	1994	intermittent failure	23		35	35	39					
TWO	1994	no aircraft data										
BERYL	1994	no attempt	9									
CHRIS	1994	no attempt	14									
FIVE	1994	complete failure	13	27	26	26						
DEBBY	1994	no attempt	5									
ERNESTO	1994	no aircraft data										
EIGHT	1994	no aircraft data										
NINE	1994	no aircraft data										

continued on next page

Table B.3: *continued*

Storm	Year	Case Type	# of fixes	B	A	A1	A2	IR1	IR2	IR3	IR4	IR5
TEN	1994	no aircraft data										
FLORENCE	1994	insufficient data	2									
GORDON	1994	no attempt	50									
ALLISON	1995	no attempt	25									
BARRY	1995	insufficient data	4									
CHANTAL	1995	intermittent failure	40	36	38	38	39					
DEAN	1995	no attempt	17									
ERIN	1995	intermittent failure	44		65	65	63	67	68	68	64	
SIX	1995	no attempt	6									
FELIX	1995	insufficient data	70								78	79
GABRIELLE	1995	no attempt	11									
HUMBERTO	1995	no aircraft data										
IRIS	1995	insufficient data	49					83	74	74		
JERRY	1995	no attempt	9									
KAREN	1995	no aircraft data										
LUIS	1995	insufficient data	47									
FOURTEEN	1995	no aircraft data										
MARILYN	1995	complete success	56		48		48				95	99
NOEL	1995	no aircraft data										
OPAL	1995	insufficient data	38					44	44	88	88	
PABLO	1995	no aircraft data										
ROXANNE	1995	complete success	72	44	44		44			82	82	
SEBASTIEN	1995	no attempt	10									
TANYA	1995	no aircraft data										
ARTHUR	1996	no attempt	12									
BERTHA	1996	complete success	58		73	73	75			73	96	101
CESAR	1996	complete failure	15					47	47			
DOLLY	1996	complete failure	18		44	44	43					
EDOUARD	1996	insufficient data	67									
FRAN	1996	delayed success	71				55		60	59	66	95
GUSTAV	1996	no aircraft data										
HORTENSE	1996	intermittent failure	17		71		71	30	68			
ISIDORE	1996	no aircraft data										
JOSEPHINE	1996	intermittent failure	24		49	49						
KYLE	1996	no attempt	2									
LILI	1996	intermittent failure	35		44	44	100		61	69	69	

continued on next page

Table B.3: *continued*

Storm	Year	Case Type	# of fixes	B	A	A1	A2	IR1	IR2	IR3	IR4	IR5
MARCO	1996	complete failure	41					31	31			
SUBTROP	1997	no aircraft data										
ANA	1997	no attempt	4									
BILL	1997	no attempt	3									
CLAUDETTE	1997	insufficient data	8					34				
DANNY	1997	complete success	43		57	57	61			61	61	
FIVE	1997	no aircraft data										
ERIKA	1997	delayed success	33		62	62	64				77	81
FABIAN	1997	no aircraft data										
GRACE	1997	no aircraft data										
ALEX	1998	no attempt	4									
BONNIE	1998	complete success	75	49	57	57	75				59	85
CHARLEY	1998	no attempt	7									
DANIELLE	1998	delayed success	43	67								
EARL	1998	no attempt	23					39	39	39		
FRANCES	1998	no attempt	14									
GEORGES	1998	insufficient data	79									
HERMINE	1998	no attempt	24									
IVAN	1998	no aircraft data										
JEANNE	1998	no aircraft data										
KARL	1998	no aircraft data										
LISA	1998	no aircraft data										
MITCH	1998	complete success	48	38	73	73	72	47	62	62	72	85
NICOLE	1998	no aircraft data										
ARLENE	1999	no attempt	8									
TWO	1999	no aircraft data										
BRET	1999	delayed success	42	32	32		32	33	33	33	98	104
CINDY	1999	no aircraft data										
DENNIS	1999	delayed success	84	43	54		54	36	36	70	102	
EMILY	1999	no attempt	14									
SEVEN	1999	no aircraft data										
FLOYD	1999	complete success	69		74	74	92				90	108
GERT	1999	insufficient data	13									
HARVEY	1999	no attempt	15					41	41			
ELEVEN	1999	no attempt	12									
TWELVE	1999	no aircraft data										

continued on next page

Table B.3: *continued*

Storm	Year	Case Type	# of fixes	B	A	A1	A2	IR1	IR2	IR3	IR4	IR5
IRENE	1999	intermittent failure	44	40	46	46	58			56		
JOSE	1999	intermittent failure	31		63	63	86	65	67	67		
KATRINA	1999	no attempt	5									
LENNY	1999	complete success	44	56	59		59					59
ONE	2000	no aircraft data										
TWO	2000	no aircraft data										
ALBERTO	2000	no aircraft data										
FOUR	2000	no attempt	6									
BERYL	2000	no attempt	9					41				
CHRIS	2000	no attempt	3									
DEBBY	2000	intermittent failure	26		58		58					
ERNESTO	2000	no aircraft data										
NINE	2000	no aircraft data										
FLORENCE	2000	intermittent failure	22					58	58	58	52	
GORDON	2000	complete failure	29	46	67		67	37				
HELENE	2000	no attempt	15									
ISAAC	2000	no aircraft data										
JOYCE	2000	no attempt	3									
KEITH	2000	complete success	34					41	66	66		84
LESLIE	2000	no attempt	11					25				
MICHAEL	2000	insufficient data	6									
NADINE	2000	no aircraft data										
SUBTROP	2000	no attempt	4									
ALLISON	2001	no attempt	3									
TWO	2001	no aircraft data										
BARRY	2001	no attempt	30									
CHANTAL	2001	no attempt	29						45	61		
DEAN	2001	no attempt	2									
ERIN	2001	complete success	21	26	60	60	90				64	
FELIX	2001	no aircraft data										
GABRIELLE	2001	no attempt	20									
NINE	2001	no aircraft data										
HUMBERTO	2001	complete success	8		49	49	77					
IRIS	2001	insufficient data	30						48	48	103	115
JERRY	2001	no attempt	3									
KAREN	2001	no aircraft data										

continued on next page

Table B.3: *continued*

Storm	Year	Case Type	# of fixes	B	A	A1	A2	IR1	IR2	IR3	IR4	IR5
LORENZO	2001	no aircraft data										
MICHELLE	2001	complete success	39		72		72			63	63	77
NOEL	2001	no aircraft data										
OLGA	2001	no aircraft data										
ARTHUR	2002	no aircraft data										
BERTHA	2002	no attempt	3									
CRISTOBAL	2002	no attempt	8									
DOLLY	2002	no aircraft data										
EDOUARD	2002	no attempt	23									
FAY	2002	no aircraft data										
SEVEN	2002	no aircraft data										
GUSTAV	2002	complete failure	22		46	46		41				
HANNA	2002	no attempt	26									
ISIDORE	2002	complete success	73	50	50	50	59	33	33	45	91	98
JOSEPHINE	2002	no aircraft data										
KYLE	2002	no attempt	12									
LILI	2002	complete success	67		40		42			47	84	90
FOURTEEN	2002	no aircraft data										
ANA	2003	no aircraft data										
TWO	2003	no aircraft data										
BILL	2003	no attempt	8					46				
CLAUDETTE	2003	intermittent failure	57	65	59		59		61	67	74	
DANNY	2003	no aircraft data										
SIX	2003	no aircraft data										
SEVEN	2003	no attempt	2									
ERIKA	2003	complete failure	16		60	60	60	35	35	35		
NINE	2003	no aircraft data										
FABIAN	2003	insufficient data	30									
GRACE	2003	no attempt	5									
HENRI	2003	complete failure	27					29				
ISABEL	2003	insufficient data	35									
FOURTEEN	2003	no aircraft data										
JUAN	2003	no aircraft data										
KATE	2003	no aircraft data										
LARRY	2003	no attempt	23					47				
MINDY	2003	no attempt	10									

continued on next page

Table B.3: *continued*

Storm	Year	Case Type	# of fixes	B	A	A1	A2	IR1	IR2	IR3	IR4	IR5
NICHOLAS	2003	no aircraft data										
ODETTE	2003	no attempt	10					53				
PETER	2003	no aircraft data										
ALEX	2004	complete success	25		52	52			44	85		
BONNIE	2004	intermittent failure	29		40		40		36			
CHARLEY	2004	insufficient data	39						82		93	113
DANIELLE	2004	no aircraft data										
EARL	2004	no aircraft data										
FRANCES	2004	insufficient data	73									
GASTON	2004	insufficient data	4						45	45		
HERMINE	2004	no aircraft data										
IVAN	2004	insufficient data	107									
TEN	2004	no aircraft data										
JEANNE	2004	insufficient data	58									
KARL	2004	no aircraft data										
LISA	2004	no aircraft data										
MATTHEW	2004	no attempt	10					33				
NICOLE	2004	no aircraft data										
OTTO	2004	no aircraft data										
ARLENE	2005	no attempt	21					31	46	49		
BRET	2005	no aircraft data										
CINDY	2005	no attempt	8							53		
DENNIS	2005	insufficient data	53								103	128
EMILY	2005	delayed success	68	46	78		78			88	88	100
FRANKLIN	2005	intermittent failure	19	41	44	44						
GERT	2005	no aircraft data										
HARVEY	2005	no aircraft data										
IRENE	2005	insufficient data	23						55	55		
TEN	2005	no aircraft data										
JOSE	2005	no aircraft data										
KATRINA	2005	delayed success	56		35	35				89	90	121
LEE	2005	no aircraft data										
MARIA	2005	no aircraft data										
NATE	2005	insufficient data	2									
OPHELIA	2005	intermittent failure	96		46	46	53			69	68	
PHILIPPE	2005	insufficient data	4									

continued on next page

Table B.3: *continued*

Storm	Year	Case Type	# of fixes	B	A	A1	A2	IR1	IR2	IR3	IR4	IR5
RITA	2005	delayed success	71	61	71	71	72			67	83	
NINETEEN	2005	no aircraft data										
STAN	2005	complete failure	12	46	62	62						
UNNAMED	2005	no aircraft data										
TAMMY	2005	no attempt	4						39			
TWENTY-TWO	2005	no aircraft data										
VINCE	2005	no aircraft data										
WILMA	2005	delayed success	56		42	42	72		54	54	66	123
ALPHA	2005	no aircraft data										
BETA	2005	insufficient data	4									
GAMMA	2005	no attempt	6									
DELTA	2005	no aircraft data										
EPSILON	2005	no aircraft data										
ZETA	2005	no aircraft data										
ALBERTO	2006	no attempt	19									
NONAME	2006	no aircraft data										
BERYL	2006	complete failure	19		50	50		48	51	51		
CHRIS	2006	no attempt	32					50				
DEBBY	2006	no aircraft data										
ERNESTO	2006	intermittent failure	55						48	58		
FLORENCE	2006	intermittent failure	13		75		75				80	
GORDON	2006	no aircraft data										
HELENE	2006	insufficient data	7									
ISAAC	2006	no aircraft data										
ANDREA	2007	no attempt	2									
BARRY	2007	no attempt	2									
CHANTAL	2007	no aircraft data										
DEAN	2007	insufficient data	47								116	121
ERIN	2007	no attempt	4									
FELIX	2007	complete success	23		69	69	110			89	89	100
GABRIELLE	2007	no attempt	13									
INGRID	2007	no attempt	2									
HUMBERTO	2007	insufficient data	4									
TEN	2007	no aircraft data										
JERRY	2007	no aircraft data										
KAREN	2007	no attempt	5									

continued on next page

Table B.3: *continued*

Storm	Year	Case Type	# of fixes	B	A	A1	A2	IR1	IR2	IR3	IR4	IR5
LORENZO	2007	no aircraft data										
MELISSA	2007	no aircraft data										
FIFTEEN	2007	no aircraft data										
NOEL	2007	no attempt	21									
OLGA	2007	no aircraft data										
ARTHUR	2008	no aircraft data										
BERTHA	2008	insufficient data	8									
CRISTOBAL	2008	no attempt	13									
DOLLY	2008	intermittent failure	33		53		60	43	43	61	66	
EDOUARD	2008	no attempt	16					37				
FAY	2008	intermittent failure	43		46	46						
GUSTAV	2008	insufficient data	56								93	96
HANNA	2008	no attempt	39									
IKE	2008	insufficient data	70									
JOSEPHINE	2008	no aircraft data										
KYLE	2008	no attempt	14									
LAURA	2008	no aircraft data										
MARCO	2008	no aircraft data										
NANA	2008	no aircraft data										
OMAR	2008	intermittent failure	19	50	51	51	94	30	30	101	101	
SIXTEEN	2008	no attempt	2									
PALOMA	2008	complete success	27		49		49	46	53	53	94	98
Summary statistics for all valid eye formation case types												
N			180	21	57	38	45	33	34	38	36	24
mean			25.9	44.8	53.9	53.6	62.6	42.6	50.1	63.6	82.3	98.3
std. dev.			22.1	11.1	12.3	12.0	17.8	12.3	13.3	15.6	15.5	16.8
minimum			2	26	26	26	32	25	30	33	52	59
lower quartile			9	38	44	44	48	33	39	53	66	85
median			19.0	44.3	51.9	51.5	59.6	41.3	47.4	61.6	83.8	98.6
upper quartile			39	49	62	62	72	47	60	69	93	108
maximum			107	67	78	74	110	83	82	101	116	128

continued on next page

Table B.3: *continued*

Storm	Year	Case Type	# of fixes	B	A	A1	A2	IR1	IR2	IR3	IR4	IR5
Summary statistics for only 'Complete Failure' cases												
N			17	3	13	10	5	7	4	2	0	0
mean			18.5		52.8	52.6	52.6	38.4				
std. dev.			7.9		12.3	13.1	10.1	7.3				
minimum			12	27	26	26	43	29	31	35	−999	−999
lower quartile			12		44	43	43	29				
median			16.0		50.2	54.4	47.8	37.2				
upper quartile			19		60	60	48	41				
maximum			41	46	71	71	67	48	51	51	−999	−999
Summary statistics for only 'Intermittent Failure' cases												
N			24	6	19	12	16	6	10	10	8	0
mean			35.0	45.5	51.8	49.0	62.5	48.8	54.0	67.4	71.9	
std. dev.			18.5	10.8	11.3	9.3	19.0	16.8	13.7	13.0	14.4	
minimum			13	36	35	35	39	30	30	56	52	−999
lower quartile			22	36	41	44	41	30	36	58	64	
median			32.0	40.7	49.5	46.3	59.1	50.3	59.3	67.0	68.8	
upper quartile			43	41	59	51	71	58	61	68	74	
maximum			96	65	75	65	100	67	68	101	101	−999
Summary statistics for only 'Delayed Success' cases												
N			12	6	9	6	9	2	4	7	8	6
mean			54.6	47.8	52.4	51.3	58.7			65.6	83.9	103.9
std. dev.			17.9	13.6	16.4	14.3	14.6			19.5	13.4	15.8
minimum			24	32	32	35	32	33	33	33	66	81
lower quartile			42	32	35	35	46			33	66	81
median			56.0	44.4	53.9	49.9	56.9			66.9	85.6	101.9
upper quartile			68	46	58	58	64			70	90	104
maximum			84	67	78	71	78	36	60	89	102	123
Summary statistics for only 'Complete Success' cases												
N			17	6	16	10	15	4	5	11	13	12
mean			46.0	43.8	57.9	61.4	68.4		51.6	66.0	80.0	90.3
std. dev.			21.0	10.6	11.3	10.0	19.4		13.5	14.9	14.1	13.5
minimum			8	26	40	49	42	33	33	45	59	59
lower quartile			25	26	49	50	48		33	47	63	84

continued on next page

Table B.3: *continued*

Storm	Year	Case Type	# of fixes	B	A	A1	A2	IR1	IR2	IR3	IR4	IR5
median			44.0	46.5	57.3	58.7	71.8		53.0	62.6	84.3	94.3
upper quartile			58	49	69	69	75		53	73	90	99
maximum			75	56	74	74	110	47	66	89	96	108

Table B.4: The actual change (kt (6 h)$^{-1}$) in the interpolated best track intensity for each 6-h period before and after the first report of an aircraft eye (A). Data from the period when the storm was over land do not contribute to these statistics.

			6-h change in best track maximum wind speed from previous period (kt (6 h)$^{-1}$)														
Storm	Year	Case Type	-60	-48	-36	-24	-18	-12	-06	+00	+06	+12	+18	+24	+36	+48	+60	+72
CHANTAL	1989	complete failure				5	5	13	7	9	6	1						
IRIS	1989	complete failure	3	0	3	5	5	5	5	3	−4	−10	−8	−3	−3	−3		
JERRY	1989	intermittent failure				5	5	5	5	5	1	0	0	0	4	9		
ARTHUR	1990	complete failure	0	0	1	1	4	5	5	9	2	−8	−6	−5	−5			
DIANA	1990	complete failure	5				9	6	9	10								
KLAUS	1990	intermittent failure				8	7	2	3	2	3	8	4	−3	−2	−2	−3	−10
LILI	1990	complete failure	−9	0	5	5	0	0	0	0	0	0	0	0	−5	−1	0	−5
NANA	1990	delayed success						3	2	5	5	7	10	8	3	−5	5	−7
BOB	1991	delayed success				5	5	5	5	10	10	5	5	5	10	−4	−24	
GRACE	1991	complete failure	5	0	5	5	5	5	0	0	0	5	5	9				
ANDREW	1992	delayed success	0	0	−0	0	0	0	5	0	5	0	5	10	15	20	4	
DANIELLE	1992	complete failure	1	−5	0	0	0	5	0	9	1							
EARL	1992	intermittent failure	0	0	0	5	3	0	2	5	3	0	0	2	−2	−5	−3	−3
EMILY	1993	intermittent failure	0	5	5	5	5	−5	−0	0	5	10	0	0	−5	0	0	5
GERT	1993	intermittent failure					5	5	5	10	10	14						
ALBERTO	1994	intermittent failure			0	0	0	5	0	5	5	0	5	5				
FIVE	1994	complete failure				0	0	0	0	0								
CHANTAL	1995	intermittent failure	0	0	5	0	5	0	5	0	0	0	5	0	5	0	−0	−5
ERIN	1995	intermittent failure							5	5	8	7	2	0			5	
MARILYN	1995	complete success					5	10	10	5	5	5	0	0	5	5	5	5
ROXANNE	1995	complete success					5	5	5	6	10	10	11	13			−2	0
BERTHA	1996	complete success	3	0	5	5	5	7	8	3	−2	−0	5	12	−5	−5	0	−3
CESAR	1996	complete failure	5	0	5	5	10	3	−0									
DOLLY	1996	complete failure	10					10	0	5	5	5						
FRAN	1996	delayed success	5	5	5	0	0	0	0	0	−3	−2	0	3	0	3	2	0
HORTENSE	1996	intermittent failure	0	5	4	5	3	0	4	6	0	0			2	9	5	7
JOSEPHINE	1996	intermittent failure		0	0	0	5	5	10	10	1	0				0		
LILI	1996	intermittent failure		0	5	0	5	10	5	5	5	5	5	0			10	−10
MARCO	1996	complete failure	9	4	−15	1	4	1	4	1	1	−9	−6	−8	−4	1	2	5
DANNY	1997	complete success				0	9	10	6	9	6	1	0	−4	−4	−14		
ERIKA	1997	delayed success	2	7	7	0	0	0	0	2	3	2	3	0	5	5	5	0
BONNIE	1998	complete success		0	0	5	5	5	10	5	5	10	5	5	0	0	0	0
DANIELLE	1998	delayed success	6	14	6	−5	−4	1	5	3	−5	−4	0	0	−5	0	−4	0
MITCH	1998	complete success		0	5	3	2	5	7	10	12	13	8	7	8	7	7	−3
BRET	1999	delayed success					0	0	4	5	5	5	5	9	6	28	1	
DENNIS	1999	delayed success	2	3	2	8	5	3	2	1	−3	0	0	2	7	3	0	0

continued on next page

Table B.4: *continued*

			6-h change in best track maximum wind speed from previous period (kt (6 h)$^{-1}$)															
Storm	Year	Case Type	-60	-48	-36	-24	-18	-12	-06	+00	+06	+12	+18	+24	+36	+48	+60	+72
FLOYD	1999	complete success	5	5	0	10	0	0	10	0	10	14	−0	−5	10	10	10	−10
IRENE	1999	intermittent failure		0	7	10	7	2	0	0	3	2	0			0	0	8
JOSE	1999	intermittent failure			5	1	4	9	6	5	5	9	6	−3	−9	−5	−1	0
LENNY	1999	complete success				0	10	15	15	5	10	−10	0	0	0	5	20	−5
DEBBY	2000	intermittent failure		3	5	10	10	5	−3	−5	−2	0	0	0	−8	−7		
FLORENCE	2000	intermittent failure					0	9	18	8	−3	−2	3	2	−3	−5	−2	0
GORDON	2000	complete failure				5	5	5	5	−4	−0	−5						
KEITH	2000	complete success			5	10	5	10	10	10	25	19	−5	−5	−20	−5		
ERIN	2001	complete success	1	4	4	4	1	5	8	15	15	12	6	8	−1	−10	0	0
HUMBERTO	2001	complete success			0	6	10	9	4	1	11	14	3	−9	−1	0	0	11
MICHELLE	2001	complete success			10	0	5	5	10	10	10	15	10	−5	5			−5
GUSTAV	2002	complete failure			3	0	2	5	3	2	3	2	7	12	−5		−5	−3
ISIDORE	2002	complete success	2	2	0	5	5	5	3	3	8	7	12	8			7	0
LILI	2002	complete success	−5	0	5	5	0	0	0	0	−5	5	5	5	5	5	15	0
CLAUDETTE	2003	intermittent failure	0	0	5	−5	0	0	0	15	−15	−5			0	0	0	5
ERIKA	2003	complete failure				3	2	5	5	5								
HENRI	2003	complete failure				1	4	0	1	5	6	2	−14			0	0	0
ALEX	2004	complete success			0	5	1	4	9	2	8	10	14	2	−1	9	2	−9
BONNIE	2004	intermittent failure	−2	0	2	0	3	5	5	5	2	3	−2	−5	3	0	−2	
GASTON	2004	insufficient data				2	5	7	8	5	5	5						2
EMILY	2005	delayed success	5	5	0	5	5	15	5	10	15	10	5	0	14	10	5	−5
FRANKLIN	2005	intermittent failure				7	2	4	0	2	6	7	−2	−4	−7	−4	0	−4
KATRINA	2005	delayed success					0	2	5	5	5	5	5			8	5	0
OPHELIA	2005	intermittent failure			0	5	5	5	4	1	5	5	5	1	3	−4	5	1
RITA	2005	delayed success		5	10	5	5	0	0	10	15	10	15	10	5	−15	−5	−0
STAN	2005	complete failure	3				7	8	7									
WILMA	2005	delayed success			2	0	3	5	5	8	7	5	8	36	14	−11	−2	0
BETA	2005	insufficient data			7	3	0	0	0	4	10	8	3	6				
BERYL	2006	complete failure				0	5	10	1	0	0	−5	−0	0	−5			
ERNESTO	2006	intermittent failure		5	5	5	5	0	9	−8	−10	−5	−0				0	
FLORENCE	2006	intermittent failure	−0	0	4	0	0	0	9	10	6	5	0	−9	0	−5	0	0
FELIX	2007	complete success				5	5	9	10	6	17	8	21	33	−8	−5		
DOLLY	2008	intermittent failure			5			0	0	9	5	5	5	14				
FAY	2008	intermittent failure	1	0	0	1	4	0	1							0		
OMAR	2008	intermittent failure				2	5	7	10	8	5	5	5	8	6	−15	5	−10
PALOMA	2008	complete success						5	5	14	11	1	9	6	11	2		
N			29	34	45	59	67	71	72	69	66	65	57	53	47	48	45	41

continued on next page

Table B.4: *continued*

			6-h change in best track maximum wind speed from previous period (kt (6 h)$^{-1}$)														
Storm	Year	Case Type	-60	-48	-36	-24	-18	-12	-06	+00	+06	+12	+18	+24	+36	+48	+60	+72
mean			1.9	1.9	3.0	3.2	3.7	4.3	4.6	4.8	4.5	3.7	3.3	3.3	0.9	0.2	1.5	−1.1
std. dev.			3.8	3.3	3.9	3.3	3.0	4.0	4.0	4.5	6.3	6.3	5.7	8.5	6.9	8.0	6.3	5.0
minimum			−9	−5	−15	−5	−4	−5	−3	−8	−15	−10	−14	−9	−20	−15	−24	−10
lower quartile			0	0	0	0	0	0	0	1	0	0	0	−3	−5	−5	−1	−5
median			1.7	0.0	4.5	3.8	4.7	5.0	5.0	5.0	5.0	5.0	3.9	0.6	0.0	0.0	0.0	0.0
upper quartile			5	4	5	5	5	5	7	8	8	7	5	7	5	5	5	0
maximum			10	14	10	10	10	15	18	15	25	19	21	36	15	28	20	11

Table B.5: The actual change (kt (6 h)$^{-1}$) in the interpolated reduced maximum flight level wind (rFL v_{max}) for each 6-h period before and after the first report of an aircraft eye (A).

			6-h change in combined maximum flight level wind speed from previous period (kt (6 h)$^{-1}$)															
Storm	Year	Case Type	-60	-48	-36	-24	-18	-12	-06	+00	+06	+12	+18	+24	+36	+48	+60	+72
CHANTAL	1989	complete failure								9	16	−3						
IRIS	1989	complete failure							12	10	−3	−13	−13	−13	−0			
JERRY	1989	intermittent failure					7	7	−1	3	−4	−4	3	1	8			
ARTHUR	1990	complete failure						−0	−0	35	−9	−6	−7					
DIANA	1990	complete failure		−0	2	2	8	9	16									
KLAUS	1990	intermittent failure					4	1	1	1	1	1	1	−2	−3	2	0	−13
LILI	1990	complete failure									−0	−3	−3	3	−4			
NANA	1990	delayed success									1	1	1	10	8	−4	−4	−4
BOB	1991	delayed success				5	4	0	−2	4	13	3	8	6	16	−2		
GRACE	1991	complete failure						7	1	−0	−0	4	1					
ANDREW	1992	delayed success				3	3	3	3	−6	−6	0	6	7	13	22	2	−12
DANIELLE	1992	complete failure		0	0	−1	1	2	2	4	14							
EARL	1992	intermittent failure	2	0	3	−2	6	6	1	1	5	2	−2	−1				
EMILY	1993	intermittent failure	5	4	−3	10	7	−3	−3	−3	6	10	3	−3	−3	−3	8	3
GERT	1993	intermittent failure							15	9	10	12	1					
ALBERTO	1994	intermittent failure					14	−1	1	2	5	3	1	5				
FIVE	1994	complete failure					−4	1	1	−0	1							
CHANTAL	1995	intermittent failure			0	−9	2	3	8	2	1	3	5	2	−1	−4	0	1
ERIN	1995	intermittent failure							7	7	3	1	0	−0	−3	0	3	−7
MARILYN	1995	complete success									8	13	9	−2	8	5	5	−1
ROXANNE	1995	complete success					4	4	4	9	4	14	18	14	−12	−12	−4	−0
BERTHA	1996	complete success							−1	−0	3	5	9	15	−6	−7	4	−1
CESAR	1996	complete failure			0	7	7	2	−1									
DOLLY	1996	complete failure	3	−2	−2	−2	0	9	−2	6	−2	5						
FRAN	1996	delayed success							−2	−1	−3	−3	2	6	1	−0	8	−3
HORTENSE	1996	intermittent failure		11	3	−0	−0	2	12	11	−6							
JOSEPHINE	1996	intermittent failure		−2	6	10	5	0	0	9	3	4						
LILI	1996	intermittent failure				3	8	8	7	−5	2	5	1	5	4	3	7	−2
MARCO	1996	complete failure	5	7	−8	1	4	−5	10	10	−4	−4	−4	−3	−1	−1	−1	−1
DANNY	1997	complete success				0	0	7	5	15	3	−1	0	3	−3	−4	0	0
ERIKA	1997	delayed success							−1	1	7	1	0	8	−0	0	9	−1
BONNIE	1998	complete success				0	0	1	1	8	5	3	5	13	3	3	3	−2
DANIELLE	1998	delayed success							13	6	−7	−7	−2	0	−7	−5	1	−0
MITCH	1998	complete success		4	4	−0	−0	−0	18	18	−0	5	15	14	15	0	10	−10
BRET	1999	delayed success					1	1	1	−1	6	4	7	7	9	20	3	−5
DENNIS	1999	delayed success		3	1	11	14	−2	−4	−3	−2	2	0	4	18	−3	−4	−3

continued on next page

Table B.5: *continued*

			6-h change in combined maximum flight level wind speed from previous period (kt (6 h)$^{-1}$)														
Storm	Year	Case Type	-60	-48	-36	-24	-18	-12	-06	+00	+06	+12	+18	+24	+36	+48	+60	+72
FLOYD	1999	complete success				9	1	4	12	2	8	14	−2	−3	8	6	2	−8
IRENE	1999	intermittent failure					1	0	0	4	14	10	3	1	−2	−5	−2	0
JOSE	1999	intermittent failure						9	9	8	7	18	−2	−5	−11	−9	2	−3
LENNY	1999	complete success				6	6	6	8	2	−2	−2	12	17	11	1	9	−2
DEBBY	2000	intermittent failure							−5	−2	8	−6	−3	5	−17	−5		
FLORENCE	2000	intermittent failure									−1	−1	−4	0	−5	−0	−1	−2
GORDON	2000	complete failure	0	0	4	6	2	6	9	−5	1	−5						
KEITH	2000	complete success			4	4	7	7	14	14	11	17	−0	−0	−19	−8	−14	0
ERIN	2001	complete success	−4	−4	5	4	1	3	11	10	16	16	5	7				
HUMBERTO	2001	complete success							3	3	14	14	−7	−8				
MICHELLE	2001	complete success				2	3	3	9	14	16	22	6	0	6	−8	−11	−2
GUSTAV	2002	complete failure			0	10	1	4	2	−1	4	−2	1	18				
ISIDORE	2002	complete success	0	0	8	7	4	1	1	5	5	6	12	10	−8	4	5	6
LILI	2002	complete success	−2	−2	−2	2	−1	7	−1	−5	3	2	8	2	2	5	5	5
CLAUDETTE	2003	intermittent failure				−8	−6	−3	−1	12	8	−4	−4	−4	−4	−1	2	0
ERIKA	2003	complete failure					9	2	2	11	−1							
HENRI	2003	complete failure				8	−1	−1	2	2	3	−2	−1	−1	−1			
ALEX	2004	complete success				5	3	7	9	3	2	10	28	−5				
BONNIE	2004	intermittent failure	1	1	1	1	1	1	1	−2	−0	−1	−3	−1	6	2	0	
GASTON	2004	insufficient data																
EMILY	2005	delayed success						9	9	9	14	16	5	1	1	11	−1	−6
FRANKLIN	2005	intermittent failure							3	1	2	3	−2	−1	−1	−1	−1	
KATRINA	2005	delayed success									4	4	4	13	4	11	4	8
OPHELIA	2005	intermittent failure								5	3	5	5	−6	3	−3	9	1
RITA	2005	delayed success					−1	6	10	4	7	14	13	12	8	−10	−7	−2
STAN	2005	complete failure					−0	4	3	20								
WILMA	2005	delayed success									7	5	3	13	27	−6	−1	−4
BETA	2005	insufficient data									5	5	5					
BERYL	2006	complete failure						2	3	3	−0	−4	−2	8				
ERNESTO	2006	intermittent failure				3	2	2	11	0	−7	−7	−7	−5	2	−1	0	1
FLORENCE	2006	intermittent failure					0	0	12	14	6	5	−11	−9				
FELIX	2007	complete success								19	13	11	15	28	6	−6		
DOLLY	2008	intermittent failure				−1	0	0	1	9	7	6	3	12				
FAY	2008	intermittent failure		1	0	−2	14	6	−3	−0	−1	−1	−1	−1	4	−0	1	−2
OMAR	2008	intermittent failure						4	4	15	5	7	9	9				
PALOMA	2008	complete success						8	8	7	4	8	21	12	6	4		
N			9	16	20	33	44	51	61	62	68	64	60	56	46	42	38	36

continued on next page

Table B.5: *continued*

Storm	Year	Case Type	6-h change in combined maximum flight level wind speed from previous period (kt (6 h)$^{-1}$)														
			-60	-48	-36	-24	-18	-12	-06	+00	+06	+12	+18	+24	+36	+48	+60	+72
mean			1.1	1.4	1.3	2.9	3.2	3.1	4.4	5.5	3.7	3.7	2.9	3.9	1.8	−0.3	1.4	−1.9
std. dev.			2.9	3.7	3.6	4.9	4.3	3.5	5.6	7.3	6.0	7.2	7.3	7.8	8.7	7.0	5.2	4.3
minimum			−4	−4	−8	−9	−6	−5	−5	−6	−9	−13	−13	−13	−19	−12	−14	−13
lower quartile			−2	−2	0	−0	0	0	0	−0	−0	−2	−2	−1	−3	−5	−1	−4
median			1.0	0.4	0.9	2.9	2.3	2.5	2.7	4.1	3.3	3.1	1.3	2.3	1.4	−1.1	1.2	−1.6
upper quartile			2	3	4	6	6	6	9	9	7	7	6	9	6	2	4	0
maximum			5	11	8	11	14	9	18	35	16	22	28	28	27	22	10	8

Appendix C

OBSERVATIONS OF WARM RINGS

C.1 Introduction

This appendix contains the seedlings for a future paper which will conduct a systematic observational study of warm rings, eye moats, and hub clouds. The VDM data set has been mined to obtain all the cases of warm rings. These data will be used in conjunction with the already assembled collection of microwave and infrared satellite imagery to construct a climatology of warm ring incidence and to ascertain where in the storm cycle warm rings and hub clouds tend to occur. Intensity trends and strutural changes are calculated for the periods leading up to, and following the warm ring episodes. The HRD flight level data will then be used for several case studies in which we will create radial profiles of tangential wind, temperature, and dew point for several storms which possessed warm rings. A composite profile will be constructued for a broad set of warm ring cases to show common characteristics of warm rings. Finally, we will seek to reconcile these observations with the theoretical prediction that warm rings should be more prevalent when the dynamical eye size is large. The occurrences and implications of this rather rare structure will examined. After considerable work beyond this dissertation, this material will be submitted for publication to *Quarterly Journal of the Royal Meteorological Society* as Vigh and Schubert (2010).

C.2 Methodology

To identify cases with qualified warm rings, the following criteria are used:

(1) The reconaissance aircraft must report a supplementary maximum flight level temperature more than 5 n mi from the flight level center,

(2) The temperature of this supplementary maximum temperature must be at least $+2\,^{\circ}\mathrm{C}$ greater than the maximum temperature reported within 5 n mi of the center, and

(3) The radius of the supplementary maximum temperature report must not exceed the eye radius by more than 3 n mi (it is permitted to be upto 3 n mi within the eyewall).

Table C.1: All cases in the VDM dataset which meet the following qualifications of a warm ring structure: (1) the reconaissance aircraft must report a supplementary maximum flight level temperature more than 5 n mi from the flight level center, (2) the temperature of this supplementary maximum temperature must be at least 2 °C greater than the maximum temperature reported *within* 5 n mi of the center, and (3) the radius of the supplementary maximum temperature report must not exceed the eye radius by more than 3 n mi (it is permitted to be upto 3 n mi within the eyewall).

The storm name, basin (AL = Atlantic, EP = Eastern Pacific), and date and time (UTC) of these warm ring cases are given in the third, fourth, and fifth columns, respectively. The fourth column gives the flight level of the aircraft fix. The fifth, sixth, and seventh columns display the maximum flight level temperatures reported just outside the eyewall ("Outside"), within the eye but greater than 5 n mi of the center ("Ring"), and within 5 n mi of the center ("Center"), respectively. The warm ring strength (maximum temperature of ring - maximum temperature near center) is shown in the ninth column. The radii of the supplementary maximum temperature report ("Ring"), the primary eye ("Eye"), and the radius of maximum wind ("RMW", which is the radius of the maximum inbound flight level wind speed reported for the fix), are given in the tenth, eleventh, and twelfth columns, respectively. The thirteenth column gives the maximum inbound flight level wind speed ("VMAX"), while the fourteenth column lists the minimum Rossby length. Summary statistics of the values in the columns follow the main table.The dynamical eye size is given in the final column.

			Fix	**Maximum FL Temp.**			Ring					Min	Dynamical
		Fix	flight		Warm		strength	Ring	Eye			Rossby	eye
Storm	Basin	Date / time UTC	level	Outside °C	Ring °C	Center °C	ΔT °C	radius n mi	radius n mi	RMW n mi	VMAX kt	length n mi	size
NANA	AL	19 Oct 1990 / 20:05	850 mb	18	25	23	+2	6	4	11	50	14.7	
ERIN	AL	03 Aug 1995 / 06:38	850 mb	18	22	20	+2	13	16	26	65	26.4	0.6
MARILYN	AL	15 Sep 1995 / 08:43	700 mb	8	22	18	+4	9	11	13	77	6.8	1.6
MARILYN	AL	15 Sep 1995 / 20:00	700 mb	10	18	15	+3	8	15	19	67	11.9	1.3
EDOUARD	AL	27 Aug 1996 / 11:22	700 mb	10	18	16	+2	8	15	15	113	6.3	2.4
EDOUARD	AL	29 Aug 1996 / 01:00	700 mb	12	24	17	+7	11	15	16	87	10.0	1.5
EDOUARD	AL	01 Sep 1996 / 03:03	700 mb	8	19	14	+5	14	15	18	102	13.9	1.1
FRAN	AL	31 Aug 1996 / 05:18	850 mb	24	24	21	+3	12	10	10	44	11.1	0.9
FRAN	AL	01 Sep 1996 / 09:30	850 mb	20	23	20	+3	10	20	17	58	15.1	1.3
FRAN	AL	04 Sep 1996 / 20:15	700 mb	14	18	16	+2	15	18	20	96	13.6	1.3
FRAN	AL	05 Sep 1996 / 00:23	700 mb	10	17	15	+2	9	10	50	95	33.6	0.3
LILI	AL	19 Oct 1996 / 08:39	700 mb	20	21	18	+3	13	20	21	77	15.3	1.3
MARCO	AL	22 Nov 1996 / 07:27	850 mb	21	28	17	+11	5	2	6	71	3.3	0.8
BONNIE	AL	22 Aug 1998 / 11:26	850 mb	20	26	24	+2	10	14	24	51	24.2	0.6
BONNIE	AL	24 Aug 1998 / 15:12	700 mb	11	18	15	+3	20	25	45	101	26.2	1.0
DANIELLE	AL	28 Aug 1998 / 01:26	850 mb	20	26	20	+6	6	10	10	54	9.8	1.0
GEORGES	AL	21 Sep 1998 / 16:16	700 mb	10	21	19	+2	8	8	19	67	12.0	0.6
GEORGES	AL	21 Sep 1998 / 17:57	700 mb	13	17	15	+2	8	8	23	70	13.9	0.5
GEORGES	AL	26 Sep 1998 / 14:53	850 mb	21	24	22	+2	12	10	18	69	15.8	0.6
GEORGES	AL	27 Sep 1998 / 11:00	850 mb	18	23	21	+2	11	10	52	81	39.8	0.3
MITCH	AL	24 Oct 1998 / 07:53	850 mb	16	22	20	+2	6	15	23	91	8.6	1.8
MITCH	AL	28 Oct 1998 / 18:03	700 mb	11	16	14	+2	7	6	7	74	3.8	

continued on next page

Table C.1: *continued*

Storm	Basin	Fix Date / time UTC	Fix flight level	Maximum FL Temp. Outside °C	Warm Ring °C	Center °C	Ring strength ΔT °C	Ring radius n mi	Eye radius n mi	RMW n mi	VMAX kt	Min Rossby length n mi	Dynamical eye size
DENNIS	AL	28 Aug 1999 / 04:06	700 mb	11	17	15	+2	9	22	29	78	22.4	1.0
DENNIS	AL	29 Aug 1999 / 17:22	700 mb	9	17	15	+2	7	22	69	89	50.9	0.4
DENNIS	AL	30 Aug 1999 / 03:50	700 mb	11	18	15	+3	18	18	83	84	65.9	0.3
FLOYD	AL	10 Sep 1999 / 23:07	700 mb	9	19	17	+2	10	9	31	82	18.3	
FLOYD	AL	11 Sep 1999 / 07:31	700 mb	10	20	16	+4	9	12	19	77	12.5	1.0
FLOYD	AL	11 Sep 1999 / 09:13	700 mb	10	21	17	+4	11	12	17	102	8.6	1.5
FLOYD	AL	11 Sep 1999 / 17:41	700 mb	11	22	18	+4	13	10	31	75	21.5	0.5
FLOYD	AL	11 Sep 1999 / 19:19	700 mb	12	19	17	+2	6	12	40	66	31.0	0.4
FLOYD	AL	14 Sep 1999 / 09:17	700 mb	11	18	16	+2	8	15	44	103	24.5	
FLOYD	AL	14 Sep 1999 / 20:27	700 mb	13	19	16	+3	14	18	34	97	21.3	0.8
FLOYD	AL	16 Sep 1999 / 04:59	700 mb	11	20	16	+4	20	18	26	105	18.7	
GERT	AL	17 Sep 1999 / 06:54	700 mb	13	18	16	+2	11	18	25	118	9.9	1.8
IRENE	AL	18 Oct 1999 / 05:42	850 mb	19	27	21	+6	4	2	29	67	32.8	0.0
LENNY	AL	15 Nov 1999 / 17:58	850 mb	15	20	18	+2	12	15	25	44	19.8	0.8
LENNY	AL	18 Nov 1999 / 06:37	700 mb	10	23	21	+2	9	9	9	121	3.2	
LENNY	AL	18 Nov 1999 / 11:01	700 mb	16	22	17	+5	10	9	8	101	3.4	2.6
LENNY	AL	18 Nov 1999 / 21:20	700 mb	9	21	17	+4	5	15	6	107	2.4	6.1
DORA	EP	17 Aug 1999 / 11:48	700 mb	10	14	12	+2	15	15	17	78	8.1	1.8
DORA	EP	17 Aug 1999 / 23:46	700 mb	8	16	14	+2	15	12	38	53	26.0	0.5
DORA	EP	18 Aug 1999 / 01:31	700 mb	8	14	11	+3	15	12	18	55	12.2	1.0
EUGENE	EP	12 Aug 1999 / 23:26	700 mb	8	16	14	+2	9	12	53	49	36.3	0.3
FLORENCE	AL	12 Sep 2000 / 16:29	850 mb	18	20	18	+2	7	12	19	64	20.5	
DANIEL	EP	30 Jul 2000 / 01:17	700 mb	9	15	13	+2	13	12	19	45	19.3	
ERIN	AL	09 Sep 2001 / 06:10	700 mb	7	13	11	+2	18	20	17	78	15.3	1.3
IRIS	AL	08 Oct 2001 / 18:07	700 mb	9	16	14	+2	6	5	4	107	1.5	3.3
IRIS	AL	08 Oct 2001 / 22:59	700 mb	9	20	15	+5	6	5	5	126	1.6	3.1
ISIDORE	AL	21 Sep 2002 / 20:55	700 mb	13	18	16	+2	8	8	13	92	7.4	1.0
LILI	AL	30 Sep 2002 / 12:29	850 mb	18	22	20	+2	6	8	12	60	9.4	0.8
KENNA	EP	25 Oct 2002 / 11:58	700 mb	10	23	18	+5	7	10	30	128	11.3	0.9
KENNA	EP	25 Oct 2002 / 13:35	700 mb	10	23	16	+7	13	10	19	96	9.8	1.0
CLAUDETTE	AL	15 Jul 2003 / 02:08	850 mb	16	22	20	+2	10	14	20	60	21.1	0.7
CLAUDETTE	AL	15 Jul 2003 / 12:52	700 mb	9	15	13	+2	8	15	20	51	25.1	0.6
ERIKA	AL	16 Aug 2003 / 06:50	700 mb	11	18	16	+2	8	8	28	62	26.3	0.3
FABIAN	AL	05 Sep 2003 / 05:38	700 mb	11	19	17	+2	9	20	35	113	20.2	1.0
ISABEL	AL	13 Sep 2003 / 17:18	700 mb	8	18	15	+3	15	22	24	147	8.7	2.6

continued on next page

Table C.1: *continued*

Storm	Basin	Fix Date / time UTC	Fix flight level	Maximum FL Temp. Outside °C	Warm Ring °C	Center °C	Ring strength ΔT °C	Ring radius n mi	Eye radius n mi	RMW n mi	VMAX kt	Min Rossby length n mi	Dynamical eye size
ISABEL	AL	13 Sep 2003 / 18:53	700 mb	10	18	15	+3	5	20	22	132	8.9	2.2
ISABEL	AL	15 Sep 2003 / 17:13	700 mb	14	18	15	+3	18	28	36	95	22.0	
OLAF	EP	05 Oct 2003 / 22:26	850 mb	17	25	23	+2	10	15	57	59	37.9	
ALEX	AL	04 Aug 2004 / 01:33	700 mb	9	18	16	+2	19	25	27	75	28.5	0.9
FRANCES	AL	31 Aug 2004 / 06:55	700 mb	10	18	16	+2	13	18	18	121	7.0	
FRANCES	AL	01 Sep 2004 / 20:35	700 mb	9	20	17	+3	7	15	17	126	7.1	2.1
FRANCES	AL	02 Sep 2004 / 08:55	700 mb	16	21	19	+2	11	12	8	97	4.5	2.6
FRANCES	AL	02 Sep 2004 / 18:18	700 mb	14	18	15	+3	8	10	17	81	11.8	0.8
FRANCES	AL	02 Sep 2004 / 20:07	700 mb	14	18	16	+2	10	10	15	104	8.2	1.2
IVAN	AL	08 Sep 2004 / 07:51	700 mb	8	20	16	+4	7	9	13	133	2.9	3.1
IVAN	AL	08 Sep 2004 / 19:28	700 mb	9	20	16	+4	9	6	8	128	2.0	3.0
IVAN	AL	11 Sep 2004 / 17:30	700 mb	10	19	17	+2	6	9	12	141	3.7	2.4
IVAN	AL	13 Sep 2004 / 10:12	700 mb	9	19	17	+2	10	15	18	151	5.8	2.6
IVAN	AL	13 Sep 2004 / 22:27	700 mb	12	19	17	+2	7	10	15	120	6.4	1.6
IVAN	AL	14 Sep 2004 / 07:11	700 mb	11	24	18	+6	11	10	14	112	6.7	1.5
IVAN	AL	14 Sep 2004 / 08:07	700 mb	11	21	17	+4	9	10	16	116	7.4	1.4
IVAN	AL	14 Sep 2004 / 11:36	700 mb	10	20	16	+4	15	12	33	112	15.8	0.8
IVAN	AL	14 Sep 2004 / 12:51	700 mb	10	21	17	+4	18	15	29	126	12.5	1.2
IVAN	AL	14 Sep 2004 / 14:03	700 mb	12	21	16	+5	11	22	28	117	13.0	
IVAN	AL	14 Sep 2004 / 15:40	700 mb	13	20	16	+4	19	20	27	102	14.5	1.4
IVAN	AL	14 Sep 2004 / 17:21	700 mb	11	18	16	+2	15	20	25	119	11.7	1.7
JEANNE	AL	21 Sep 2004 / 06:10	850 mb	18	24	22	+2	8	22	24	88	17.3	1.3
JEANNE	AL	25 Sep 2004 / 12:47	700 mb	11	19	17	+2	12	18	19	99	11.9	
JEANNE	AL	25 Sep 2004 / 16:06	700 mb	11	18	16	+2	11	12	27	94	17.7	
DENNIS	AL	09 Jul 2005 / 14:59	700 mb	13	15	13	+2	9	8	13	64	11.8	0.6
EMILY	AL	14 Jul 2005 / 23:46	700 mb	7	16	14	+2	6	4	6	101	1.9	2.1
EMILY	AL	16 Jul 2005 / 00:56	700 mb	11	19	14	+5	6	4	5	103	1.8	
EMILY	AL	16 Jul 2005 / 02:20	700 mb	12	23	17	+6	5	5	7	77	3.3	1.5
EMILY	AL	17 Jul 2005 / 12:01	700 mb	9	17	15	+2	7	5	7	119	2.6	1.9
EMILY	AL	18 Jul 2005 / 00:14	700 mb	15	22	17	+5	8	6	8	77	4.9	1.2
EMILY	AL	18 Jul 2005 / 01:35	700 mb	7	23	16	+7	6	6	15	118	6.0	1.0
EMILY	AL	18 Jul 2005 / 03:29	700 mb	10	23	15	+8	5	6	11	141	3.8	1.6
EMILY	AL	19 Jul 2005 / 09:29	700 mb	9	16	13	+3	11	15	49	79	32.9	
KATRINA	AL	27 Aug 2005 / 11:07	700 mb	16	23	20	+3	7	4	31	85	20.5	0.2
KATRINA	AL	27 Aug 2005 / 17:15		9	21	18	+3	16	25	38	83	25.6	1.0

continued on next page

Table C.1: *continued*

Storm	Basin	Fix Date / time UTC	Fix flight level	Maximum FL Temp. Outside °C	Warm Ring °C	Center °C	Ring strength ΔT °C	Ring radius n mi	Eye radius n mi	RMW n mi	VMAX kt	Min Rossby length n mi	Dynamical eye size
NATE	AL	08 Sep 2005 / 05:59	700 mb	13	16	14	+2	18	18	27	59	30.6	0.6
OPHELIA	AL	15 Sep 2005 / 13:21	850 mb	16	26	20	+6	16	16	35	69	38.1	
PHILIPPE	AL	19 Sep 2005 / 05:17	700 mb	7	18	14	+4	6	8	6	72	3.4	2.4
RITA	AL	20 Sep 2005 / 15:17	700 mb	11	20	15	+5	6	19	19	77	13.8	
RITA	AL	20 Sep 2005 / 15:43	700 mb	11	20	15	+5	6	19	19	77	13.8	
RITA	AL	23 Sep 2005 / 08:31	700 mb	11	18	16	+2	8	16	22	126	10.9	1.5
WILMA	AL	24 Oct 2005 / 01:12	700 mb	8	16	14	+2	24	22	27	114	13.4	1.7
WILMA	AL	24 Oct 2005 / 02:46	700 mb	9	18	15	+3	15	28	36	105	19.3	1.4
WILMA	AL	24 Oct 2005 / 05:54	700 mb	11	18	15	+3	14	30	24	80	17.4	1.7
WILMA	AL	24 Oct 2005 / 09:32	700 mb	10	18	16	+2	12	30	19	84	13.6	2.2
ADRIAN	EP	19 May 2005 / 16:55	850 mb	14	27	23	+4	10	10	6	83	2.2	4.5
DEAN	AL	16 Aug 2007 / 17:33	700 mb	14	21	19	+2	6	6	6	75	2.7	
FELIX	AL	03 Sep 2007 / 19:00	700 mb	9	20	17	+3	6	8	7	95	2.6	2.9
FELIX	AL	03 Sep 2007 / 20:41		9	15	13	+2	6	8	14	79	6.1	1.2
GUSTAV	AL	26 Aug 2008 / 07:36	700 mb	8	17	15	+2	7	10	14	91	6.3	1.6
IKE	AL	06 Sep 2008 / 17:11	700 mb	7	18	14	+4	13	15	11	100	5.7	2.6
PALOMA	AL	06 Nov 2008 / 19:20	850 mb	17	21	19	+2	9	8	17	52	12.6	0.7
PALOMA	AL	07 Nov 2008 / 19:43	700 mb	10	18	16	+2	7	8	18	90	8.9	0.9
N				110	110	110	110	110	110	110	110	110	90
minimum				7	13	11	+2	4	2	4	44	1.5	0.0
maximum				24	28	24	+11	24	30	83	151	65.9	6.1
average				12.0	19.8	16.6	3.1	10.3	13.3	22.0	89.7	14.59	1.41
std. dev.				3.8	3.1	2.6	1.6	4.1	6.2	13.7	25.3	11.15	0.97

Appendix D

UNREFERENCED TABLES

The Vortex Data Message data set has proven to be a veritable gold mine for a more general exploration of the inner core structure of tropical cyclones. Because these data have not been previously available, extensive summary tables have been prepared to document selected aspects of hurricane structure and intensity that may be of interest to the broader tropical cyclone research community.

The first table is a summary of the top 30 aircraft-observed storms ranked by the highest maximum flight level wind speed observed in each storm. Following tables list the storms which had largest and smallest eye diameters, the largest and smallest radii of maximum winds, and the largest and smallest minimum Rossby radius of deformation. Additional tables list all of the storms which had dynamically-large and dynamically-small eyes, all storms with central dew point temperature depressions exceeding (15 °C), and all storms with a horizontal temperature difference across the eyewall exceeding 10 °C. The final table lists all cases for which aircraft observed concentric eyewalls.

D.1 Tables summarizing extreme observations

This section presents tables which summarize the top 15 or top 30 extreme measurements from the VDM data set for the following parameters: highest FL maximum wind speed (FL v_{max}), largest and smallest radius of maximum winds at flight level (FL r_{max}), largest and smallest eye diameter (d_{eye}), largest and smallest minimum Rossby length computed from flight level winds (FL $\lambda_{R,min}$), largest and smallest dynamical eye size. The values of additional intensity, thermodynamic, and structure parameters

are given for the fix time in which the extreme value was measured.

Table D.1: A summary of the top 30 cases with the highest maximum flight level wind speed in the VDM data set. This maximum wind speed is the combined maximum value of the inbound and outbound legs and may not match the fix time exactly. The storm name, basin (AL = Atlantic, EP = Eastern Pacific), and date and time (UTC) of fix are given in the first, second, and third columns, respectively. The fourth column gives the flight level of the aircraft fix. The minimum sea level pressure ("MSLP", hPa) measured during the fix is given fifth column. The maximum flight level temperatures reported just outside the eyewall ("Outside") and within 5 n mi of the center ("Eye") are given in the sixth and seventh columns, respectively. The corresponding dew point temperature at the location of maximum flight level temperature in the eye is given in the eighth column.The flight level dew point temperature depression, $T - T_d$, at the location of maximum flight temperature (°C, measured within 5 n mi of the storm center) is given in the ninth column. The flight level baroclinity (°C, tenth column). The diameter of the primary eye and the radius of maximum wind ("RMW", given by the radius of the maximum inbound flight level wind speed reported for the fix), are given in the eleventh and twelfth columns, respectively. The thirteenth column gives the maximum inbound flight level wind speed ("VMAX"), while the fourteenth column lists the minimum Rossby length. The dynamical eye size is given in the final column.

Storm	Basin	Fix date / time UTC	Fix flight level	MSLP hPa	Outside T °C	Eye T °C	Eye T_d °C	T - T_d °C	Baro-clinity °C	Eye diameter n mi	RMW n mi	VMAX kt	Min Rossby length n mi	Dynamical eye size
ANDREW	AL	23 Aug 1992 / 15:27	700 mb	926	10	21	3	18	11	8	7	170	2.5	1.6
WILMA	AL	19 Oct 2005 / 06:11	700 mb	892	10	24	11	13	14	2	3	168	0.7	1.4
MITCH	AL	26 Oct 1998 / 19:00	700 mb	905	10	22	11	11	12	20	14	168	3.4	2.9
WILMA	AL	19 Oct 2005 / 08:00	700 mb	884	10	24	10	14	14	4	3	166	0.8	2.7
KATRINA	AL	28 Aug 2005 / 14:17	700 mb	907	12	26	6	20	14	22	14	166	6.1	1.8
DEAN	AL	21 Aug 2007 / 06:48	700 mb	907	9	21	14	7	12	15	9	165	3.3	2.3
RITA	AL	22 Sep 2005 / 05:38	700 mb	898	9	28	3	25	19	16	12	165	4.3	1.9
DEAN	AL	21 Aug 2007 / 08:14	700 mb	906	11	23	12	11	12	15	8	164	3.1	2.4
FELIX	AL	03 Sep 2007 / 12:27	700 mb	942	10	22	6	16	12	8	3	162	0.9	4.3
DEAN	AL	20 Aug 2007 / 23:46	700 mb	914	9	21	17	4	12	16	8	162	2.3	3.5
WILMA	AL	19 Oct 2005 / 04:32	850 mb	901	17	26	25	1	9	4	3	162	0.8	2.6
HUGO	AL	15 Sep 1989 / 23:40	700 mb	923	11	24	6	18	13	9	5	162	1.3	3.5
RITA	AL	21 Sep 2005 / 19:36	700 mb	914	8	27	2	25	19	20	16	161	5.7	1.7
IVAN	AL	11 Sep 2004 / 19:17	700 mb	918	9	22	11	11	13	17	12	161	3.3	2.6
DEAN	AL	21 Aug 2007 / 07:31	700 mb	909	15	22	13	9	7	15	9	160	2.5	3.0
KATRINA	AL	28 Aug 2005 / 17:55	700 mb	902	14	29	6	23	15	25	22	160	8.5	1.5
RITA	AL	22 Sep 2005 / 11:10	700 mb	907	11	27	5	22	16	18	9	159	4.0	
ISABEL	AL	13 Sep 2003 / 18:53	700 mb	932	10	15	15	0	5	40	22	158	8.9	2.2
JOHN	EP	23 Aug 1994 / 01:28	700 mb	929	8	19	10	9	11	22	14	157	3.6	3.0
JOHN	EP	22 Aug 1994 / 23:35	700 mb	929	10	20	9	11	10	25	16	157	3.5	3.6
DEAN	AL	21 Aug 2007 / 06:05	700 mb	909	12	23	12	11	11	15	12	156	3.4	2.2
IVAN	AL	09 Sep 2004 / 11:41	700 mb	921	9	20	13	7	11	10	7	156	1.6	3.2
ISABEL	AL	12 Sep 2003 / 19:01	700 mb	920	11	20	12	8	9	30	18	156	6.6	2.3
JOHN	EP	23 Aug 1994 / 12:14	700 mb	936	10	20	10	10	10	15	15	156	3.3	2.2
FELIX	AL	03 Sep 2007 / 06:57	700 mb	931	9	26	12	14	17	10	6	155	1.7	2.9

continued on next page

Table D.1: *continued*

Storm	Basin	Fix date / time UTC	Fix flight level	MSLP hPa	Outside T °C	Eye T °C	Eye T_d °C	T - T_d °C	Baro-clinity °C	Eye diameter n mi	RMW n mi	VMAX kt	Min Rossby length n mi	Dynamical eye size
DEAN	AL	20 Aug 2007 / 23:02	700 mb	915	11	21	18	3	10	16	9	155	3.6	2.2
IVAN	AL	12 Sep 2004 / 23:59	700 mb	916	13	19	17	2	6	17	18	155	5.4	1.6
MITCH	AL	26 Oct 1998 / 17:12	700 mb	906	11	21	13	8	10	20	7	155	1.9	5.4
MITCH	AL	25 Oct 1998 / 19:03	700 mb	924	13	22	5	17	9	17	6	155	1.6	5.5
JOHN	EP	23 Aug 1994 / 23:01	700 mb	937	13	19	10	9	6	17	9	155	3.0	2.9

Table D.2: A summary of the fifteen smallest and largest reported eye diameters in the VDM data set. The storm name, basin (AL = Atlantic, EP = Eastern Pacific), and date and time (UTC) of fix are given in the first, second, and third columns, respectively. The fourth column gives the flight level of the aircraft fix. The minimum sea level pressure ("MSLP", hPa) measured during the fix is given fifth column. The maximum flight level temperatures reported just outside the eyewall ("Outside") and within 5 n mi of the center ("Eye") are given in the sixth and seventh columns, respectively. The corresponding dew point temperature at the location of maximum flight level temperature in the eye is given in the eighth column.The flight level dew point temperature depression, $T - T_d$, at the location of maximum flight temperature (°C, measured within 5 n mi of the storm center) is given in the ninth column. The flight level baroclinity (°C, tenth column). The diameter of the primary eye and the radius of maximum wind ("RMW", given by the radius of the maximum inbound flight level wind speed reported for the fix), are given in the eleventh and twelfth columns, respectively. The thirteenth column gives the maximum inbound flight level wind speed ("VMAX"), while the fourteenth column lists the minimum Rossby length. The dynamical eye size is given in the final column.

Storm	Basin	Fix date / time UTC	Fix flight level	MSLP hPa	Outside T °C	Eye T °C	Eye T_d °C	$T - T_d$ °C	Baro-clinity °C	Eye diameter n mi	RMW n mi	VMAX kt	Min Rossby length n mi	Dynamical eye size
Smallest eye diameters														
EMILY	AL	27 Aug 1993 / 11:53	850 mb	993	16	18	18	0	2	2	67	56	65.9	0.0
WILMA	AL	19 Oct 2005 / 06:11	700 mb	892	10	24	11	13	14	2	3	168	0.7	1.4
IRENE	AL	18 Oct 1999 / 05:42	850 mb	964	19	21			2	3	29	67	32.8	0.0
FLORENCE	AL	13 Sep 2000 / 16:54	850 mb	989	18	20	18	2	2	3	12	48	17.4	0.1
IRIS	AL	08 Oct 2001 / 11:19	700 mb	954	11	18	9	9	7	3	4	134	1.2	1.2
WILMA	AL	20 Oct 2005 / 08:34	700 mb	906	16	22	17	5	6	3	21	120	7.6	0.2
GERT	AL	20 Sep 1993 / 04:01	850 mb	984	16	20	18	2	4	4	62	80	37.0	0.1
WILMA	AL	19 Oct 2005 / 04:32	850 mb	901	17	26	25	1	9	4	3	162	0.8	2.6
WILMA	AL	19 Oct 2005 / 08:00	700 mb	884	10	24	10	14	14	4	3	166	0.8	2.7
WILMA	AL	19 Oct 2005 / 18:06	700 mb	892	12	20	15	5	8	4	2	128	0.7	3.0
WILMA	AL	19 Oct 2005 / 21:39	700 mb	892	13	16	16	0	3	4	2	114	0.8	2.6
WILMA	AL	20 Oct 2005 / 05:13	700 mb	899	16	18	18	0	2	4	34	120	12.1	0.2
WILMA	AL	20 Oct 2005 / 06:49	700 mb	903	16	17	17	0	1	4	26	112	10.0	0.2
IKE	AL	11 Sep 2008 / 09:05	700 mb	947	7	16	13	3	9	4	98	93	56.9	0.0
CHANTAL	AL	01 Aug 1989 / 09:23	850 mb	984	17	19	19	0	2	5	25	66	24.9	0.1
Largest eye diameters														
OPHELIA	AL	12 Sep 2005 / 20:26	850 mb	988	19	19	16	3	0	90	50	65	51.9	
IRENE	AL	12 Aug 2005 / 19:29	850 mb	997	13	21	16	5	8	80	42	61	42.9	0.9
WILMA	AL	22 Oct 2005 / 19:20	700 mb	957	11	14	14	0	3	75	51	81	30.6	1.2
WILMA	AL	22 Oct 2005 / 23:02	700 mb	959	11	14	14	0	3	70	31	87	17.9	2.0
WILMA	AL	22 Oct 2005 / 17:49	700 mb	958	11	14	14	0	3	70	40	90	21.9	
IRENE	AL	12 Aug 2005 / 20:23	850 mb	997	16	20	16	4	4	70	34	75	29.0	
FELIX	AL	18 Aug 1995 / 00:34	850 mb	973	18	20	19	1	2	70	45	73	47.7	0.7

continued on next page

Table D.2: *continued*

Storm	Basin	Fix date / time UTC	Fix flight level	MSLP hPa	Outside T °C	Eye T °C	Eye T_d °C	T - T_d °C	Baro-clinity °C	Eye diameter n mi	RMW n mi	VMAX kt	Min Rossby length n mi	Dynamical eye size
WILMA	AL	24 Oct 2005 / 07:47	700 mb	953	9	14	14	0	5	65	20	80	14.8	2.2
WILMA	AL	24 Oct 2005 / 06:59	700 mb	952	8	17	12	5	9	65	46	135	19.8	1.6
WILMA	AL	23 Oct 2005 / 11:06	700 mb	961	10	14	14	0	4	65	93	68	64.8	0.5
WILMA	AL	23 Oct 2005 / 09:17	700 mb	960	10	14	14	0	4	65	76	81	45.9	0.7
WILMA	AL	23 Oct 2005 / 08:05	700 mb	961	8	14	14	0	6	65	35	84	21.2	1.5
WILMA	AL	22 Oct 2005 / 20:41	700 mb	958	12	14	14	0	2	65	36	90	19.9	
GEORGES	AL	24 Sep 1998 / 12:08	850 mb	990	18	20	18	2	2	65	40	44	43.0	0.8
IKE	AL	12 Sep 2008 / 20:38	700 mb	955	11	19	11	8	8	60	71	105	41.4	0.7

Table D.3: A summary of the fifteen smallest and largest reported radii of maximum wind speeds in the VDM data set. The storm name, basin (AL = Atlantic, EP = Eastern Pacific), and date and time (UTC) of fix are given in the first, second, and third columns, respectively. The fourth column gives the flight level of the aircraft fix. The minimum sea level pressure ("MSLP", hPa) measured during the fix is given fifth column. The maximum flight level temperatures reported just outside the eyewall ("Outside") and within 5 n mi of the center ("Eye") are given in the sixth and seventh columns, respectively. The corresponding dew point temperature at the location of maximum flight level temperature in the eye is given in the eighth column.The flight level dew point temperature depression, $T - T_d$, at the location of maximum flight temperature (°C, measured within 5 n mi of the storm center) is given in the ninth column. The flight level baroclinity (°C, tenth column). The diameter of the primary eye and the radius of maximum wind ("RMW", given by the radius of the maximum inbound flight level wind speed reported for the fix), are given in the eleventh and twelfth columns, respectively. The thirteenth column gives the maximum inbound flight level wind speed ("VMAX"), while the fourteenth column lists the minimum Rossby length. The dynamical eye size is given in the final column.

Storm	Basin	Fix date / time UTC	Fix flight level	MSLP hPa	Outside T °C	Eye T °C	Eye T_d °C	T - T_d °C	Baro-clinity °C	Eye diameter n mi	RMW n mi	VMAX kt	Min Rossby length n mi	Dynamical eye size
Smallest radii of maximum wind speed														
HARVEY	AL	21 Sep 1999 / 11:05	850 mb	996	22	23	18	5	1		1	50	8.8	
IRIS	AL	08 Oct 2001 / 09:15	700 mb	956	11	18	9	9	7	5	1	112	0.5	5.5
ERIKA	AL	14 Aug 2003 / 23:43	1500 ft	1008	22	25	24	1	3		1	22	2.9	
CHARLEY	AL	13 Aug 2004 / 19:30	700 mb	945	10	18	8	10	8	5	1	138	0.5	5.5
NANA	AL	18 Oct 1990 / 07:47	850 mb	992	19	23	14	9	4	14	2	64	1.8	
BOB	AL	17 Aug 1991 / 22:32	850 mb	980	18	21	20	1	3	10	2	66	2.6	1.9
ANDREW	AL	21 Aug 1992 / 13:12	1500 ft	1007	24	26	23	3	2	18	2	51	3.2	
GORDON	AL	11 Nov 1994 / 03:37	1500 ft	1003	24	26	21	5	2		2	48	1.6	
ALLISON	AL	04 Jun 1995 / 12:00	850 mb	988	24	19	18	1	−5		2	69	1.7	
MARCO	AL	20 Nov 1996 / 09:23	700 mb	989	11	15	13	2	4		2	64	1.1	
DANNY	AL	17 Jul 1997 / 14:48	1500 ft	1001	26	25	23	2	−1		2	41	3.3	
DANNY	AL	17 Jul 1997 / 23:28	1500 ft	997	24	24	22	2	0		2	57	2.4	
HERMINE	AL	18 Sep 1998 / 16:26	1500 ft	1001	27	28	25	3	1		2	26	4.7	
BRET	AL	19 Aug 1999 / 23:20	1500 ft	1000	23	25	24	1	2	9	2	35	2.7	1.6
EMILY	AL	27 Aug 1999 / 18:47	1500 ft	1007	22	24	24	0	2		2	49	2.0	
Largest radii of maximum wind speed														
TD11	AL	03 Oct 1999 / 12:36	1500 ft	1007	22	24	23	1	2		176	31	180.6	
ISIDORE	AL	24 Sep 2002 / 17:47	850 mb	987	19	19	18	1	0		158	40	151.6	
NOEL	AL	01 Nov 2007 / 23:22	850 mb	981	19	25	15	10	6		155	81	184.1	
KYLE	AL	11 Oct 2002 / 23:09	925 mb	1011	23	21	21	0	−2		144	38	202.9	
TAMMY	AL	05 Oct 2005 / 18:16	1500 ft	1003	21	24	23	1	3		143	53	143.9	
FLOYD	AL	08 Sep 1993 / 12:15	1500 ft	1012	23	23	22	1	0		138	47	154.0	
GRACE	AL	31 Aug 2003 / 07:09	850 mb	1009	18	20	14	6	2		136	32	186.7	

continued on next page

Table D.3: *continued*

Storm	Basin	Fix date / time UTC	Fix flight level	MSLP hPa	Outside T °C	Eye T °C	Eye T_d °C	T - T_d °C	Baro-clinity °C	Eye diameter n mi	RMW n mi	VMAX kt	Min Rossby length n mi	Dynamical eye size
TAMMY	AL	05 Oct 2005 / 20:05	1500 ft	1001	21	24	23	1	3		135	51	152.2	
OPHELIA	AL	16 Sep 2005 / 17:55	700 mb	993	12	15	10	5	3		134	73	120.1	
BERTHA	AL	31 Jul 1990 / 05:32	850 mb	976	17	20	16	4	3		133	63	136.6	
FRANCES	AL	11 Sep 1998 / 01:11	1500 ft	995	26	27	23	4	1		130	59	113.1	
ISIDORE	AL	24 Sep 2002 / 19:32	850 mb	988	17	19	18	1	2		125	54	101.2	
LESLIE	AL	06 Oct 2000 / 06:21	850 mb	1006	18	19	16	3	1		124	33	180.9	
DEBBY	AL	23 Aug 2000 / 10:25	700 mb	1008	10	12	8	4	2		123	65	99.5	
BERTHA	AL	30 Jul 1990 / 23:27	700 mb	974	9	14	10	4	5		122	62	127.7	

Table D.4: A summary of the top 30 cases with the largest minimum Rossby lengths in the VDM data set. The storm name, basin (AL = Atlantic, EP = Eastern Pacific), and date and time (UTC) of fix are given in the first, second, and third columns, respectively. The fourth column gives the flight level of the aircraft fix. The minimum sea level pressure ("MSLP", hPa) measured during the fix is given fifth column. The maximum flight level temperatures reported just outside the eyewall ("Outside") and within 5 n mi of the center ("Eye") are given in the sixth and seventh columns, respectively. The corresponding dew point temperature at the location of maximum flight level temperature in the eye is given in the eighth column.The flight level dew point temperature depression, $T - T_d$, at the location of maximum flight temperature (°C, measured within 5 n mi of the storm center) is given in the ninth column. The flight level baroclinity (°C, tenth column). The diameter of the primary eye and the radius of maximum wind ("RMW", given by the radius of the maximum inbound flight level wind speed reported for the fix), are given in the eleventh and twelfth columns, respectively. The thirteenth column gives the maximum inbound flight level wind speed ("VMAX"), while the fourteenth column lists the minimum Rossby length. The dynamical eye size is given in the final column.

Storm	Basin	Fix date / time UTC	Fix flight level	MSLP hPa	Outside T °C	Eye T °C	Eye T_d °C	T - T_d °C	Baro-clinity °C	Eye diameter n mi	RMW n mi	VMAX kt	Min Rossby length n mi	Dynamical eye size
Smallest minimum Rossby length														
IRIS	AL	08 Oct 2001 / 09:15	700 mb	956	11	18	9	9	7	5	1	112	0.5	5.5
CHARLEY	AL	13 Aug 2004 / 19:30	700 mb	945	10	18	8	10	8	5	1	138	0.5	5.5
WILMA	AL	19 Oct 2005 / 19:56	700 mb	892	12	19	15	4	7	5	2	141	0.6	4.1
WILMA	AL	19 Oct 2005 / 18:06	700 mb	892	12	20	15	5	8	4	2	128	0.7	3.0
WILMA	AL	19 Oct 2005 / 06:11	700 mb	892	10	24	11	13	14	2	3	168	0.7	1.4
WILMA	AL	19 Oct 2005 / 08:00	700 mb	884	10	24	10	14	14	4	3	166	0.8	2.7
WILMA	AL	19 Oct 2005 / 21:39	700 mb	892	13	16	16	0	3	4	2	149	0.8	2.6
WILMA	AL	19 Oct 2005 / 04:32	850 mb	901	17	26	25	1	9	4	3	162	0.8	2.6
FELIX	AL	03 Sep 2007 / 12:27	700 mb	942	10	22	6	16	12	8	3	162	0.9	4.3
IRIS	AL	08 Oct 2001 / 10:38	700 mb	955	13	17	9	8	4	5	3	119	1.1	2.4
MARCO	AL	20 Nov 1996 / 09:23	700 mb	989	11	15	13	2	4		2	64	1.1	
KENNA	EP	24 Oct 2002 / 17:18	700 mb	921	8	19	11	8	11	10	4	145	1.2	4.3
IRIS	AL	08 Oct 2001 / 21:33	700 mb	955	8	15	13	2	7	10	3	100	1.2	4.1
IRIS	AL	08 Oct 2001 / 11:19	700 mb	954	11	18	9	9	7	3	4	134	1.2	1.2
IVAN	AL	09 Sep 2004 / 08:44	700 mb	921	11	20	15	5	9	11	5	134	1.3	4.3
Largest minimum Rossby length														
GORDON	AL	19 Nov 1994 / 09:52	700 mb	994	10	15			5		105	18	239.0	
HENRI	AL	04 Sep 2003 / 06:57	850 mb	1009	17	18	17	1	1		103	29	222.7	
HENRI	AL	04 Sep 2003 / 05:07	850 mb	1012	18	18	16	2	0		103	18	222.0	
KYLE	AL	26 Sep 2008 / 17:34	850 mb	1007	17	20	14	6	3		90	56	216.3	
CHRIS	AL	03 Aug 2006 / 23:19	1500 ft	1012	24	24	24	0	0		79	11	215.7	
CHANTAL	AL	15 Jul 1995 / 01:56	1500 ft	1009	24	24	20	4	0		103	16	209.3	
FLORENCE	AL	15 Sep 2000 / 20:33	850 mb	995	16	22			6		119	26	204.1	

continued on next page

Table D.4: *continued*

Storm	Basin	Fix date / time UTC	Fix flight level	MSLP hPa	Outside T °C	Eye T °C	Eye T_d °C	T - T_d °C	Baro-clinity °C	Eye diameter n mi	RMW n mi	VMAX kt	Min Rossby length n mi	Dynamical eye size
KYLE	AL	11 Oct 2002 / 23:09	925 mb	1011	23	21	21	0	−2		144	38	202.9	
JOSEPHINE	AL	06 Oct 1996 / 12:20	1500 ft	1004	23	24	22	2	1		68	13	201.1	
HANNA	AL	13 Sep 2002 / 17:08	1500 ft	1003	24	25	23	2	1		107	22	200.8	
DENNIS	AL	25 Aug 1999 / 01:30	1500 ft	1008	26	26			0		93	31	200.5	
KYLE	AL	09 Oct 2002 / 17:17	1500 ft	1011	23	24	23	1	1		98	28	198.9	
DEAN	AL	29 Jul 1995 / 00:20	1500 ft	1008	24	24	21	3	0		71	27	197.9	
ANDREW	AL	21 Aug 1992 / 02:13	surface	1014	24	24	19	5	0		89	16	197.8	
EARL	AL	29 Sep 1992 / 02:01	1500 ft	1005	24	25			1		88	20	194.9	

Table D.5: A summary of the cases with the smallest and largest dynamical eye sizes the VDM data set. The storm name, basin (AL = Atlantic, EP = Eastern Pacific), and date and time (UTC) of fix are given in the first, second, and third columns, respectively. The fourth column gives the flight level of the aircraft fix. The minimum sea level pressure ("MSLP", hPa) measured during the fix is given fifth column. The maximum flight level temperatures reported just outside the eyewall ("Outside") and within 5 n mi of the center ("Eye") are given in the sixth and seventh columns, respectively. The corresponding dew point temperature at the location of maximum flight level temperature in the eye is given in the eighth column.The flight level dew point temperature depression, $T - T_d$, at the location of maximum flight temperature (°C, measured within 5 n mi of the storm center) is given in the ninth column. The flight level baroclinity (°C, tenth column). The diameter of the primary eye and the radius of maximum wind ("RMW", given by the radius of the maximum inbound flight level wind speed reported for the fix), are given in the eleventh and twelfth columns, respectively. The thirteenth column gives the maximum inbound flight level wind speed ("VMAX"), while the fourteenth column lists the minimum Rossby length. The dynamical eye size is given in the final column.

Storm	Basin	Fix date / time UTC	Fix flight level	MSLP hPa	Outside T °C	Eye T °C	Eye T_d °C	T - T_d °C	Baro-clinity °C	Eye diameter n mi	RMW n mi	VMAX kt	Min Rossby length n mi	Dynamical eye size
Smallest dynamical eye sizes														
EMILY	AL	27 Aug 1993 / 11:53	850 mb	993	16	18	18	0	2	2	67	56	65.9	0.02
CHANTAL	AL	15 Jul 1995 / 15:35	1500 ft	1007	25	25	24	1	0	8	88	26	138.9	0.03
IKE	AL	11 Sep 2008 / 09:05	700 mb	947	7	16	13	3	9	4	98	93	56.9	0.04
EMILY	AL	27 Aug 1993 / 13:41	850 mb	993	18	17	17	0	−1	6	58	37	83.8	0.04
DENNIS	AL	10 Jul 2005 / 22:19		961	5	11	6	5	6	8	97	62	94.5	0.04
GUSTAV	AL	27 Aug 2008 / 09:18	700 mb	998	6	11	9	2	5	8	93	38	92.4	0.04
IRENE	AL	18 Oct 1999 / 05:42	850 mb	964	19	21			2	3	29	67	32.8	0.05
ROXANNE	AL	14 Oct 1995 / 03:04	850 mb	983	18	20	17	3	2	7	75	53	66.3	0.05
GERT	AL	20 Sep 1993 / 04:01	850 mb	984	16	20	18	2	4	4	62	80	37.0	0.05
ROXANNE	AL	14 Oct 1995 / 05:02	850 mb	983	16	20	18	2	4	8	87	55	73.7	0.05
ALBERTO	AL	02 Jul 1994 / 15:29	1500 ft	1003	24	25	24	1	1	12	63	30	105.3	0.06
ERIKA	AL	16 Aug 2003 / 05:22	700 mb	991	9	16	11	5	7	15	101	36	130.2	0.06
EMILY	AL	27 Aug 1993 / 15:40	850 mb	992	18	17	17	0	−1	5	42	62	39.6	0.06
IKE	AL	11 Sep 2008 / 17:21	700 mb	953	10	16	16	0	6	8	87	75	63.2	0.06
DANIELLE	AL	25 Sep 1992 / 13:23	1500 ft	1003	19	21	19	2	2	10	57	59	70.2	0.07
Largest dynamical eye sizes														
LENNY	AL	18 Nov 1999 / 21:20	700 mb	971	9	17	11	6	8	30	6	107	2.4	6.12
EMILIA	EP	19 Jul 1994 / 23:30	700 mb	926	11	18	12	6	7	15	6	136	1.3	5.81
EMILIA	EP	19 Jul 1994 / 19:59	700 mb	927	9	18	12	6	9	20	8	132	1.7	5.73
MITCH	AL	25 Oct 1998 / 19:03	700 mb	924	13	22	5	17	9	17	6	155	1.6	5.48
IRIS	AL	08 Oct 2001 / 09:15	700 mb	956	11	18	9	9	7	5	1	91	0.5	5.46
CHARLEY	AL	13 Aug 2004 / 19:30	700 mb	945	10	18	8	10	8	5	1	138	0.5	5.46
MITCH	AL	26 Oct 1998 / 17:12	700 mb	906	11	21	13	8	10	20	7	155	1.9	5.38

continued on next page

Table D.5: *continued*

Storm	Basin	Fix date / time UTC	Fix flight level	MSLP hPa	Outside T °C	Eye T °C	Eye T_d °C	T - T_d °C	Baro-clinity °C	Eye diameter n mi	RMW n mi	VMAX kt	Min Rossby length n mi	Dynamical eye size
EMILIA	EP	19 Jul 1994 / 18:14	700 mb	926	10	17	12	5	7	16	8	148	1.5	5.19
KEONI	CP	15 Aug 1993 / 19:43	700 mb	956	10	18	6	12	8	23	8	118	2.3	5.00
GEORGES	AL	19 Sep 1998 / 17:28	700 mb	949	10	20	10	10	10	30	9	112	3.0	4.99
DEAN	AL	18 Aug 2007 / 02:58	700 mb	935	11	20	10	10	9	15	5	117	1.6	4.83
EMILIA	EP	21 Jul 1994 / 03:27	700 mb	935	8	19	11	8	11	24	9	119	2.5	4.73
EMILIA	EP	20 Jul 1994 / 17:10	700 mb	937	9	17	13	4	8	21	9	127	2.2	4.69
ADRIAN	EP	19 May 2005 / 16:55	850 mb	982	14	23	16	7	9	20	6	83	2.2	4.55
KEITH	AL	01 Oct 2000 / 22:23	850 mb	957	17	20	20	0	3	20	7	133	2.3	4.41

D.2 Tables listing all observations exceeding a given threshold

This section of the appendix gives more extensive tables that list all the observations which exceed a given threshold. The following tables are included for all observations for which: eye diameter ≥ 50 n mi, eye diameter ≤ 8 n mi, dynamical eye size ≥ 1.8, dynamical eye size ≤ 0.6, dew point depression $\geq 15\,^{\circ}$C, horizontal temperature difference between the eye and outside the eyewall $\geq 10\,^{\circ}$C, and all cases with aircraft-observed concentric eyewalls. Treating these upper and lower thresholds as a class of storms, summary statistics are given at the bottom of each table which characterize the mean, standard deviation, minimum, and maximum values for the various accompanying thermodynamic and structure information observed along with the parameter of interest.

Table D.6: All cases of the VDM data set which had very large eyes (eye diameter $\geq$ 50 n mi).The storm name, basin (AL = Atlantic, EP = Eastern Pacific), and date and time (UTC) of fix are given in the first, second, and third columns, respectively. The fourth column gives the flight level of the aircraft fix. The minimum sea level pressure ("MSLP", hPa) measured during the fix is given fifth column. The maximum flight level temperatures reported just outside the eyewall ("Outside") and within 5 n mi of the center ("Eye") are given in the sixth and seventh columns, respectively. The corresponding dew point temperature at the location of maximum flight level temperature in the eye is given in the eighth column.The flight level dew point temperature depression, $T - T_d$, at the location of maximum flight temperature (°C, measured within 5 n mi of the storm center) is given in the ninth column. The flight level baroclinity, defined as the difference between the maximum flight level temperature within 5 n mi of the storm center, T_{inside}, and the representative flight level temperature just outside the eyewall, $T_{outside}$ (°C) is given in the tenth column); The diameter of the primary eye and the radius of maximum wind ("RMW", given by the radius of the maximum inbound flight level wind speed reported for the fix), are given in the eleventh and twelfth columns, respectively. The thirteenth column gives the maximum inbound flight level wind speed ("VMAX"), while the fourteenth column lists the minimum Rossby length. The dynamical eye size is given in the final column. Summary statistics of the values in the columns follow the main table.

Storm	Basin	Fix date / time UTC	Fix flight level	MSLP hPa	Outside T °C	Eye T °C	Eye T_d °C	T - T_d °C	Baro-clinity °C	Eye diameter n mi	RMW n mi	VMAX kt	Min Rossby length n mi	Dynamical eye size
GABRIELLE	AL	05 Sep 1989 / 07:57	700 mb		16	17	11	6	1	50	35	90	18.4	1.4
GABRIELLE	AL	06 Sep 1989 / 00:36	700 mb	945	12	16	13	3	4	50	37	110	17.5	1.4
GABRIELLE	AL	07 Sep 1989 / 08:42	700 mb	949	12	15	15	0	3	50	20	78	16.6	1.5
BERTHA	AL	01 Aug 1990 / 12:15	850 mb	977	19	19	16	3	0	50	46	55	67.9	0.4
FERNANDA	EP	16 Aug 1993 / 13:34	700 mb	977	12	15	11	4	3	50	27	87	15.4	
FERNANDA	EP	16 Aug 1993 / 15:17	700 mb	978	10	14	11	3	4	50	28	86	16.2	
FERNANDA	EP	16 Aug 1993 / 17:08	700 mb	977	10	13	11	2	3	50	24	77	15.5	
FELIX	AL	18 Aug 1995 / 00:34	850 mb	973	18	20	19	1	2	70	45	73	47.7	0.7
FELIX	AL	18 Aug 1995 / 02:32	850 mb	973	18	20	20	0	2	60	78	73	78.3	
FELIX	AL	18 Aug 1995 / 05:19	850 mb	971	17	20	19	1	3	60	69	59	84.2	0.4
LUIS	AL	07 Sep 1995 / 23:52	700 mb	935	11	18	14	4	7	58	37	110	18.6	1.6
LUIS	AL	08 Sep 1995 / 02:08	700 mb	936	10	19	14	5	9	58	30	121	14.0	2.1
LUIS	AL	08 Sep 1995 / 23:47	700 mb	945	12	16	13	3	4	50	26	103	16.2	1.5
LUIS	AL	09 Sep 1995 / 01:59	700 mb	947	13	17	12	5	4	50	20	91	14.4	1.7
LUIS	AL	09 Sep 1995 / 05:42	700 mb	949	11	16	13	3	5	50	29	107	18.1	1.4
EDOUARD	AL	30 Aug 1996 / 02:33	700 mb	940	10	19	12	7	9	60	31	87	21.2	1.4
ERIKA	AL	07 Sep 1997 / 03:09	700 mb	981	10	16	6	10	6	55	34	66	23.4	1.2
BONNIE	AL	24 Aug 1998 / 15:12	700 mb	964	11	15	14	1	4	50	45	101	26.2	1.0
GEORGES	AL	24 Sep 1998 / 12:08	850 mb	990	18	20	18	2	2	65	40	44	43.0	0.8
GEORGES	AL	25 Sep 1998 / 11:41	850 mb	982	21	22	17	5	1	55	35	70	27.2	1.0
GEORGES	AL	25 Sep 1998 / 13:17	850 mb	982	17	23	17	6	6	60	30	105	16.1	1.9
GEORGES	AL	25 Sep 1998 / 14:20	850 mb	981	19	24	16	8	5	50	30	66	25.1	1.0
FLOYD	AL	15 Sep 1999 / 01:04	700 mb	933	12	19	15	4	7	50	24	122	12.5	2.0
FLOYD	AL	15 Sep 1999 / 02:57	700 mb	933	11	19	15	4	8	50	36	134	17.2	1.5

continued on next page

Table D.6: *continued*

Storm	Basin	Fix date / time UTC	Fix flight level	MSLP hPa	Outside T °C	Eye T °C	Eye T_d °C	T - T_d °C	Baro-clinity °C	Eye diameter n mi	RMW n mi	VMAX kt	Min Rossby length n mi	Dynamical eye size
FLOYD	AL	15 Sep 1999 / 08:29	700 mb	938	15	18	14	4	3	50	33	97	22.2	1.1
FLOYD	AL	15 Sep 1999 / 10:15	700 mb	941	13	18	13	5	5	50	29	98	19.6	
FLOYD	AL	15 Sep 1999 / 12:02	700 mb	943	12	17	11	6	5	50	36	117	20.6	1.2
FLOYD	AL	15 Sep 1999 / 15:25	700 mb	946	12	18	13	5	6	50	37	109	23.0	1.1
FLOYD	AL	15 Sep 1999 / 19:47	700 mb	949	12	15	14	1	3	50	41	98	28.9	0.9
FLOYD	AL	15 Sep 1999 / 21:04	700 mb	948	13	15	12	3	2	50	48	95	34.9	0.7
FLOYD	AL	15 Sep 1999 / 23:01	700 mb	950	11	16	13	3	5	50	25	82	21.9	1.1
LENNY	AL	15 Nov 1999 / 19:55	850 mb	982	16	19	19	0	3	50	28	69	14.4	1.7
LENNY	AL	16 Nov 1999 / 05:17	850 mb	977	18	23	17	6	5	55	40	55	25.7	
LENNY	AL	16 Nov 1999 / 12:01	700 mb	977	15	16	10	6	1	50	44	59	26.2	1.0
LENNY	AL	16 Nov 1999 / 13:19	700 mb	973	11	18	11	7	7	50	27	65	15.0	1.7
ERIN	AL	09 Sep 2001 / 09:18	700 mb	981	6	11	7	4	5	50	24	105	16.2	
MICHELLE	AL	04 Nov 2001 / 13:20	700 mb	950	16	17	13	4	1	50	24	133	9.0	2.8
MICHELLE	AL	04 Nov 2001 / 17:13	700 mb	949	19	21	10	11	2	50	27	126	10.9	2.3
ISABEL	AL	15 Sep 2003 / 17:13	700 mb	950	14	15	14	1	1	55	36	95	22.0	
ISABEL	AL	17 Sep 2003 / 17:10	700 mb	956	9	15	13	2	6	60	40	95	28.7	1.0
ISABEL	AL	17 Sep 2003 / 20:35	700 mb	955	9	14	13	1	5	50	55	97	38.4	0.7
ALEX	AL	04 Aug 2004 / 01:33	700 mb	973	9	16	9	7	7	50	27	75	28.5	0.9
ALEX	AL	04 Aug 2004 / 03:16	700 mb	972	9	17	10	7	8	60	37	58	48.8	
ALEX	AL	04 Aug 2004 / 05:05	700 mb	973	10	18	14	4	8	55	17	68	20.4	
FRANCES	AL	04 Sep 2004 / 22:24	700 mb	957	9	15	15	0	6	60	39	100	23.9	1.3
IVAN	AL	15 Sep 2004 / 07:15	700 mb	938	13	19	16	3	6	60	25	132	11.5	2.6
IVAN	AL	15 Sep 2004 / 09:17	700 mb	939	13	19	16	3	6	50	25	113	13.5	1.9
IVAN	AL	15 Sep 2004 / 11:05	700 mb	939	15	19	16	3	4	50	24	96	15.4	1.6
IVAN	AL	16 Sep 2004 / 04:07	700 mb	939	19	20	14	6	1	50	43	116	24.7	1.0
JEANNE	AL	20 Sep 2004 / 09:51	850 mb	991	15	19	18	1	4	50	66	59	61.9	0.4
JEANNE	AL	24 Sep 2004 / 21:09	700 mb	964	10	14	11	3	4	50	33	92	21.7	1.2
JEANNE	AL	26 Sep 2004 / 00:28	700 mb	951	11	17	11	6	6	50	33	108	19.0	1.3
JEANNE	AL	26 Sep 2004 / 02:16	700 mb	953	15	16	11	5	1	60	45	102	27.1	1.1
EMILY	AL	18 Jul 2005 / 20:12	700 mb	984	10	16	9	7	6	60	29	59	25.2	1.2
IRENE	AL	12 Aug 2005 / 19:29	850 mb	997	13	21	16	5	8	80	42	61	42.9	0.9
IRENE	AL	12 Aug 2005 / 20:23	850 mb	997	16	20	16	4	4	70	34	75	29.0	
KATRINA	AL	27 Aug 2005 / 17:15		950	9	18	18	0	9	50	38	83	25.6	1.0
OPHELIA	AL	12 Sep 2005 / 20:26	850 mb	988	19	19	16	3	0	90	50	65	51.9	
OPHELIA	AL	14 Sep 2005 / 05:49	700 mb	980	10	15	7	8	5	50	46	62	51.6	0.5

continued on next page

Table D.6: *continued*

Storm	Basin	Fix date / time UTC	Fix flight level	MSLP hPa	Outside T °C	Eye T °C	Eye T_d °C	T - T_d °C	Baro-clinity °C	Eye diameter n mi	RMW n mi	VMAX kt	Min Rossby length n mi	Dynamical eye size
OPHELIA	AL	14 Sep 2005 / 07:06	700 mb	980	9	15	8	7	6	50	39	66	42.1	0.6
OPHELIA	AL	14 Sep 2005 / 08:50	700 mb	980	9	14	8	6	5	50	47	64	51.5	0.5
OPHELIA	AL	14 Sep 2005 / 11:19	700 mb	980	9	14	10	4	5	55	32	80	29.5	
OPHELIA	AL	14 Sep 2005 / 18:37	700 mb	979	10	15	11	4	5	50	27	75	27.1	0.9
OPHELIA	AL	14 Sep 2005 / 20:05	700 mb	979	11	15	10	5	4	50	34	83	30.6	0.8
OPHELIA	AL	14 Sep 2005 / 23:43	700 mb	979	10	14	8	6	4	60	29	74	29.5	1.0
OPHELIA	AL	15 Sep 2005 / 01:07	700 mb	980	8	14	13	1	6	55	27	74	27.6	
OPHELIA	AL	15 Sep 2005 / 02:35	700 mb	980	10	14	9	5	4	50	32	80	30.2	0.8
OPHELIA	AL	15 Sep 2005 / 03:53	700 mb	981	7	14	13	1	7	50	38	75	37.7	0.7
OPHELIA	AL	15 Sep 2005 / 05:39	700 mb	982	7	14	10	4	7	50	32	81	30.0	0.8
RITA	AL	20 Sep 2005 / 16:01		979	14	20	13	7	6	50	43	83	28.1	0.9
WILMA	AL	22 Oct 2005 / 17:49	700 mb	958	11	14	14	0	3	70	40	90	21.9	
WILMA	AL	22 Oct 2005 / 19:20	700 mb	957	11	14	14	0	3	75	51	81	30.6	1.2
WILMA	AL	22 Oct 2005 / 20:41	700 mb	958	12	14	14	0	2	65	36	90	19.9	
WILMA	AL	22 Oct 2005 / 21:53	700 mb	957	12	14	14	0	2	60	34	93	18.3	1.6
WILMA	AL	22 Oct 2005 / 23:02	700 mb	959	11	14	14	0	3	70	31	87	17.9	2.0
WILMA	AL	23 Oct 2005 / 08:05	700 mb	961	8	14	14	0	6	65	35	84	21.2	1.5
WILMA	AL	23 Oct 2005 / 09:17	700 mb	960	10	14	14	0	4	65	76	81	45.9	0.7
WILMA	AL	23 Oct 2005 / 11:06	700 mb	961	10	14	14	0	4	65	93	68	64.8	0.5
WILMA	AL	23 Oct 2005 / 17:50	700 mb	963	8	14	13	1	6	60	59	85	35.9	0.8
WILMA	AL	24 Oct 2005 / 02:46	700 mb	957	9	15	15	0	6	55	36	105	19.3	1.4
WILMA	AL	24 Oct 2005 / 04:21	700 mb	954	12	16	13	3	4	60	36	112	18.4	1.6
WILMA	AL	24 Oct 2005 / 05:54	700 mb	955	11	15	15	0	4	60	24	80	17.4	1.7
WILMA	AL	24 Oct 2005 / 06:59	700 mb	952	8	17	12	5	9	65	46	135	19.8	1.6
WILMA	AL	24 Oct 2005 / 07:47	700 mb	953	9	14	14	0	5	65	20	80	14.8	2.2
WILMA	AL	24 Oct 2005 / 08:39	700 mb	953	9	14	13	1	5	60	40	123	19.1	1.6
WILMA	AL	24 Oct 2005 / 09:32	700 mb	950	10	16	13	3	6	60	19	84	13.6	2.2
WILMA	AL	24 Oct 2005 / 10:14	700 mb	951	13	14	12	2	1	60	25	86	17.4	1.7
HELENE	AL	17 Sep 2006 / 15:46	850 mb	976	17	20	16	4	3	50	18	76	11.6	2.1
BERTHA	AL	11 Jul 2008 / 17:08	700 mb	977	7	12	5	7	5	55	35	80	28.2	1.0
BERTHA	AL	11 Jul 2008 / 18:47	700 mb	976	8	13	5	8	5	55	34	91	24.4	1.1
BERTHA	AL	12 Jul 2008 / 17:06	700 mb	983	8	12	8	4	4	50	40	67	39.2	0.6
BERTHA	AL	12 Jul 2008 / 18:43	700 mb	984	9	12	12	0	3	50	45	72	40.7	0.6
FAY	AL	21 Aug 2008 / 02:10	850 mb	994	16	19	18	1	3	50	47	59	49.6	0.5
IKE	AL	12 Sep 2008 / 20:38	700 mb	955	11	19	11	8	8	60	71	105	41.4	0.7

continued on next page

Table D.6: *continued*

Storm	Basin	Fix date / time UTC	Fix flight level	MSLP hPa	Outside T °C	Eye T °C	Eye T_d °C	T - T_d °C	Baro-clinity °C	Eye diameter n mi	RMW n mi	VMAX kt	Min Rossby length n mi	Dynamical eye size
IKE	AL	12 Sep 2008 / 22:24	700 mb	954	9	16	15	1	7	50	41	90	28.8	0.9
IKE	AL	13 Sep 2008 / 00:46	700 mb	952	9	17	14	3	8	50	27	89	19.7	
IKE	AL	13 Sep 2008 / 01:52	700 mb	953	13	16	14	2	3	50	43	96	28.6	0.9
IKE	AL	13 Sep 2008 / 02:35	700 mb	953	10	16	12	4	6	50	36	83	27.8	0.9
N				97	98	98	98	98	98	98	98	98	98	81
minimum				933	6	11	5	0	0	50	17	44	9.0	0.4
maximum				997	21	24	20	11	9	90	93	135	84.2	2.8
average				963.5	11.9	16.5	13.0	3.5	4.6	55.5	36.9	87.2	27.66	1.22
std. dev.				16.8	3.4	2.7	3.1	2.6	2.2	7.6	13.2	20.1	14.53	0.54

Table D.7: All cases of the VDM data set which had very small eyes (eye diameter $\leq$ 8 n mi).The storm name, basin (AL = Atlantic, EP = Eastern Pacific), and date and time (UTC) of fix are given in the first, second, and third columns, respectively. The fourth column gives the flight level of the aircraft fix. The minimum sea level pressure ("MSLP", hPa) measured during the fix is given fifth column. The maximum flight level temperatures reported just outside the eyewall ("Outside") and within 5 n mi of the center ("Eye") are given in the sixth and seventh columns, respectively. The corresponding dew point temperature at the location of maximum flight level temperature in the eye is given in the eighth column.The flight level dew point temperature depression, $T - T_d$, at the location of maximum flight temperature (°C, measured within 5 n mi of the storm center) is given in the ninth column. The flight level baroclinity, defined as the difference between the maximum flight level temperature within 5 n mi of the storm center, T_{inside}, and the representative flight level temperature just outside the eyewall, $T_{outside}$ (°C) is given in the tenth column); The diameter of the primary eye and the radius of maximum wind ("RMW", given by the radius of the maximum inbound flight level wind speed reported for the fix), are given in the eleventh and twelfth columns, respectively. The thirteenth column gives the maximum inbound flight level wind speed ("VMAX"), while the fourteenth column lists the minimum Rossby length. The dynamical eye size is given in the final column. Summary statistics of the values in the columns follow the main table.

Storm	Basin	Fix date / time UTC	Fix flight level	MSLP hPa	Outside T °C	Eye T °C	Eye T_d °C	T - T_d °C	Baro-clinity °C	Eye diameter n mi	RMW n mi	VMAX kt	Min Rossby length n mi	Dynamical eye size
CHANTAL	AL	01 Aug 1989 / 08:50	850 mb	985	19	19	18	1	0	8	15	50	19.8	0.2
CHANTAL	AL	01 Aug 1989 / 09:23	850 mb	984	17	19	19	0	2	5	25	66	24.9	0.1
HUGO	AL	16 Sep 1989 / 07:06	700 mb	933	11	22	3	19	11	6	10	96	3.8	0.8
HUGO	AL	16 Sep 1989 / 08:42	700 mb	930	12	20	3	17	8	6	10	114	3.3	0.9
HUGO	AL	16 Sep 1989 / 11:49	700 mb	940	14	19	7	12	5	8	6	94	2.4	1.7
KLAUS	AL	06 Oct 1990 / 11:35	1500 ft	995	22	24	21	3	2	5	25	54	19.9	0.1
KLAUS	AL	06 Oct 1990 / 13:31	1500 ft	997	24	25	22	3	1	5	30	50	25.6	0.1
KLAUS	AL	06 Oct 1990 / 15:28	1500 ft	997	25	24	22	2	−1	5	45	56	34.0	0.1
KLAUS	AL	06 Oct 1990 / 17:22	1500 ft	996	24	25	22	3	1	5	15	58	11.5	0.2
NANA	AL	17 Oct 1990 / 23:54	850 mb	990	17	24	9	15	7	8	15	62	13.3	0.3
NANA	AL	18 Oct 1990 / 18:59	700 mb	995	10	14	2	12	4	8	30	48	36.8	0.1
NANA	AL	19 Oct 1990 / 09:20	850 mb	990	16	20	15	5	4	8	15	48	20.3	0.2
CLAUDETTE	AL	06 Sep 1991 / 18:41	850 mb	965	17	20	20	0	3	6	7	112	3.9	0.8
CLAUDETTE	AL	06 Sep 1991 / 20:16	850 mb	961	18	21	19	2	3	6	9	107	5.3	0.6
ANDREW	AL	22 Aug 1992 / 11:54	850 mb	981	16	22	13	9	6	6	9	99	5.6	
ANDREW	AL	23 Aug 1992 / 14:03	700 mb	930	9	19	6	13	10	8	6	143	2.5	1.6
ANDREW	AL	23 Aug 1992 / 15:27	700 mb	926	10	21	3	18	11	8	7	170	2.5	1.6
ANDREW	AL	23 Aug 1992 / 16:48	700 mb	922	12	22	3	19	10	8	6	136	2.7	1.5
ANDREW	AL	23 Aug 1992 / 17:53	700 mb	923	12	22	4	18	10	8	7	154	2.8	1.5
ANDREW	AL	23 Aug 1992 / 20:45	700 mb	927	10	20	7	13	10	8	6	119	3.1	1.3
ANDREW	AL	23 Aug 1992 / 22:32	700 mb	923	8	15	10	5	7	8	5	127	2.4	1.7
ANDREW	AL	24 Aug 1992 / 00:13	700 mb	931	7	14	12	2	7	8	6	116	3.1	1.3
EMILY	AL	27 Aug 1993 / 11:53	850 mb	993	16	18	18	0	2	2	67	56	65.9	0.0
EMILY	AL	27 Aug 1993 / 13:41	850 mb	993	18	17	17	0	−1	6	58	37	83.8	0.0

continued on next page

Table D.7: *continued*

Storm	Basin	Fix date / time UTC	Fix flight level	MSLP hPa	Outside T °C	Eye T °C	Eye T_d °C	T - T_d °C	Baro-clinity °C	Eye diameter n mi	RMW n mi	VMAX kt	Min Rossby length n mi	Dynamical eye size
EMILY	AL	27 Aug 1993 / 15:40	850 mb	992	18	17	17	0	−1	5	42	62	39.6	0.1
EMILY	AL	27 Aug 1993 / 17:36	850 mb	990	18	18	17	1	0	6	15	68	13.6	0.2
GERT	AL	20 Sep 1993 / 04:01	850 mb	984	16	20	18	2	4	4	62	80	37.0	0.1
GERT	AL	20 Sep 1993 / 05:36	850 mb	982	19	20	18	2	1	5	36	69	25.3	0.1
CHANTAL	AL	15 Jul 1995 / 15:35	1500 ft	1007	25	25	24	1	0	8	88	26	138.9	0.0
OPAL	AL	01 Oct 1995 / 09:23	1500 ft	985	24	26	25	1	2	8	6	49	6.2	0.6
OPAL	AL	04 Oct 1995 / 11:31	700 mb	917	13	25	11	14	12	8	8	152	3.4	1.2
OPAL	AL	04 Oct 1995 / 12:31	700 mb	921	15	26	13	13	11	7	10	86	7.5	0.5
OPAL	AL	04 Oct 1995 / 14:31	700 mb	930	12	23	13	10	11	8	57	83	41.9	0.1
OPAL	AL	04 Oct 1995 / 16:16	700 mb	934	15	25	15	10	10	5	10	109	6.1	0.4
ROXANNE	AL	14 Oct 1995 / 00:59	850 mb	981	18	21	17	4	3	8	5	50	5.2	0.8
ROXANNE	AL	14 Oct 1995 / 03:04	850 mb	983	18	20	17	3	2	7	75	53	66.3	0.1
ROXANNE	AL	14 Oct 1995 / 05:02	850 mb	983	16	20	18	2	4	8	87	55	73.7	0.1
ROXANNE	AL	14 Oct 1995 / 13:25	850 mb	981	19	22	20	2	3	8	63	63	49.0	0.1
HORTENSE	AL	09 Sep 1996 / 08:29	850 mb	986	15	20	16	4	5	6	33	89	14.1	
LILI	AL	16 Oct 1996 / 23:25	1500 ft	991	24	26	24	2	2	8	6	47	5.6	0.7
LILI	AL	17 Oct 1996 / 00:10	1500 ft	991	23	25	24	1	2	5	4	51	3.5	0.7
MARCO	AL	22 Nov 1996 / 07:27	850 mb	985	21	17	17	0	−4	5	6	71	3.3	0.8
DANNY	AL	19 Jul 1997 / 11:42	850 mb	984	16	19	17	2	3	6	7	64	7.7	0.4
DANNY	AL	19 Jul 1997 / 12:59	850 mb	984	16	19	17	2	3	6	14	68	14.3	0.2
DANNY	AL	19 Jul 1997 / 15:54	850 mb	986	16	20	18	2	4	8	5	56	6.3	0.6
LINDA	EP	14 Sep 1997 / 19:46	700 mb	963	11	15	14	1	4	6	42	84	25.3	0.1
LINDA	EP	14 Sep 1997 / 21:19	700 mb	961	11	14	14	0	3	6	43	68	31.7	0.1
DANIELLE	AL	29 Aug 1998 / 15:19	850 mb	987	18	22	20	2	4	8	26	58	25.7	0.2
MITCH	AL	26 Oct 1998 / 05:08	700 mb	922	14	19	15	4	5	8	9	124	2.9	1.4
MITCH	AL	28 Oct 1998 / 09:41	700 mb	947	11	20	12	8	9	8	7	88	3.2	1.3
MITCH	AL	28 Oct 1998 / 11:02	700 mb	948	11	21	14	7	10	8	6	95	2.5	1.6
BRET	AL	21 Aug 1999 / 01:22	850 mb	981	19	22	19	3	3	8	6	68	4.7	0.9
BRET	AL	21 Aug 1999 / 11:51	850 mb	979	19	23	20	3	4	7	10	79	7.0	0.5
IRENE	AL	18 Oct 1999 / 02:05	850 mb	973	17	21	19	2	4	8	33	43	54.2	0.1
IRENE	AL	18 Oct 1999 / 05:42	850 mb	964	19	21			2	3	29	67	32.8	0.0
FLORENCE	AL	13 Sep 2000 / 16:54	850 mb	989	18	20	18	2	2	3	12	48	17.4	0.1
IRIS	AL	08 Oct 2001 / 06:20	700 mb	971	11	15	8	7	4	8	6	105	2.4	1.7
IRIS	AL	08 Oct 2001 / 07:51	700 mb	963	17	17	9	8	0	8	3	97	1.3	3.1
IRIS	AL	08 Oct 2001 / 09:15	700 mb	956	11	18	9	9	7	5	1	91	0.5	5.5

continued on next page

Table D.7: *continued*

Storm	Basin	Fix date / time UTC	Fix flight level	MSLP hPa	Outside T °C	Eye T °C	Eye T_d °C	T - T_d °C	Baro-clinity °C	Eye diameter n mi	RMW n mi	VMAX kt	Min Rossby length n mi	Dynamical eye size
IRIS	AL	08 Oct 2001 / 10:38	700 mb	955	13	17	9	8	4	5	3	119	1.1	2.4
IRIS	AL	08 Oct 2001 / 11:19	700 mb	954	11	18	9	9	7	3	4	134	1.2	1.2
JULIETTE	EP	26 Sep 2001 / 17:22	700 mb	940	14	17	15	2	3	7	6	97	2.8	1.3
JULIETTE	EP	26 Sep 2001 / 19:00	700 mb	940	15	17	15	2	2	7	3	81	1.7	2.1
ISIDORE	AL	20 Sep 2002 / 10:03	700 mb	967	11	18	13	5	7	8	5	95	2.7	1.5
LILI	AL	28 Sep 2002 / 23:56	850 mb	1001	18	21	18	3	3	8	18	50	16.0	
LILI	AL	29 Sep 2002 / 01:52	850 mb	1002	16	20	19	1	4	8	9	43	9.4	
LILI	AL	29 Sep 2002 / 13:42	850 mb	996	16	22	17	5	6	8	9	57	7.1	0.6
LILI	AL	29 Sep 2002 / 17:09	850 mb	995	17	22	16	6	5	8	6	66	4.1	1.0
LILI	AL	03 Oct 2002 / 01:07	700 mb	942	14	23	10	13	9	8	10	93	6.8	0.6
BONNIE	AL	09 Aug 2004 / 21:54	1500 ft	1006	22	26	23	3	4	8	13	53	13.3	0.3
CHARLEY	AL	11 Aug 2004 / 14:13	850 mb	996	17	21	16	5	4	5	6	48	5.0	0.5
CHARLEY	AL	12 Aug 2004 / 00:17	850 mb	992	16	19	19	0	3	8	6	60	4.2	0.9
CHARLEY	AL	12 Aug 2004 / 02:12	850 mb	993	16	20	18	2	4	8	7	76	3.9	1.0
CHARLEY	AL	13 Aug 2004 / 17:01	700 mb	954	9	18	11	7	9	8	10	141	4.3	0.9
CHARLEY	AL	13 Aug 2004 / 18:33	700 mb	946	9	20	8	12	11	8	6	102	3.7	1.1
CHARLEY	AL	13 Aug 2004 / 19:04	700 mb	943	13	19	14	5	6	6	7	123	3.6	0.8
CHARLEY	AL	13 Aug 2004 / 19:30	700 mb	945	10	18	8	10	8	5	1	138	0.5	5.5
CHARLEY	AL	13 Aug 2004 / 19:57	700 mb	941	9	20	7	13	11	5	3	148	1.3	1.9
IVAN	AL	06 Sep 2004 / 17:29	700 mb	969	9	18	8	10	9	6	4	53	2.1	
IVAN	AL	06 Sep 2004 / 20:58	700 mb	964	10	17	9	8	7	8	6	106	1.6	2.5
IVAN	AL	06 Sep 2004 / 23:14	700 mb	963	16	19	11	8	3	6	5	79	1.7	1.7
DENNIS	AL	07 Jul 2005 / 19:40	700 mb	957	11	17	12	5	6	8	9	93	4.4	
DENNIS	AL	10 Jul 2005 / 07:57	700 mb	932	11	20	13	7	9	8	6	104	3.8	1.1
DENNIS	AL	10 Jul 2005 / 11:43	700 mb	930	9	21	17	4	12	8	9	131	4.6	0.9
DENNIS	AL	10 Jul 2005 / 13:23	700 mb	930	12	20	14	6	8	8	8	109	5.0	0.8
DENNIS	AL	10 Jul 2005 / 15:13	700 mb	937	12	20	11	9	8	8	5	93	3.7	1.1
DENNIS	AL	10 Jul 2005 / 17:25	700 mb	942	14	19	13	6	5	8	7	112	4.4	0.9
DENNIS	AL	10 Jul 2005 / 17:46	700 mb	942	16	19	12	7	3	8	4	89	3.2	1.3
DENNIS	AL	10 Jul 2005 / 18:18	700 mb	943	11	19	14	5	8	8	5	81	4.3	0.9
DENNIS	AL	10 Jul 2005 / 19:30	700 mb	946	14	20	12	8	6	8	7	117	4.3	0.9
DENNIS	AL	10 Jul 2005 / 22:19		961	5	11	6	5	6	8	97	62	94.5	0.0
EMILY	AL	14 Jul 2005 / 23:46	700 mb	962	7	14	13	1	7	8	6	101	1.9	2.1
EMILY	AL	15 Jul 2005 / 01:30	700 mb	958	7	13	13	0	6	8	6	125	1.6	2.5
EMILY	AL	15 Jul 2005 / 05:03	700 mb	952	9	21	4	17	12	8	5	81	2.1	1.9

continued on next page

Table D.7: *continued*

Storm	Basin	Fix date / time UTC	Fix flight level	MSLP hPa	Outside T °C	Eye T °C	Eye T_d °C	T - T_d °C	Baro-clinity °C	Eye diameter n mi	RMW n mi	VMAX kt	Min Rossby length n mi	Dynamical eye size
EMILY	AL	15 Jul 2005 / 11:57	700 mb	964	9	20	7	13	11	8	10	126	2.7	1.5
EMILY	AL	15 Jul 2005 / 13:30	700 mb	968	13	22	7	15	9	8	8	88	3.2	1.3
IRENE	AL	12 Aug 2005 / 18:14	850 mb	997	17	22	16	6	5	8	24	57	27.0	0.1
KATRINA	AL	24 Aug 2005 / 19:49	1500 ft	1002	23	26	26	0	3	6	12	39	18.3	
KATRINA	AL	27 Aug 2005 / 20:09	700 mb	945	11	19	13	6	8	8	29	85	19.4	0.2
WILMA	AL	18 Oct 2005 / 21:42	850 mb	963	17	20	20	0	3	7	9	82	4.4	0.8
WILMA	AL	18 Oct 2005 / 23:09	850 mb	954	18	22	20	2	4	8	7	80	3.5	1.1
WILMA	AL	19 Oct 2005 / 04:32	850 mb	901	17	26	25	1	9	4	3	162	0.8	2.6
WILMA	AL	19 Oct 2005 / 06:11	700 mb	892	10	24	11	13	14	2	3	168	0.7	1.4
WILMA	AL	19 Oct 2005 / 08:00	700 mb	884	10	24	10	14	14	4	3	166	0.8	2.7
WILMA	AL	19 Oct 2005 / 18:06	700 mb	892	12	20	15	5	8	4	2	128	0.7	3.0
WILMA	AL	19 Oct 2005 / 19:56	700 mb	892	12	19	15	4	7	5	2	141	0.6	4.1
WILMA	AL	19 Oct 2005 / 21:39	700 mb	892	13	16	16	0	3	4	2	114	0.8	2.6
WILMA	AL	20 Oct 2005 / 05:13	700 mb	899	16	18	18	0	2	4	34	120	12.1	0.2
WILMA	AL	20 Oct 2005 / 06:49	700 mb	903	16	17	17	0	1	4	26	112	10.0	0.2
WILMA	AL	20 Oct 2005 / 08:34	700 mb	906	16	22	17	5	6	3	21	120	7.6	0.2
WILMA	AL	20 Oct 2005 / 10:20	700 mb	910	12	19	18	1	7	7	23	122	8.2	0.4
ERNESTO	AL	27 Aug 2006 / 11:30	700 mb	997	6	14	6	8	8	6	15	48	12.8	
LANE	EP	15 Sep 2006 / 19:05	700 mb	985	8	13	13	0	5	8	10	56	8.7	0.5
LANE	EP	16 Sep 2006 / 18:09	700 mb	955	7	20	14	6	13	8	6	110	3.1	1.3
FELIX	AL	03 Sep 2007 / 11:09	700 mb	938	12	25	12	13	13	8	52	130	13.5	0.3
FELIX	AL	03 Sep 2007 / 12:27	700 mb	942	10	22	6	16	12	8	3	112	0.9	4.3
FELIX	AL	03 Sep 2007 / 17:23	700 mb	953	7	19	9	10	12	8	8	114	2.4	1.6
HUMBERTO	AL	13 Sep 2007 / 04:47	850 mb	992	13	21	0	21	8	8	8	79	6.9	0.6
HUMBERTO	AL	13 Sep 2007 / 05:24	850 mb	990	17	22	0	22	5	6	7	55	8.7	0.3
FAY	AL	19 Aug 2008 / 08:18	850 mb	989	16	19	14	5	3	8	14	43	19.4	0.2
GUSTAV	AL	27 Aug 2008 / 07:57	700 mb	999	6	10	10	0	4	6	20	22	38.3	0.1
GUSTAV	AL	27 Aug 2008 / 09:18	700 mb	998	6	11	9	2	5	8	93	38	92.4	0.0
IKE	AL	09 Sep 2008 / 06:18	700 mb	967	11	14	8	6	3	8	20	69	14.9	0.3
IKE	AL	09 Sep 2008 / 07:08	700 mb	966	11	14	8	6	3	6	8	53	7.9	0.4
IKE	AL	09 Sep 2008 / 11:06	700 mb	965	10	14	8	6	4	7	15	49	16.0	0.2
IKE	AL	10 Sep 2008 / 23:06	700 mb	947	11	17	13	4	6	8	35	68	28.8	0.1
IKE	AL	11 Sep 2008 / 02:19		944	16	22	12	10	6	7	7	71	5.8	0.6
IKE	AL	11 Sep 2008 / 05:41	700 mb	947	13	18	10	8	5	8	6	82	4.3	0.9
IKE	AL	11 Sep 2008 / 07:25	700 mb	946	11	17	11	6	6	8	36	97	21.4	0.2

continued on next page

Table D.7: *continued*

Storm	Basin	Fix date / time UTC	Fix flight level	MSLP hPa	Outside T °C	Eye T °C	Eye T_d °C	T - T_d °C	Baro-clinity °C	Eye diameter n mi	RMW n mi	VMAX kt	Min Rossby length n mi	Dynamical eye size
IKE	AL	11 Sep 2008 / 09:05	700 mb	947	7	16	13	3	9	4	98	93	56.9	0.0
IKE	AL	11 Sep 2008 / 11:02	700 mb	946	12	17	10	7	5	8	36	70	29.5	0.1
IKE	AL	11 Sep 2008 / 17:21	700 mb	953	10	16	16	0	6	8	87	75	63.2	0.1
IKE	AL	11 Sep 2008 / 19:14	700 mb	952	8	17	16	1	9	8	61	101	35.0	0.1
N				133	133	133	132	132	133	133	133	133	133	125
minimum				884	5	10	0	0	−4	2	1	22	0.5	0.0
maximum				1007	25	26	26	22	14	8	98	170	138.9	5.5
average				959.9	14.0	19.6	13.6	6.0	5.6	6.8	18.7	86.8	15.23	0.94
std. dev.				29.7	4.5	3.4	5.6	5.3	3.6	1.6	22.3	33.3	22.07	1.03

Table D.8: All cases of the VDM data set which had dynamically-large eyes ($\geq$ 1.8).The storm name, basin (AL = Atlantic, EP = Eastern Pacific), and date and time (UTC) of these dynamically-large eye cases cases are given in the third, fourth, and fifth columns, respectively. The fourth column gives the flight level (FL) of the aircraft fix. The fifth, sixth, and seventh columns display the maximum flight level temperatures reported just outside the eyewall ("Outside"), within the eye but greater than 5 n mi of the center ("Ring"), and within 5 n mi of the center ("Center"), respectively. The warm ring magnitude (maximum temperature of ring - maximum temperature near center) is shown in the eighth column. The radii of the supplementary maximum temperature report ("Ring"), the primary eye ("Eye"), and the radius of maximum wind ("RMW", given by the radius of the maximum inbound flight level wind speed reported for the fix), are given in the ninth, tenth, and eleventh columns, respectively. The thirteenth column gives the maximum inbound flight level wind speed ("VMAX"), while the thirteenth column lists the minimum Rossby length. The dynamical eye size is given in the final column. Values are given in the native units of the VDM data set. Summary statistics of the values in the columns follow the main table.

Storm	Basin	Fix Date / Time UTC	Fix flight level	**Maximum FL Temp.** Outside °C	Warm Ring °C	Center °C	Ring strength ΔT °C	Ring radius n mi	Eye radius n mi	RMW n mi	VMAX kt	Min Rossby length n mi	Dynamical eye size
GABRIELLE	AL	05 Sep 1989 / 05:40	700 mb	14		15			20	20	90	10.6	1.9
GABRIELLE	AL	05 Sep 1989 / 20:59	700 mb	11		15			18	23	124	9.6	1.8
HUGO	AL	15 Sep 1989 / 23:40	700 mb	11		24			4	5	141	1.3	3.5
HUGO	AL	16 Sep 1989 / 23:12	300 mb	11		18			12	13	115	4.4	2.9
HUGO	AL	16 Sep 1989 / 23:17	300 mb	11		18			12	13	115	4.4	2.9
HUGO	AL	17 Sep 1989 / 01:12	700 mb	8		16			15	10	113	3.5	4.3
HUGO	AL	17 Sep 1989 / 03:02	700 mb	9		15			10	12	135	3.5	2.9
HUGO	AL	18 Sep 1989 / 01:04	700 mb	13		19			13	15	93	6.7	1.9
BOB	AL	17 Aug 1991 / 22:32	850 mb	18		21			5	2	53	2.6	1.9
ANDREW	AL	22 Aug 1992 / 13:34	850 mb	18		23			5	3	99	1.9	2.7
ANDREW	AL	22 Aug 1992 / 17:05	700 mb	8		16			8	6	110	3.3	2.2
EMILY	AL	31 Aug 1993 / 17:29	850 mb	17		21			22	16	132	9.6	2.4
KEONI	CP	15 Aug 1993 / 05:48	850 mb	18		24			15	17	106	5.2	2.9
KEONI	CP	15 Aug 1993 / 07:33	850 mb	18		24			12	19	100	6.2	2.0
KEONI	CP	15 Aug 1993 / 17:42	700 mb	10		18			10	13	111	3.9	2.6
KEONI	CP	15 Aug 1993 / 19:43	700 mb	10		18			12	8	118	2.3	5.0
DANIEL	EP	14 Jul 1994 / 05:14	1500 ft	24		24			15	5	27	7.0	2.1
EMILIA	EP	19 Jul 1994 / 18:14	700 mb	10		17			8	8	148	1.5	5.2
EMILIA	EP	19 Jul 1994 / 19:59	700 mb	9		18			10	8	132	1.7	5.7
EMILIA	EP	19 Jul 1994 / 23:30	700 mb	11		18			8	6	136	1.3	5.8
EMILIA	EP	20 Jul 1994 / 01:09	700 mb	11		17			8	9	151	1.8	4.3
EMILIA	EP	20 Jul 1994 / 03:13	700 mb	9		19			6	11	131	2.5	2.4
EMILIA	EP	20 Jul 1994 / 05:05	700 mb	10		18			6	7	118	1.8	3.4
EMILIA	EP	20 Jul 1994 / 11:45	700 mb	9		15			11	13	132	3.0	3.6
EMILIA	EP	20 Jul 1994 / 13:35	700 mb	9		16			11	13	143	2.8	3.9
EMILIA	EP	20 Jul 1994 / 15:12	700 mb	9		15			11	13	150	2.7	4.1

continued on next page

Table D.8: *continued*

Storm	Basin	Fix Date / Time UTC	Fix flight level	Maximum FL Temp. Outside °C	Maximum FL Temp. Warm Ring °C	Maximum FL Temp. Center °C	Ring strength ΔT °C	Ring radius n mi	Eye radius n mi	RMW n mi	VMAX kt	Min Rossby length n mi	Dynamical eye size
EMILIA	EP	20 Jul 1994 / 17:10	700 mb	9		17			10	9	127	2.2	4.7
EMILIA	EP	21 Jul 1994 / 00:12	700 mb	8		19			10	11	132	2.8	3.6
EMILIA	EP	21 Jul 1994 / 03:27	700 mb	8		19			12	9	119	2.5	4.7
EMILIA	EP	21 Jul 1994 / 05:14	700 mb	9		18			10	13	125	3.5	2.8
EMILIA	EP	21 Jul 1994 / 11:39	700 mb	11		17			10	8	110	2.6	3.8
EMILIA	EP	21 Jul 1994 / 13:43	700 mb	10		16			6	9	134	2.4	2.5
GILMA	EP	25 Jul 1994 / 12:28	700 mb	9		15			8	11	96	3.3	2.4
GILMA	EP	25 Jul 1994 / 13:56	700 mb	9		14			8	7	99	2.1	3.9
GILMA	EP	25 Jul 1994 / 15:23	700 mb	10		17			8	6	77	2.3	3.5
GILMA	EP	25 Jul 1994 / 17:11	700 mb	10		18			9	8	113	2.1	4.3
GILMA	EP	26 Jul 1994 / 11:31	700 mb	10		19			15	16	59	8.0	1.9
GILMA	EP	26 Jul 1994 / 13:22	700 mb	9		18			12	15	84	5.3	2.3
GILMA	EP	26 Jul 1994 / 17:01	700 mb	8		18			14	12	60	6.0	2.3
JOHN	EP	22 Aug 1994 / 17:42	700 mb	11		18			12	10	124	2.7	4.2
JOHN	EP	22 Aug 1994 / 23:35	700 mb	10		20			12	16	157	3.5	3.6
JOHN	EP	23 Aug 1994 / 01:28	700 mb	8		19			11	14	133	3.6	3.0
JOHN	EP	23 Aug 1994 / 12:14	700 mb	10		20			8	15	156	3.3	2.2
JOHN	EP	23 Aug 1994 / 15:07	700 mb	10		19			10	14	143	3.4	2.9
JOHN	EP	23 Aug 1994 / 17:28	700 mb	9		20			8	9	128	2.5	3.4
JOHN	EP	23 Aug 1994 / 19:16	700 mb	10		21			9	15	116	4.5	2.0
JOHN	EP	23 Aug 1994 / 20:54	700 mb	9		19			8	8	99	2.9	3.0
JOHN	EP	23 Aug 1994 / 23:01	700 mb	13		19			8	9	110	3.0	2.9
JOHN	EP	24 Aug 1994 / 05:04	700 mb	11		17			9	10	144	2.5	3.5
JOHN	EP	24 Aug 1994 / 06:44	700 mb	12		17			9	10	136	2.7	3.4
JOHN	EP	24 Aug 1994 / 08:33	700 mb	10		17			9	7	106	2.4	3.7
JOHN	EP	24 Aug 1994 / 11:02	700 mb	10		19			9	6	99	2.2	4.0
JOHN	EP	24 Aug 1994 / 17:24	700 mb	10		14			9	13	112	4.3	2.1
JOHN	EP	24 Aug 1994 / 19:13	700 mb	10		17			9	13	124	4.0	2.3
JOHN	EP	24 Aug 1994 / 23:13	700 mb	9		15			9	10	85	4.5	2.0
JOHN	EP	25 Aug 1994 / 06:53	700 mb	9		16			15	14	102	5.3	2.8
FELIX	AL	12 Aug 1995 / 10:44	700 mb	13		18			9	6	117	2.9	3.1
LUIS	AL	03 Sep 1995 / 22:47	700 mb	9		16			18	24	130	7.6	2.3
LUIS	AL	04 Sep 1995 / 01:01	700 mb	11		17			18	30	138	8.9	2.0
LUIS	AL	04 Sep 1995 / 05:24	700 mb	12		17			20	25	122	8.4	2.4
LUIS	AL	04 Sep 1995 / 11:02	700 mb	12		18			20	21	127	6.7	3.0

continued on next page

Table D.8: *continued*

Storm	Basin	Fix Date / Time UTC	Fix flight level	Maximum FL Temp. Outside °C	Warm Ring °C	Center °C	Ring strength ΔT °C	Ring radius n mi	Eye radius n mi	RMW n mi	VMAX kt	Min Rossby length n mi	Dynamical eye size
LUIS	AL	04 Sep 1995 / 13:14	700 mb	10		19			20	28	146	7.8	2.6
LUIS	AL	04 Sep 1995 / 15:19	700 mb	12		18			19	23	123	7.6	2.5
LUIS	AL	04 Sep 1995 / 17:01	700 mb	12		17			15	16	110	6.0	2.5
LUIS	AL	04 Sep 1995 / 23:30	700 mb	12		17			19	15	101	6.1	3.1
LUIS	AL	05 Sep 1995 / 02:02	700 mb	14		17			18	19	117	6.7	2.7
LUIS	AL	05 Sep 1995 / 03:48	700 mb	11		17			17	22	120	7.5	2.3
LUIS	AL	05 Sep 1995 / 05:23	700 mb	11		16			15	18	102	7.3	2.1
LUIS	AL	05 Sep 1995 / 18:19	700 mb	9		14			18	28	126	9.6	1.8
LUIS	AL	05 Sep 1995 / 23:53	700 mb	12		15			20	23	131	7.8	2.6
LUIS	AL	06 Sep 1995 / 02:49	700 mb	10		18			16	20	127	7.0	2.3
LUIS	AL	06 Sep 1995 / 04:24	700 mb	12		17			14	14	96	6.6	2.1
LUIS	AL	06 Sep 1995 / 11:22	700 mb	11		21			16	20	122	7.6	2.0
LUIS	AL	06 Sep 1995 / 13:59	700 mb	11	19	17	+2		15	16	105	7.2	2.1
LUIS	AL	06 Sep 1995 / 15:57	700 mb	14	20	18	+2		14	15	100	7.1	2.0
LUIS	AL	06 Sep 1995 / 17:37	700 mb	11		18			16	17	120	6.8	2.3
LUIS	AL	08 Sep 1995 / 02:08	700 mb	10		19			29	30	121	14.0	2.1
MARILYN	AL	14 Sep 1995 / 12:52	700 mb	8		17			9	9	78	4.0	2.2
MARILYN	AL	15 Sep 1995 / 05:26	700 mb	12		19			8	9	91	3.9	1.9
MARILYN	AL	15 Sep 1995 / 10:29	700 mb	8		20			11	12	98	5.0	2.2
MARILYN	AL	15 Sep 1995 / 12:10	700 mb	10		22			11	8	99	3.3	3.3
MARILYN	AL	15 Sep 1995 / 18:05	700 mb	10		19			20	13	81	6.7	3.0
MARILYN	AL	16 Sep 1995 / 01:33	700 mb	13		17			10	14	110	5.5	1.8
MARILYN	AL	16 Sep 1995 / 06:00	700 mb	8		16			10	9	105	3.8	2.6
MARILYN	AL	16 Sep 1995 / 23:17	700 mb	10		17			8	9	97	4.5	1.9
MARILYN	AL	17 Sep 1995 / 01:00	700 mb	9		17			8	9	116	3.8	2.0
ROXANNE	AL	10 Oct 1995 / 11:06	850 mb	19		23			20	19	88	10.0	2.0
ROXANNE	AL	10 Oct 1995 / 12:54	850 mb	18		22			20	15	98	7.1	2.8
ROXANNE	AL	10 Oct 1995 / 23:09	700 mb	12		20			12	10	98	4.9	2.5
EDOUARD	AL	26 Aug 1996 / 23:34	700 mb	12		17			10	13	125	4.7	2.1
EDOUARD	AL	27 Aug 1996 / 01:24	700 mb	12		22			10	16	136	5.4	1.9
EDOUARD	AL	27 Aug 1996 / 11:22	700 mb	10	18	16	+2	8	15	15	113	6.3	2.4
EDOUARD	AL	27 Aug 1996 / 13:00	700 mb	9	19	18	+1	9	15	18	128	6.7	2.2
EDOUARD	AL	27 Aug 1996 / 17:10	700 mb	11	17	16	+1	10	18	16	111	7.0	2.5
EDOUARD	AL	28 Aug 1996 / 23:13	700 mb	12	22	18	+4		15	10	100	5.5	2.8
EDOUARD	AL	29 Aug 1996 / 20:49	700 mb	4		13			8	7	106	3.9	1.9

continued on next page

Table D.8: *continued*

Storm	Basin	Fix Date / Time UTC	Fix flight level	Maximum FL Temp. Outside °C	Maximum FL Temp. Warm Ring °C	Maximum FL Temp. Center °C	Ring strength ΔT °C	Ring radius n mi	Eye radius n mi	RMW n mi	VMAX kt	Min Rossby length n mi	Dynamical eye size
EDOUARD	AL	30 Aug 1996 / 16:30	700 mb	10		16			15	16	134	7.9	1.9
ERIKA	AL	07 Sep 1997 / 23:38	850 mb	19		25			14	14	88	8.0	1.8
GEORGES	AL	19 Sep 1998 / 17:28	700 mb	10		20			15	9	112	3.0	5.0
GEORGES	AL	19 Sep 1998 / 19:13	700 mb	8		18			12	15	146	3.9	3.2
GEORGES	AL	19 Sep 1998 / 20:48	700 mb	9		20			12	11	118	3.5	3.5
GEORGES	AL	20 Sep 1998 / 06:13	700 mb	10		23			10	15	144	4.0	2.5
GEORGES	AL	21 Sep 1998 / 09:08	700 mb	10		21			15	13	89	6.1	2.5
GEORGES	AL	21 Sep 1998 / 11:03	700 mb	11		20			8	8	72	4.7	1.8
GEORGES	AL	22 Sep 1998 / 13:33	700 mb	9		15			16	17	104	7.2	2.3
GEORGES	AL	25 Sep 1998 / 13:17	850 mb	17		23			30	30	105	16.1	1.9
MITCH	AL	24 Oct 1998 / 19:19	850 mb	17		22			18	21	86	8.9	2.0
MITCH	AL	25 Oct 1998 / 07:57	700 mb	11		19			10	15	119	4.9	2.0
MITCH	AL	25 Oct 1998 / 11:32	700 mb	9		18			10	13	111	4.6	2.2
MITCH	AL	25 Oct 1998 / 13:26	700 mb	11		19			9	14	124	4.4	2.0
MITCH	AL	25 Oct 1998 / 17:15	700 mb	13		19			9	10	138	2.9	3.1
MITCH	AL	25 Oct 1998 / 19:03	700 mb	13		22			8	6	155	1.6	5.5
MITCH	AL	26 Oct 1998 / 17:12	700 mb	11		21			10	7	155	1.9	5.4
MITCH	AL	26 Oct 1998 / 19:00	700 mb	10		22			10	14	168	3.4	2.9
MITCH	AL	26 Oct 1998 / 20:00	700 mb	13		20			10	12	146	3.4	2.9
MITCH	AL	27 Oct 1998 / 05:18	700 mb	11		18			10	13	148	3.7	2.6
MITCH	AL	27 Oct 1998 / 06:52	700 mb	12		17			11	12	145	3.5	3.2
MITCH	AL	27 Oct 1998 / 08:15	700 mb	15		16			10	12	131	3.8	2.6
MITCH	AL	27 Oct 1998 / 20:48	700 mb	12		19			10	13	112	4.7	2.1
MITCH	AL	27 Oct 1998 / 21:33	700 mb	13		17			11	16	120	5.4	2.0
MITCH	AL	27 Oct 1998 / 22:40	700 mb	10		16			10	10	123	3.3	3.0
MITCH	AL	27 Oct 1998 / 23:40	700 mb	12		16			10	15	128	4.7	2.1
MITCH	AL	28 Oct 1998 / 05:48	700 mb	12		21			8	10	99	4.0	1.9
LESTER	EP	17 Oct 1998 / 11:30	700 mb	8		14			10	12	93	4.6	2.2
LESTER	EP	17 Oct 1998 / 13:16	700 mb	4		14			10	11	93	4.2	2.4
LESTER	EP	17 Oct 1998 / 14:16	700 mb	6		14			10	12	90	4.7	2.1
LESTER	EP	18 Oct 1998 / 17:53	700 mb	12		19			8	9	80	3.9	1.9
BRET	AL	22 Aug 1999 / 08:01	700 mb	11		20			10	10	134	4.6	2.2
BRET	AL	22 Aug 1999 / 11:30	700 mb	12		18			10	9	107	5.2	1.9
BRET	AL	22 Aug 1999 / 23:41	700 mb	11		17			8	6	118	3.2	2.3
FLOYD	AL	12 Sep 1999 / 19:46	700 mb	11		21			20	16	113	7.8	2.6

continued on next page

Table D.8: *continued*

Storm	Basin	Fix Date / Time UTC	Fix flight level	Maximum FL Temp. Outside °C	Warm Ring °C	Center °C	Ring strength ΔT °C	Ring radius n mi	Eye radius n mi	RMW n mi	VMAX kt	Min Rossby length n mi	Dynamical eye size
FLOYD	AL	12 Sep 1999 / 21:29	700 mb	12		21			18	21	131	8.9	2.0
FLOYD	AL	13 Sep 1999 / 17:35	700 mb	13		25			12	12	111	6.2	2.0
FLOYD	AL	13 Sep 1999 / 19:20	700 mb	12		25			15	16	113	8.1	1.9
FLOYD	AL	15 Sep 1999 / 01:04	700 mb	12		19			25	24	122	12.5	2.0
GERT	AL	16 Sep 1999 / 10:07	700 mb	12		15			18	23	121	8.2	2.1
JOSE	AL	20 Oct 1999 / 03:34	850 mb	21	25	24	+1	6	20	13	78	6.5	3.1
JOSE	AL	20 Oct 1999 / 06:05	700 mb	9		18			15	16	87	7.3	2.1
LENNY	AL	15 Nov 1999 / 06:00	850 mb	18		21			12	10	71	5.3	2.4
LENNY	AL	15 Nov 1999 / 07:42	850 mb	19		22			8	6	70	3.2	2.3
LENNY	AL	16 Nov 1999 / 07:07	850 mb	17		24			22	33	109	11.0	2.1
LENNY	AL	16 Nov 1999 / 21:26	700 mb	10		18			15	15	80	7.1	2.1
LENNY	AL	16 Nov 1999 / 23:03	700 mb	9		20			18	14	115	4.6	3.8
LENNY	AL	17 Nov 1999 / 07:28	700 mb	10		17			15	10	97	4.1	3.6
LENNY	AL	17 Nov 1999 / 11:04	700 mb	9		17			15	14	130	4.4	3.4
LENNY	AL	17 Nov 1999 / 19:29	700 mb	12		25			11	11	120	3.9	2.8
LENNY	AL	17 Nov 1999 / 21:24	700 mb	11		24			11	13	114	4.8	2.3
LENNY	AL	17 Nov 1999 / 23:10	700 mb	10		22			10	16	128	5.3	1.9
LENNY	AL	18 Nov 1999 / 03:32	700 mb	10		20			10	12	119	4.3	2.3
LENNY	AL	18 Nov 1999 / 04:37	700 mb	8		21			9	10	119	3.6	2.5
LENNY	AL	18 Nov 1999 / 05:34	700 mb	8		22			10	14	118	5.1	2.0
LENNY	AL	18 Nov 1999 / 06:02	700 mb	13		20			9	11	107	4.4	2.0
LENNY	AL	18 Nov 1999 / 09:27	700 mb	10		21			9	11	113	4.2	2.2
LENNY	AL	18 Nov 1999 / 11:01	700 mb	16	22	17	+5	10	9	8	101	3.4	2.6
LENNY	AL	18 Nov 1999 / 17:59	700 mb	11		20			12	13	121	4.7	2.7
LENNY	AL	18 Nov 1999 / 21:20	700 mb	9	21	17	+4	5	15	6	107	2.4	6.1
LENNY	AL	18 Nov 1999 / 23:07	700 mb	10		18			15	16	95	7.3	2.1
LENNY	AL	19 Nov 1999 / 05:35	700 mb	13		18			15	10	66	6.6	2.3
LENNY	AL	19 Nov 1999 / 07:24	700 mb	9		17			15	11	68	7.0	2.1
DORA	EP	15 Aug 1999 / 11:00	700 mb	9		16			9	6	67	3.4	2.7
DORA	EP	15 Aug 1999 / 17:45	700 mb	9		15			12	16	108	5.6	2.2
DORA	EP	15 Aug 1999 / 20:06	700 mb	9		16			12	16	114	5.3	2.3
DORA	EP	15 Aug 1999 / 23:19	700 mb	8		16			12	9	81	4.3	2.9
DORA	EP	17 Aug 1999 / 11:48	700 mb	10	14	12	+2	15	15	17	78	8.1	1.8
KEITH	AL	30 Sep 2000 / 18:08	850 mb	17		21			20	15	82	7.9	2.5
KEITH	AL	30 Sep 2000 / 19:48	850 mb	16		21			12	15	96	6.7	1.9

continued on next page

Table D.8: *continued*

Storm	Basin	Fix Date / Time UTC	Fix flight level	Maximum FL Temp. Outside °C	Warm Ring °C	Center °C	Ring strength ΔT °C	Ring radius n mi	Eye radius n mi	RMW n mi	VMAX kt	Min Rossby length n mi	Dynamical eye size
KEITH	AL	30 Sep 2000 / 21:18	850 mb	17		22			10	12	101	5.2	1.9
KEITH	AL	01 Oct 2000 / 05:55	700 mb	9		22			10	14	119	5.1	2.0
KEITH	AL	01 Oct 2000 / 18:16	700 mb	11		25			10	8	103	3.4	3.0
KEITH	AL	01 Oct 2000 / 19:39	700 mb	9		24			10	13	102	5.5	1.8
KEITH	AL	01 Oct 2000 / 22:23	850 mb	17		20			10	7	133	2.3	4.4
KEITH	AL	01 Oct 2000 / 23:04	850 mb	17		23			10	10	124	3.5	2.9
ERIN	AL	09 Sep 2001 / 19:52	700 mb	9		18			15	10	103	7.3	2.0
IRIS	AL	05 Oct 2001 / 23:46	1500 ft	23		25			6	3	37	3.1	1.9
IRIS	AL	06 Oct 2001 / 19:35	850 mb	15		20			8	6	75	3.3	2.3
IRIS	AL	07 Oct 2001 / 07:15	700 mb	8		16			8	5	52	4.0	1.9
IRIS	AL	08 Oct 2001 / 07:51	700 mb	17		17			4	3	97	1.3	3.1
IRIS	AL	08 Oct 2001 / 09:15	700 mb	11		18			2	1	91	0.5	5.5
IRIS	AL	08 Oct 2001 / 10:38	700 mb	13		17			2	3	119	1.1	2.4
IRIS	AL	08 Oct 2001 / 18:07	700 mb	9	16	14	+2	6	5	4	107	1.5	3.3
IRIS	AL	08 Oct 2001 / 19:16	700 mb	8		15			5	4	112	1.5	3.4
IRIS	AL	08 Oct 2001 / 21:33	700 mb	8		15			5	3	100	1.2	4.1
IRIS	AL	08 Oct 2001 / 22:59	700 mb	9	20	15	+5	6	5	5	126	1.6	3.1
MICHELLE	AL	03 Nov 2001 / 09:28	700 mb	11		20			8	9	125	3.3	2.3
MICHELLE	AL	03 Nov 2001 / 11:15	700 mb	12		20			8	8	128	2.9	2.6
MICHELLE	AL	03 Nov 2001 / 19:21	700 mb	12		18			8	8	106	3.5	2.4
MICHELLE	AL	03 Nov 2001 / 21:01	700 mb	13		17			8	7	107	3.1	2.4
MICHELLE	AL	04 Nov 2001 / 11:57	700 mb	16		18			15	11	108	5.1	3.0
MICHELLE	AL	04 Nov 2001 / 13:20	700 mb	16		17			25	24	133	9.0	2.8
MICHELLE	AL	04 Nov 2001 / 17:13	700 mb	19		21			25	27	126	10.9	2.3
JULIETTE	EP	24 Sep 2001 / 16:25	700 mb	10		13			8	9	92	3.6	2.1
JULIETTE	EP	24 Sep 2001 / 18:00	700 mb	11		14			8	9	88	3.7	2.0
JULIETTE	EP	25 Sep 2001 / 18:19	700 mb	13		19			6	6	131	1.8	3.3
JULIETTE	EP	25 Sep 2001 / 20:06	700 mb	13		19			4	5	123	1.6	2.8
JULIETTE	EP	26 Sep 2001 / 19:00	700 mb	15		17			4	3	81	1.7	2.1
ISIDORE	AL	22 Sep 2002 / 10:31	700 mb	11		16			10	11	122	4.7	2.0
ISIDORE	AL	22 Sep 2002 / 18:48	700 mb	12		16			10	10	110	4.7	2.1
ISIDORE	AL	22 Sep 2002 / 20:26	700 mb	13		17			10	8	86	4.8	2.1
ISIDORE	AL	22 Sep 2002 / 21:49	700 mb	12		16			10	7	99	3.6	2.8
LILI	AL	29 Sep 2002 / 11:43	850 mb	18		23			6	3	47	2.9	1.9
LILI	AL	02 Oct 2002 / 16:13	700 mb	12		20			8	7	103	4.1	1.9

continued on next page

Table D.8: *continued*

Storm	Basin	Fix Date / Time UTC	Fix flight level	Maximum FL Temp. Outside °C	Maximum FL Temp. Warm Ring °C	Maximum FL Temp. Center °C	Ring strength ΔT °C	Ring radius n mi	Eye radius n mi	RMW n mi	VMAX kt	Min Rossby length n mi	Dynamical eye size
LILI	AL	02 Oct 2002 / 18:01	700 mb	13		20			8	5	100	3.0	2.5
LILI	AL	02 Oct 2002 / 21:41	700 mb	12		22			6	5	120	2.6	2.1
KENNA	EP	24 Oct 2002 / 17:18	700 mb	8		19			5	4	145	1.2	4.3
KENNA	EP	24 Oct 2002 / 18:59	700 mb	9		19			5	6	146	1.7	2.9
CLAUDETTE	AL	10 Jul 2003 / 15:26	700 mb	9		14			4	3	76	1.7	2.6
FABIAN	AL	01 Sep 2003 / 05:25	700 mb	9		16			12	14	121	5.1	2.4
FABIAN	AL	01 Sep 2003 / 07:09	700 mb	11		17			10	14	128	4.9	2.0
FABIAN	AL	01 Sep 2003 / 07:28	700 mb	12	18	16	+2	14	10	13	133	4.4	2.3
FABIAN	AL	01 Sep 2003 / 17:19	700 mb	10		15			12	11	126	4.0	3.1
FABIAN	AL	01 Sep 2003 / 19:17	700 mb	9		14			10	12	140	3.9	2.5
FABIAN	AL	02 Sep 2003 / 05:32	700 mb	11		18			10	11	130	4.0	2.5
FABIAN	AL	02 Sep 2003 / 07:15	700 mb	11	23	22	+1	11	10	13	128	4.8	2.1
FABIAN	AL	02 Sep 2003 / 17:18	700 mb	12	17	16	+1	9	18	14	99	6.9	2.5
FABIAN	AL	02 Sep 2003 / 19:09	700 mb	11		16			14	17	122	6.9	2.1
FABIAN	AL	03 Sep 2003 / 17:27	700 mb	11	18	17	+1	13	12	13	111	6.2	1.8
FABIAN	AL	04 Sep 2003 / 04:16	700 mb	13		18			12	8	91	4.9	2.5
FABIAN	AL	04 Sep 2003 / 19:35	700 mb	14		16			12	10	89	6.9	1.8
ISABEL	AL	12 Sep 2003 / 17:12	700 mb	10		21			15	15	128	6.1	2.5
ISABEL	AL	12 Sep 2003 / 19:01	700 mb	11		20			15	18	141	6.6	2.3
ISABEL	AL	13 Sep 2003 / 17:18	700 mb	8	18	15	+3	15	22	24	147	8.7	2.6
ISABEL	AL	13 Sep 2003 / 18:53	700 mb	10	18	15	+3	5	20	22	132	8.9	2.2
ISABEL	AL	14 Sep 2003 / 07:25	700 mb	10		17			20	27	143	10.4	1.9
ISABEL	AL	14 Sep 2003 / 17:17	700 mb	10		19			22	18	120	8.4	2.7
CHARLEY	AL	12 Aug 2004 / 13:33	700 mb	9		17			10	6	65	4.3	2.2
CHARLEY	AL	12 Aug 2004 / 15:16	700 mb	9		18			9	7	80	4.2	2.2
CHARLEY	AL	12 Aug 2004 / 17:04	700 mb	9		19			10	9	105	4.2	2.3
CHARLEY	AL	12 Aug 2004 / 20:59	700 mb	11		17			10	6	62	4.9	2.0
CHARLEY	AL	13 Aug 2004 / 06:56	700 mb	7		14			9	5	81	3.4	2.6
CHARLEY	AL	13 Aug 2004 / 08:32	700 mb	7		14			8	7	104	3.8	2.0
CHARLEY	AL	13 Aug 2004 / 15:22	700 mb	10		18			5	3	107	1.7	3.0
CHARLEY	AL	13 Aug 2004 / 19:30	700 mb	10		18			2	1	138	0.5	5.5
CHARLEY	AL	13 Aug 2004 / 19:57	700 mb	9		20			2	3	148	1.3	1.9
FRANCES	AL	29 Aug 2004 / 21:16	700 mb	9		20			8	9	118	3.5	2.3
FRANCES	AL	31 Aug 2004 / 10:28	700 mb	11		21			15	19	120	7.5	2.0
FRANCES	AL	31 Aug 2004 / 11:14	700 mb	11		19			15	21	138	7.3	2.1

continued on next page

Table D.8: *continued*

Storm	Basin	Fix Date / Time UTC	Fix flight level	Maximum FL Temp. Outside °C	Maximum FL Temp. Warm Ring °C	Maximum FL Temp. Center °C	Ring strength ΔT °C	Ring radius n mi	Eye radius n mi	RMW n mi	VMAX kt	Min Rossby length n mi	Dynamical eye size
FRANCES	AL	31 Aug 2004 / 17:30	700 mb	13		24			14	9	105	4.2	3.2
FRANCES	AL	31 Aug 2004 / 19:07	700 mb	13		24			14	11	123	4.4	3.2
FRANCES	AL	31 Aug 2004 / 20:57	700 mb	14		22			13	12	124	4.8	2.7
FRANCES	AL	31 Aug 2004 / 23:07	700 mb	14		22			15	12	130	4.6	3.3
FRANCES	AL	01 Sep 2004 / 18:59	700 mb	9		17			16	17	111	8.0	2.0
FRANCES	AL	01 Sep 2004 / 20:35	700 mb	9	20	17	+3	7	15	17	126	7.1	2.1
FRANCES	AL	01 Sep 2004 / 22:15	700 mb	10		18			14	17	134	6.7	2.1
FRANCES	AL	01 Sep 2004 / 23:23	700 mb	13		18			14	16	119	7.1	2.0
FRANCES	AL	02 Sep 2004 / 05:43	700 mb	13		23			15	15	138	5.9	2.6
FRANCES	AL	02 Sep 2004 / 07:18	700 mb	15		21			12	12	115	5.7	2.2
FRANCES	AL	02 Sep 2004 / 08:55	700 mb	16	21	19	+2	11	12	8	97	4.5	2.6
IVAN	AL	06 Sep 2004 / 20:58	700 mb	10		17			4	6	106	1.6	2.5
IVAN	AL	07 Sep 2004 / 06:13	700 mb	10		15			10	13	85	4.2	2.4
IVAN	AL	07 Sep 2004 / 11:16	700 mb	9		16			8	8	92	2.4	3.5
IVAN	AL	07 Sep 2004 / 17:45	700 mb	11		18			8	9	111	2.3	3.2
IVAN	AL	07 Sep 2004 / 19:30	700 mb	11		16			7	11	118	2.7	2.6
IVAN	AL	07 Sep 2004 / 20:43	700 mb	10		18			5	8	89	2.6	1.9
IVAN	AL	07 Sep 2004 / 22:08	700 mb	12		18			5	5	94	1.5	3.2
IVAN	AL	08 Sep 2004 / 06:00	700 mb	11		18			10	12	114	3.2	3.2
IVAN	AL	08 Sep 2004 / 07:51	700 mb	8	20	16	+4	7	9	13	133	2.9	3.1
IVAN	AL	08 Sep 2004 / 09:29	700 mb	9		17			9	13	94	4.2	2.1
IVAN	AL	08 Sep 2004 / 11:10	700 mb	8		17			10	9	95	2.9	3.5
IVAN	AL	08 Sep 2004 / 17:48	700 mb	10		17			8	7	130	1.7	4.4
IVAN	AL	08 Sep 2004 / 19:28	700 mb	9	20	16	+4	9	6	8	128	2.0	3.0
IVAN	AL	08 Sep 2004 / 21:08	700 mb	9		18			5	7	111	2.0	2.4
IVAN	AL	08 Sep 2004 / 23:11	700 mb	9		19			5	8	120	2.2	2.3
IVAN	AL	09 Sep 2004 / 07:10	700 mb	10		20			6	7	146	1.6	3.7
IVAN	AL	09 Sep 2004 / 08:44	700 mb	11		20			6	5	134	1.3	4.3
IVAN	AL	09 Sep 2004 / 10:10	700 mb	11		20			4	5	118	1.5	3.1
IVAN	AL	09 Sep 2004 / 11:41	700 mb	9		20			5	7	156	1.6	3.2
IVAN	AL	09 Sep 2004 / 17:40	700 mb	13		20			6	6	132	1.6	4.0
IVAN	AL	09 Sep 2004 / 18:37	700 mb	9		18			5	7	144	1.7	2.9
IVAN	AL	09 Sep 2004 / 20:12	700 mb	9		18			5	5	124	1.5	3.4
IVAN	AL	09 Sep 2004 / 21:45	700 mb	11		17			5	5	111	1.7	3.0
IVAN	AL	10 Sep 2004 / 05:19	700 mb	9		19			9	12	133	3.4	2.6

continued on next page

Table D.8: *continued*

Storm	Basin	Fix Date / Time UTC	Fix flight level	Maximum FL Temp. Outside °C	Maximum FL Temp. Warm Ring °C	Maximum FL Temp. Center °C	Ring strength ΔT °C	Ring radius n mi	Eye radius n mi	RMW n mi	VMAX kt	Min Rossby length n mi	Dynamical eye size
IVAN	AL	10 Sep 2004 / 06:56	700 mb	9	18	17	+1	10	10	9	123	2.8	3.4
IVAN	AL	10 Sep 2004 / 08:41	700 mb	10		17			10	12	129	3.6	2.8
IVAN	AL	10 Sep 2004 / 10:23	700 mb	8		18			10	11	141	3.1	3.3
IVAN	AL	10 Sep 2004 / 11:05	700 mb	13		18			10	8	107	2.9	3.4
IVAN	AL	10 Sep 2004 / 17:38	700 mb	9		17			8	10	112	3.6	2.2
IVAN	AL	10 Sep 2004 / 19:13	700 mb	9		17			8	9	103	3.6	2.2
IVAN	AL	10 Sep 2004 / 20:37	700 mb	9		18			8	8	118	2.8	2.7
IVAN	AL	10 Sep 2004 / 23:31	700 mb	12		18			6	7	106	2.8	2.2
IVAN	AL	11 Sep 2004 / 09:47	700 mb	10		18			15	15	135	4.7	3.2
IVAN	AL	11 Sep 2004 / 17:30	700 mb	10	19	17	+2	6	9	12	141	3.7	2.4
IVAN	AL	11 Sep 2004 / 19:17	700 mb	9		22			8	12	161	3.3	2.6
IVAN	AL	11 Sep 2004 / 20:44	700 mb	11		24			8	9	150	2.6	3.2
IVAN	AL	11 Sep 2004 / 22:18	700 mb	12		22			8	10	135	3.2	2.6
IVAN	AL	12 Sep 2004 / 00:05	700 mb	12		22			8	10	146	3.0	2.5
IVAN	AL	12 Sep 2004 / 05:47	700 mb	11		21			10	11	133	3.7	2.7
IVAN	AL	12 Sep 2004 / 07:29	700 mb	11		19			8	12	140	3.8	2.0
IVAN	AL	13 Sep 2004 / 01:42	700 mb	10		18			14	19	146	6.1	2.3
IVAN	AL	13 Sep 2004 / 03:18	700 mb	11	20	19	+1	9	16	17	140	5.7	2.8
IVAN	AL	13 Sep 2004 / 05:03	700 mb	13		20			18	16	113	6.7	2.6
IVAN	AL	13 Sep 2004 / 08:31	700 mb	9		18			14	14	153	4.4	3.2
IVAN	AL	13 Sep 2004 / 10:12	700 mb	9	19	17	+2	10	15	18	151	5.8	2.6
IVAN	AL	13 Sep 2004 / 11:49	700 mb	12		20			15	12	132	4.4	3.4
IVAN	AL	13 Sep 2004 / 14:04	700 mb	12		18			14	15	140	5.3	2.7
IVAN	AL	13 Sep 2004 / 17:47	700 mb	11		20			12	10	136	3.7	3.4
IVAN	AL	14 Sep 2004 / 20:46	700 mb	11		18			22	24	147	9.3	2.4
IVAN	AL	14 Sep 2004 / 22:01	700 mb	17		18			22	22	126	10.0	2.2
IVAN	AL	14 Sep 2004 / 23:19	700 mb	13		19			22	19	116	9.5	2.3
IVAN	AL	15 Sep 2004 / 00:45	700 mb	17		18			22	23	143	9.4	2.3
IVAN	AL	15 Sep 2004 / 02:04	700 mb	11		18			22	20	135	8.7	2.5
IVAN	AL	15 Sep 2004 / 03:08	700 mb	13		19			22	17	110	9.1	2.5
IVAN	AL	15 Sep 2004 / 07:15	700 mb	13		19			30	25	132	11.5	2.6
IVAN	AL	15 Sep 2004 / 09:17	700 mb	13		19			25	25	113	13.5	1.9
IVAN	AL	15 Sep 2004 / 16:12	700 mb	11		19			20	14	98	9.2	2.2
IVAN	AL	16 Sep 2004 / 01:30	700 mb	22		22			20	13	100	8.8	2.3
JEANNE	AL	25 Sep 2004 / 02:39	850 mb	18		20			22	19	110	10.7	2.1

continued on next page

Table D.8: *continued*

Storm	Basin	Fix Date / Time UTC	Fix flight level	Maximum FL Temp. Outside °C	Warm Ring °C	Center °C	Ring strength ΔT °C	Ring radius n mi	Eye radius n mi	RMW n mi	VMAX kt	Min Rossby length n mi	Dynamical eye size
DENNIS	AL	07 Jul 2005 / 09:39	700 mb	9		14			10	10	80	5.2	1.9
DENNIS	AL	07 Jul 2005 / 22:16	700 mb	7		18			10	10	110	4.2	2.4
DENNIS	AL	08 Jul 2005 / 05:24	700 mb	13		17			8	10	119	4.1	1.8
DENNIS	AL	08 Jul 2005 / 06:24	700 mb	10		19			8	7	106	3.2	2.3
DENNIS	AL	08 Jul 2005 / 06:53	700 mb	10		18			8	9	121	3.6	2.1
DENNIS	AL	08 Jul 2005 / 11:59	700 mb	9		20			8	8	136	3.0	2.7
DENNIS	AL	08 Jul 2005 / 15:17	700 mb	9		20			6	6	107	2.9	2.1
DENNIS	AL	08 Jul 2005 / 17:06	700 mb	9		19			5	5	129	2.0	2.5
DENNIS	AL	09 Jul 2005 / 21:16	700 mb	11		18			6	4	89	2.8	2.2
DENNIS	AL	10 Jul 2005 / 01:31	700 mb	11		19			6	5	107	2.9	1.9
DENNIS	AL	10 Jul 2005 / 06:05	700 mb	11		20			5	4	99	2.6	1.9
EMILY	AL	14 Jul 2005 / 15:27	700 mb	8	18	18	+0	8	5	6	85	2.2	2.3
EMILY	AL	14 Jul 2005 / 17:11	700 mb	10		16			6	6	65	2.9	1.9
EMILY	AL	14 Jul 2005 / 23:46	700 mb	7	16	14	+2	6	4	6	101	1.9	2.1
EMILY	AL	15 Jul 2005 / 01:30	700 mb	7		13			4	6	125	1.6	2.5
EMILY	AL	15 Jul 2005 / 05:03	700 mb	9		21			4	5	81	2.1	1.9
EMILY	AL	15 Jul 2005 / 14:53	700 mb	11		20			8	4	60	2.3	3.2
EMILY	AL	15 Jul 2005 / 23:22	700 mb	10		14			5	8	108	2.7	1.9
EMILY	AL	16 Jul 2005 / 05:41	700 mb	9		16			6	6	77	2.9	2.2
EMILY	AL	16 Jul 2005 / 11:52	700 mb	7	15	14	+1	6	6	10	148	2.6	2.5
EMILY	AL	16 Jul 2005 / 13:28	700 mb	10		17			6	5	114	1.7	3.8
EMILY	AL	16 Jul 2005 / 15:14	700 mb	10		15			6	6	101	2.3	2.8
EMILY	AL	16 Jul 2005 / 17:17	700 mb	9		20			6	8	141	2.3	2.4
EMILY	AL	16 Jul 2005 / 23:40	700 mb	13		23			7	6	149	1.7	4.2
EMILY	AL	17 Jul 2005 / 01:17	700 mb	7		23			5	5	127	1.6	3.0
EMILY	AL	17 Jul 2005 / 12:01	700 mb	9	17	15	+2	7	5	7	119	2.6	1.9
EMILY	AL	19 Jul 2005 / 23:18	700 mb	10		19			8	7	101	4.0	2.1
KATRINA	AL	28 Aug 2005 / 19:23	700 mb	14		28			14	18	148	7.6	1.8
KATRINA	AL	28 Aug 2005 / 20:38	700 mb	16		28			14	14	130	6.8	2.1
KATRINA	AL	28 Aug 2005 / 22:31	700 mb	14		27			14	16	139	7.3	1.9
KATRINA	AL	28 Aug 2005 / 23:26	700 mb	14		28			14	16	139	7.3	1.9
KATRINA	AL	29 Aug 2005 / 02:36	700 mb	13		25			15	15	122	7.9	1.9
PHILIPPE	AL	19 Sep 2005 / 05:17	700 mb	7	18	14	+4	6	8	6	72	3.4	2.4
RITA	AL	21 Sep 2005 / 15:17	700 mb	12		22			12	9	137	3.8	3.3
RITA	AL	21 Sep 2005 / 17:53	700 mb	9		26			10	7	153	2.7	3.8

continued on next page

Table D.8: *continued*

Storm	Basin	Fix Date / Time UTC	Fix flight level	Maximum FL Temp. Outside °C	Warm Ring °C	Center °C	Ring strength ΔT °C	Ring radius n mi	Eye radius n mi	RMW n mi	VMAX kt	Min Rossby length n mi	Dynamical eye size
RITA	AL	21 Sep 2005 / 21:16	700 mb	9		30			10	9	145	3.6	2.8
RITA	AL	21 Sep 2005 / 23:09	700 mb	8		28			10	11	142	4.5	2.2
RITA	AL	21 Sep 2005 / 23:13	700 mb	8		28			10	11	142	4.5	2.2
RITA	AL	22 Sep 2005 / 05:38	700 mb	9		28			8	12	165	4.3	1.9
RITA	AL	22 Sep 2005 / 09:12	700 mb	14		29			9	10	134	4.4	2.0
RITA	AL	22 Sep 2005 / 17:45	700 mb	12		21			8	8	120	4.0	1.9
RITA	AL	22 Sep 2005 / 19:13	700 mb	13		20			9	10	133	4.6	2.0
STAN	AL	04 Oct 2005 / 08:48	700 mb	13		15			8	6	67	4.1	2.0
WILMA	AL	19 Oct 2005 / 04:32	850 mb	17		26			2	3	162	0.8	2.6
WILMA	AL	19 Oct 2005 / 08:00	700 mb	10		24			2	3	166	0.8	2.7
WILMA	AL	19 Oct 2005 / 18:06	700 mb	12		20			2	2	128	0.7	3.0
WILMA	AL	19 Oct 2005 / 19:56	700 mb	12		19			2	2	141	0.6	4.1
WILMA	AL	19 Oct 2005 / 21:39	700 mb	13		16			2	2	114	0.8	2.6
WILMA	AL	20 Oct 2005 / 18:43	700 mb	13		20			18	15	145	4.7	3.7
WILMA	AL	20 Oct 2005 / 20:16	700 mb	12		23			20	21	135	7.0	2.9
WILMA	AL	20 Oct 2005 / 21:16	700 mb	12		23			20	21	135	7.0	2.9
WILMA	AL	20 Oct 2005 / 21:39	700 mb	13		22			18	15	127	5.4	3.3
WILMA	AL	20 Oct 2005 / 23:05	700 mb	11		22			20	20	130	7.0	2.9
WILMA	AL	21 Oct 2005 / 05:01	700 mb	10		20			18	19	128	6.9	2.5
WILMA	AL	21 Oct 2005 / 06:44	700 mb	10		18			15	18	130	6.5	2.3
WILMA	AL	21 Oct 2005 / 08:21	700 mb	11		17			15	15	112	6.3	2.4
WILMA	AL	21 Oct 2005 / 10:11	700 mb	12		16			15	16	115	6.6	2.3
WILMA	AL	22 Oct 2005 / 23:02	700 mb	11		14			35	31	87	17.9	2.0
WILMA	AL	24 Oct 2005 / 07:47	700 mb	9	15	14	+1	11	32	20	80	14.8	2.2
WILMA	AL	24 Oct 2005 / 09:32	700 mb	10	18	16	+2	12	30	19	84	13.6	2.2
ADRIAN	EP	19 May 2005 / 16:55	850 mb	14	27	23	+4	10	10	6	83	2.2	4.5
ADRIAN	EP	19 May 2005 / 18:30	850 mb	15		26			12	8	71	3.4	3.6
HELENE	AL	17 Sep 2006 / 15:46	850 mb	17		20			25	18	76	11.6	2.1
HELENE	AL	18 Sep 2006 / 16:19	500 mb	1		5			20	13	65	11.1	1.8
HELENE	AL	19 Sep 2006 / 16:37	700 mb	18		19			20	12	79	8.7	2.3
HELENE	AL	19 Sep 2006 / 17:40	850 mb	18		20			20	16	96	9.6	2.1
JOHN	EP	30 Aug 2006 / 11:13	700 mb	17		20			6	6	107	2.2	2.8
JOHN	EP	30 Aug 2006 / 12:53	700 mb	11		18			6	5	87	2.3	2.7
JOHN	EP	01 Sep 2006 / 15:49	700 mb	9		16			6	6	98	3.2	1.9
JOHN	EP	01 Sep 2006 / 16:45	700 mb	10		16			6	5	85	3.1	1.9

continued on next page

Table D.8: *continued*

Storm	Basin	Fix Date / Time UTC	Fix flight level	Maximum FL Temp. Outside °C	Warm Ring °C	Center °C	Ring strength ΔT °C	Ring radius n mi	Eye radius n mi	RMW n mi	VMAX kt	Min Rossby length n mi	Dynamical eye size
DEAN	AL	17 Aug 2007 / 12:36	700 mb	6		17			8	12	100	4.2	2.0
DEAN	AL	17 Aug 2007 / 14:17	200 mb	12		18			8	8	82	3.5	2.5
DEAN	AL	17 Aug 2007 / 15:59	700 mb			18			8	5	65	2.7	3.1
DEAN	AL	17 Aug 2007 / 17:17	700 mb	7		19			8	11	124	3.2	2.7
DEAN	AL	18 Aug 2007 / 02:58	700 mb	11		20			8	5	117	1.6	4.8
DEAN	AL	18 Aug 2007 / 05:00	700 mb	12		20			6	5	117	1.6	4.2
DEAN	AL	18 Aug 2007 / 11:51	700 mb	11		23			6	8	145	2.1	2.9
DEAN	AL	18 Aug 2007 / 13:23	700 mb	11		18			6	7	117	2.3	2.7
DEAN	AL	18 Aug 2007 / 15:02	700 mb	11		21			6	5	91	2.1	2.6
DEAN	AL	18 Aug 2007 / 16:14	700 mb	9		20			6	8	128	2.4	2.3
DEAN	AL	18 Aug 2007 / 17:02	700 mb	11		16			6	7	110	2.4	2.2
DEAN	AL	19 Aug 2007 / 02:09	700 mb	8		16			12	12	92	5.1	2.5
DEAN	AL	19 Aug 2007 / 05:11	700 mb	8		16			12	12	105	4.5	2.5
DEAN	AL	20 Aug 2007 / 02:19	700 mb	7		18			8	9	108	3.5	2.3
DEAN	AL	20 Aug 2007 / 17:39		9		19			9	10	140	3.1	2.9
DEAN	AL	20 Aug 2007 / 19:23	700 mb	9		19			9	15	151	4.3	2.1
DEAN	AL	20 Aug 2007 / 21:02	700 mb	10	21	20	+1	7	8	11	126	3.8	2.1
DEAN	AL	20 Aug 2007 / 21:37	700 mb	10	21	20	+1	7	8	11	126	3.8	2.1
DEAN	AL	20 Aug 2007 / 23:02	700 mb	11		21			8	9	110	3.6	2.2
DEAN	AL	20 Aug 2007 / 23:46	700 mb	9		21			8	8	156	2.3	3.5
DEAN	AL	21 Aug 2007 / 06:05	700 mb	12		23			8	12	156	3.4	2.2
DEAN	AL	21 Aug 2007 / 06:48	700 mb	9		21			8	9	123	3.3	2.3
DEAN	AL	21 Aug 2007 / 07:31	700 mb	15		22			8	9	160	2.5	3.0
DEAN	AL	21 Aug 2007 / 08:14	700 mb	11		23			8	8	116	3.1	2.4
FELIX	AL	01 Sep 2007 / 22:41	700 mb	16		17			15	14	77	5.5	2.7
FELIX	AL	02 Sep 2007 / 05:13	700 mb	10		13			15	15	93	5.0	3.0
FELIX	AL	02 Sep 2007 / 05:40	700 mb	6		13			15	12	55	6.7	2.2
FELIX	AL	02 Sep 2007 / 06:38	700 mb	13	15	14	+1	8	15	11	79	4.3	3.5
FELIX	AL	02 Sep 2007 / 09:54	700 mb	14		15			12	15	90	5.2	2.4
FELIX	AL	02 Sep 2007 / 11:32	700 mb	8		15			12	7	70	3.2	3.9
FELIX	AL	02 Sep 2007 / 17:24	700 mb	8		16			10	13	122	3.5	2.9
FELIX	AL	02 Sep 2007 / 18:54	700 mb	8		16			6	7	114	2.0	3.0
FELIX	AL	02 Sep 2007 / 23:07	700 mb	25		26			8	12	152	2.6	2.9
FELIX	AL	03 Sep 2007 / 05:11	700 mb	7		24			5	8	132	2.1	2.4
FELIX	AL	03 Sep 2007 / 06:57	700 mb	9		26			5	6	121	1.7	2.9

continued on next page

Table D.8: *continued*

Storm	Basin	Fix Date / Time UTC	Fix flight level	Maximum FL Temp. Outside °C	Warm Ring °C	Center °C	Ring strength ΔT °C	Ring radius n mi	Eye radius n mi	RMW n mi	VMAX kt	Min Rossby length n mi	Dynamical eye size
FELIX	AL	03 Sep 2007 / 12:27	700 mb	10		22			4	3	112	0.9	4.3
FELIX	AL	03 Sep 2007 / 19:00	700 mb	9	20	17	+3	6	8	7	95	2.6	2.9
FELIX	AL	04 Sep 2007 / 05:33	700 mb	8		18			8	9	143	2.2	3.4
FELIX	AL	04 Sep 2007 / 06:22	700 mb	8		17			8	7	116	2.1	3.6
FELIX	AL	04 Sep 2007 / 07:02	700 mb	9		18			8	7	125	2.0	3.8
HUMBERTO	AL	13 Sep 2007 / 06:52	850 mb	17		27			8	4	65	4.3	2.0
GUSTAV	AL	30 Aug 2008 / 12:20	700 mb	16		17			15	11	90	6.1	2.5
GUSTAV	AL	30 Aug 2008 / 16:54	700 mb	9		19			15	18	141	6.5	2.3
GUSTAV	AL	30 Aug 2008 / 20:08	700 mb	9		19			12	10	98	5.4	2.2
GUSTAV	AL	30 Aug 2008 / 21:54	700 mb	10		22			12	14	123	6.1	2.0
IKE	AL	06 Sep 2008 / 17:11	700 mb	7	18	14	+4	13	15	11	100	5.7	2.6
IKE	AL	06 Sep 2008 / 19:06	700 mb	10		15			14	15	109	7.1	2.0
IKE	AL	06 Sep 2008 / 23:12	700 mb	8		17			14	16	115	7.1	2.0
IKE	AL	07 Sep 2008 / 06:25	700 mb	11		16			12	12	105	5.8	2.0
IKE	AL	07 Sep 2008 / 07:54	700 mb	13		15			12	10	95	5.3	2.2
OMAR	AL	15 Oct 2008 / 09:12	700 mb	12		15			6	3	48	2.2	2.7
PALOMA	AL	07 Nov 2008 / 07:04	850 mb	14		22			9	8	82	4.1	2.2
PALOMA	AL	07 Nov 2008 / 21:26	700 mb	10		17			9	11	106	4.7	1.9
PALOMA	AL	08 Nov 2008 / 05:59	700 mb	6		19			11	11	110	4.6	2.4
PALOMA	AL	08 Nov 2008 / 07:44	700 mb	7		20			13	9	118	3.6	3.7
PALOMA	AL	08 Nov 2008 / 09:34	700 mb	6		20			13	13	134	4.6	2.9
PALOMA	AL	08 Nov 2008 / 11:11	700 mb	7		22			9	9	112	3.8	2.4
PALOMA	AL	08 Nov 2008 / 16:11		7		20			8	8	108	3.6	2.2
N				433	39	434	39	36	434	434	434	434	434
minimum				1	14	5	+0	5	2	1	27	0.5	1.8
maximum				25	27	30	+5	15	35	33	168	17.9	6.1
average				11.1	19.0	18.7	2.2	8.8	11.2	11.5	113.7	4.60	2.65
std. dev.				3.0	2.7	3.2	1.3	2.8	5.3	5.6	24.0	2.62	0.77

Table D.9: All cases of the VDM data set which had dynamically-small eyes (≤ 0.6).The storm name, basin (AL = Atlantic, EP = Eastern Pacific), and date and time (UTC) of these dynamically-large eye cases cases are given in the third, fourth, and fifth columns, respectively. The fourth column gives the flight level (FL) of the aircraft fix. The fifth, sixth, and seventh columns display the maximum flight level temperatures reported just outside the eyewall ("Outside"), within the eye but greater than 5 n mi of the center ("Ring"), and within 5 n mi of the center ("Center"), respectively. The warm ring magnitude (maximum temperature of ring - maximum temperature near center) is shown in the eighth column. The radii of the supplementary maximum temperature report ("Ring"), the primary eye ("Eye"), and the radius of maximum wind ("RMW", given by the radius of the maximum inbound flight level wind speed reported for the fix), are given in the ninth, tenth, and eleventh columns, respectively. The thirteenth column gives the maximum inbound flight level wind speed ("VMAX"), while the thirteenth column lists the minimum Rossby length. The dynamical eye size is given in the final column. Values are given in the native units of the VDM data set. Summary statistics of the values in the columns follow the main table.

Storm	Basin	Fix Date / Time UTC	Fix flight level	**Maximum FL Temp.** Outside °C	Warm Ring °C	Center °C	Ring strength ΔT °C	Ring radius n mi	Eye radius n mi	RMW n mi	VMAX kt	Min Rossby length n mi	Dynamical eye size
CHANTAL	AL	01 Aug 1989 / 01:13	1500 ft	24		24			12	50	48	61.2	0.20
CHANTAL	AL	01 Aug 1989 / 02:33	850 mb	17		19			12	30	58	32.5	0.38
CHANTAL	AL	01 Aug 1989 / 05:04	850 mb	17		20			10	30	50	37.7	0.26
CHANTAL	AL	01 Aug 1989 / 07:21	850 mb	18		20			8	26	58	29.0	0.26
CHANTAL	AL	01 Aug 1989 / 08:50	850 mb	19		19			4	15	50	19.8	0.20
CHANTAL	AL	01 Aug 1989 / 09:23	850 mb	17		19			2	25	66	24.9	0.10
DEAN	AL	04 Aug 1989 / 02:55	700 mb	11		17			10	23	62	17.5	0.57
DEAN	AL	04 Aug 1989 / 04:19	700 mb	11		14			11	25	58	20.3	0.54
DEAN	AL	04 Aug 1989 / 05:42	700 mb	8		15			10	90	75	53.5	0.19
DEAN	AL	05 Aug 1989 / 02:19	700 mb	10		16			8	15	42	19.0	0.39
DEAN	AL	05 Aug 1989 / 23:24	700 mb	13		16			12	24	68	22.2	0.56
DEAN	AL	06 Aug 1989 / 01:18	700 mb	13		15			12	26	51	31.9	0.39
DEAN	AL	06 Aug 1989 / 02:59	700 mb	12		15			10	36	59	38.3	0.26
DEAN	AL	06 Aug 1989 / 05:05	700 mb	12		15			8	41	70	37.4	0.20
GABRIELLE	AL	06 Sep 1989 / 20:40	700 mb	13		19			22	95	105	50.6	0.45
GABRIELLE	AL	07 Sep 1989 / 05:30	700 mb	13		16			20	90	95	55.3	0.36
GABRIELLE	AL	07 Sep 1989 / 11:04	700 mb	13		16			22	70	82	52.5	0.43
HUGO	AL	19 Sep 1989 / 06:03	700 mb	20		18			8	30	45	31.5	0.24
HUGO	AL	20 Sep 1989 / 12:10	700 mb	19		17			10	30	73	23.8	0.42
HUGO	AL	20 Sep 1989 / 13:55	700 mb	15		18			10	30	64	27.3	0.37
HUGO	AL	20 Sep 1989 / 15:23	700 mb	17		18			10	30	63	27.9	0.36
HUGO	AL	20 Sep 1989 / 17:09	700 mb	16		18			10	30	57	31.0	0.32
HUGO	AL	21 Sep 1989 / 22:15	700 mb	13		21			15	30	69	30.1	0.50
HUGO	AL	21 Sep 1989 / 23:58	700 mb	13		19			15	60	72	55.7	0.27
HUGO	AL	22 Sep 1989 / 01:39	700 mb	13		22			15	30	76	28.2	0.53
IRIS	AL	19 Sep 1989 / 18:09	surface	24		26			9	25	72	16.3	0.55

continued on next page

Table D.9: *continued*

Storm	Basin	Fix Date / Time UTC	Fix flight level	Maximum FL Temp. Outside °C	Maximum FL Temp. Warm Ring °C	Maximum FL Temp. Center °C	Ring strength ΔT °C	Ring radius n mi	Eye radius n mi	RMW n mi	VMAX kt	Min Rossby length n mi	Dynamical eye size
JERRY	AL	13 Oct 1989 / 23:12	1500 ft	14		23			5	25	66	20.7	0.24
JERRY	AL	15 Oct 1989 / 05:17	1500 ft	21		24			5	16	54	18.0	0.28
JERRY	AL	15 Oct 1989 / 11:36	1500 ft	22		24			5	17	73	14.9	0.34
KAREN	AL	30 Nov 1989 / 12:24	1500 ft	24		24			5	10	50	9.9	0.51
KAREN	AL	30 Nov 1989 / 13:39	1500 ft	22		24			5	15	65	11.2	0.44
BERTHA	AL	01 Aug 1990 / 12:15	850 mb	19		19			25	46	55	67.9	0.37
GUSTAV	AL	29 Aug 1990 / 11:26		9		15			12	26	64	22.3	0.54
GUSTAV	AL	31 Aug 1990 / 13:41	700 mb	5		17			12	71	71	66.1	0.19
KLAUS	AL	04 Oct 1990 / 21:38	1500 ft	27		25			10	30	47	25.2	0.40
KLAUS	AL	06 Oct 1990 / 11:35	1500 ft	22		24			2	25	54	19.9	0.13
KLAUS	AL	06 Oct 1990 / 13:31	1500 ft	24		25			2	30	50	25.6	0.10
KLAUS	AL	06 Oct 1990 / 15:28	1500 ft	25		24			2	45	56	34.0	0.07
KLAUS	AL	06 Oct 1990 / 17:22	1500 ft	24		25			2	15	58	11.5	0.22
LILI	AL	11 Oct 1990 / 23:29	850 mb	19		17			12	25	67	25.2	0.50
NANA	AL	17 Oct 1990 / 23:54	850 mb	17		24			4	15	62	13.3	0.30
NANA	AL	18 Oct 1990 / 18:59	700 mb	10		14			4	30	48	36.8	0.11
NANA	AL	19 Oct 1990 / 05:58	850 mb	15		20			5	15	73	13.3	0.38
NANA	AL	19 Oct 1990 / 09:20	850 mb	16		20			4	15	48	20.3	0.20
NANA	AL	19 Oct 1990 / 11:09	850 mb	16		20			5	15	51	19.2	0.26
NANA	AL	19 Oct 1990 / 18:06	850 mb	18		23			5	15	62	16.1	0.31
BOB	AL	17 Aug 1991 / 11:42	1500 ft	24		26			5	10	35	18.6	0.27
BOB	AL	17 Aug 1991 / 13:03	1500 ft	23		25			5	10	48	13.7	0.36
BOB	AL	17 Aug 1991 / 14:26	1500 ft	24		25			4	35	60	37.0	0.12
BOB	AL	17 Aug 1991 / 15:43	1500 ft	24		25			4	10	58	11.5	0.39
BOB	AL	17 Aug 1991 / 17:19	1500 ft	23		25			4	10	71	9.5	0.47
BOB	AL	17 Aug 1991 / 23:50	850 mb	17		22			6	60	59	61.7	0.10
BOB	AL	18 Aug 1991 / 05:51	850 mb	20		21			5	8	47	11.9	0.42
BOB	AL	18 Aug 1991 / 07:31	850 mb	18		20			8	35	61	38.5	0.19
BOB	AL	18 Aug 1991 / 09:10	850 mb	17		20			10	30	82	25.4	0.39
BOB	AL	18 Aug 1991 / 10:41	850 mb	18		21			8	15	64	16.7	0.45
BOB	AL	18 Aug 1991 / 15:06	700 mb	13		17			10	60	64	62.6	0.16
BOB	AL	18 Aug 1991 / 16:39	700 mb	11		16			10	15	65	17.0	0.59
BOB	AL	18 Aug 1991 / 17:52	700 mb	10		17			10	45	63	49.8	0.20
BOB	AL	18 Aug 1991 / 19:10	700 mb	11		17			10	30	95	23.4	0.43
BOB	AL	19 Aug 1991 / 05:23	700 mb	16		18			8	17	88	15.8	0.54

continued on next page

Table D.9: *continued*

Storm	Basin	Fix Date / Time UTC	Fix flight level	Maximum FL Temp. Outside °C	Maximum FL Temp. Warm Ring °C	Maximum FL Temp. Center °C	Ring strength ΔT °C	Ring radius n mi	Eye radius n mi	RMW n mi	VMAX kt	Min Rossby length n mi	Dynamical eye size
BOB	AL	19 Aug 1991 / 08:54	700 mb	8		16			8	10	59	14.3	0.53
BOB	AL	19 Aug 1991 / 12:20	700 mb	8		15			10	42	97	36.0	0.28
CLAUDETTE	AL	06 Sep 1991 / 20:16	850 mb	18		21			3	9	107	5.3	0.57
CLAUDETTE	AL	07 Sep 1991 / 23:37	700 mb	10		14			5	16	90	11.7	0.43
CLAUDETTE	AL	08 Sep 1991 / 23:39	700 mb	11		19			10	39	99	27.9	0.36
CLAUDETTE	AL	09 Sep 1991 / 01:11	700 mb	7		15			10	18	74	17.7	0.56
CLAUDETTE	AL	09 Sep 1991 / 04:20	700 mb	8		14			5	20	102	14.5	0.34
CLAUDETTE	AL	09 Sep 1991 / 05:05	700 mb	8		17			5	28	94	21.9	0.23
GRACE	AL	28 Oct 1991 / 12:11	1500 ft	16		18			15	15	43	25.2	0.59
GRACE	AL	28 Oct 1991 / 13:55	1500 ft	16		18			18	20	44	32.5	0.54
GRACE	AL	28 Oct 1991 / 17:25	850 mb	14		14			12	35	57	43.1	0.29
GRACE	AL	28 Oct 1991 / 19:10	850 mb	14		14			12	20	56	25.9	0.48
ANDREW	AL	21 Aug 1992 / 16:43	1500 ft	24		25			12	35	47	40.9	0.28
ANDREW	AL	22 Aug 1992 / 03:41	1500 ft	22		24			8	15	60	14.9	0.54
ANDREW	AL	25 Aug 1992 / 06:11	700 mb	10		14			7	25	107	14.5	0.48
ANDREW	AL	25 Aug 1992 / 08:07	700 mb	8		13			6	23	105	13.7	0.44
ANDREW	AL	25 Aug 1992 / 09:37	700 mb	11		13			6	18	86	13.1	0.46
ANDREW	AL	25 Aug 1992 / 11:20	700 mb	10		13			5	15	103	9.3	0.54
ANDREW	AL	26 Aug 1992 / 11:02	700 mb	9		13			6	21	96	15.0	0.40
DANIELLE	AL	25 Sep 1992 / 11:33	1500 ft	22		21			5	25	42	45.3	0.11
DANIELLE	AL	25 Sep 1992 / 13:23	1500 ft	19		21			5	57	59	70.2	0.07
DANIELLE	AL	25 Sep 1992 / 15:11	1500 ft	22		20			8	25	58	34.0	0.22
DANIELLE	AL	25 Sep 1992 / 17:04	1500 ft	20		20			5	23	61	30.2	0.17
DANIELLE	AL	25 Sep 1992 / 18:31	1500 ft	20		20			8	24	55	34.8	0.22
EARL	AL	30 Sep 1992 / 13:59	1500 ft	23		23			5	26	55	31.7	0.16
EARL	AL	02 Oct 1992 / 01:54	1500 ft	22		23			5	42	51	49.4	0.10
EMILY	AL	27 Aug 1993 / 11:53	850 mb	16		18			1	67	56	65.9	0.02
EMILY	AL	27 Aug 1993 / 13:41	850 mb	18		17			3	58	37	83.8	0.04
EMILY	AL	27 Aug 1993 / 15:40	850 mb	18		17			2	42	62	39.6	0.06
EMILY	AL	27 Aug 1993 / 17:36	850 mb	18		18			3	15	68	13.6	0.22
EMILY	AL	28 Aug 1993 / 17:03	850 mb	18		26			8	26	74	22.3	0.34
EMILY	AL	29 Aug 1993 / 03:13	850 mb	17		21			8	20	83	16.0	0.47
EMILY	AL	29 Aug 1993 / 13:22	850 mb	18		21			10	37	76	32.7	0.31
EMILY	AL	30 Aug 1993 / 05:07	850 mb	17		22			11	29	76	26.9	0.41
EMILY	AL	30 Aug 1993 / 11:46	850 mb	18		20			10	23	63	25.9	0.39

continued on next page

Table D.9: *continued*

Storm	Basin	Fix Date / Time UTC	Fix flight level	Maximum FL Temp. Outside °C	Maximum FL Temp. Warm Ring °C	Maximum FL Temp. Center °C	Ring strength ΔT °C	Ring radius n mi	Eye radius n mi	RMW n mi	VMAX kt	Min Rossby length n mi	Dynamical eye size
EMILY	AL	31 Aug 1993 / 05:33	850 mb	18		20			15	39	75	37.2	0.40
EMILY	AL	01 Sep 1993 / 05:21	700 mb	9		15			15	35	80	34.5	0.43
EMILY	AL	01 Sep 1993 / 08:27	700 mb	7		15			15	38	118	26.2	0.57
GERT	AL	20 Sep 1993 / 00:20	1500 ft	24		25			10	55	58	43.9	0.23
GERT	AL	20 Sep 1993 / 04:01	850 mb	16		20			2	62	80	37.0	0.05
GERT	AL	20 Sep 1993 / 05:36	850 mb	19		20			2	36	69	25.3	0.10
GERT	AL	20 Sep 1993 / 13:40	700 mb	9		15			18	78	77	47.6	0.37
KEONI	CP	14 Aug 1993 / 20:21	850 mb	18		21			9	33	47	21.9	0.41
ALBERTO	AL	02 Jul 1994 / 11:47	1500 ft	23		24			12	16	42	22.3	0.56
ALBERTO	AL	02 Jul 1994 / 13:40	1500 ft	23		24			8	68	42	84.2	0.09
ALBERTO	AL	02 Jul 1994 / 15:29	1500 ft	24		25			6	63	30	105.3	0.06
ALBERTO	AL	02 Jul 1994 / 17:15	1500 ft	23		24			10	20	40	29.8	0.34
ALBERTO	AL	03 Jul 1994 / 14:07	1500 ft	23		25			10	18	67	18.5	0.54
TD05	AL	30 Aug 1994 / 18:35	1500 ft	24		26			20	29	35	39.7	0.50
FLORENCE	AL	06 Nov 1994 / 19:41	700 mb	7		11			15	29	72	29.5	0.51
EMILIA	EP	22 Jul 1994 / 05:02	700 mb	9		17			5	23	68	13.6	0.37
GILMA	EP	27 Jul 1994 / 00:03	700 mb	11		19			10	30	46	18.9	0.53
BARRY	AL	08 Jul 1995 / 11:39	1500 ft	22		23			18	15	38	30.8	0.57
CHANTAL	AL	15 Jul 1995 / 11:52	1500 ft	25		27			10	105	51	93.4	0.11
CHANTAL	AL	15 Jul 1995 / 15:35	1500 ft	25		25			4	88	26	138.9	0.03
ERIN	AL	31 Jul 1995 / 15:46	850 mb	16		21			10	48	81	31.0	0.32
ERIN	AL	31 Jul 1995 / 17:10	700 mb	11		14			10	25	41	31.9	0.31
ERIN	AL	02 Aug 1995 / 02:24	850 mb	18		22			10	15	52	18.0	0.55
ERIN	AL	02 Aug 1995 / 18:58	1500 ft	23		24			10	25	72	22.5	0.44
ERIN	AL	02 Aug 1995 / 20:18	1500 ft	23		24			10	25	46	34.5	0.29
ERIN	AL	02 Aug 1995 / 21:57	1500 ft	23		25			10	16	57	18.5	0.54
ERIN	AL	03 Aug 1995 / 03:59	850 mb	18		22			10	26	81	21.2	0.47
ERIN	AL	03 Aug 1995 / 05:18	850 mb	19		22			12	20	60	22.1	0.52
ERIN	AL	03 Aug 1995 / 09:57	850 mb	19		23			10	19	70	18.4	0.54
FELIX	AL	11 Aug 1995 / 11:22	850 mb	19		25			9	26	66	18.8	0.48
FELIX	AL	14 Aug 1995 / 02:36	700 mb	13		18			10	64	60	63.9	0.16
FELIX	AL	14 Aug 1995 / 05:46	700 mb	13		15			10	70	76	56.5	0.18
FELIX	AL	14 Aug 1995 / 23:22	700 mb	13		15			10	15	63	16.9	0.59
FELIX	AL	15 Aug 1995 / 01:25	700 mb	13		15			10	13	54	17.1	0.58
FELIX	AL	15 Aug 1995 / 03:04	700 mb	13		15			10	98	80	77.6	0.13

continued on next page

Table D.9: *continued*

Storm	Basin	Fix Date / Time UTC	Fix flight level	Maximum FL Temp. Outside °C	Maximum FL Temp. Warm Ring °C	Maximum FL Temp. Center °C	Ring strength ΔT °C	Ring radius n mi	Eye radius n mi	RMW n mi	VMAX kt	Min Rossby length n mi	Dynamical eye size
FELIX	AL	15 Aug 1995 / 05:08	700 mb	11		15			10	95	77	78.6	0.13
FELIX	AL	15 Aug 1995 / 11:50	700 mb	12		15			10	100	51	117.1	0.09
FELIX	AL	15 Aug 1995 / 15:42	700 mb	11		14			10	77	83	63.2	0.16
FELIX	AL	15 Aug 1995 / 17:20	700 mb	12		14			10	100	76	85.6	0.12
FELIX	AL	15 Aug 1995 / 22:56	700 mb	12		16			8	76	57	87.4	0.09
FELIX	AL	16 Aug 1995 / 02:24	700 mb	12		17			8	103	72	93.1	0.08
FELIX	AL	16 Aug 1995 / 05:17	700 mb	12		15			6	17	53	24.3	0.27
FELIX	AL	18 Aug 1995 / 05:19	850 mb	17		20			30	69	59	84.2	0.36
IRIS	AL	23 Aug 1995 / 21:31	850 mb	23		21			12	41	48	30.0	0.42
IRIS	AL	29 Aug 1995 / 23:15	700 mb	12		21			10	24	76	17.2	0.58
IRIS	AL	30 Aug 1995 / 11:01	700 mb	11		16			10	28	83	18.7	0.54
LUIS	AL	07 Sep 1995 / 11:32	700 mb	10		16			12	47	103	23.2	0.54
LUIS	AL	07 Sep 1995 / 13:54	700 mb	11		17			10	47	91	26.4	0.38
LUIS	AL	08 Sep 1995 / 11:23	700 mb	12		16			10	26	88	17.5	0.57
MARILYN	AL	19 Sep 1995 / 00:15	700 mb	11		15			10	23	70	21.3	0.47
MARILYN	AL	19 Sep 1995 / 09:27	700 mb	12		14			7	37	56	43.4	0.16
MARILYN	AL	19 Sep 1995 / 11:37	700 mb	9		14			7	43	50	56.0	0.12
MARILYN	AL	19 Sep 1995 / 18:10	700 mb	11		14			20	62	90	47.9	0.42
OPAL	AL	02 Oct 1995 / 12:02	850 mb	20		22			12	32	60	25.8	0.49
OPAL	AL	02 Oct 1995 / 17:52	850 mb	17		22			15	44	60	35.0	0.43
OPAL	AL	02 Oct 1995 / 19:51	850 mb	19		22			15	33	48	33.2	0.45
OPAL	AL	03 Oct 1995 / 09:44	700 mb	15		16			15	28	50	28.7	0.52
OPAL	AL	03 Oct 1995 / 17:51	700 mb	15		16			11	19	49	21.0	0.52
OPAL	AL	03 Oct 1995 / 19:50	700 mb	13		18			11	25	71	19.4	0.57
OPAL	AL	04 Oct 1995 / 12:31	700 mb	15		26			4	10	86	7.5	0.47
OPAL	AL	04 Oct 1995 / 14:31	700 mb	12		23			4	57	83	41.9	0.10
OPAL	AL	04 Oct 1995 / 16:16	700 mb	15		25			2	10	109	6.1	0.41
ROXANNE	AL	09 Oct 1995 / 19:24	1500 ft	24		25			5	26	47	23.9	0.21
ROXANNE	AL	09 Oct 1995 / 21:16	1500 ft	24		25			5	35	50	30.2	0.17
ROXANNE	AL	09 Oct 1995 / 22:55	1500 ft	22		25			12	30	56	23.6	0.53
ROXANNE	AL	14 Oct 1995 / 03:04	850 mb	18		20			4	75	53	66.3	0.05
ROXANNE	AL	14 Oct 1995 / 05:02	850 mb	16		20			4	87	55	73.7	0.05
ROXANNE	AL	14 Oct 1995 / 11:42	850 mb	18		21			5	74	60	58.7	0.09
ROXANNE	AL	14 Oct 1995 / 13:25	850 mb	19		22			4	63	63	49.0	0.08
ROXANNE	AL	14 Oct 1995 / 15:28	850 mb	18		21			4	70	70	48.9	0.09

continued on next page

Table D.9: *continued*

Storm	Basin	Fix Date / Time UTC	Fix flight level	Maximum FL Temp. Outside °C	Warm Ring °C	Center °C	Ring strength ΔT °C	Ring radius n mi	Eye radius n mi	RMW n mi	VMAX kt	Min Rossby length n mi	Dynamical eye size
BERTHA	AL	08 Jul 1996 / 05:19	850 mb	16		20			12	77	76	39.7	0.32
BERTHA	AL	08 Jul 1996 / 07:00	850 mb	18		19			10	24	42	23.5	0.43
BERTHA	AL	08 Jul 1996 / 09:38	700 mb	10		14			15	70	55	50.2	0.30
BERTHA	AL	09 Jul 1996 / 15:30	700 mb	15		16			10	28	67	21.3	0.47
BERTHA	AL	10 Jul 1996 / 02:16	700 mb	9		14			10	104	56	89.3	0.11
BERTHA	AL	10 Jul 1996 / 05:58	850 mb	20		24			10	40	80	27.9	0.36
BERTHA	AL	10 Jul 1996 / 07:26	850 mb	20		22			8	40	99	23.0	0.33
BERTHA	AL	10 Jul 1996 / 08:48	850 mb	20		23			8	40	65	34.6	0.22
BERTHA	AL	10 Jul 1996 / 10:11	850 mb	20		23			8	34	75	26.0	0.29
BERTHA	AL	10 Jul 1996 / 11:54	850 mb	20		23			10	35	77	26.3	0.38
BERTHA	AL	10 Jul 1996 / 14:54	700 mb	11		16			8	78	63	67.1	0.12
BERTHA	AL	10 Jul 1996 / 16:41	700 mb	13		15			8	37	95	23.3	0.32
BERTHA	AL	10 Jul 1996 / 18:15	700 mb	10		16			8	32	79	24.5	0.31
BERTHA	AL	10 Jul 1996 / 20:41	700 mb	11		15			6	62	96	38.5	0.16
BERTHA	AL	11 Jul 1996 / 02:00	700 mb	11		16			9	26	68	24.1	0.37
BERTHA	AL	11 Jul 1996 / 04:09	700 mb	10		15			10	68	85	48.4	0.21
CESAR	AL	28 Jul 1996 / 02:56	850 mb	16		20			8	58	40	40.4	0.19
DOLLY	AL	22 Aug 1996 / 17:51	1500 ft	23		24			8	66	59	50.1	0.15
DOLLY	AL	22 Aug 1996 / 23:16	850 mb	19		21			5	10	42	11.7	0.43
DOLLY	AL	23 Aug 1996 / 00:59	850 mb	19		20			10	37	48	36.4	0.28
DOLLY	AL	23 Aug 1996 / 02:56	850 mb	18	22	21	+1	10	10	26	35	35.3	0.28
DOLLY	AL	23 Aug 1996 / 05:10	850 mb	19		21			12	81	46	77.8	0.16
EDOUARD	AL	30 Aug 1996 / 04:21	700 mb	10		18			5	23	115	12.2	0.41
EDOUARD	AL	30 Aug 1996 / 05:19	700 mb	12		18			5	22	104	13.0	0.39
EDOUARD	AL	30 Aug 1996 / 06:21	700 mb	12		17			5	21	108	12.0	0.42
EDOUARD	AL	30 Aug 1996 / 23:32	700 mb	12		18			8	33	110	20.1	0.37
EDOUARD	AL	31 Aug 1996 / 01:10	700 mb	11		21			10	31	106	19.8	0.50
EDOUARD	AL	31 Aug 1996 / 02:50	700 mb	9		16			10	32	109	20.0	0.50
EDOUARD	AL	31 Aug 1996 / 05:07	700 mb	9	18	18	+0	7	11	31	107	19.9	0.55
EDOUARD	AL	31 Aug 1996 / 13:27	700 mb	12		15			5	31	83	26.5	0.19
EDOUARD	AL	31 Aug 1996 / 15:09	700 mb	10		15			5	29	98	21.4	0.23
EDOUARD	AL	31 Aug 1996 / 17:07	700 mb	10		16			5	25	111	16.6	0.30
EDOUARD	AL	01 Sep 1996 / 05:05	700 mb	14		15			10	28	104	21.0	0.48
EDOUARD	AL	01 Sep 1996 / 12:15	700 mb	11		16			6	55	70	59.2	0.10
EDOUARD	AL	01 Sep 1996 / 14:39	700 mb	10		15			6	54	86	48.8	0.12

continued on next page

Table D.9: *continued*

Storm	Basin	Fix Date / Time UTC	Fix flight level	Maximum FL Temp. Outside °C	Warm Ring °C	Center °C	Ring strength ΔT °C	Ring radius n mi	Eye radius n mi	RMW n mi	VMAX kt	Min Rossby length n mi	Dynamical eye size
EDOUARD	AL	01 Sep 1996 / 15:33	700 mb	12		14			6	58	85	52.7	0.11
EDOUARD	AL	01 Sep 1996 / 17:03	700 mb	8		13			8	101	83	87.7	0.09
EDOUARD	AL	02 Sep 1996 / 10:39	700 mb	10		13			6	28	75	32.2	0.19
EDOUARD	AL	02 Sep 1996 / 11:35	700 mb	7		11			8	71	62	88.1	0.09
FRAN	AL	30 Aug 1996 / 09:14	850 mb	17		23			15	64	58	47.9	0.31
FRAN	AL	30 Aug 1996 / 12:22	850 mb	19	25	24	+1	9	15	49	55	39.7	0.38
FRAN	AL	01 Sep 1996 / 19:36	850 mb	19		21			12	32	71	23.4	0.53
FRAN	AL	01 Sep 1996 / 21:22	850 mb	18		21			12	29	63	24.1	0.52
FRAN	AL	01 Sep 1996 / 23:07	850 mb	18		22			12	41	75	28.5	0.44
FRAN	AL	03 Sep 1996 / 06:38	700 mb	9		14			15	45	64	38.3	0.39
FRAN	AL	03 Sep 1996 / 10:26	700 mb	11		15			15	44	79	31.1	0.48
FRAN	AL	05 Sep 1996 / 00:23	700 mb	10	17	15	+2	9	10	50	95	33.6	0.30
FRAN	AL	05 Sep 1996 / 02:53	700 mb	12		18			10	28	102	18.2	0.55
FRAN	AL	05 Sep 1996 / 11:05	700 mb	13		14			12	48	94	34.6	0.36
FRAN	AL	05 Sep 1996 / 12:37	700 mb	11		14			12	32	78	28.4	0.44
FRAN	AL	05 Sep 1996 / 20:58	700 mb	8		14			10	86	73	77.7	0.13
FRAN	AL	05 Sep 1996 / 22:09	700 mb	7		15			10	63	107	42.2	0.24
JOSEPHINE	AL	07 Oct 1996 / 15:36	1500 ft	25		26			10	73	60	69.6	0.14
JOSEPHINE	AL	07 Oct 1996 / 17:31	1500 ft	23		25			12	39	51	46.6	0.27
LILI	AL	18 Oct 1996 / 05:32	850 mb	18		21			8	48	73	32.4	0.23
DANNY	AL	18 Jul 1997 / 12:27	1500 ft	22		24			8	12	61	13.4	0.56
DANNY	AL	18 Jul 1997 / 16:18	1500 ft	22		24			5	10	75	9.2	0.54
DANNY	AL	18 Jul 1997 / 17:12	1500 ft	23		24			5	9	70	8.9	0.56
DANNY	AL	18 Jul 1997 / 18:48	1500 ft	23		25			8	13	59	15.0	0.50
DANNY	AL	18 Jul 1997 / 23:25	1500 ft	22		24			5	20	69	19.7	0.25
DANNY	AL	19 Jul 1997 / 04:55	850 mb	22		20			6	13	78	11.6	0.52
DANNY	AL	19 Jul 1997 / 08:54	850 mb	16		20			6	11	67	11.5	0.52
DANNY	AL	19 Jul 1997 / 11:42	850 mb	16		19			3	7	64	7.7	0.39
DANNY	AL	19 Jul 1997 / 12:59	850 mb	16		19			3	14	68	14.3	0.21
DANNY	AL	19 Jul 1997 / 14:10	850 mb	17		21			5	9	60	10.5	0.47
ERIKA	AL	06 Sep 1997 / 03:53	850 mb	17		22			10	88	76	46.2	0.22
ERIKA	AL	06 Sep 1997 / 05:03	850 mb	17		24			10	84	48	67.3	0.15
ERIKA	AL	06 Sep 1997 / 09:00	850 mb	20		23			5	21	64	14.3	0.35
ERIKA	AL	07 Sep 1997 / 08:06	700 mb	9		16			11	36	83	20.1	0.55
ERIKA	AL	07 Sep 1997 / 09:48	700 mb	9		16			15	53	63	38.1	0.39

continued on next page

Table D.9: *continued*

Storm	Basin	Fix Date / Time UTC	Fix flight level	Maximum FL Temp. Outside °C	Maximum FL Temp. Warm Ring °C	Maximum FL Temp. Center °C	Ring strength ΔT °C	Ring radius n mi	Eye radius n mi	RMW n mi	VMAX kt	Min Rossby length n mi	Dynamical eye size
ERIKA	AL	09 Sep 1997 / 17:30	700 mb	10		16			15	41	77	33.0	0.45
LINDA	EP	14 Sep 1997 / 19:46	700 mb	11		15			3	42	84	25.3	0.12
LINDA	EP	14 Sep 1997 / 21:19	700 mb	11		14			3	43	68	31.7	0.09
LINDA	EP	14 Sep 1997 / 23:07	700 mb	11		14			5	25	65	19.8	0.25
BONNIE	AL	22 Aug 1998 / 05:35	1500 ft	24		25			10	27	76	18.0	0.56
BONNIE	AL	22 Aug 1998 / 11:26	850 mb	20	26	24	+2	10	14	24	51	24.2	0.58
BONNIE	AL	22 Aug 1998 / 13:50	850 mb	19		24			16	30	53	29.0	0.57
BONNIE	AL	22 Aug 1998 / 16:32	850 mb	19		23			12	35	80	23.1	0.54
BONNIE	AL	22 Aug 1998 / 23:37	850 mb	19		22			10	31	79	21.2	0.47
BONNIE	AL	24 Aug 1998 / 00:17	700 mb	12		18			10	51	78	36.3	0.28
BONNIE	AL	24 Aug 1998 / 01:51	700 mb	14		19			12	44	88	28.4	0.44
BONNIE	AL	24 Aug 1998 / 03:44	700 mb	10		15			12	40	105	21.9	0.57
BONNIE	AL	24 Aug 1998 / 23:40	700 mb	16		21			15	44	81	32.5	0.46
BONNIE	AL	26 Aug 1998 / 18:43	700 mb	11		15			8	36	103	26.1	0.33
BONNIE	AL	26 Aug 1998 / 20:32	700 mb	10		17			10	41	108	28.4	0.35
BONNIE	AL	27 Aug 1998 / 02:24	700 mb	10		15			15	60	86	50.4	0.30
BONNIE	AL	27 Aug 1998 / 03:25	700 mb	11		15			15	44	85	38.4	0.39
BONNIE	AL	27 Aug 1998 / 05:01	700 mb	10		16			12	74	78	66.6	0.19
BONNIE	AL	27 Aug 1998 / 06:00	700 mb	12		15			12	35	76	34.6	0.36
BONNIE	AL	27 Aug 1998 / 07:01	700 mb	11		15			12	59	79	54.0	0.23
BONNIE	AL	27 Aug 1998 / 08:01	700 mb	10		15			5	69	71	68.4	0.07
DANIELLE	AL	27 Aug 1998 / 13:19	700 mb	10		15			8	89	60	67.6	0.11
DANIELLE	AL	27 Aug 1998 / 15:05	700 mb	10		13			10	43	56	37.3	0.27
DANIELLE	AL	29 Aug 1998 / 11:42	850 mb	18		22			5	27	57	26.6	0.19
DANIELLE	AL	29 Aug 1998 / 13:30	850 mb	18		23			5	33	42	43.1	0.12
DANIELLE	AL	29 Aug 1998 / 15:19	850 mb	18		22			4	26	58	25.7	0.16
DANIELLE	AL	29 Aug 1998 / 17:16	850 mb	18		22			5	29	67	25.1	0.20
DANIELLE	AL	29 Aug 1998 / 23:23	850 mb	16		22			5	34	68	29.2	0.17
DANIELLE	AL	30 Aug 1998 / 01:12	850 mb	20		22			6	34	42	45.9	0.14
DANIELLE	AL	30 Aug 1998 / 05:10	850 mb	18		21			10	34	69	29.3	0.34
DANIELLE	AL	30 Aug 1998 / 11:48	850 mb	18		20			8	43	62	41.0	0.18
DANIELLE	AL	30 Aug 1998 / 13:35	850 mb	18		21			8	23	48	29.2	0.26
DANIELLE	AL	30 Aug 1998 / 15:26	850 mb	17		20			8	43	55	46.4	0.16
DANIELLE	AL	30 Aug 1998 / 17:26	850 mb	18		21			10	41	68	36.6	0.27
DANIELLE	AL	31 Aug 1998 / 00:00	700 mb	10		16			10	23	66	22.2	0.45

continued on next page

Table D.9: *continued*

Storm	Basin	Fix Date / Time UTC	Fix flight level	Maximum FL Temp. Outside °C	Maximum FL Temp. Warm Ring °C	Maximum FL Temp. Center °C	Ring strength ΔT °C	Ring radius n mi	Eye radius n mi	RMW n mi	VMAX kt	Min Rossby length n mi	Dynamical eye size
DANIELLE	AL	31 Aug 1998 / 01:39	700 mb	10		15			10	21	67	20.1	0.50
DANIELLE	AL	31 Aug 1998 / 03:12	700 mb	11		16			10	17	66	16.7	0.60
DANIELLE	AL	01 Sep 1998 / 03:03	700 mb	9		16			10	52	71	49.1	0.20
GEORGES	AL	21 Sep 1998 / 17:57	700 mb	13	17	15	+2	8	8	23	70	13.9	0.54
GEORGES	AL	24 Sep 1998 / 23:32	850 mb	19		21			18	80	68	57.5	0.30
GEORGES	AL	25 Sep 1998 / 20:12	850 mb	19		23			8	26	71	20.8	0.36
GEORGES	AL	25 Sep 1998 / 21:36	850 mb	19		24			8	34	77	24.9	0.30
GEORGES	AL	25 Sep 1998 / 22:21	850 mb	19		24			8	51	82	34.5	0.22
GEORGES	AL	26 Sep 1998 / 02:22	850 mb	16		24			12	85	82	55.7	0.22
GEORGES	AL	26 Sep 1998 / 08:48	850 mb	18		21			10	24	77	18.4	0.54
GEORGES	AL	26 Sep 1998 / 17:55	850 mb	19		23			15	36	85	25.3	0.59
GEORGES	AL	27 Sep 1998 / 11:00	850 mb	18	23	21	+2	11	10	52	81	39.8	0.25
GEORGES	AL	27 Sep 1998 / 11:07	850 mb	18	23	22	+1	11	10	95	88	63.7	0.16
GEORGES	AL	27 Sep 1998 / 17:53	700 mb	13		16			10	24	66	23.7	0.42
GEORGES	AL	27 Sep 1998 / 19:35	700 mb	11		15			10	32	76	27.4	0.37
GEORGES	AL	27 Sep 1998 / 23:12	700 mb	11		15			10	35	78	29.3	0.34
GEORGES	AL	28 Sep 1998 / 03:15	700 mb	12	16	15	+1	9	10	20	64	21.0	0.48
GEORGES	AL	28 Sep 1998 / 04:08	700 mb	11	16	15	+1	11	10	36	72	32.9	0.30
GEORGES	AL	28 Sep 1998 / 06:05	700 mb	11		16			10	27	90	20.3	0.49
BRET	AL	20 Aug 1999 / 23:30	850 mb	18		22			5	22	49	22.8	0.22
BRET	AL	21 Aug 1999 / 03:09	850 mb	18		23			6	18	65	14.5	0.42
BRET	AL	21 Aug 1999 / 05:06	850 mb	19		24			4	17	56	15.9	0.28
BRET	AL	21 Aug 1999 / 11:51	850 mb	19		23			4	10	79	7.0	0.50
BRET	AL	21 Aug 1999 / 17:03	850 mb	19		22			5	13	72	10.1	0.49
DENNIS	AL	27 Aug 1999 / 13:43	850 mb	17		23			10	44	67	37.5	0.27
DENNIS	AL	27 Aug 1999 / 15:18	700 mb	9		15			12	91	53	88.6	0.14
DENNIS	AL	27 Aug 1999 / 17:03	700 mb	11		16			20	41	53	43.9	0.46
DENNIS	AL	28 Aug 1999 / 08:24	700 mb	11		18			18	34	59	34.5	0.51
DENNIS	AL	28 Aug 1999 / 11:43	700 mb	11		16			18	48	66	43.1	0.41
DENNIS	AL	28 Aug 1999 / 13:08	700 mb	11		16			18	60	69	51.0	0.34
DENNIS	AL	28 Aug 1999 / 14:12	surface	9	16	15	+1	11	18	58	102	34.6	0.51
DENNIS	AL	29 Aug 1999 / 11:39	700 mb	11		16			15	37	84	29.4	0.51
DENNIS	AL	29 Aug 1999 / 17:22	700 mb	9	17	15	+2	7	22	69	89	50.9	0.44
DENNIS	AL	30 Aug 1999 / 00:12	700 mb	9		16			18	81	74	71.4	0.25
DENNIS	AL	30 Aug 1999 / 03:50	700 mb	11	18	15	+3	18	18	83	84	65.9	0.27

continued on next page

Table D.9: *continued*

Storm	Basin	Fix Date / Time UTC	Fix flight level	Maximum FL Temp. Outside °C	Maximum FL Temp. Warm Ring °C	Maximum FL Temp. Center °C	Ring strength ΔT °C	Ring radius n mi	Eye radius n mi	RMW n mi	VMAX kt	Min Rossby length n mi	Dynamical eye size
DENNIS	AL	30 Aug 1999 / 05:43	700 mb	10		20			20	73	84	59.3	0.34
DENNIS	AL	30 Aug 1999 / 07:09	700 mb	11	18	17	+1	18	20	59	73	55.9	0.36
DENNIS	AL	30 Aug 1999 / 10:17	700 mb	12	18	17	+1	10	20	76	95	55.8	0.36
DENNIS	AL	30 Aug 1999 / 11:27	700 mb	12		17			20	34	72	34.5	0.58
DENNIS	AL	31 Aug 1999 / 00:25	700 mb	10	21	17	+4	25	20	66	74	63.8	0.31
DENNIS	AL	04 Sep 1999 / 17:18	850 mb	20		21			12	29	50	42.8	0.29
DENNIS	AL	04 Sep 1999 / 18:41	850 mb	18		21			12	21	71	22.8	0.55
DENNIS	AL	04 Sep 1999 / 19:56	850 mb	17		20			12	34	56	44.8	0.28
DENNIS	AL	04 Sep 1999 / 20:51	850 mb	17		21			12	71	48	97.9	0.13
FLOYD	AL	11 Sep 1999 / 17:41	700 mb	11	22	18	+4	13	10	31	75	21.5	0.47
FLOYD	AL	11 Sep 1999 / 19:19	700 mb	12	19	17	+2	6	12	40	66	31.0	0.40
FLOYD	AL	11 Sep 1999 / 23:11	700 mb	10	17	16	+1	7	12	42	83	26.3	0.48
FLOYD	AL	14 Sep 1999 / 23:23	700 mb	13		17			8	28	103	17.0	0.50
GERT	AL	20 Sep 1999 / 17:48	700 mb	9		13			10	73	81	54.2	0.18
GERT	AL	20 Sep 1999 / 19:41	700 mb	9		14			10	59	91	40.5	0.25
IRENE	AL	14 Oct 1999 / 22:10	850 mb	18		22			5	8	38	11.5	0.44
IRENE	AL	14 Oct 1999 / 23:38	850 mb	20		21			6	69	59	58.1	0.10
IRENE	AL	17 Oct 1999 / 23:40		18		20			10	28	48	41.8	0.24
IRENE	AL	18 Oct 1999 / 01:08	850 mb	16		22			6	58	62	64.4	0.09
IRENE	AL	18 Oct 1999 / 02:05	850 mb	17		21			4	33	43	54.2	0.07
IRENE	AL	18 Oct 1999 / 05:42	850 mb	19	27	21	+6	4	2	29	67	32.8	0.05
DORA	EP	17 Aug 1999 / 23:46	700 mb	8	16	14	+2	15	12	38	53	26.0	0.48
EUGENE	EP	12 Aug 1999 / 23:26	700 mb	8	16	14	+2	9	12	53	49	36.3	0.34
DEBBY	AL	22 Aug 2000 / 17:53	700 mb	9		15			12	29	41	30.4	0.41
FLORENCE	AL	13 Sep 2000 / 16:54	850 mb	18		20			2	12	48	17.4	0.09
GORDON	AL	17 Sep 2000 / 11:38	700 mb	5		18			15	54	52	59.6	0.25
GORDON	AL	17 Sep 2000 / 13:28	700 mb	7		19			15	65	65	58.3	0.26
GORDON	AL	17 Sep 2000 / 15:24	850 mb	19		23			15	40	66	37.1	0.40
GORDON	AL	17 Sep 2000 / 17:06	850 mb	14		22			15	67	46	82.1	0.18
KEITH	AL	05 Oct 2000 / 05:51	700 mb	14	14	13	+1	8	10	38	77	24.1	0.41
KEITH	AL	05 Oct 2000 / 07:26	700 mb	11	13	12	+1	6	10	62	62	47.1	0.21
IRIS	AL	05 Oct 2001 / 19:26	850 mb	15		18			5	26	58	16.5	0.30
IRIS	AL	06 Oct 2001 / 07:10	850 mb	16		20			8	53	47	41.1	0.18
MICHELLE	AL	04 Nov 2001 / 00:13	700 mb	10		16			6	26	116	10.5	0.57
GUSTAV	AL	10 Sep 2002 / 14:49	1500 ft	23		26			9	40	51	56.4	0.16

continued on next page

Table D.9: *continued*

Storm	Basin	Fix Date / Time UTC	Fix flight level	Maximum FL Temp. Outside °C	Warm Ring °C	Center °C	Ring strength ΔT °C	Ring radius n mi	Eye radius n mi	RMW n mi	VMAX kt	Min Rossby length n mi	Dynamical eye size
GUSTAV	AL	10 Sep 2002 / 17:59	850 mb	17		19			18	21	53	30.5	0.57
LILI	AL	29 Sep 2002 / 03:38	850 mb	20		21			6	11	37	13.3	0.45
LILI	AL	29 Sep 2002 / 05:05	850 mb	18		22			5	19	53	15.9	0.32
LILI	AL	29 Sep 2002 / 13:42	850 mb	16		22			4	9	57	7.1	0.57
LILI	AL	29 Sep 2002 / 15:04	850 mb	17		24			5	8	40	8.9	0.56
LILI	AL	01 Oct 2002 / 03:32	700 mb	10		14			8	16	62	12.6	0.59
LILI	AL	03 Oct 2002 / 01:07	700 mb	14		23			4	10	93	6.8	0.59
LILI	AL	03 Oct 2002 / 05:18	700 mb	12		22			5	12	92	8.5	0.59
CLAUDETTE	AL	10 Jul 2003 / 13:52	700 mb	10		16			5	14	69	8.6	0.58
CLAUDETTE	AL	14 Jul 2003 / 09:28	850 mb	20		21			8	20	60	20.2	0.37
CLAUDETTE	AL	14 Jul 2003 / 11:06	850 mb	17		23			8	21	49	25.9	0.29
CLAUDETTE	AL	15 Jul 2003 / 03:54	850 mb	15		20			12	23	43	33.3	0.35
CLAUDETTE	AL	15 Jul 2003 / 12:52	700 mb	9	15	13	+2	8	15	20	51	25.1	0.60
ERIKA	AL	16 Aug 2003 / 02:20	700 mb	14	17	16	+1	13	6	25	67	22.0	0.27
ERIKA	AL	16 Aug 2003 / 03:47	700 mb	10		15			10	19	44	25.3	0.40
ERIKA	AL	16 Aug 2003 / 05:22	700 mb	9	18	16	+2	15	8	101	36	130.2	0.06
ERIKA	AL	16 Aug 2003 / 06:50	700 mb	11	18	16	+2	8	8	28	62	26.3	0.29
ERIKA	AL	16 Aug 2003 / 08:25	700 mb	14	18	15	+3		8	17	66	15.2	0.49
FABIAN	AL	06 Sep 2003 / 05:57	700 mb	13		18			10	29	101	22.3	0.45
ISABEL	AL	16 Sep 2003 / 07:01	700 mb	13		17			20	57	92	36.4	0.55
ISABEL	AL	16 Sep 2003 / 19:53	700 mb	9		15			12	53	83	39.1	0.32
ISABEL	AL	16 Sep 2003 / 22:13	700 mb	10	16	15	+1	9	12	52	103	31.7	0.39
ISABEL	AL	17 Sep 2003 / 14:49	700 mb	11	16	15	+1	21	20	46	80	38.0	0.53
ISABEL	AL	17 Sep 2003 / 23:44	700 mb	15		17			22	73	97	50.4	0.45
ISABEL	AL	18 Sep 2003 / 01:17	700 mb	14	17	17	+0	36	12	41	85	33.6	0.37
ISABEL	AL	18 Sep 2003 / 02:56	700 mb	13		17			14	41	93	31.2	0.45
ISABEL	AL	18 Sep 2003 / 04:00	700 mb	14		16			15	50	109	32.5	0.46
ISABEL	AL	18 Sep 2003 / 05:03	700 mb	15		16			20	52	90	40.5	0.49
ISABEL	AL	18 Sep 2003 / 08:57	700 mb	11	15	14	+1		20	40	76	37.9	0.53
ISABEL	AL	18 Sep 2003 / 10:53	700 mb	9		15			15	42	91	33.8	0.44
ISABEL	AL	18 Sep 2003 / 13:02	700 mb	8		15			12	47	111	31.6	0.40
JIMENA	EP	01 Sep 2003 / 05:51	700 mb	10		17			10	30	57	21.9	0.46
JIMENA	EP	01 Sep 2003 / 11:04	700 mb	11		16			10	13	28	18.9	0.53
ALEX	AL	02 Aug 2004 / 17:04	850 mb	17		19			10	13	50	18.7	0.54
ALEX	AL	03 Aug 2004 / 00:18	850 mb	17		19			12	16	52	22.4	0.56

continued on next page

Table D.9: *continued*

Storm	Basin	Fix Date / Time UTC	Fix flight level	Maximum FL Temp. Outside °C	Warm Ring °C	Center °C	Ring strength ΔT °C	Ring radius n mi	Eye radius n mi	RMW n mi	VMAX kt	Min Rossby length n mi	Dynamical eye size
ALEX	AL	03 Aug 2004 / 01:19	850 mb	17		21			5	10	62	12.0	0.42
ALEX	AL	03 Aug 2004 / 03:09	850 mb	16		21			8	17	67	18.7	0.40
ALEX	AL	03 Aug 2004 / 05:16	850 mb	18		21			5	17	81	15.7	0.32
ALEX	AL	03 Aug 2004 / 12:58	700 mb	11		19			10	19	72	20.3	0.49
ALEX	AL	03 Aug 2004 / 14:29	700 mb	16	19	19	+0	6	12	21	71	22.8	0.55
BONNIE	AL	09 Aug 2004 / 21:54	1500 ft	22		26			4	13	53	13.3	0.30
BONNIE	AL	10 Aug 2004 / 05:39	850 mb	18		21			5	14	30	25.1	0.20
BONNIE	AL	10 Aug 2004 / 07:26	850 mb	17		21			5	8	49	9.1	0.55
BONNIE	AL	11 Aug 2004 / 08:15	850 mb	18		21			10	13	44	17.4	0.57
BONNIE	AL	11 Aug 2004 / 10:04	850 mb	17		23			8	22	52	24.7	0.30
CHARLEY	AL	11 Aug 2004 / 14:13	850 mb	17		21			2	6	48	5.0	0.50
CHARLEY	AL	12 Aug 2004 / 04:04	850 mb	18		21			5	18	47	16.1	0.31
FRANCES	AL	02 Sep 2004 / 21:12		20		21			15	52	81	34.7	0.43
FRANCES	AL	03 Sep 2004 / 17:28	700 mb	10		17			10	64	74	48.2	0.21
FRANCES	AL	04 Sep 2004 / 14:12	700 mb	11	16	15	+1	11	15	50	79	37.7	0.40
FRANCES	AL	04 Sep 2004 / 15:22	700 mb	11		16			15	37	85	26.5	0.57
IVAN	AL	16 Sep 2004 / 06:49	700 mb	15		17			10	25	72	23.7	0.42
IVAN	AL	16 Sep 2004 / 07:12	700 mb	14		17			10	20	67	20.6	0.49
JEANNE	AL	18 Sep 2004 / 11:24	1500 ft	24		26			5	16	50	15.8	0.32
JEANNE	AL	20 Sep 2004 / 06:10	850 mb	16		20			12	37	46	45.2	0.28
JEANNE	AL	20 Sep 2004 / 09:51	850 mb	15		19			25	66	59	61.9	0.40
JEANNE	AL	20 Sep 2004 / 18:15	850 mb	17		23			15	35	65	32.8	0.46
JEANNE	AL	24 Sep 2004 / 05:12	700 mb	10		13			15	39	74	30.9	0.48
JEANNE	AL	24 Sep 2004 / 17:57	700 mb	10		15			12	28	72	23.4	0.53
DENNIS	AL	09 Jul 2005 / 05:26	700 mb	9		12			6	28	69	21.8	0.28
DENNIS	AL	09 Jul 2005 / 06:06	700 mb	10		12			6	31	71	23.5	0.26
DENNIS	AL	09 Jul 2005 / 07:11	700 mb	11		13			6	8	43	10.3	0.58
DENNIS	AL	09 Jul 2005 / 08:24	700 mb	11		14			6	22	66	18.4	0.33
DENNIS	AL	09 Jul 2005 / 08:46	700 mb	12		14			5	14	53	14.7	0.34
DENNIS	AL	10 Jul 2005 / 22:19		5		11			4	97	62	94.5	0.04
EMILY	AL	20 Jul 2005 / 07:45	700 mb	12		19			8	35	107	18.7	0.43
FRANKLIN	AL	23 Jul 2005 / 01:48	850 mb	17		19			8	21	39	33.8	0.22
FRANKLIN	AL	23 Jul 2005 / 23:59	850 mb	18	21	20	+1	10	5	7	31	14.6	0.34
IRENE	AL	12 Aug 2005 / 18:14	850 mb	17		22			4	24	57	27.0	0.15
IRENE	AL	14 Aug 2005 / 17:18	850 mb	17		20			8	15	50	22.7	0.35

continued on next page

Table D.9: *continued*

Storm	Basin	Fix Date / Time UTC	Fix flight level	Maximum FL Temp. Outside °C	Maximum FL Temp. Warm Ring °C	Maximum FL Temp. Center °C	Ring strength ΔT °C	Ring radius n mi	Eye radius n mi	RMW n mi	VMAX kt	Min Rossby length n mi	Dynamical eye size
IRENE	AL	14 Aug 2005 / 17:32	850 mb	16		19			9	17	54	23.8	0.38
IRENE	AL	14 Aug 2005 / 19:45	850 mb	17		19			8	15	67	17.3	0.43
IRENE	AL	14 Aug 2005 / 21:18	850 mb	14		20			10	19	79	18.6	0.54
KATRINA	AL	24 Aug 2005 / 23:05	1500 ft	21	25	24	+1	11	8	19	35	31.7	0.25
KATRINA	AL	25 Aug 2005 / 17:18	850 mb	19		22			6	16	64	15.2	0.39
KATRINA	AL	26 Aug 2005 / 14:34	700 mb	10		17			4	13	81	9.5	0.48
KATRINA	AL	26 Aug 2005 / 15:56	700 mb	13		18			5	19	74	15.0	0.33
KATRINA	AL	27 Aug 2005 / 11:07	700 mb	16	23	20	+3	7	4	31	85	20.5	0.22
KATRINA	AL	27 Aug 2005 / 15:14	700 mb	12		16			6	44	87	28.1	0.23
KATRINA	AL	27 Aug 2005 / 17:59	700 mb	12		17			4	31	89	19.7	0.23
KATRINA	AL	27 Aug 2005 / 20:09	700 mb	11		19			4	29	85	19.4	0.21
KATRINA	AL	29 Aug 2005 / 10:02	700 mb	11		18			12	35	109	21.2	0.59
KATRINA	AL	29 Aug 2005 / 10:55	700 mb	11		18			11	40	88	29.7	0.37
KATRINA	AL	29 Aug 2005 / 12:09	700 mb	10	19	18	+1	10	12	34	116	19.7	0.58
KATRINA	AL	29 Aug 2005 / 12:47		12		20			15	58	117	32.7	0.46
NATE	AL	08 Sep 2005 / 05:59	700 mb	13	16	14	+2	18	18	27	59	30.6	0.57
OPHELIA	AL	08 Sep 2005 / 01:45	850 mb	17		21			9	24	48	32.2	0.28
OPHELIA	AL	08 Sep 2005 / 03:16	850 mb	18		20			10	36	39	56.4	0.18
OPHELIA	AL	09 Sep 2005 / 02:24	850 mb	19	24	22	+2	12	12	19	57	21.8	0.57
OPHELIA	AL	09 Sep 2005 / 17:09	850 mb	18		24			5	32	60	35.0	0.14
OPHELIA	AL	10 Sep 2005 / 17:17	700 mb	9		15			17	40	77	36.1	0.47
OPHELIA	AL	11 Sep 2005 / 11:25	700 mb	10		13			16	25	63	27.9	0.57
OPHELIA	AL	12 Sep 2005 / 00:29	700 mb	11		14			10	58	74	52.0	0.19
OPHELIA	AL	13 Sep 2005 / 13:20	700 mb	10		12			9	64	66	64.5	0.14
OPHELIA	AL	13 Sep 2005 / 15:08	700 mb	9		12			8	42	56	51.1	0.16
OPHELIA	AL	14 Sep 2005 / 01:54	700 mb	9		14			18	37	69	38.0	0.46
OPHELIA	AL	14 Sep 2005 / 02:54	700 mb	9		13			22	39	72	38.5	0.58
OPHELIA	AL	14 Sep 2005 / 05:49	700 mb	10		15			25	46	62	51.6	0.48
OPHELIA	AL	14 Sep 2005 / 07:06	700 mb	9		15			25	39	66	42.1	0.59
OPHELIA	AL	14 Sep 2005 / 08:50	700 mb	9		14			25	47	64	51.5	0.49
OPHELIA	AL	14 Sep 2005 / 17:15	700 mb	10		16			20	34	73	34.4	0.58
OPHELIA	AL	15 Sep 2005 / 08:32	700 mb	14	15	13	+2	27	20	27	59	34.6	0.58
RITA	AL	24 Sep 2005 / 04:31	700 mb	10	18	17	+1	26	15	43	107	26.4	0.57
RITA	AL	24 Sep 2005 / 07:03		9		19			12	47	108	28.9	0.42
WILMA	AL	20 Oct 2005 / 05:13	700 mb	16		18			2	34	120	12.1	0.16

continued on next page

Table D.9: *continued*

Storm	Basin	Fix Date / Time UTC	Fix flight level	Maximum FL Temp. Outside °C	Warm Ring °C	Center °C	Ring strength ΔT °C	Ring radius n mi	Eye radius n mi	RMW n mi	VMAX kt	Min Rossby length n mi	Dynamical eye size
WILMA	AL	20 Oct 2005 / 06:49	700 mb	16		17			2	26	112	10.0	0.20
WILMA	AL	20 Oct 2005 / 08:34	700 mb	16		22			2	21	120	7.6	0.20
WILMA	AL	20 Oct 2005 / 10:20	700 mb	12		19			4	23	122	8.2	0.43
WILMA	AL	23 Oct 2005 / 05:28	700 mb	8		14			10	30	79	19.3	0.52
WILMA	AL	23 Oct 2005 / 07:06	700 mb	9		14			10	36	78	23.4	0.43
WILMA	AL	23 Oct 2005 / 11:06	700 mb	10		14			32	93	68	64.8	0.50
WILMA	AL	23 Oct 2005 / 14:58	700 mb	12		14			5	34	67	26.4	0.19
WILMA	AL	23 Oct 2005 / 16:34	700 mb	12		14			5	97	80	59.5	0.08
BERYL	AL	20 Jul 2006 / 05:36	850 mb	16		20			18	37	44	63.8	0.27
ERNESTO	AL	31 Aug 2006 / 08:17	850 mb	17		18			12	33	33	62.3	0.20
ERNESTO	AL	31 Aug 2006 / 09:18	850 mb	17		18			12	49	50	61.4	0.20
ERNESTO	AL	31 Aug 2006 / 11:02	850 mb	16		18			12	23	61	25.6	0.49
ERNESTO	AL	31 Aug 2006 / 23:51	850 mb	15		19			10	17	48	26.2	0.38
FLORENCE	AL	10 Sep 2006 / 05:24	850 mb	16		22			15	29	45	38.5	0.39
LANE	EP	15 Sep 2006 / 17:27	700 mb	9		14			4	24	58	19.4	0.23
LANE	EP	15 Sep 2006 / 18:44	700 mb	9		14			4	24	58	19.4	0.23
LANE	EP	15 Sep 2006 / 19:05	700 mb	8		13			4	10	56	8.7	0.46
DEAN	AL	22 Aug 2007 / 14:40	700 mb	6	16	15	+1	26	8	37	86	20.6	0.41
DEAN	AL	22 Aug 2007 / 15:10	700 mb	13		15			9	28	83	16.2	0.55
FELIX	AL	03 Sep 2007 / 11:09	700 mb	12		25			4	52	130	13.5	0.30
HUMBERTO	AL	13 Sep 2007 / 04:47	850 mb	13		21			4	8	79	6.9	0.58
HUMBERTO	AL	13 Sep 2007 / 05:24	850 mb	17		22			3	7	55	8.7	0.35
DOLLY	AL	22 Jul 2008 / 12:51	700 mb	9	13	12	+1	7	10	51	54	49.1	0.20
DOLLY	AL	22 Jul 2008 / 13:43	700 mb	19		22			10	21	48	24.0	0.42
DOLLY	AL	23 Jul 2008 / 03:42	700 mb	13	13	13	+0	18	12	31	61	29.0	0.43
DOLLY	AL	23 Jul 2008 / 08:07	700 mb	9		14			10	26	73	21.0	0.48
FAY	AL	19 Aug 2008 / 08:18	850 mb	16		19			4	14	43	19.4	0.21
FAY	AL	21 Aug 2008 / 02:10	850 mb	16	20	19	+1	18	25	47	59	49.6	0.50
GUSTAV	AL	27 Aug 2008 / 05:51	700 mb	6		11			6	30	42	30.4	0.20
GUSTAV	AL	27 Aug 2008 / 07:57	700 mb	6		10			3	20	22	38.3	0.08
GUSTAV	AL	27 Aug 2008 / 09:18	700 mb	6		11			4	93	38	92.4	0.04
GUSTAV	AL	27 Aug 2008 / 18:06	850 mb	16		19			8	88	31	105.0	0.08
GUSTAV	AL	29 Aug 2008 / 09:43	700 mb	10		11			5	19	54	15.1	0.33
GUSTAV	AL	29 Aug 2008 / 17:20	700 mb	10		13			8	36	48	32.1	0.23
GUSTAV	AL	29 Aug 2008 / 23:05				14			10	31	58	23.7	0.42

continued on next page

Table D.9: *continued*

Storm	Basin	Fix Date / Time UTC	Fix flight level	Maximum FL Temp. Outside °C	Warm Ring °C	Center °C	Ring strength ΔT °C	Ring radius n mi	Eye radius n mi	RMW n mi	VMAX kt	Min Rossby length n mi	Dynamical eye size
GUSTAV	AL	31 Aug 2008 / 17:37	700 mb	9		16			8	24	105	13.8	0.55
GUSTAV	AL	01 Sep 2008 / 12:30	700 mb			16			15	44	81	34.7	0.43
IKE	AL	06 Sep 2008 / 05:11	700 mb	11		15			8	21	82	13.5	0.59
IKE	AL	08 Sep 2008 / 20:13	700 mb	9		13			5	23	53	21.5	0.23
IKE	AL	08 Sep 2008 / 21:08	700 mb	8		12			5	27	58	23.1	0.22
IKE	AL	08 Sep 2008 / 23:06	700 mb	10	14	14	+0	7	5	20	63	16.1	0.31
IKE	AL	09 Sep 2008 / 06:18	700 mb	11		14			4	20	69	14.9	0.27
IKE	AL	09 Sep 2008 / 07:08	700 mb	11		14			3	8	53	7.9	0.38
IKE	AL	09 Sep 2008 / 09:50	700 mb	11		14			4	14	56	13.0	0.35
IKE	AL	09 Sep 2008 / 11:06	700 mb	10		14			4	15	49	16.0	0.22
IKE	AL	09 Sep 2008 / 11:33	700 mb	12		14			4	7	43	8.6	0.52
IKE	AL	09 Sep 2008 / 20:00	700 mb	12		12			8	65	60	53.7	0.14
IKE	AL	09 Sep 2008 / 21:15	700 mb	9		14			8	99	61	76.8	0.11
IKE	AL	09 Sep 2008 / 23:02	700 mb	10		13			6	74	51	70.0	0.09
IKE	AL	10 Sep 2008 / 17:29	700 mb	10	16	15	+1	6	5	53	73	39.1	0.13
IKE	AL	10 Sep 2008 / 19:09	700 mb	11	16	15	+1	9	5	91	89	53.8	0.09
IKE	AL	10 Sep 2008 / 23:06	700 mb	11		17			4	35	68	28.8	0.14
IKE	AL	11 Sep 2008 / 07:25	700 mb	11		17			4	36	97	21.4	0.19
IKE	AL	11 Sep 2008 / 09:05	700 mb	7	17	16	+1	8	2	98	93	56.9	0.04
IKE	AL	11 Sep 2008 / 11:02	700 mb	12		17			4	36	70	29.5	0.14
IKE	AL	11 Sep 2008 / 14:31	700 mb	22		22			5	25	90	16.4	0.31
IKE	AL	11 Sep 2008 / 17:21	700 mb	10	17	16	+1	50	4	87	75	63.2	0.06
IKE	AL	11 Sep 2008 / 19:14	700 mb	8		17			4	61	101	35.0	0.11
IKE	AL	11 Sep 2008 / 20:50	700 mb	16		17			8	82	77	58.8	0.14
IKE	AL	13 Sep 2008 / 07:45	700 mb	11		16			20	64	71	56.1	0.36
PALOMA	AL	07 Nov 2008 / 08:39		5		12			8	77	61	49.5	0.17
PALOMA	AL	07 Nov 2008 / 17:57	700 mb	10	15	14	+1	8	8	27	63	18.5	0.43
N				506	53	508	53	51	508	508	508	508	508
minimum				5	13	10	+0	4	1	6	22	5.0	0.02
maximum				27	27	27	+6	50	32	105	130	138.9	0.60
average				14.5	18.1	18.4	1.5	12.9	9.5	37.5	68.4	33.37	0.34
std. dev.				4.7	3.4	3.8	1.1	8.5	5.0	22.4	19.2	20.60	0.16

Table D.10: All cases of the VDM data set which had a dew point depression of ($\geq 15\,^{\circ}$C). The storm name, basin (AL = Atlantic, EP = Eastern Pacific), and date and time (UTC) of fix are given in the first, second, and third columns, respectively. The fourth column gives the flight level of the aircraft fix. The minimum sea level pressure ("MSLP", hPa) measured during the fix is given fifth column. The maximum flight level temperatures reported just outside the eyewall ("Outside") and within 5 n mi of the center ("Eye") are given in the sixth and seventh columns, respectively. The corresponding dew point temperature at the location of maximum flight level temperature in the eye is given in the eighth column.The flight level dew point temperature depression, $T - T_d$, at the location of maximum flight temperature ($^{\circ}$C, measured within 5 n mi of the storm center) is given in the ninth column. The flight level baroclinity, defined as the difference between the maximum flight level temperature within 5 n mi of the storm center, T_{inside}, and the representative flight level temperature just outside the eyewall, $T_{outside}$ ($^{\circ}$C) is given in the tenth column); The radii of the primary eye ("Eye"), and the radius of maximum wind ("RMW", given by the radius of the maximum inbound flight level wind speed reported for the fix), are given in the eleventh and twelfth columns, respectively. The thirteenth column gives the maximum inbound flight level wind speed ("VMAX"), while the fourteenth column lists the minimum Rossby length. The dynamical eye size is given in the final column. Summary statistics of the values in the columns follow the main table.

Storm	Basin	Fix date / time UTC	Fix flight level	MSLP hPa	Outside T °C	Eye T °C	Eye T_d °C	T - T_d °C	Baro-clinity °C	Eye radius n mi	RMW n mi	VMAX kt	Min Rossby length n mi	Dynamical eye size
HUGO	AL	15 Sep 1989 / 23:40	700 mb	923	11	24	6	18	13	4	5	141	1.3	3.5
HUGO	AL	16 Sep 1989 / 05:25	700 mb	927	13	21	5	16	8	9	15	90	6.1	1.5
HUGO	AL	16 Sep 1989 / 07:06	700 mb	933	11	22	3	19	11	3	10	96	3.8	0.8
HUGO	AL	16 Sep 1989 / 08:42	700 mb	930	12	20	3	17	8	3	10	114	3.3	0.9
ARTHUR	AL	25 Jul 1990 / 23:39	850 mb	1000	18	25	10	15	7		11	68	5.4	
ARTHUR	AL	26 Jul 1990 / 05:11	850 mb	1002	18	27	9	18	9		10	23	14.6	
GUSTAV	AL	28 Aug 1990 / 23:44	700 mb	983	17	21	4	17	4		45	66	33.9	
GUSTAV	AL	29 Aug 1990 / 03:15	700 mb		15	20	4	16	5		20	73	14.6	
GUSTAV	AL	29 Aug 1990 / 05:10	700 mb	984	12	22	1	21	10		40	78	26.8	
GUSTAV	AL	31 Aug 1990 / 00:27	700 mb	958	12	21	3	18	9	12	12	107	7.6	1.5
GUSTAV	AL	31 Aug 1990 / 01:56	700 mb	957	10	18	3	15	8	12	15	107	9.5	1.3
NANA	AL	17 Oct 1990 / 23:54	850 mb	990	17	24	9	15	7	4	15	62	13.3	0.3
ANDREW	AL	23 Aug 1992 / 12:24	700 mb	934	9	19	4	15	10	6	8	124	3.9	1.4
ANDREW	AL	23 Aug 1992 / 15:27	700 mb	926	10	21	3	18	11	4	7	170	2.5	1.6
ANDREW	AL	23 Aug 1992 / 16:48	700 mb	922	12	22	3	19	10	4	6	136	2.7	1.5
ANDREW	AL	23 Aug 1992 / 17:53	700 mb	923	12	22	4	18	10	4	7	154	2.8	1.5
EMILIA	EP	22 Jul 1994 / 13:28	700 mb	992	10	19	3	16	9		23	69	13.9	
MARILYN	AL	14 Sep 1995 / 10:48	700 mb	985	10	20	5	15	10	8	12	52	7.8	1.0
MARILYN	AL	14 Sep 1995 / 14:38	700 mb	987	10	20	4	16	10	12	16	50	11.1	1.1
MARILYN	AL	15 Sep 1995 / 12:10	700 mb	974	10	22	4	18	12	11	8	99	3.3	3.3
MARILYN	AL	17 Sep 1995 / 06:24	700 mb	953	14	22	7	15	8	7	11	86	6.5	1.1
MARCO	AL	20 Nov 1996 / 06:11	850 mb	983	20	31	9	22	11		7	63	3.7	
MARCO	AL	22 Nov 1996 / 10:31	850 mb	989	17	27	12	15	10		34	54	23.4	
EARL	AL	01 Sep 1998 / 11:51	1500 ft	999	26	25	−3	28	−1		20	19	55.5	

continued on next page

Table D.10: *continued*

Storm	Basin	Fix date / time UTC	Fix flight level	MSLP hPa	Outside T °C	Eye T °C	Eye T_d °C	T - T_d °C	Baro-clinity °C	Eye radius n mi	RMW n mi	VMAX kt	Min Rossby length n mi	Dynamical eye size
EARL	AL	01 Sep 1998 / 13:29	1500 ft	1000	25	25	−3	28	0		41	49	46.2	
EARL	AL	01 Sep 1998 / 15:30	1500 ft	1000	25	25	−2	27	0		93	45	102.5	
EARL	AL	01 Sep 1998 / 17:30	1500 ft	998	25	25	−1	26	0		70	15	190.6	
GEORGES	AL	20 Sep 1998 / 06:13	700 mb	937	10	23	6	17	13	10	15	144	4.0	2.5
GEORGES	AL	20 Sep 1998 / 07:59	700 mb	939	10	23	6	17	13	10	16	146	4.2	
GEORGES	AL	20 Sep 1998 / 21:17	700 mb	957	9	24	8	16	15		23	104	8.8	
MITCH	AL	25 Oct 1998 / 19:03	700 mb	924	13	22	5	17	9	8	6	155	1.6	5.5
FLOYD	AL	13 Sep 1999 / 05:23	700 mb	923	11	24	5	19	13	10	17	126	7.5	1.3
FLOYD	AL	13 Sep 1999 / 07:45	700 mb	922	11	24	5	19	13	10	12	120	5.6	1.8
FLOYD	AL	13 Sep 1999 / 09:33	700 mb	923	11	24	5	19	13	10	22	149	8.3	1.2
FLOYD	AL	13 Sep 1999 / 11:21	700 mb	921	11	26	4	22	15	10	19	142	7.6	1.3
FLOYD	AL	13 Sep 1999 / 17:35	700 mb	926	13	25	5	20	12	12	12	111	6.2	2.0
FLOYD	AL	13 Sep 1999 / 19:20	700 mb	923	12	25	6	19	13	15	16	113	8.1	1.9
FLOYD	AL	13 Sep 1999 / 20:59	700 mb	922	13	24	6	18	11	12	18	118	8.7	1.4
LENNY	AL	17 Nov 1999 / 19:29	700 mb	934	12	25	7	18	13	11	11	120	3.9	2.8
LENNY	AL	17 Nov 1999 / 21:24	700 mb	929	11	24	6	18	13	11	13	114	4.8	2.3
LENNY	AL	18 Nov 1999 / 05:34	700 mb	937	8	22	6	16	14	10	14	118	5.1	2.0
LENNY	AL	18 Nov 1999 / 06:37	700 mb	940	10	21	6	15	11	9	9	121	3.2	
LENNY	AL	18 Nov 1999 / 07:27	700 mb	941	13	23	5	18	10	8	13	102	5.5	1.5
LENNY	AL	18 Nov 1999 / 07:44	700 mb	947	11	23	6	17	12	9	13	97	5.7	1.6
LENNY	AL	18 Nov 1999 / 08:15	700 mb	941	14	21	6	15	7	8	14	120	5.0	1.6
GORDON	AL	16 Sep 2000 / 23:13	850 mb	985	18	28	12	16	10		18	70	15.1	
GORDON	AL	17 Sep 2000 / 11:38	700 mb	987	5	18	2	16	13	15	54	52	59.6	0.3
KEITH	AL	01 Oct 2000 / 05:55	700 mb	943	9	22	3	19	13	10	14	119	5.1	2.0
KEITH	AL	01 Oct 2000 / 07:08	700 mb	942	8	24	5	19	16	10	16	116	6.0	1.7
KEITH	AL	01 Oct 2000 / 07:34	700 mb	942	9	23	2	21	14	8	12	114	4.6	1.6
KEITH	AL	01 Oct 2000 / 18:16	700 mb	950	11	25	2	23	14	10	8	103	3.4	3.0
KEITH	AL	01 Oct 2000 / 19:39	700 mb	951	9	24	5	19	15	10	13	102	5.5	1.8
KEITH	AL	01 Oct 2000 / 21:02	700 mb	955	10	23	6	17	13	10	13	92	6.0	1.7
HUMBERTO	AL	24 Sep 2001 / 07:43	700 mb	989	8	21	0	21	13	12	20	66	23.1	
LILI	AL	02 Oct 2002 / 23:24	700 mb	940	14	26	6	20	12	4	7	89	4.9	0.9
JIMENA	EP	31 Aug 2003 / 22:27	700 mb	1000	10	19	4	15	9		19	71	11.6	
FRANCES	AL	31 Aug 2004 / 10:28	700 mb	949	11	21	6	15	10	15	19	120	7.5	2.0
FRANCES	AL	31 Aug 2004 / 17:30	700 mb	942	13	24	8	16	11	14	9	105	4.2	3.2
FRANCES	AL	01 Sep 2004 / 05:40	700 mb	939	10	22	5	17	12	11	15	123	6.1	1.8

continued on next page

Table D.10: *continued*

Storm	Basin	Fix date / time UTC	Fix flight level	MSLP hPa	Outside T °C	Eye T °C	Eye T_d °C	T - T_d °C	Baro-clinity °C	Eye radius n mi	RMW n mi	VMAX kt	Min Rossby length n mi	Dynamical eye size
FRANCES	AL	01 Sep 2004 / 07:12	700 mb	935	9	23	8	15	14	11	25	111	11.2	1.0
FRANCES	AL	01 Sep 2004 / 09:03	700 mb	936	9	22	6	16	13	11	12	96	6.3	1.7
EMILY	AL	15 Jul 2005 / 05:03	700 mb	952	9	21	4	17	12	4	5	81	2.1	1.9
EMILY	AL	15 Jul 2005 / 13:30	700 mb	968	13	22	7	15	9	4	8	88	3.2	1.3
EMILY	AL	17 Jul 2005 / 01:17	700 mb	931	7	23	4	19	16	5	5	127	1.6	3.0
KATRINA	AL	28 Aug 2005 / 11:04	700 mb	910	10	25	10	15	15	12	18	153	7.1	1.8
KATRINA	AL	28 Aug 2005 / 12:57	700 mb	908	10	26	6	20	16	11	18	145	7.6	1.5
KATRINA	AL	28 Aug 2005 / 14:17	700 mb	907	12	26	6	20	14	11	14	140	6.1	1.8
KATRINA	AL	28 Aug 2005 / 15:00	700 mb	907	11	27	7	20	16	11	18	154	7.2	1.5
KATRINA	AL	28 Aug 2005 / 17:55	700 mb	902	14	29	6	23	15	12	22	160	8.5	1.5
KATRINA	AL	28 Aug 2005 / 19:23	700 mb	902	14	28	9	19	14	14	18	148	7.6	1.8
KATRINA	AL	28 Aug 2005 / 20:38	700 mb	903	16	28	6	22	12	14	14	130	6.8	2.1
KATRINA	AL	28 Aug 2005 / 22:31	700 mb	904	14	27	10	17	13	14	16	139	7.3	1.9
KATRINA	AL	28 Aug 2005 / 23:26	700 mb	904	14	28	9	19	14	14	16	139	7.3	1.9
RITA	AL	21 Sep 2005 / 15:17	700 mb	934	12	22	7	15	10	12	9	137	3.8	3.3
RITA	AL	21 Sep 2005 / 17:53	700 mb	920	9	26	3	23	17	10	7	153	2.7	3.8
RITA	AL	21 Sep 2005 / 19:36	700 mb	914	8	27	2	25	19	10	16	161	5.7	1.7
RITA	AL	21 Sep 2005 / 21:16	700 mb	904	9	30	−1	31	21	10	9	145	3.6	2.8
RITA	AL	21 Sep 2005 / 23:09	700 mb	899	8	28	1	27	20	10	11	142	4.5	2.2
RITA	AL	21 Sep 2005 / 23:13	700 mb	899	8	28	1	27	20	10	11	142	4.5	2.2
RITA	AL	22 Sep 2005 / 05:38	700 mb	898	9	28	3	25	19	8	12	165	4.3	1.9
RITA	AL	22 Sep 2005 / 07:14	700 mb	899	9	31	−3	34	22	8	13	148	5.2	1.5
RITA	AL	22 Sep 2005 / 09:12	700 mb	902	14	29	8	21	15	9	10	134	4.4	2.0
RITA	AL	22 Sep 2005 / 11:10	700 mb	907	11	27	5	22	16	9	9	133	4.0	
ERNESTO	AL	27 Aug 2006 / 07:26	850 mb	994	22	26	10	16	4		4	46	3.6	
FELIX	AL	02 Sep 2007 / 23:07	700 mb	936	25	26	4	22	1	8	12	152	2.6	2.9
FELIX	AL	03 Sep 2007 / 05:11	700 mb	937	7	24	7	17	17	5	8	132	2.1	2.4
FELIX	AL	03 Sep 2007 / 12:27	700 mb	942	10	22	6	16	12	4	3	112	0.9	4.3
HUMBERTO	AL	13 Sep 2007 / 04:47	850 mb	992	13	21	0	21	8	4	8	79	6.9	0.6
HUMBERTO	AL	13 Sep 2007 / 05:24	850 mb	990	17	22	0	22	5	3	7	55	8.7	0.3
HUMBERTO	AL	13 Sep 2007 / 06:09	850 mb	989	16	26	0	26	10		10	78	8.8	
HUMBERTO	AL	13 Sep 2007 / 06:52	850 mb	986	17	27	0	27	10	8	4	65	4.3	2.0
GUSTAV	AL	30 Aug 2008 / 18:28	700 mb	943	13	20	5	15	7	12	15	115	6.7	1.8
GUSTAV	AL	30 Aug 2008 / 21:54	700 mb	941	10	22	6	16	12	12	14	123	6.1	2.0
HANNA	AL	03 Sep 2008 / 11:01	850 mb	996	14	17	0	17	3		48	50	43.7	

continued on next page

Table D.10: *continued*

Storm	Basin	Fix date / time UTC	Fix flight level	MSLP hPa	Outside T °C	Eye T °C	Eye T_d °C	T - T_d °C	Baro-clinity °C	Eye radius n mi	RMW n mi	VMAX kt	Min Rossby length n mi	Dynamical eye size
PALOMA	AL	08 Nov 2008 / 09:34	700 mb	945	6	20	5	15	14	13	13	134	4.6	2.9
PALOMA	AL	08 Nov 2008 / 16:11		948	7	20	4	16	13	8	8	108	3.6	2.2
PALOMA	AL	08 Nov 2008 / 19:33	700 mb	952	9	23	5	18	14	8	9	142	3.1	
PALOMA	AL	08 Nov 2008 / 21:23	700 mb	961	10	26	2	24	16	9	10	102	4.8	
PALOMA	AL	08 Nov 2008 / 23:05	700 mb	968	9	22	5	17	13		14	92	7.5	
N				98	99	99	99	99	99	80	99	99	99	74
minimum				898	5	17	−3	15	−1	3	3	15	0.9	0.3
maximum				1002	26	31	12	34	22	15	93	170	190.6	5.5
average				946.1	12.3	23.7	4.7	19.1	11.5	9.3	15.9	107.4	11.45	1.90
std. dev.				31.0	4.3	3.0	3.1	4.0	4.5	3.2	13.1	36.1	22.91	0.89

Table D.11: All cases of the VDM data set which had a flight level baroclinity of greater than 10 °C, where baroclinity is defined as the difference between the maximum flight level temperature within 5 n mi of the storm center, T_{inside}, and the representative flight level temperature just outside the eyewall, $T_{outside}$ (°C). The storm name, basin (AL = Atlantic, EP = Eastern Pacific), and date and time (UTC) of fix are given in the first, second, and third columns, respectively. The fourth column gives the flight level of the aircraft fix. The minimum sea level pressure ("MSLP", hPa) measured during the fix is given fifth column. The maximum flight level temperatures reported just outside the eyewall ("Outside") and within 5 n mi of the center ("Eye") are given in the sixth and seventh columns, respectively. The corresponding dew point temperature at the location of maximum flight level temperature in the eye is given in the eighth column.The flight level dew point temperature depression, $T-T_d$, at the location of maximum flight temperature (°C, measured within 5 n mi of the storm center) is given in the ninth column. The flight level baroclinity (°C, tenth column). The diameter of the primary eye and the radius of maximum wind ("RMW", given by the radius of the maximum inbound flight level wind speed reported for the fix), are given in the eleventh and twelfth columns, respectively. The thirteenth column gives the maximum inbound flight level wind speed ("VMAX"), while the fourteenth column lists the minimum Rossby length. The dynamical eye size is given in the final column. Summary statistics of the values in the columns follow the main table.

Storm	Basin	Fix date / time UTC	Fix flight level	MSLP hPa	Outside T °C	Eye T °C	Eye T_d °C	T - T_d °C	Baro-clinity °C	Eye diameter n mi	RMW n mi	VMAX kt	Min Rossby length n mi	Dynamical eye size
HUGO	AL	15 Sep 1989 / 23:40	700 mb	923	11	24	6	18	13	9	5	141	1.3	3.5
HUGO	AL	16 Sep 1989 / 07:06	700 mb	933	11	22	3	19	11	6	10	96	3.8	0.8
HUGO	AL	18 Sep 1989 / 02:53	700 mb	935	10	20	10	10	10	18	15	105	6.0	1.5
GUSTAV	AL	29 Aug 1990 / 05:10	700 mb	984	12	22	1	21	10		40	78	26.8	
GUSTAV	AL	31 Aug 1990 / 13:41	700 mb	962	5	17	11	6	12	25	71	71	66.1	0.2
BOB	AL	19 Aug 1991 / 14:10	700 mb	959	8	18	14	4	10	22	45	95	39.8	
ANDREW	AL	23 Aug 1992 / 12:24	700 mb	934	9	19	4	15	10	11	8	124	3.9	1.4
ANDREW	AL	23 Aug 1992 / 14:03	700 mb	930	9	19	6	13	10	8	6	143	2.5	1.6
ANDREW	AL	23 Aug 1992 / 15:27	700 mb	926	10	21	3	18	11	8	7	170	2.5	1.6
ANDREW	AL	23 Aug 1992 / 16:48	700 mb	922	12	22	3	19	10	8	6	136	2.7	1.5
ANDREW	AL	23 Aug 1992 / 17:53	700 mb	923	12	22	4	18	10	8	7	154	2.8	1.5
ANDREW	AL	23 Aug 1992 / 20:45	700 mb	927	10	20	7	13	10	8	6	119	3.1	1.3
ANDREW	AL	24 Aug 1992 / 05:46	700 mb	936	6	16	12	4	10	20	13	132	5.9	1.7
ANDREW	AL	24 Aug 1992 / 08:04	700 mb	932	4	16	13	3	12	13	8	133	3.6	1.8
EMILIA	EP	20 Jul 1994 / 03:13	700 mb	928	9	19	11	8	10	12	11	131	2.5	2.4
EMILIA	EP	21 Jul 1994 / 00:12	700 mb	934	8	19	11	8	11	20	11	132	2.8	3.6
EMILIA	EP	21 Jul 1994 / 03:27	700 mb	935	8	19	11	8	11	24	9	119	2.5	4.7
EMILIA	EP	22 Jul 1994 / 01:39	700 mb	970	7	18	14	4	11	18	8	122	2.7	
EMILIA	EP	22 Jul 1994 / 03:23	700 mb	969	9	19	6	13	10	15	14	94	6.0	1.2
GILMA	EP	26 Jul 1994 / 02:05	700 mb	975	10	22	8	14	12		12	53	6.7	
GILMA	EP	26 Jul 1994 / 03:56	700 mb	978	10	20	8	12	10		11	91	3.6	
GILMA	EP	26 Jul 1994 / 05:35	700 mb	977	9	21	7	14	12		12	84	4.2	
GILMA	EP	26 Jul 1994 / 15:09	700 mb	980	7	17	8	9	10	22	17	74	6.9	1.6
GILMA	EP	26 Jul 1994 / 17:01	700 mb	981	8	18	8	10	10	28	12	60	6.0	2.3

continued on next page

Table D.11: *continued*

Storm	Basin	Fix date / time UTC	Fix flight level	MSLP hPa	Outside T °C	Eye T °C	Eye T_d °C	T - T_d °C	Baro-clinity °C	Eye diameter n mi	RMW n mi	VMAX kt	Min Rossby length n mi	Dynamical eye size
JOHN	EP	22 Aug 1994 / 23:35	700 mb	929	10	20	9	11	10	25	16	157	3.5	3.6
JOHN	EP	23 Aug 1994 / 01:28	700 mb	929	8	19	10	9	11	22	14	133	3.6	3.0
JOHN	EP	23 Aug 1994 / 12:14	700 mb	936	10	20	10	10	10	15	15	156	3.3	2.2
JOHN	EP	23 Aug 1994 / 17:28	700 mb	935	9	20	11	9	11	17	9	128	2.5	3.4
JOHN	EP	23 Aug 1994 / 19:16	700 mb	934	10	21	8	13	11	18	15	116	4.5	2.0
JOHN	EP	23 Aug 1994 / 20:54	700 mb	937	9	19	9	10	10	17	8	99	2.9	3.0
JOHN	EP	25 Aug 1994 / 17:51	700 mb	968	7	17	10	7	10		21	115	7.3	
IRIS	AL	25 Aug 1995 / 15:33	850 mb	997	17	27	13	14	10		31	44	23.4	
IRIS	AL	29 Aug 1995 / 13:36	700 mb	974	9	20	7	13	11	25	32	81	20.8	0.6
LUIS	AL	06 Sep 1995 / 08:03	700 mb	939	9	19	12	7	10	25	25	119	9.6	1.3
LUIS	AL	06 Sep 1995 / 11:22	700 mb	941	11	21	11	10	10	31	20	122	7.6	2.0
MARILYN	AL	14 Sep 1995 / 10:48	700 mb	985	10	20	5	15	10	15	12	52	7.8	1.0
MARILYN	AL	14 Sep 1995 / 14:38	700 mb	987	10	20	4	16	10	25	16	50	11.1	1.1
MARILYN	AL	15 Sep 1995 / 08:43	700 mb	974	8	18	6	12	10	22	13	77	6.8	1.6
MARILYN	AL	15 Sep 1995 / 10:29	700 mb	975	8	20	6	14	12	22	12	98	5.0	2.2
MARILYN	AL	15 Sep 1995 / 12:10	700 mb	974	10	22	4	18	12	22	8	99	3.3	3.3
MARILYN	AL	16 Sep 1995 / 17:03	700 mb	950	10	20	8	12	10	15	11	98	5.3	1.4
MARILYN	AL	17 Sep 1995 / 11:33	700 mb	964	14	24	10	14	10		14	81	9.0	
MARILYN	AL	17 Sep 1995 / 13:17	700 mb	969	10	20	10	10	10		36	84	22.0	
OPAL	AL	04 Oct 1995 / 11:31	700 mb	917	13	25	11	14	12	8	8	152	3.4	1.2
OPAL	AL	04 Oct 1995 / 12:31	700 mb	921	15	26	13	13	11	7	10	86	7.5	0.5
OPAL	AL	04 Oct 1995 / 14:31	700 mb	930	12	23	13	10	11	8	57	83	41.9	0.1
OPAL	AL	04 Oct 1995 / 16:16	700 mb	934	15	25	15	10	10	5	10	109	6.1	0.4
OPAL	AL	04 Oct 1995 / 17:42	700 mb	940	12	23	12	11	11		94	90	63.0	
OPAL	AL	04 Oct 1995 / 20:24	700 mb	944	11	25	11	14	14		59	126	31.0	
OPAL	AL	04 Oct 1995 / 21:44	700 mb	940	11	22	11	11	11		77	48	94.4	
OPAL	AL	04 Oct 1995 / 22:19	700 mb	946	12	22	11	11	10		54	115	31.7	
ROXANNE	AL	16 Oct 1995 / 01:21	850 mb	979	14	24	16	8	10		69	84	37.7	
BERTHA	AL	11 Jul 1996 / 12:04	700 mb	977	9	19	9	10	10	18	56	86	41.6	
BERTHA	AL	12 Jul 1996 / 12:57	700 mb	974	8	19	6	13	11		35	80	31.4	
BERTHA	AL	12 Jul 1996 / 14:40	700 mb	974	5	16	9	7	11		72	106	47.6	
EDOUARD	AL	27 Aug 1996 / 01:24	700 mb	942	12	22	10	12	10	20	16	136	5.4	1.9
EDOUARD	AL	28 Aug 1996 / 01:48	700 mb	948	9	19	12	7	10	22	16	124	6.5	1.7
EDOUARD	AL	29 Aug 1996 / 12:56	700 mb	950	11	21	7	14	10	15	8	90	5.1	1.5
EDOUARD	AL	31 Aug 1996 / 01:10	700 mb	944	11	21	13	8	10	20	31	106	19.8	0.5

continued on next page

Table D.11: *continued*

Storm	Basin	Fix date / time UTC	Fix flight level	MSLP hPa	Outside T °C	Eye T °C	Eye T_d °C	T - T_d °C	Baro-clinity °C	Eye diameter n mi	RMW n mi	VMAX kt	Min Rossby length n mi	Dynamical eye size
MARCO	AL	20 Nov 1996 / 06:11	850 mb	983	20	31	9	22	11		7	63	3.7	
MARCO	AL	22 Nov 1996 / 10:31	850 mb	989	17	27	12	15	10		34	54	23.4	
GEORGES	AL	19 Sep 1998 / 17:28	700 mb	949	10	20	10	10	10	30	9	112	3.0	5.0
GEORGES	AL	19 Sep 1998 / 19:13	700 mb	944	8	18	10	8	10	25	15	146	3.9	3.2
GEORGES	AL	19 Sep 1998 / 20:48	700 mb	938	9	20	9	11	11	25	11	118	3.5	3.5
GEORGES	AL	20 Sep 1998 / 06:13	700 mb	937	10	23	6	17	13	20	15	144	4.0	2.5
GEORGES	AL	20 Sep 1998 / 07:59	700 mb	939	10	23	6	17	13	20	16	146	4.2	
GEORGES	AL	20 Sep 1998 / 19:33	700 mb	956	10	21	11	10	11		20	129	6.2	
GEORGES	AL	20 Sep 1998 / 21:17	700 mb	957	9	24	8	16	15		23	104	8.8	
GEORGES	AL	21 Sep 1998 / 09:08	700 mb	964	10	21	15	6	11	30	13	89	6.1	2.5
GEORGES	AL	21 Sep 1998 / 14:37	700 mb	971	8	19	11	8	11	15	19	78	10.3	0.7
MITCH	AL	26 Oct 1998 / 17:12	700 mb	906	11	21	13	8	10	20	7	155	1.9	5.4
MITCH	AL	26 Oct 1998 / 19:00	700 mb	905	10	22	11	11	12	20	14	168	3.4	2.9
MITCH	AL	28 Oct 1998 / 08:18	700 mb	942	10	21	12	9	11		7	99	2.8	
MITCH	AL	28 Oct 1998 / 11:02	700 mb	948	11	21	14	7	10	8	6	95	2.5	1.6
LESTER	EP	17 Oct 1998 / 13:16	700 mb	976	4	14	10	4	10	20	11	93	4.2	2.4
DENNIS	AL	30 Aug 1999 / 05:43	700 mb	962	10	20	11	9	10	40	73	84	59.3	0.3
DENNIS	AL	31 Aug 1999 / 02:12	700 mb	974	7	19	10	9	12		78	89	62.6	
FLOYD	AL	12 Sep 1999 / 19:46	700 mb	940	11	21	9	12	10	40	16	113	7.8	2.6
FLOYD	AL	13 Sep 1999 / 05:23	700 mb	923	11	24	5	19	13	20	17	126	7.5	1.3
FLOYD	AL	13 Sep 1999 / 07:45	700 mb	922	11	24	5	19	13	20	12	120	5.6	1.8
FLOYD	AL	13 Sep 1999 / 09:33	700 mb	923	11	24	5	19	13	20	22	149	8.3	1.2
FLOYD	AL	13 Sep 1999 / 11:21	700 mb	921	11	26	4	22	15	20	19	142	7.6	1.3
FLOYD	AL	13 Sep 1999 / 17:35	700 mb	926	13	25	5	20	12	25	12	111	6.2	2.0
FLOYD	AL	13 Sep 1999 / 19:20	700 mb	923	12	25	6	19	13	30	16	113	8.1	1.9
FLOYD	AL	13 Sep 1999 / 20:59	700 mb	922	13	24	6	18	11	25	18	118	8.7	1.4
JOSE	AL	20 Oct 1999 / 13:30	700 mb	978	8	18	7	11	10	28	15	92	6.6	
JOSE	AL	20 Oct 1999 / 17:13	700 mb	987	9	23			14	35	19	50	15.5	1.1
LENNY	AL	16 Nov 1999 / 23:03	700 mb	960	9	20	7	13	11	35	14	115	4.6	3.8
LENNY	AL	17 Nov 1999 / 19:29	700 mb	934	12	25	7	18	13	22	11	120	3.9	2.8
LENNY	AL	17 Nov 1999 / 21:24	700 mb	929	11	24	6	18	13	22	13	114	4.8	2.3
LENNY	AL	17 Nov 1999 / 23:10	700 mb	939	10	22	8	14	12	20	16	128	5.3	1.9
LENNY	AL	18 Nov 1999 / 03:32	700 mb	944	10	20	7	13	10	20	12	119	4.3	2.3
LENNY	AL	18 Nov 1999 / 04:37	700 mb	944	8	21	9	12	13	18	10	119	3.6	2.5
LENNY	AL	18 Nov 1999 / 05:34	700 mb	937	8	22	6	16	14	20	14	118	5.1	2.0

continued on next page

Table D.11: *continued*

Storm	Basin	Fix date / time UTC	Fix flight level	MSLP hPa	Outside T °C	Eye T °C	Eye T_d °C	T - T_d °C	Baro-clinity °C	Eye diameter n mi	RMW n mi	VMAX kt	Min Rossby length n mi	Dynamical eye size
LENNY	AL	18 Nov 1999 / 06:37	700 mb	940	10	21	6	15	11	18	9	121	3.2	
LENNY	AL	18 Nov 1999 / 07:27	700 mb	941	13	23	5	18	10	16	13	102	5.5	1.5
LENNY	AL	18 Nov 1999 / 07:44	700 mb	947	11	23	6	17	12	18	13	97	5.7	1.6
LENNY	AL	18 Nov 1999 / 09:27	700 mb	951	10	21	7	14	11	18	11	113	4.2	2.2
DORA	EP	16 Aug 1999 / 06:15	700 mb	968	8	18	5	13	10	22	15	111	5.2	
DORA	EP	16 Aug 1999 / 11:03	700 mb	971	8	18	6	12	10	22	10	59	6.4	1.7
GORDON	AL	16 Sep 2000 / 23:13	850 mb	985	18	28	12	16	10		18	70	15.1	
GORDON	AL	17 Sep 2000 / 01:20	850 mb	987	17	27	13	14	10		42	79	30.5	
GORDON	AL	17 Sep 2000 / 11:38	700 mb	987	5	18	2	16	13	30	54	52	59.6	0.3
GORDON	AL	17 Sep 2000 / 13:28	700 mb	990	7	19	8	11	12	30	65	65	58.3	0.3
KEITH	AL	01 Oct 2000 / 05:55	700 mb	943	9	22	3	19	13	20	14	119	5.1	2.0
KEITH	AL	01 Oct 2000 / 07:08	700 mb	942	8	24	5	19	16	20	16	116	6.0	1.7
KEITH	AL	01 Oct 2000 / 07:34	700 mb	942	9	23	2	21	14	15	12	114	4.6	1.6
KEITH	AL	01 Oct 2000 / 18:16	700 mb	950	11	25	2	23	14	20	8	103	3.4	3.0
KEITH	AL	01 Oct 2000 / 19:39	700 mb	951	9	24	5	19	15	20	13	102	5.5	1.8
KEITH	AL	01 Oct 2000 / 21:02	700 mb	955	10	23	6	17	13	20	13	92	6.0	1.7
KEITH	AL	02 Oct 2000 / 07:58	700 mb	976	9	19	8	11	10	25	16	85	8.0	
ERIN	AL	09 Sep 2001 / 21:32	700 mb	969	7	17	5	12	10	28	18	100	13.5	
ERIN	AL	09 Sep 2001 / 23:08	700 mb	969	7	18	4	14	11	30	21	114	13.9	1.1
HUMBERTO	AL	24 Sep 2001 / 07:43	700 mb	989	8	21	0	21	13	25	20	66	23.1	
ISIDORE	AL	20 Sep 2002 / 08:24	700 mb	967	12	23	10	13	11	10	5	71	3.6	1.4
LILI	AL	02 Oct 2002 / 21:41	700 mb	939	12	22	9	13	10	11	5	120	2.6	2.1
LILI	AL	02 Oct 2002 / 23:24	700 mb	940	14	26	6	20	12	9	7	89	4.9	0.9
LILI	AL	03 Oct 2002 / 02:59	700 mb	948	11	24	14	10	13	9	10	126	5.1	0.9
LILI	AL	03 Oct 2002 / 05:18	700 mb	955	12	22	10	12	10	10	12	92	8.5	0.6
LILI	AL	03 Oct 2002 / 06:52	700 mb	957	10	20	11	9	10		20	70	18.5	
KENNA	EP	24 Oct 2002 / 17:18	700 mb	921	8	19	11	8	11	10	4	145	1.2	4.3
KENNA	EP	24 Oct 2002 / 18:59	700 mb	918	9	19	6	13	10	10	6	146	1.7	2.9
CLAUDETTE	AL	13 Jul 2003 / 15:14	850 mb	994	15	25	17	8	10		52	60	47.7	
CLAUDETTE	AL	13 Jul 2003 / 20:39	850 mb	997	14	25	16	9	11		68	69	53.7	
FABIAN	AL	02 Sep 2003 / 07:15	700 mb	945	11	22	10	12	11	20	13	128	4.8	2.1
FABIAN	AL	03 Sep 2003 / 06:53	700 mb	945	10	20	12	8	10	35	15	105	7.3	
ISABEL	AL	12 Sep 2003 / 17:12	700 mb	920	10	21	17	4	11	30	15	128	6.1	2.5
CHARLEY	AL	12 Aug 2004 / 17:04	700 mb	981	9	19	8	11	10	19	9	105	4.2	2.3
CHARLEY	AL	13 Aug 2004 / 18:33	700 mb	946	9	20	8	12	11	8	6	102	3.7	1.1

continued on next page

Table D.11: *continued*

Storm	Basin	Fix date / time UTC	Fix flight level	MSLP hPa	Outside T °C	Eye T °C	Eye T_d °C	T - T_d °C	Baro-clinity °C	Eye diameter n mi	RMW n mi	VMAX kt	Min Rossby length n mi	Dynamical eye size
CHARLEY	AL	13 Aug 2004 / 19:57	700 mb	941	9	20	7	13	11	5	3	148	1.3	1.9
FRANCES	AL	29 Aug 2004 / 19:35	700 mb	949	10	20	8	12	10	12	9	97	4.2	1.4
FRANCES	AL	29 Aug 2004 / 21:16	700 mb	952	9	20	7	13	11	16	9	118	3.5	2.3
FRANCES	AL	31 Aug 2004 / 10:28	700 mb	949	11	21	6	15	10	30	19	120	7.5	2.0
FRANCES	AL	31 Aug 2004 / 17:30	700 mb	942	13	24	8	16	11	27	9	105	4.2	3.2
FRANCES	AL	31 Aug 2004 / 19:07	700 mb	940	13	24	10	14	11	28	11	123	4.4	3.2
FRANCES	AL	01 Sep 2004 / 05:40	700 mb	939	10	22	5	17	12	22	15	123	6.1	1.8
FRANCES	AL	01 Sep 2004 / 07:12	700 mb	935	9	23	8	15	14	22	25	111	11.2	1.0
FRANCES	AL	01 Sep 2004 / 09:03	700 mb	936	9	22	6	16	13	22	12	96	6.3	1.7
FRANCES	AL	01 Sep 2004 / 11:05	700 mb	937	9	21	7	14	12	22	21	121	8.8	1.2
FRANCES	AL	02 Sep 2004 / 05:43	700 mb	937	13	23	11	12	10	30	15	138	5.9	2.6
FRANCES	AL	06 Sep 2004 / 09:03	850 mb	981	9	19	18	1	10	28	42	36	69.5	
IVAN	AL	08 Sep 2004 / 23:11	700 mb	938	9	19	12	7	10	10	8	120	2.2	2.3
IVAN	AL	09 Sep 2004 / 05:27	700 mb	925	9	21	11	10	12	12	6	154	1.3	
IVAN	AL	09 Sep 2004 / 07:10	700 mb	922	10	20	13	7	10	12	7	146	1.6	3.7
IVAN	AL	09 Sep 2004 / 11:41	700 mb	921	9	20	13	7	11	10	7	156	1.6	3.2
IVAN	AL	10 Sep 2004 / 05:19	700 mb	930	9	19	13	6	10	18	12	133	3.4	2.6
IVAN	AL	10 Sep 2004 / 10:23	700 mb	934	8	18	14	4	10	20	11	141	3.1	3.3
IVAN	AL	10 Sep 2004 / 22:22	700 mb	927	9	19	10	9	10	12	13	122	4.4	1.4
IVAN	AL	11 Sep 2004 / 19:17	700 mb	918	9	22	11	11	13	17	12	161	3.3	2.6
IVAN	AL	11 Sep 2004 / 20:44	700 mb	913	11	24	14	10	13	17	9	150	2.6	3.2
IVAN	AL	11 Sep 2004 / 22:18	700 mb	912	12	22	12	10	10	17	10	135	3.2	2.6
IVAN	AL	12 Sep 2004 / 00:05	700 mb	910	12	22	13	9	10	15	10	146	3.0	2.5
IVAN	AL	12 Sep 2004 / 05:47	700 mb	915	11	21	13	8	10	20	11	133	3.7	2.7
IVAN	AL	15 Sep 2004 / 20:12	700 mb	933	10	20	12	8	10	30	19	118	10.6	1.4
DENNIS	AL	07 Jul 2005 / 22:16	700 mb	955	7	18	10	8	11	20	10	110	4.2	2.4
DENNIS	AL	08 Jul 2005 / 11:59	700 mb	938	9	20	10	10	11	16	8	136	3.0	2.7
DENNIS	AL	08 Jul 2005 / 13:23	700 mb	938	8	20	9	11	12	13	7	96	3.7	1.8
DENNIS	AL	08 Jul 2005 / 15:17	700 mb	937	9	20	9	11	11	12	6	107	2.9	2.1
DENNIS	AL	08 Jul 2005 / 17:06	700 mb	941	9	19	9	10	10	10	5	129	2.0	2.5
DENNIS	AL	10 Jul 2005 / 03:29	700 mb	940	9	19	10	9	10	10	8	131	3.9	1.3
DENNIS	AL	10 Jul 2005 / 11:43	700 mb	930	9	21	17	4	12	8	9	131	4.6	0.9
EMILY	AL	14 Jul 2005 / 15:27	700 mb	976	8	18	6	12	10	10	6	85	2.2	2.3
EMILY	AL	15 Jul 2005 / 05:03	700 mb	952	9	21	4	17	12	8	5	81	2.1	1.9
EMILY	AL	15 Jul 2005 / 11:57	700 mb	964	9	20	7	13	11	8	10	126	2.7	1.5

continued on next page

Table D.11: *continued*

Storm	Basin	Fix date / time UTC	Fix flight level	MSLP hPa	Outside T °C	Eye T °C	Eye T_d °C	T - T_d °C	Baro-clinity °C	Eye diameter n mi	RMW n mi	VMAX kt	Min Rossby length n mi	Dynamical eye size
EMILY	AL	15 Jul 2005 / 16:45	700 mb	970	7	17	10	7	10	15	11	100	3.9	
EMILY	AL	16 Jul 2005 / 17:17	700 mb	937	9	20	12	8	11	11	8	141	2.3	2.4
EMILY	AL	16 Jul 2005 / 23:40	700 mb	929	13	23	9	14	10	14	6	149	1.7	4.2
EMILY	AL	17 Jul 2005 / 01:17	700 mb	931	7	23	4	19	16	10	5	127	1.6	3.0
EMILY	AL	17 Jul 2005 / 03:20	700 mb	939	10	20	10	10	10	12	5	96	2.2	
EMILY	AL	17 Jul 2005 / 05:34	700 mb	943	7	19	10	9	12	12	8	119	2.9	
EMILY	AL	17 Jul 2005 / 17:15	700 mb	948	9	19	12	7	10	10	10	132	3.4	1.5
EMILY	AL	17 Jul 2005 / 22:58	700 mb	951	8	18	13	5	10	10	10	109	4.3	1.2
EMILY	AL	19 Jul 2005 / 18:01	700 mb	959	8	18	11	7	10	15	15	94	9.1	0.8
EMILY	AL	19 Jul 2005 / 22:46	700 mb	949	9	19	11	8	10	17	11	110	5.8	1.5
EMILY	AL	20 Jul 2005 / 03:31	700 mb	945	9	20	8	12	11	16	8	99	4.7	1.7
EMILY	AL	20 Jul 2005 / 05:57	700 mb	944	10	20	8	12	10	15	10	99	5.9	1.3
KATRINA	AL	28 Aug 2005 / 09:21	700 mb	915	8	20	13	7	12	28	16	144	6.7	
KATRINA	AL	28 Aug 2005 / 11:04	700 mb	910	10	25	10	15	15	25	18	153	7.1	1.8
KATRINA	AL	28 Aug 2005 / 12:57	700 mb	908	10	26	6	20	16	22	18	145	7.6	1.5
KATRINA	AL	28 Aug 2005 / 14:17	700 mb	907	12	26	6	20	14	22	14	140	6.1	1.8
KATRINA	AL	28 Aug 2005 / 15:00	700 mb	907	11	27	7	20	16	22	18	154	7.2	1.5
KATRINA	AL	28 Aug 2005 / 17:55	700 mb	902	14	29	6	23	15	25	22	160	8.5	1.5
KATRINA	AL	28 Aug 2005 / 19:23	700 mb	902	14	28	9	19	14	28	18	148	7.6	1.8
KATRINA	AL	28 Aug 2005 / 20:38	700 mb	903	16	28	6	22	12	28	14	130	6.8	2.1
KATRINA	AL	28 Aug 2005 / 22:31	700 mb	904	14	27	10	17	13	28	16	139	7.3	1.9
KATRINA	AL	28 Aug 2005 / 23:26	700 mb	904	14	28	9	19	14	28	16	139	7.3	1.9
KATRINA	AL	29 Aug 2005 / 02:36	700 mb	908	13	25	17	8	12	30	15	122	7.9	1.9
KATRINA	AL	29 Aug 2005 / 07:00	700 mb	915	9	20	18	2	11	32	39	122	20.7	0.8
OPHELIA	AL	16 Sep 2005 / 20:42	850 mb	995	16	26	13	13	10		81	32	153.5	
RITA	AL	21 Sep 2005 / 15:17	700 mb	934	12	22	7	15	10	25	9	137	3.8	3.3
RITA	AL	21 Sep 2005 / 17:53	700 mb	920	9	26	3	23	17	20	7	153	2.7	3.8
RITA	AL	21 Sep 2005 / 19:36	700 mb	914	8	27	2	25	19	20	16	161	5.7	1.7
RITA	AL	21 Sep 2005 / 21:16	700 mb	904	9	30	−1	31	21	20	9	145	3.6	2.8
RITA	AL	21 Sep 2005 / 23:09	700 mb	899	8	28	1	27	20	20	11	142	4.5	2.2
RITA	AL	21 Sep 2005 / 23:13	700 mb	899	8	28	1	27	20	20	11	142	4.5	2.2
RITA	AL	22 Sep 2005 / 05:38	700 mb	898	9	28	3	25	19	16	12	165	4.3	1.9
RITA	AL	22 Sep 2005 / 07:14	700 mb	899	9	31	−3	34	22	16	13	148	5.2	1.5
RITA	AL	22 Sep 2005 / 09:12	700 mb	902	14	29	8	21	15	18	10	134	4.4	2.0
RITA	AL	22 Sep 2005 / 11:10	700 mb	907	11	27	5	22	16	18	9	133	4.0	

continued on next page

Table D.11: *continued*

Storm	Basin	Fix date / time UTC	Fix flight level	MSLP hPa	Outside T °C	Eye T °C	Eye T_d °C	T - T_d °C	Baro-clinity °C	Eye diameter n mi	RMW n mi	VMAX kt	Min Rossby length n mi	Dynamical eye size
RITA	AL	22 Sep 2005 / 22:11	700 mb	913	9	19	15	4	10	14	19	124	9.3	0.7
RITA	AL	24 Sep 2005 / 07:03		936	9	19	9	10	10	24	47	108	28.9	0.4
WILMA	AL	19 Oct 2005 / 06:11	700 mb	892	10	24	11	13	14	2	3	168	0.7	1.4
WILMA	AL	19 Oct 2005 / 08:00	700 mb	884	10	24	10	14	14	4	3	166	0.8	2.7
WILMA	AL	20 Oct 2005 / 20:16	700 mb	918	12	23	10	13	11	40	21	135	7.0	2.9
WILMA	AL	20 Oct 2005 / 21:16	700 mb	918	12	23	10	13	11	40	21	135	7.0	2.9
WILMA	AL	20 Oct 2005 / 23:05	700 mb	923	11	22	14	8	11	40	20	130	7.0	2.9
WILMA	AL	21 Oct 2005 / 05:01	700 mb	930	10	20	9	11	10	35	19	128	6.9	2.5
WILMA	AL	21 Oct 2005 / 17:44	700 mb	926	7	20	12	8	13	30	35	116	14.5	1.0
WILMA	AL	21 Oct 2005 / 20:06	700 mb	926	8	18	17	1	10	25	17	119	7.0	1.8
WILMA	AL	21 Oct 2005 / 21:42	700 mb	928	7	18	18	0	11	24	28	115	11.9	1.0
ADRIAN	EP	19 May 2005 / 18:30	850 mb	984	15	26	15	11	11	25	8	71	3.4	3.6
CHRIS	AL	02 Aug 2006 / 17:52	850 mb	1006	11	23	14	9	12		52	47	47.9	
JOHN	EP	31 Aug 2006 / 19:10	700 mb	973	9	19	8	11	10	15	12	77	7.6	1.0
JOHN	EP	31 Aug 2006 / 20:47	700 mb	968	7	18	10	8	11	15	6	66	4.5	1.7
LANE	EP	16 Sep 2006 / 18:09	700 mb	955	7	20	14	6	13	8	6	110	3.1	1.3
DEAN	AL	17 Aug 2007 / 12:36	700 mb	965	6	17	11	6	11	17	12	100	4.2	2.0
DEAN	AL	17 Aug 2007 / 17:17	700 mb	966	7	19	9	10	12	17	11	124	3.2	2.7
DEAN	AL	17 Aug 2007 / 23:32	700 mb	946	8	18	13	5	10		10	130	2.8	
DEAN	AL	18 Aug 2007 / 01:15	700 mb	937	10	20	8	12	10		11	138	2.9	
DEAN	AL	18 Aug 2007 / 11:51	700 mb	926	11	23	11	12	12	12	8	145	2.1	2.9
DEAN	AL	18 Aug 2007 / 15:02	700 mb	930	11	21	10	11	10	11	5	91	2.1	2.6
DEAN	AL	18 Aug 2007 / 16:14	700 mb	930	9	20	11	9	11	11	8	128	2.4	2.3
DEAN	AL	19 Aug 2007 / 03:17	700 mb	919	6	18	15	3	12	25	31	118	10.2	1.2
DEAN	AL	19 Aug 2007 / 04:17	700 mb	920	7	18	15	3	11	23	20	122	6.4	1.8
DEAN	AL	20 Aug 2007 / 02:19	700 mb	927	7	18	15	3	11	16	9	108	3.5	2.3
DEAN	AL	20 Aug 2007 / 05:16	700 mb	926	6	17	14	3	11	15	16	129	5.3	1.4
DEAN	AL	20 Aug 2007 / 17:39		924	9	19	18	1	10	18	10	140	3.1	2.9
DEAN	AL	20 Aug 2007 / 19:23	700 mb	918	9	19	18	1	10	18	15	151	4.3	2.1
DEAN	AL	20 Aug 2007 / 21:02	700 mb	916	10	20	13	7	10	16	11	126	3.8	2.1
DEAN	AL	20 Aug 2007 / 21:37	700 mb	916	10	20	13	7	10	16	11	126	3.8	2.1
DEAN	AL	20 Aug 2007 / 23:02	700 mb	915	11	21	18	3	10	16	9	110	3.6	2.2
DEAN	AL	20 Aug 2007 / 23:46	700 mb	914	9	21	17	4	12	16	8	156	2.3	3.5
DEAN	AL	21 Aug 2007 / 06:05	700 mb	909	12	23	12	11	11	15	12	156	3.4	2.2
DEAN	AL	21 Aug 2007 / 06:48	700 mb	907	9	21	14	7	12	15	9	123	3.3	2.3

continued on next page

Table D.11: *continued*

Storm	Basin	Fix date / time UTC	Fix flight level	MSLP hPa	Outside T °C	Eye T °C	Eye T_d °C	T - T_d °C	Baro-clinity °C	Eye diameter n mi	RMW n mi	VMAX kt	Min Rossby length n mi	Dynamical eye size
DEAN	AL	21 Aug 2007 / 08:14	700 mb	906	11	23	12	11	12	15	8	116	3.1	2.4
ERIN	AL	15 Aug 2007 / 20:32	850 mb	1003	10	23	15	8	13		75	37	103.1	
FELIX	AL	03 Sep 2007 / 05:11	700 mb	937	7	24	7	17	17	10	8	132	2.1	2.4
FELIX	AL	03 Sep 2007 / 06:57	700 mb	931	9	26	12	14	17	10	6	121	1.7	2.9
FELIX	AL	03 Sep 2007 / 11:09	700 mb	938	12	25	12	13	13	8	52	130	13.5	0.3
FELIX	AL	03 Sep 2007 / 12:27	700 mb	942	10	22	6	16	12	8	3	112	0.9	4.3
FELIX	AL	03 Sep 2007 / 17:23	700 mb	953	7	19	9	10	12	8	8	114	2.4	1.6
FELIX	AL	04 Sep 2007 / 05:33	700 mb	941	8	18	12	6	10	15	9	143	2.2	3.4
HUMBERTO	AL	13 Sep 2007 / 06:09	850 mb	989	16	26	0	26	10		10	78	8.8	
HUMBERTO	AL	13 Sep 2007 / 06:52	850 mb	986	17	27	0	27	10	17	4	65	4.3	2.0
DOLLY	AL	23 Jul 2008 / 15:26	700 mb	966	8	18	11	7	10		10	69	8.9	
GUSTAV	AL	30 Aug 2008 / 16:54	700 mb	945	9	19	5	14	10	30	18	141	6.5	2.3
GUSTAV	AL	30 Aug 2008 / 20:08	700 mb	942	9	19	7	12	10	24	10	98	5.4	2.2
GUSTAV	AL	30 Aug 2008 / 21:54	700 mb	941	10	22	6	16	12	24	14	123	6.1	2.0
GUSTAV	AL	31 Aug 2008 / 11:03	700 mb	960	9	19	10	9	10	25	12	83	8.4	1.5
GUSTAV	AL	31 Aug 2008 / 23:03	700 mb	953	7	17	8	9	10	32	55	79	41.0	
GUSTAV	AL	01 Sep 2008 / 08:30	700 mb	956	12	22	8	14	10		36	101	22.9	
OMAR	AL	15 Oct 2008 / 07:28	700 mb	986	6	16	7	9	10	20	23	62	12.8	
OMAR	AL	16 Oct 2008 / 05:43	700 mb	959	8	21			13	12	9	99	4.0	1.5
PALOMA	AL	08 Nov 2008 / 05:59	700 mb	951	6	19	11	8	13	22	11	110	4.6	2.4
PALOMA	AL	08 Nov 2008 / 07:44	700 mb	950	7	20	6	14	13	26	9	118	3.6	3.7
PALOMA	AL	08 Nov 2008 / 09:34	700 mb	945	6	20	5	15	14	26	13	134	4.6	2.9
PALOMA	AL	08 Nov 2008 / 11:11	700 mb	939	7	22	12	10	15	18	9	112	3.8	2.4
PALOMA	AL	08 Nov 2008 / 16:11		948	7	20	4	16	13	16	8	108	3.6	2.2
PALOMA	AL	08 Nov 2008 / 17:32	700 mb	952	10	20	8	12	10	30	8	104	3.7	
PALOMA	AL	08 Nov 2008 / 19:33	700 mb	952	9	23	5	18	14	16	9	142	3.1	
PALOMA	AL	08 Nov 2008 / 21:23	700 mb	961	10	26	2	24	16	18	10	102	4.8	
PALOMA	AL	08 Nov 2008 / 23:05	700 mb	968	9	22	5	17	13		14	92	7.5	
N				262	262	262	260	260	262	227	262	262	262	204
minimum				884	4	14	−3	0	10	2	3	32	0.7	0.1
maximum				1006	20	31	18	34	22	40	94	170	153.5	5.4
average				943.2	9.9	21.4	9.1	12.3	11.6	19.0	17.4	112.8	10.39	2.04
std. dev.				24.5	2.5	3.1	4.0	5.6	2.1	7.7	16.1	28.8	17.24	0.93

Table D.12: All cases in the VDM data set for which reconnaissance aircraft reported concentric eyewalls. All data on each row of the table correspond to the indicated fix date/time (third column). The fix flight level and minimum sea level pressure ("MSLP", hPa) measured during the fix, are given in the fourth, and fifth columns, respectively. The flight level dew point temperature depression, $T - T_d$, measured within 5 n mi of the storm center (°C) is displayed in the sixth column); The flight level baroclinity, defined as the difference between the maximum flight level temperature within 5 n mi of the storm center, T_{inside}, and the representative flight level temperature just outside the eyewall, $T_{outside}$ (°C) is given in the seventh column); The aircraft-measured diameters of the primary, secondary, and tertiary (if present) eyewalls are indicated in the eighth column (n mi). The maximum inbound flight level wind speed (VMAX, m s^{-1}), and the range from the center (RMW, n mi) are given in the ninth and tenth columns, respectively. Similarly, the VMAX, m s^{-1} and RMW n mi for the secondary eyewall are given in the eleventh and twelfth columns, respectively. The last column indicates the minimum Rossby length (n mi). Summary statistics of the values in the columns follow the main table.

Storm	Basin	Fix date / time UTC	Fix flight level	MSLP hPa	T - T_d °C	Baro-clinity °C	Concentric eye diameters n mi	**Primary eyewall** VMAX kt	**Primary eyewall** RMW n mi	**Secondary eyewall** VMAX kt	**Secondary eyewall** RMW n mi	Min Rossby length n mi
CHANTAL	AL	01 Aug 1989 / 05:04	850 mb	988	0	3	20 – 40	50	30			37.7
GABRIELLE	AL	04 Sep 1989 / 05:25	700 mb	940	6	3	15 – 35	75	20			10.9
HUGO	AL	16 Sep 1989 / 11:49	700 mb	940	12	5	8 – 30	94	6			2.4
BOB	AL	18 Aug 1991 / 09:10	850 mb	978	0	3	20 – 40	82	30			25.4
ANDREW	AL	23 Aug 1992 / 20:45	700 mb	927	13	10	8 – 20	119	6			3.1
ANDREW	AL	23 Aug 1992 / 22:32	700 mb	923	5	7	8 – 20	127	5			2.4
ANDREW	AL	24 Aug 1992 / 00:13	700 mb	931	2	7	8 – 20	116	6			3.1
EMILIA	EP	20 Jul 1994 / 01:09	700 mb	927	4	6	15 – 30	151	9			1.8
EMILIA	EP	20 Jul 1994 / 03:13	700 mb	928	8	10	12 – 30	131	11			2.5
EMILIA	EP	20 Jul 1994 / 05:05	700 mb	929	6	8	12 – 24	118	7			1.8
GILMA	EP	25 Jul 1994 / 12:28	700 mb	966	5	6	16 – 40	96	11			3.3
JOHN	EP	23 Aug 1994 / 12:14	700 mb	936	10	10	15 – 20	156	15			3.3
LUIS	AL	07 Sep 1995 / 23:52	700 mb	935	4	7	20 – 58	110	37			18.6
LUIS	AL	08 Sep 1995 / 02:08	700 mb	936	5	9	21 – 58	121	30			14.0
LUIS	AL	08 Sep 1995 / 11:23	700 mb	941	1	4	20 – 50	88	26			17.5
LUIS	AL	08 Sep 1995 / 13:33	700 mb	942	3	7	20 – 50	104	25			14.6
MARILYN	AL	19 Sep 1995 / 00:15	700 mb	969	4	4	20 – 40	70	23			21.3
BERTHA	AL	10 Jul 1996 / 05:58	850 mb	970	4	4	20 – 85	80	40			27.9
BERTHA	AL	10 Jul 1996 / 07:26	850 mb	970	2	2	15 – 70	99	40			23.0
BERTHA	AL	10 Jul 1996 / 08:48	850 mb	969	3	3	15 – 70	65	40			34.6
BERTHA	AL	10 Jul 1996 / 10:11	850 mb	968	2	3	15 – 70	75	34			26.0
BERTHA	AL	10 Jul 1996 / 11:54	850 mb	968	2	3	20 – 70	77	35	72		26.3
BERTHA	AL	10 Jul 1996 / 14:54	700 mb	969	4	5	16 – 60	63	78			67.1
BERTHA	AL	10 Jul 1996 / 16:41	700 mb	968	2	2	15 – 40	95	37			23.3
EDOUARD	AL	29 Aug 1996 / 20:49	700 mb	944	5	9	15 – 50	106	7			3.9
EDOUARD	AL	29 Aug 1996 / 23:09	700 mb	943	2	1	12 – 55	99	9			5.5
EDOUARD	AL	30 Aug 1996 / 00:53	700 mb	941	5	3	10 – 50	86	10			7.0

continued on next page

Table D.12: *continued*

Storm	Basin	Fix date / time UTC	Fix flight level	MSLP hPa	T - T_d °C	Baro-clinity °C	Concentric eye diameters n mi	**Primary eyewall** VMAX kt	**Primary eyewall** RMW n mi	**Secondary eyewall** VMAX kt	**Secondary eyewall** RMW n mi	Min Rossby length n mi
EDOUARD	AL	30 Aug 1996 / 02:33	700 mb	940	7	9	10 – 40 – 60	87	31			21.2
EDOUARD	AL	30 Aug 1996 / 04:21	700 mb	937	7	8	10 – 30	115	23			12.2
EDOUARD	AL	31 Aug 1996 / 13:27	700 mb	954	1	3	10 – 30	83	31			26.5
EDOUARD	AL	31 Aug 1996 / 15:09	700 mb	954	1	5	10 – 30	98	29			21.4
EDOUARD	AL	31 Aug 1996 / 17:07	700 mb	954	3	6	10 – 30	111	25			16.6
DANNY	AL	19 Jul 1997 / 04:55	850 mb	987	2	−2	12 – 30	78	13			11.6
DANNY	AL	19 Jul 1997 / 06:12	850 mb	987	3	4	15 – 30	63	9			10.0
ERIKA	AL	06 Sep 1997 / 09:00	850 mb	986	5	3	10 – 25	64	21			14.3
MITCH	AL	26 Oct 1998 / 05:08	700 mb	922	4	5	8 – 15	124	9			2.9
FLOYD	AL	14 Sep 1999 / 23:23	700 mb	934	1	4	17 – 50	103	28			17.0
GERT	AL	16 Sep 1999 / 08:20	700 mb	941	2	4	18 – 30	95	29			13.1
FLORENCE	AL	13 Sep 2000 / 16:54	850 mb	989	2	2	3 – 5	48	12			17.4
IRIS	AL	08 Oct 2001 / 06:20	700 mb	971	7	4	8 – 22	105	6			2.4
IRIS	AL	08 Oct 2001 / 11:19	700 mb	954	9	7	3 – 9 – 18	134	4			1.2
IRIS	AL	08 Oct 2001 / 19:16	700 mb	956	1	7	10 – 30	112	4			1.5
JULIETTE	EP	26 Sep 2001 / 17:22	700 mb	940	2	3	7 – 38	97	6			2.8
JULIETTE	EP	26 Sep 2001 / 19:00	700 mb	940	2	2	7 – 40	81	3			1.7
ISIDORE	AL	21 Sep 2002 / 07:23	700 mb	964	1	3	15 – 25	84	13			8.2
LILI	AL	01 Oct 2002 / 23:41	700 mb	968	1	4	18 – 35	77	11			7.8
LILI	AL	02 Oct 2002 / 18:01	700 mb	941	8	7	15 – 35	100	5			3.0
ISABEL	AL	13 Sep 2003 / 05:05	700 mb	935	1	5	25 – 35	100	25			12.9
ISABEL	AL	13 Sep 2003 / 06:49	700 mb	936	0	4	25 – 35	124	31			12.9
ISABEL	AL	17 Sep 2003 / 14:49	700 mb	956	2	4	40 – 60	80	46			38.0
CHARLEY	AL	11 Aug 2004 / 14:13	850 mb	996	5	4	5 – 12	48	6			5.0
FRANCES	AL	30 Aug 2004 / 18:13	700 mb	948	0	5	18 – 48	89	26			13.4
FRANCES	AL	01 Sep 2004 / 11:05	700 mb	937	14	12	22 – 50	121	21			8.8
FRANCES	AL	01 Sep 2004 / 17:19	700 mb	941	2	8	30 – 40	105	23			11.3
IVAN	AL	11 Sep 2004 / 06:12	700 mb	923	1	7	12 – 40	138	16			4.9
IVAN	AL	11 Sep 2004 / 07:43	700 mb	924	2	8	15 – 20	129	16			5.2
IVAN	AL	11 Sep 2004 / 09:16	700 mb	925	3	8	12 – 30	115	19			6.9
IVAN	AL	11 Sep 2004 / 19:17	700 mb	918	11	13	17 – 20	161	12			3.3
IVAN	AL	11 Sep 2004 / 20:44	700 mb	913	10	13	17 – 20	150	9			2.6
IVAN	AL	12 Sep 2004 / 00:05	700 mb	910	9	10	15 – 17	146	10			3.0
IVAN	AL	12 Sep 2004 / 09:06	700 mb	919	1	7	15 – 30	115	29	113	10	11.2
IVAN	AL	12 Sep 2004 / 11:08	700 mb	919	0	6	12 – 60	116	10			3.9

continued on next page

Table D.12: *continued*

Storm	Basin	Fix date / time UTC	Fix flight level	MSLP hPa	T - T_d °C	Baro-clinity °C	Concentric eye diameters n mi	**Primary eyewall** VMAX kt	**Primary eyewall** RMW n mi	**Secondary eyewall** VMAX kt	**Secondary eyewall** RMW n mi	Min Rossby length n mi
IVAN	AL	12 Sep 2004 / 14:39	700 mb	921	0	8	15 – 50	131	25			8.6
IVAN	AL	12 Sep 2004 / 16:20	700 mb	922	0	7	15 – 30	122	27			10.0
IVAN	AL	12 Sep 2004 / 18:06	700 mb	920	0	7	15 – 30	114	25			10.0
IVAN	AL	12 Sep 2004 / 20:08	700 mb	916	0	6	14 – 40	118	21			8.2
IVAN	AL	12 Sep 2004 / 23:59	700 mb	916	2	6	17 – 40	155	18			5.4
JEANNE	AL	24 Sep 2004 / 17:57	700 mb	968	4	5	25 – 60	72	28			23.4
EMILY	AL	15 Jul 2005 / 11:57	700 mb	964	13	11	8 – 20	126	10			2.7
EMILY	AL	15 Jul 2005 / 13:30	700 mb	968	15	9	8 – 25	88	8			3.2
EMILY	AL	20 Jul 2005 / 05:57	700 mb	944	12	10	15 – 50	99	10			5.9
EMILY	AL	20 Jul 2005 / 07:45	700 mb	943	6	7	16 – 50	107	35	98		18.7
EMILY	AL	20 Jul 2005 / 08:56	700 mb	944	4	5	15 – 50	94	11			6.8
KATRINA	AL	27 Aug 2005 / 15:14	700 mb	949	4	4	13 – 40	87	44			28.1
KATRINA	AL	27 Aug 2005 / 17:59	700 mb	948	3	5	9 – 55	89	31			19.7
KATRINA	AL	27 Aug 2005 / 20:09	700 mb	945	6	8	8 – 50	85	29			19.4
RITA	AL	22 Sep 2005 / 14:49	700 mb	913	8	4	17 – 55	135	13			5.8
RITA	AL	22 Sep 2005 / 16:19	700 mb	915	4	8	18 – 45	120	11			5.5
RITA	AL	22 Sep 2005 / 17:45	700 mb	914	5	9	15 – 50	120	8			4.0
RITA	AL	22 Sep 2005 / 19:13	700 mb	913	4	7	18 – 48	133	10			4.6
RITA	AL	22 Sep 2005 / 20:43	700 mb	911	3	7	15 – 40	123	12			6.0
RITA	AL	22 Sep 2005 / 21:20	700 mb	913	3	8	16 – 41	102	22			13.0
RITA	AL	22 Sep 2005 / 22:11	700 mb	913	4	10	14 – 35	124	19			9.3
RITA	AL	22 Sep 2005 / 23:28	700 mb	913	3	7	16 – 35	125	24			11.7
RITA	AL	23 Sep 2005 / 00:10	700 mb	915	1	7	17 – 32	123	20			9.9
RITA	AL	23 Sep 2005 / 00:27		916	1	4	18 – 35	114	21			11.2
RITA	AL	23 Sep 2005 / 01:44	700 mb	917	1	5	18 – 32	109	17			9.5
WILMA	AL	19 Oct 2005 / 19:56	700 mb	892	4	7	5 – 10	141	2			0.6
WILMA	AL	20 Oct 2005 / 06:49	700 mb	903	0	1	4 – 40	112	26			10.0
WILMA	AL	20 Oct 2005 / 08:34	700 mb	906	5	6	3 – 35	120	21			7.6
WILMA	AL	20 Oct 2005 / 10:20	700 mb	910	1	7	7 – 35	122	23			8.2
WILMA	AL	23 Oct 2005 / 05:28	700 mb	962	0	6	20 – 60	79	30			19.3
WILMA	AL	23 Oct 2005 / 07:06	700 mb	960	0	5	20 – 60	78	36			23.4
WILMA	AL	23 Oct 2005 / 14:58	700 mb	964	1	2	10 – 60	67	34			26.4
WILMA	AL	23 Oct 2005 / 16:34	700 mb	963	0	2	10 – 60	80	97			59.5
WILMA	AL	24 Oct 2005 / 01:12	700 mb	958	0	6	45 – 60	114	27			13.4
HELENE	AL	19 Sep 2006 / 16:37	700 mb	958	6	1	40 – 100	79	12	79		8.7

continued on next page

Table D.12: *continued*

Storm	Basin	Fix date / time UTC	Fix flight level	MSLP hPa	T - T_d °C	Baro-clinity °C	Concentric eye diameters n mi	**Primary eyewall** VMAX kt	**Primary eyewall** RMW n mi	**Secondary eyewall** VMAX kt	**Secondary eyewall** RMW n mi	Min Rossby length n mi
DEAN	AL	17 Aug 2007 / 15:59	700 mb	963	7		17 – 32	65	5			2.7
DEAN	AL	18 Aug 2007 / 17:02	700 mb	930	1	5	11 – 22	110	7			2.4
DEAN	AL	19 Aug 2007 / 01:05	700 mb	918	2	6		105	5			1.9
DEAN	AL	19 Aug 2007 / 12:19	700 mb	923	6	8	16 – 34	110	13			4.8
DEAN	AL	19 Aug 2007 / 13:58	700 mb	926	5		16 – 32	111	23			8.4
DEAN	AL	19 Aug 2007 / 15:22	700 mb	927	1			132	21			6.5
DEAN	AL	19 Aug 2007 / 17:01	700 mb	930	1	9	16 – 36	130	26			8.2
DEAN	AL	20 Aug 2007 / 05:16	700 mb	926	3	11	15 – 27	129	16			5.3
DEAN	AL	20 Aug 2007 / 21:02	700 mb	916	7	10	16 – 30	126	11			3.8
DEAN	AL	20 Aug 2007 / 21:37	700 mb	916	7	10	16 – 30	126	11			3.8
DOLLY	AL	23 Jul 2008 / 03:42	700 mb	982	1	0	25 – 40	61	31			29.0
IKE	AL	07 Sep 2008 / 20:09	700 mb	945	3	6	16 – 48	106	16			7.6
IKE	AL	08 Sep 2008 / 20:13	700 mb	965	0	4	10 – 50	53	23			21.5
IKE	AL	08 Sep 2008 / 21:08	700 mb	967	0	4	10 – 50	58	27			23.1
IKE	AL	11 Sep 2008 / 09:05	700 mb	947	3	9	4 – 12	93	98			56.9
IKE	AL	11 Sep 2008 / 11:02	700 mb	946	7	5	8 – 42	70	36			29.5
PALOMA	AL	08 Nov 2008 / 11:11	700 mb	939	10	15	18 – 32	112	9			3.8
N				114	114	111		114	114	4	1	114
minimum				892	0	−2		48	2	72	10	0.6
maximum				996	15	15		161	98	113	10	67.1
average				941.5	3.8	6.0		103.1	21.3	90.5	10.0	12.64
std. dev.				22.8	3.5	3.0		25.4	15.7	18.6	0.0	11.94

Appendix E

STRUCTURE AND INTENSITY PLOTS FROM THE VORTEX DATA MESSAGE DATA SET

In order to visualize and quality-control the massive quantities of VDM data, a suite of specialized 5-panel plots have been created to illustrate the temporal changes in intensity and structure over the lifetimes of each of the 205 storms in the VDM data set. A detailed description of these 'structure and intensity' plots has been provided in chapter 5.4.3.

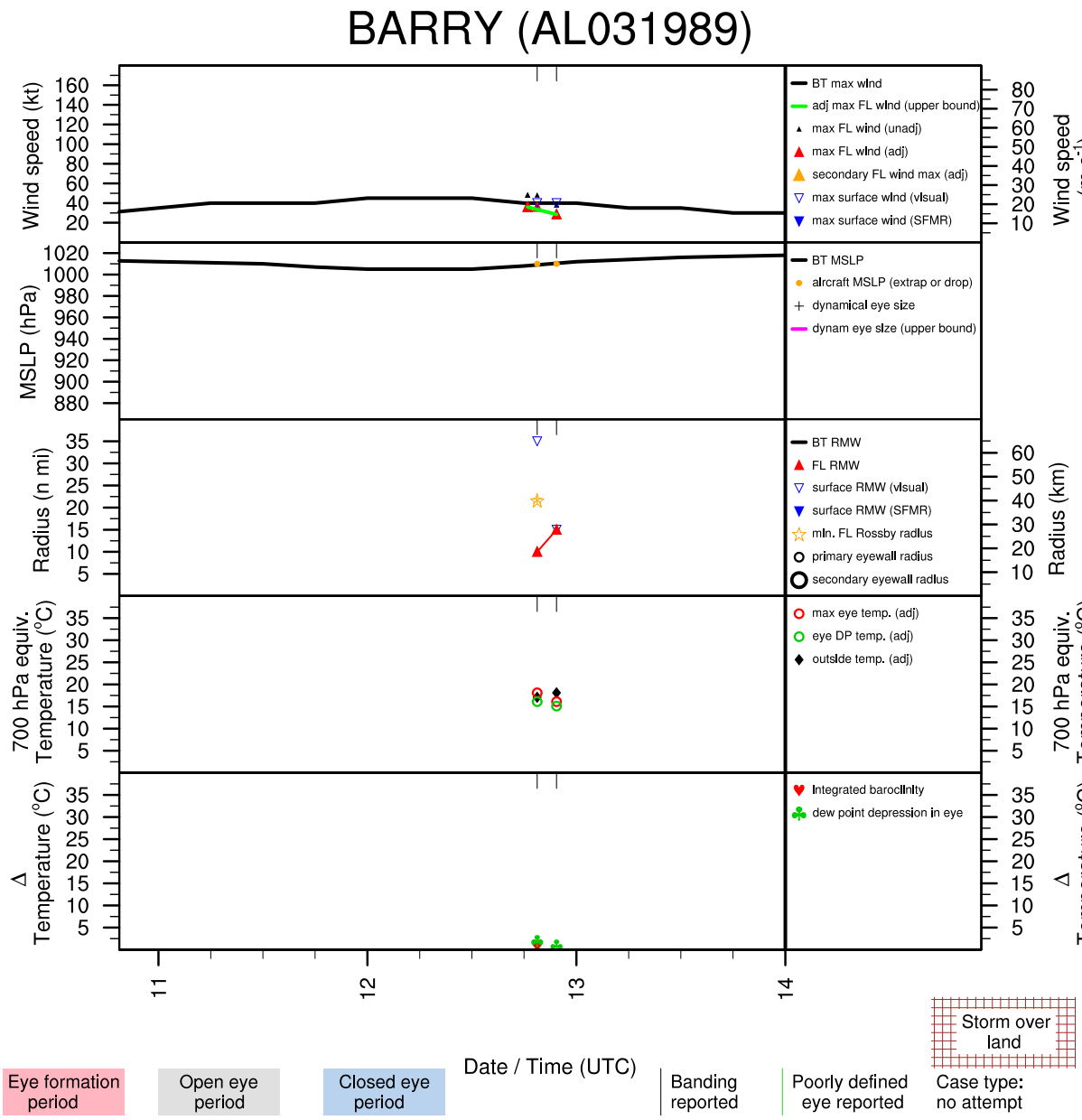

Figure E.1: Structure and intensity parameters for Tropical Storm Barry (1989).

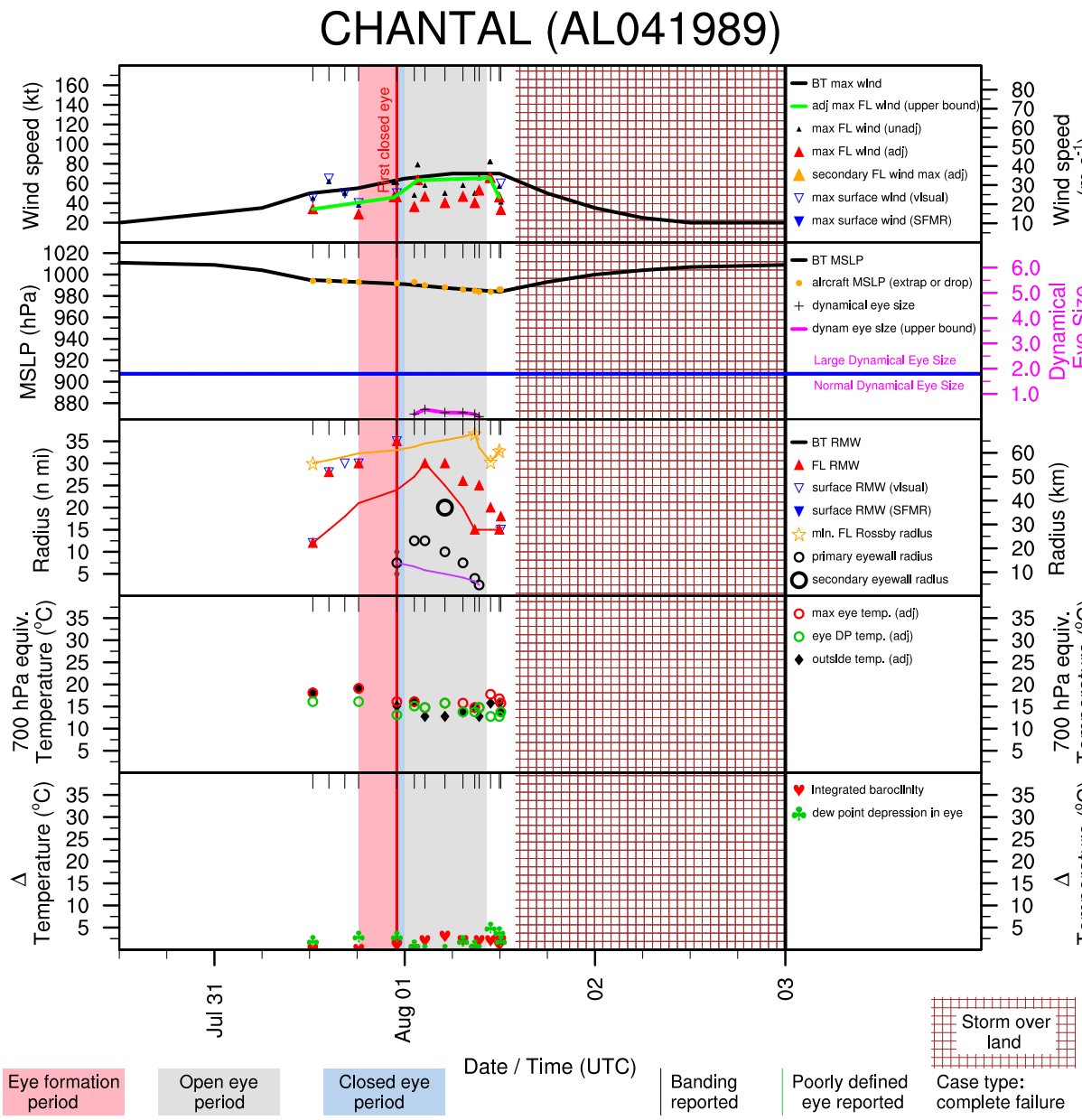

Figure E.2: Structure and intensity parameters for Hurricane Chantal (1989).

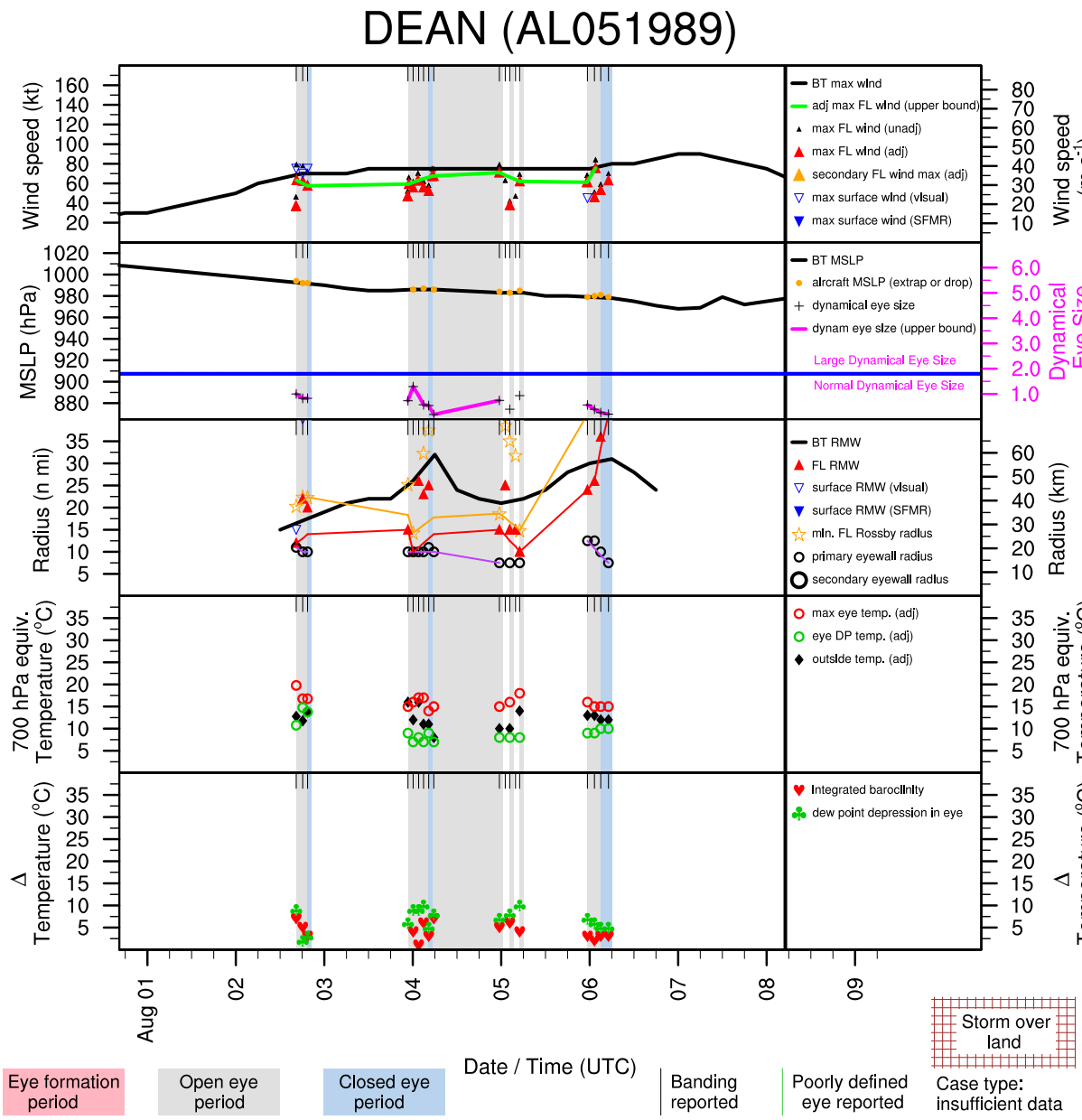

Figure E.3: Structure and intensity parameters for Hurricane Dean (1989).

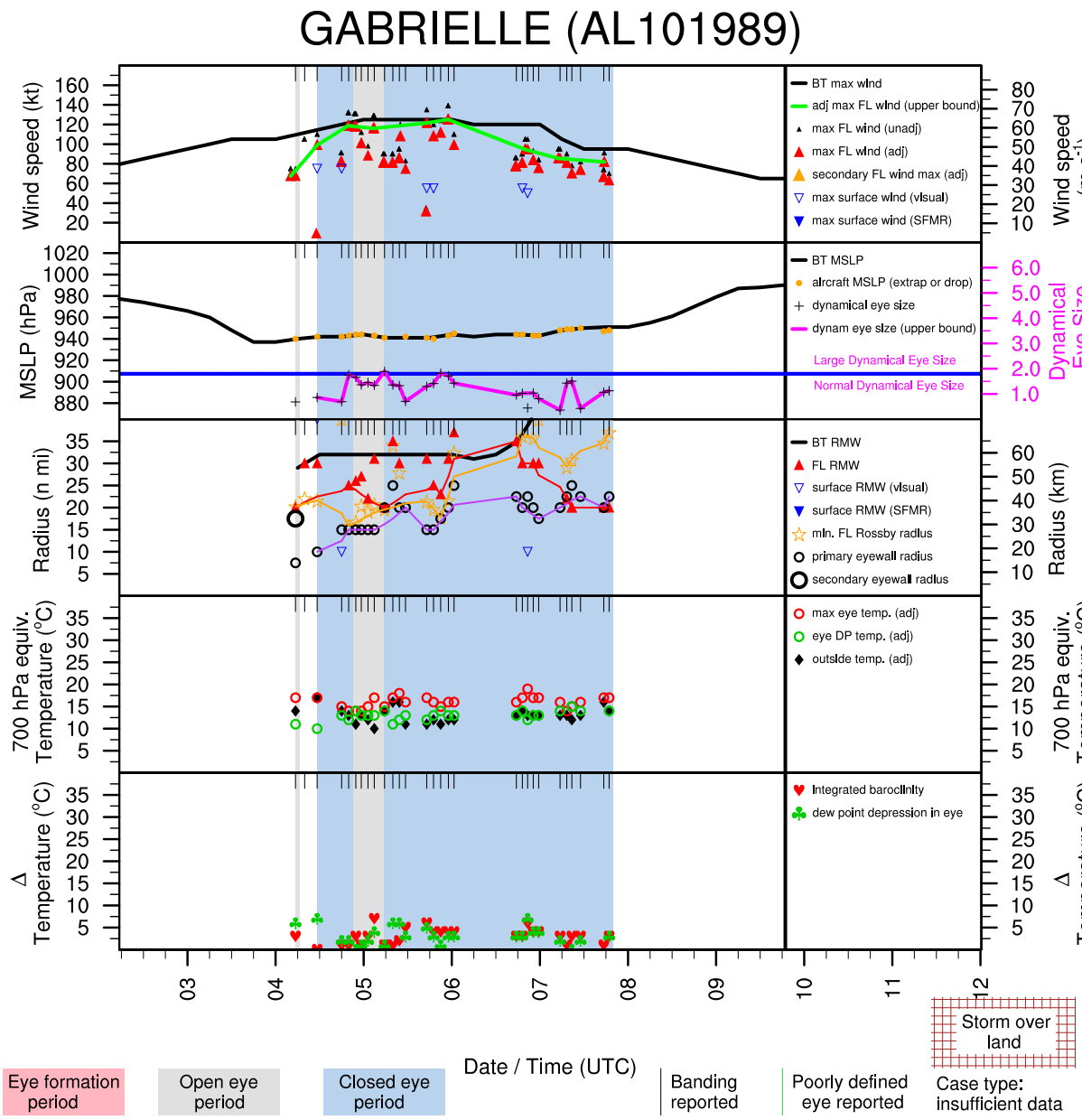

Figure E.4: Structure and intensity parameters for Hurricane Gabrielle (1989).

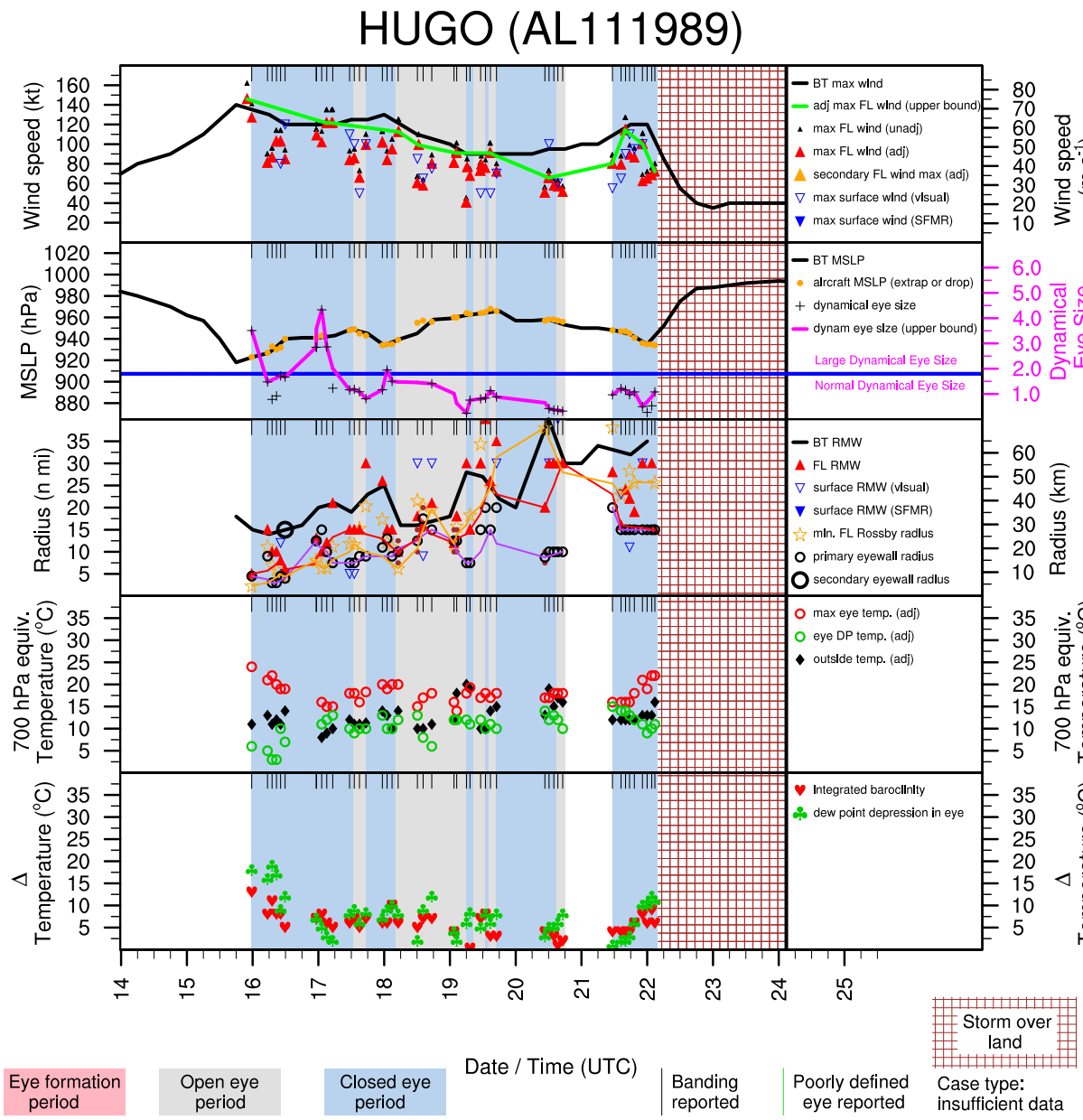

Figure E.5: Structure and intensity parameters for Hurricane Hugo (1989).

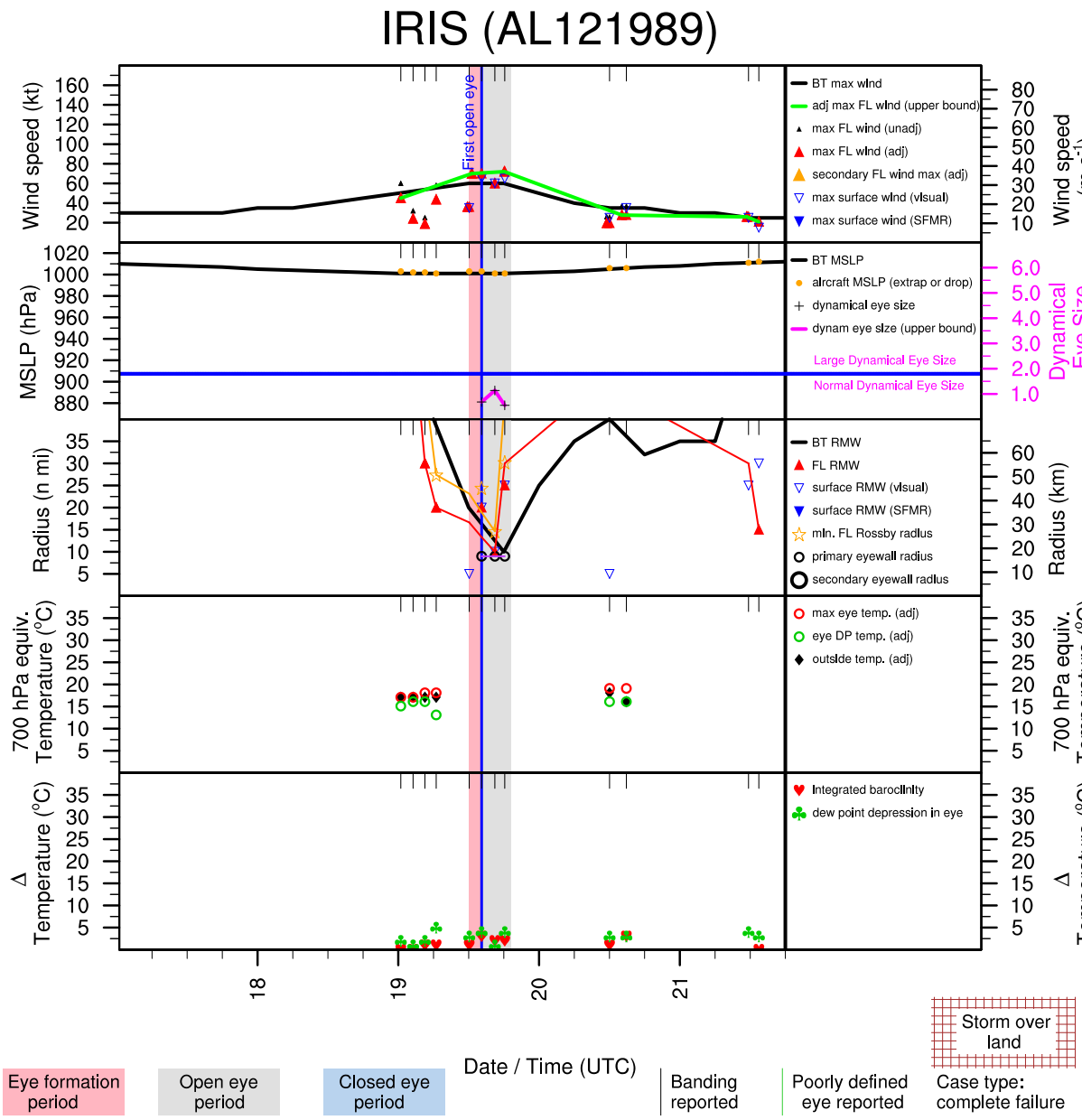

Figure E.6: Structure and intensity parameters for Tropical Storm Iris (1989).

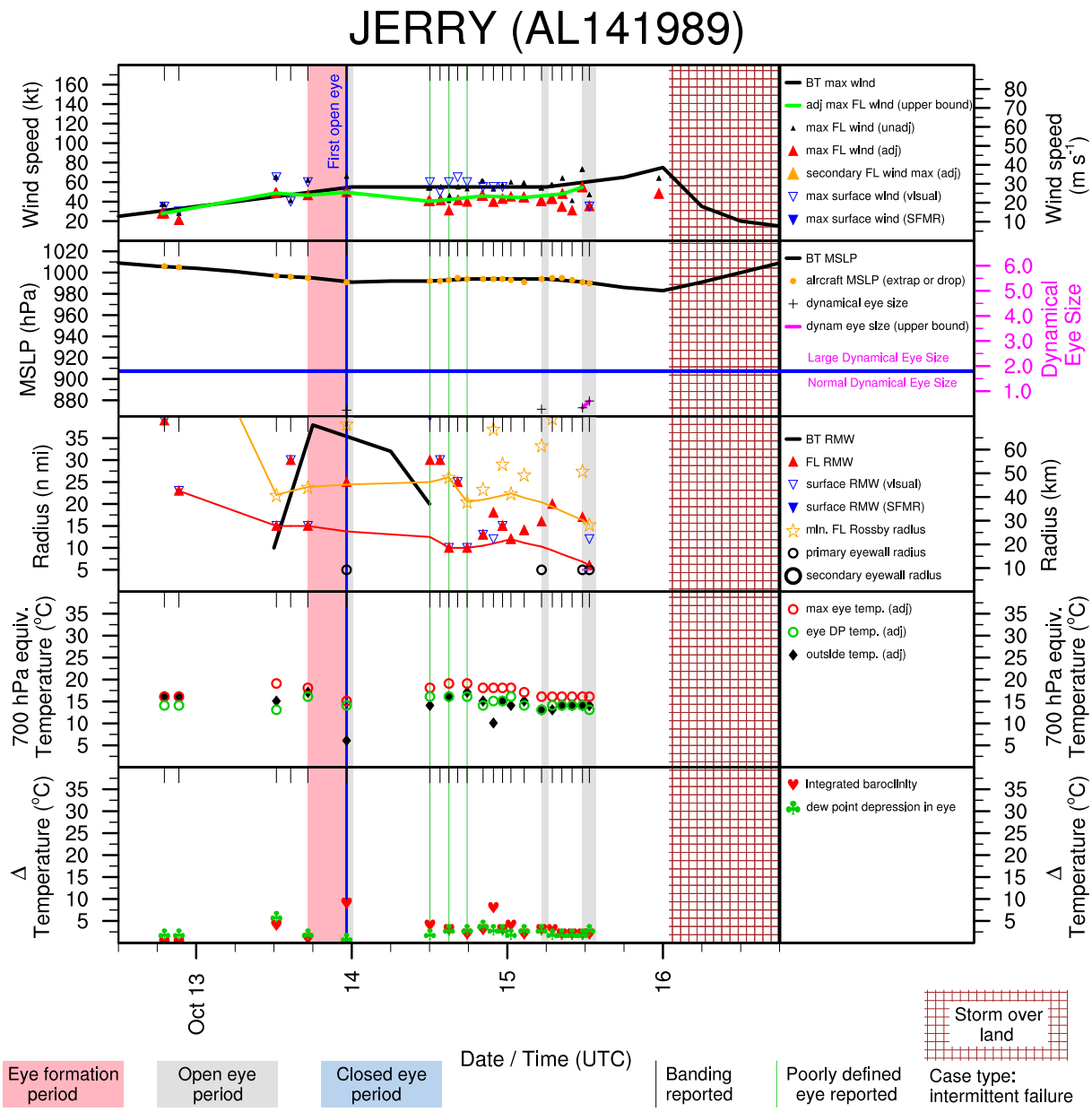

Figure E.7: Structure and intensity parameters for Hurricane Jerry (1989).

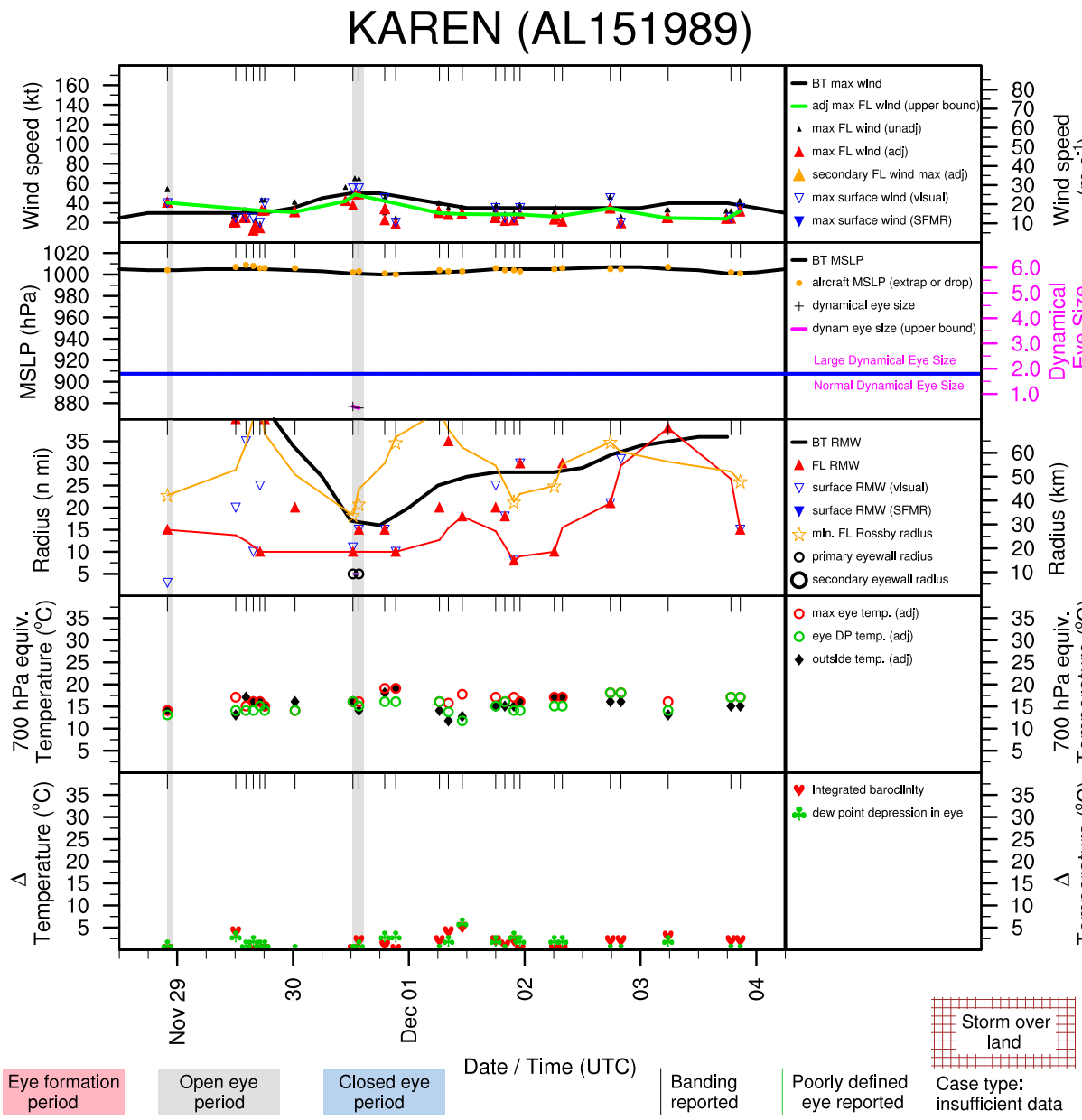

Figure E.8: Structure and intensity parameters for Tropical Storm Karen (1989).

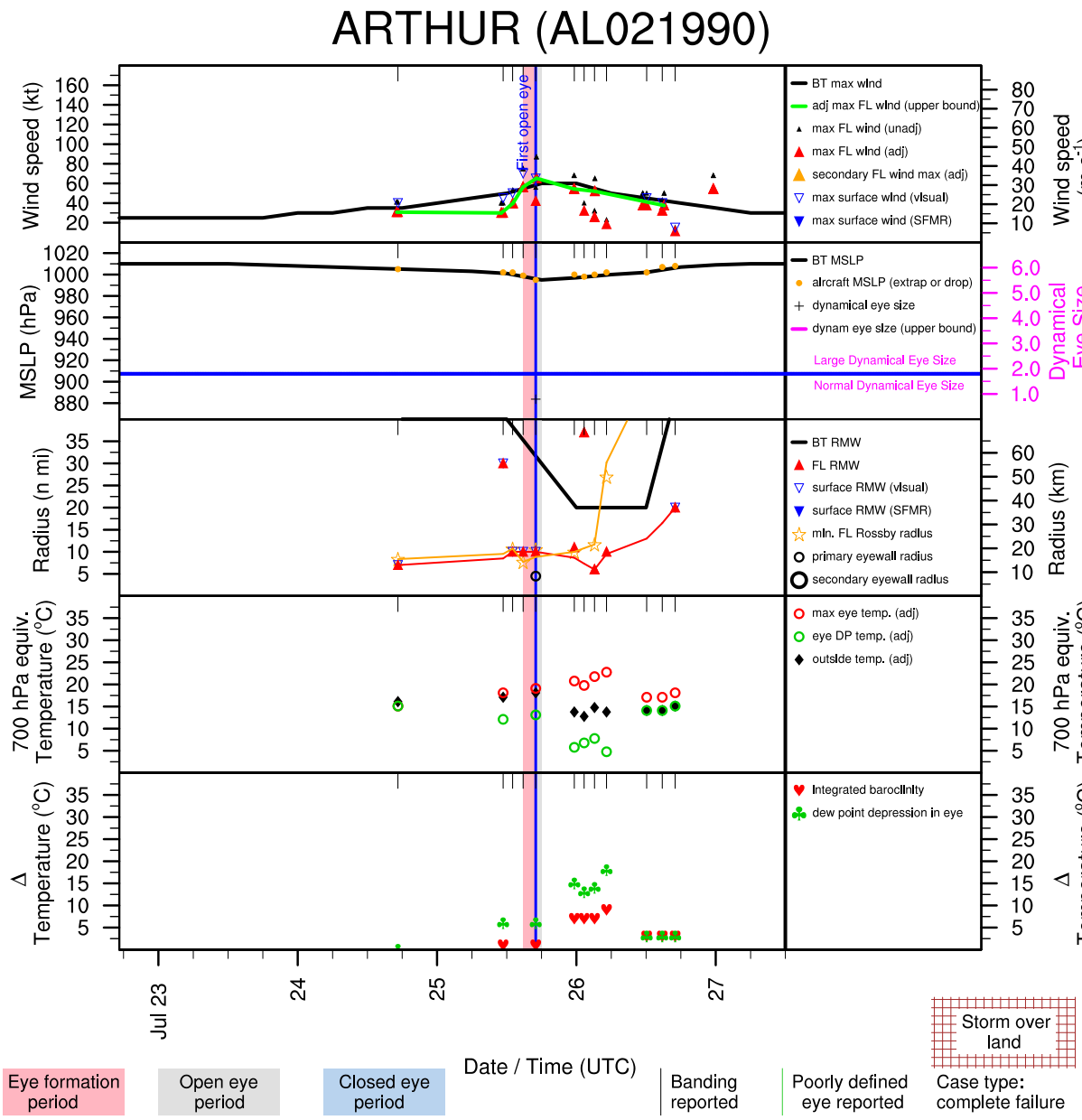

Figure E.9: Structure and intensity parameters for Tropical Storm Arthur (1990).

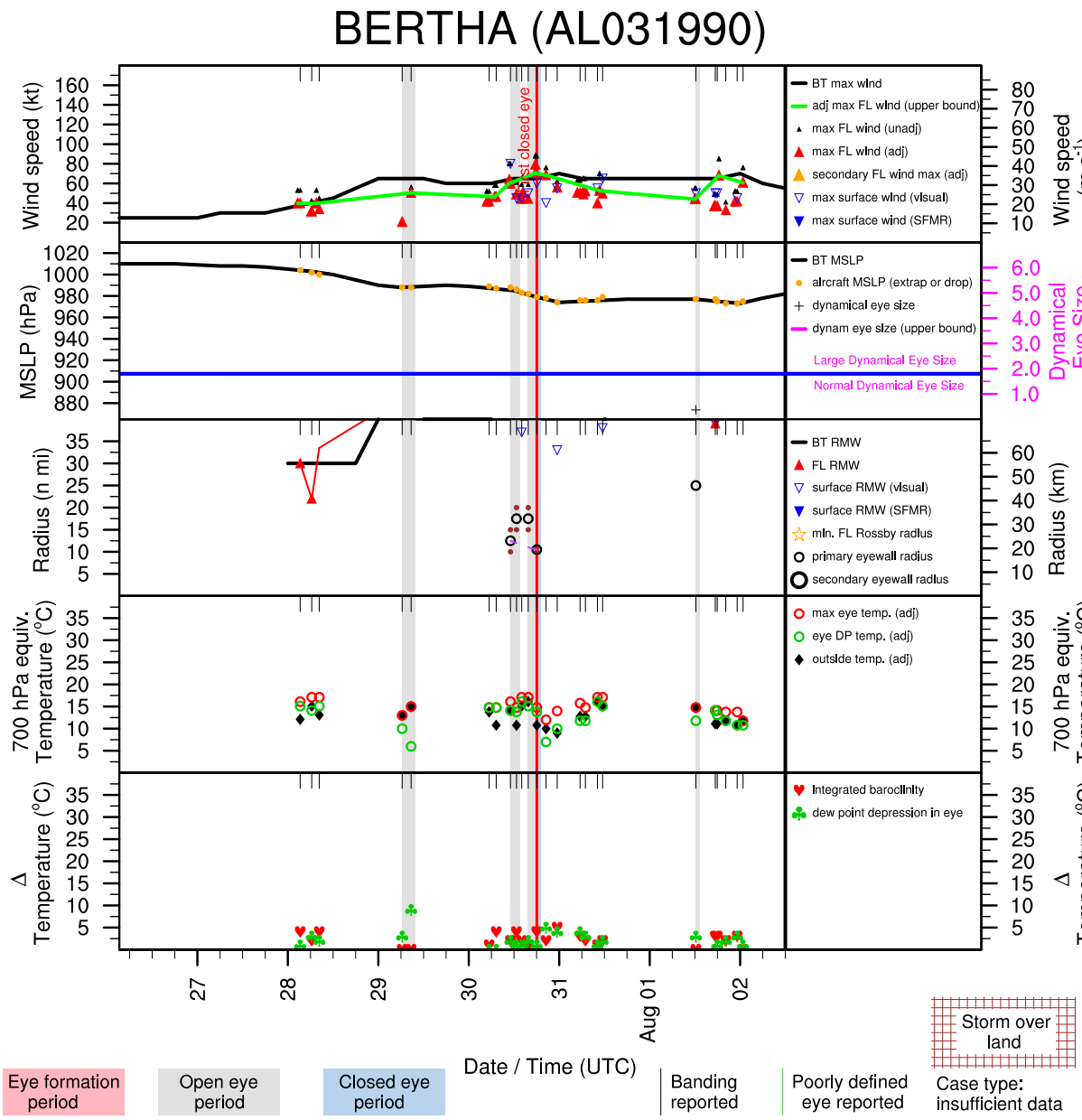

Figure E.10: Structure and intensity parameters for Hurricane Bertha (1990).

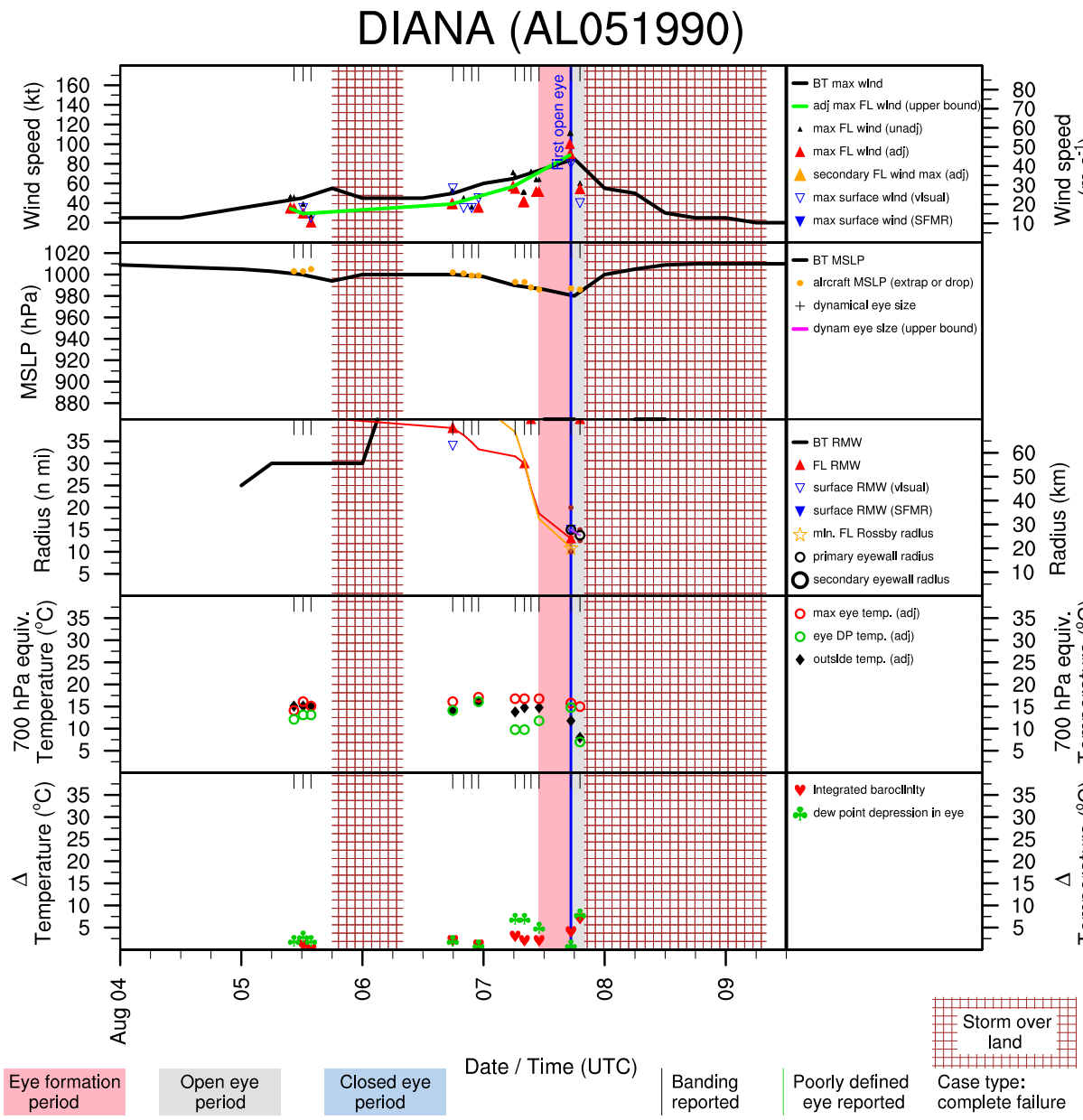

Figure E.11: Structure and intensity parameters for Hurricane Diana (1990).

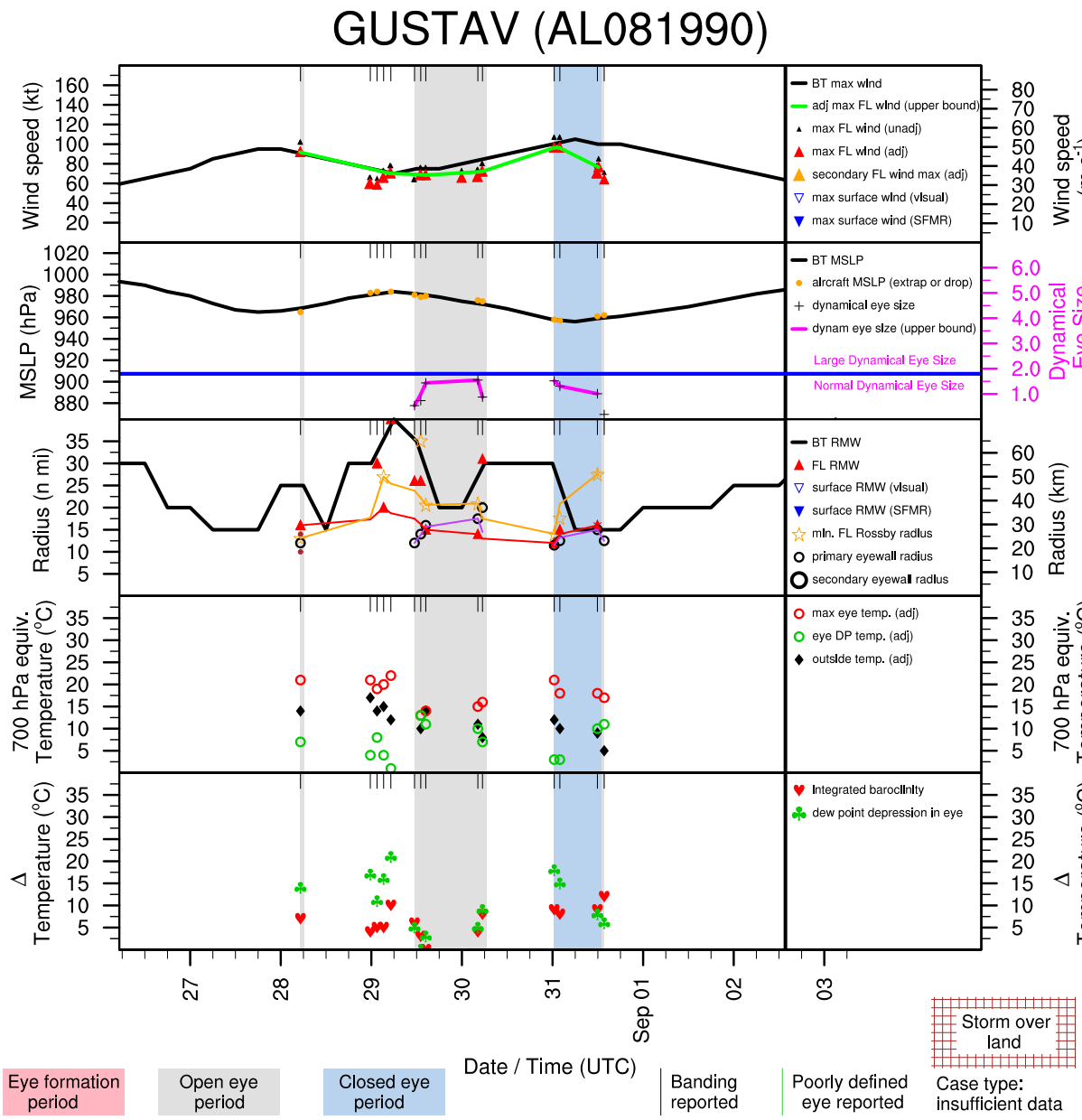

Figure E.12: Structure and intensity parameters for Hurricane Gustav (1990).

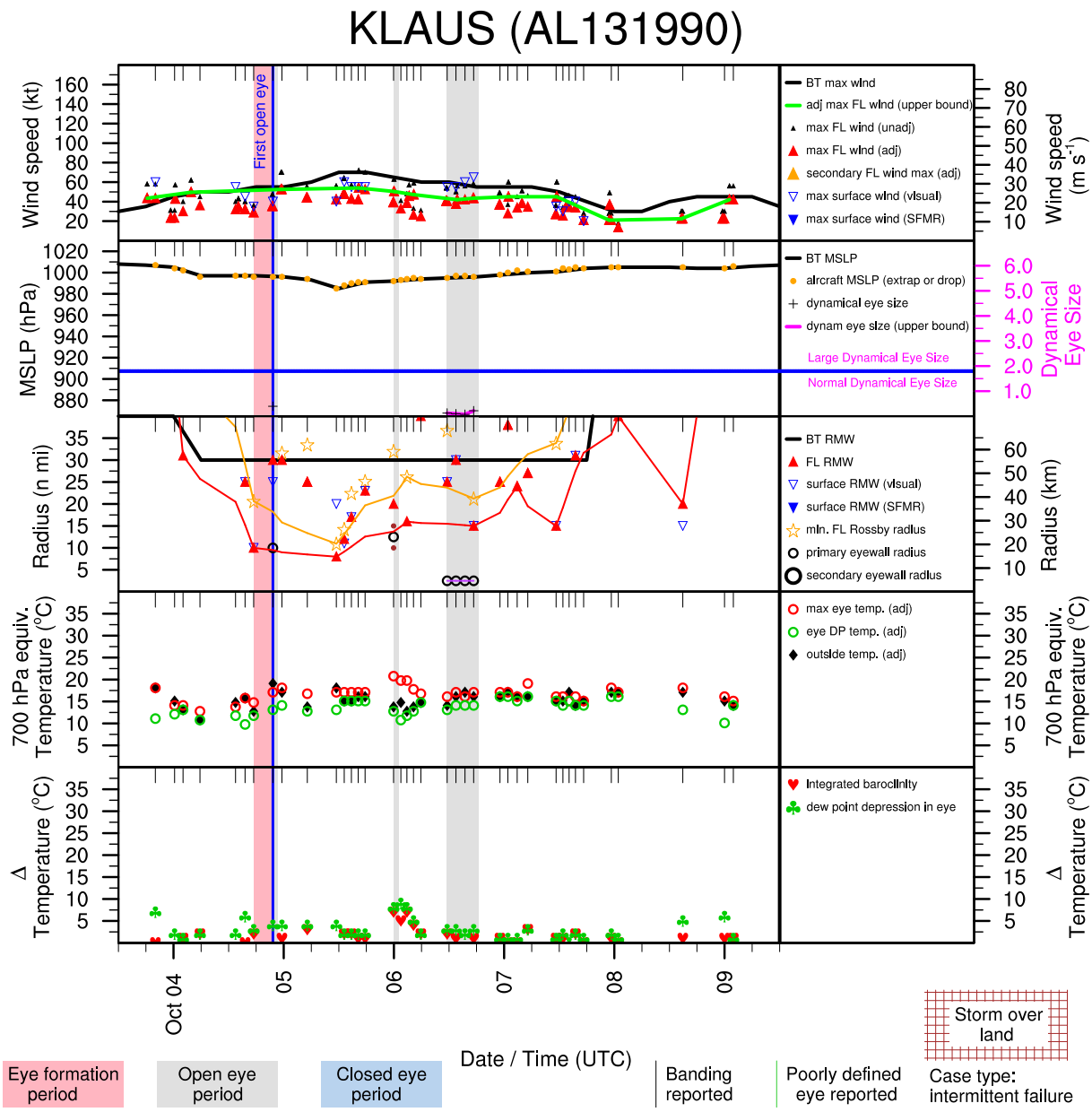

Figure E.13: Structure and intensity parameters for Hurricane Klaus (1990).

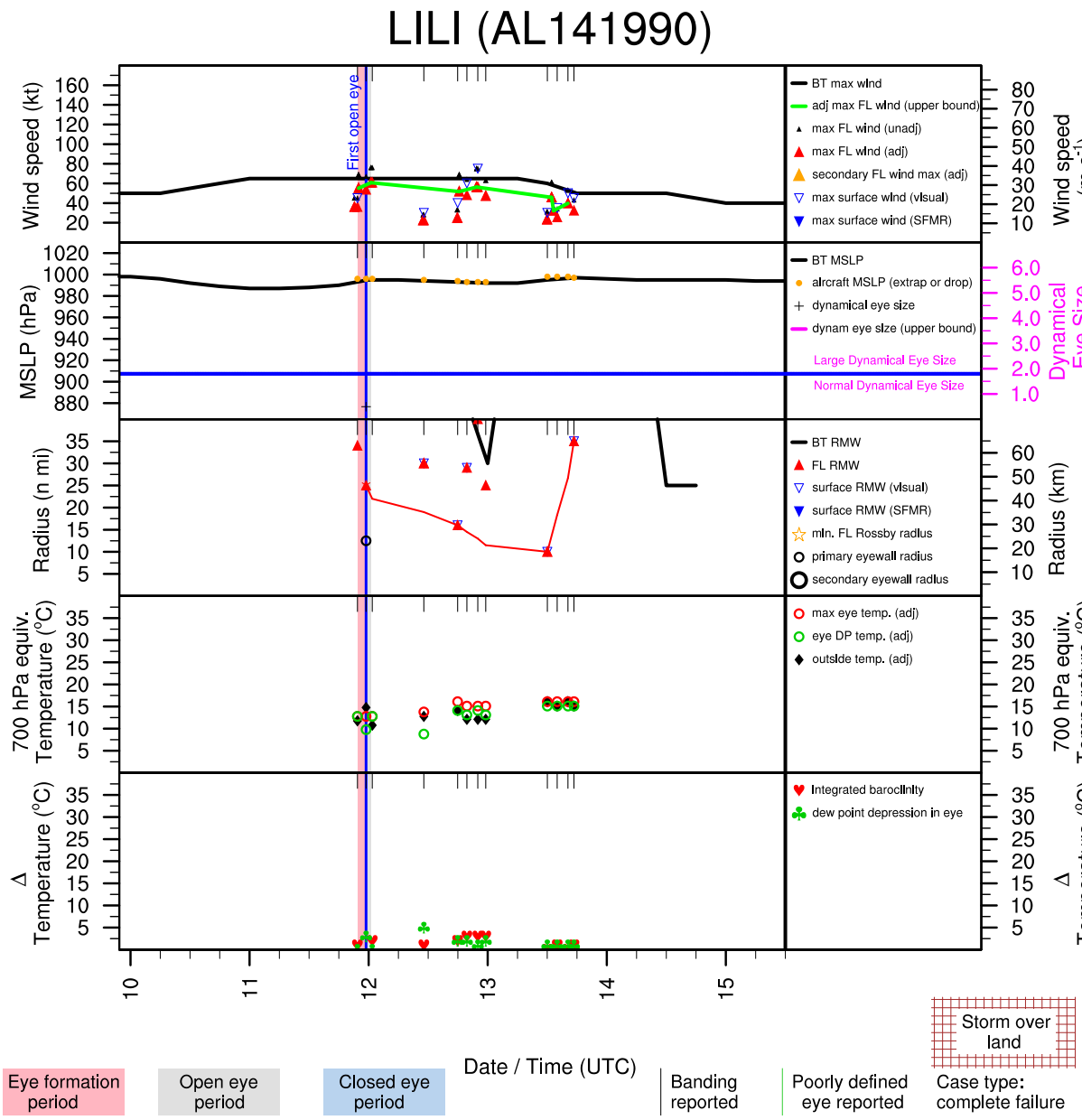

Figure E.14: Structure and intensity parameters for Hurricane Lili (1990).

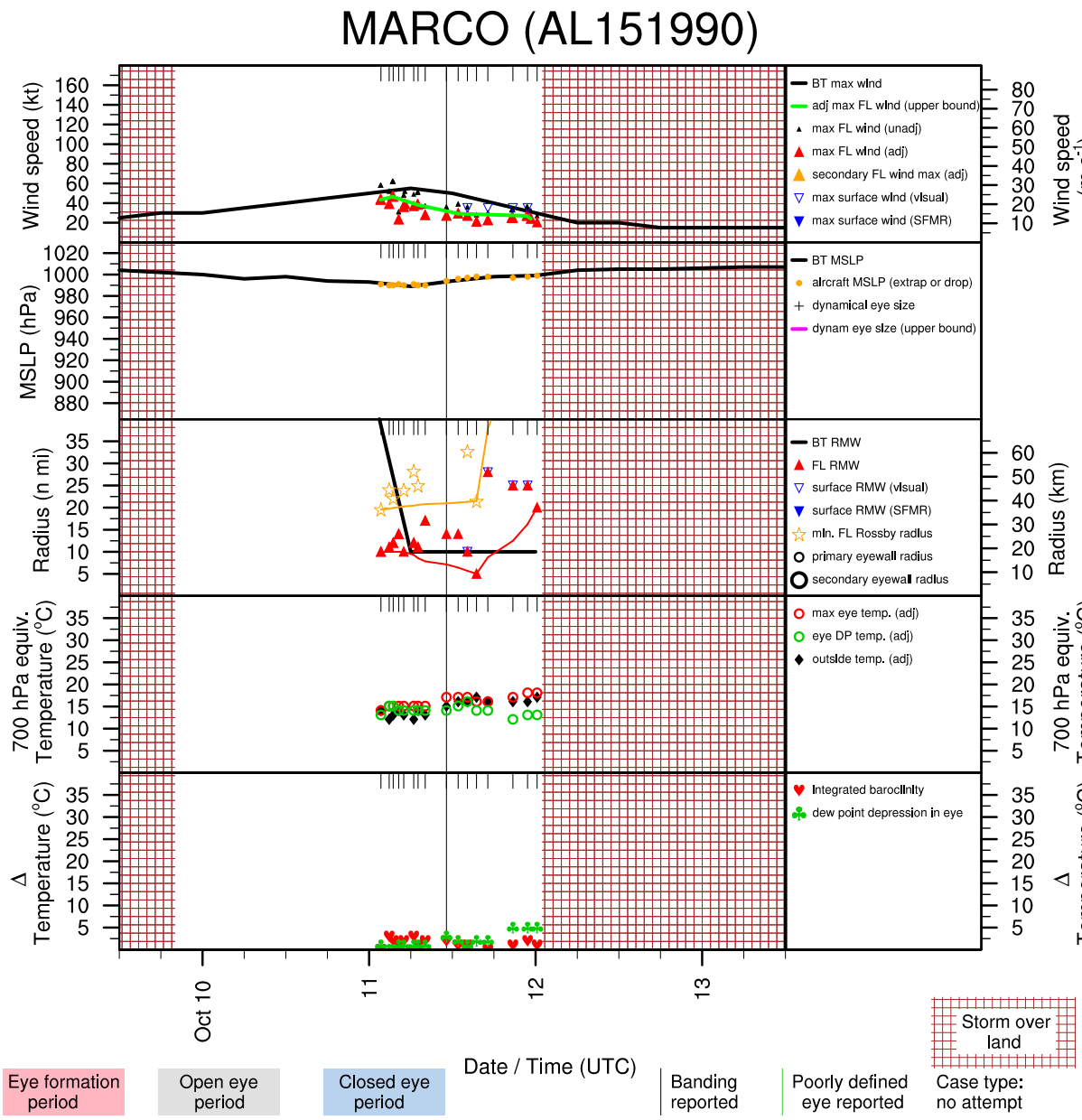

Figure E.15: Structure and intensity parameters for Tropical Storm Marco (1990).

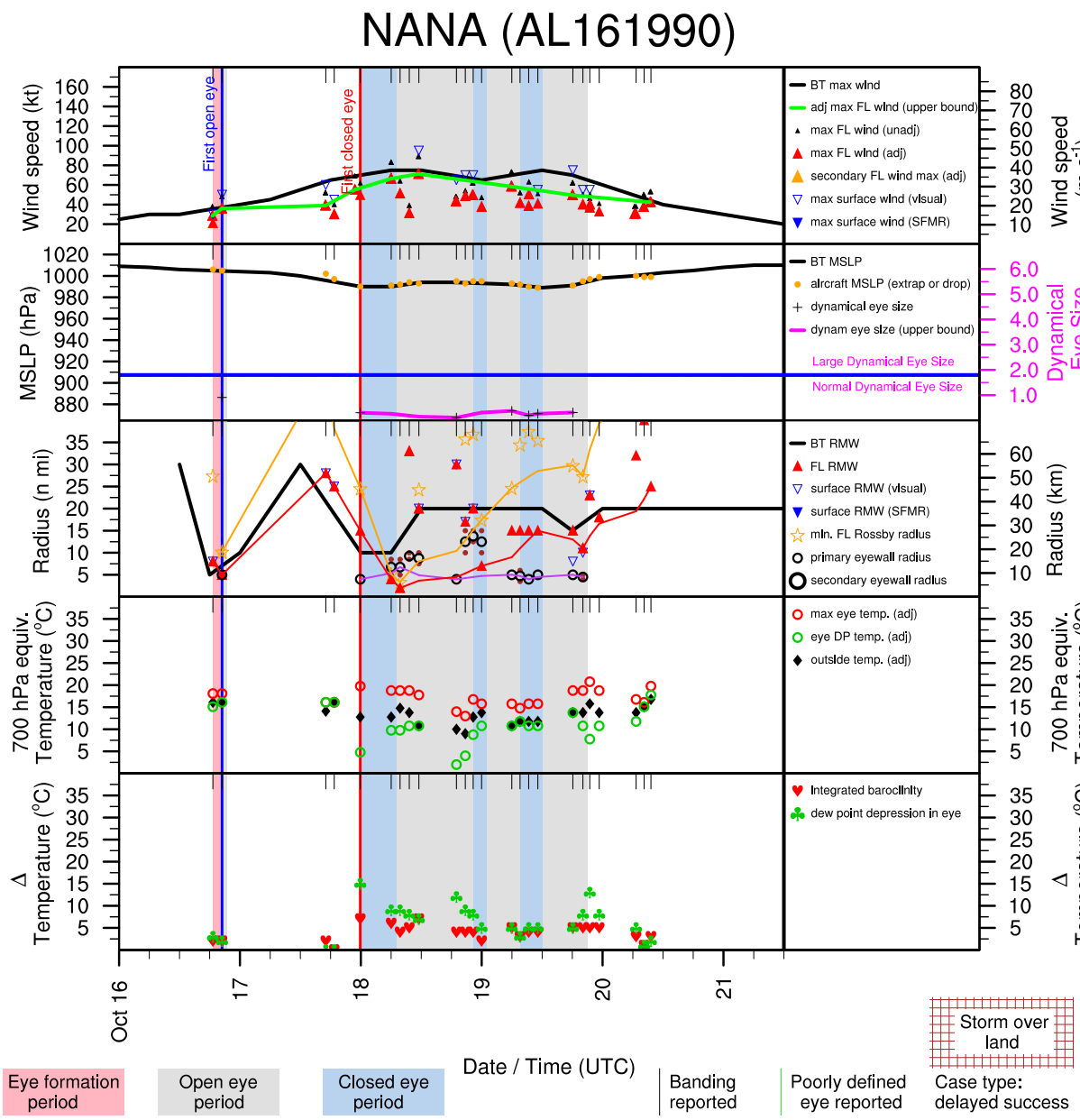

Figure E.16: Structure and intensity parameters for Hurricane Nana (1990).

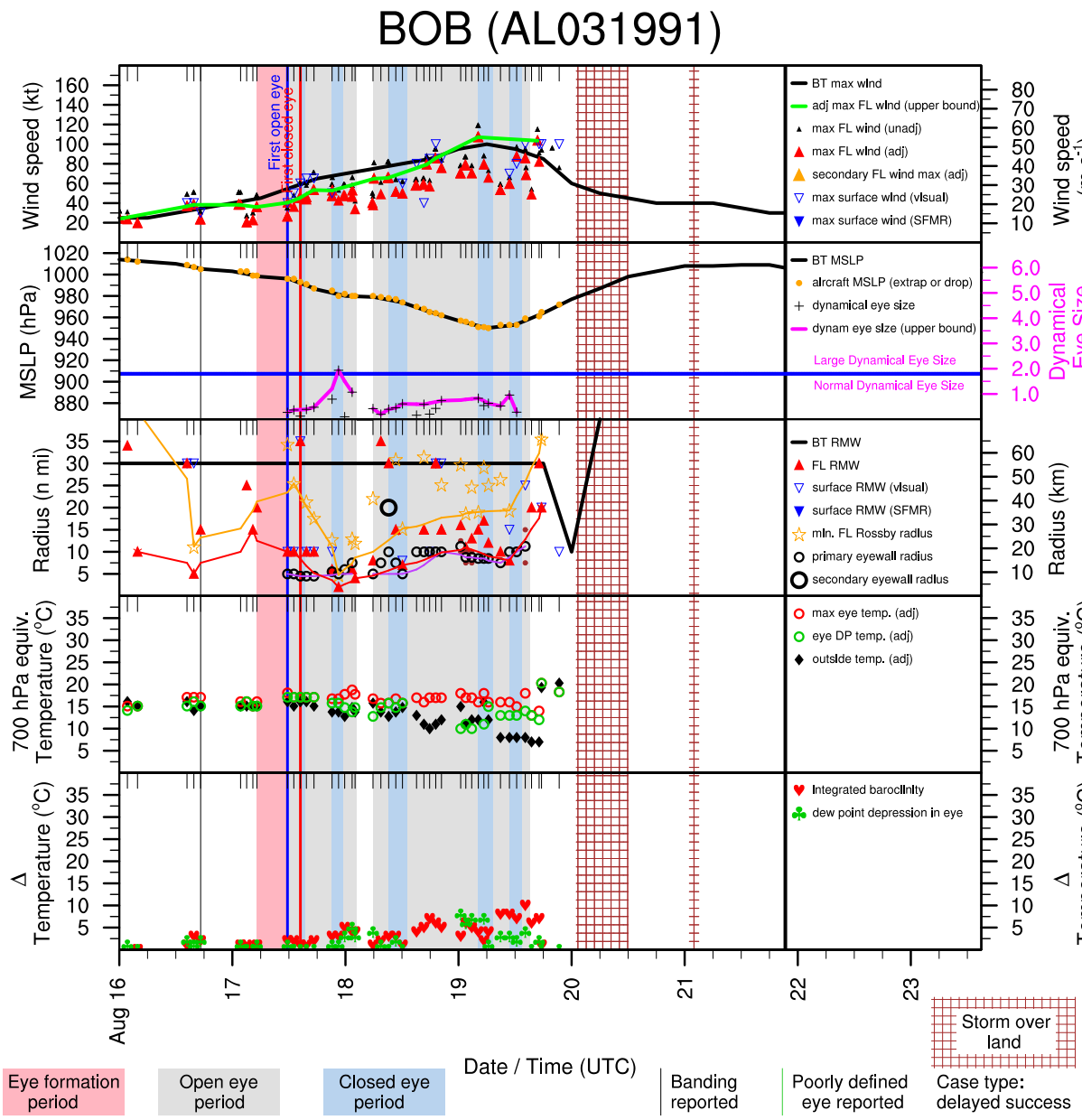

Figure E.17: Structure and intensity parameters for Hurricane Bob (1991).

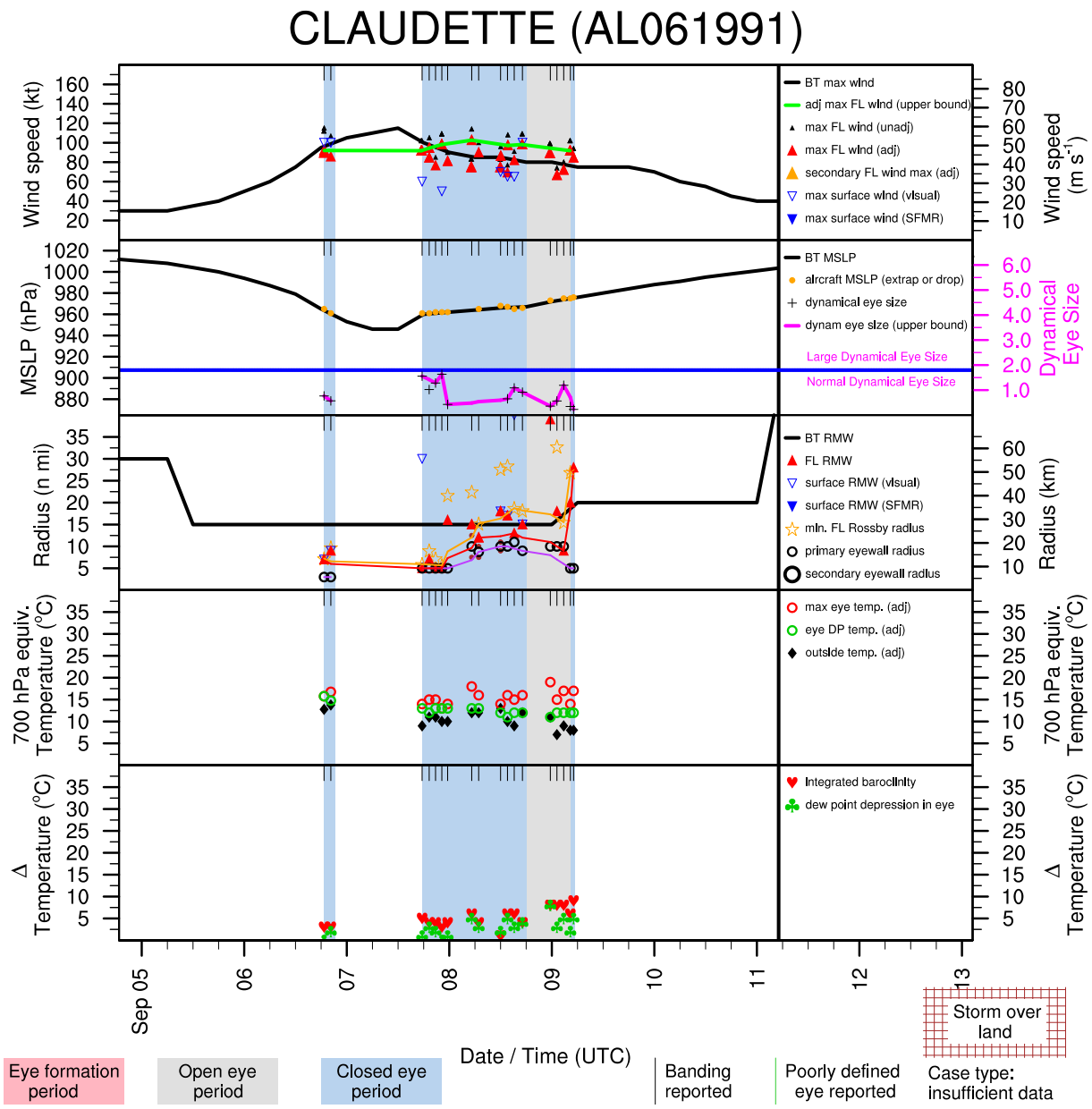

Figure E.18: Structure and intensity parameters for Hurricane Claudette (1991).

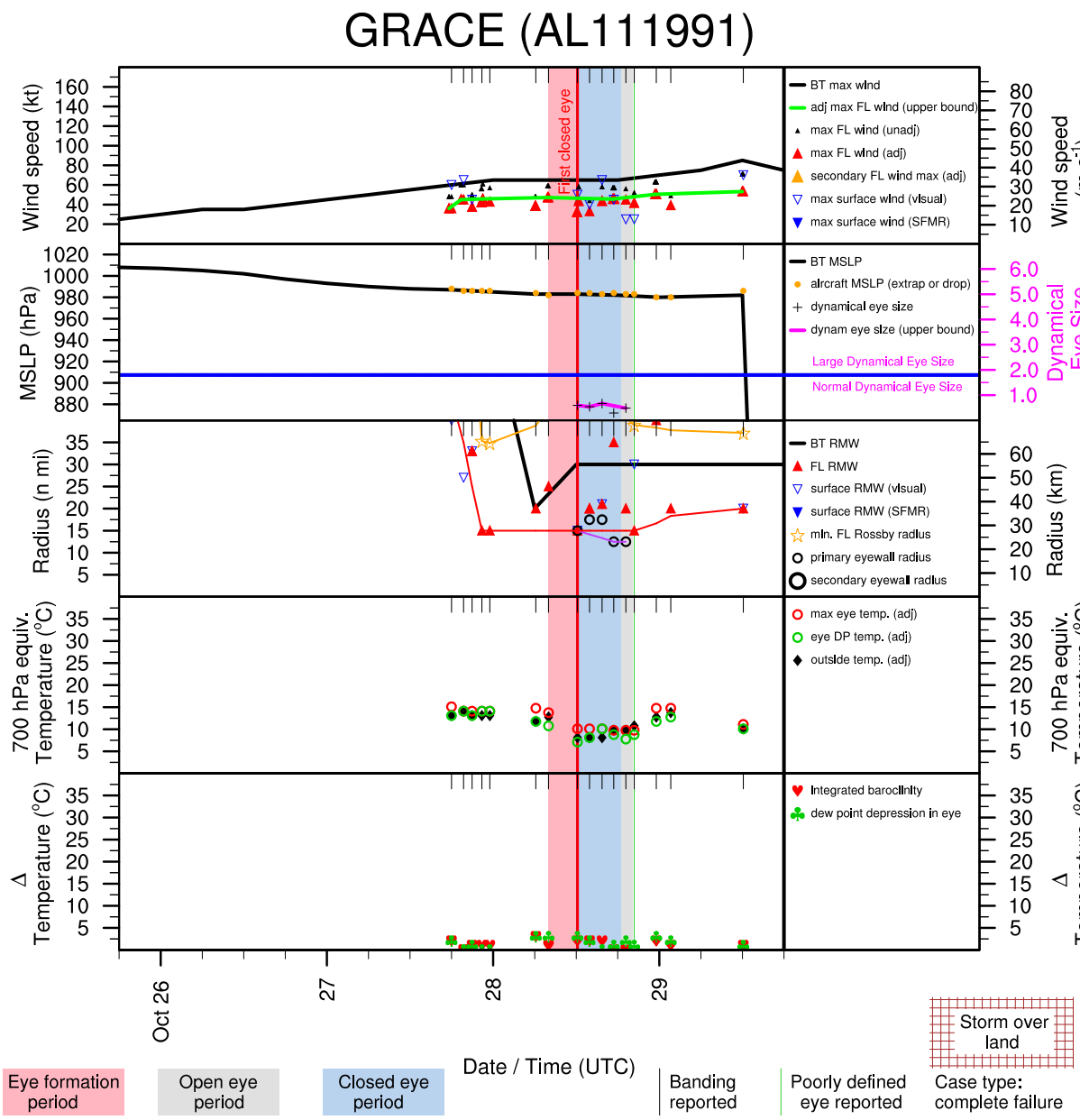

Figure E.19: Structure and intensity parameters for Hurricane Grace (1991).

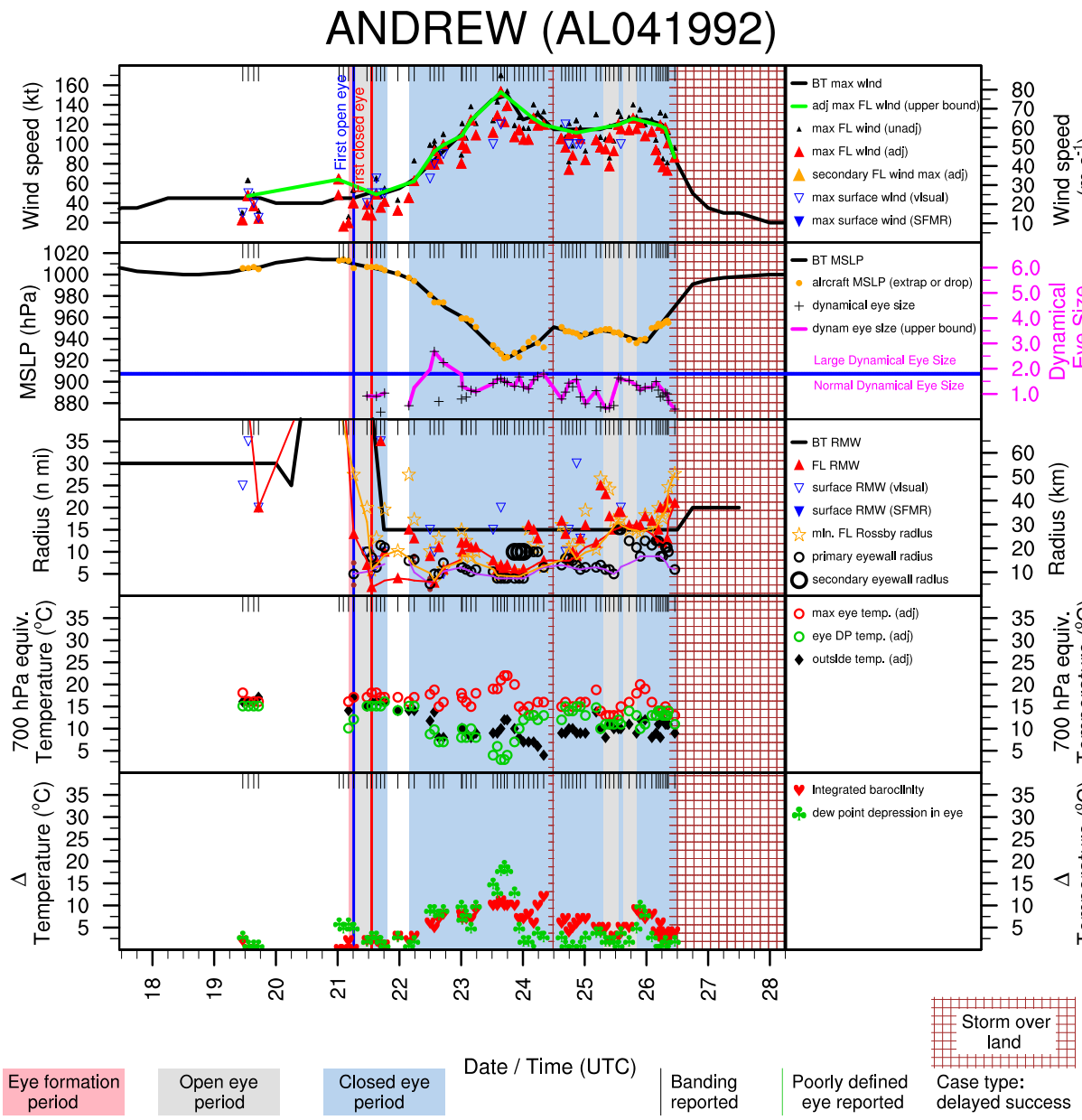

Figure E.20: Structure and intensity parameters for Hurricane Andrew (1992).

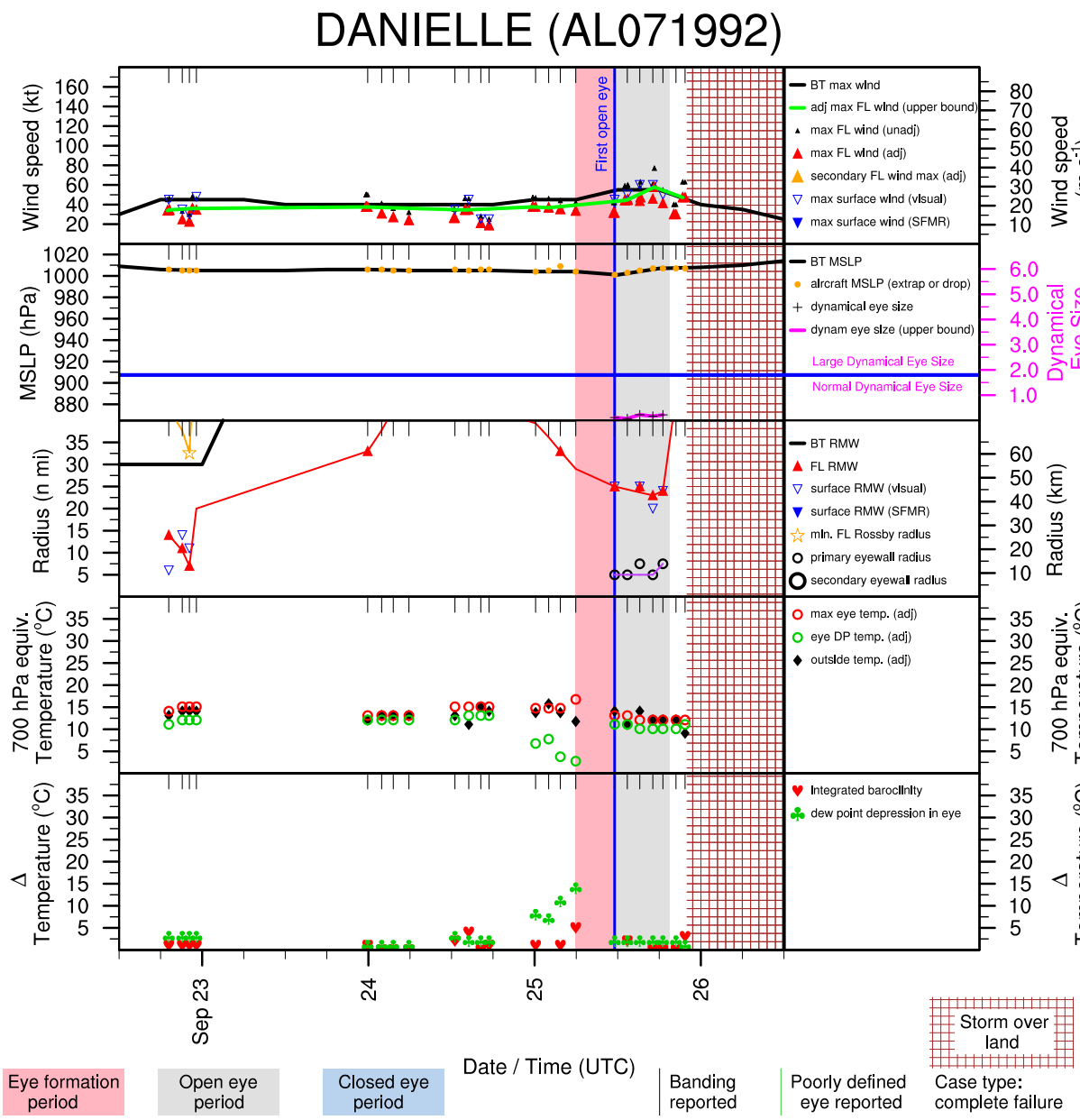

Figure E.21: Structure and intensity parameters for Tropical Storm Danielle (1992).

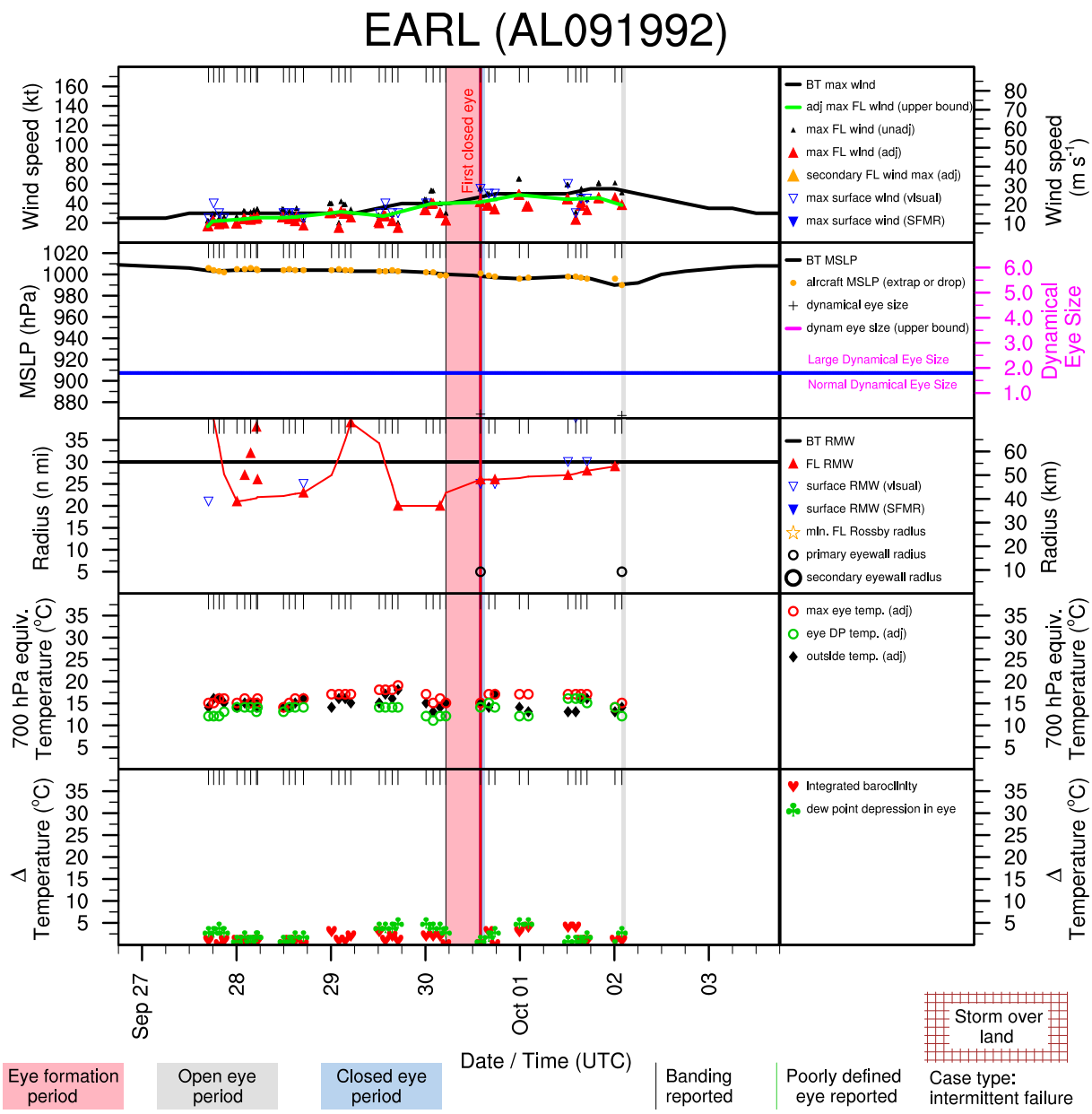

Figure E.22: Structure and intensity parameters for Tropical Storm Earl (1992).

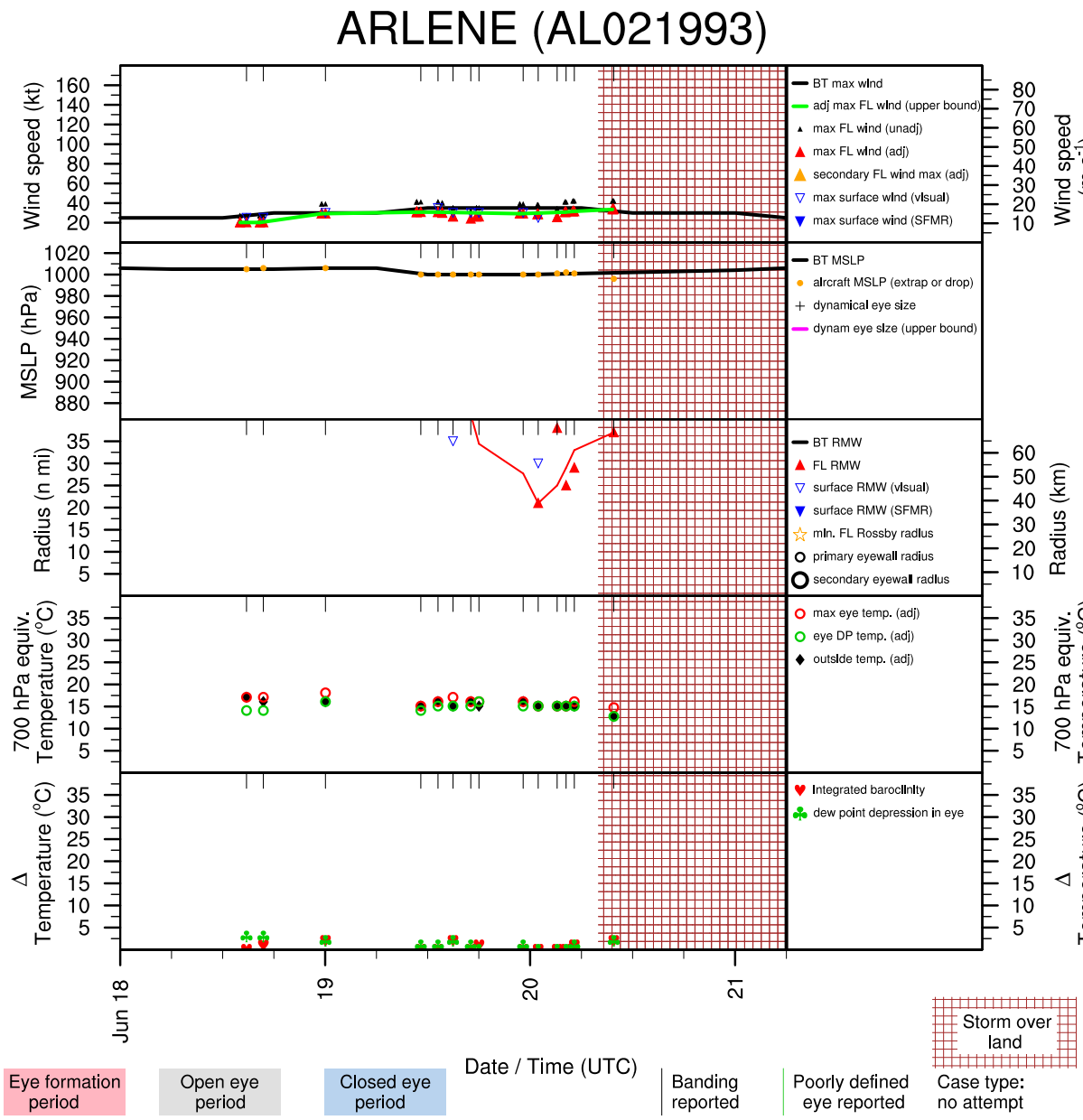

Figure E.23: Structure and intensity parameters for Tropical Storm Arlene (1993).

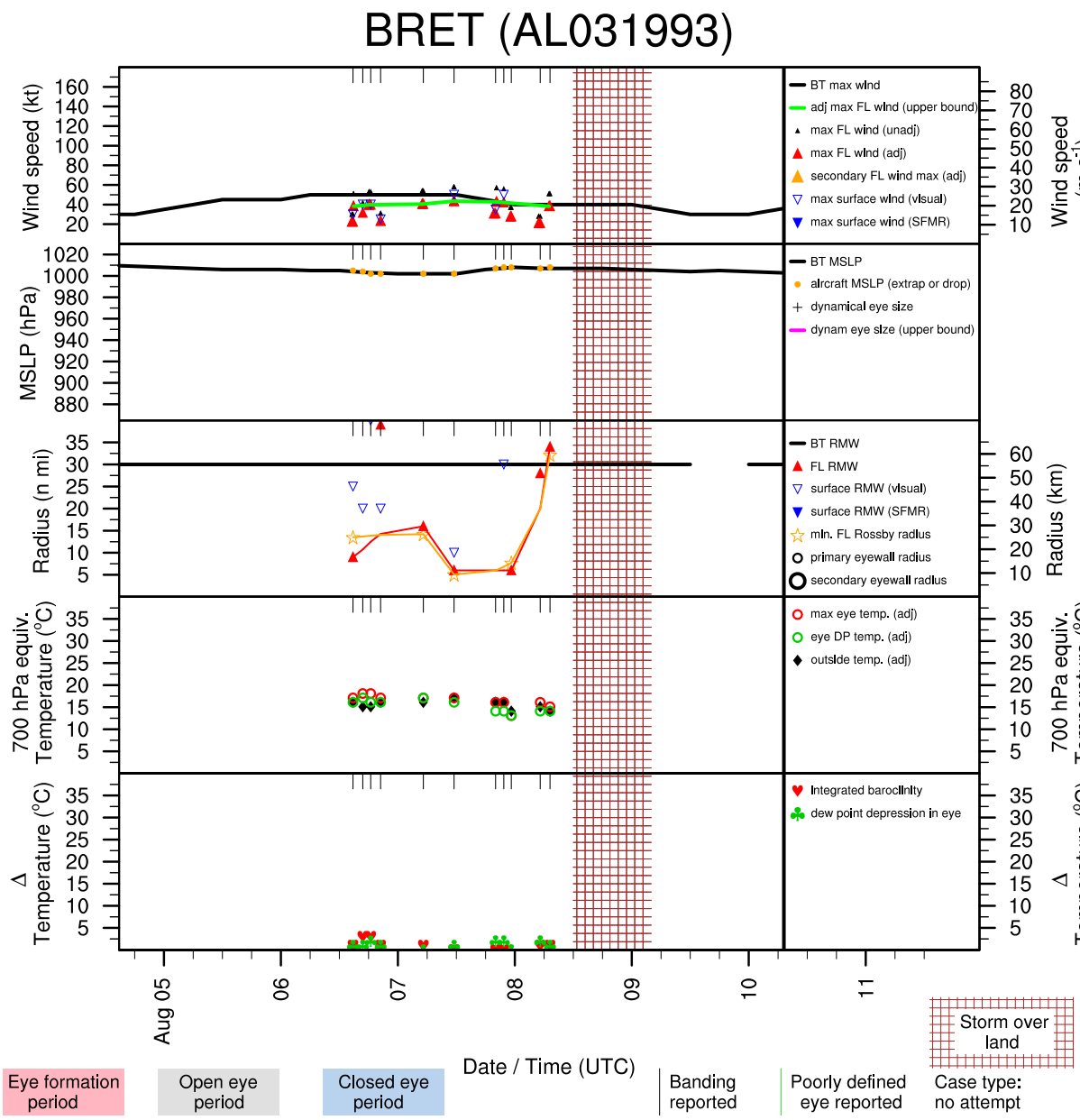

Figure E.24: Structure and intensity parameters for Tropical Storm Bret (1993).

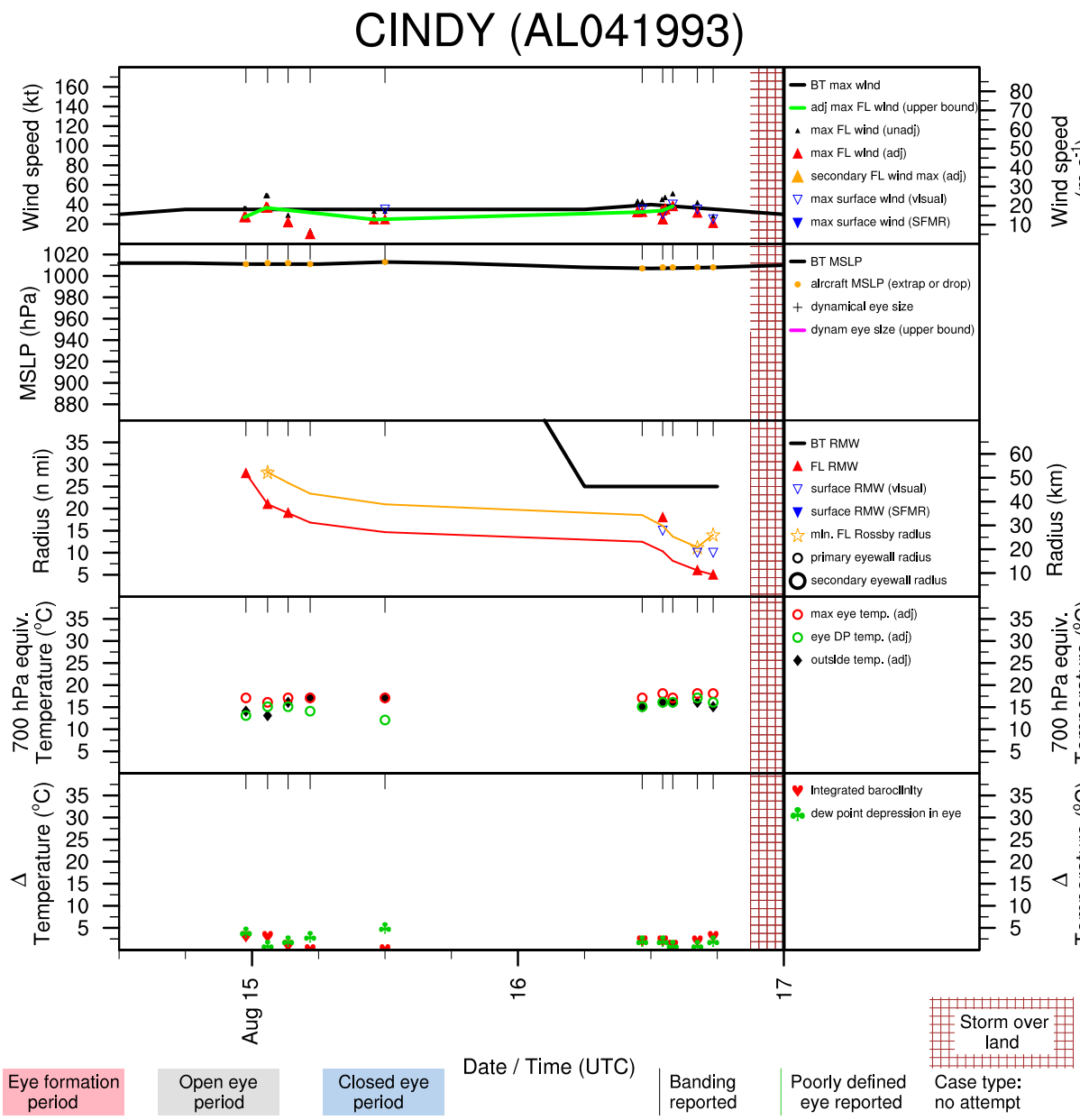

Figure E.25: Structure and intensity parameters for Tropical Storm Cindy (1993).

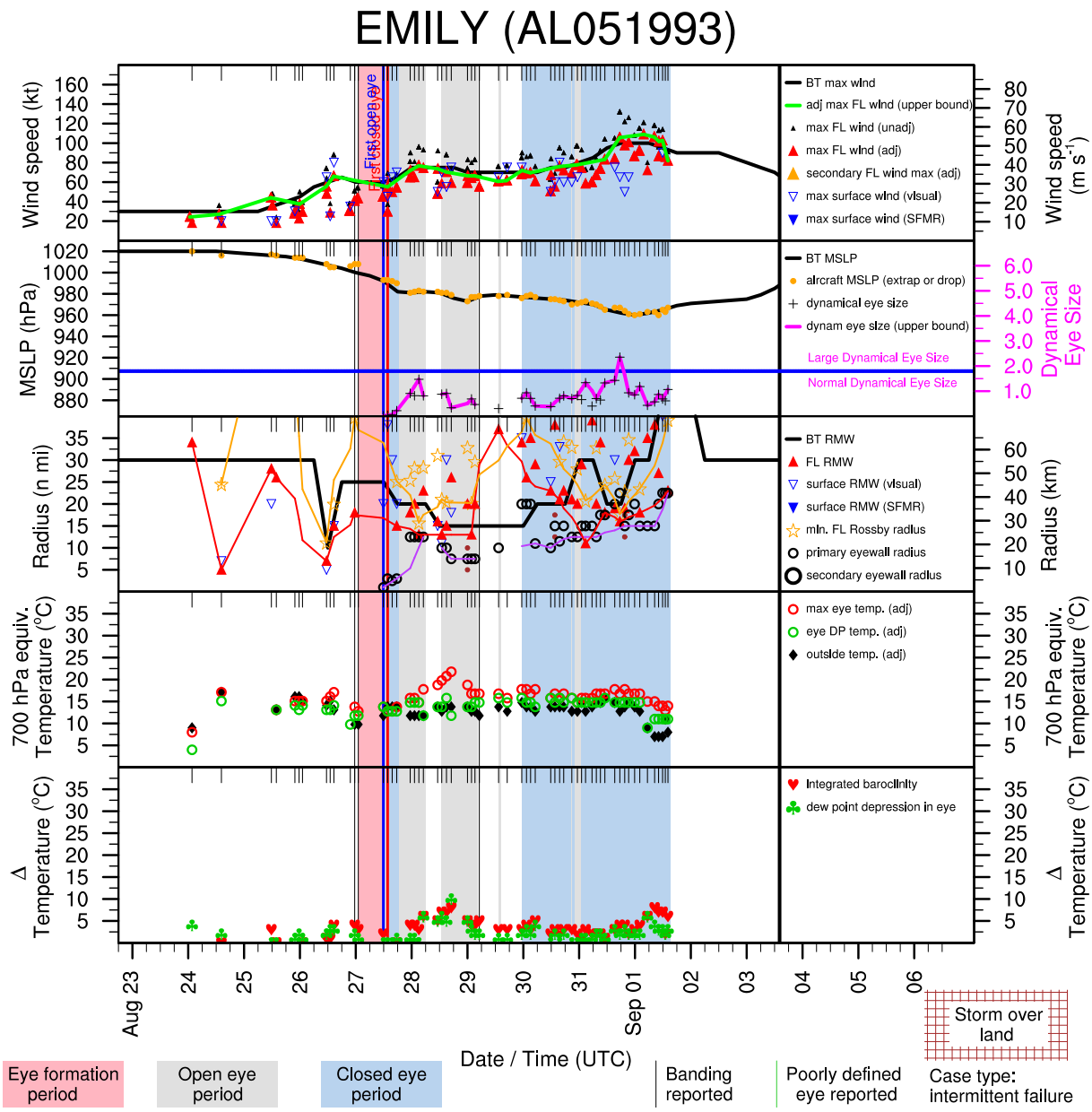

Figure E.26: Structure and intensity parameters for Hurricane Emily (1993).

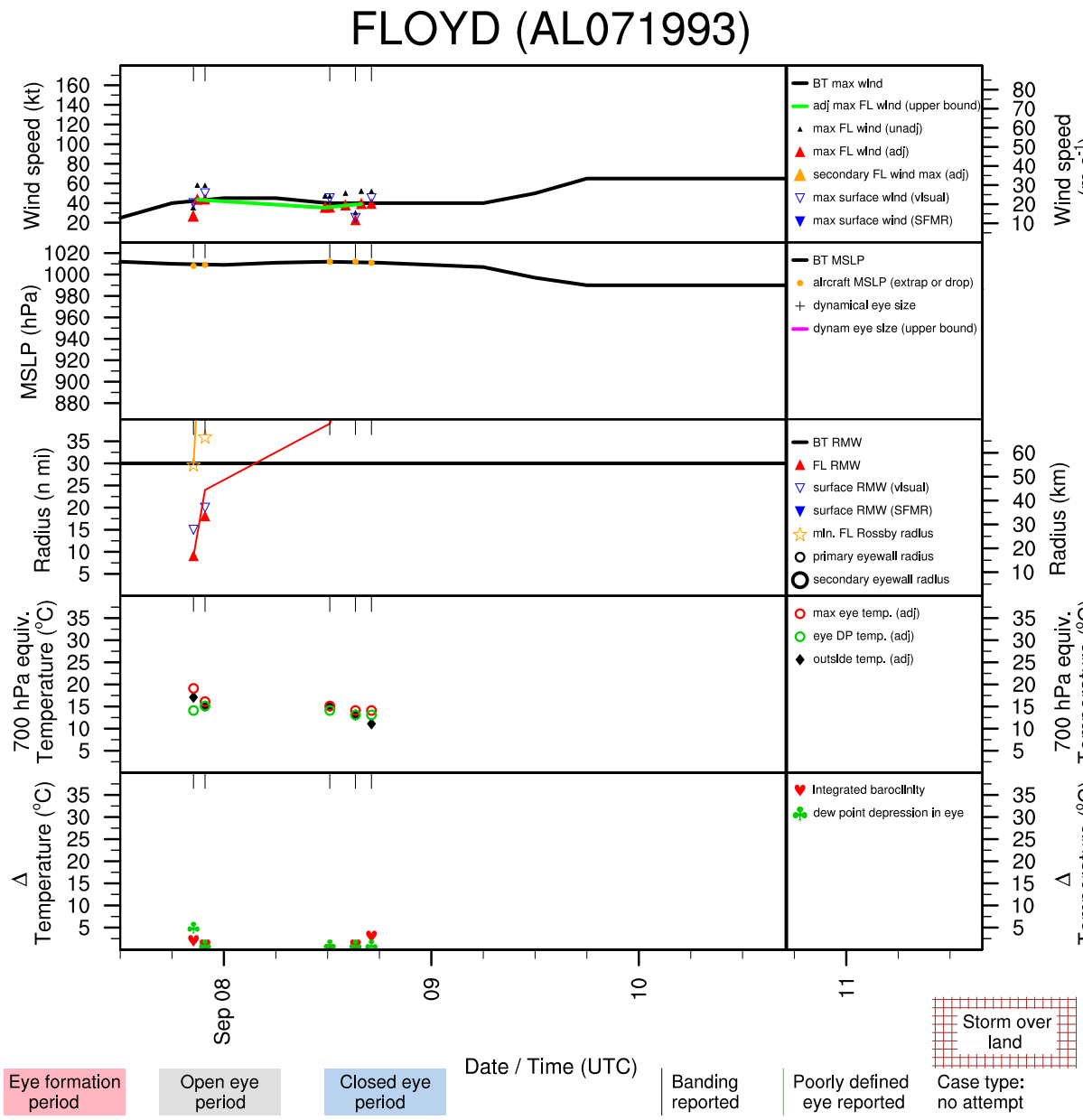

Figure E.27: Structure and intensity parameters for Hurricane Floyd (1993).

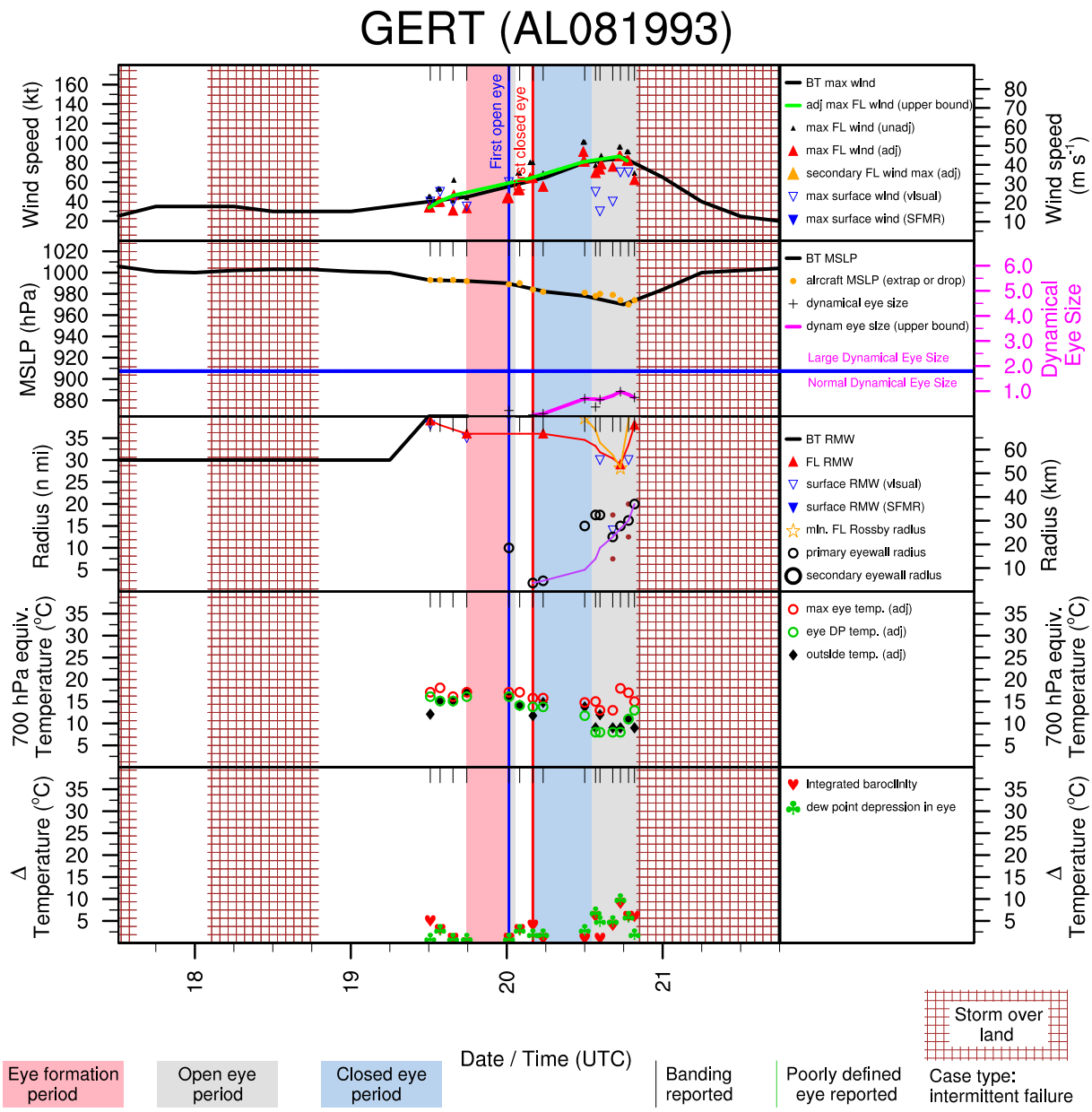

Figure E.28: Structure and intensity parameters for Hurricane Gert (1993).

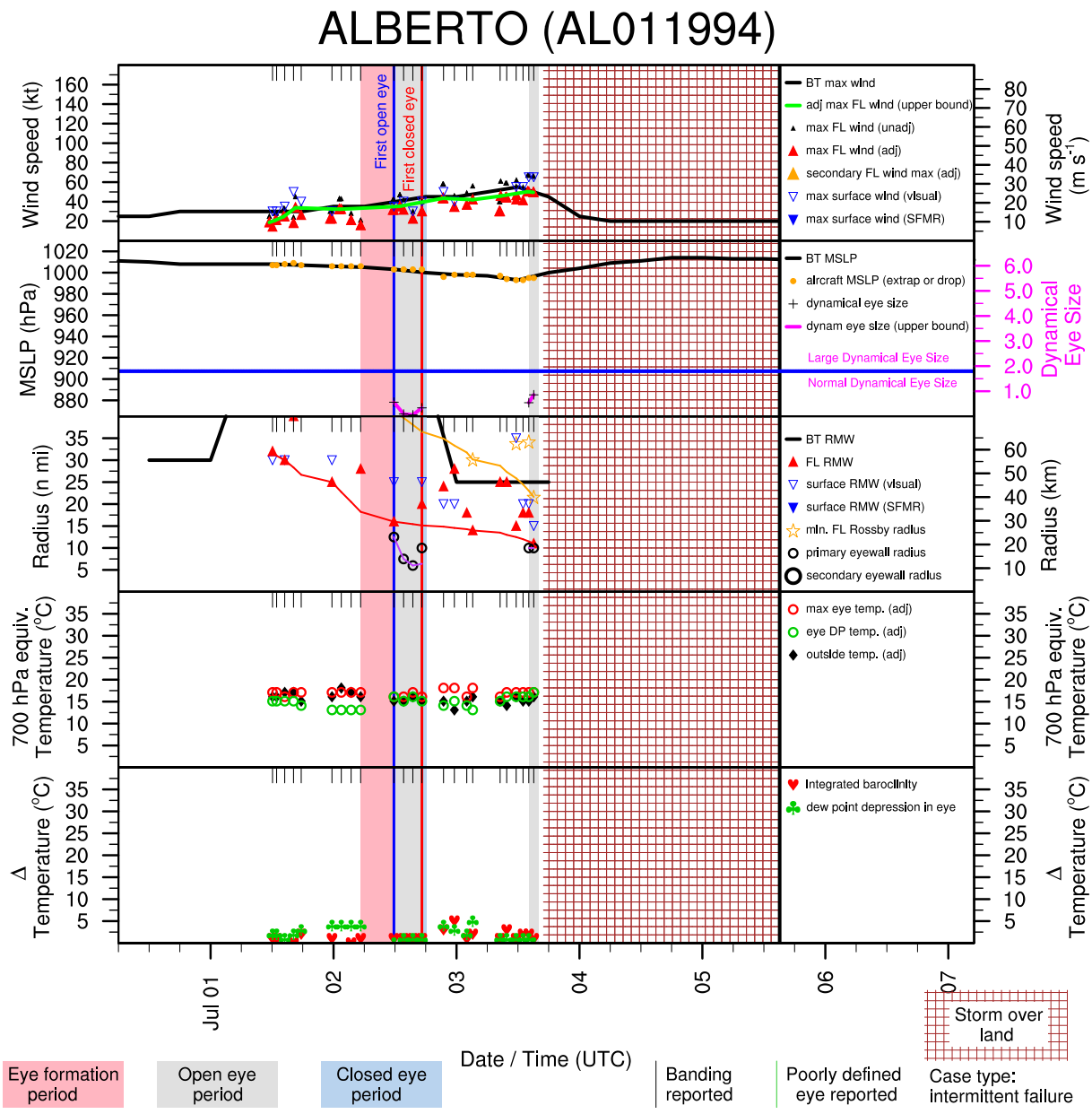

Figure E.29: Structure and intensity parameters for Tropical Storm Alberto (1994).

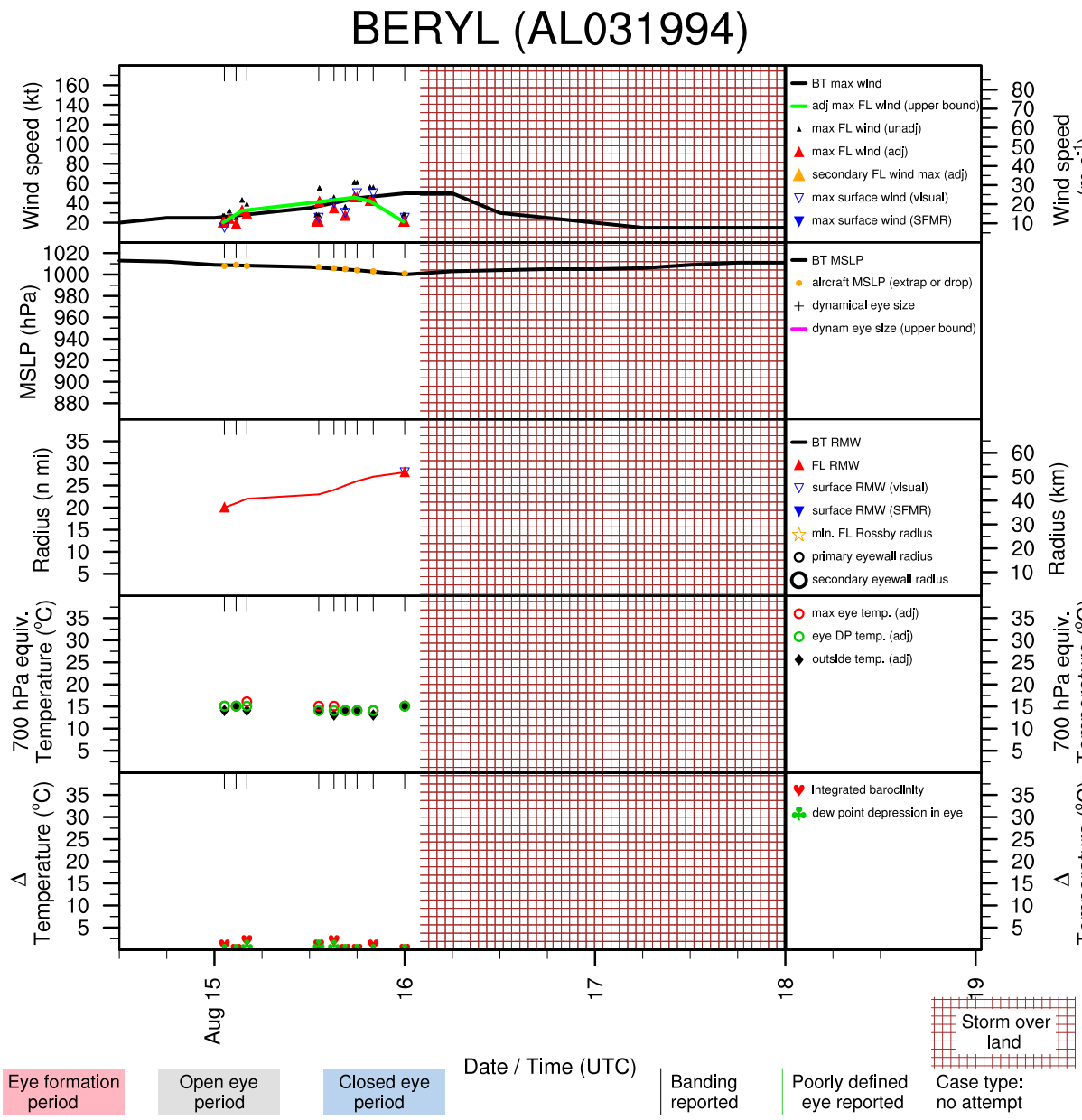

Figure E.30: Structure and intensity parameters for Tropical Storm Beryl (1994).

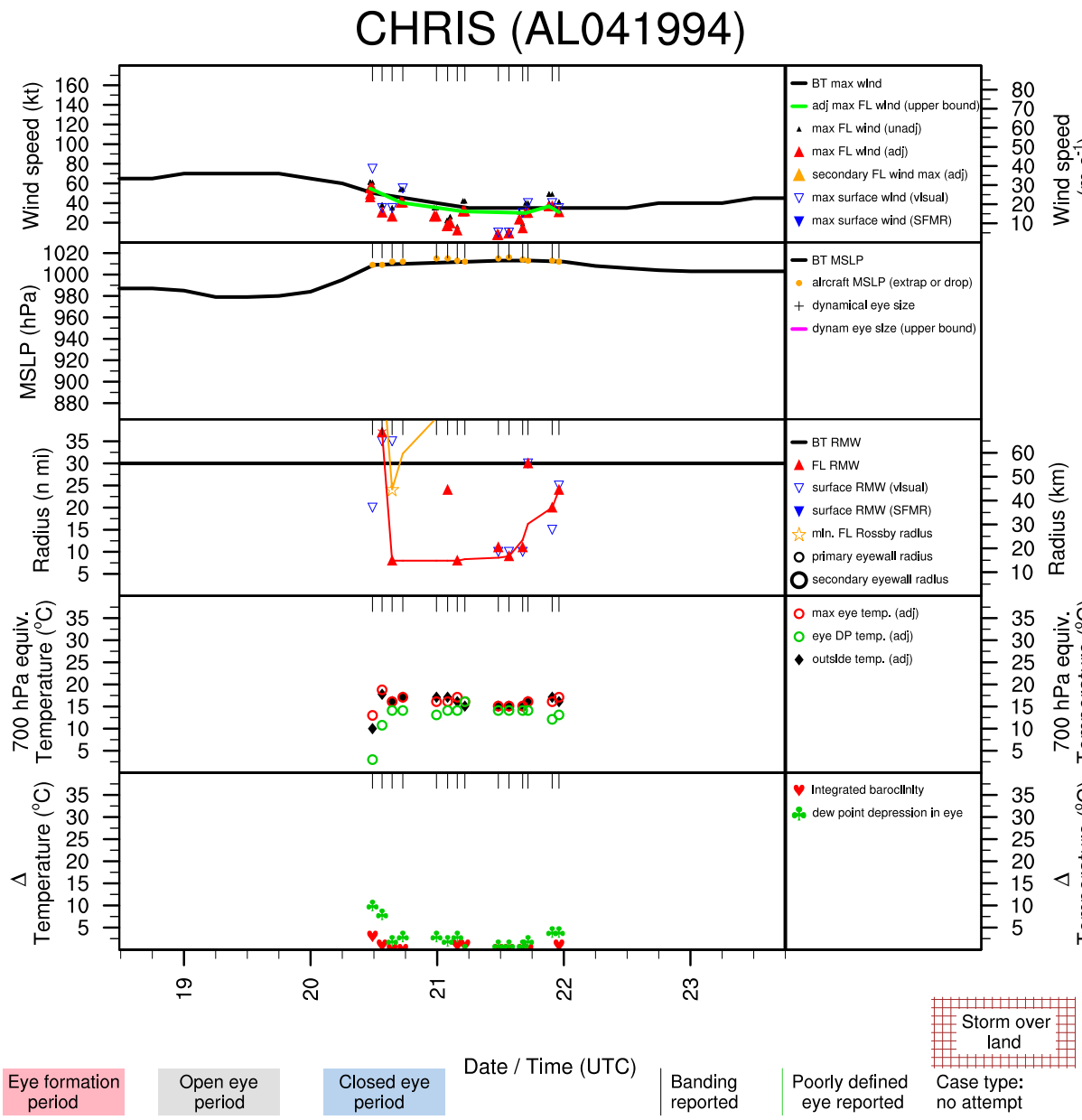

Figure E.31: Structure and intensity parameters for Hurricane Chris (1994).

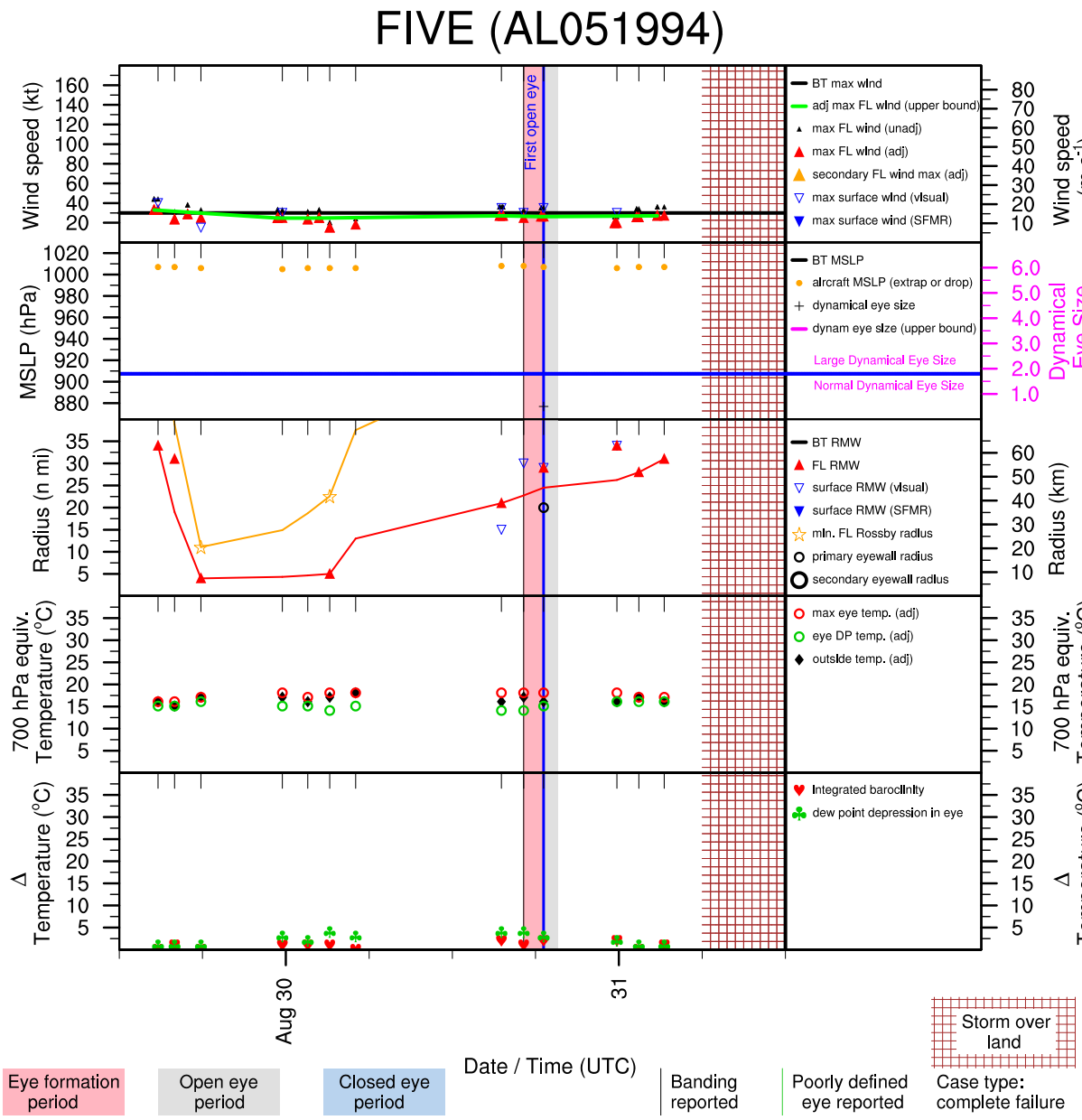

Figure E.32: Structure and intensity parameters for Tropical Depression Five (1994).

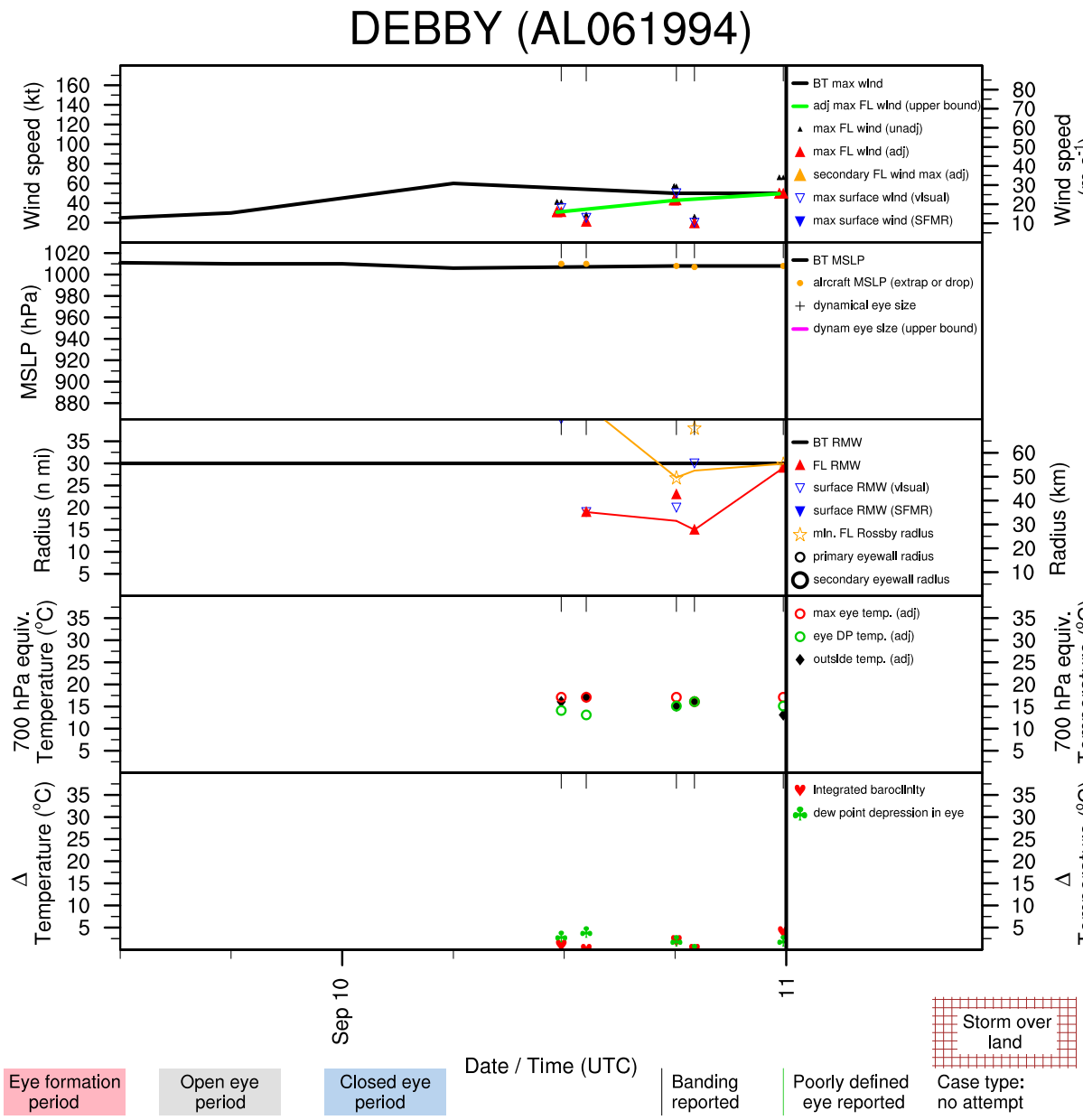

Figure E.33: Structure and intensity parameters for Tropical Storm Debby (1994).

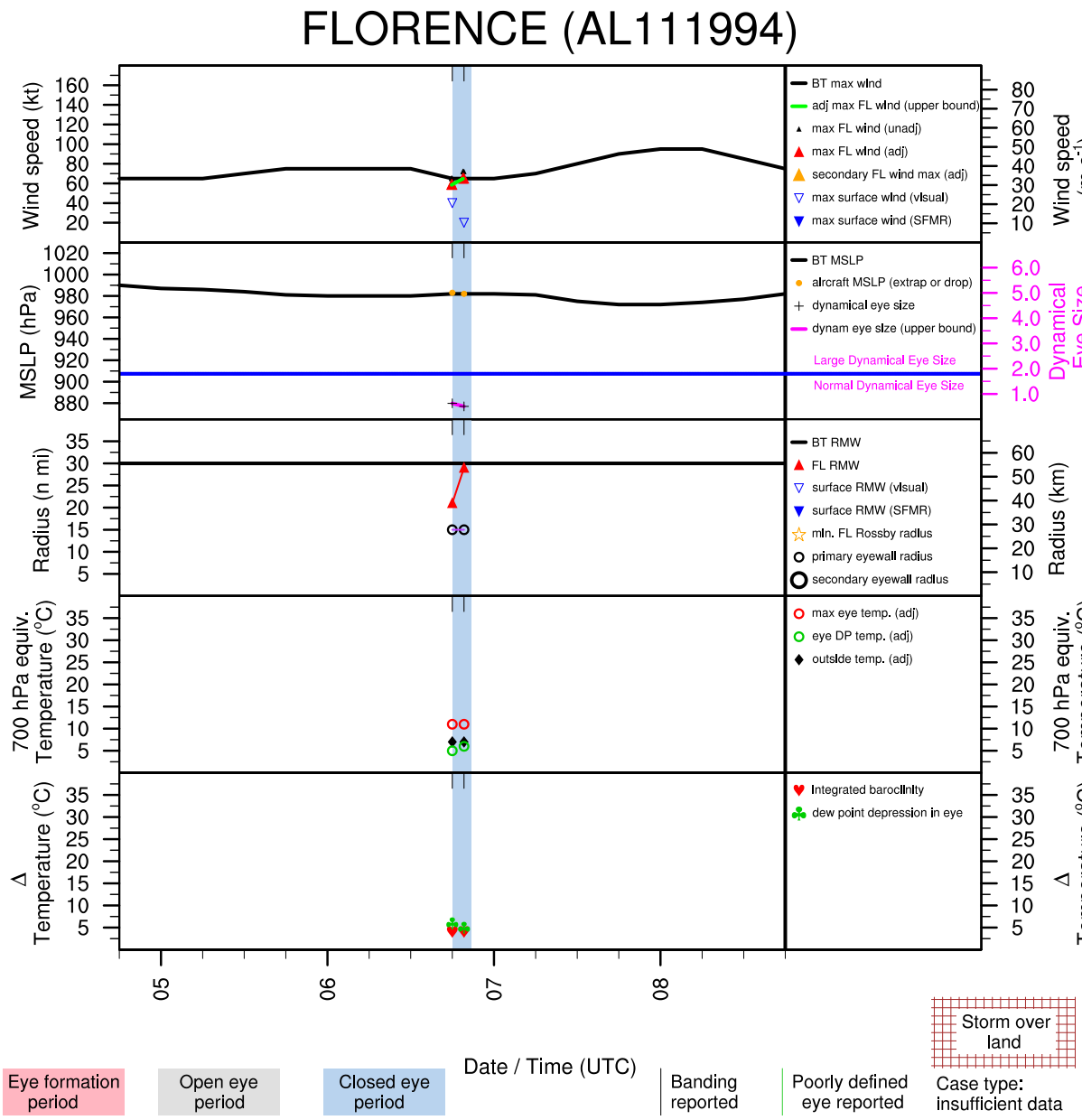

Figure E.34: Structure and intensity parameters for Hurricane Florence (1994).

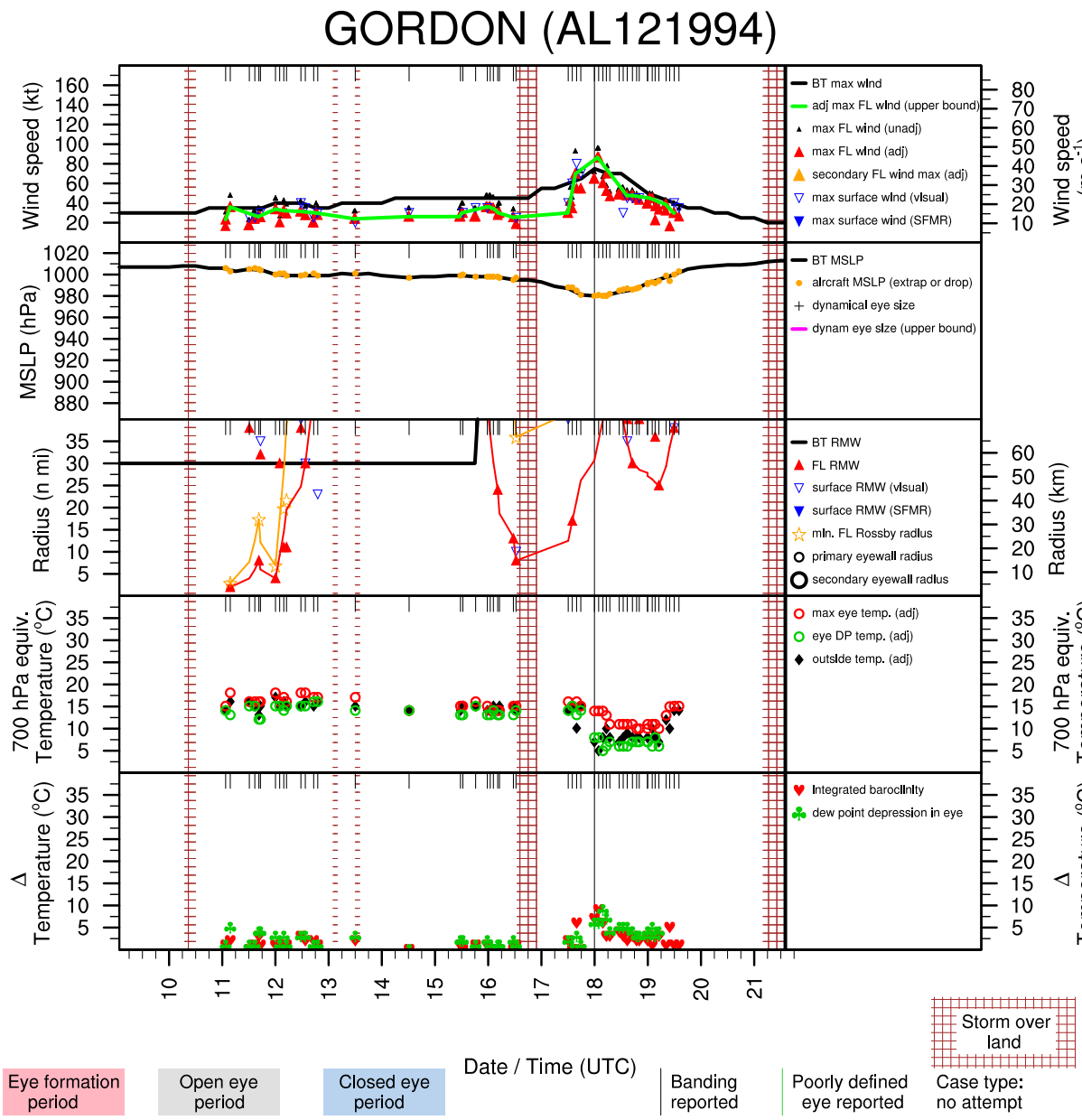

Figure E.35: Structure and intensity parameters for Hurricane Gordon (1994).

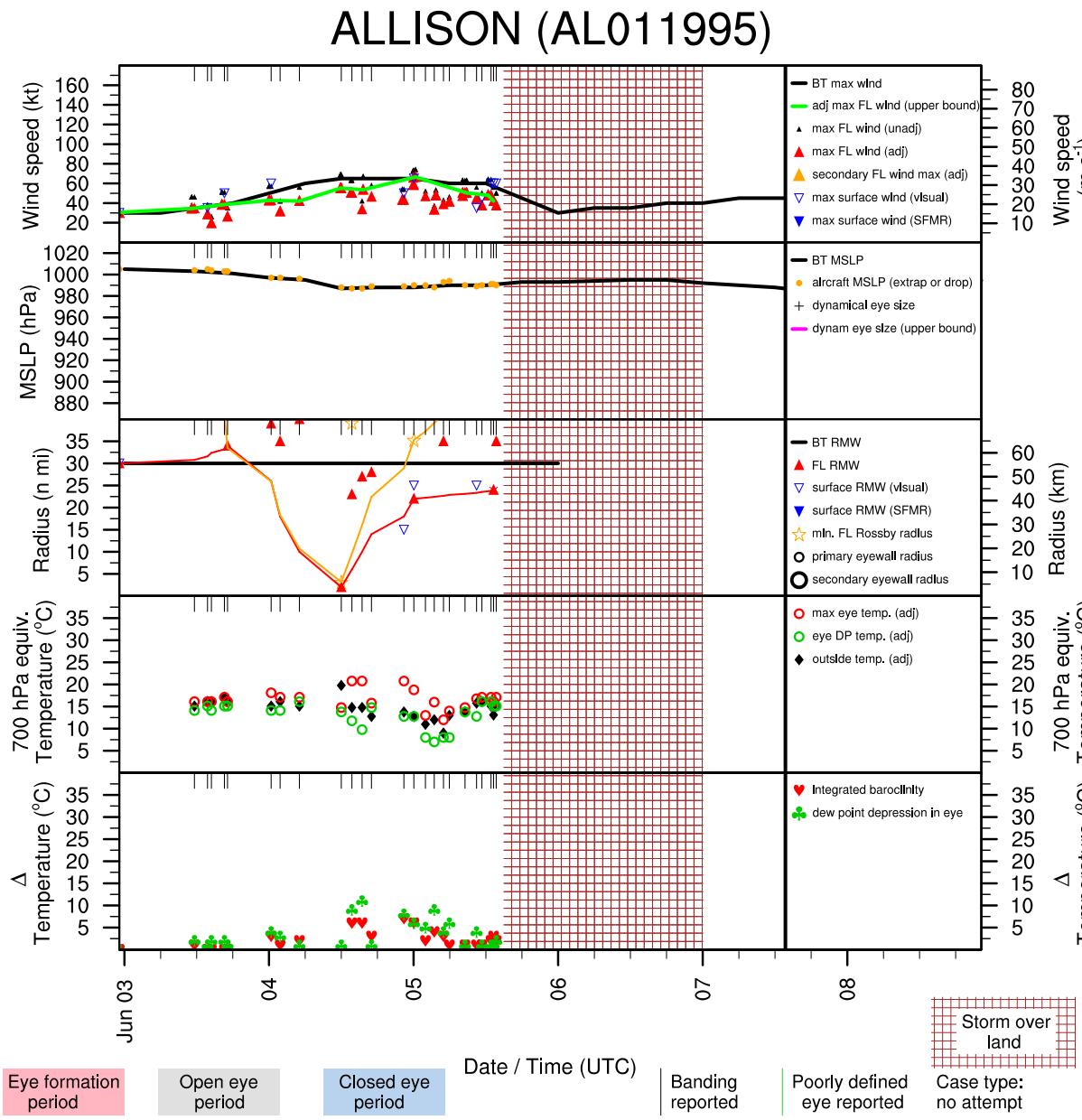

Figure E.36: Structure and intensity parameters for Hurricane Allison (1995).

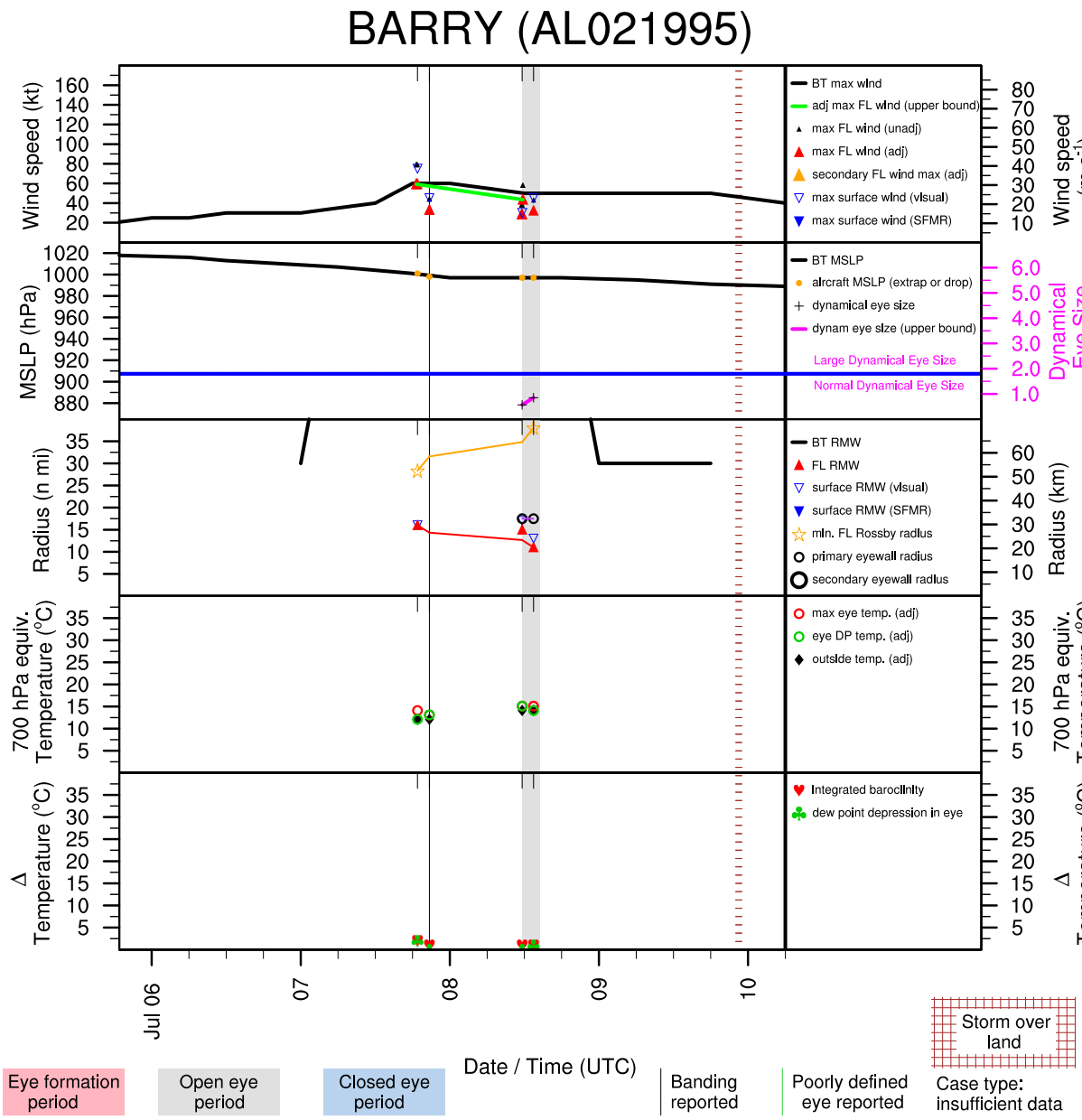

Figure E.37: Structure and intensity parameters for Tropical Storm Barry (1995).

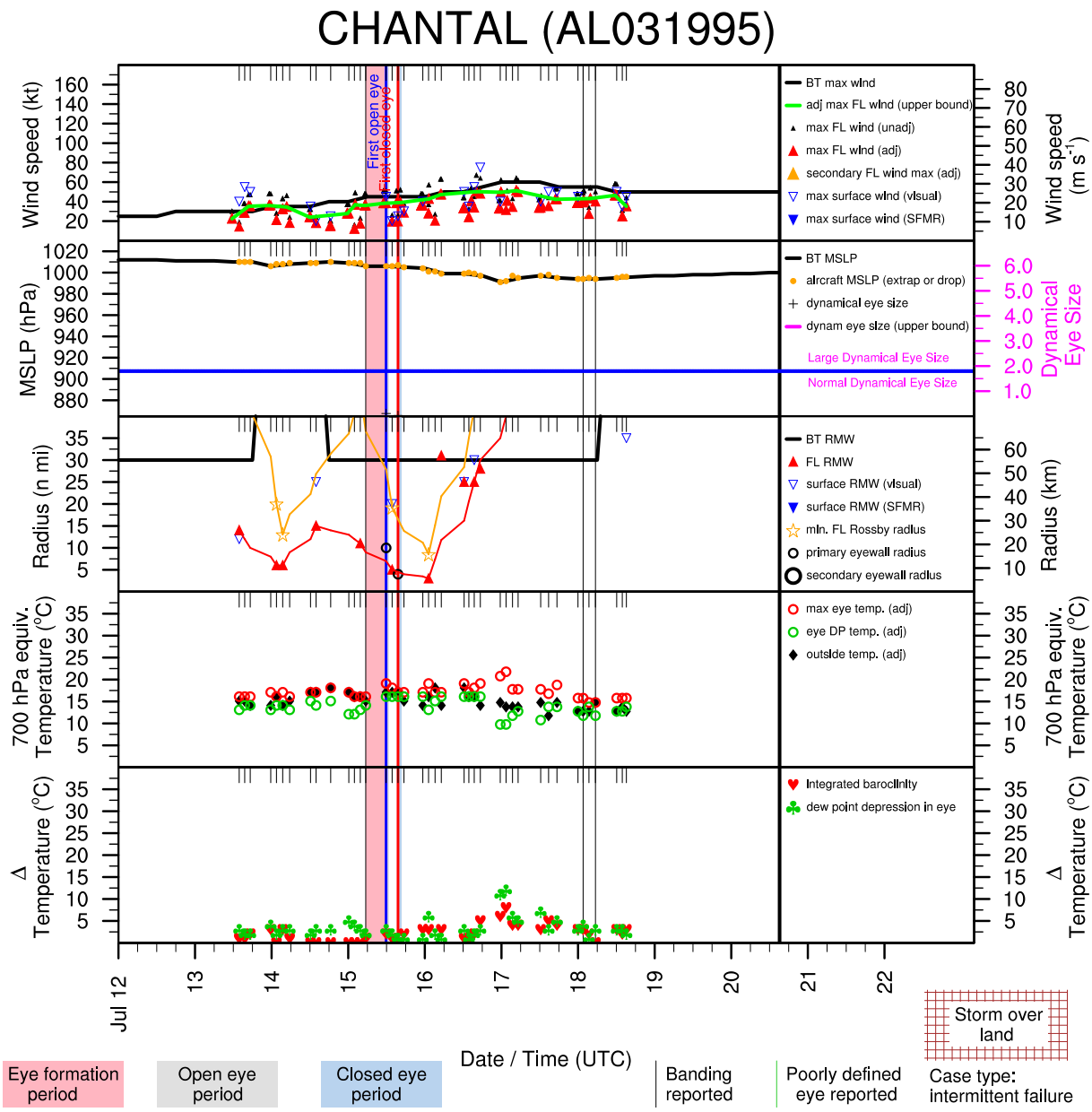

Figure E.38: Structure and intensity parameters for Tropical Storm Chantal (1995).

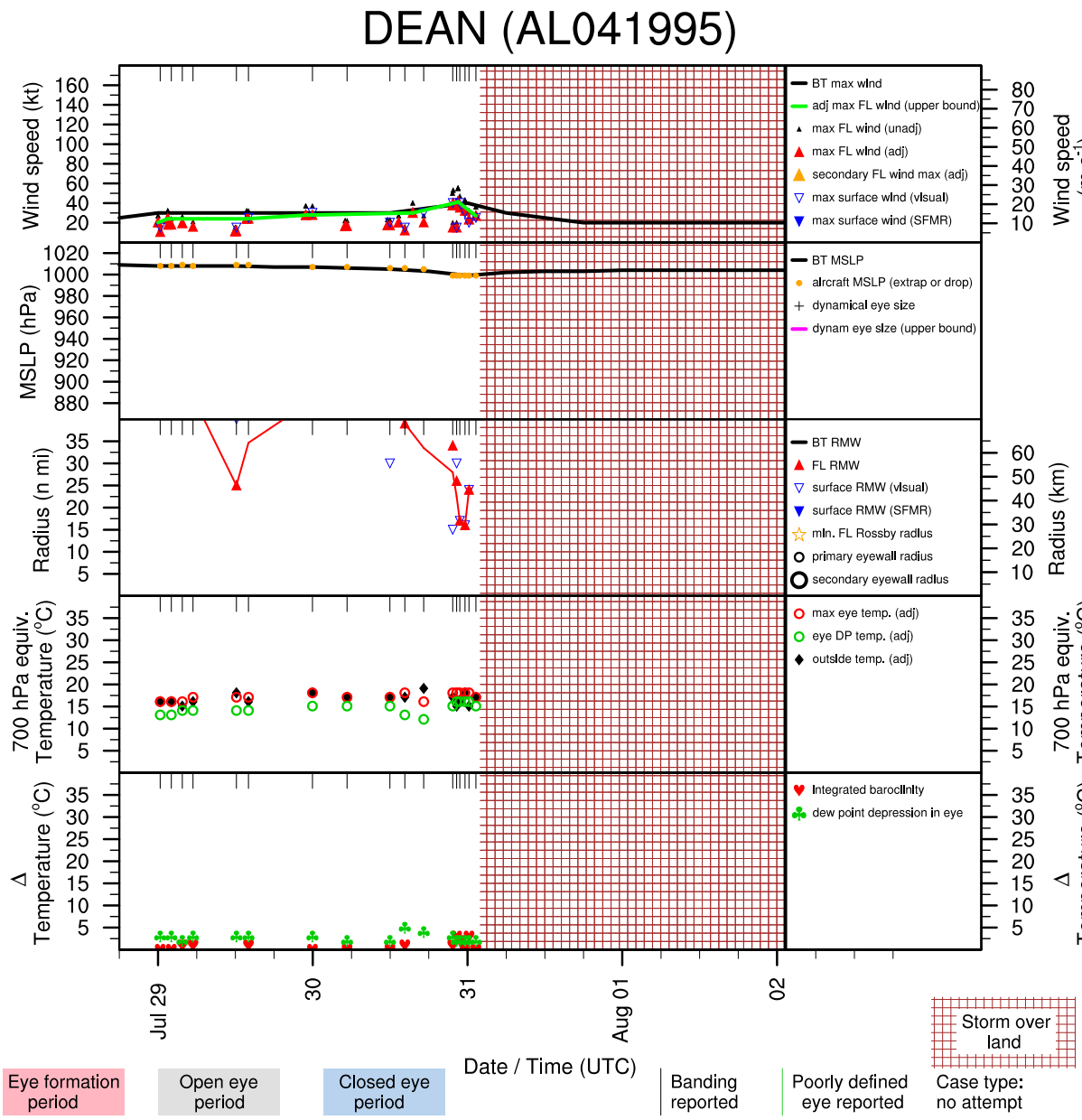

Figure E.39: Structure and intensity parameters for Tropical Storm Dean (1995).

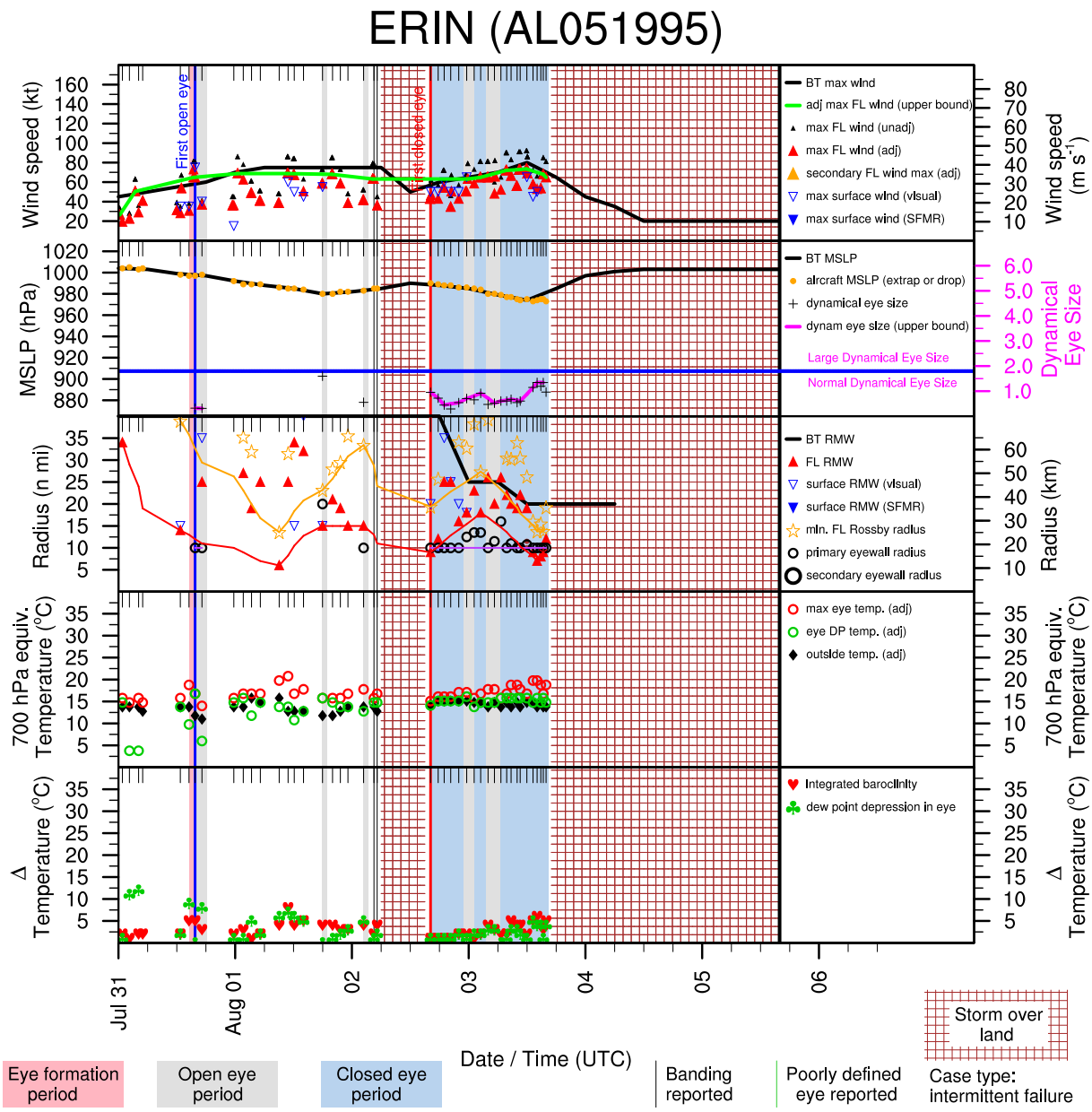

Figure E.40: Structure and intensity parameters for Hurricane Erin (1995).

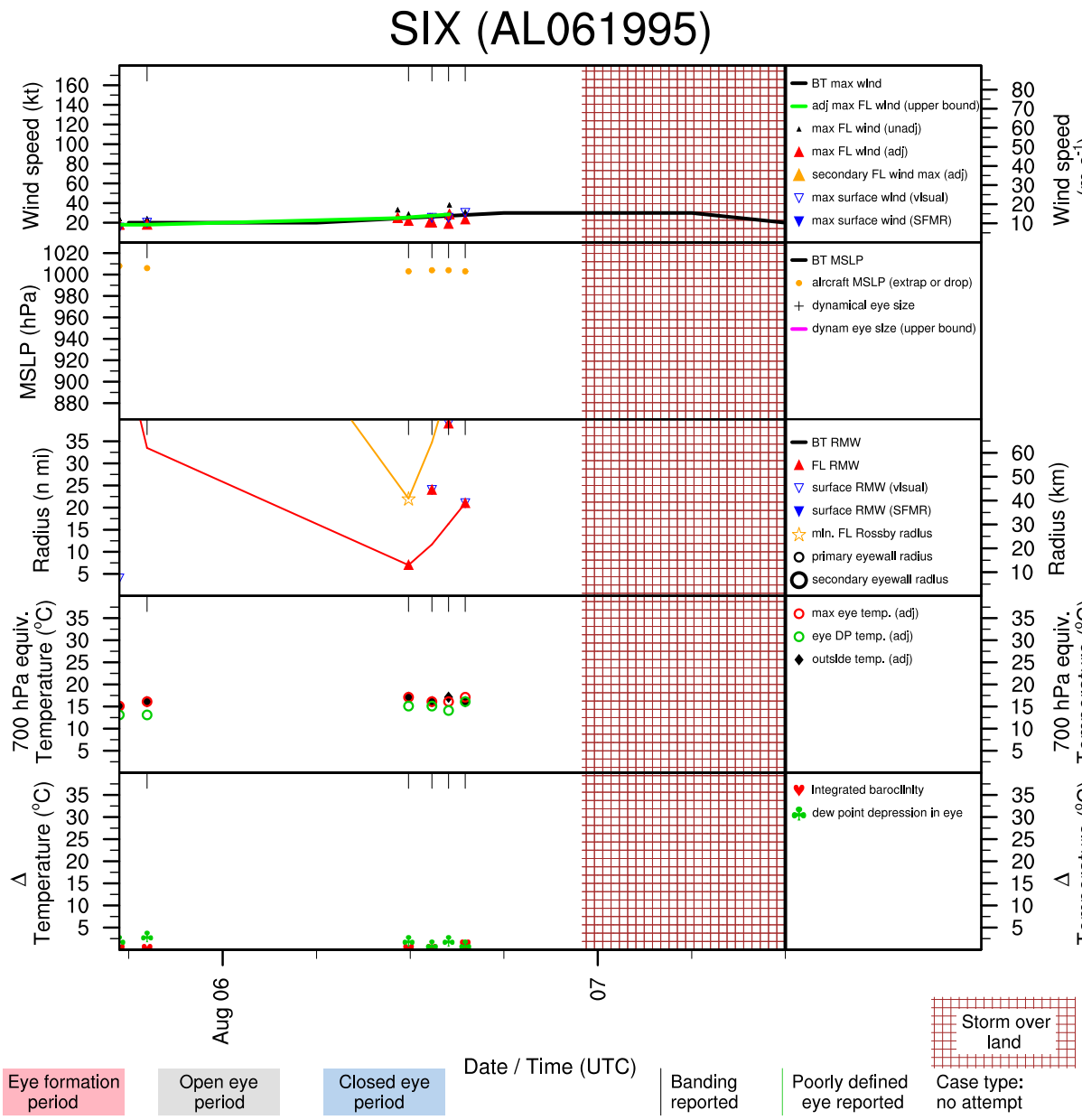

Figure E.41: Structure and intensity parameters for Tropical Depression Six (1995).

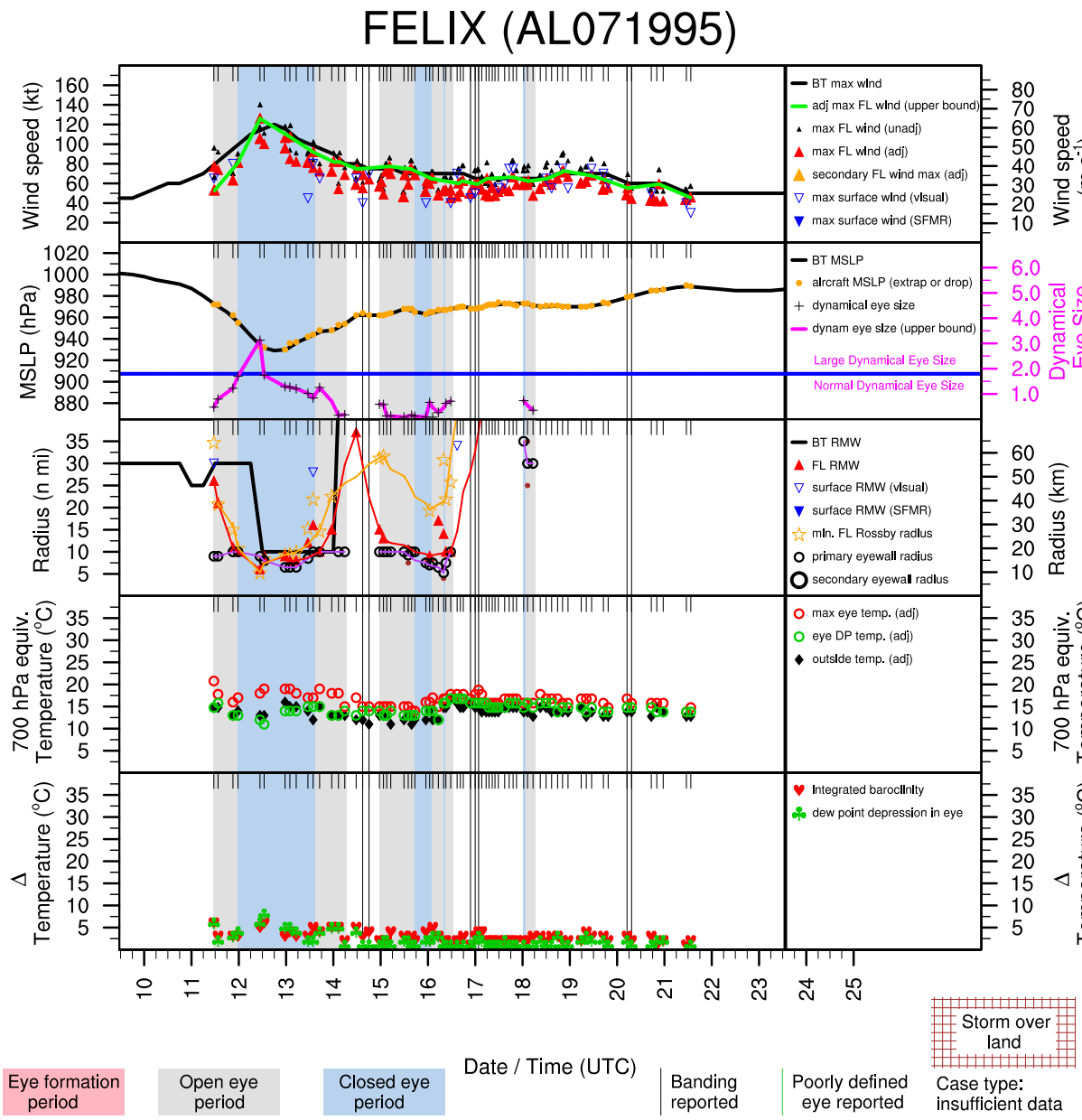

Figure E.42: Structure and intensity parameters for Hurricane Felix (1995).

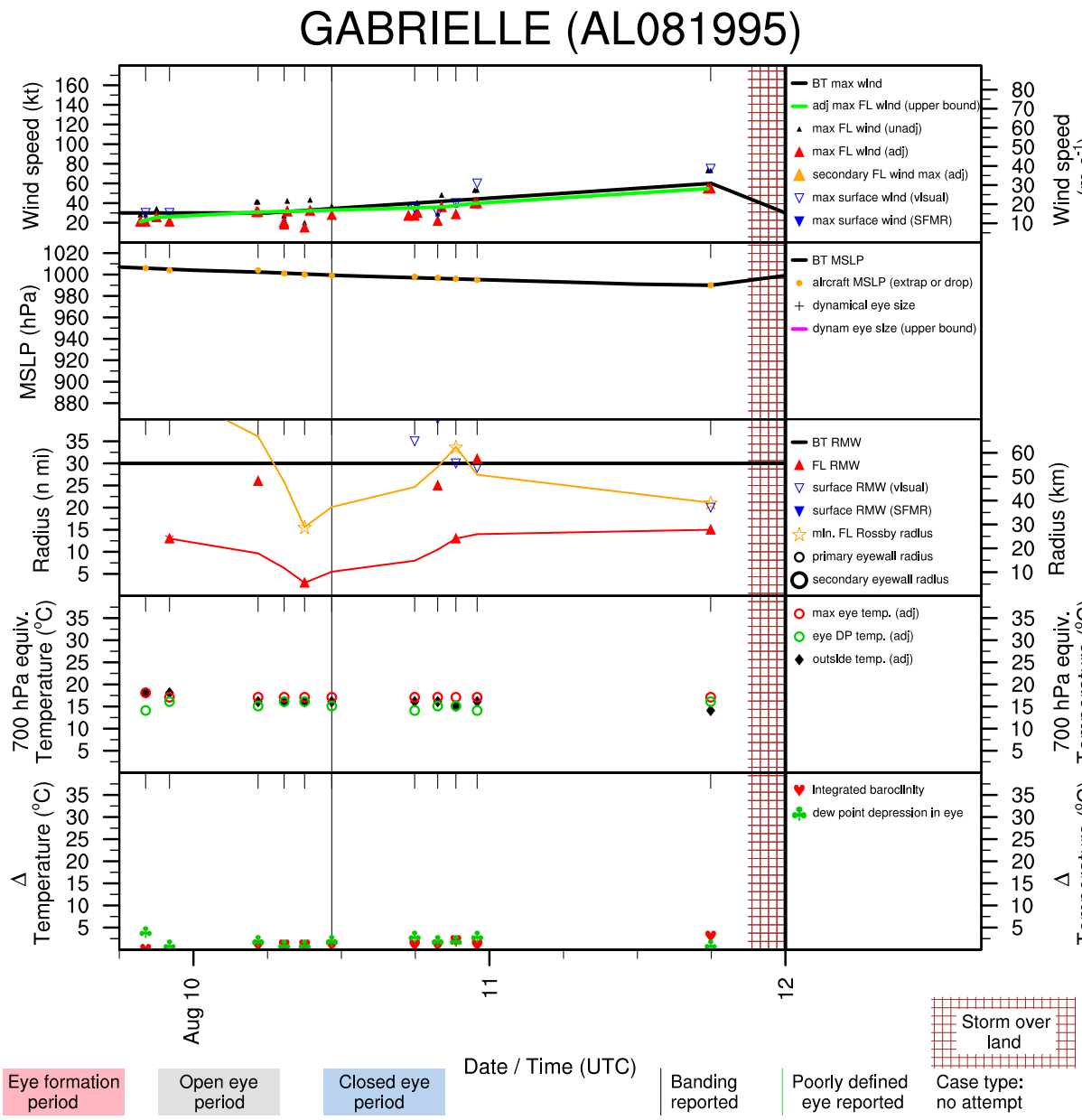

Figure E.43: Structure and intensity parameters for Tropical Storm Gabrielle (1995).

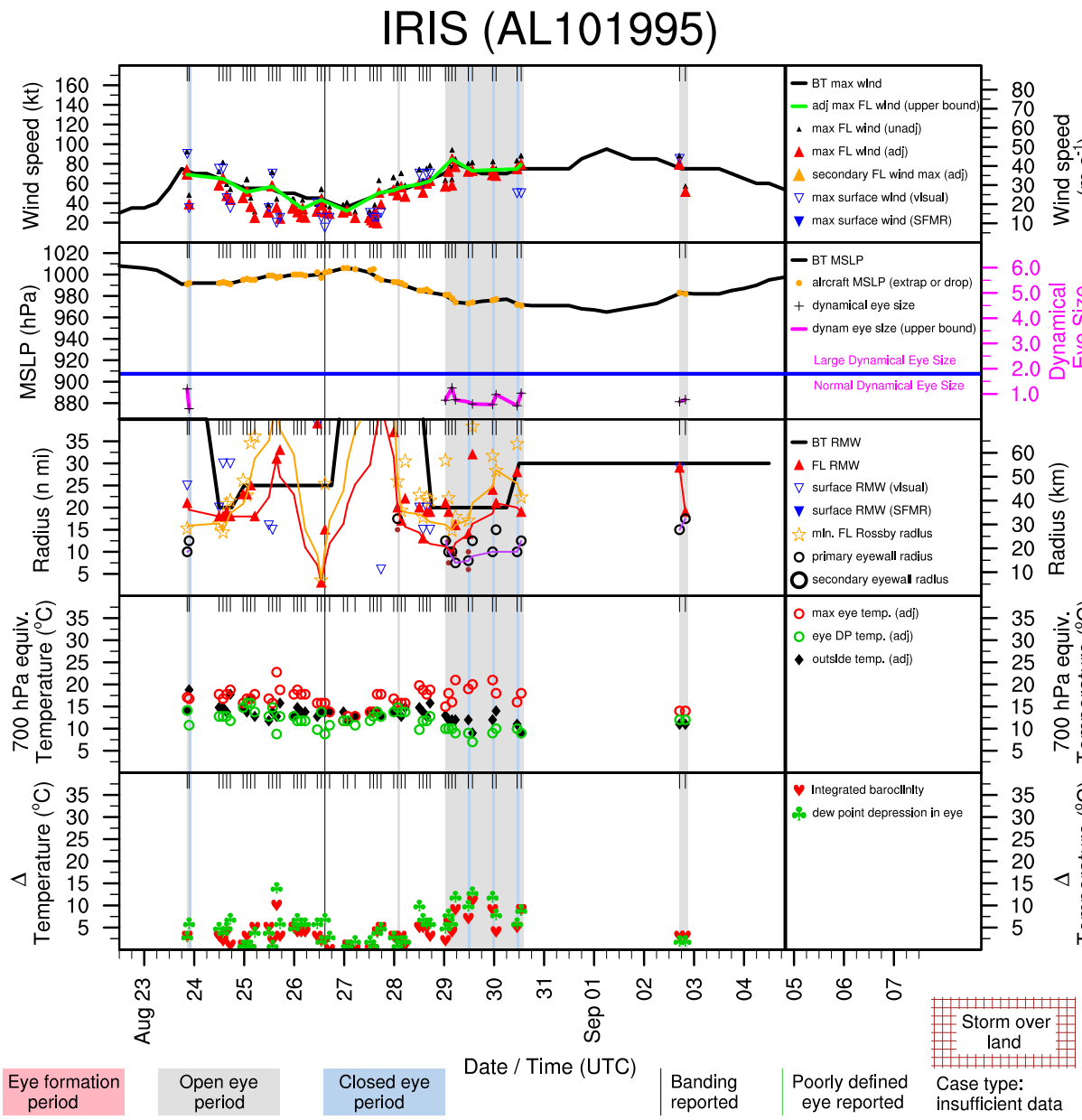

Figure E.44: Structure and intensity parameters for Hurricane Iris (1995).

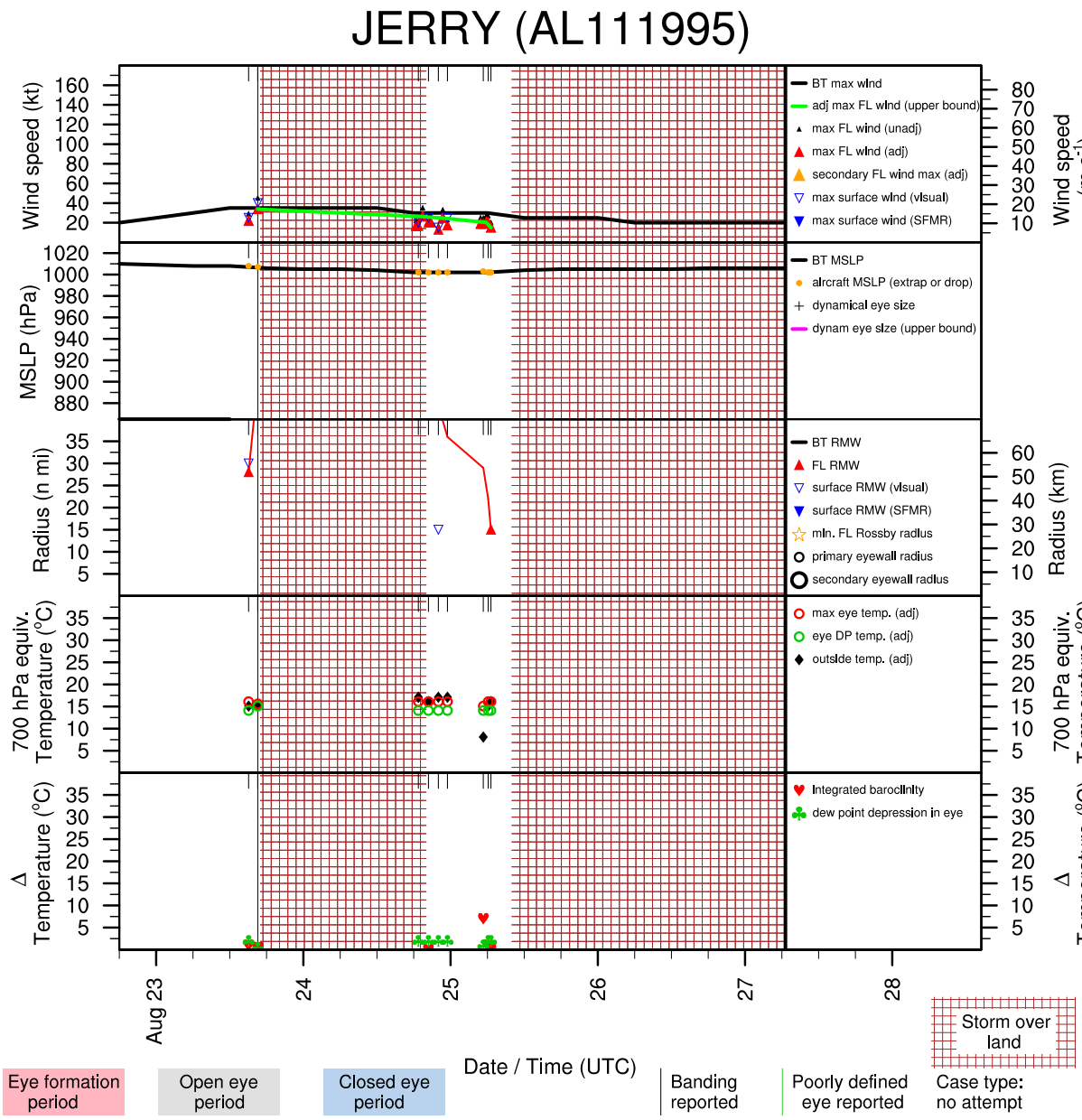

Figure E.45: Structure and intensity parameters for Tropical Storm Jerry (1995).

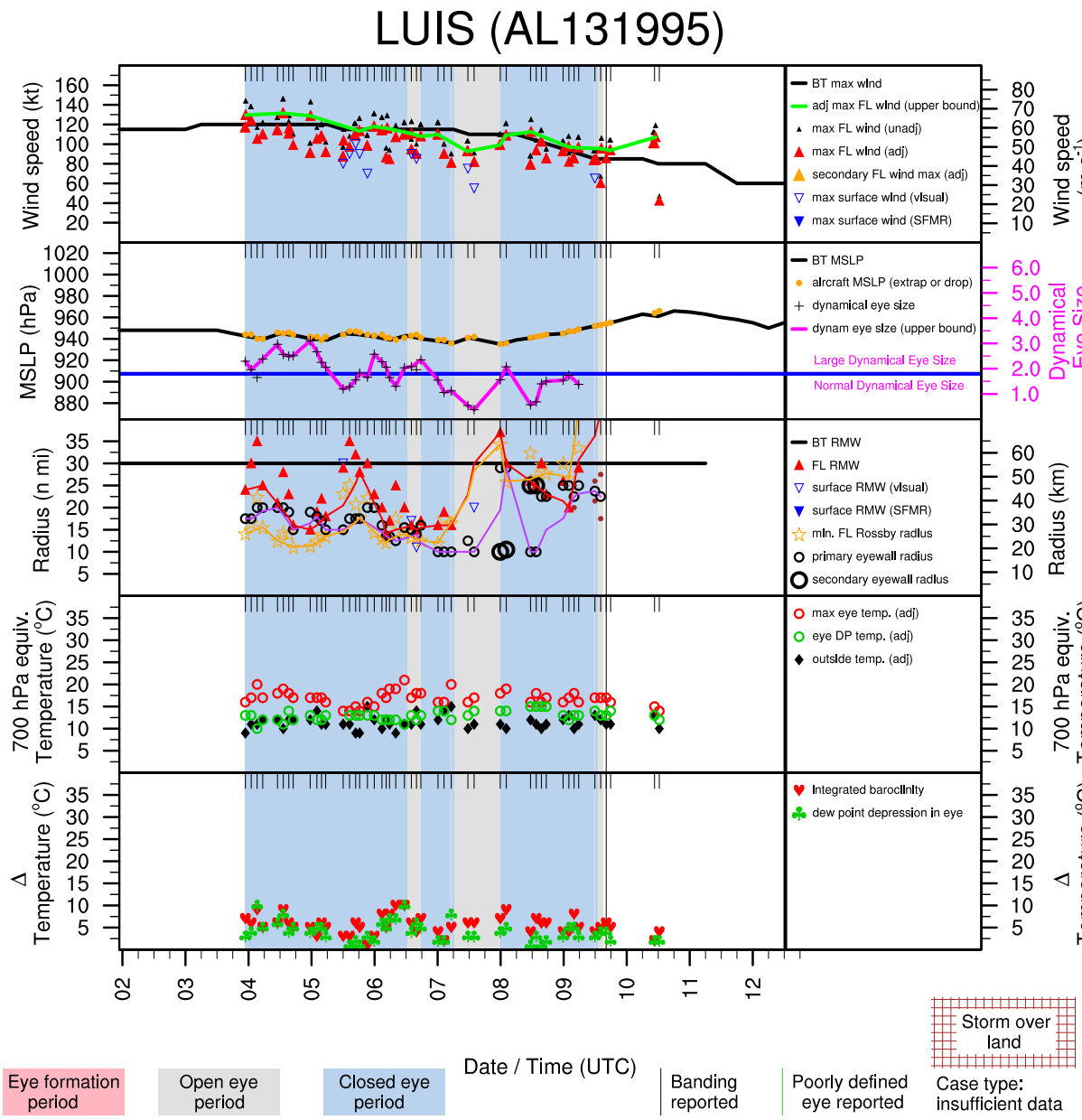

Figure E.46: Structure and intensity parameters for Hurricane Luis (1995).

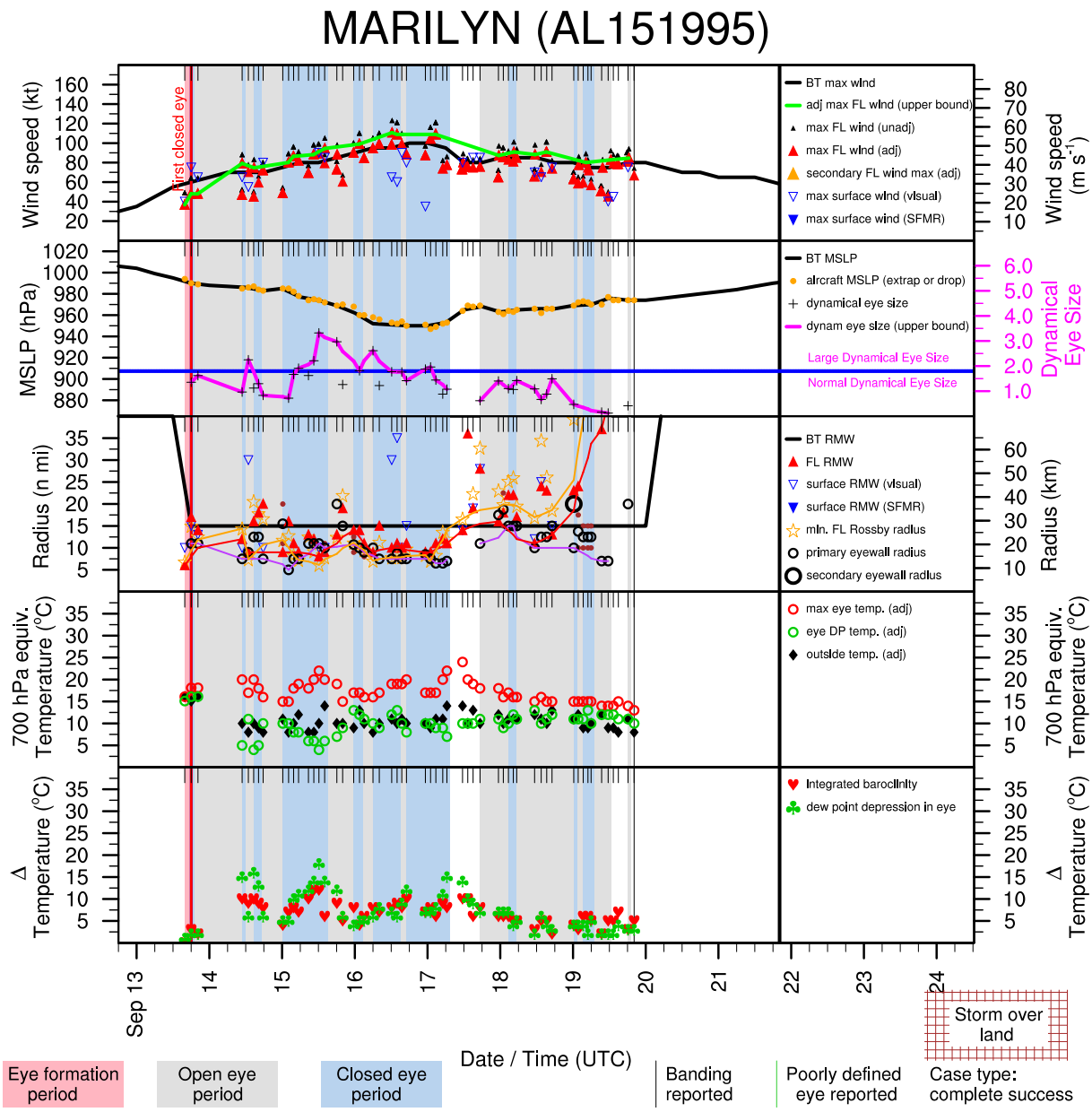

Figure E.47: Structure and intensity parameters for Hurricane Marilyn (1995).

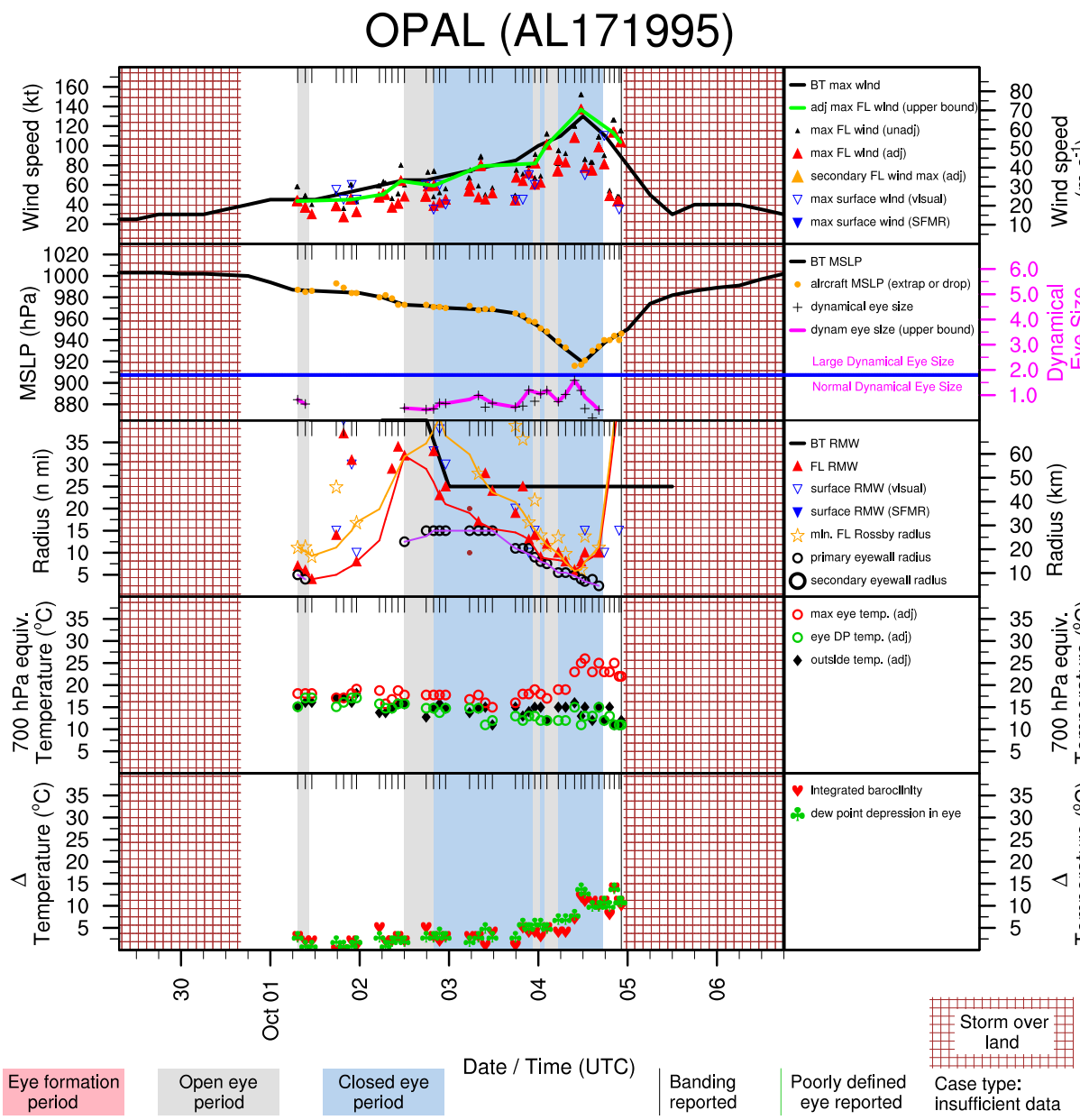

Figure E.48: Structure and intensity parameters for Hurricane Opal (1995).

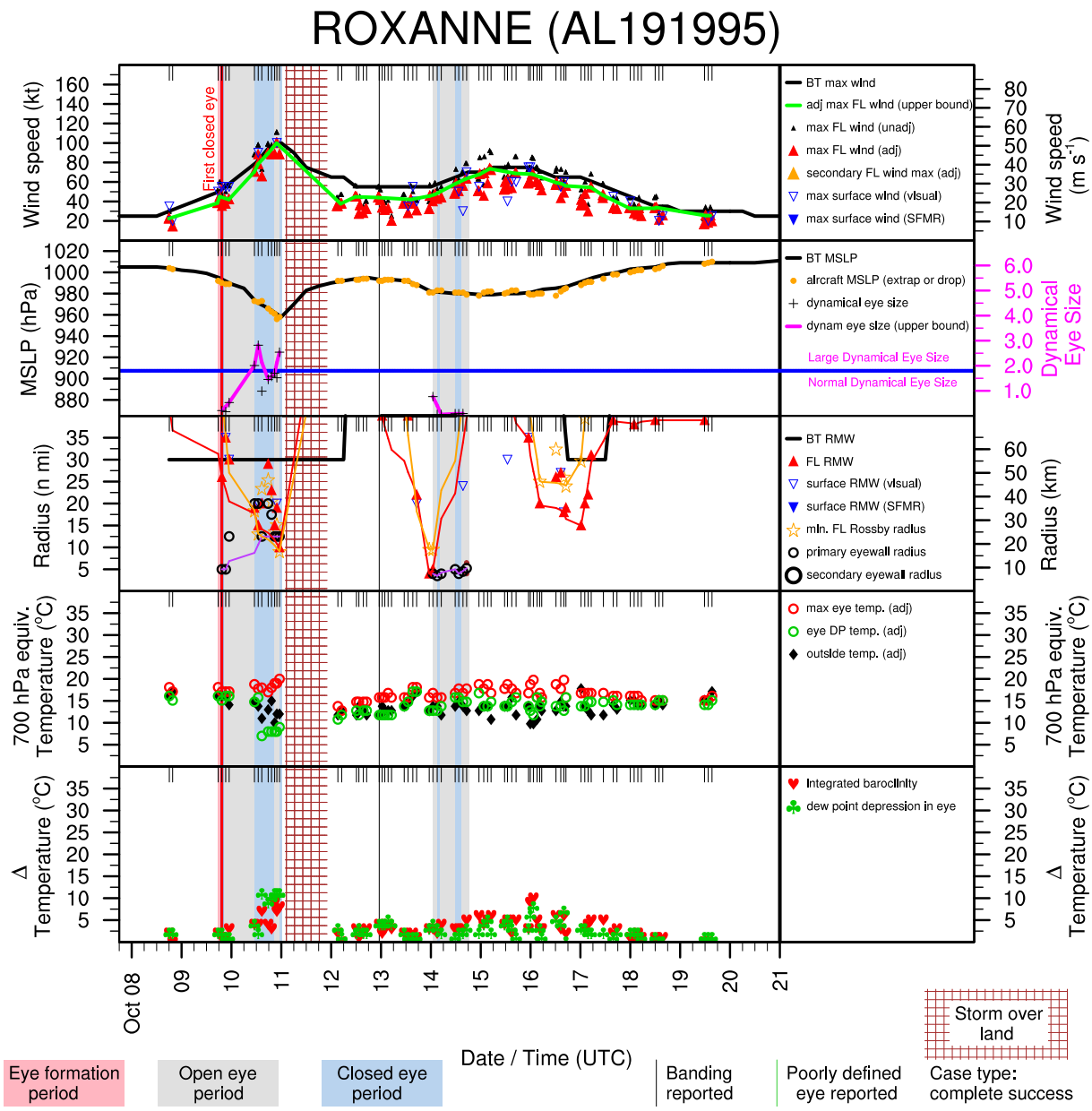

Figure E.49: Structure and intensity parameters for Hurricane Roxanne (1995).

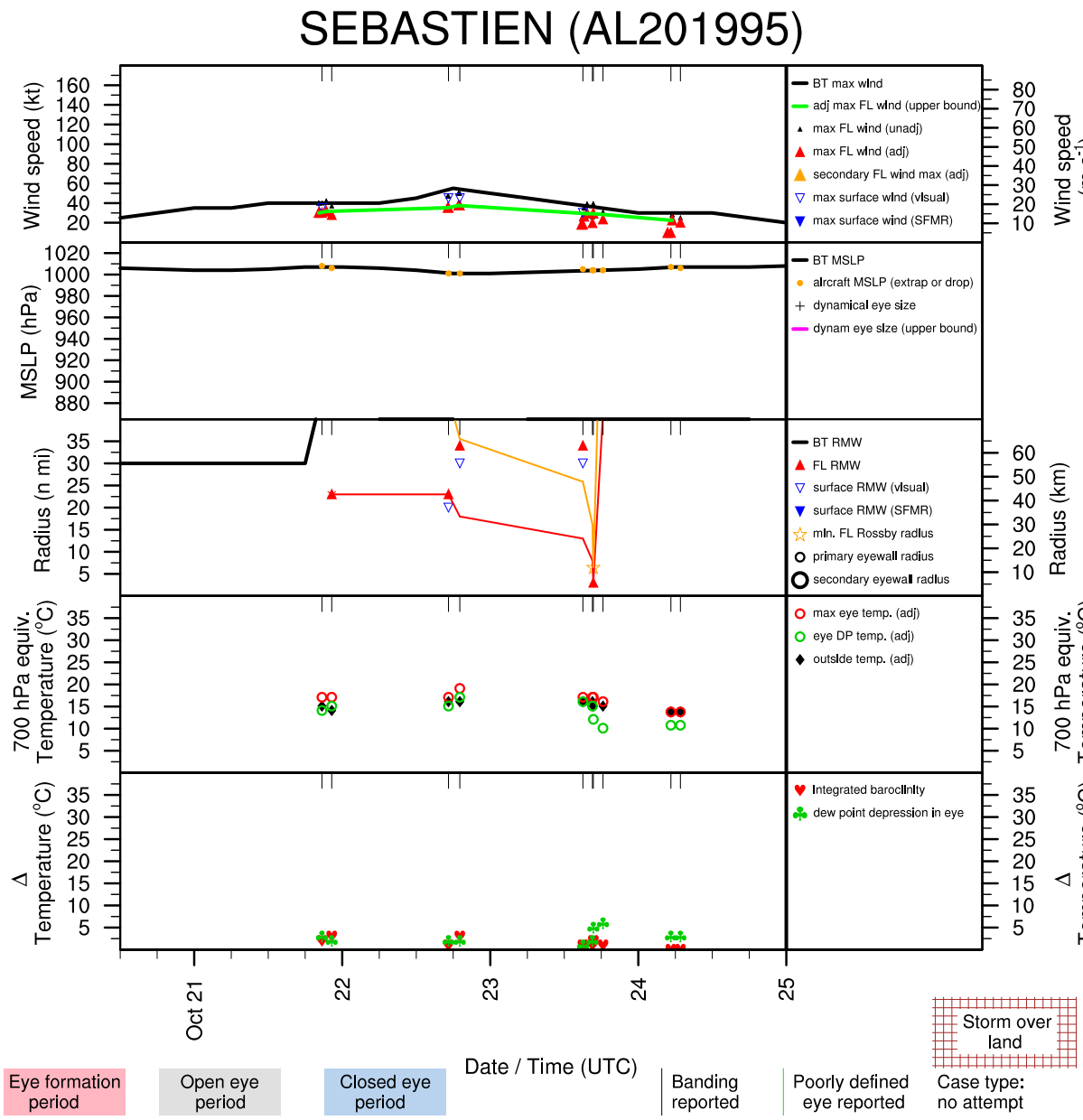

Figure E.50: Structure and intensity parameters for Tropical Storm Sebastien (1995).

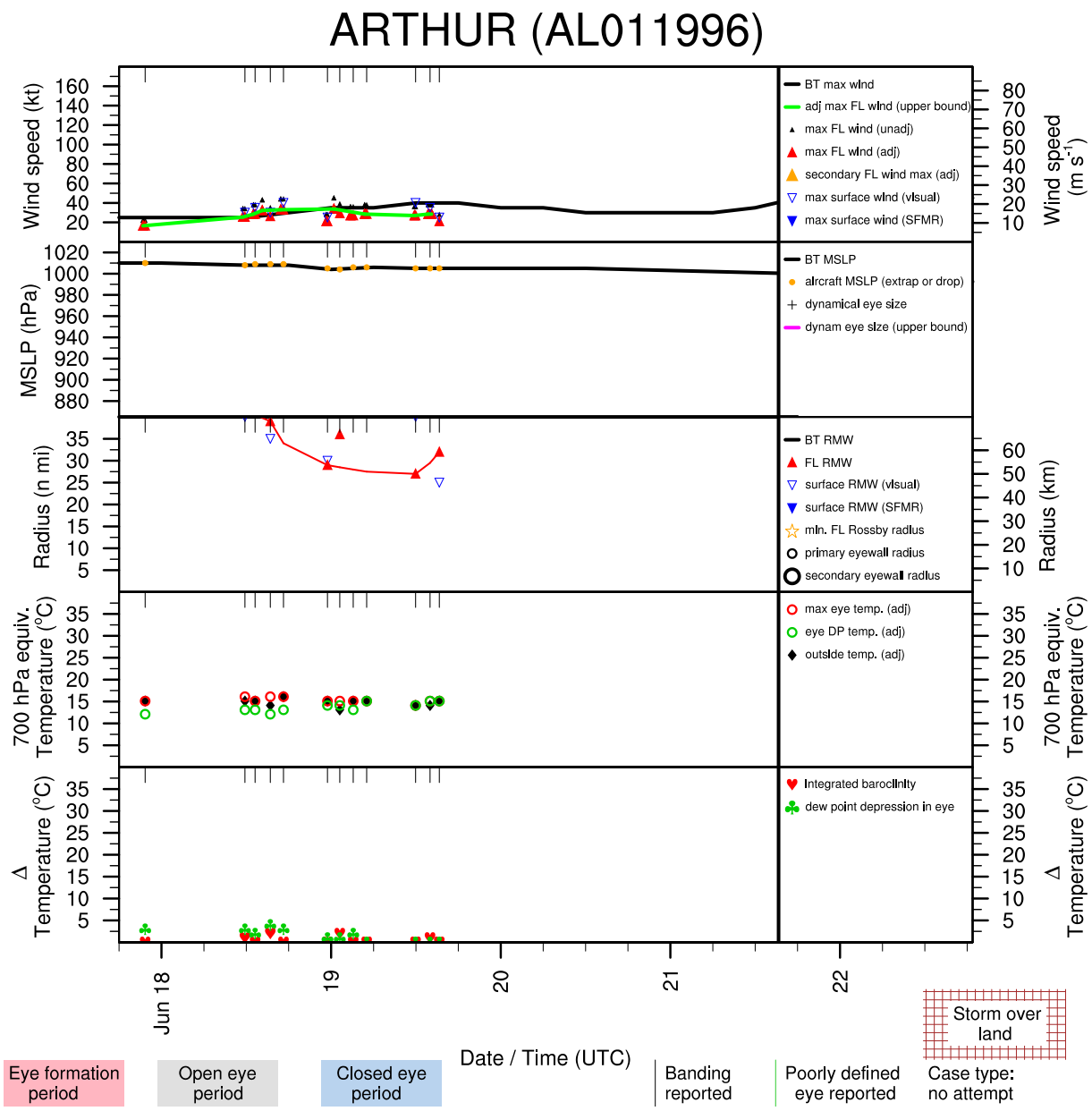

Figure E.51: Structure and intensity parameters for Tropical Storm Arthur (1996).

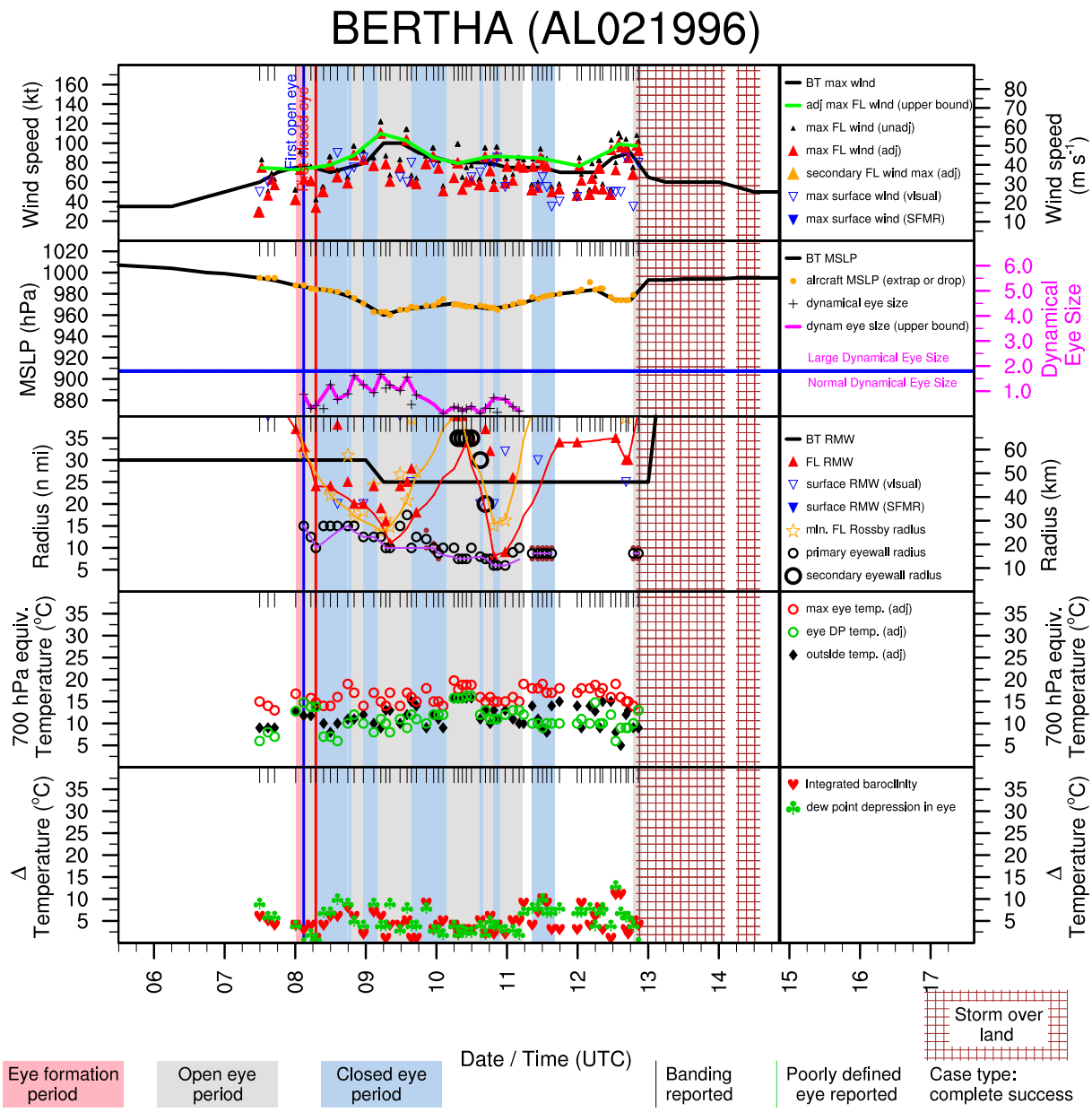

Figure E.52: Structure and intensity parameters for Hurricane Bertha (1996).

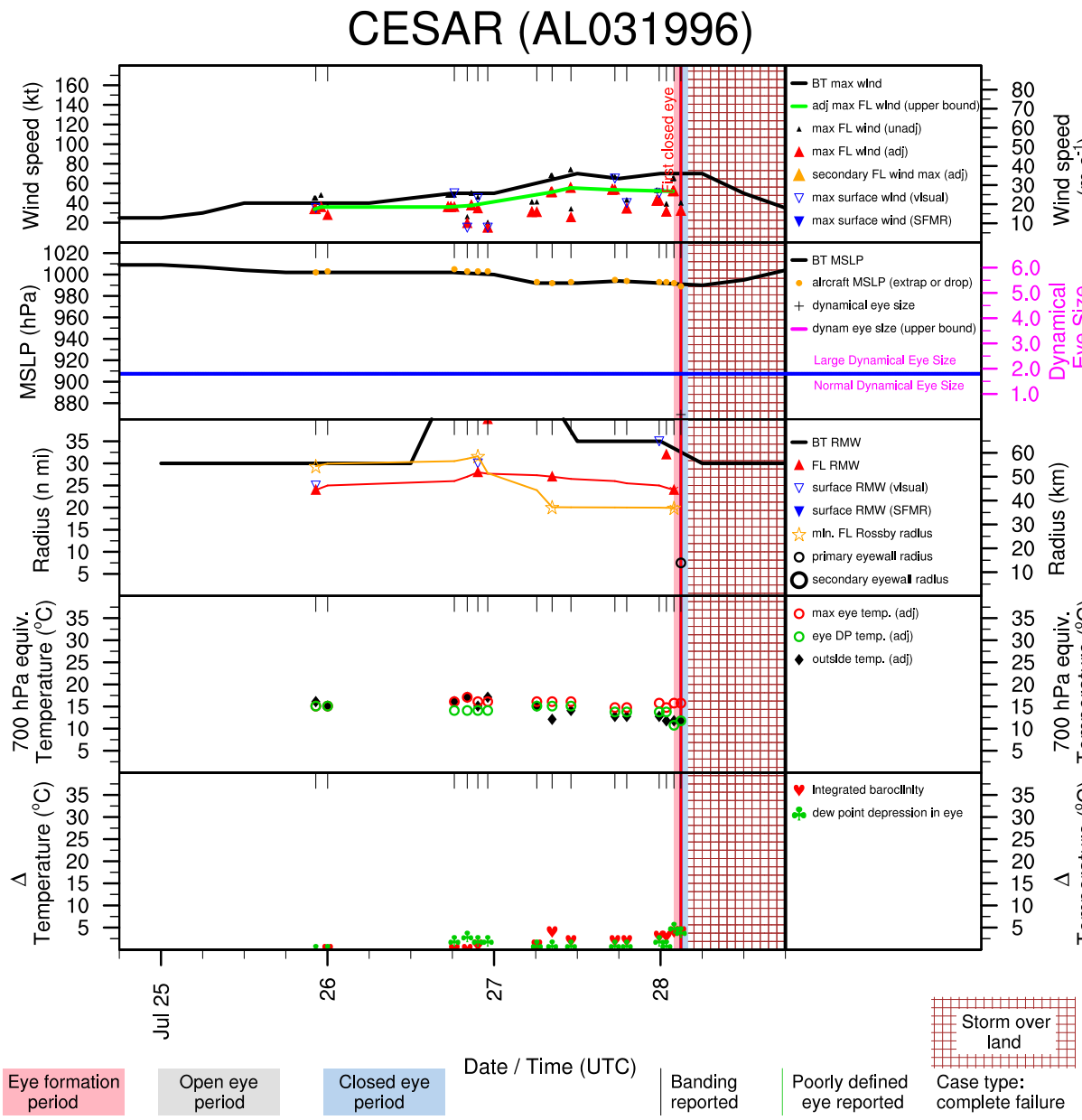

Figure E.53: Structure and intensity parameters for Hurricane Cesar (1996).

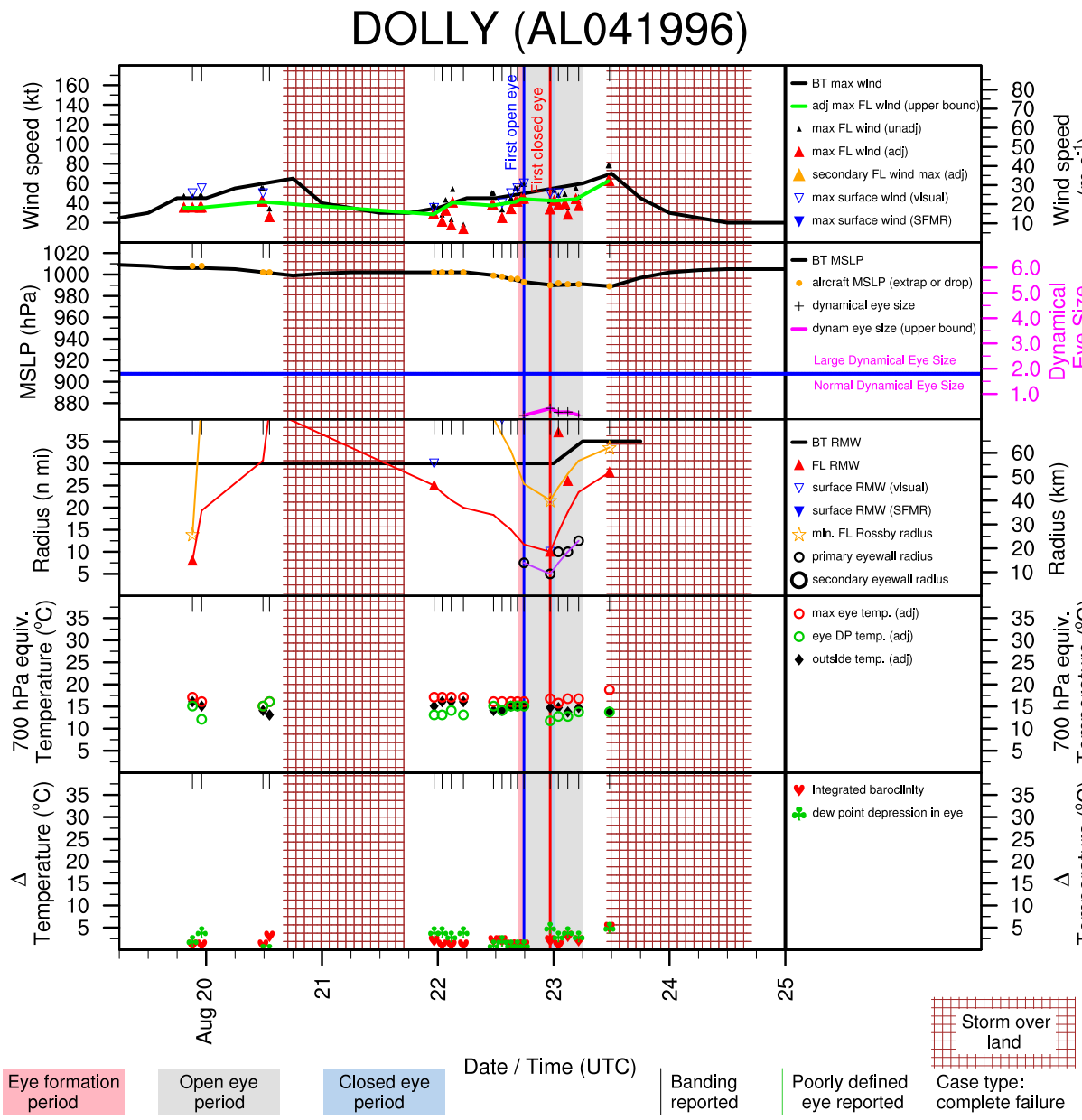

Figure E.54: Structure and intensity parameters for Hurricane Dolly (1996).

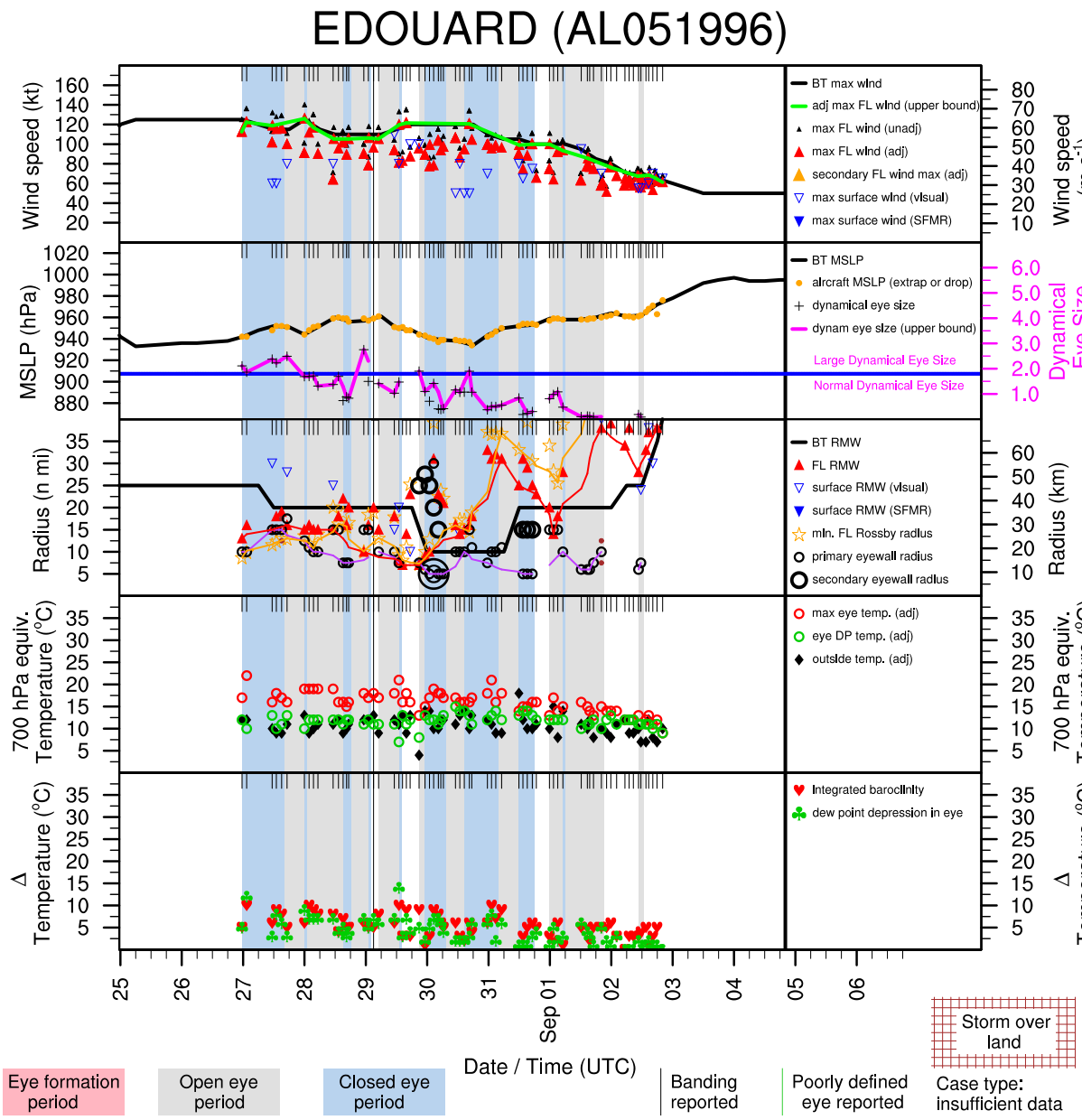

Figure E.55: Structure and intensity parameters for Hurricane Edouard (1996).

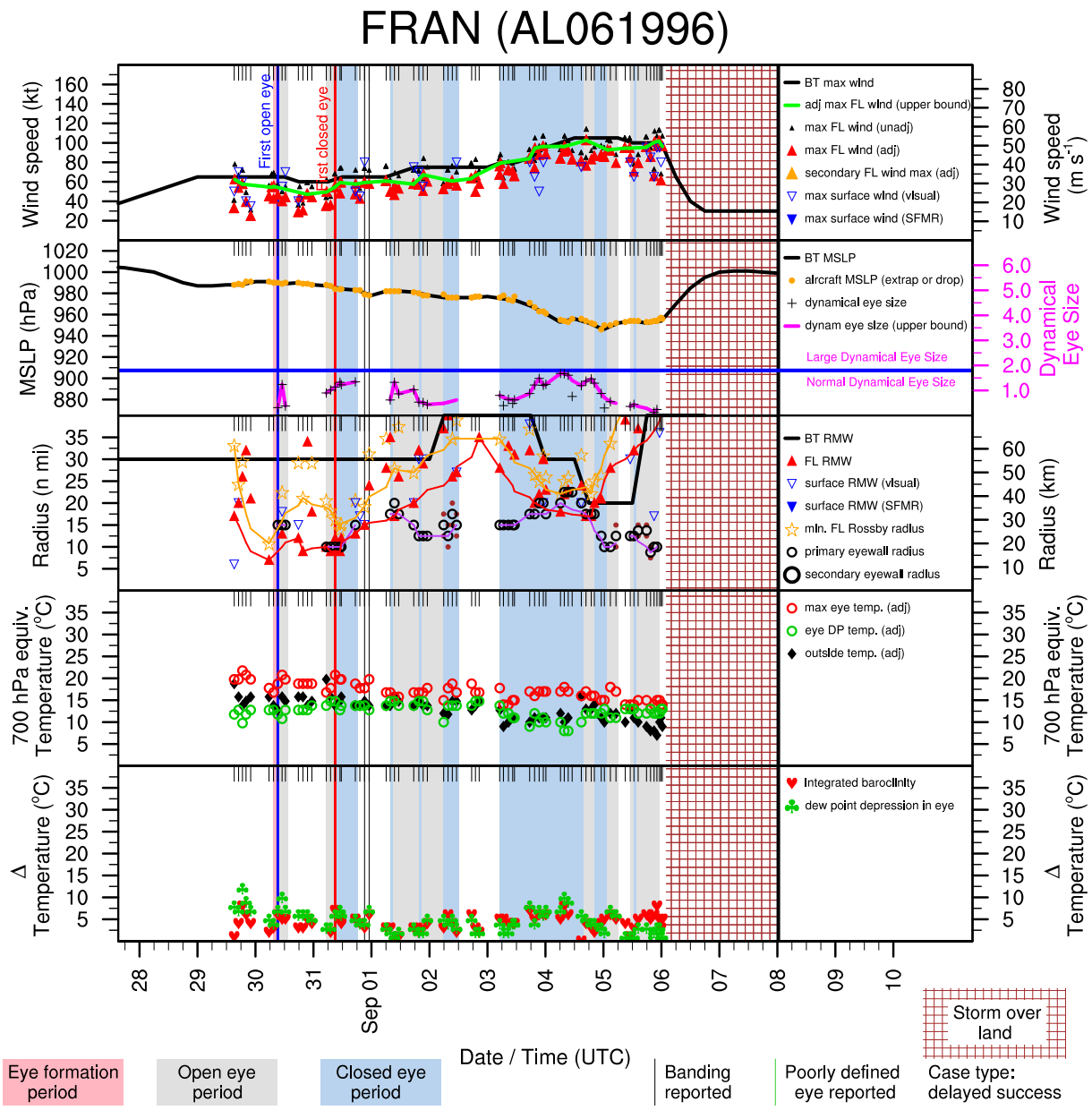

Figure E.56: Structure and intensity parameters for Hurricane Fran (1996).

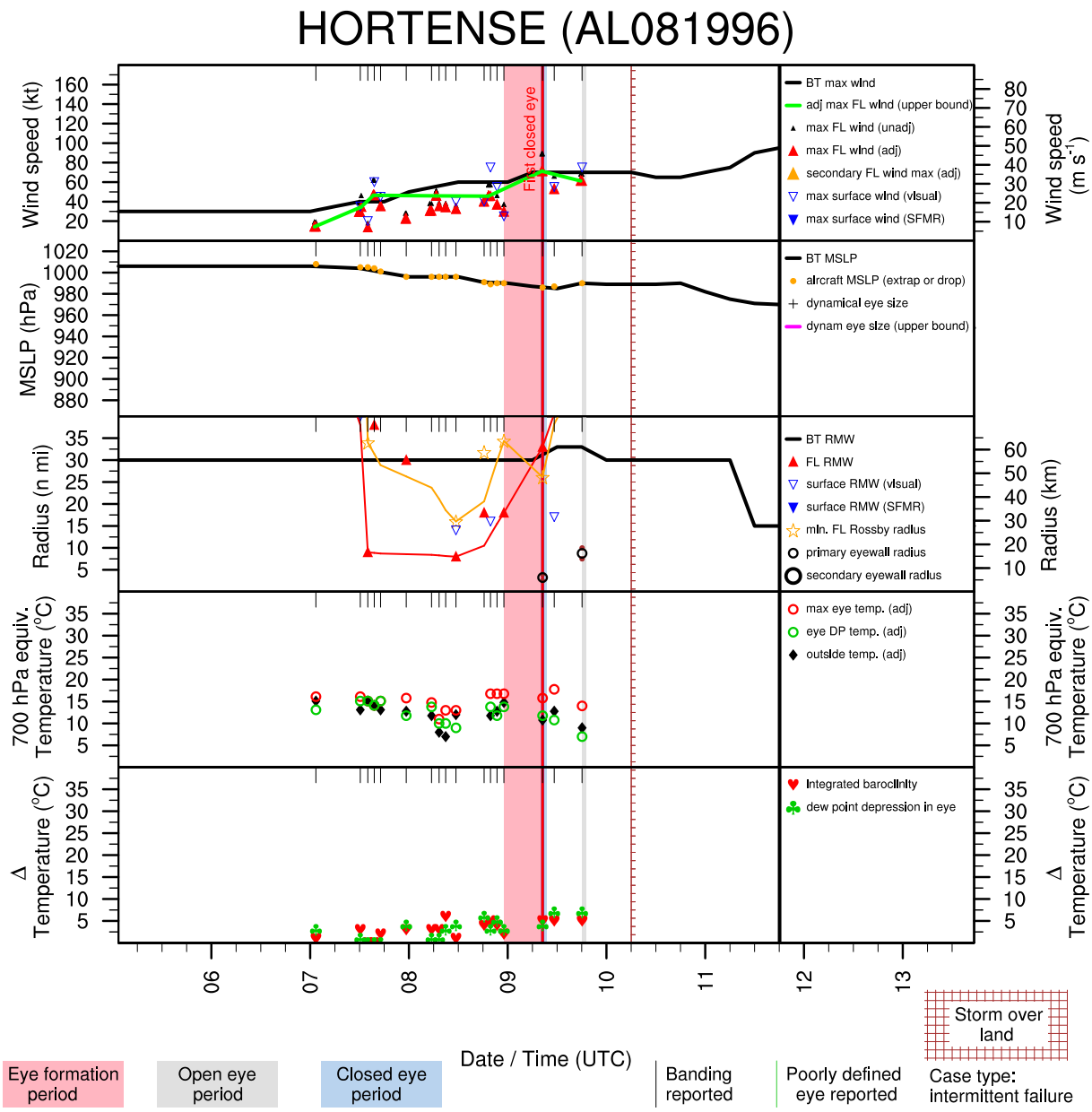

Figure E.57: Structure and intensity parameters for Hurricane Hortense (1996).

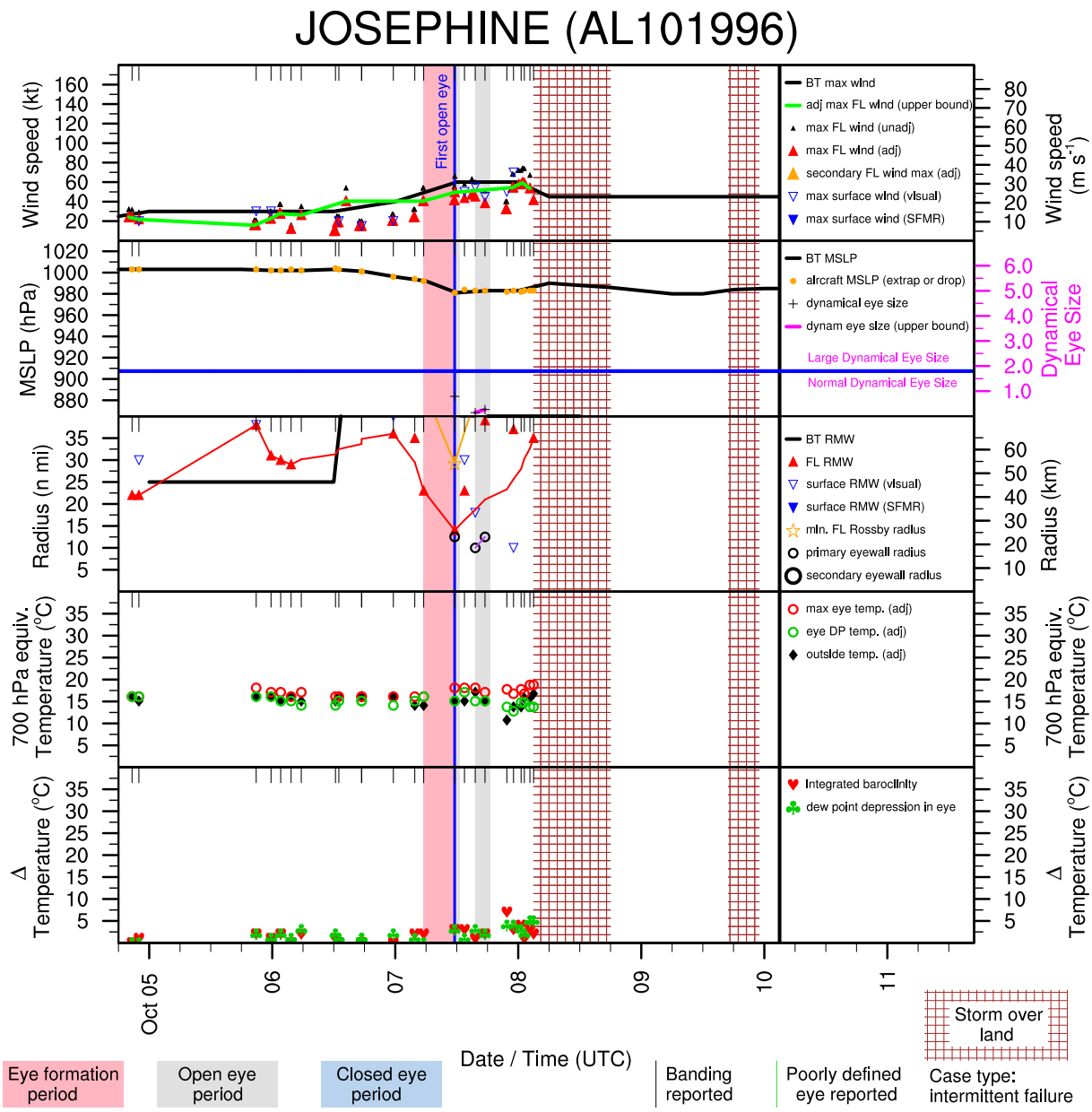

Figure E.58: Structure and intensity parameters for Tropical Storm Josephine (1996).

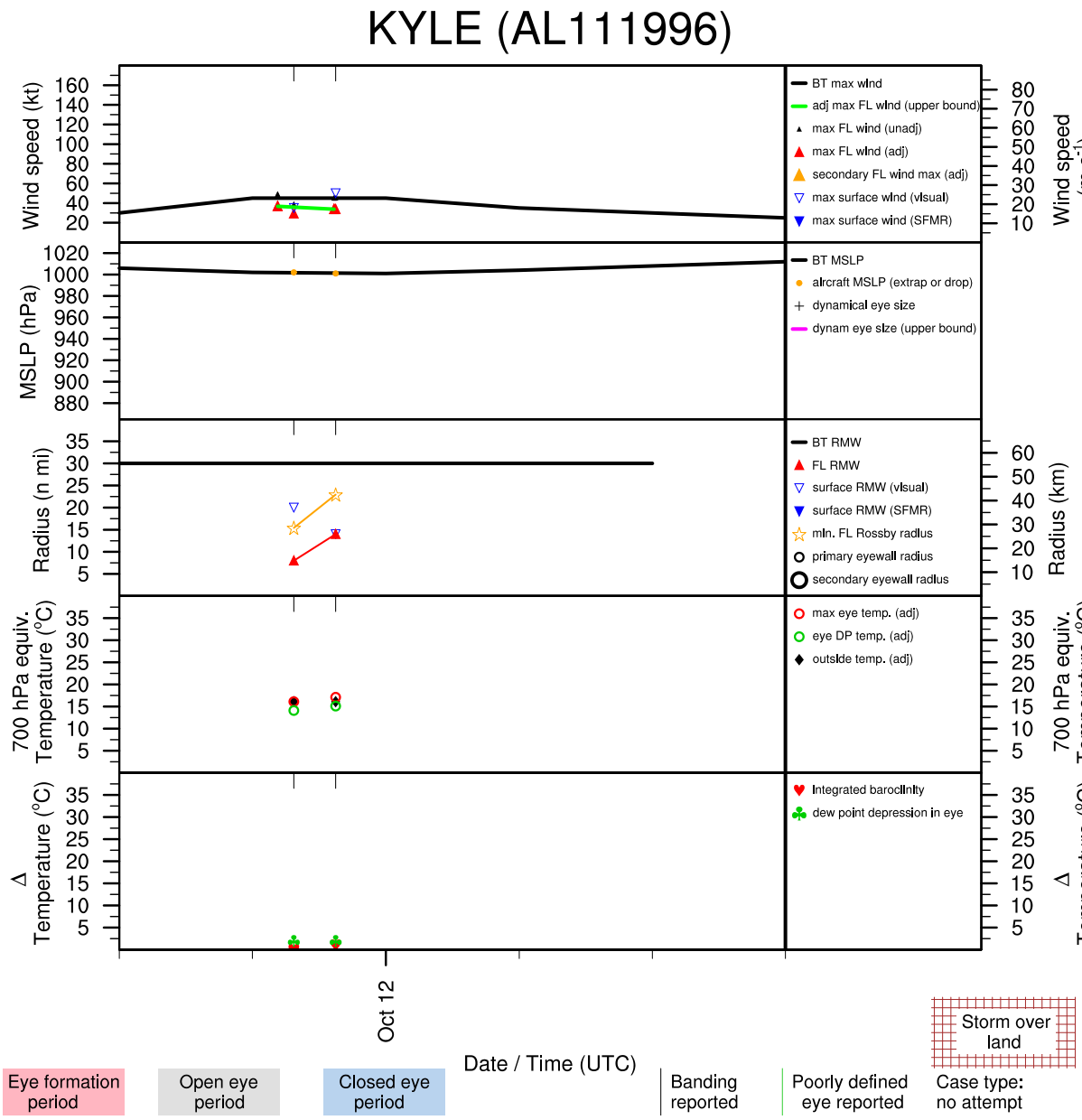

Figure E.59: Structure and intensity parameters for Tropical Storm Kyle (1996).

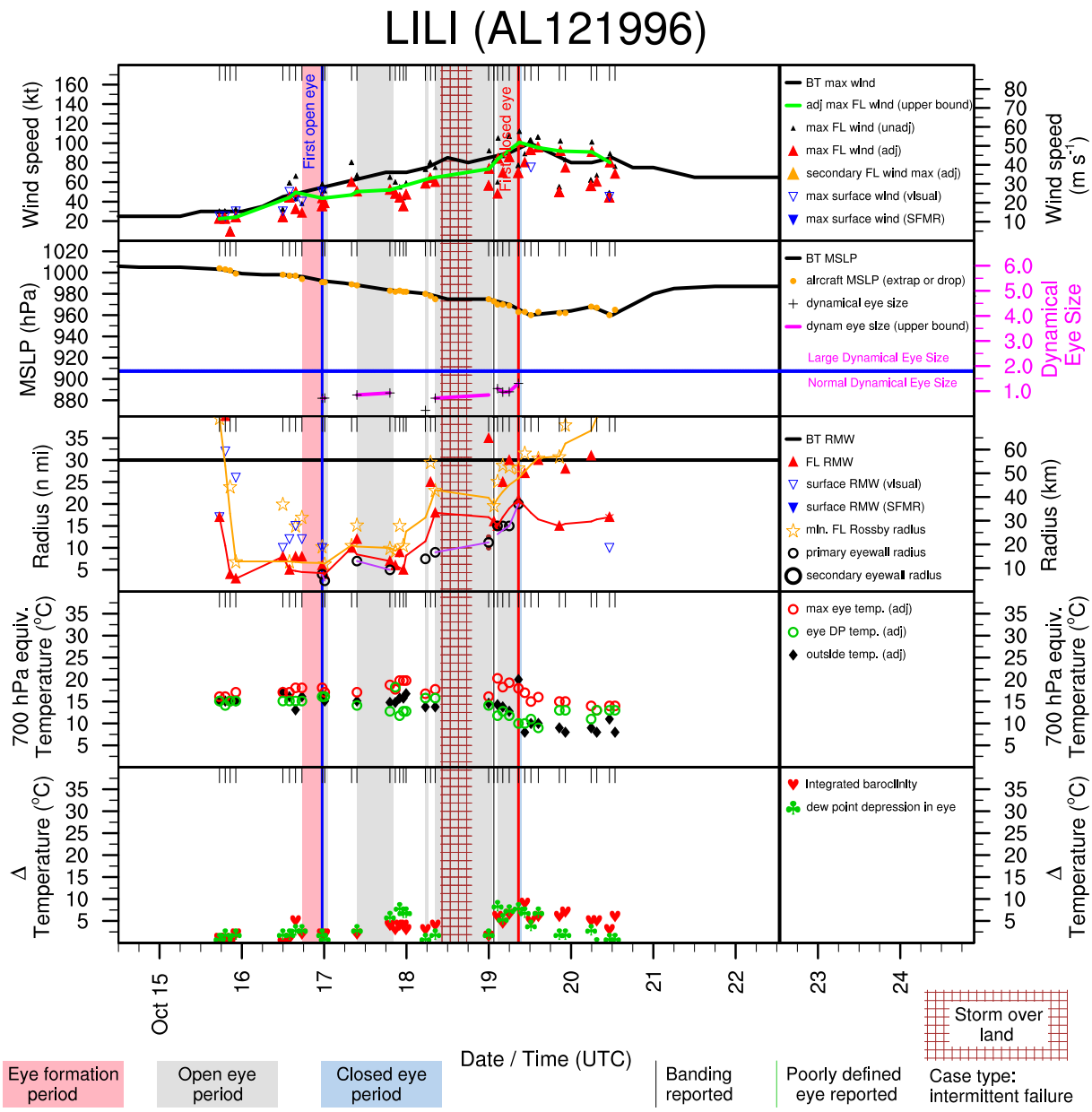

Figure E.60: Structure and intensity parameters for Hurricane Lili (1996).

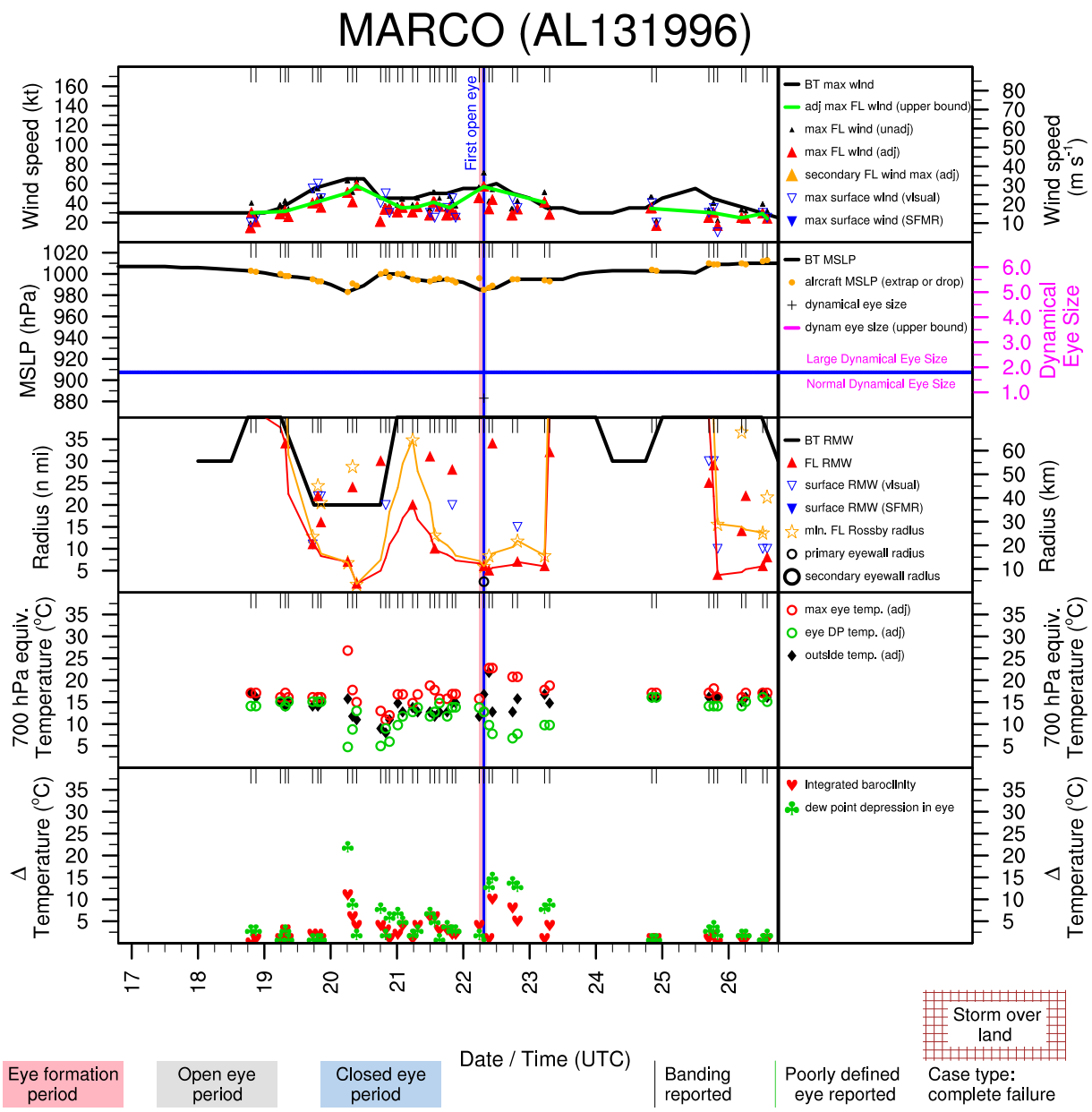

Figure E.61: Structure and intensity parameters for Hurricane Marco (1996).

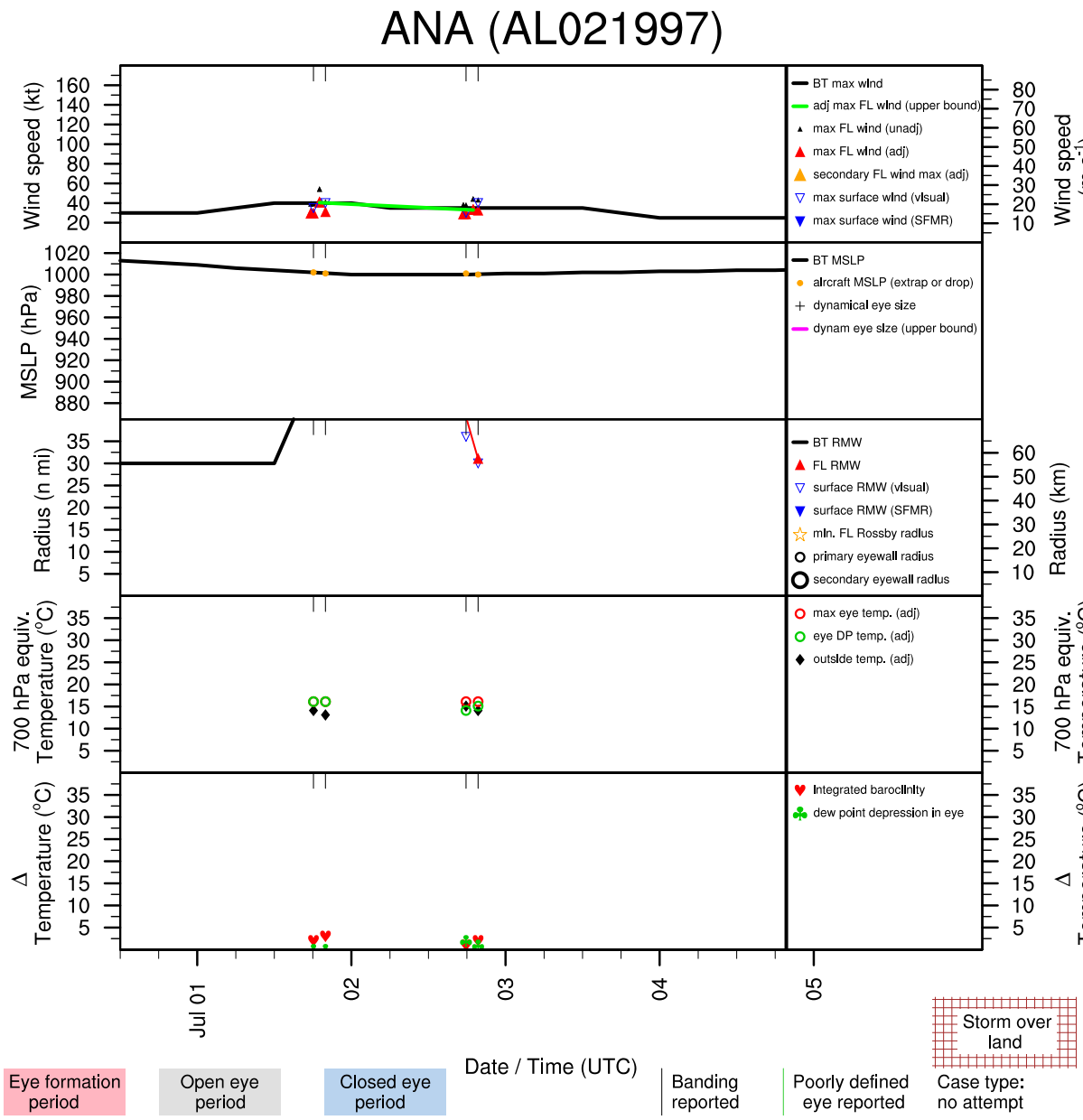

Figure E.62: Structure and intensity parameters for Tropical Storm Ana (1997).

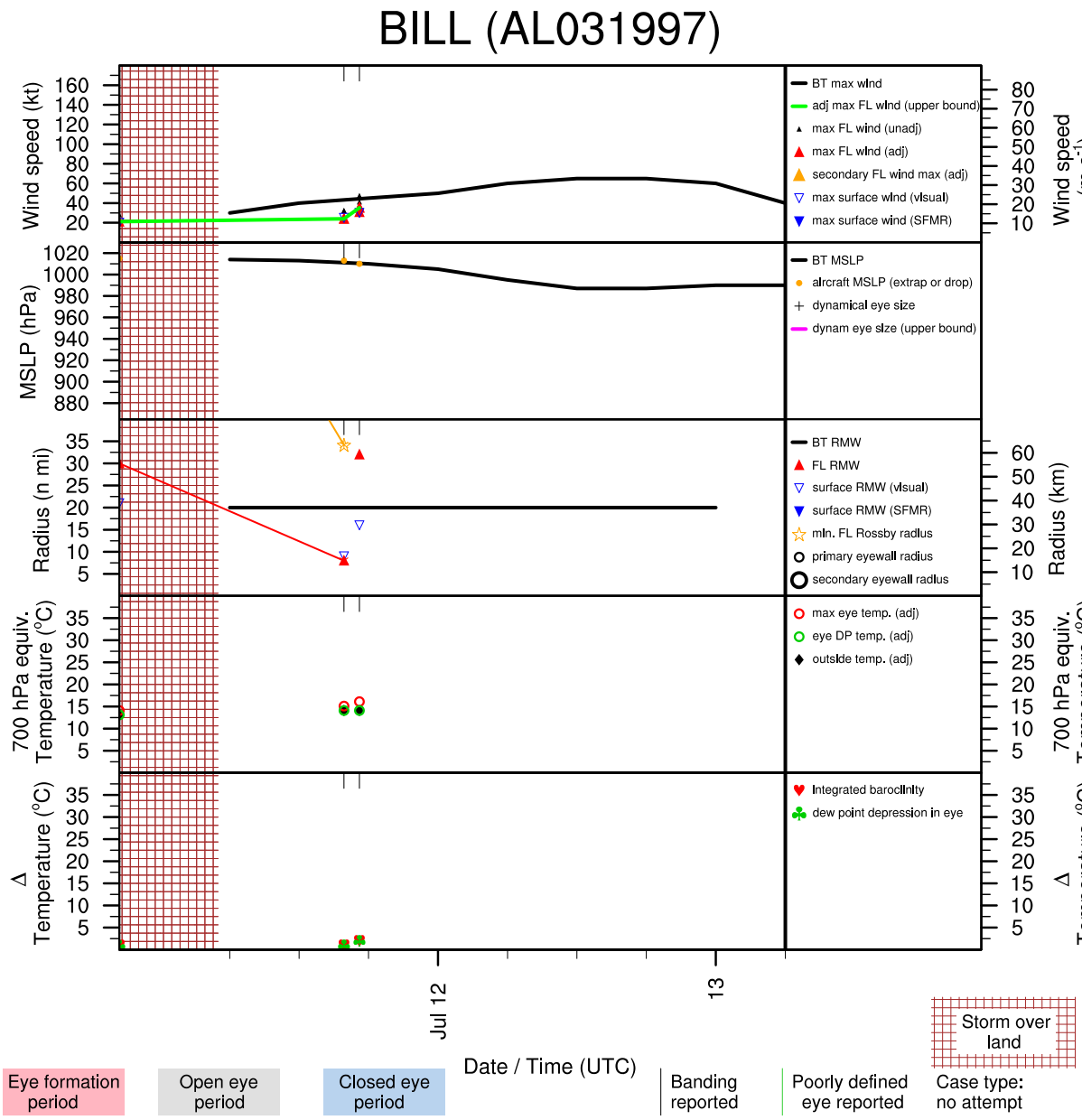

Figure E.63: Structure and intensity parameters for Hurricane Bill (1997).

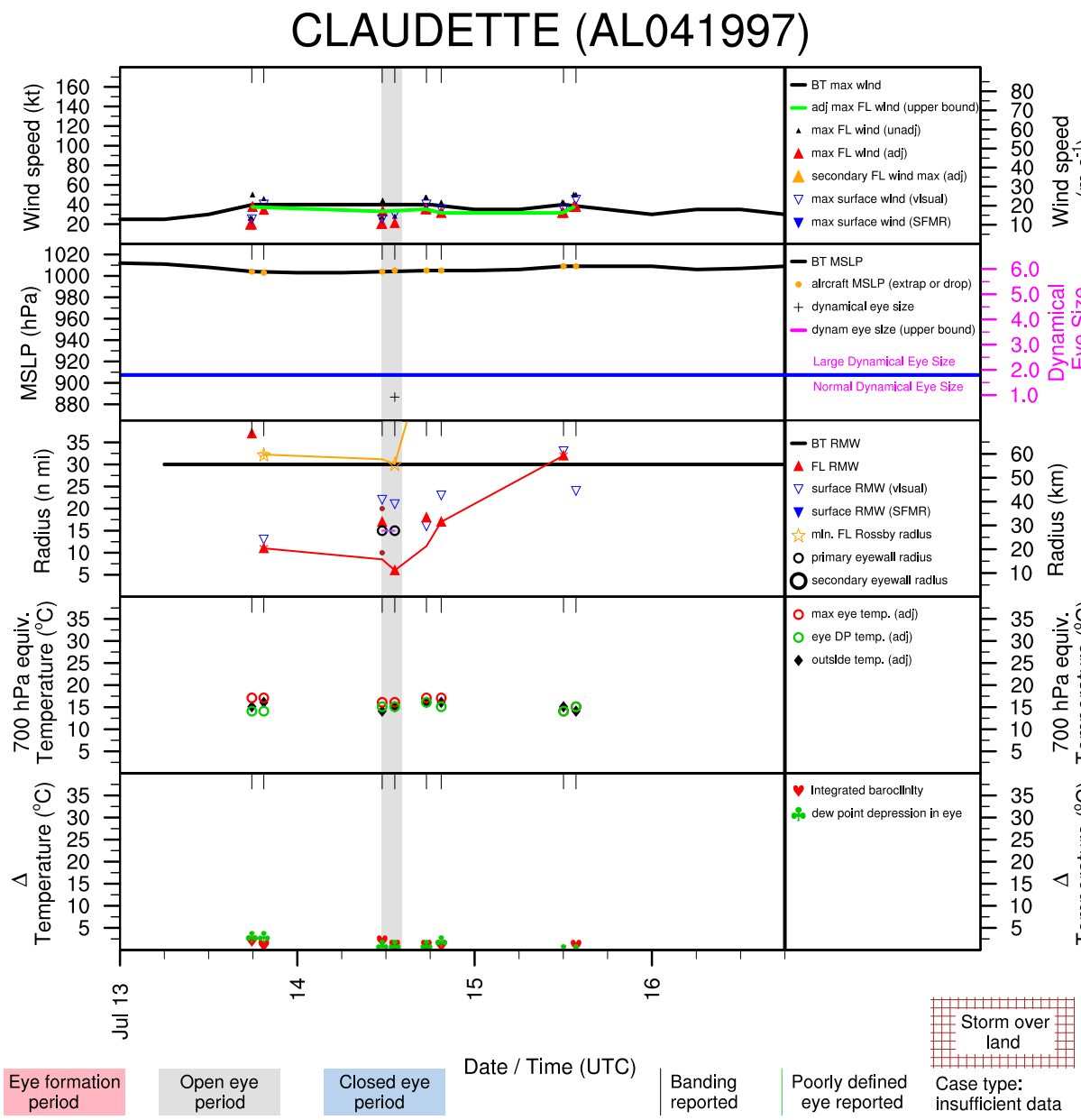

Figure E.64: Structure and intensity parameters for Tropical Storm Claudette (1997).

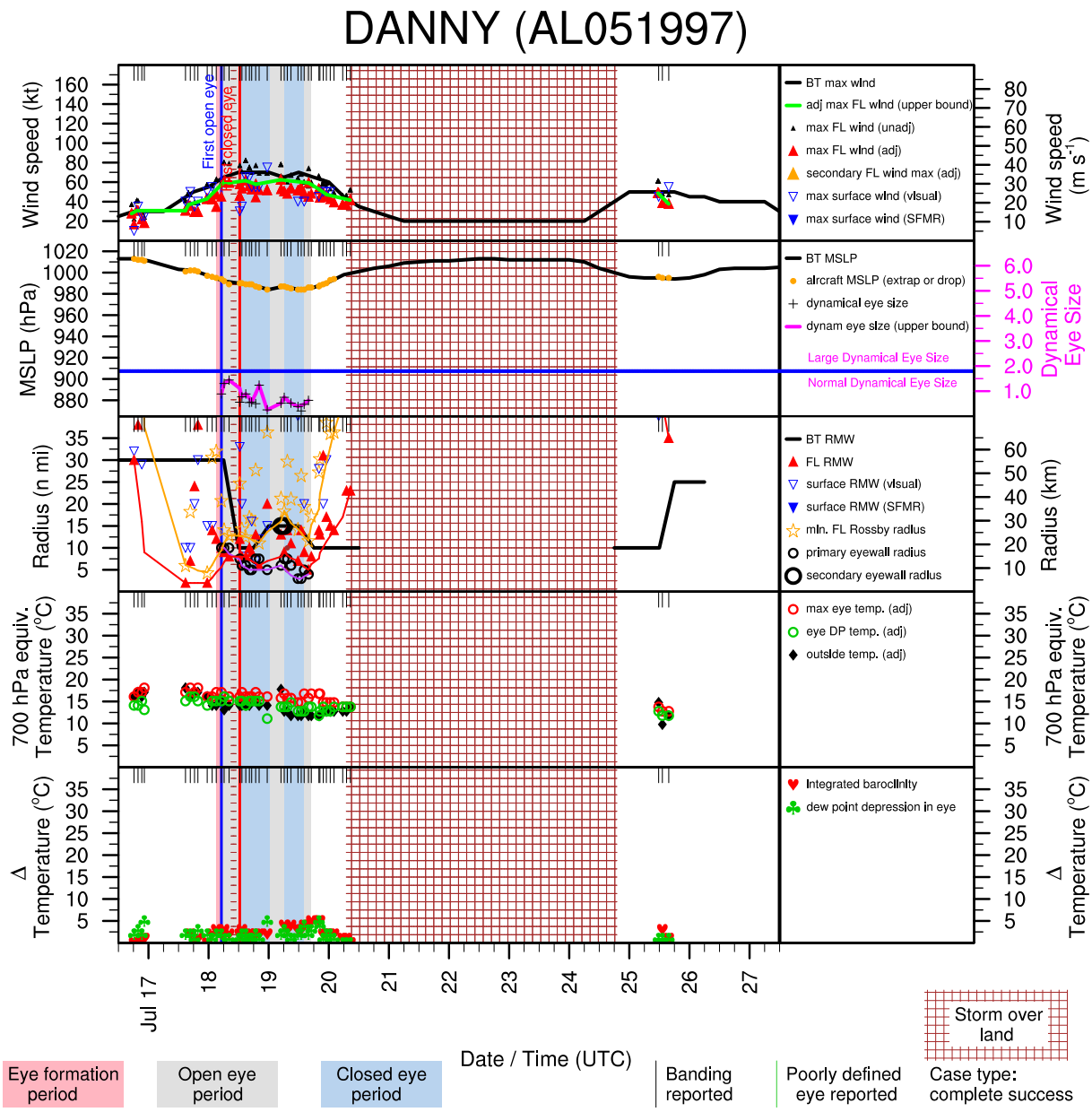

Figure E.65: Structure and intensity parameters for Hurricane Danny (1997).

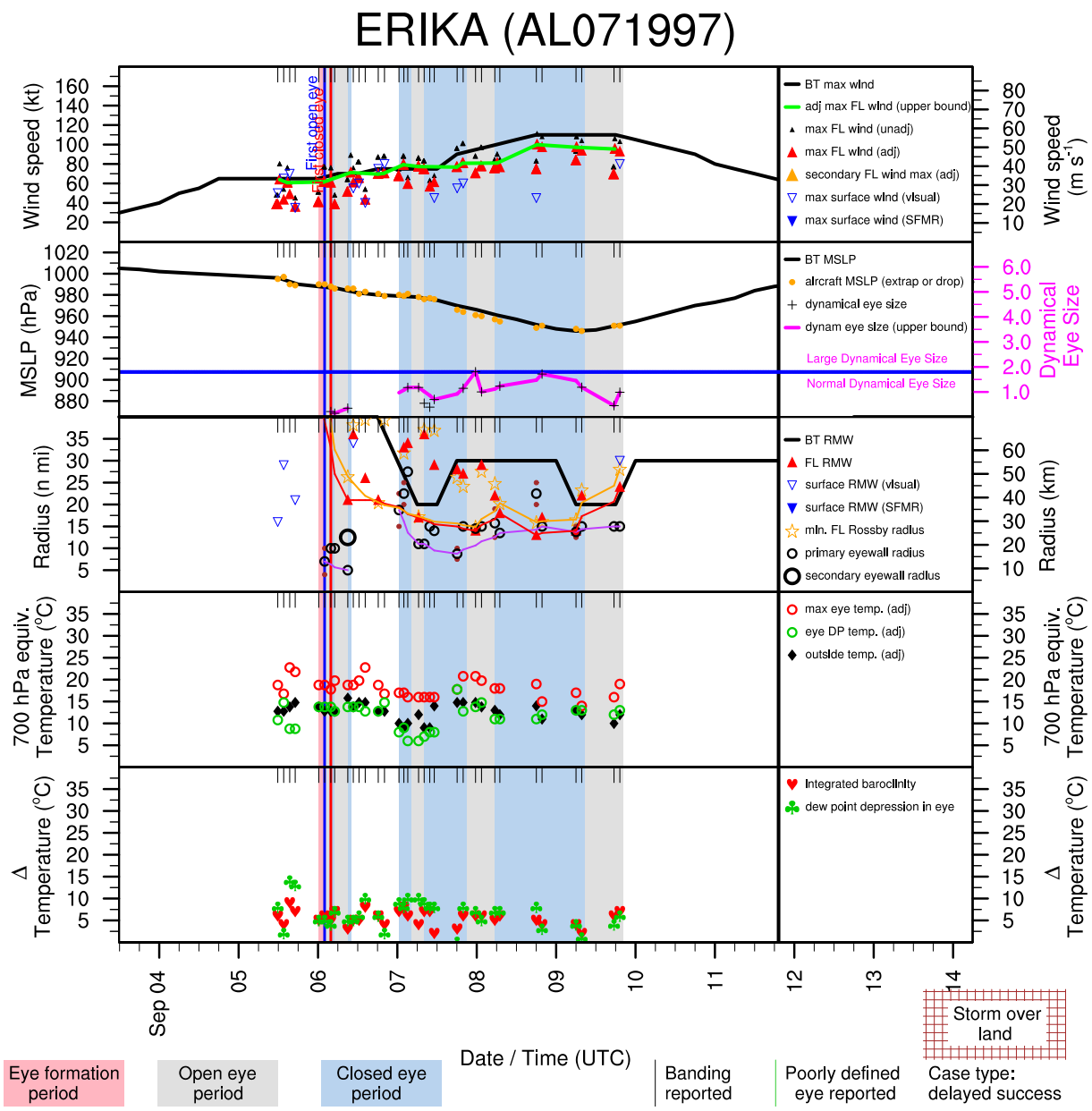

Figure E.66: Structure and intensity parameters for Hurricane Erika (1997).

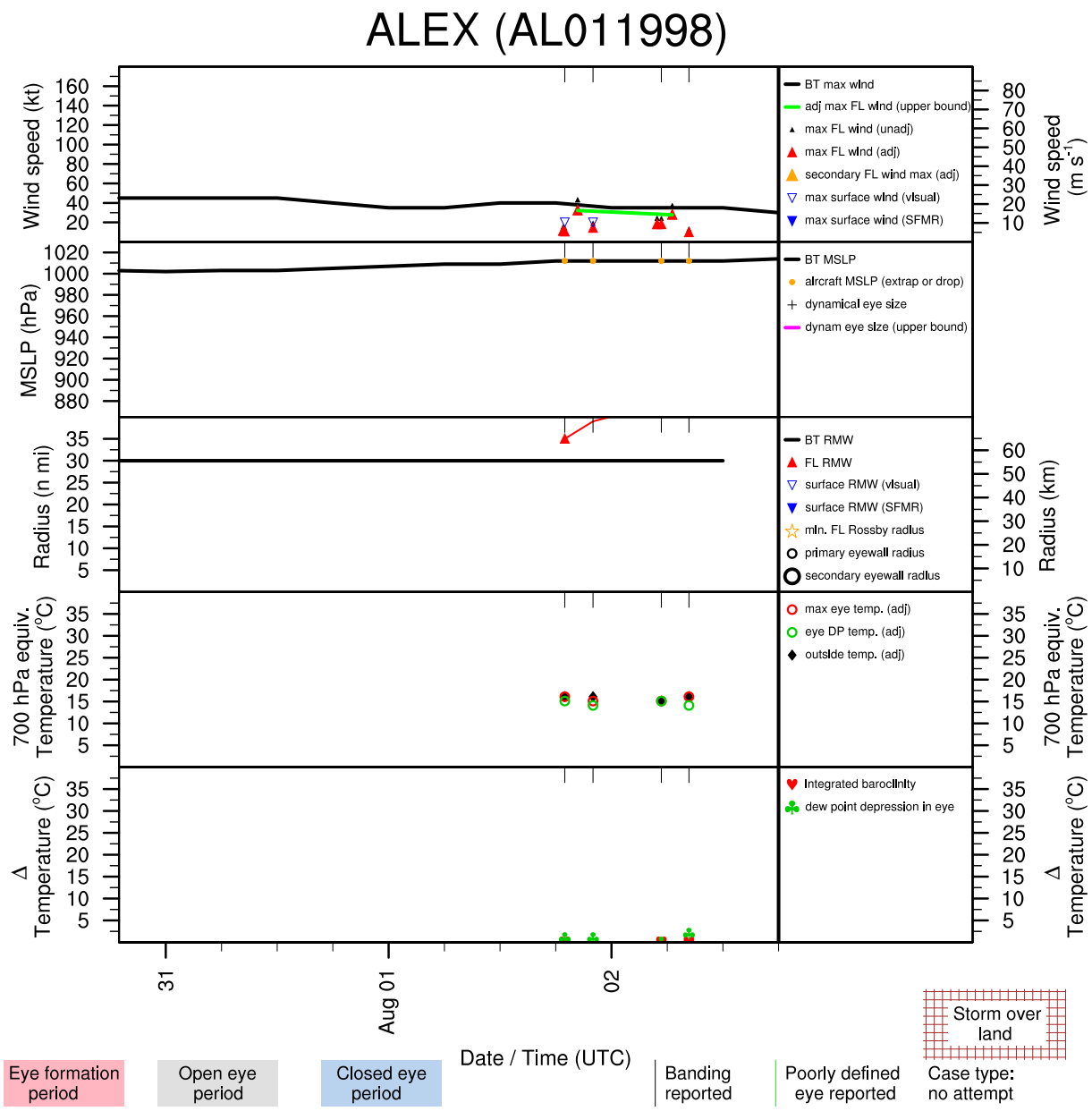

Figure E.67: Structure and intensity parameters for Tropical Storm Alex (1998).

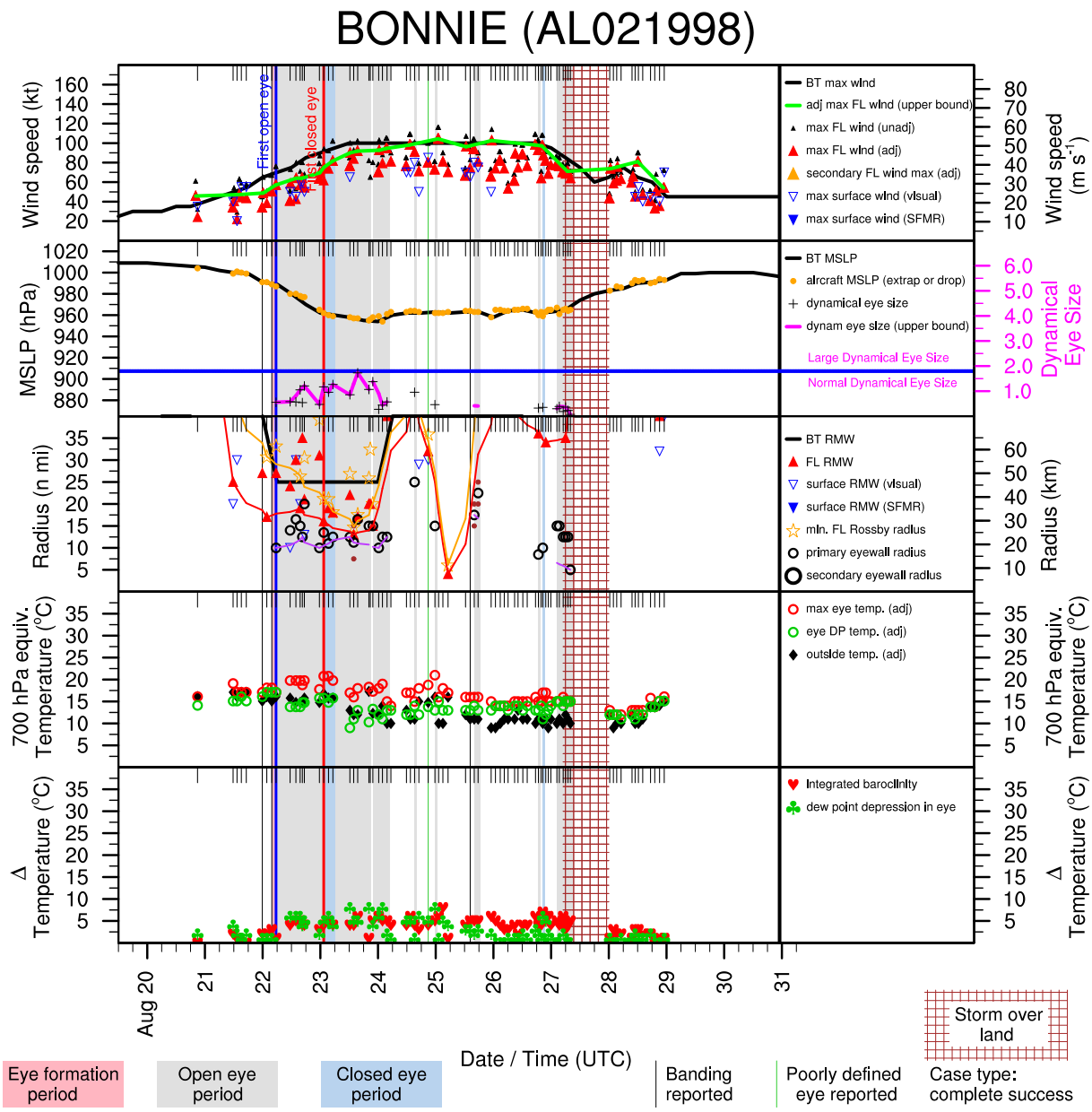

Figure E.68: Structure and intensity parameters for Hurricane Bonnie (1998).

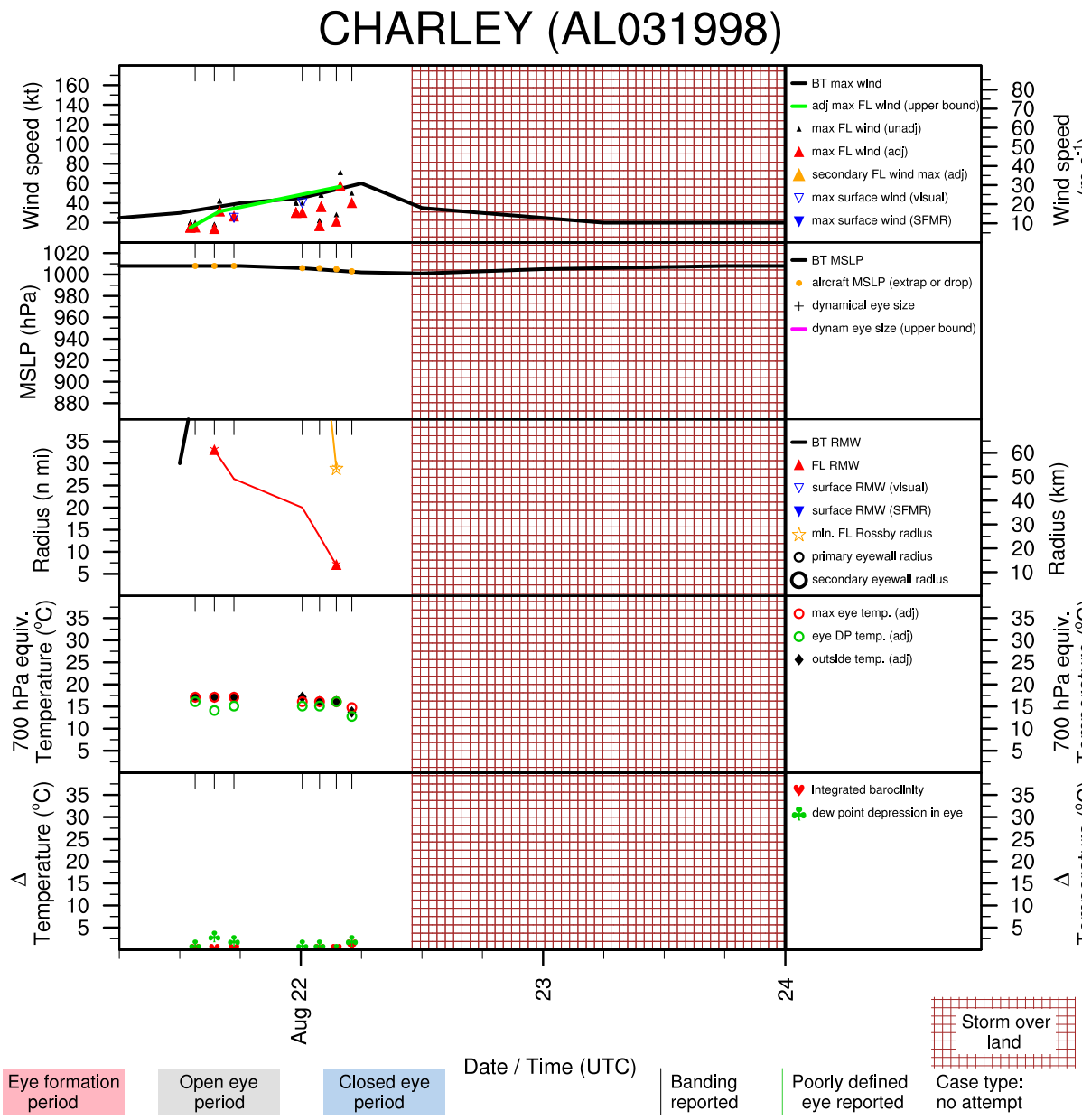

Figure E.69: Structure and intensity parameters for Tropical Storm Charley (1998).

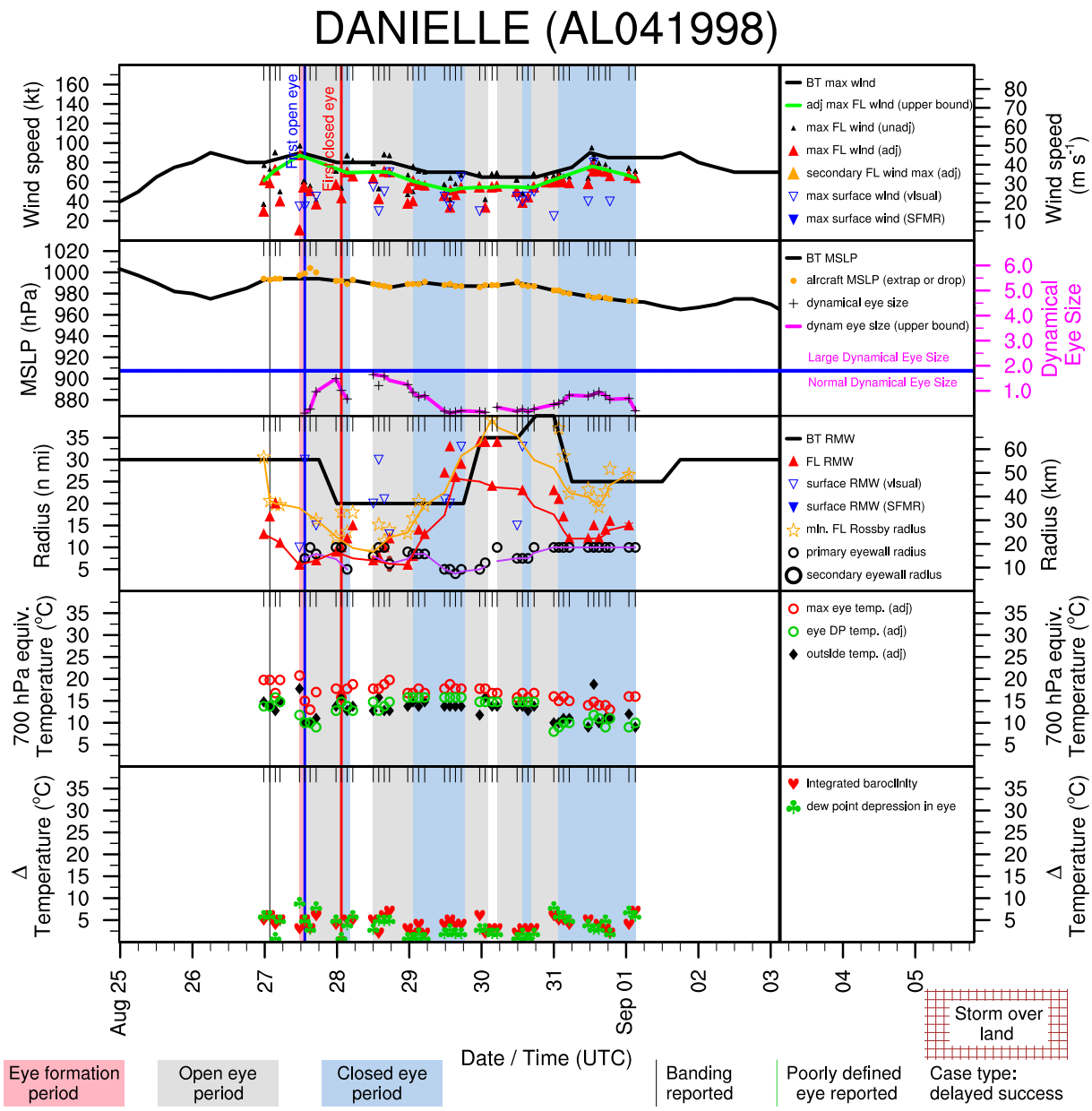

Figure E.70: Structure and intensity parameters for Hurricane Danielle (1998).

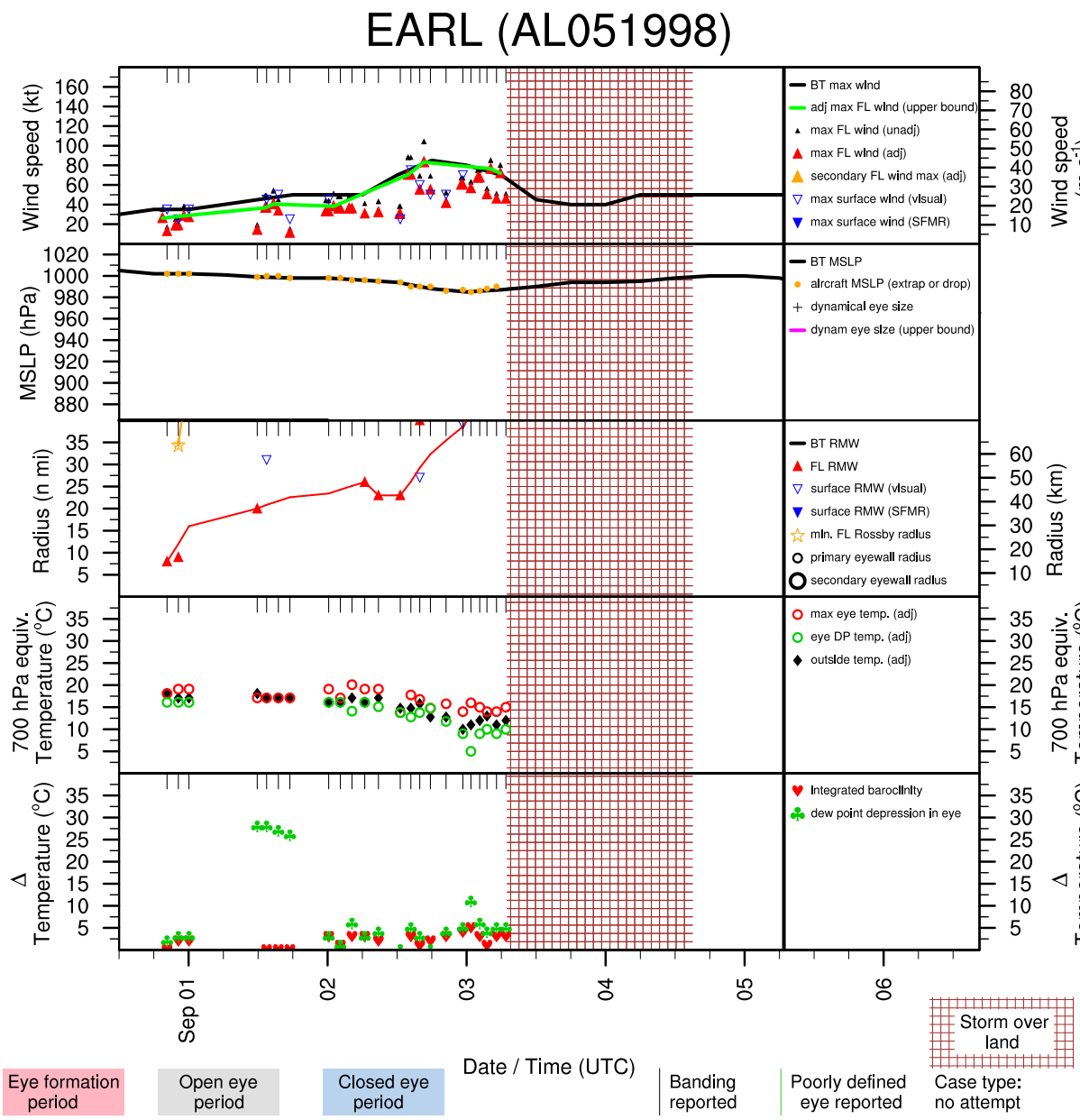

Figure E.71: Structure and intensity parameters for Hurricane Earl (1998).

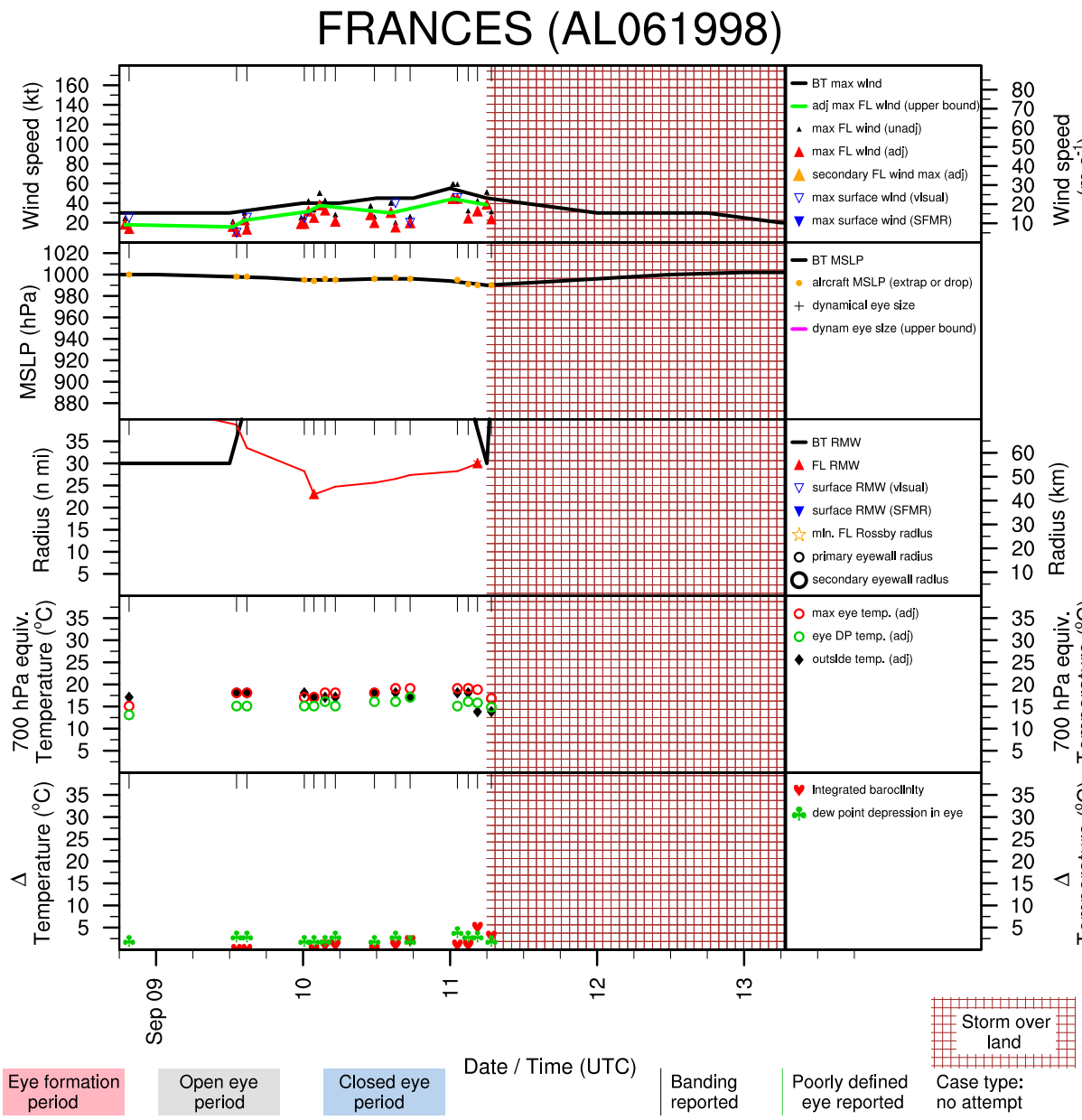

Figure E.72: Structure and intensity parameters for Tropical Storm Frances (1998).

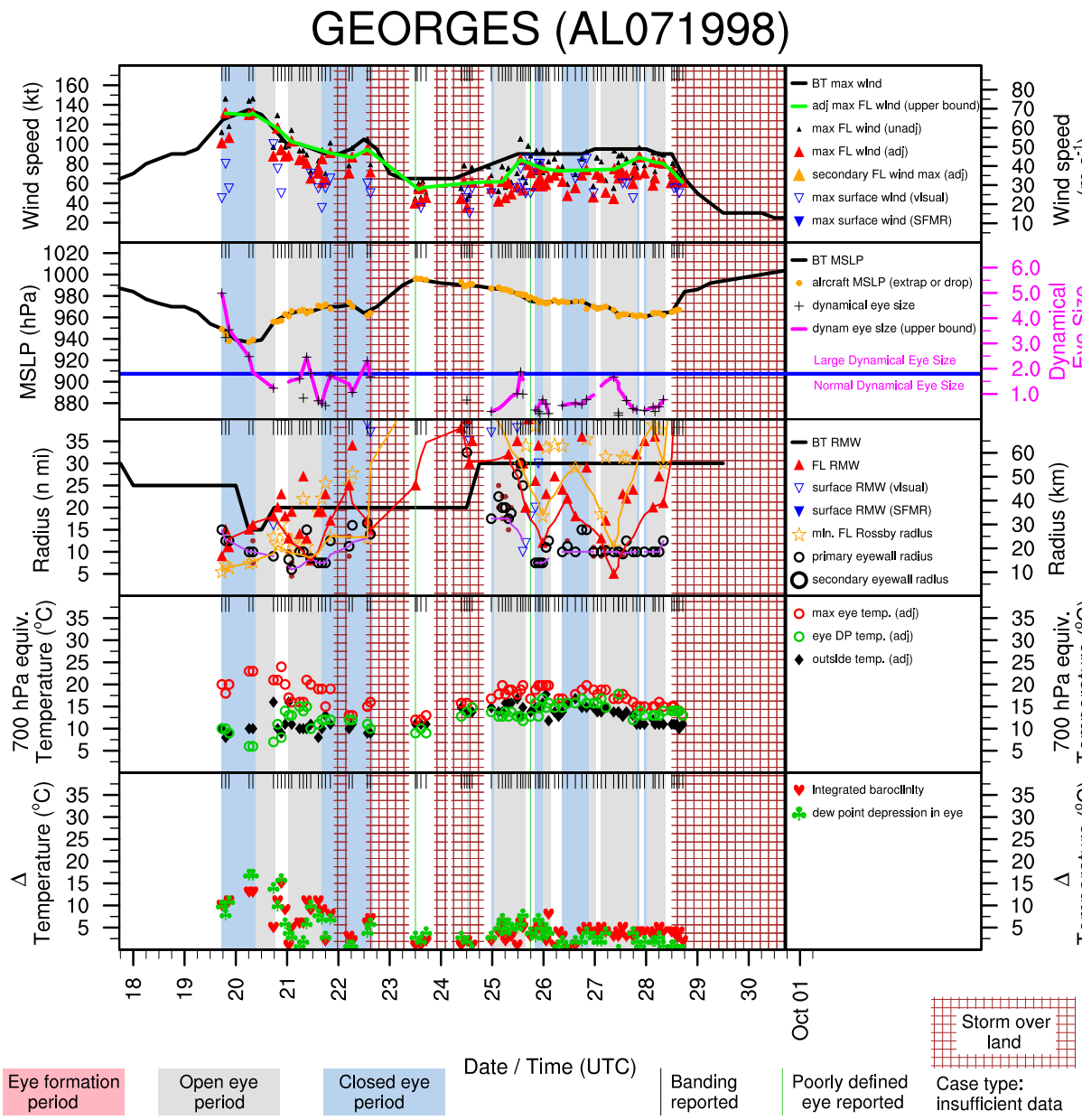

Figure E.73: Structure and intensity parameters for Hurricane Georges (1998).

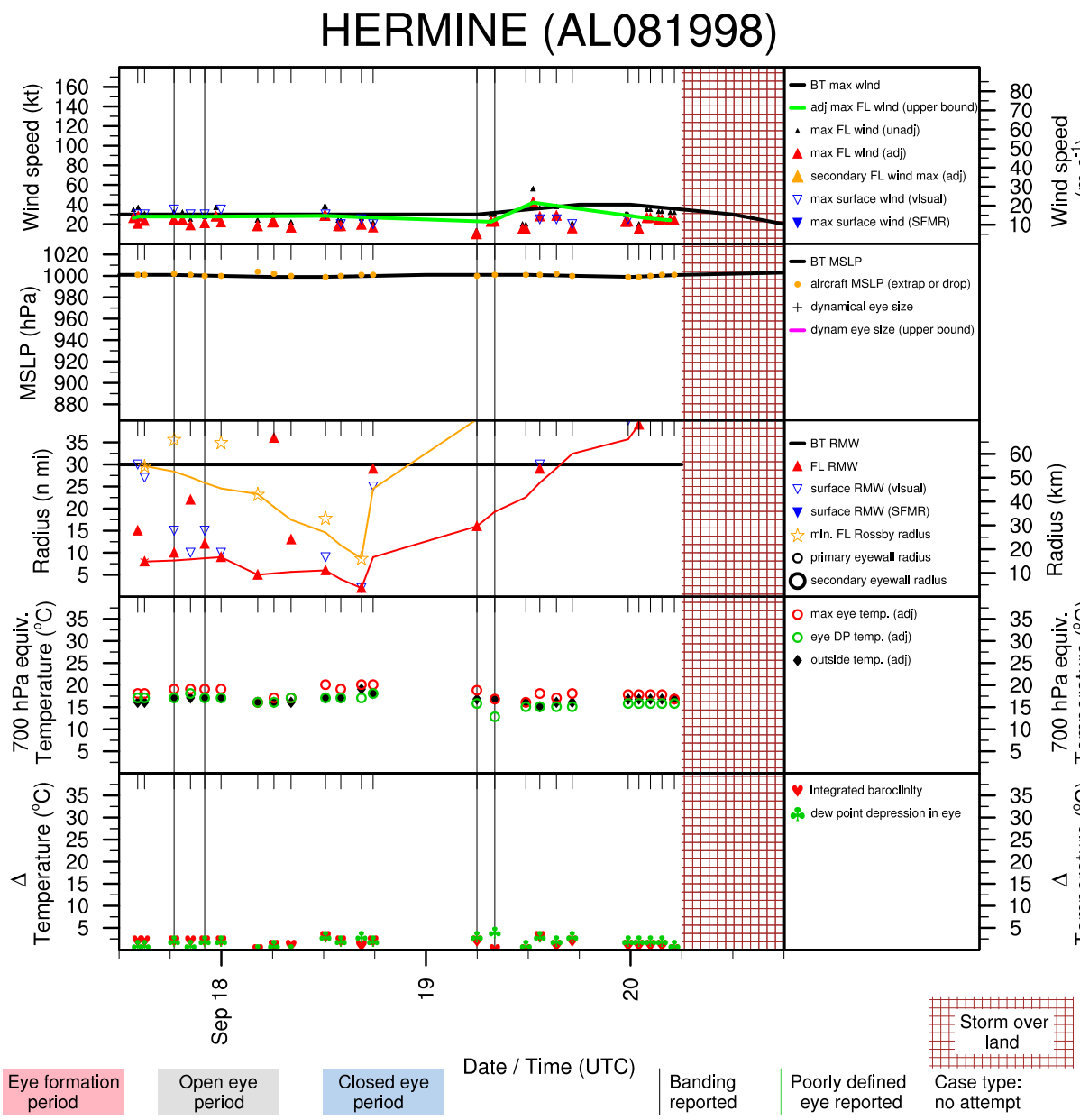

Figure E.74: Structure and intensity parameters for Tropical Storm Hermine (1998).

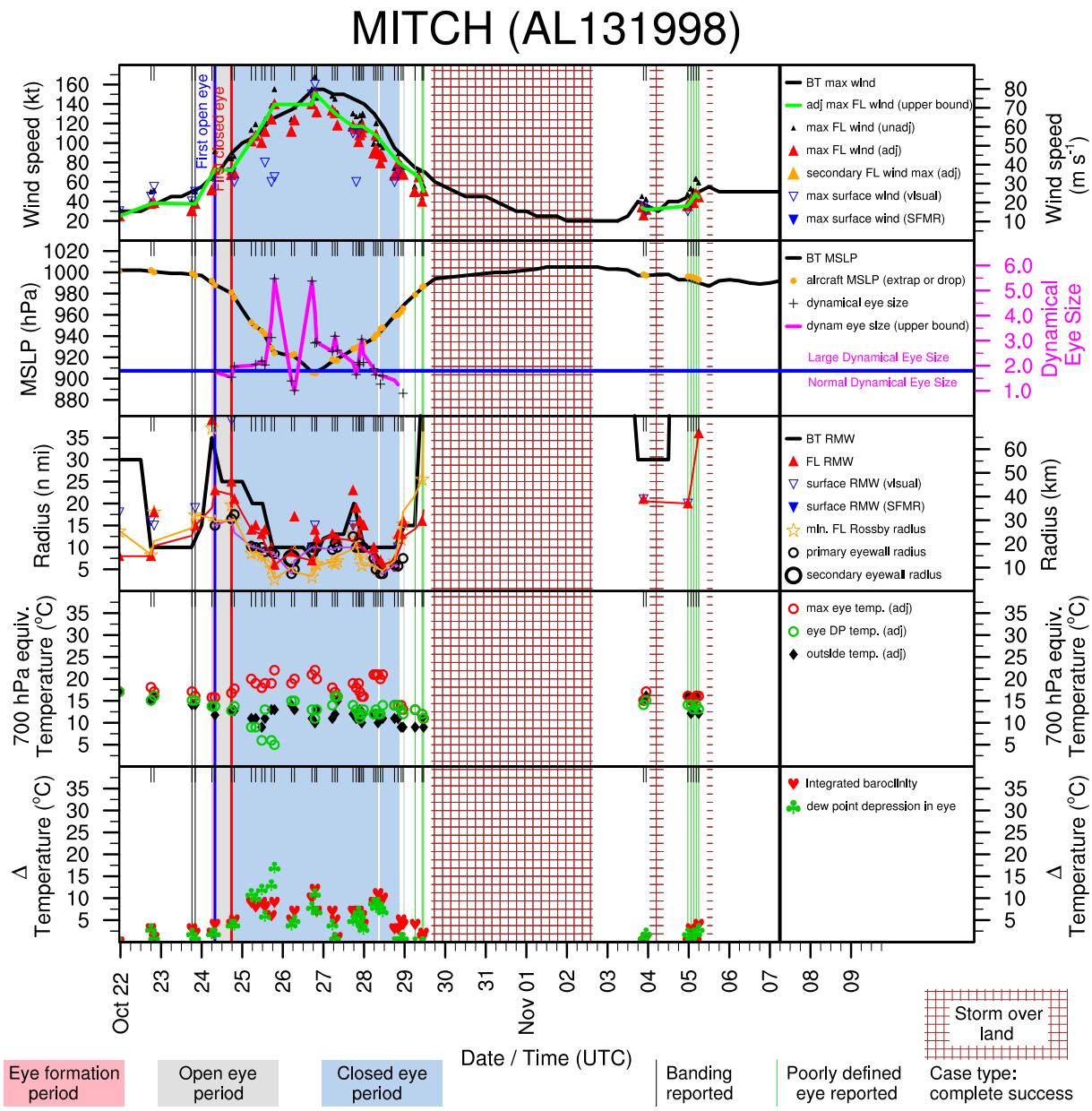

Figure E.75: Structure and intensity parameters for Hurricane Mitch (1998).

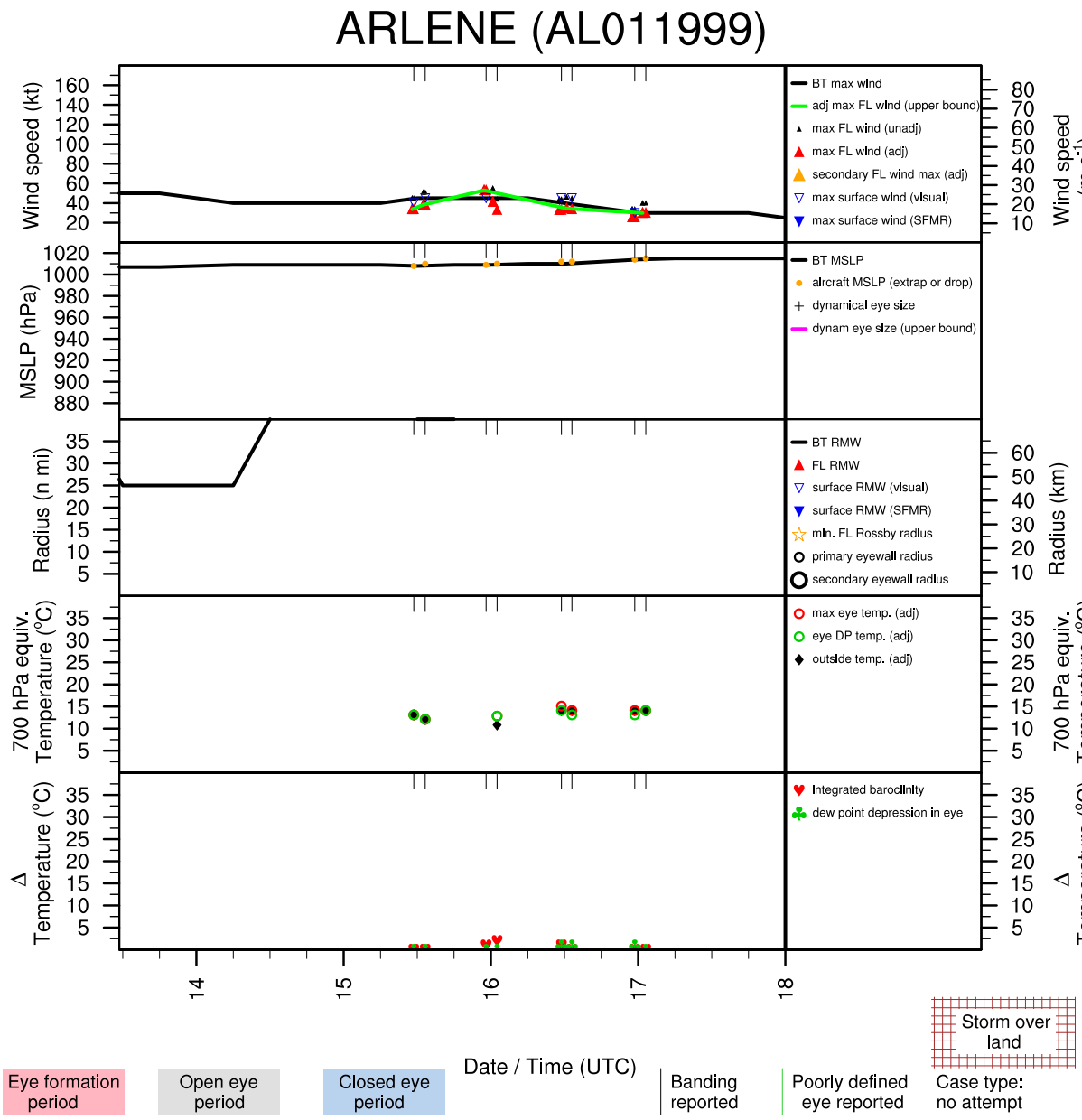

Figure E.76: Structure and intensity parameters for Tropical Storm Arlene (1999).

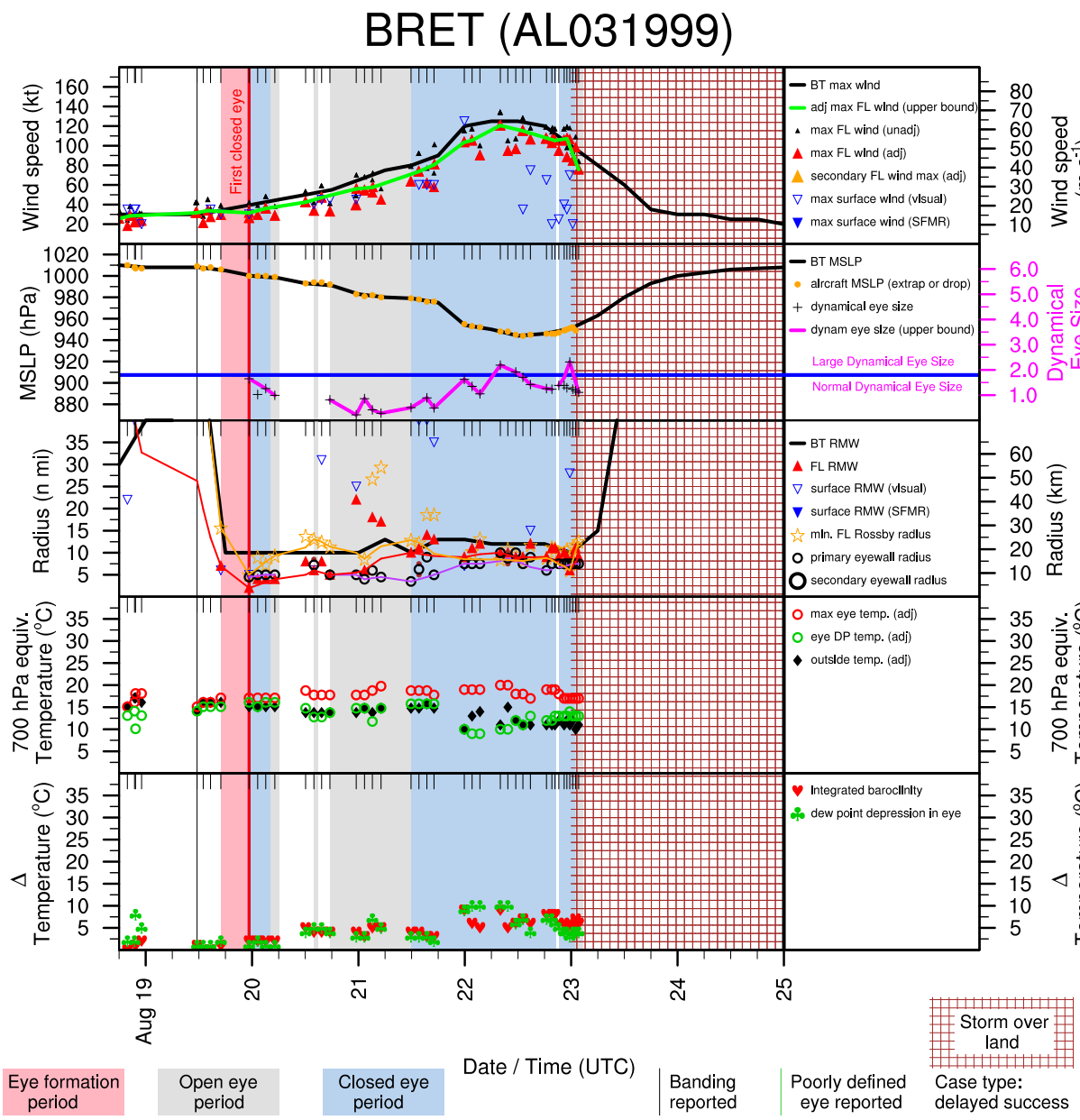

Figure E.77: Structure and intensity parameters for Hurricane Bret (1999).

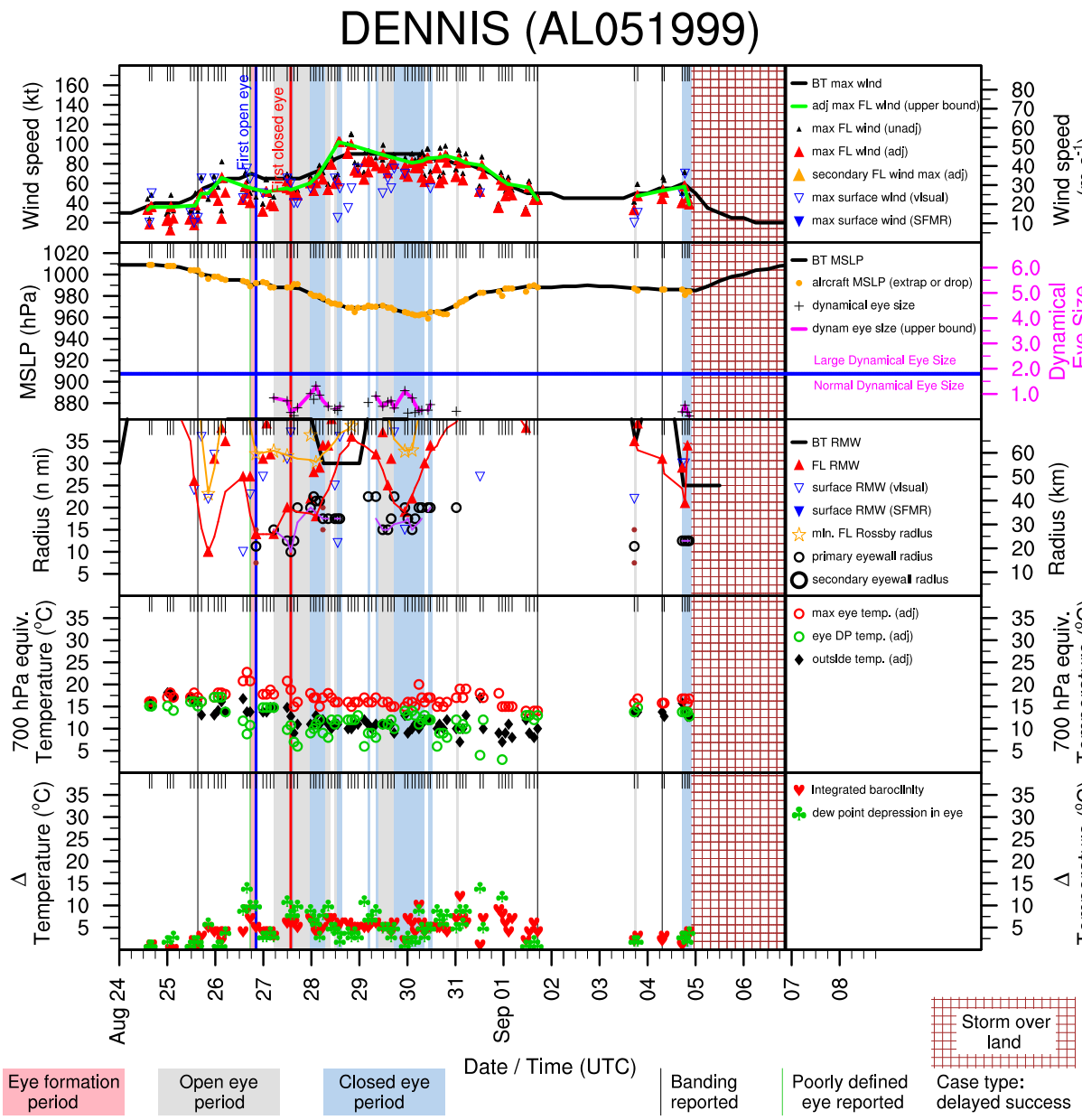

Figure E.78: Structure and intensity parameters for Hurricane Dennis (1999).

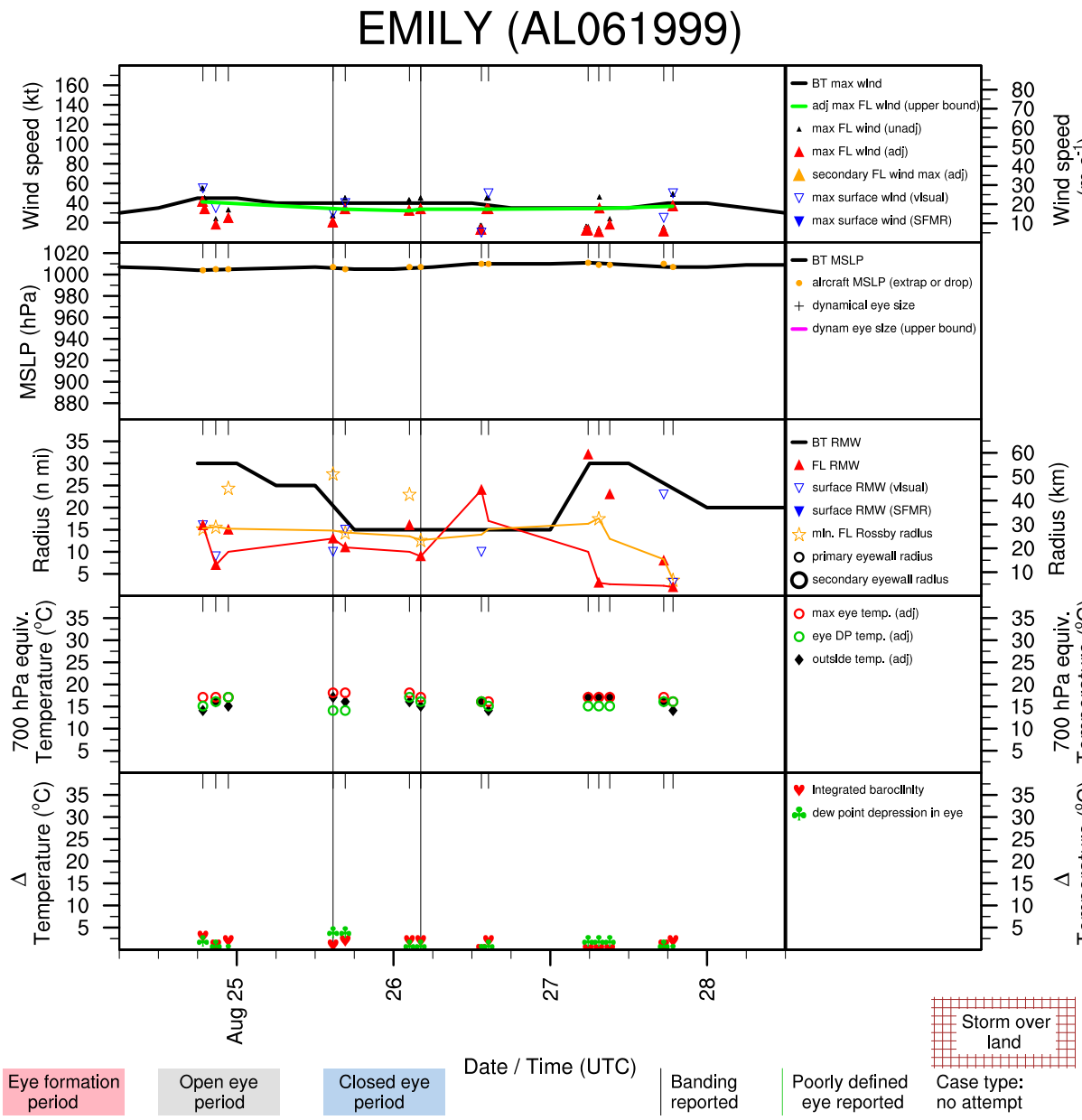

Figure E.79: Structure and intensity parameters for Tropical Storm Emily (1999).

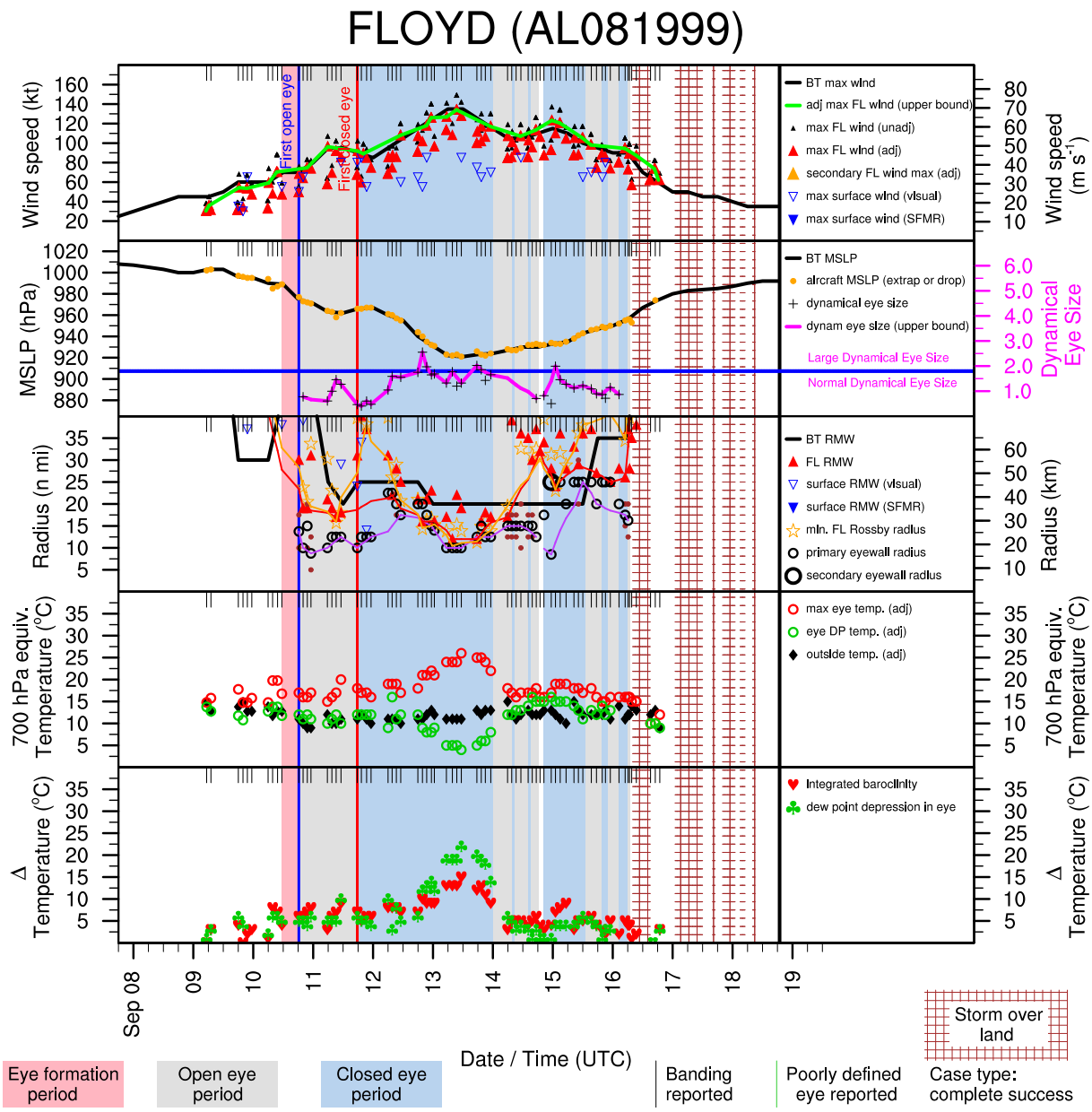

Figure E.80: Structure and intensity parameters for Hurricane Floyd (1999).

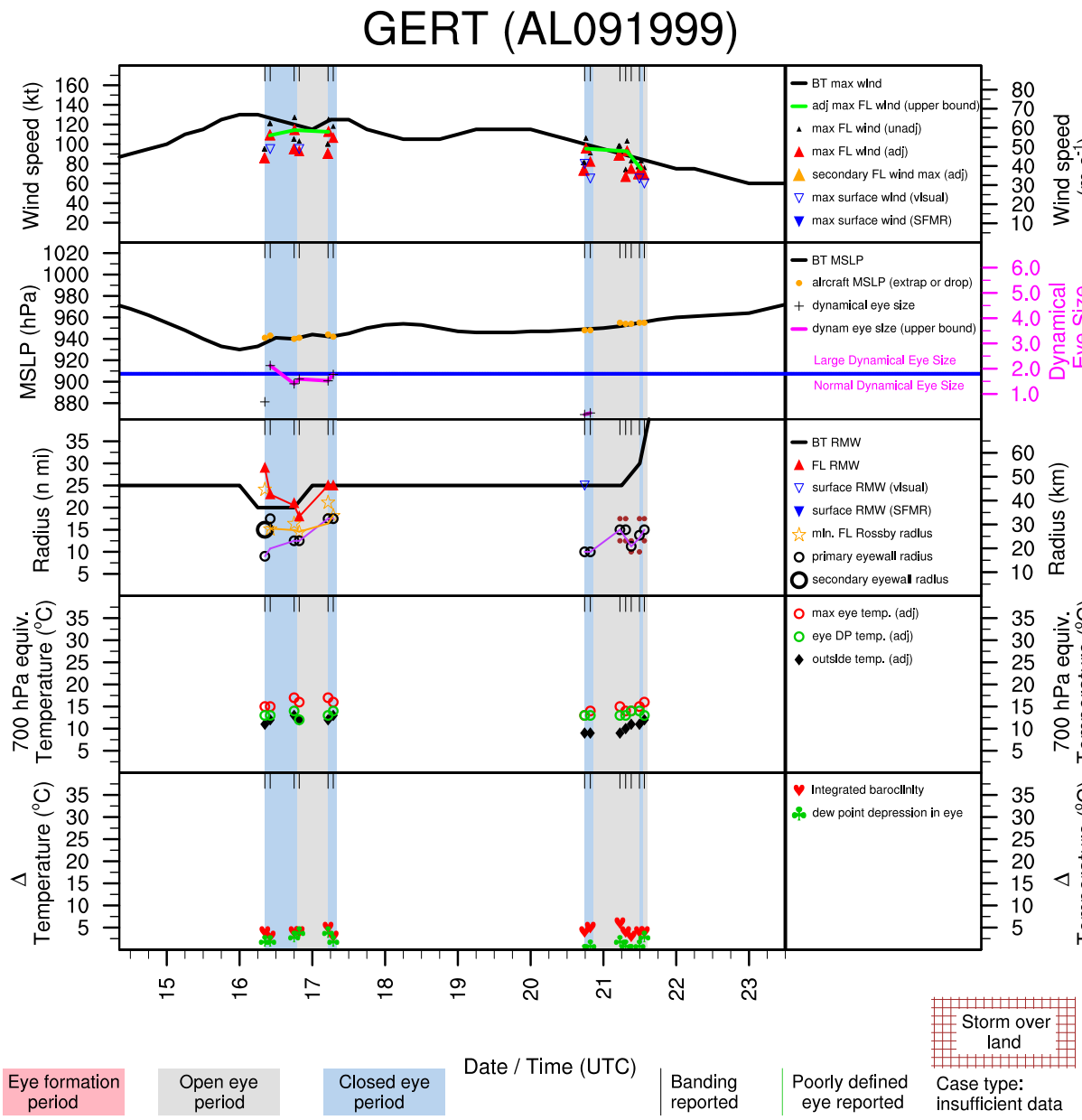

Figure E.81: Structure and intensity parameters for Hurricane Gert (1999).

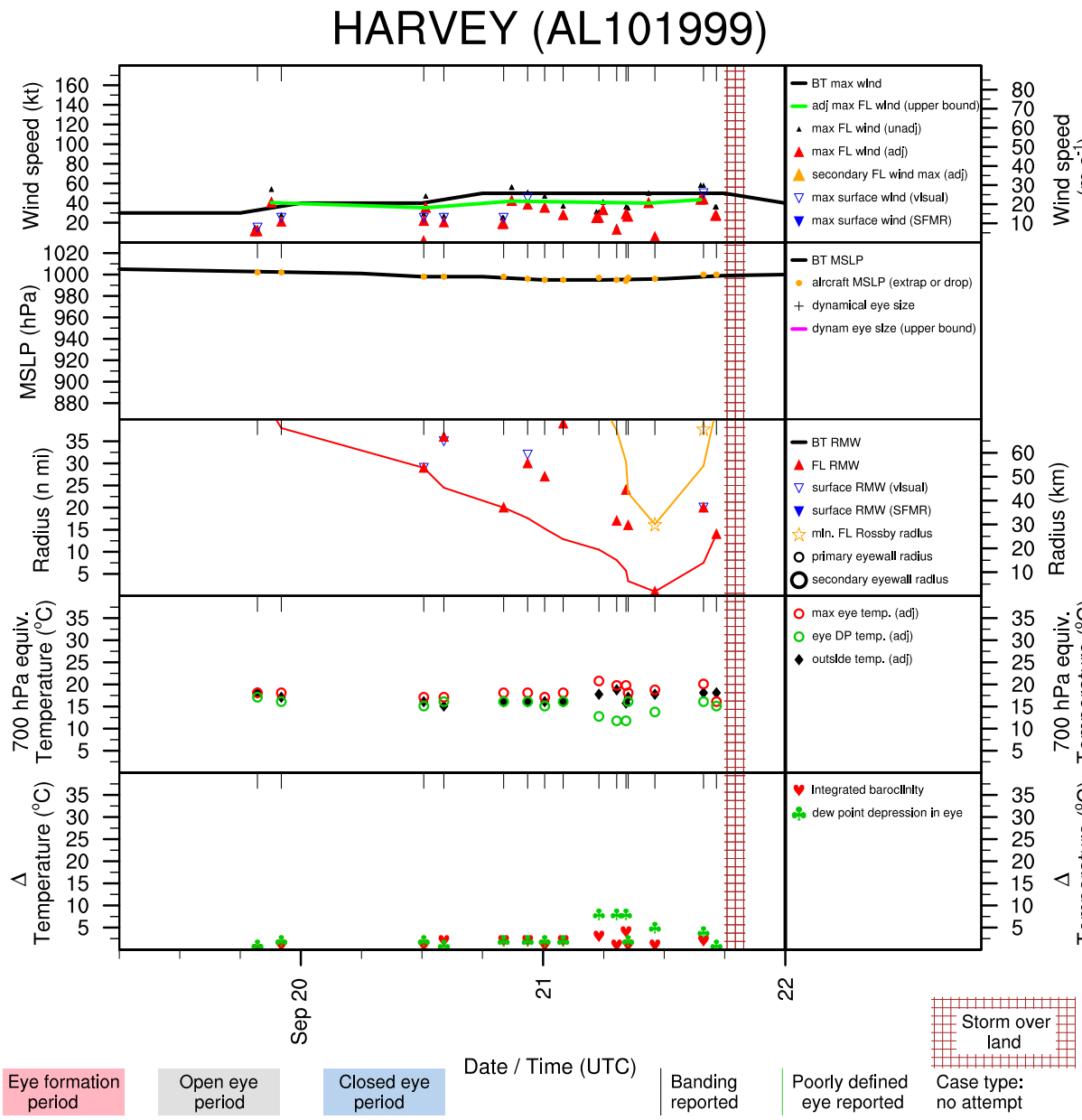

Figure E.82: Structure and intensity parameters for Tropical Storm Harvey (1999).

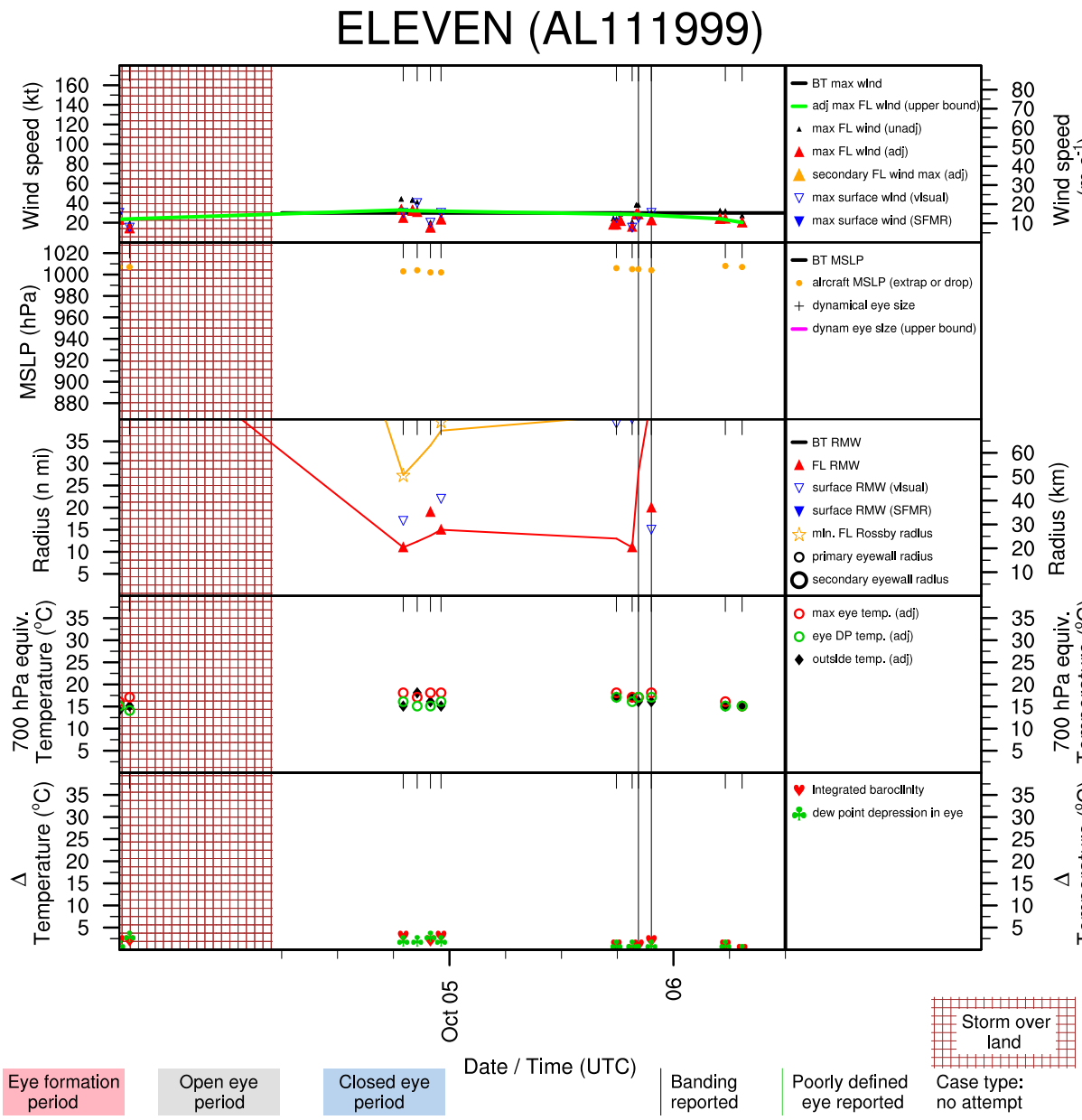

Figure E.83: Structure and intensity parameters for Tropical Depression Eleven (1999).

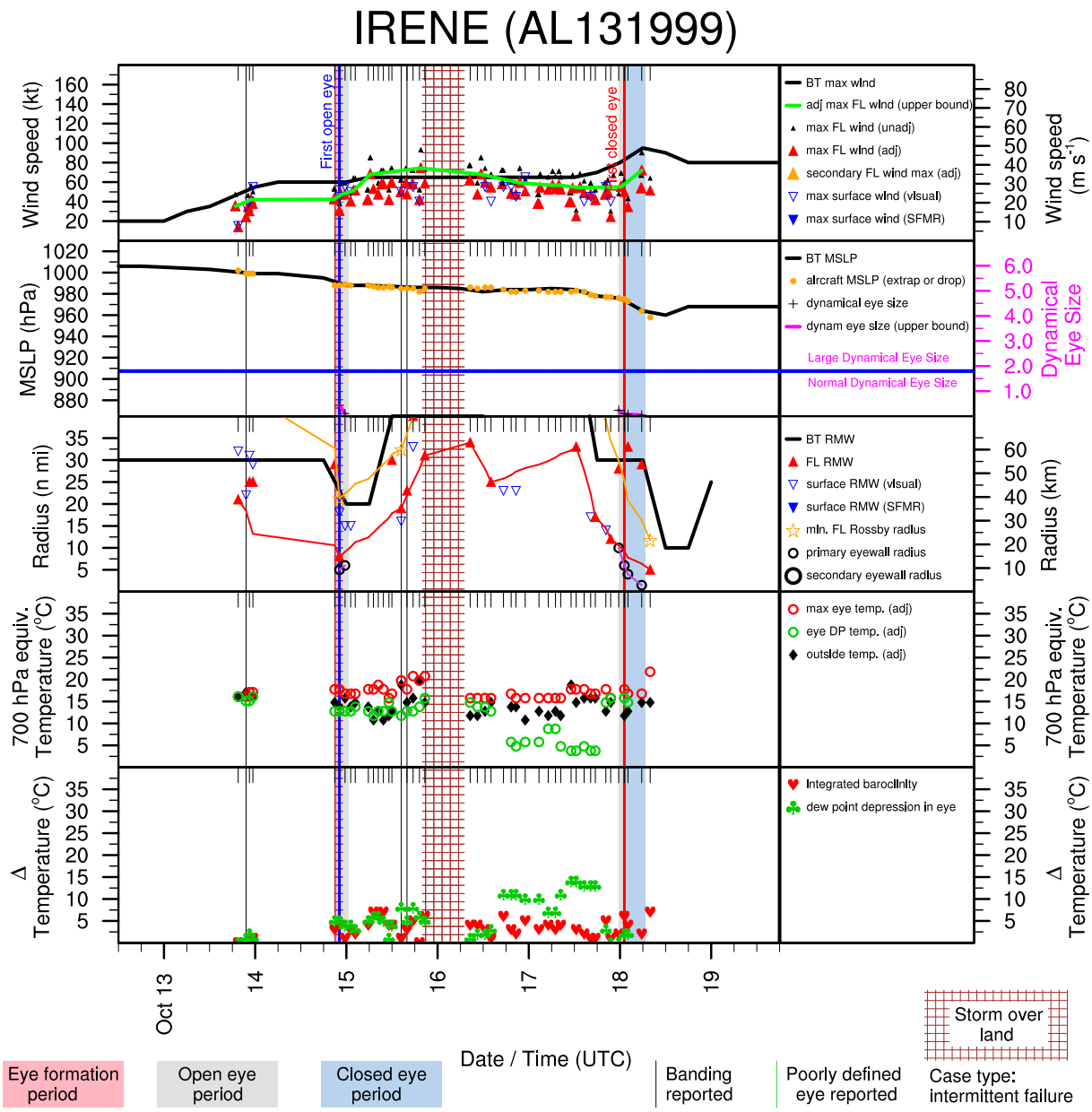

Figure E.84: Structure and intensity parameters for Hurricane Irene (1999).

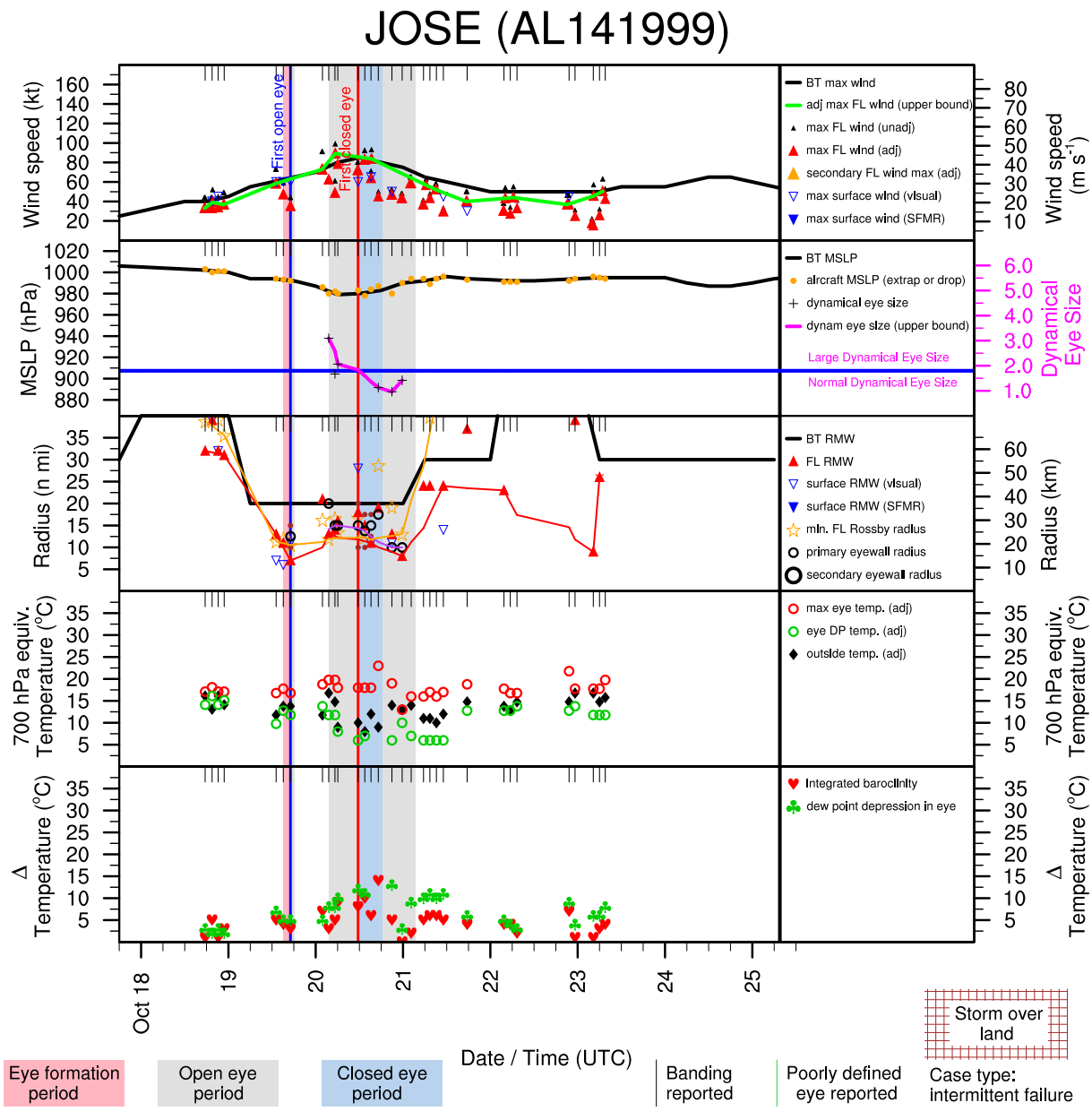

Figure E.85: Structure and intensity parameters for Hurricane Jose (1999).

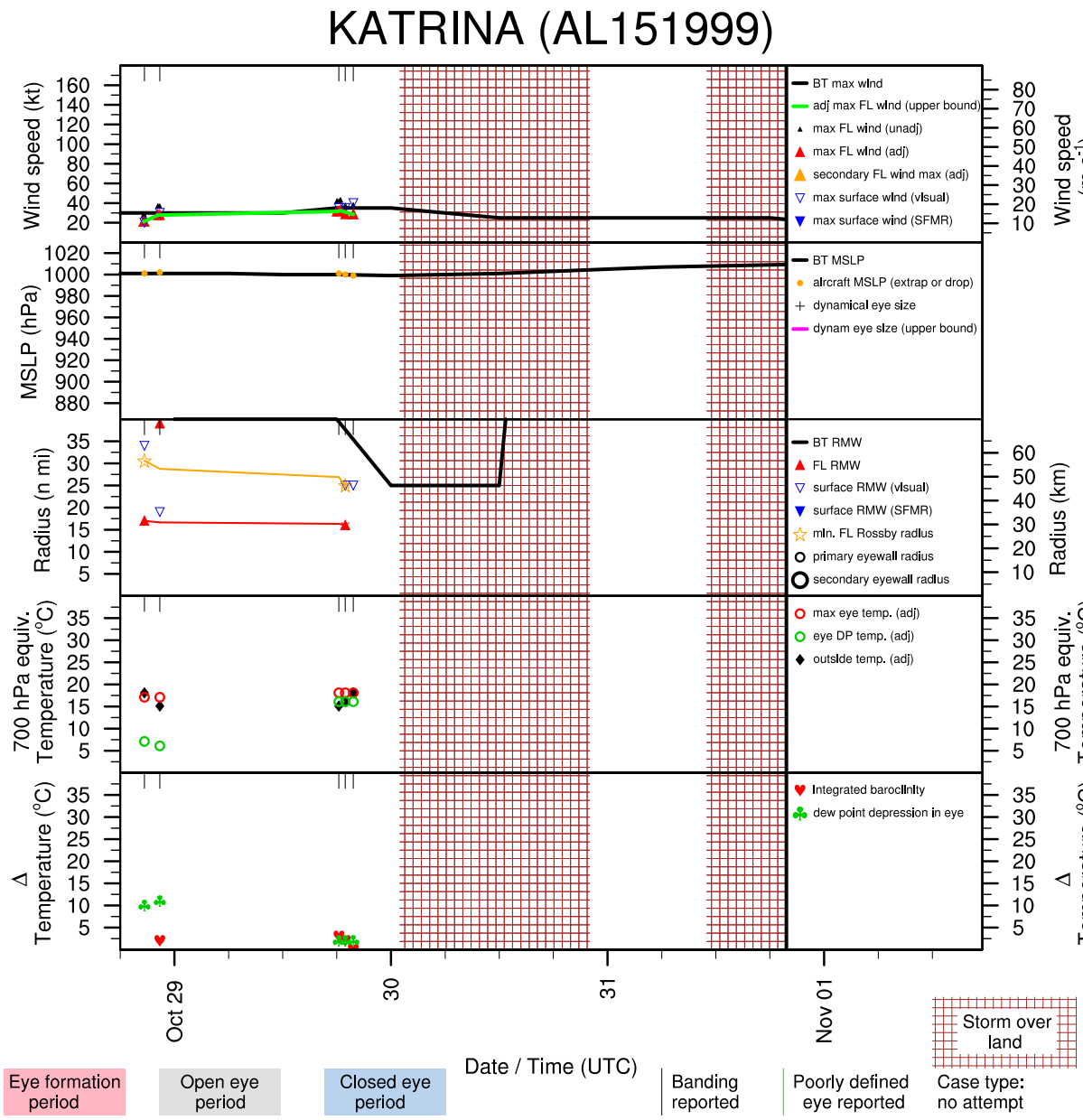

Figure E.86: Structure and intensity parameters for Tropical Storm Katrina (1999).

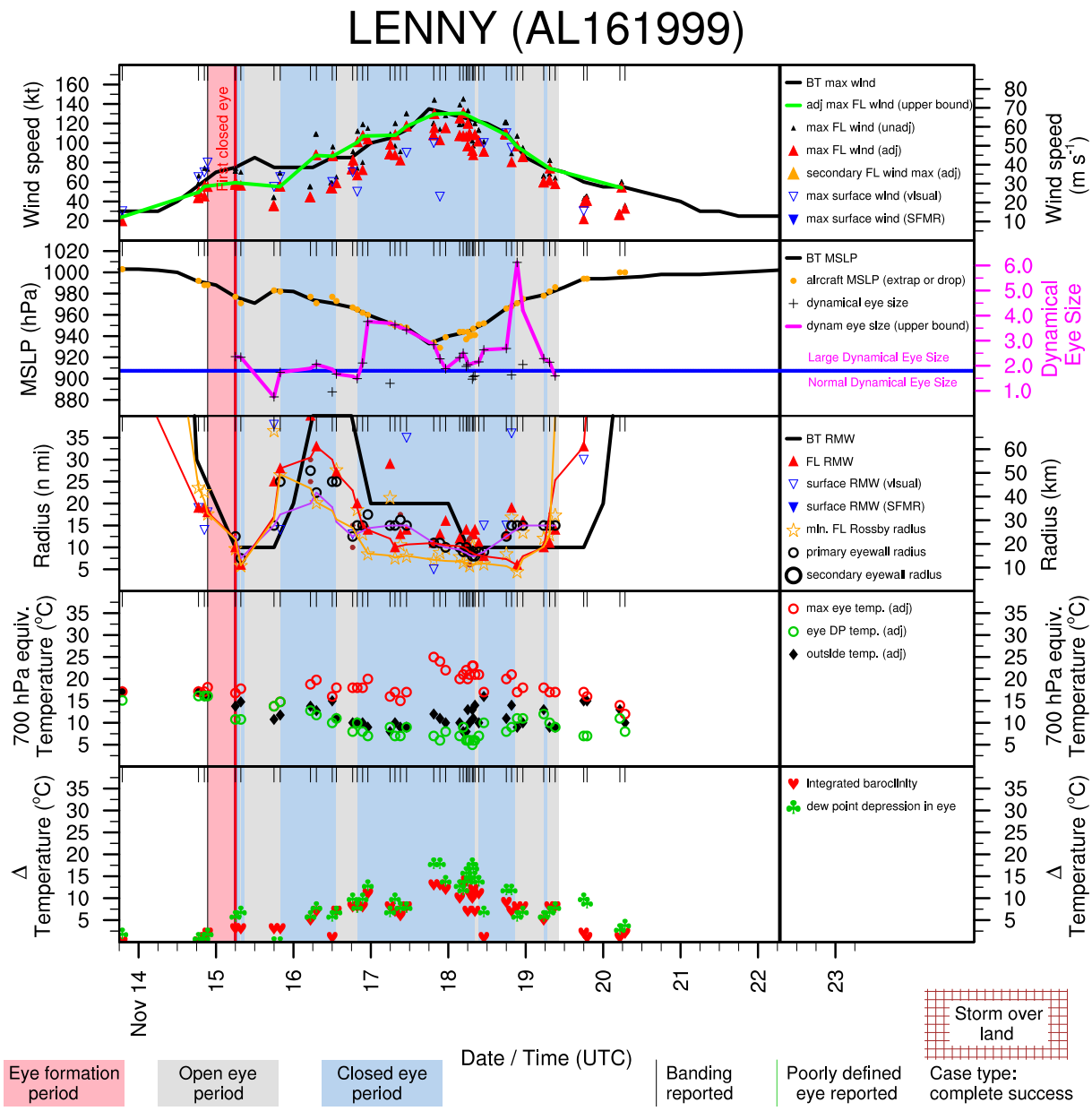

Figure E.87: Structure and intensity parameters for Hurricane Lenny (1999).

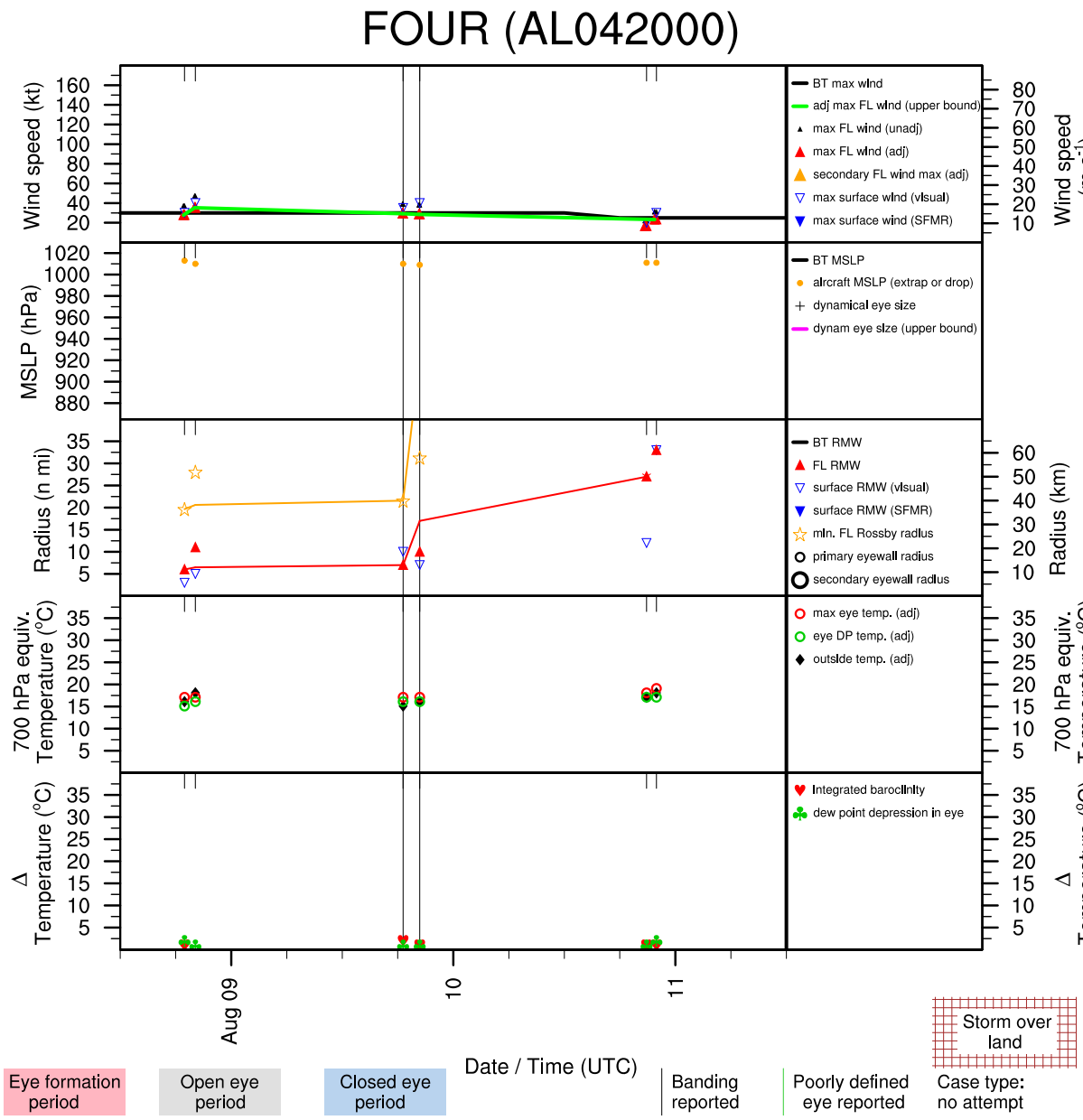

Figure E.88: Structure and intensity parameters for Tropical Depression Four (2000).

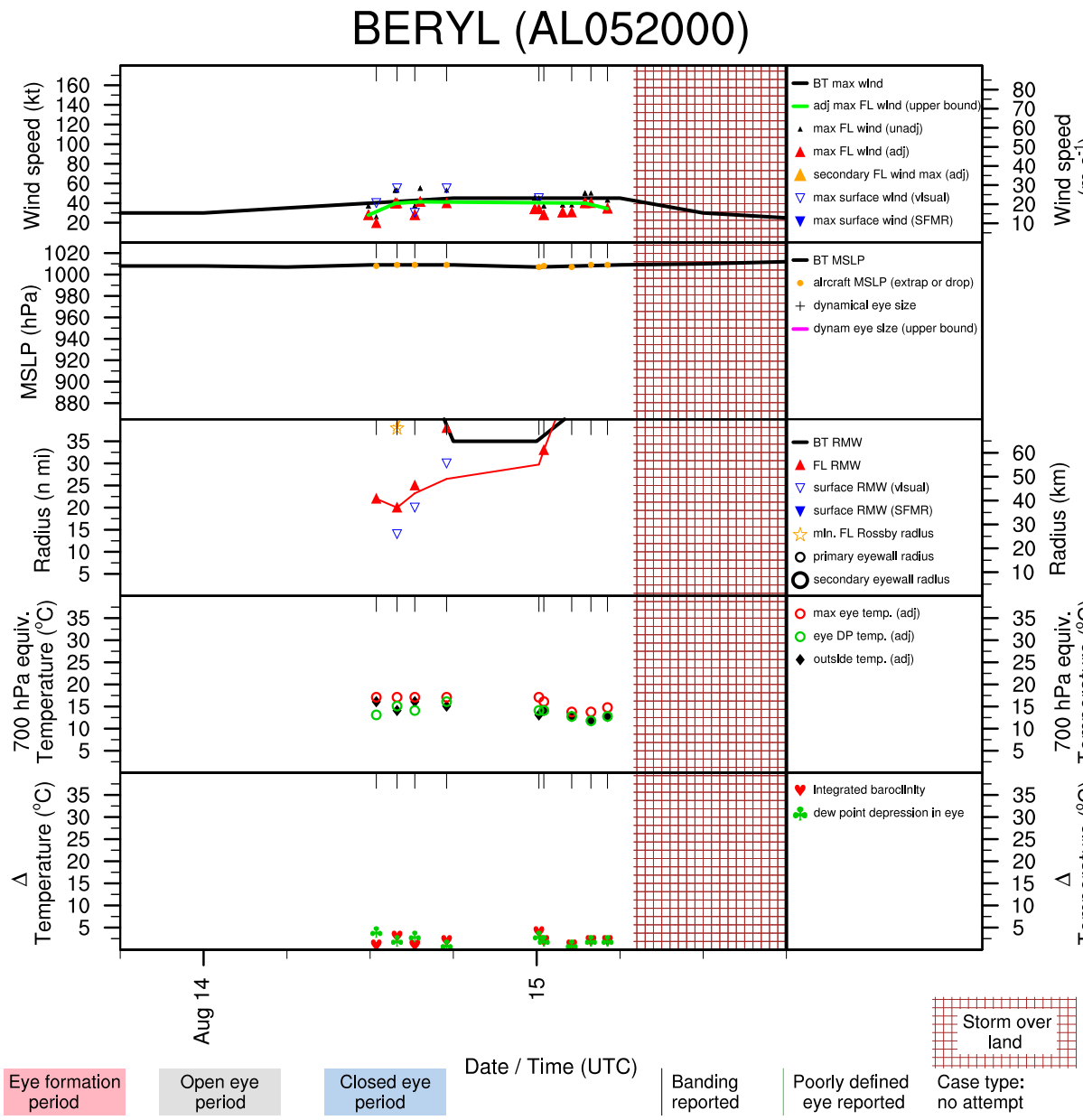

Figure E.89: Structure and intensity parameters for Tropical Storm Beryl (2000).

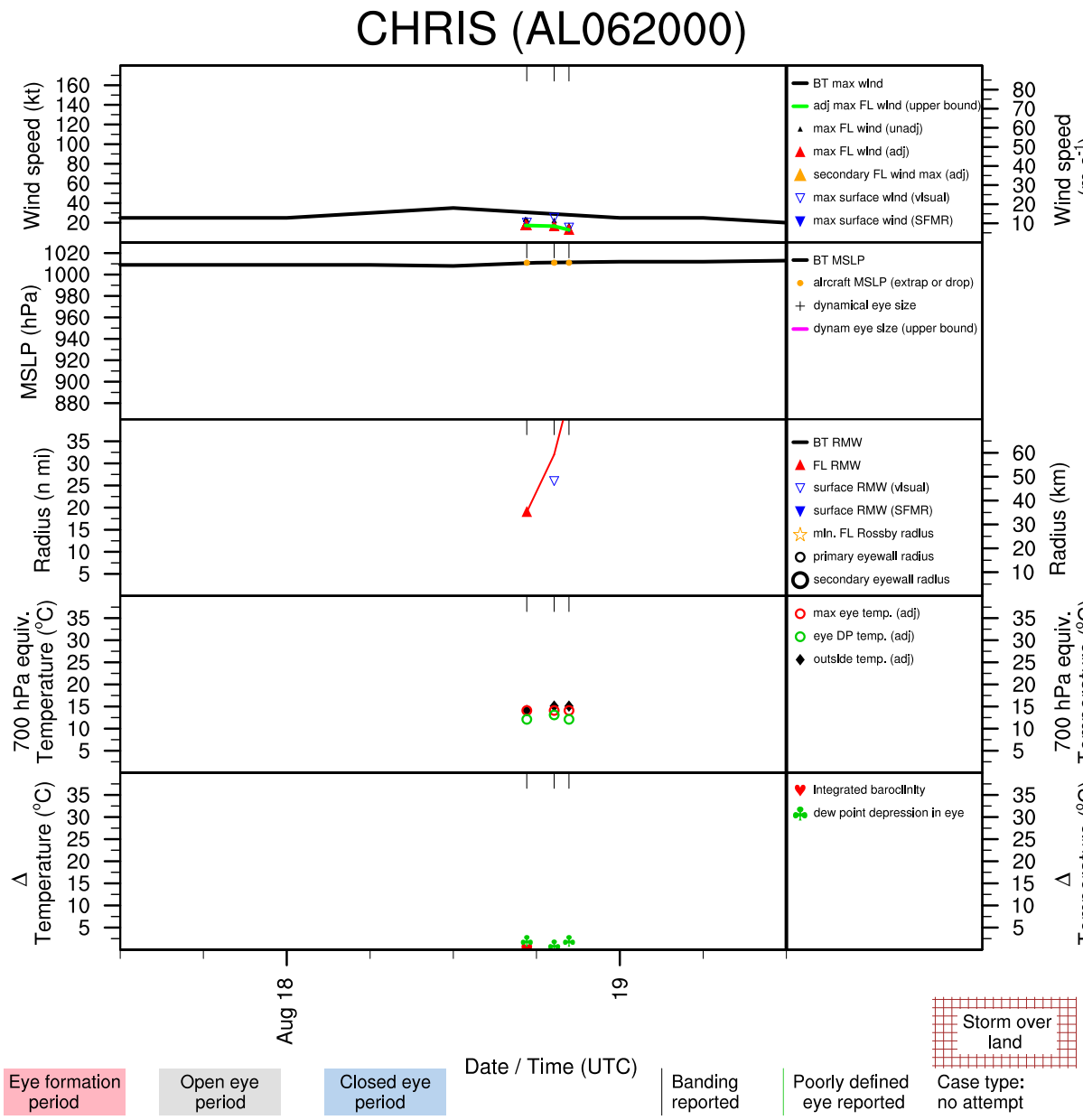

Figure E.90: Structure and intensity parameters for Tropical Storm Chris (2000).

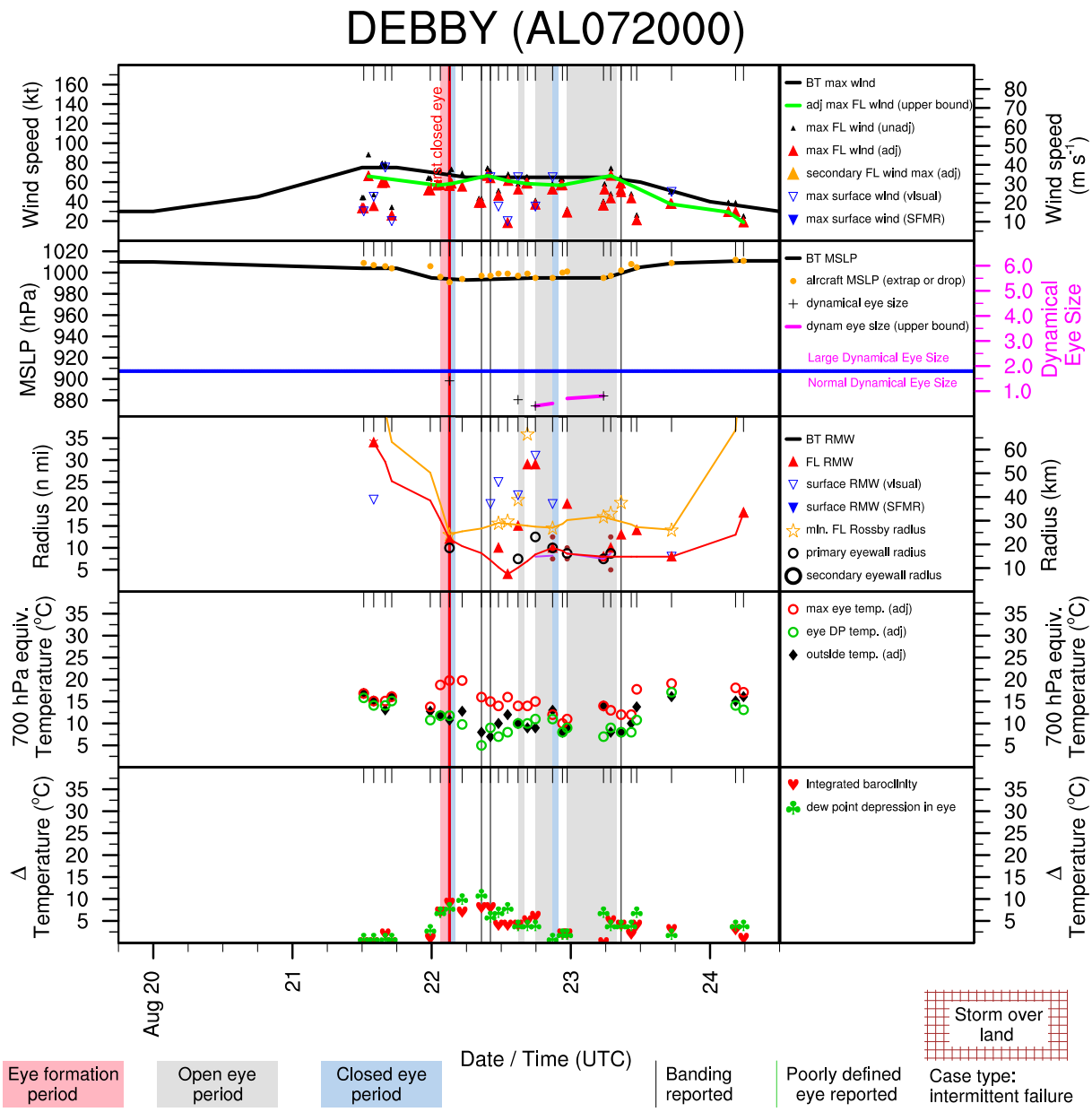

Figure E.91: Structure and intensity parameters for Hurricane Debby (2000).

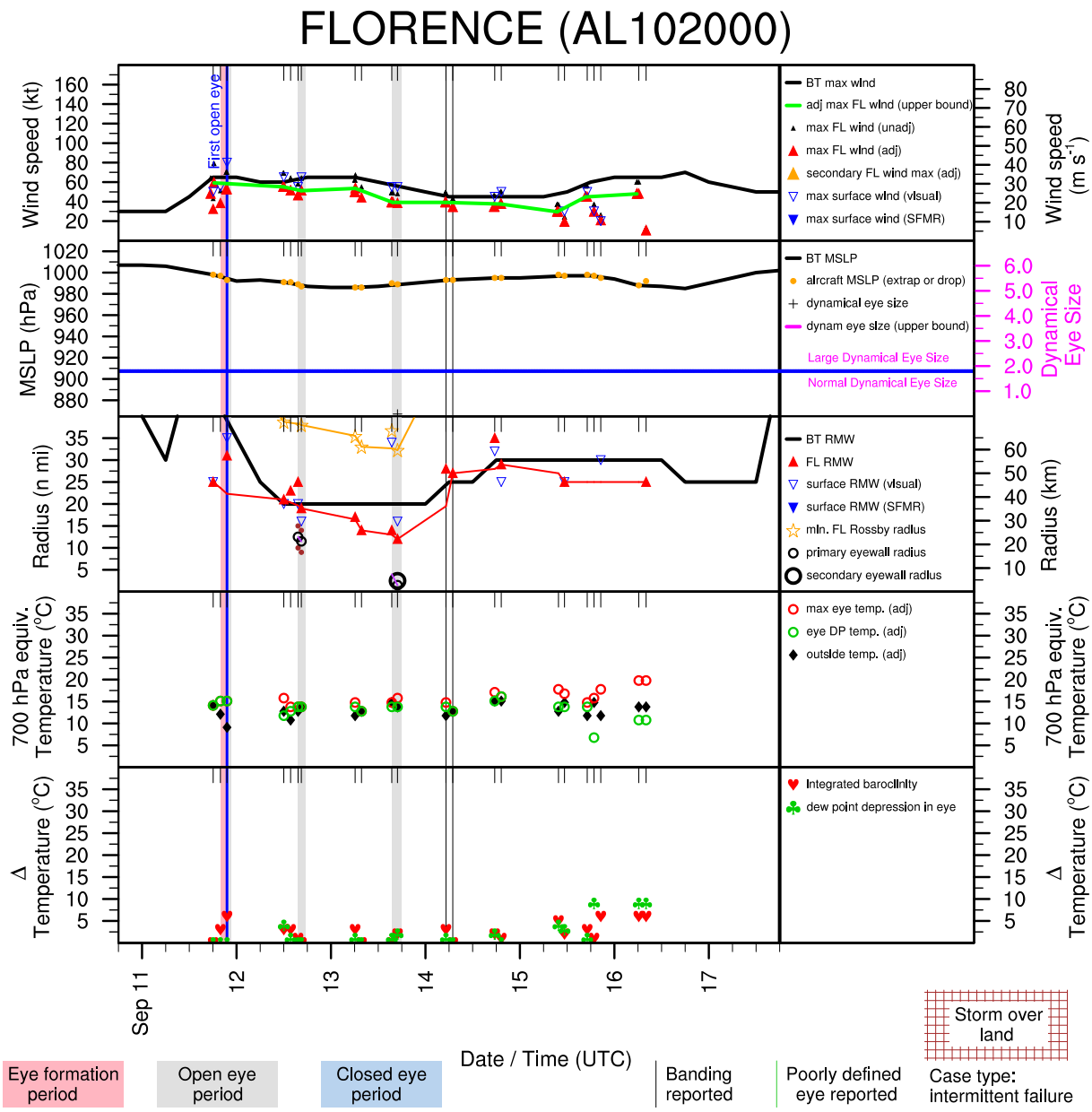

Figure E.92: Structure and intensity parameters for Hurricane Florence (2000).

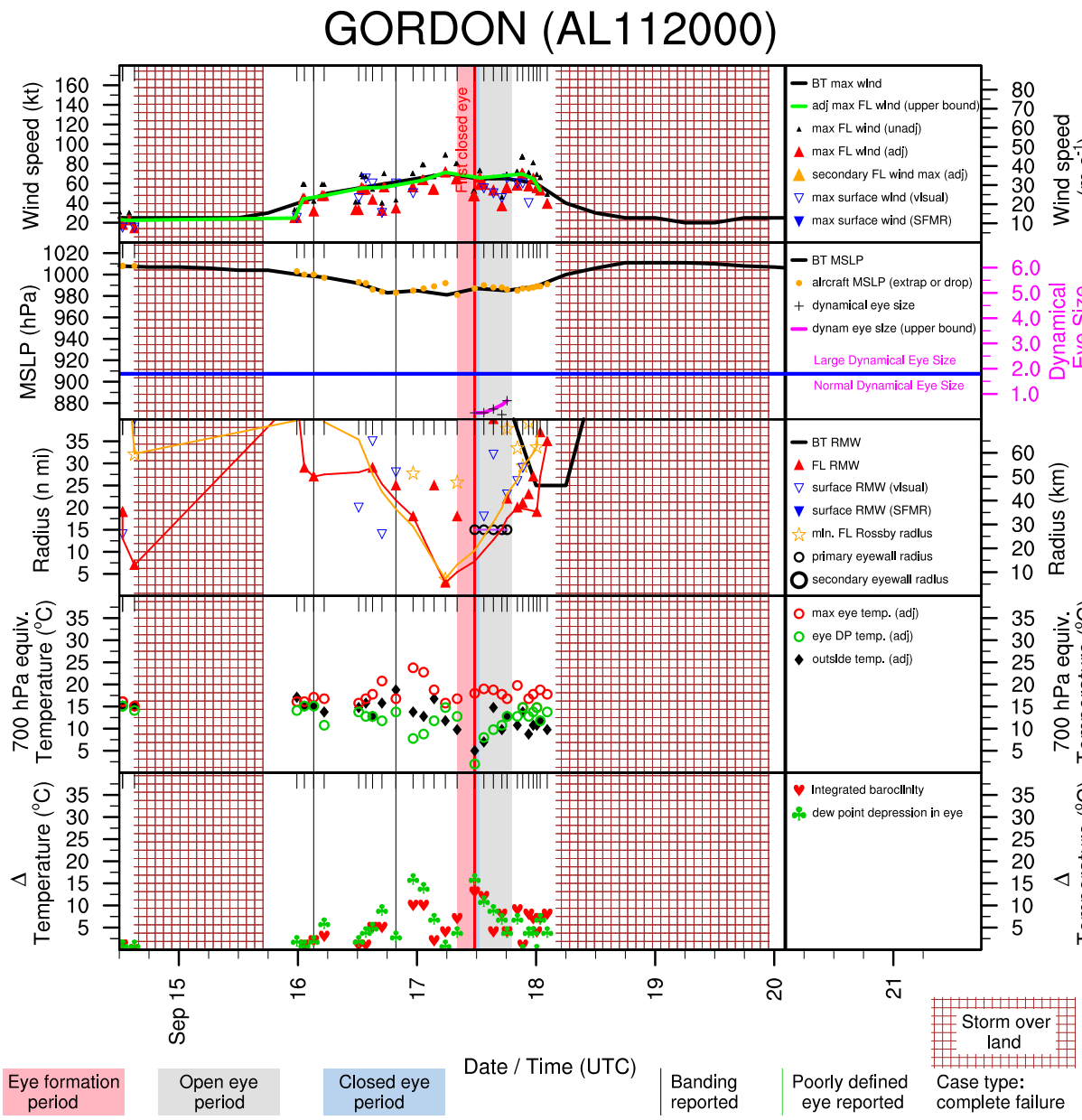

Figure E.93: Structure and intensity parameters for Hurricane Gordon (2000).

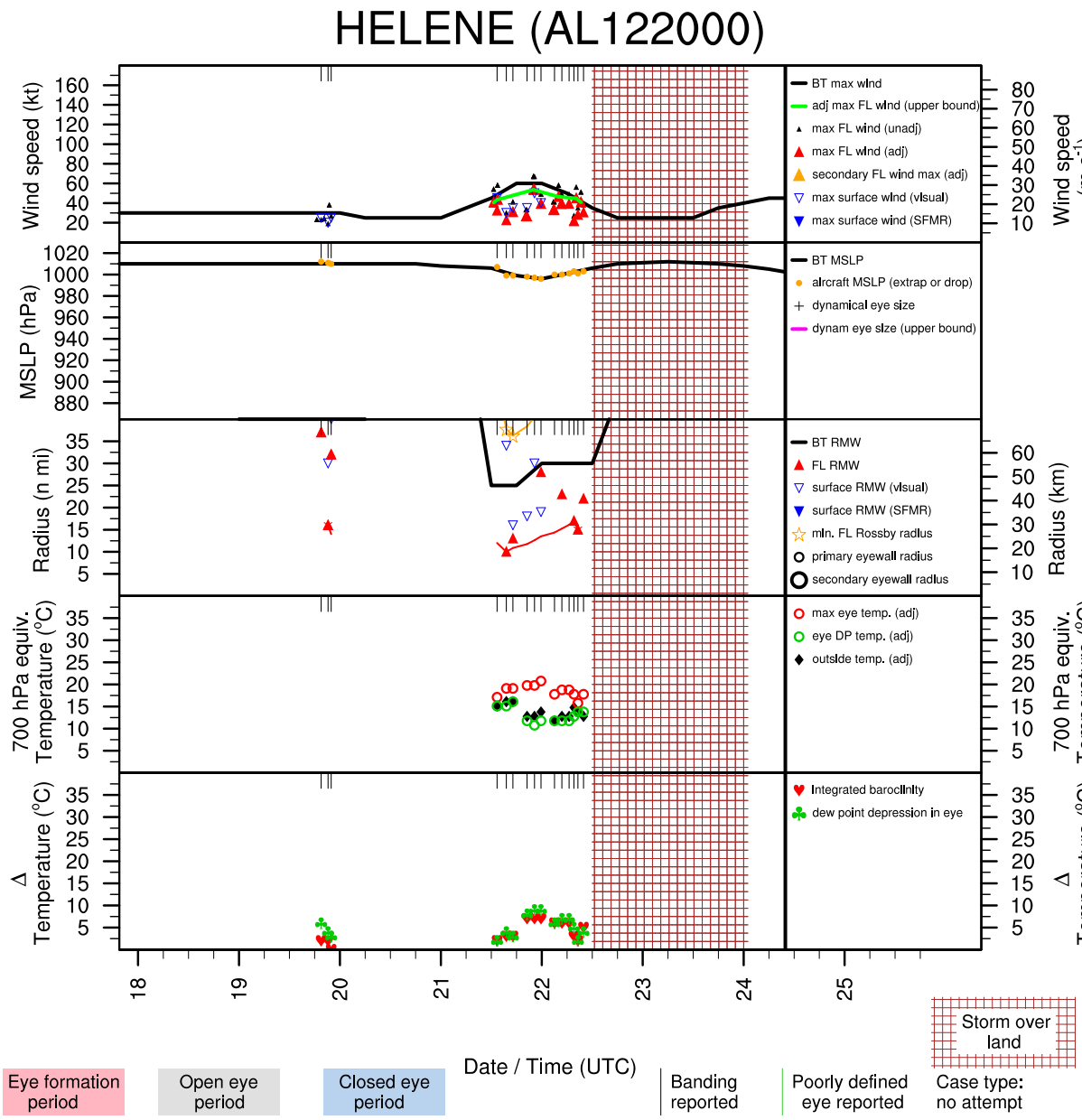

Figure E.94: Structure and intensity parameters for Tropical Storm Helene (2000).

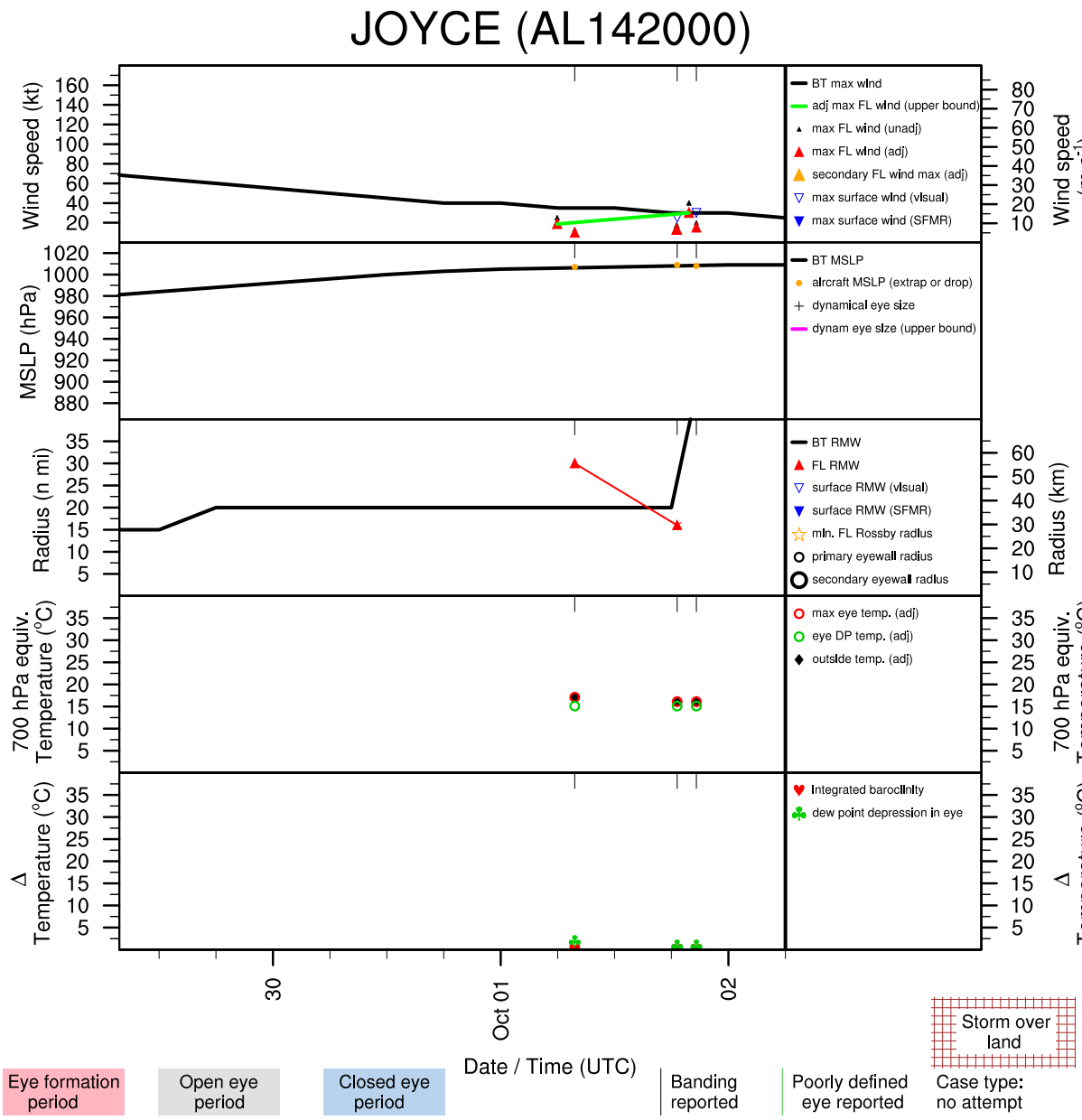

Figure E.95: Structure and intensity parameters for Hurricane Joyce (2000).

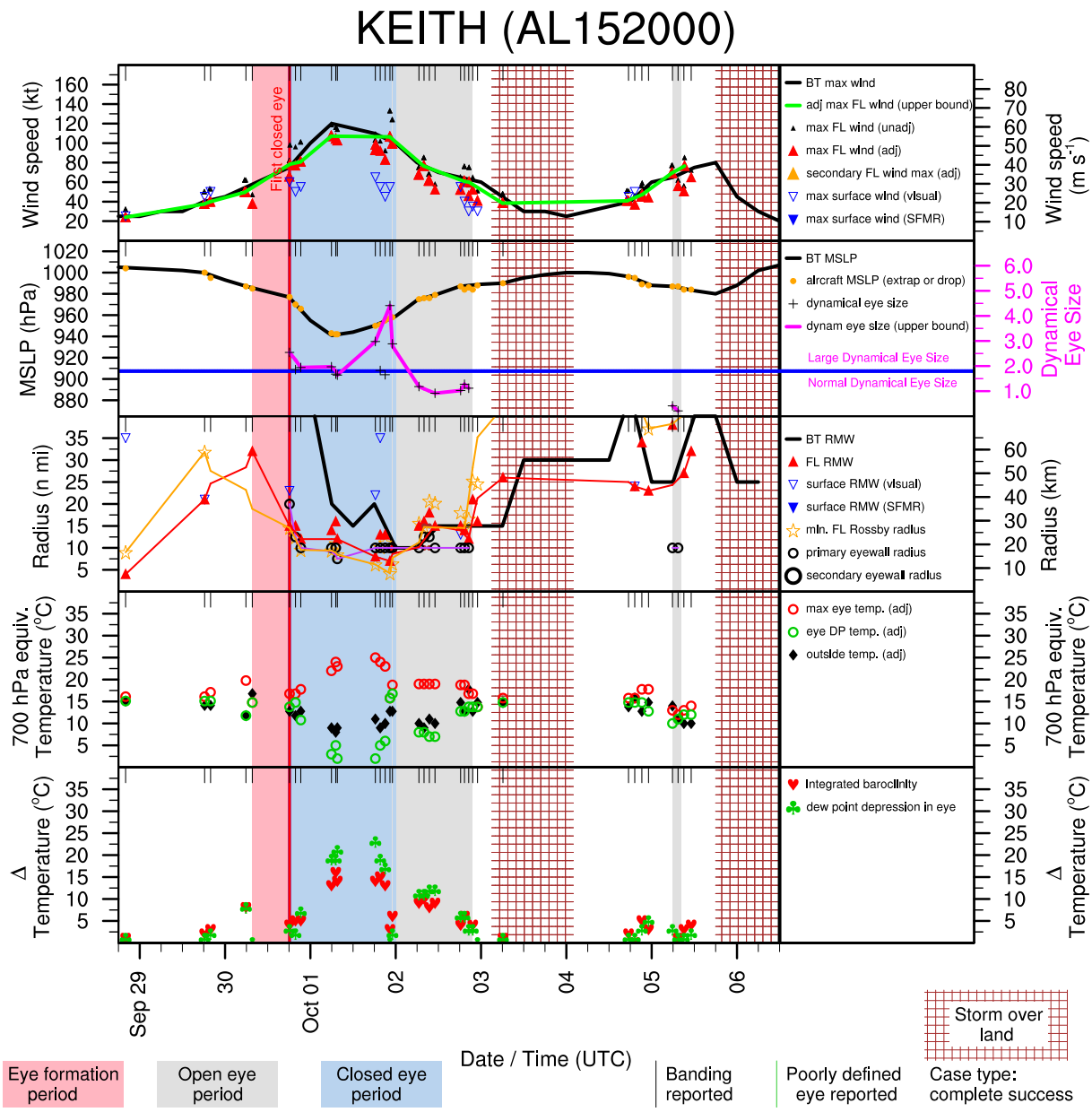

Figure E.96: Structure and intensity parameters for Hurricane Keith (2000).

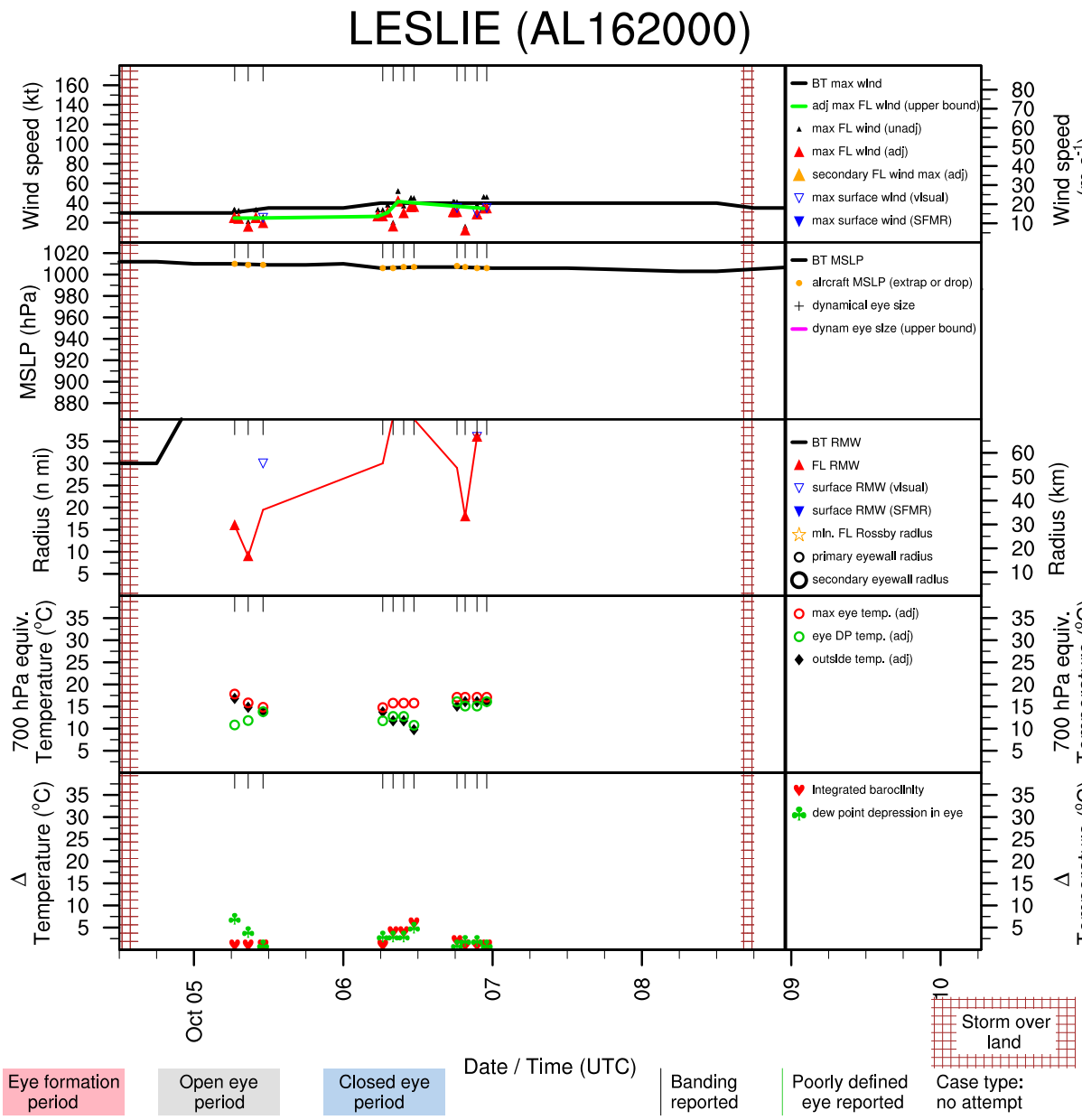

Figure E.97: Structure and intensity parameters for Tropical Storm Leslie (2000).

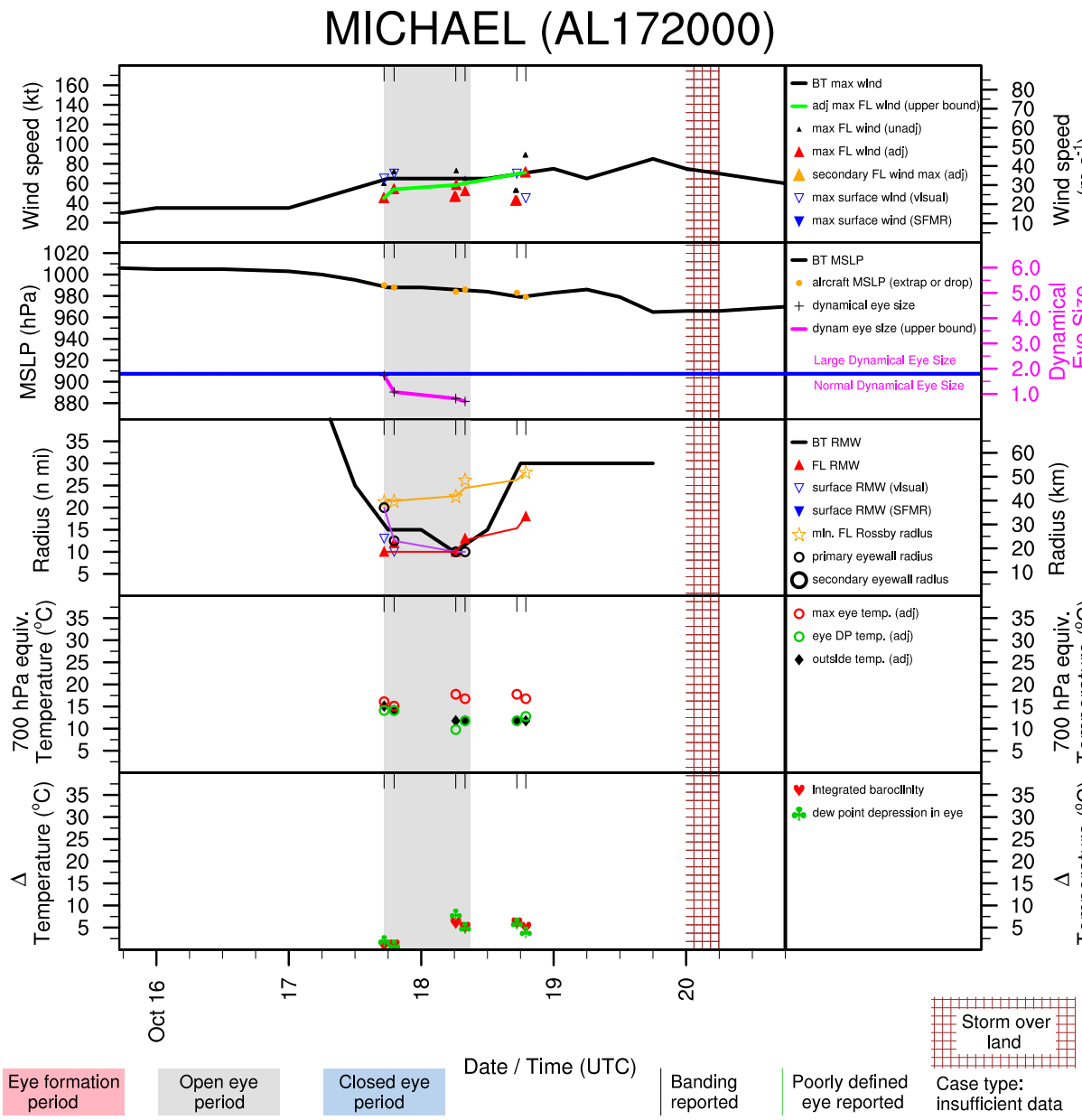

Figure E.98: Structure and intensity parameters for Hurricane Michael (2000).

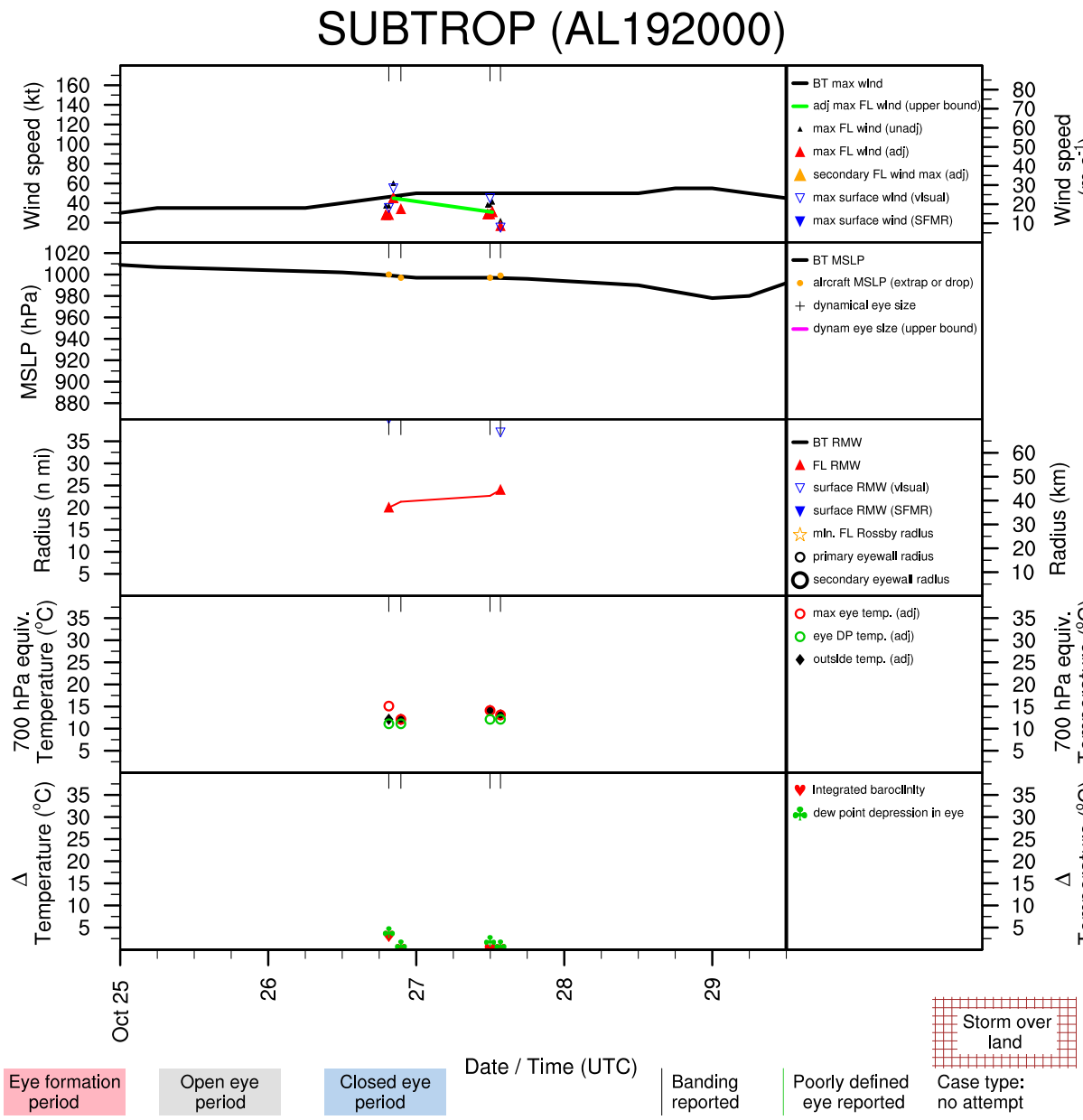

Figure E.99: Structure and intensity parameters for Tropical Storm Subtrop (2000).

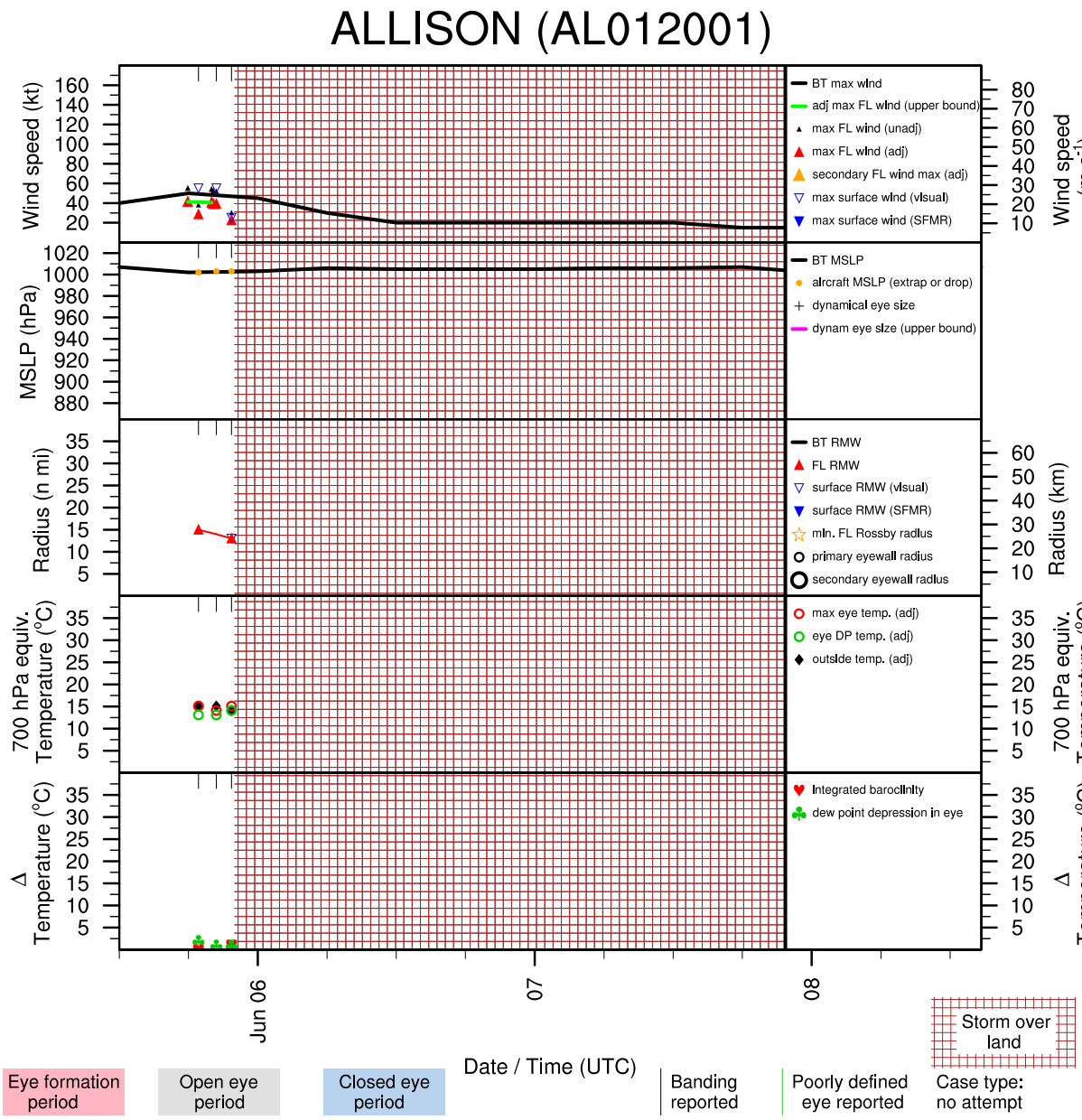

Figure E.100: Structure and intensity parameters for Tropical Storm Allison (2001).

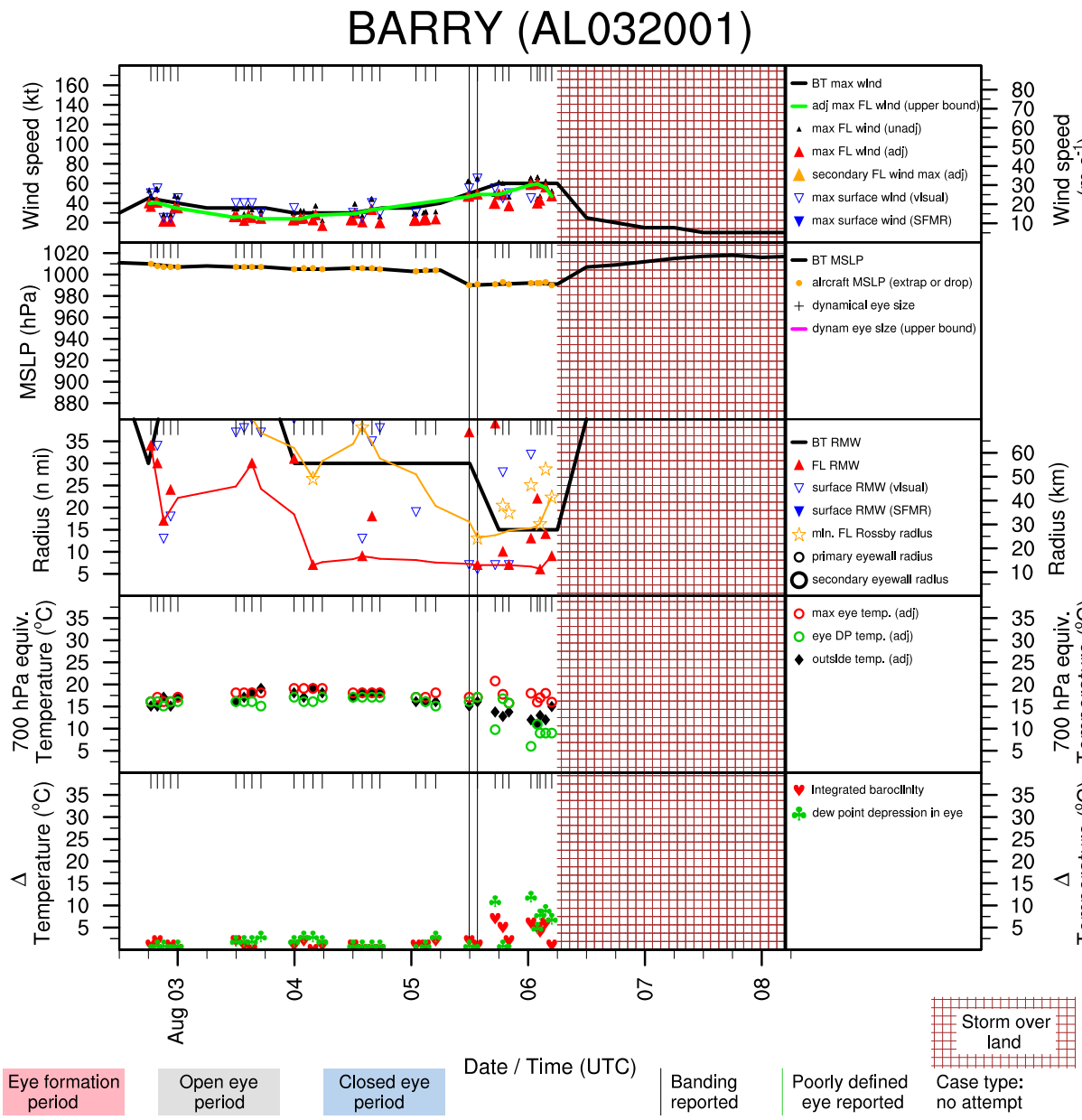

Figure E.101: Structure and intensity parameters for Tropical Storm Barry (2001).

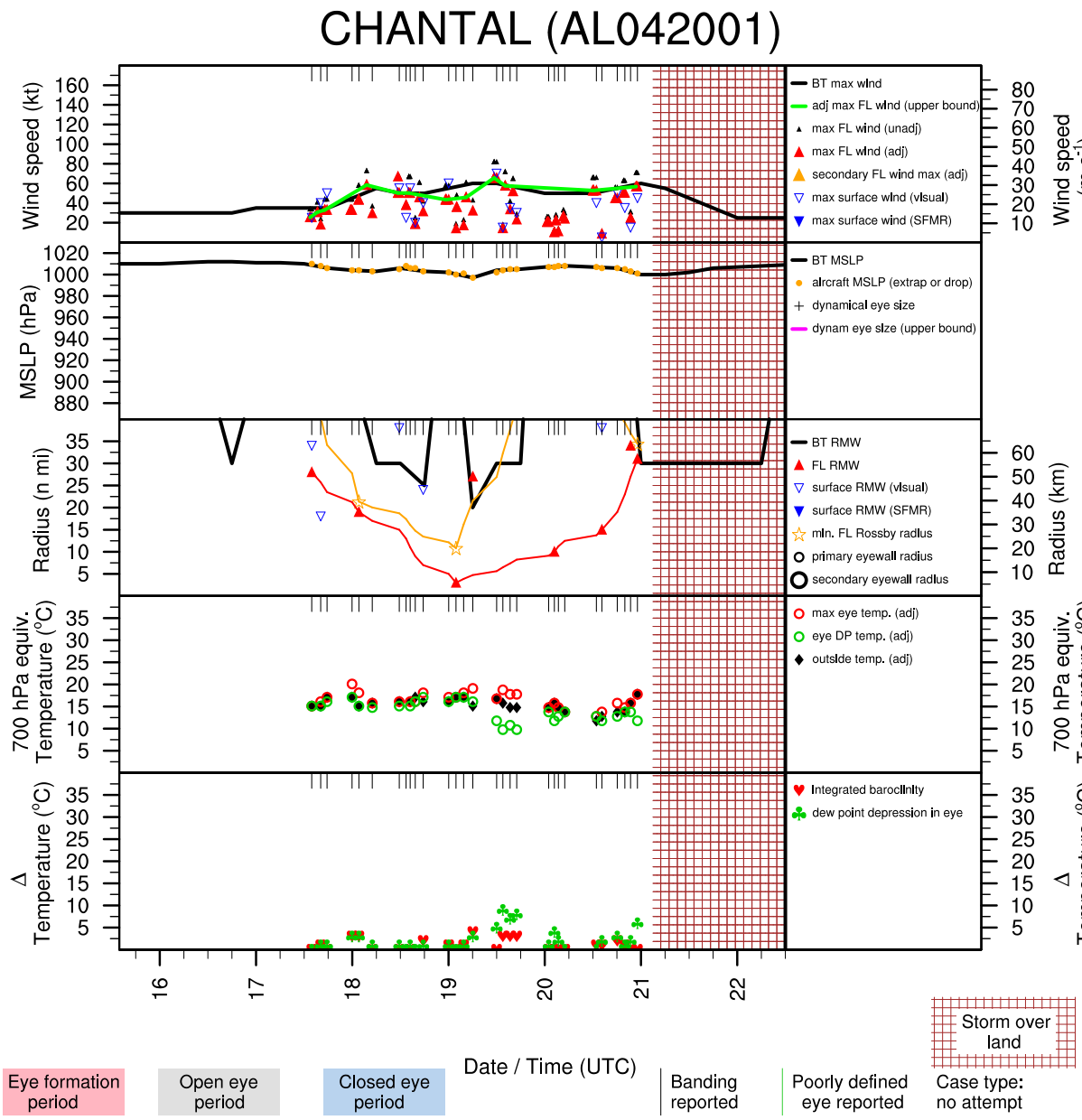

Figure E.102: Structure and intensity parameters for Tropical Storm Chantal (2001).

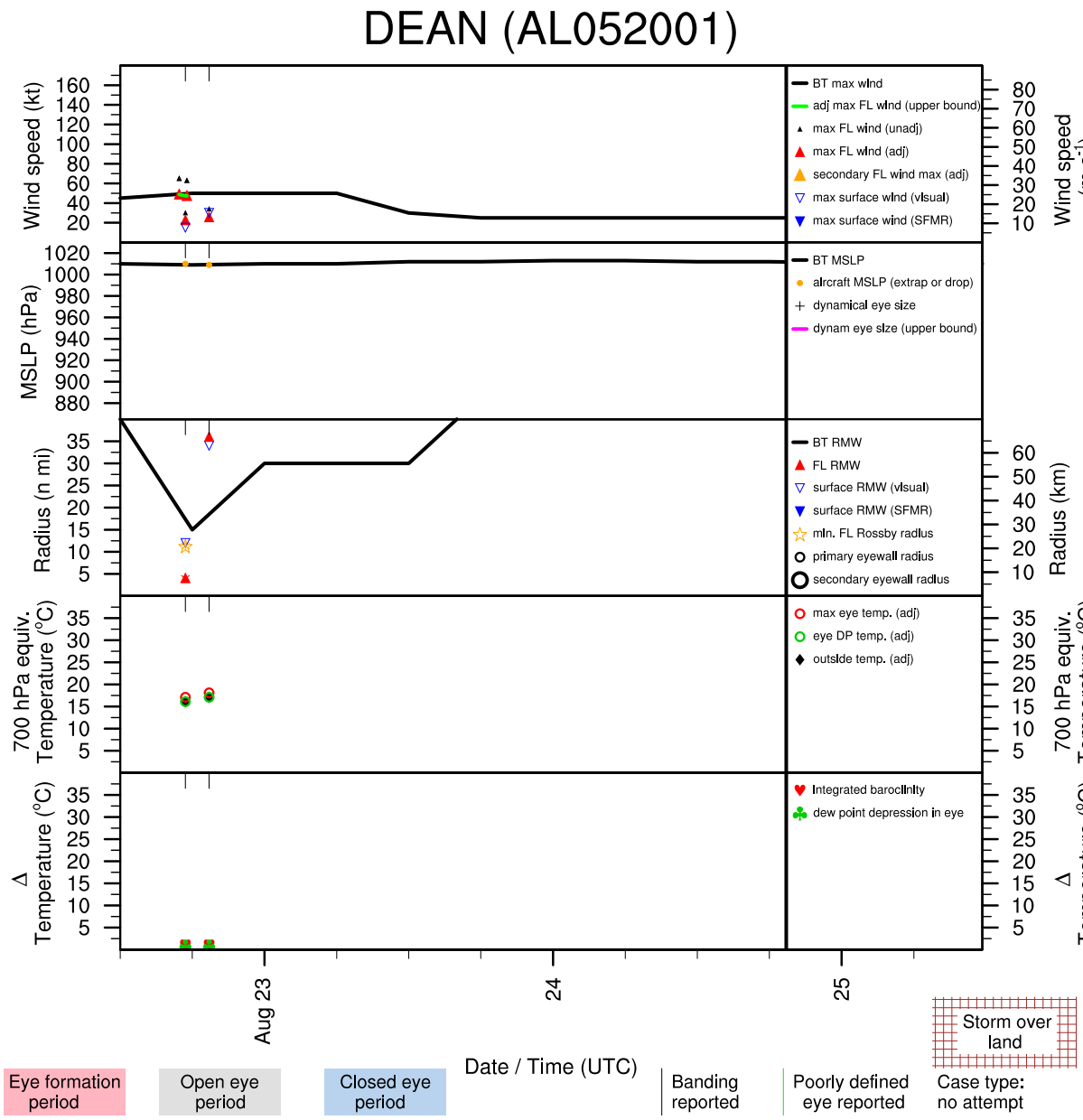

Figure E.103: Structure and intensity parameters for Tropical Storm Dean (2001).

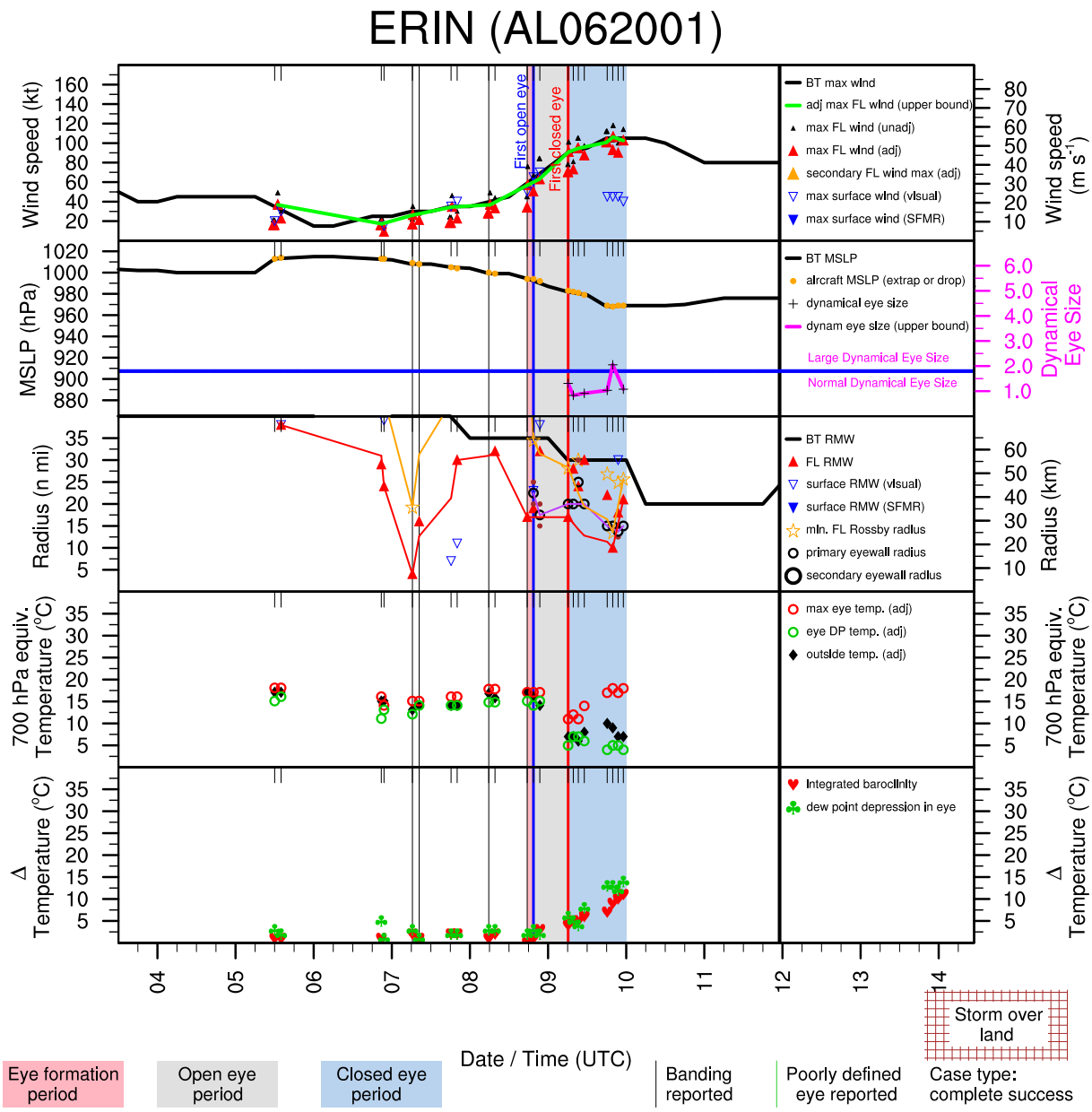

Figure E.104: Structure and intensity parameters for Hurricane Erin (2001).

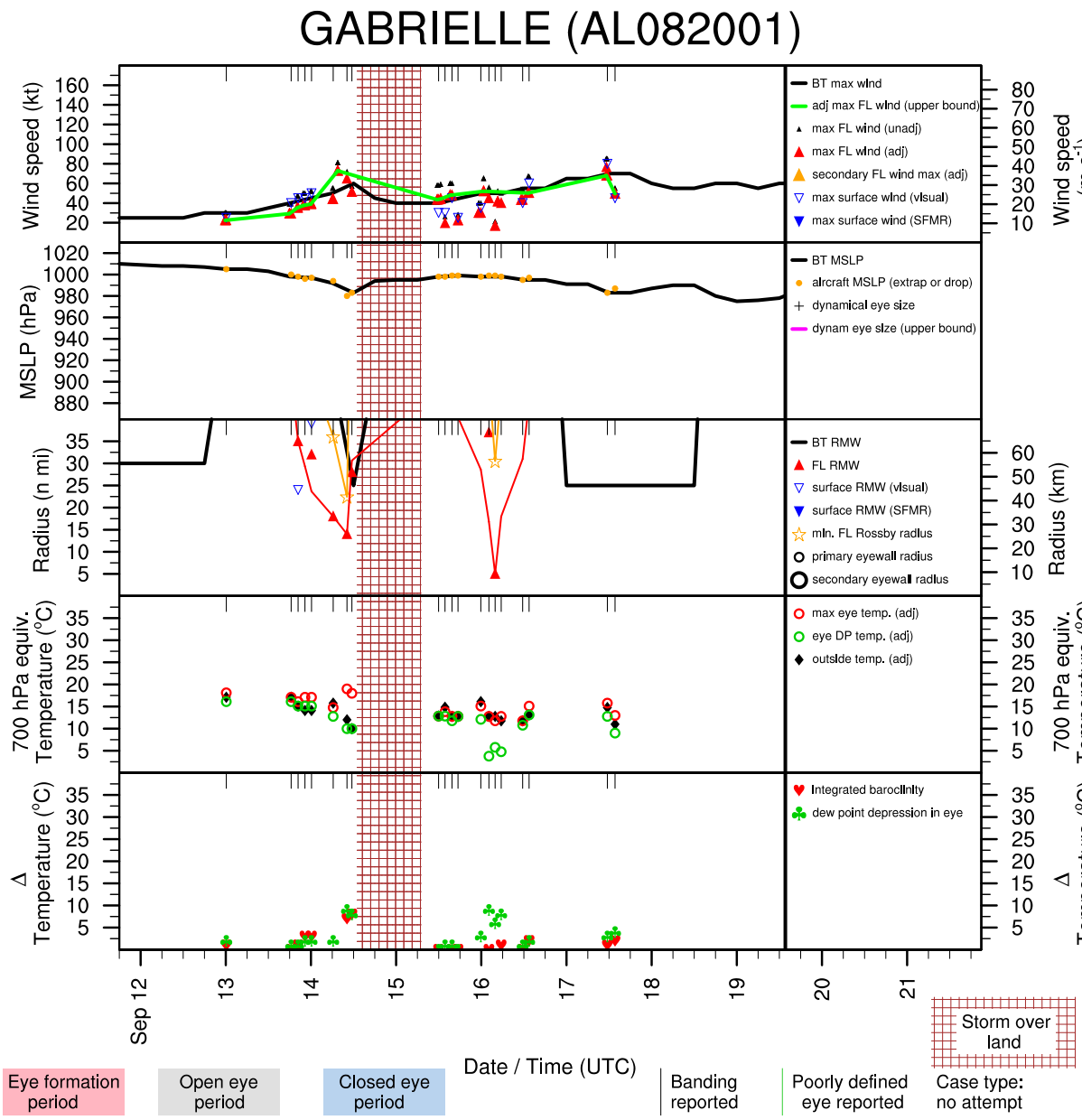

Figure E.105: Structure and intensity parameters for Hurricane Gabrielle (2001).

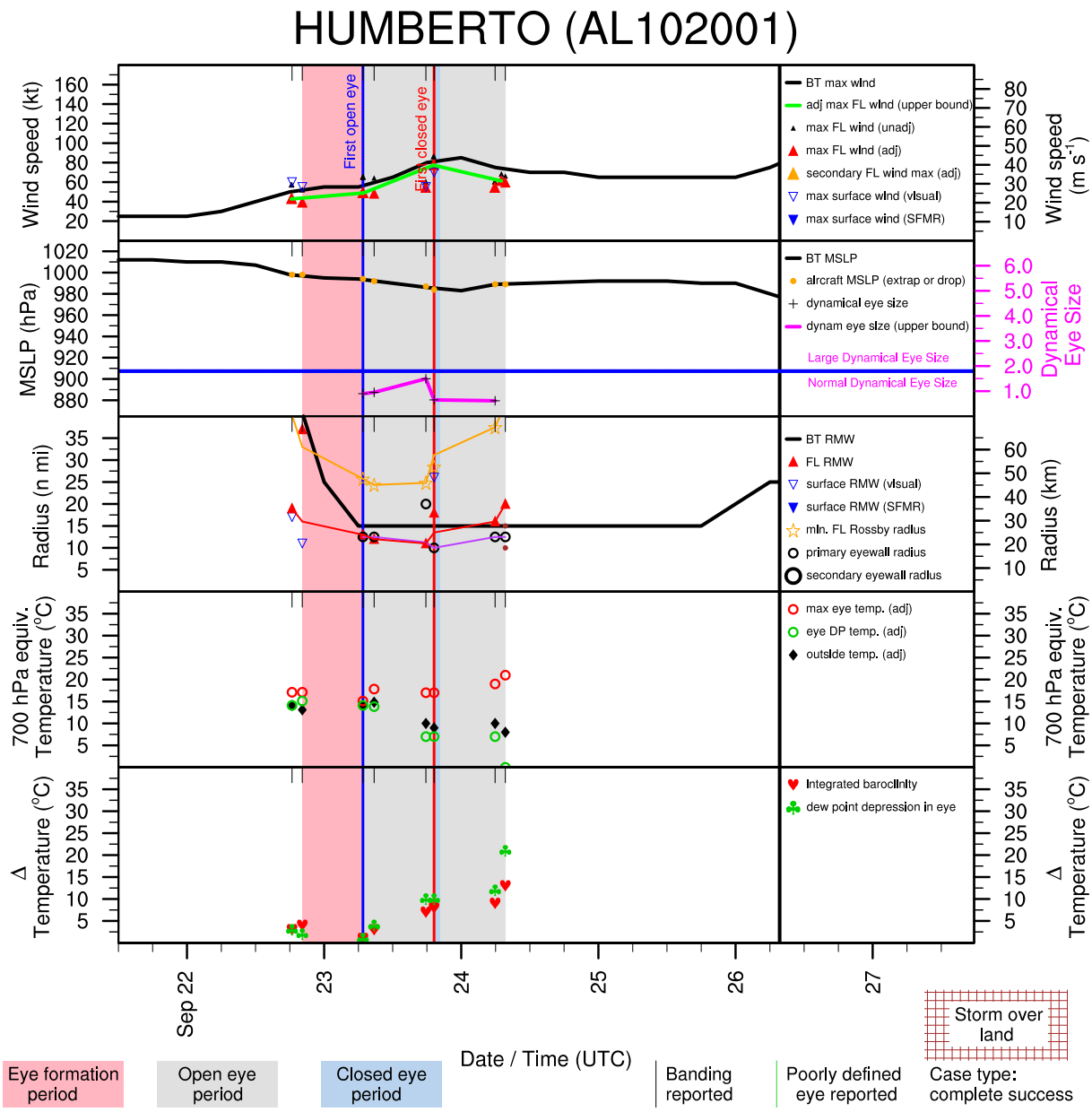

Figure E.106: Structure and intensity parameters for Hurricane Humberto (2001).

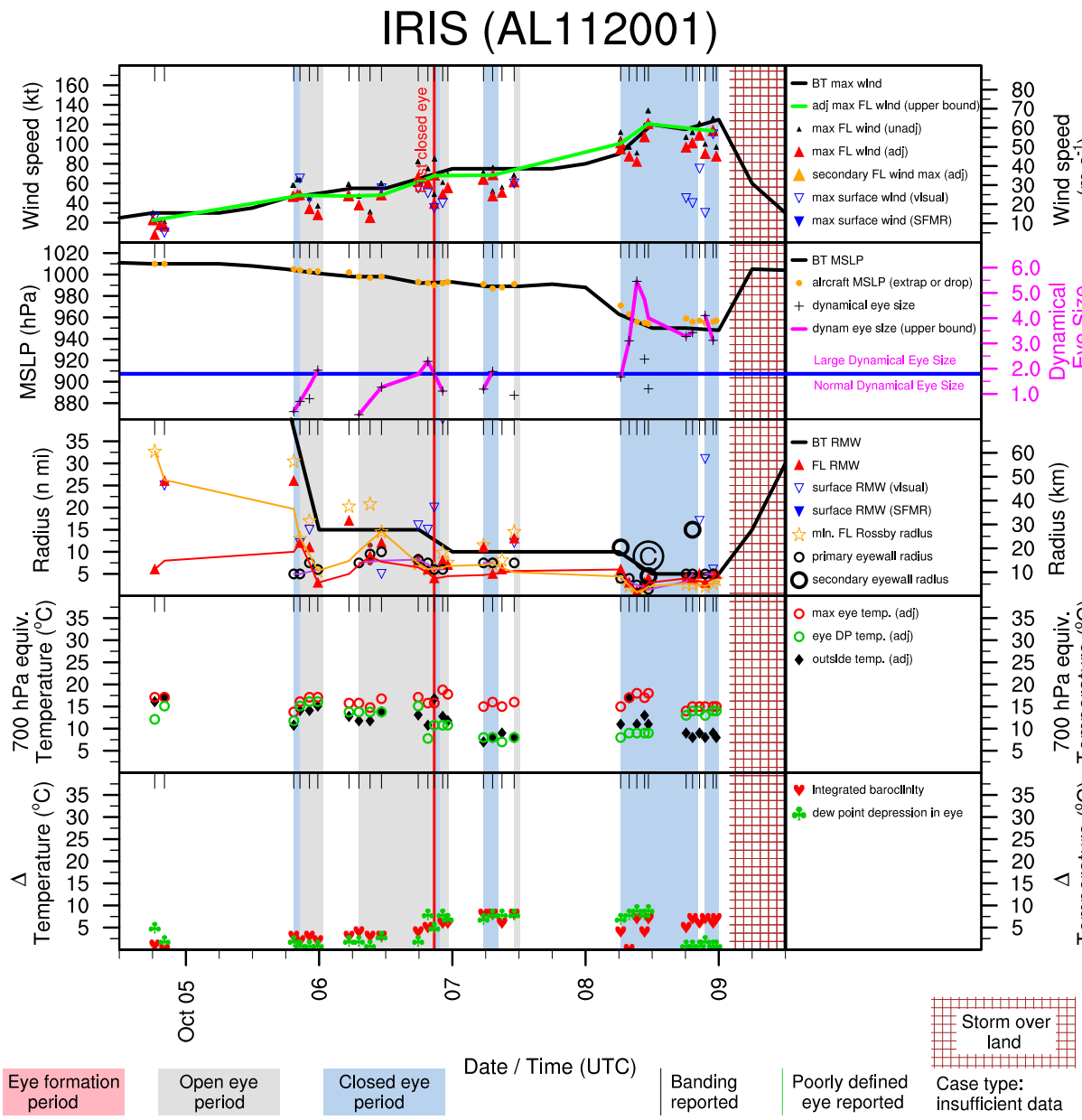

Figure E.107: Structure and intensity parameters for Hurricane Iris (2001).

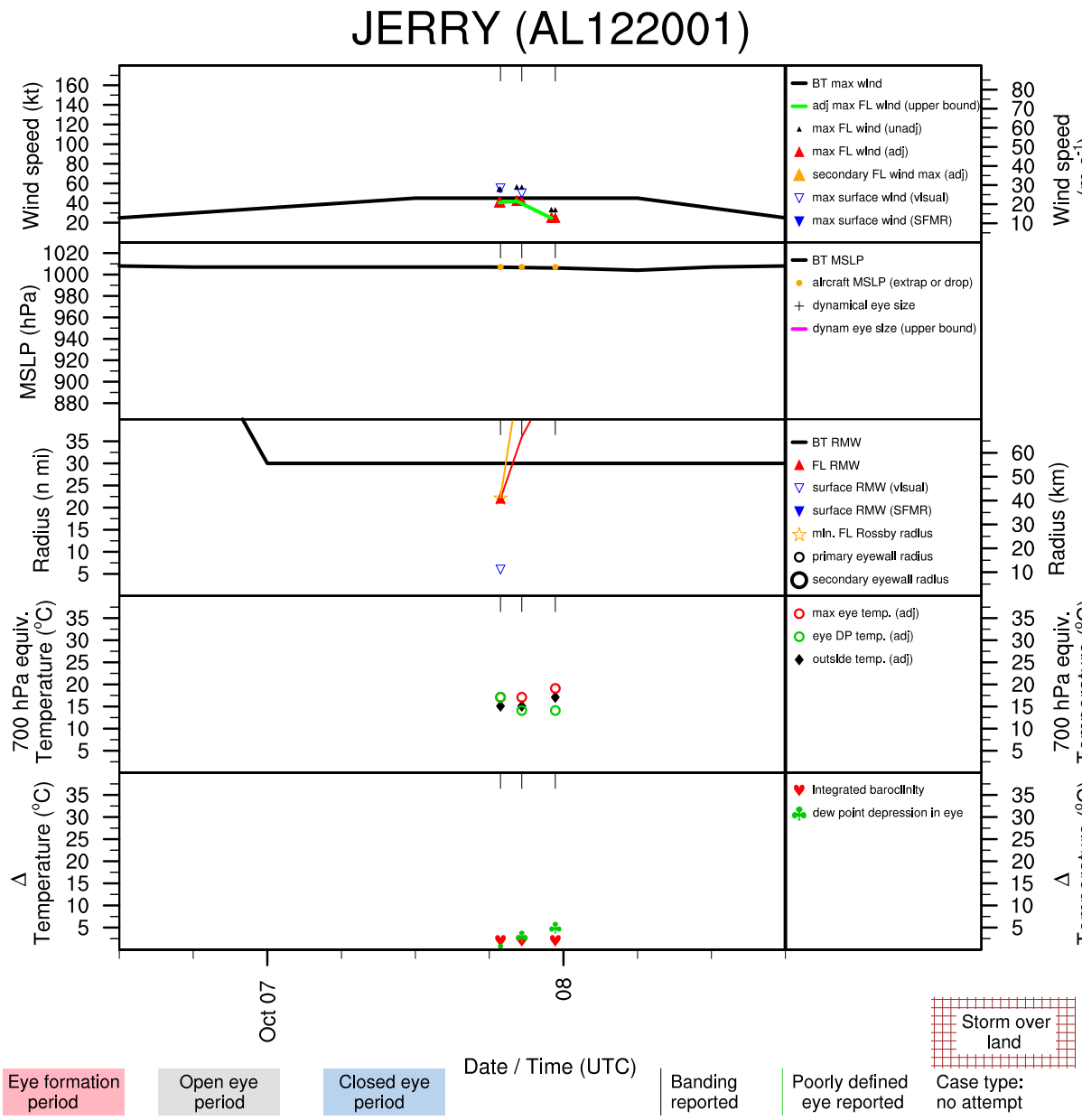

Figure E.108: Structure and intensity parameters for Tropical Storm Jerry (2001).

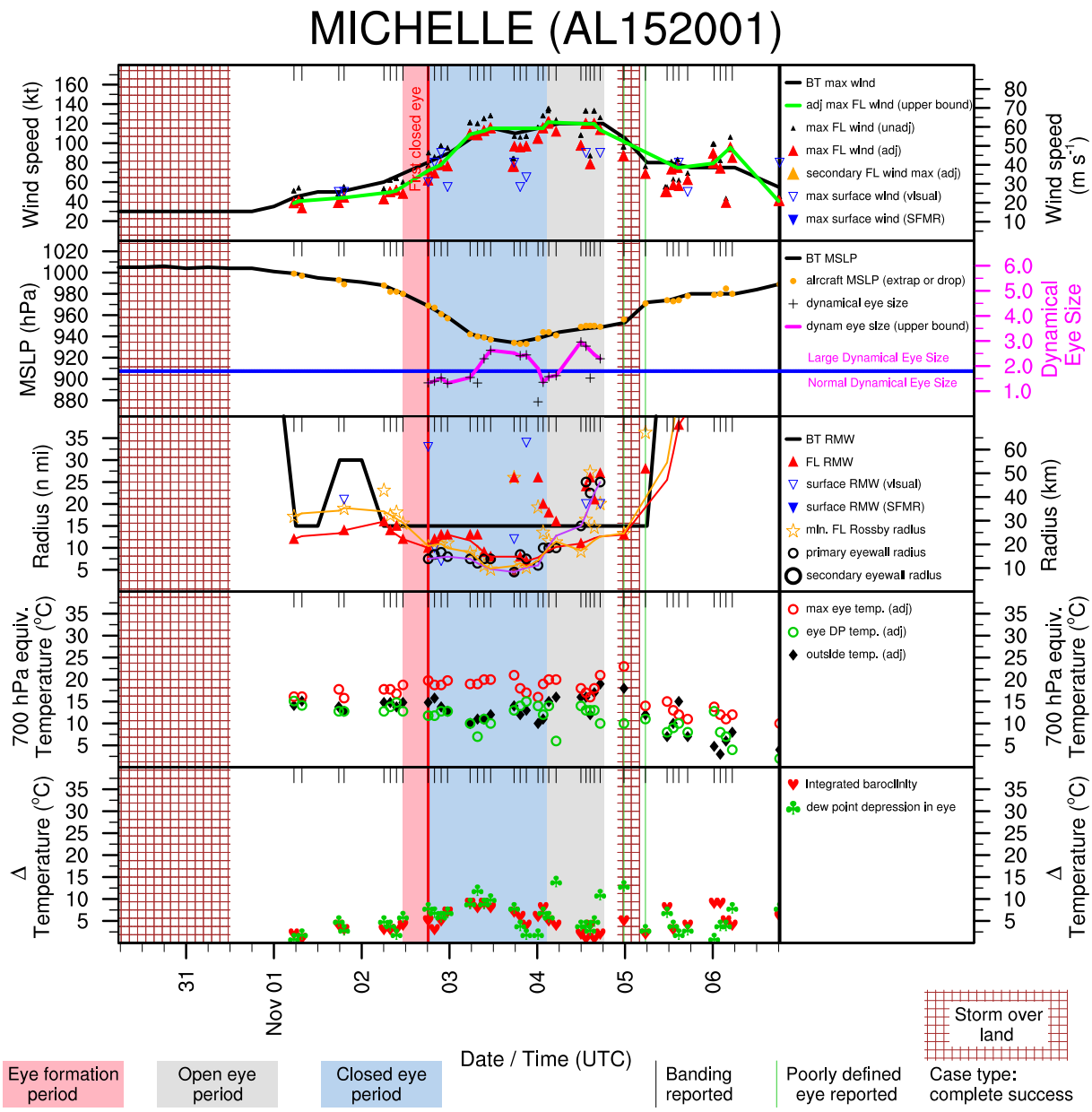

Figure E.109: Structure and intensity parameters for Hurricane Michelle (2001).

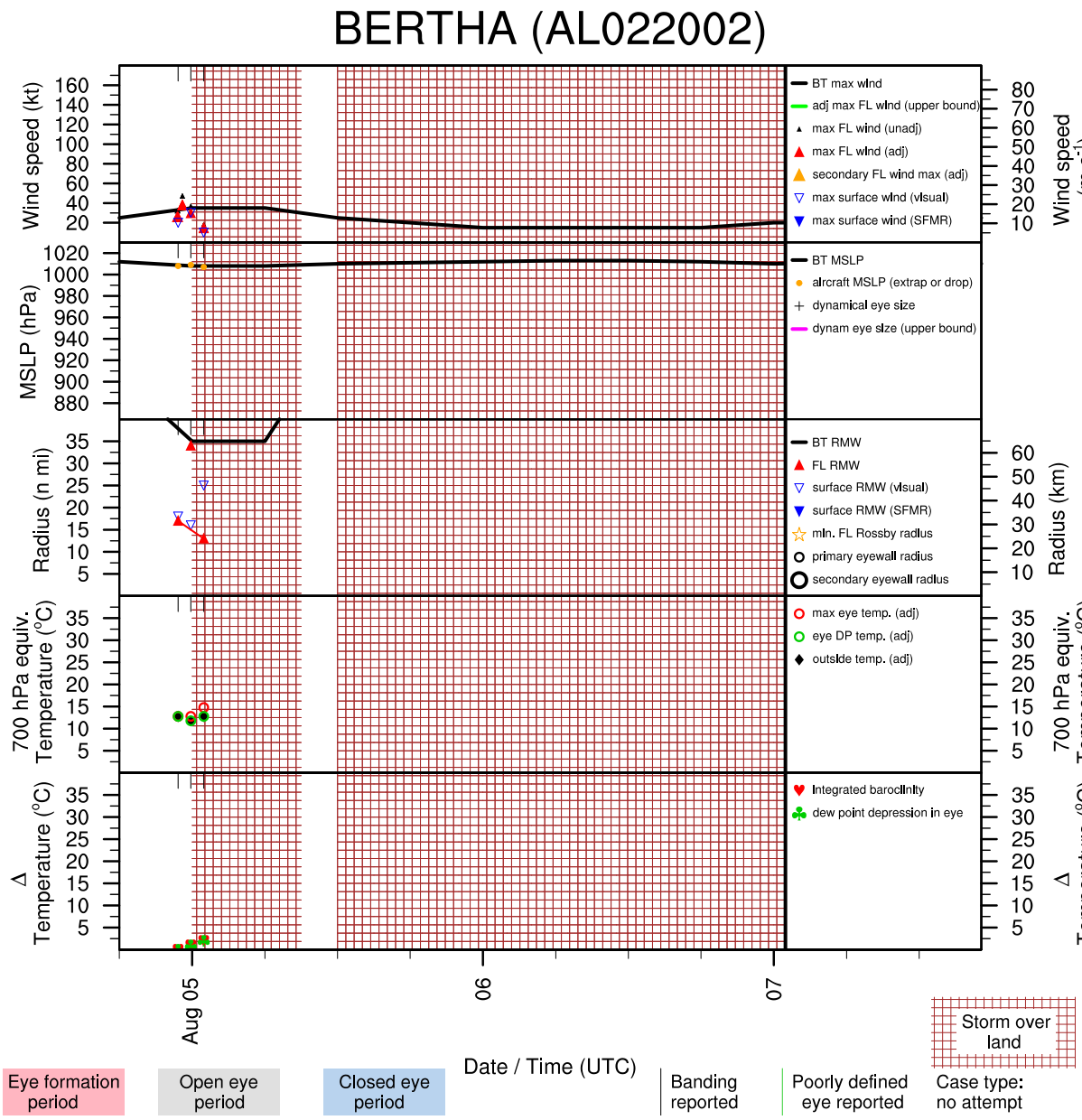

Figure E.110: Structure and intensity parameters for Tropical Storm Bertha (2002).

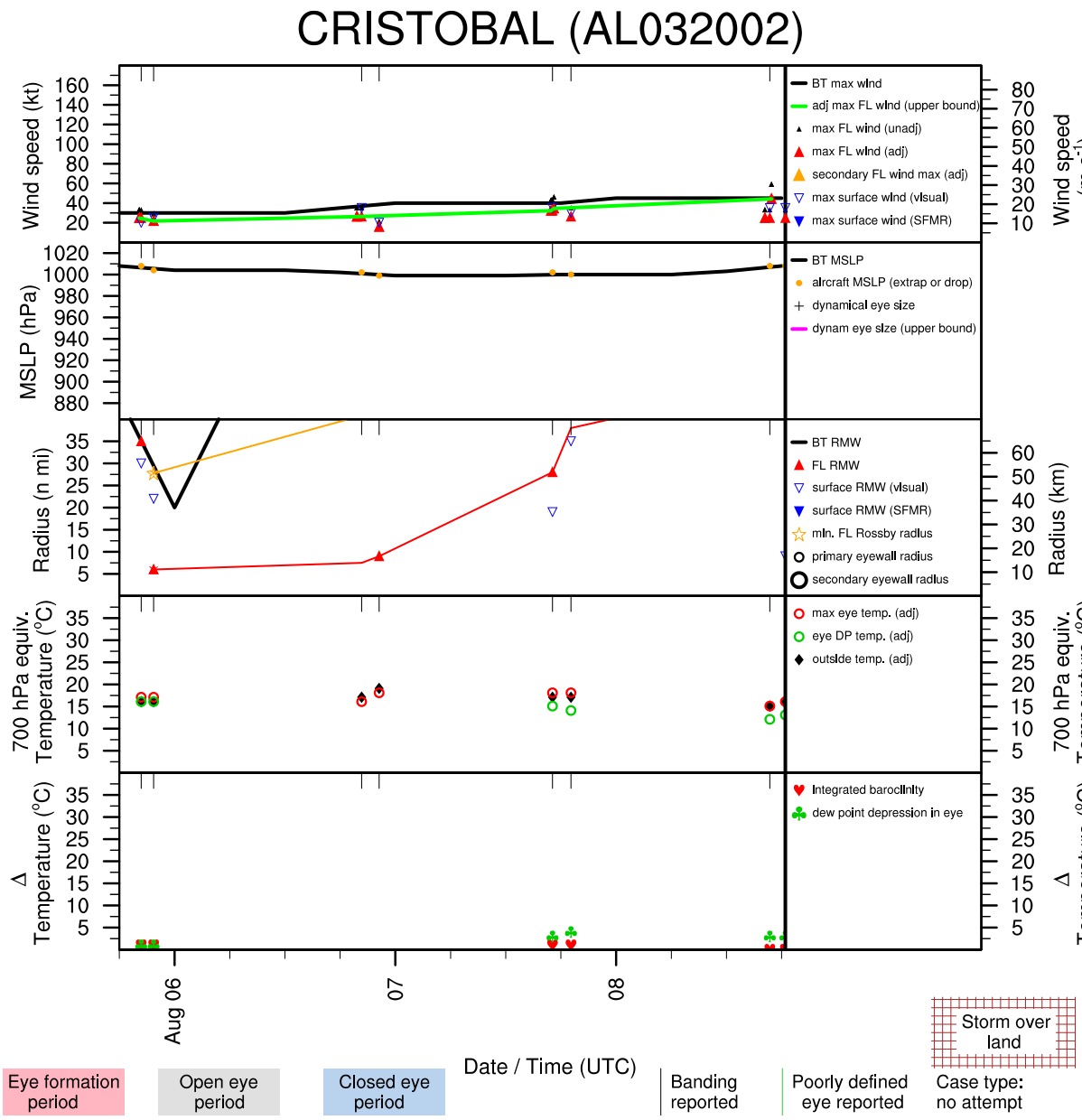

Figure E.111: Structure and intensity parameters for Tropical Storm Cristobal (2002).

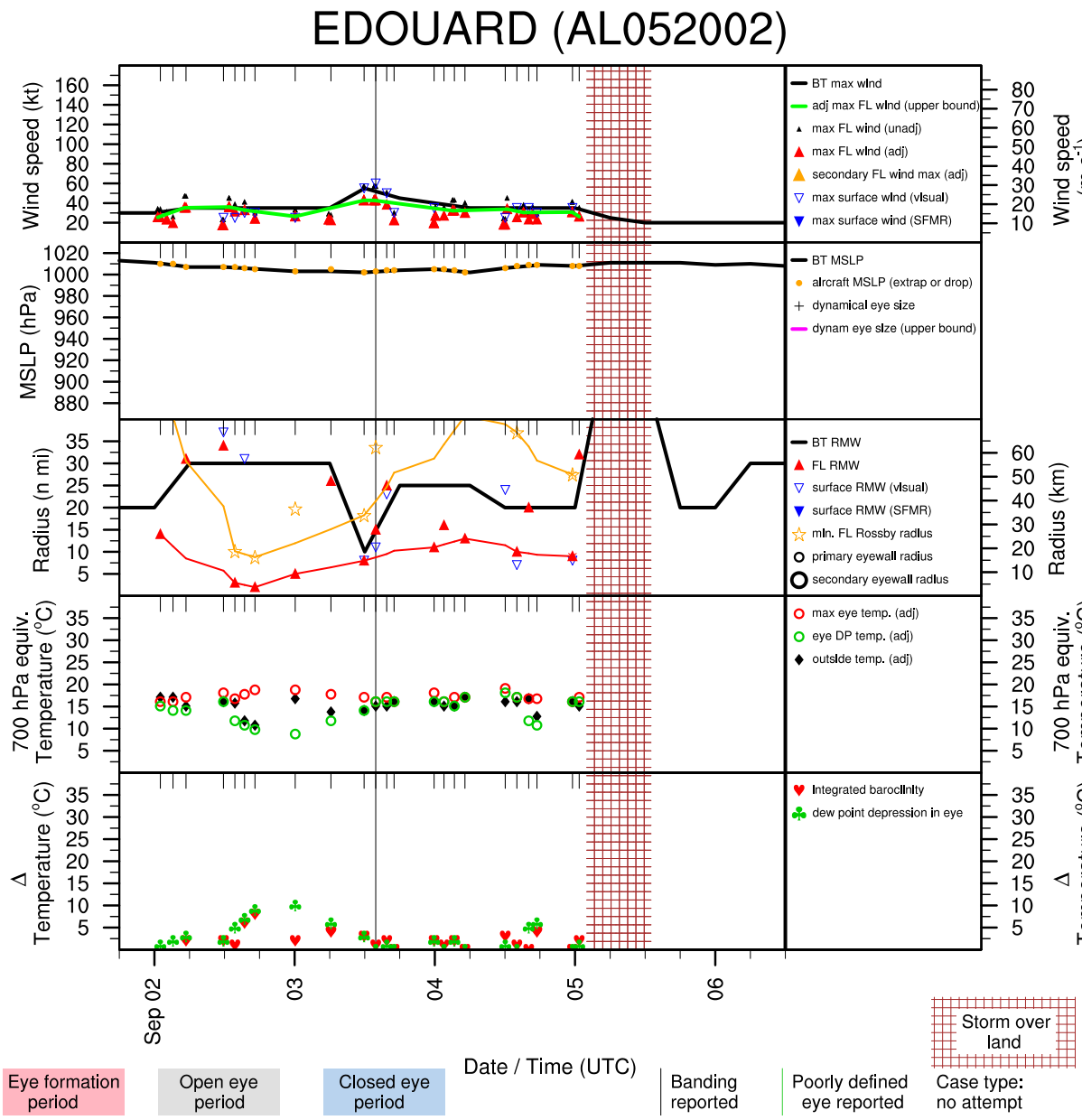

Figure E.112: Structure and intensity parameters for Tropical Storm Edouard (2002).

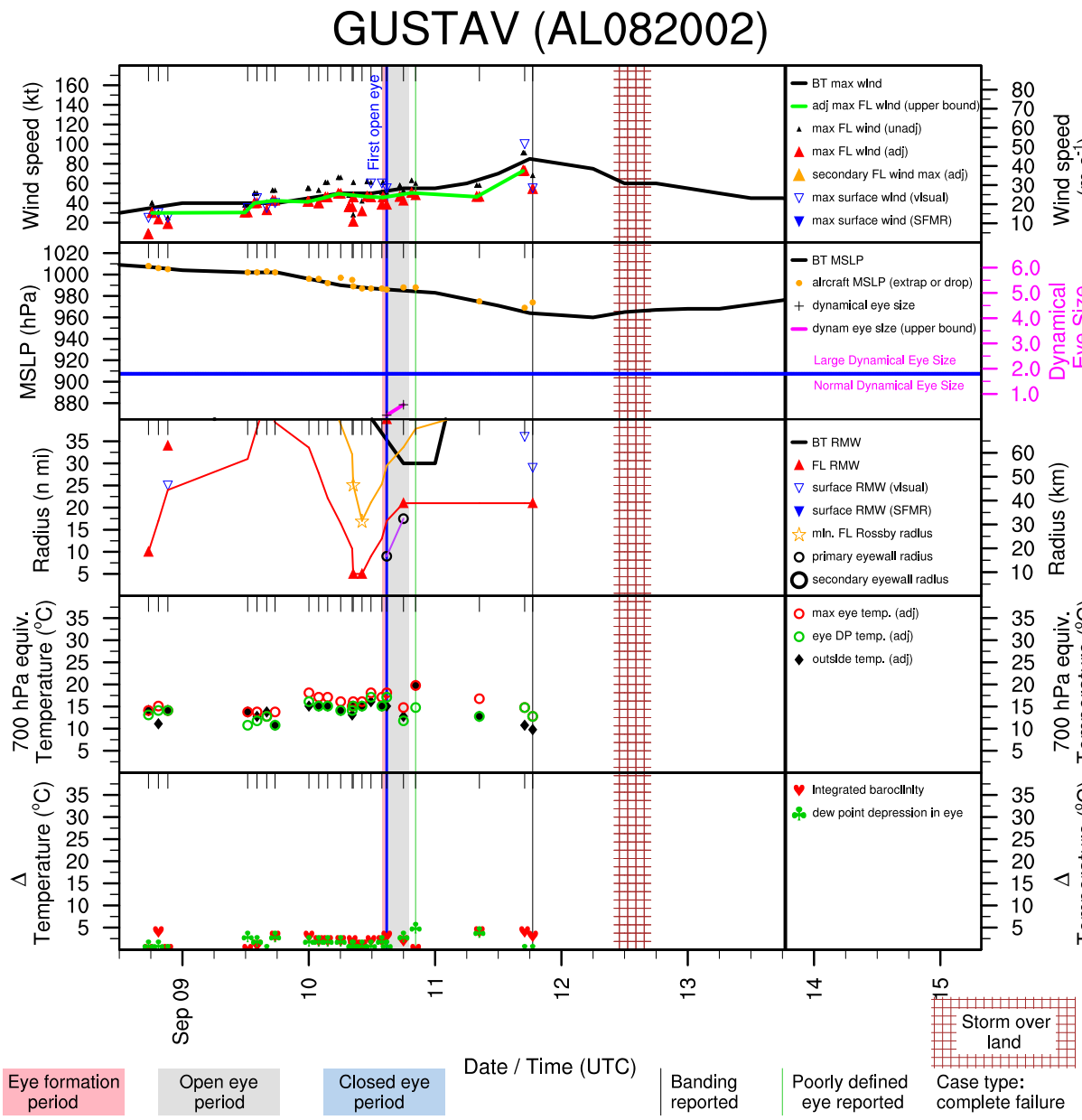

Figure E.113: Structure and intensity parameters for Hurricane Gustav (2002).

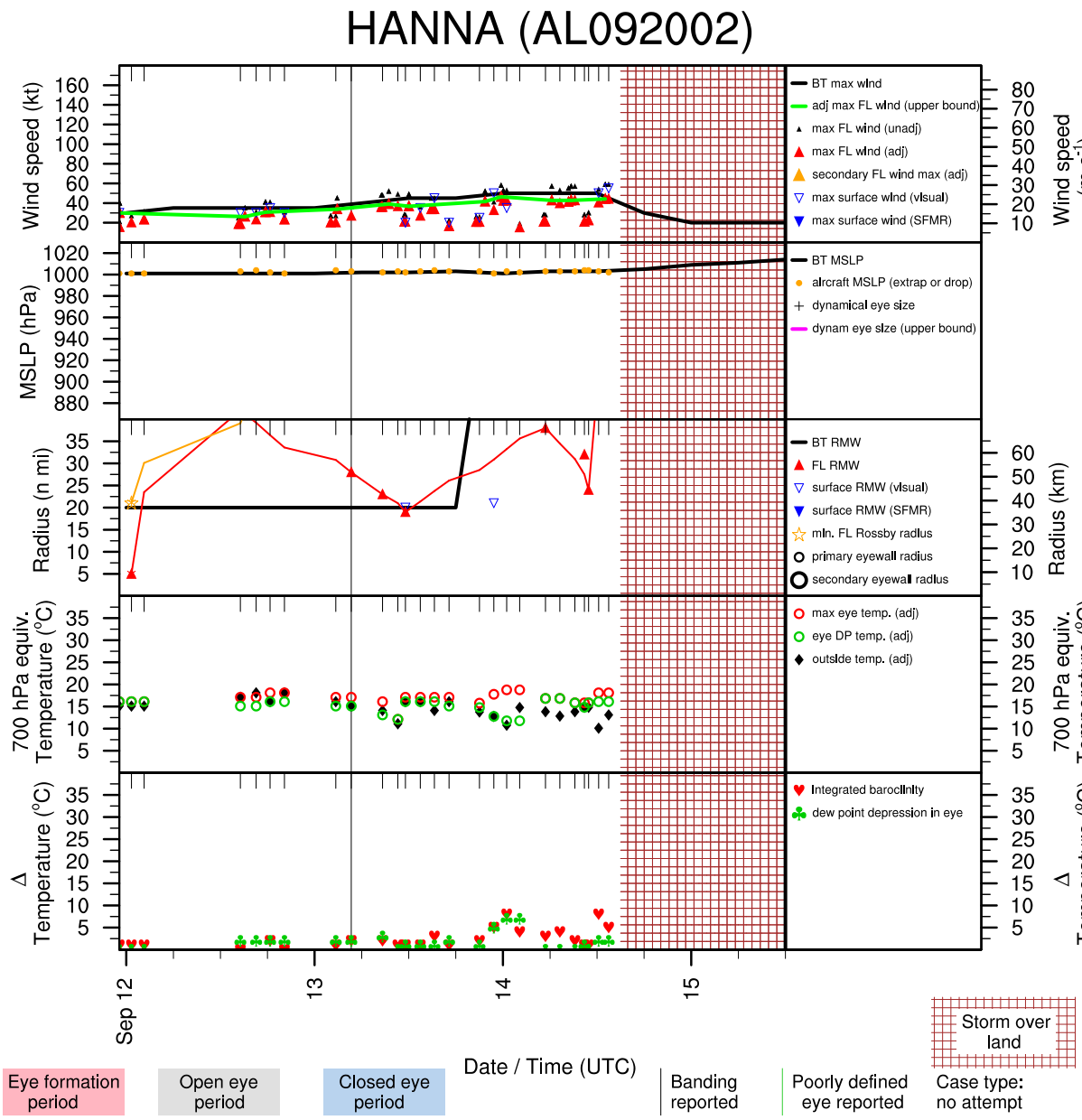

Figure E.114: Structure and intensity parameters for Tropical Storm Hanna (2002).

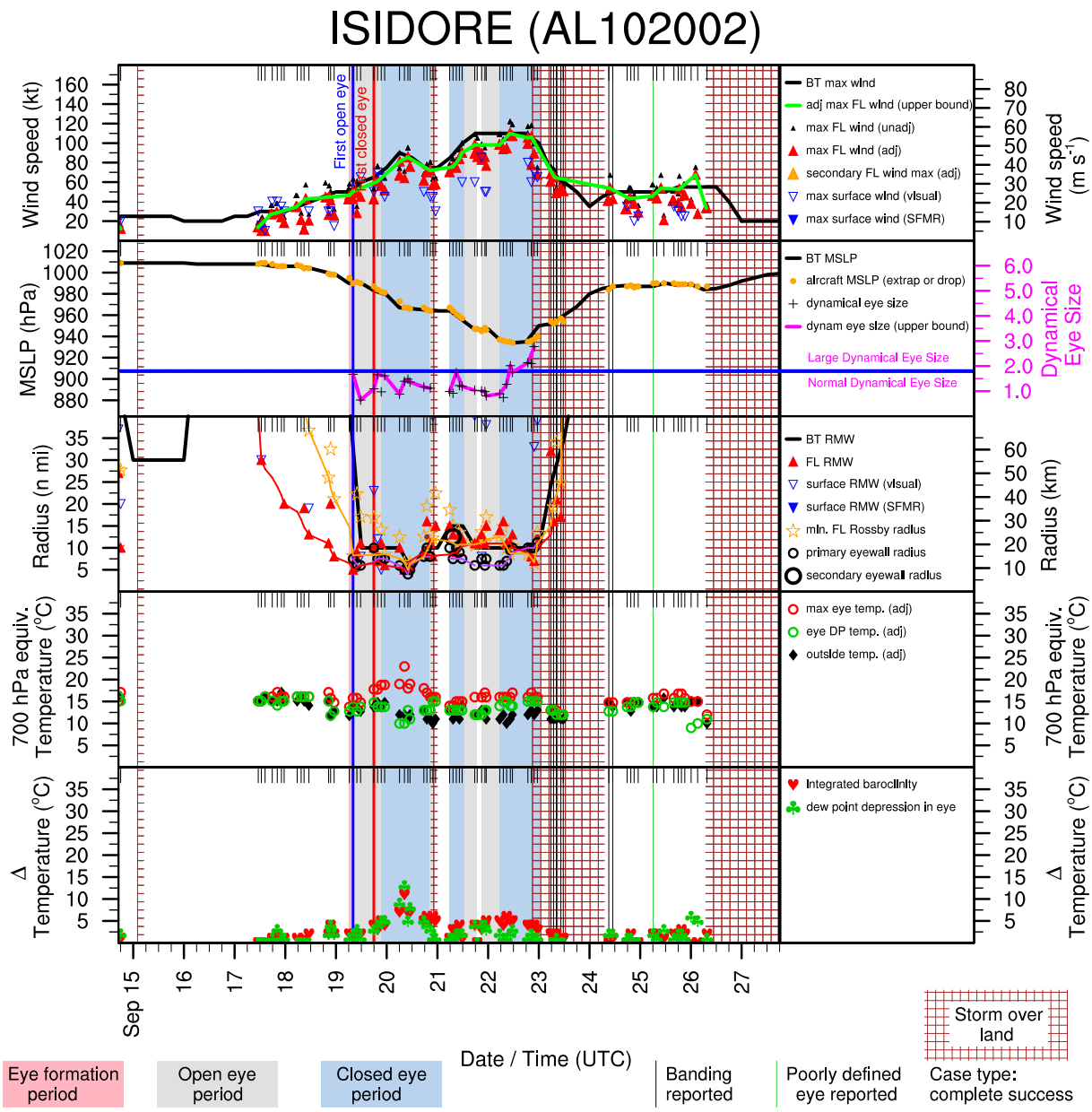

Figure E.115: Structure and intensity parameters for Hurricane Isidore (2002).

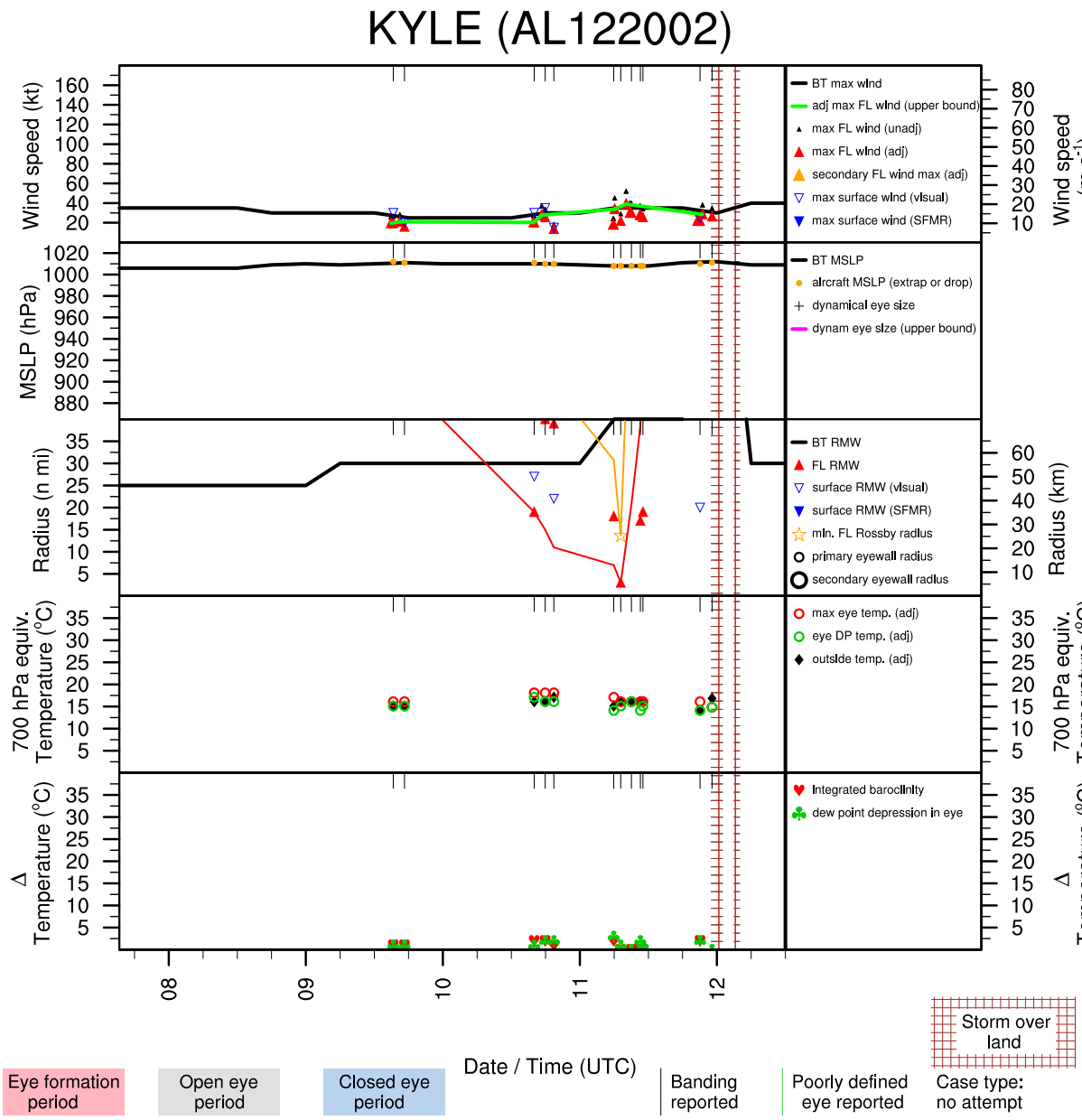

Figure E.116: Structure and intensity parameters for Hurricane Kyle (2002).

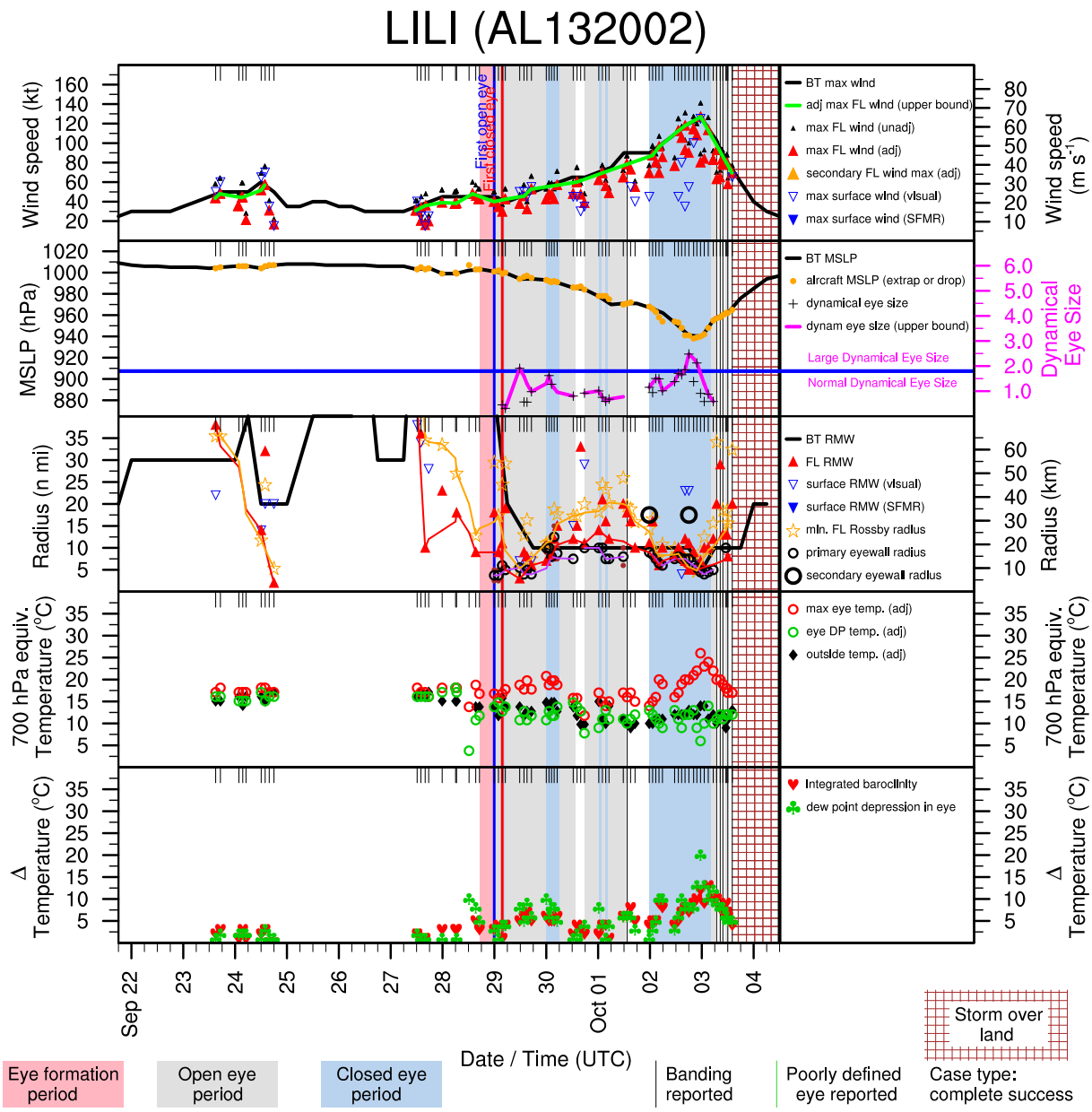

Figure E.117: Structure and intensity parameters for Hurricane Lili (2002).

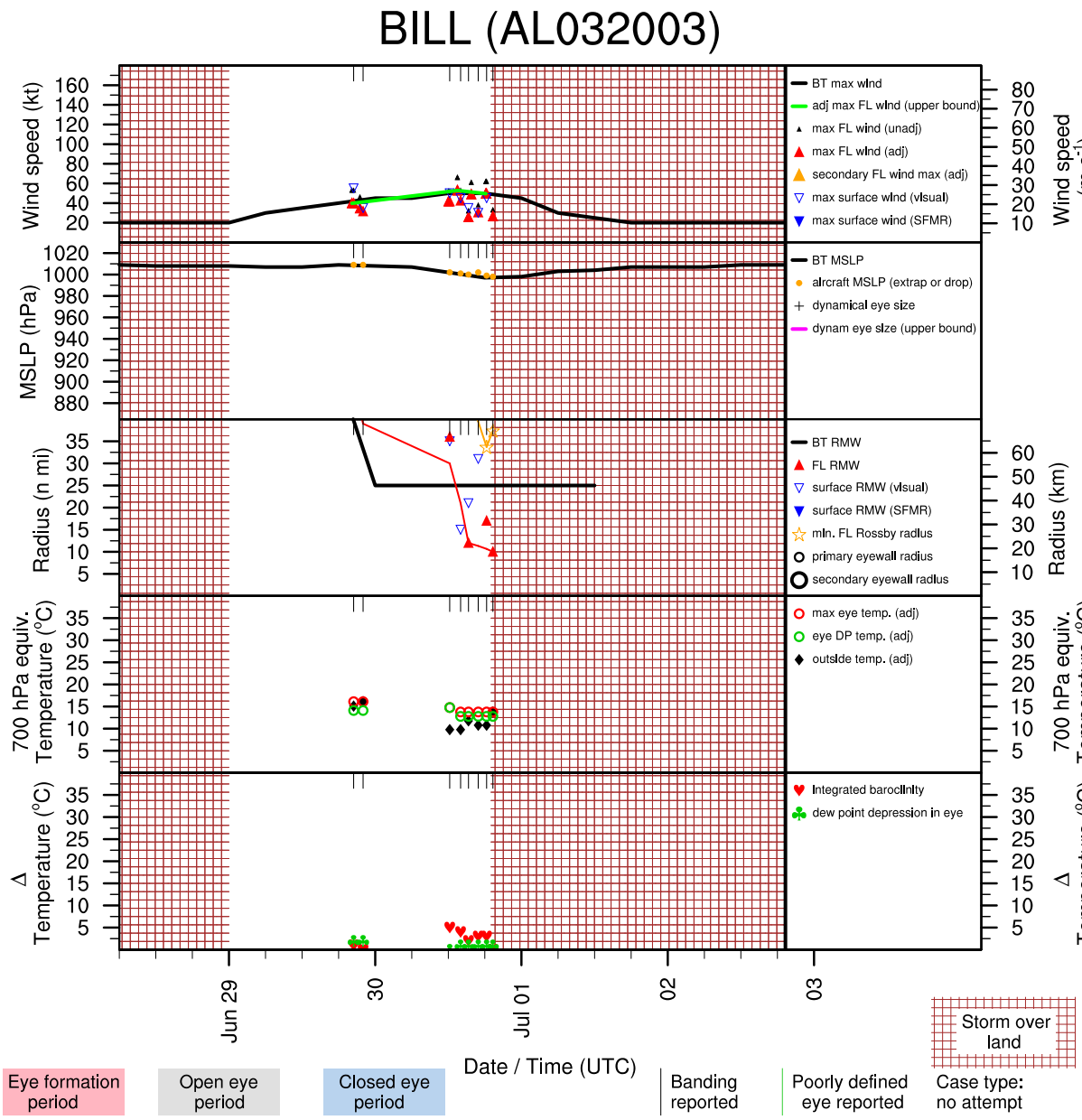

Figure E.118: Structure and intensity parameters for Tropical Storm Bill (2003).

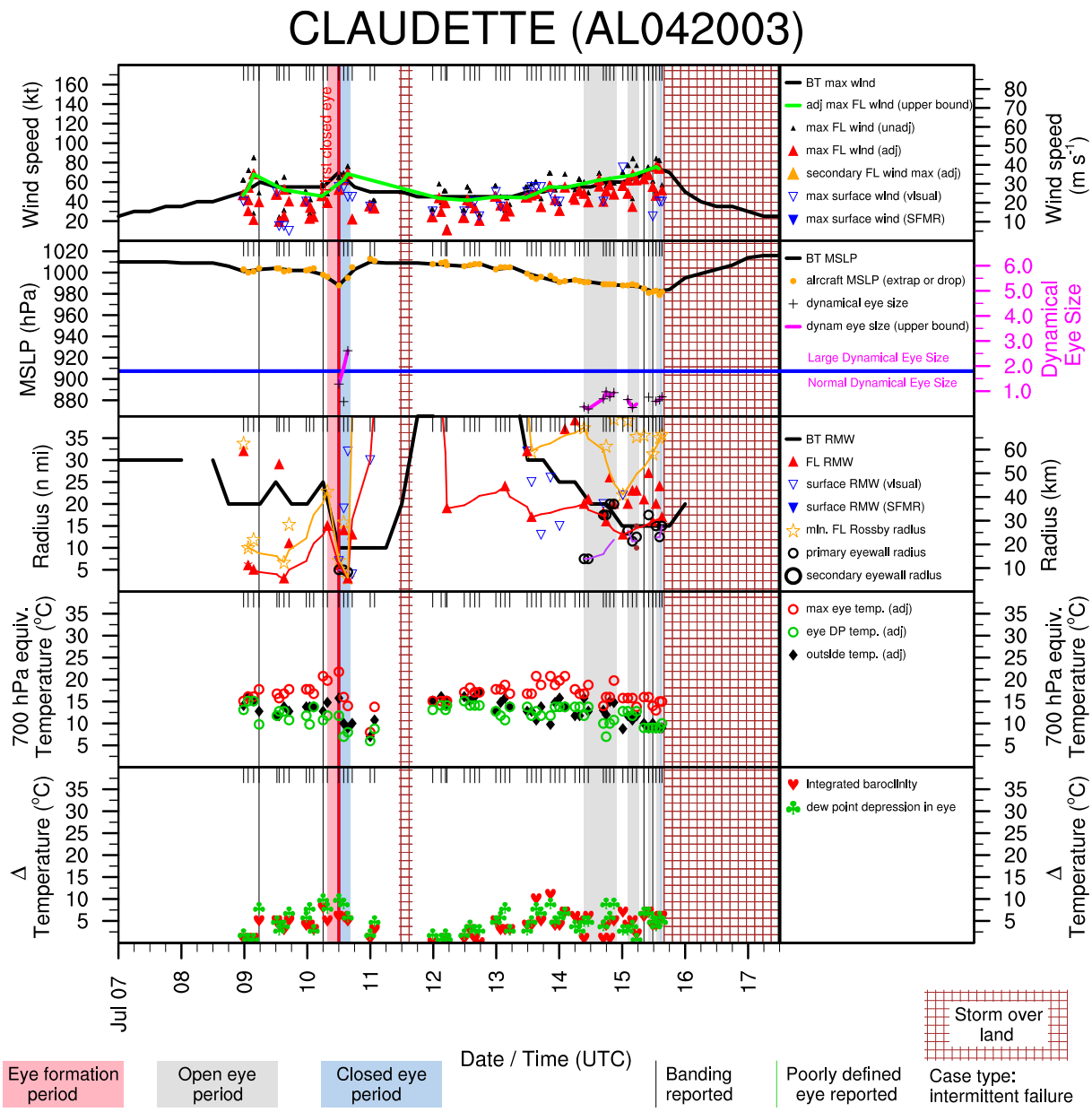

Figure E.119: Structure and intensity parameters for Hurricane Claudette (2003).

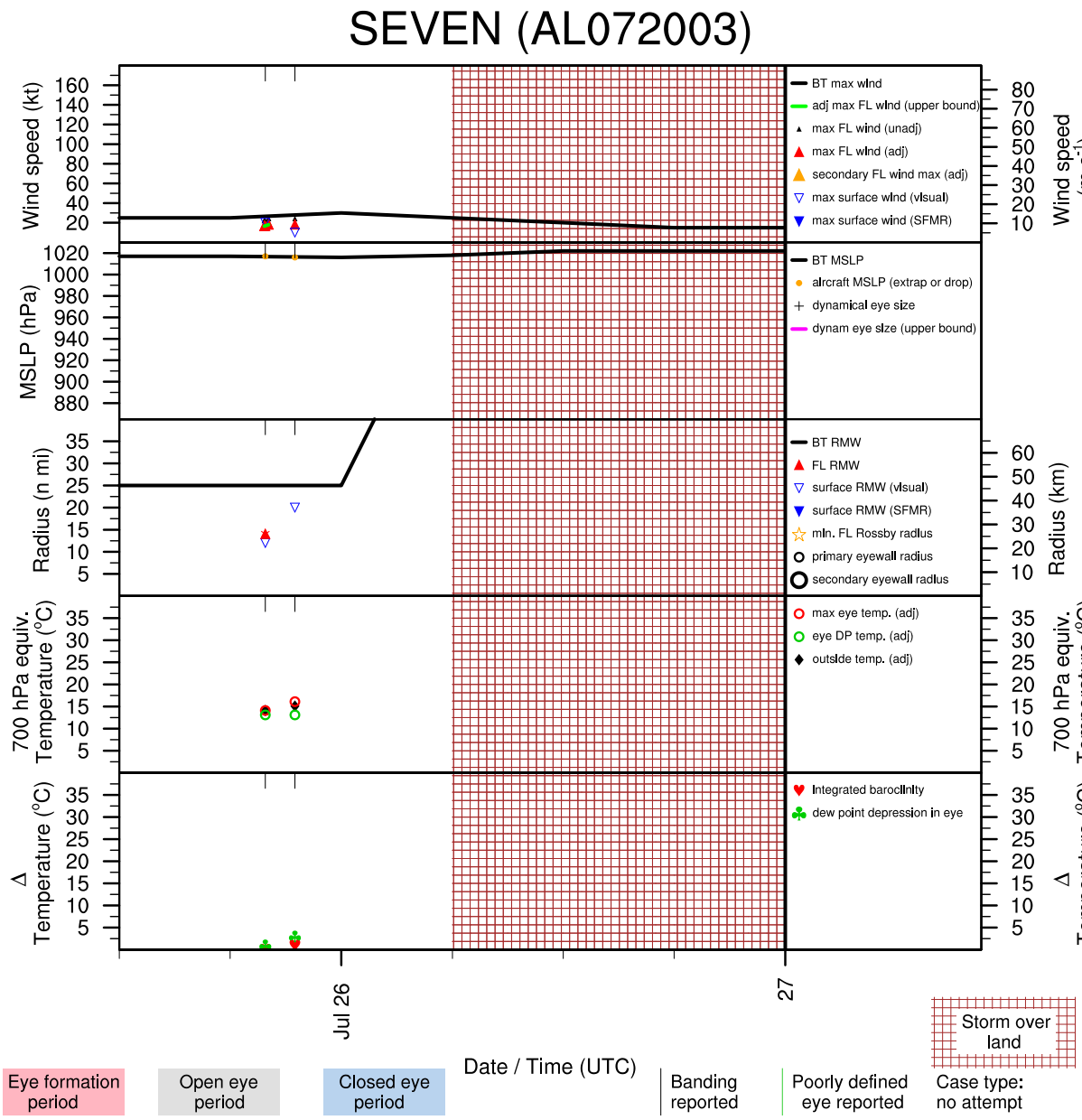

Figure E.120: Structure and intensity parameters for Tropical Depression Seven (2003).

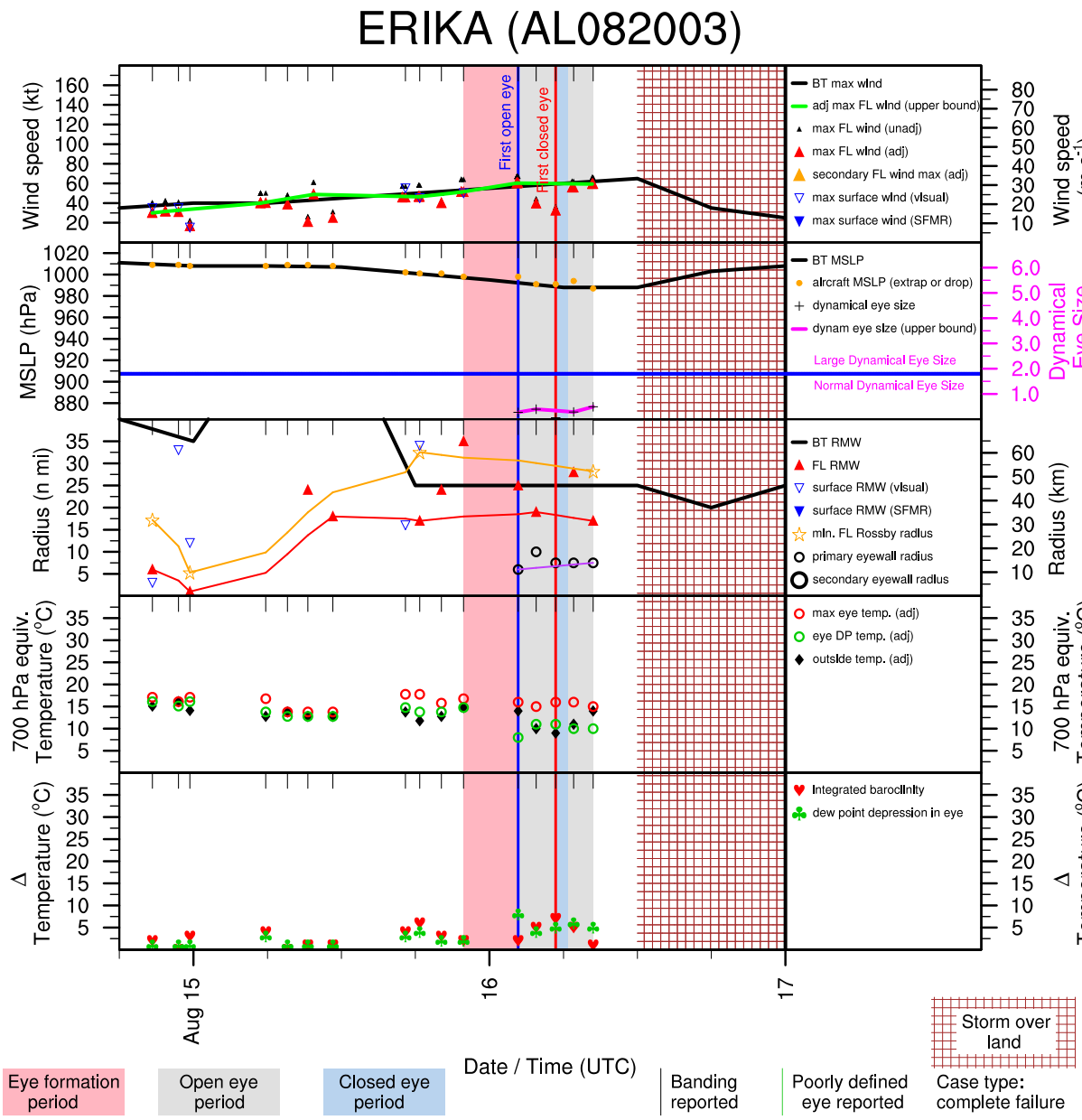

Figure E.121: Structure and intensity parameters for Hurricane Erika (2003).

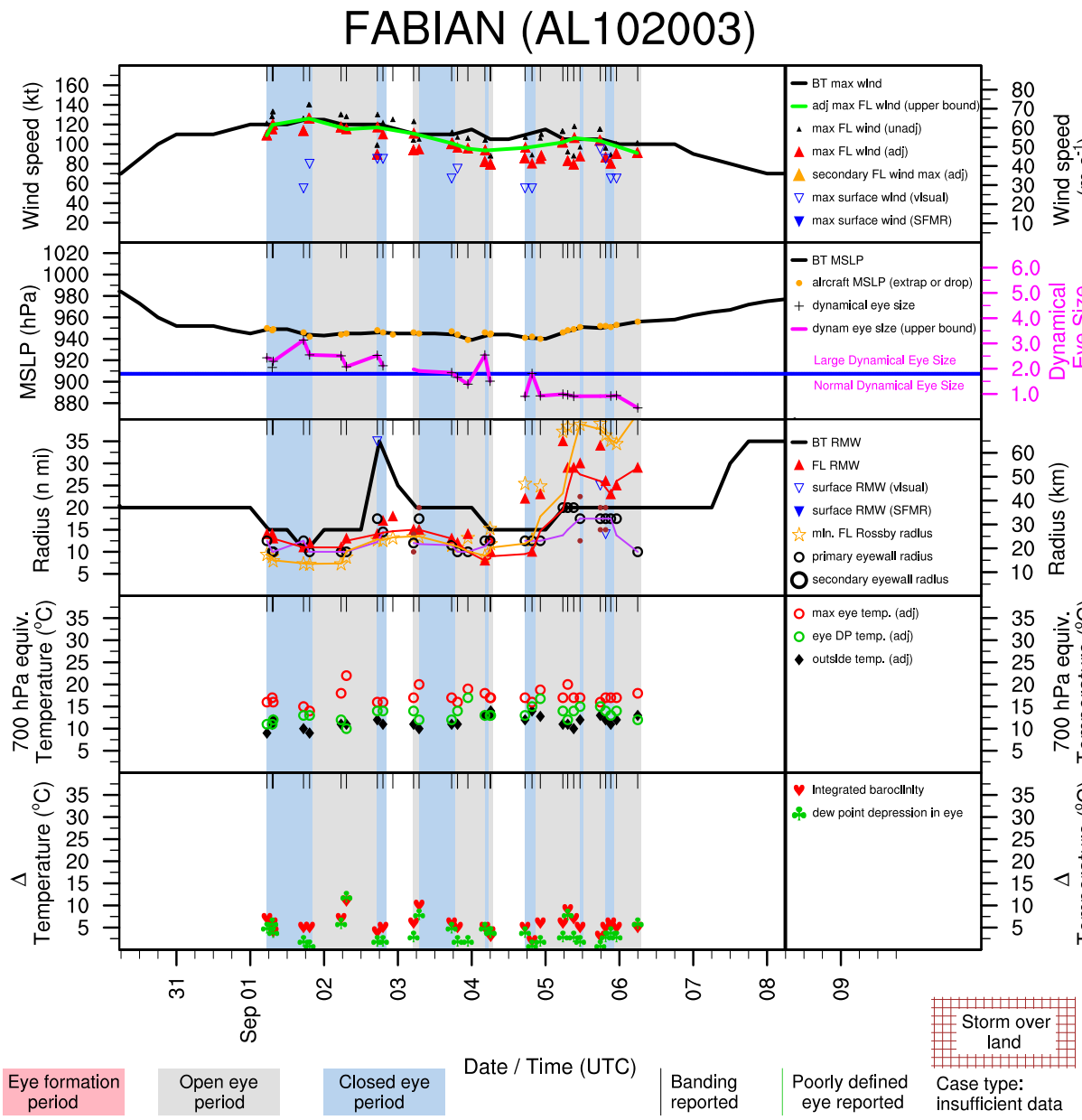

Figure E.122: Structure and intensity parameters for Hurricane Fabian (2003).

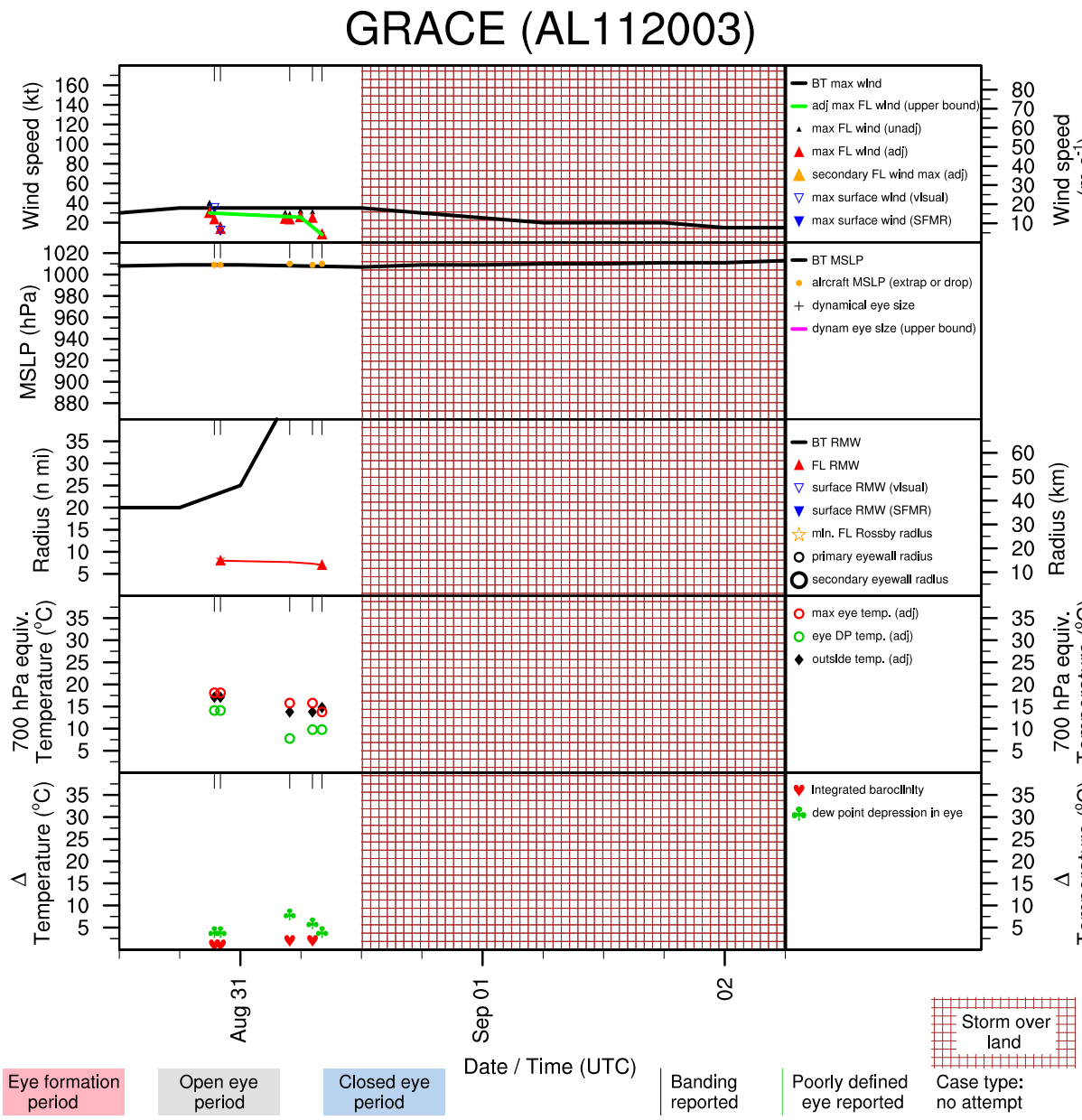

Figure E.123: Structure and intensity parameters for Tropical Storm Grace (2003).

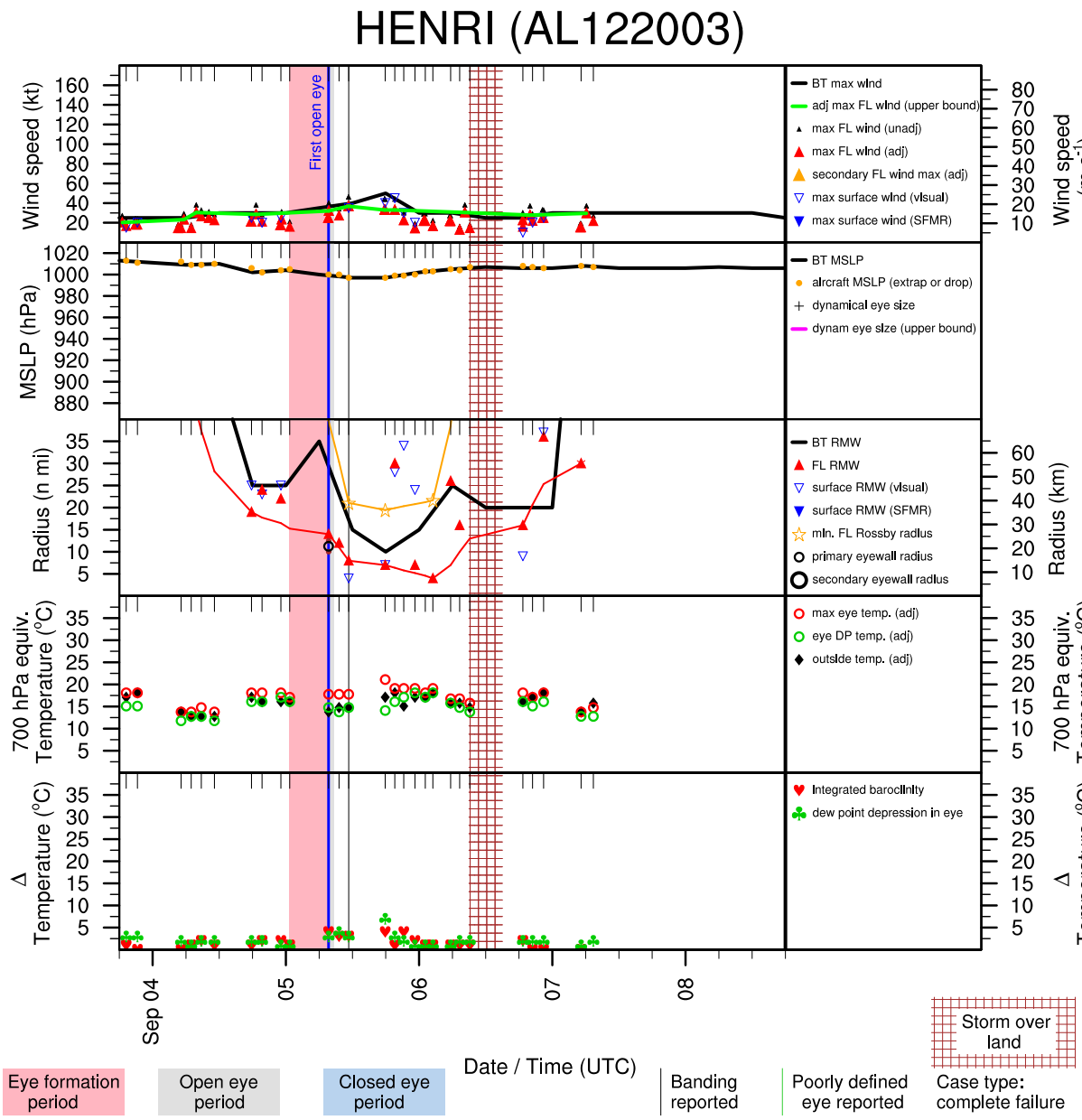

Figure E.124: Structure and intensity parameters for Tropical Storm Henri (2003).

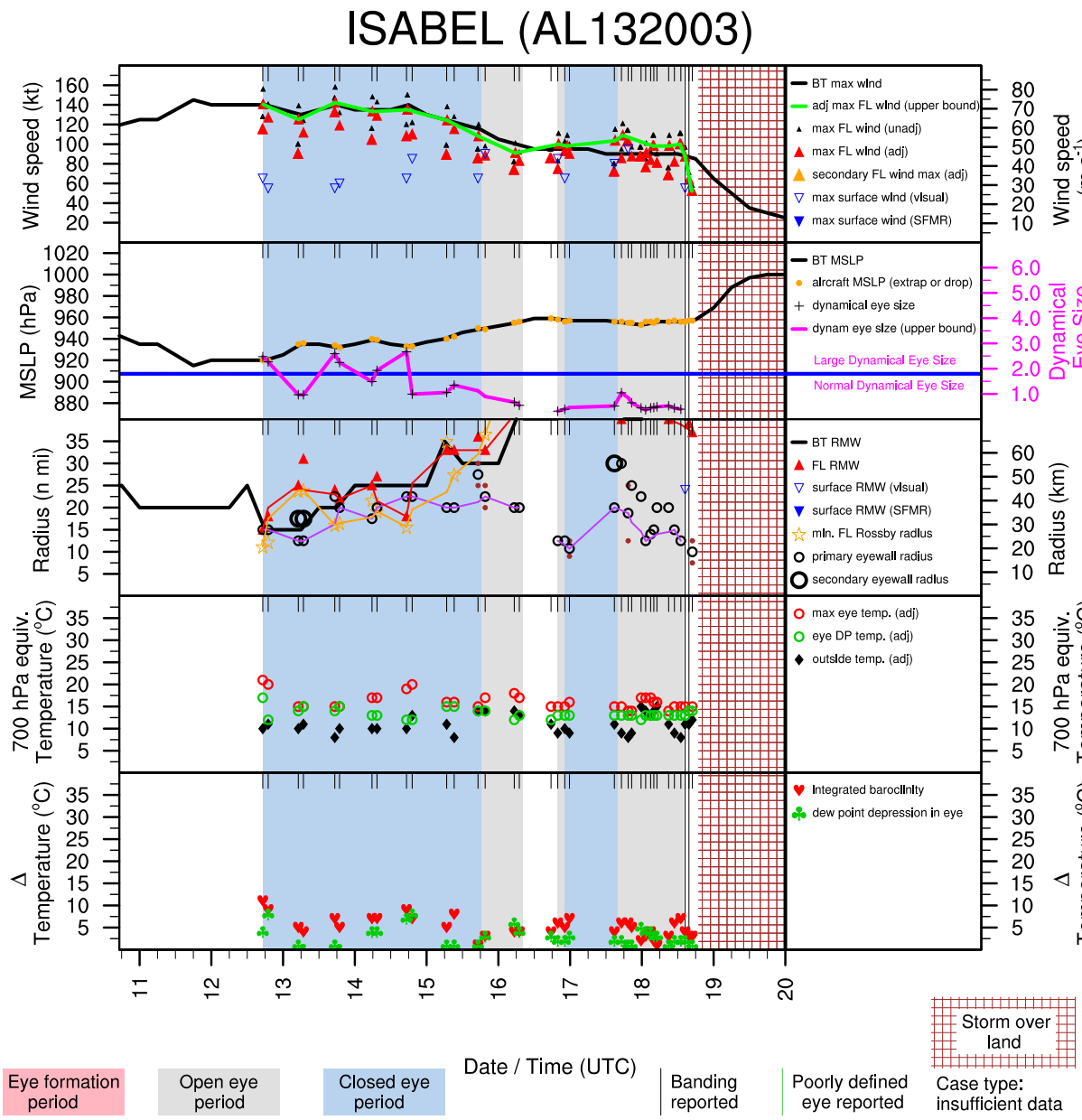

Figure E.125: Structure and intensity parameters for Hurricane Isabel (2003).

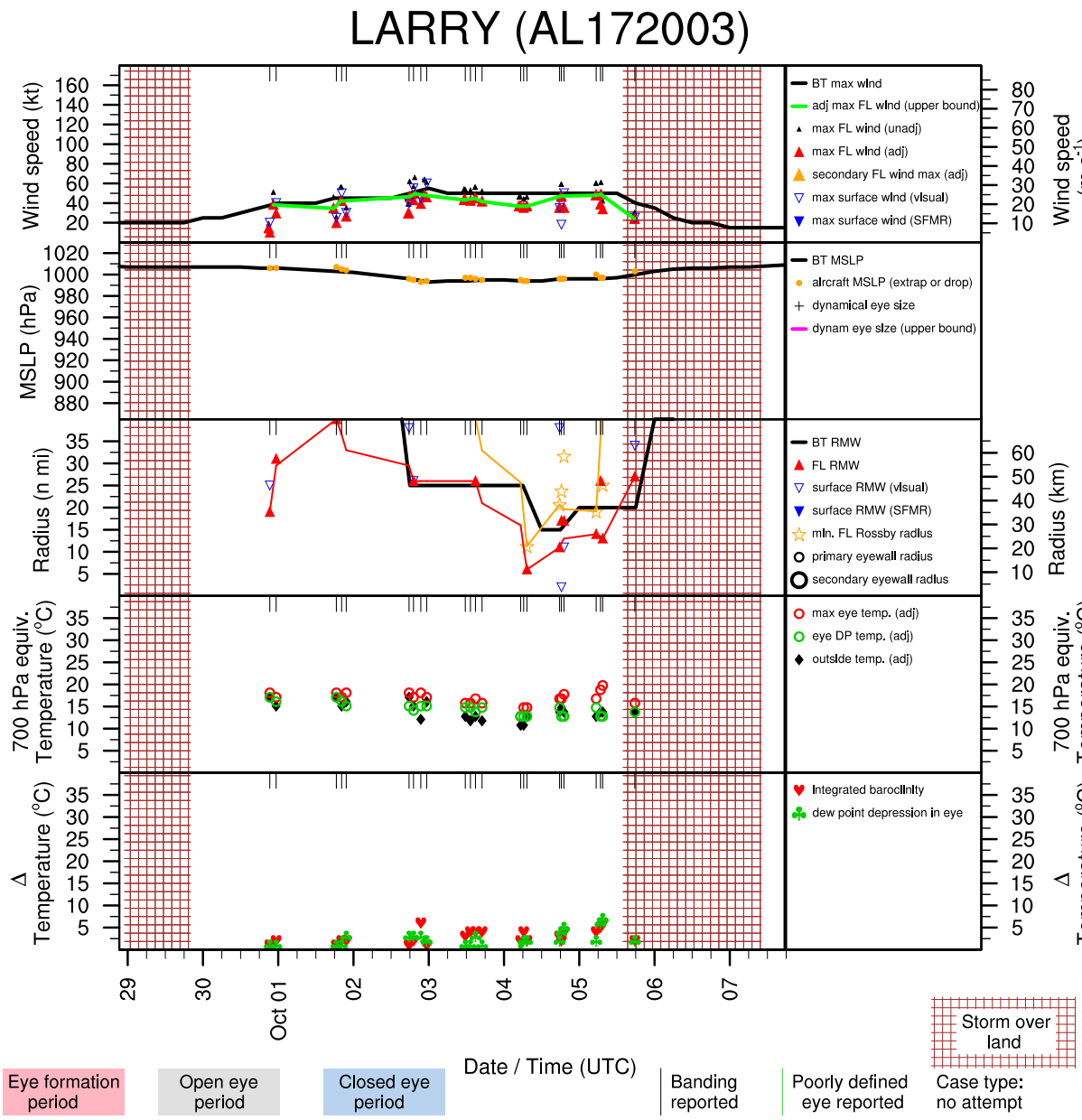

Figure E.126: Structure and intensity parameters for Tropical Storm Larry (2003).

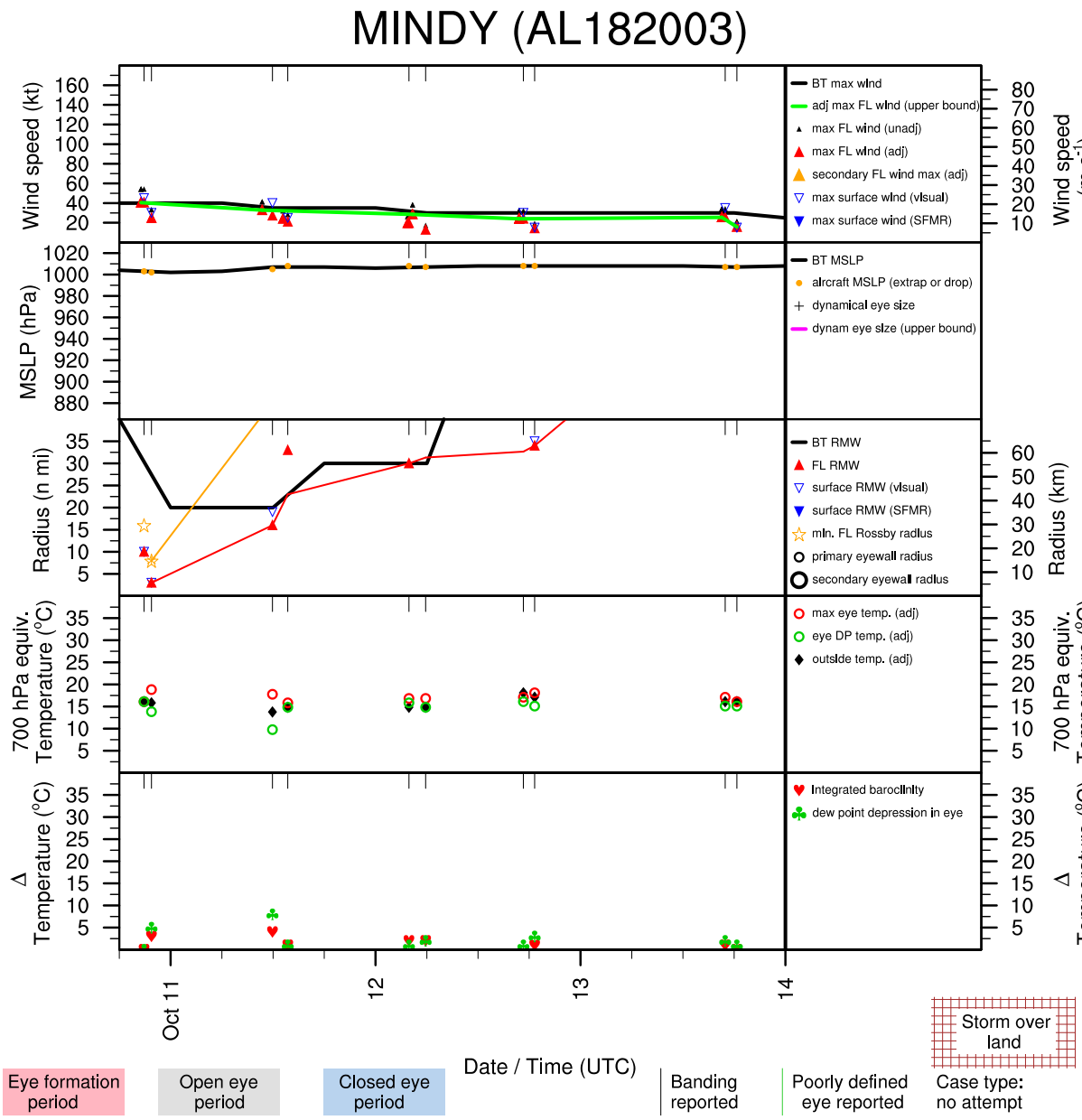

Figure E.127: Structure and intensity parameters for Tropical Storm Mindy (2003).

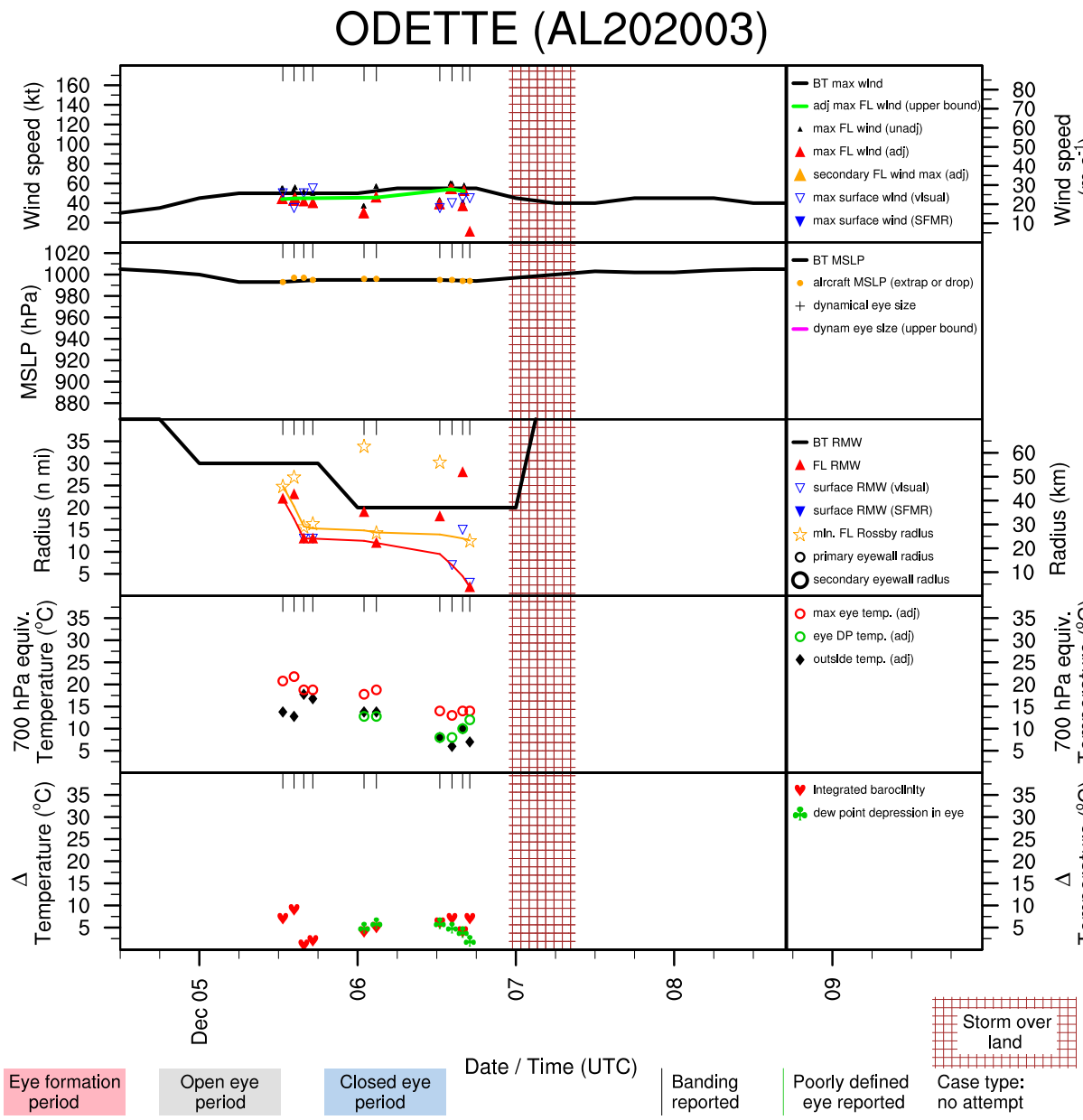

Figure E.128: Structure and intensity parameters for Tropical Storm Odette (2003).

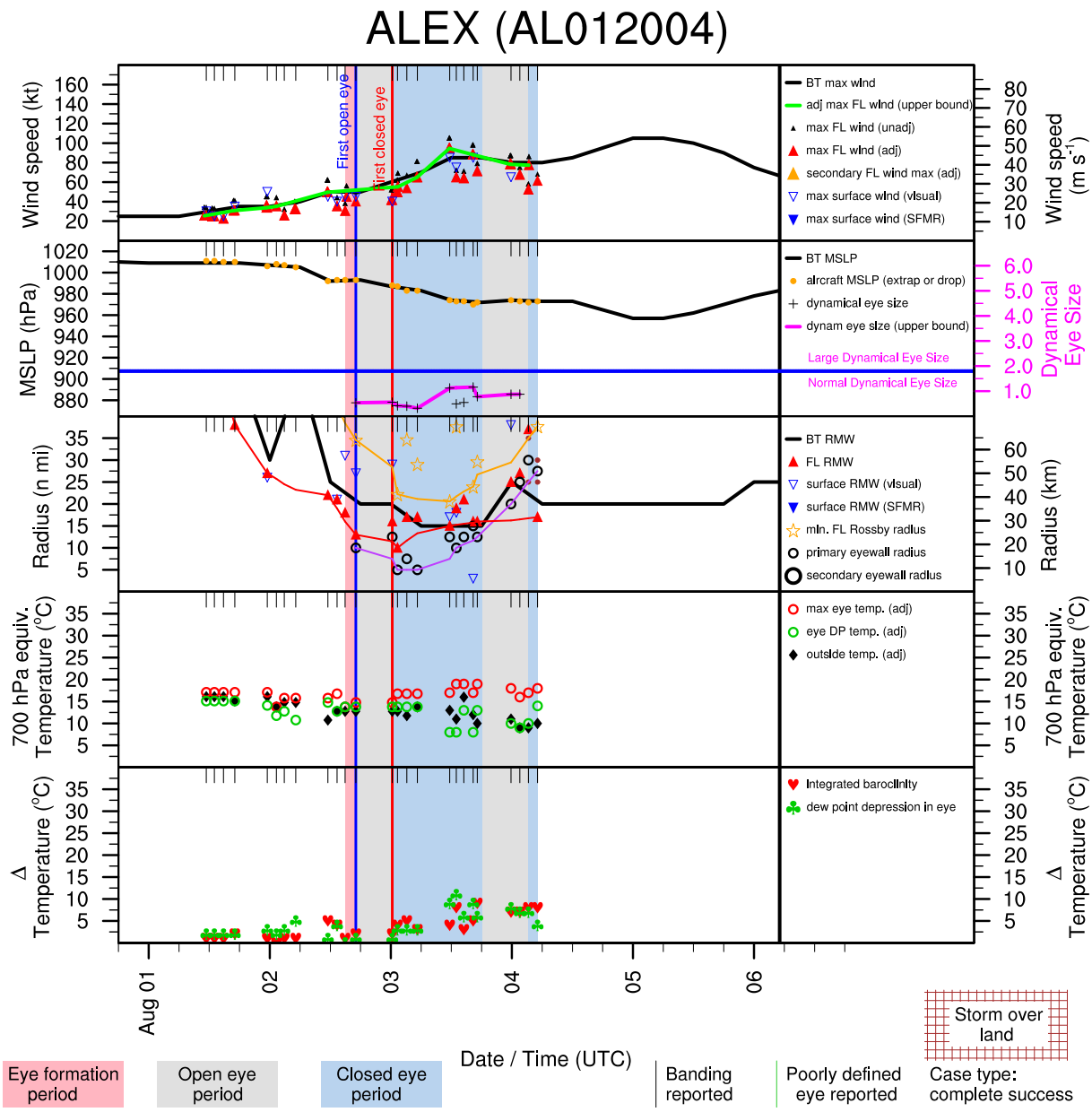

Figure E.129: Structure and intensity parameters for Hurricane Alex (2004).

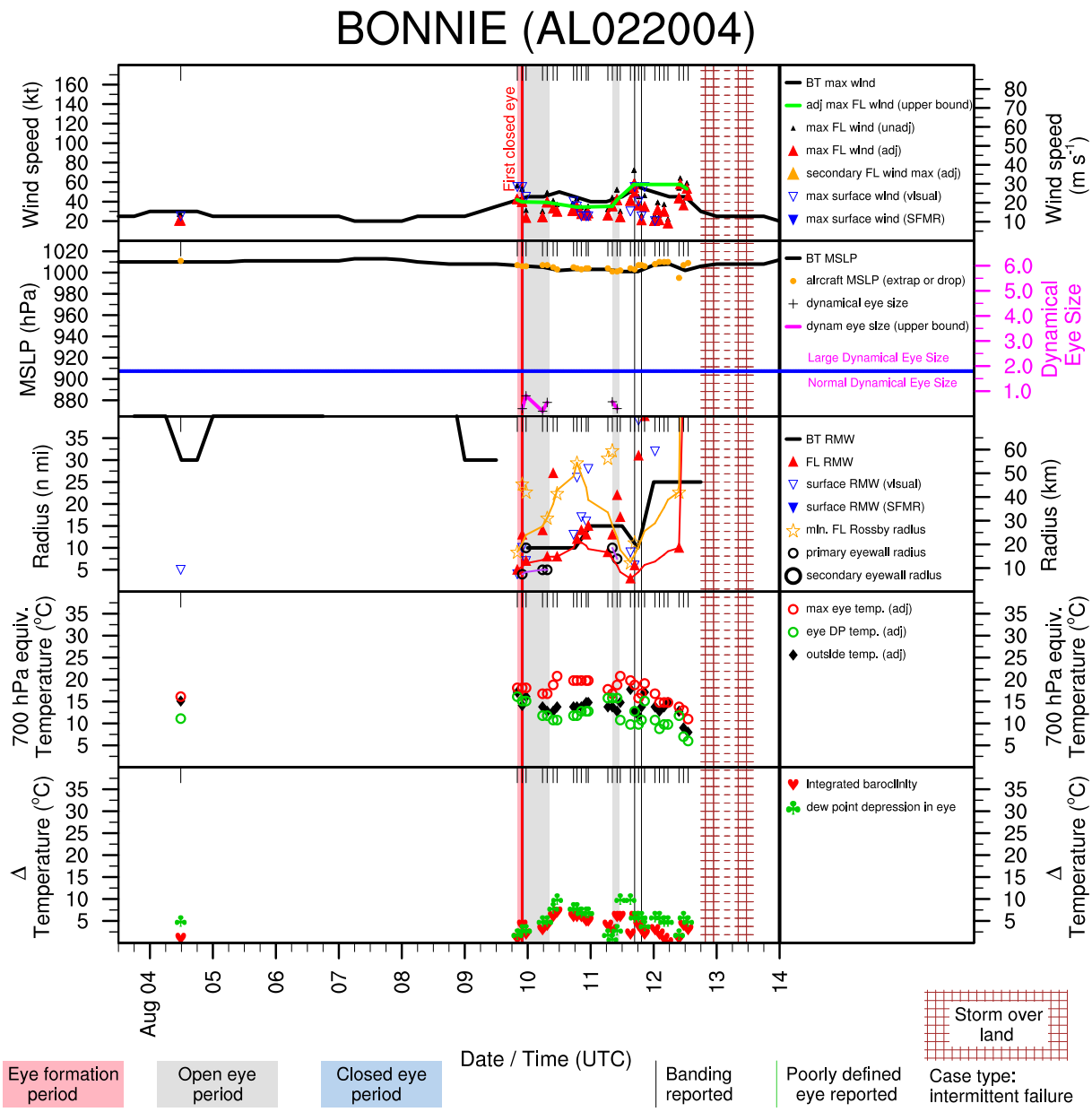

Figure E.130: Structure and intensity parameters for Tropical Storm Bonnie (2004).

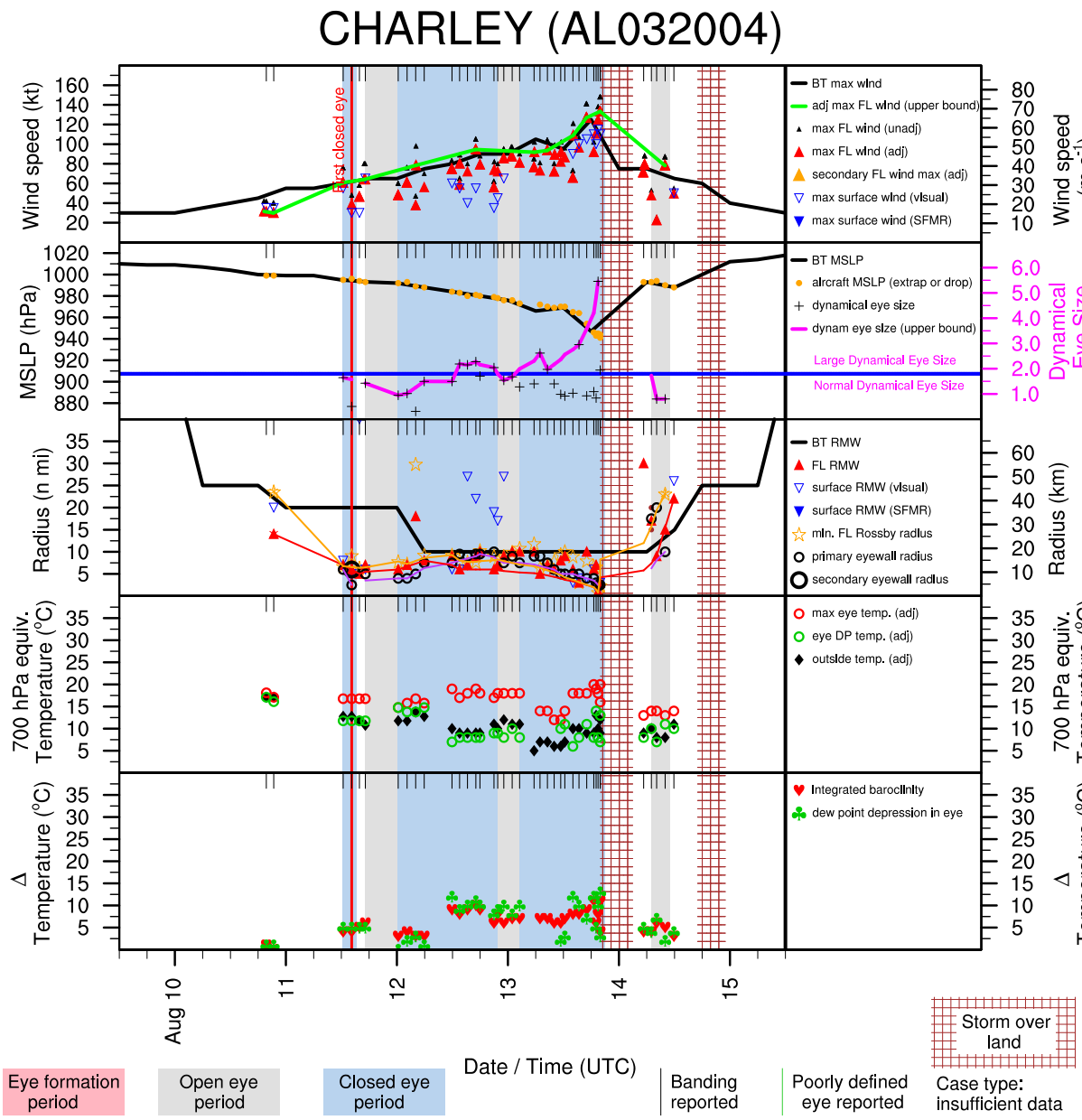

Figure E.131: Structure and intensity parameters for Hurricane Charley (2004).

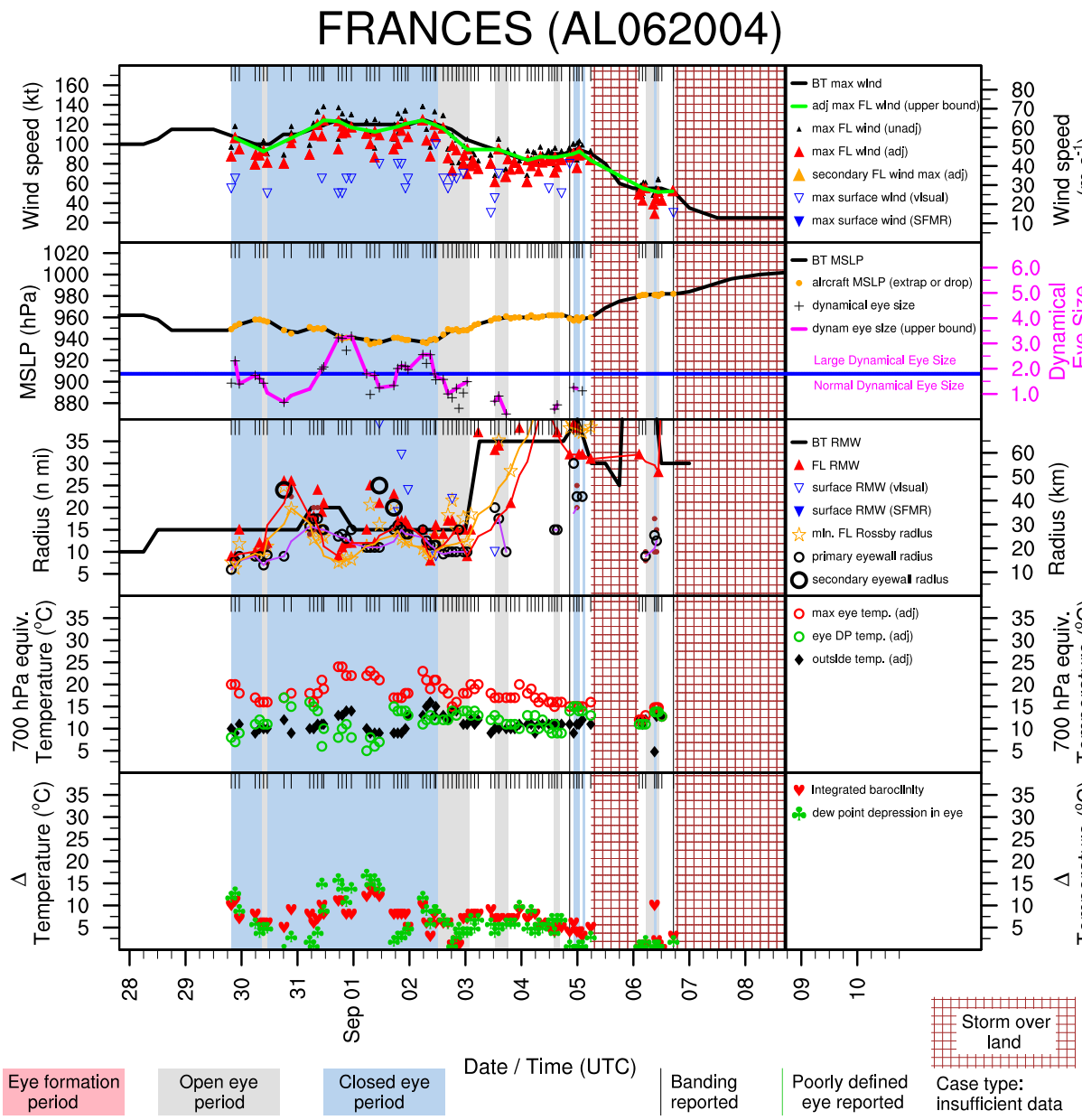

Figure E.132: Structure and intensity parameters for Hurricane Frances (2004).

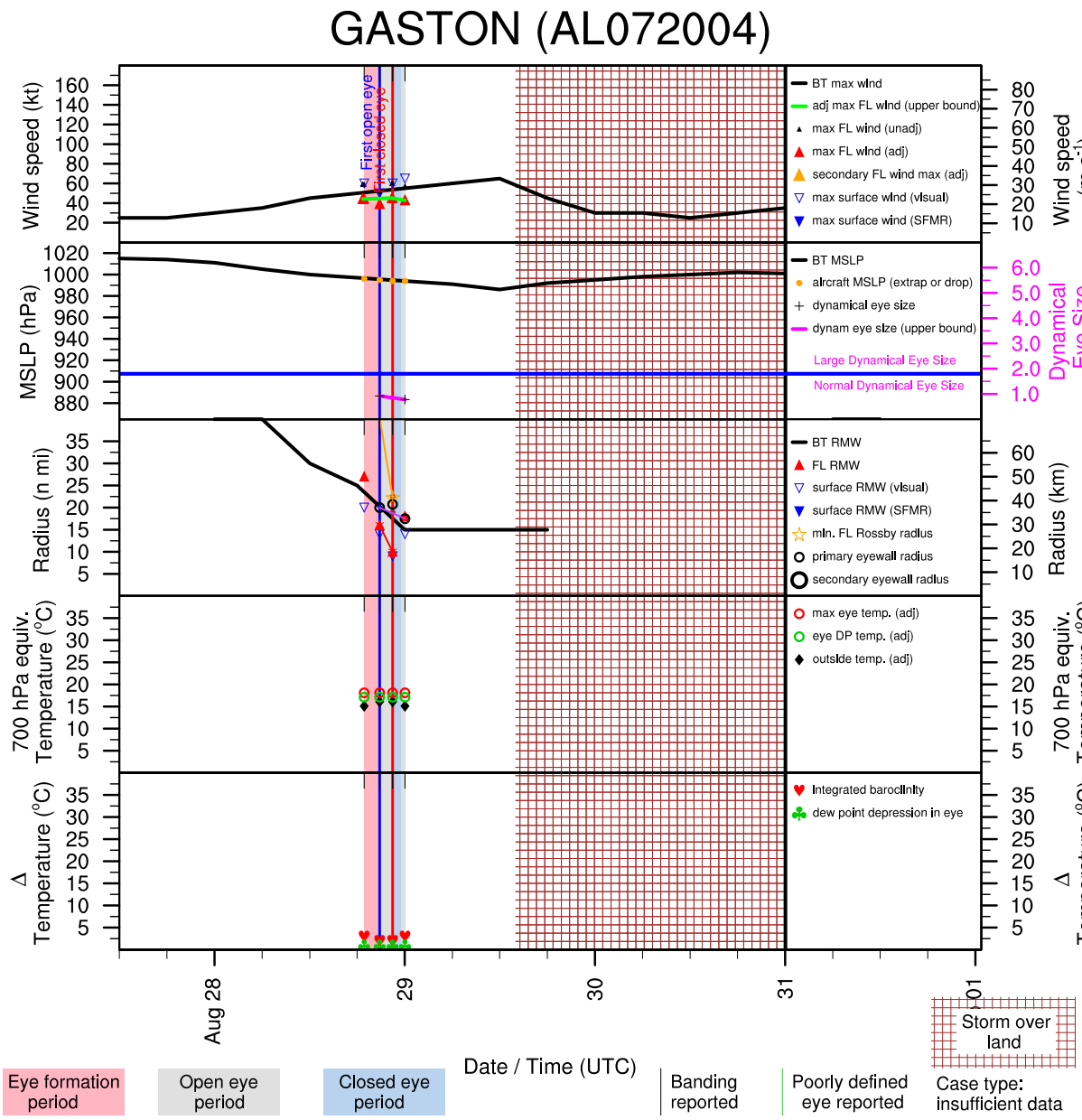

Figure E.133: Structure and intensity parameters for Hurricane Gaston (2004).

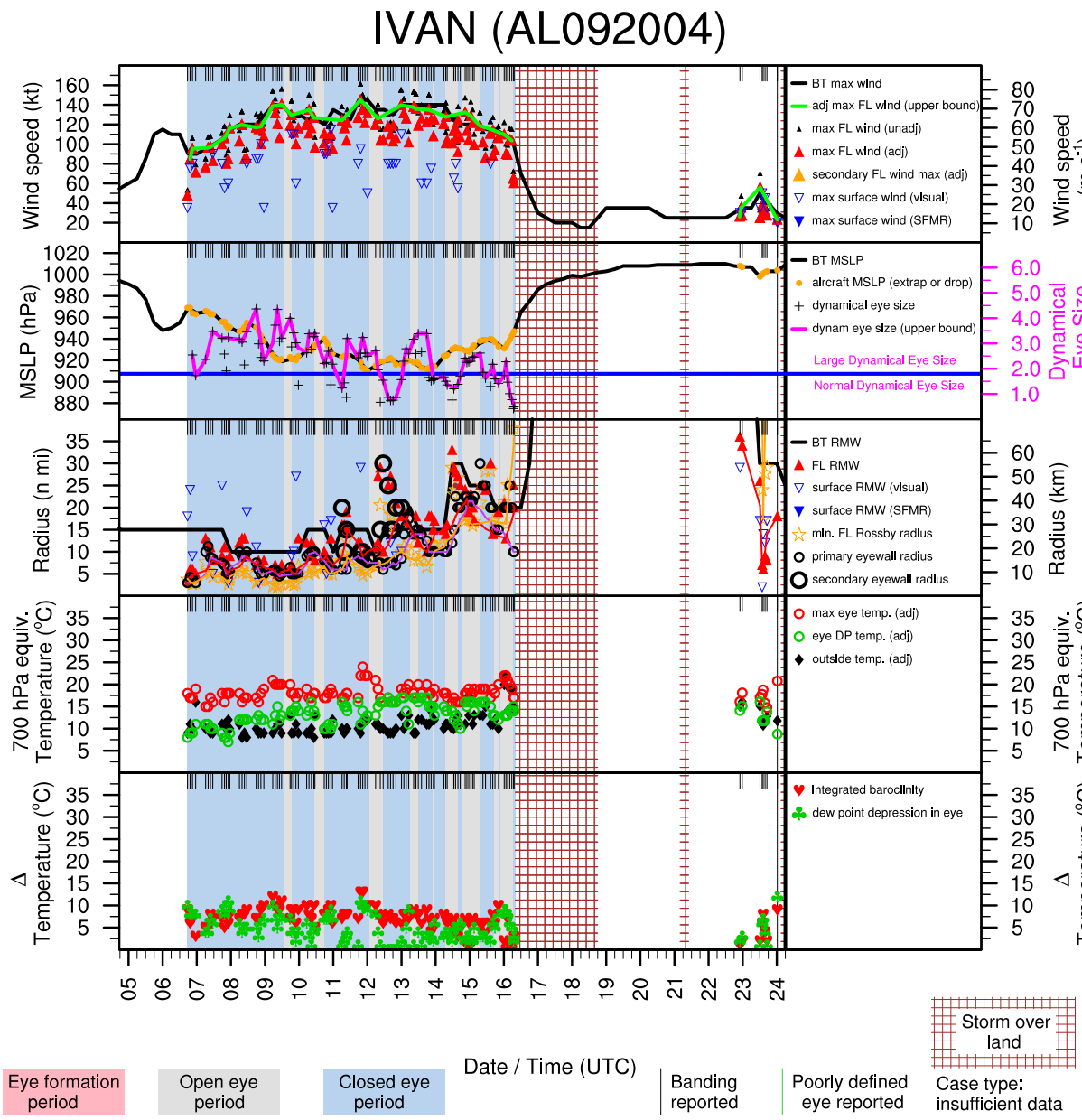

Figure E.134: Structure and intensity parameters for Hurricane Ivan (2004).

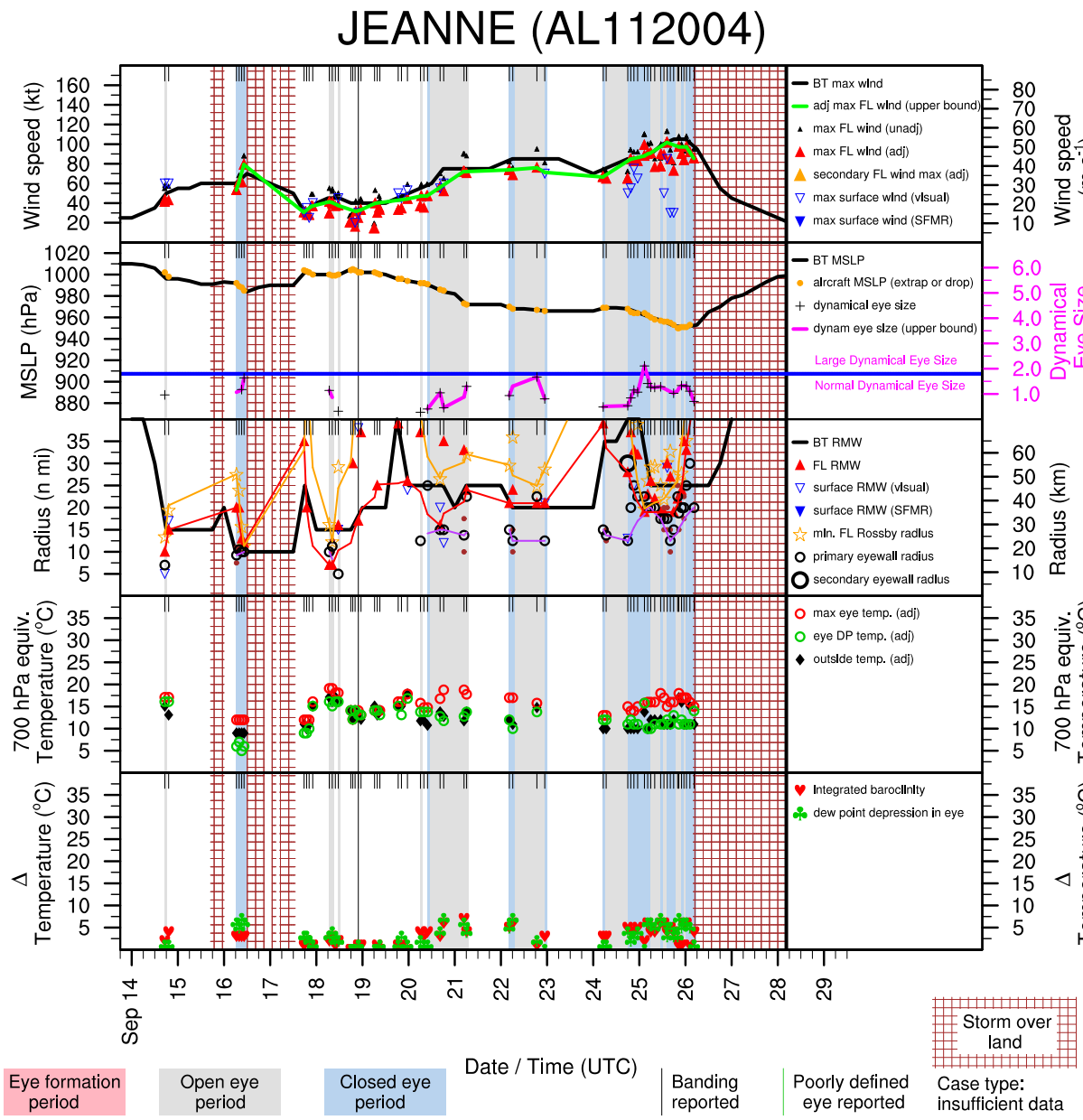

Figure E.135: Structure and intensity parameters for Hurricane Jeanne (2004).

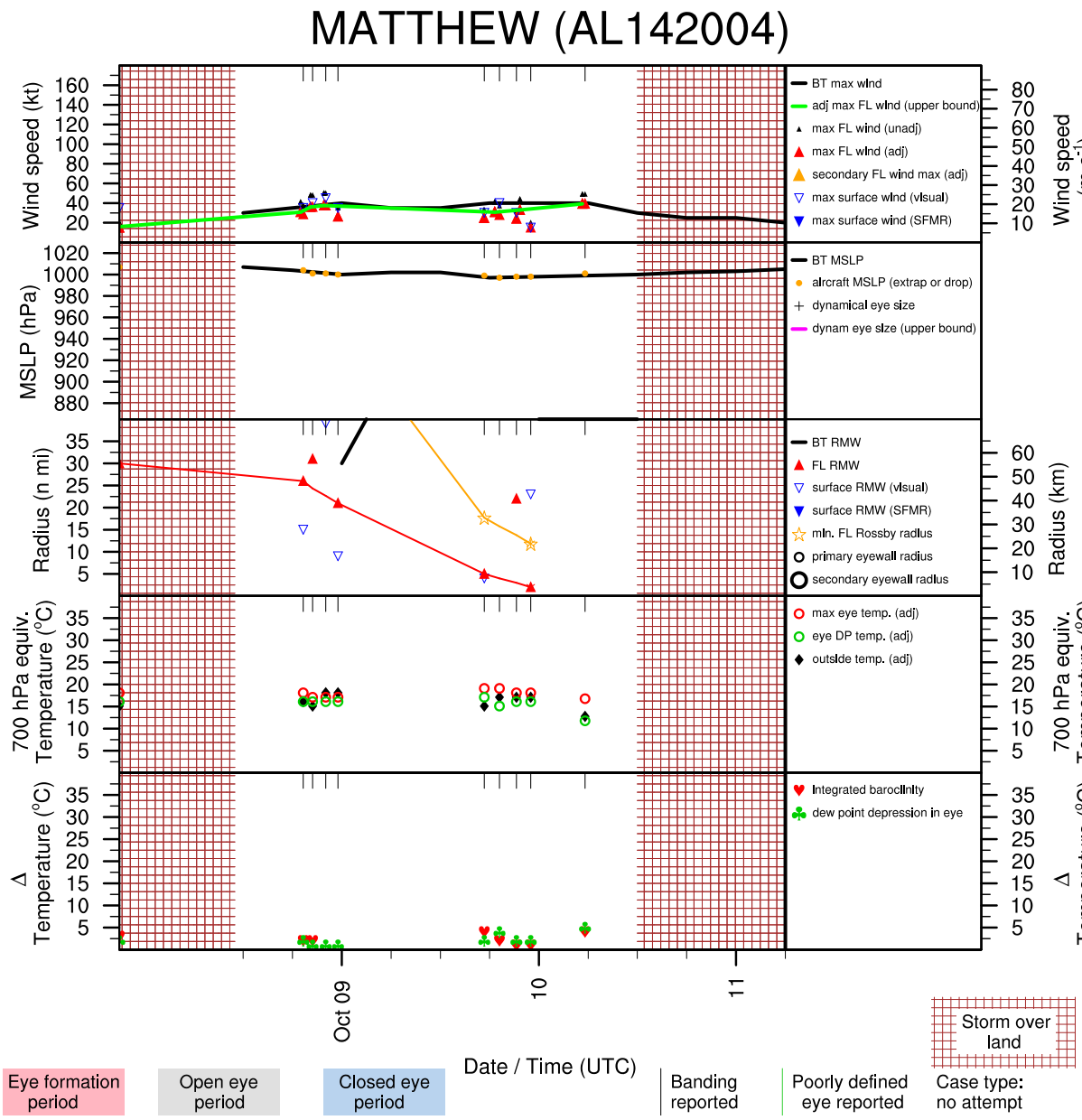

Figure E.136: Structure and intensity parameters for Tropical Storm Matthew (2004).

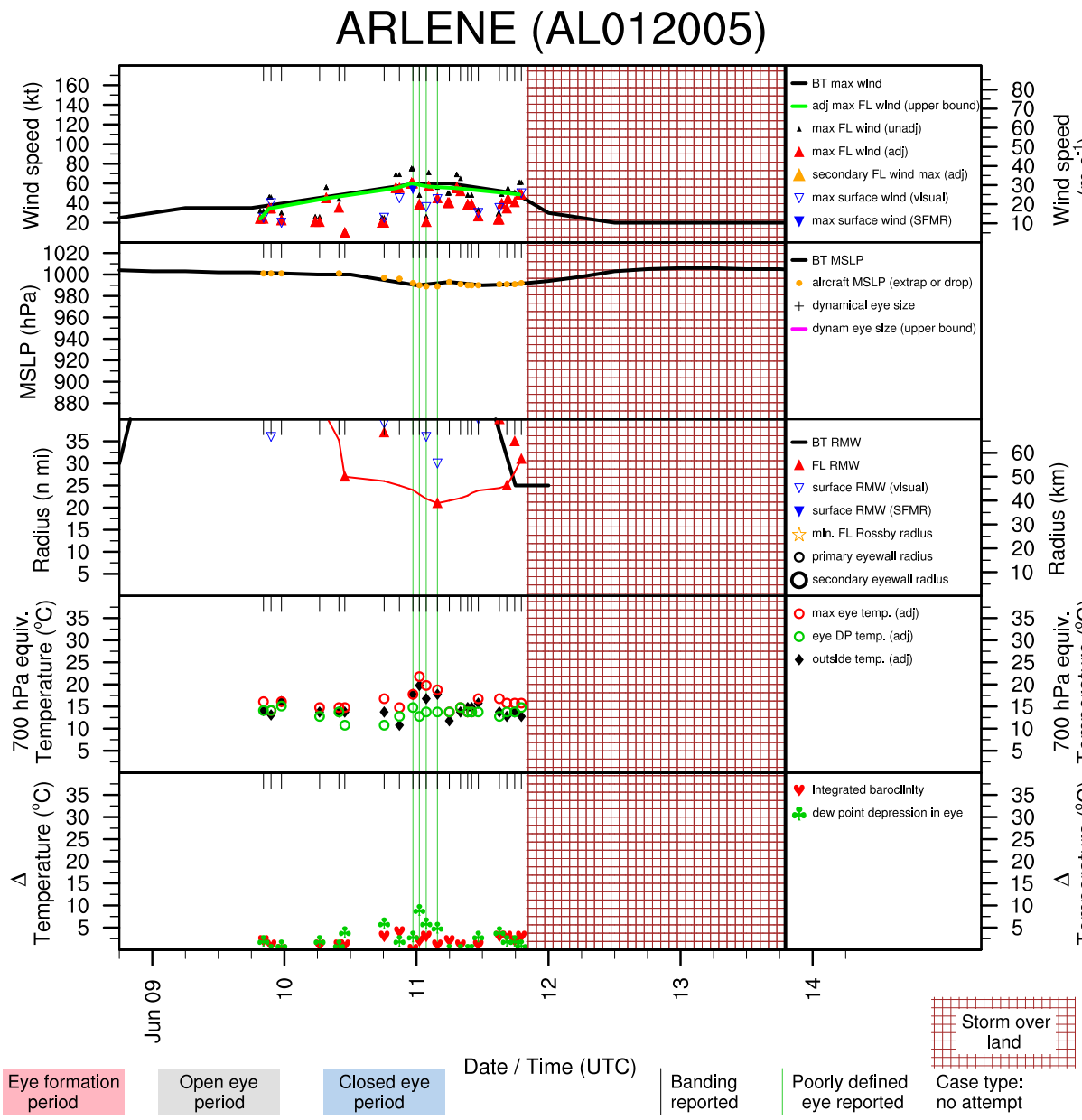

Figure E.137: Structure and intensity parameters for Tropical Storm Arlene (2005).

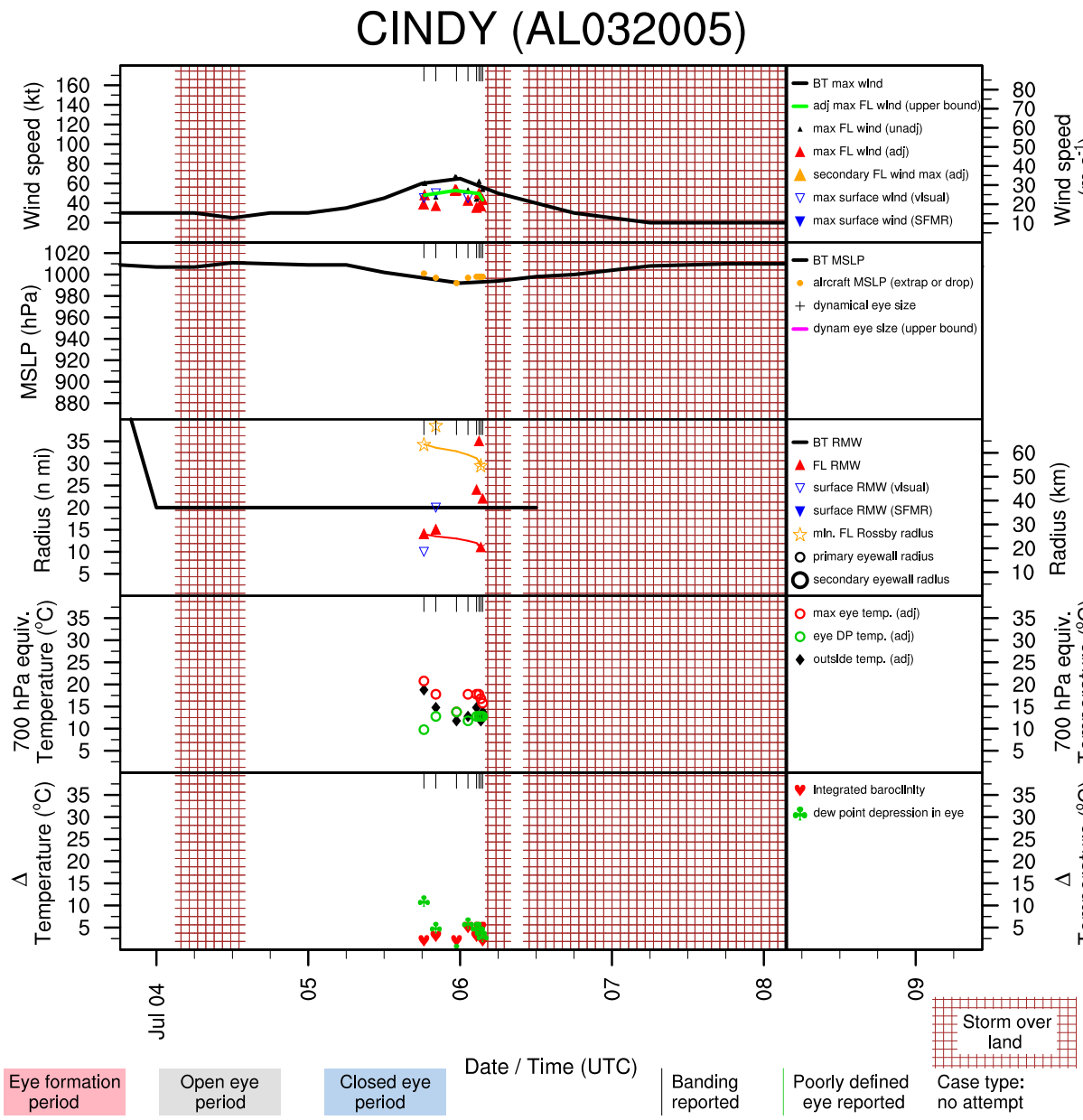

Figure E.138: Structure and intensity parameters for Hurricane Cindy (2005).

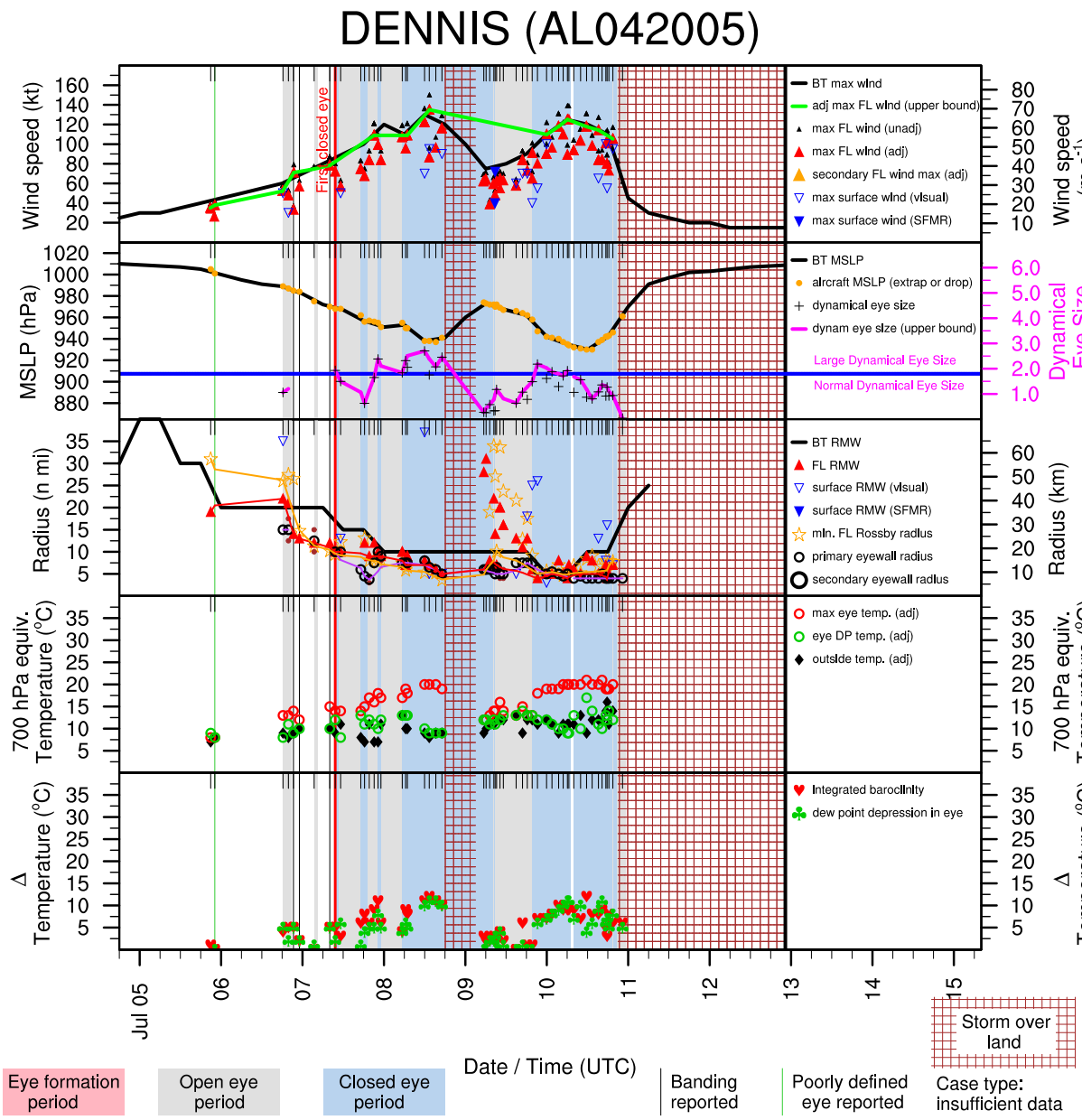

Figure E.139: Structure and intensity parameters for Hurricane Dennis (2005).

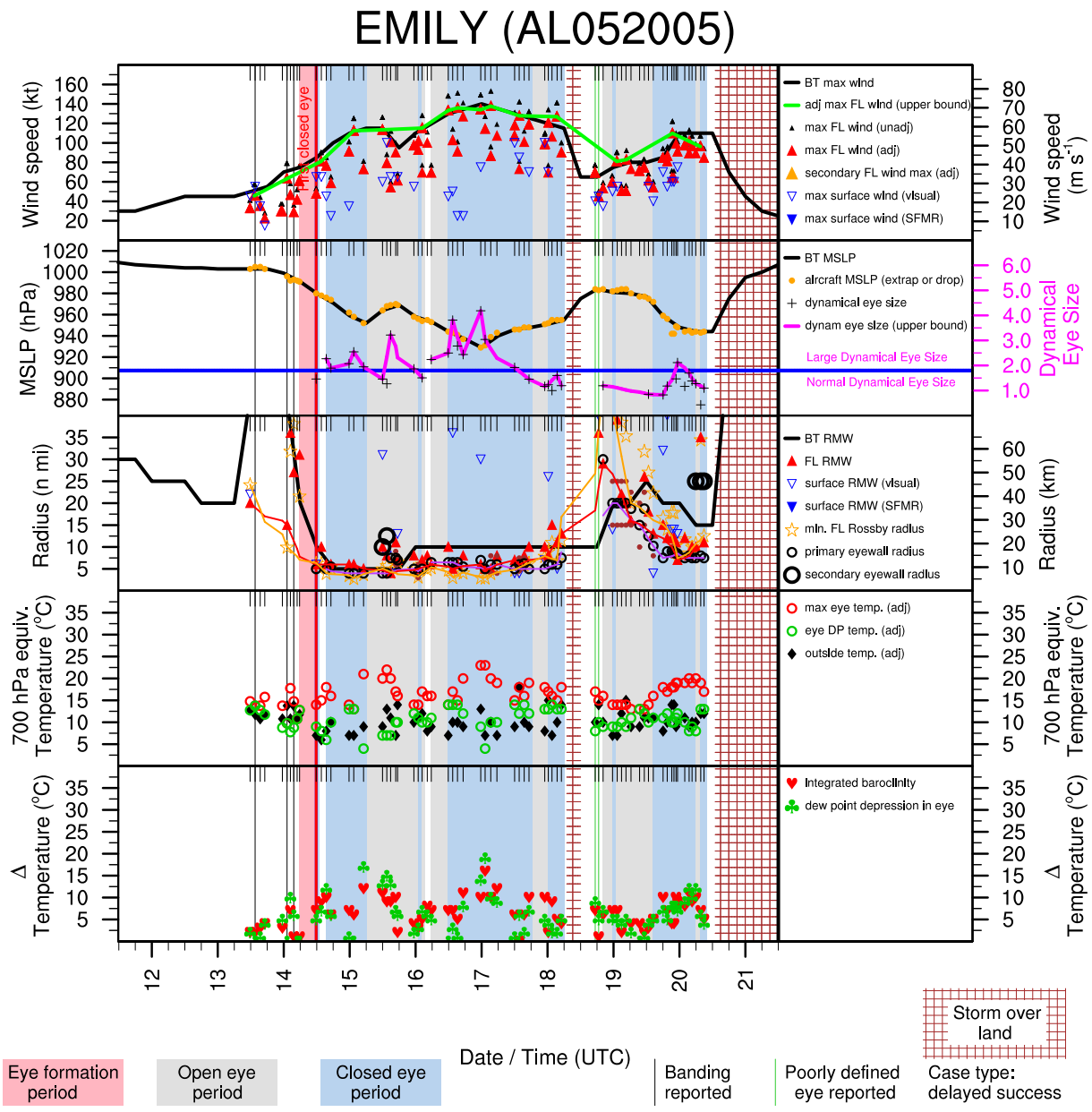

Figure E.140: Structure and intensity parameters for Hurricane Emily (2005).

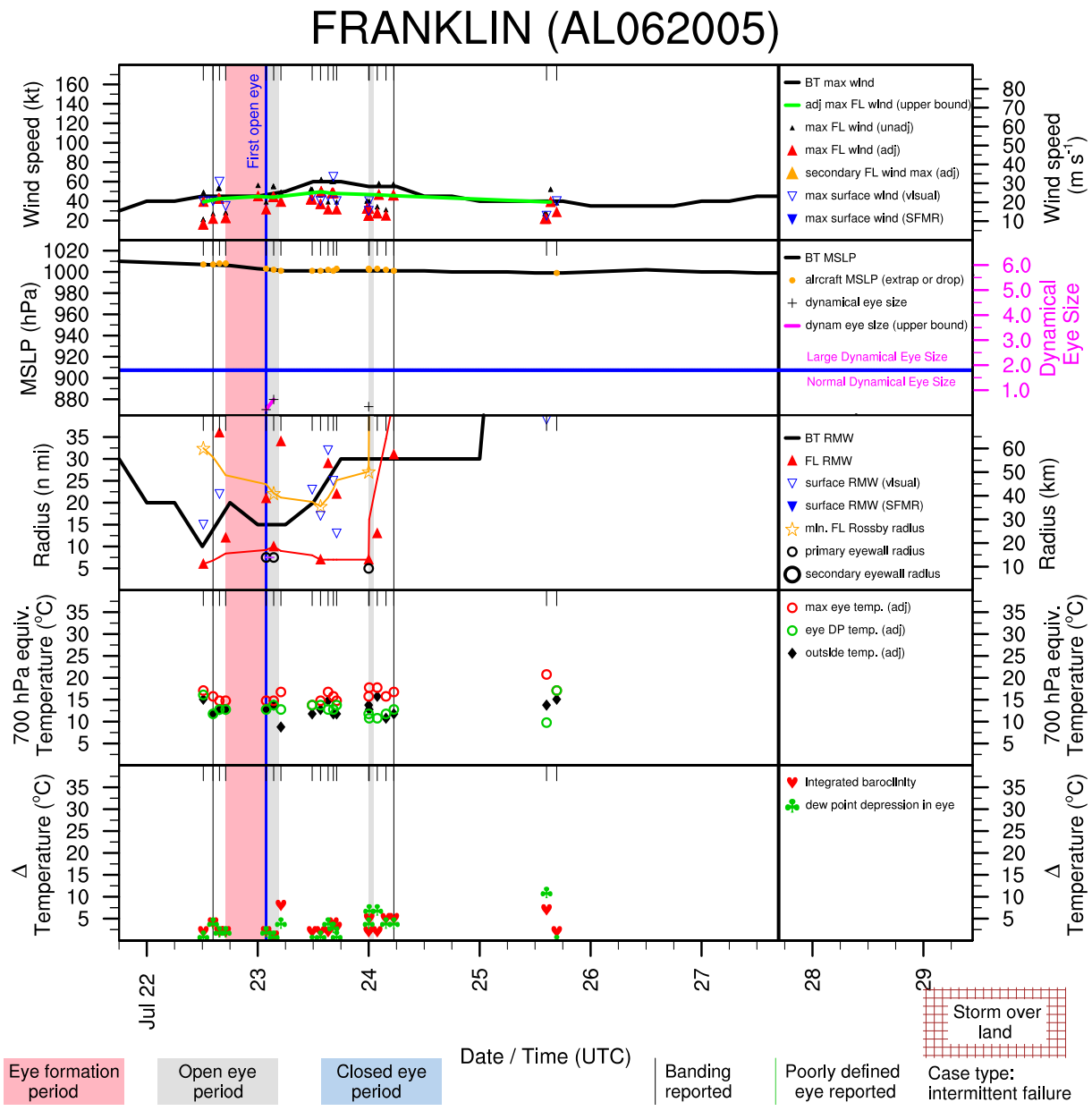

Figure E.141: Structure and intensity parameters for Tropical Storm Franklin (2005).

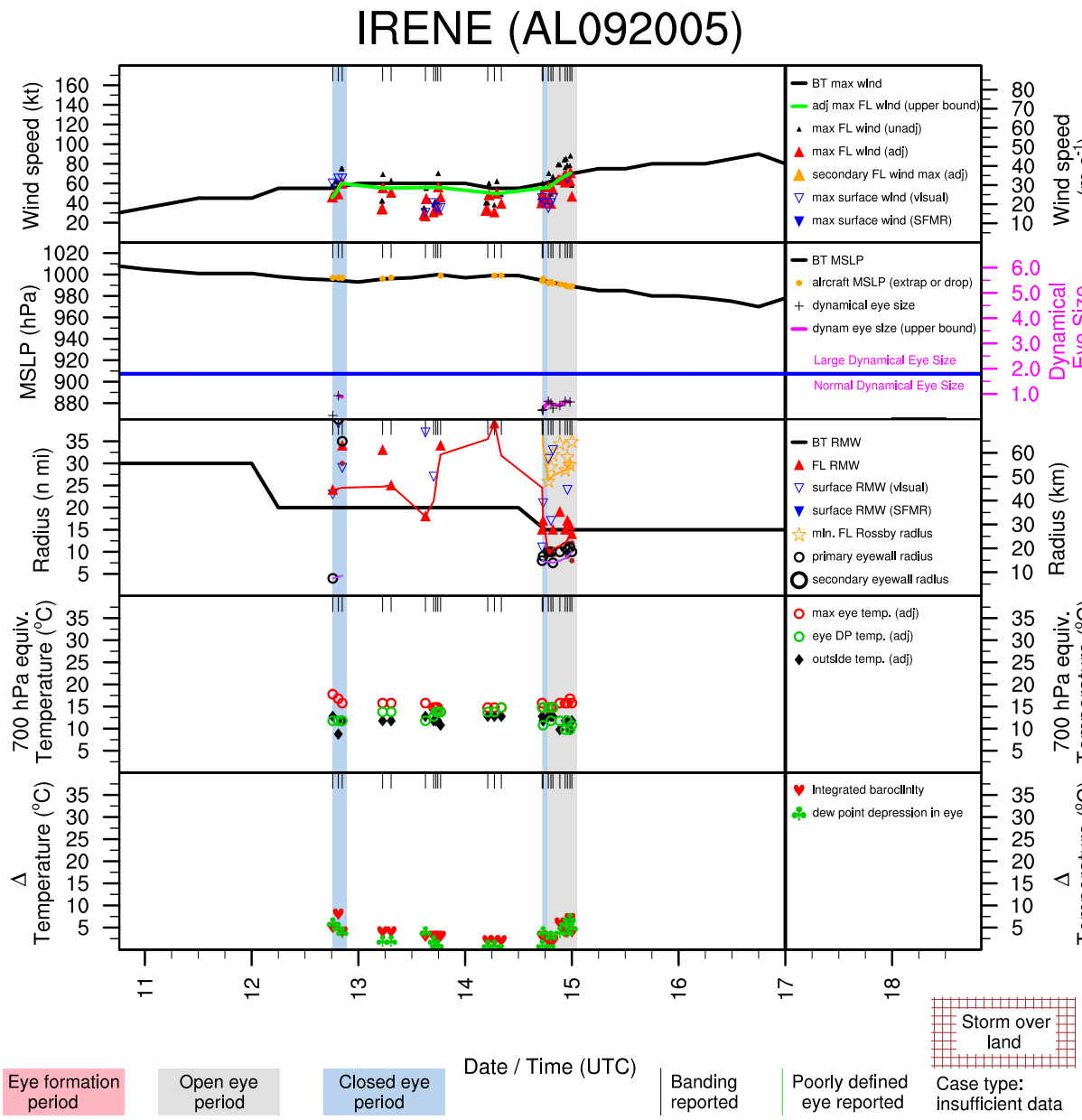

Figure E.142: Structure and intensity parameters for Hurricane Irene (2005).

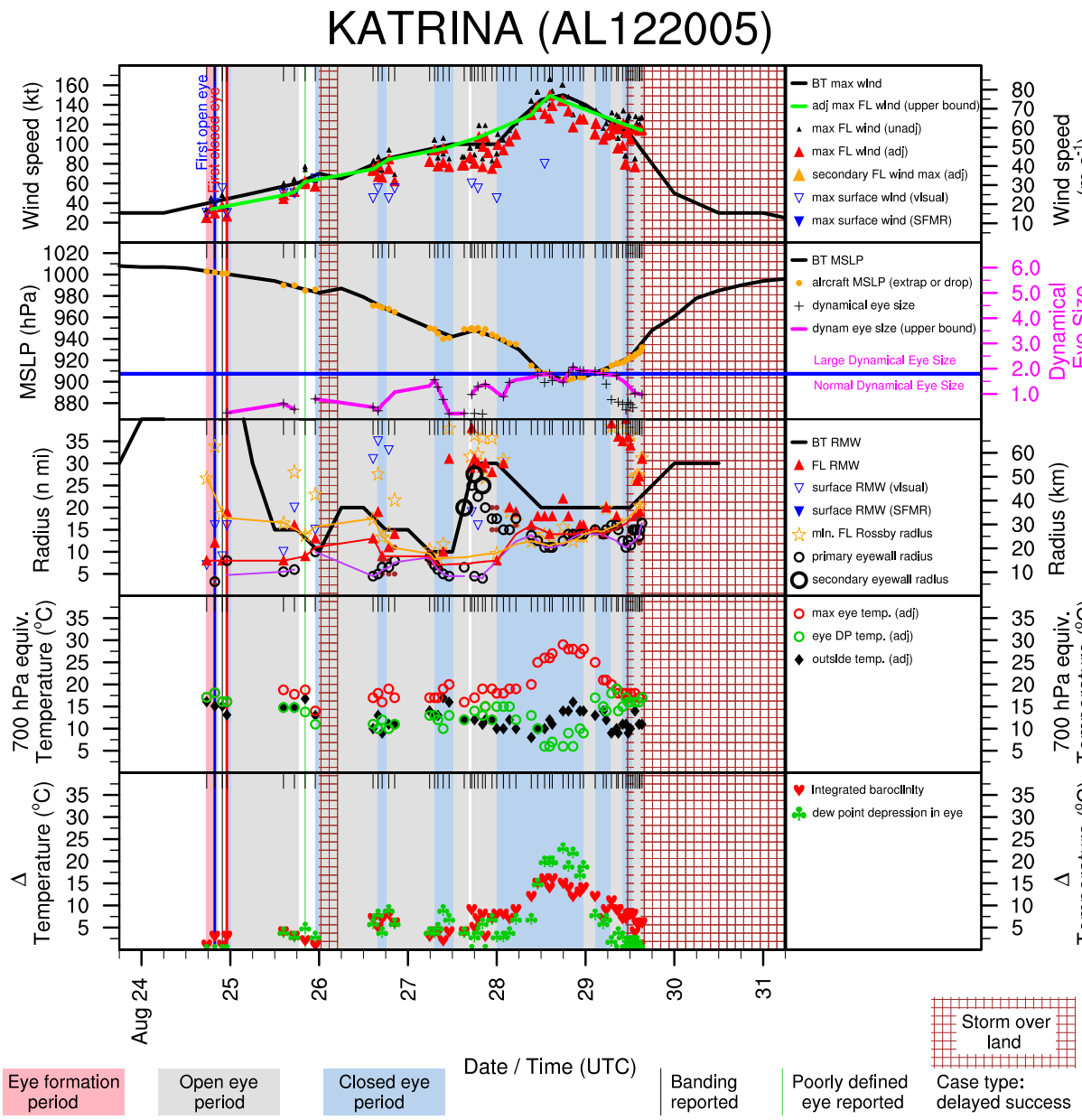

Figure E.143: Structure and intensity parameters for Hurricane Katrina (2005).

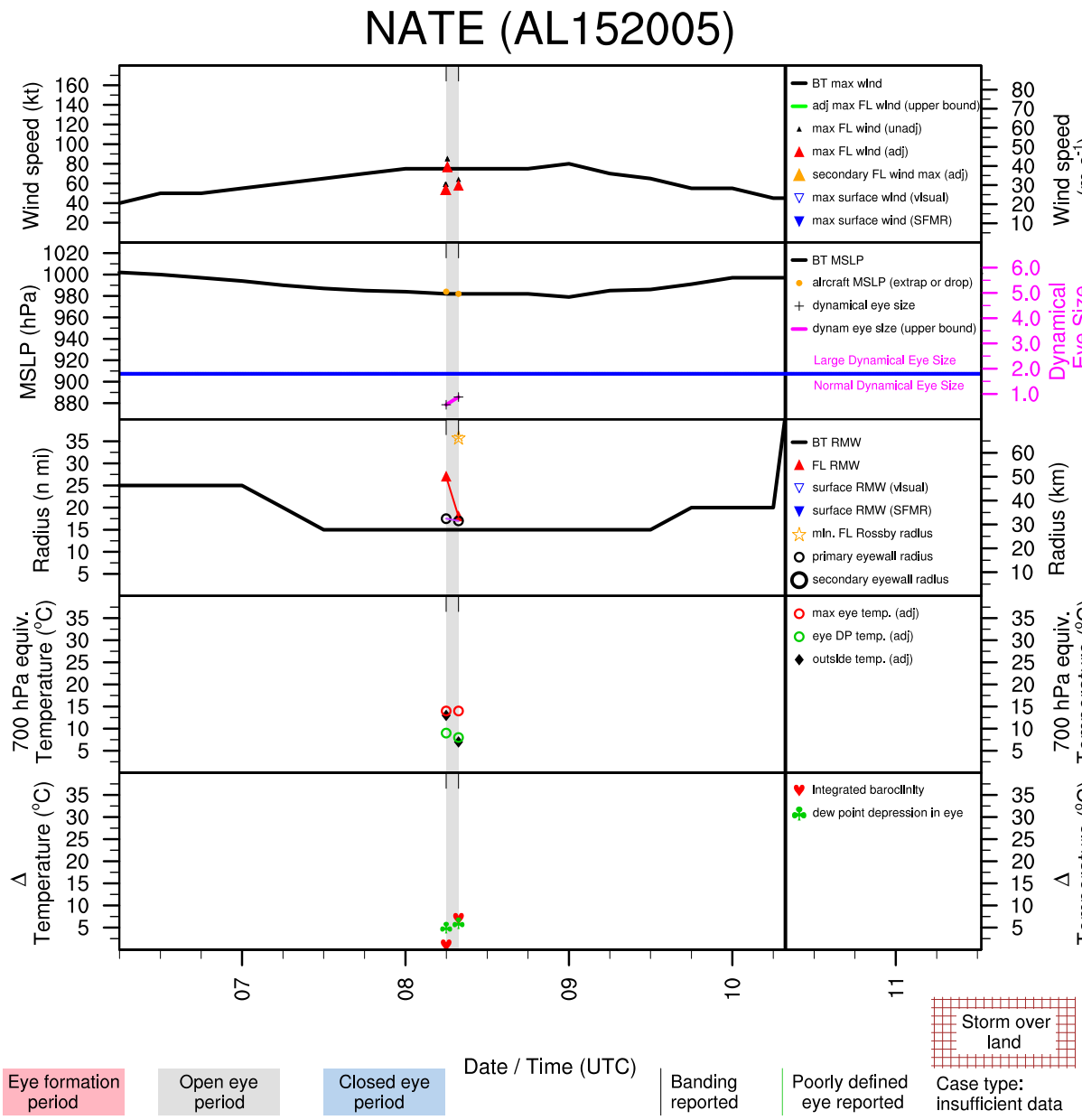

Figure E.144: Structure and intensity parameters for Hurricane Nate (2005).

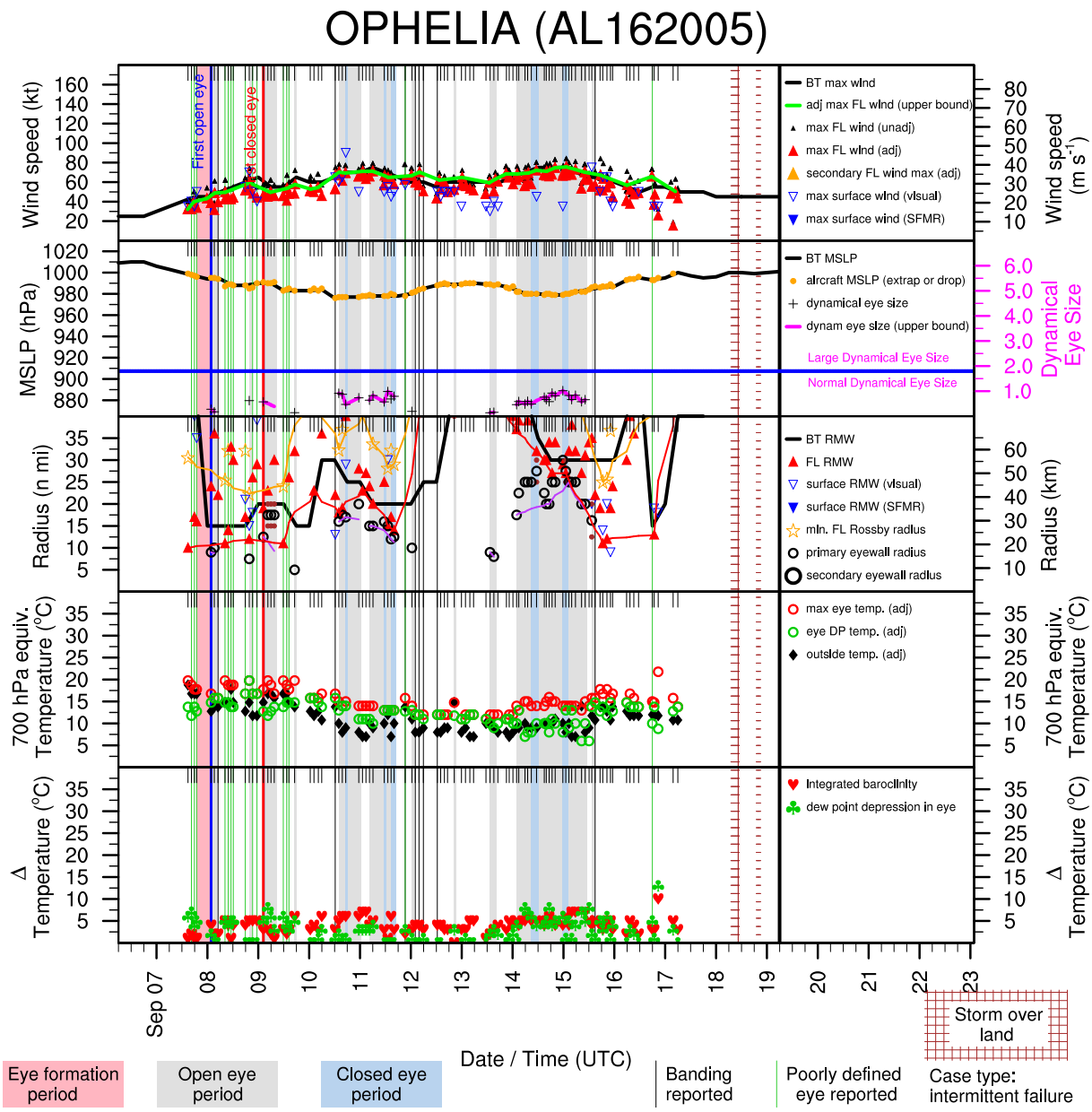

Figure E.145: Structure and intensity parameters for Hurricane Ophelia (2005).

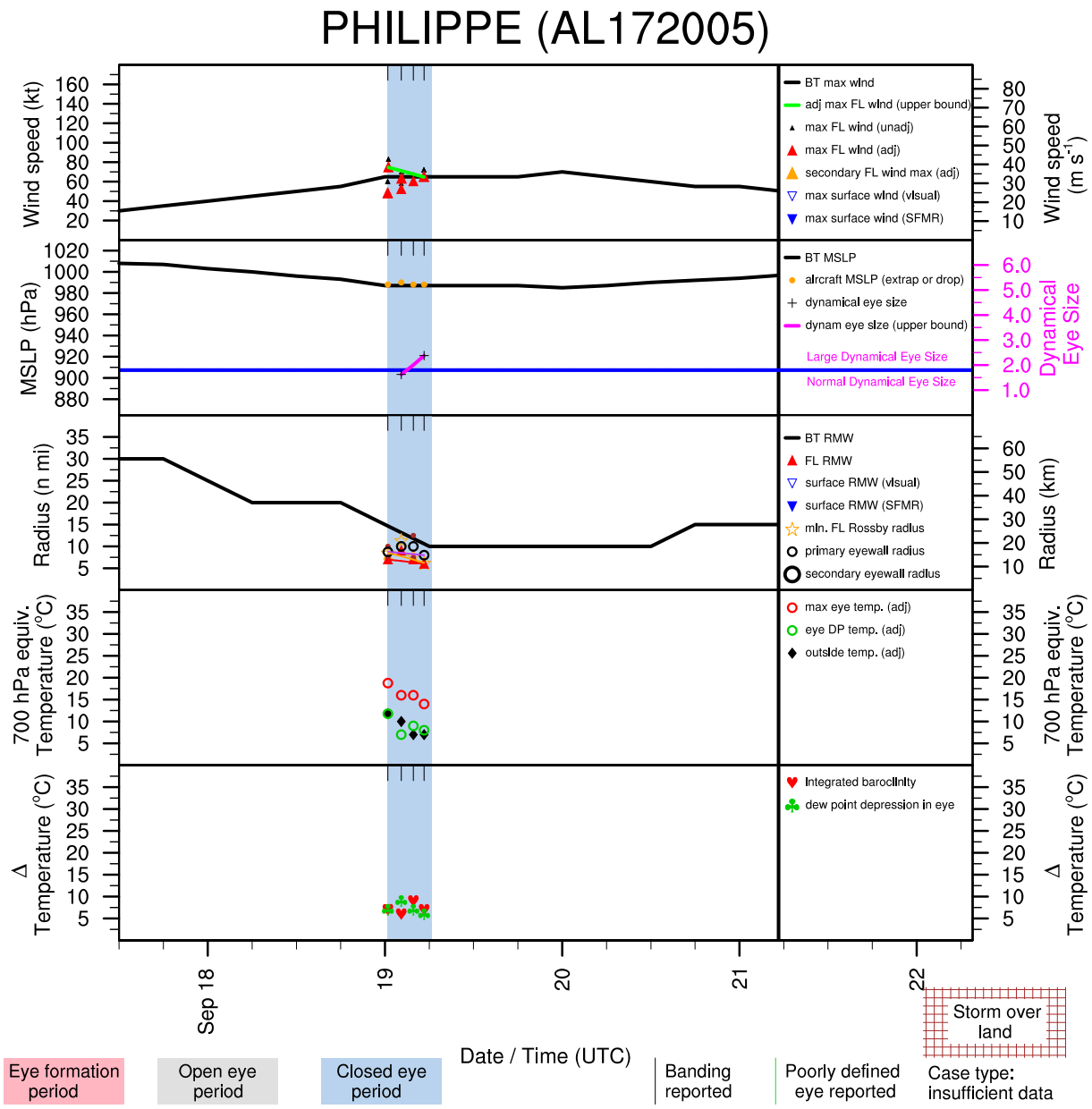

Figure E.146: Structure and intensity parameters for Hurricane Philippe (2005).

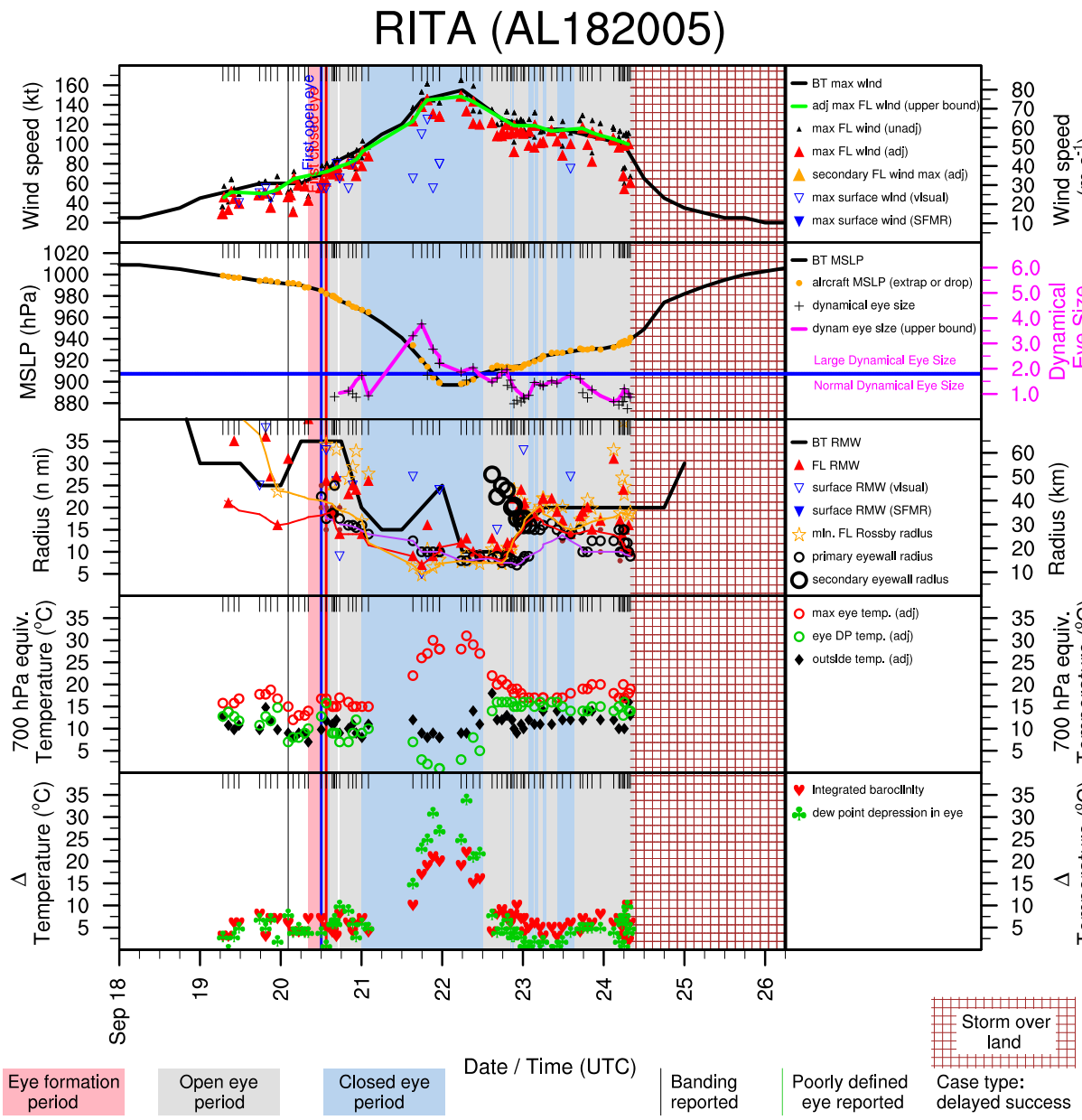

Figure E.147: Structure and intensity parameters for Hurricane Rita (2005).

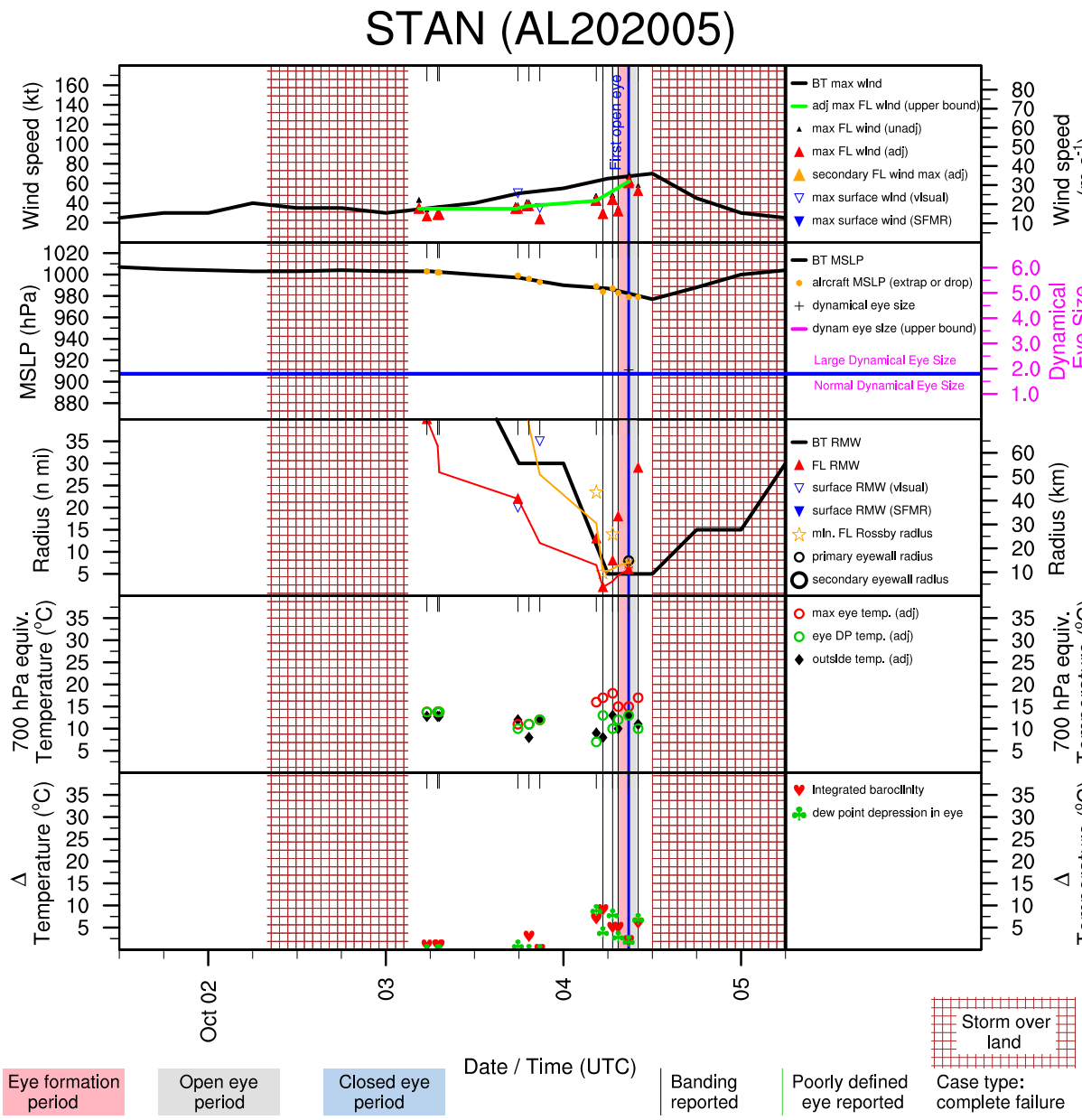

Figure E.148: Structure and intensity parameters for Hurricane Stan (2005).

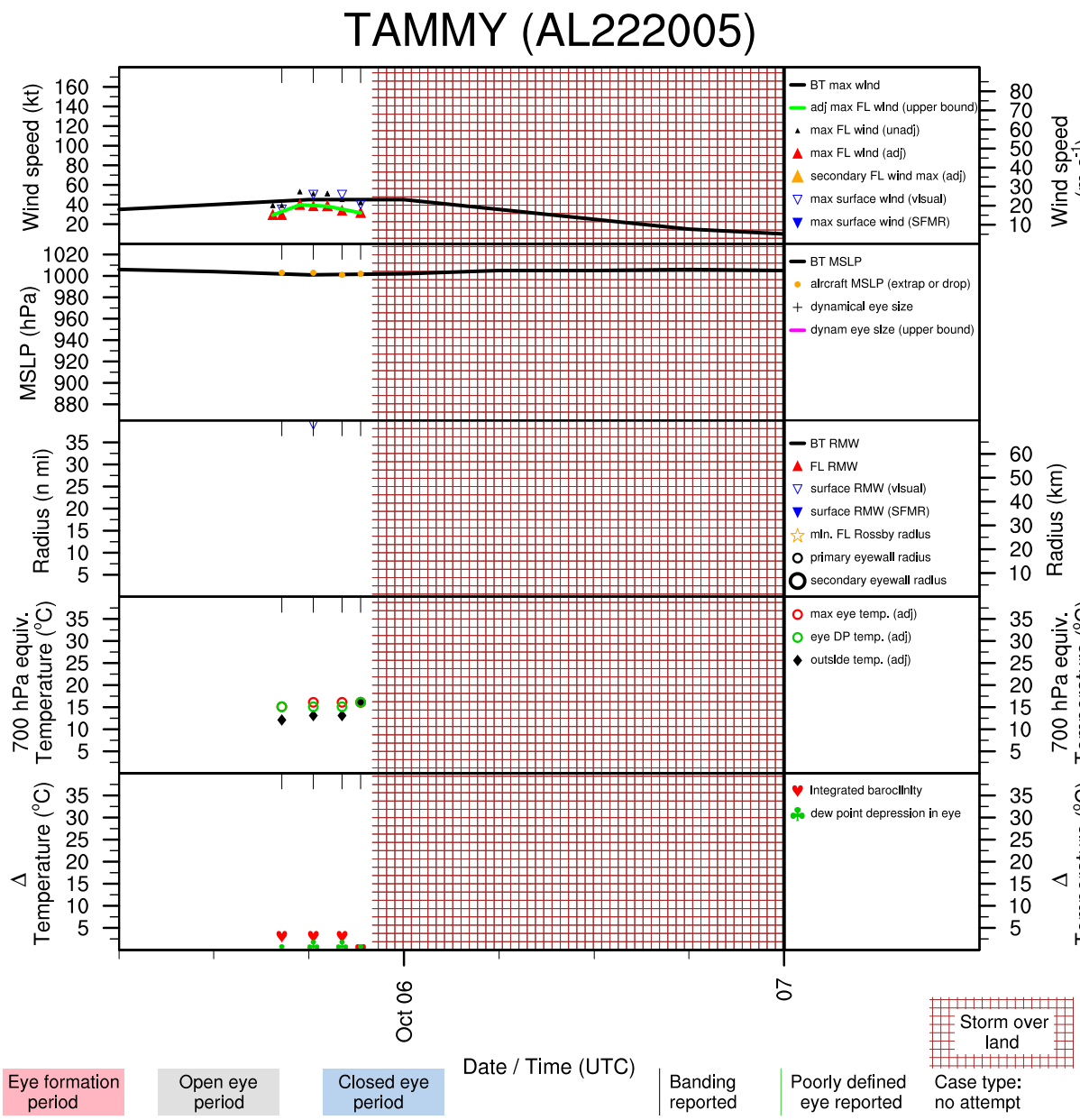

Figure E.149: Structure and intensity parameters for Tropical Storm Tammy (2005).

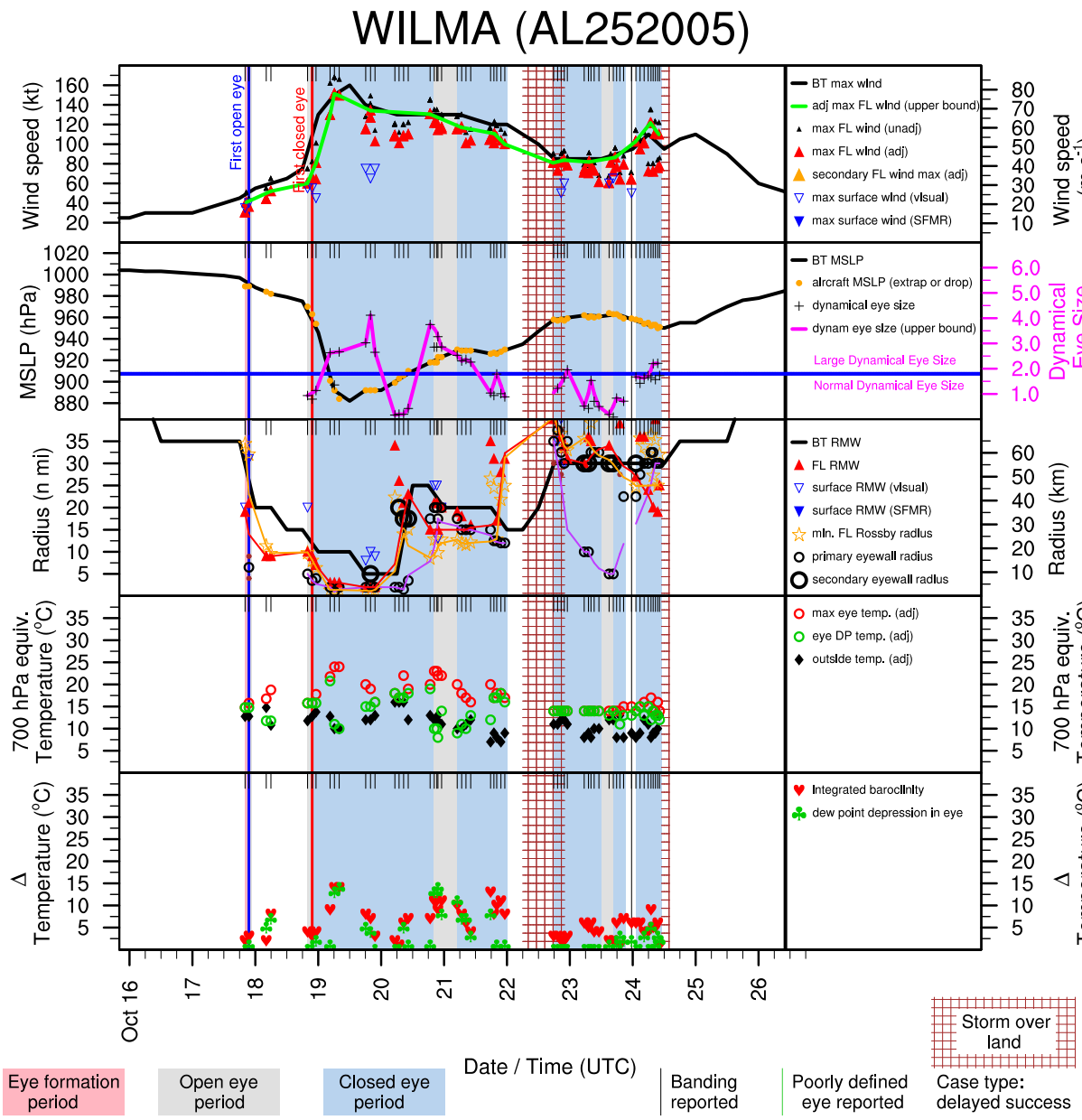

Figure E.150: Structure and intensity parameters for Hurricane Wilma (2005).

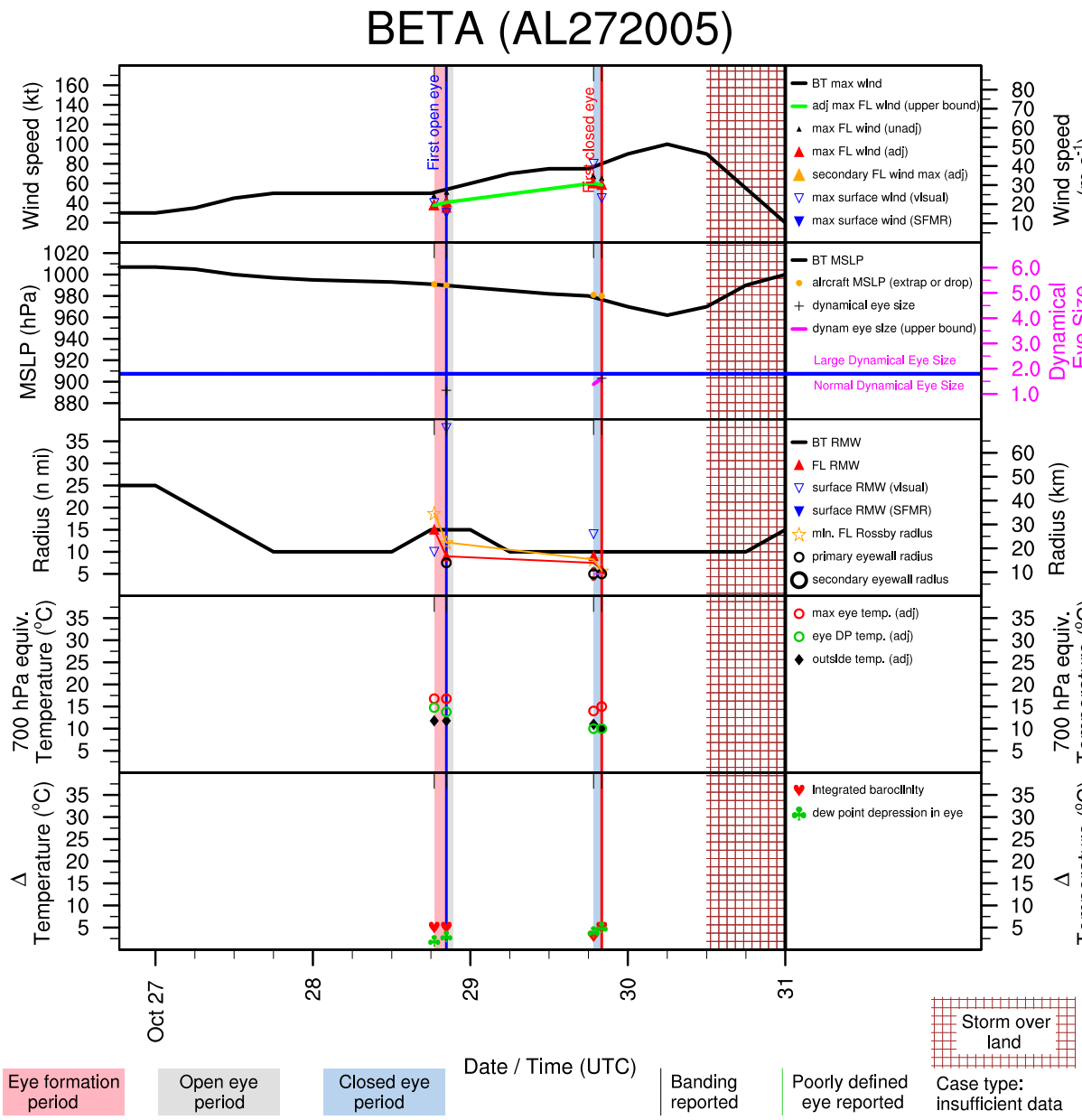

Figure E.151: Structure and intensity parameters for Hurricane Beta (2005).

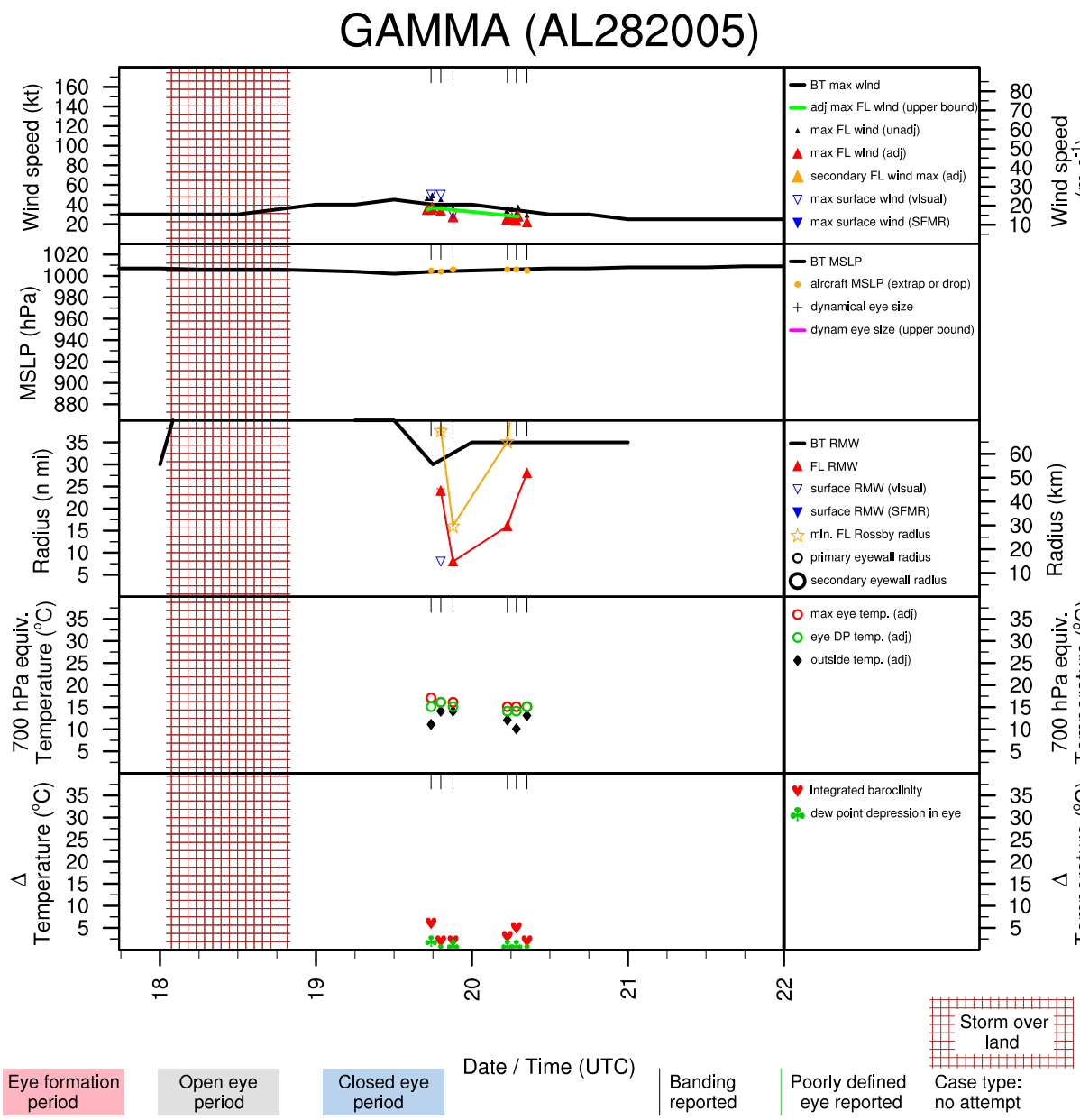

Figure E.152: Structure and intensity parameters for Tropical Storm Gamma (2005).

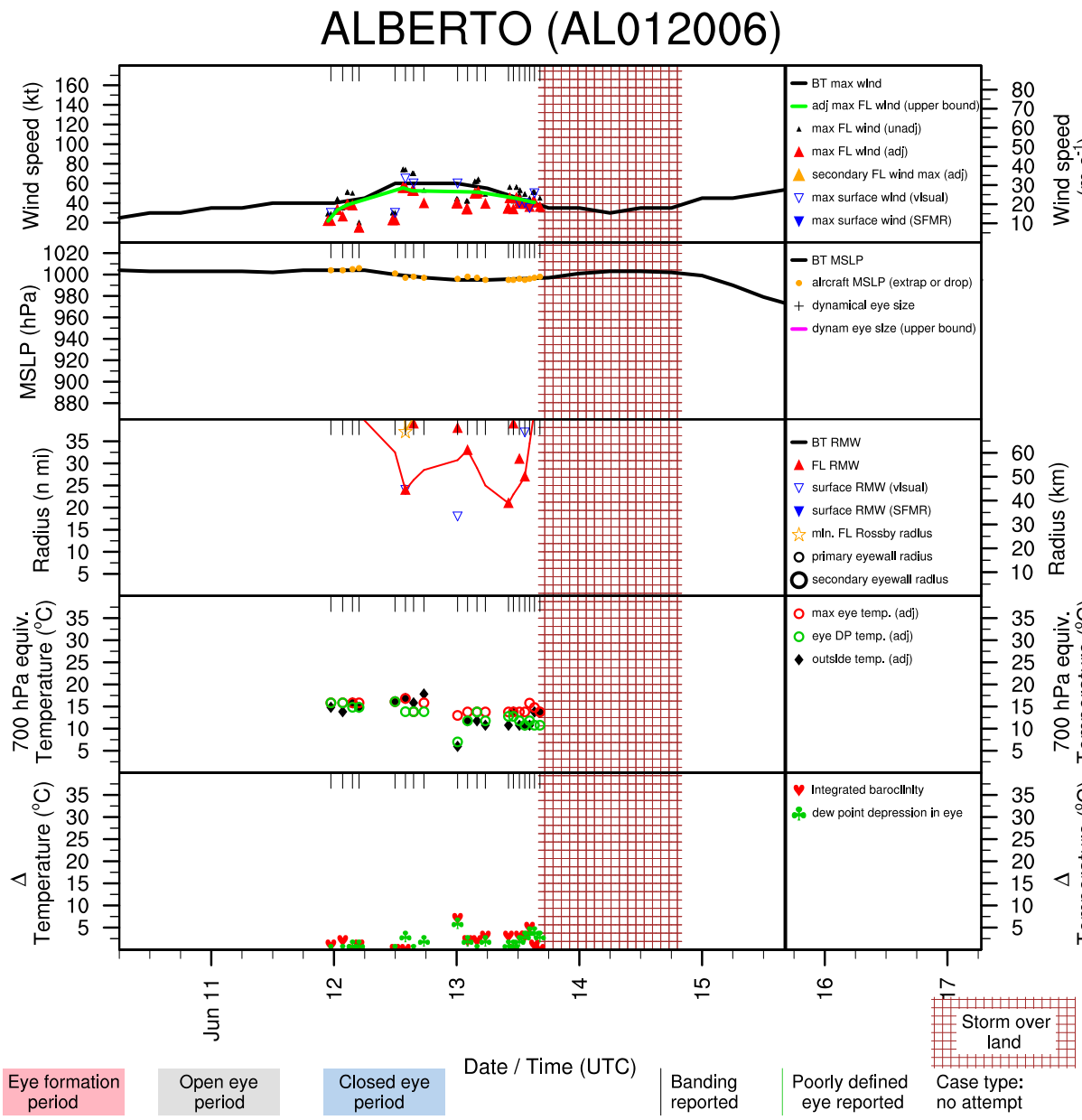

Figure E.153: Structure and intensity parameters for Tropical Storm Alberto (2006).

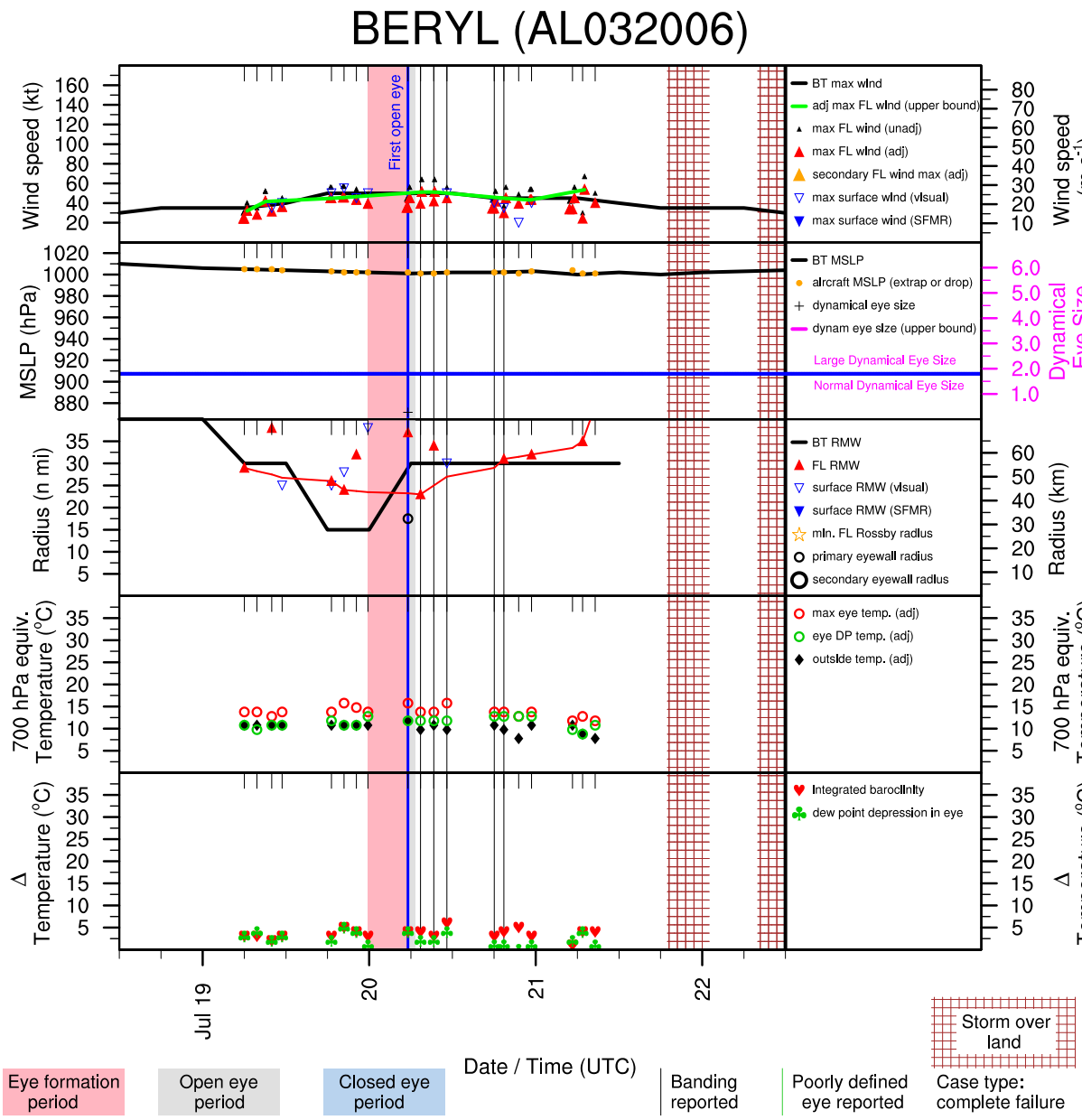

Figure E.154: Structure and intensity parameters for Tropical Storm Beryl (2006).

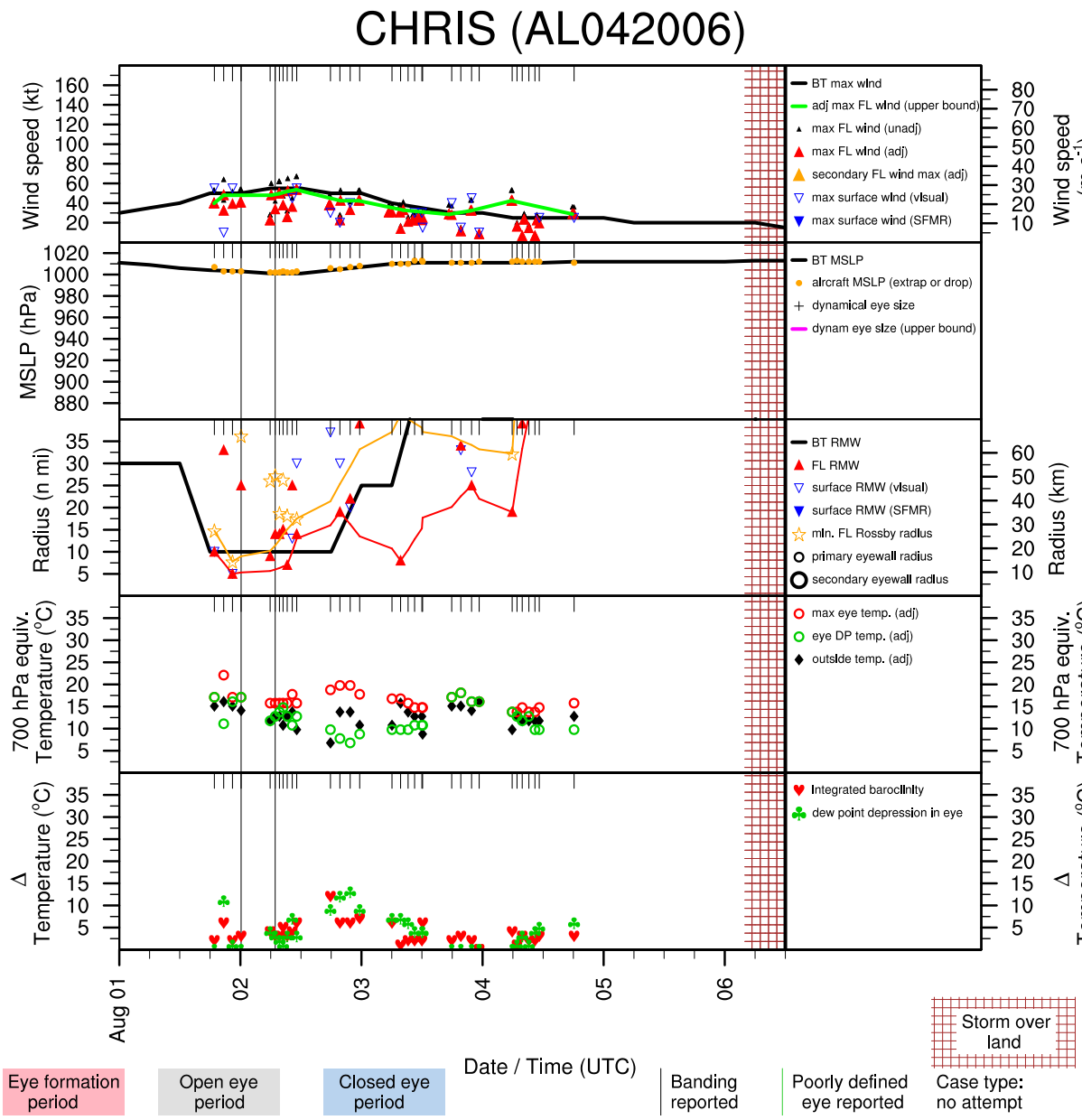

Figure E.155: Structure and intensity parameters for Tropical Storm Chris (2006).

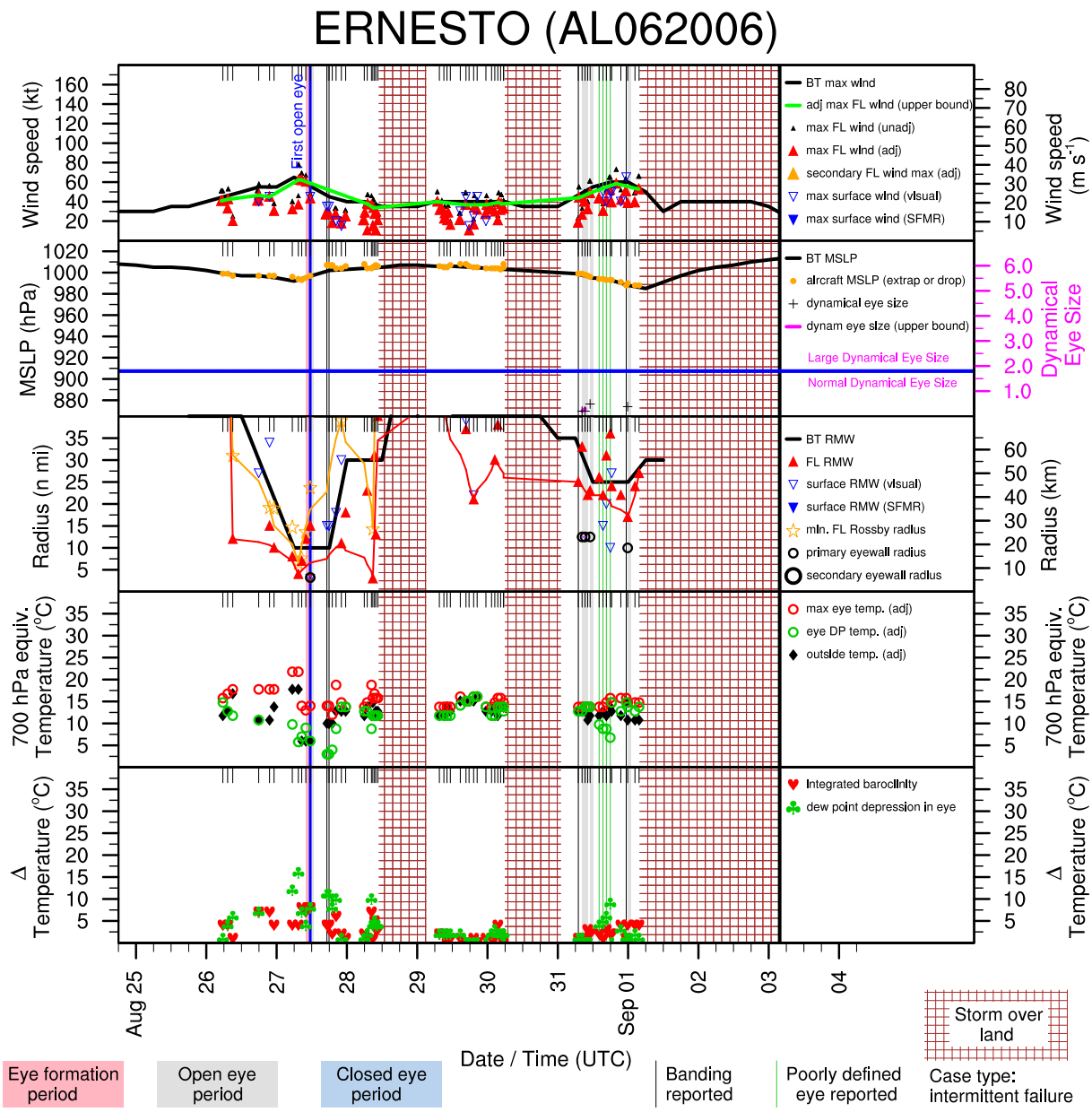

Figure E.156: Structure and intensity parameters for Hurricane Ernesto (2006).

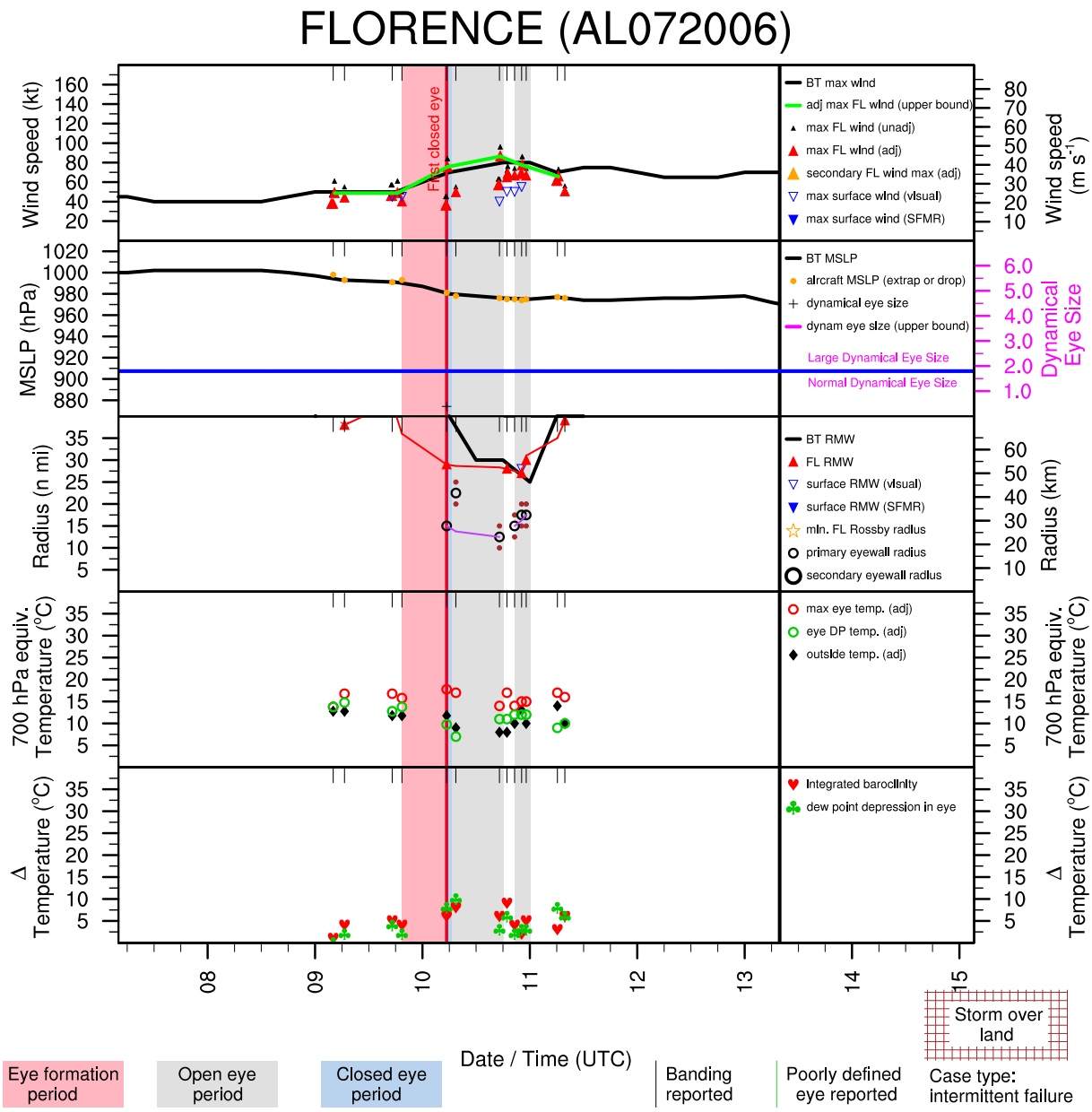

Figure E.157: Structure and intensity parameters for Hurricane Florence (2006).

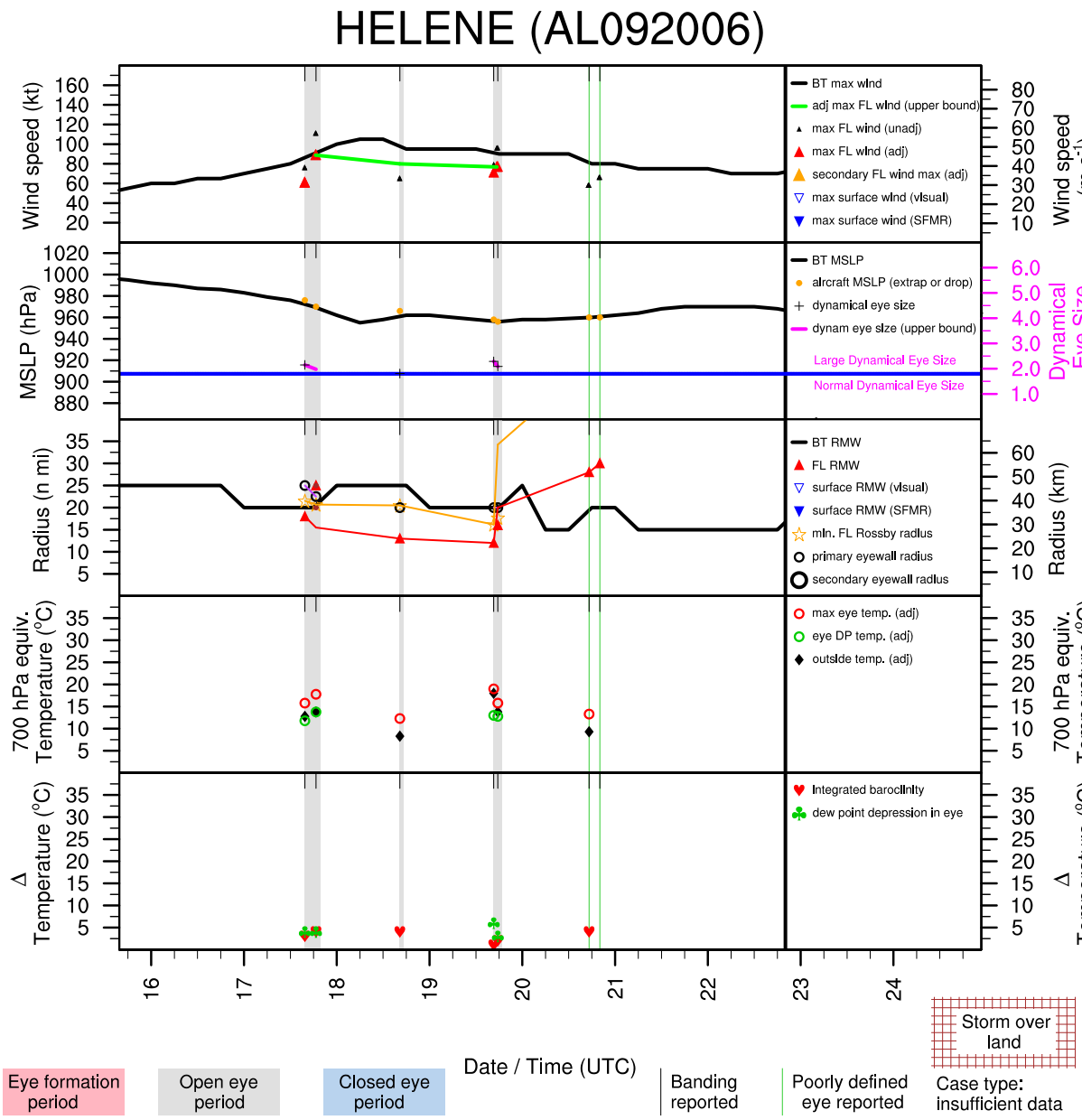

Figure E.158: Structure and intensity parameters for Hurricane Helene (2006).

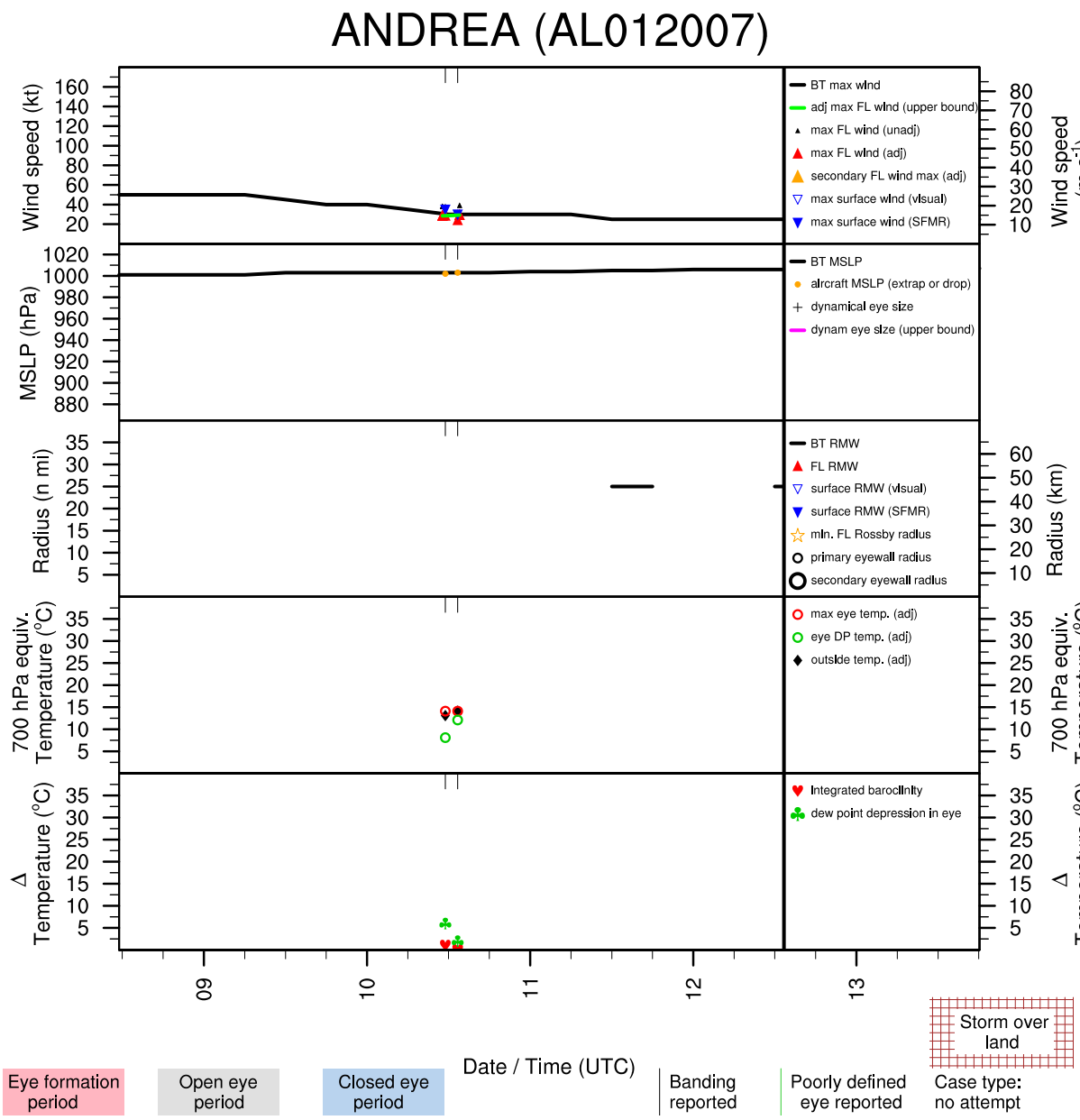

Figure E.159: Structure and intensity parameters for Hurricane Andrea (2007).

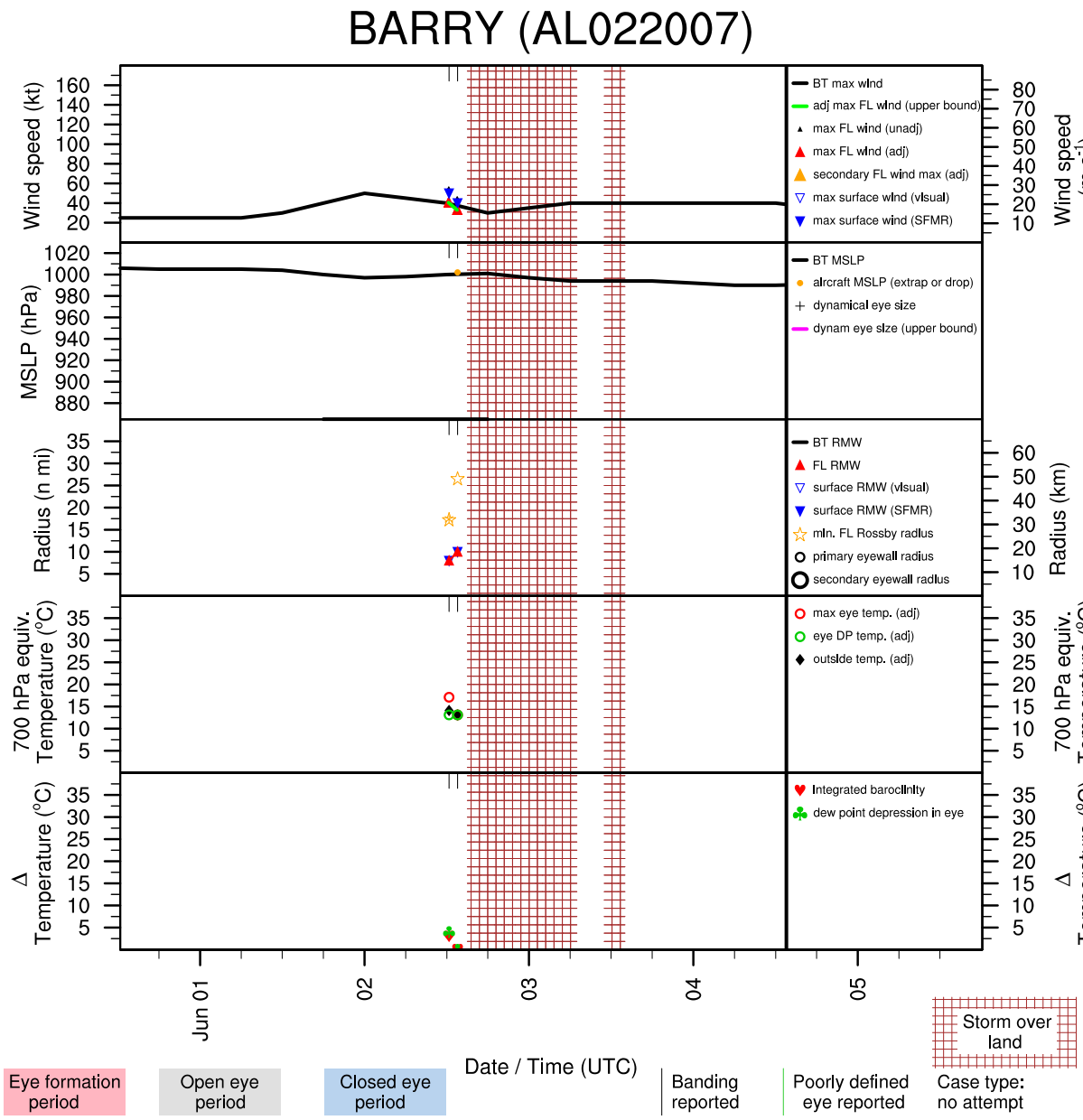

Figure E.160: Structure and intensity parameters for Tropical Storm Barry (2007).

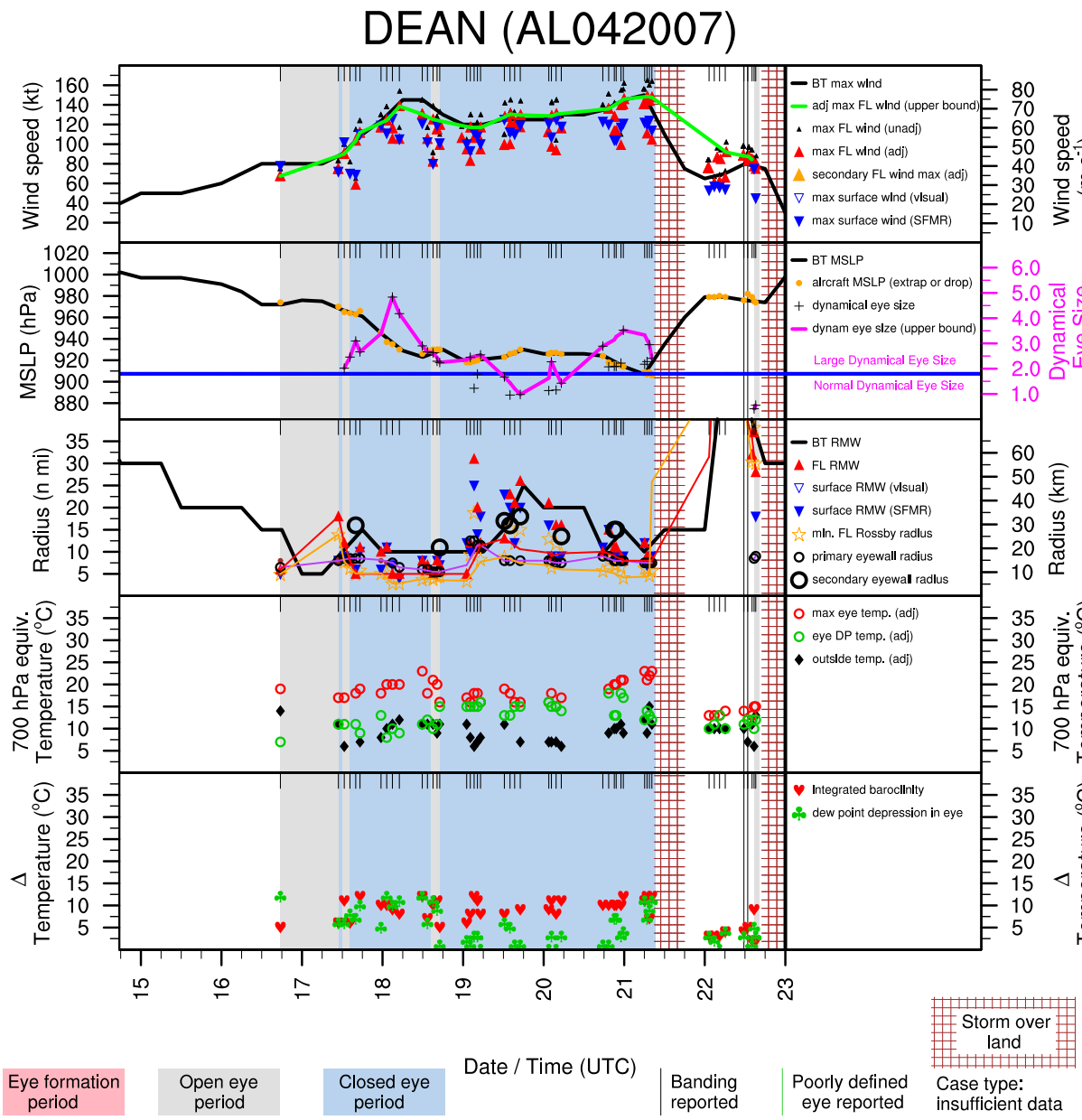

Figure E.161: Structure and intensity parameters for Hurricane Dean (2007).

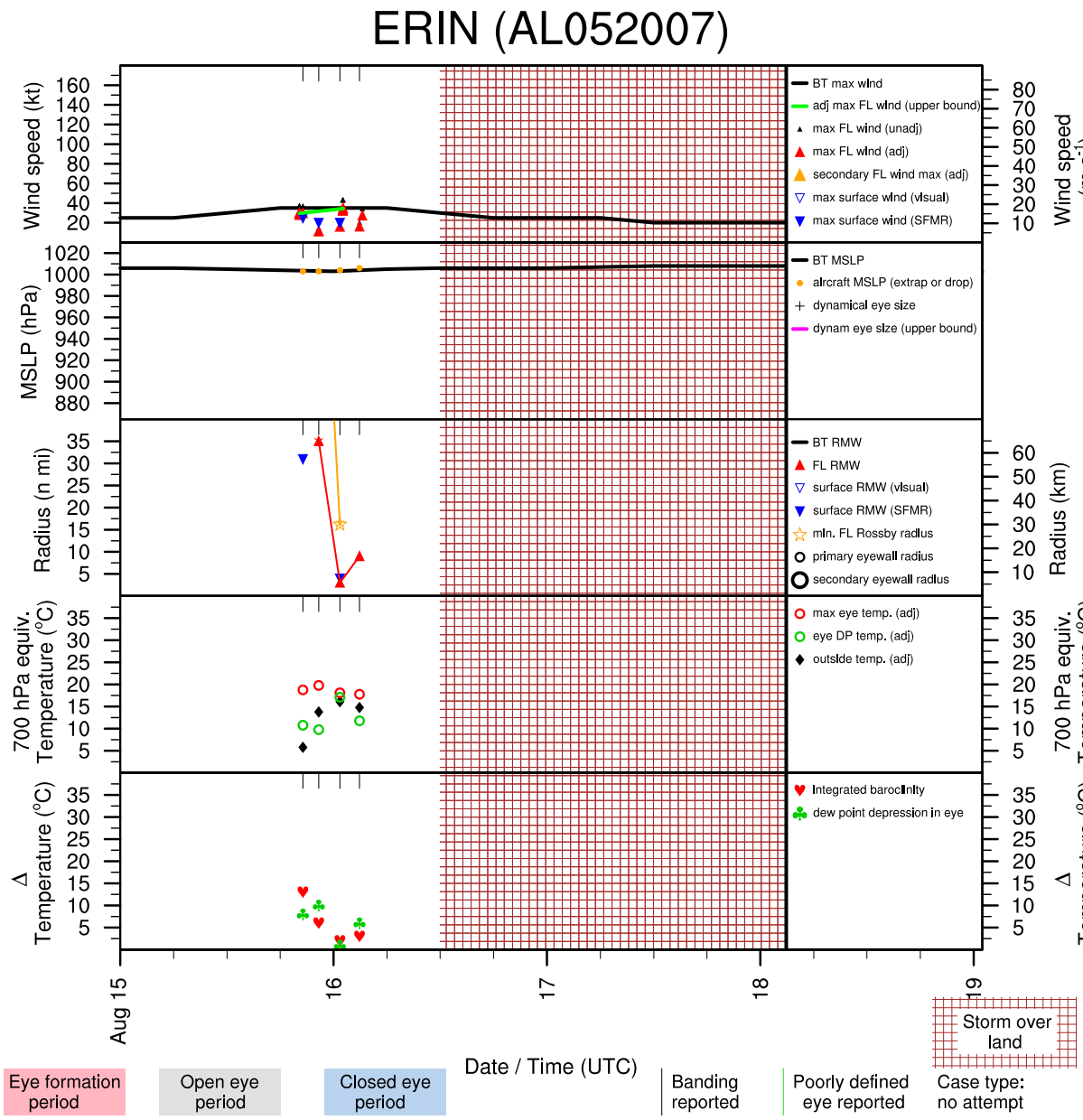

Figure E.162: Structure and intensity parameters for Tropical Storm Erin (2007).

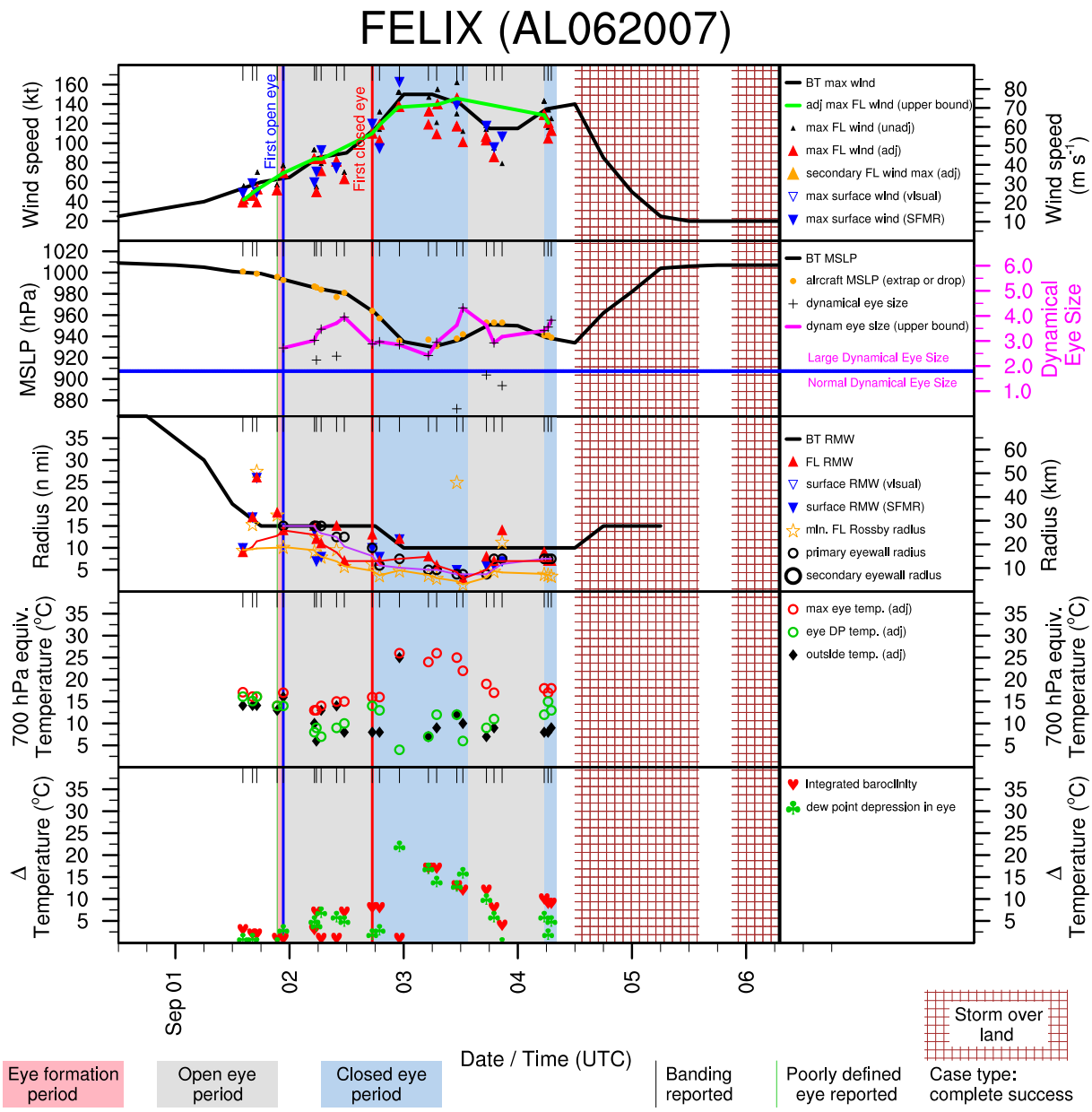

Figure E.163: Structure and intensity parameters for Hurricane Felix (2007).

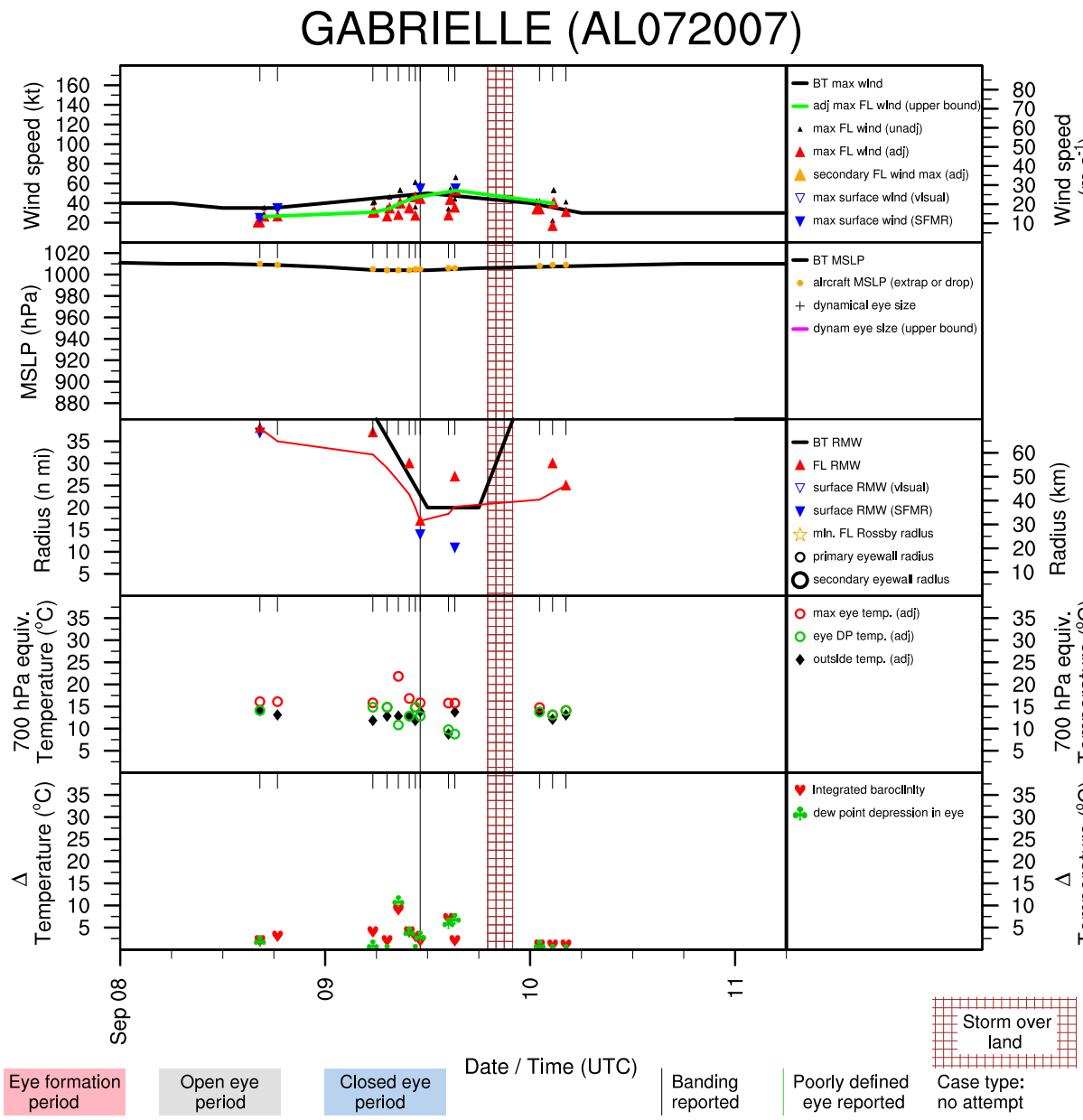

Figure E.164: Structure and intensity parameters for Tropical Storm Gabrielle (2007).

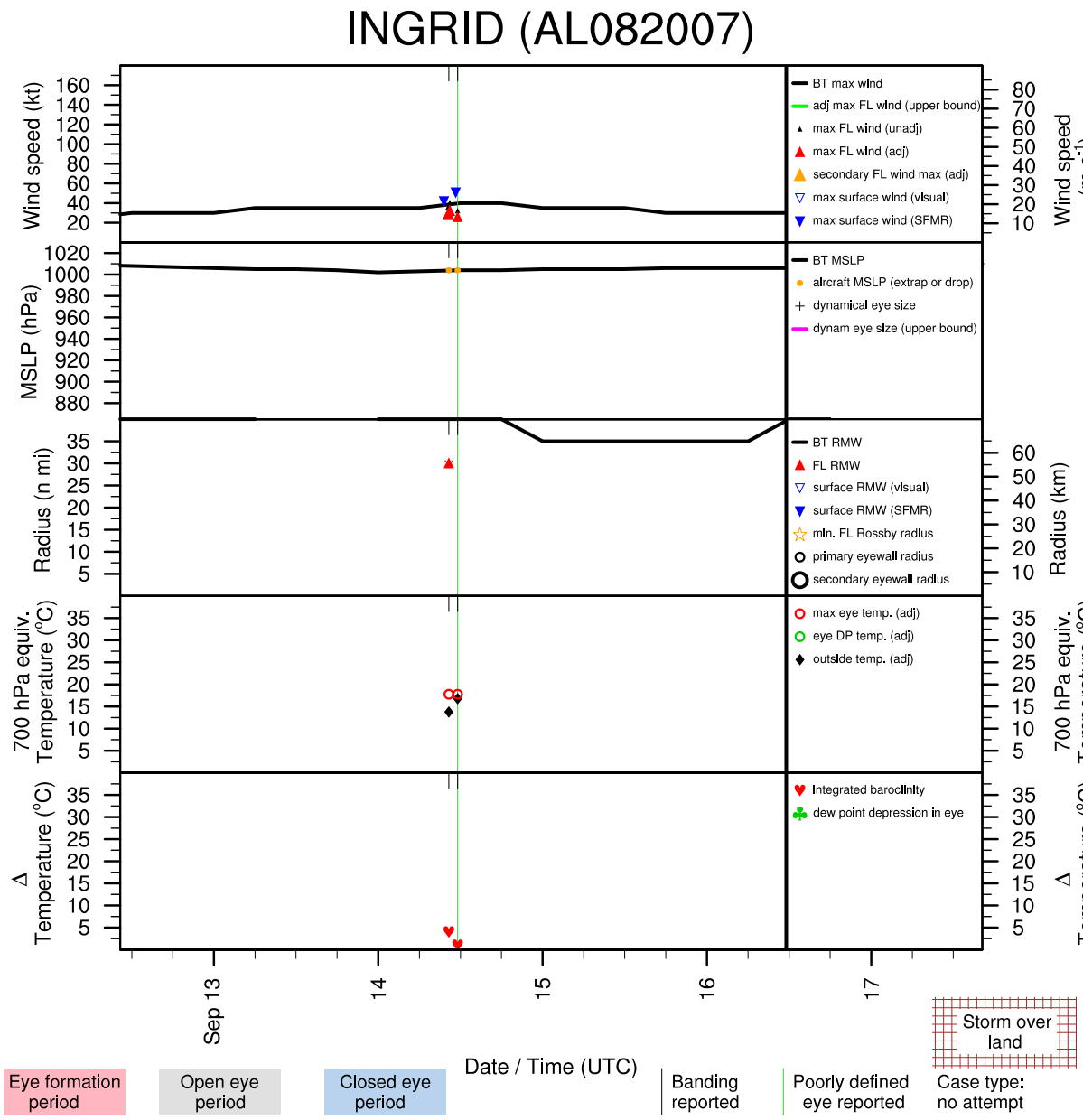

Figure E.165: Structure and intensity parameters for Tropical Storm Ingrid (2007).

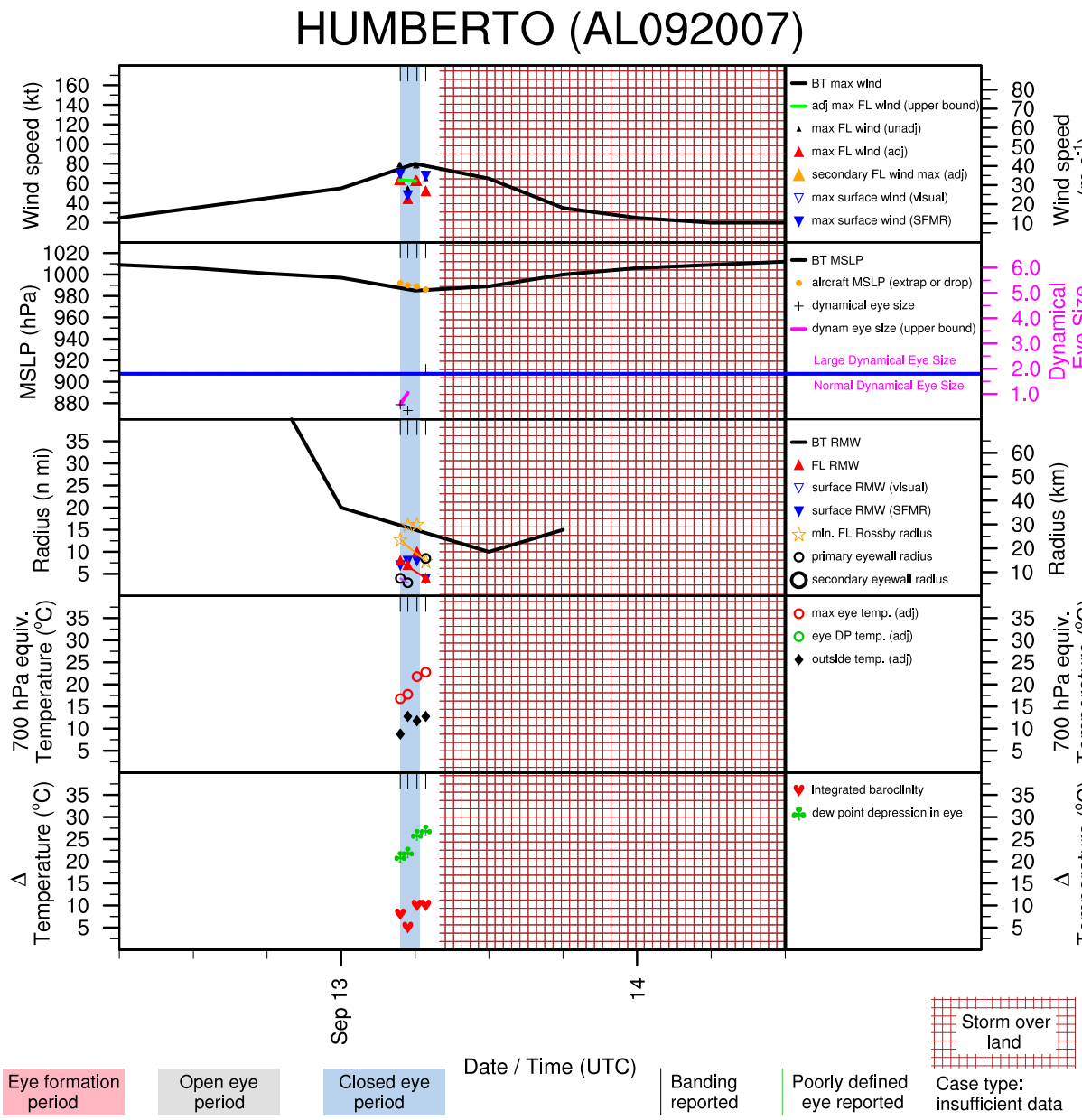

Figure E.166: Structure and intensity parameters for Hurricane Humberto (2007).

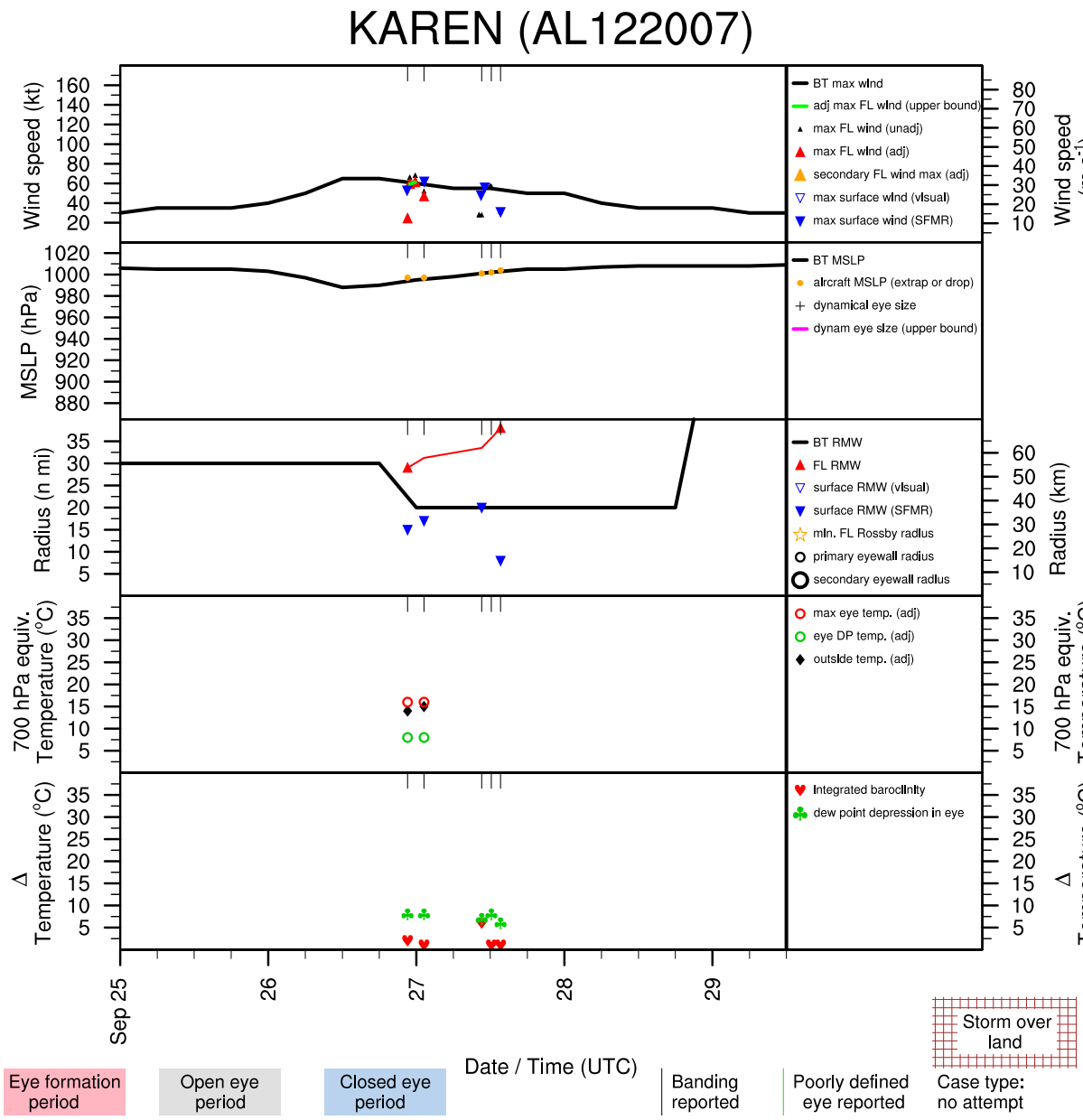

Figure E.167: Structure and intensity parameters for Hurricane Karen (2007).

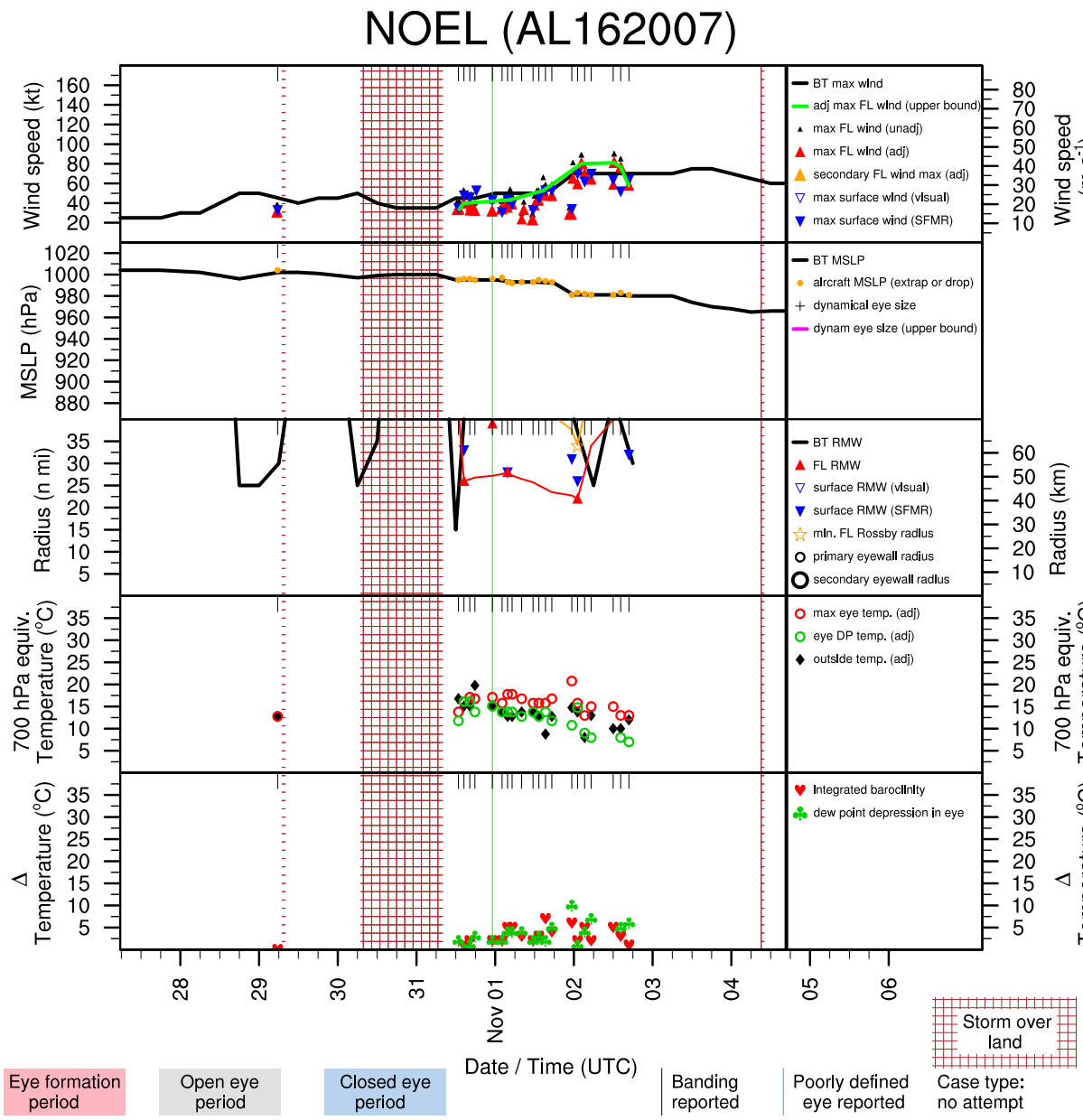

Figure E.168: Structure and intensity parameters for Hurricane Noel (2007).

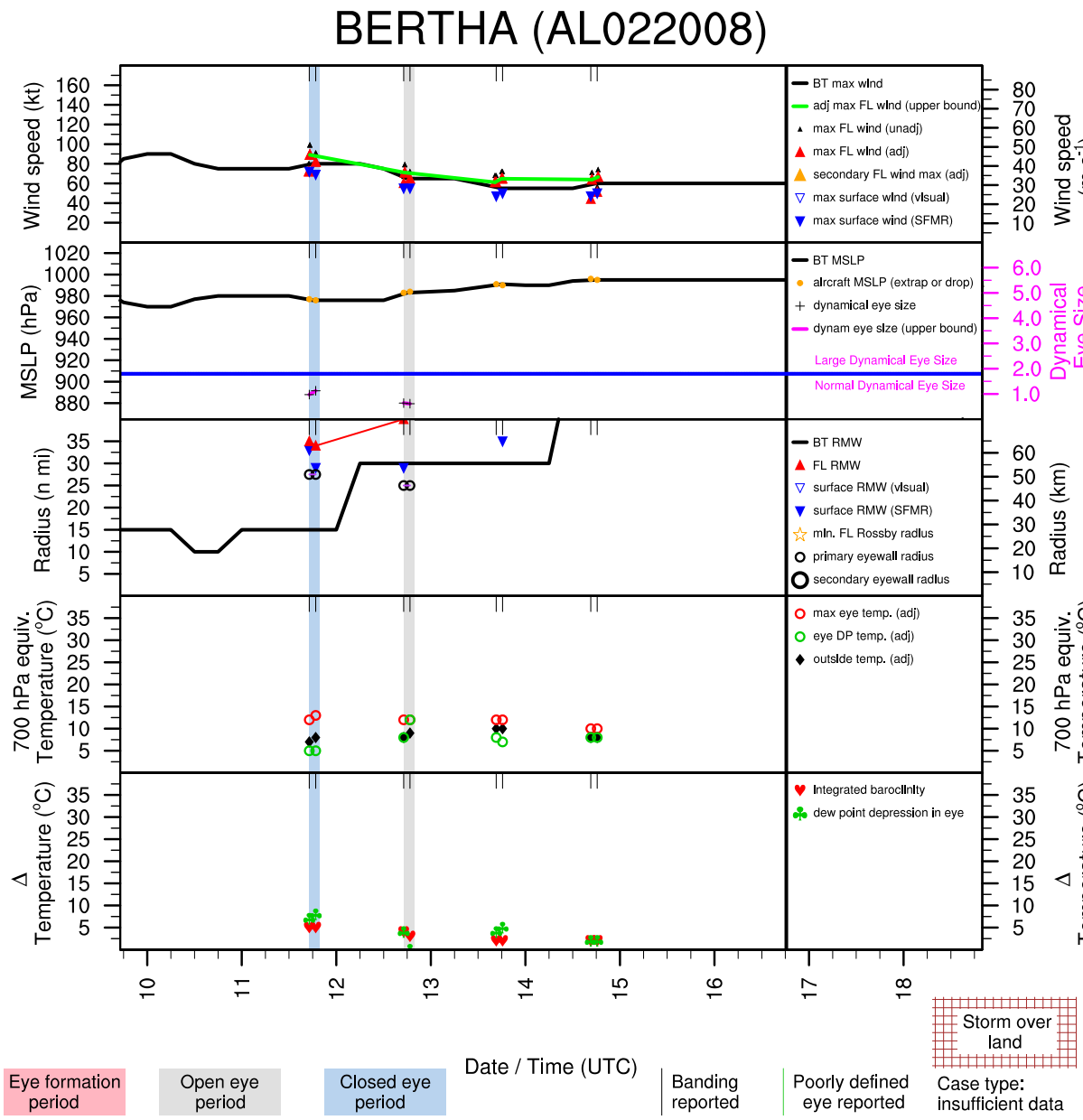

Figure E.169: Structure and intensity parameters for Hurricane Bertha (2008).

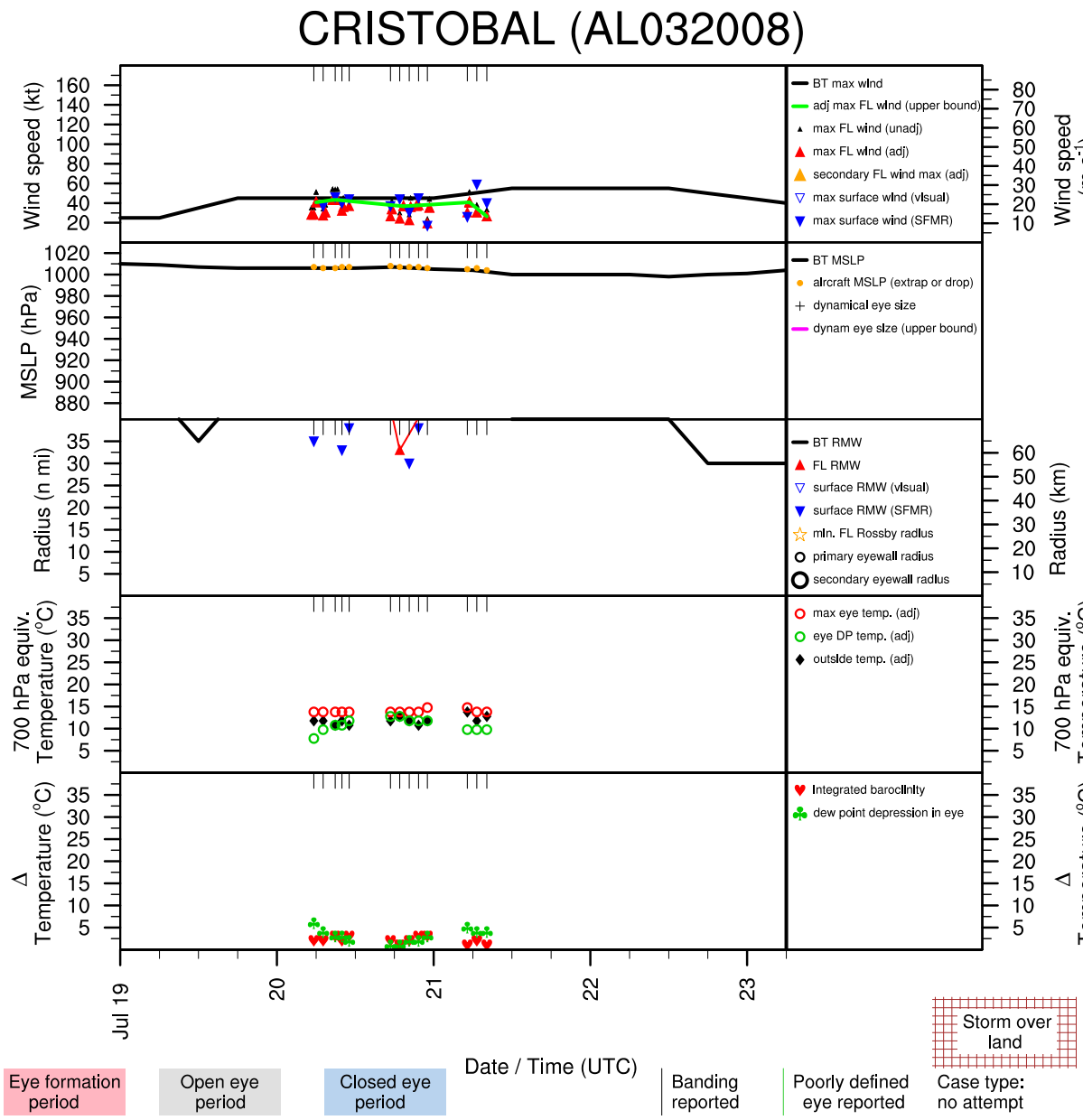

Figure E.170: Structure and intensity parameters for Tropical Storm Cristobal (2008).

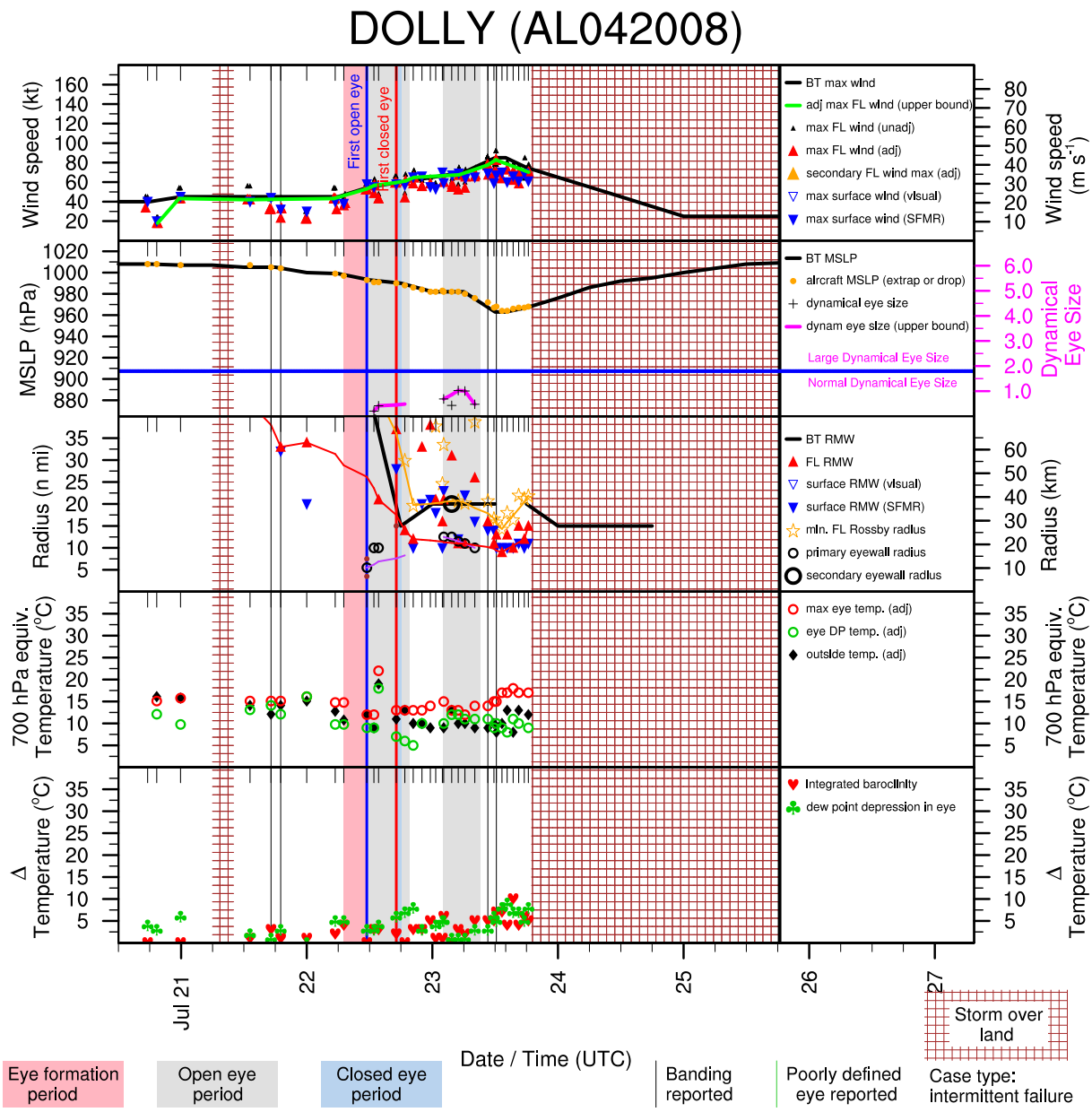

Figure E.171: Structure and intensity parameters for Hurricane Dolly (2008).

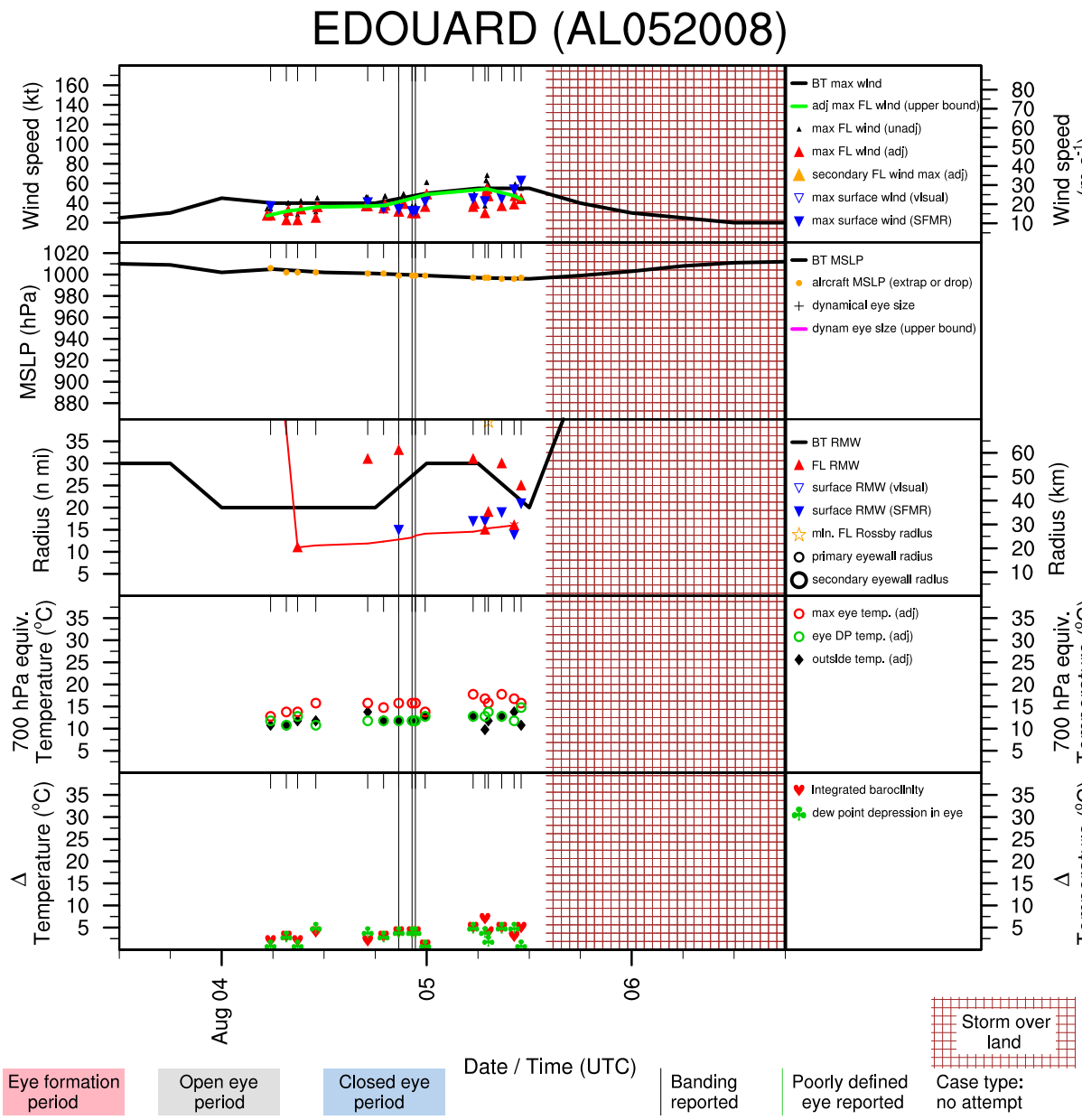

Figure E.172: Structure and intensity parameters for Tropical Storm Edouard (2008).

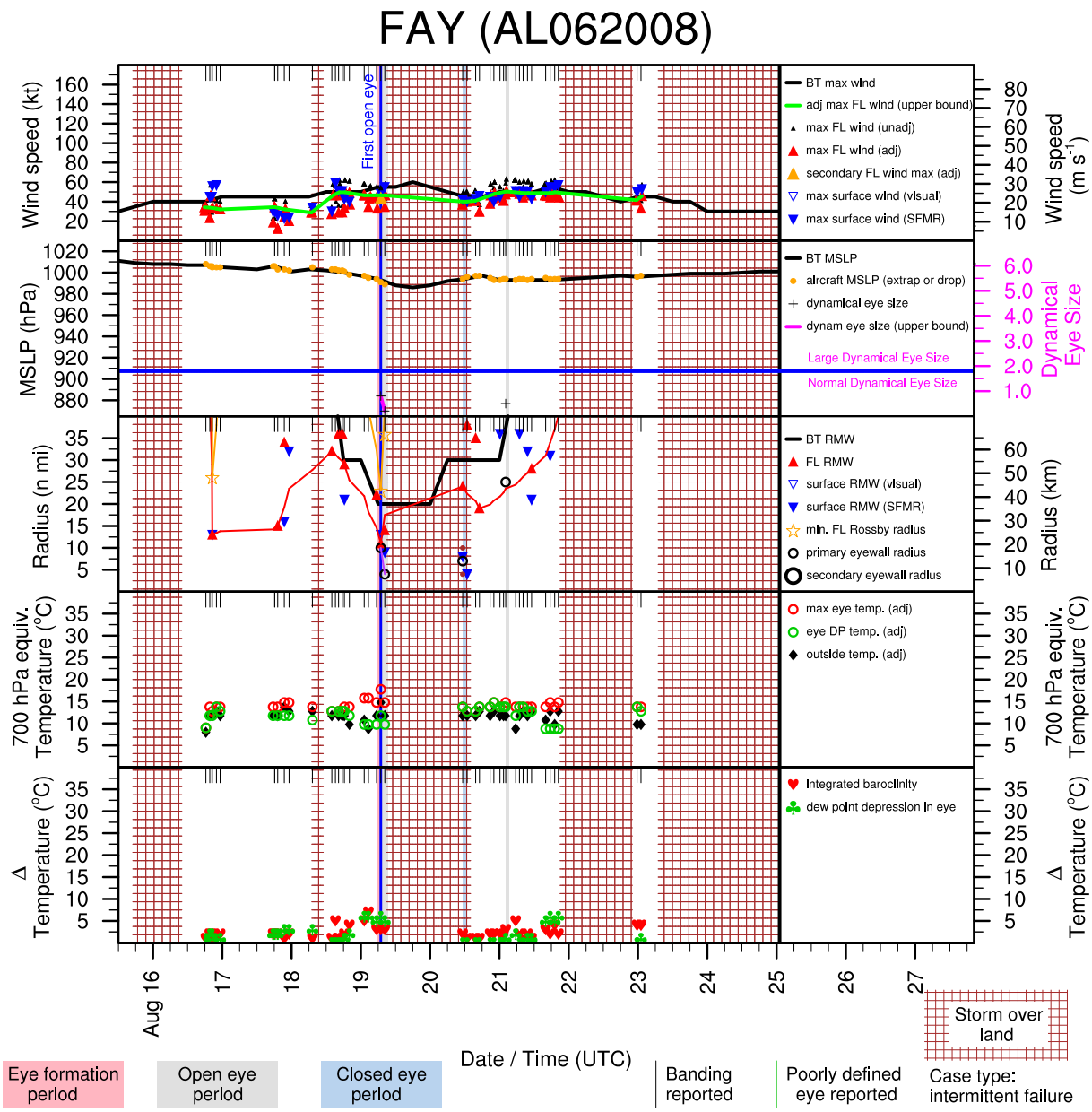

Figure E.173: Structure and intensity parameters for Tropical Storm Fay (2008).

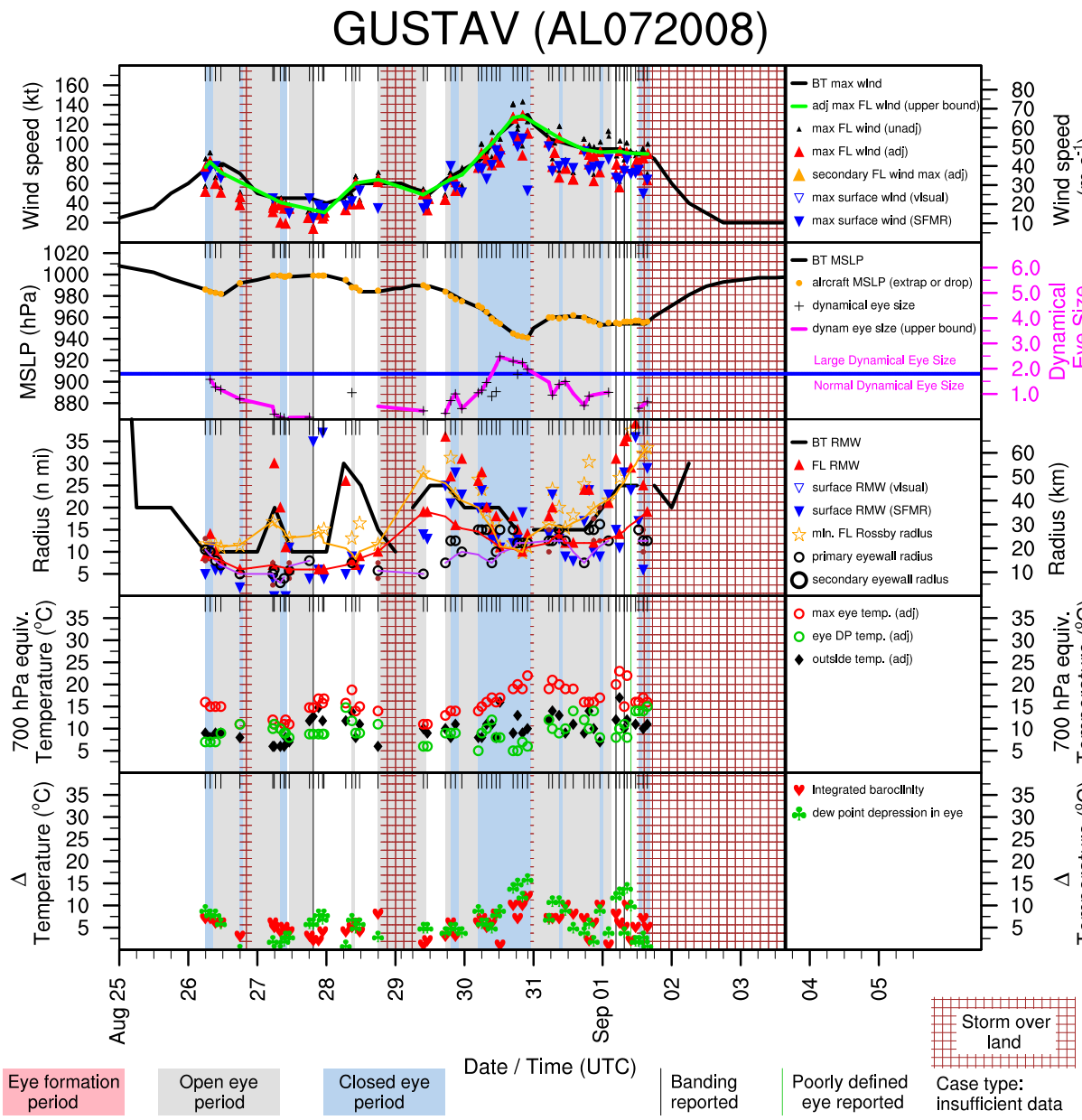

Figure E.174: Structure and intensity parameters for Hurricane Gustav (2008).

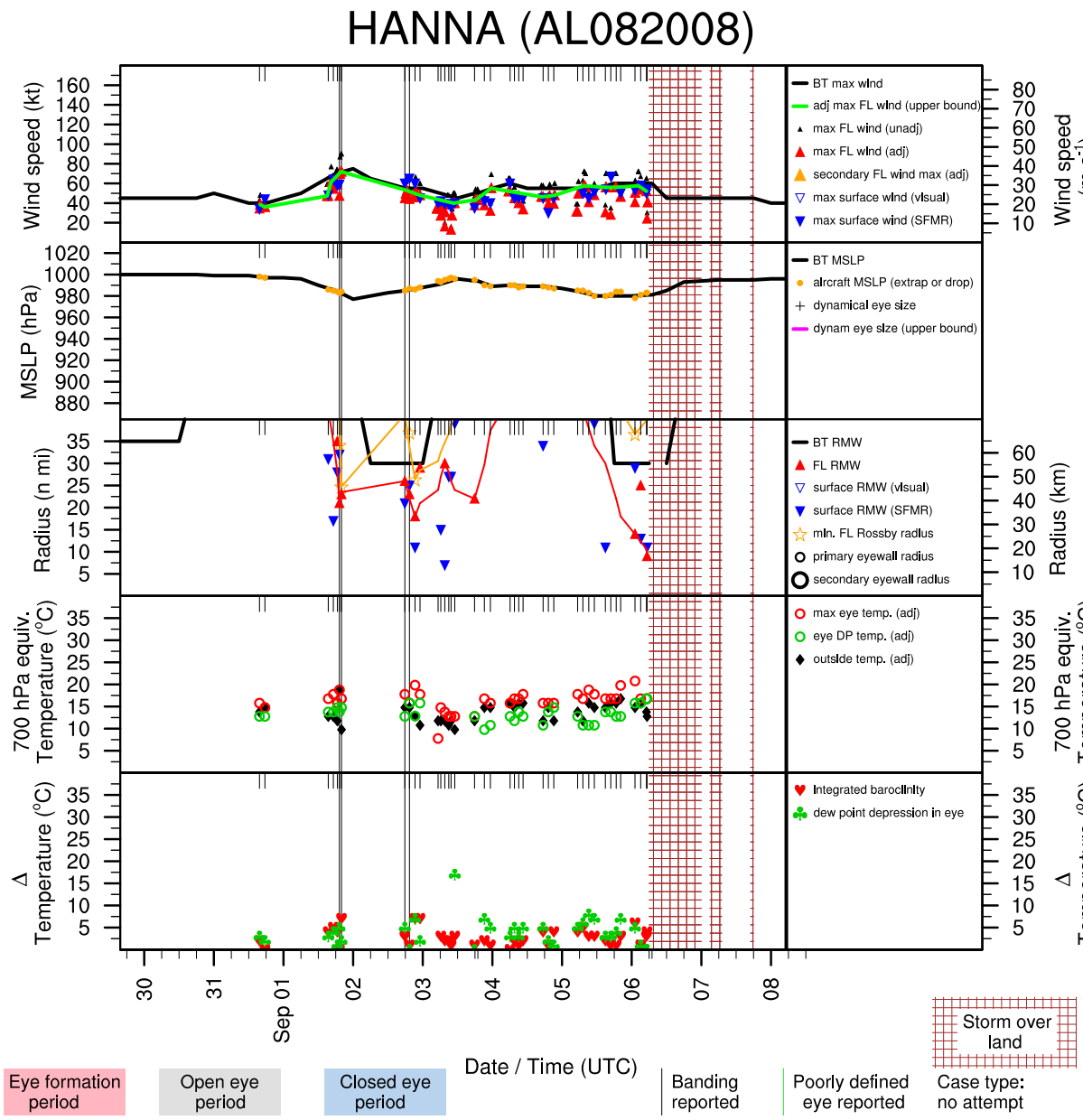

Figure E.175: Structure and intensity parameters for Hurricane Hanna (2008).

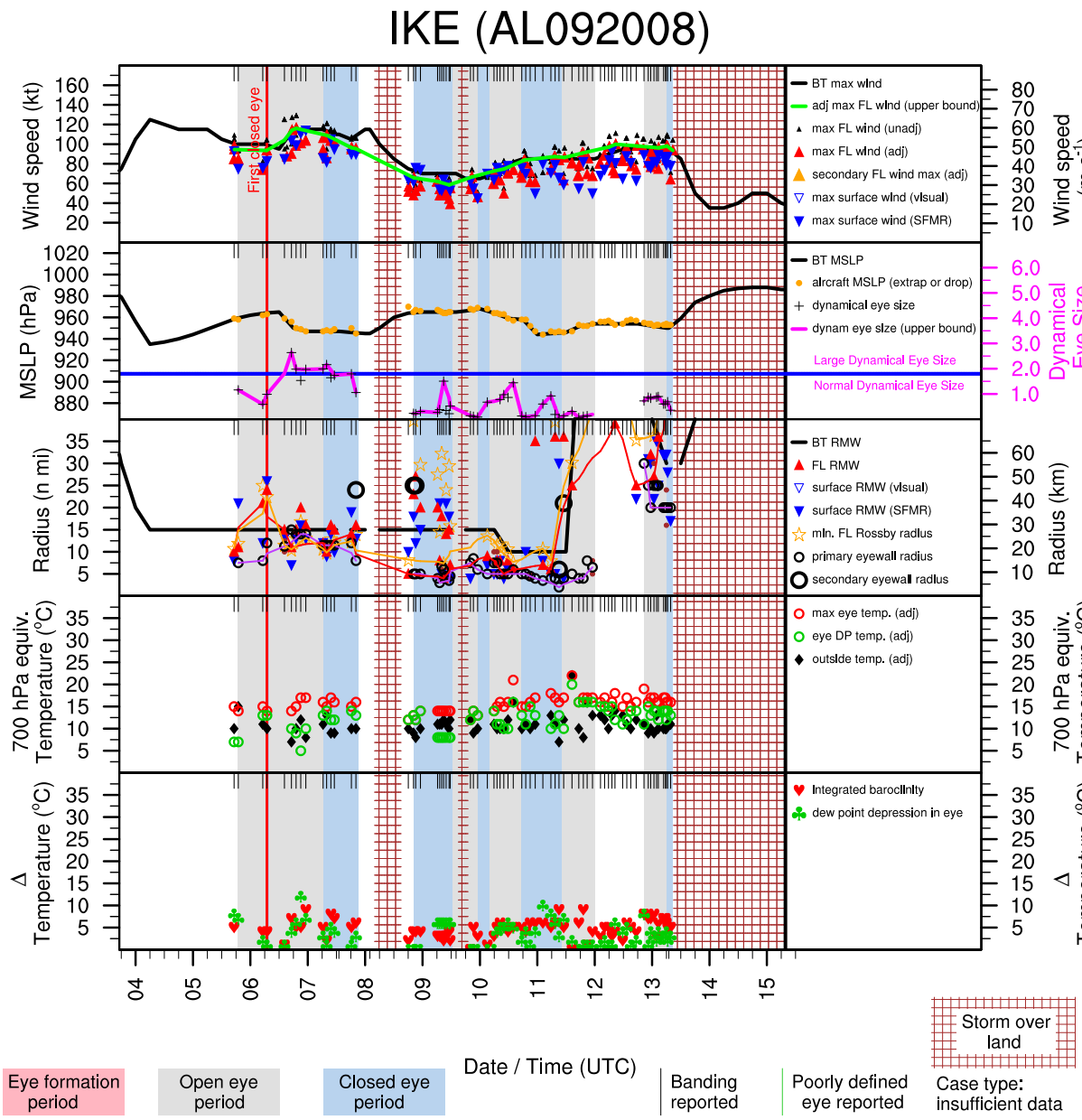

Figure E.176: Structure and intensity parameters for Hurricane Ike (2008).

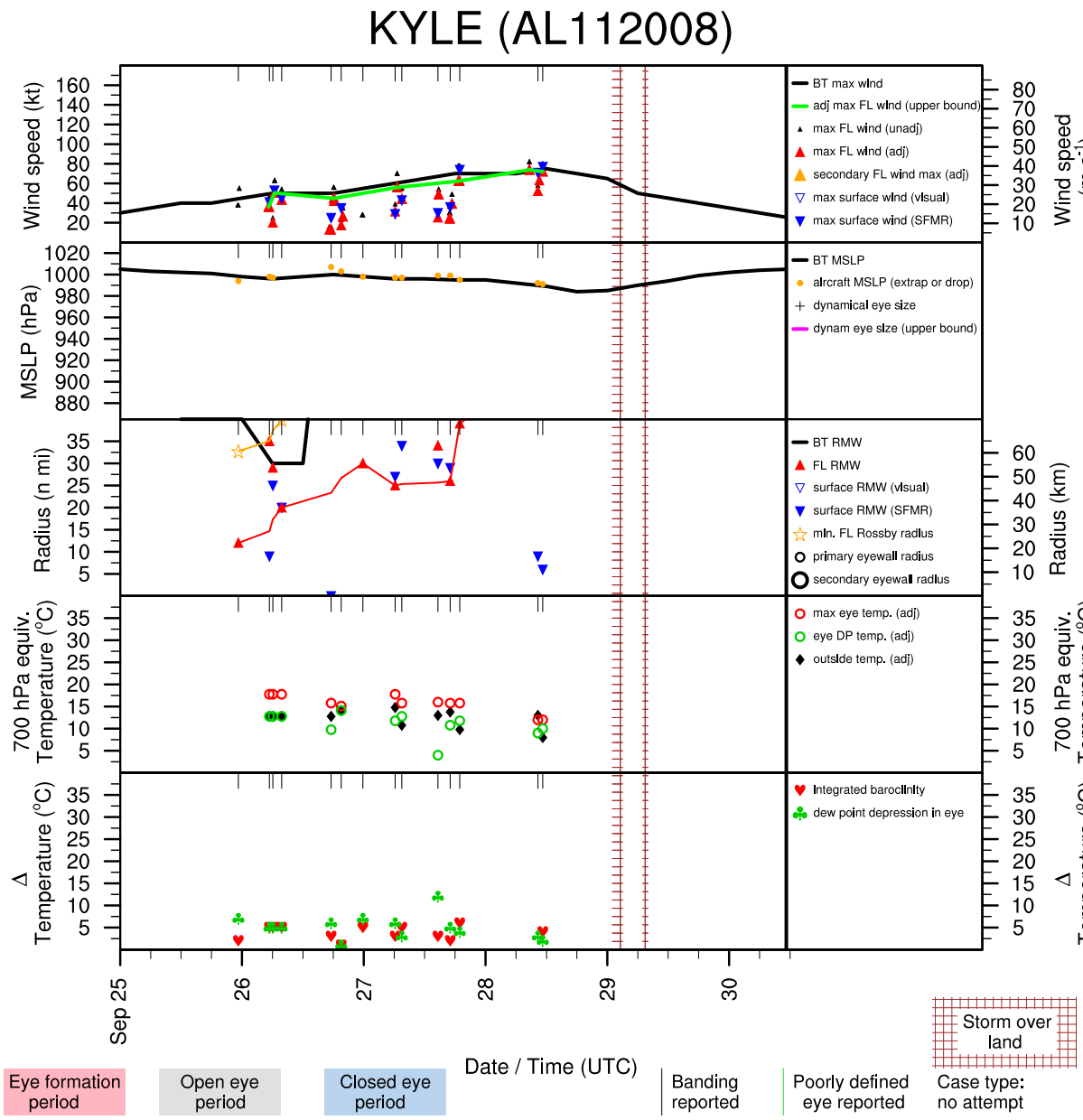

Figure E.177: Structure and intensity parameters for Hurricane Kyle (2008).

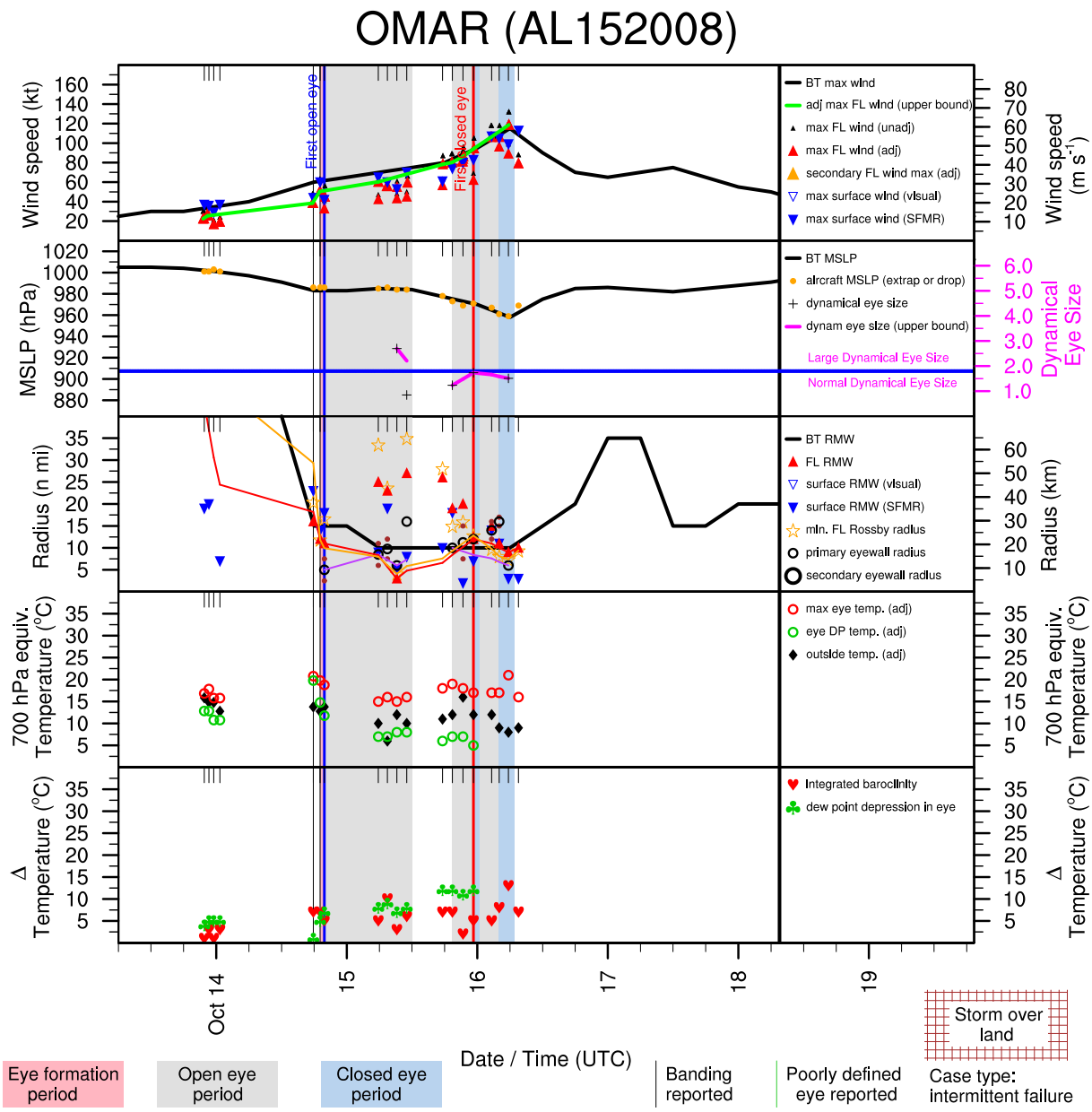

Figure E.178: Structure and intensity parameters for Hurricane Omar (2008).

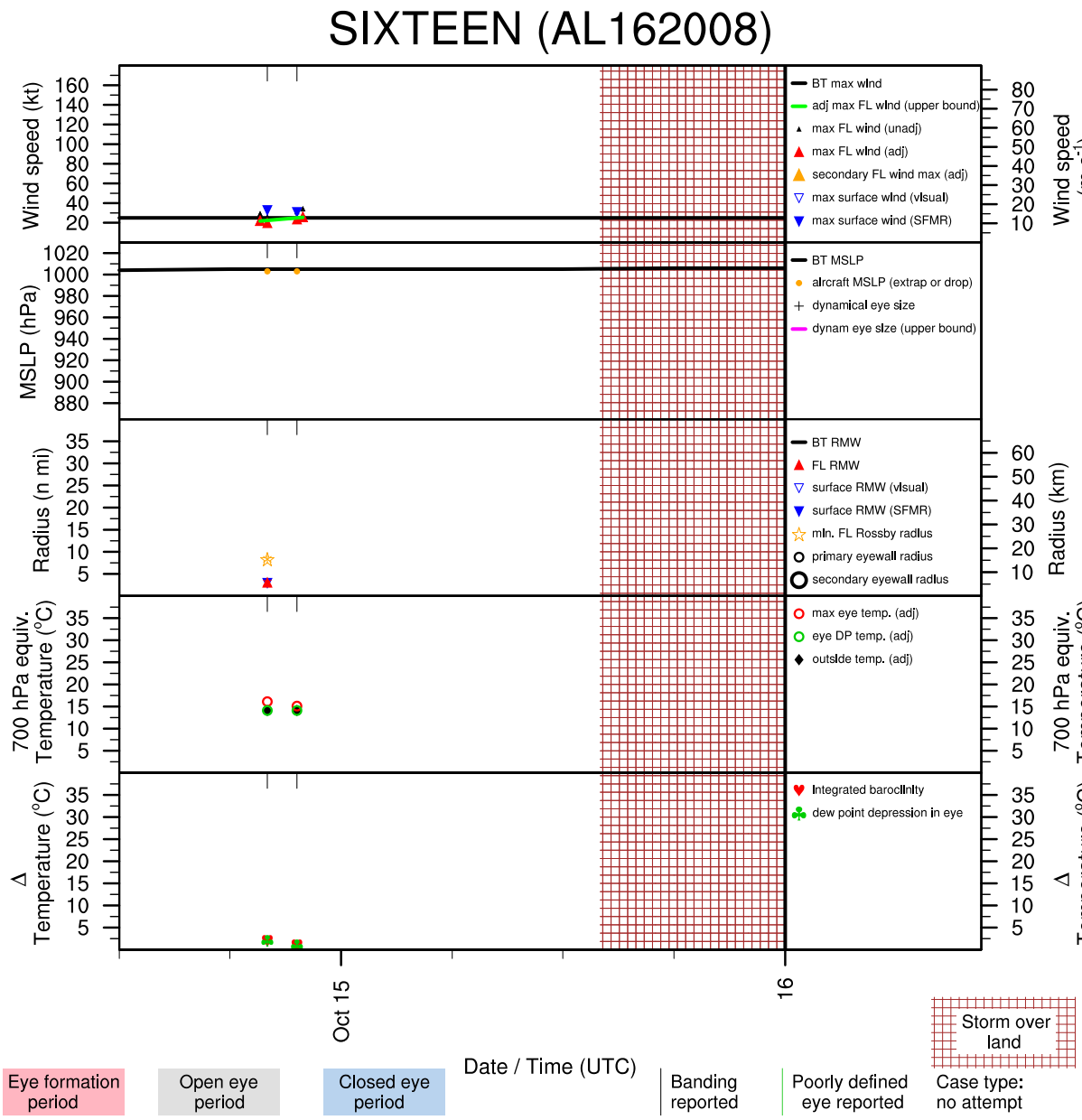

Figure E.179: Structure and intensity parameters for Tropical Depression Sixteen (2008).

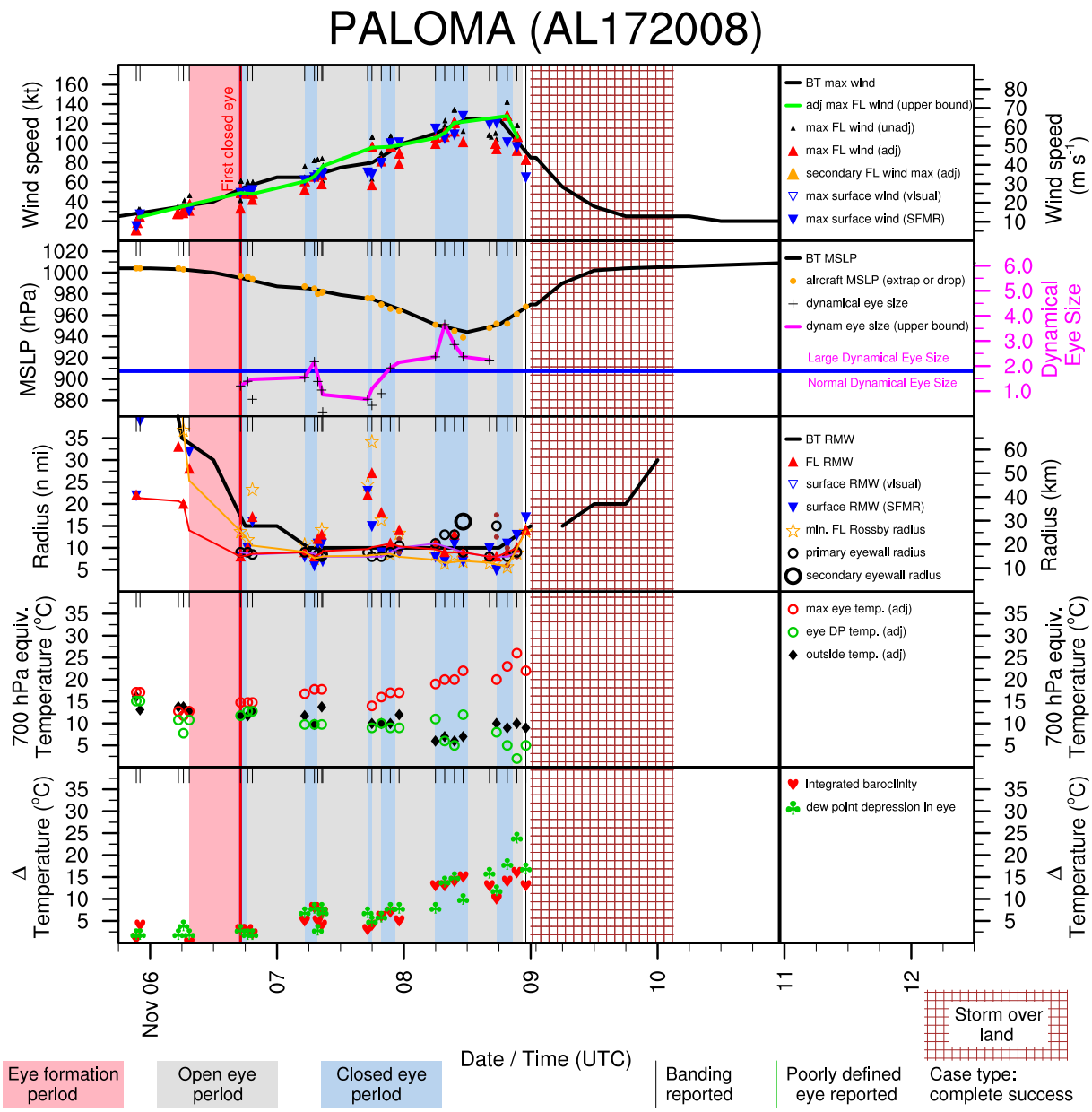

Figure E.180: Structure and intensity parameters for Hurricane Paloma (2008).